To the Graduate Council:

I am submitting herewith a dissertation written by Philip A. Jallouk, entitled "Two-Phase Flow Pressure Drop and Heat Transfer Characteristics of Refrigerants in Vertical Tubes." I recommend that it be accepted in partial fulfillment of the requirements for the degree of Doctor of Philosophy, with a major in Engineering Science.

Julian E. Mott, Major Professor

We have read this dissertation
and recommend its acceptance:

Accepted for the Council:

Vice Chancellor
Graduate Studies and Research

TWO-PHASE FLOW PRESSURE DROP AND HEAT TRANSFER CHARACTERISTICS OF REFRIGERANTS IN VERTICAL TUBES

A Dissertation

Presented for the

Doctor of Philosophy

Degree

The University of Tennessee

Philip A. Jallouk

December 1974

ACKNOWLEDGMENTS

This investigation was performed at the Oak Ridge Gaseous Diffusion Plant operated by the Union Carbide Corporation for the U.S. Atomic Energy Commission. The author wishes to express his appreciation to Union Carbide Corporation and to the Atomic Energy Commission for the use of the facilities and equipment and for the assistance of many of the staff members. The author is especially grateful to Professor Julian E. Mott who served as major professor. His interest and assistance contributed significantly to the success of this research project. Thanks are also due to Dr. George J. Kidd, Jr., head of the Special Projects Department at the Oak Ridge Gaseous Diffusion Plant. His valuable advice and timely suggestions were very helpful in the undertaking of this work. A special word of appreciation is also due to Mr. Ulys C. Fulmer, who assisted the author in the debugging of the loop and the data taking. Finally, the author wishes to thank Mrs. Donna Brewster for typing the manuscript.

1175403

ABSTRACT

Research was undertaken to study the two-phase flow characteristics of refrigerants in vertical tubes. An experimental study was made of the flow regime, pressure drop, heat transfer coefficient, and critical heat flux of R-114 boiling in a 0.785-in.-ID, 10-ft-long vertical tube. The boiling temperature was varied in the range of 100 to 250°F for all tests except the heat transfer coefficient runs where the range 100 to 200°F was studied. The mass flux range was $0.12 \leq G \leq 3.5 \times 10^6$ lbm/hr-sq ft.

The flow regime studies were made by observing the flow in a Pyrex glass section at the test section exit. They indicated that at low mass fluxes and boiling temperatures a large part of the flow was annular in nature. As the boiling temperature was increased, the bubbly flow regime increased significantly. With increasing mass flux, the flow became opaque and a frothy whitish liquid was observed, indicating that the liquid and vapor phases were mixing vigorously. Comparison of the experimental regimes with various flow maps did not yield any satisfactory results. The equations of J. L. L. Baker and the scaling of the experimental flow regimes obtained with one fluid to another on an equal density ratio basis were the only two ways found which gave close albeit not entirely satisfactory agreement.

The pressure drop results were analyzed by separating the gravitational, acceleration, and frictional components. While no entirely satisfactory formulation for the void fraction of R-114 was available, the Martinelli-Nelson model and a modified form of the Zuber et al correlation yielded results which did not differ appreciably from each

other. The frictional component was compared to numerous correlations and the equations developed by Chisholm in a 1973 publication were found to give the best agreement with experimental results. This correlation was also found to agree well with other experimental data for R-11 and R-12 over a very wide range of boiling temperatures and flow rates. Only at very low mass fluxes in horizontal flow was this correlation found to be unsatisfactory.

The experimental heat transfer coefficient results obtained were compared to the ones predicted by numerous heat transfer correlations in the literature. None was found to be satisfactory. Chen's correlation exhibited the least amount of scatter although it consistently underpredicted the experimental heat transfer coefficient results. A detailed analysis of the different components of the correlation indicated that the Forster-Zuber pool boiling correlation with a variable coefficient or the use of the Rohsenow pool boiling equation resulted in a considerable improvement in the Chen correlation, thus reinforcing the concept of superposition. The multiplication factor, F, was also slightly modified. An experimental suppression factor, S, was obtained which was quite similar to Chen's although an effect of pressure was noted. An analytical solution was presented for S. It, however, could not be definitely confirmed since it was found to depend on the frequency of bubble generation from a boiling surface and little information on this could be found. Application of the modified Chen correlation to experimental data in the literature on horizontal flow indicated a lack of agreement at low flows--possibly due to stratification.

The critical heat flux results obtained were analyzed using the scaling law of Barnett and Wood and the scaling factor approach of Stevens and Kirby. Neither was found to be as satisfactory as the compensated distortion model of Ahmad. The critical heat flux data Dix obtained with R-114 were also compared to the present results and satisfactory agreement was obtained.

Recommendations for further investigation are given.

TABLE OF CONTENTS

Chapter		Page
I.	INTRODUCTION AND STATEMENT OF PROBLEM	1
	Introduction	1
	Statement of Problem	5
II.	LITERATURE SURVEY	9
	Flow Regimes	9
	Adiabatic Flow	9
	Diabatic Flow	16
	Pressure Drop	23
	Void Fraction	39
	Heat Transfer Coefficients	51
	Pool Boiling	52
	Flow Boiling	60
	Critical Heat Flux	91
III.	EXPERIMENTAL INVESTIGATION	103
	Description of System	103
	Testing Procedure and Data Recording	114
	Range of Parameters Covered by the Tests	119
	Flow Regimes	119
	Pressure Drop	120
	Heat Transfer Coefficients	120
	Critical Heat Flux	120
IV.	RESULTS AND DISCUSSION	122
	Flow Regimes	122
	Introduction	122

Chapter

	Page
Experimental Results	126
Discussion	134
Comparison With Other Flow Regime Studies	141
Pressure Drop	157
Introduction	157
Experimental Results - This Study	158
Other Frictional Pressure Drop Models	198
Experimental Results - Other Studies, Vertical Tests	213
Experimental Results - Other Studies, Horizontal Tests	216
Heat Transfer Coefficients	235
Introduction	235
Experimental Results - This Study	237
Comparison of Experimental Results With Various Correlations	244
Derivation of an Improved Forced Convective Boiling Correlation	272
Application of an Improved Forced Convection Correlation to Refrigerant and Non-Refrigerant Data	318
Experimental Results - Other Studies, Vertical Tests	343
Experimental Results - Other Studies, Horizontal Tests	343
Critical Heat Flux	348
Introduction	348
Experimental Results - This Study	348
V. SUMMARY, CONCLUSIONS, AND RECOMMENDATIONS	396

Chapter		Page
	Summary and Conclusions	396
	Recommendations	402
REFERENCES		407
APPENDIXES		420
A.	POOL BOILING RESULTS FOR R-11, R-113, AND R-114	421
B.	DESCRIPTION OF BOILING TEST FACILITY AND ASSOCIATED INSTRUMENTATION	423
	Boiling Facility	423
	Test Section and Associated Instrumentation	428
	Heat Input System	429
	Pressure Drop Measuring System	432
	Temperature Measuring System	434
	System Start-Up	435
	Operating Procedure and Problems Encountered	439
	General Observations	442
C.	CALIBRATION TECHNIQUES	446
	Pressure Drop	446
	Flow Rates	450
	Heat Input to Test Section	460
	Thermocouple Calibrations	471
	Overall Calibration	482
D.	SAMPLE CALCULATIONS	487
	Flow Regimes - Application of Quandt [7] Analysis	487
	Data Reduction - Pressure Drop	488
	Data Analysis - Pressure Drop	496
	Application of Pressure Drop Results to Design Calculations	501

Chapter		Page
	Data Reduction - Heat Transfer Coefficients	501
	Data Analysis - Heat Transfer Coefficients	503
	Application of Heat Transfer Results to Design Calculations	504
	Data Reduction - Critical Heat Flux	505
	Data Analysis - Critical Heat Flux	505
	Application of Critical Heat Flux Results to Design Calculations	512
E.	PHYSICAL PROPERTIES OF R-114	513
	Thermodynamic Properties	513
	Transport Properties	516
	Tabulation of Results	517
F.	TABULATION OF DATA	519
G.	ERROR ANALYSIS	601
	Monte Carlo Error Analysis Code	601
	Pressure Drop	602
	Heat Transfer Coefficients	603
	Critical Heat Flux	603
VITA		610

LIST OF TABLES

Table		Page
I-1.	Properties of Benzene, Water, and Several Refrigerants	6
II-1.	Values for the Parameter B in Chisholm's [28] Pressure Drop Correlation	33
II-2.	Experimentally Determined Values of Slip Factor γ' as a Function of Pressure for Steam-Water, Thom [35]	40
II-3.	Prediction of Values for Exponent η' in Equation (2-49) Based on Various Correlations	57
II-4.	Range of Operating Conditions in Cheshire and Stirling [36] Tests	73
II-5.	Values of Constants for Equation (2-72)	74
II-6.	C_{sf} Values as Determined by Blatt and Adt [42] With R-11 and R-113	76
II-7.	Various Values for the Coefficients and Exponents in the Pierre [89] and Altman, Norris, and Staub [40] Correlations	77
II-8.	Comparison of Various Heat Transfer Coefficient Correlations With Boiling Refrigerant Data	90
II-9.	R-114 Critical Heat Flux Test Parameter Range, Dix [111]	99
II-10.	Refrigerant Modeling Constants and Critical Heat Flux Prediction Errors, Dix [111]	99
IV-1.	Comparison of ORGDP Pool Boiling Data With Various Correlations	274
IV-2.	Values Obtained for the Coefficients of the Rohsenow [61] Correlation Using the ORGDP Pool Boiling Data	276
IV-3.	Comparison of Furse's [74] R-11 Pool Boiling Data With Various Correlations	279
IV-4.	Comparison of An Analytical Model for Waiting Time With the Abdelmessih et al [129] Experimental Results for the Case of $q/A = 5.94 \times 10^4$ Btu/hr-sq ft	316

Table		Page
A-1.	Pool Boiling Coefficients for R-11, R-113, and R-114	422
B-1.	Listing of All Major Components in the Boiling Facility	425
B-2.	Listing of All the Components and Instrumentation Associated With the Test Section	437
E-1.	Tabulation of Physical Properties of R-114 . . .	518
F-1.	Tabulation of Flow Regime Data	520
F-2.	Pressure Drop - Experimental Data, $G \approx 0.12 \times 10^6$ lbm/hr-sq ft, $T \approx 100°F$	526
F-3.	Pressure Drop - Experimental Data, $G \approx 0.24 \times 10^6$ lbm/hr-sq ft, $T \approx 100°F$	529
F-4.	Pressure Drop - Experimental Data, $G \approx 0.47 \times 10^6$ lbm/hr-sq ft, $T \approx 100°F$	532
F-5.	Pressure Drop - Experimental Data, $G \approx 0.90 \times 10^6$ lbm/hr-sq ft, $T \approx 100°F$	534
F-6.	Pressure Drop - Experimental Data, $G \approx 1.77 \times 10^6$ lbm/hr-sq ft, $T \approx 100°F$	536
F-7.	Pressure Drop - Experimental Data, $G \approx 0.12 \times 10^6$ lbm/hr-sq ft, $T \approx 150°F$	537
F-8.	Pressure Drop - Experimental Data, $G \approx 0.24 \times 10^6$ lbm/hr-sq ft, $T \approx 150°F$	538
F-9.	Pressure Drop - Experimental Data, $G \approx 0.44 \times 10^6$ lbm/hr-sq ft, $T \approx 150°F$	540
F-10.	Pressure Drop - Experimental Data, $G \approx 0.87 \times 10^6$ lbm/hr-sq ft, $T \approx 150°F$	541
F-11.	Pressure Drop - Experimental Data, $G \approx 1.70 \times 10^6$ lbm/hr-sq ft, $T \approx 150°F$	543
F-12.	Pressure Drop - Experimental Data, $G \approx 3.44 \times 10^6$ lbm/hr-sq ft, $T \approx 150°F$	545
F-13.	Pressure Drop - Experimental Data, $G \approx 0.12 \times 10^6$ lbm/hr-sq ft, $T \approx 200°F$	546
F-14.	Pressure Drop - Experimental Data, $G \approx 0.24 \times 10^6$ lbm/hr-sq ft, $T \approx 200°F$	547

Table		Page
F-15.	Pressure Drop - Experimental Data, G ≈ 0.92 x 10^6 lbm/hr-sq ft, T ≈ 200°F	548
F-16.	Pressure Drop - Experimental Data, G ≈ 1.70 x 10^6 lbm/hr-sq ft, T ≈ 200°F	549
F-17.	Pressure Drop - Experimental Data, G ≈ 3.42 x 10^6 lbm/hr-sq ft, T ≈ 200°F	550
F-18.	Pressure Drop - Experimental Data, G ≈ 0.47 x 10^6 lbm/hr-sq ft, T ≈ 250°F	551
F-19.	Pressure Drop - Experimental Data, G ≈ 0.97 x 10^6 lbm/hr-sq ft, T ≈ 250°F	552
F-20.	Pressure Drop - Correlated Results, G ≈ 0.12 x 10^6 lbm/hr-sq ft, T ≈ 100°F	553
F-21.	Pressure Drop - Correlated Results, G ≈ 0.24 x 10^6 lbm/hr-sq ft, T ≈ 100°F	556
F-22.	Pressure Drop - Correlated Results, G ≈ 0.47 x 10^6 lbm/hr-sq ft, T ≈ 100°F	559
F-23.	Pressure Drop - Correlated Results, G ≈ 0.90 x 10^6 lbm/hr-sq ft, T 100°F	561
F-24.	Pressure Drop - Correlated Results, G ≈ 1.77 x 10^6 lbm/hr-sq ft, T ≈ 100°F	563
F-25.	Pressure Drop - Correlated Results, G ≈ 0.12 x 10^6 lbm/hr-sq ft, T ≈ 150°F	564
F-26.	Pressure Drop - Correlated Results, G ≈ 0.24 x 10^6 lbm/hr-sq ft, T ≈ 150°F	565
F-27.	Pressure Drop - Correlated Results, G ≈ 0.44 x 10^6 lbm/hr-sq ft, T ≈ 150°F	567
F-28.	Pressure Drop - Correlated Results, G ≈ 0.87 x 10^6 lbm/hr-sq ft, T ≈ 150°F	568
F-29.	Pressure Drop - Correlated Results, G ≈ 1.70 x 10^6 lbm/hr-sq ft, T ≈ 150°F	570
F-30.	Pressure Drop - Correlated Results, G ≈ 3.44 x 10^6 lbm/hr-sq ft, T ≈ 150°F	572
F-31.	Pressure Drop - Correlated Results, G ≈ 0.12 x 10^6 lbm/hr-sq ft, T ≈ 200°F	573

Table		Page
F-32.	Pressure Drop - Correlated Results, G ≈ 0.24 x 10^6 lbm/hr-sq ft, T ≈ 200°F	574
F-33.	Pressure Drop - Correlated Results, G ≈ 0.92 x 10^6 lbm/hr-sq ft, T ≈ 200°F	575
F-34.	Pressure Drop - Correlated Results, G ≈ 1.70 x 10^6 lbm/hr-sq ft, T ≈ 200°F	576
F-35.	Pressure Drop - Correlated Results, G ≈ 3.42 x 10^6 lbm/hr-sq ft, T ≈ 200°F	577
F-36.	Pressure Drop - Correlated Results, G ≈ 0.47 x 10^6 lbm/hr-sq ft, T ≈ 250°F	578
F-37.	Pressure Drop - Correlated Results, G ≈ 0.97 x 10^6 lbm/hr-sq ft, T ≈ 250°F	579
F-38.	Heat Transfer - Experimental Data, G ≈ 0.12 x 10^6 lbm/hr-sq ft, T ≈ 100°F	580
F-39.	Heat Transfer - Experimental Data, G ≈ 0.23 x 10^6 lbm/hr-sq ft, T ≈ 100°F	582
F-40.	Heat Transfer - Experimental Data, G ≈ 0.45 x 10^6 lbm/hr-sq ft, T ≈ 100°F	583
F-41.	Heat Transfer - Experimental Data, G ≈ 0.89 x 10^6 lbm/hr-sq ft, T ≈ 100°F	585
F-42.	Heat Transfer - Experimental Data, G ≈ 0.14 x 10^6 lbm/hr-sq ft, T ≈ 150°F	587
F-43.	Heat Transfer - Experimental Data, G ≈ 0.24 x 10^6 lbm/hr-sq ft, T ≈ 150°F	588
F-44.	Heat Transfer - Experimental Data, G ≈ 0.44 x 10^6 lbm/hr-sq ft, T ≈ 150°F	589
F-45.	Heat Transfer - Experimental Data, G ≈ 0.90 x 10^6 lbm/hr-sq ft, T ≈ 150°F	590
F-46.	Heat Transfer - Experimental Data, G ≈ 1.73 x 10^6 lbm/hr-sq ft, T ≈ 150°F	591
F-47.	Heat Transfer - Experimental Data, G ≈ 3.43 x 10^6 lbm/hr-sq ft, T ≈ 150°F	592
F-48.	Heat Transfer - Experimental Data, G ≈ 0.13 x 10^6 lbm/hr-sq ft, T ≈ 200°F	593

Table		Page
F-49.	Heat Transfer - Experimental Data, G ≈ 0.25 x 10^6 lbm/hr-sq ft, T ≈ 200°F	594
F-50.	Heat Transfer - Experimental Data, G ≈ 0.45 x 10^6 lbm/hr-sq ft, T ≈ 200°F	595
F-51.	Heat Transfer - Experimental Data, G ≈ 0.90 x 10^6 lbm/hr-sq ft, T ≈ 200°F	596
F-52.	Heat Transfer - Experimental Data, G ≈ 1.72 x 10^6 lbm/hr-sq ft, T ≈ 200°F	597
F-53.	Heat Transfer - Experimental Data, G ≈ 3.48 x 10^6 lbm/hr-sq ft, T ≈ 200°F	598
F-54.	Critical Heat Flux - Experimental Data	599

LIST OF FIGURES

Figure		Page
I-1.	Pressure-Temperature Relationships for Various Refrigerants [1]	2
II-1.	Schematic Drawings of Flow Patterns in Two-Phase Vertical Upflow	10
II-2.	Flow Regime Map, Baker [5]	12
II-3.	Classification of Gas-Liquid Flow Regimes, Quandt [7]	15
II-4.	Flow Regime Data for Steam-Water Mixtures, Hosler [14]	21
II-5.	Flow Regime Data of Hosler [14] for Steam-Water Mixtures Compared With Flow Regime Maps of Baker [5], Kozlov [6], and Quandt [7]	22
II-6.	Example of Mass Flux Effect on the Frictional Component of Two-Phase Pressure Drop, Muscettola [22]	25
II-7.	Baroczy's [23] Correlation for Two-Phase Frictional Pressure Drop	27
II-8.	Mass Flux Correction to Baroczy's [23] Frictional Pressure Drop Correlation	29
II-9.	Comparison of Chisholm's [25, 27] Analytically Derived Values for Φ_{ftt} With the Lockhart-Martinelli [19] Curve	32
II-10.	General Correlation of the Two-Phase Parameter, ε, Chawla [29, 30, 31, 32]	34
II-11.	Comparison of Martinelli-Nelson [4] and Thom [35] Void Fraction Correlations	41
II-12.	Comparison of Various Models With Shiralkar's [50] Data for the Void Fraction of R-114. $G = 0.156 \times 10^6$ lbm/hr-sq ft	47
II-13.	Comparison of Various Models With Shiralkar's [50] Data for the Void Fraction of R-114. $G = 0.303 \times 10^6$ lbm/hr-sq ft	48
II-14.	Comparison of Various Models With Shiralkar's [50] Data for the Void Fraction of R-114. $G = 0.526 \times 10^6$ lbm/hr-sq ft	49

Figure		Page
II-15.	Comparison of Shiralkar's [50] R-114 Data With Marchaterre and Hoglund [47] Correlation . . .	50
II-16.	Characteristic Pool Boiling Curves for R-114 at Various Pressures, Hesse [75]	59
II-17.	Multiplication Factor, F, as a Function of the Martinelli Parameter, Chen [80]	64
II-18.	Suppression Factor, S, as a Function of the Two-Phase Reynolds Number, Chen [80]	64
II-19.	Comparison of Experimental Data With the Separated Flow Model, Davis and David [81]	66
II-20.	Correlation of the Experimental Data at 50 psia by the Homogeneous Model, Davis and David [81]	66
II-21.	Heat Transfer Correlation and Range of Parameters in Series, E, F, and G, Shrock and Grossman [82]	67
II-22.	Comparison of the R-12 Vertical Flow Boiling Data of Lavin and Young [84] With the Correlations of Other Workers	70
II-23.	Comparison of Napendsky's [15] Heat Transfer Results at a Heat Flux of 22,500 Btu/hr-sq ft With the Guerrieri and Talty [77] Correlation	72
II-24.	Comparison of the R-113 Horizontal Flow Boiling Results of Gouse and Coumou [91] With Various Correlations	80
II-25.	Model for Suppression of Nucleation in Forced Convection Boiling [92]	81
II-26.	Comparison of the R-113 Horizontal Flow Boiling Data of Gouse and Dickson [93] With Several Correlations	83
II-27.	Comparison of the R-11 Horizontal Flow Boiling Data of Gouse and Dickson [93] With Several Correlations	84
II-28.	Comparison of the R-12 Horizontal Flow Boiling Results of Chaddock and Noerager [43] With the Correlations of Dengler and Addoms [78] and Guerrieri and Talty [77]	84

Figure		Page
II-29.	Comparison of the R-12 Horizontal Flow Boiling Results of Chaddock and Noerager [43] With the Correlation of Schrock and Grossman [82]	85
II-30.	Comparison of the R-12 Horizontal Flow Boiling Results of Chaddock and Noerager [43] With the Correlations of Pierre [89] and Altman, Norris, and Staub [40]	85
II-31.	Comparison of Purcupile, Riedle, and Schmidt [94] Vertical Flow Boiling Data With Dengler and Addoms [78] Correlation	87
II-32.	Comparison of Purcupile, Riedle, and Schmidt [94] Vertical Flow Boiling Data With Schrock and Grossman [82] Correlation	87
II-33.	Comparison of Purcupile, Riedle, and Schmidt [94] Vertical Flow Boiling Data With Chen [80] Correlation	88
II-34.	Comparison of Purcupile, Riedle, and Schmidt [94] Vertical Flow Boiling Data With Chawla's [29] Correlation for the Nucleate Boiling Regime . .	88
II-35.	Comparison of Purcupile, Riedle, and Schmidt [94] Vertical Flow Boiling Data With Riedle-Purcupile [95] Correlation	89
II-36.	Comparison of the Scaling Law in Equation (2-80) With Experimental Data. Barnett [106]	95
II-37.	Critical Heat Flux Data With R-12 and R-22 Using the Scaling Factors of Stevens and Kirby [107] and the Modification of Staub [110]	98
III-1.	Schematic Drawing of Boiling Facility	104
III-2.	Overall View of Ten-Foot Test Section	105
III-3.	Cutaway View of Test Section, Heaters, Thermon, and Insulation	107
III-4.	Detail of the Groove Separating the Zones in the Test Section	108
III-5.	Illustration of Wall and Instream Thermocouples in a Zone	109
III-6.	Detail of Instream Thermocouple Installation . . .	110

Figure		Page
III-7.	Cross Sectional View of All Thermocouple Locations	111
III-8.	Pressure Measurement Setup and Instrumentation .	112
III-9.	Visual Flow Indicator Assembly	115
IV-1.	Bubbly Flow	124
IV-2.	Bubbly-Slug Flow (Round Slug)	124
IV-3.	Bubbly-Slug Flow (Slug With Bullet-Shaped Nose) .	124
IV-4.	Transition Flow	125
IV-5.	Weak Annular Flow	125
IV-6.	Strong Annular Flow	127
IV-7.	Mist Flow	127
IV-8.	Experimental Flow Regime Map for R-114 at 110°F .	128
IV-9.	Experimental Flow Regime Map for R-114 at 150°F .	129
IV-10.	Experimental Flow Regime Map for R-114 at 200°F .	130
IV-11.	Experimental Flow Regime Map for R-114 at 250°F .	131
IV-12.	Illustration of the Nonspherical Shape of Bubbles in Bubbly Flow	136
IV-13.	Typical Size of Vapor Slug in Bubbly-Slug Flow .	136
IV-14.	Three Consecutive Frames From Video Tape Depicting Vapor Slug in Bubbly-Slug Flow	137
IV-15.	Example of the Bubble Sizes Occurring in Bubbly Flow at High Mass Fluxes	140
IV-16.	Illustration of the Unidentifiable Flow Regime .	140
IV-17.	Comparison of Experimental and Baker [5] Flow Regime Maps, T ≈ 110°F	142
IV-18.	Comparison of Experimental and Baker [5] Flow Regime Maps, T ≈ 150°F	142
IV-19.	Comparison of Experimental and Baker [5] Flow Regime Maps, T ≈ 200°F	143

Figure		Page
IV-20.	Comparison of Experimental and Baker [5] Flow Regime Maps, T ≈ 250°F	143
IV-21.	Comparison of Experimental Flow Regime Map and Quandt [7] Analysis, T ≈ 110°F	144
IV-22.	Comparison of Experimental Flow Regime Map and Quandt [7] Analysis, T ≈ 150°F	144
IV-23.	Comparison of Experimental Flow Regime Map and Quandt [7] Analysis, T ≈ 200°F	145
IV-24.	Comparison of Experimental Flow Regime Map and Quandt [7] Analysis, T ≈ 250°F	145
IV-25.	Comparison of Experimental Flow Regime Map and Zuber et al [10] Equation for the Transition From Churn-Turbulent to Annular Flow, T ≈ 110°F	149
IV-26.	Comparison of Experimental Flow Regime Map and Zuber et al [10] Equation for the Transition From Churn-Turbulent to Annular Flow, T ≈ 150°F	149
IV-27.	Comparison of Experimental Flow Regime Map and Zuber et al [10] Equation for the Transition From Churn-Turbulent to Annular Flow, T ≈ 200°F	150
IV-28.	Comparison of Experimental Flow Regime Map and Zuber et al [10] Equation for the Transition From Slug to Annular Flow, T ≈ 110°F	151
IV-29.	Comparison of Experimental Flow Regime Map and J. L. L. Baker's [17] Transitions Between Churn, Wispy Annular, and Annular. $\eta' = 1/2$, T ≈ 110°F.	152
IV-30.	Comparison of Experimental Flow Regime Map and J. L. L. Baker's [17] Transitions Between Churn, Wispy Annular, and Annular. $\eta' = 1/2$, T ≈ 150°F.	152
IV-31.	Comparison of Experimental Flow Regime Map and J. L. L. Baker's [17] Transitions Between Churn, Wispy Annular, and Annular. $\eta' = 1/2$, T ≈ 200°F.	153
IV-32.	Comparison of Experimental Flow Regime Map and J. L. L. Baker's [17] Transitions Between Churn, Wispy Annular, and Annular. $\eta' = 1/2$, T ≈ 250°F.	153

Figure		Page
IV-33.	Comparison of Experimental Flow Regime Map and J. L. L. Baker's [17] Transitions Between Churn, Wispy Annular, and Annular. $\eta' = 0$, $T \approx 110°F$ . .	155
IV-34.	Comparison of Experimental Flow Regime Map and J. L. L. Baker's [17] Transitions Between Churn, Wispy Annular, and Annular. $\eta' = 0$, $T \approx 150°F$ . .	155
IV-35.	Comparison of Experimental Flow Regime Map and J. L. L. Baker's [17] Transitions Between Churn, Wispy Annular, and Annular. $\eta' = 0$, $T \approx 200°F$ . .	156
IV-36.	Comparison of Experimental Flow Regime Map and J. L. L. Bakers [17] Transitions Between Churn, Wispy Annular, and Annular. $\eta' = 0$, $T \approx 250°F$ . .	156
IV-37.	Comparison of Experimental Pressure Drop Results With Analytically Derived Frictional Component Using the Homogeneous [3] Model, $T \approx 100°F$ . . .	159
IV-38.	Comparison of Experimental Pressure Drop Results With Analytically Derived Frictional Component Using the Homogeneous [3] Model, $T \approx 150°F$ . . .	162
IV-39.	Comparison of Experimental Pressure Drop Results With Analytically Derived Frictional Component Using the Homogeneous [3] Model, $T \approx 200°F$ . . .	165
IV-40.	Comparison of Experimental Pressure Drop Results With Analytically Derived Frictional Component Using the Homogeneous [3] Model, $T \approx 250°F$ . . .	168
IV-41.	Comparison of Experimental Pressure Drop Results With Analytically Derived Frictional Components Using the Martinelli-Nelson [4] Model, $T \approx 100°F$	169
IV-42.	Comparison of Experimental Pressure Drop Results With Analytically Derived Frictional Components Using the Martinelli-Nelson [4] Model, $T \approx 150°F$	172
IV-43.	Comparison of Experimental Pressure Drop Results With Analytically Derived Frictional Components Using the Martinelli-Nelson [4] Model, $T \approx 200°F$	175
IV-44.	Comparison of Experimental Pressure Drop Results With Analytically Derived Frictional Components Using the Martinelli-Nelson [4] Model, $T \approx 250°F$	178

Figure		Page
IV-45.	Comparison of Void Fraction Formulations From the Homogeneous [3] and Martinelli-Nelson [4] Models	180
IV-46.	Comparison of Void Fractions From a Modified Form of the Zuber et al [10] Formulation and Martinelli-Nelson [4]	182
IV-47.	Comparison of Experimental Pressure Drop Results With Analytically Derived Frictional Components Using the Martinelli-Nelson [4] Model and a Modified Form of the Zuber et al [10] General Void Fraction Correlation, T ≈ 100°F	183
IV-48.	Comparison of Experimental Pressure Drop Results With Analytically Derived Frictional Components Using the Martinelli-Nelson [4] Model and a Modified Form of the Zuber et al [10] General Void Fraction Correlation, T ≈ 150°F	186
IV-49.	Comparison of Experimental Pressure Drop Results With Analytically Derived Frictional Components Using the Martinelli-Nelson [4] Model and a Modified Form of the Zuber et al [10] General Void Fraction Correlation, T ≈ 200°F	189
IV-50.	Comparison of Experimental Pressure Drop Results With Analytically Derived Frictional Components Using the Martinelli-Nelson [4] Model and a Modified Form of the Zuber et al [10] General Void Fraction Correlation, T ≈ 250°F	192
IV-51.	Comparison of Experimental Pressure Drop Results in the Critical Heat Flux Region With the Martinelli-Nelson [4] Model and a Modified Form of the Zuber et al [10] General Void Fraction Correlation, T ≈ 100°F	194
IV-52.	Comparison of Experimental Pressure Drop Results in the Critical Heat Flux Region With the Martinelli-Nelson [4] Model and a Modified Form of the Zuber et al [10] General Void Fraction Correlation, T ≈ 150°F	195
IV-53.	Comparison of Experimental Pressure Drop Results in the Critical Heat Flux Region With the Martinelli-Nelson [4] Model and a Modified Form of the Zuber et al [10] General Void Fraction Correlation, T ≈ 200°F	196

Figure		Page
IV-54.	Comparison of Experimental Pressure Drop Results in the Critical Heat Flux Region With the Martinelli-Nelson [4] Model and a Modified Form of the Zuber et al [10] General Void Fraction Correlation, T ≈ 250°F	197
IV-55.	Comparison of Experimental Pressure Drop Results With Davis [34] Correlation, T ≈ 100°F	200
IV-56.	Comparison of Experimental Pressure Drop Results With Davis [34] Correlation, T ≈ 150°F	200
IV-57.	Comparison of Experimental Pressure Drop Results With Davis [34] Correlation, T ≈ 200°F	201
IV-58.	Comparison of Experimental Pressure Drop Results With Various Correlations, T ≈ 100°F	202
IV-59.	Comparison of Experimental Pressure Drop Results With Various Correlations, T ≈ 150°F	205
IV-60.	Comparison of Experimental Pressure Drop Results With Various Correlations, T ≈ 200°F	208
IV-61.	Comparison of Experimental Pressure Drop Results With Various Correlations, T ≈ 250°F	211
IV-62.	Comparison of Cheshire and Stirling's [36] R-114 Experimental Pressure Drop Results With Those of This Study, T ≈ 86°F	214
IV-63.	Comparison of Cheshire and Stirling's [36] R-114 Experimental Pressure Drop Results With Those of This Study, T ≈ 111°F	214
IV-64.	Comparison of Cheshire and Stirling's [36] R-114 Experimental Pressure Drop Results With Those of This Study, T ≈ 136°F	215
IV-65.	Comparison of Napadensky's [15] R-12 Experimental Pressure Drop Results With Various Correlations, T ≈ 86°F	217
IV-66.	Comparison of Napadensky's [15] R-12 Experimental Pressure Drop Results With Various Correlations, T ≈ 104°F	219
IV-67.	Comparison of Napadensky's [15] R-12 Experimental Pressure Drop Results With Various Correlations, T ≈ 140°F	221

Figure		Page
IV-68.	Comparison of Bryan and Seigel's [39] R-11 Experimental Pressure Drop Results With Various Correlations. Horizontal Boiling . .	224
IV-69.	Comparison of Johnston and Chaddock's [41] R-12 Experimental Pressure Drop Results With Various Correlations. Horizontal Boiling . .	227
IV-70.	Comparison of Johnston and Chaddock's [41] R-22 Experimental Pressure Drop Results With Various Correlations. Horizontal Boiling . .	229
IV-71.	Comparison of Chaddock and Noerager's [43] R-12 Experimental Pressure Drop Results With Various Correlations. Horizontal Boiling . .	231
IV-72.	Comparison of the Chisholm [28] 1973 and Chawla [29, 30, 31, 32] Correlations	233
IV-73.	Plot of the Heat Flux Versus the Wall-to-Bulk Temperature Difference for the Forced Convective Boiling of R-114, T ≈ 100°F	238
IV-74.	Plot of the Heat Flux Versus the Wall-to-Bulk Temperature Difference for the Forced Convective Boiling of R-114, T ≈ 150°F	239
IV-75.	Plot of the Heat Flux Versus the Wall-to-Bulk Temperature Difference for the Forced Convective Boiling of R-114, T ≈ 200°F	240
IV-76.	Plot of the Heat Transfer Coefficient Versus the Wall-to-Bulk Temperature Difference for the Forced Convective Boiling of R-114, T ≈ 100°F	241
IV-77.	Plot of the Heat Transfer Coefficient Versus the Wall-to-Bulk Temperature Difference for the Forced Convective Boiling of R-114, T ≈ 150°F	242
IV-78.	Plot of the Heat Transfer Coefficient Versus the Wall-to-Bulk Temperature Difference for the Forced Convective Boiling of R-114, T ≈ 200°F	243
IV-79.	Comparison of the Experimental Heat Transfer Coefficients With the Cheshire and Stirling [36] Correlation, T ≈ 100°F	245

Figure		Page
IV-80.	Comparison of the Experimental Heat Transfer Coefficients With the Cheshire and Stirling [36] Correlation, T ≈ 150°F	246
IV-81.	Comparison of the Experimental Heat Transfer Coefficients With the Cheshire and Stirling [36] Correlation, T ≈ 200°F	247
IV-82.	Comparison of the Experimental Heat Transfer Coefficients With the Altman, Norris, and Staub [40] Correlation	250
IV-83.	Comparison of the Experimental Heat Transfer Coefficients With the Davis and David [81] Separated Flow Model, T ≈ 100°F	252
IV-84.	Comparison of the Experimental Heat Transfer Coefficients With the Davis and David [81] Separated Flow Model, T ≈ 150°F	252
IV-85.	Comparison of the Experimental Heat Transfer Coefficients With the Davis and David [81] Separated Flow Model, T ≈ 200°F	253
IV-86.	Comparison of the Experimental Heat Transfer Coefficients With the Davis and David [81] Homogeneous Model, T ≈ 100°F	253
IV-87.	Comparison of the Experimental Heat Transfer Coefficients With the Davis and David [81] Homogeneous Model, T ≈ 150°F	254
IV-88.	Comparison of the Experimental Heat Transfer Coefficients With the Davis and David [81] Homogeneous Model, T ≈ 200°F	254
IV-89.	Comparison of the Experimental Heat Transfer Coefficients With the Dengler and Addoms [78] Correlation	256
IV-90.	Comparison of the Average Experimental Heat Transfer Coefficients Along the Length of the Boiling Test Section With the Dengler and Addoms [78] Correlation	257
IV-91.	Comparison of the Experimental Heat Transfer Coefficients With the Guerrieri and Talty [77] Correlation	259

Figure		Page
IV-92.	Comparison of the Average Experimental Heat Transfer Coefficients Along the Length of the Boiling Test Section With the Guerrieri and Talty [77] Correlation	260
IV-93.	Comparison of the Average Experimental Heat Transfer Coefficients Along the Length of the Boiling Test Section With the Bennett et al [79] Correlation	262
IV-94.	Comparison of the Experimental Heat Transfer Coefficients With the Schrock and Grossman [82] Correlation, T ≈ 100°F	264
IV-95.	Comparison of the Experimental Heat Transfer Coefficients With the Schrock and Grossman [82] Correlation, T ≈ 150°F	264
IV-96.	Comparison of the Experimental Heat Transfer Coefficients With the Schrock and Grossman [82] Correlation, T ≈ 200°F	265
IV-97.	Comparison of the Experimental Heat Transfer Coefficients With the Collier and Pulling [83] Correlation, T ≈ 100°F	265
IV-98.	Comparison of the Experimental Heat Transfer Coefficients With the Collier and Pulling [83] Correlation, T ≈ 150°F	266
IV-99.	Comparison of the Experimental Heat Transfer Coefficients With the Collier and Pulling [83] Correlation, T ≈ 200°F	266
IV-100.	Comparison of the Experimental Heat Transfer Coefficients With the Riedle and Purcupile [94, 95] Correlation, T ≈ 100°F	267
IV-101.	Comparison of the Experimental Heat Transfer Coefficients With the Riedle and Purcupile [94, 95] Correlation, T ≈ 150°F	267
IV-102.	Comparison of the Experimental Heat Transfer Coefficients With the Riedle and Purcupile [94, 95] Correlation, T ≈ 200°F	268
IV-103.	Comparison of the Experimental Heat Transfer Coefficients With the Chen [80] Correlation, T ≈ 100°F	269

Figure		Page
IV-104.	Comparison of the Experimental Heat Transfer Coefficients With the Chen [80] Correlation, T ≈ 150°F	269
IV-105.	Comparison of the Experimental Heat Transfer Coefficients With the Chen [80] Correlation, T ≈ 200°F	270
IV-106.	Comparison of the Average Experimental Heat Transfer Coefficients Along the Length of the Boiling Test Section With the Chen [80] Correlation	271
IV-107.	Correlation of the ORGDP Pool Boiling Data With the Rohsenow [61] Equation	277
IV-108.	Correlation of Furse's [74] R-11 Data With the Rohsenow [61] Equation	280
IV-109.	Correlation of Furse's [74] R-12 Data With the Rohsenow [61] Equation	280
IV-110.	Correlation of Hesse's [75] R-12 Data With the Rohsenow [61] Equation	282
IV-111.	Correlation of Hesse's [75] R-113 Data With the Rohsenow [61] Equation	282
IV-112.	Correlation of Hesse's [75] R-114 Data With the Rohsenow [61] Equation	283
IV-113.	Comparison of F Function Calculated by Momentum Transfer Analogy With Empirical Curve, Chen [80]	287
IV-114.	Comparison of Chen's [80] Empirical Curve With Various Formulations for the Multiplication Factor F, T = 100°F	287
IV-115.	Comparison of Chen's [80] Empirical Curve With Various Formulations for the Multiplication Factor F, T = 150°F	288
IV-116.	Comparison of Chen's [80] Empirical Curve With Various Formulations for the Multiplication Factor F, T = 200°F	288
IV-117.	Temperature Profiles for Pool Boiling and for Convective Boiling With the Same Total Superheat, Chen [80]	290

Figure		Page
IV-118.	Radius of Curvature Versus Vapor Volume and Distance From the Wall in a Cavity	291
IV-119.	Subcooled Flow Boiling Curve For R-113 in a Stainless Steel Tube, Murphy and Bergles [120]	294
IV-120.	Temperature Profiles in the Vicinity of a Bubble in Pool Boiling and Flow Boiling	294
IV-121.	Steady State Solution for the Suppression Factor for Various Values of Wall-to-Bulk Temperature Differences and m	301
IV-122.	Effect of Boiling Temperature on the Suppression Factor According to the Steady State Solution .	303
IV-123.	Plot of the Number of Active Nucleation Sites Versus Cavity Size for a Variety of Materials and Surface Finishes, Brown [121]	304
IV-124.	Transient Behavior of the Thermal Boundary Layer in the Vicinity of an Active Nucleation Site .	308
IV-125.	Transient Behavior of the Thermal Boundary Layer in the Vicinity of the Wall for One of the Tests Conducted by Abdelmessih et al [129] . .	315
IV-126.	Plot of the Experimentally Determined C_{sf} Values Versus the Two-Phase Reynolds Number Using the Original Multiplication Factor F. T ≈ 100°F . .	320
IV-127.	Plot of the Experimentally Determined C_{sf} Values Versus the Two-Phase Reynolds Number Using the Original Multiplication Factor F. T ≈ 150°F . .	320
IV-128.	Plot of the Experimentally Determined C_{sf} Values Versus the Two-Phase Reynolds Number Using the Original Multiplication Factor F. T ≈ 200°F . .	321
IV-129.	Plot of Experimentally Determined C_{sf} Values Versus the Two-Phase Reynolds Number Using $F=(1/1-\alpha)^{0.9}$ and the Modified Zuber et al [10] Void Fraction Formulation. T ≈ 100°F	322
IV-130.	Plot of Experimentally Determined C_{sf} Values Versus the Two-Phase Reynolds Number Using $F=(1/1-\alpha)^{0.9}$ and the Modified Zuber et al [10] Void Fraction Formulation. T ≈ 150°F	322

Figure		Page
IV-131.	Plot of Experimentally Determined C_{sf} Values Versus the Two-Phase Reynolds Number Using $F=(1/1-\alpha)^{0.9}$ and the Modified Zuber et al [10] Void Fraction Formulation. T ≈ 200°F	323
IV-132.	Plot of the Experimentally Determined C_{sf} Values Versus the Two-Phase Reynolds Number Using $F=(\Phi_{ftt})^{0.89}$. T ≈ 100°F	323
IV-133.	Plot of the Experimentally Determined C_{sf} Values Versus the Two-Phase Reynolds Number Using $F=(\Phi_{ftt})^{0.89}$. T ≈ 150°F	324
IV-134.	Plot of the Experimentally Determined C_{sf} Values Versus the Two-Phase Reynolds Number Using $F=(\Phi_{ftt})^{0.89}$. T ≈ 200°F	324
IV-135.	Plot of the Experimentally Determined Suppression Factor Versus the Two-Phase Reynolds Number Using the Forster-Zuber [52] Pool Boiling Correlation With a 0.3802 Coefficient. T ≈ 100°F	326
IV-136.	Plot of the Experimentally Determined Suppression Factor Versus the Two-Phase Reynolds Number Using the Forster-Zuber [52] Pool Boiling Correlation With a 0.3802 Coefficient. T ≈ 150°F	326
IV-137.	Plot of the Experimentally Determined Suppression Factor Versus the Two-Phase Reynolds Number Using the Forster-Zuber [52] Pool Boiling Correlation With a 0.3802 Coefficient. T ≈ 200°F	327
IV-138.	Comparison of the Experimental Heat Transfer Coefficients With a Modified Form of the Chen [80] Correlation Using the Forster-Zuber [52] Pool Boiling Equation With a 0.3802 Coefficient. T ≈ 100°F	329
IV-139.	Comparison of the Experimental Heat Transfer Coefficients With a Modified Form of the Chen [80] Correlation Using the Forster-Zuber [52] Pool Boiling Equation With a 0.3802 Coefficient. T ≈ 150°F	330
IV-140.	Comparison of the Experimental Heat Transfer Coefficients With a Modified Form of the Chen [80] Correlation Using the Forster-Zuber [52] Pool Boiling Equation With a 0.3802 Coefficient. T ≈ 200°F	331

Figure		Page
IV-141.	Plot of Experimentally Determined Suppression Factor Versus Two-Phase Reynolds Number Using the Rohsenow [61] Pool Boiling Correlation With C_{sf} = 0.0047. T ≈ 100°F	333
IV-142.	Plot of Experimentally Determined Suppression Factor Versus Two-Phase Reynolds Number Using the Rohsenow [61] Pool Boiling Correlation With C_{sf} = 0.0047. T ≈ 150°F	334
IV-143.	Plot of Experimentally Determined Suppression Factor Versus Two-Phase Reynolds Number Using the Rohsenow [61] Pool Boiling Correlation With C_{sf} = 0.0047. T ≈ 200°F	335
IV-144.	Comparison of the Experimental Heat Transfer Coefficients With a Modified Form of the Chen [80] Correlation Using the Rohsenow [61] Pool Boiling Equation With C_{sf} = 0.0047. T ≈ 100°F	336
IV-145.	Comparison of the Experimental Heat Transfer Coefficients With a Modified Form of the Chen [80] Correlation Using the Rohsenow [61] Pool Boiling Equation With C_{sf} = 0.0047. T ≈ 150°F	337
IV-146.	Comparison of the Experimental Heat Transfer Coefficients With a Modified Form of the Chen [80] Correlation Using the Rohsenow [61] Pool Boiling Equation With C_{sf} = 0.0047. T ≈ 200°F	338
IV-147.	Comparison of Allen's [88] Experimental Heat Transfer Coefficients For R-114 With a Modified Form of the Chen [80] Correlation Using the Rohsenow [61] Pool Boiling Equation With C_{sf} = 0.0026. T ≈ 160°F	344
IV-148.	Comparison of Chaddock and Noerager's [43] Experimental Heat Transfer Coefficients For R-12 With a Modified Form of the Chen [80] Correlation Using the Forster-Zuber [52] Pool Boiling Equation With a Coefficient of 0.292. T ≈ 54°F	346
IV-149.	Comparison of Chaddock and Noerager's [43] Experimental Heat Transfer Coefficients For R-12 With a Modified Form of the Chen [80] Correlation Using the Rohsenow [61] Pool Boiling Equation With C_{sf} = 0.007. T ≈ 54°F .	347

Figure		Page
IV-150.	Plot of the Exit Quality at Which the Critical Heat Flux Occurs Versus the L/D Ratio for Various Mass Fluxes	350
IV-151.	Plot of the Exit Quality at Which the Critical Heat Flux Occurs Versus the Boiling Temperature for Various Mass Fluxes	352
IV-152.	Comparison of the Experimentally Determined Critical Heat Fluxes With Values Obtained Using the Macbeth [101] and Biasi et al [112] Correlations and the Scaling Laws of Barnett and Wood [105]. T ≈ 100°F	355
IV-153.	Comparison of the Experimentally Determined Critical Heat Fluxes With Values Obtained Using the Macbeth [101] and Biasi et al [112] Correlations and the Scaling Laws of Barnett and Wood [105]. T ≈ 150°F	357
IV-154.	Comparison of the Experimentally Determined Critical Heat Fluxes With Values Obtained Using the Macbeth [101] and Biasi et al [112] Correlations and the Scaling Laws of Barnett and Wood [105]. T ≈ 200°F	360
IV-155.	Comparison of the Experimentally Determined Critical Heat Fluxes With Values Obtained Using the Macbeth [101] and Biasi et al [112] Correlations and the Scaling Laws of Barnett and Wood [105]. T ≈ 250°F	363
IV-156.	Comparison of the Experimentally Determined Qualities at the Critical Heat Flux With the Correlation of Stevens and Kirby [107] As Modified by Staub [110] for the Case of $\Delta h/h_{fg}$ = 0. T ≈ 100°F	366
IV-157.	Comparison of the Experimentally Determined Qualities at the Critical Heat Flux With the Correlation of Stevens and Kirby [107] As Modified by Staub [110] for the Case of $\Delta h/h_{fg}$ = 0. T ≈ 150°F	367
IV-158.	Comparison of the Experimentally Determined Qualities at the Critical Heat Flux With the Correlation of Stevens and Kirby [107] As Modified by Staub [110] for the Case of $\Delta h/h_{fg}$ = 0. T ≈ 200°F	368

Figure | Page

IV-159. Comparison of the Experimentally Determined Qualities at the Critical Heat Flux With the Correlation of Stevens and Kirby [107] as Modified By Staub [110] for the Case of $\Delta h/h_{fg}$ = 0. T ≈ 250°F 369

IV-160. Comparison of the Critical Heat Flux Qualities Obtained for Water at 442°F Using the Biasi et al [112] Correlation With the Correlation of Stevens and Kirby [107] as Modified by Staub [110] for the Case of $\Delta h/h_{fg}$ = 0. K_s = 0.658 370

IV-161. Comparison of the Critical Heat Flux Qualities Obtained for Water at 517°F Using the Biasi et al [112] Correlation With the Correlation of Stevens and Kirby [107] as Modified by Staub [110] for the Case of $\Delta h/h_{fg}$ = 0. K_s = 0.658 371

IV-162. Comparison of the Critical Heat Flux Qualities Obtained for Water at 587°F Using the Biasi et al [112] Correlation With the Correlation of Stevens and Kirby [107] as Modified by Staub [110] for the Case of $\Delta h/h_{fg}$ = 0. K_s = 0.658 372

IV-163. Comparison of the Critical Heat Flux Qualities Obtained for Water at 652°F Using the Biasi et al [112] Correlation With the Correlation of Stevens and Kirby [107] as Modified by Staub [110] for the Case of $\Delta h/h_{fg}$ = 0. K_s = 0.658 373

IV-164. Normalized Pressure Effect on Mass Velocity Modeling 375

IV-165. Comparison of the Critical Heat Flux Qualities Obtained for Water at 442°F Using the Biasi et al [112] Correlation With the Correlation of Stevens and Kirby [107] as Modified by Staub [110] for the Case of $\Delta h/h_{fg}$ = 0. K_s Is as Defined in Equation (4-93) 376

IV-166. Comparison of the Critical Heat Flux Qualities Obtained for Water at 517°F Using the Biasi et al [112] Correlation With the Correlation of Stevens and Kirby [107] as Modified by Staub [110] for the Case of $\Delta h/h_{fg}$ = 0. K_s Is as Defined in Equation (4-93) 377

Figure		Page
IV-167.	Comparison of the Critical Heat Flux Qualities Obtained for Water at 587°F Using the Biasi et al [112] Correlation With the Correlation of Stevens and Kirby [107] as Modified by Staub [110] for the Case of $\Delta h/h_{fg} = 0$. K_s Is as Defined in Equation (4-93)	378
IV-168.	Comparison of the Critical Heat Flux Qualities Obtained for Water at 652°F Using the Biasi et al [112] Correlation With the Correlation of Stevens and Kirby [107] as Modified by Staub [110] for the Case of $\Delta h/h_{fg} = 0$. K_s Is as Defined in Equation (4-93)	379
IV-169.	Comparison of the Experimentally Determined Qualities at the Critical Heat Flux With the Compensated Distortion Model of Ahmad [116]. T ≈ 100°F	381
IV-170.	Comparison of the Experimentally Determined Qualities at the Critical Heat Flux With the Compensated Distortion Model of Ahmad [116]. T ≈ 150°F	382
IV-171.	Comparison of the Experimentally Determined Qualities at the Critical Heat Flux With the Compensated Distortion Model of Ahmad [116]. T ≈ 200°F	383
IV-172.	Comparison of the Experimentally Determined Qualities at the Critical Heat Flux With the Compensated Distortion Model of Ahmad [116]. T ≈ 250°F	384
IV-173.	Comparison of the Critical Heat Flux Qualities Obtained for Water At 442°F Using the Biasi et al [112] Correlation With the Compensated Distortion Model of Ahmad [116]	385
IV-174.	Comparison of the Critical Heat Flux Qualities Obtained for Water At 517°F Using the Biasi et al [112] Correlation With the Compensated Distortion Model of Ahmad [116]	386
IV-175.	Comparison of the Critical Heat Flux Qualities Obtained for Water At 587°F Using the Biasi et al [112] Correlation With the Compensated Distortion Model of Ahmad [116]	387

Figure		Page
IV-176.	Comparison of the Critical Heat Flux Qualities Obtained for Water At 652°F Using the Biasi et al [112] Correlation With the Compensated Distortion Model of Ahmad [116]	388
IV-177.	Plot of the Compensated Distortion Model for R-114 Boiling in a 0.785-In.-ID Tube. T = 100°F . . .	391
IV-178.	Plot of the Compensated Distortion Model for R-114 Boiling in a 0.785-In.-ID Tube. T = 150°F . . .	392
IV-179.	Plot of the Compensated Distortion Model for R-114 Boiling in a 0.785-In.-ID Tube. T = 200°F . . .	393
IV-180.	Plot of the Compensated Distortion Model for R-114 Boiling in a 0.785-In.-ID Tube. T = 250°F . . .	394
B-1.	Detailed Schematic Drawing of the Boiling Facility	424
B-2.	Circuit Diagram for Heat Input Control System Shown Here in the Heat Flux Control Position	431
B-3.	Thermocouple Wiring Diagram	436
C-1.	Experimentally Determined Friction Factors for Single-Phase Flow of Water Inside Test Section .	447
C-2.	Calibration Curve for the DP Cell and Receiver Gage	451
C-3.	Calibration Curve for FE 105B	452
C-4.	Calibration Curve for FE 105A	453
C-5.	Calibration Curve for FE 119A	454
C-6.	Calibration Curve for FE 123A	455
C-7.	Calibration Curve for FE 119B	457
C-8.	Calibration Curve for FE 123B	458
C-9.	Calibration Curve for FE 126	459
C-10.	Heat Loss Calibration Results	461
C-11.	In-Stream Thermocouple Calibration Results	472
C-12.	Overall Calibration of Instrumentation	483

Figure		Page
D-1.	In-Stream Temperature Profile for Run 17	495
G-1.	Experimental Uncertainty in Frictional Pressure Drop Results. Martinelli-Nelson [4] Model With Zuber et al [10] Modified Void Fraction Correlation	604
G-2.	Experimental Uncertainty in Heat Transfer Coefficient Results. Chen [80] Correlation Using the Forster-Zuber [52] Pool Boiling Equation With a Coefficient of 0.3802, T ≈ 100°F	607
G-3.	Experimental Uncertainty in Heat Transfer Coefficient Results. Chen [80] Correlation Using the Rohsenow [61] Pool Boiling Equation With C_{sf} = 0.0047, T ≈ 100°F	608

LIST OF SYMBOLS

a	thermal diffusivity = $k_f/(\rho_f c_{pf})$
a'	exponent used in Gilmour correlation, Equation (2-53)
A	area
A_p	apparatus parameter - used in Zuber et al void fraction correlation for pseudo-jet flow
A_w	area of the annular orifice in a rotameter
A_1	coefficient used in Macbeth critical heat flux correlation
b	exponent used by Pierre and Altman and Norris and Staub, Equation (2-76)
b_a	coefficient used in the equation of state for R-114, Equation (E-2)
b_2	exponent in Groeneveld scaling factor, Equation (2-87)
b'	exponent used in Gilmour correlation, Equation (2-53)
B	coefficient used in the Chisholm correlation [Equation (2-21)]; values of which are given in Table II-1 on page 33
Bo	Boiling number, defined in Equation (2-68)
c_p	specific heat at constant pressure
c_v	specific heat at constant volume
c'	exponent used in Gilmour correlation, Equation (2-53)
C	constant used in Chisholm correlation and defined in Equation (2-15)
C_a	empirical constant used in Gilmour correlation, Equation (2-53)
C_o	distribution parameter in Zuber et al void fraction correlation, Equation (2-31)
C_{sf}	coefficient in Equation (2-45) which depends on heating surface-fluid combination
C_T	modeling constant used in Equation (2-84)

C_{vf}	relative volumetric flow rate of gas
C_i	constants; i = 1,2,3,....
$\bar{C}$	parameter used in Chisholm correlation and defined in Equation (2-19)
C'	discharge coefficient of a rotameter, Equation (C-2)
C_2'	parameter used in Chisholm correlation and defined in Equation (2-16)
d'	exponent used in Gilmour correlation, Equation (2-53)
D	diameter
D_1	parameter in Equation (2-10) which, in this case, is taken to be approximately equal to one
e	exponent in O'Donnell, Robinson, and Webb correlation, Equation (2-72)
E	empirical coefficient used by Pierre and Altman, Norris, and Staub, Equation (2-76)
E_s	empirical function used by Stevens and Kirby, Equation (2-83)
f	Darcy-Weisbach friction factor
f_i	functions; i = 1,2,3,....
f'	Fanning friction factor
f(p)	term used in Biasi et al critical heat flux correlation
F	Reynolds number multiplication factor
Fr	Froude number
g	gravitational acceleration
g_c	universal gravitational constant
G	total mass flux based on the entire pipe cross-sectional area
G_o	mass velocity parameter used by Gilmour, Equation (2-53)
h	heat transfer coefficient
h_{fg}	latent heat of vaporization

Δh	subcooled enthalpy at tube inlet
$h(p)$	term used in Biasi et al critical heat flux correlation
H	coefficient used in equation of state of R-114, Equation (E-2)
j	volumetric flux density
j'	dummy variable in Equation (G-2)
J	mechanical equivalent of heat; 778.26 ft-lbf/Btu
J'	coefficient in Equation (E-6)
k	thermal conductivity
k_o	dimensional relative roughness of a wall
k'	dummy variable in Equation (G-2)
K	constant used by Lombardi and Pedrocchi, Equation (2-25)
K_f	load factor, Equation (2-77)
K_i	coefficient used by Baker, Touloukian, and Hawkins in Equation (2-75)
K_o	coefficient used by O'Donnell, Robinson, and Webb, Equation (2-72)
K_s	critical heat flux scaling factor
K'	parameter used in the Bankoff variable density void fraction model and computed by Hughmark
K"	constant used in Equation (C-4)
ln	natural logarithm
L	length, usually tube length
m	exponent in Equation (4-37)
$\dot{m}$	mass flow rate
m'	constant used by Lombardi and Pedrocchi in Equation (2-25)
n	number of sites per unit area with radii larger than r, Equation (4-37)
n_o	parameter used by Chisholm in Equation (2-21)

n'	exponent in Equation (2-49)
N	number of sites per unit area per unit radius, Equation (4-38)
Nu	Nusselt number
P, p	pressure
Pr	Prandtl number
P_r	reduced pressure
q	amount of heat transferred per unit time
Q	volumetric flow rate
R, r	bubble or cavity radius
r_s	radius for which n would be one per unit area in Equation (4-37)
r'	exponent in Rohsenow pool boiling correlation, Equation (2-45)
R_o	initial radius of bubble, Equation (4-14)
$\dot{R}$	rate of change of bubble radius with time
R'	scale reading on a rotameter
Re	Reynolds number
RMS 1, RMS 2	root mean squared error, Equations (G-3) and (G-4)
s	exponent in Rohsenow pool boiling correlation, Equation (2-45)
S	suppression factor
S_1	first component of suppression factor, Equation (4-45)
S_2	second component of suppression factor, Equation (4-48)
S_{tot}	total suppression factor, Equation (4-50)
St*	Stanton number based on the frictional velocity, Equation (4-16)
t	time
T	temperature

T_o parameter used in Chisholm correlation and defined in Equation (2-20)

u dummy variable

v specific volume

v_{fg} latent specific volume

v_f' volume of float in a rotameter

V velocity

$\bar{V}_{gj}$ weighted mean drift velocity in Zuber et al void fraction correlation as used in Equation (2-31)

We Weber number

x quality. Defined in the saturated region as the fraction or percent of the total flow by weight that is vapor. In the subcooled region, it is $h_f - \Delta h/h_{fg}$. In the superheated region, it is $h_g + \Delta h/h_{fg}$.

X Martinelli parameter

X_{ttl} modified Martinelli parameter for the turbulent-turbulent case according to Davis, Equation (4-5)

X' independent variable in Equation (G-1)

y coordinate axis taken away from the wall

y_i coefficients and exponents used in Macbeth critical heat flux correlation; i = 1,2,3,....

y^+ parameter in Equation (4-94)

Y dependent variable in Equation (G-1)

z coordinate axis taken along the length of the tube

z_o dummy variable used in Equation (4-53)

Greek Symbols

α void fraction, or fraction of the total flow by volume that is vapor

γ rate of change of the density ratio with pressure, Equation (2-81)

γ' slip factor; used in Thom's void fraction correlation

Γ	parameter used in Chisholm correlation and defined in Equation (2-22)
δ	boundary layer thickness
Δ	difference between two quantities
ε	ratio of the mean liquid velocity to the mean vapor velocity as used by Chawla and given in Figure II-10 on page 34
η	dummy variable used in Equation (4-59)
η'	dummy variable used in Equation (2-8)
θ	angle of inclination with respect to the vertical
θ'	temperature difference as used in Equation (4-53)
λ	parameter used in Chisholm correlation
μ	dynamic viscosity
ν	kinematic viscosity
ξ	dummy variable defined in Equation (4-69)
ρ	density
$\Delta\rho$	the difference between the liquid and vapor densities
σ	surface tension
σ'	standard deviation
τ	dimensionless parameter defined in Equation (4-60)
Φ_{ftt}	square root of Martinelli multiplier
Φ_{fo}	square root of two-phase multiplier
Φ'_{ftt}	square root of Martinelli multiplier based on Lockhart-Martinelli correlation
Ψ^*	property parameter, Equation (4-99)
Ψ	parameter used in compensated distortion model
Ψ'	parameter used in Chisholm correlation and defined in Equation (2-18)
Ω	Baroczy's two-phase multiplier ratio

Subscripts

acc	acceleration component
at CHF	denotes condition at critical heat flux
avg	average
conv	convective
crit, c	critical condition
CHF	critical heat flux
exp	experimental quantity
f	liquid
fa	liquid alone
fo	liquid only
float	refers to the float in a rotameter
g	gas or vapor
grav	gravitational component
i	refers to condition at tube inlet
m	mean or average condition
mac	macroconvective
max	maximum
min	minimum
o	refers to condition at tube outlet
sat	saturated
tot	total
TP	two-phase quantity
TPF	two-phase frictional quantity
tt	turbulent-turbulent
w	wall
ω	refers to annular orifice in a rotameter

Symbols

$\langle\ \rangle$	average conditions, usually across the tube cross section

CHAPTER I

INTRODUCTION AND STATEMENT OF PROBLEM

A. INTRODUCTION

The transfer of heat to a boiling liquid is a very efficient means of heat transfer in that large heat fluxes can be supported through small cross-sectional areas at moderately low temperature differences. As a consequence, this mode of heat transfer, which can be identified as a convection process, coupled with a change in phase from liquid to vapor is applied in numerous industrial systems such as boilers in steam power plants, air-conditioning and refrigeration equipment, nuclear reactors, and electronic power tubes.

There are two basic areas in boiling where considerable research has been done. They are pool boiling and flow boiling. Pool boiling is boiling on a heated surface submerged in a pool of initially quiescent liquid. Flow boiling is boiling in a flowing stream of fluid, where the heating surface may be the channel wall confining the flow. In this investigation, the main interest will be in the latter, although some reference will made to pool boiling, especially when correlations obtained from pool boiling experiments are used to help predict flow boiling results.

A variety of organic refrigerants are available today with temperature-pressure relationships covering, at least, the range of 0.1 to 800 psia and -180 to 300°F, as illustrated in Figure I-1. In general, these organic compounds are quite stable, nonflammable materials with low toxicity levels [1].* As a rule, the selection of a refrigerant for

---

*Numbers in brackets designate references at the end of the dissertation.

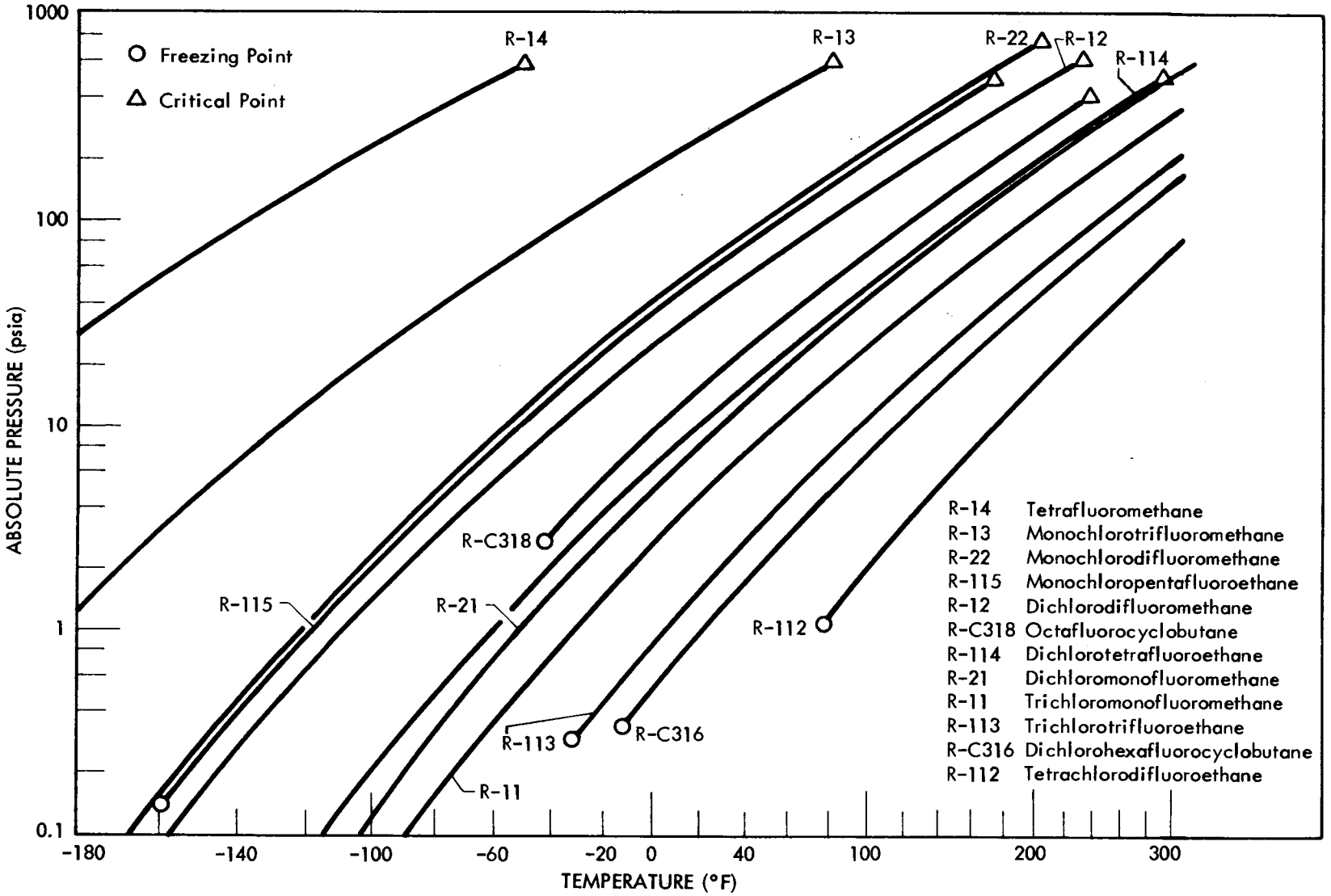


Figure I-1. PRESSURE-TEMPERATURE RELATIONSHIPS FOR VARIOUS REFRIGERANTS [1].

a particular application is a compromise between conflicting desirable properties; while low viscosity and low surface tension are desirable boiling properties, they make it difficult to achieve dropwise condensation. In general, it is advantageous to select a refrigerant with as high a latent heat of vaporization as possible [2]. While the refrigerants whose boiling points at moderate pressures are significantly below ambient are used in refrigeration cycles, those whose boiling points are above ambient can be used in boilers where it is not feasible or desirable to use water.

To optimize heat exchanger or boiler performance, it is necessary for the design engineer to compute (for a given geometry, heat load, and/or mass flow rate) the following quantities:

Pressure drop

Heat transfer coefficient

Critical heat flux

Pressure drop information is important since this dictates the pumping power needed to maintain a certain mass flow rate or, in the case of a natural circulation system, the amount of "head" required. The amount of heat transferred and the tube wall temperature will be dependent on the heat transfer coefficient subject, of course, to the amount of thermal resistance between the boiling surface and the source of heat (i.e., hotter gas or liquid). Further, in a two-phase boiling system, there is usually a limit to the amount of heat that the system can remove under a given set of flow and temperature conditions. Thus, the design engineer will have to also know this parameter, commonly referred to as the critical heat flux. This limit is also described as the boiling crisis and can occur under two basic types of flow regimes. In the

bubbly flow regime at high heat fluxes, the bubbles become crowded together and form a continuous layer of bubbles which impedes the transfer of heat from the heating surface to the predominantly liquid core. This type of crisis, also referred to as departure from nucleate boiling (DNB), usually occurs at low qualities and in some instances where the average condition at the tube cross section is subcooled. In the annular flow regime, the phenomena is quite different. The liquid film on the wall breaks up, and patches of vapor are observed to form. This is referred to as dryout. The qualities at which this phenomenon occurs are higher than those observed in the bubbly flow regime. Dryout occurs only in saturated flow. The associated decrease in heat transfer coefficient usually results in either a sharp decrease in the heat flux or a sharp increase in the wall temperature, depending on whether the system is heat flux controlled or temperature controlled. The maximum heat flux that the system experiences at a given operating condition just before this boiling crisis occurs is referred to as the critial heat flux [3].

The analysis of two-phase systems is significantly more complex than single-phase systems. Not only are there twice as many equations as in the single-phase system, but the boundary conditions are more complicated and involve such fators as surface tension and phase change. It is interesting to note that the interaction between the liquid and gas phases in flow boiling leads to the development of different flow regimes. The occurrence of the bubbly, slug, annular, and mist flow regimes, as well as variations of those basic flow regions in vertical upflow has been well documented in the literature [3]. In addition, the pressure drop and heat transfer coefficients obtained are believed

to depend on the flow regime [4]. As a result, only a limited number of equations exist for predicting the performance of a boiling system, and they are generally associated with the various flow regimes. Numerous empirical and semi-empirical correlations are, however, available. They are based on tests conducted for a limited number of geometries and working fluids. As with all empirical correlations, care should be taken in applying these equations to geometries and working fluids where the accuracy of such correlations has not been experimentally verified. This is especially true in situations where the thermodynamic and transport properties of a fluid are quite different from those on which available correlations are based. Refrigerants are a case in point. In Table I-1, the properties of five refrigerants are compared to those of water and benzene. It can be seen that significant differences do exist in the critical pressure, vapor density, specific heats, latent heat of vaporization, thermal conductivities, and surface tension. Indeed, boiling studies with refrigerants have indicated discrepancies between experimental results and predicted values. Several correlations which have been used for such fluids as water, methanol, and benzene are not applicable to refrigerants. As a result, because of the increased use of refrigerants, it is necessary to be able to more reliably predict their boiling behavior. Indeed, it would be quite desirable to be able to modify the correlations existing in the literature today in order to make them more applicable to the fluorocarbon family of working fluids.

B. STATEMENT OF PROBLEM

Because of the significant discrepancies that have been noted between the behavior of boiling refrigerants and other working fluids

Table I-1

PROPERTIES OF BENZENE, WATER, AND SEVERAL REFRIGERANTS

Property	Fluid						
	Benzene	Water	R-113	R-114	R-21	R-12	R-22
Molecular Weight	78.1	18	187.39	170.93	102.93	120.93	86.48
Boiling Point at 1 atm (°F)	177	212	117.63	38.39	48.06	-21.62	-41.44
Freezing Point (°F)		32	-31	-137	-211	-252	-256
Critical Temperature (°F)	552	705.3	417.4	294.3	353.3	233.6	204.8
Critical Pressure (psia)	714	3206.7	495	474	750	596.9	716
Liquid Density (at 86°F) (lbm/cu ft)	54.5	62.1	96.96	89.91	84.52	80.67	73.36
Vapor Density (at boiling point) (lbm/cu ft)	0.172	0.0373	0.461	0.488	0.285	0.395	0.301
Liquid c_p (at 86°F) (Btu/lbm-°F)	0.43	1.023	0.218	0.238	0.256	0.240	0.335
Vapor c_p (at 86°F) (Btu/lbm-°F)	0.260*	0.45	0.161**	0.160	0.140	0.145	0.152
h_{fg} (at boiling point) (Btu/lbm)	170	970.3	63.12	59.00	104.15	71.04	100.66
Liquid Viscosity (at 86°F) (centipoise)	0.55	0.8131	0.619	0.356	0.330	0.351	0.229
Vapor Viscosity (at 1 atm) (centipoise)	0.0076	0.0133	0.0104†	0.0117	0.0116	0.0127	0.0131
Liquid Thermal Conductivity (at 86°F) (Btu/hr-ft-°F)	0.092	0.3633	0.0521	0.0447	0.0697	0.0492	0.0595
Vapor Thermal Conductivity (at 1 atm) (Btu/hr-ft-°F)	0.0092	0.0129	0.00450††	0.00646	0.00569	0.00557	0.00678
Surface tension (at 77°F) (dynes/cm)	28.9	72	19	13	19	9	9

*At 176°F.

**At 140°F.

†At 0.1 atm.

††At 0.5 atm.

such as water, it is the aim of the present work to use both analytic and experimental techniques to study the heat transfer and pressure drop characteristics of a boiling refrigerant in a vertical tube. From this, improvement in the prediction of system behavior for this situation will be sought. To accomplish this goal, four interrelated areas of endeavor will be investigated.

1. The flow regimes occurring with R-114 two-phase flow in a vertical tube with heat transfer will be studied. This will be done experimentally in the entire quality range of zero to one, the mass flux range 0.10×10^6 to 3.5×10^6 lbm/hr-sq ft, and the boiling temperature range 100 to 250°F. To clarify some of the regimes, video tape pictures will be taken for later playback at much slower speeds. A comparison with published flow maps will be made to determine their applicability to boiling R-114.

2. The experimental results for pressure drop obtained from the present tests will be compared with the Martinelli-Nelson [4] and Homogeneous [3] models, as well as with other correlations which attempt to correct for the mass flow, as well as the particular fluid tested. The mass flux and temperature ranges to be covered are the same as those mentioned in part 1.

3. Boiling coefficients in the mass flow range described in part 1 and in the temperature range of 100 to 200°F will be obtained. The quality will be varied in the range from approximately zero to that at which critical heat flux occurs. The results will be compared with numerous correlations existing in the literature.

4. The amount of information available on the critical heat flux with R-114 in the range described in part 1 will be extended.

In addition, the experimental scaling factors, which allow the results obtained with one fluid to be applied to a different fluid, will be calculated. The values obtained will be compared with those obtained from other R-114 tests previously conducted. In addition, through flow visualization studies, an attempt will be made to observe the hydrodynamic changes associated with the occurrence of critical heat flux.

CHAPTER II

LITERATURE SURVEY

A. FLOW REGIMES

In order to gain an understanding of heat transfer in two-phase flows, an accurate description of the flow regimes is necessary. This understanding, when achieved, should lead to the improved prediction of the heat transfer coefficient, the pressure drop, and the critical heat flux.

To date, no general set of terminologies has been adopted in the literature to describe the various ways in which a liquid and a vapor behave in cocurrent flow. The subjective nature of flow regime studies has undoubtedly contributed to this undesirable situation. It has therefore become necessary for anyone conducting a survey of the research done on flow regimes to define a fundamental set of flow regimes and attempt to fit the observations of other experimenters to the defined set. One set of flow regimes and their definition has been advanced by Collier and Wallis [3]. This set of terminologies which constituted some of the more common flow regime descriptions at the time of publication has become increasingly more popular since then. The regimes applicable to vertical cocurrent flow are shown in Figure II-1.

Adiabatic Flow

For adiabatic flow, one of the earliest correlations of flow regime information was performed by Baker [5]. Using the results of numerous previous tests on adiabatic horizontal flow of air-water

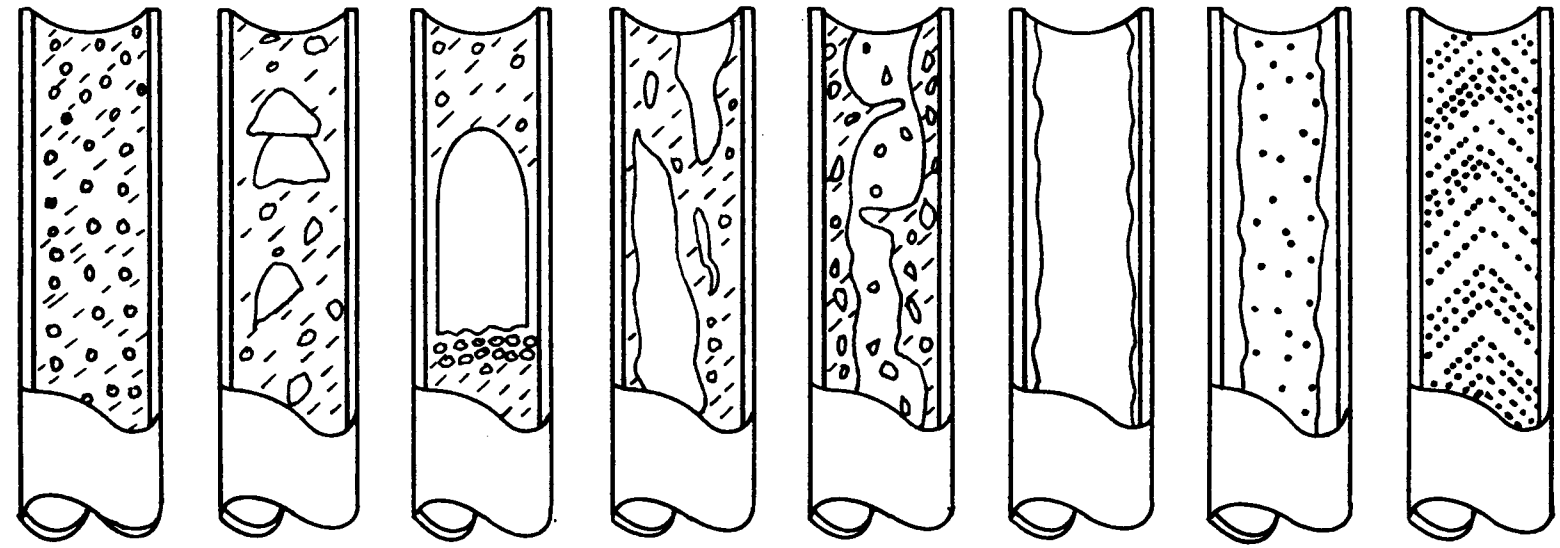


Figure II-1. SCHEMATIC DRAWINGS OF FLOW PATTERNS IN TWO-PHASE VERTICAL UPFLOW.

mixtures, the flow map shown in Figure II-2 was presented. Baker [5] hypothesized that the flow regime was a function of:

$$\frac{xG}{\left[\frac{\rho_g}{0.075}\,\frac{\rho_f}{62.3}\right]^{1/2}}$$

and

$$\frac{1-x}{x}\left[\frac{\rho_g}{0.075}\,\frac{\rho_f}{62.3}\right]^{1/2}\frac{0.0050}{\sigma}\left[\frac{\mu_f}{2.419}\left(\frac{62.3}{\rho_f}\right)^2\right]^{1/3}$$

where

x is the quality,

G is the total mass flux based on total pipe cross-sectional area (lbm/hr-sq ft),

ρ_g is the density of the gas phase (lbm/cu ft),

ρ_f is the density of the liquid phase (lbm/cu ft),

σ is the surface tension (lbf/ft), and

μ_f is the liquid viscosity (lbm/ft-hr).

It is interesting to note that all of the physical properties used in the above equations with the exception of μ_f were presented in terms of ratios which reduced to one for air and water at standard conditions of temperature and pressure.

Kozlov [6] studied vertical flow patterns in a 25-mm-diameter glass tube, using air and water, and correlated the results with the Froude number, Fr_m, based on the mean velocity and a quantity he called the relative volumetric flux rate of the gas, C_{vf}. Kozlov [6] identified six flow regimes and presented equations to define the boundaries between the regions. They are:

$$C_{vf} = 0.05\ Fr_m^{0.2} \qquad (2\text{-}1)$$

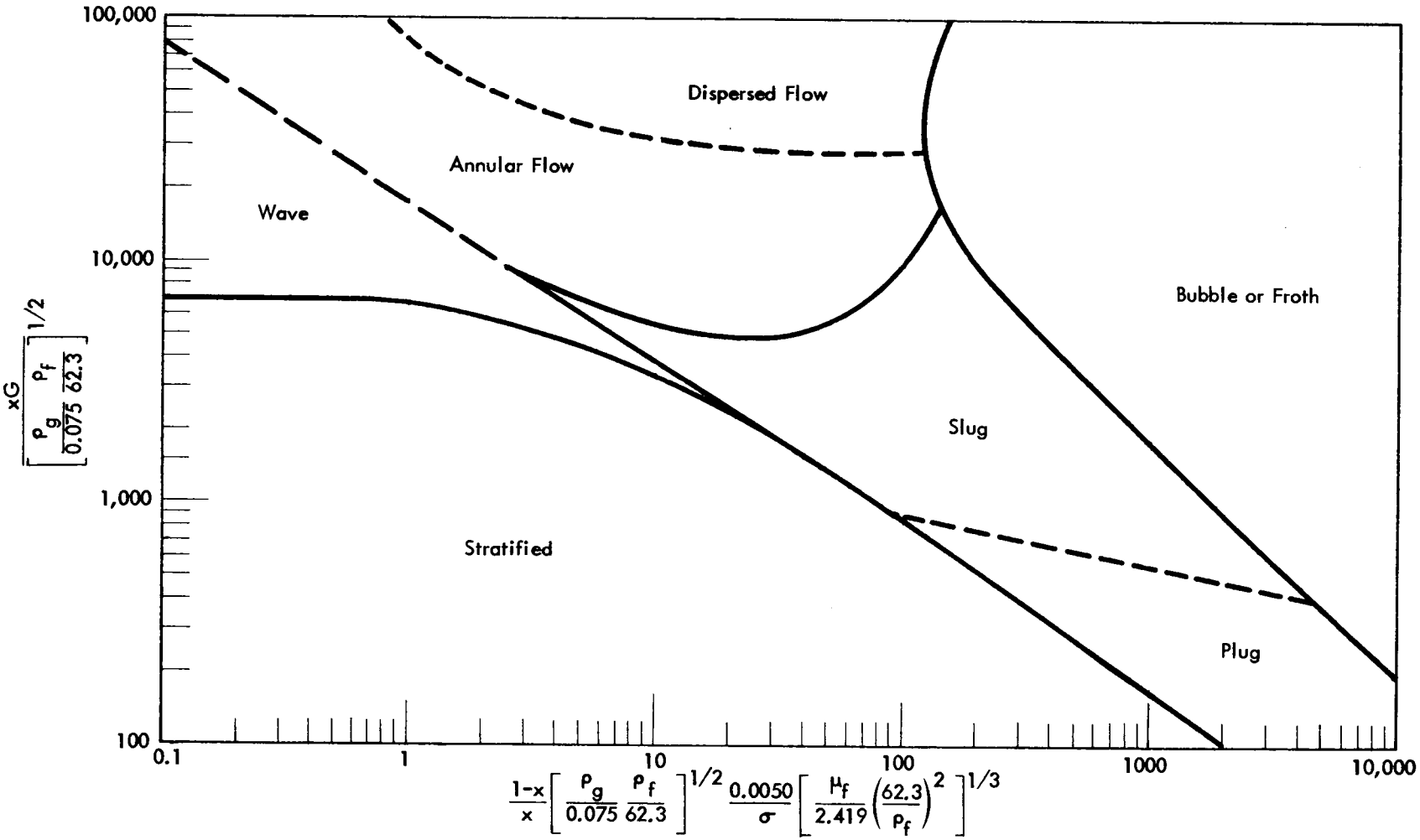


Figure II-2. FLOW REGIME MAP, BAKER [5].

for the boundary between the bubble and plug type of flow. Here

$C_{vf} = \frac{Q_g}{Q_g + Q_f}$ is the relative volumetric flow rate of the gas,

Q_g is the volumetric flow rate of the gas phase (cu ft/sec),

Q_f is the volumetric flow rate of the liquid phase (cu ft/sec),

$Fr_m = \frac{V_m^2}{gD}$ is the Froude number based on the mean velocity,

$V_m = \frac{(Q_f + Q_g)}{0.785D^2}$ is the mean velocity of the two-phase mixture (ft/sec),

g is the gravitational acceleration (ft/sec^2), and

D is the tube diameter (ft).

$$C_{vf} = 0.12\ Fr_m^{0.15} \tag{2-2}$$

was recommended for the boundary between the plug and plug-dispersion type of flow,

$$C_{vf} = 0.5\ Fr_m^{0.10} \tag{2-3}$$

for the boundary between the plug-dispersion and emulsion type of flow,

$$C_{vf} = 0.65\ Fr_m^{0.05} \tag{2-4}$$

for the boundary between the emulsion and film-emulsion type of flow, and

$$C_{vf} = 0.85\ Fr_m^{0.02} \tag{2-5}$$

for the boundary between the film-emulsion and drop type of flow. From the descriptions Kozlov [6] gave of each of his flow regimes, a different set of names, more closely related to the flow regimes categorized in Figure II-1 can be attempted. For example, the plug flow regime, consisting of alternating bullet-shaped gas plugs and liquid

plugs can quite confidently be renamed the slug flow regime. The plug-dispersion region, where a portion of the liquid in the center of the tube is thrown to the sides by the gas stream may be classified as semi-annular flow or a transition from slug to annular flow. The emulsion type of flow where films of liquid between gas bubbles form a continuously breaking and reforming three-dimensional cell structure may also be considered as a semi-annular type of flow. The film-emulsion regime in which a liquid film flows along the wall and the gas carrying dispersed moisture flows through the center of the tube may be renamed as a semi-annular or spray-annular type of flow regime. Drop flow is analogous to spray-annular flow.

Quandt [7], in 1962 analyzed gas-liquid flow in a duct from the standpoint of the dominant forces on the system. For adiabatic flow (considering only the pressure gradient, gravitational forces, and interfacial surface tension), he was able to derive expressions--based on force balances--showing that bubbly, annular, and dispersed flow were subclasses of pressure gradient-controlled flow while slug, wave, and stratified flow were subclasses of gravity-controlled flow. The particular flow regime existing in each case was dependent on the magnitude of the Froude and Weber numbers. Figure II-3 summarizes the essential results of the Quandt [7] analysis.

The plots of Baker [5], Kozlov [6], and Quandt [7] represent an attempt to correlate the flow regimes in terms of parameters which hopefully generalize these plots to other flow conditions and fluids. Numerous other flow pattern investigations have been reported in the literature for adiabatic flow. Most of the results, however, were plotted in terms of variations of total mass flux versus quality.

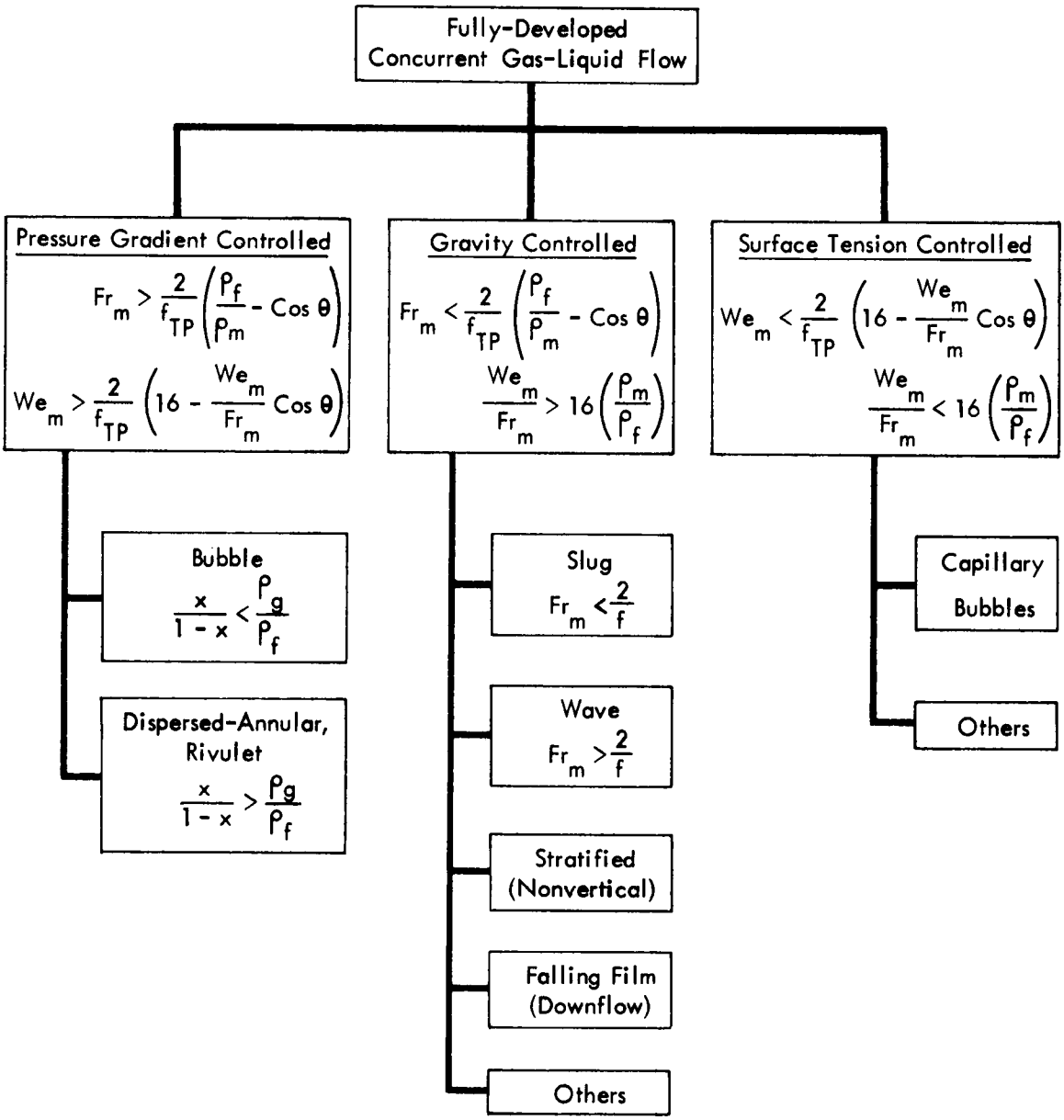


Figure II-3. CLASSIFICATION OF GAS-LIQUID FLOW REGIMES, QUANDT [7].

Diabatic Flow

For the case of diabatic flow in a vertical tube, the quality and void fraction are not uniform along the length of the tube and the flow patterns may conceivably differ from those of adiabatic or isothermal flow. No universal agreement exists on this point, however. Wallis and Griffith [8] conducted tests in which they used a porous wall to force air into a rectangular channel to approximately model the change in quality and void fraction along the length of the tube. From this two-phase boiling analogy, they concluded that the flow pattern was generally determined more by the rate of bubble formation at the wall rather than local flow quality or length along the passage in which the flow had time to develop. Also, the distribution of liquid and vapor across the channel was markedly different when the vapor was generated along the wall. Hsu and Graham [9] boiling water in a vertical glass tube at what is assumed to be atmospheric pressure, substantiated to some degree Wallis and Griffith's [8] findings. Hsu and Graham [9] noted that the flow pattern was determined to a large extent by whether there were a large number of active nucleation sites or not. Also, the flow pattern was affected by both the heating length and by the total heat flux. In contrast, Zuber et al [10] boiling R-22 in a vertical tube noted a negligible effect of heat flux on the flow mechanism transition, with local quality, total flow rate, and pressure as the dominant control variables. In addition, they presented the following equations for flow regime transition:

$$\frac{23}{(Re_f)^{1/2}} \frac{V_{fo}\Delta\rho}{j_f\rho_f} \left(\frac{\rho_f}{\rho_g} - 1.41\right)^{1/2} \frac{\left(\frac{\sigma g \Delta\rho}{\rho_f^2}\right)^{1/4}}{\langle j \rangle} = 0.25 \qquad (2\text{-}6)$$

for the boundary between churn turbulent and annular flow. Here,

$Re_f = \frac{\rho_f V_{fo} D}{\mu_f}$ is the Reynolds number for the liquid only,

$V_{fo} = \frac{G}{\rho_f}$ is the velocity for the liquid only (ft/sec),

$\Delta\rho = \rho_f - \rho_g$ is the difference between the densities of the liquid and vapor phases (lbm/cu ft),

$j_g = \alpha V_g$ is volumetric flux density of the vapor (ft/sec),

α is the void fraction,

$V_g = \frac{xG}{\alpha\rho_g}$ is the local velocity of the vapor phase (ft/sec),

$\langle j \rangle = \langle j_f \rangle + \langle j_g \rangle$ is the average volumetric flux density of the mixture over the cross-sectional area of the duct (ft/sec), and

$j_f = \frac{(1-x)G}{\rho_f}$ is the volumetric flux density of the liquid phase (ft/sec).

For the boundary between slug and annular flow in adiabatic systems, Zuber et al [10] proposed:

$$\frac{23}{(Re_f)^{1/2}} \frac{V_{fo}}{\langle j \rangle} \frac{\Delta\rho}{\rho_f} \left(\frac{\rho_f}{\rho_g}\right)^{1/2} - \frac{0.35}{\langle j \rangle} \left(\frac{g\Delta\rho D}{\rho_f}\right)^{1/2} = 0.20 \quad . \qquad (2\text{-}7)$$

They, however, cautioned that the above equations had not been tested against experimental data.

Other investigators who were concerned with the application of correlations obtained for adiabatic flow conditions to diabatic flow included Bergles and Suo [11] and Bergles, Roos, and Bourne [12]. Boiling water in a 0.4-in.-diameter vertical tube at 500 and 1000 psia, they

concluded that some adiabatic correlations can be used to estimate flow regime transitions in low heat flux situations. Bergles, Lopina, and Fiori [13], who ran flow pattern observation tests of boiling water at pressures below 100 psia, concluded that conventional adiabatic flow regime plots cannot be used to predict the flow regimes in boiling water, since the effect of nonequilibrium voids and heat flux are particularly important at low pressures.

In recent years, flow regime information for a large number of working fluids and various test section orientations has been published. An excellent compilation can be found in Hosler's publication [14]. In flow regime studies with heat transfer, the location of the visualization section is important. While it is desirable to observe the flow in a heated portion of the test section, this is not always possible. The use of glass tubes, heated electrically by a thin metallic coating on the outside surface of the tube, results in serious limitations on the operating pressures, temperatures, and heat fluxes that can be achieved. The use of metallic tubes on the other hand limits the observer to either visually observing the flow at the exit of the test section or using an indirect observation technique such as X-ray pictures, radiation attenuation, hot-wire probes, or other electrical probes. Many investigators have chosen to use a flow visualization section at the end of their boiling tube because of the inherent simplicity. How representative the regime observed in this adiabatic section is, of the flow regime in the heated length of tube is open to debate. Some differences between the two certainly exist, and Hsu and Graham [9] in their tests refer to an important one. Since the bubbles

are ejected from a heated surface into the mainstream at a high velocity, the void fraction profile is different at a heated cross section than at an adiabatic one. In addition, the acceleration of the two-phase flow while it is heated is not modeled in the nonheated length. On the other hand, one does not expect a radical change in flow regime to occur in a length of a few inches, especially if the quality is approximately constant. It may thus be stated that while the microscopic differences in flow regime between adiabatic and nonadiabatic sections are significant, the macroscopic ones may not be.

Napadensky [15] who observed flow patterns in R-12 upstream and downstream of his vertical test section seemed to agree with the Baker [5] plot although he did not take a sufficient amount of data to clearly delineate the transition regions. In addition, a comparison of Baker's [5] flow map with Isbin et al's [16] high pressure steam-water results is encouraging. It is interesting to note that Napadensky [15] did not at any time observe a slug flow regime. Zuber et al [10] also did not observe a slug flow regime in two-phase systems with heat transfer. He did, however, see vapor slugs in adiabatic sections following the heated sections. J. L. L. Baker [17], who boiled R-11 in a vertical rectangular test section, also noted the absence of slug flow at elevated pressures. Modeling water and R-11 in terms of orthobaric density ratios, he obtained the following equations for flow regime transitions:

$$j_g = 0.9\,(gD)^{1/2}\left(\frac{\rho_f}{\rho_g} - 1\right)^{1/2}\left(\frac{\rho_{gH_2O}}{\rho_g}\right)^{1-\eta'}\left(\frac{\sigma}{\sigma_{H_2O}}\right)^{\eta'} + 0.6\left(\frac{\rho_f}{\rho_g}\right)^{1/2} j_f \qquad (2\text{-}8)$$

for the boundary between churn and annular flow where η' can be equal to either 1/2 or 0. This equation is based on a modification of the Haberstroh and Griffith [18] result. In addition:

$$\frac{j_g}{\left(\frac{\rho_f}{\rho_g}\right)^{1/2}} + 0.194\, j_f = 1.6 \left(\frac{\rho_{gR-11}}{\rho_g}\right)^{1/2} \qquad (2\text{-}9)$$

for the boundary between churn and wispy-annular. This wispy-annular regime had the usual characteristics of annular flow with the added feature of rather large agglomerates of liquid in the vapor core. Also:

$$j_g = 25\, j_f - \frac{150\, D_1}{\left(\frac{\rho_f}{\rho_g}\right)^{1/3}} \qquad (2\text{-}10)$$

for the boundary between wispy-annular and annular flow. D_1 in this case is taken to be approximately equal to one. In Equations (2-8) to (2-10), j_f and j_g are in ft/sec.

Hosler [14], in 1968, ran tests with boiling water in a vertical rectangular channel at pressures of between 150 and 2000 psia. His results are shown in Figure II-4. He compared his results with the correlations suggested by Baker [5], Kozlov [6], and Quandt [7]. The results for the 1400-psia case are shown in Figure II-5. None of these did an entirely adequate job of predicting the flow pattern. Based on the results, however, Hosler [14] was able to discount the validity of the Kozlov [6] map. The Baker [5] map predicted the annular type of flow reasonably well. It, however, did not adequately predict bubbly flow, especially at low pressures, nor did it predict the bubble-slug transition. The Quandt [7] analysis predicted the largest fraction of

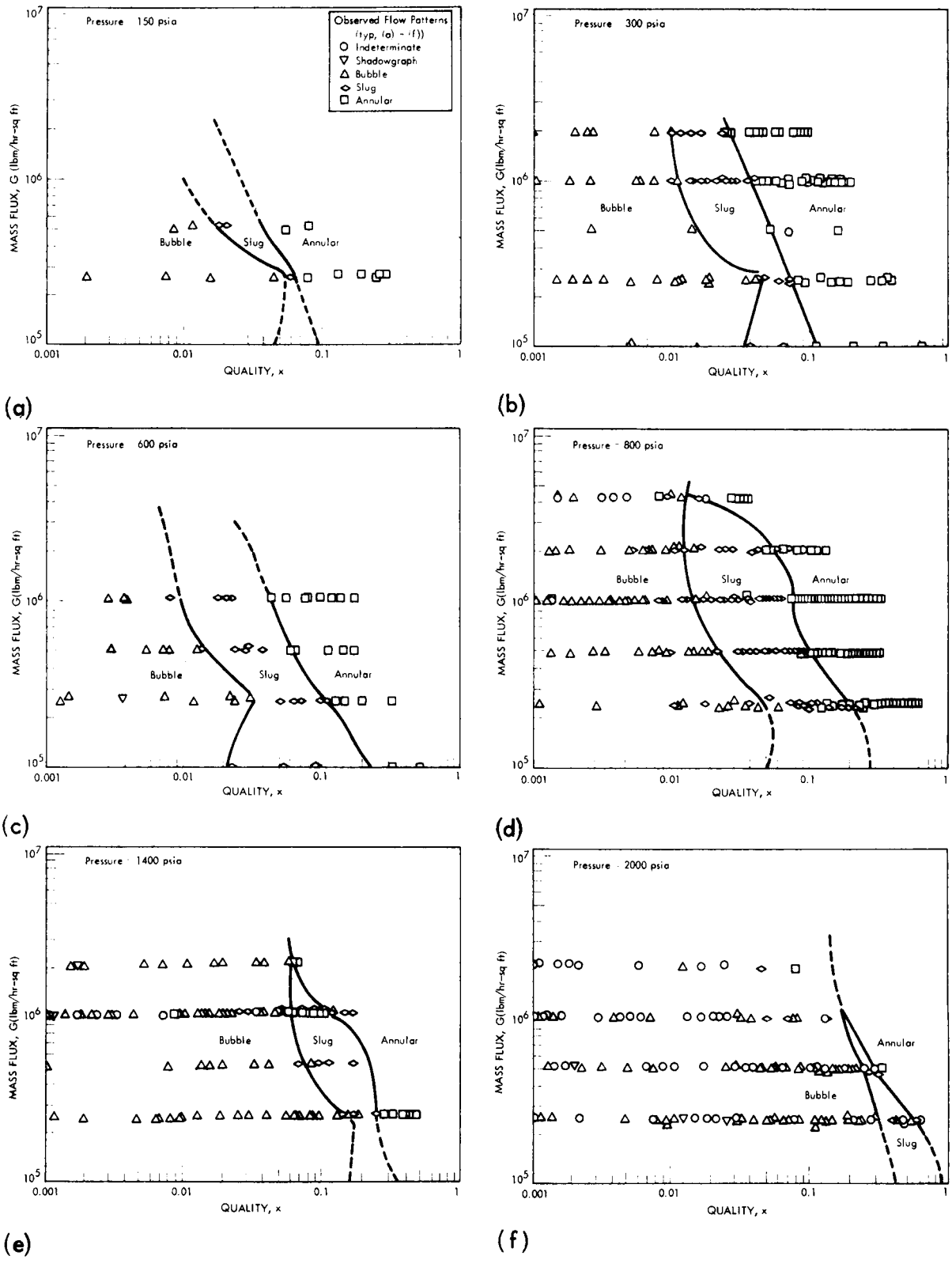


Figure II-4. FLOW REGIME DATA FOR STEAM-WATER MIXTURES, HOSLER [14].

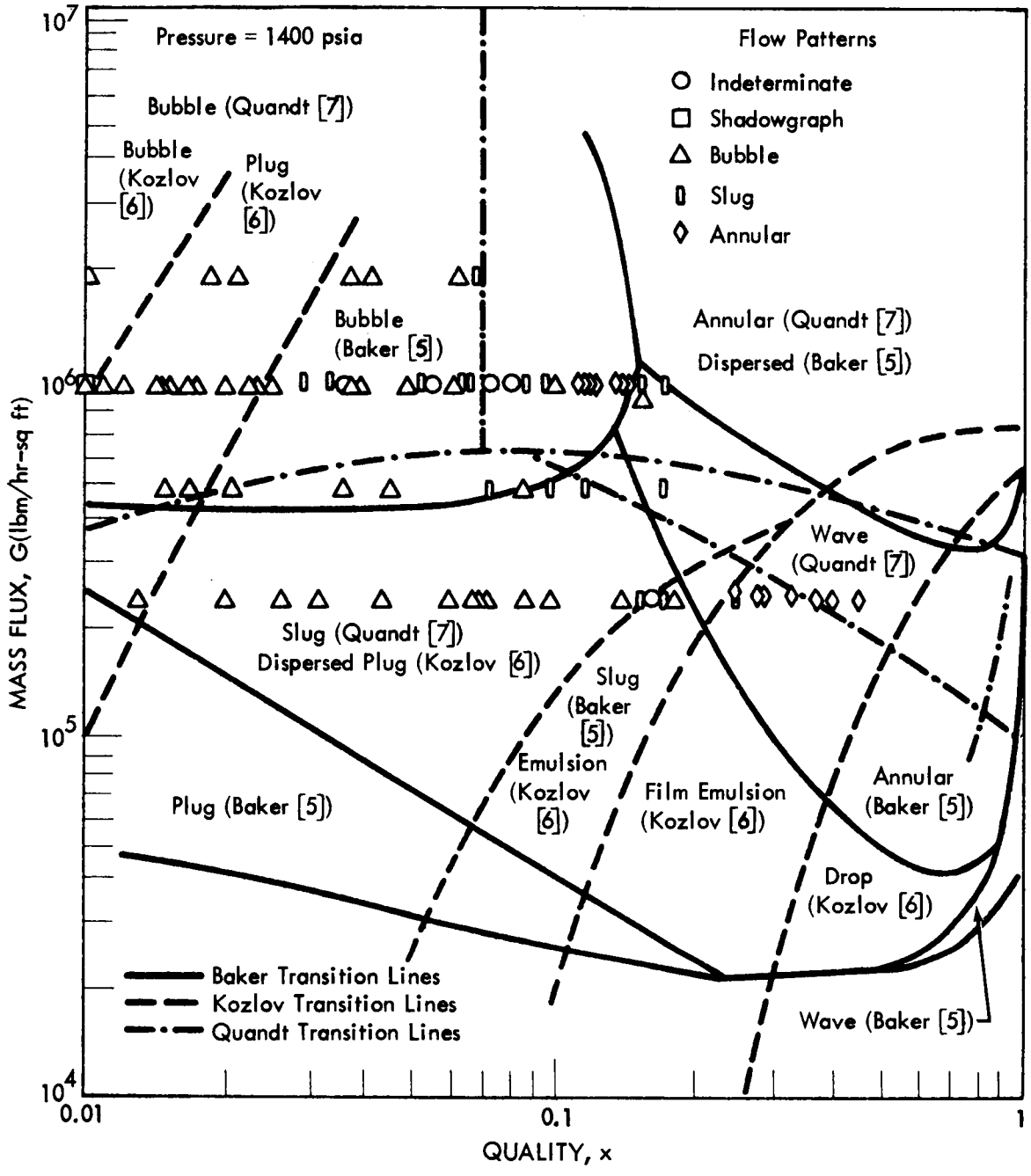


Figure II-5. FLOW REGIME DATA OF HOSLER [14] FOR STEAM-WATER MIXTURES COMPARED WITH FLOW REGIME MAPS OF BAKER [5], KOZLOV [6], AND QUANDT [7].

the data correctly, although some gaps were found in this analysis. Hosler [14] felt that an extension of the Quandt [7] analysis to account for the effect of heat transfer and developing flow would be useful.

In conclusion, it can be summarized that at present, no reliable method of predicting which flow regime would occur under a given set of operating conditions exists. Neither the Zuber et al [10] nor the Baker [17] equations for regime transitions have been compared to flow observations other than those of the respective authors. Therefore, unless a designer can find flow pattern studies in the literature for the exact tube size, working fluid, heat flux, flow rate, and quality he is interested in, the Baker [5] map and Quandt [7] analysis seem to offer the best choices for predicting the flow regimes, despite the lack of knowledge on the limits of their applicability.

B. PRESSURE DROP

It is generally agreed that the Lockhart-Martinelli (L-M) [19] and Martinelli-Nelson (M-N) [4] models are the most widely used and best developed models to date. A comparison between the L-M [19] model and four other correlations which have found wide use in the literature was presented by Dukler, Wicks, and Cleveland [20]. It was shown there that the L-M [19] model was superior to the others in most flow regimes.

As an extension of this work Dukler et al [21] compared the L-M [19] model to two other models, one for homogeneous flow and the other for constant slip. These models, developed through similarity analysis, were based on the assumption that by matching the Reynolds and Euler numbers of two different systems, the experimental results and physical

relationships that exist in one system can be expected to apply to the other. For one-component, steam-water systems, the L-M [19] correlation was most satisfactory for the low- and high-pressure data although one of Dukler et al's [21] models was better at the intermediate pressure level. Since it does not include pressure drop terms to account for the two-phase change (acceleration) or body force effects, the L-M [19] model is applicable only to two-phase isothermal flow in horizontal tubes. The M-N [4] model, on the other hand, accounts for the acceleration of flow and is therefore applicable to forced circulation boiling with any tube orientation.

Another model which has been developed to predict pressure drops in two-phase flows in tubes is the Homogeneous [3] model. In this model, it is assumed that both liquid and vapor flow at the same velocity and that both phases are sufficiently well mixed for the equations to be developed by using the mean physical properties of this pseudo-fluid. This is in contrast to the L-M [19] and M-N [4] models where the two phases are allowed to have different velocities.

From a comparison of the M-N [4] model with the data of numerous investigators, it is noted that the M-N [4] model overestimates the pressure drop in most cases. It is generally applicable at low flow rates and high qualities where the annular type flow regime is believed to exist [3]. At high flow rates and low qualities, where the buoyancy effect of bubbles is negligible and where the flow regime is chaotic and dominated by turbulent mixing, the Homogeneous [3] model is superior. Pressure drops for intermediate flow rates and qualities lie between these two models. An example of this is shown in Figure II-6 where the

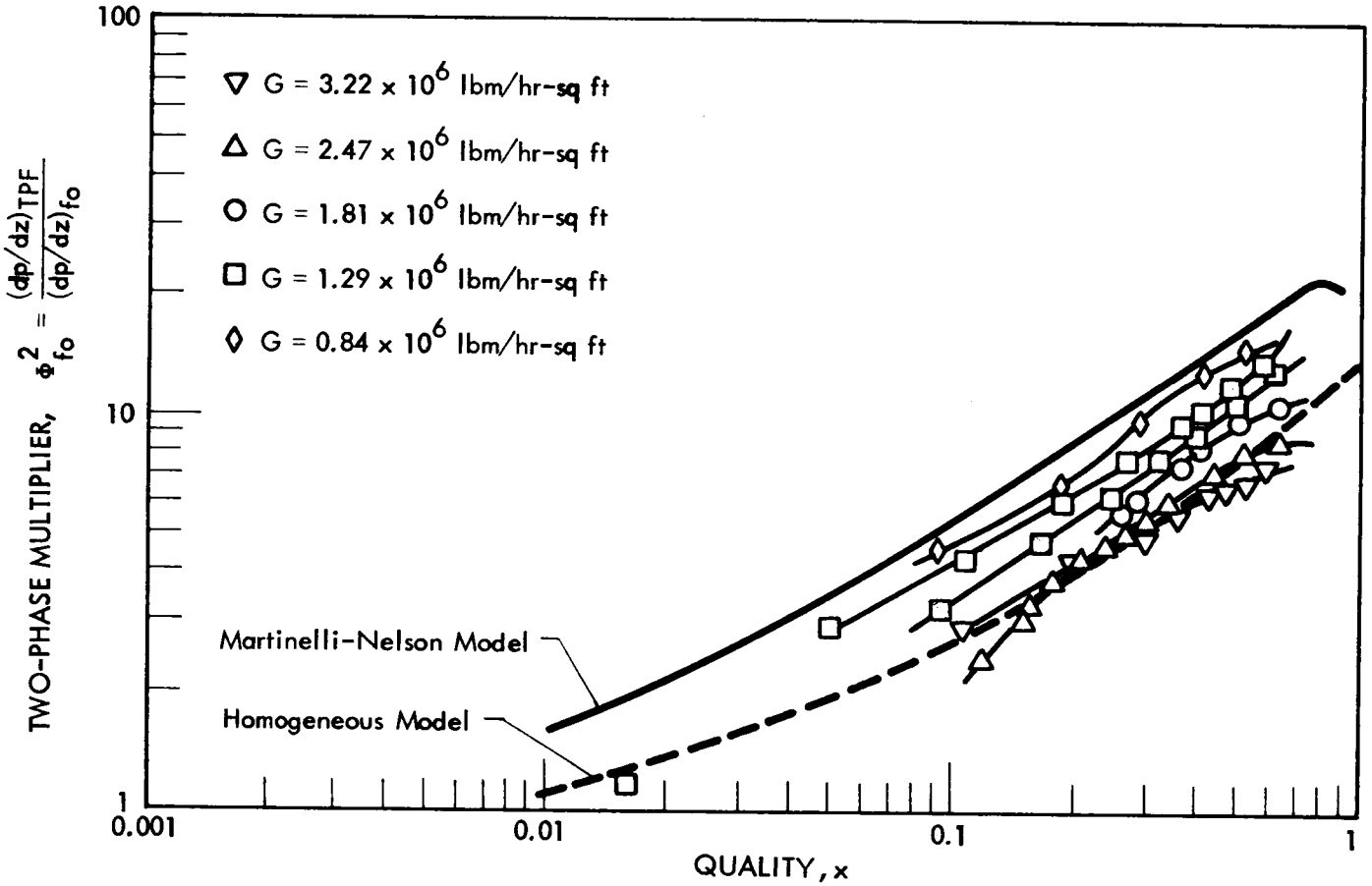


Figure II-6. EXAMPLE OF MASS FLUX EFFECT ON THE FRICTIONAL COMPONENT OF TWO-PHASE PRESSURE DROP, MUSCETTOLA [22].

frictional pressure drop results of Muscettola [22] for the adiabatic flow of water in a 0.197 in. tube at various mass fluxes is shown. The ordinate in the graph of Figure II-6 is the two-phase multiplier Φ^2_{fo} which is the ratio of the two-phase frictional pressure gradient to the single-phase frictional pressure gradient, assuming both liquid and vapor components are in the liquid phase. It is worthwhile at this time to explain the difference between the two-phase multiplier Φ^2_{fo} and the Martinelli multiplier for the turbulent-turbulent case Φ^2_{ftt}. This latter term which was developed and discussed extensively in the two Martinelli publications [4,19] can be defined as

$$\Phi^2_{ftt} = \frac{(dp/dz)_{TPF}}{(dp/dz)_{fa}} \quad . \tag{2-11}$$

The denominator on the right hand side of the expression is the single-phase pressure drop gradient assuming the liquid component alone was flowing in the tube (i.e., the vapor component is removed). These two-phase multipliers are related by:

$$\Phi^2_{fo} = \Phi^2_{ftt} (1 - x)^{1.8} \quad . \tag{2-12}$$

Several experimenters have attempted to correct for the mass flux effect noted in Figure II-6. Baroczy [23], using air-water and steam data from the literature, correlated the results for a mass flux of 1 x 10^6 lbm/hr-sq ft using the expressions Φ^2_{fo}, a property index $(\mu_f/\mu_g)^{0.2}/(\rho_f/\rho_g)$, and x, the quality.

The correlation obtained is shown in Figure II-7. For mass fluxes different from 1 x 10^6 lbm/hr-sq ft, multiplier ratios as a function of the property index cited above were presented. These ratios are shown

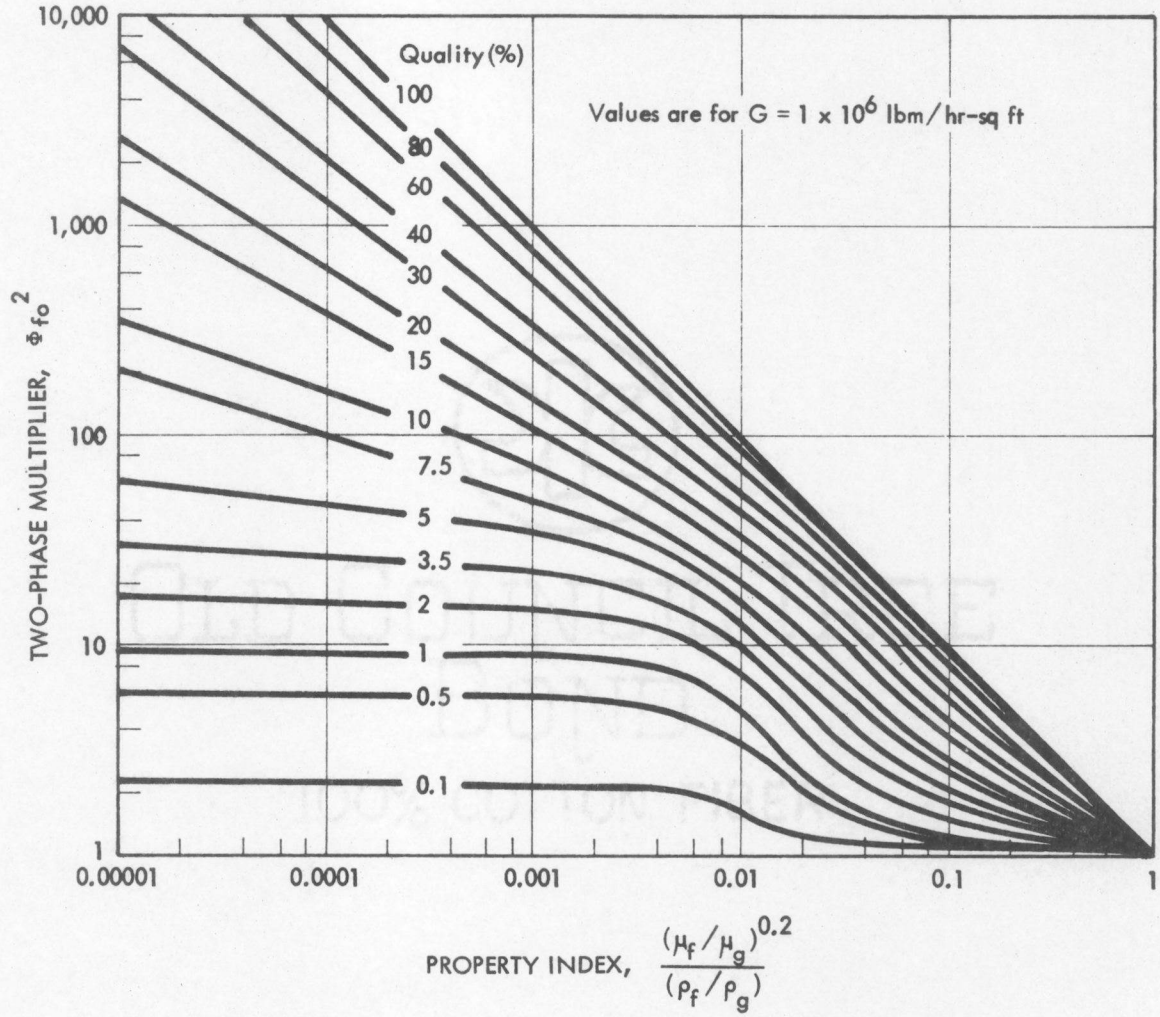


Figure II-7. BAROCZY'S [23] CORRELATION FOR TWO-PHASE FRICTIONAL PRESSURE DROP.

in Figure II-8. No explanation was advanced for the complex behavior of the multiplier ratios although changing flow patterns very likely exerted some influence. Baroczy [23] compared his correlation with pressure drop results for mercury-nitrogen, kerosene-air, diesel oil-air, sodium potassium-nitrogen, and boiling potassium. Satisfactory agreement was obtained in most cases.

Chisholm, Head of the Applied Heat Transfer Division of the National Engineering Laboratory, Glascow, Scotland has over the years published numerous papers [24, 25, 26, 27, 28] among others, on the pressure gradients due to friction during the flow of evaporating two-phase mixtures. Combining the continuity and momentum equations for mixtures, he was able to obtain an equation of the form:

$$\frac{(\Delta P)_{TPF}}{(\Delta P)_{fa}} = 1 + \frac{C}{X} + \frac{1}{X^2} = \Phi^2_{ftt} \qquad (2\text{-}13)$$

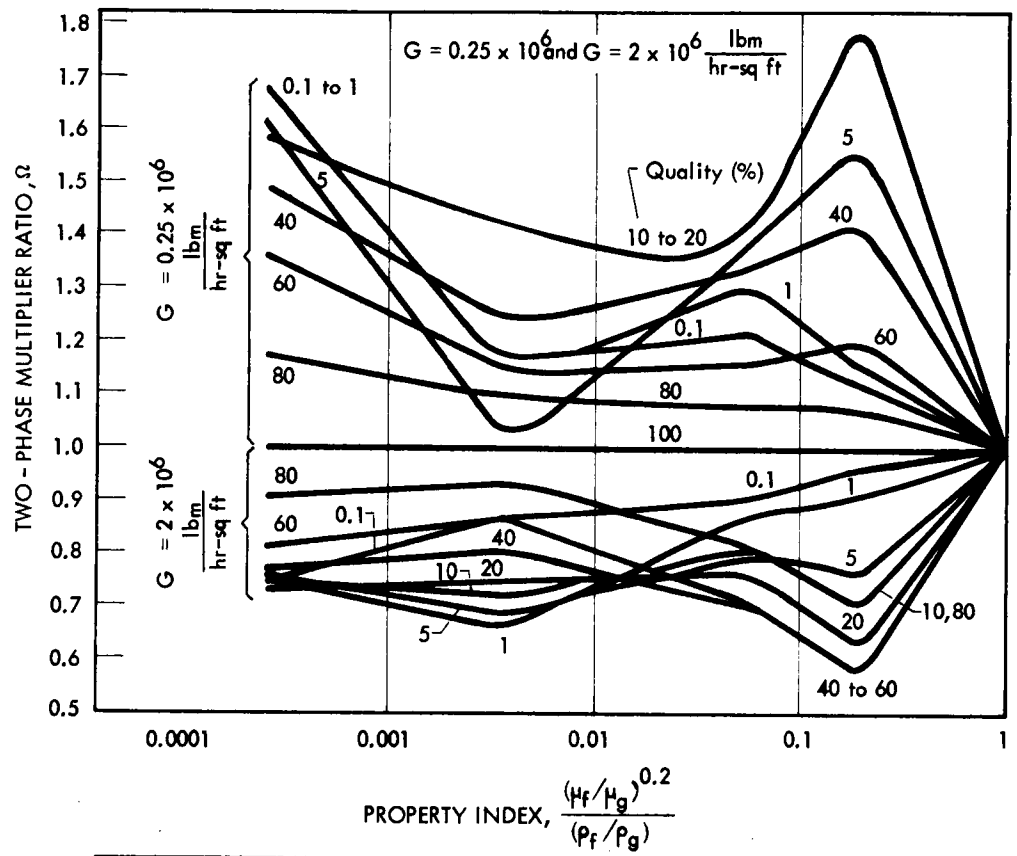
where X is the Martinelli parameter. For the case of turbulent-turbulent flow:

$$X_{tt} = \left(\frac{1 - x}{x}\right)^{0.9} \left(\frac{\rho_g}{\rho_f}\right)^{0.5} \left(\frac{\mu_f}{\mu_g}\right)^{0.1} . \qquad (2\text{-}14)$$

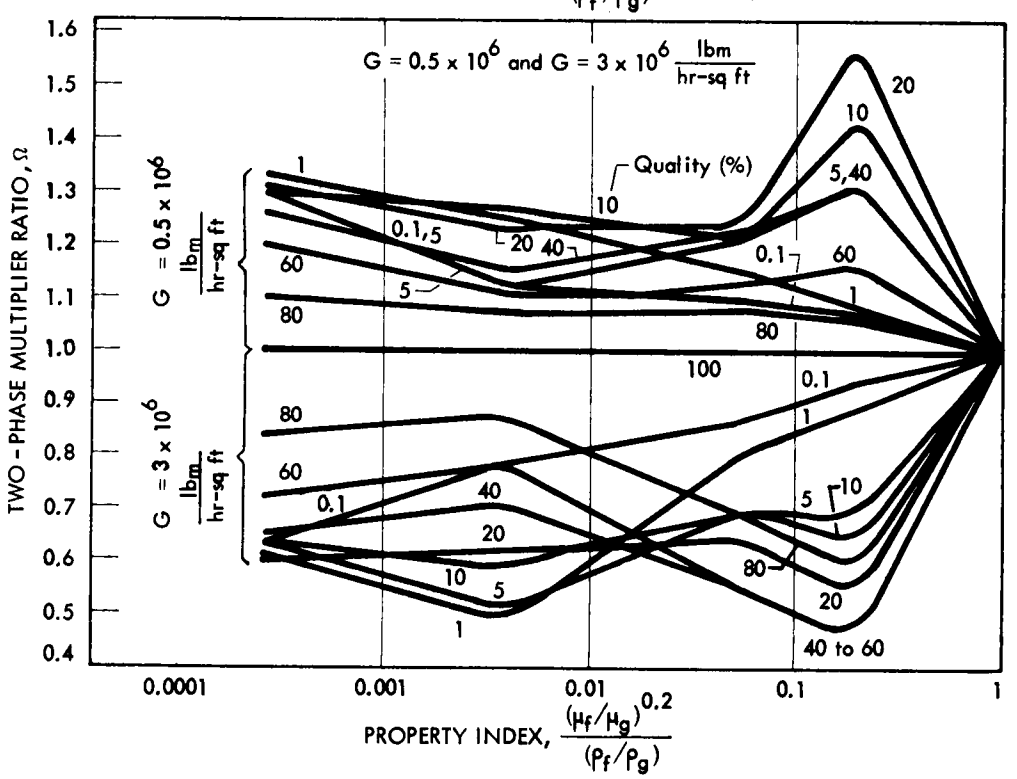
The variations among his papers consisted of obtaining values for C as a function of numerous parameters or transforming Equation (2-13) into different forms. In one of Chisholm's more widely used correlations [25, 27], the following equations were recommended for smooth tubes:

If $G \leq 1.47 \times 10^6$ lbm/hr-sq ft

$$\Phi^2_{ftt} = 1 + \frac{C}{X} + \frac{1}{X^2} \qquad (2\text{-}13)$$



(a)



(b)

Figure II-8. MASS FLUX CORRECTION TO BAROCZY'S [23] FRICTIONAL PRESSURE DROP CORRELATION.

and

$$C = \left\{ \lambda + (C_2' - \lambda)(\rho_g v_{fg})^{0.5} \right\} \left\{ \left(\frac{\rho_f}{\rho_g} \right)^{0.5} + \left(\frac{\rho_g}{\rho_f} \right)^{0.5} \right\} \qquad (2\text{-}15)$$

where $\lambda = 0.75$

$$C_2' = 1.47 \times 10^6 / G \qquad (2\text{-}16)$$

and v_{fg} is the latent specific volume (cu ft/lbm)

if $C_2' > 4$, let $C_2' = 4$.

If $G > 1.47 \times 10^6$ lbm/hr-sq ft

$$\Phi_{ftt}^2 = \left[1 + \frac{\bar{C}}{X} + \frac{1}{X^2} \right] \Psi' \qquad (2\text{-}17)$$

where

$$\Psi' = \left[1 + \frac{C}{T_o} + \frac{1}{T_o^2} \right] \Big/ \left[1 + \frac{\bar{C}}{T_o} + \frac{1}{T_o^2} \right] \qquad (2\text{-}18)$$

$$\bar{C} = \left(\frac{\rho_f}{\rho_g} \right)^{0.5} + \left(\frac{\rho_g}{\rho_f} \right)^{0.5} \qquad (2\text{-}19)$$

and

$$T_o = \left(\frac{x}{1 - x} \right)^{0.9} \left(\frac{\mu_f}{\mu_g} \right)^{0.1} \left(\frac{\rho_g}{\rho_f} \right)^{0.5} . \qquad (2\text{-}20)$$

It should be noted that additional limitations based on the values of the system pressure and the liquid-to-vapor density ratio exist. In most cases, they represent conditions beyond those that will be of interest in the present study of refrigerants. The original publications [25, 27] should be consulted for these limitations. Chisholm [25, 27] compared his results to the Baroczy [23] results shown in Figure II-7. Excellent agreement was obtained in all cases except those where the quality was very low. Comparison with Baroczy's [23] two-phase

multiplier ratio, Ω (Figure II-8), gave good agreement for high mass flux values. At low mass flux values, however, the Baroczy [23] correlation gave lower friction pressure gradients. A comparison of Chisholm's [25, 27] analytical equations with the L-M [19] model is shown in Figure II-9. Instead of obtaining one Φ_{ftt} vs X curve, a series of curves each representing a different value of C (and therefore mass flux) were obtained.

In his latest paper, Chisholm [28] transformed Equation (2-13) into one of the form:

$$\Phi_{fo}^2 = 1 + (\Gamma^2 - 1)\left\{Bx^{(2-n_o)/2}(1-x)^{(2-n_o)/2} + x^{(2-n_o)}\right\}. \quad (2\text{-}21)$$

For $n_o = 0.2$:

$$\Gamma = \left(\frac{\rho_f}{\rho_g}\right)^{0.5}\left(\frac{\mu_g}{\mu_f}\right)^{0.1} \quad (2\text{-}22)$$

which is the reciprocal of the square root of Baroczy's [23] property index. Recommended values for B as a function of G and Γ are given in Table II-1. These values are a compromise between the correlations of Baroczy [23], L-M [19], and Chisholm [25, 27].

Chawla [29, 30, 31, 32] developed a new theory for frictional pressure gradient independent of whether either or both of the phases in a tube were laminar or turbulent. The equation obtained was:

$$\left(\frac{dp}{dz}\right)_{TPF} = \frac{0.3164}{(GD/\mu_g)^{1/4}}\,\frac{G^2x^{1.75}}{2D\rho_g}\left(1 + \frac{1-x}{x\varepsilon(\rho_f/\rho_g)}\right)^{2.375}. \quad (2\text{-}23)$$

The parameter ε is the ratio of the mean liquid velocity to the mean vapor velocity. In a broader sense, however, ε embodies the flow pattern effect, the roughness increase of the liquid surface, and particularly,

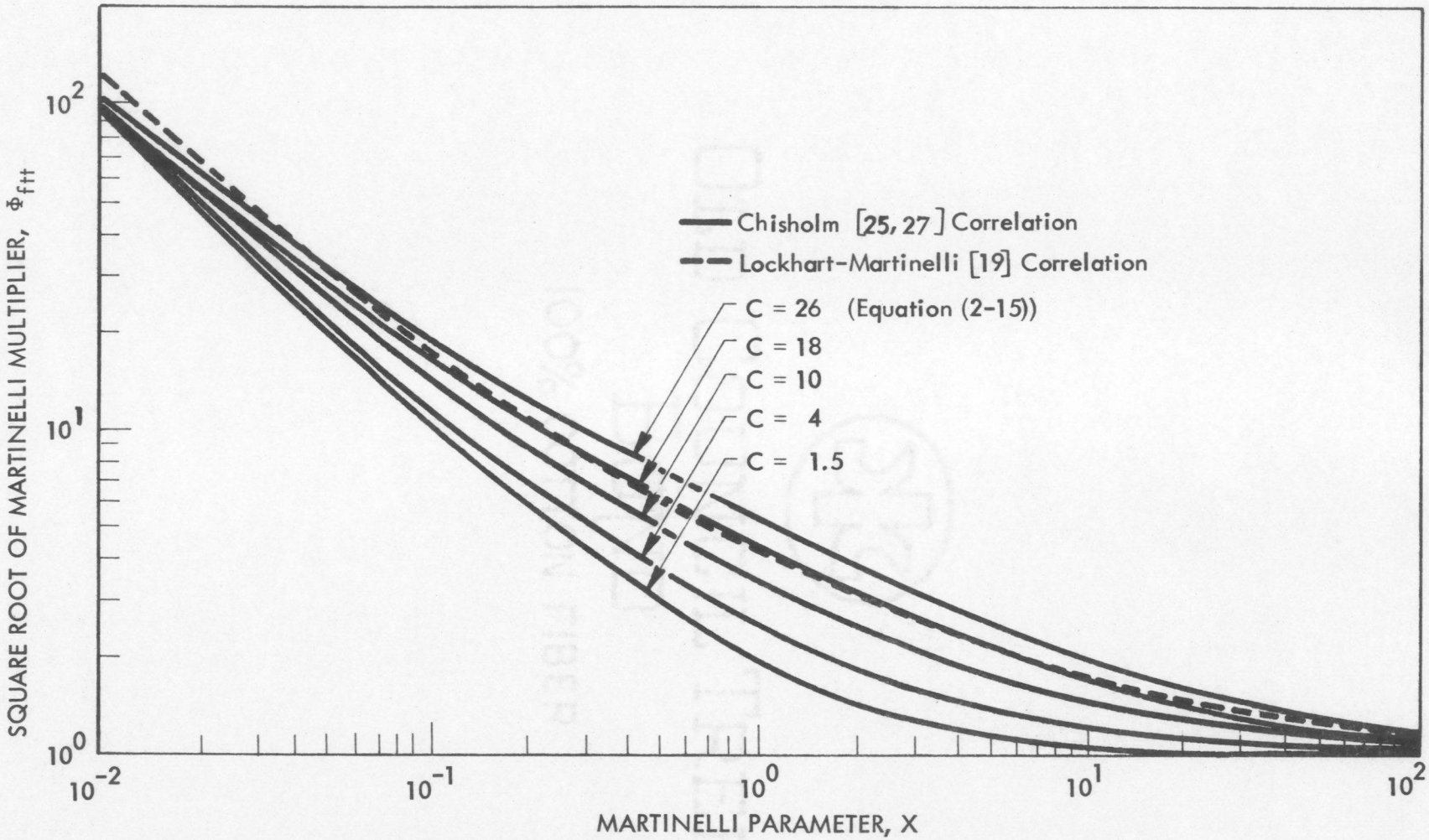


Figure II-9. COMPARISON OF CHISHOLM'S [25,27] ANALYTICALLY DERIVED VALUES FOR Φ_{ftt} WITH THE LOCKHART-MARTINELLI [19] CURVE.

Table II-1

VALUES FOR THE PARAMETER B IN CHISHOLM'S [28]
PRESSURE DROP CORRELATION

Γ	G(lbm/hr-sq ft)	B
≤ 9.5	$\leq 0.369 \times 10^6$	4.8
	$0.369 \times 10^6 < G < 1.401 \times 10^6$	$1.769 \times 10^6/G$
	$\geq 1.401 \times 10^6$	$1{,}493.4/G$
$9.5 < \Gamma < 28$	$\leq 0.442 \times 10^6$	$14{,}119/(\Gamma G^{0.5})$
	$> 0.442 \times 10^6$	$21/\Gamma$
≥ 28		$0.4073 \times 10^6/(\Gamma^2 G^{0.5})$

the exchange of momentum between the phases. While Chawla [29, 30, 31, 32] presented various formulations, the values of ε shown in Figure II-10 are probably the most reliable. Here,

$$\varepsilon = \varepsilon \left\{ \frac{1 - x}{x} (Re\ Fr)_{fa}^{-1/6} \left(\frac{\rho_g}{\rho_f}\right)^{0.9} \left(\frac{\mu_g}{\mu_f}\right)^{0.5} ; \frac{k_o}{D} \right\} \qquad (2\text{-}24)$$

where k_o/D is the relative roughness of the tube wall. Equations (2-23) and (2-24) were verified by an extensive testing program Chawla [29] undertook with R-11 in horizontal tubes.

Lombardi and Pedrocchi [33] have recently proposed a correlation for the two-phase pressure drop of the form:

$$\left(\frac{dp}{dz}\right)_{TPF} = KG^{m'} \left[\frac{v_m^{0.86} \sigma^{0.4}}{D^{1.2}} \right] \qquad (2\text{-}25)$$

where $\left(\frac{dp}{dz}\right)_{TPF}$ is the two-phase frictional pressure gradient in (lbm/cu ft), K and m' are empirically-obtained constants, and

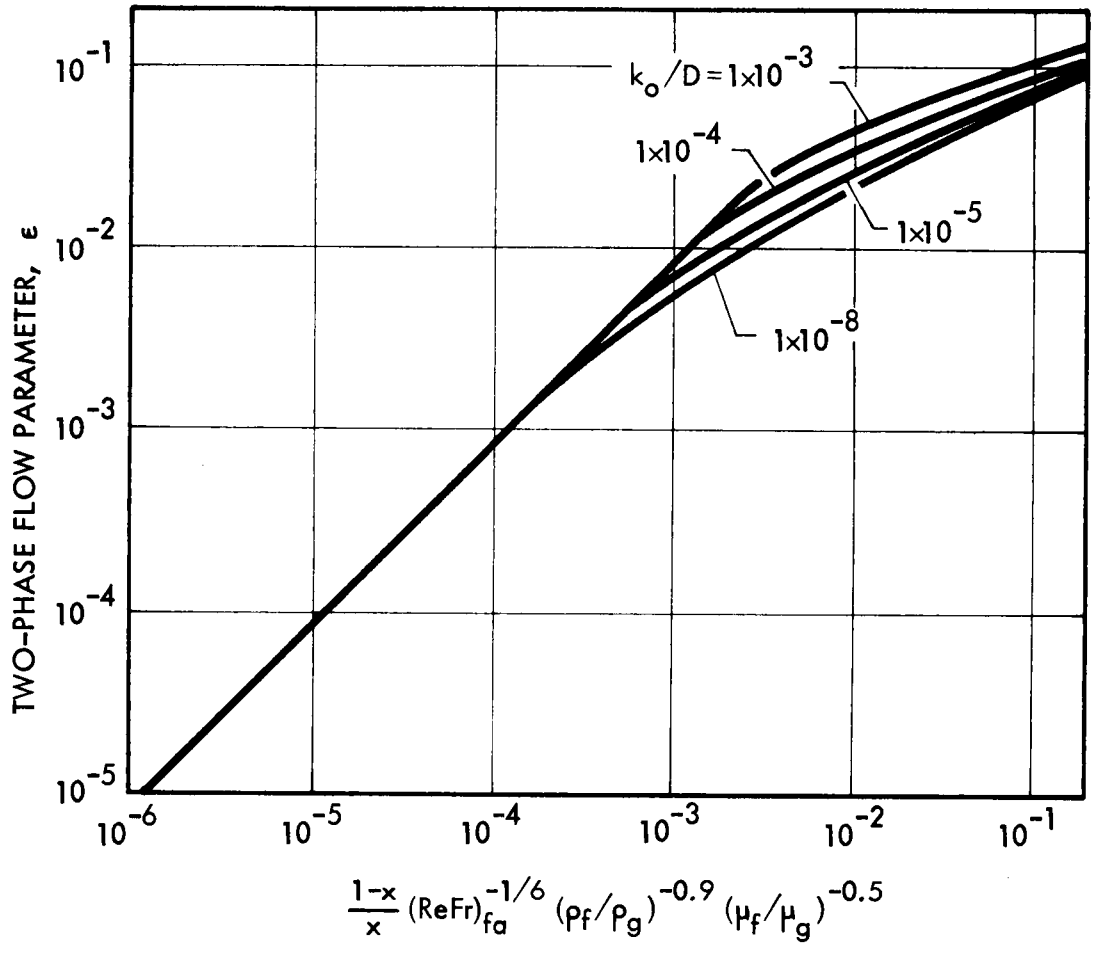


Figure II-10. GENERAL CORRELATION OF THE TWO-PHASE FLOW PARAMETER ϵ, CHAWLA [29, 30, 31, 32].

$$v_m = [x\, v_g + (1 - x)\, v_f] \qquad (2\text{-}26)$$

is the mean specific volume.

For flow in round tubes, values of 5.675×10^{-7} for K and 1.4 for m' are recommended. This correlation, as well as a similar one proposed for rod clusters and annuli, was verified against 1400 experimental data points for the following range of parameters for vertical upflow:

$0.369 \times 10^6 < G < 3.686 \times 10^6$, lbm/hr-sq ft

$0.0164 < D < 0.0820$, ft

$0.3281 < L < 13.124$, ft

$15 < \rho_f/\rho_g < 100$

$0.00137 < \sigma < 0.00548$, lbf/ft

$0.01 < x < 0.98$

As a result, it was found that 87% of all experimental data were between ± 15% of the predicted values. Mention was not made of which working fluids were included in the 1400 experimental data points, although it is believed that the majority were obtained with steam-water. The flow regime was either dispersed or annular-dispersed. It is interesting to note the correlation of Lombardi and Pedrocchi [33] differs from those of M-N [4], Baroczy [23], and Chisholm [25, 27, 28] in three major ways:

(1) the viscosity of neither phase affects frictional pressure losses

(2) a new controlling parameter appears to be the surface tension

(3) the exponents of mass flux and mean specific volume are lower.

In addition to Chawla [29, 30, 31, 32], several investigators have studied the pressure drop in boiling refrigerants. Napadensky [15] who boiled R-12 in a vertical stainless-steel tube observed the strong influence of flow patterns on the agreement between his data and the L-M [19] model. In applying his data, he subtracted out the gravitational term and assumed that the acceleration term was small compared to the frictional pressure drop term (which is not always true). Napadensky [15], also, did not correct his curve for elevated pressures as illustrated by M-N [4], but instead used the atmospheric pressure curve published by L-M [19]. A scaling of the M-N [4] curves on, possibly, an equal reduced pressure basis for water and R-12 would have resulted in a lower curve and could conceivably have given better agreement with the R-12 data, especially at the higher boiling temperatures. A correlation similar to the one Davis [34] used, in which the Froude number raised to a power was incorporated into the Martinelli parameter, X_{tt}, significantly decreased the scatter in Napadensky's [15] data. This correction, however, did not seem to be valid over the entire flow range. Davis [34] found it applicable only in the turbulent-turbulent flow regime in a limited range of liquid and gas Reynolds numbers - mainly those which he thought corresponded to annular flow. Napadensky [15], who was able to visually inspect the flow regime, found that the Froude number correlation did indeed apply to the annular flow regime only for vertical flow.

It is interesting to note that Napadensky [15] did not compare his data to the M-N [4] model. He did, however, compare his non-adiabatic data with Thom's [35] correlation. This correlation was very similar to the one by M-N [4] but was based on more recent experimental

data on steam-water pressure drops. The results of the comparison were not satisfactory. Napadensky [15] attributed this failure to correlate to the lack of success in scaling some of the steam-water parameters to R-12. He however, did not mention how he attempted to go about this.

Additional work on the pressure drop in boiling refrigerants was performed by Cheshire and Stirling [36], who boiled R-114 in a natural circulation evaporator. They obtained experimental pressure drops which were on the average, 25% higher than those predicted by the M-N [4] model. It should be pointed out that Cheshire and Stirling [36] also used the atmospheric pressure values of the Martinelli multiplier, Φ^2_{ftt}, and did not apply the pressure correction curve M-N [4] recommended. Foltz and Murray [37] ran tests on four vertical pipes using R-114. The pressure drop results obtained were compared to a homogeneous model and were found to be 25% higher than those predicted by the model. In addition to the effect of slip, an unknown length of subcooled liquid may have contributed to the experimental uncertainty.

Hatch and Jacobs [38] measured the pressure drop in a horizontal two-phase mixture of R-11 under adiabatic and diabatic conditions. Data were obtained in the mass flux range of 0.081×10^6 to 3.19×10^6 lbm/hr-sq ft, with qualities from zero to unity and with saturation temperatures from 86 to 154°F. The experimental frictional pressure drops for both cases were about 40% lower than the M-N [4] values. Hatch and Jacobs [38] did not mention any mass flux or boiling temperature effect on the data, nor did they explain how they modeled the M-N [4] curve when they applied it to R-11. Bryan and Seigel [39] who also boiled R-11 in a horizontal tube did not correlate their results.

Altman, Norris, and Staub [40] boiled R-22 in two horizontal copper tubes, 4 ft long and 0.343 in. ID. For boiling temperatures of 40 and 75°F, and mass fluxes of between 0.592×10^5 and 4.68×10^5 lbm/hr-sq ft, they scaled the graph of M-N [4] for the ratio of the two-phase pressure drop to the single-phase pressure drop assuming liquid only flows. Using apparently, an equal density ratio as the scaling parameter, Altman, Norris, and Staub [40] were able to correlate their pressure drop data with the M-N [4] model to within 25%. Johnston and Chaddock [41] confirmed this for R-22 and also for R-12. For both fluids, the tests were conducted at sub-zero temperatures and in a lower range of mass fluxes than the Altman, Norris, and Staub [40] tests.

Blatt and Adt [42] boiled R-11 and R-113 in stainless steel and copper horizontal tubes at mass fluxes of 0.432×10^5 and 0.540×10^5 lbm/hr-sq ft and unspecified boiling temperatures. The results were correlated by a modified version of the M-N [4] model in which zero slip between the phases was assumed, thus enabling a calculation to be made of the void fraction from the quality and the densities of the two phases. Agreement was good in all ranges except for qualities below 0.25 where the correlation underestimated the pressure drop. Chaddock and Noerager [43], who boiled R-12 in a horizontal tube did not correlate their pressure drop results.

In conclusion, it can be said that the M-N [4] model probably gives good results at high qualities and low mass fluxes while the Homogeneous [3] model is better at high flow rates and low qualities. The correlations of Baroczy [23], Chisholm [24, 25, 26, 27, 28], Chawla [29, 30, 31, 32], Lombardi and Pedrocchi [33], and Davis [34] each in a

different way attempted to predict, among other things, the effect of the mass flow rate. Much work has been done on measuring the pressure drop of various boiling refrigerants. The methods of analysis have been quite varied and in many cases, undesirable simplifications were made due to the lack of reliable information on such things as a scaling parameter or the void fraction. At this point, no reliable information exists as to which of the above-mentioned correlations is the best nor are the limits of applicability of such a correlation known.

C. VOID FRACTION

One of the main problems encountered in vertical flow pressure drop analysis is the determination of accurate values for the void fraction, α. This parameter is used in computing the gravitational component of the pressure drop and, as shown in the sample calculations in Appendix D, affects the momentum term also. For any two-phase system where one-dimensional flow is assumed, the equation

$$\frac{1 - x}{x} = \frac{V_f}{V_g}\left(\frac{\rho_f}{\rho_g}\right)\frac{1 - \alpha}{\alpha} \qquad (2\text{-}27)$$

is valid. In the Homogeneous [3] model, both the liquid and vapor are assumed to have the same velocity and thus the void fraction is readily obtainable from the quality and density ratio. In a separated flow model, the V_f/V_g ratio, commonly referred to as the slip ratio is usually a complex function of flow regime, fluid properties, velocity, and test section geometry and orientation. A large amount of data has been gathered and numerous correlations presented for attempting to predict the void fraction. A complete discussion of this subject is beyond

the scope of this study although the results from some of the more important publications will be discussed here.

Probably one of the earliest and more widely used void fraction models was presented by M-N [4]. It was shown that when the assumption of annular flow was made:

$$\Phi_{ftt} \approx \frac{1}{1 - \alpha} \tag{2-28}$$

and the M-N [4] curves for Φ_{ftt} vs X_{tt} could be used to obtain α. Another void fraction correlation based on steam-water data obtained in the 1950's at the University of Cambridge was published by Thom [35]. In this case a direct relationship between the quality and the void fraction was presented in the form:

$$\alpha = \frac{\gamma' x}{1 + x(\gamma' - 1)} \quad . \tag{2-29}$$

A tabulation of the slip factor γ', as a function of steam-water pressure is given in Table II-2.

Table II-2

EXPERIMENTALLY DETERMINED VALUES OF SLIP FACTOR γ' AS A FUNCTION OF PRESSURE FOR STEAM-WATER, THOM [35]

Pressure (psia)	14.7	250	600	1250	2100	3000	3206
Slip Factor, γ'	246	40.0	20.0	9.80	4.95	2.15	1.00

The results were in good agreement with those of M-N [4] at intermediate and high pressures. At low pressures however, Thom's [35] results yielded void fractions higher than those predicted by M-N [4]. A comparison is given in Figure II-11.

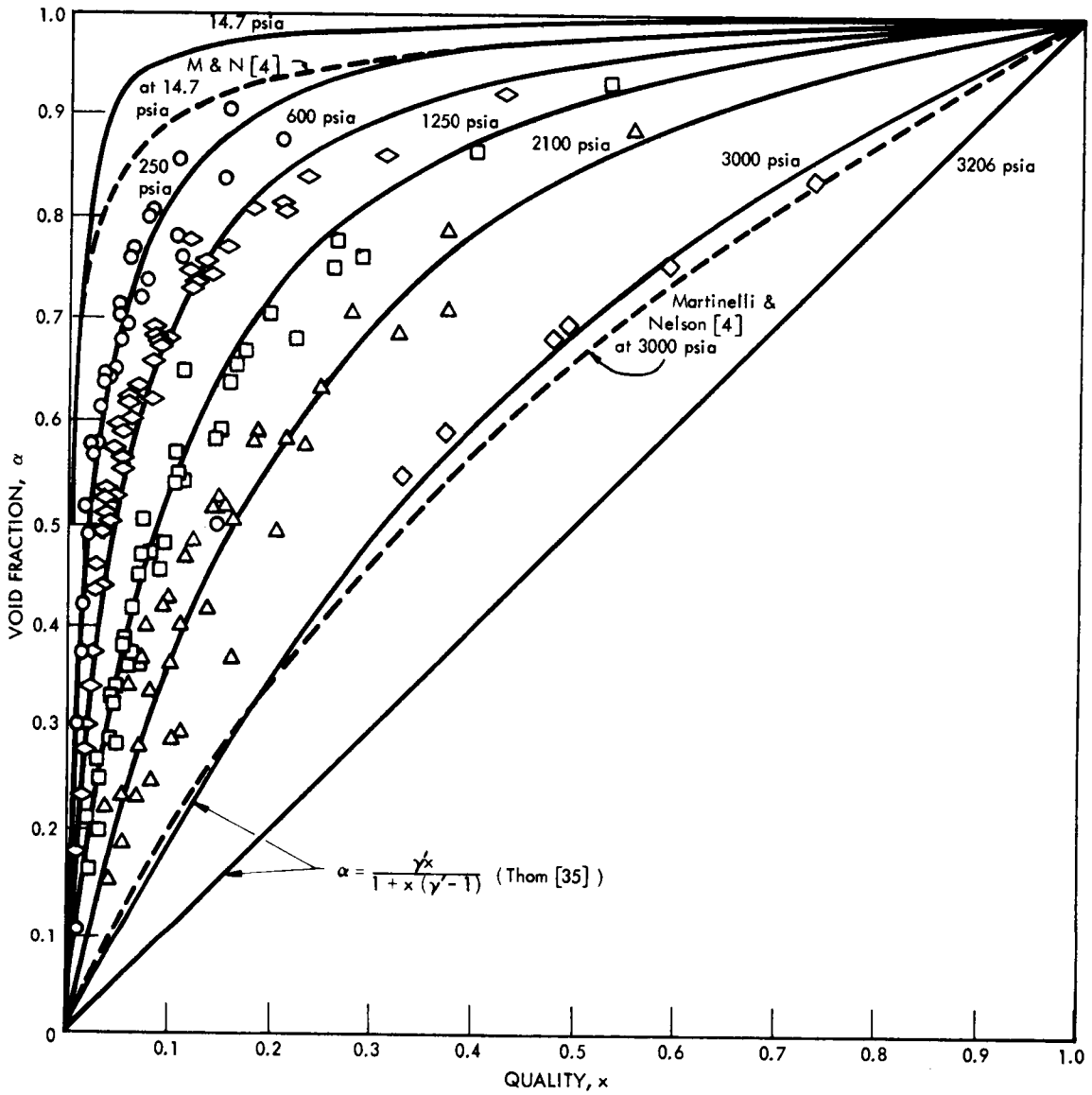


Figure II-11. COMPARISON OF MARTINELLI-NELSON [4] AND THOM [35] VOID FRACTION CORRELATIONS.

In 1960, Levy [44] presented his momentum exchange model in which he assumed that the pressure drop in the liquid phase was equal to that in the vapor phase. When compared to experimental results for steam-water, the model tended to underestimate the void fraction in most cases. Bankoff [45] whose variable density model for the bubbly flow regime was published at the same time, assumed that the velocity and void fraction followed a power law distribution at any cross-section. From this analysis, the following relationship was obtained:

$$\alpha = \frac{K'\rho_f\, x}{\rho_g + x\, \Delta\rho} \quad . \tag{2-30}$$

A value of $K' = 0.89$ was found to correlate steam-water data well. Hughmark [46] extended the above analysis by obtaining a correlation for K' as a function of Reynolds number, Froude number, density ratio and quality. When compared to the M-N [4] correlation, Bankoff's [45] variable density model showed the same trend Thom [35] observed experimentally--namely that the M-N [4] model was accurate at higher pressures but tended to underestimate the void fraction at low pressures.

Marchaterre and Hoglund [47] have presented yet another correlation for void fraction. Observing that the relative velocity between the liquid and vapor phases was the only unknown parameter in relating the void fraction to the quality as shown in Equation (2-27), they presented curves based on a large amount of data from various sources which correlated the slip ratio, V_f/V_g, with the Froude number and the volumetric flow rate. This correlation is valid only for cases where the velocity, assuming liquid only flows through the tube, is greater than 0.8 ft/sec.

Baroczy [48], in 1965, presented a generalized correlation for void fraction in two-phase flow which was proposed for use with all fluids including liquid metals. A plot was presented of the liquid fraction, $(1 - \alpha)$, as a function of the Baroczy property index $(\mu_f/\mu_g)^{0.2}/(\rho_f/\rho_g)$. A comparison of the results with the M-N [4] void fraction correlation exhibited the same trends Bankoff [45] and Thom [35] observed.

One of the earliest reported experiments with refrigerants was reported by Kowalczewski [49] who measured the void fraction of R-12 over a limited range of flow conditions. An empirical expression was obtained, but its application to conditions beyond the range of experimental data obtained by Kowalczewski [49] was not recommended.

Probably the most complete and exhaustive study of void fractions was reported by Zuber et al [10]. Published for the joint U.S. - EURATOM research and development program, this report summarized the results of an experimental and analytical investigation for determining, among other things, the effects of mass flux, heat flux, inlet subcooling, and system pressure on the void fraction under steady state conditions.

Generally, analysis of the volumetric concentration of liquid and vapor must take into account the effect of the non-uniform flow and concentration distributions across a duct, as well as the effect of the local relative velocity between the two phases. For the specific case of adiabatic dispersed two-phase flow systems with constant velocity and concentration profiles, Zuber et al [10] obtained the following expression which they claimed was also applicable to cases of non-uniform flow and concentration profiles, as well as non-zero local relative velocity:

$$\langle\alpha\rangle = \frac{\langle j_g \rangle}{C_o \langle j \rangle + \bar{V}_{gj}} \tag{2-31}$$

where C_o is the distribution parameter which accounts for the effect of non-uniform flow and concentration profiles. It is the reciprocal of the term K' used by Bankoff [45] and Hughmark [46]. $\bar{V}_{gj}$ is the weighted mean drift velocity which accounts for the relative velocity between the two phases. The above equation can also be expressed in terms of quality so that:

$$\langle\alpha\rangle = \frac{x}{C_o\,(\Delta\rho/\rho_f)\,x + \left[C_o + \bar{V}_{gj}/V_{fo}\right](\rho_g/\rho_f)} \,. \tag{2-32}$$

The expressions for C_o and $\bar{V}_{gj}$ are dependent on flow regime, as well as on other parameters. By examining their own results for R-22 and the results of numerous other tests, Zuber et al [10] formulated the following expressions for those two parameters:

For bubbly flow (D ≤ two inches; round tubes):

$$P_r < 0.5,\ C_o \simeq 1.2 \tag{2-33}$$

$$P_r > 0.5,\ C_o \simeq 1.2\text{-}0.4\,(P_r - 0.5) \tag{2-34}$$

$$\bar{V}_{gj} = 1.41 \left[\frac{\sigma g\,\Delta\rho}{\rho_f^{\,2}}\right]^{1/4} \tag{2-35}$$

where P_r is the reduced pressure.

For slug flow:

$$C_o = 1.2 \tag{2-36}$$

$$\bar{V}_{gj} = 0.35 \left[\frac{g\,\Delta\rho D}{\rho_f}\right]^{1/2} \,. \tag{2-37}$$

For annular flow:

$$C_o = 1.0 \tag{2-38}$$

$$\bar{V}_{gj} = 23 \left[\frac{\mu_f \bar{V}_{fo}}{\rho_g D}\right]^{1/2} \frac{\Delta\rho}{\rho_f} \quad . \tag{2-39}$$

For pseudo-jet flow:

$$1.0 \leq C_o \leq 1.25 \tag{2-40}$$

$$\bar{V}_{gj} = A_p \left[\frac{\sigma g \Delta\rho}{\rho_g^2}\right]^{1/4} \tag{2-41}$$

where A_p, the apparatus parameter, depends on the L/D ratio and the mode of injection of the vapor into the stream. Generally A_p is between the values of 0.50 and 0.89.

If the flow regime is unknown or if a simplified form of the void fraction equation is desired, the following expressions were recommended:

$$C_o \simeq 1.13 \tag{2-42}$$

$$\bar{V}_{gj} = 1.41 \left[\frac{\sigma g \Delta\rho}{\rho_f^2}\right]^{1/4} \quad . \tag{2-43}$$

Equations (2-42) and (2-43) when inserted into (2-32) generally overestimate the void fraction in bubbly flow but underestimate it in the annular flow regime. It should be noted that none of the expressions Zuber et al [10] recommended can be considered accurate at very high qualities since the void fraction is not unity when the quality is one. This deviation increases with decreasing velocity.

Zuber et al [10] compared their analytical results with a wide variety of refrigerant and non-refrigerant data from numerous sources including their own tests. Agreement was generally better than that obtained by the Homogeneous [3], M-N [4], Levy momentum exchange [44], Bankoff variable density [45] or Marchaterre and Hoglund [47] models.

Subsequent to the publication of the Zuber et al [10] report, experimental results on the subcooled and saturated void fraction of two-phase R-114 were obtained by Shiralkar [50]. Using a hot wire in an annulus, void fractions were obtained at different radial positions at a given cross-section. While data were only taken at one pressure, namely 123 psia, the mass flux was varied from 0.156 x 10^6 to 0.527 x 10^6 lbm/hr-sq ft. The results obtained were found to be in very good agreement with the Zuber et al [10] general correlation represented by Equations (2-32), (2-42), and (2-43). The results are shown in Figures II-12, II-13, and II-14. Also shown in these figures is a comparison of the Shiralkar [50] data with the M-N [4], Thom [35], and Baroczy [48] models. Of these, only the Baroczy [48] model gave reasonably good predictions. It should be noted that the void fraction curves of M-N [4] and Thom [35], obtained for steam-water, were applied to R-114 by modeling the two fluids on an equal reduced pressure basis. If the modeling had been done on an equal density ratio basis, both M-N [4] and Thom [35] curves would have come down slightly, giving a better agreement with the data. The improvement would however have been so slight that neither model would have surpassed the Zuber et al [10] or the Baroczy [48] correlations.

In Figure II-15, a comparison of Shiralkar's [50] data with the Marchaterre and Hoglund [47] correlation is illustrated. Because this correlation is valid only in cases where the velocity, assuming liquid only flows through the tube, is greater than 0.8 ft/sec, Shiralkar's [50] results for a mass flux of 0.156 x 10^6 lbm/hr-sq ft could not be used. For the other flow rates, as can be seen, the agreement is not very good.

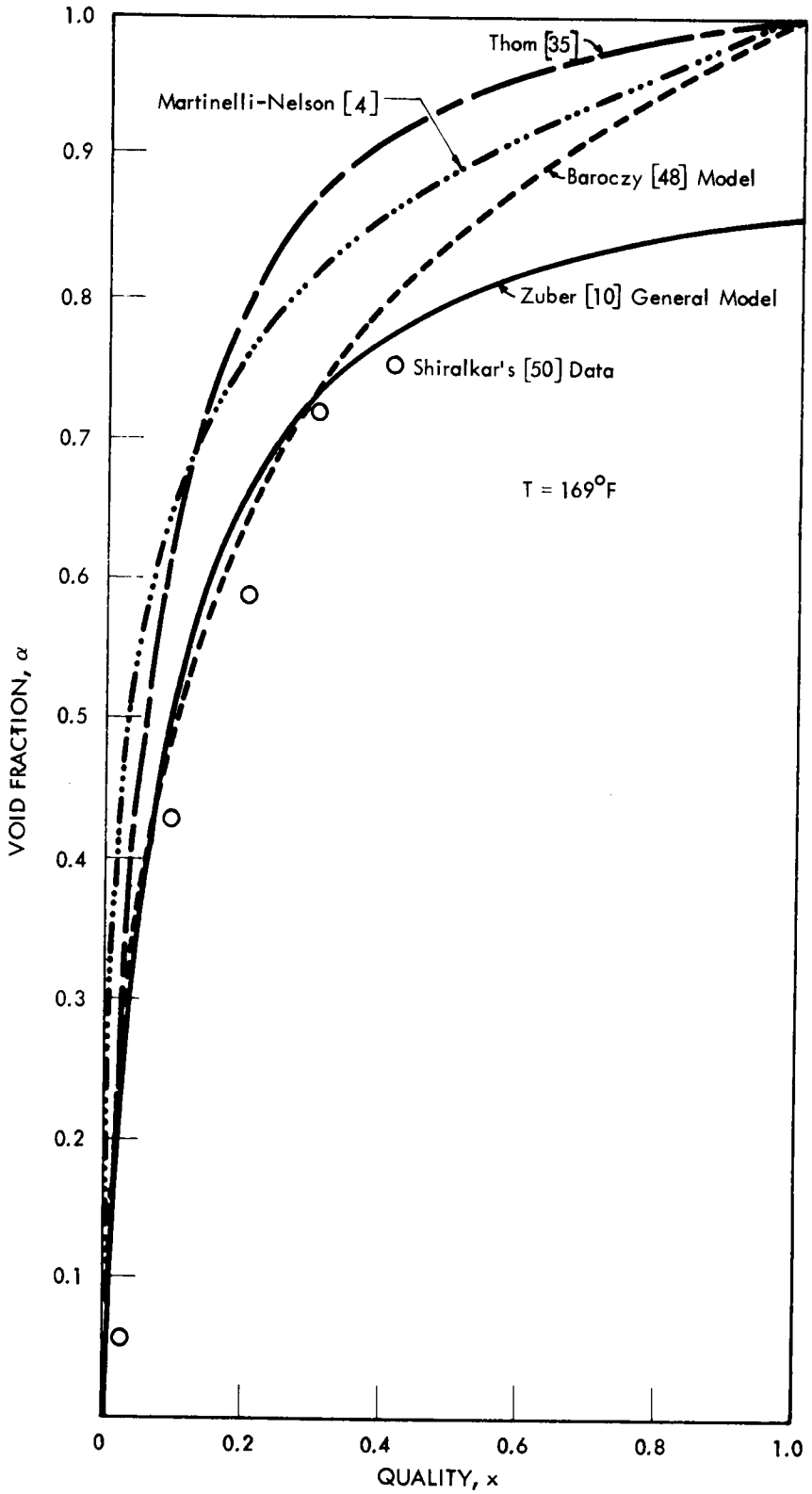


Figure II-12. COMPARISON OF VARIOUS MODELS WITH SHIRALKAR'S [50] DATA FOR THE VOID FRACTION OF R-114. $G = 0.156 \times 10^6$ lbm/hr-sq ft.

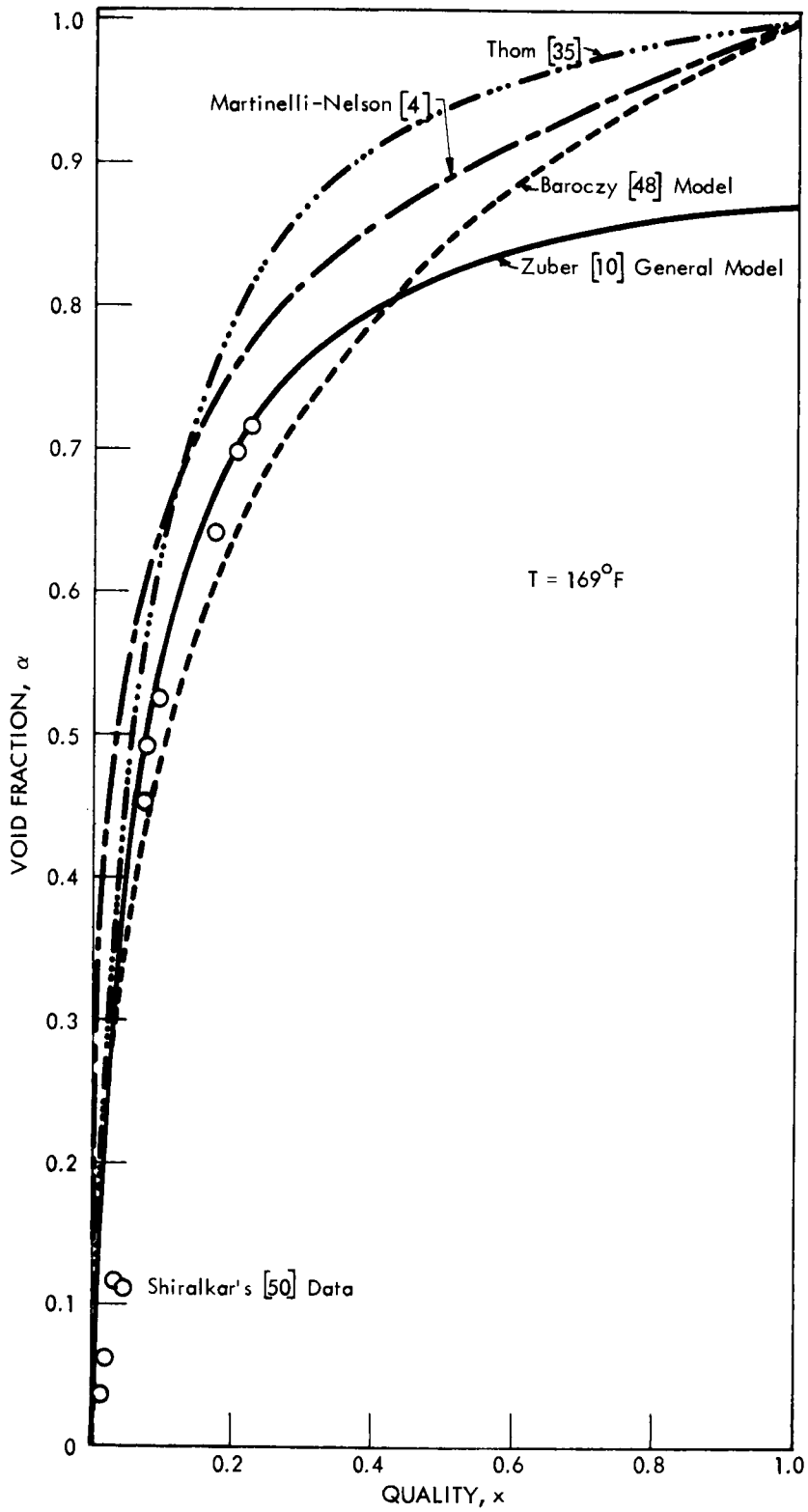


Figure II-13. COMPARISON OF VARIOUS MODELS WITH SHIRALKAR'S [50] DATA FOR THE VOID FRACTION OF R-114. $G = 0.303 \times 10^6$ lbm/hr-sq ft.

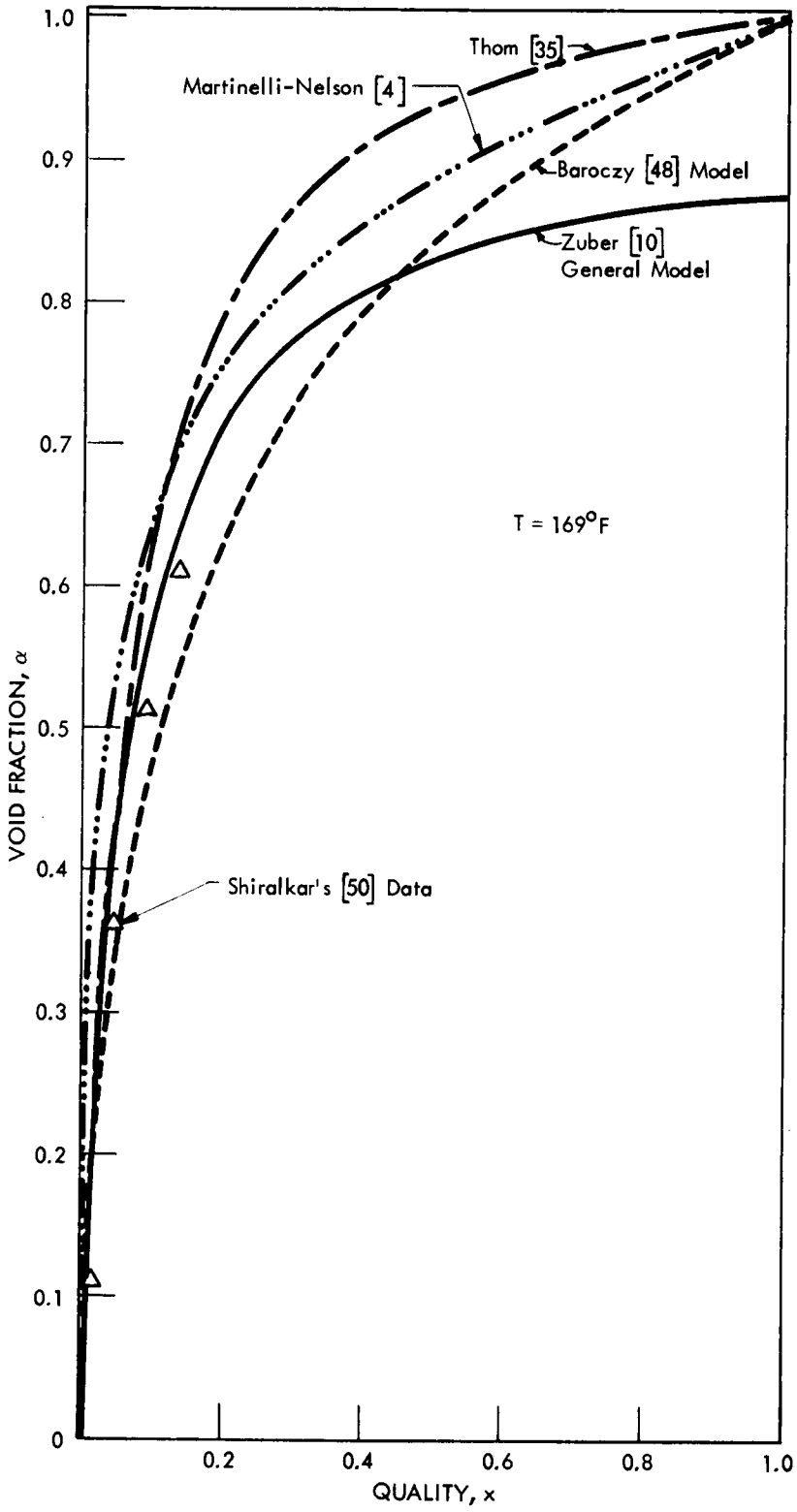
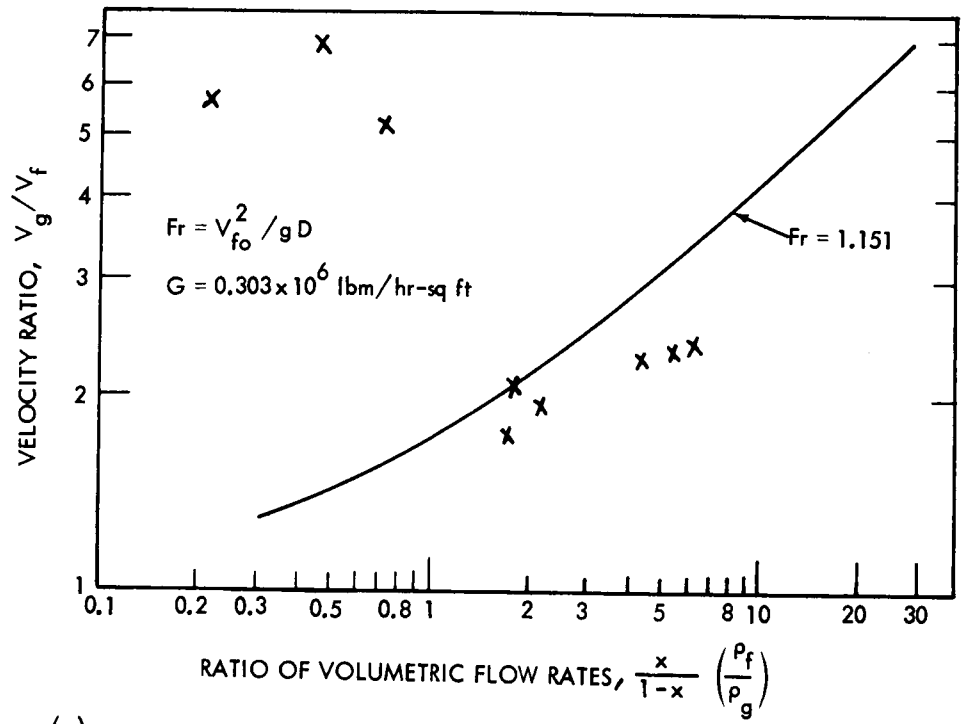
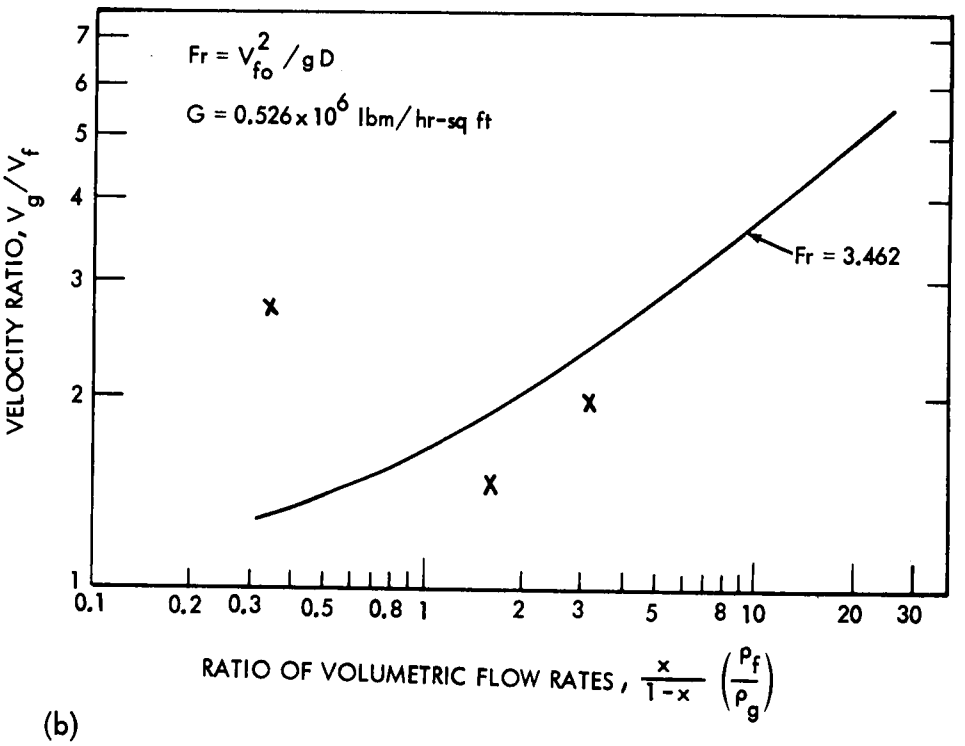


Figure II-14. COMPARISON OF VARIOUS MODELS WITH SHIRALKAR'S [50] DATA FOR THE VOID FRACTION OF R-114. $G = 0.526 \times 10^6$ lbm/hr-sq ft.



(a)



(b)

Figure II-15. COMPARISON OF SHIRALKAR'S [50] R-114 DATA WITH MARCHATERRE AND HOGLUND [47] CORRELATION.

In summation, it appears that the Zuber et al [10] general void fraction correlation gives the best agreement with experimental data. While the Baroczy [48] void fraction correlation was also quite successful in predicting R-114 void fractions, its principal weakness lies in the fact that it does not correct for the mass flux effect. The errors can be significant in the mass flux range of less than 0.10×10^6 lbm/hr-sq ft. This is illustrated in the R-22 plots in Zuber et al [10]. It should however be remembered that the Zuber et al [10] general correlation is not accurate in the high quality range and appropriate corrections need to be made in that region.

D. HEAT TRANSFER COEFFICIENTS

The ability to predict the heat transfer boiling coefficient as a function of the numerous variables that exist in a two-phase mixture is probably the most important task in the design of such things as heat exchangers and in nuclear reactors. To this end, a large number of experiments has been conducted and numerous correlations have been presented for a variety of working fluids. The most elementary correlations usually define the heat transfer coefficient as a function of only a few variables. Such relations are usually limited in application to conditions not significantly different from those at which the tests were run and do not lead to any insight into the fundamental boiling mechanism. The two basic areas in boiling where considerable research has been done--pool boiling and flow boiling--will be discussed here. However, interest in the former will be limited to those experimental investigations and correlations which will be used later to attempt to formulate more reliable flow boiling correlations.

Pool Boiling

The phenomena of boiling a fluid from a heated surface submerged in a pool of initially quiescent liquid without external agitation has been studied extensively by a variety of investigators for numerous fluids and boiling surfaces over a wide range of temperatures and pressures. Many correlations have been derived including those of Chang [51], Forster and Zuber [52], Forster and Grief [53], Gilmour [54], Hara [55], Hughmark [56], Kutateladze [57], Borishanskiy and Minchenko [58], Levy [59], Nishikawa and Yamagata [60], Rohsenow [61], and Zuber [62]. All of these correlations require the use of one or more empirically determined constants. In some cases [52, 53, 56, 57, 58] such constants were supplied and claims to the generalized use of these correlations for a wide variety of fluids and boiling surfaces were made. Other correlations [51, 54, 55, 59, 60, 61, 62] required the determination of an empirical coefficient or coefficients for different fluid-surface combinations. Not all of the above correlations will be discussed here. Those with constant coefficients whose values had been supplied by the authors will be briefly reviewed. Also, those correlations with variable coefficients which have been extensively compared with experimental pool boiling results will be considered.

One of the earliest and most widely used pool boiling correlation was presented by Rohsenow [61] in 1952. He started with the postulation that

$$Nu = Nu\ (Re, Pr) \tag{2-44}$$

where Nu is hD/k, the Nusselt number, Pr is $\mu c_p/k$, the Prandtl number, h is the heat transfer coefficient, k is the thermal conductivity and c_p

is the specific heat. Taking the diameter to be the departure diameter of the bubble and evaluating all properties at the saturation temperature, Rohsenow [61] was able to use previous work that had been done on bubble dynamics to obtain the relation:

$$\frac{c_{pf}\Delta T}{h_{fg}} = C_{sf}\left(\frac{q/A}{\mu_f h_{fg}}\sqrt{\frac{\sigma}{g\Delta\rho}}\right)^{r'}(Pr)_f^s \qquad (2\text{-}45)$$

where ΔT is the wall-to-bulk temperature difference, h_{fg} is the latent heat of vaporization, and q/A is the heat flux. Rohsenow [61] was able to correlate pool boiling data well with values of 0.33 and 1.7 for r' and s, respectively. A considerable amount of work has been undertaken to determine C_{sf}, the coefficient dependent on the heating surface--fluid combination. Brief listings of C_{sf} have been presented by Kreith [63], Tong [64], and Rohsenow and Hartnett [65], among others. Recent work mentioned by Vachon et al [66] has indicated that a better correlation can be obtained for water if the exponent of the Prandtl number is changed to one. In addition, an extensive amount of work has been done to investigate the exponent r' in Equation (2-45). Vachon et al [66, 67, 68] studied a wide variety of liquid-surface combinations to determine the effect of surface finish and wettability. They concluded from these studies that the variations in r' can be affected by the surface roughness, surface preparation technique and wettability characteristics. Mathematical formulations for the effect of these parameters were not presented because no way of adequately describing pool boiling surfaces was available. Nix and Vachon [69] and Kosky and Lyon [70] showed an additional effect of system pressure on r'.

Forster and Zuber [52] in 1955 presented another pool boiling correlation. Based on an analysis of bubble dynamics, it was shown that

the product of the bubble radius and radial velocity are constant and represented by

$$2R\dot{R} = \left[\frac{\Delta T\, c_{pf}\rho_f\sqrt{\pi a}}{h_{fg}\,\rho_g}\right]^2 \qquad (2\text{-}46)$$

where R is the bubble radius, $\dot{R}$ is the radial velocity and a is the thermal diffusivity. Integrating this equation and solving for R yields:

$$R = \frac{\Delta T\, c_{pf}\rho_f\sqrt{\pi a}}{h_{fg}\,\rho_g}\left(\frac{2\sigma}{\Delta P}\right)^{1/2}\left(\frac{\rho_f}{\Delta P}\right)^{1/4} \qquad (2\text{-}47)$$

where ΔP is the pressure difference corresponding to the wall-to-bulk temperature difference and where the second portion of Equation (2-47), $\left(2\sigma/\Delta P\right)^{1/2}\left(\rho_f/\Delta P\right)^{1/4}$ is the time constant chosen. This time constant is not the only one that may be significant and many others are possible. Postulating that the results can be correlated by Equation (2-44) and using maximum heat flux data for ethanol, n-penthane, benzene and water, the following equation was obtained:

$$h_{TP} = 0.172\left(\frac{\rho_f^{0.49}\, c_{pf}^{0.45}\, k_f^{0.79}}{h_{fg}^{0.24}\,\rho_g^{0.24}\,\sigma^{0.5}\,\mu_f^{0.29}}\right)(\Delta T)^{0.24}\,(\Delta P)^{0.75} \quad . \qquad (2\text{-}48)$$

The liquid properties are evaluated at the wall temperature while the vapor properties are taken at the saturated temperature. It should be noted that in contrast to the Rohsenow [61] pool boiling correlation, a constant coefficient is claimed by Forster and Zuber [52]. The range of validity of the Forster-Zuber [52] pool boiling correlation has been questioned because only maximum heat flux data were used in determining the constants and exponents in the correlation. Rewriting Equation (2-48) in the form:

$$q/A = \text{Constant } (\Delta T)^{n'} \tag{2-49}$$

one obtains:

$$\frac{q}{A} = \left(\frac{0.172\ k_f^{0.79}\ c_{pf}^{0.45}\ \rho_f^{0.49}}{\sigma^{0.5}\ h_{fg}^{0.24}\ \rho_g^{0.24}\ \mu_f^{0.29}} \right) (\Delta T)^{1.24}\ (\Delta P)^{0.75}. \tag{2-50}$$

Since ΔP is approximately proportional to ΔT,

$$\frac{q}{A} = \text{Constant } (\Delta T)^{2.00} \tag{2-51}$$

In contrast, if the Rohsenow [61] pool boiling equation with an r' of 0.33 is recast into this form:

$$\frac{q}{A} = \left(\frac{k_f^{5.1}\ (\Delta\rho)^{0.5}\ g^{0.5}}{c_{pf}^{2.1}\ \mu_f^{4.1}\ \sigma^{0.5}\ h_{fg}^{2}\ g_c^{0.5}\ (C_{sf})^3} \right) (\Delta T)^3. \tag{2-52}$$

While much data has been found to follow the temperature difference to the third power rule, the value of the coefficient n' in Equation (2-49) can in reality vary rather widely [71]. Corty and Foust [72], as well as Chapman [73] have observed values as high as 10.2 for R-113 and 6.9 for water. Indeed, at a constant pressure and for the same surface-fluid combination, the value of the exponent n' can be varied from 3 to 24 by changing the surface roughness [71]. Despite this inconsistency, the Forster-Zuber [52] pool boiling equation has been shown to correlate additional data for boiling methanol and liquid metals [71].

In 1958, Gilmour [54] used a different approach to correlate pool boiling results. He expressed a nucleate boiling Colburn j factor as a function of the Prandtl number, Reynolds number and an additional new dimensionless group which took into account the pressure and surface tension. In the equation:

$$\left(\frac{h_{TP}}{c_{pf}G_o}\right)^{a'}\left(\frac{\mu_f c_{pf}}{k_f}\right)^{b'}\left(\frac{\rho_f \sigma}{P^2}\right)^{c'} = \frac{C_a}{\left(\frac{DG_o}{\mu_f}\right)^{d'}} . \qquad (2\text{-}53)$$

G_o is the term Gilmour [54] called the mass velocity. It is the mass of liquid per hour per square foot that returns to the heating surface as a quantity of vapor of equal volume leaves. C_a is an empirical constant which is dependent on surface material and roughness. In comparing this type of correlation to an extensive collection of experimental pool boiling results, Gilmour [54] was able to obtain the following values for the various constants:

$$\left.\begin{aligned} a' &= 1 \\ b' &= 0.6 \\ c' &= 0.425 \\ d' &= 0.3 \end{aligned}\right\} \qquad (2\text{-}54)$$

$$\left.\begin{aligned} C_a &= 1 \times 10^{-3} \text{ for copper and steel surfaces} \\ C_a &= 5.9 \times 10^{-4} \text{ for stainless steel or chromium-nickel alloys} \\ C_a &= 4 \times 10^{-4} \text{ for polished surfaces} \end{aligned}\right\} \qquad (2\text{-}55)$$

In the Gilmour [54] correlation, it is assumed that the fluid properties are evaluated at the bulk fluid temperature.

Hughmark [56] obtained a pool boiling correlation using a statistical technique to determine the coefficient and exponents in an eight-variable equation using data from a large number of sources. He obtained the following equation:

$$\frac{q}{A} = 2.67 \times 10^{-9}\left(\frac{\Delta P^{1.867}\,\Delta\rho^{2.27}\,c_{pf}^{0.945}\,T_{wall}^{1.618}}{\rho_g^{1.385}\,h_{fg}^{1.15}\,\mu_f^{1.630}\,P_r^{0.202}}\right) . \qquad (2\text{-}56)$$

Here, T_{wall} is the wall temperature (°R) and P_r is the reduced pressure. All the fluid properties are evaluated at the wall temperature. The pressure used in computing P_r is the bulk fluid pressure.

Two relatively important and quite similar correlations have appeared in the Russian literature. Kutateladze [57] presented the following equation:

$$h_{TP} = 0.0007\ (Pr)^{0.35} \left(\frac{(q/A)P}{h_{fg}\ \rho_g \nu_f} \right)^{0.7} \frac{1}{\sqrt{\sigma}} \Delta\rho^{-0.2}\ k_f \qquad (2\text{-}57)$$

where $\nu_f = \mu_f/\rho_f$ is the kinematic viscosity of the liquid. Borishanskiy and Minchenko [58] changed the exponent of the Prandtl number and varied the coefficient. They obtained:

$$h_{TP} = 0.00087\ (Pr)^{0.7} \left(\frac{(q/A)P}{h_{fg}\ \rho_g \nu_f} \right)^{0.7} \frac{1}{\sqrt{\sigma}} \Delta\rho^{-0.2}\ k_f \ . \qquad (2\text{-}58)$$

In both Equations (2-57) and (2-58) all properties are evaluated at the saturation temperature.

These last four correlations will now be checked to see what values they predict for the exponent n' in Equation (2-49). The values obtained are presented in Table II-3.

Table II-3

PREDICTION OF VALUES FOR EXPONENT n' IN EQUATION (2-49) BASED ON VARIOUS CORRELATIONS

Correlation	n'
Gilmour [54]	3.333
Hughmark [56]	1.867
Kutateladze [57]	3.333
Borishanskiy-Minchenko [58]	3.333

From this it appears that the Gilmour [54], Kutateladze [57], and Borishanskiy-Minchenko [58] correlations yield exponents which are in general agreement with the Rohsenow [61] correlation. The Hughmark [56] exponent is similar to that obtained by Forster-Zuber [52].

Relatively little reliable work has been done on measuring the pool boiling coefficients of refrigerants. Corty and Foust [72] obtained an extensive amount of data on R-113 boiling from horizontal blocks of copper and nickel polished in a variety of different ways. They, however, did not correlate their results in any way other than by heat transfer coefficient versus wall-to-bulk temperature difference plots. Furse [74] boiled R-11 and R-12 from a heated horizontal copper surface at boiling temperatures ranging from -25 to +50°F. He also presented only heat transfer coefficient versus temperature difference plots.

Additional pool boiling information was obtained at the Oak Ridge Gaseous Diffusion Plant (ORGDP). This previously unpublished data is given in Appendix A. All tests were run at a boiling temperature of 112°F utilizing an electrically-heated copper disk. R-11, R-113, and R-114 were the test fluids. The only other source of R-114 pool boiling data that has been found was a recent publication by Hesse [75]. In addition to R-114, R-12 and R-113 were boiled on the outside of a horizontal nickel tube. Only plots of heat flux versus wall-to-bulk temperature difference were furnished. An example is shown in Figure II-16. Data were taken not only in the nucleate boiling range, but also in the critical heat flux and film boiling regions. The boiling temperature range over which tests were run was quite extensive. For R-114, for

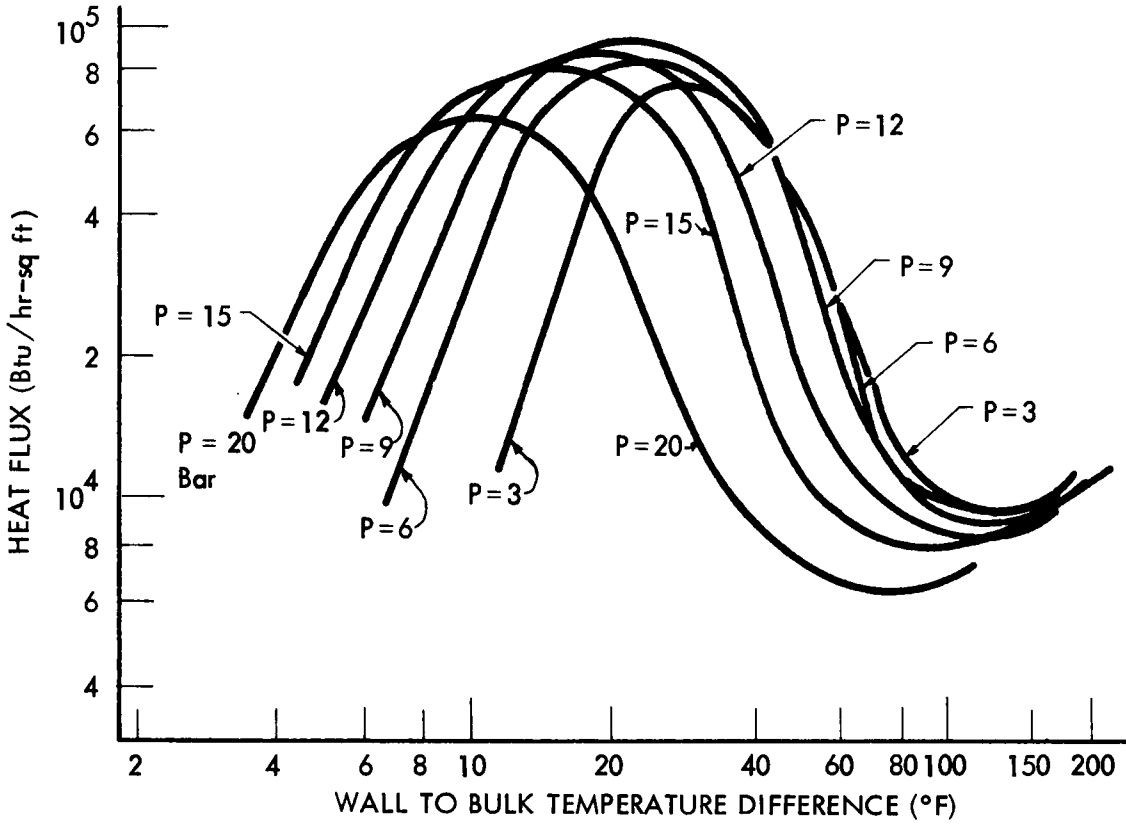


Figure II-16. CHARACTERISTIC POOL BOILING CURVES FOR R-114 AT VARIOUS PRESSURES, HESSE [75].

example, the range was 97 to 245°F. These results will be discussed in greater detail later.

Lippert and Dougall [76] conducted tests with R-113 boiling from a horizontal copper surface. While their primary objective was to measure the temperature profile in the thermal sublayer, they did obtain some pool boiling data and correlated it using the Rohsenow [61] pool boiling correlation. The C_{sf} coefficient in Equation (2-45) for R-113 was found to be 0.0048. An exponent r' of 0.20 was found to correlate the results best. The value of s used was 1.7. Another extensive series of pool boiling tests with R-113 was performed by Chapman [73]. Boiling from a vertical and horizontal copper surface lapped with a 400-grit compound, he was able to correlate his results using the Rohsenow [61] equation. For both vertical and horizontal positions, average values of 0.00272 and 0.092 were obtained for C_{sf} and r' respectively.

Flow Boiling

One of the more widely-used relations for predicting the heat transfer coefficient in flow boiling is based on the analogy between energy transport and momentum transport. Using the fact that the L-M [19] and M-N [4] models are among the most reliable models available to date, and since the Martinelli parameter, X_{tt}, can be considered as a measure of the degree to which a two-phase mixture acts as a liquid rather than a vapor, a correlation of the form:

$$\frac{h_{TP}}{h_{fa}} = C_2 \left(\frac{1}{X_{tt}}\right)^{C_3} \qquad (2\text{-}59)$$

has received widespread attention. Here, h_{TP} is the two-phase heat transfer coefficient, h_{fa} is the single-phase heat transfer coefficient,

assuming liquid alone flows through the pipe, and C_2 and C_3 are experimentally determined constants. Generally, a C_2 of approximately 3.4 and a C_3 of 0.45 as obtained by Guerrieri and Talty [77] with various organic fluids has been accepted. Dengler and Addoms [78] boiling water in a 1-in.-dia copper tube, 20 ft long, obtained the following equation:

$$\frac{h_{TP}}{h_{fo}} = 3.5 \left(\frac{1}{X_{tt}}\right)^{0.50} . \qquad (2\text{-}60)$$

This equation differs from Equation (2-59) in that h_{fo} is defined as the single-phase coefficient assuming liquid only flows through the pipe. The differences between the two definitions were discussed in Section C above. Bennett et al [79] boiling water at approximately atmospheric pressure in two different sized annuli correlated their data by an equation similar to that of Guerrieri and Talty [77]. Bennett et al [79], however, noted an effect of heat flux and thus proposed:

$$\frac{h_{TP}}{h_{fa}} \left(\frac{q}{A}\right)^{-0.11} = 0.64 \left(\frac{1}{X_{tt}}\right)^{0.74} \qquad (2\text{-}61)$$

where (q/A) is in Btu/hr-sq ft. Other correlations similar to Equation (2-61) have been obtained. In many of these, however, additional empirical constants are presented and the original form of the expression, as embodied in Equation (2-59) is modified by so many constants as to render any such correlation of limited use.

Another correlation which is widely used today is the Chen [80] correlation. Here:

$$h_{TP} = 0.023(Re)_{fa}^{0.8} (Pr)_f^{0.4} \left(\frac{k_f}{D}\right) F$$

$$+ 0.172 \left(\frac{k_f^{0.79} c_{pf}^{0.45} \rho_f^{0.49}}{h_{fg}^{0.24} \rho_g^{0.24} \sigma^{0.5} \mu_f^{0.29}} \right) (\Delta T)^{0.24} (\Delta P)^{0.75} S. \quad (2\text{-}62)$$

$(Re)_{fa}$ is the Reynolds number based on the velocity assuming the liquid alone flows in the tube, F is a multiplication factor and S is a suppression factor. Applicability of this equation is claimed in the vertical, saturated forced convective region where the annular or annular-mist flow regime exists. It is assumed that the contribution of both the nucleate boiling and two-phase forced convective coefficients are additive. The convective component, represented by the first part of Equation (2-62) is the Dittus-Boelter relation modified by the factor F. The factor F is the ratio of the two-phase Reynolds number to the liquid Reynolds number based on the liquid fraction of flow. Basically, it accounts for the more rapid movement of the liquid due to the presence of the vapor phase, and also accounts for the complex interrelationships between the liquid and vapor phases in the various flow regimes. By claiming F was strictly a flow parameter, Chen [80] reasoned that by analogy to momentum transfer in two-phase flow, F may be assumed to be a function of the Martinelli parameter, X_{tt}, only. The nucleate boiling portion, constituting the second part of Equation (2-62) was based on the formulation of Forster and Zuber [52]. Since the temperature profiles close to the wall in a forced-convective system are much steeper than would exist in the pool boiling case, the growth of the bubbles formed at the wall is necessarily smaller. This is due to the fact that as a bubble is formed at the wall and begins to grow, it protrudes into a region where the liquid is considerably cooler than the temperature of the liquid adjacent to the wall and probably similar

to the bulk or mixing cup temperature. As a result, heat is transferred from the gas in the bubble to the adjacent liquid and the rate of bubble growth is decreased. The degree to which this occurs is represented by the term S which is defined as:

$$S = \left(\frac{T_{\text{fluid around bubble}} - T_{\text{saturated}}}{T_{\text{wall}} - T_{\text{saturated}}} \right)^{0.99} \qquad (2\text{-}63)$$

S was assumed to be a function of both F and the Reynolds number. Since both F and S are unknown and occur in the same equation, their respective values were obtained from experimental data using an iterative procedure described in Chen's [80] paper. The curves obtained for F and S are presented in Figures II-17 and II-18, respectively.

Numerous other correlations have been proposed in the last few years for a variety of boiling conditions and working fluids. Davis and David [81], who worked with steam-water mixtures, used two different flow models to develop their correlations. In the first model, they assumed that the flow was separated and annular in character and that nucleation was suppressed. The resistance to heat transfer occurred within the thin layer of liquid at the wall and was governed by the Reynolds number and physical properties of the liquid. Using a Dittus-Boelter type equation, they were able to correlate their data with the equation:

$$\frac{h_{TP} D}{k_f} = 0.060 \left(\frac{\rho_f}{\rho_g} \right)^{0.28} \left(\frac{D \times G}{\mu_f} \right)^{0.87} \left(\frac{\mu\, c_p}{k} \right)_f^{0.4} \qquad (2\text{-}64)$$

The second model was based on the homogeneous flow concept characteristic of the dispersed or dispersed annular flow regime. Assuming no

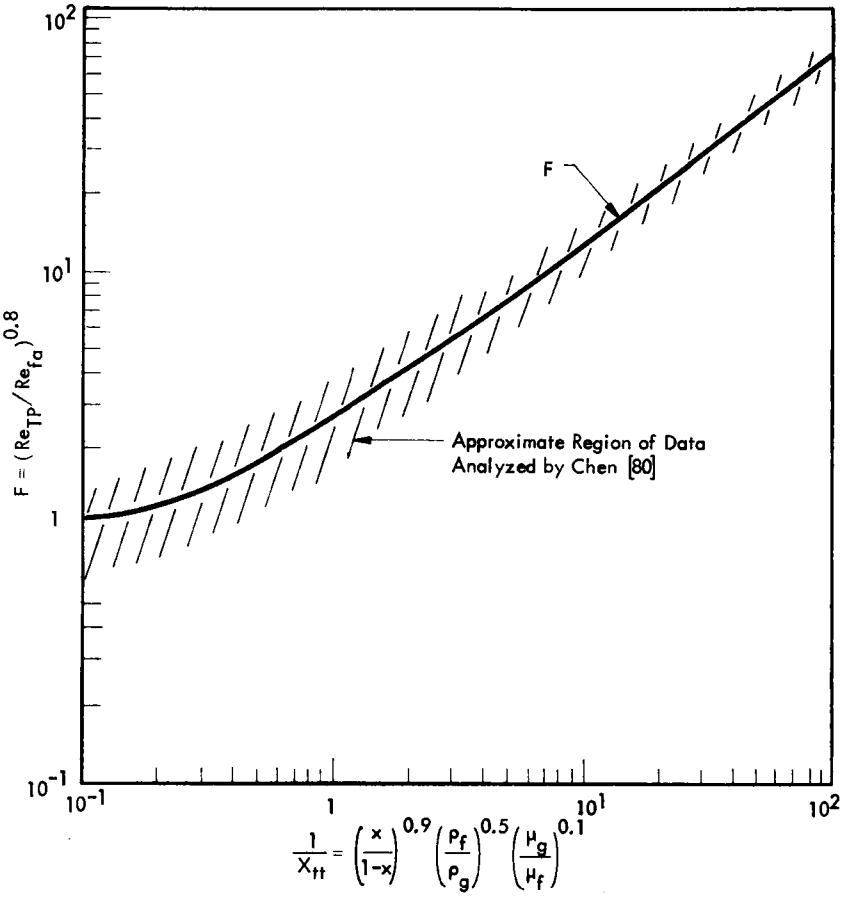


Figure II-17. MULTIPLICATION FACTOR, F, AS A FUNCTION OF THE MARTINELLI PARAMETER, CHEN [80].

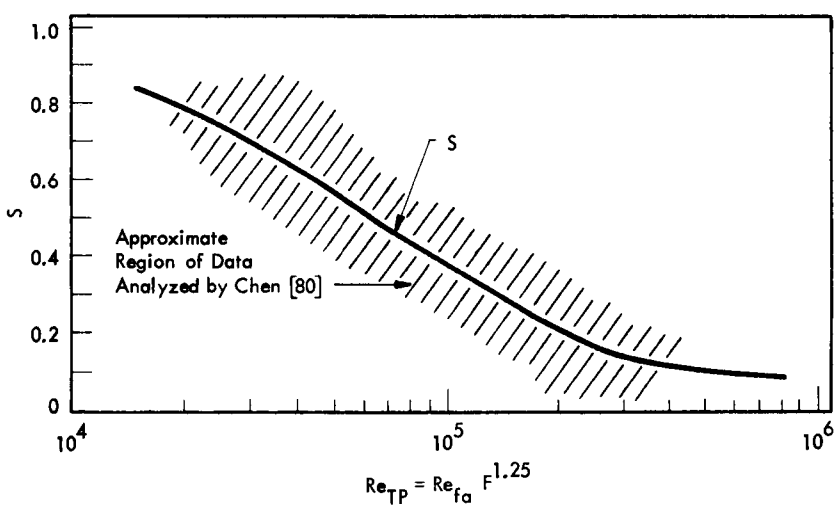


Figure II-18. SUPPRESSION FACTOR, S, AS A FUNCTION OF THE TWO-PHASE REYNOLDS NUMBER, CHEN [80].

slip occurred and that thermodynamic equilibrium existed between the two phases, the following equation was developed:

$$\frac{h_{TP}D}{k_f} = 0.033 \left(\frac{DG}{\mu_{TP}}\right)^{0.87} \left(\frac{\mu c_p}{k}\right)_f^{0.4} \tag{2-65}$$

where:

$$\frac{1}{\mu_{TP}} = \left[\frac{x}{\mu_g} + \frac{1 - x}{\mu_f}\right] \tag{2-66}$$

is the two-phase viscosity. Both Equations (2-64) and (2-65) predicted experimental data to within ± 15%. A flow visualization test section downstream of the heated portion of the tube enabled the experimental runs to be classified according to flow regime. Data were taken over a range of total mass fluxes from 50,000 to 600,000 lbm/hr-sq ft, qualities from 0.30 to 0.90, pressures from 25 to 150 psia and heat fluxes from 60,000 to 260,000 Btu/hr-sq ft. The results are shown in Figures II-19 and II-20.

Another correlation based on experiments with water and steam in vertical tubes was put forth by Schrock and Grossman [82] who proposed the expression:

$$\frac{h_{TP}D/k_f}{(Re)_{fa}^{0.8}\ Pr^{1/3}} = 170 \left[Bo + 1.50 \times 10^{-4} \left(\frac{1}{X_{tt}}\right)^{2/3}\right] \tag{2-67}$$

where

$$Bo = \frac{q/A}{G\ h_{fg}} \tag{2-68}$$

is the Boiling number. This equation was found to correlate the data to within ± 35%. The results are given in Figure II-21 along with the range of parameters tested. This correlation was based on the assumption that at low heat fluxes, the flow is annular and that sufficient

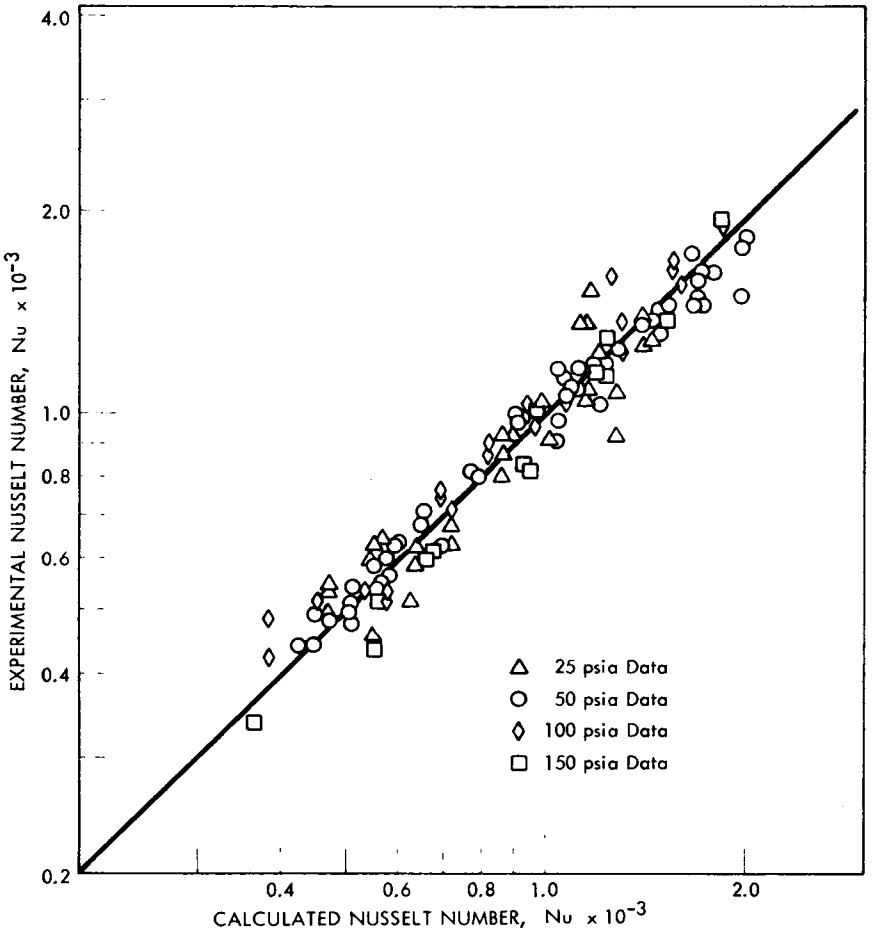


Figure II-19. COMPARISON OF EXPERIMENTAL DATA WITH THE SEPARATED FLOW MODEL, DAVIS AND DAVID [81] .

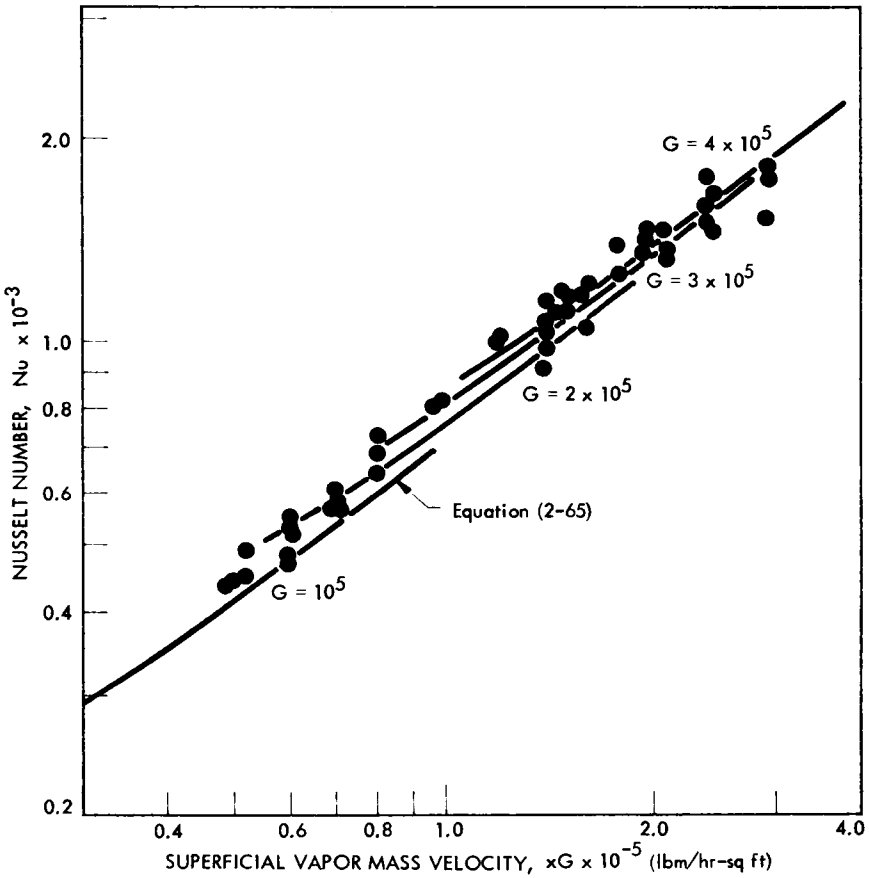
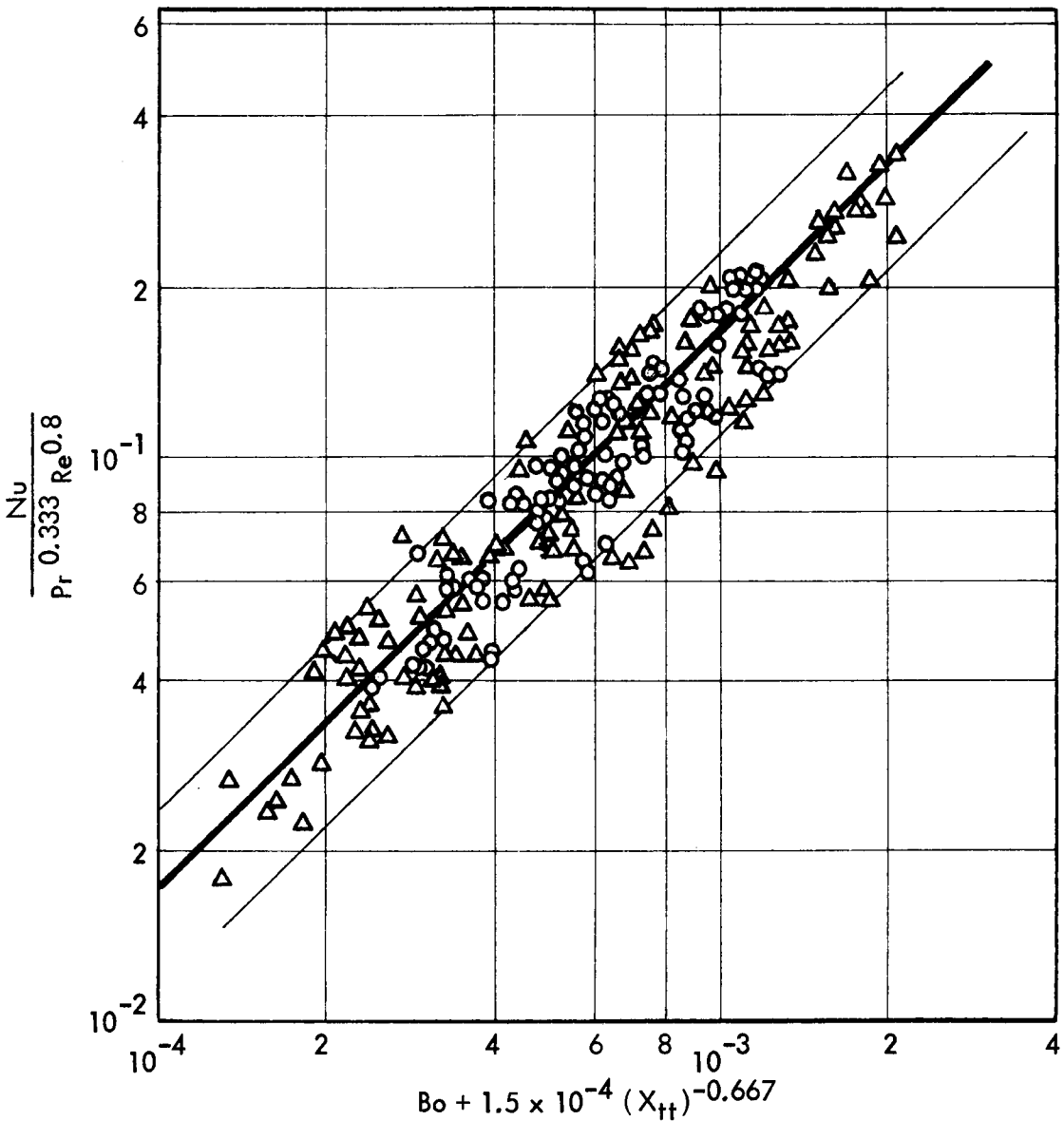


Figure II-20. CORRELATION OF THE EXPERIMENTAL DATA AT 50 PSIA BY THE HOMOGENEOUS MODEL, DAVIS AND DAVID [81] .



Series	Test Section		Range of Variables		Exit Quality
	Length (inches)	Diameter (inch)	q/A (Btu/hr-sq ft)	G (lbm/sec-sq ft)	
E	15, 30, 40	0.1181	1.43×10^5 to 1.45×10^5	197 to 911	0.08 to 0.56
F	15, 30	0.2370	1.23×10^5 to 7.59×10^5	81 to 230	0.08 to 0.57
G	30	0.4317	0.653×10^5 to 2.46×10^5	49 to 69	0.10 to 0.43

Figure II-21. HEAT TRANSFER CORRELATION AND RANGE OF PARAMETERS IN SERIES E, F, AND G, SCHROCK AND GROSSMAN [82].

heat is transmitted through the thin liquid layer for nucleation to be suppressed. Thus, the Martinelli parameter dominates the correlation. At higher heat fluxes, where the liquid superheat at the wall is large enough for nucleation to occur, thereby augmenting the forced convection component, the heat transfer characteristics are governed by both the Boiling number and Martinelli parameter. At even higher heat fluxes, the Boiling number effect dominates, indicating that the heat transfer has become independent of the two-phase flow characteristics of the system. Collier and Pulling [83] used a similar equation but with different coefficients.

Chawla [29, 30, 31, 32] presented correlations for boiling in two regimes - the nucleate boiling regime (in which heat transfer depends primarily on the heat flux) and the convective range (in which the heat transfer coefficient is a function of only the mass flow and not the heat flux). In the nucleate boiling regime which is similar to pool boiling, the flow regime is generally bubbly or chaotic in nature while in the convective range, annular flow exists. A rather complex equation embodying wetting angles, bubble frequencies and numerous empirically-determined constants was presented for calculating the heat transfer coefficient in the nucleate boiling regime. For the convective flow case, the following two empirical equations from Chawla's [32] 1970 publication are presented:

$$\frac{h_{TP}D}{k_f}\left[1+\left(1-\frac{1-x}{x\varepsilon\left(\frac{\rho_f}{\rho_g}\right)}\right)^{-1/2}\right]=0.0066\,(Re_{fa}\,Fr_{fa})^{0.475}\left(\frac{x}{1-x}\right)$$

$$\left(\frac{\rho_f}{\rho_g}\right)^{0.3}\left(\frac{\mu_f}{\mu_g}\right)^{0.8}(Re_{fa})^{0.35}\,(Pr_f)^{0.42} \qquad (2\text{-}69)$$

for $Re_{fa}Fr_{fa}$ less than 109. For values greater than 109, the following equation was recommended:

$$\frac{h_{TP}D}{k_f}\left[1+\left(1-\frac{1-x}{x\varepsilon\left(\frac{\rho_f}{\rho_g}\right)}\right)^{-1/2}\right]=0.015\,(Re_{fa}Fr_{fa})^{0.3}\left(\frac{x}{1-x}\right)$$

$$\left(\frac{\rho_f}{\rho_g}\right)^{0.3}\left(\frac{\mu_f}{\mu_g}\right)^{0.8}(Re_{fa})^{0.35}\,(Pr_f)^{0.42}. \quad (2\text{-}70)$$

Applicability is claimed over the entire quality range from zero to one. Here, the parameter ε is the same one Chawla [32] introduced in his pressure drop studies and is illustrated in Figure II-10 on page 34. Chawla [32] obtained very good agreement when he compared Equations (2-69) and (2-70) to a wide variety of refrigerant and non-refrigerant data.

While the agreement obtained by Chawla [32] between his correlations and R-11, R-12, and R-22 data is gratifying, many of the other correlations mentioned above have not fared as well. Lavin and Young [84], boiling R-12 in a plain vertical tube, correlated their annular flow regime data in a manner similar to that represented by Equation (2-59). Their correlating line fell considerably below that of Dengler and Addoms [78] and other investigators as shown in Figure II-22. Lavin and Young [84] attributed the difference to the fact that the Martinelli parameter by itself was not sufficient and such important quantities as the vapor-liquid velocity ratio and hence the vapor-liquid density ratio may have been improperly modeled. Lavin and Young [84] pointed out that the liquid-to-vapor density ratio range for R-12 was considerably below that of the fluids used by Dengler and Addoms [78], Guerrieri and Talty [77], and Bennett et al [79]. Napadensky's [15] heat transfer

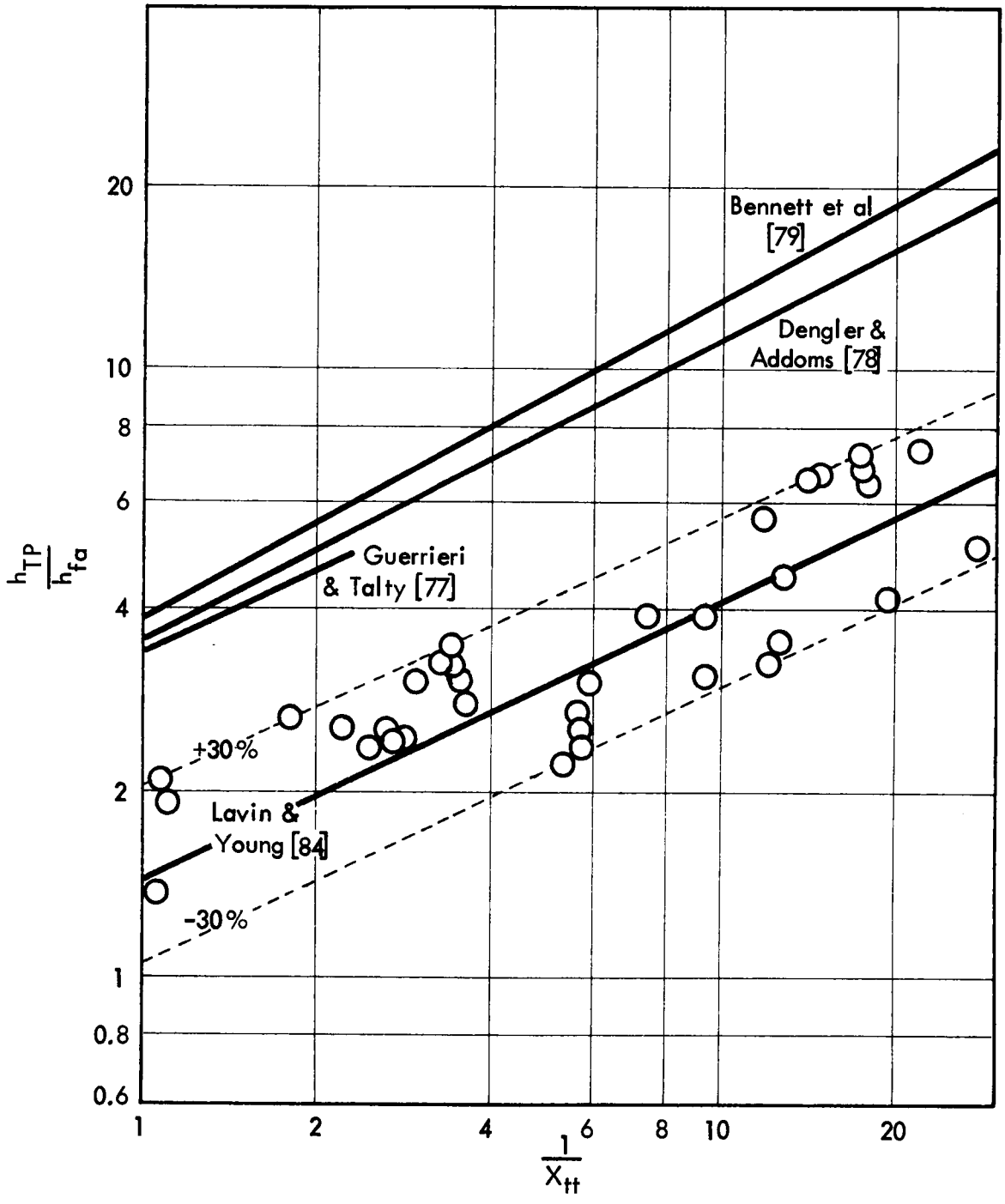


Figure II-22. COMPARISON OF THE R-12 VERTICAL FLOW BOILING DATA OF LAVIN AND YOUNG [84] WITH THE CORRELATIONS OF OTHER WORKERS.

results seemed to only partially confirm Lavin and Young's [84] findings. Despite the fact that in Napadensky's [15] tests the liquid-to-vapor density ratios were the same, or even lower than those in Lavin and Young's [84] tests, Napadensky [15] obtained reasonably good agreement with the Guerrieri and Talty [77] correlation as shown in Figure II-23. On the other hand, Napadensky [15] was able to improve the correlation by using a so-called Flux number (which is the reciprocal of the Boiling number) raised to the 0.1 power. This significantly reduced the scatter in his data. The excessive use of empirical constants, however, seriously limited the applicability of the correlation obtained.

Cheshire and Stirling [36] in 1949 boiled R-114 in a vertical copper tube under natural circulation conditions. They obtained the correlation:

$$h_{TP} = \frac{1.093 \times 10^{-11}}{\mu_f^{0.6}} \left(\frac{(T + 460)\ \Delta T}{\sigma} \right)^2 . \qquad (2\text{-}71)$$

All properties were evaluated at the bulk fluid temperature. This correlation was based on data taken in the range of operating conditions given in Table II-4.

One would expect this correlation to be valid in a very limited range of operating conditions, since such important parameters as quality and mass flow rate were not included. This was found to be the case. A comparison by the present author of the Cheshire and Stirling [36] and Chen [80] correlations showed little agreement. While the heat transfer coefficient increased as the second power of the boiling temperature and the wall-to-bulk temperature difference in the Cheshire

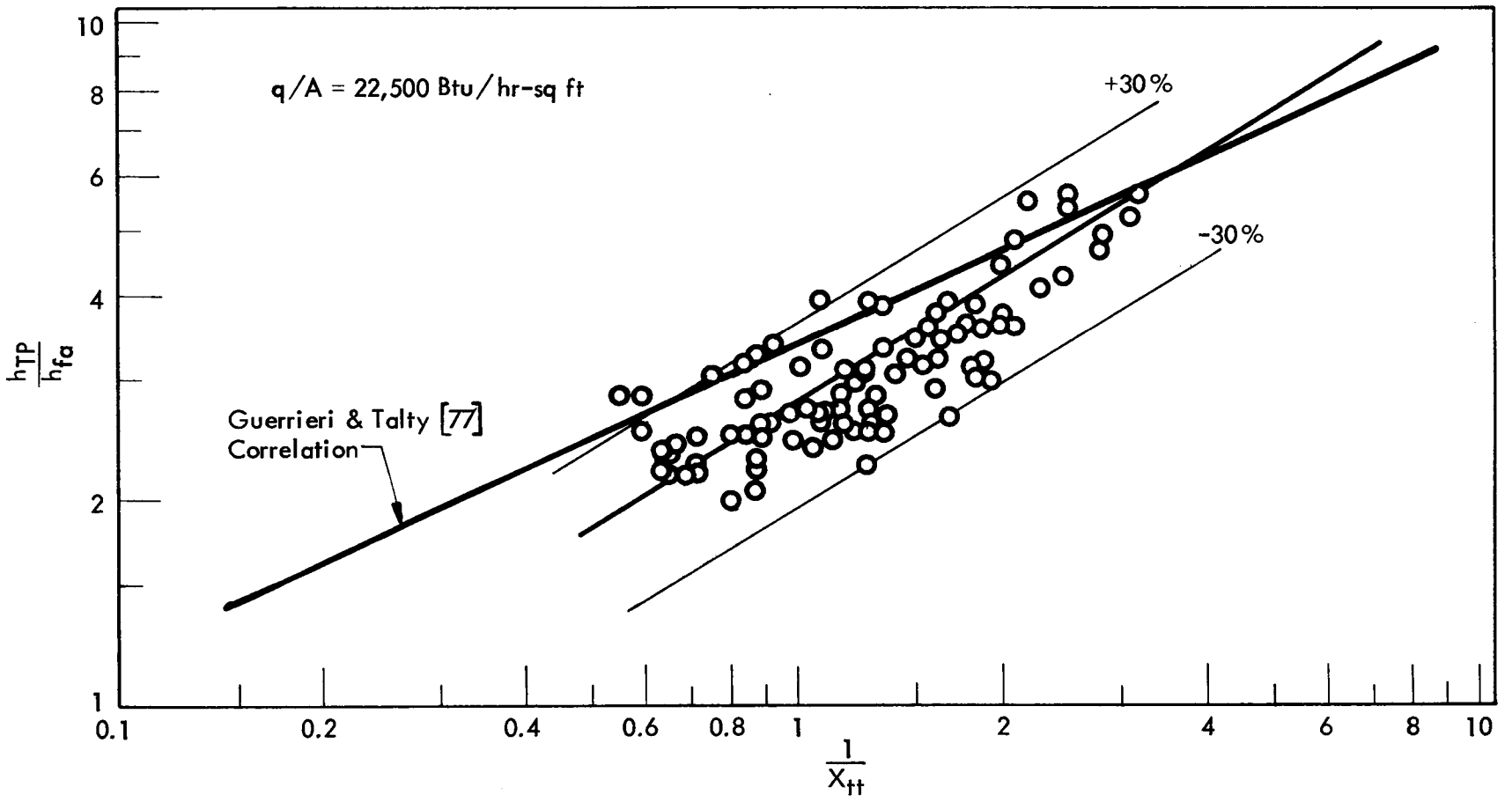


Figure II-23. COMPARISON OF NAPADENSKY'S [15] HEAT TRANSFER RESULTS AT A HEAT FLUX OF 22,500 BTU/HR-SQ FT WITH THE GUERRIERI AND TALTY [77] CORRELATION.

Table II-4

RANGE OF OPERATING CONDITIONS IN CHESHIRE AND STIRLING [36] TESTS

Boiling Temperature, T (°F):	85, 110, 135
Total Mass Flux (lbm/hr-sq ft):	$0.0611 \times 10^6 \leq G \leq 0.2446 \times 10^6$
Heat Flux (Btu/hr-sq ft):	$5000 \leq q/A \leq 33,200$
Wall-to-Bulk Temperature Difference (°F):	$10.0 \leq \Delta T \leq 17.5$
Heat Transfer Coefficients (Btu/hr-sq ft-°F):	$500 \leq h \leq 2500$

and Stirling [36] correlation, the effect of these two parameters is much less pronounced in the Chen [80] correlation.

O'Donnell, Robinson, and Webb [85], using the same test section as Cheshire and Stirling [36] boiled R-114, R-11, R-113, and water. They correlated their data in the form:

$$h_{TP} = K_o\left(\frac{q}{A}\right)^e \quad . \tag{2-72}$$

The values for K_o and e are given in Table II-5. Equation (2-72) can be rewritten to yield:

$$\frac{q}{A} = K_o^{(1/1-e)} \, (\Delta T)^{(1/1-e)} \quad . \tag{2-73}$$

When Equation (2-73) is compared to Equation (2-49) which is of a similar form, it is noted that the values for the exponent 1/1-e in Equation (2-73), using the values in Table II-5, are slightly lower than, but of the same magnitude as, the values of n' in Equation (2-49) as given in Table II-3 on page 57. A reason for this may be that the boiling occurring was in a regime similar to Chawla's [29, 30, 31, 32] nucleate boiling regime and therefore possessed many of the characteristics of pool boiling.

It is interesting to note that Equation (2-72) is a more empirical form of Cheshire and Stirling's [36] correlation as represented by Equation (2-71). For R-114, the K_o and e values in Table II-5 can be quantitatively deduced from the Cheshire and Stirling [36] correlation. Both investigators [36, 85] noted a significant effect of the surface characteristics and finish on the heat transfer coefficient but made no attempt to study this effect.

Table II-5

VALUES OF CONSTANTS FOR EQUATION (2-72)

Fluid	T (°F)	K_o	e
R-114	85	1.8	0.65
	110	2.1	0.65
	135	2.4	0.65
R-11	85	8.7	0.47
	110	7.4	0.47
	135	9.9	0.47
	160	11.1	0.47
R-113	110	12.0	0.44
	135	12.8	0.44
	160	14.0	0.44
Water	110 to 210	1.4	0.48

Wasserman, Erickson, and Mann [86] boiled R-113 in a natural circulation vertical tube evaporator. They correlated their results in a Rohensow [61] type of correlation and obtained a coefficient and exponents that differed significantly from those observed in pool boiling. Since Wasserman et al [86] did not subtract out the forced convective term, a strict comparison with pool boiling results is premature. Here again, a strong effect due to surface finish was detected.

Baker, Touloukian, and Hawkins [87], boiling R-12 and methyl chloride in a horizontal tube, also obtained expressions similar in form to the Rohsenow [61] correlation but with additional terms to account for the inlet and exit qualities and mass flow rate. For R-12, when temperature differences of less than 12°F and flow rates of less than 120 lbm/hr were encountered:

$$\frac{c_{pf}\Delta T}{h_{fg}} = 0.0125 \left[\frac{q/A}{\mu_f h_{fg}} \sqrt{\frac{\sigma}{g\Delta\rho}}\right]^{1/3} (Pr)_f^{1.7} \left(\frac{x_o}{x_i}\right)^{-0.042} \qquad (2\text{-}74)$$

correlated the data to within ± 10%. Here x_o and x_i are the outlet and inlet qualities, respectively. This expression, which does not include the Reynolds number, is believed to hold in the nucleate boiling regime described above by Chawla [29, 30, 31, 32]. For all methyl chloride runs and for R-12 where wall-to-bulk temperature differences exceeded 12°F, the following relation was obtained:

$$\frac{c_{pf}\Delta T}{h_{fg}} = K_i \left[\frac{q/A}{\mu_f h_{fg}} \sqrt{\frac{\sigma}{g\Delta\rho}}\right]^{3/4} (Pr)_f^{1.7} \left(\frac{x_o}{x_i}\right)^{-0.042} \left[\frac{GD}{\mu_f}(1 - x_{avg}) \frac{\rho_g}{\rho_f}\right]^{-1/3} . \qquad (2\text{-}75)$$

For R-12, K_i was 0.073. This equation represented 97% of the data within ± 15%. It illustrates the reduced effect of heat flux and the increased importance of mass flux on the heat transfer coefficient.

Blatt and Adt [42], boiling R-11 and R-113 in horizontal channels, also correlated their data using the Rohsenow [61] correlation. They did subtract out the forced convection term but did not account for the increased liquid velocity in computing the single-phase heat

transfer coefficient. The nucleate boiling portion of their heat transfer correlated well with the Rohsenow [61] equation. The average deviation was 30%. Some of the experimentally determined values of C_{sf}, obtained for the various heating surface-fluid combinations are given in Table II-6. Suppression of boiling, as discussed by Chen [80], was not accounted for and quite possibly the C_{sf} values in Table II-6 have the suppression factor term included in them.

Table II-6

C_{sf} VALUES AS DETERMINED BY BLATT AND ADT [42] WITH R-11 AND R-113

Fluid-Surface Combinations	C_{sf}
R-11 - Stainless Steel	0.006
R-11 - Copper	0.010
R-113 - Stainless Steel	0.004
R-113 - Copper	0.007

Allen [88], in 1961, ran additional tests with R-114 in a three-foot vertical tube. Although he did not correlate his results, a comparison by the present author indicated that the heat transfer coefficients obtained were below those predicted by the Cheshire and Stirling [36] correlation, but above those one would expect with the Chen [80] correlation. These results will be discussed in greater detail later.

Altman, Norris, and Staub [40], boiling R-22 in a horizontal tube, were able to correlate their data, as well as those of Baker, Touloukian, and Hawkins [87] by using an extension of Pierre's [89] correlation:

$$Nu = E\,(Re_{fo}^2 K_f)^b \tag{2-76}$$

where

$$K_f = \frac{J\,\Delta x\,h_{fg}}{L} \tag{2-77}$$

is the load factor, Δx is the difference in quality between the inlet and outlet and J is the mechanical equivalent of heat, 778.26 ft-lbf/Btu. The various values of E and b are given in Table II-7.

Table II-7

VARIOUS VALUES FOR THE COEFFICIENTS AND EXPONENTS IN THE PIERRE [89] AND ALTMAN, NORRIS, AND STAUB [40] CORRELATIONS

Fluid	Quality Ranges	$(Re_{fo}^2 K_f)$ Range	E, b
R-11, R-12, R-22	$x_o < 0.7$	$10^9 < (Re_{fo}^2 K_f) < 0.6 \times 10^{12}$	E = 0.0009 b = 0.5
R-22	$x_o < 0.8$	$0.6 \times 10^{12} < (Re_{fo}^2 K_f) < 1.5 \times 10^{12}$	E = 0.0225 b = 0.375
R-12, R-22	$x_i < 0.5$ $x_o \geq 1.0$ (but exit superheat less than 11°F)	$10^9 < (Re_{fo}^2 K_f) < 0.7 \times 10^{12}$	E = 0.0082 b = 0.4

Johnston and Chaddock [41] boiled R-12 and R-22 in the sub-zero temperature range and found Pierre's [89] equation, with slightly different coefficients, quite satisfactory. It should, however, be pointed out that these equations utilize the difference in quality between the inlet and the outlet of the tube in computing the load factor K_f. Most experimenters have observed and Anderson in the discussion of Altman, Norris, and Staub's [40] paper pointed out that the heat transfer coefficient is a strong function of the local quality at high values of

mass flux rather than the quality difference between inlet and exit. Since most of Altman, Norris, and Staub's [40] data and all of Johnston and Chaddock's [41] tests were at low mass fluxes, this strong dependency did not appear.

An extensive study of boiling R-113 in the upflow and downflow directions was undertaken by Pujol and Stenning [90]. As in Chawla's [29, 30, 31, 32] case, different equations were presented for the nucleate boiling and convective ranges. For nucleate boiling,

$$\frac{h_{TP}}{h_{fo}} = 0.90 \left[Bo \times 10^4 + 4.45 \left(\frac{1}{X_{tt}} \right)^{0.37} \right] \qquad (2\text{-}78)$$

correlated the upflow data successfully. Note that both the heat flux and the mass flow have an effect. For the convective region, which Pujol and Stenning [90] called the nucleation suppressed region,

$$\frac{h_{TP}}{h_{fo}} = 4.0 \left(\frac{1}{X_{tt}} \right)^{0.37} \qquad (2\text{-}79)$$

correlated the data within ± 15%.

Several publications on boiling refrigerants based on work supported by ASHRAE have appeared in the literature recently. Gouse and Coumou [91] undertook an extensive study of boiling R-113 in horizontal tubes. Using heat-resistant glass tubes coated on the outside with a transparent, electrically conducting film, they were able to photograph the flow regimes, as well as obtain heat transfer coefficients along the length of the tube. The results obtained confirmed Anderson's [40] point that the Pierre [89] equation fails to predict the heat transfer coefficient accurately at high mass fluxes. In addition, a comparison of the experimental heat transfer coefficients with the correlations of

numerous other investigators yielded the conclusion that the Guerrieri and Talty [77] and Chen [80] correlations were closest to reasonably approximating the data. Figure II-24 illustrating the results for two tests indicates this. The Guerrieri and Talty [77] equation lay partially above and partially below the experimental results. The Chen [80] correlation was consistently slightly lower. The visual observations indicated that annular flow was established at rather low qualities and that nucleation was suppressed in this annular flow regime. A model presented by Bergles and Rohsenow [92] was applied to show why this would occur. As shown in Figure II-25, this model compares the degree of superheat required for nucleation to start at the wall to the temperature distribution in the liquid near the wall. While the degree of superheat is a reciprocal function of the cavity radius, thus resulting in a hyperbolic curve, the temperature distribution in the liquid near the wall is linear. Thus, the intersection of the curve and the straight line defines the range of active nucleation sites where bubbles are generated. Since the slope of the temperature distribution in the liquid near the wall is a function of the fluid velocity, some cases could occur where the curve and straight line do not intersect. These extreme cases denote the occurrence of total suppression and no bubbles can grow. Of course, this model only predicts the cavity range in which nucleation can occur. That cavity size must exist on the heated surface for boiling to actually occur.

An extension of the Gouse and Coumou [91] study was made by Gouse and Dickson [93] with a different test section. In addition to R-113 studies, one test with R-11 was conducted. For the R-113 cases, the experimental results were higher than those predicted by the numerous

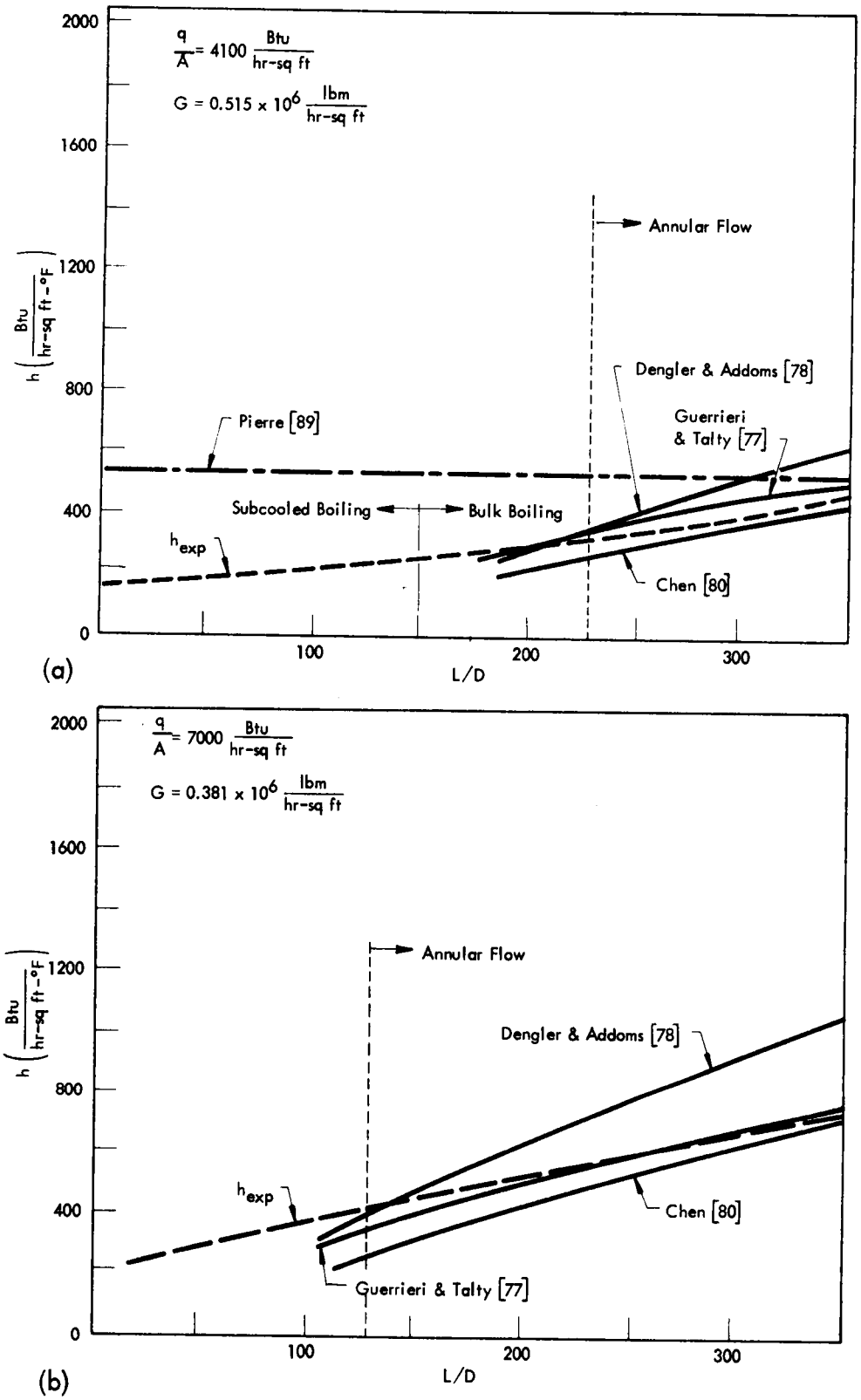


Figure II-24. COMPARISON OF THE R-113 HORIZONTAL FLOW BOILING RESULTS OF GOUSE AND COUMOU [91] WITH VARIOUS CORRELATIONS.

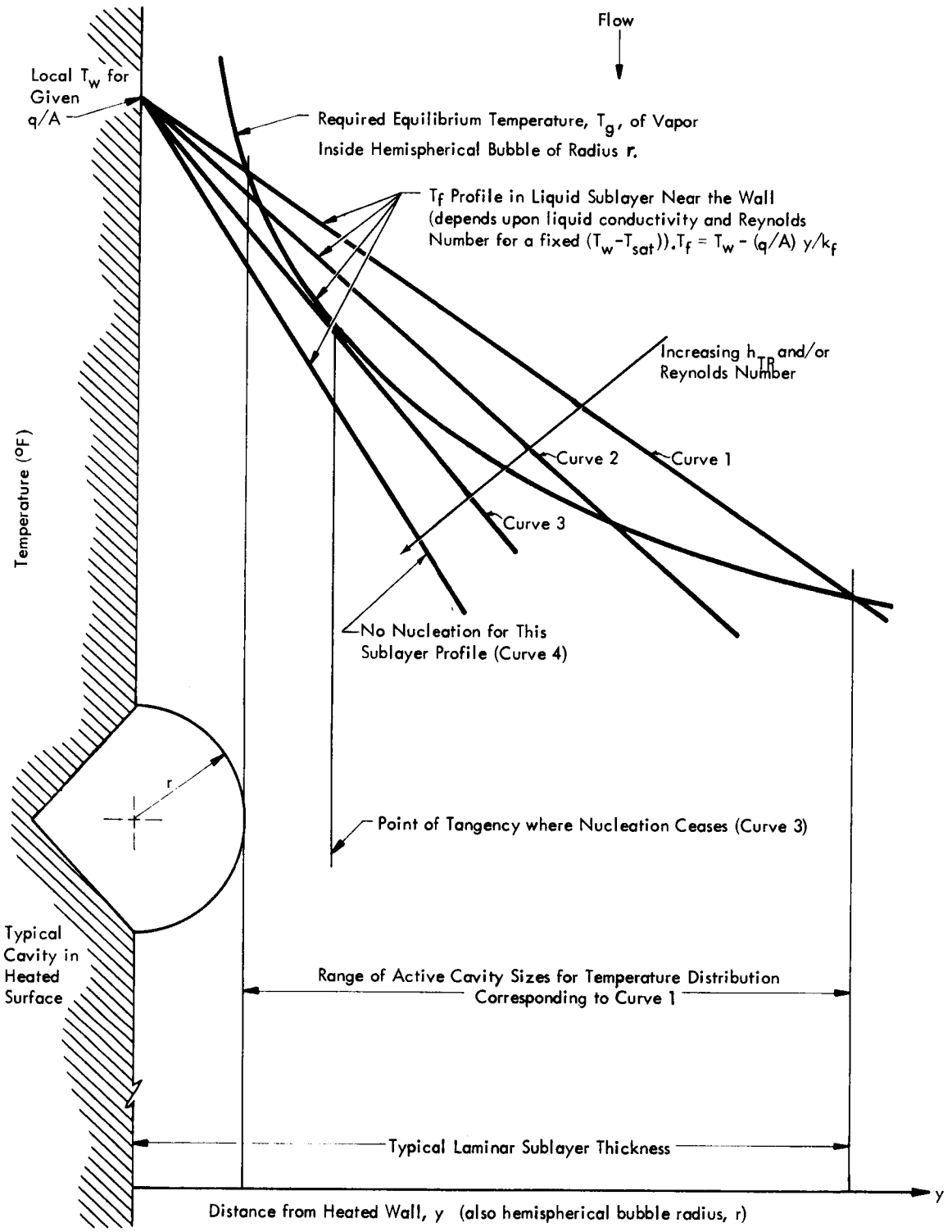


Figure II-25. MODEL FOR SUPPRESSION OF NUCLEATION IN FORCED CONVECTION BOILING [92].

correlations that were checked. This is shown in Figure II-26. The correlations of Davis and David (annular flow model) [81], Dengler and Addoms [78], Schrock and Grossman [82], and Chen [80] gave the closest albeit not entirely satisfactory agreement. Insufficient data were taken with R-11 to formulate any definite conclusions. As can be seen in Figure II-27, however, both the Dengler and Addoms [78] and Chen [80] correlations were close, with Chen [80] being consistently lower. In general, the experimental heat transfer coefficients obtained by Gouse and Dickson [93] were higher than those measured by Gouse and Coumou [91].

Another study, supported by ASHRAE, on boiling refrigerants in horizontal tubes was performed by Chaddock and Noerager [43] who boiled R-12 in a horizontal tube with constant heat flux. Using stainless steel tubes, they studied the temperature distribution of the tube wall in the circumferential direction and, based on this, were able to make some general remarks about the flow regime existing in their test section. Reasonably good agreement was found between their experimental heat transfer results and the Dengler and Addoms [78] and Pierre [89] correlations, as shown in Figures II-28, II-29, and II-30. Agreement was not good when a comparison was made with the Schrock and Grossman [82], Guerrieri and Talty [77], and Chen [80] correlations. Agreement was excellent with Altman, Norris, and Staub's [40] modification to the Pierre [89] equation where a slightly different coefficient and exponent were used. Chaddock and Noerager [43] concluded that both heat flux and mass velocity have a marked effect on the heat transfer coefficient.

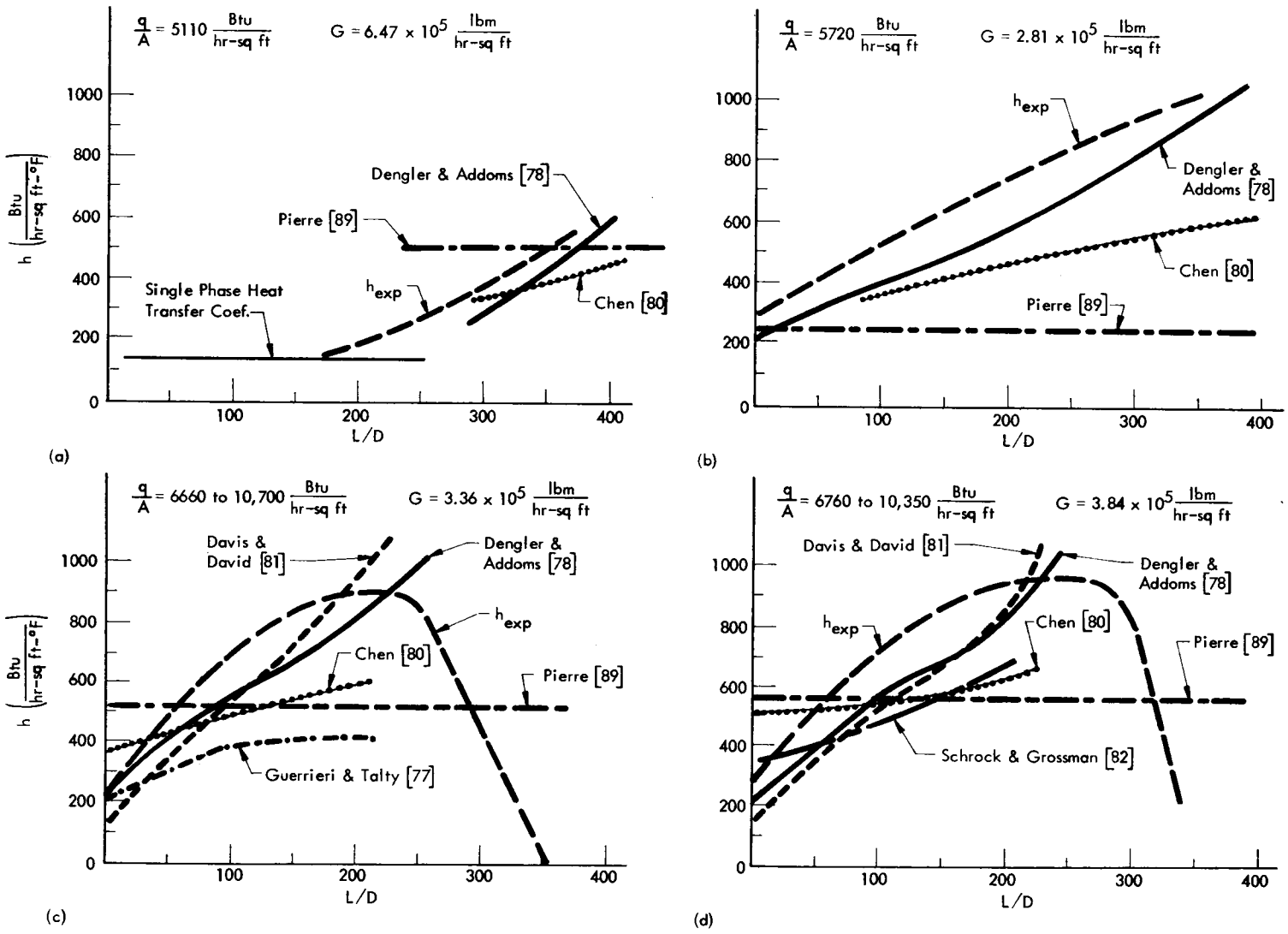


Figure II-26. COMPARISON OF THE R-113 HORIZONTAL FLOW BOILING DATA OF GOUSE AND DICKSON [93] WITH SEVERAL CORRELATIONS.

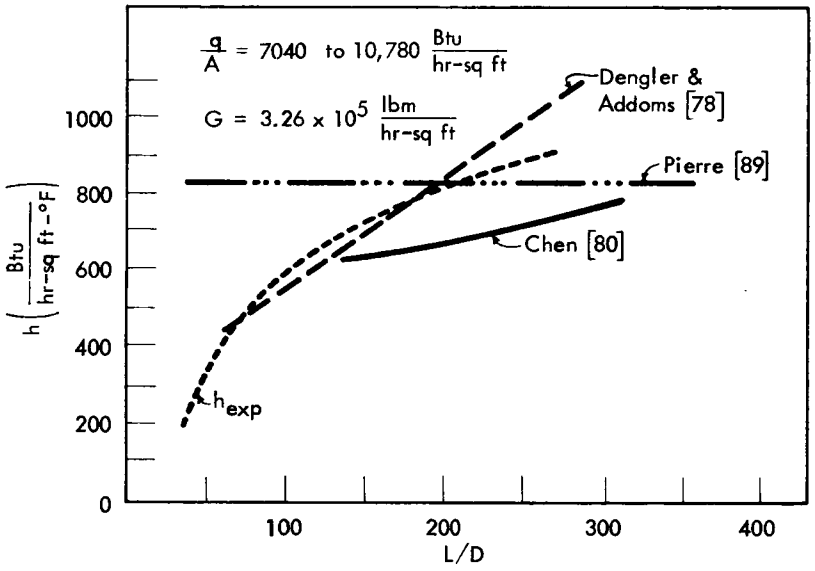


Figure II-27. COMPARISON OF THE R-11 HORIZONTAL FLOW BOILING DATA OF GOUSE AND DICKSON [93] WITH SEVERAL CORRELATIONS.

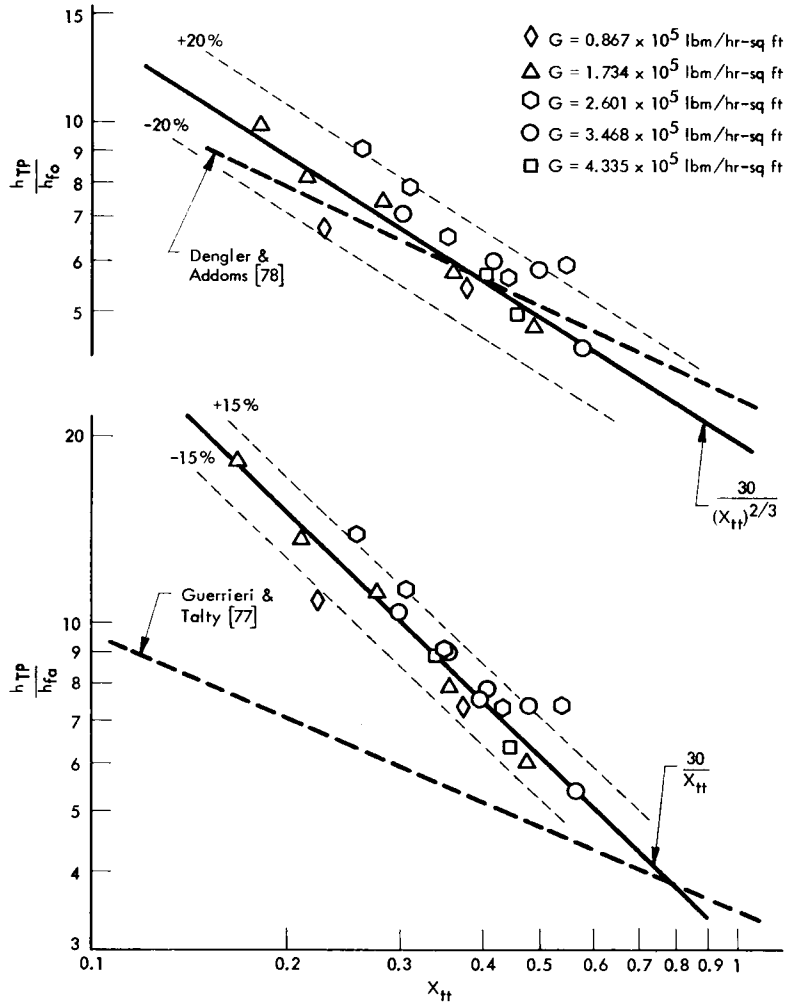


Figure II-28. COMPARISON OF THE R-12 HORIZONTAL FLOW BOILING RESULTS OF CHADDOCK AND NOERAGER [43] WITH THE CORRELATIONS OF DENGLER AND ADDOMS [78] AND GUERRIERI AND TALTY [77].

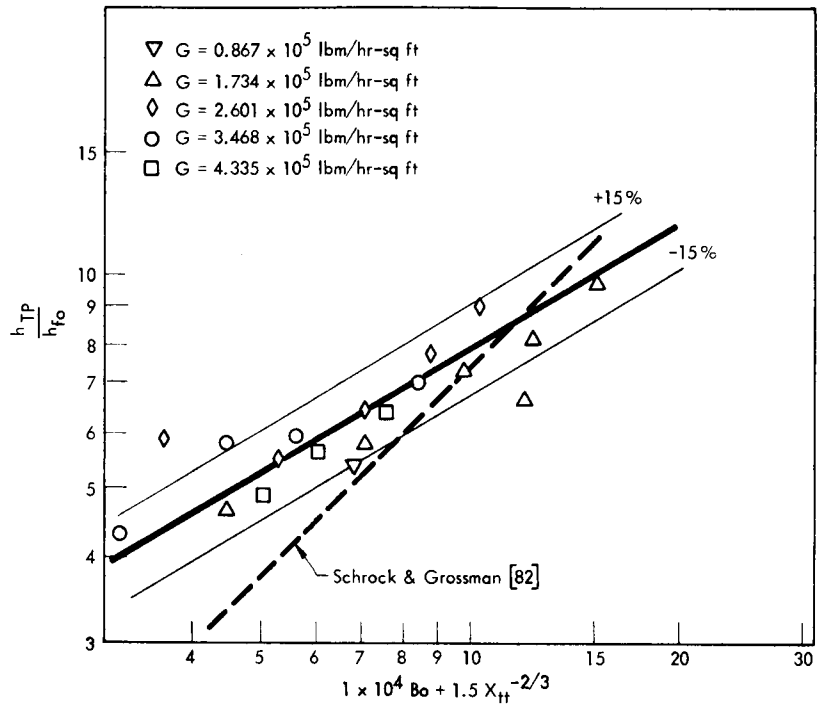


Figure II-29. COMPARISON OF THE R-12 HORIZONTAL FLOW BOILING RESULTS OF CHADDOCK AND NOERAGER [43] WITH THE CORRELATION OF SCHROCK AND GROSSMAN [82].

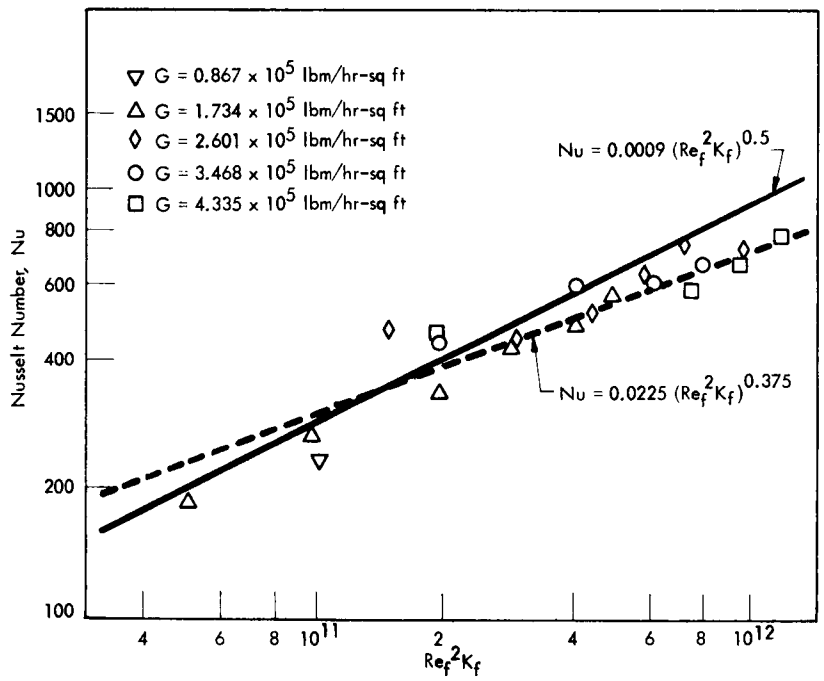


Figure II-30. COMPARISON OF THE R-12 HORIZONTAL FLOW BOILING RESULTS OF CHADDOCK AND NOERAGER [43] WITH THE CORRELATIONS OF PIERRE [89] AND ALTMAN, NORRIS, AND STAUB [40].

One of the most recent investigations of boiling refrigerants in vertical tubes was reported by Purcupile, Riedle, and Schmidt [94]. Using R-11, R-12, and R-113, in 0.740 in. and 0.236 in. ID stainless steel tubes, they ran tests mainly in the low quality region ($-0.06 < x_o < 0.21$) for both saturated and subcooled boiling cases. The results obtained were compared with the correlations of Dengler and Addoms [78], Schrock and Grossman [82], Chen [80], and Chawla [29, 30, 31, 32] in the nucleate boiling regime. In addition Purcupile, Riedle, and Schmidt [94] applied an equation which they had previously developed [95] to this data. Comparison of these correlations with the data is shown in Figures II-31 to II-35.

In conclusion, it can be stated that while numerous correlations exist in the literature today for predicting heat transfer coefficients, no single correlation has been found adequate for refrigerants. While the Chen [80] correlation seems to be superior for water and various organic fluids, it does not fare as well with refrigerants in the few publications where it was used for comparison with experimental data. Opinion is divided on the Guerrieri and Talty [77] correlation with only some experimenters obtaining good agreement with this correlation. No disagreement was found with the Dengler and Addoms [78] correlation by any experimenters but the number of comparisons is limited. In Table II-8 a comparison of some of the correlations reported with the results of numerous experimenters is shown. It should be pointed out that no attempt was made to differentiate between horizontal and vertical boiling since correlations derived for one orientation seemed to hold equally well for the other in some cases. Quite possibly at high

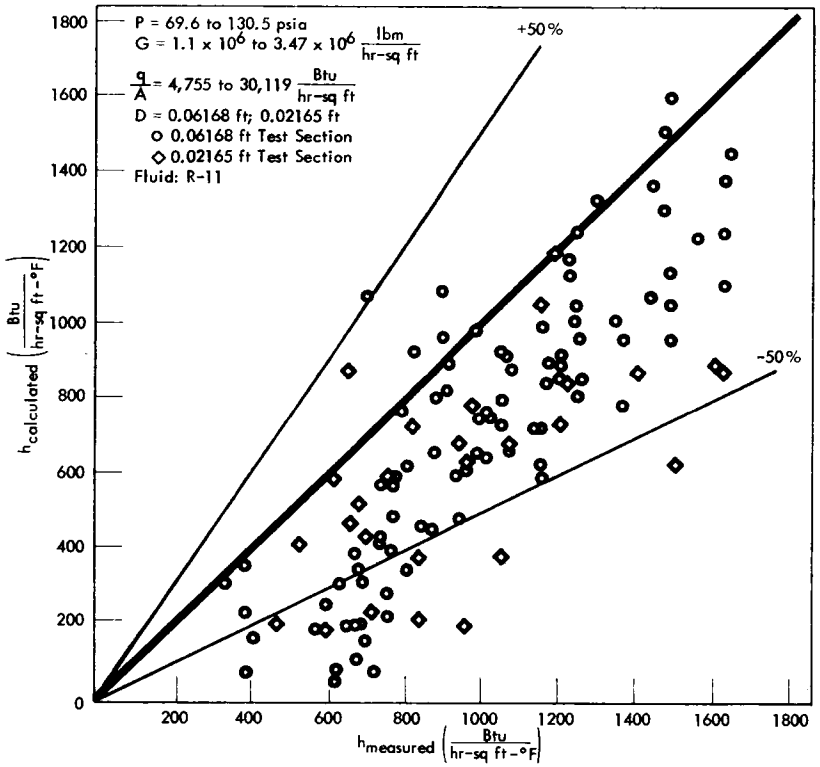


Figure II - 31. COMPARISON OF PURCUPILE, RIEDLE, AND SCHMIDT [94] VERTICAL FLOW BOILING DATA WITH DENGLER AND ADDOMS [78] CORRELATION.

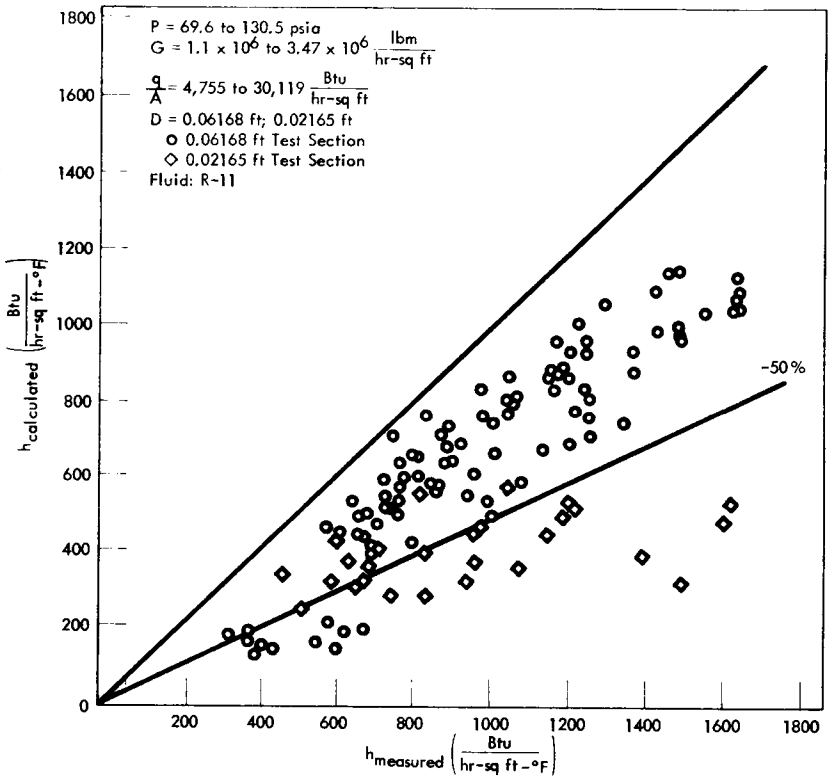


Figure II - 32. COMPARISON OF PURCUPILE, RIEDLE, AND SCHMIDT [94] VERTICAL FLOW BOILING DATA WITH SCHROCK AND GROSSMAN [82] CORRELATION.

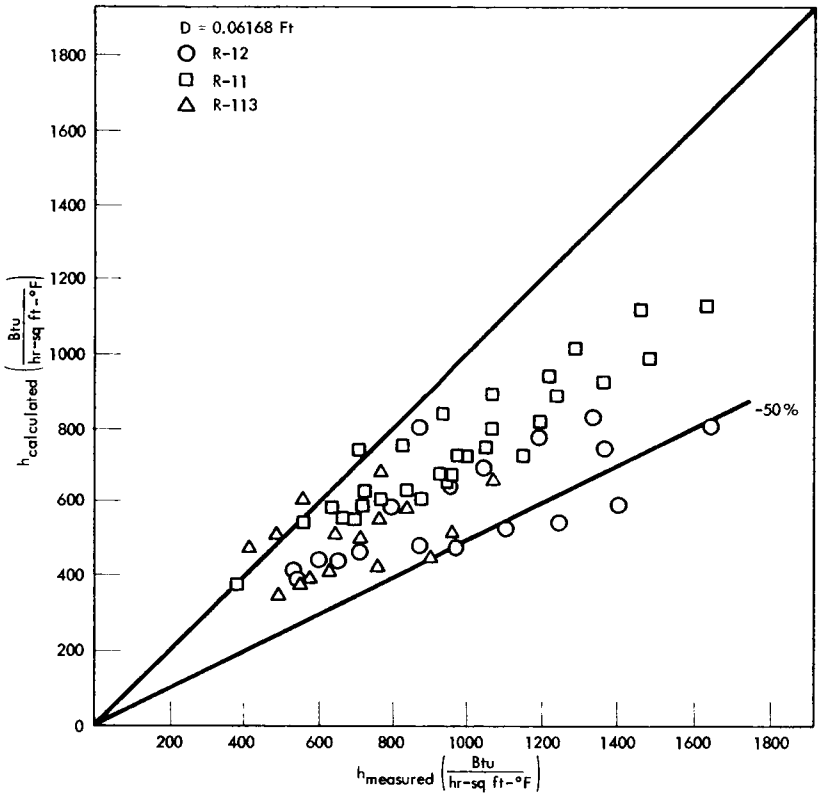


Figure II-33. COMPARISON OF PURCUPILE, RIEDLE, AND SCHMIDT [94] VERTICAL FLOW BOILING DATA WITH CHEN [80] CORRELATION.

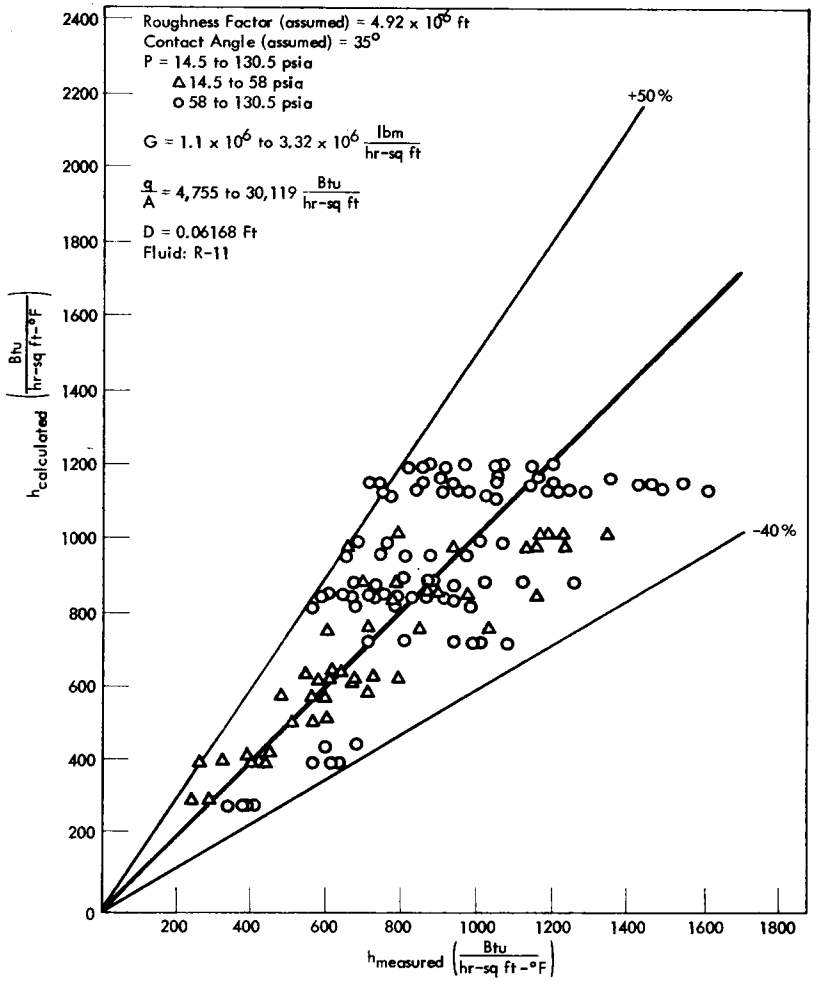


Figure II-34. COMPARISON OF PURCUPILE, RIEDLE, AND SCHMIDT [94] VERTICAL FLOW BOILING DATA WITH CHAWLA'S [29] CORRELATION FOR THE NUCLEATE BOILING REGIME.

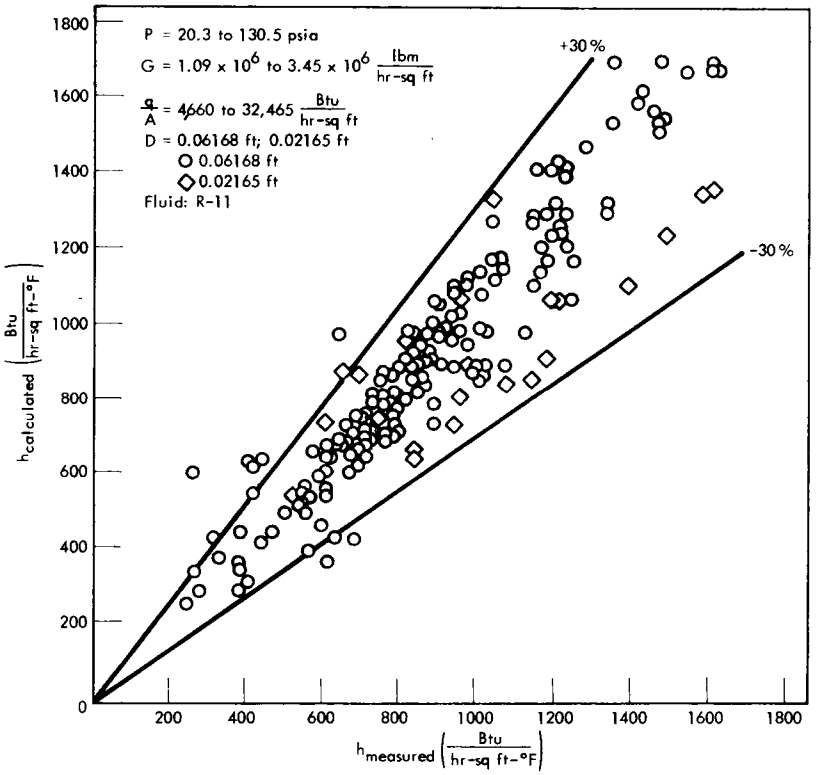


Figure II - 35. COMPARISON OF PURCUPILE, RIEDLE, AND SCHMIDT [94] VERTICAL FLOW BOILING DATA WITH RIEDLE-PURCUPILE [95] CORRELATION.

TABLE II-8

COMPARISON OF VARIOUS HEAT TRANSFER COEFFICIENT CORRELATIONS WITH BOILING REFRIGERANT DATA

Experiments with Refrigerants	Correlations									
	Guerrieri and Talty [77]	Chen [80]	Schrock and Grossman [82]	Dengler and Addoms [78]	Rohsenow (Pool) [61]	Pierre [89]	Davis and David [81]	Bennett et al [79]	Chawla (Nucleate Boiling Regime) [29]	Cheshire and Stirling [36]
Lavin and Young, R-12 [84]	Correlation too high			Correlation too high				Correlation too high		
Napadensky, R-12 [15]	Good agreement (slightly different exponent, however)							Different coefficient and exponent	No agreement	
Cheshire and Stirling, R-114 [36]		Very different								
O'Donnell, Robinson, and Webb, R-114, R-113, R-11 [85]		Very different								Good agreement
Wasserman, Erickson, and Mann, R-113 [86]					Different coefficients in equation					
Baker, Touloukian, and Hawkins, R-12 [87]					Approximate agreement (additional coefficients used)					
Blatt and Adt, R-11, R-113 [42]					Good agreement					
Allen, R-114 [88]		Very different								Correlation too high
Altman, Norris, and Staub, R-22 [40]						Good agreement				
Johnston and Chaddock, R-12, R-22 [41]						Good agreement (with slightly different coefficients)				
Pujol and Stenning, R-113 [90]	Slightly different coefficient and exponent		Different coefficient and exponent							
Gouse and Coumou, R-113 [91]	Good agreement	Fair agreement*		Correlation a bit too high		Agreement over a very limited range				
Gouse and Dickson, R-113, R-11 [93]	Correlation too low	Fair agreement*	Correlation generally too low	Good agreement		Generally poor agreement	Good agreement			
Chaddock and Noerager, R-12 [43]	Correlation too low	Unsatisfactory agreement	Different coefficients and exponent	Good agreement		Good agreement				
Purcupile, Riedle, and Schmidt, R-11, R-12, R-113 [94]		Fair agreement*	Correlation generally a bit too low	Good agreement					Good agreement	

*Correlation is consistently slightly too low.

flows, stratification does not occur in the horizontal mode and the flow regimes agree with those in the vertical position.

One final work is in order on the large amount of data available at the present in the Soviet literature on boiling refrigerants. While the amount of information is indeed massive, most of the results obtained were correlated in the most empirical fashion. Recent attempts to correlate the results on a common basis have been published for pool boiling [96, 97]. The correlations, however, are not similar to any published in the Western literature and will not be discussed here.

E. CRITICAL HEAT FLUX

A knowledge of the conditions under which the critical heat flux occurs in a boiling system is necessary in order to enable an engineer to properly design the system. The critical heat flux is essentially the maximum upper limit on the heat transfer coefficient at which a system can be operated since exceeding this limit results in a sharp decrease in heat transfer effectiveness.

Two types of boiling crisis can occur in flow boiling:

(1) Departure from nucleate boiling (DNB) - when the number of vapor bubbles close to the wall is large and these crowded bubbles form an insulating layer. This layer as it becomes thicker, impedes boiling and liquid can no longer come in contact with the hot surface. The boiling then changes from nucleate boiling to film boiling. Liquid still remains in the tube, predominantly in the core. The bulk enthalpy is usually significantly below the saturated vapor enthalpy. For the heat flux-controlled case, the increase in wall temperature is large and occurs rapidly. This is usually referred to as fast burnout.

(2) Dryout - when the liquid film on the wall evaporates. This usually occurs in a transition from the two-phase annular or dispersed flow pattern. The liquid film becomes thin and breaks down into dry patches. For the heat flux-controlled case, the increase in wall temperature is small and occurs rather slowly. This mechanism can be called slow burnout.

There are numerous parameters which have an effect on the critical heat flux. They include: (1) flow rate, (2) system pressure, (3) local quality, (4) tube diameter, (5) tube length, (6) material and surface finish, and (7) method of heating. Of these, parameters (1) to (5) are the most important. The effects of (6) and (7) are not well understood. An excellent review of recent work in this field has been written by L. S. Tong [98]. He presents several correlations developed at Westinghouse, Babcock and Wilcox, United Kingdom Atomic Energy Authority (including the famous Macbeth [99, 100, 101] correlation), United Nuclear Corporation, General Electric, and CISE. These predict the critical heat flux for water as a function of local pressure, local enthalpy, mass velocity, and degree of subcooling. An overall review of flow boiling critical heat flux mechanisms is presented by Tong and Hewitt [102].

It is interesting to note that tests conducted by Bergles and Rohsenow [92] and Farber [103] indicate that pool boiling and flow boiling heat fluxes are quite different. The effect of subcooling, for example, has been found to be stronger in pool boiling critical heat flux than in flow boiling. In contrast, Gambill [104] has proposed an equation which superimposes a forced convection heat transfer

component on the critical heat flux determined in the absence of forced flow (i.e., pool boiling). He was able to correlate most of his data within ± 40% for various fluids and numerous flow conditions.

Tests conducted have indicated that surface deposits or scale have no adverse effect on the critical heat flux in flow boiling. Some surface roughness effects have, however, been noted. In subcooled flow boiling, if the roughness is greater than the bubble layer thickness, the increase in flow agitation improves critical heat flux. For small roughness heights, smaller than the thickness of the bubble layer, the effect on critical heat flux is insignificant. In the high quality region, the surface roughness increases the liquid entrainment thereby reducing the liquid film thickness and lowering the critical heat flux.

While most of the above tests have been conducted with water, numerous tests have been run with other fluids, such as refrigerants. Much lower system pressures and heat fluxes are encountered when refrigerants are used, thus making testing easier. However, in order to successfully apply these results to the prediction of critical heat flux in water, an appropriate scaling method must be used.

For exact modeling, both geometric and dynamic simulitude are required. Geometric similitude implies a similar flow field, channel geometry and bubble size, where the bubble size is a function of fluid and surface properties and system pressure. Hydrodynamic similitude requires a similar flow pattern and similar velocity and shear distributions in the pipe. The flow pattern is a function of the Froude, Weber, and Reynolds numbers, as well as the relative volumetric flow rate of the gas and the liquid to vapor density ratio. The velocity and

shear distributions in the pipe are functions of the Reynolds number. Thermodynamic similitude requires the same heat transfer mechanism and equivalent thermodynamic properties of the two coolants [98].

Two approaches to scaling are in use today. Macbeth [101] called them the scaling law approach and the scaling factor approach. To establish a set of scaling laws, the key operation is to find what fluid properties are important in the behavior of the phenomenon being studied and combine them with the salient geometric scaling parameters.

Barnett and Wood [105] used the scaling-law approach to compare critical heat flux data for water, R-12 and R-21. They found that an equation of the following type modeled the critical heat flux to within ± 7% in uniformly heated round tubes:

$$\frac{(q/A)_{crit}\,\gamma^{1/2}}{\rho_f^{1/2} h_{fg}} = f_2\left(\left[\frac{L}{D}\right], \left[\frac{Dc_{pf}\rho_f^{1/2}}{k_f \gamma^{1/2}}\right], \left[\frac{G\gamma^{1/2}}{\rho_f^{1/2}}\right], \left[\frac{\rho_f}{\rho_g}\right], \left[\frac{\Delta h}{h_{fg}}\right]\right) \quad (2\text{-}80)$$

here,

$$\gamma = -\frac{d\left(\frac{\rho_f}{\rho_g}\right)}{dp} \quad (2\text{-}81)$$

is the rate of change of the density ratio with pressure (1/psia) and Δh is the subcooled enthalpy at the inlet. Equation (2-80) was based on water data at 560 and 1000 psia, R-12 data at 83.5 and 154.8 psia and R-21 results at 106.3 and 200 psia. A very lucid explanation of the reasoning behind the choice of variables in the scaling law given in Equation (2-80) is presented by Barnett [106]. An illustration of the results obtained is shown in Figure II-36.

Physically speaking, by equating the L/D ratio, one is achieving similarity in channel geometry. By using the same liquid to vapor

	P (psia)	L (in)	D (in)	Best Line to Data
Water	1000	68.0	0.220	
R-12	155	95.0	0.303	
Water Equiv. of R-12	1000	68.2	0.217	
R-21	200	83.5	0.264	
Water Equiv. of R-21	1000	68.1	0.215	

$G \times 10^{-6}$ $\frac{lbm}{hr\text{-}sq\ ft}$	0.75	1.5	3.0
Water	◊	▮	◇
Water Equiv. of R-12	□	○	○
Water Equiv. of R-21	△	▽	▮

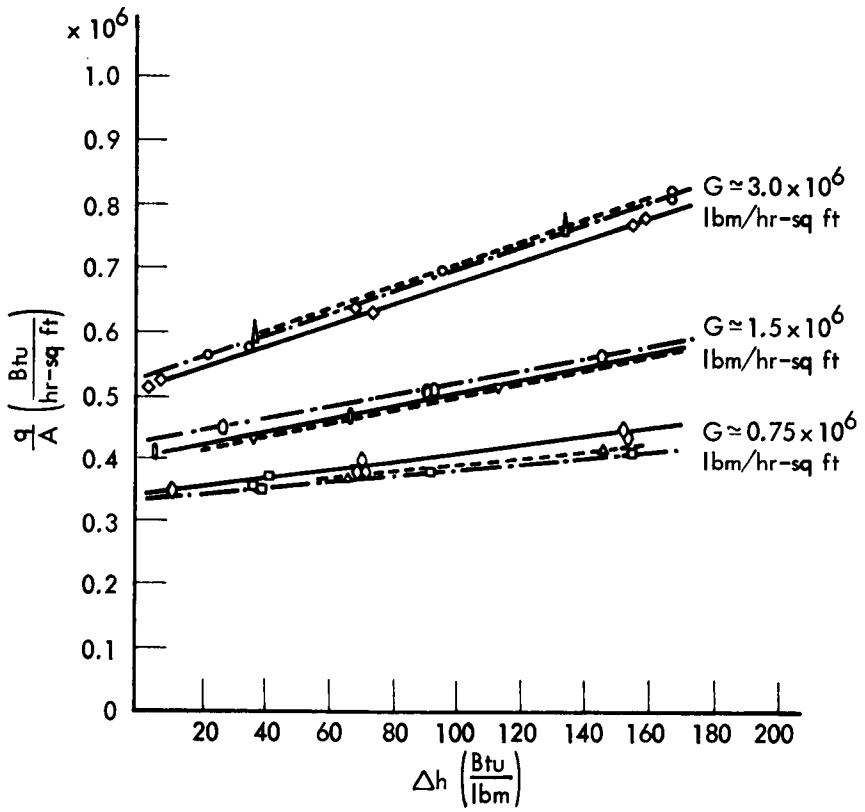


Figure II-36. COMPARISON OF THE SCALING LAW IN EQUATION (2-80) WITH EXPERIMENTAL DATA. BARNETT [106]

density ratio and quality in model and prototype, the void fraction is approximately the same (a comparison with Equation (2-43) indicates that $\bar{V}_{gj}$ is not modeled). Similar void fractions at the same mass flux signify that hydrodynamic similitude has been approximately achieved. In addition, from a simple heat balance on a tube element containing a moving fluid subjected to a uniform heat flux, one obtains the dimensionless equation:

$$x = \frac{4L}{D} \frac{(q/A)_{crit}}{G\, h_{fg}} - \frac{\Delta h}{h_{fg}} \quad . \tag{2-82}$$

Note that by using the same $\Delta h/h_{fg}$ ratio for the two fluids, the inlet subcooling in the model is fixed. The other terms in the scaling equation are fluid properties.

The use of scaling factors is a less rigorous approach than the use of scaling laws. Here data for a given fluid and geometry are linked with those of another fluid by numerical scaling factors without actually identifying the fluid properties which make up the factors. Stevens and Kirby [107] were able to obtain a graphical correlation for uniform flux round tubes using the empirical function:

$$E_s = \left[GD^{1/4} \left(\frac{D}{L}\right)^{0.59}\right] 10^{-4} \frac{\text{lbm-in.}^{1/4}}{\text{hr-sq ft}} \tag{2-83}$$

where x_{crit} is obtained by using Equation (2-82).

In order to superimpose the curves of x_{crit} vs. E_s for R-12 and water, Stevens and Kirby [107] multiplied their E_s factor for water by the scaling factor K_s which was found to be 0.658. Subsequent work by Coffield, Rohrer, and Tong [108] and Tong, Motley, and Cermak [109] has shown that the scaling factor, K_s, is a function of the density ratio and the degree of subcooling. Staub [110] extended Stevens and Kirby's

[107] work by suggesting that the boiling length be used for L rather than the total heated length. The improvement obtained by this modification is shown in Figure II-37. Staub [110] also noted a small effect of density ratio on the scaling factor K_s.

Dix [111] was the only investigator in the literature to obtain critical heat flux data for R-114. Using his results along with previously published data for R-12, R-21, and R-22, he was able to confirm the effect of ρ_f/ρ_g on K_s as Coffield, Rohrer, and Tong [108] had previously indicated. Dix [111] noted that K_s was also a function of other parameters- varying approximately 20% with mass flux and 5% with L/D ratio. A 20% variation with ρ_f/ρ_g was noted. Over the limited range, shown in Table II-9 in which Dix [111] took data, the following correlation for the scaling factor was obtained:

$$K_s = C_T\left(1.00 - 0.09 \times 10^{-6}\, G_{water}\right)\left(1.04 - 0.0005\,\frac{L}{D}\right)\left(1.41 - 0.02\,\frac{\rho_f}{\rho_g}\right). \qquad (2\text{-}84)$$

C_T is a modeling constant which is dependent on the fluid used, and G_{water} is the corresponding mass flux of water. Values of C_T for four different fluids along with the heat flux prediction errors are given in Table II-10. Critical heat flux values for water used for comparison with the refrigerant data were generated from the Biasi et al [112] correlation. From the studies of Paleev and Filippovich [113] with annular flow, for matching geometries and equal qualities:

$$C_T \approx \frac{\left(\sqrt{\sigma\rho_g}\right)_{Refrigerant}}{\left(\sqrt{\sigma\rho_g}\right)_{Water}} \qquad (2\text{-}85)$$

	$\Delta h / h_{fg}$	
□	0.04 - 0.26	R-12 Data, Correlation of Stevens and Kirby [107], 155 psia
o	0.04 - 0.26	R-12 Data, Staub [110] Modification; L = L_{boil}, 155 psia
△	0.03 - 0.29	R-22 Data, L = L_{boil}, 190 psia

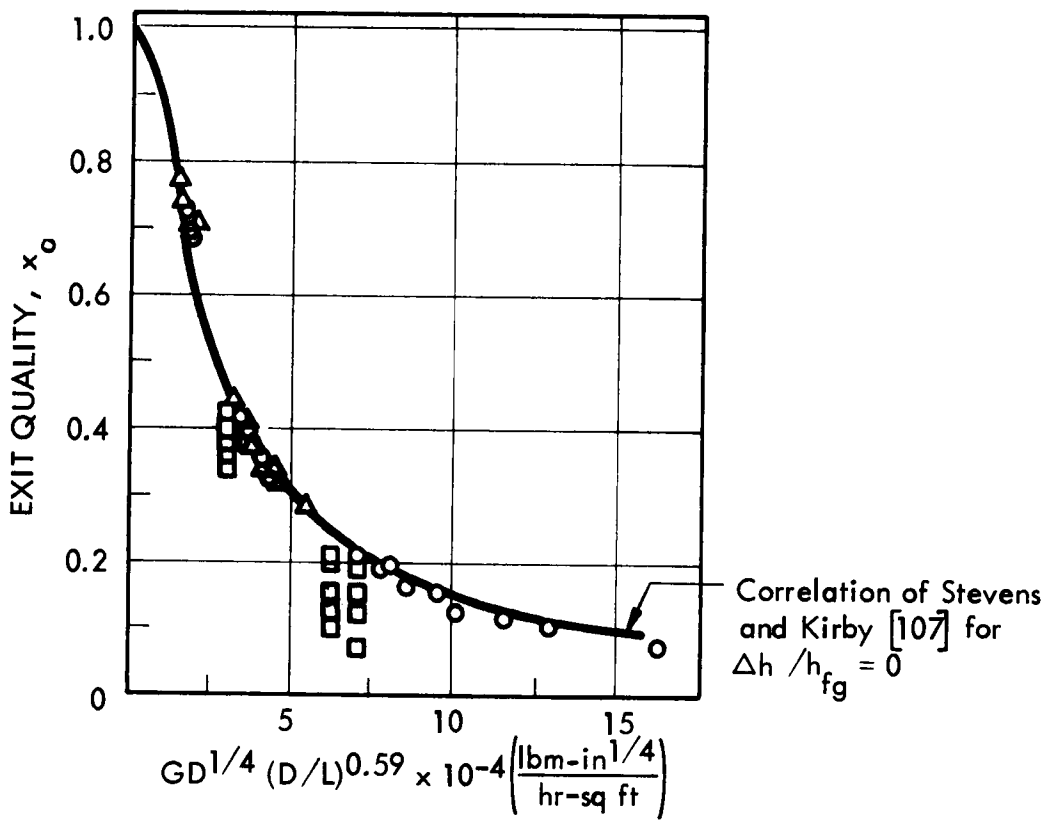


Figure II-37. CRITICAL HEAT FLUX DATA WITH R-12 AND R-22 USING THE SCALING FACTORS OF STEVENS AND KIRBY [107] AND THE MODIFICATION OF STAUB [110].

Table II-9

R-114 CRITICAL HEAT FLUX TEST PARAMETER RANGE, DIX [111]

Parameter	Minimum	Maximum
ρ_f/ρ_g	10.7	20.6
Pressure (psia)	123.8	207.6
Temperature (°F)	169.5	213.5
Mass Flux, G $\frac{\text{lbm}}{\text{hr-sq ft}}$	0.3×10^6	1.5×10^6
$\Delta h/h_{fg}$	0.03	0.54
D (in.)	0.393	0.555
$L_{\text{subcooled + boiling}}$ (in.)	25	76
L_{boiling} (in.)	0.291	65.61

Table II-10

REFRIGERANT MODELING CONSTANTS AND
CRITICAL HEAT FLUX PREDICTION ERRORS, DIX [111]

Refrigerant	C_T	K_s Range, Equation (2-84)	No. of Points	RMS Error, %
R-114	0.740	0.54 - 0.87	424	4.2
R-12	0.800	0.51 - 0.80	973	6.3
R-22	0.807	0.65 - 0.72	11	3.6
R-21	0.920	0.61 - 0.90	557	8.5

Stevens and Macbeth [114] studied the effect of test section size on the applicability of refrigerant modeling. They noted that for uniformly heated round tubes, little restriction on the size of the model needs to be made. For more complex geometries such as annuli and multi-rod clusters, the model test section should not be much smaller than the prototype under consideration.

Groeneveld [115] presented results of work done by the Atomic Energy of Canada Ltd. at Chalk River, Ontario. The data obtained for R-12 agreed very well with the previous work of Barnett and Wood [105], as well as others at the Atomic Energy Establishment in Winfrith, England. Groeneveld [115], however, used an optimization technique to obtain his scaling factors. For the form of the equation:

$$\left(\frac{q}{A}\right)_{crit} = f_3\left(D, \frac{L}{D}, G, x\right) \tag{2-86}$$

he obtained:

$$\left(\frac{q}{A}\right)_{crit} = D^{b_2} f_4\left(\frac{L}{D}\right) f_5(G) f_6(x) \tag{2-87}$$

where:

$$b_2 = -0.362713 \tag{2-88}$$

$$f_4(L/D) = 9.71043 \times 10^6 - 2.17140 \times 10^4 (L/D) + 42.2492 (L/D)^2 \tag{2-89}$$

$$f_5(G) = 1.16244 \times 10^{-2} - 1.150610 \times 10^{-2} (G/10^6) + 6.28448 \times 10^{-3} (G/10^6)^2 - 1.17288 \times 10^{-3} (G/10^6)^3 \tag{2-90}$$

$$f_6(x) = 1.36368 - 2.88422x + 3.52880x^2 - 2.2307x^3 . \tag{2-91}$$

Groeneveld [115] also presented a slightly different form of Equation (2-86):

$$\left(\frac{q}{A}\right)_{crit} = f_7\left(D, \frac{L}{D}, G, \Delta h\right) . \qquad (2\text{-}92)$$

These scaling parameters predicted the water critical heat flux with an rms error of 7.8%. Ahmad [116] has recently proposed a set of parameters to be used in fluid to fluid modeling. The resulting "compensated distortion model" was successfully tested at different liquid to vapor density ratios for refrigerants, water, potassium, and carbon dioxide over a large range of mass flux and inlet subcooling and in both subcooled and quality regions. From an application of the Buckingham Pi Theorem and a judicious choice of important parameters, Ahmad [116] was able to show that plots of a modeling parameter Ψ_{CHF} vs. the Boiling number yielded the same curve for model and prototype assuming the liquid to vapor density ratio and the degree of subcooling ($\Delta h/h_{fg}$) were the same in both systems. The modeling parameter proposed was defined as:

$$\Psi_{CHF} = \left[\left(\frac{GD}{\mu_f}\right)\left(\frac{\mu_f^2}{\sigma D \rho_f}\right)^{2/3}\left(\frac{\mu_g}{\mu_f}\right)^{1/5}\right] . \qquad (2\text{-}93)$$

In order to avoid using the surface tension because it may not be reliably known for many refrigerants, a different property grouping was chosen and the following modeling parameter was obtained instead:

$$\Psi_{CHF} = \left[\left(\frac{GD}{\mu_f}\right)\left(\frac{\gamma^{1/2}\mu_f}{D\rho_f^{1/2}}\right)^{2/3}\left(\frac{\mu_f}{\mu_g}\right)^{1/8}\right] . \qquad (2\text{-}94)$$

Agreement between this theory and experimental data is quite good and numerous results can be found in Ahmad's [116] publication. In order for this correlation to be applicable in predicting critical heat flux

behavior, a correlation function was developed. Based on this correlation function, for the case of zero inlet subcooling, critical heat flux results can be presented in the form of exit quality, x_o vs. $\Psi_{CHF}\ (D/L)^{0.6}$ plots where Ψ_{CHF} is defined by Equation (2-94).

In addition to attempting to solve for the critical heat flux by using empirical and semi-empirical correlations, scaling laws, and scaling factors as was discussed above, some strictly analytical work has been done. The analyses obtained usually require the determination of one or two empirical constants to fit the data. The fundamental equations can be derived by using either (1) the thermal or mass balance near the tube wall or (2) the hydrodynamic behavior of the main stream. In general, the empirical correlations have proved more accurate. A good review of some of the analytical work done to date is given in Tong's [98] book.

In summation, it can be said that for the case of a uniformly heated round tube, sufficient equations exist to give reasonably good predictions of critical heat fluxes for water. In addition, because of the advantages of using refrigerants and then scaling the results for use in water, a significant number of contributions have been made in the literature towards that end. While the empirical scaling equations determined by Stevens and Kirby [107] are the most widely used, the scaling factor K_s is subject to variations and the effect of mass flux, density ratio, etc., on this parameter is not completely understood. In this respect, the compensated distortion model may look more attractive. Considerably more tests need to be performed, however, before more reliable answers are available.

CHAPTER III

EXPERIMENTAL INVESTIGATION

A. DESCRIPTION OF SYSTEM

The experimental work was performed in the boiling facility in the K-1401 building at the Oak Ridge Gaseous Diffusion Plant. This facility was built and operated under the direction of the author. The working fluid used was R-114 (Dichlorotetrafluoroethane).

In the test loop sketched in Figure III-1, the R-114, after leaving the storage tank, was either pumped or traveled by natural circulation through one of the two turbine flowmeters--each accurate in a different flow range--and on to a preheater. The preheater heated the fluid either to saturation or to the desired degree of subcooling. From there, the R-114 traveled through the boiling test section to two entrainment separators where the liquid and vapor were separated. The vapor was condensed and, along with the liquid, flowed back to the storage tank. The flow rates of both liquid and vapor were measured to determine the quality and provide a mass balance. In addition, the heat removed in the condenser was calculated from the flow rate and temperature change of the cooling water and compared to the heat input from the test section and preheater (and pump in forced circulation cases) to provide a heat balance. Additional information, as well as a more detailed drawing of the test facility, can be found in Appendix B.

The test section shown in Figure III-2 was constructed from drawn copper tubing with a 0.785-in. inside diameter and a 1.750-in. outside diameter. The 10-ft heated length was divided into 10 individually controlled zones. Each zone was heated by tubular heaters wrapped

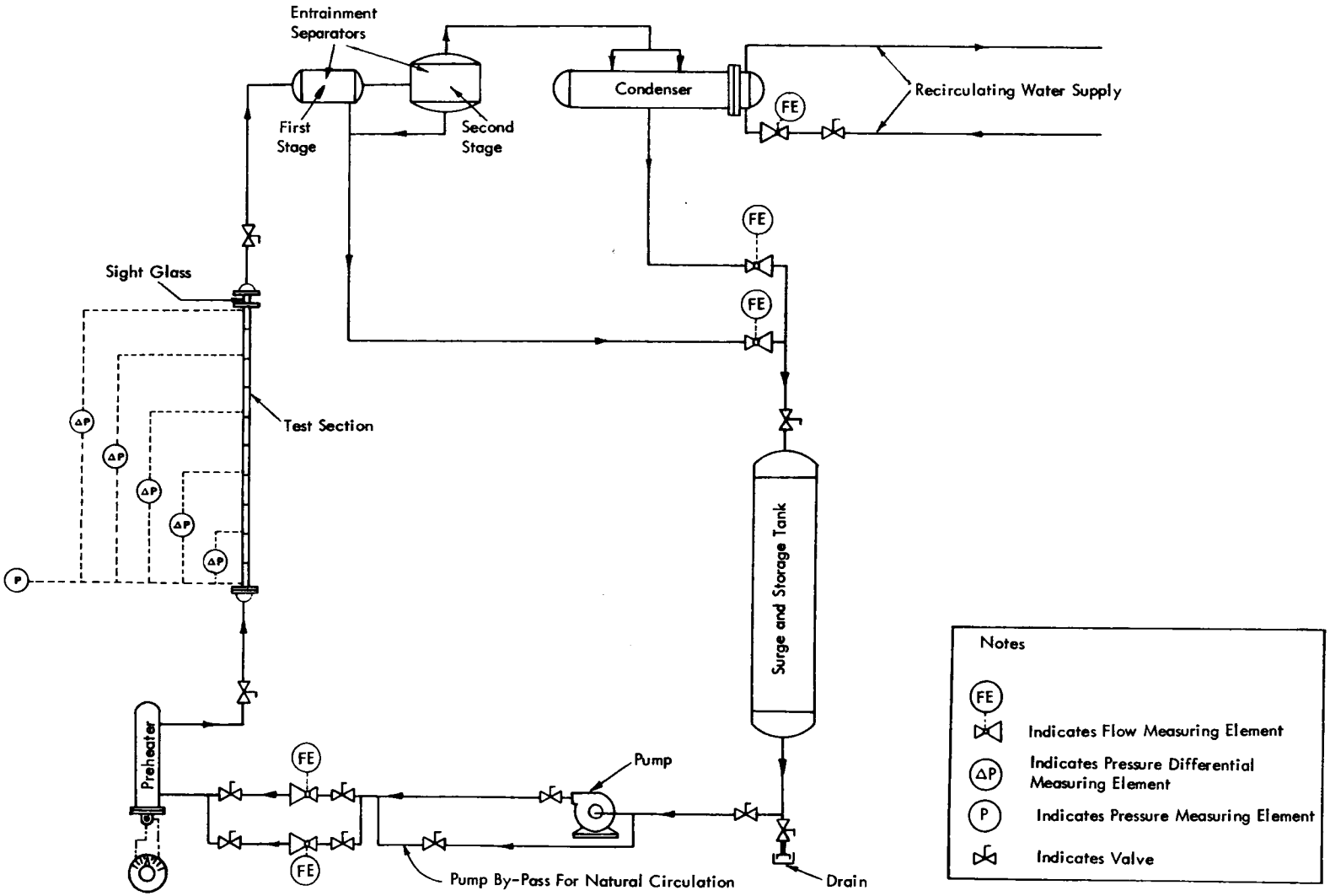


Figure III - 1. SCHEMATIC DRAWING OF BOILING FACILITY.

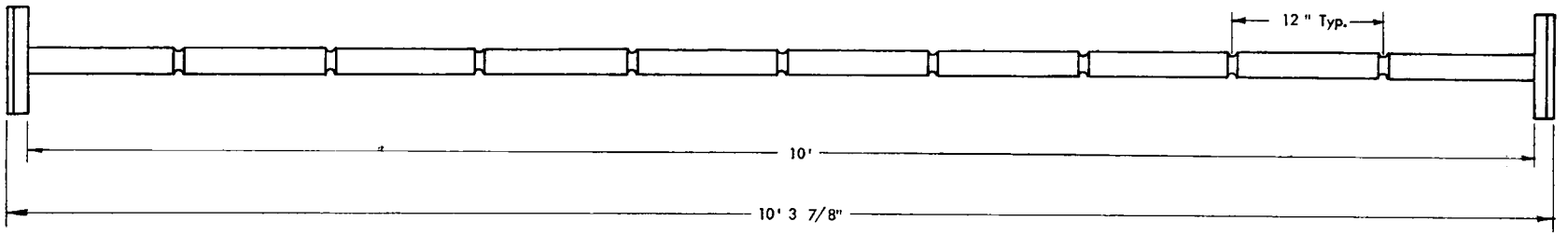


Figure III - 2. OVERALL VIEW OF TEN-FOOT TEST SECTION.

around the outside of the copper tube. Heat-conducting cement was then placed over the heaters to provide a good thermal bond with the tube. Each 1-ft zone was isolated from adjacent zones as much as possible in order to minimize axial conduction. Grooves 1/2-in. wide were cut into the copper tube at 1-ft intervals deep enough to leave a wall thickness of 0.100 in. This not only enhanced the accuracy of the zone-by-zone heat transfer measurements, but also provided better data during the critical heat flux measurements where steep changes in the wall temperature could have led to significant axial conduction. The grooves were filled with an epoxy capable of withstanding 500°F. The entire test section was then covered with at least 3 in. of insulation to minimize heat loss to the atmosphere. This is illustrated in Figures III-3 and III-4.

Wall temperature measurements in each of the 10 zones of the tube consisted of four, 24-gage Chromel-Constantan thermocouples embedded in the wall so that the bead was at a distance of 7/64 of an inch from the inside tube surface in each zone. A calibrated 32-gage Chromel-Alumel thermocouple measured the refrigerant temperature in the center of each zone (Figures III-5, III-6, and III-7). Additional thermocouples were spot-welded to the heaters to monitor sheath temperature in order to prevent overheating and possible burnout of any of the heaters.

Pressure instrumentation consisted of pressure taps at approximately 2-ft intervals in the test section. The absolute pressure was measured at the inlet and differential pressures between this inlet tap and any other tap were sensed by a DP cell (Figure III-8).

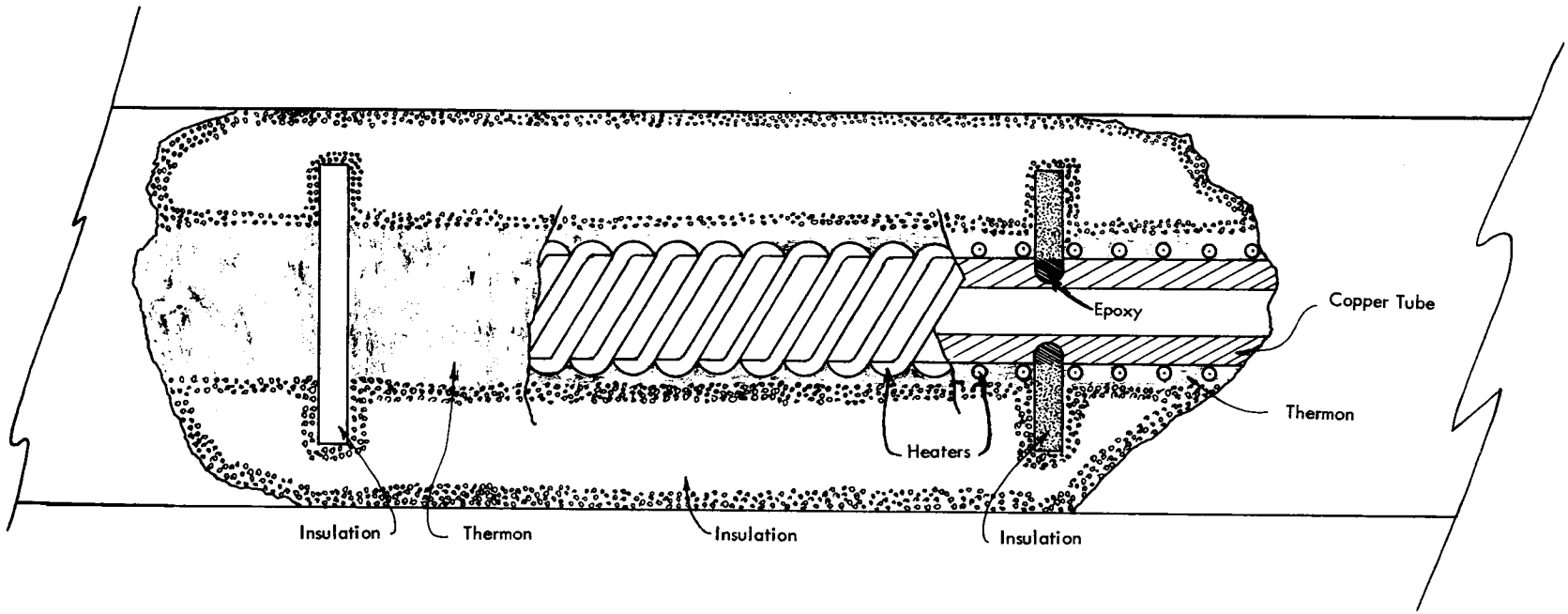


Figure III-3. CUTAWAY VIEW OF TEST SECTION, HEATERS, THERMON, AND INSULATION.

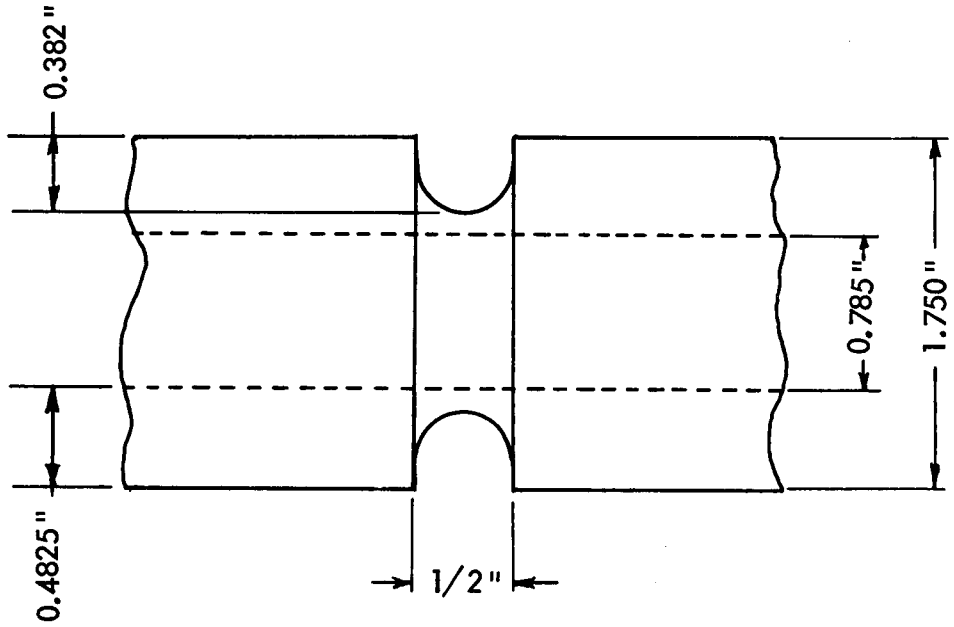


Figure III-4. DETAIL OF THE GROOVE SEPARATING THE ZONES IN THE TEST SECTION.

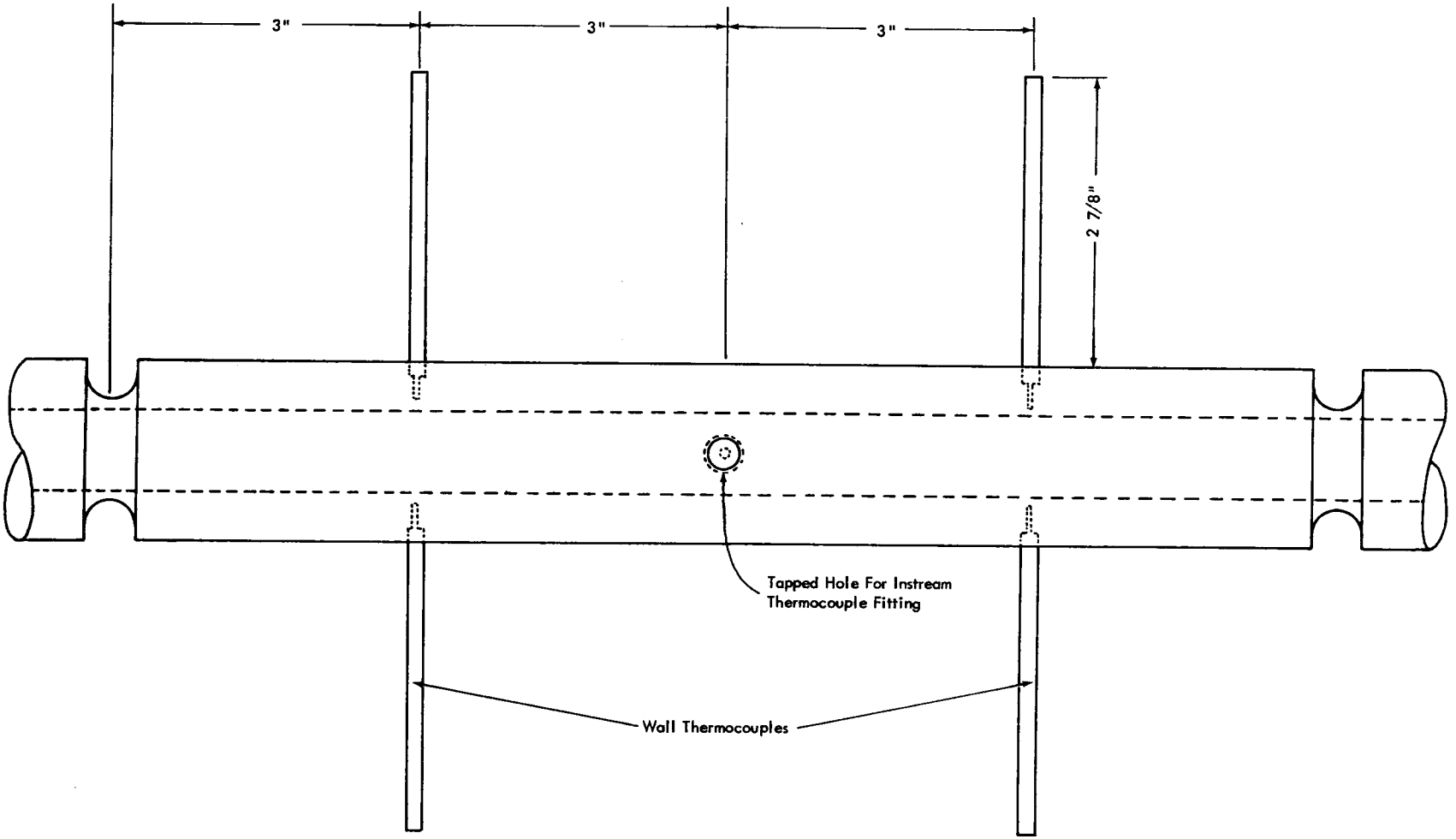


Figure III - 5. ILLUSTRATION OF WALL AND INSTREAM THERMOCOUPLES IN A ZONE.

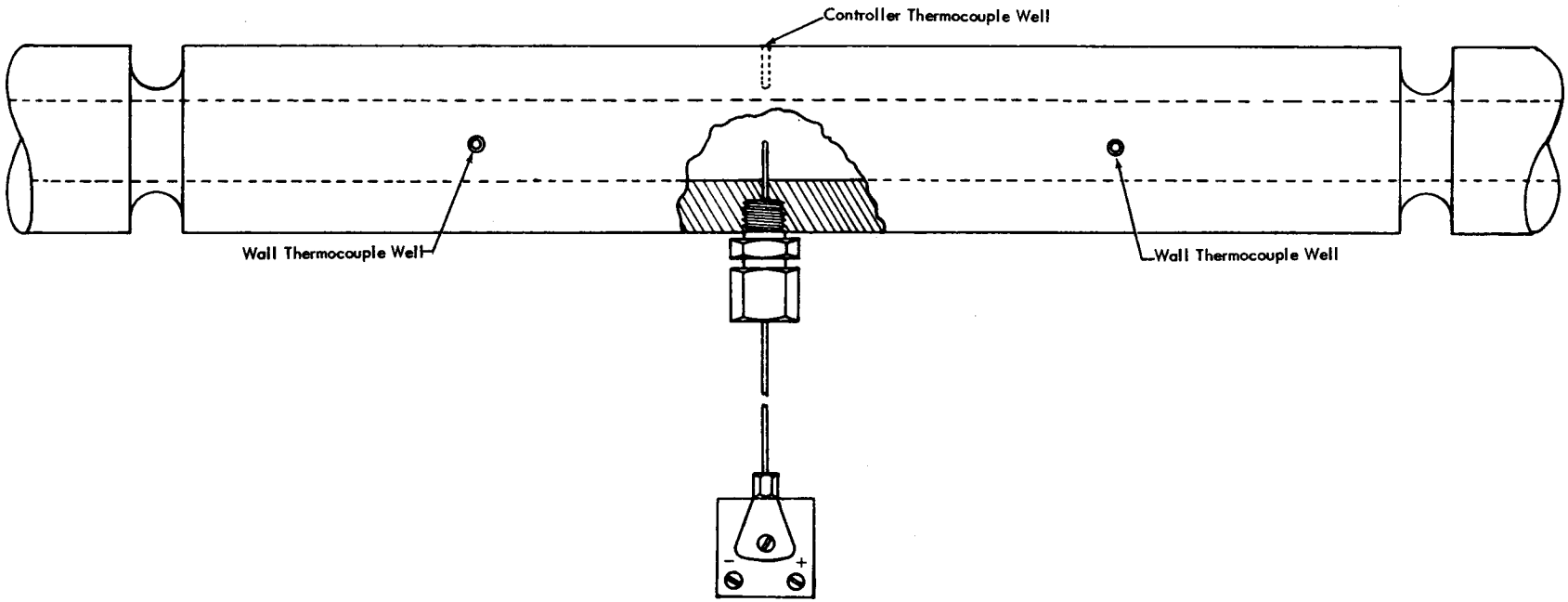
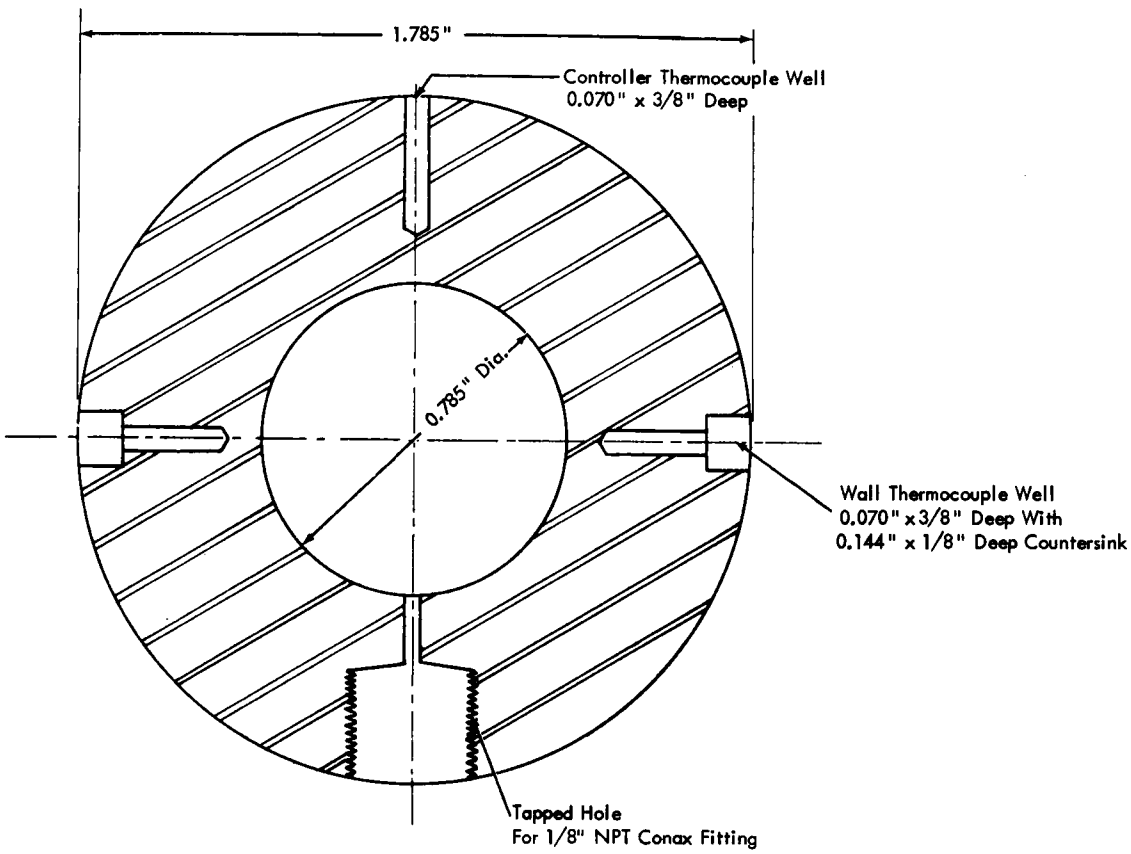


Figure III-6. DETAIL OF INSTREAM THERMOCOUPLE INSTALLATION.



NOTE: Not All Holes Are In The Same Plane

Figure III - 7. CROSS SECTIONAL VIEW OF ALL THERMOCOUPLE LOCATIONS.

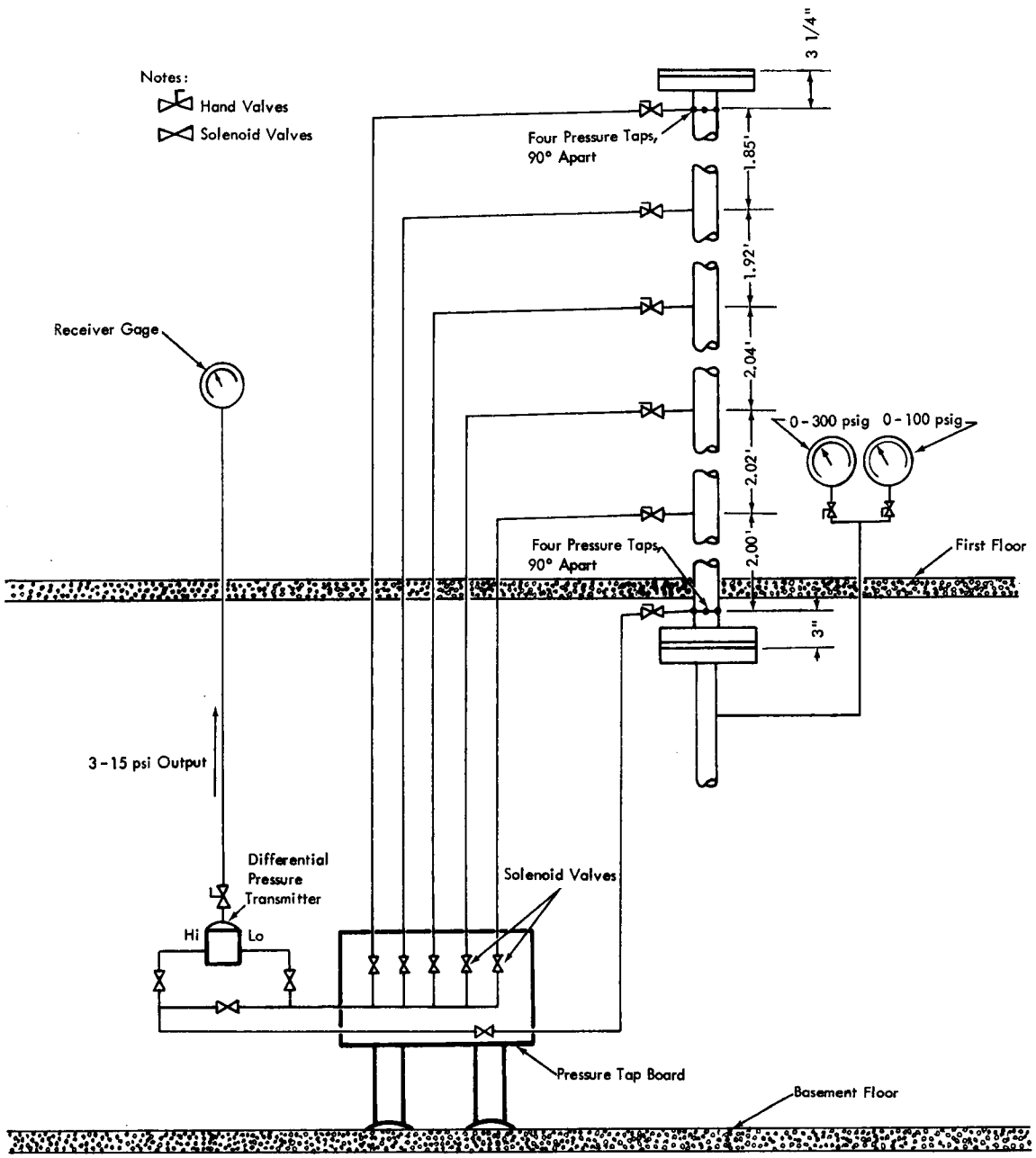


Figure III-8. PRESSURE MEASUREMENT SETUP AND INSTRUMENTATION.

In order to increase the versatility of this system and because at some future date it may be desirable to run tests to check the effect of heat flux or temperature distribution on the critical heat flux, a unique method of heat addition was devised to enable operation by either controlling the heat flux or the wall temperature. For the case of wall temperature control, a thermocouple sensed the wall temperature of the tube and fed the voltage signal to a controller. This controller compared the wall temperature to the desired temperature which was manually set. A signal was then sent to a zero-firing SCR. If the wall temperature was too low, the signal from the controller slowly rose, thus increasing the on-time and decreasing the off-time of the SCR. If the wall temperature was too high, the signal from the controller decreased. The on-off cycling of the SCR was rapid enough so that the fluctuations were completely damped out by the thick copper tube wall. For the case where it was desirable to control the heat flux, the controller was switched out of the circuit and a potentiometer switched in. With this setup, it was possible to set any heat flux distribution or any wall temperature distribution. It should be remembered that the desired distributions were actually approximated by 10 step functions, each representing an individual zone. Within each zone only a uniform heat flux distribution was possible. The wattage into each zone was recorded on a calibrated watt-hour meter over a period of one minute and converted to watts. A calibration of the heat loss through the insulation was also made in order to subtract this loss from the total heat input. In all tests reported here, a uniform heat flux was the only wall boundary condition used. A wiring diagram and additional information on any of the above-mentioned system components can be found in Appendix B.

At the exit of the test section, a flow visualization apparatus was located. The Pyrex glass in this apparatus was 1-7/8 in. long with an inside diameter of 0.785 in. As smooth a transition as possible was made between the copper tube and the flow visualization apparatus to minimize any disruption in the flow regime existing at the exit. This is illustrated in Figure III-9.

All instrumentation used was calibrated in order to minimize experimental error. The instrumentation in question included thermocouples and millivolt recording devices, pressure taps and pressure measuring devices, and flow measuring devices. All calibration curves are given in Appendix C.

B. TESTING PROCEDURE AND DATA RECORDING

The testing procedure in the natural and forced circulation runs consisted of maintaining a constant flow rate, setting a desired boiling temperature, and varying the heat flux over the entire range from 3000 Btu/hr-sq ft upwards, in 3000-Btu/hr-sq ft intervals until the critical heat flux was attained. This was evidenced by a sharp rise in wall temperature in Zone 10. After the data were recorded for this operating condition, the electrical input to the tenth zone was cut off and sufficient time was allowed for the wall temperature to drop back to approximately the boiling temperature. The heat flux in the other 9 zones was then increased. This procedure was continued until the critical heat flux occurred in the fourth zone. In all runs undertaken, the flow at the inlet was slightly subcooled.

Once this set of tests had been completed, the boiling temperature was maintained constant and the flow rate was varied. The range of heat

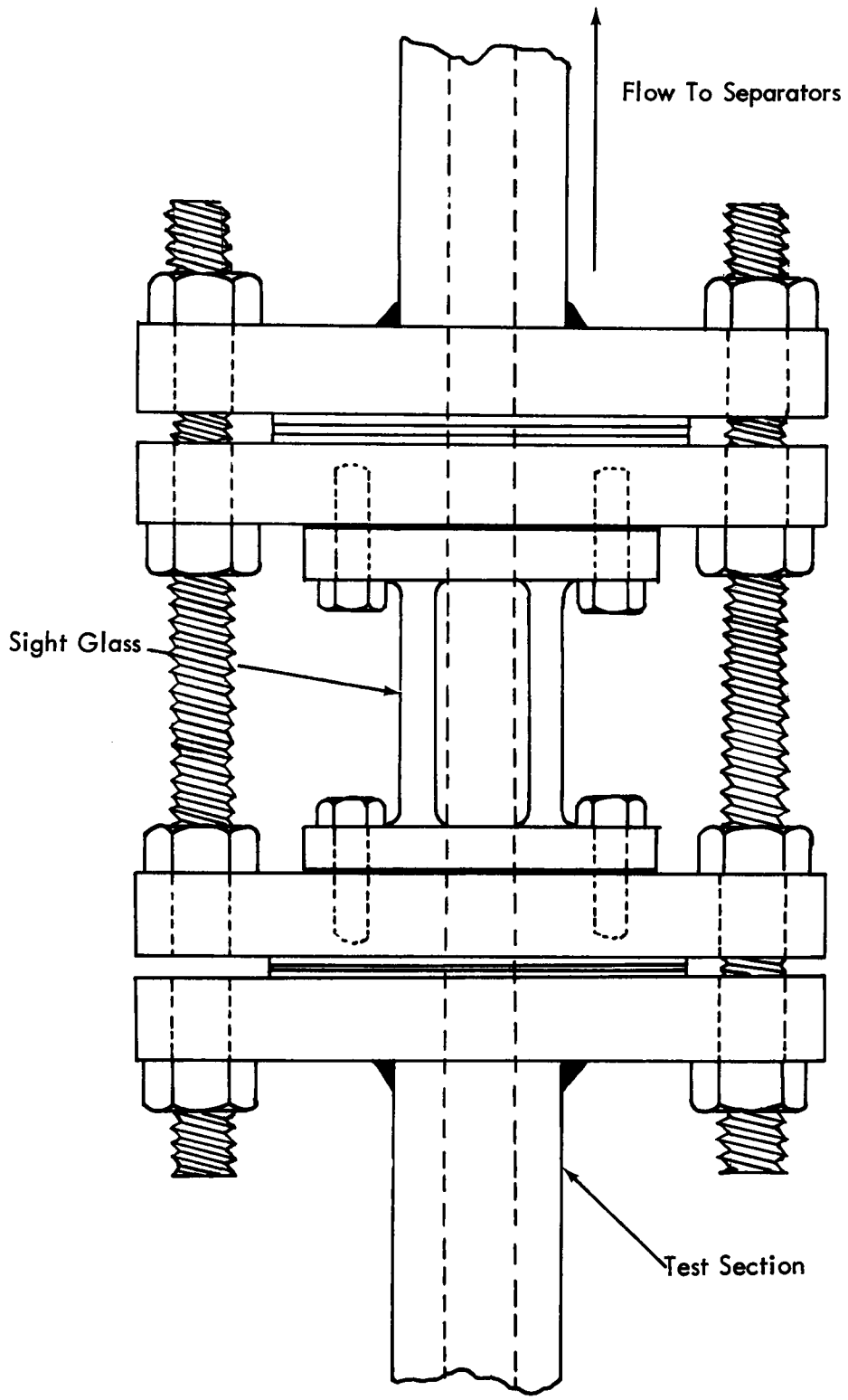


Figure III-9. VISUAL FLOW INDICATOR ASSEMBLY

fluxes outlined above was then repeated at this flow rate. Once the mass fluxes between 0.1 x 10^6 and 3.5 x 10^6 lbm/hr-sq ft were covered, a new boiling temperature was set and the entire procedure repeated again. Thus, essentially, the heat flux was the parameter most frequently varied, the mass flow rate the second most frequently varied, and the boiling temperature the least frequently varied.

While the majority of tests did adhere to the schedule outlined above, several tests were repeated at frequent intervals to assure that no time-dependent changes were taking place in the system. Since the data-taking process was approximately 6 months long, pressure drop tests were repeated to make sure that none of the pressure tap lines or DP cells used were damaged. Heat transfer coefficient tests were repeated to check for any drifts due to thermocouple problems or due to fundamental changes in the characteristics of the boiling surface because of the frequent excursions of the wall temperatures during critical heat flux runs. The pressure drop results yielded no time-dependent trends. One problem was, however, encountered with the wall thermocouples. Initially, the thermocouples were attached to the wall using a type of adhesive frequently used for this purpose. In addition to providing good thermal contact with the wall, a thin layer between the thermocouple bead and the copper tube wall served as an electrical insulator. This adhesive, however, can begin to char if a sufficiently high temperature is attained. This did occur during the critical heat flux runs, and the thermocouple bead was no longer attached to the tube wall. Because of the proximity of the heaters and despite the use of tubular porcelain insulators to isolate the thermocouple wire from the heaters (see Appendix B), conduction through the Chromel-Constantan wire to the

bead was significant enough to result in a consistently higher thermocouple reading. While a calibration of this error was obtained, it was felt that this additional source of uncertainty affected the accuracy of the data. Hence, all wall thermocouples were removed and reattached to the wall using a 30% tin - 70% lead solder. Heat transfer coefficient tests were then rerun, and no additional problems were encountered.

For numerous runs, covering the entire range of test variables, flow regime studies were conducted using a closed circuit video system. This unit had the desirable feature of allowing a playback at a variety of speeds all the way down to a frame-by-frame manual control. This enabled a close inspection to be made of particularly interesting frames. This video system recorded 60 frames per second. The exposure time for each frame was 30 microseconds. At the higher flow rates, especially at high qualities, it was not always possible to clearly see the individual liquid droplets entrained in the vapor flow since, in many cases, they appeared as streaks on the video tape. It was, however, possible to clearly discern the individual flow regimes and the transition between these regimes. The video tape pictures taken were augmented by quality, temperature, and flow rate information to enable a flow map to be drawn. All tests except those at 250°F were performed in the forced-circulation mode. This was necessary since, at extremely low qualities, insufficient liquid head existed to cause any appreciable natural circulation.

In addition to the flow visualization runs described above in which definite values of quality, temperature, and mass flow rate were set and steady state occurred before the flow regime was studied, a

series of "summary" runs was made. In these runs, the heat input to the test section was continuously varied while the boiling temperature and flow rate were held steady. Exit qualities from zero to those corresponding to critical heat flux were thereby achieved. In many runs, it was possible to increase the heat flux until mist flow or dryout was achieved. This was, however, not always possible. In the higher flow rate runs, the heat fluxes needed and the wall temperatures associated with these heat fluxes in the CHF region, it was felt, would have resulted in damage to the test section, alteration of the characteristics of the boiling surface, or both. Thus, as a rule, it was decided that a wall temperature of less than 350°F would be maintained at all times. In some cases, temperatures of 400 to 450°F were inadvertently obtained. Careful study of the heat transfer coefficient data before and after some of these high wall temperature excursions indicated no change in the boiling characteristics. The advantage of these "summary" runs was that despite the lack of data on quality, the dynamic behavior of the boiling fluid could be observed. The mechanisms that took place as the fluid underwent a regime transformation were carefully observed. In addition, the existence of certain flow regimes in narrow quality ranges which may have been missed in the steady state runs could be observed. "Summary" runs were made at all boiling temperatures and mass flow rates at which steady state runs were obtained.

For the pressure drop, heat transfer coefficient and critical heat flux runs, the following data were recorded:

(1) Gage pressure at the inlet of the test section.

(2) Barometric pressure.

(3) Pressure drop at 2-ft intervals along the entire length of the test section.

(4) Wall and instream temperatures in each of the 10 zones.

(5) Temperature of the liquid in the pressure tap lines.

(6) Gross heat input to each of the 10 zones.

(7) Heater sheath temperatures in each of the 10 zones.

(8) Flow rate at inlet of test section, as well as temperature at the flow measuring instrument.

(9) Liquid and vapor flow rates at test section exit and temperatures at the flow measuring instruments.

(10) Inlet and outlet water temperatures as well as water flow rate to the condenser.

A sample calculation is presented in Appendix D. The thermodynamic and transport properties of R-114 are given in Appendix E.

C. RANGE OF PARAMETERS COVERED BY THE TESTS

Flow Regimes

Number of Runs (Excluding Summary Runs): 207 (Tabulated in Appendix F).

Boiling Temperatures, °F: 110, 150, 200, and 250.

Mass Fluxes, lbm/hr-sq ft:

At 110°F: $0.113 \times 10^6 \leq G \leq 3.59 \times 10^6$
At 150°F: $0.111 \times 10^6 \leq G \leq 3.30 \times 10^6$
At 200°F: $0.115 \times 10^6 \leq G \leq 0.95 \times 10^6$
At 250°F: $0.257 \times 10^6 \leq G \leq 1.00 \times 10^6$

Qualities:

At 110°F: $0.0013 \leq x \leq 0.9247$
At 150°F: $0.0020 \leq x \leq 0.9023$
At 200°F: $0.0119 \leq x \leq 0.9001$
At 250°F: $0.1240 \leq x \leq 0.5991$

Pressure Drop

Number of Runs:

Below Critical Heat Flux: 710 (Tabulated in Appendix F).
Above Critical Heat Flux: 121

Boiling Temperatures, °F: 100, 150, 200, and 250.

Mass Fluxes, lbm/hr-sq ft:

At 100°F: $G \approx 0.12, 0.24, 0.47, 0.90, 1.77 \times 10^6$
At 150°F: $G \approx 0.12, 0.24, 0.44, 0.87, 1.70, 3.44 \times 10^6$
At 200°F: $G \approx 0.12, 0.24, 0.92, 1.70, 3.42 \times 10^6$
At 250°F: $G \approx 0.47, 0.97 \times 10^6$

Note: No differentiation is made here between natural and forced circulation runs.

Qualities:

At 100°F: $0.000 \leq x \leq 1.036$
At 150°F: $0.000 \leq x \leq 1.019$
At 200°F: $0.010 \leq x \leq 1.042$
At 250°F: $0.017 \leq x \leq 0.350$

Heat Transfer Coefficients

Number of Runs:

Below Critical Heat Flux: 445 (Tabulated in Appendix F).

Boiling Temperatures, °F: 100, 150, and 200.

Mass Fluxes, lbm/hr-sq ft:

At 100°F: $G \approx 0.12, 0.23, 0.45, 0.89 \times 10^6$
At 150°F: $G \approx 0.14, 0.24, 0.44, 0.90, 1.73, 3.43 \times 10^6$
At 200°F: $G \approx 0.13, 0.25, 0.45, 0.90, 1.72, 3.48 \times 10^6$

Note: No differentiation is made here between natural and forced circulation runs.

Qualities:

At 100°F: $0.004 \leq x \leq 0.932$
At 150°F: $-0.008 \leq x \leq 0.745$
At 200°F: $0.012 \leq x \leq 0.699$

Critical Heat Flux

Number of Runs: 150 (Tabulated in Appendix F).

Boiling Temperatures, °F: 100, 150, 200, and 250.

Mass Fluxes, lbm/hr-sq ft:

At 100°F: $G \approx 0.12, 0.235, 0.46, 0.92 \times 10^6$
At 150°F: $G \approx 0.12, 0.23, 0.45, 0.89, 1.70 \times 10^6$
At 200°F: $G \approx 0.13, 0.24, 0.46, 0.92, 1.70 \times 10^6$
At 250°F: $G \approx 0.26, 0.48, 0.97 \times 10^6$

CHAPTER IV

RESULTS AND DISCUSSION

A. FLOW REGIMES

Introduction

Flow regime observations were made in the ranges described in Chapter III, Section C. A total of 207 runs were analyzed. Whereas no definitive set of flow regimes and regime definitions has been formulated to date, the following regime delineations will be used. They not only adequately cover the different observations made in this study, but for the most part conform with the terminology used by many of the previous experimenters:

(1) Bubbly Flow

(2) Bubbly-Slug Flow

(3) Transition

(4) Weak Annular

(5) Strong Annular--Mist

In addition to these five, numerous runs yielded regimes which could not be identified. The conditions under which non-identifiable regimes occurred will be discussed later and some explanations will be offered.

Bubbly Flow. The bubbly flow regime is that regime in which individual discrete bubbles of vapor of a diameter considerably smaller than the tube diameter are present and are completely surrounded by liquid.

Bubbly-Slug Flow. The bubbly-slug flow regime is that regime in which a combination of small bubbles (diameters considerably smaller than the tube diameter) and large bubbles or slugs (diameters approximately

the same as the tube diameter) appear simultaneously in the flow. Usually, the small bubbles are in the wake of vapor slugs. An example of bubbly flow is shown in Figure IV-1. Bubbly-slug flow can be seen in Figures IV-2 and IV-3.

Transition Flow. The transition flow regime occurs between bubbly or bubbly-slug and annular flow. In this unsteady regime, the flow is seen to alternate between bubbly and annular. Great turbulence exists in the flow with the possibility at low mass fluxes of flow reversal in some of the liquid eddies. While this behavior of the two-phase flow mixture was considered a flow regime in itself, it could possibly have been regarded as a transition between two different flow regimes. This is illustrated in Figure IV-4.

Weak Annular Flow. The weak annular flow regime is that regime where there is a separation between the two phases with a vapor core in the center surrounded by a liquid film. The liquid-vapor interface is however quite rough with the liquid waves in certain rare instances bridging the gap across the tube diameter. This is shown in Figure IV-5.

Strong Annular-Mist Flow. In the strong annular flow regime the liquid and vapor phases are more distinctly separated. While the interface is much smoother, some ripples do exist. Also, the liquid film on the wall is generally thin. In the mist flow regime, liquid droplets are entrained in and are carried along by the vapor that has otherwise completely filled the tube. Generally, the annular-mist flow regime is believed to exist also. In this case, the vapor core in

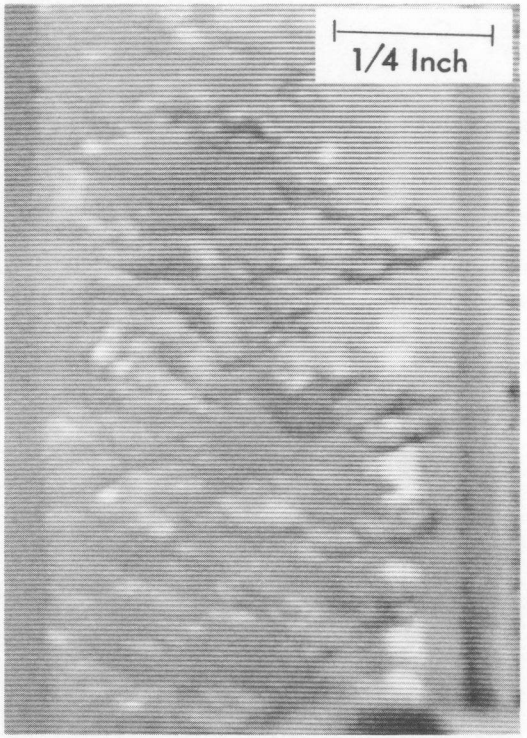


Figure IV-1. BUBBLY FLOW.



Figure IV-2. BUBBLY-SLUG FLOW (ROUND SLUG).



Figure IV-3. BUBBLY-SLUG FLOW (SLUG WITH BULLET-SHAPED NOSE).

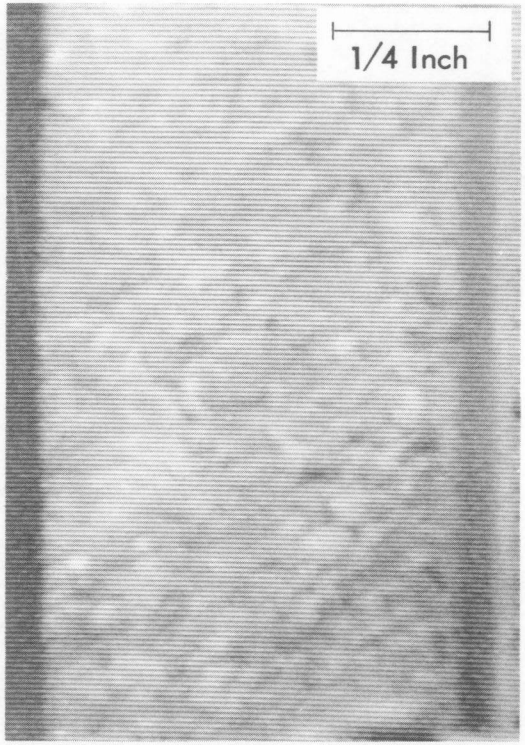


Figure IV-4. TRANSITION FLOW.

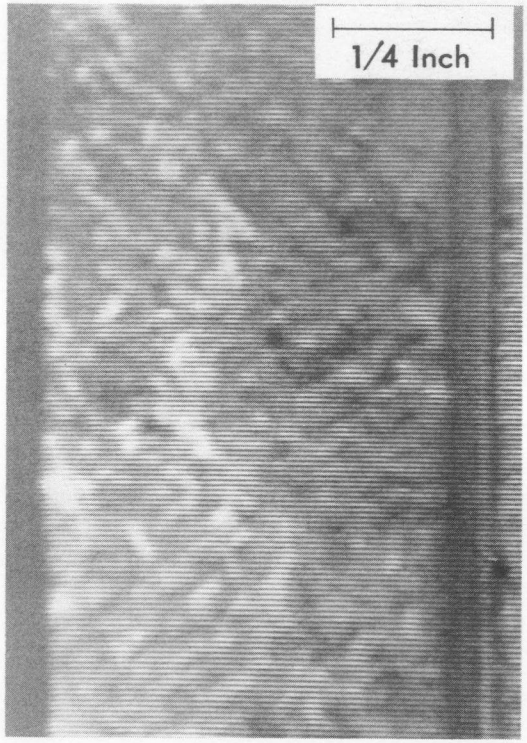


Figure IV-5. WEAK ANNULAR FLOW.

annular flow contains liquid droplets which were sheared from the waves at the liquid-vapor interface. This was visually confirmed only when very thin liquid films existed because only then was the film sufficiently transparent to allow the observation of the high speed liquid particles. When the film on the wall dried up, in all cases mist flow was observed. An example of strong annular flow is shown in Figure IV-6. Mist flow is illustrated in Figure IV-7. Note the liquid droplets in the vapor stream.

Numerous runs were made where the regime was unidentifiable. This generally occurred at all high velocity runs regardless of boiling temperature. It became more widespread however as the boiling temperature increased until at the 250°F boiling temperature, it was found to occur at all flow rates including some of the lowest tested. The reason that the regime was unidentifiable was that the two-phase mixture became opaque. It began to take on the appearance of a frothy, whitish liquid. This could possibly have been due to vigorous mixing of the liquid and vapor phases resulting in a homogeneous mixture. At high flows one would generally expect a two-phase mixture to take on some of the characteristics of homogeneous flow and the pressure drop results to be presented in a later section will also indicate this trend. Also, at the 250°F boiling temperature, the liquid and vapor densities are rapidly approaching each other. This facilitates mixing between the two phases.

Experimental Results

The results of the 207 runs made are given in Figures IV-8 to IV-11 for boiling temperatures of 110, 150, 200, and 250°F,

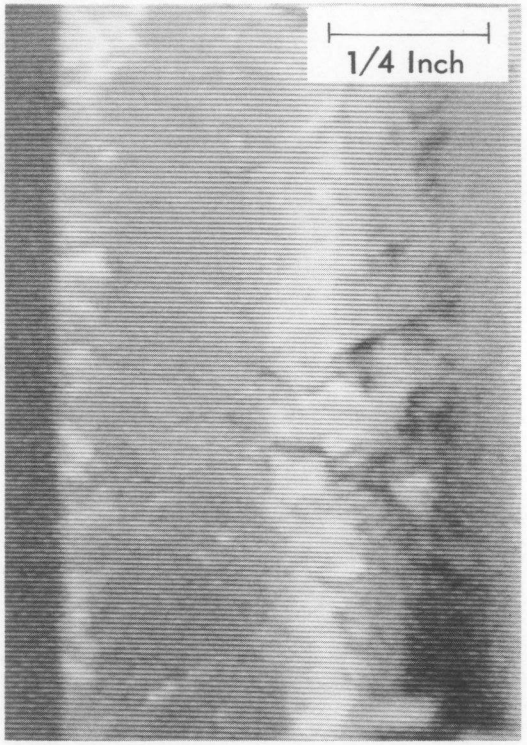


Figure IV-6. STRONG ANNULAR FLOW.

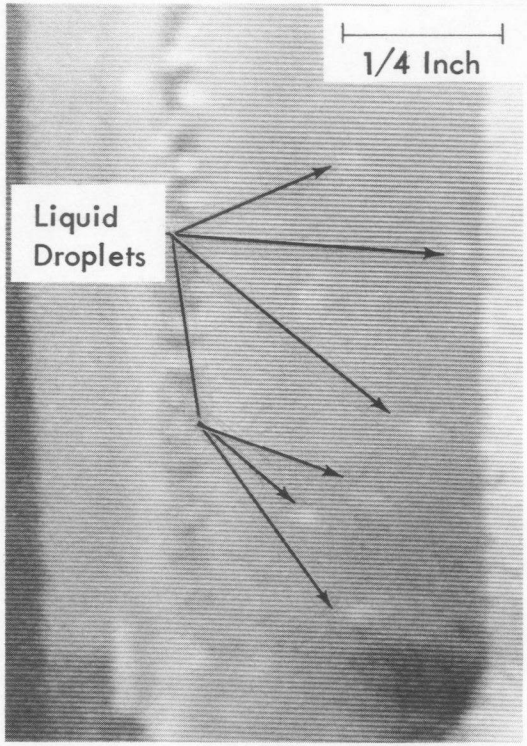


Figure IV-7. MIST FLOW.

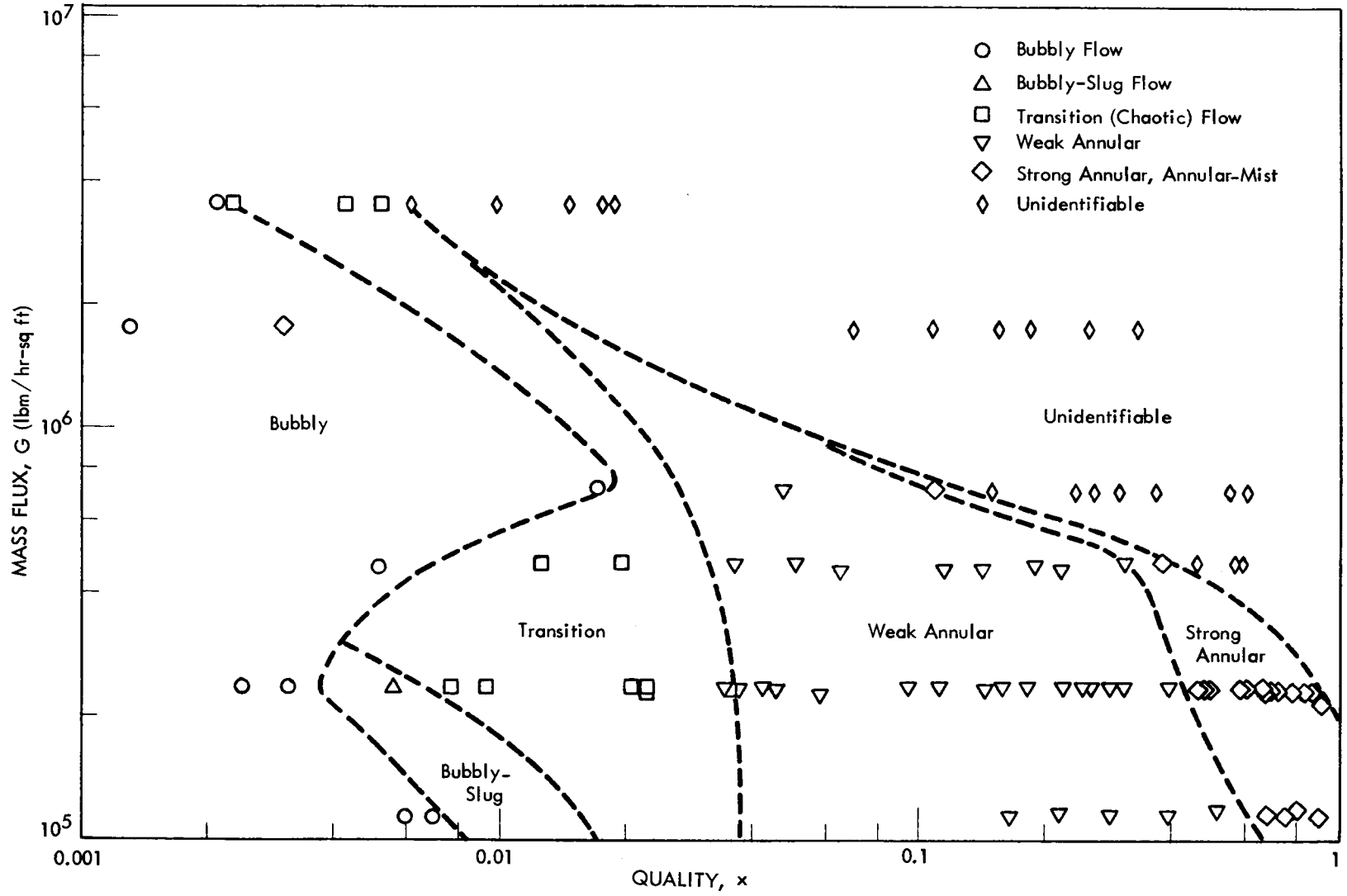


Figure IV-8. EXPERIMENTAL FLOW REGIME MAP FOR R-114 AT 110°F.

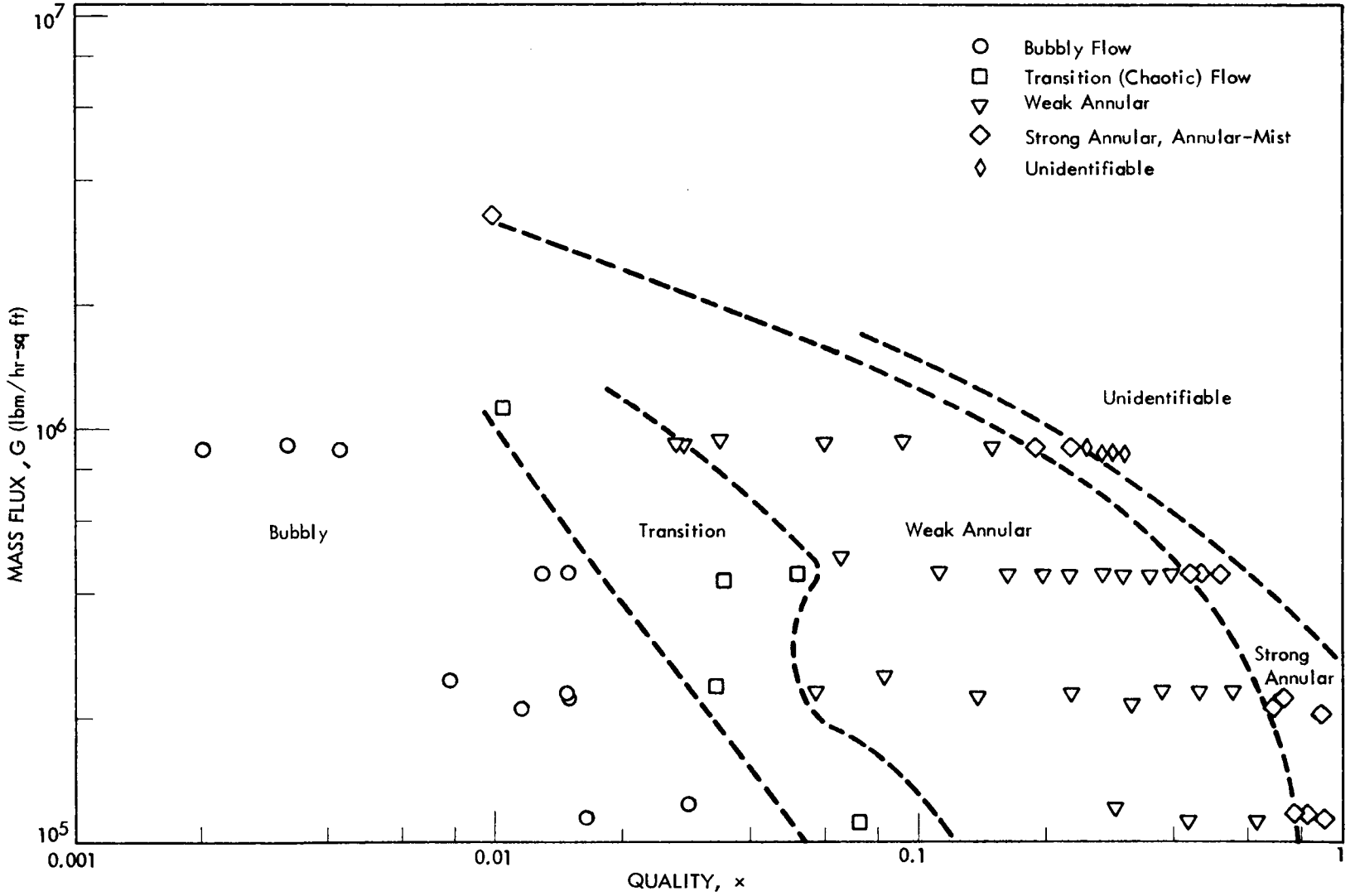


Figure IV-9. EXPERIMENTAL FLOW REGIME MAP FOR R-114 AT 150°F.

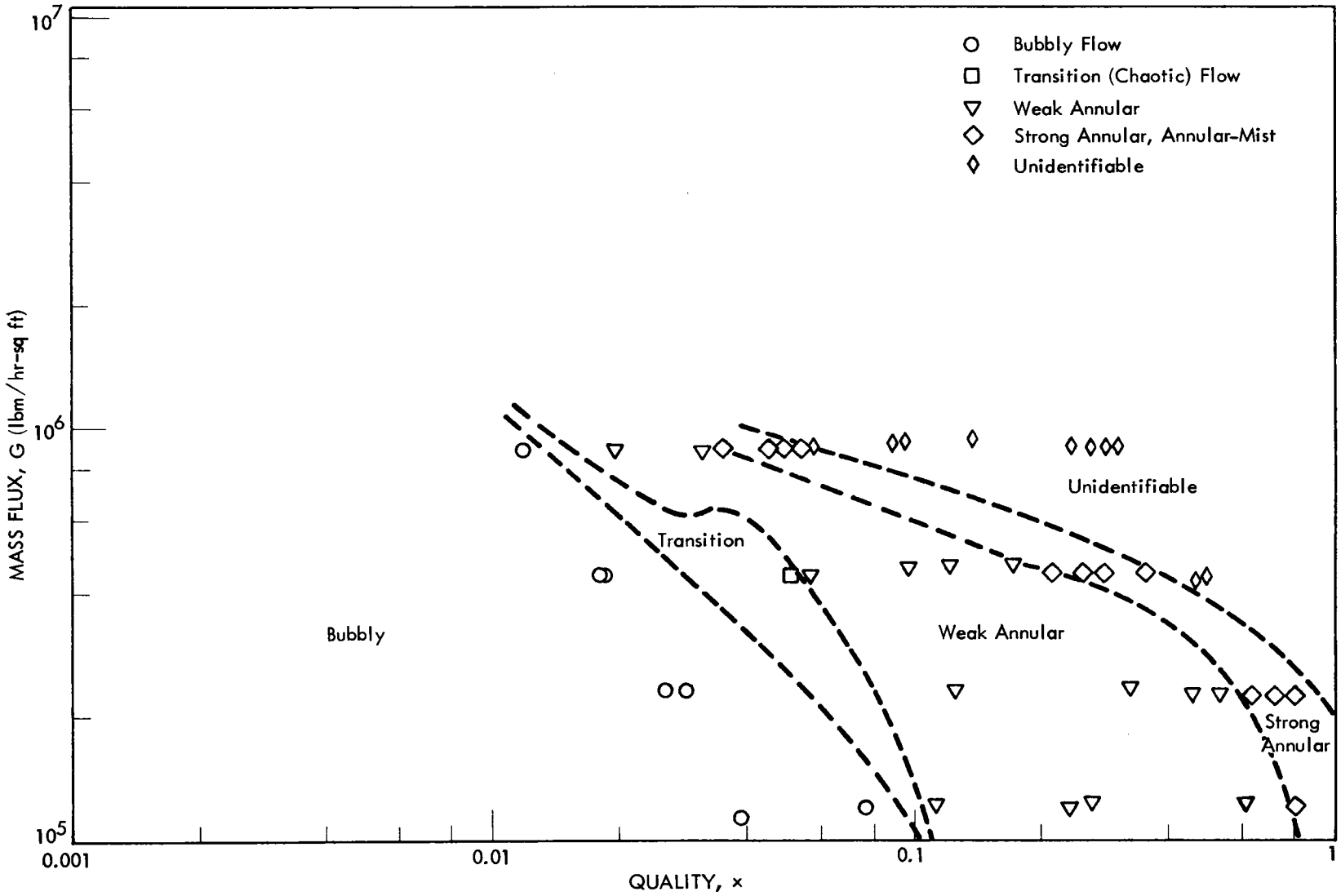


Figure IV-10. EXPERIMENTAL FLOW REGIME MAP FOR R-114 AT 200°F.

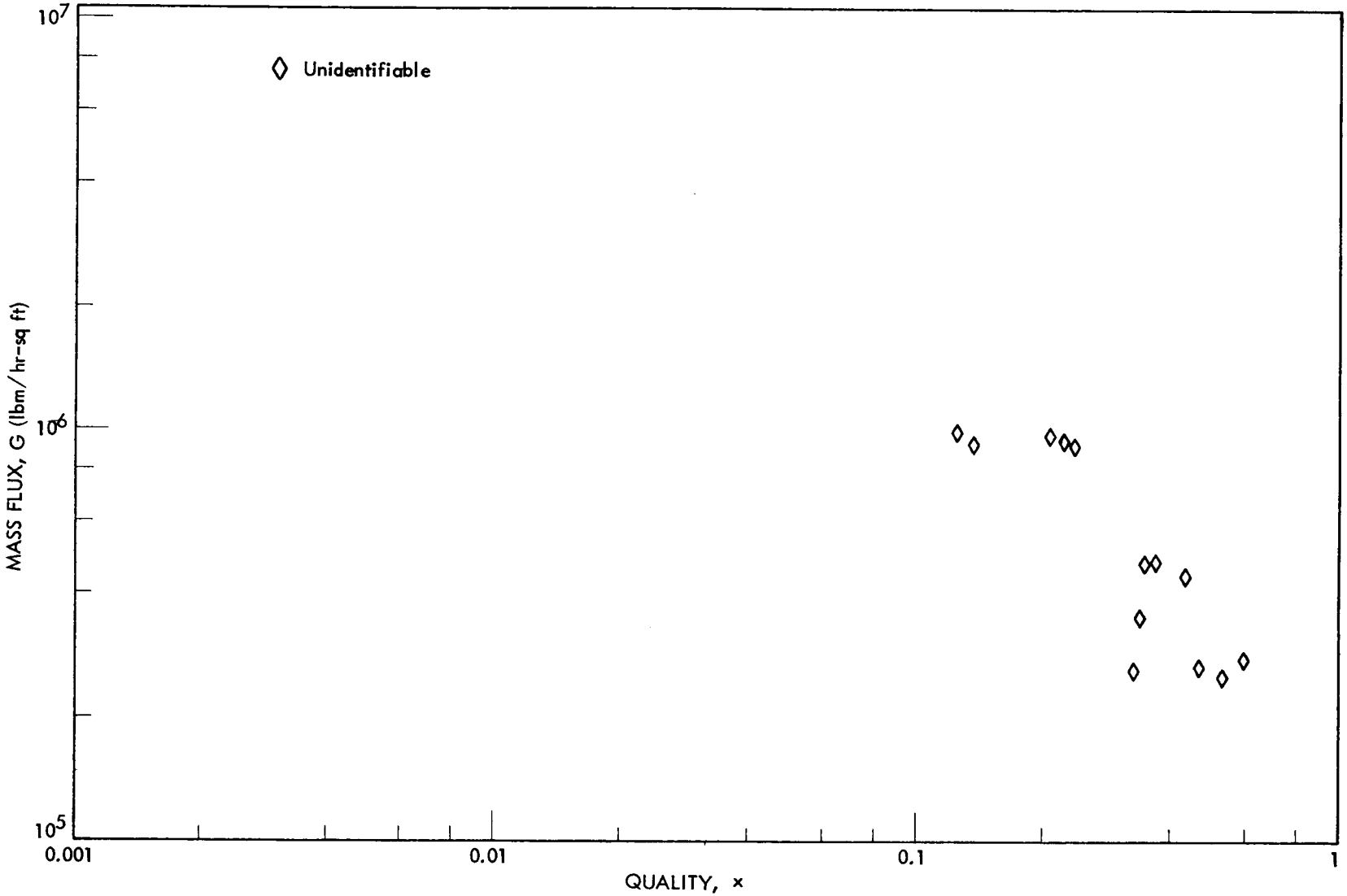


Figure IV-11. EXPERIMENTAL FLOW REGIME MAP FOR R-114 at 250°F.

respectively. From the graphs, the following general comments can be made.

(1) The bubbly-slug flow regime was found to occur only at the 100°F boiling temperature and then only at mass flux values of less than approximately 0.3×10^6 lbm/hr-sq ft.

(2) As the flow rate was increased, while the boiling temperature was kept constant, there was a decrease in the size of the bubbly and weak annular flow regime. There were corresponding increases in the strong annular flow regime and the region of unidentifiable flow.

(3) As the boiling temperature was increased while the flow rate was kept constant, the range of the bubbly flow regime was found to increase significantly. The other flow regimes were each found to correspondingly shrink a bit.

(4) No discernable change in the flow pattern was noted as the critical heat flux occurred. While numerous observers have attributed the critical heat flux to the dryout of the liquid film on the wall and the formation of a dry patch or possibly to the formation of a vapor bubbly layer between the tube wall and fluid, no such phenomenon was observed in the present tests. This could be attributed to the fact that, strictly speaking, in the present tests, the flow observations were made in the adiabatic portion of the system immediately downstream of the test section. Any dry patches that may have formed on the copper tube probably disappeared in the Pyrex glass flow visualization section. Not only was there no heat input into the fluid in this region, there was a small loss of heat to the ambient air. Also, any layer of bubbles forming on the copper surface may have been completely swept into the

mainstream of the flow by the time that fluid reached the Pyrex glass test section. This behavior was noted by Hsu and Graham [9]. As a result, no claims to flow regime transformation as a result of CHF can be made on the basis of the present study.

(5) No effect of adiabatic vs. diabatic boundary condition was noted on the flow regimes or on the transition points between flow regimes. The runs made at a boiling temperature of 110°F and a mass flux of 0.23×10^6 lbm/hr-sq ft were divided into two groups. In one group, the zone or zones immediately below the Pyrex glass visualization test section were used to supply all the heat. In the other group, all heating was done by the preheater or by the heaters in the first two or three zones so that a distance of at least 100 L/D ratios lay between the heated wall and the flow visualization section. In all these tests, particular attention was paid to the location of the transition points between the various flow regimes. On the basis of these tests, no difference was observed between the two groups despite the fact that Bergles, Lopina, and Fiori [13] pointed out that any effect of a diabatic boundary condition on the flow regime would have been particularly observable at low boiling temperatures. Of course the same reasoning used in (4) above can be applied here and it can be pointed out that the Pyrex glass test section in use here actually constituted an adiabatic boundary condition. Zuber et al [10] made some interesting observations regarding the effect of heat flux on the nucleation in the annular flow regime. Using high speed motion pictures, they were able to observe that bubbles were locally generated at the wall and that they did "empty themselves" into the vapor core. The extent of

the bubble nucleation depended on numerous factors in addition to the magnitude of the heat flux. This observation is at odds with the conclusions of numerous other studies which claimed that no bubble nucleation was observed in the annular flow regime. Most of these conclusions were however based on observations made with the naked eye. The existence of locally generated bubbles at the wall is important both with regard to the analysis of burnout, as well as the correct formulation of the heat transfer mechanism in the annular flow regime.

Discussion

The 110°F boiling runs. From the "summary" runs made, as well as from the individual runs plotted in Figure IV-8 on page 128, the following brief descriptions of the various flow regimes can be made:

(a) $G \approx 0.12 \times 10^6$ lbm/hr-sq ft: When the fluid was heated to the saturation temperature, individual bubbles began to appear. They were fairly large, some as large as 1/4 in. Unlike what one is usually accustomed to seeing in water, the bubbles were not spherical in shape. They tended to be ellipsoidal and/or odd-shaped, sometimes even exhibiting an upward concavity. In some cases, these large bubbles fractured into two smaller bubbles. This behavior was attributed to the low surface tension of R-114. As the heat flux was further increased, the quality at the visualization test section increased also, resulting in a higher void fraction and a corresponding increase in the two-phase velocity. This caused a decrease in the size of the bubbles and an increase in the number of bubbles. At a quality of approximately 1%, slugs of vapor started to appear. These slugs were of approximately the same diameter as the tube. They were rarely more than 1-1/2 in. long and

seldom had a bullet-shaped nose. An example of non-spherical bubbles is given in Figure IV-12. A typical vapor slug is shown in Figure IV-13. A rare bullet-shaped slug can be seen in Figure IV-14 where three consecutive video tape frames are depicted. The large number of small bubbles in the wake of each slug is worth noting. Quite possibly the high degree of turbulence in the wake of a vapor slug caused the fracture of the succeeding slug. As the quality was increased, the slugs appeared with greater frequency. Eventually, this flow pattern completely broke down into a chaotic mixture of liquid and vapor. Eddies of liquid were seen to move in a direction opposite to the main flow. The flow was also seen to transform to weak annular and back to bubbly-slug flow. Numerous observations of the video tape did not lead to any insight into the breakdown mechanism. It was however hypothesized that with increasing frequency, the liquid portion separating the end of one slug from the next became thinner until finally, when a sufficiently small thickness was obtained, this film was unable to bridge the cross-sectional area of the tube due to the low surface tension of R-114. With increasing quality, the transition flow regime began to take on a more orderly appearance with the vapor forming a core surrounded by a liquid film. The evolution from the transition flow regime to the weak annular regime was a gradual one. The existence of an interface between the liquid and vapor phases in weak annular flow was, however, obvious. At first, this film was quite thick and the interface rough. With increasing quality, the large velocity difference between the liquid and vapor phases caused most of the crests in the liquid waves to be sheared off and entrained in the vapor. Eventually, a considerably smoother interface was observed. This was called the strong annular flow regime.

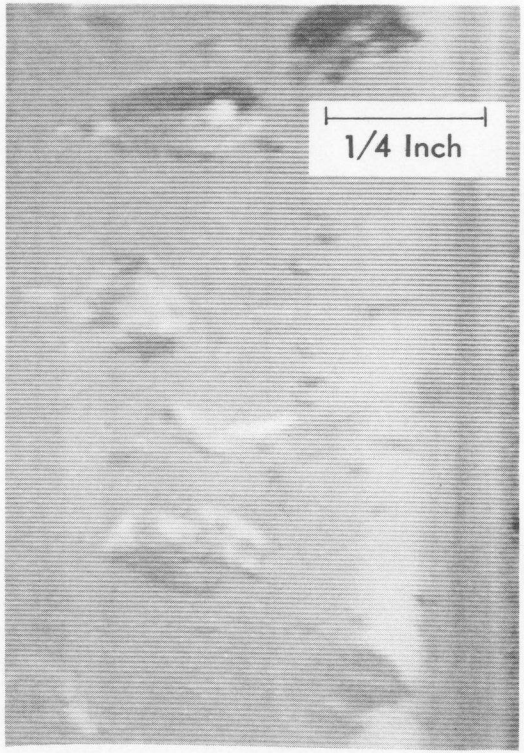


Figure IV-12. ILLUSTRATION OF THE NONSPHERICAL SHAPE OF BUBBLES IN BUBBLY FLOW.

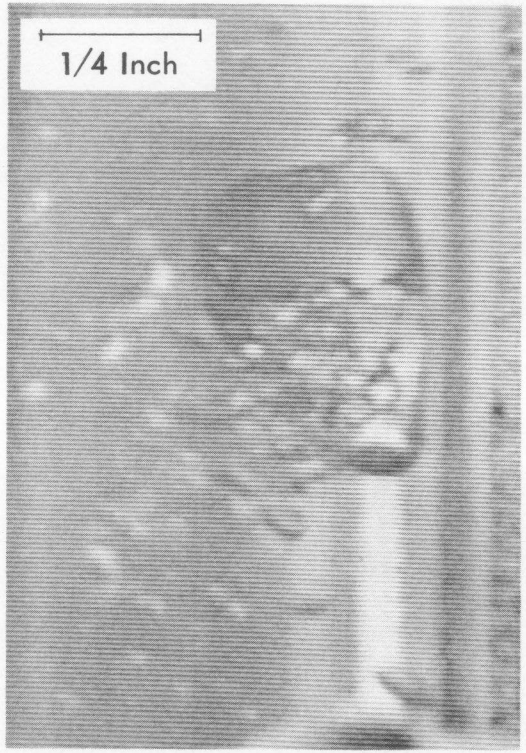


Figure IV-13. TYPICAL SIZE OF VAPOR SLUG IN BUBBLY-SLUG FLOW.

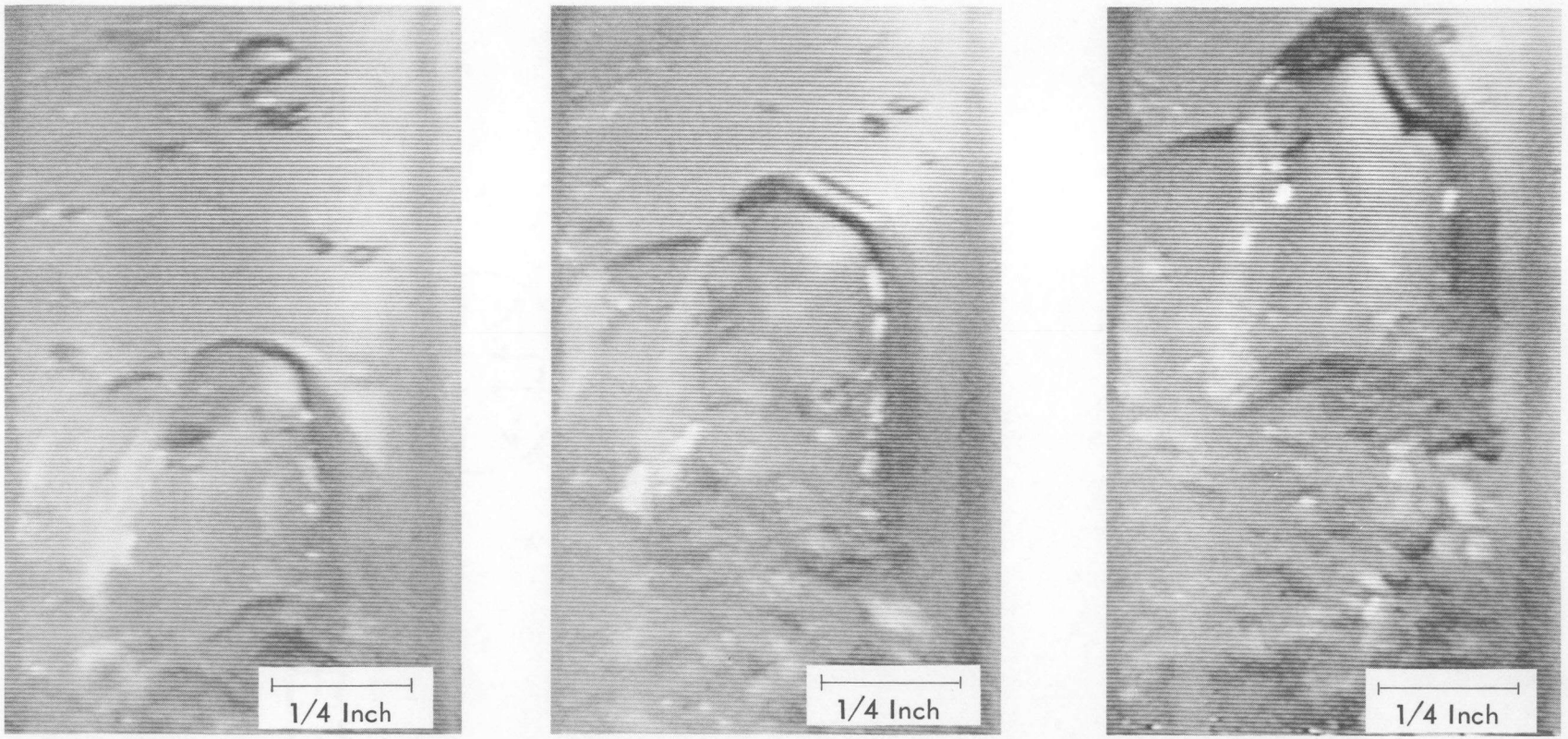


Figure IV-14. THREE CONSECUTIVE FRAMES FROM VIDEO TAPE DEPICTING VAPOR SLUG IN BUBBLY-SLUG FLOW.

The location of the transition point necessarily entailed a value judgment and various transition points may have been selected by different observers. The interface in strong annular flow while considerably smoother, still had small ripples. As the quality increased further, the liquid film on the wall became thinner and therefore more transparent. It eventually became possible to see the droplets in the vapor stream. These high velocity particles were easily observable since light was reflected from their surface. At higher qualities, the film on the wall became increasingly thinner and eventually disappeared, leaving a pure mist flow. With increasing heat flux, the droplets became fewer in number until they finally disappeared and only single phase vapor remained.

(b) $G \approx 0.23 \times 10^6$ lbm/hr-sq ft: The behavior of the flow regimes at this mass flux were identical to those at $G \approx 0.12 \times 10^6$ lbm/hr-sq ft with one exception. At the very high qualities (in the CHF region), the liquid film on the wall was seen to turn opaque and the flow regime was no longer identifiable. This regime was however very short-lived before pure mist flow occurred.

(c) $G \approx 0.46 \times 10^6$ lbm/hr-sq ft: In the bubbly flow regime, the bubble sizes encountered were quite a bit smaller than those observed in (a) or (b) above. In addition, the bubbly-slug regime completely disappeared. In the bubbly flow regime, the number of bubbles was seen to increase until the entire tube was filled with them. The regime was then seen to change, due possibly to the breakdown of the liquid film between the bubbles and the occurrence of coalescence. Again, in this case, an unidentifiable region where the flow became

frothy and opaque was observed. It occurred at a considerably lower quality than in (b) above.

(d) $G \approx 0.7 \times 10^6$ lbm/hr-sq ft: In the bubbly flow regime, the bubbles were found to be even smaller than those observed at the lower mass fluxes. This is shown in Figure IV-15. A slight change was also seen to occur in the transition regime. No longer were the eddies moving in a haphazard fashion and sometimes reversing their flow. They now all moved continuously in the upward direction and at a considerably higher velocity. The region of opaque flow occurred at an even lower quality.

(e) $G \approx 1.7 \times 10^6$ lbm/hr-sq ft: The bubbles in the bubbly flow regime were a bit smaller than those in (d). Apparently there is a lower limit to bubble size and it was being approached in these runs. The unidentifiable opaque regime was prominent in a considerably wider portion of the quality range. An example of this opaque region is shown in Figure IV-16.

The 150 and 200°F boiling runs. The flow regimes occurring were identically the same as those observed at the 110°F boiling temperature with the exception that the bubbly-slug flow regime never occurred. Also bubbles as large as those in (a) above were not observed. The largest bubbles seen were of approximately the same size as those noted in (b) above. Differences in the qualities at which regime transitions occurred and the breadth of the individual flow regimes was different for each temperature as can be observed in Figures IV-9 and IV-10 on pages 128 and 129.

The 250°F boiling run. Although the rather limited amount of information given in Figure IV-11 on page 131 indicated that the unidentifiable

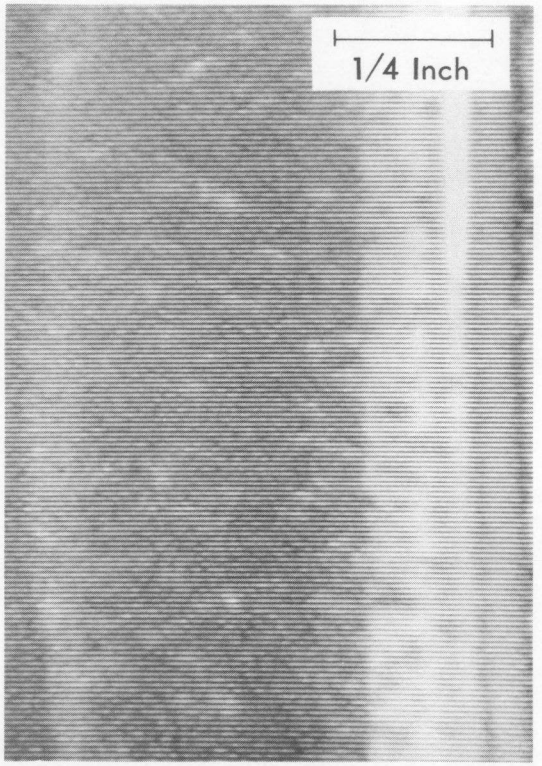


Figure IV-15. EXAMPLE OF THE BUBBLE SIZES OCCURRING IN BUBBLY FLOW AT HIGH MASS FLUXES.

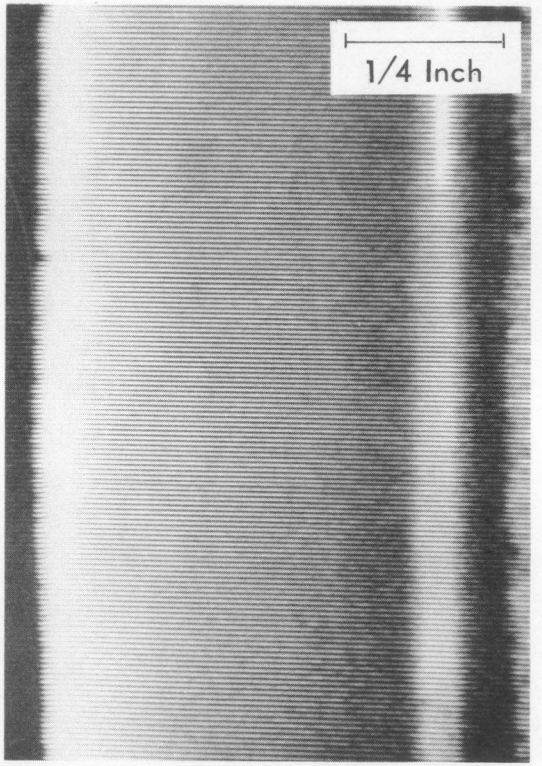


Figure IV-16. ILLUSTRATION OF THE UNIDENTIFIABLE FLOW REGIME.

opaque regime existed over a wide range of operating conditions, the "summary" runs taken at this temperature yielded additional information on the flow regimes. At low qualities, a bubbly flow regime of considerable size existed. The bubbles were quite small, even at low flow rates. A change to the transition flow regime took place only when the flow visualization section contained a very large number of these small bubbles. Beyond the transition region, only a small annular flow regime occurred before the two-phase flow became opaque.

Comparison With Other Flow Regime Studies

Based on the studies Hosler [14] made with steam-water mixtures, as discussed in the literature survey, the Quandt [7] analysis and the Baker [5] map gave the most reasonable agreement with experimental results. A comparison of the present R-114 results with the Baker [5] and Quandt [7] predictions is presented in Figures IV-17 through IV-24.

The Baker [5] map in general, did not satisfactorily predict the flow regimes at any of the boiling temperatures. A much broader bubbly flow regime was predicted than actually existed. This was especially true at the higher boiling temperatures. The trend of a larger bubbly flow regime with increasing boiling temperature was correctly predicted by Baker [5]. His assertion of a lower mass flux limit on the bubbly flow regime was however not in agreement with the present data. No lower limit was observed in the mass flux range investigated in this study. It is worth noting that the same discrepancies were noted between the Baker [5] plot and the experimental flow regimes of Hosler [14] with steam-water. This was shown in Figure II-5 on page 22.

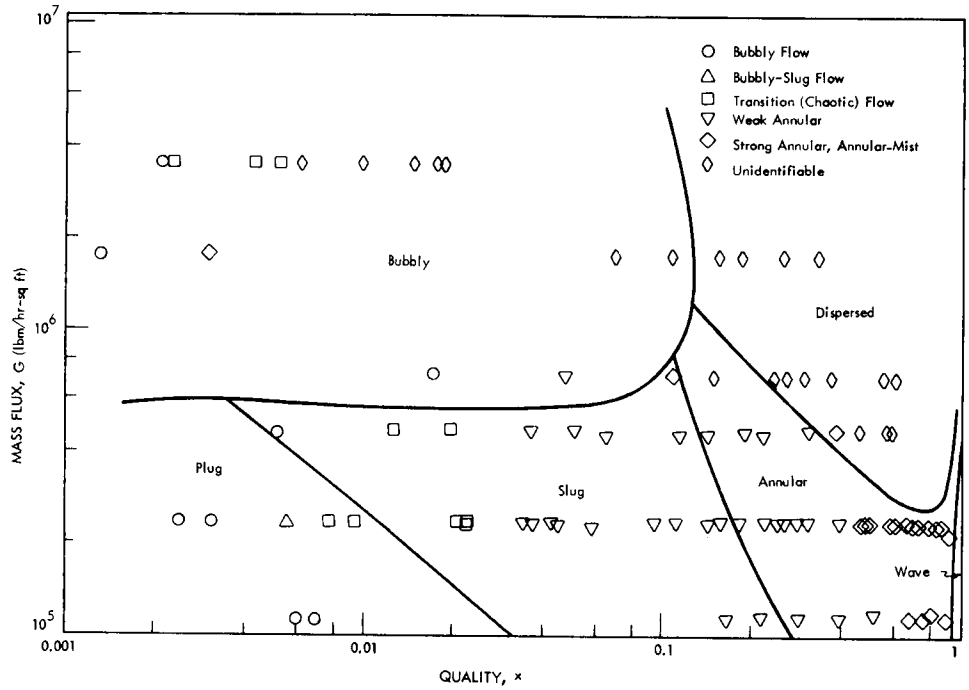


Figure IV-17. COMPARISON OF EXPERIMENTAL AND BAKER [5] FLOW REGIME MAPS, T≈110°F.

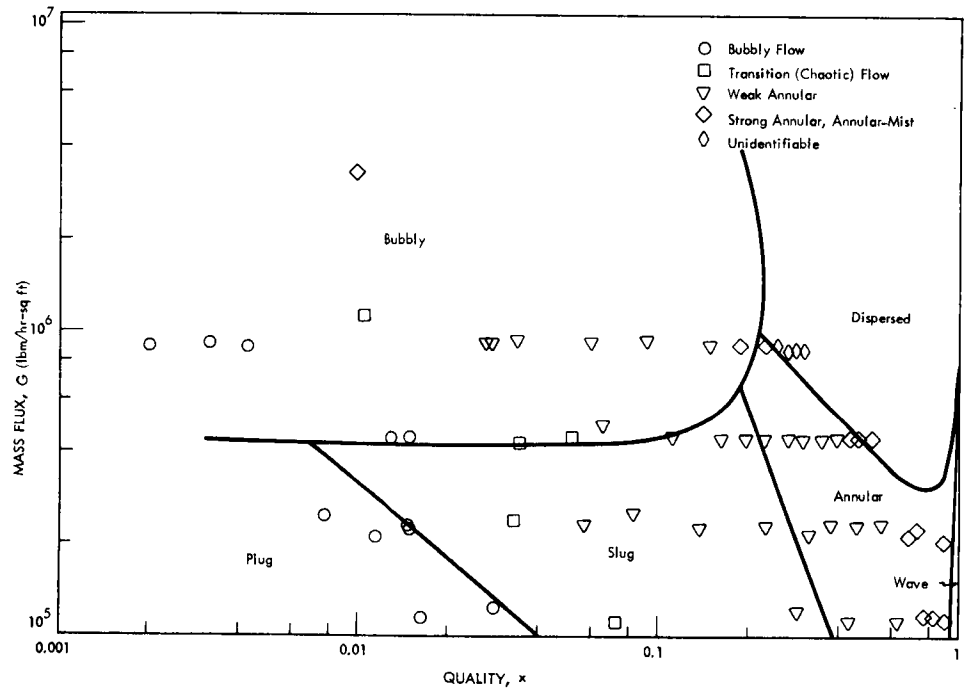


Figure IV-18. COMPARISON OF EXPERIMENTAL AND BAKER [5] FLOW REGIME MAPS, T≈150°F.

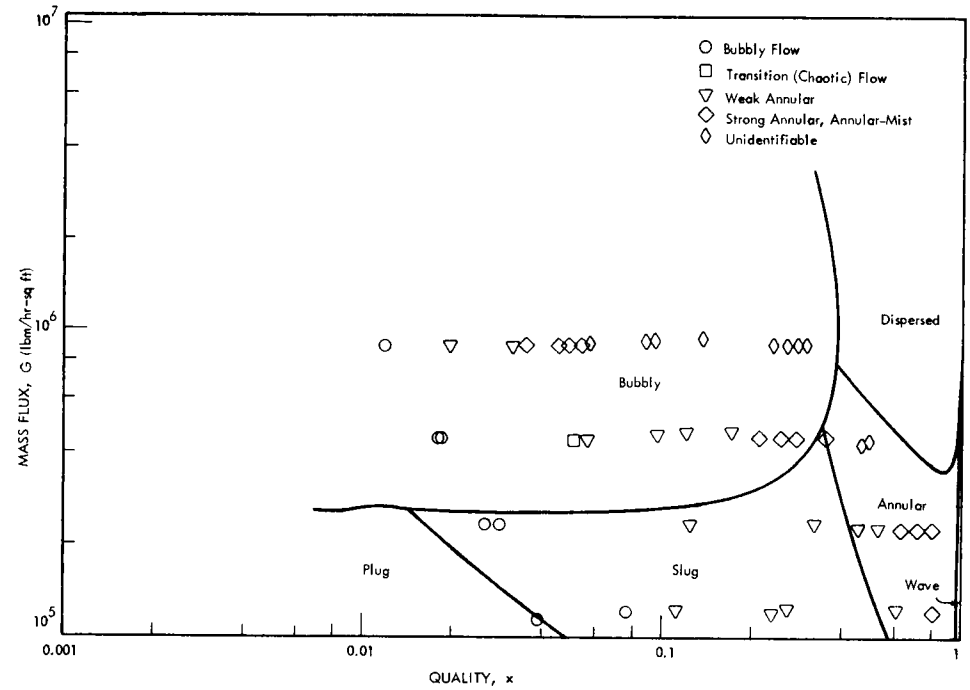


Figure IV-19. COMPARISON OF EXPERIMENTAL AND BAKER [5] FLOW REGIME MAPS, T ≈200°F.

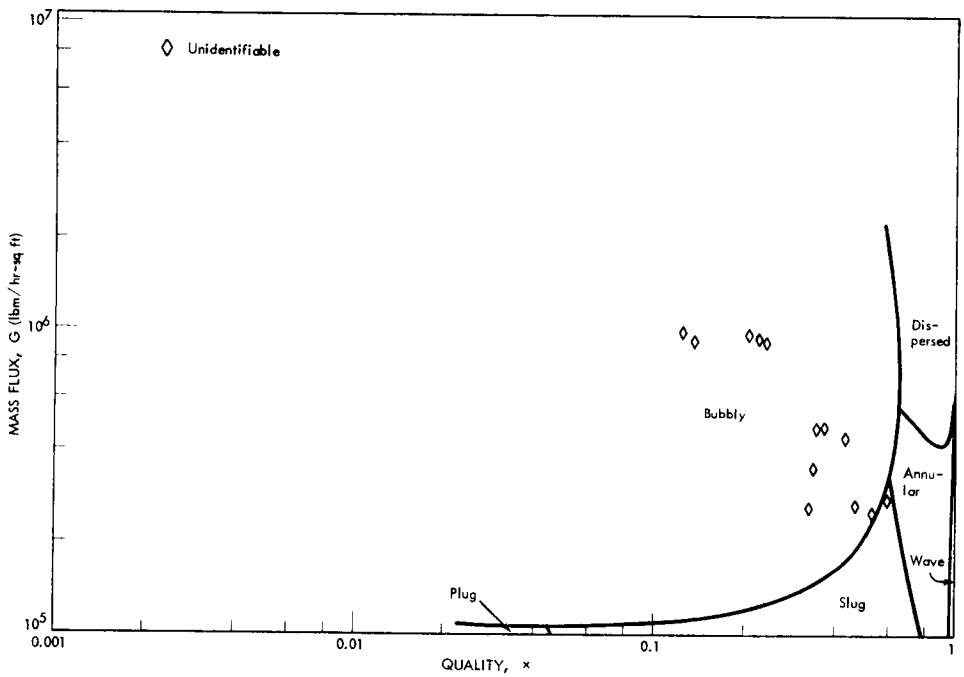


Figure IV-20. COMPARISON OF EXPERIMENTAL AND BAKER [5] FLOW REGIME MAPS, T ≈250°F.

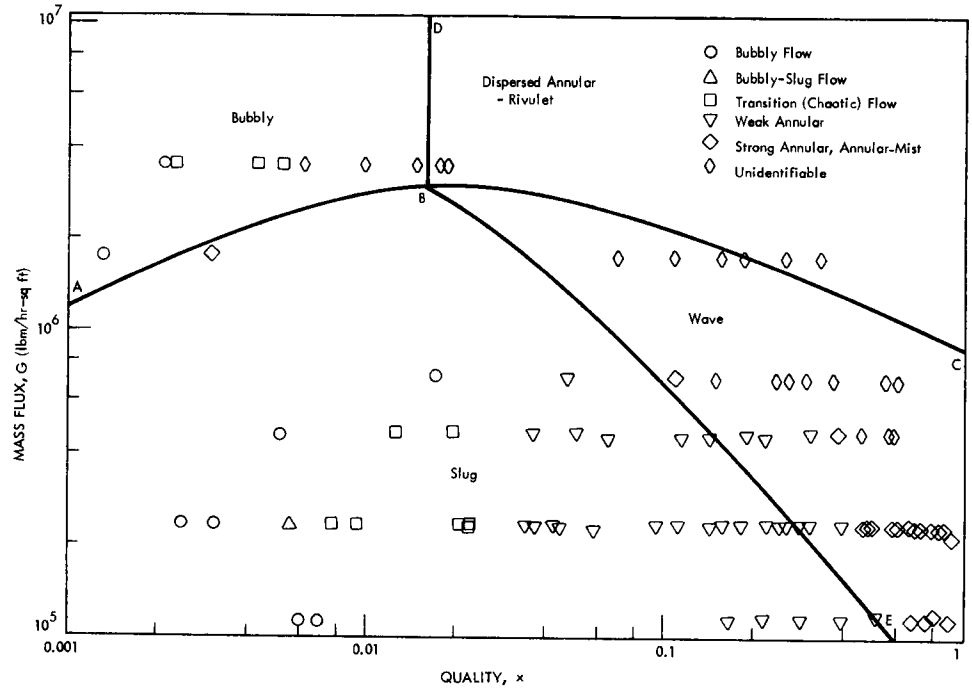


Figure IV-21. COMPARISON OF EXPERIMENTAL FLOW REGIME MAP AND QUANDT [7] ANALYSIS, T ≈ 110°F

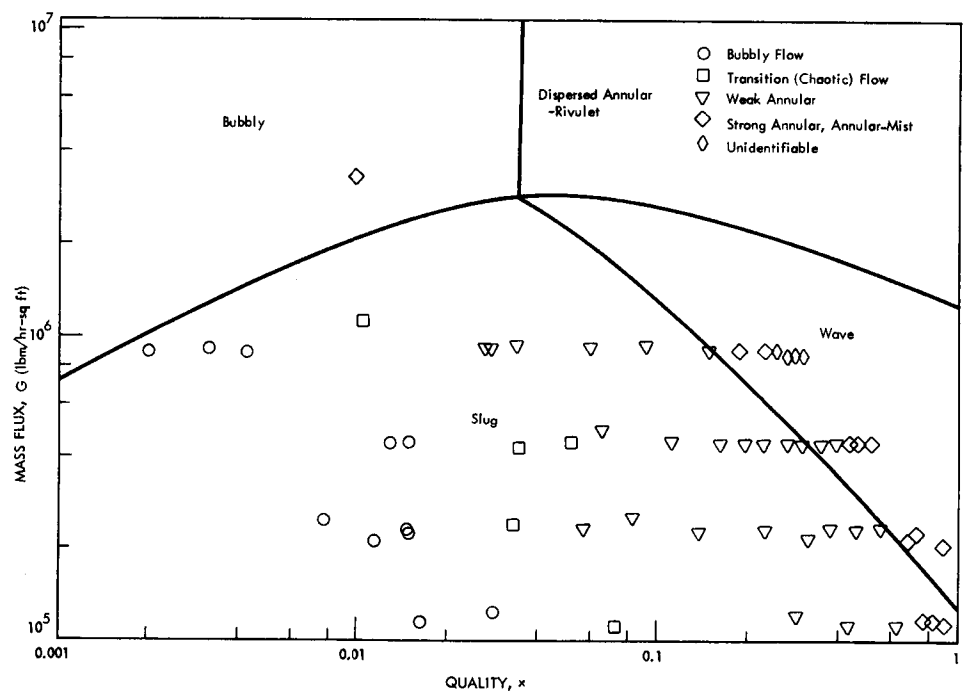


Figure IV-22. COMPARISON OF EXPERIMENTAL FLOW REGIME MAP AND QUANDT [7] ANALYSIS, T ≈ 150°F

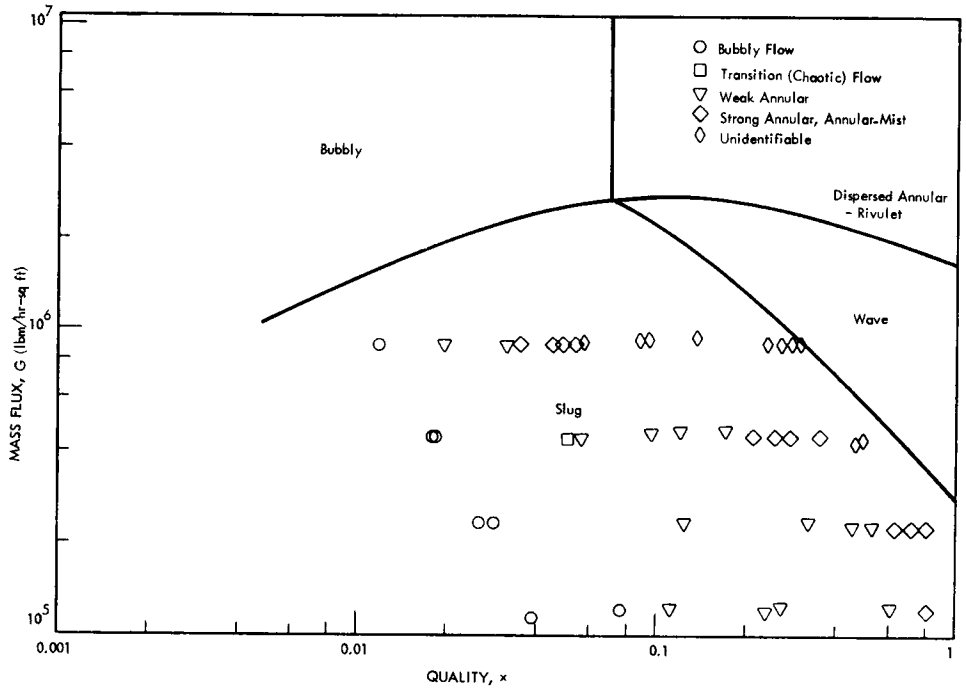


Figure IV-23. COMPARISON OF EXPERIMENTAL FLOW REGIME MAP AND QUANDT [7] ANALYSIS, T≈200°F

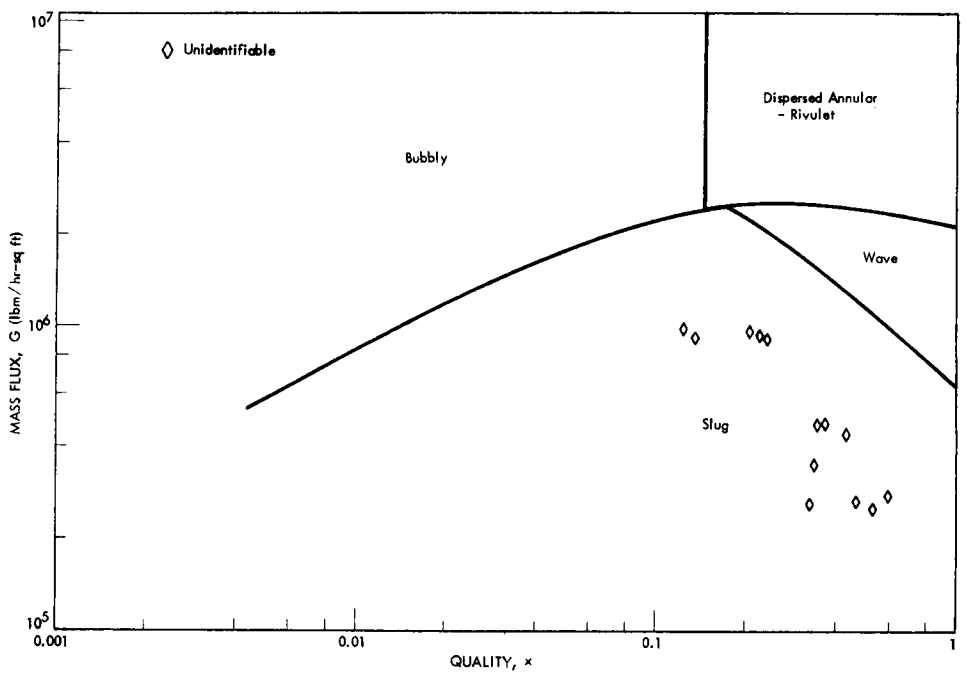


Figure IV-24. COMPARISON OF EXPERIMENTAL FLOW REGIME MAP AND QUANDT [7] ANALYSIS, T≈250°F

The slug flow regime in R-114 was considerably smaller than that predicted by the Baker [5] map. While slug flow was found to occur in only a narrow range for the 110°F boiling temperature case, a wider band was claimed by Baker [5] at all temperature levels. The same discrepancy was noted by Hosler [14] although to a smaller extent.

Combining the annular and dispersed regimes Baker [5] defined, and noting their resemblence to the weak annular and strong annular-mist flow regimes of this study, it is seen that the Baker [5] map underestimated the size of the annular flow regime. The greatest deviations seemed to occur at the higher boiling temperatures. Hosler [14], on the other hand, obtained reasonably good agreement between his annular flow steam-water visualization tests and those predicted by the Baker [5] map. No stratified or plug flow was noted in the present experiments. These may, however, exist in the horizontal flow mode for which the Baker [5] map was originally obtained.

Before comparing the Quandt [7] analysis which was summarized in Figure II-3 on page 15 with the present R-114 flow regime studies, the classification of the various flow patterns will be summarized. At the 110°F boiling temperature, the pressure gradient-controlled region was that part of the map above the line ABC in Figure IV-21. The gravity-controlled portion was below the ABC line. The bubbly flow regime was defined as that portion of the pressure gradient-controlled region where

$$\frac{x}{1 - x} < \frac{\rho_g}{\rho_f} \quad . \tag{4-1}$$

This was represented by the ABD portion of Figure IV-21. In the region where

$$\frac{x}{1 - x} > \frac{\rho_g}{\rho_f} \tag{4-2}$$

dispersed annular or rivulent flow occurred (DBC). The former was associated with a continuous film on the wall with additional liquid droplets entrained in the vapor, while in the latter, the liquid film ceased to be continuous. In the gravity-controlled region

$$Fr_m < \frac{2}{f} \tag{4-3}$$

with f as the single-phase Darcy-Weisbach friction factor, represented the slug flow regime (ABE) while for

$$Fr_m > \frac{2}{f} \tag{4-4}$$

the wave flow regime existed (EBC). With R-114, no case of surface tension-controlled flow existed in the temperature and flow rate ranges investigated here. A sample calculation is given in Appendix D.

On the basis of the comparisons in Figures IV-21 through IV-24 it can be seen that the quality at which transition occurred from bubbly flow to dispersed-annular flow was predicted reasonably well by the Quandt [7] analysis. A lower mass flux limit below which slug flow occurred was however incorrectly predicted. If the bubbly flow regime had been extended to both the gravity and pressure gradient controlled regions, the agreemment would have been considerably improved. The analysis still did not predict the experimentally observed negative slope of the bubbly regime-transition regime boundary. The slug flow regime predicted by Quandt [5] was considerably larger than the one experimentally observed. In addition, the wave regime which corresponded to the weak annular flow regime in this study actually occurred in a slightly different portion of Figures IV-21 through IV-24 than predicted by the Quandt [7] analysis. The dispersed annular-rivulet flow regime which corresponded to the strong annular-mist flow regime in this study did not agree well with experimental observations.

Despite the deivations between the Quandt [7] analysis and the present flow regime observations, it is believed that an extension of this analysis would yield improved results. For example, the Quandt [7] analysis is valid for the case of a fully developed flow field which is uniform over the duct length. This limits the analysis to the case of adiabatic flow--a situation which is somewhat different from the one occurring in this case where a constant addition of heat yielded a continuous change in flow pattern along the length of the tube. In addition, the assumption of a homogeneous mixture of liquid and vapor is not entirely valid for many of these regimes. Thom's [35] work among others, indicated that at low pressures, slip ratios significantly in excess of one do exist. Therefore the addition of an acceleration term to the analysis of the forces on an element of liquid along with the use of the more reasonable separated flow model for the wave, as well as the dispersed annular-rivulet flow regime should enhance the accuracy of this type of analysis.

In contrast to the Baker [5] and Quandt [7] studies which are applicable only for adiabatic flow, Zuber et al [10] boiling R-22 and J. L. L. Baker [17] working with R-11 presented Equations (2-6), (2-8), (2-9), and (2-10) as the boundaries between various diabatic flow regimes. Equation (2-7) represented the transition between slug and annular flow for the adiabatic case. The results of Zuber et al's [10] equation for the transition from churn-turbulent (similar to the transition regime in this study) to annular flow are shown in Figures IV-25 to IV-27 for the 110, 150, and 200°F boiling temperatures, respectively. Agreement with experimental data was not very good. In all cases, a

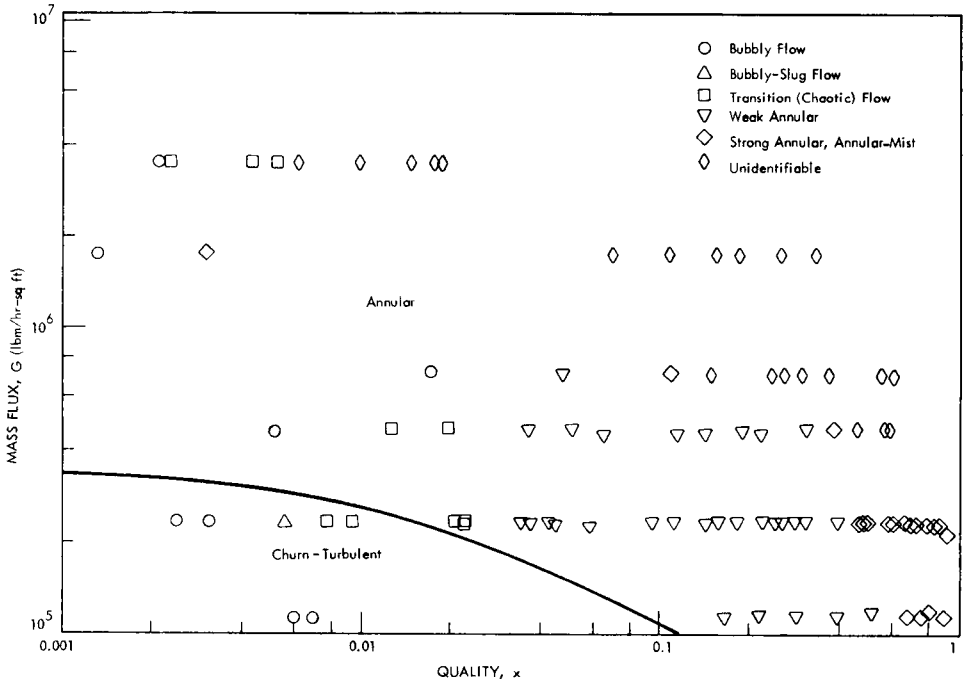


Figure IV-25. COMPARISON OF EXPERIMENTAL FLOW REGIME MAP AND ZUBER ET AL [10] EQUATION FOR THE TRANSITION FROM CHURN-TURBULENT TO ANNULAR FLOW, T≈110°F

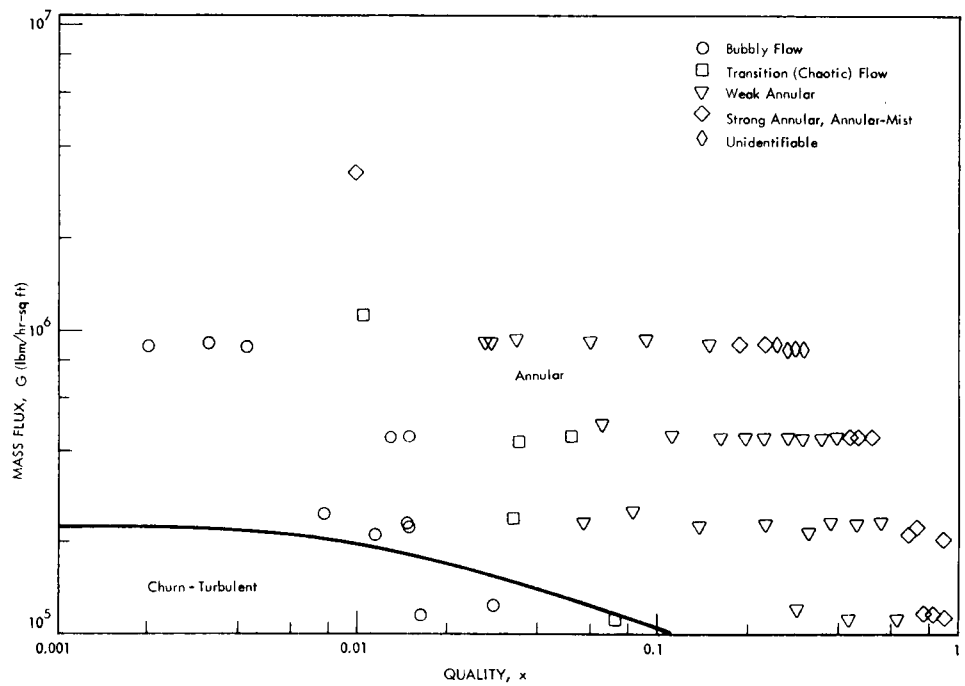


Figure IV-26. COMPARISON OF EXPERIMENTAL FLOW REGIME MAP AND ZUBER ET AL [10] EQUATION FOR THE TRANSITION FROM CHURN-TURBULENT TO ANNULAR FLOW, T≈150°F

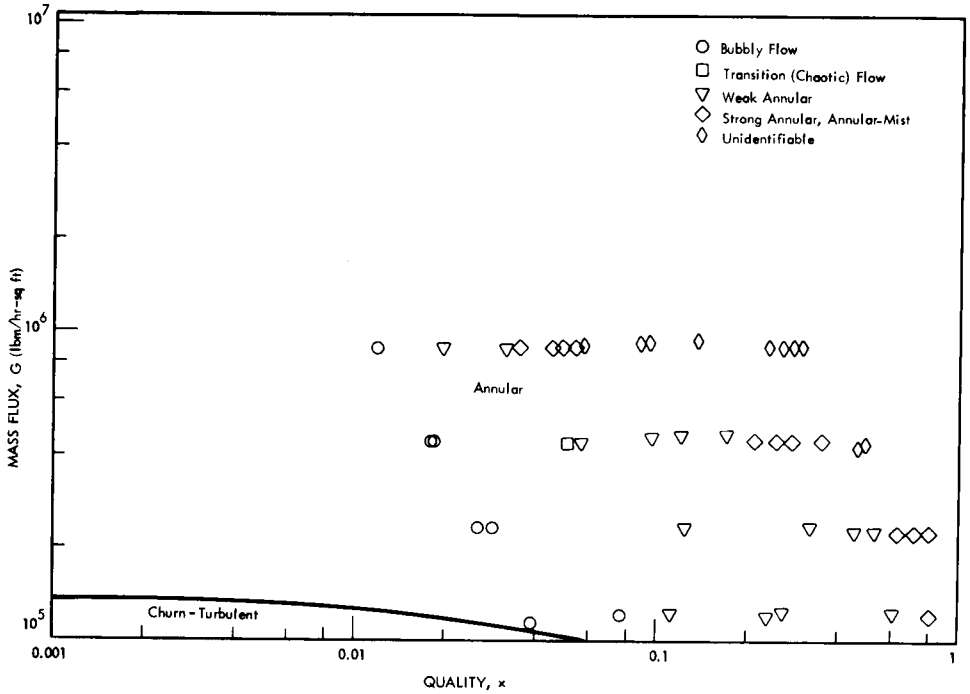


Figure IV-27. COMPARISON OF EXPERIMENTAL FLOW REGIME MAP AND ZUBER ET AL [10] EQUATION FOR THE TRANSITION FROM CHURN-TURBULENT TO ANNULAR FLOW, T ≈ 200°F

larger annular flow region was predicted than actually existed. This was especially true at high mass fluxes and high boiling temperatures. At 250°F, annular flow was predicted for the entire flow and quality range covered in this study.

For adiabatic flow, the transition from slug to annular flow, predicted by Zuber et al [10] in Equation (2-7) is shown in Figure IV-28 for the 110°F boiling temperature. The slug region predicted was considerably larger than the bubbly-slug region experimentally observed. Equation (2-7) however correctly predicted the absence of slug flow at the 150, 200, and 250°F boiling temperatures for the range of parameters investigated here.

J. L. L. Baker [17] in Equations (2-8), (2-9), and (2-10) defined the transitions between three regimes, namely churn or semiannular (cor-

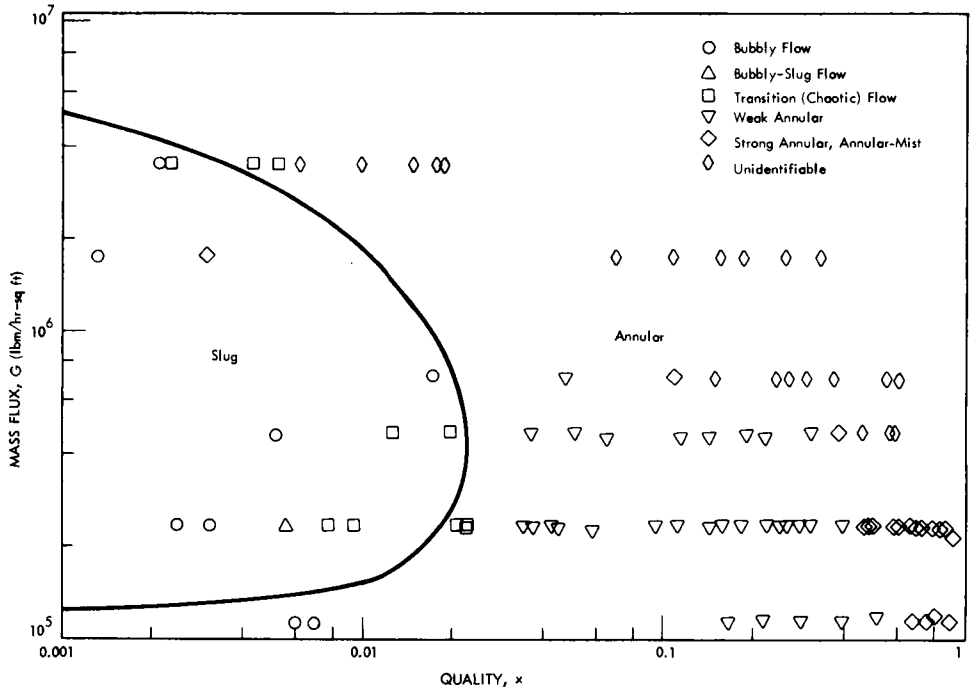


Figure IV-28. COMPARISON OF EXPERIMENTAL FLOW REGIME MAP AND ZUBER ET AL [10] EQUATION FOR THE TRANSITION FROM SLUG TO ANNULAR FLOW, T≈110°F

responding to weak annular), wispy annular or ligament flow (corresponding to the unidentifiable flow regime) and annular. J. L. L. Baker [17] supplemented his high-speed photographs with X-ray observations of the flow and was therefore able to penetrate the liquid film on the wall and view the inner core. He observed that this inner flow was not continuous and was probably caused by sheets or ligaments of liquid being torn from the highly disturbed liquid film and transported by the vapor in the core. For the case of $\eta' = 1/2$ in Equation (2-8), signifying the importance of both inertial and interfacial forces, the regime transitions illustrated in Figures IV-29 through IV-32 were obtained. The agreement was satisfactory. While the transition between the churn and annular regimes in J. L. L. Baker's [17] map did not exactly correspond to the transition between weak annular and annular in this study, a part of this may be attributed to subjective differences between the two observers.

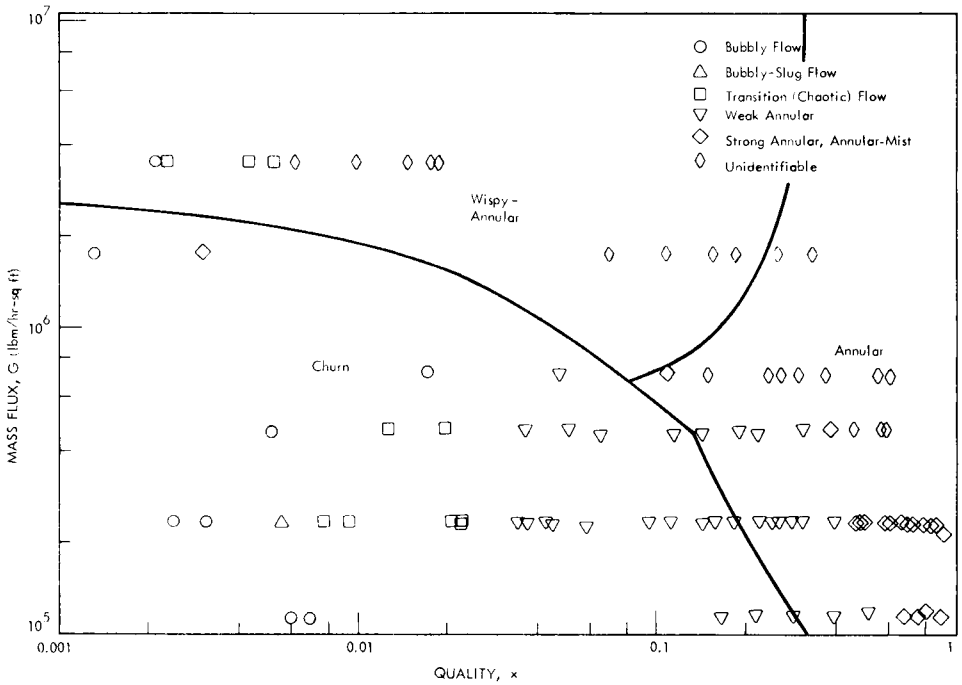


Figure IV-29. COMPARISON OF EXPERIMENTAL FLOW REGIME MAP AND J. L. L. BAKER'S [17] TRANSITIONS BETWEEN CHURN, WISPY ANNULAR, AND ANNULAR. $\eta' = 1/2$, $T \approx 110°F$.

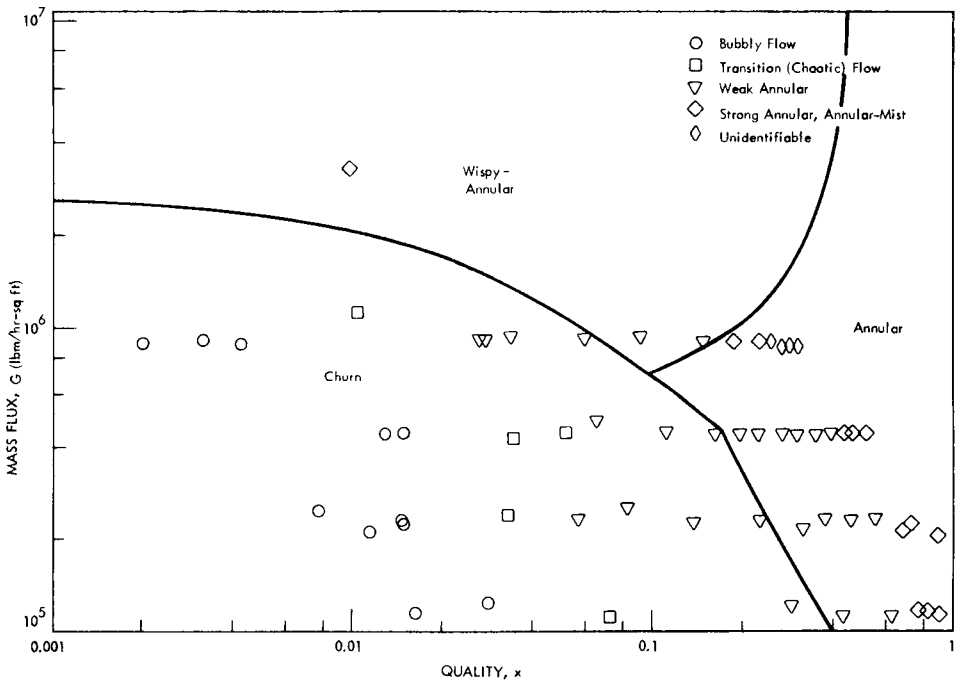


Figure IV-30. COMPARISON OF EXPERIMENTAL FLOW REGIME MAP AND J. L. L. BAKER'S [17] TRANSITIONS BETWEEN CHURN, WISPY ANNULAR, AND ANNULAR. $\eta' = 1/2$, $T \approx 150°F$.

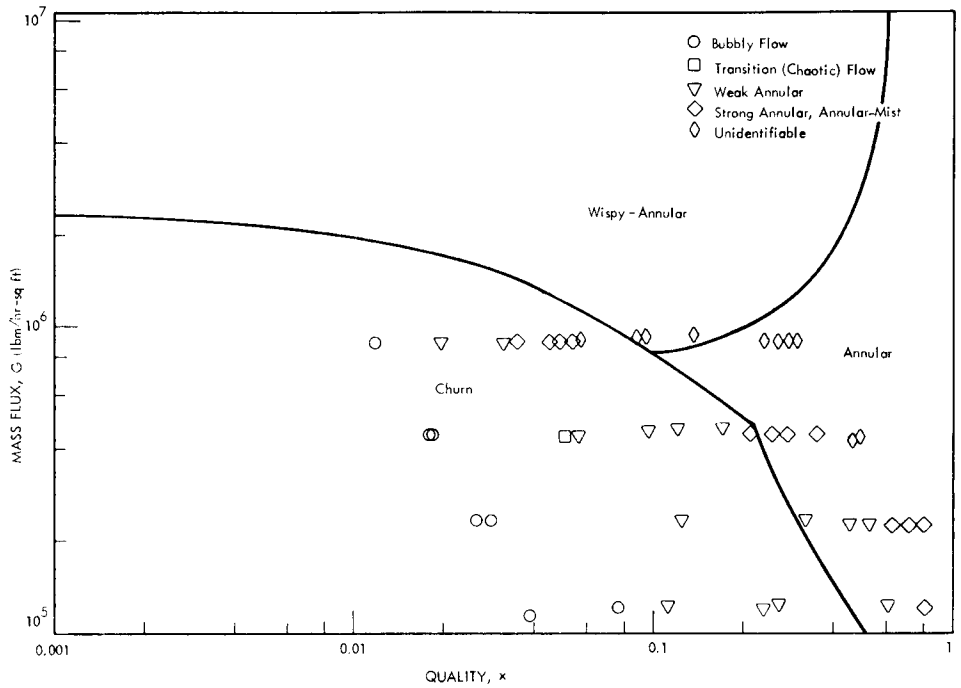


Figure IV-31. COMPARISON OF EXPERIMENTAL FLOW REGIME MAP AND J. L. L. BAKER'S [17] TRANSITIONS BETWEEN CHURN, WISPY ANNULAR, AND ANNULAR. $\eta' = 1/2$, T≈200°F.

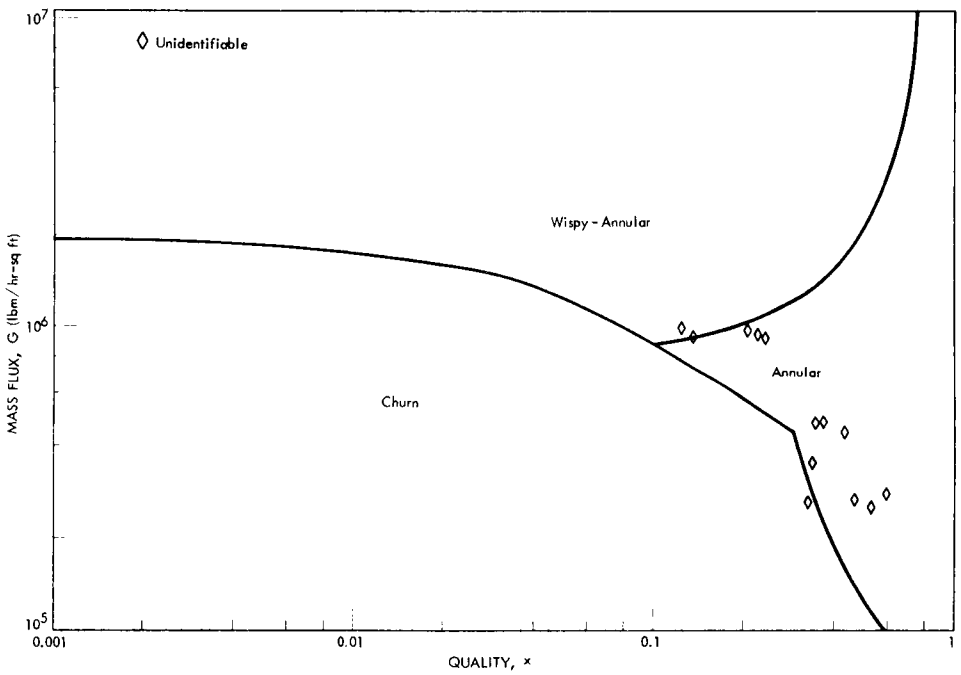


Figure IV-32. COMPARISON OF EXPERIMENTAL FLOW REGIME MAP AND J. L. L. BAKER'S [17] TRANSITIONS BETWEEN CHURN, WISPY ANNULAR, AND ANNULAR. $\eta' = 1/2$, T≈250°F.

The churn to wispy-annular transition of Baker [17] followed quite closely the boundary of the unidentifiable flow regime in this study. No correspondence to the wispy-annular to annular transition was observed in this study.

Using an η' of zero, signifying an inertial-controlled system yielded results which showed a slight improvement in the churn to annular transition. This is shown in Figures IV-33 through IV-36.

An attempt will now be made to compare Hosler's [14] steam-water results and the present R-114 studies. This comparison will be made on an equal density ratio basis as suggested by J. L. L. Baker [17]. The 110°F boiling run corresponded to a boiling water pressure of 453 psia. This is halfway between the 300 and 600 psia runs in Figure II-4 on page 21. In addition to the fact that a significantly smaller slug flow regime existed in the R-114 runs, the upper limit of the bubbly flow regime and the lower limit of the annular flow regime occurred at lower qualities in R-114 than in either the 300 or 600 psia water runs. The 150°F, R-114 boiling runs corresponded quite closely to the 800 psia water runs. Good agreement between the two working fluids was observed at the bubbly and annular flow regime transitions. No slug flow regime was noted in the R-114 runs, however. The 200°F, R-114 runs corresponded to the 1400 psia water runs. Again, as in the 110°F runs, agreement was not very good and the same trends noted at 110°F apply to the 200°F case. Insufficient data were available at the 250°F boiling temperature in R-114 to obtain a meaningful comparison with the water runs.

Despite only fair agreement between the R-114 observations in this study and the transitions proposed by J. L. L. Baker [17], Equations

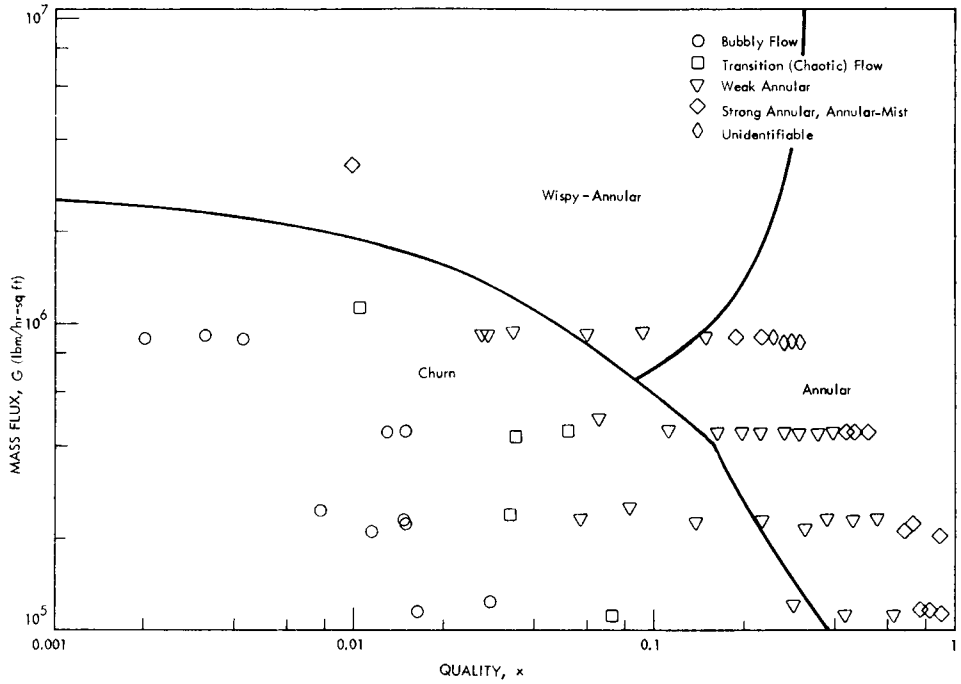


Figure IV-33. COMPARISON OF EXPERIMENTAL FLOW REGIME MAP AND J. L. L. BAKER'S [17] TRANSITIONS BETWEEN CHURN, WISPY ANNULAR, AND ANNULAR. $\eta' = 0$, T≈110°F.

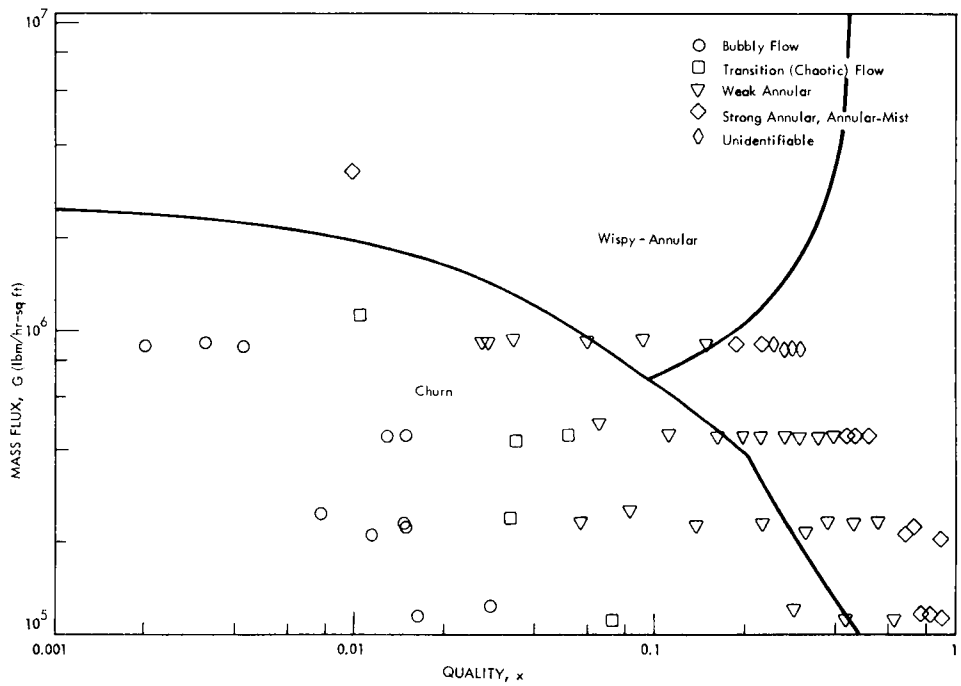


Figure IV-34. COMPARISON OF EXPERIMENTAL FLOW REGIME MAP AND J. L. L. BAKER'S [17] TRANSITIONS BETWEEN CHURN, WISPY ANNULAR, AND ANNULAR. $\eta' = 0$, T≈150°F.

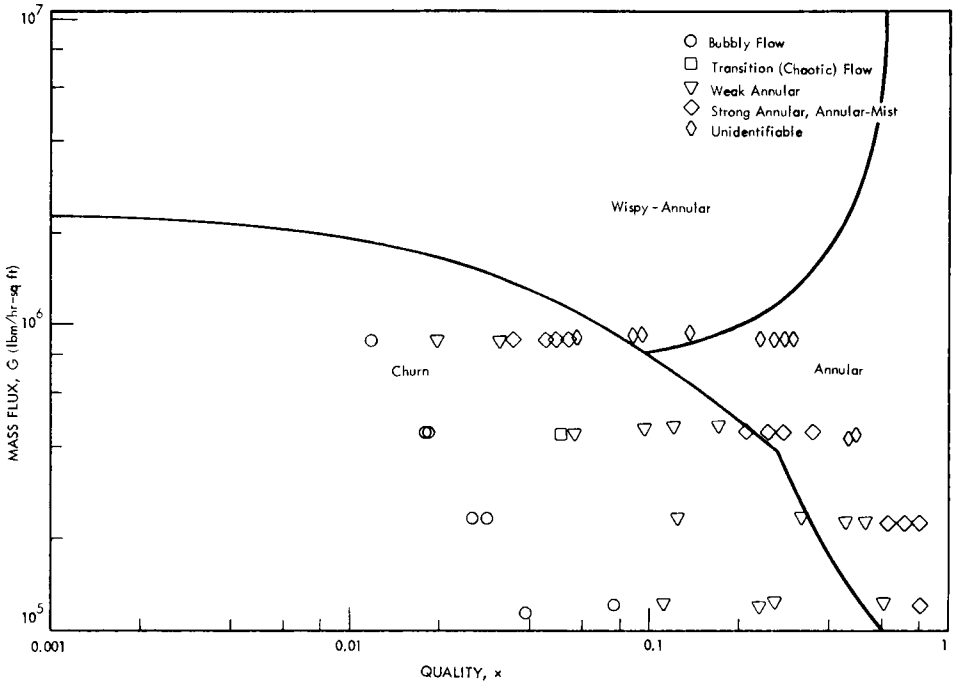


Figure IV-35. COMPARISON OF EXPERIMENTAL FLOW REGIME MAP AND J. L. L. BAKER'S [17] TRANSITIONS BETWEEN CHURN, WISPY ANNULAR, AND ANNULAR. $\eta' = 0$, $T \approx 200°F$.

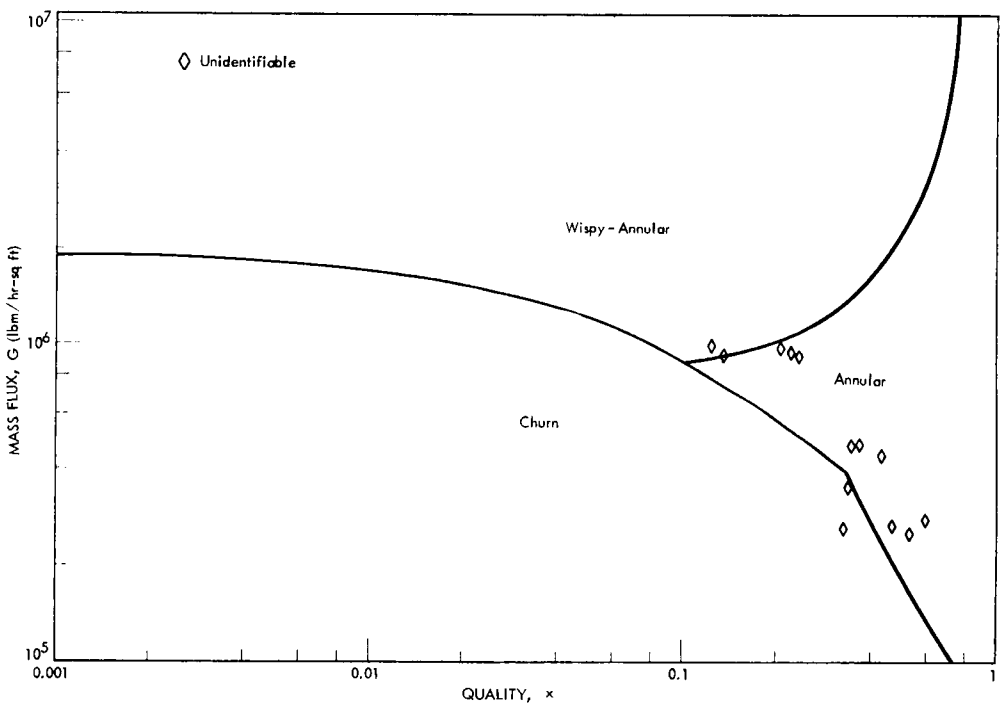


Figure IV-36. COMPARISON OF EXPERIMENTAL FLOW REGIME MAP AND J. L. L. BAKER'S [17] TRANSITIONS BETWEEN CHURN, WISPY ANNULAR, AND ANNULAR. $\eta' = 0$, $T \approx 250°F$.

(2-8), (2-9), and (2-10), as well as the scaling of Hosler's [14] water data on an equal density ratio from one fluid to another yielded the most accurate predictions and are therefore recommended for use with fluids for which no flow regime information exists.

B. PRESSURE DROP

Introduction

Pressure drop results were acquired in the range described in Chapter III, Section C. A total of 710 runs were obtained in the pre-critical heat flux region. An additional 121 runs were made while at least a portion of the tube between two adjacent pressure taps was beyond the critical heat flux. While runs were undertaken in both the natural circulation and forced circulation modes, no differences in the results were noted and consequently no differentiation between the modes will be made.

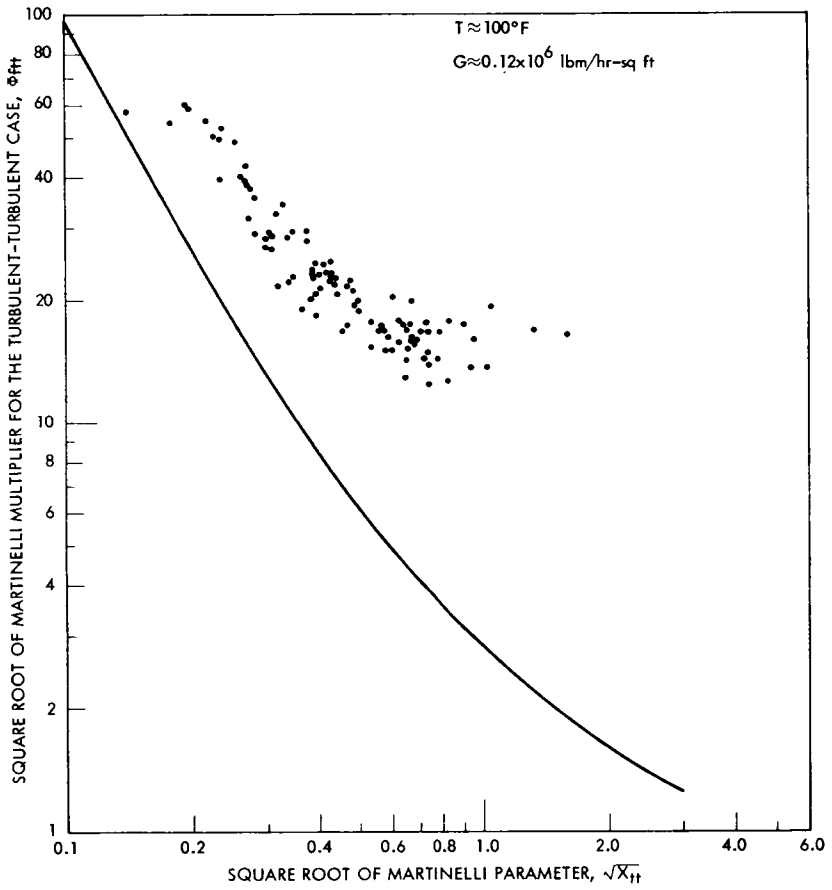
In a vertical test section with heat transfer, the gravitational, frictional, and acceleration components contribute to the pressure drop and all three must be taken into account. The equations obtained for each of these components by the Homogeneous [3] model, and by the Martinelli-Nelson [4] separated flow analysis are presented in Appendix D along with a sample calculation. A computer program was written to calculate the magnitudes of the three different components. Every one-foot zone in the test section was divided into 12 increments and the physical properties were assumed constant in each increment. An interative technique was used to obtain the conditions at the exit of each zone once the inlet condition was known. The total pressure drop was

the sum of the components in each of the increments. As a check on this iterative technique, the number of increments per zone was changed. The iteration was found to converge and the difference in the computed pressure drop between one increment per zone and forty-eight increments per zone was less than 1 percent.

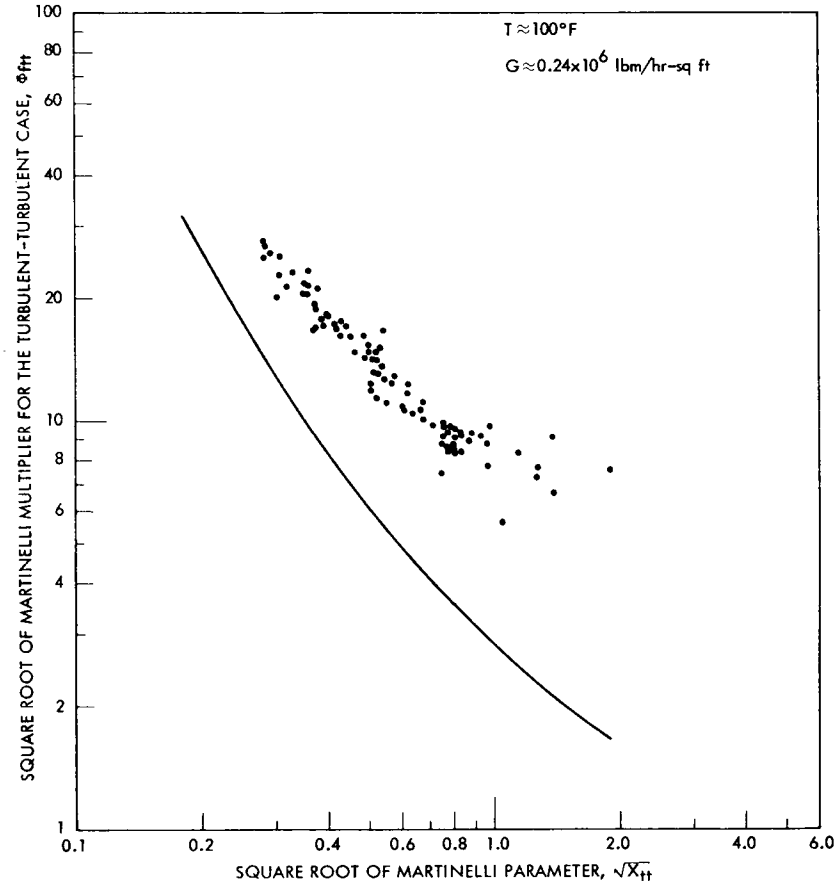
Experimental Results - This Study

The non-critical heat flux results obtained are shown in Figures IV-37 to IV-44. They were obtained from a comparison of the experimental frictional component and the analytically derived frictional component using the Homogeneous [3] model and the Martinelli-Nelson [4] model with the M-N [4] formulation for the void fraction. The Φ_{ftt} vs $\sqrt{X_{tt}}$ parameters were chosen since the former represents a meaningful dimensionless pressure drop formulation and the latter includes the important two-phase physical properties. This type of plot also makes it possible to easily compare the experimental results with the curves proposed by Martinelli and Nelson [4].

Homogeneous [3] Model. The application of the Homogeneous [3] model is straightforward since the void fraction, which is the only important unknown, can be easily computed when the liquid and vapor components are assumed to have the same velocity. The results, shown in Figures IV-37 to IV-40, indicated that at all boiling temperatures and for all mass fluxes in the range studied here, the experimental friction factor was higher than the calculated value. A portion of this discrepancy may be associated with the fact that this formulation overpredicts the void fraction. A study of the data tabulation in Appendix

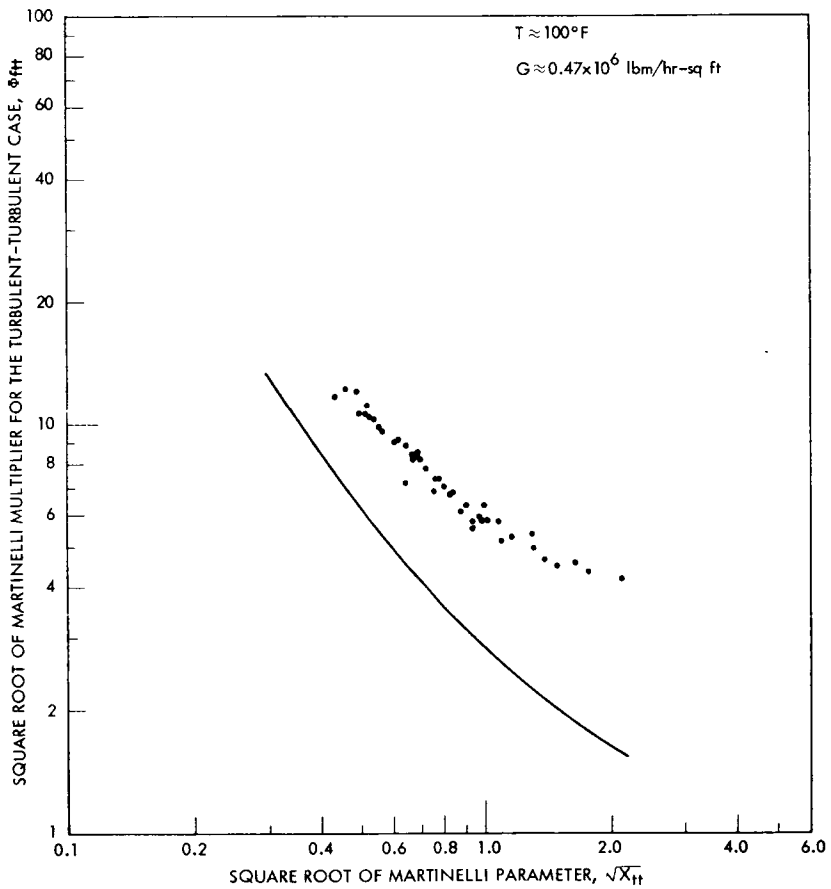


(a)

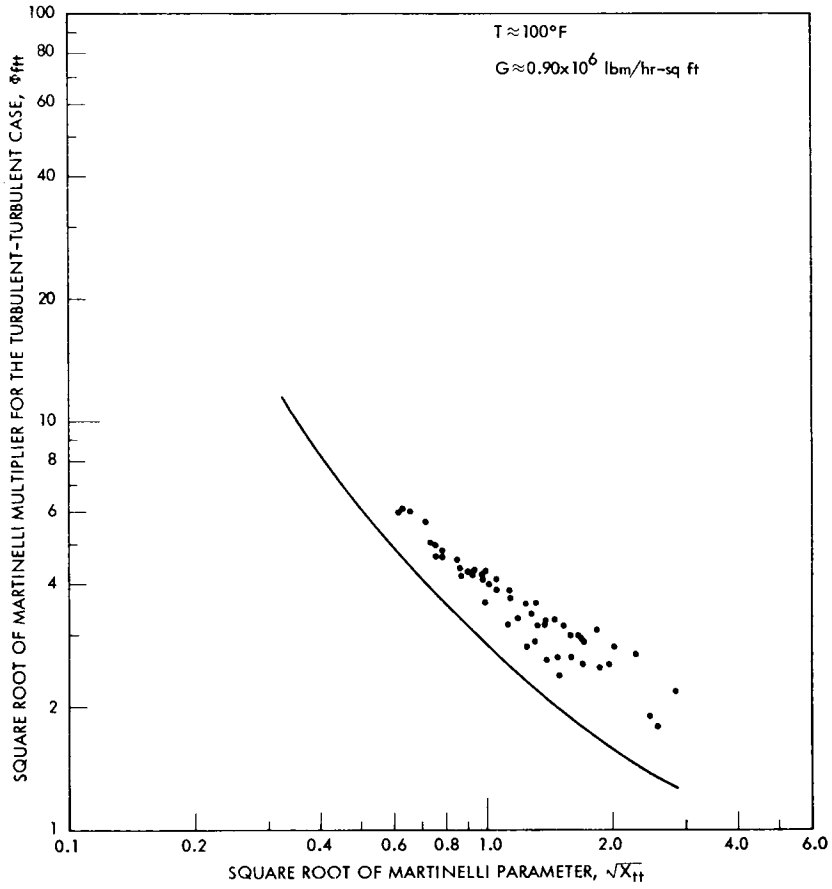


(b)

Figure IV-37. COMPARISON OF EXPERIMENTAL PRESSURE DROP RESULTS WITH ANALYTICALLY DERIVED FRICTIONAL COMPONENT USING THE HOMOGENEOUS [3] MODEL, T≈100°F.

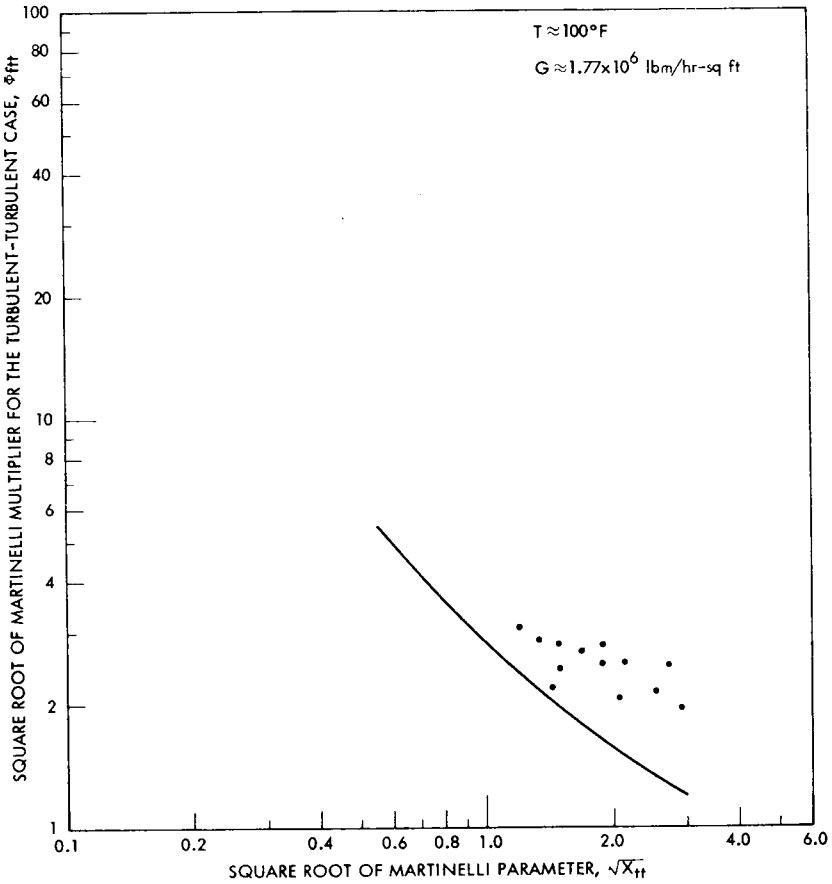


(c)



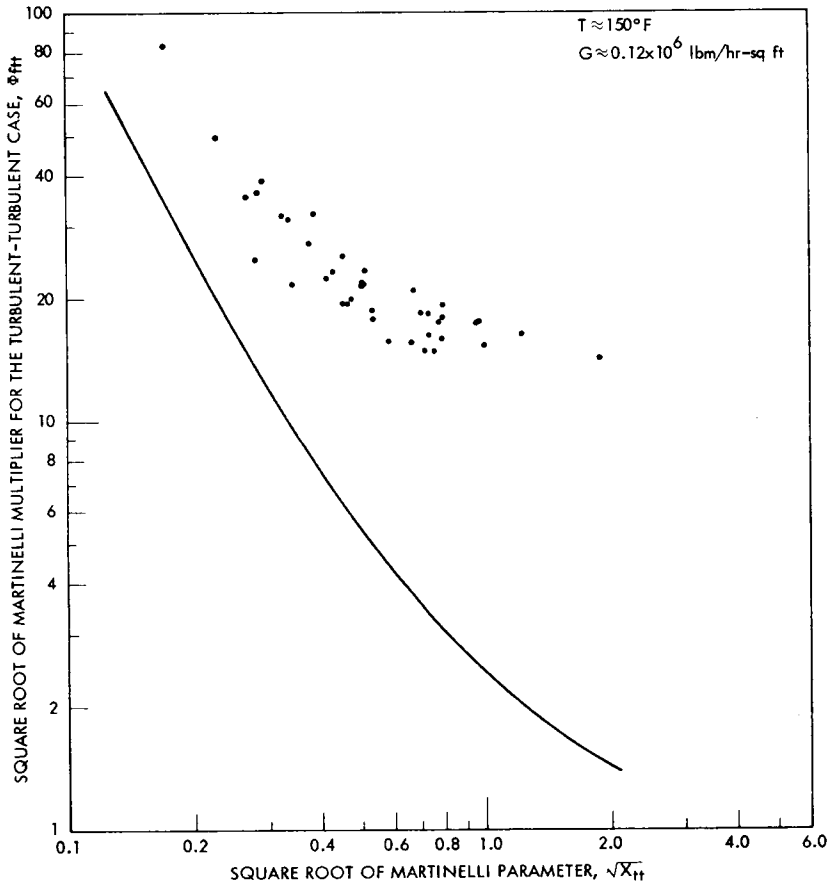
(d)

Figure IV-37. (continued)

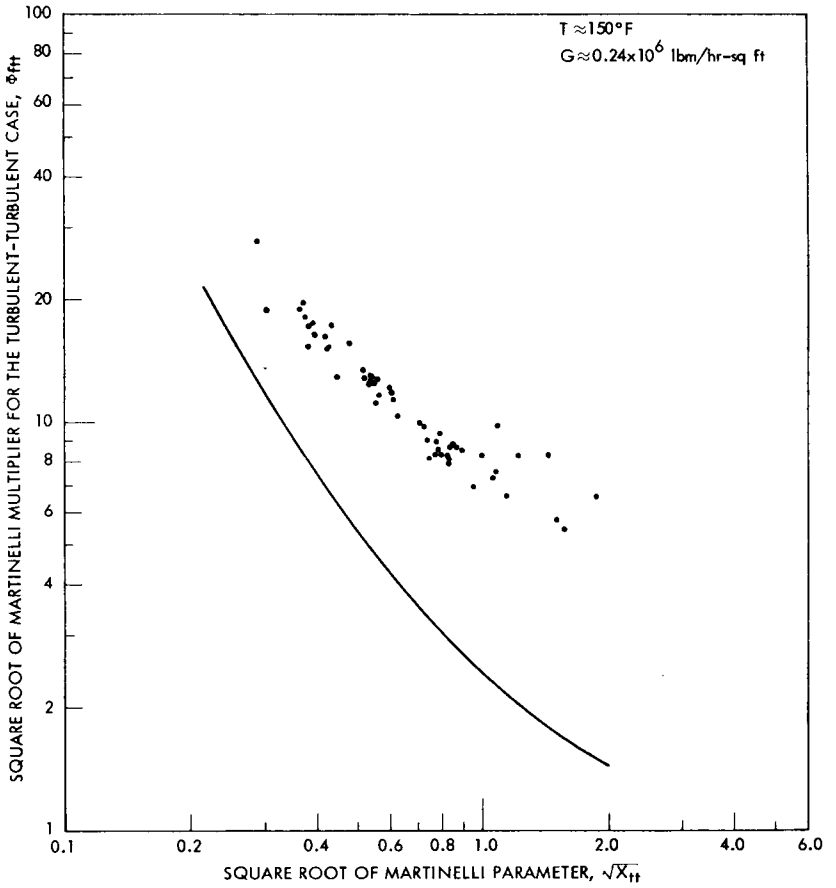


(e)

Figure IV-37. (continued)

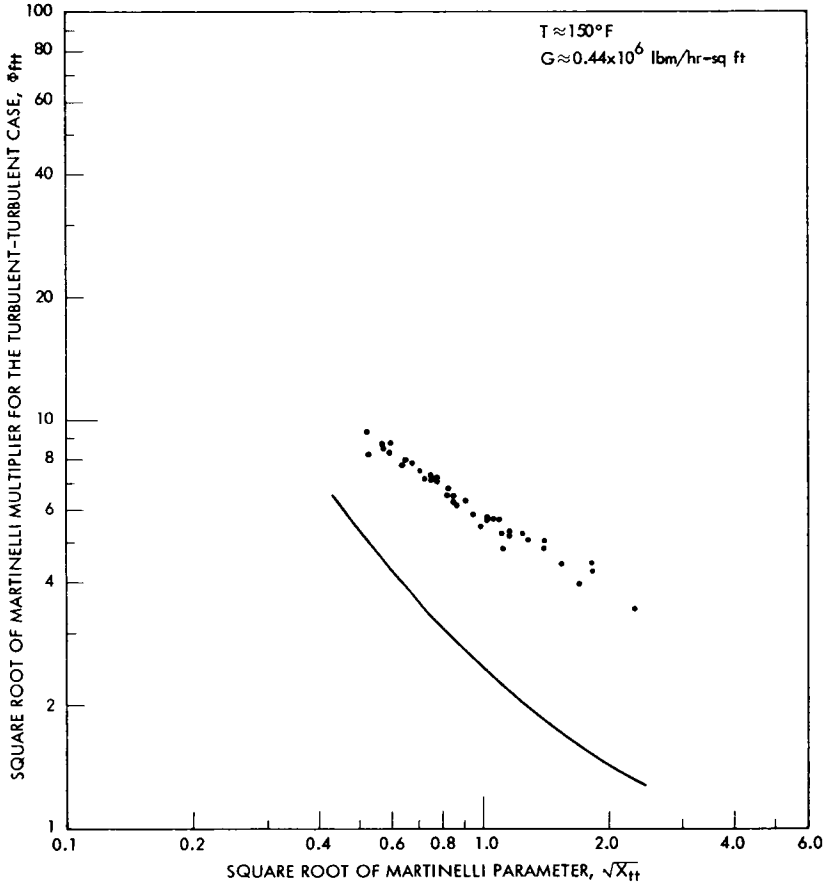


(a)

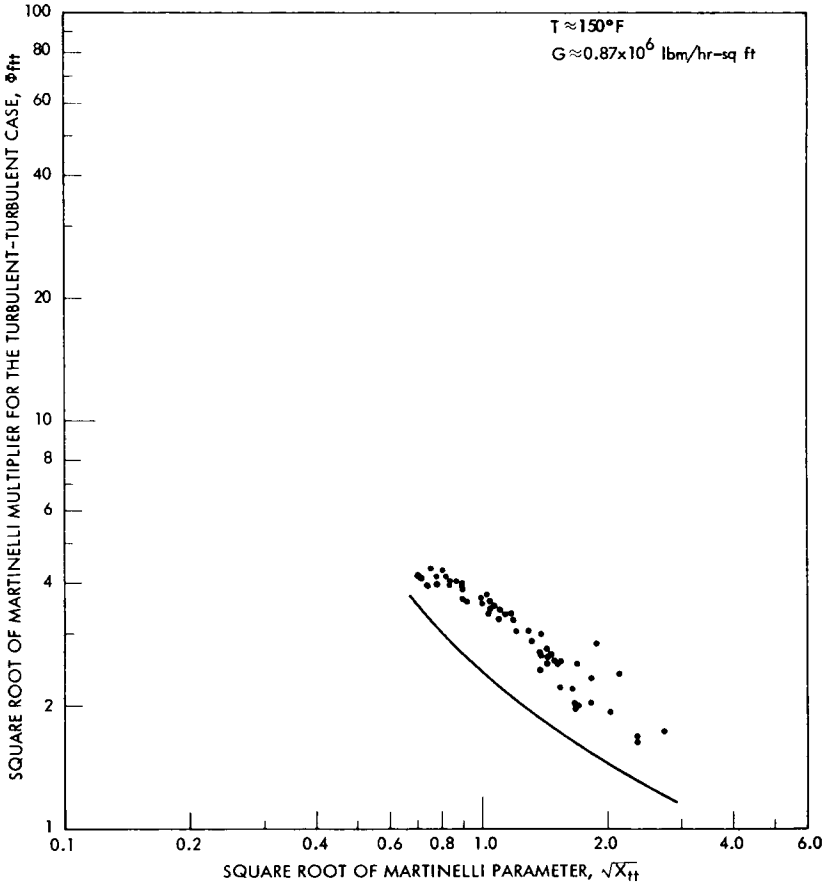


(b)

Figure IV-38. COMPARISON OF EXPERIMENTAL PRESSURE DROP RESULTS WITH ANALYTICALLY DERIVED FRICTIONAL COMPONENT USING THE HOMOGENEOUS [3] MODEL, T≈150°F.

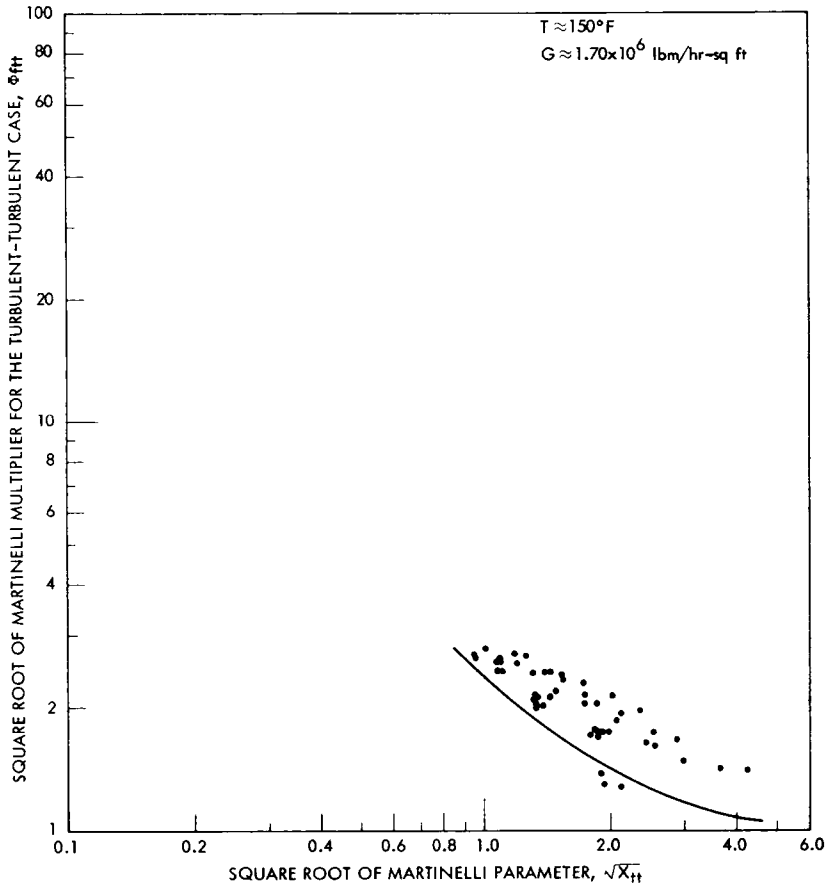


(c)

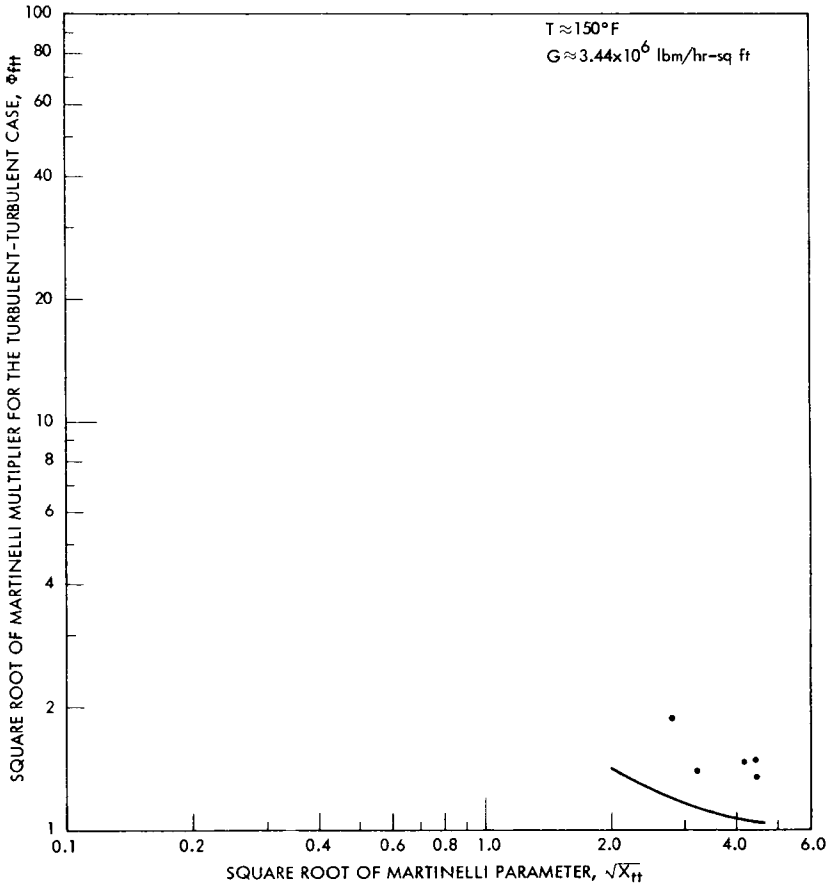


(d)

Figure IV-38. (continued)

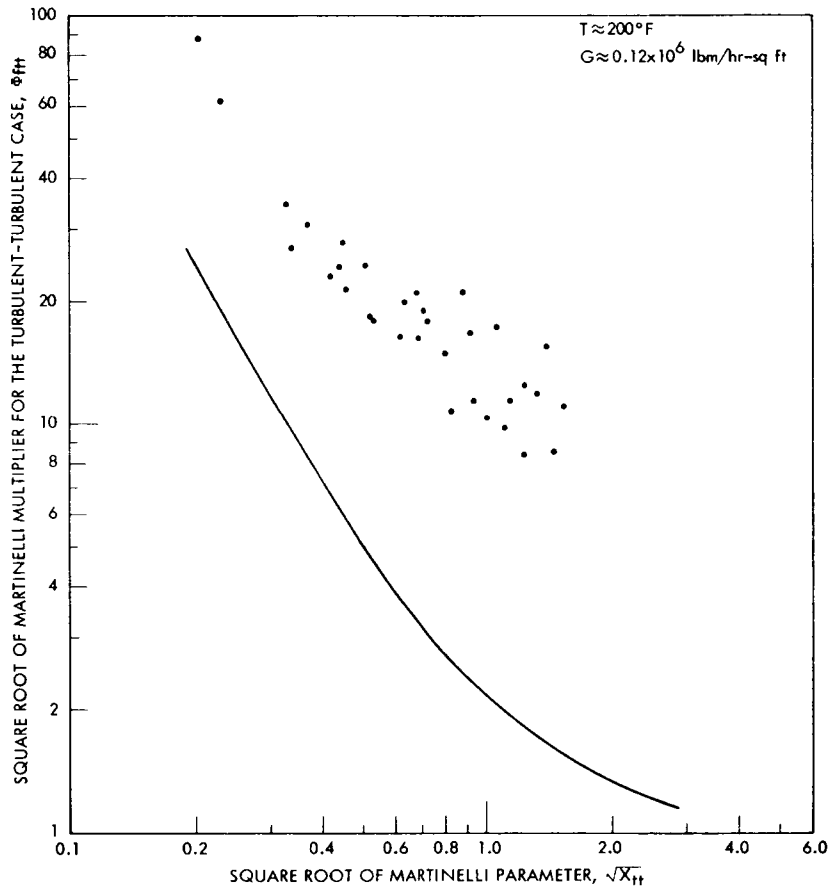


(e)

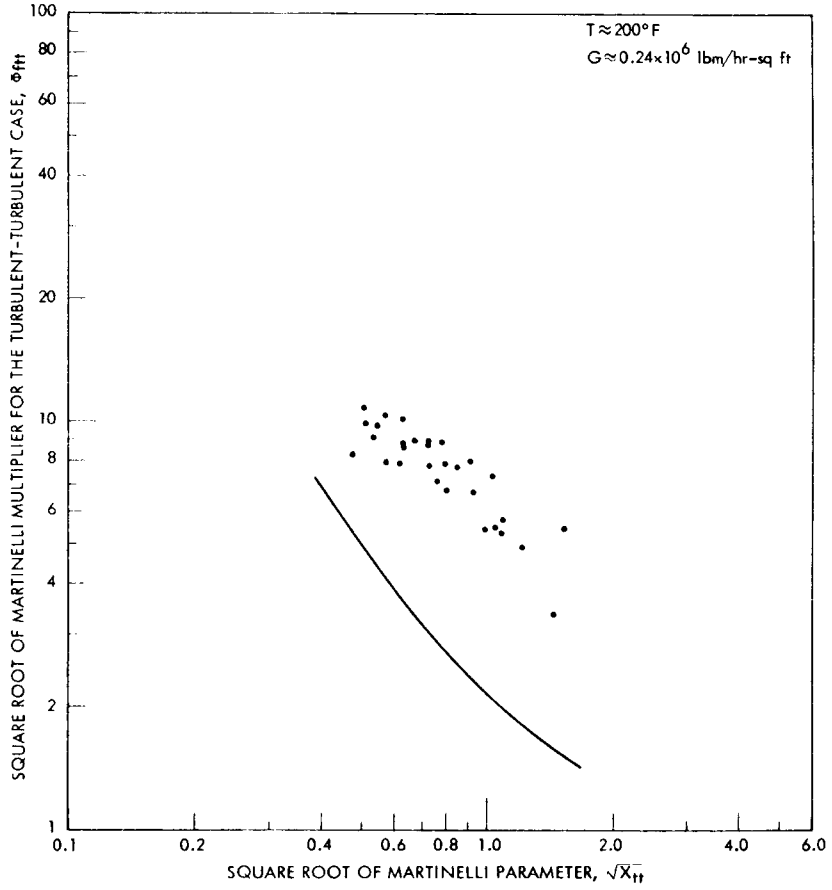


(f)

Figure IV-38. (continued)

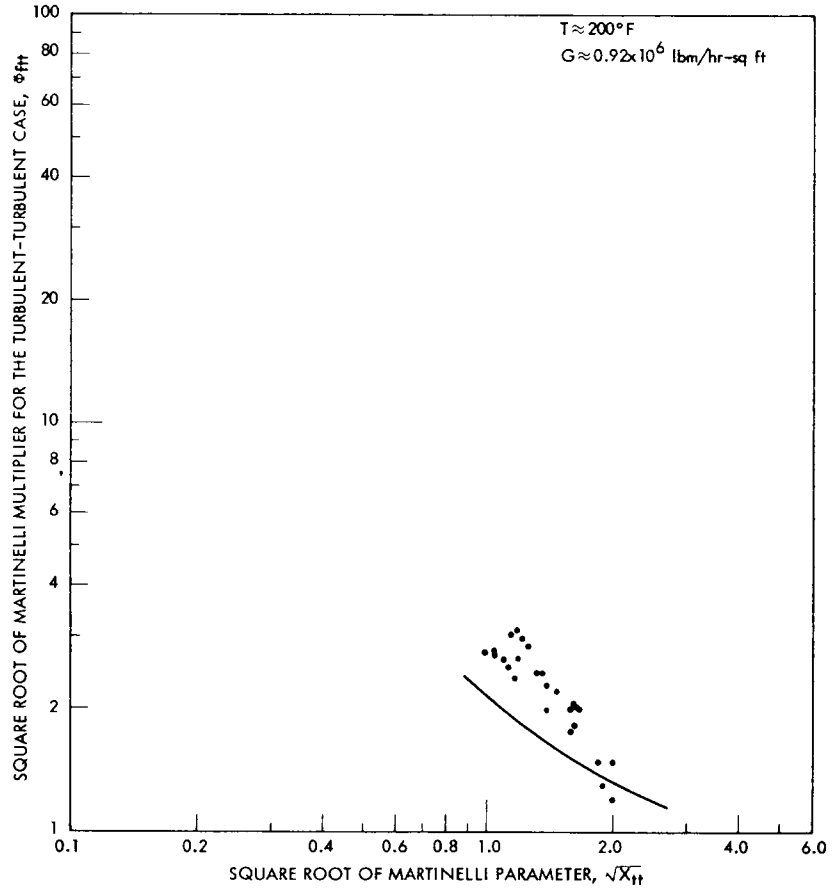


(a)

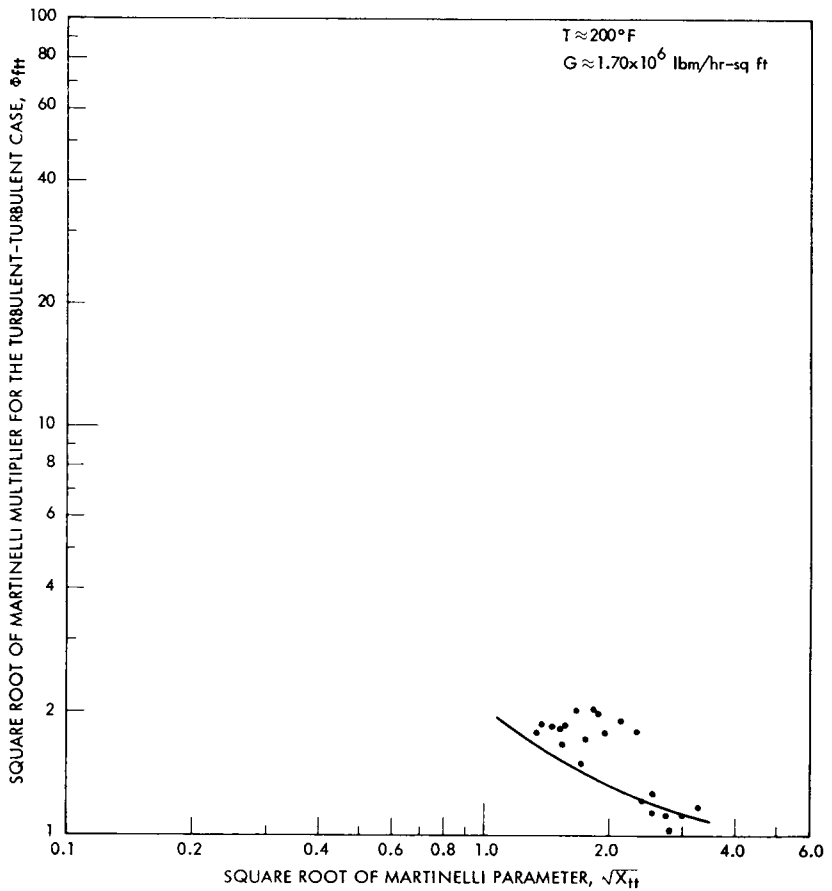


(b)

Figure IV-39. COMPARISON OF EXPERIMENTAL PRESSURE DROP RESULTS WITH ANALYTICALLY DERIVED FRICTIONAL COMPONENT USING THE HOMOGENEOUS [3] MODEL, T≈200°F.

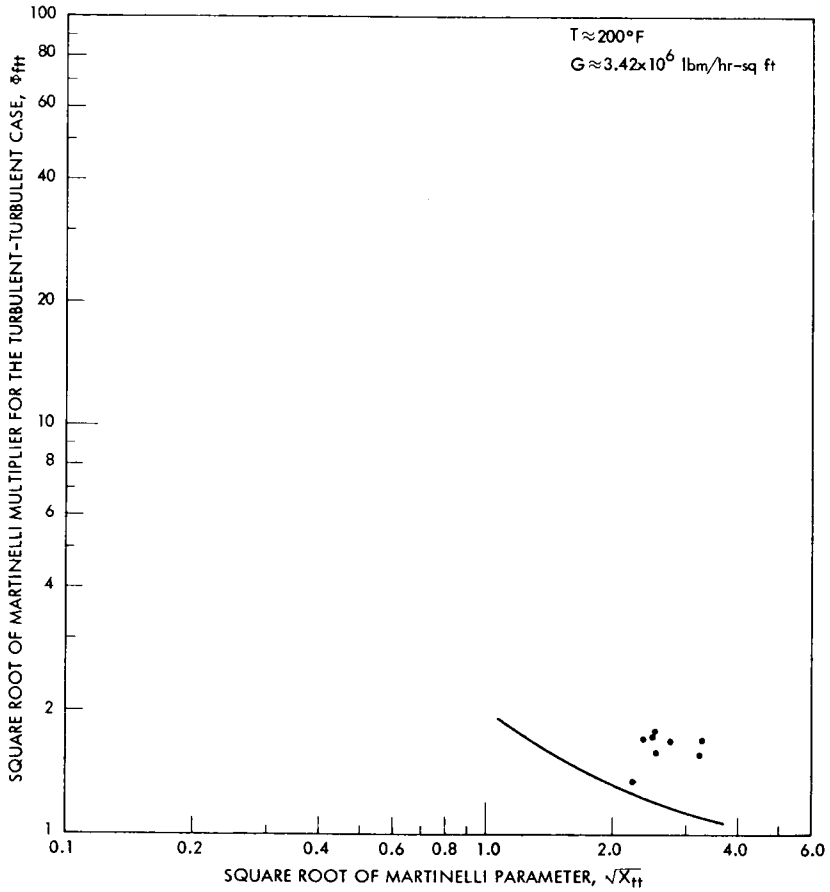


(c)



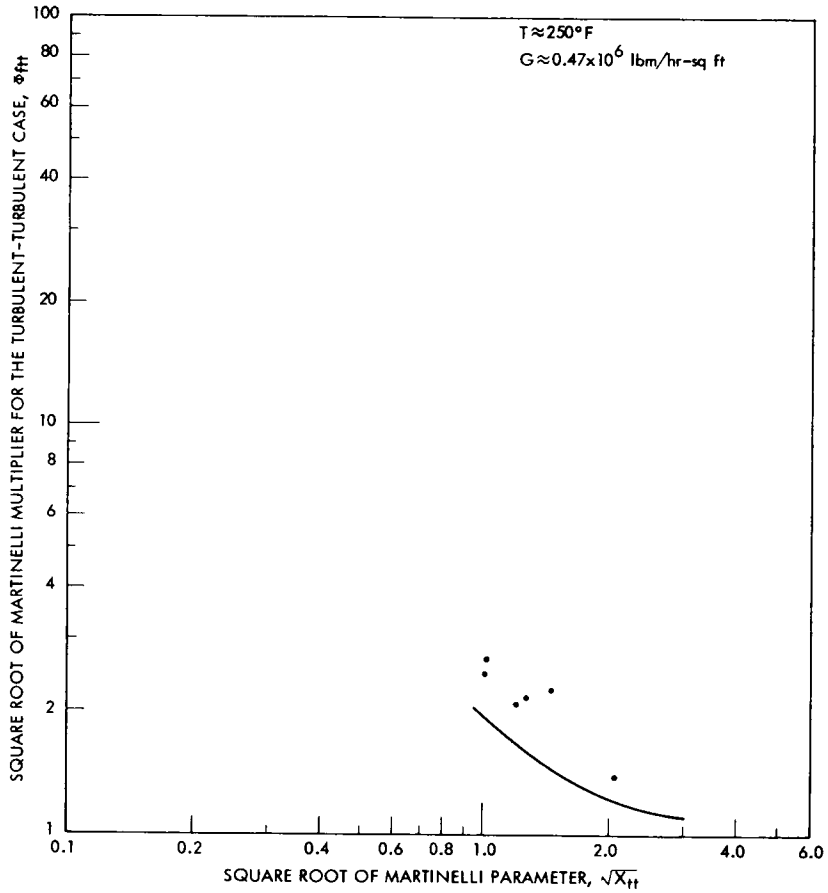
(d)

Figure IV-39. (continued)

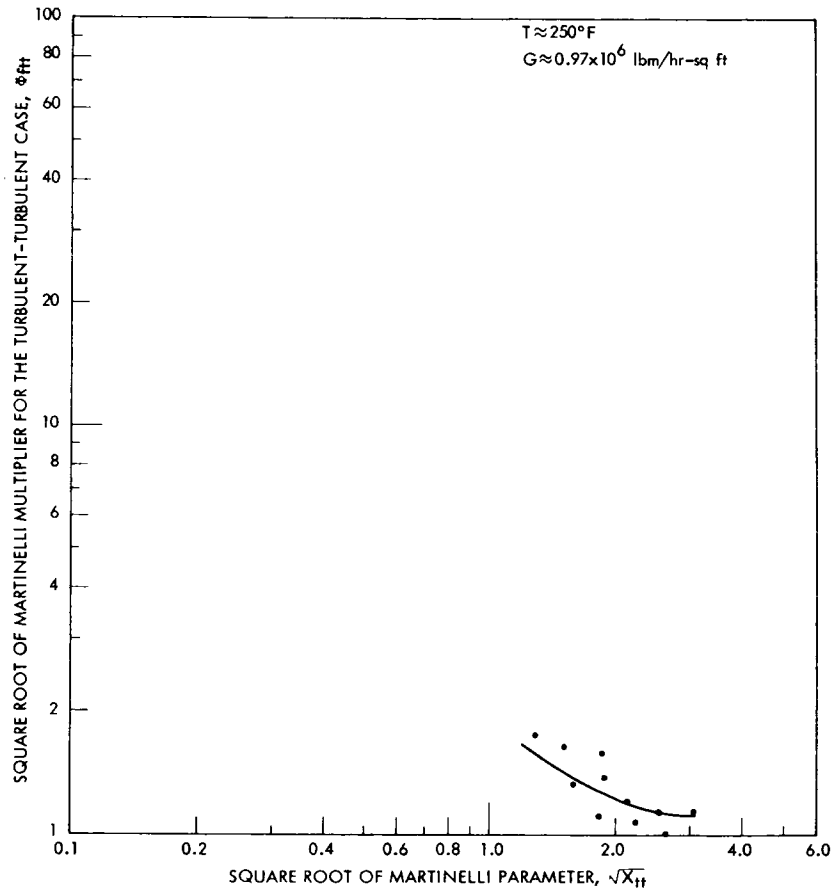


(e)

Figure IV-39. (continued)

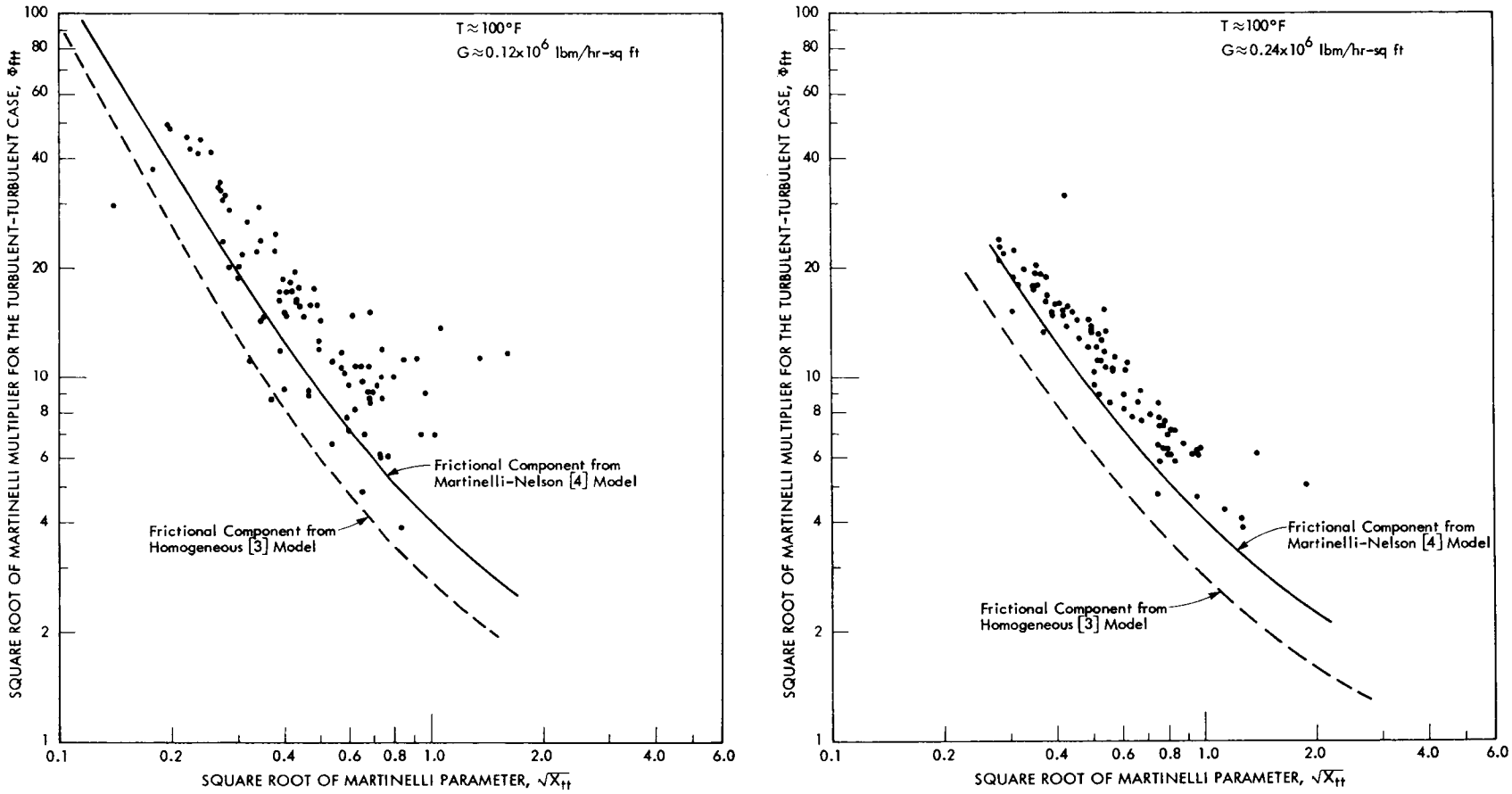


(a)



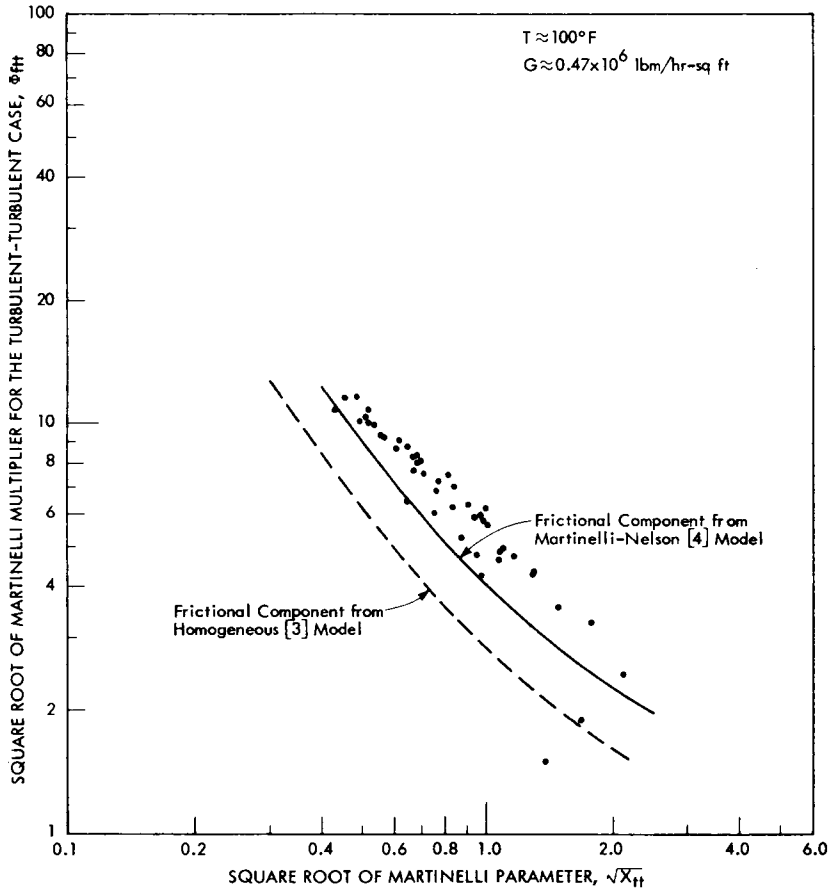
(b)

Figure IV-40. COMPARISON OF EXPERIMENTAL PRESSURE DROP RESULTS WITH ANALYTICALLY DERIVED FRICTIONAL COMPONENT USING THE HOMOGENEOUS [3] MODEL, T≈250°F.

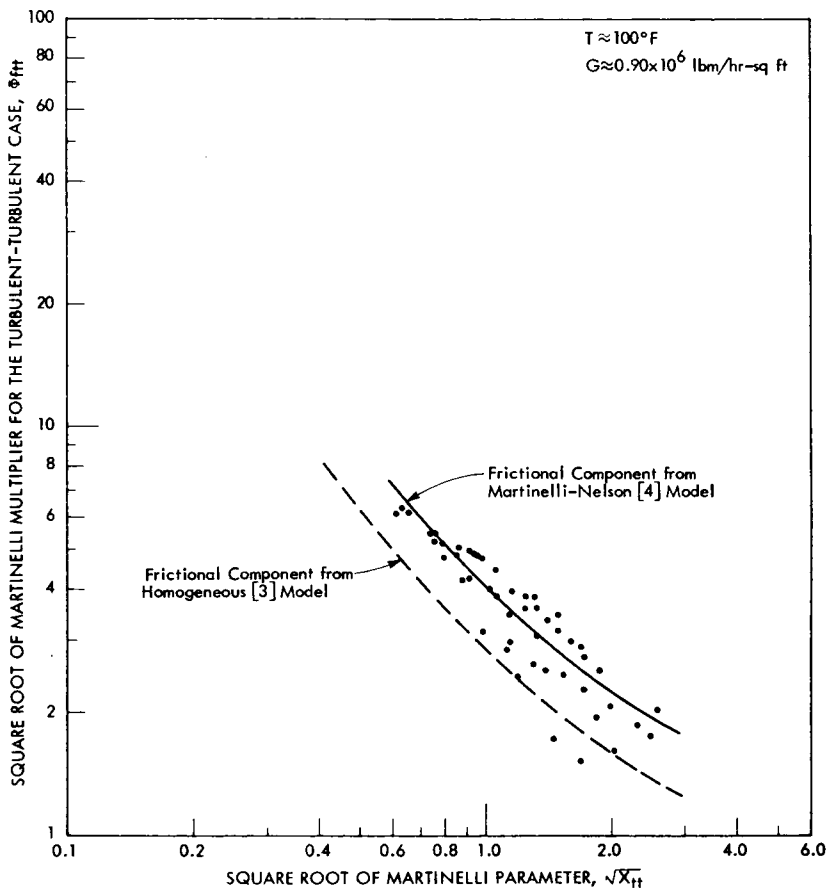


(a) (b)

Figure IV-41. COMPARISON OF EXPERIMENTAL PRESSURE DROP RESULTS WITH ANALYTICALLY DERIVED FRICTIONAL COMPONENTS USING THE MARTINELLI-NELSON [4] MODEL, T≈100°F.

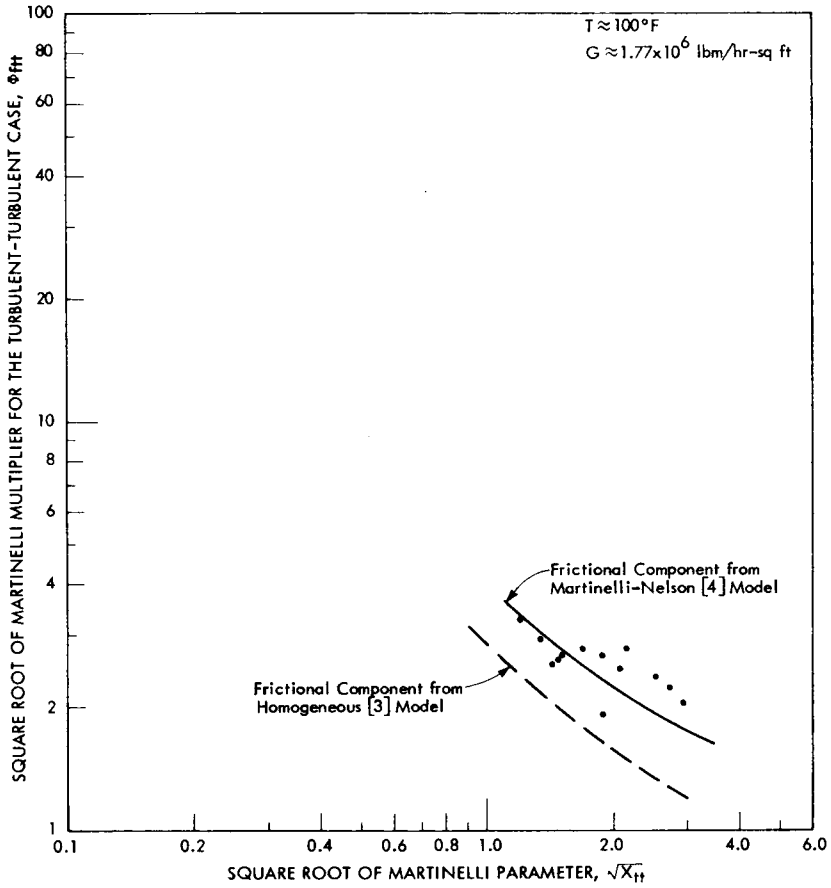


(c)



(d)

Figure IV-41. (continued)



(e)

Figure IV-41. (continued)

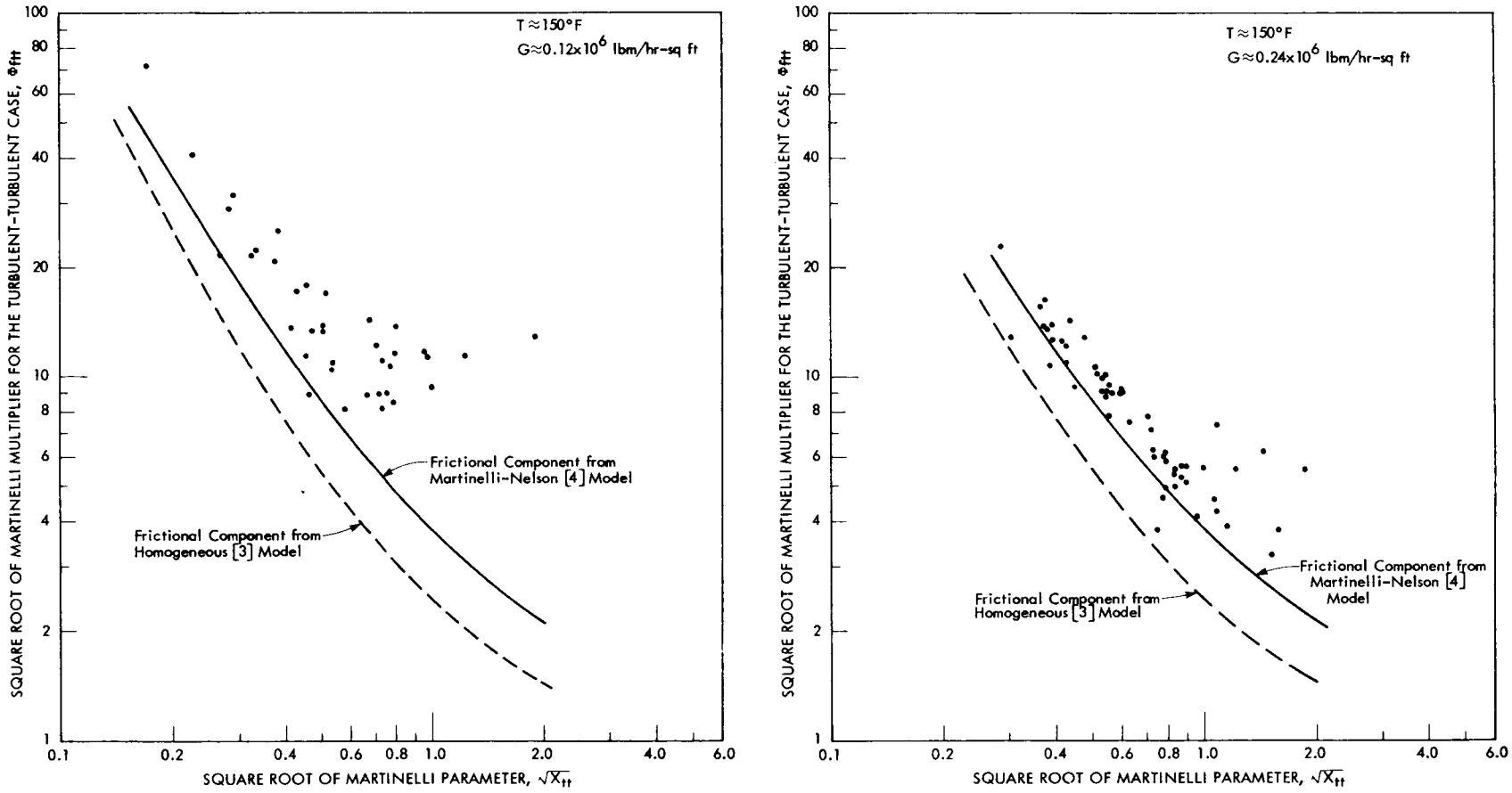
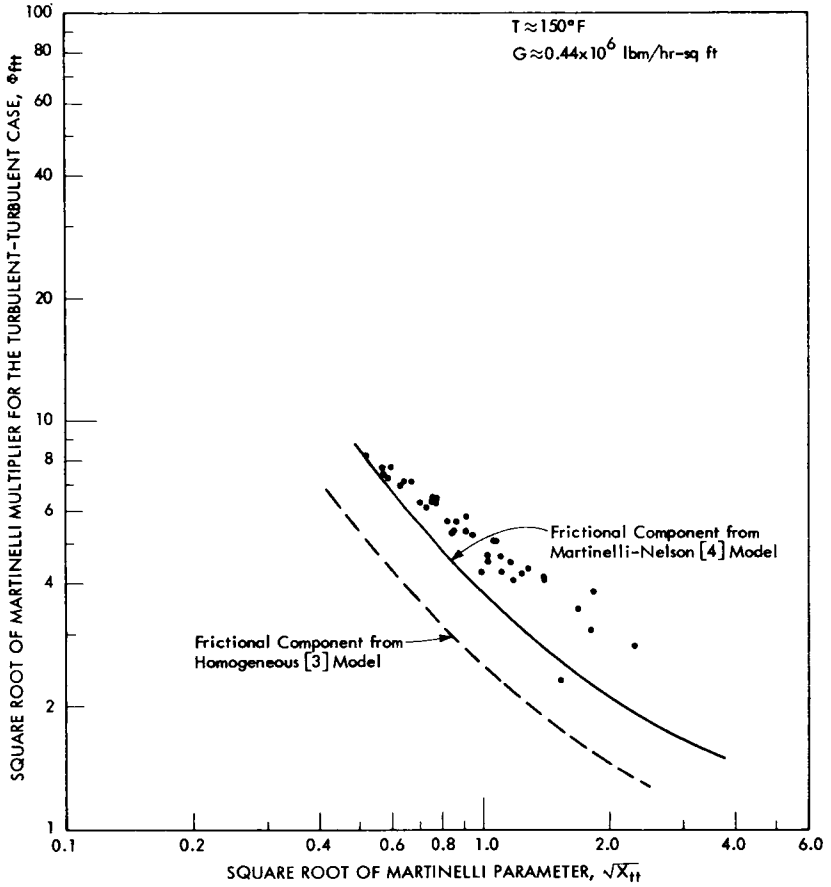
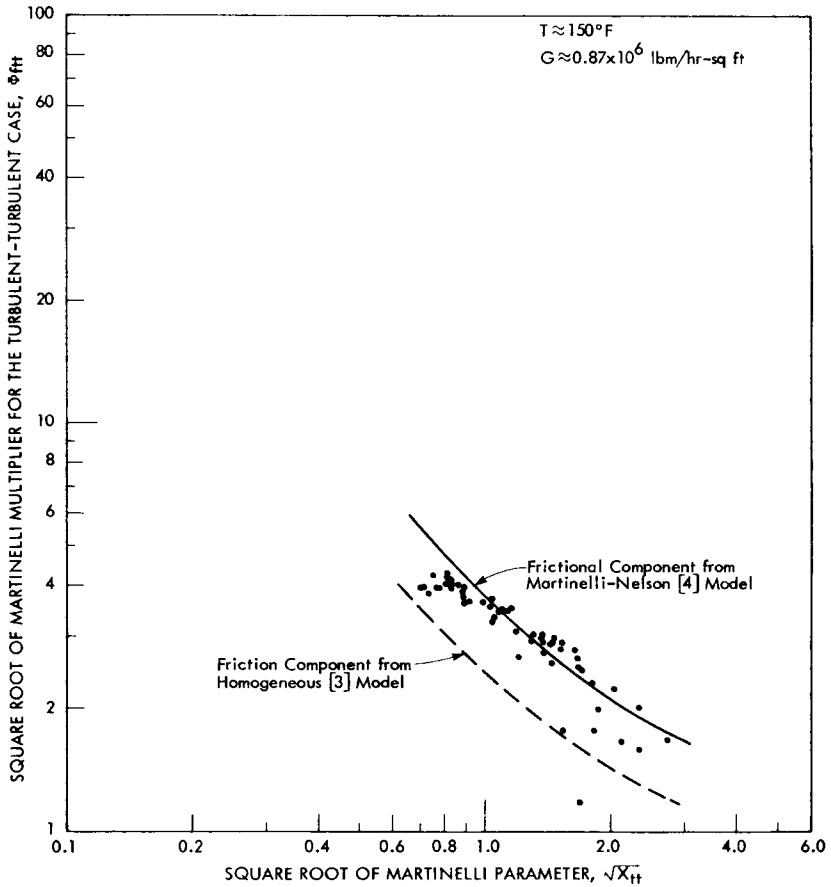


Figure IV-42. COMPARISON OF EXPERIMENTAL PRESSURE DROP RESULTS WITH ANALYTICALLY DERIVED FRICTIONAL COMPONENTS USING THE MARTINELLI-NELSON [4] MODEL, T≈150°F.

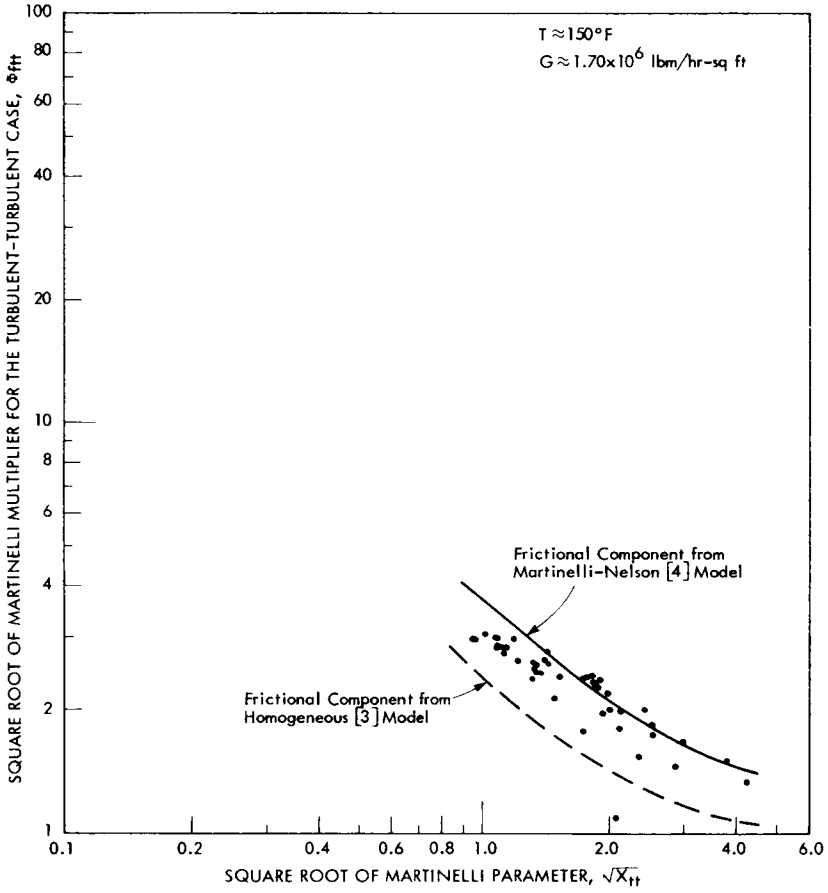


(c)

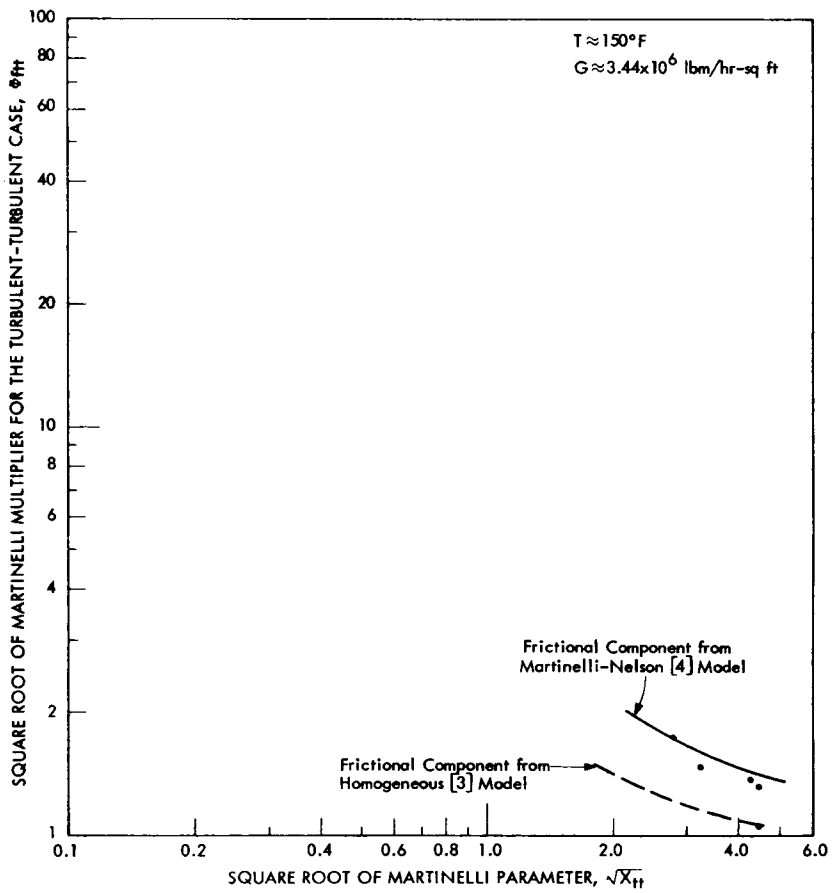


(d)

Figure IV-42. (continued)



(e)



(f)

Figure IV-42. (continued)

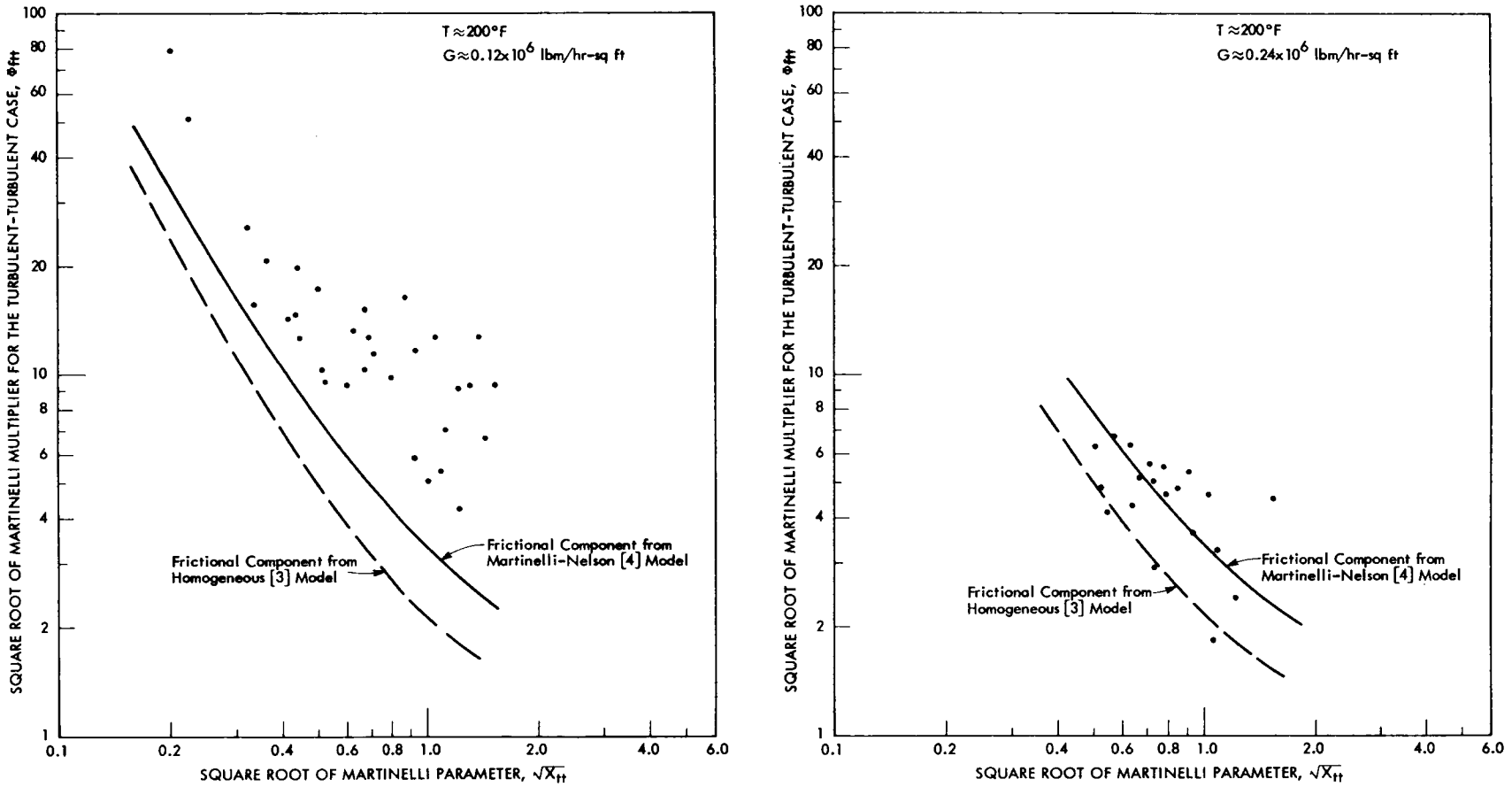
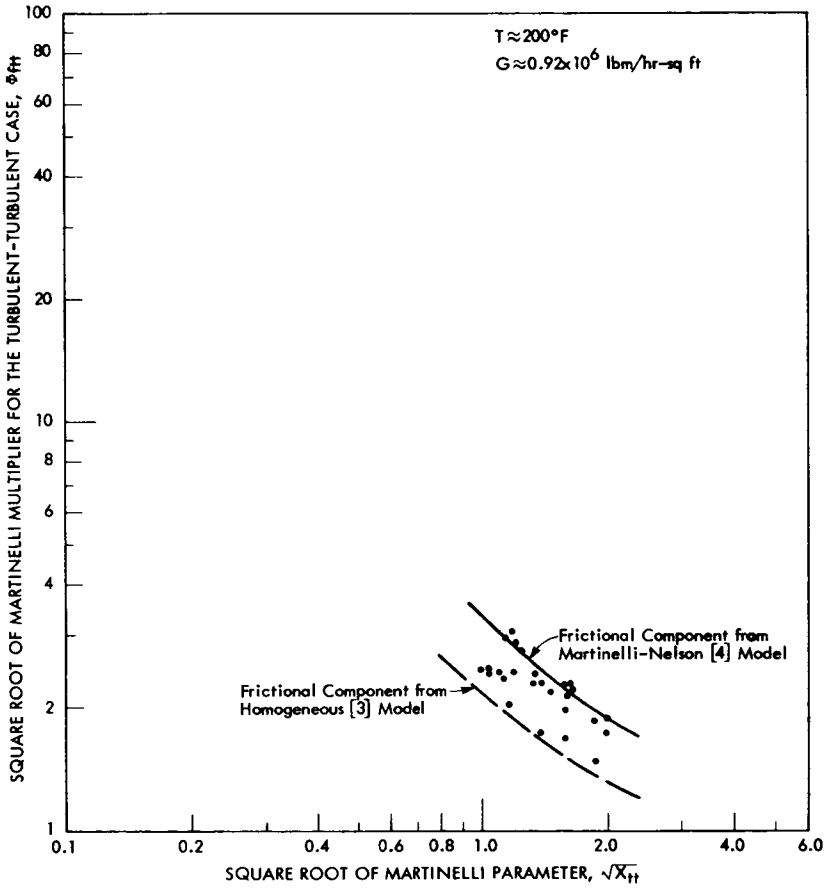
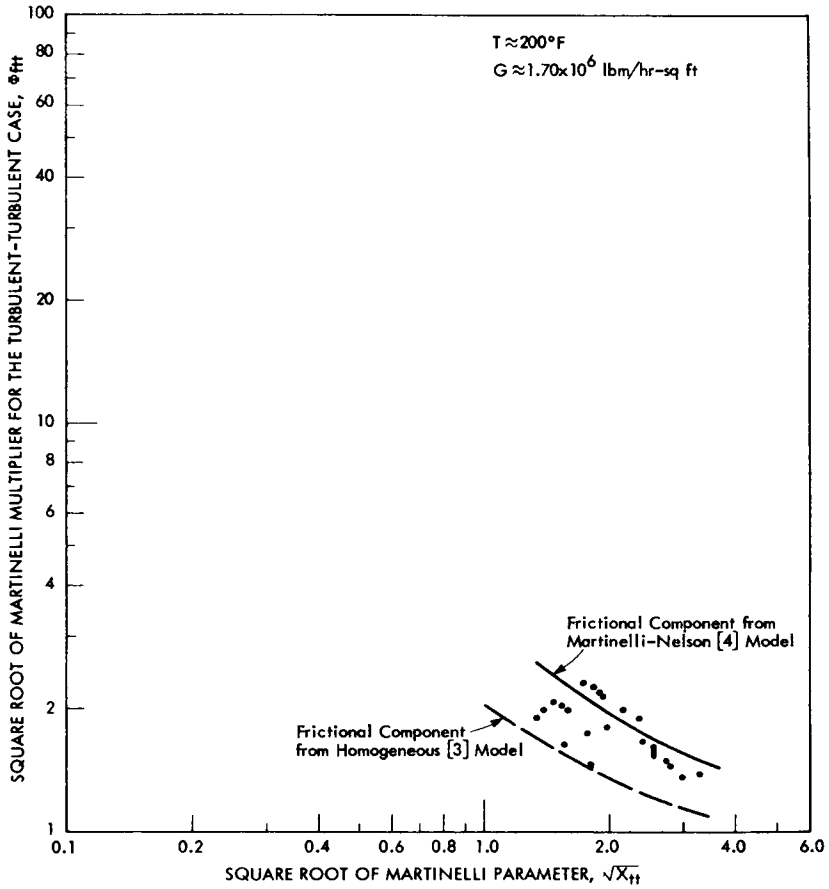


Figure IV-43. COMPARISON OF EXPERIMENTAL PRESSURE DROP RESULTS WITH ANALYTICALLY DERIVED FRICTIONAL COMPONENTS USING THE MARTINELLI-NELSON [4] MODEL, T≈ 200°F.

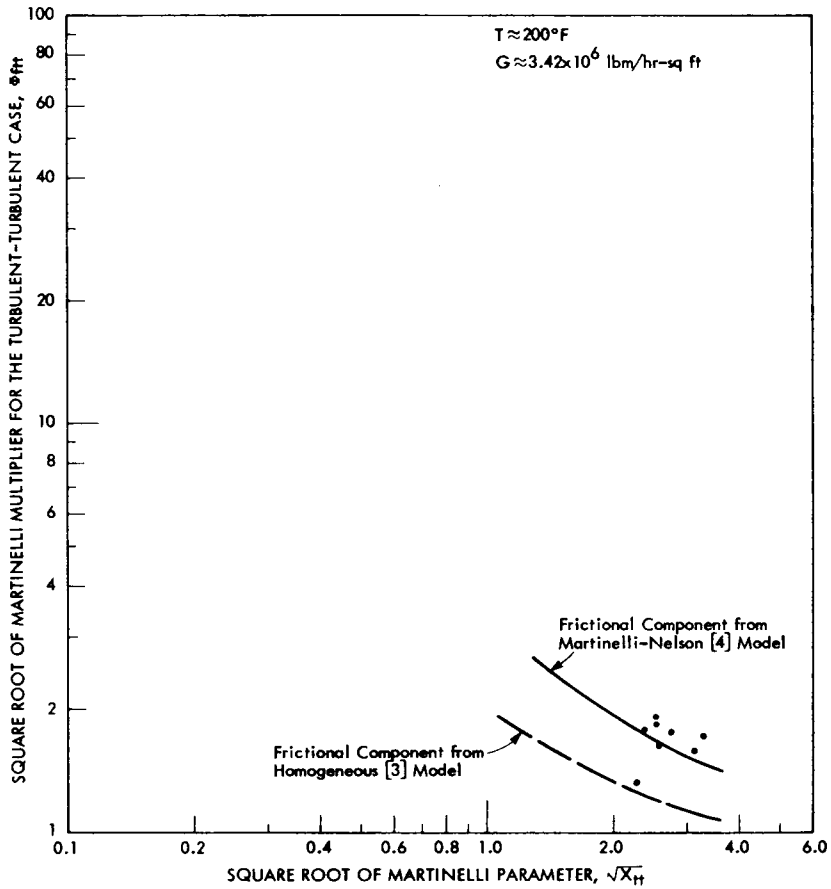


(c)



(d)

Figure IV-43. (continued)



(e)

Figure IV-43. (continued)

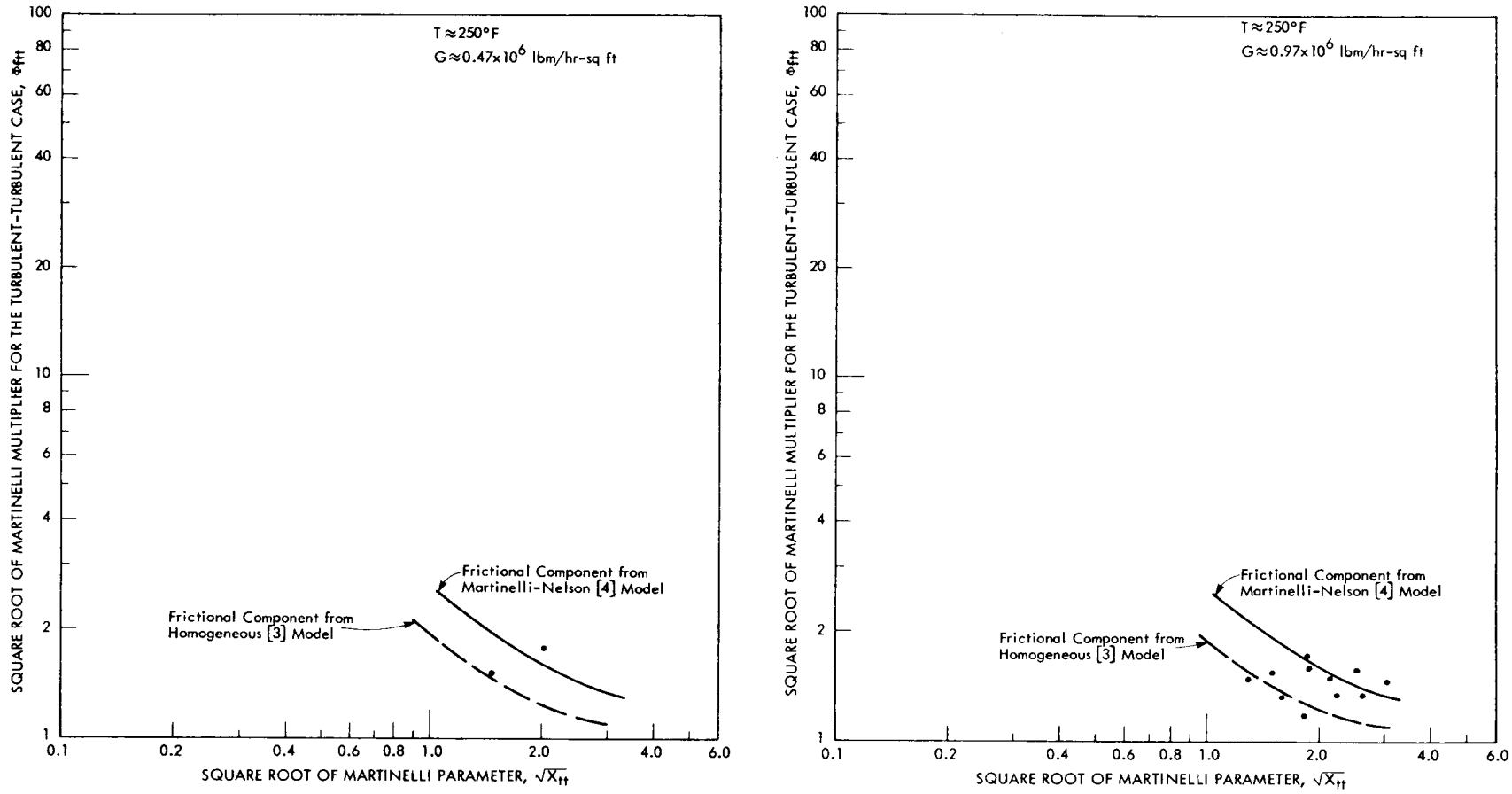


Figure IV-44. COMPARISON OF EXPERIMENTAL PRESSURE DROP RESULTS WITH ANALYTICALLY DERIVED FRICTIONAL COMPONENTS USING THE MARTINELLI-NELSON [4] MODEL, T≈250°F.

F shows that the gravity and acceleration components are a significant portion of the total pressure drop especially at low qualities. Thus, any inaccuracies can be expected to appreciably affect the frictional component. As the mass flows increase, closer agreement is found to occur between the experimental results and the Homogeneous [3] model. Two factors contribute to this. First of all, at high flows, the frictional portion constitutes a greater percentage of the total pressure drop. Thus, any inaccuracies in the void fraction have a smaller effect on the Martinelli multiplier Φ^2_{ftt}. Secondly, at high flow rates the flow does exhibit more of the characteristics of homogeneous flow as the flow regime results in Chaper IV, Section A indicate. At the 250°F boiling temperature the agreement of this experimental data with the Homogeneous [3] model is good even at the low flow rates studied here. The homogeneous nature of the flow at this boiling temperature was confirmed in the flow regime studies.

Martinelli-Nelson [4] Model. Because a very large percentage of two-phase R-114 flowing in a vertical tube is annular in nature, the application of a separated flow model, such as the one presented by Martinelli-Nelson [4] should yield results better than those obtained by the Homogeneous [3] model. The results in Figures IV-41 to IV-44 attest to this. The Martinelli-Nelson [4] formulation for the void fraction applied here by modeling the water and R-114 values on an equal reduced pressure basis was used in the calculation of the gravitational and acceleration components. A comparison of the void fraction curves of the Homogeneous [3] model and Martinelli-Nelson [4] are given in Figure IV-45. The Homogeneous [3] model curve is higher in all quality ranges except for the very low ones.

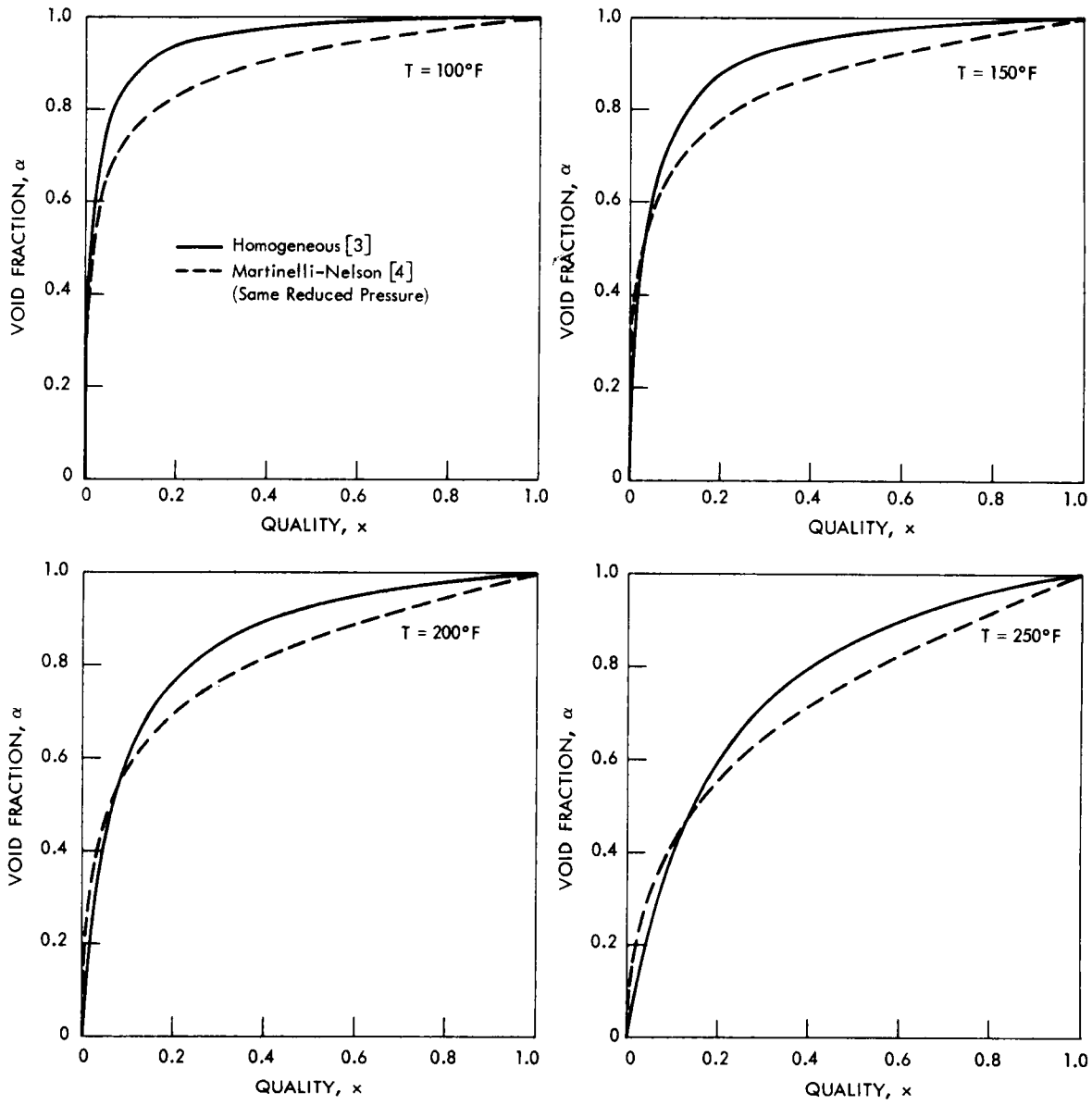


Figure IV-45. COMPARISON OF VOID FRACTION FORMULATIONS FROM THE HOMOGENEOUS [3] AND MARTINELLI-NELSON [4] MODELS.

Since it was found that the Zuber et al [10] general expression for the void fraction gave the best agreement when compared to the R-114 void fraction data of Shiralkar [50] and with the larger body of R-22 data of Zuber et al [10], it was used in the analysis of the present data. Because the expression in Equations (2-32), (2-42), and (2-43) is not accurate at high qualities (the void fraction does not go to one as the quality approaches one), it was modified by assuming a linear relationship between void fraction and quality in the range ($0.40 < x < 1.0$). Any discrepancies between this formulation and the true void fraction are believed to be small since the shape of this curve is in good agreement with all other void fraction equations. In addition since the void fraction is large in this region, the gravitational component is considerably smaller than it would be in the lower quality region. A comparison of this modified Zuber et al [10] void fraction correlation and the Martinelli-Nelson [4] formulation is shown in Figure IV-46. In the mass flux range covered in this study, the Martinelli-Nelson [4] void fraction is generally higher than that predicted by Zuber et al [10].

The results from the application of the Martinelli-Nelson [4] model with the modified Zuber et al [10] general void fraction formulation are shown in Figures IV-47 to IV-50. In general, the results obtained differed little from those in Figures IV-41 to IV-44 where the Martinelli-Nelson [4] form of the void fraction was used. The only improvements that resulted were in the low mass flux region at the 100, 150, and 200°F boiling temperatures. The use of the modified Zuber et al [10] void fraction correlation resulted in experimental values of

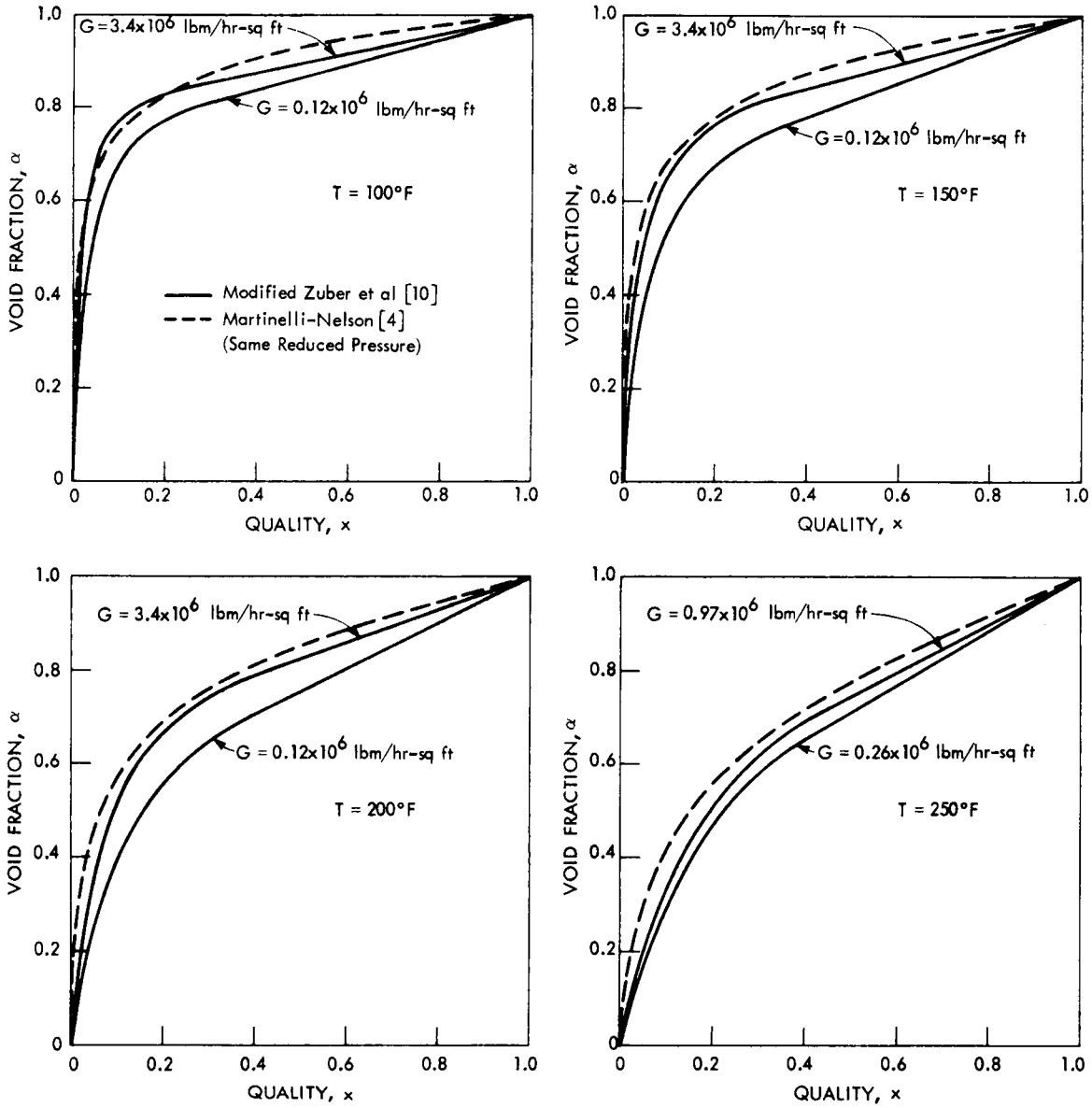
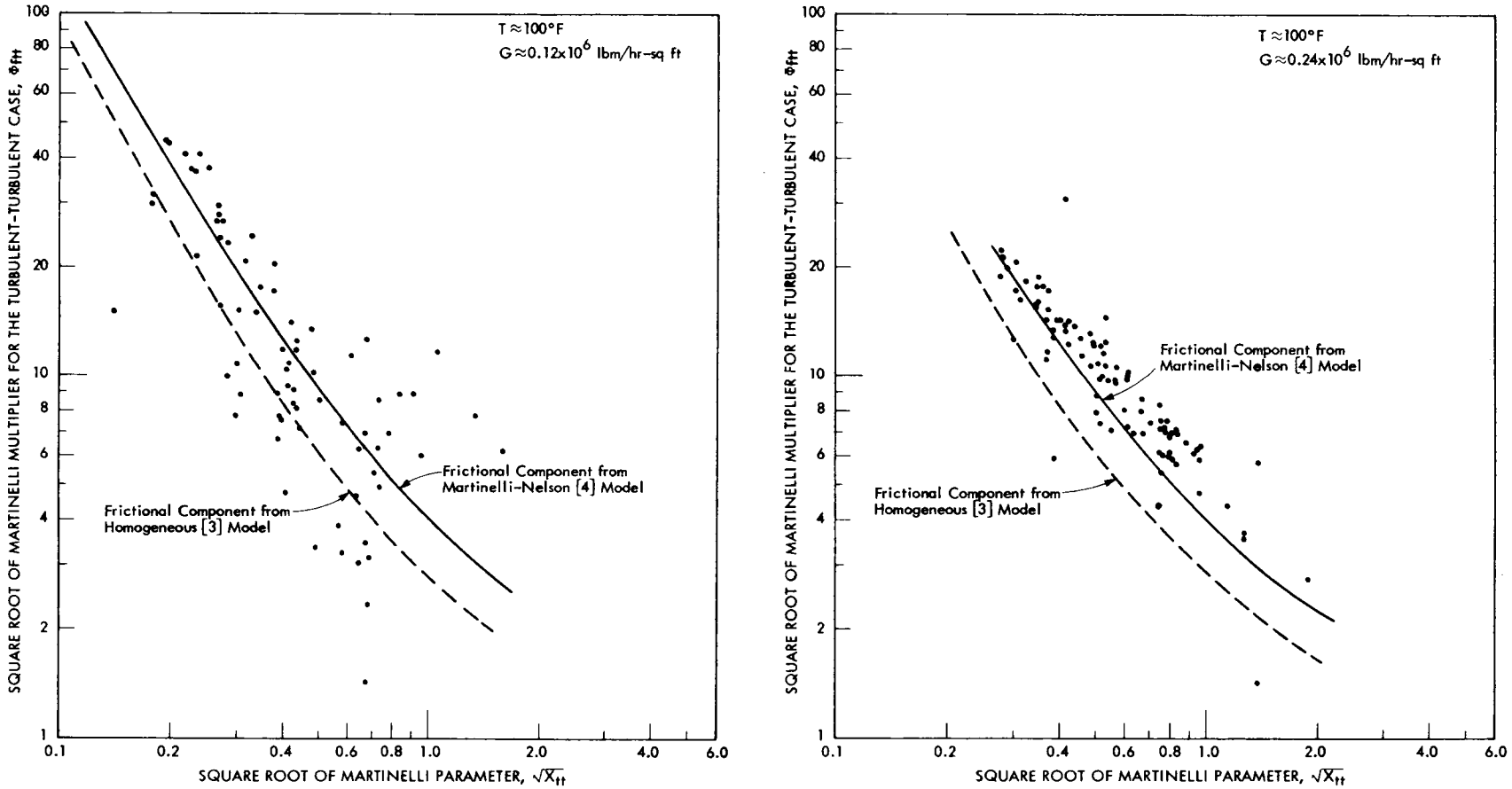
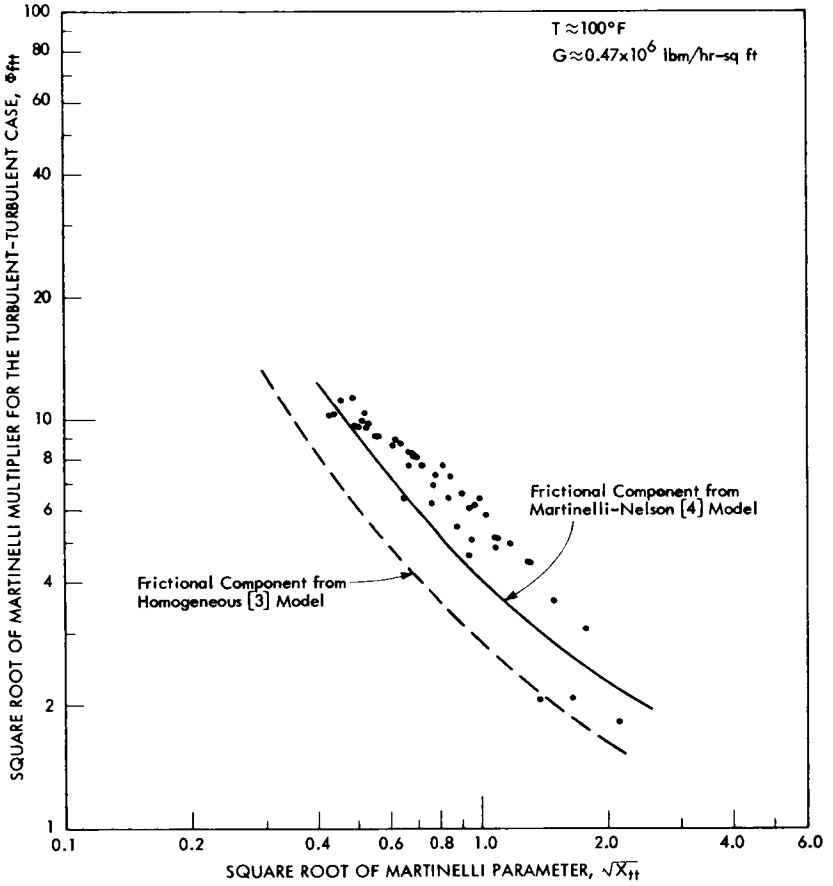


Figure IV-46. COMPARISON OF VOID FRACTIONS FROM A MODIFIED FORM OF THE ZUBER ET AL [10] FORMULATION AND MARTINELLI-NELSON [4].

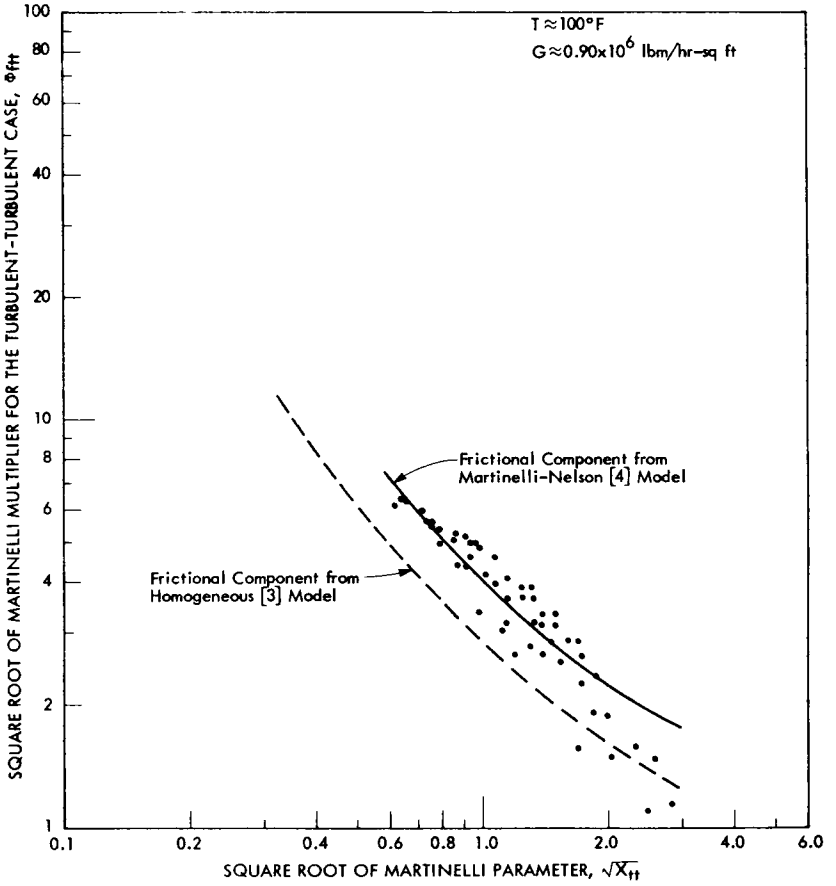


(a) (b)

Figure IV-47. COMPARISON OF EXPERIMENTAL PRESSURE DROP RESULTS WITH ANALYTICALLY DERIVED FRICTIONAL COMPONENTS USING THE MARTINELLI-NELSON [4] MODEL AND A MODIFIED FORM OF THE ZUBER ET AL [10] GENERAL VOID FRACTION CORRELATION, T≈100°F.

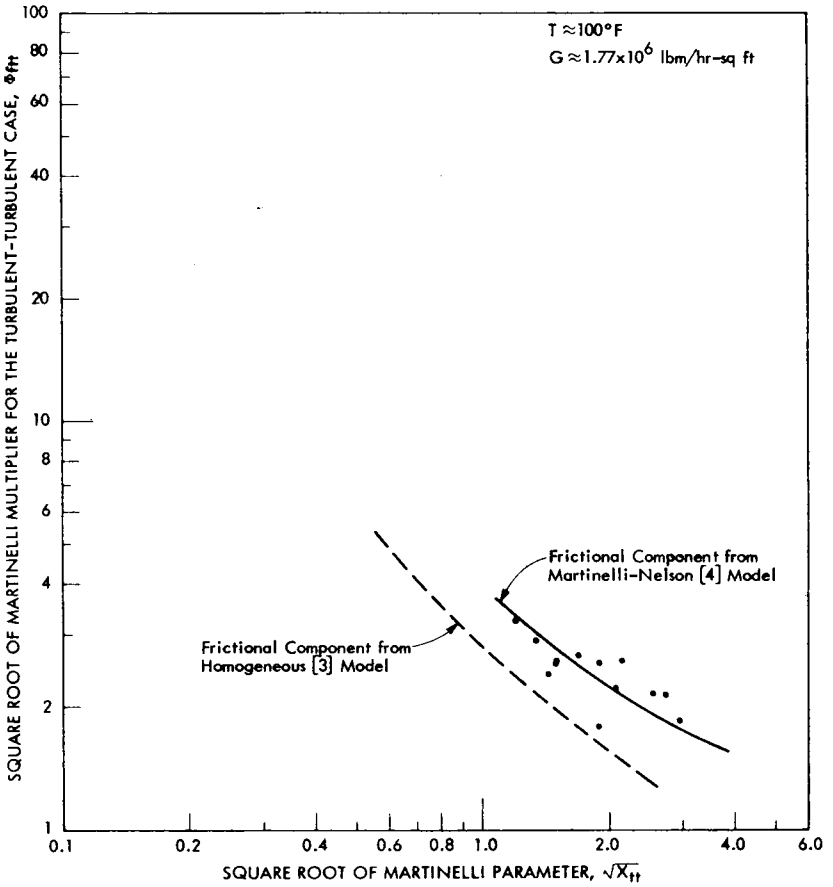


(c)



(d)

Figure IV-47. (continued)



(e)

Figure IV-47. (continued)

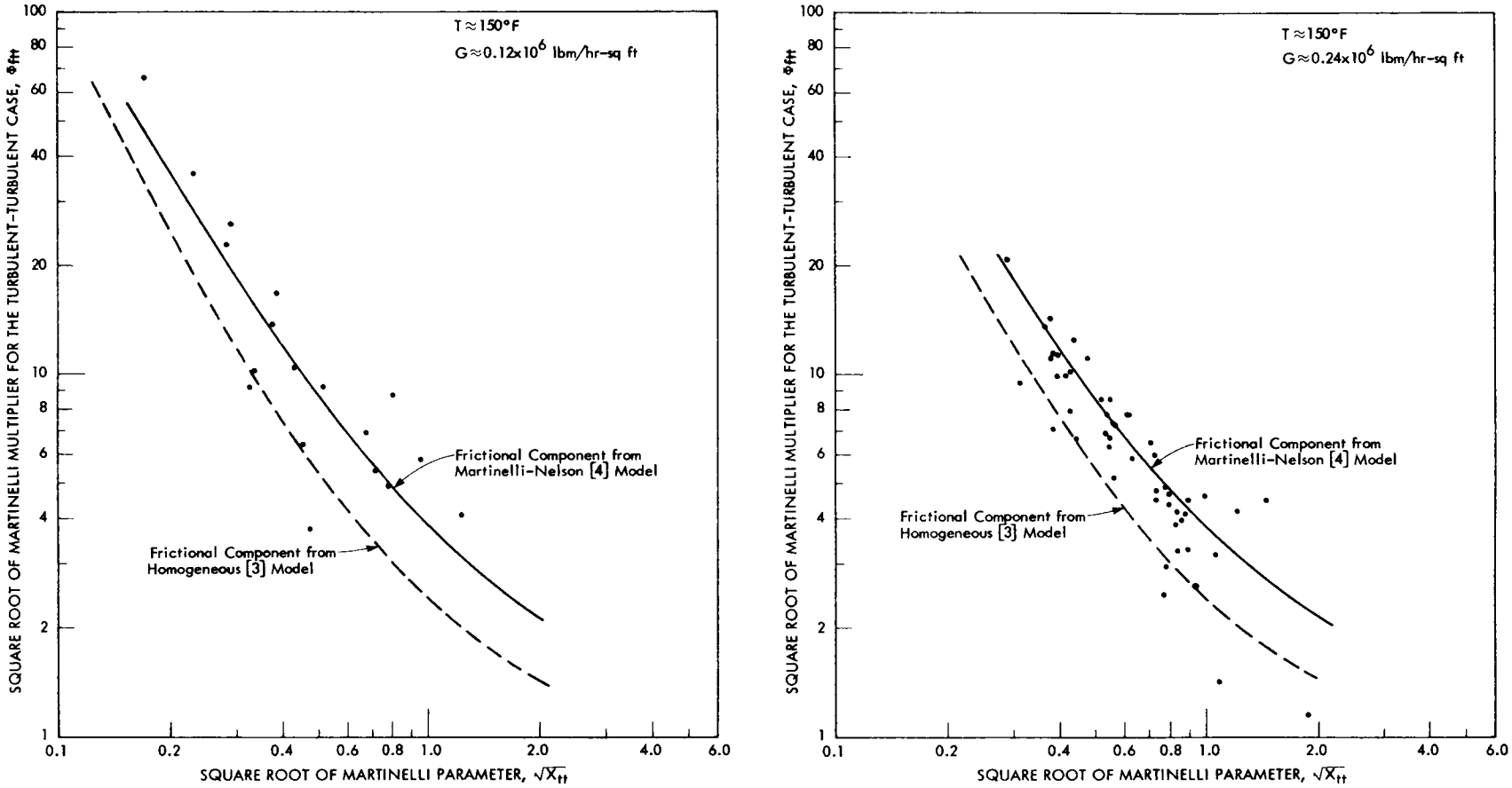
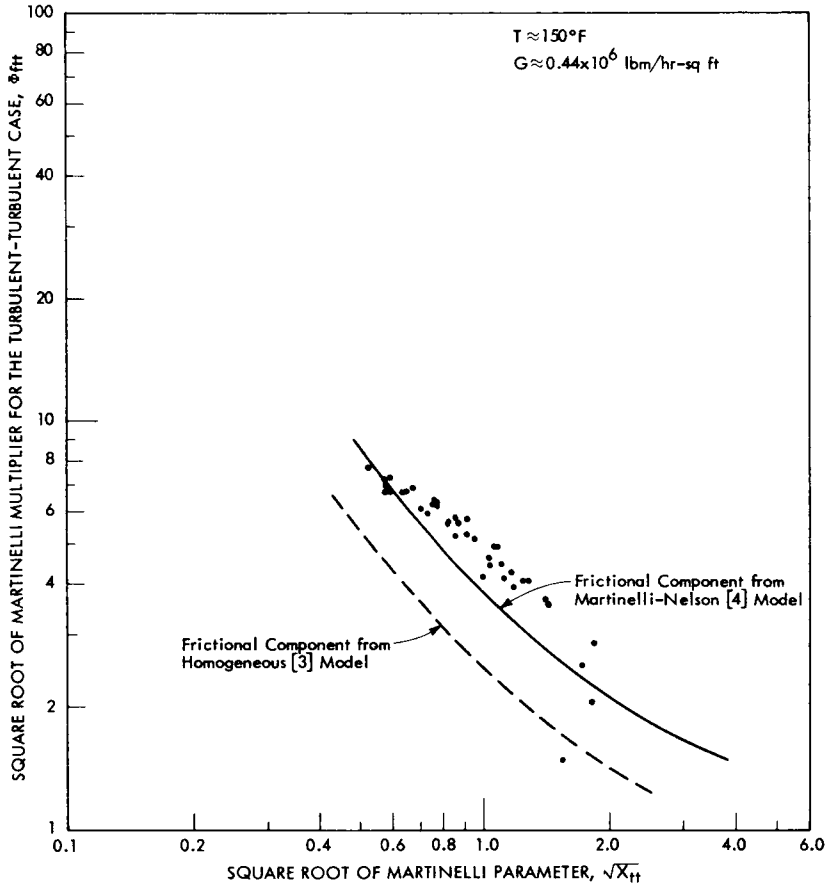
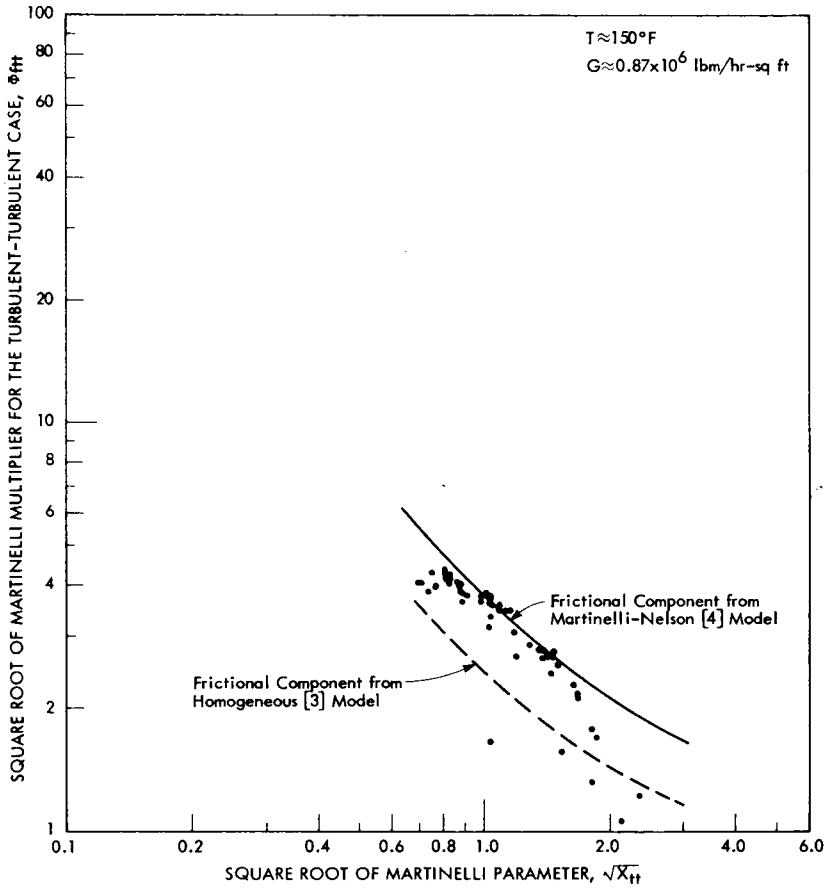


Figure IV-48. COMPARISON OF EXPERIMENTAL PRESSURE DROP RESULTS WITH ANALYTICALLY DERIVED FRICTIONAL COMPONENTS USING THE MARTINELLI-NELSON [4] MODEL AND A MODIFIED FORM OF THE ZUBER ET AL [10] GENERAL VOID FRACTION CORRELATION, T≈150°F.

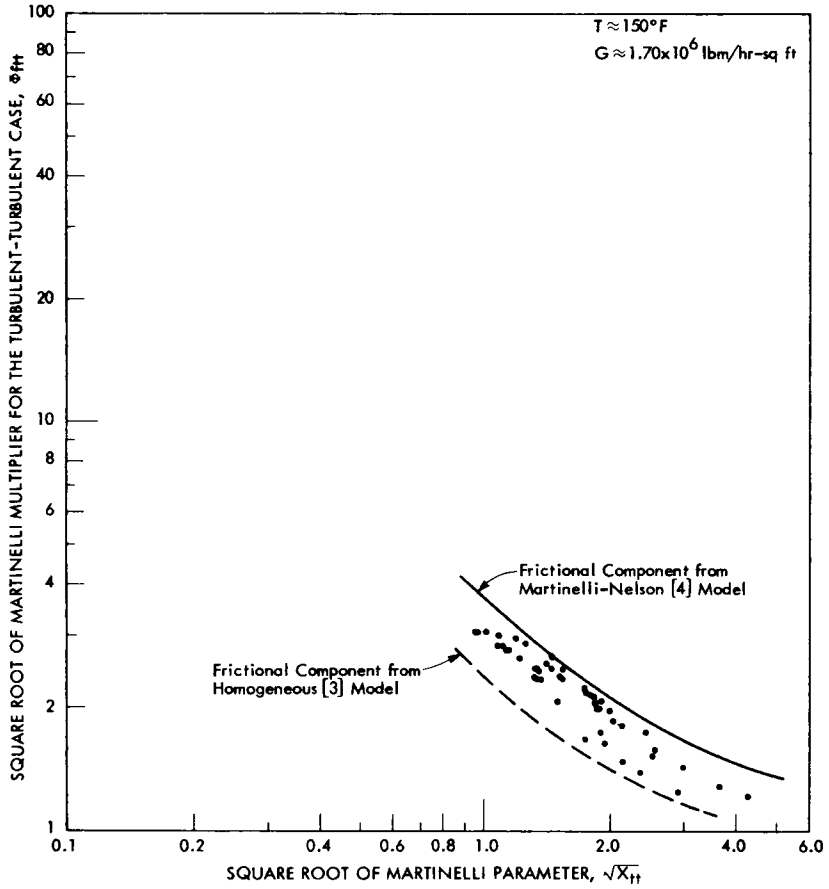


(c)

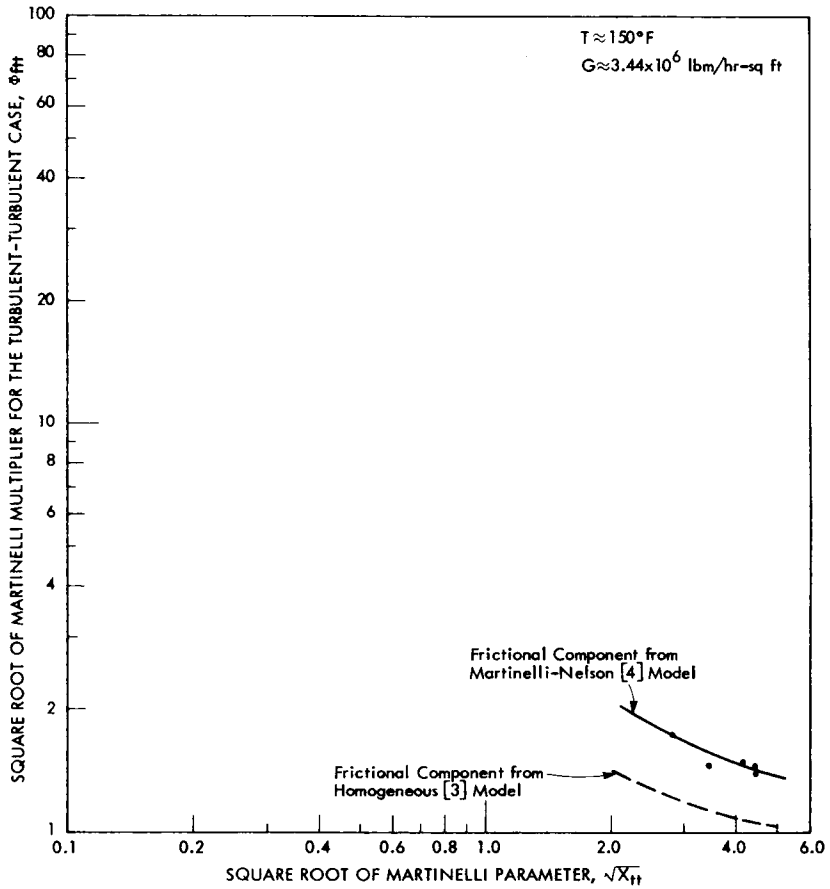


(d)

Figure IV-48. (continued)

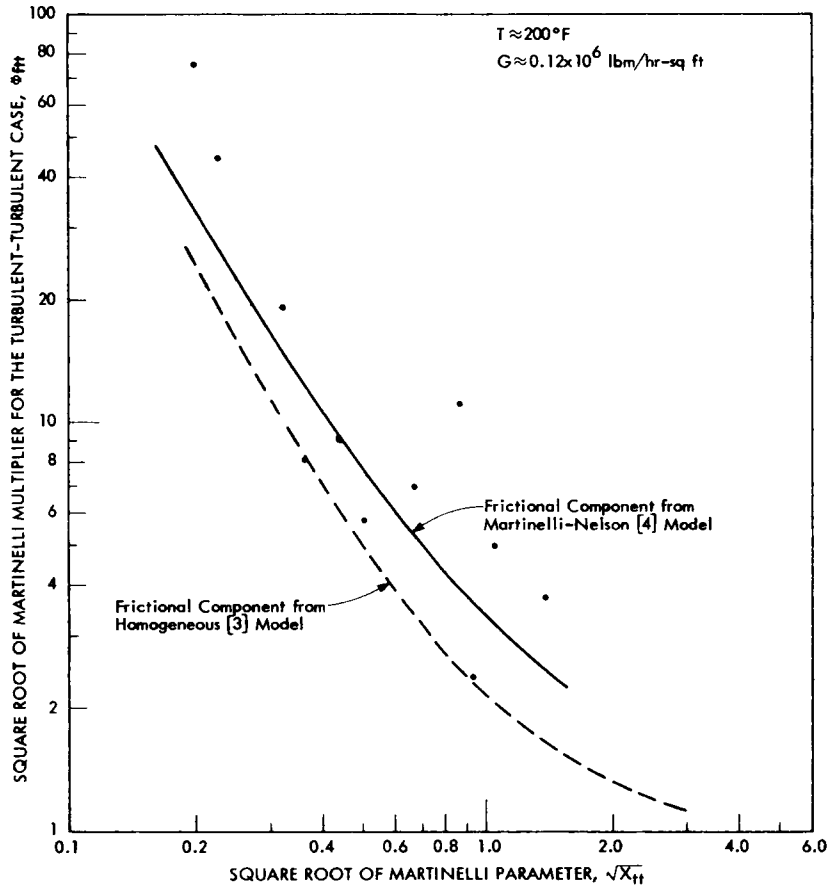


(e)

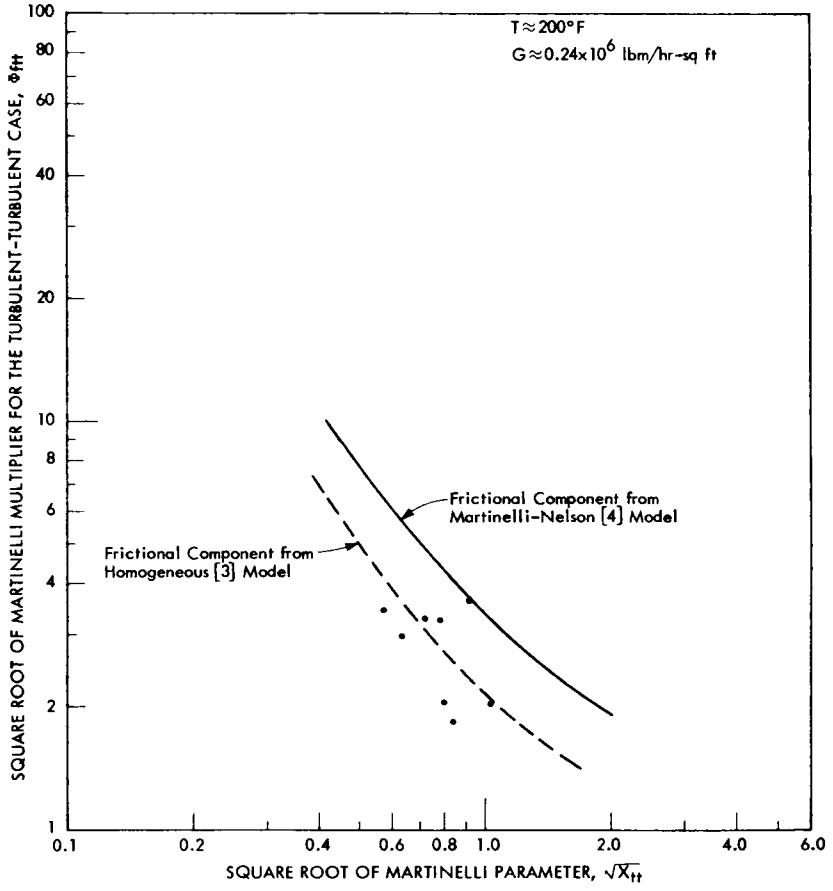


(f)

Figure IV-48. (continued)

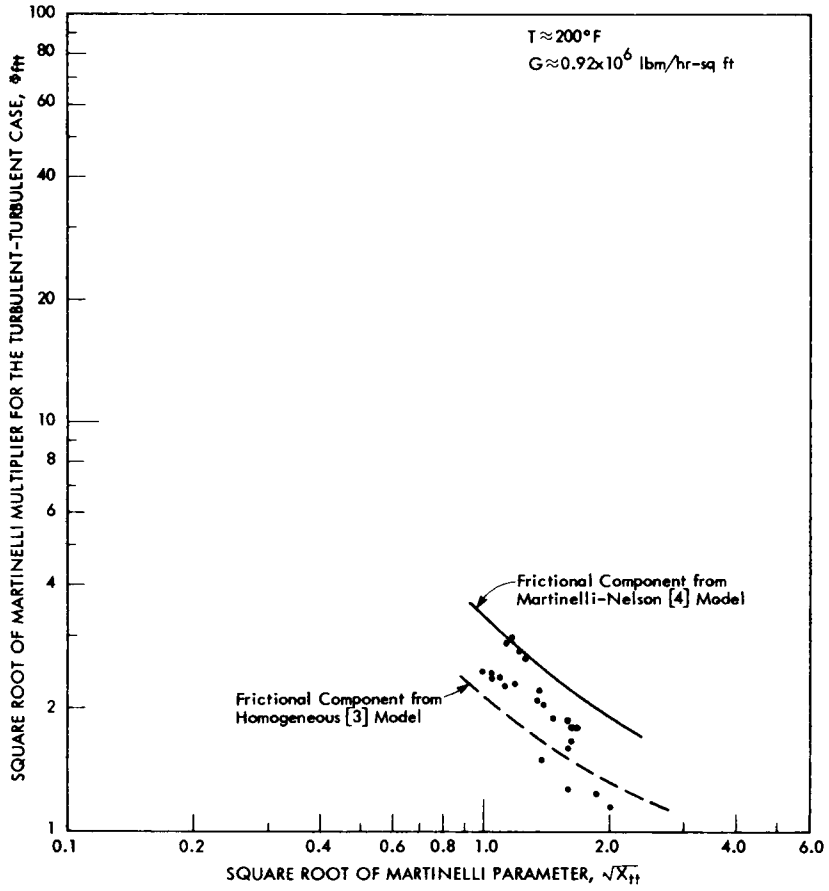


(a)

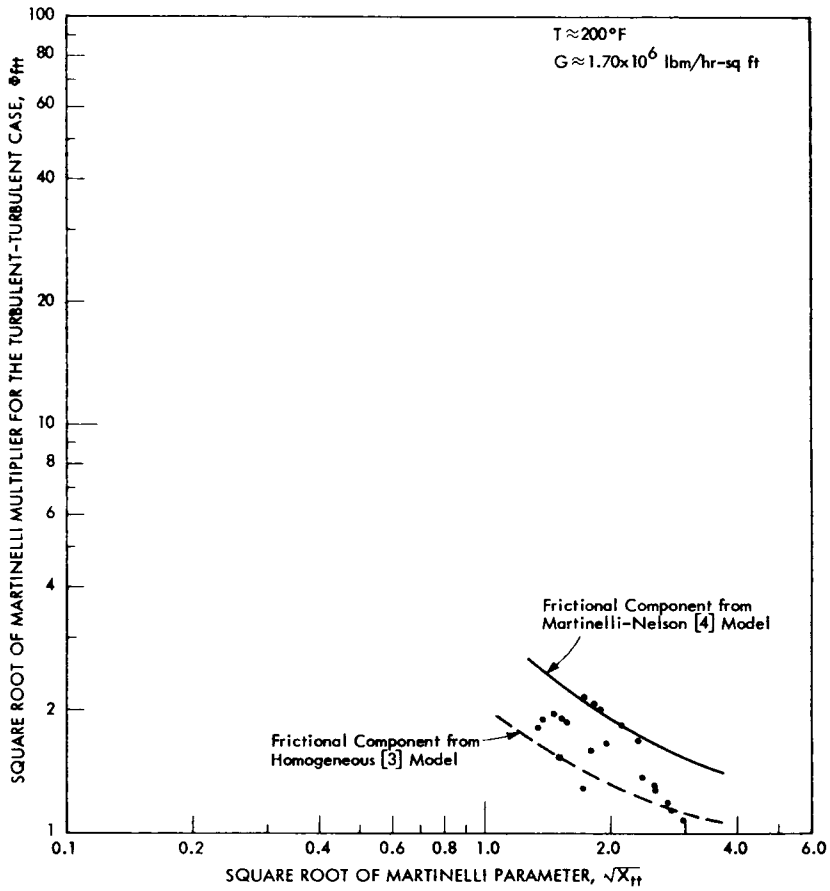


(b)

Figure IV-49. COMPARISON OF EXPERIMENTAL PRESSURE DROP RESULTS WITH ANALYTICALLY DERIVED FRICTIONAL COMPONENTS USING THE MARTINELLI-NELSON [4] MODEL AND A MODIFIED FORM OF THE ZUBER ET AL [10] GENERAL VOID FRACTION CORRELATION, T ≈200°F.

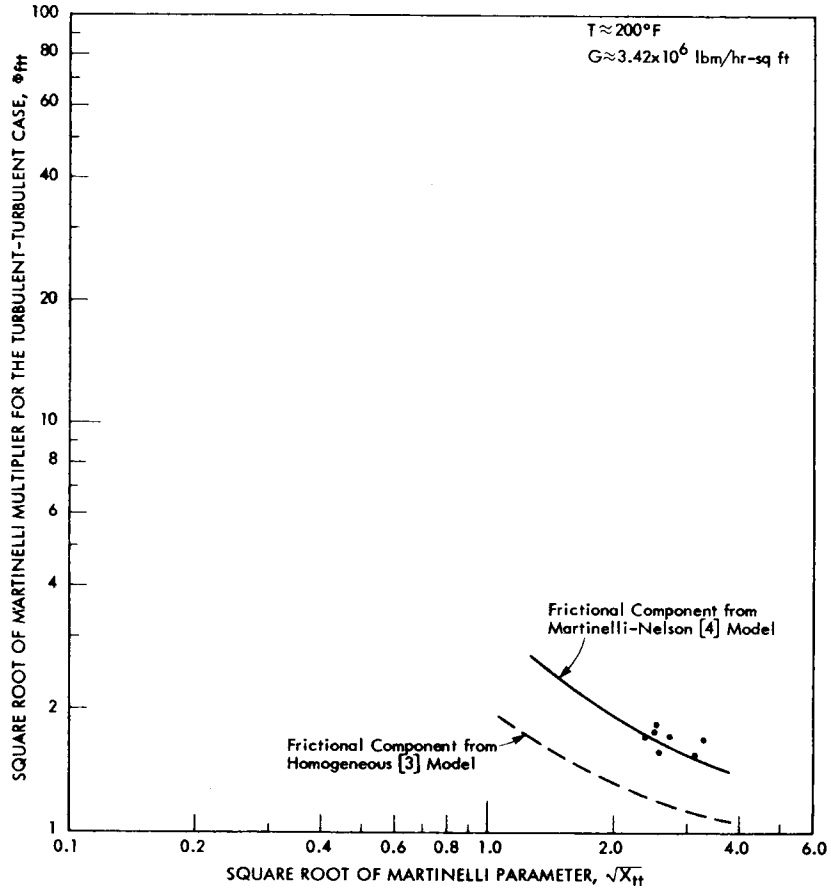


(c)



(d)

Figure IV-49. (continued)



(e)

Figure IV-49. (continued)

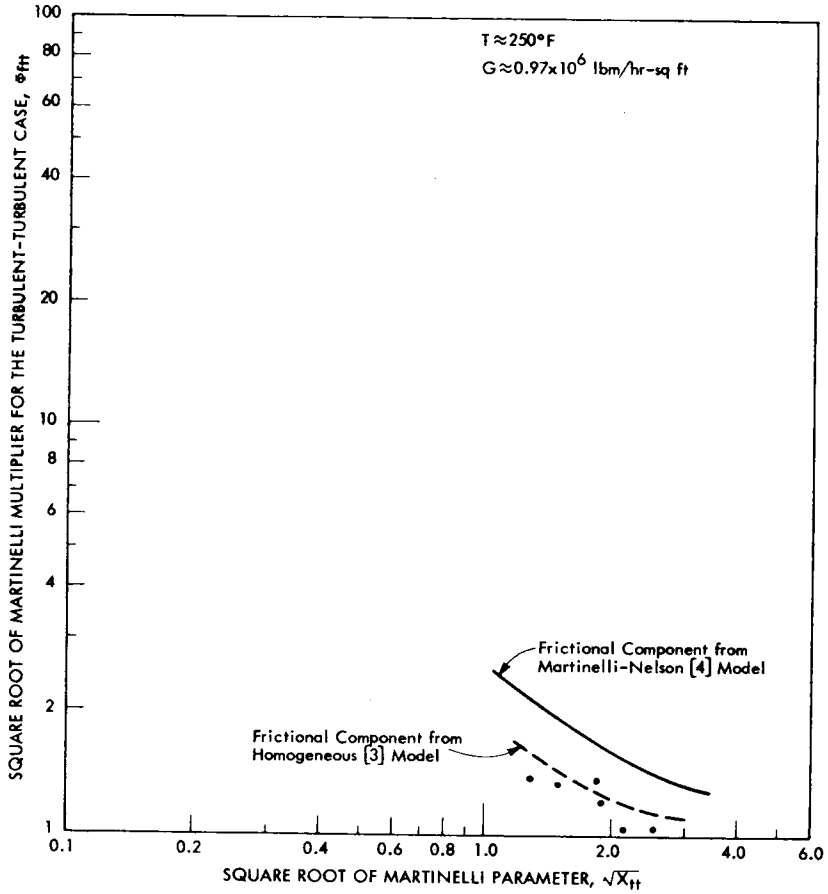


Figure IV-50. COMPARISON OF EXPERIMENTAL PRESSURE DROP RESULTS WITH ANALYTICALLY DERIVED FRICTIONAL COMPONENTS USING THE MARTINELLI-NELSON [4] MODEL AND A MODIFIED FORM OF THE ZUBER ET AL [10] GENERAL VOID FRACTION CORRELATION, T≈250°F.

Φ_{ftt} considerably closer to the Martinelli-Nelson [4] curve at the higher values of $\sqrt{X_{tt}}$. It should, however, be pointed out that for many runs, the computed sum of the gravitational and acceleration terms obtained using the Zuber et al [10] modified void fraction correlation was greater than the total experimentally measured pressure drop. These runs are denoted by asterisks in the tabulation of the correlated results for pressure drop in Appendix F. This raises some questions as to the range of applicability of the Zuber et al [10] modified void fraction correlation. Despite this uncertainty, the correlation will continue to be used in the analysis of the subsequent results because of the lack of more reliable information over a wide range on the void fraction of R-114.

Frictional Pressure Drop in the Critical Heat Flux Region. All of the pressure drop results presented above were taken in the region where no critical heat flux occurred. Data obtained in the critical heat flux region was found to correlate differently. As shown in Figures IV-51 to IV-54, the experimental Martinelli multiplier was below that observed in the non-critical heat flux runs at the higher values of $\sqrt{X_{tt}}$. An explanation of the phenomena can be found by recalling the two basic critical heat flux mechanisms explained in Section E of Chapter II. At high qualities, critical heat flux occurs when the liquid film on the wall dries up. Under these conditions, little change in the frictional component of the pressure drop can be expected. Figures IV-51 to IV-54 bear out this fact. When the critical heat flux occurs at lower qualities, however, a radically different phenomenon takes place. The bubbles generated close to the wall become so numerous

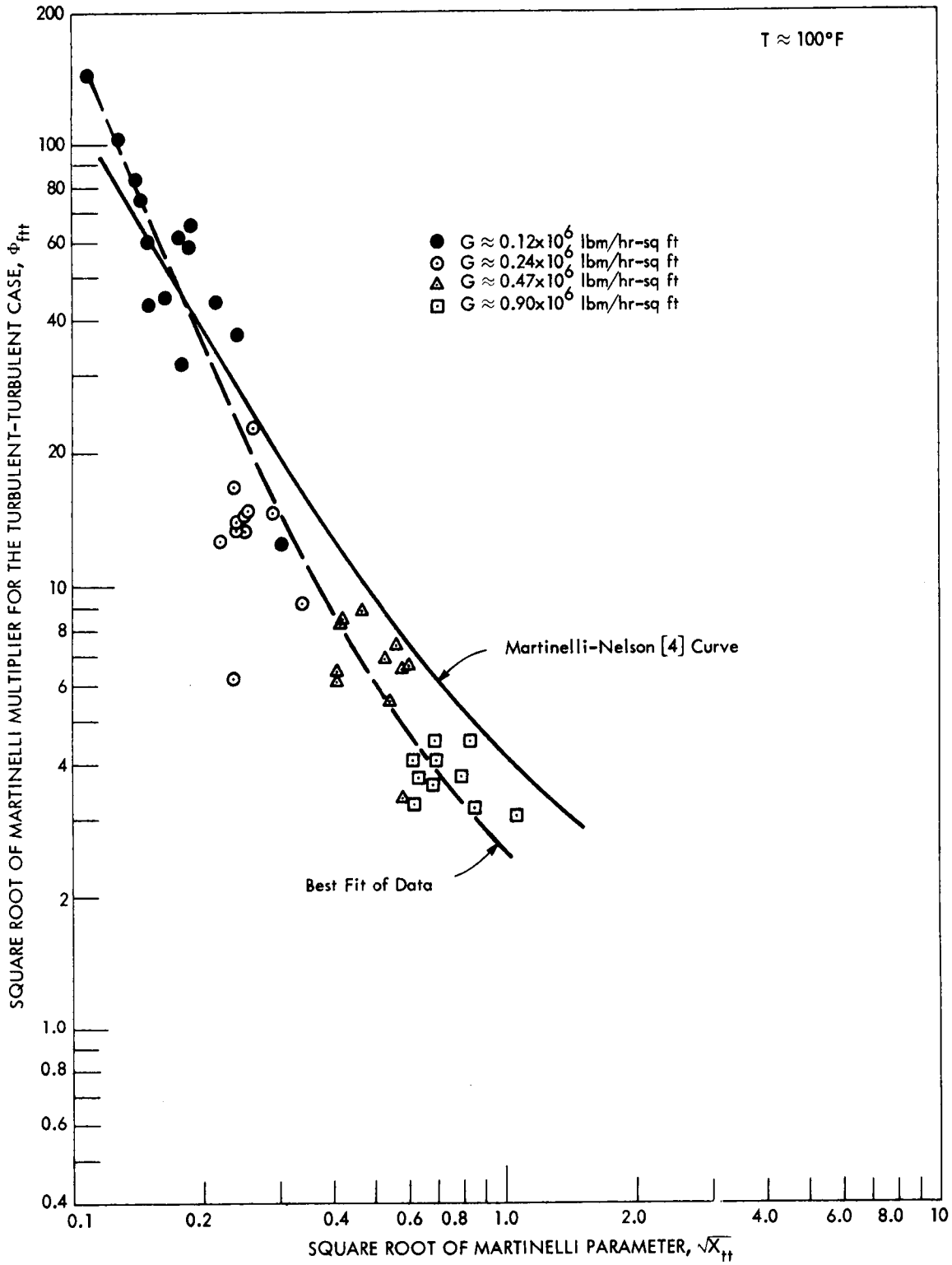


Figure IV-51. COMPARISON OF EXPERIMENTAL PRESSURE DROP RESULTS IN THE CRITICAL HEAT FLUX REGION WITH THE MARTINELLI-NELSON [4] MODEL AND A MODIFIED FORM OF THE ZUBER ET AL [10] GENERAL VOID FRACTION CORRELATION, T ≈ 100°F.

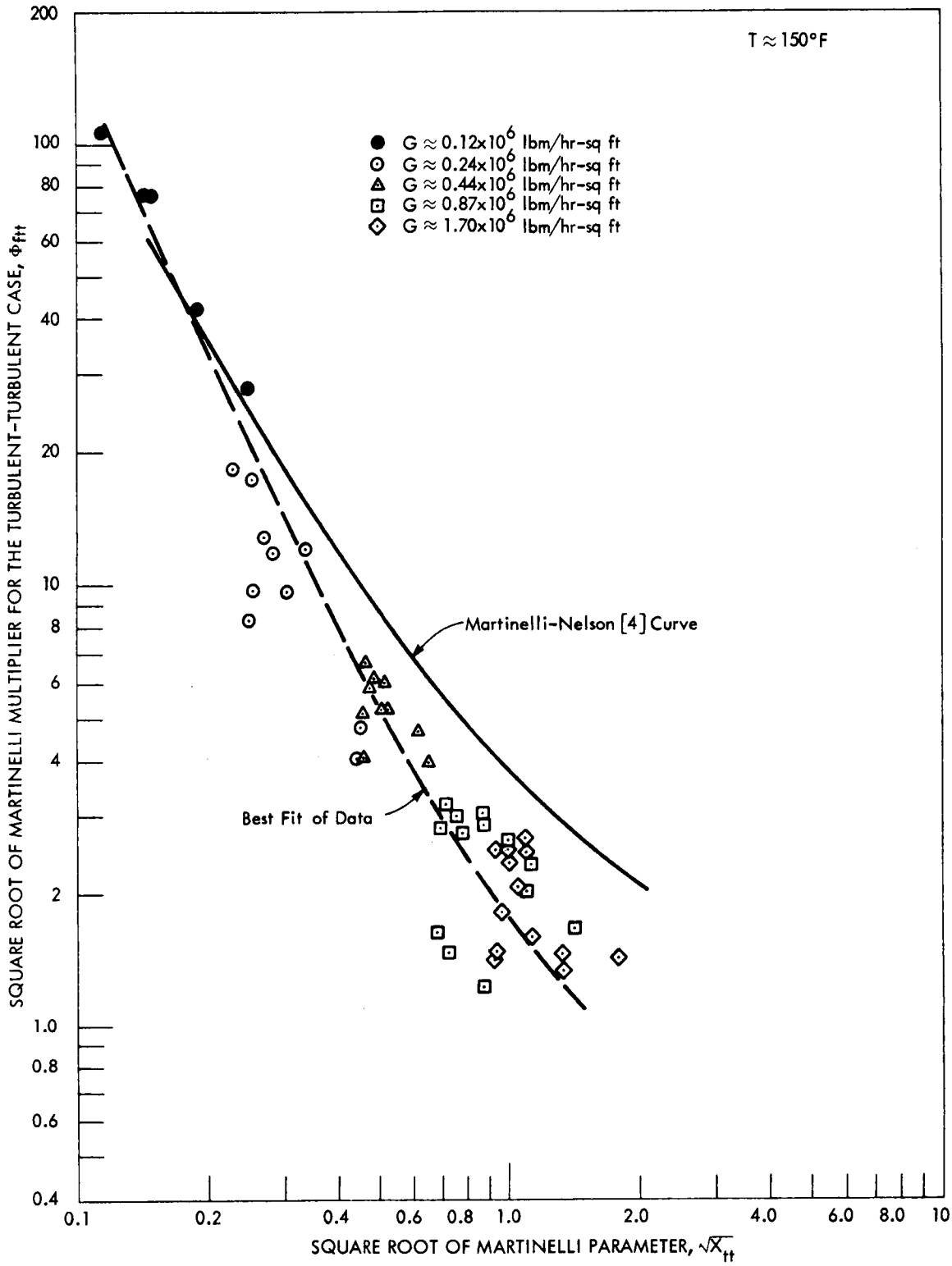


Figure IV-52. COMPARISON OF EXPERIMENTAL PRESSURE DROP RESULTS IN THE CRITICAL HEAT FLUX REGION WITH THE MARTINELLI-NELSON [4] MODEL AND A MODIFIED FORM OF THE ZUBER ET AL [10] GENERAL VOID FRACTION CORRELATION, T ≈ 150°F.

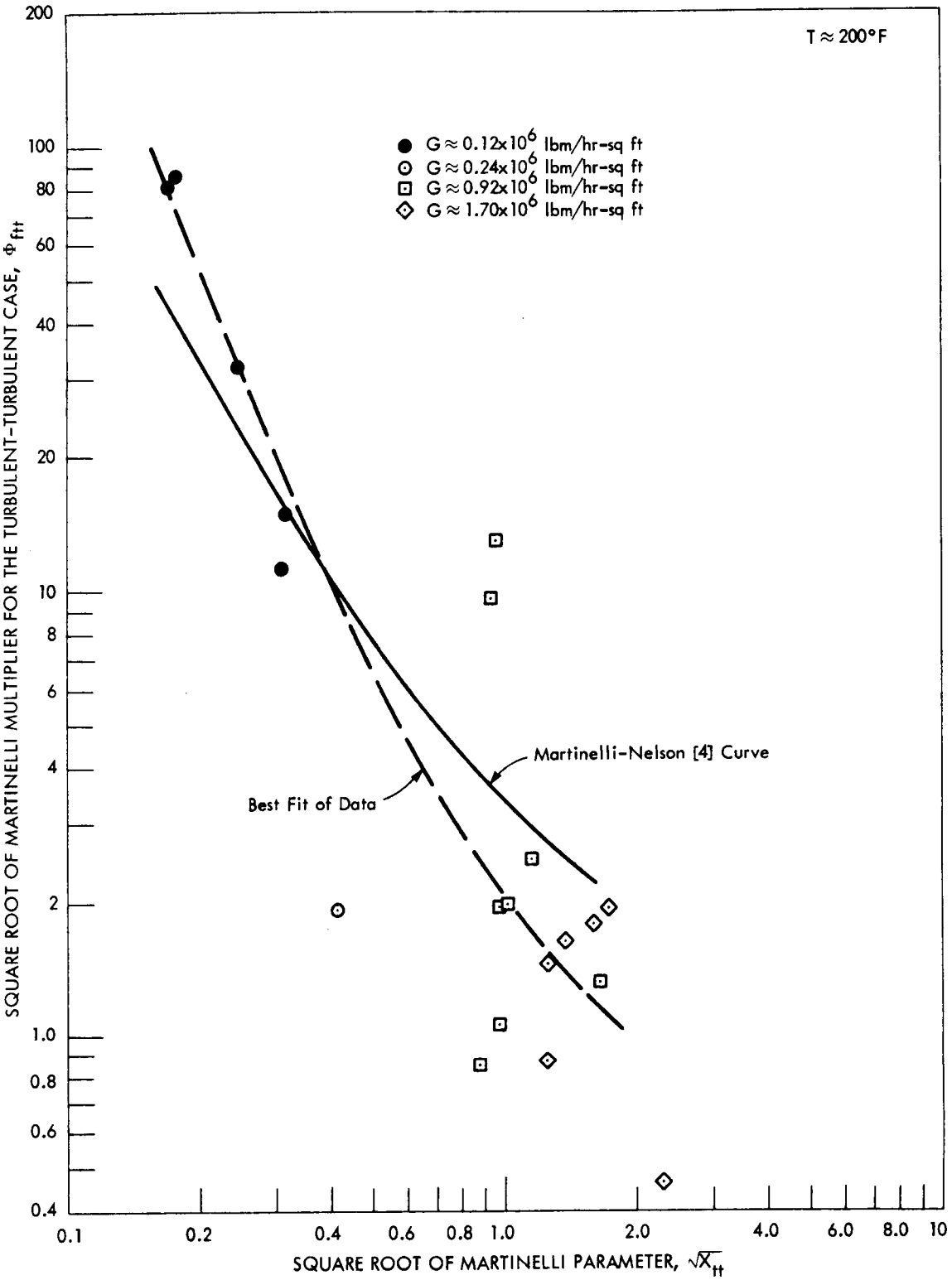
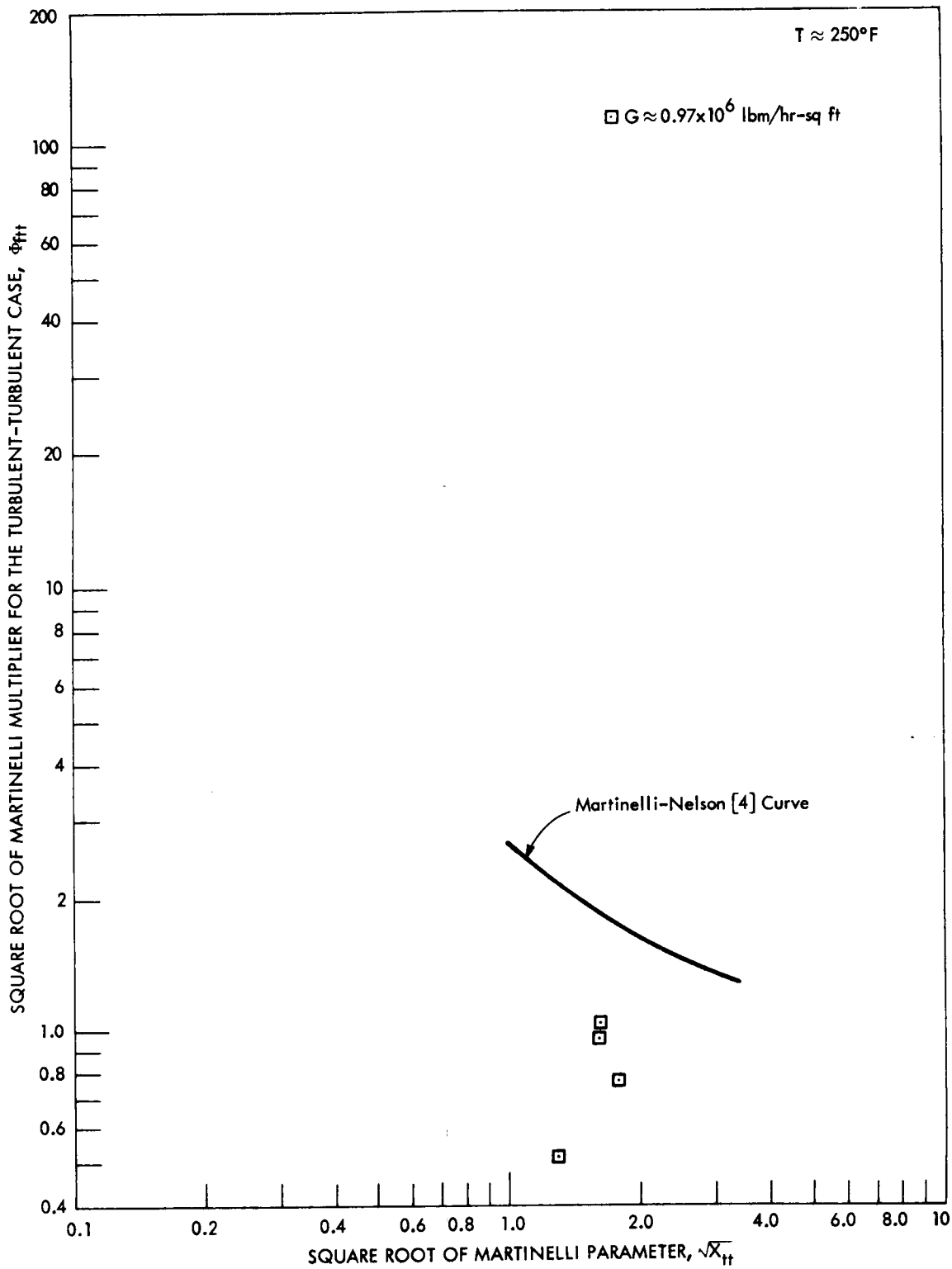


Figure IV-53. COMPARISON OF EXPERIMENTAL PRESSURE DROP RESULTS IN THE CRITICAL HEAT FLUX REGION WITH THE MARTINELLI-NELSON [4] MODEL AND A MODIFIED FORM OF THE ZUBER ET AL [10] GENERAL VOID FRACTION CORRELATION, T ≈ 200°F.



Form IV-54. COMPARISON OF EXPERIMENTAL PRESSURE DROP RESULTS IN THE CRITICAL HEAT FLUX REGION WITH THE MARTINELLI-NELSON [4] MODEL AND A MODIFIED FORM OF THE ZUBER ET AL [10] GENERAL VOID FRACTION CORRELATION, T ≈ 250°F.

that they form an insulating layer between the liquid core and the wall. Under these conditions, the frictional component can be expected to change markedly. This bubble layer decreases the wall shear stress and results in a lower frictional pressure drop. The thickness of this bubble layer is an important parameter and is believed to depend on numerous parameters such as the heat flux, mass flow rate and quality. No attempt to determine the effect of these parameters on the frictional component of the pressure drop was attempted in this study because the amount of data was limited. For design purposes, the non-critical heat flux values for frictional pressure drop can be used as a first approximation. They will lead to quite conservative designs. The other alternative is to use the best fit of the data in Figures IV-51 to IV-54.

Other Frictional Pressure Drop Models

The results plotted in Figures IV-37 to IV-44 on pages 159 to 178 indicate that the experimental Martinelli parameter, Φ^2_{ftt} is mass flux dependent. This trend was also noted by other investigators for other working fluids and a number of correlations, reviewed in Chapter II, Section B, have been proposed. A comparison of many of these correlations with the present non-critical heat flux data will now be attempted.

Davis [34] Correlation. The mass flux modification presented by this correlation is quite straightforward. It involves defining a modified Martinelli parameter such that:

$$X_{tt_1} = C_4\left(\frac{1-x}{x}\right)^{0.9}\left(\frac{\rho_g}{\rho_f}\right)^{0.5}\left(\frac{\mu_f}{\mu_g}\right)^{0.1}(Fr_m)^{0.185}. \qquad (4\text{-}5)$$

Davis [34] correlated air-water and air-trichloroethylene data with a C_4 of 0.19. Napadensky [15] used a C_4 of one. In the present tests, a

C_4 of 0.549 was found to correlate the data best. The results in Figures IV-55 to IV-57 for the 100, 150, and 200°F tests include representative points for the various flow rates.

It should be noted that the same Martinelli-Nelson [4] curve was used in the Φ_{ftt} versus $\sqrt{X_{tt_1}}$ curves as in the Φ_{ftt} versus $\sqrt{X_{tt}}$ curves. As can be seen, this correlation works quite well. Its only detraction is the fact that C_4 is not constant and can only be determined experimentally. It varies over a wide range as witnessed by the values of 0.19, 0.549, and 1.0 obtained so far.

Baroczy [23] Correlation. The mass flux correction utilized in this correlation involves the use of the graphs in Figures II-7 and II-8 on pages 27 and 29. The results are shown in Figures IV-58 to IV-61. The agreement is generally quite good. The plots are seen to exhibit some unusual curvature in certain cases and this is believed to be due to the two-phase multiplier ratio, Ω, in Figure II-8 on page 29. Since values for the multiplier ratio were presented only in the mass flux range:

$$0.25 \times 10^6 \leq G \leq 3.0 \times 10^6 \text{ lbm/hr-sq ft}$$

the curves obtained for $G \approx 0.12 \times 10^6$ and $G \approx 3.4 \times 10^6$ lbm/hr-sq ft were extrapolations. This could be partially responsible for the difference between the experimental results and the correlation at $G \approx 3.4 \times 10^6$ lbm/hr-sq ft for both 150 and 200°F boiling cases.

Chisholm [24, 25, 26, 27, 28] Correlation. Both Chisholm [24, 25, 26, 27, 28] correlations represented by Equations (2-13) to (2-20) and (2-21) and (2-22) are also plotted in Figures IV-58 to IV-61. In all cases, the 1973 correlation [28] lay slightly below the earlier one.

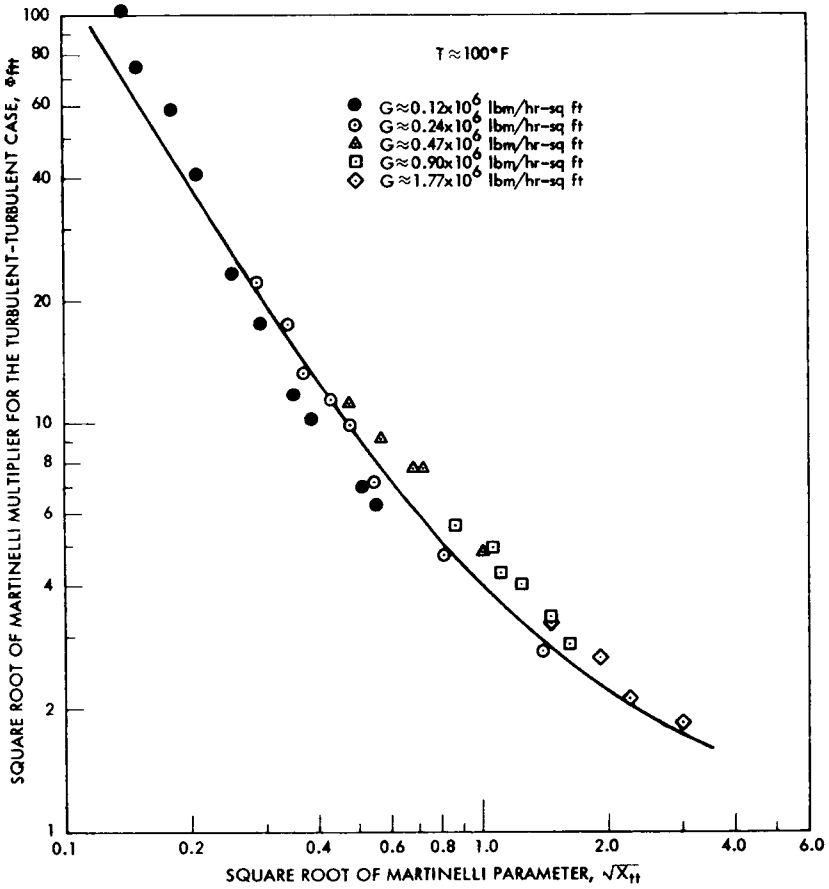


Figure IV-55. COMPARISON OF EXPERIMENTAL PRESSURE DROP RESULTS WITH DAVIS [34] CORRELATION, T≈100°F.

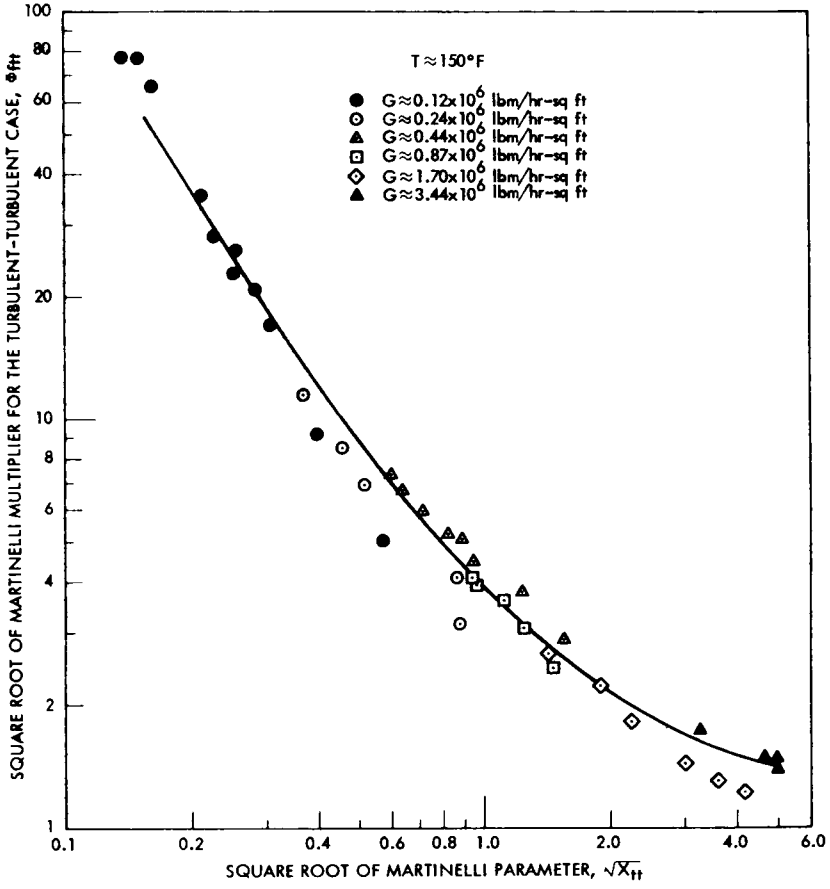


Figure IV-56. COMPARISON OF EXPERIMENTAL PRESSURE DROP RESULTS WITH DAVIS [34] CORRELATION, T≈150°F.

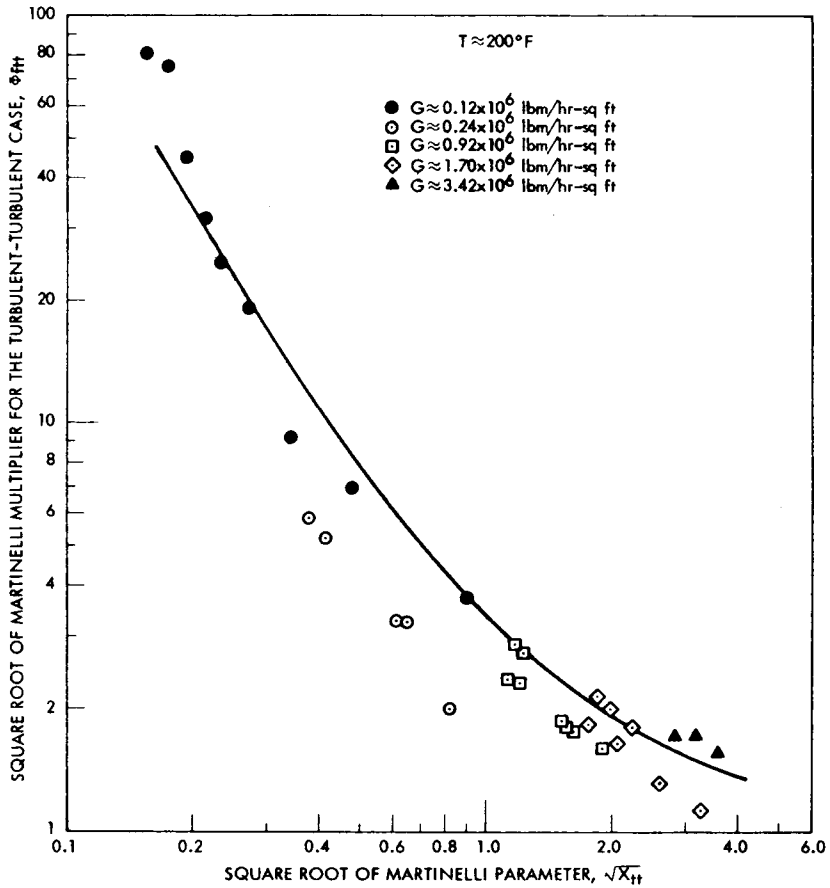
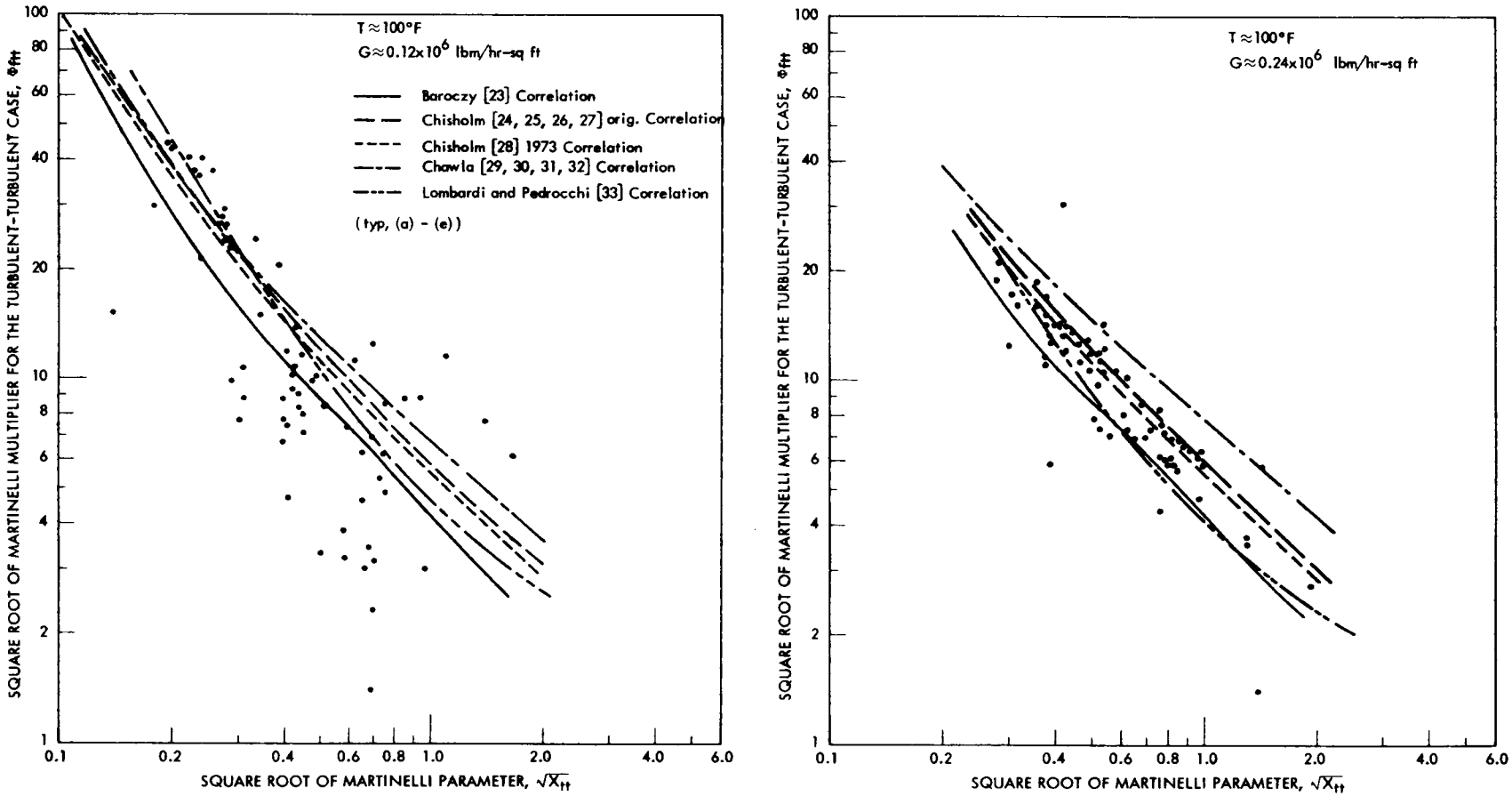
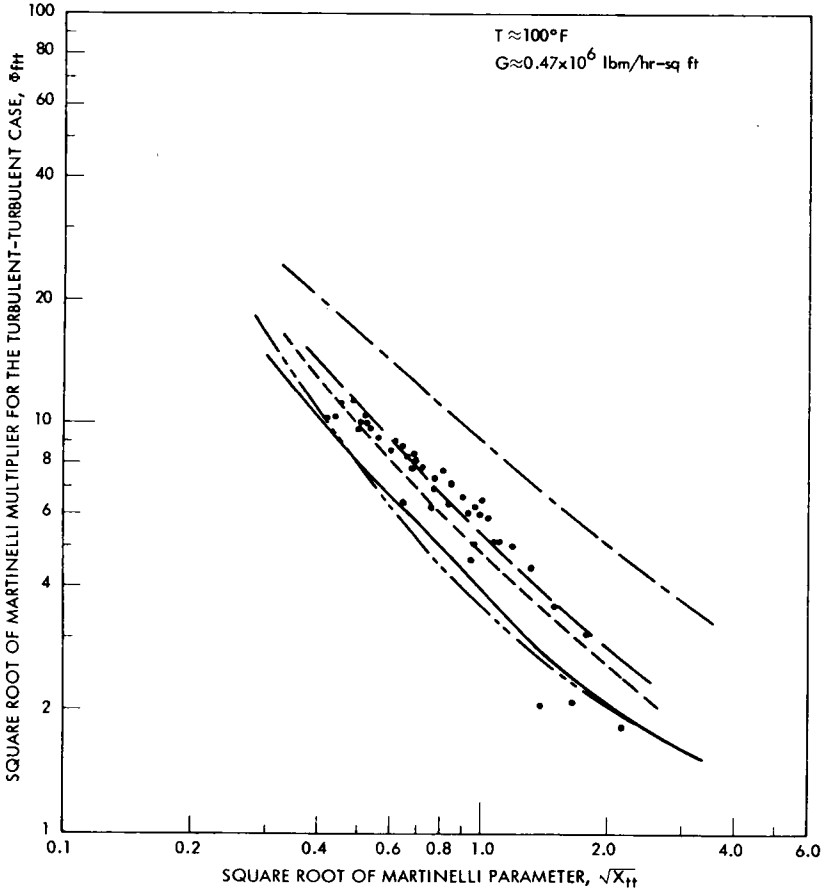


Figure IV-57. COMPARISON OF EXPERIMENTAL PRESSURE DROP RESULTS WITH DAVIS [34] CORRELATION, T≈200°F.

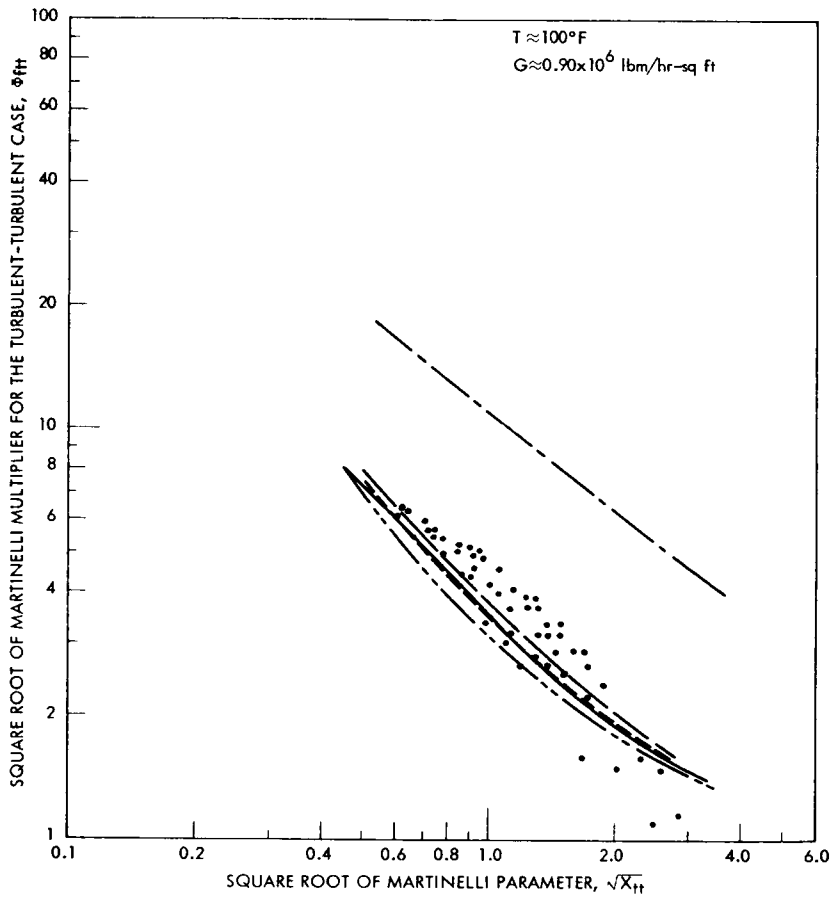


(a) (b)

Figure IV-58. COMPARISON OF EXPERIMENTAL PRESSURE DROP RESULTS WITH VARIOUS CORRELATIONS, T ≈ 100°F.

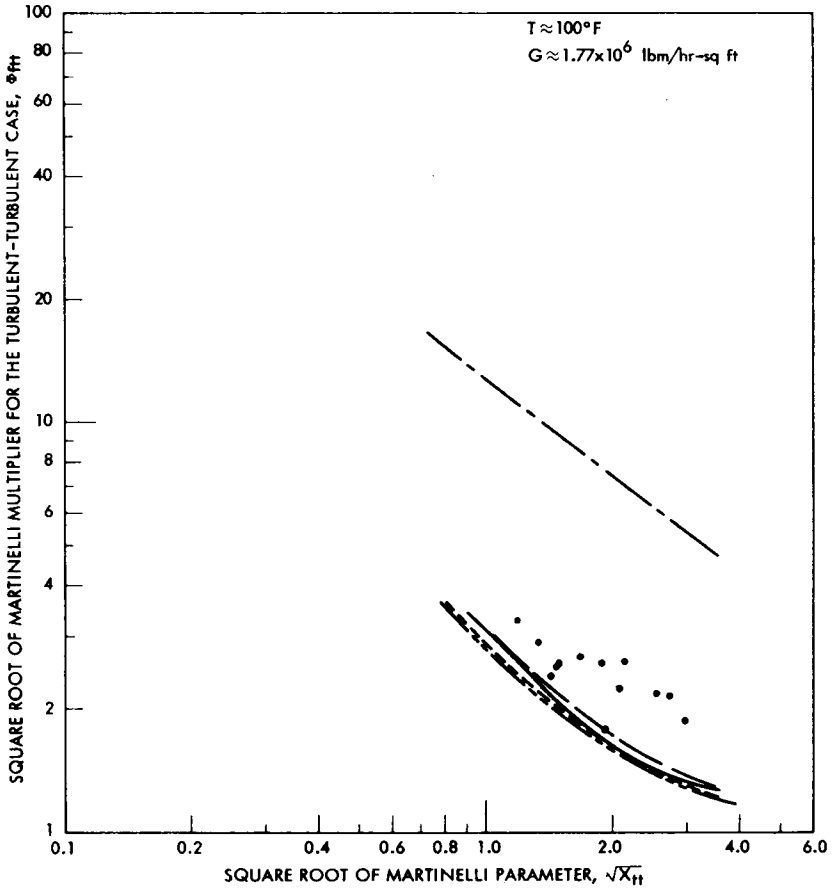


(c)



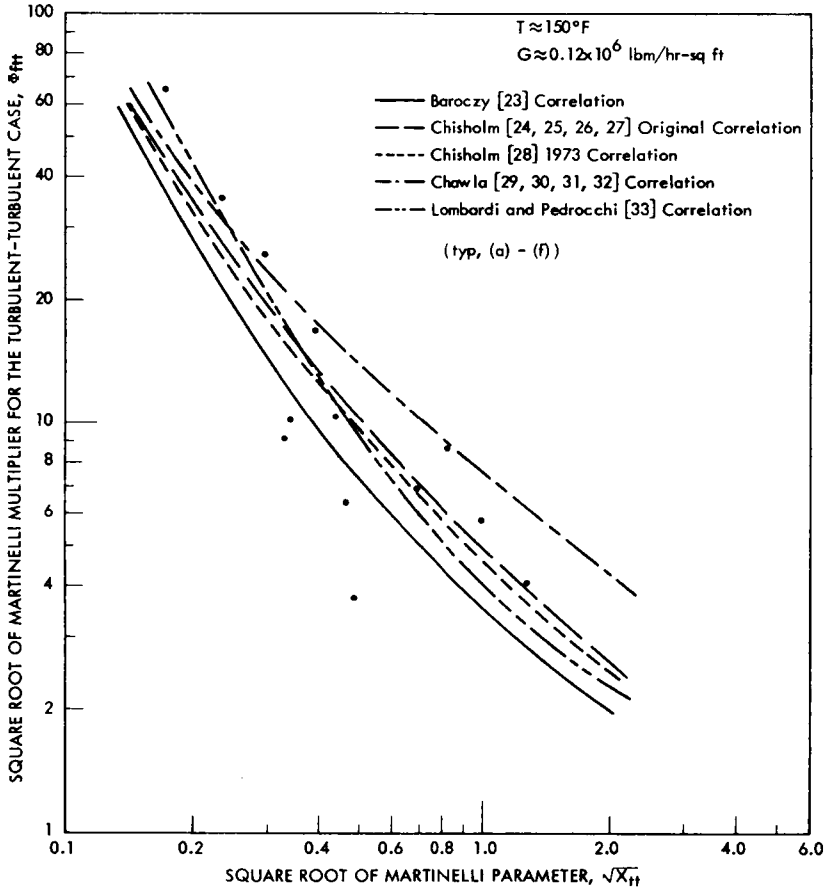
(d)

Figure IV-58. (continued)

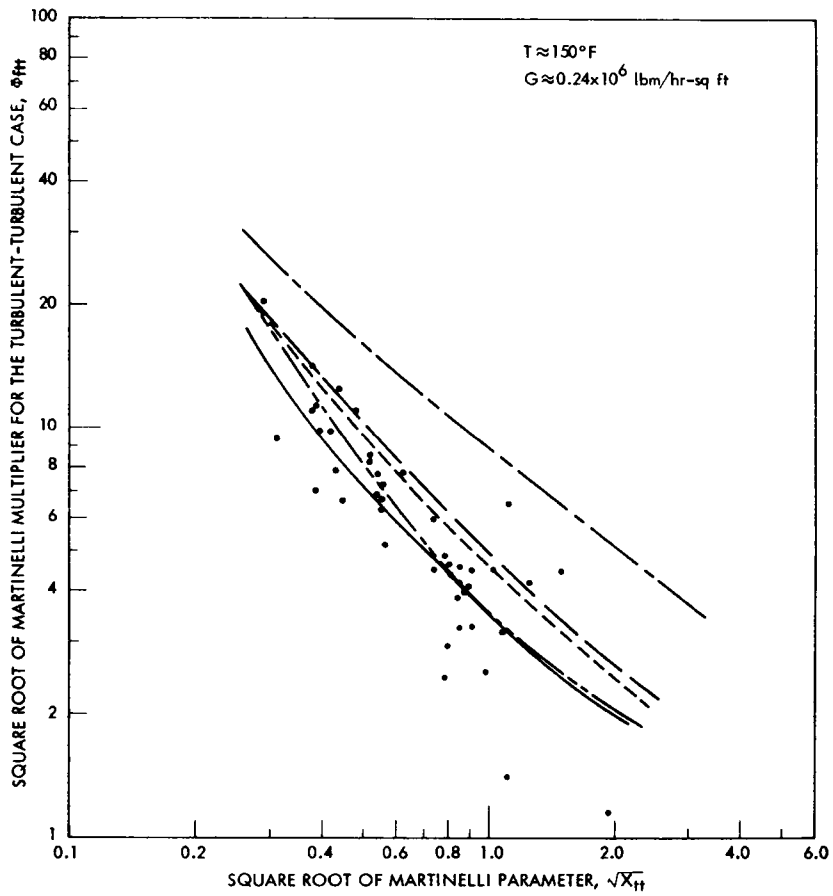


(e)

Figure IV-58. (continued)

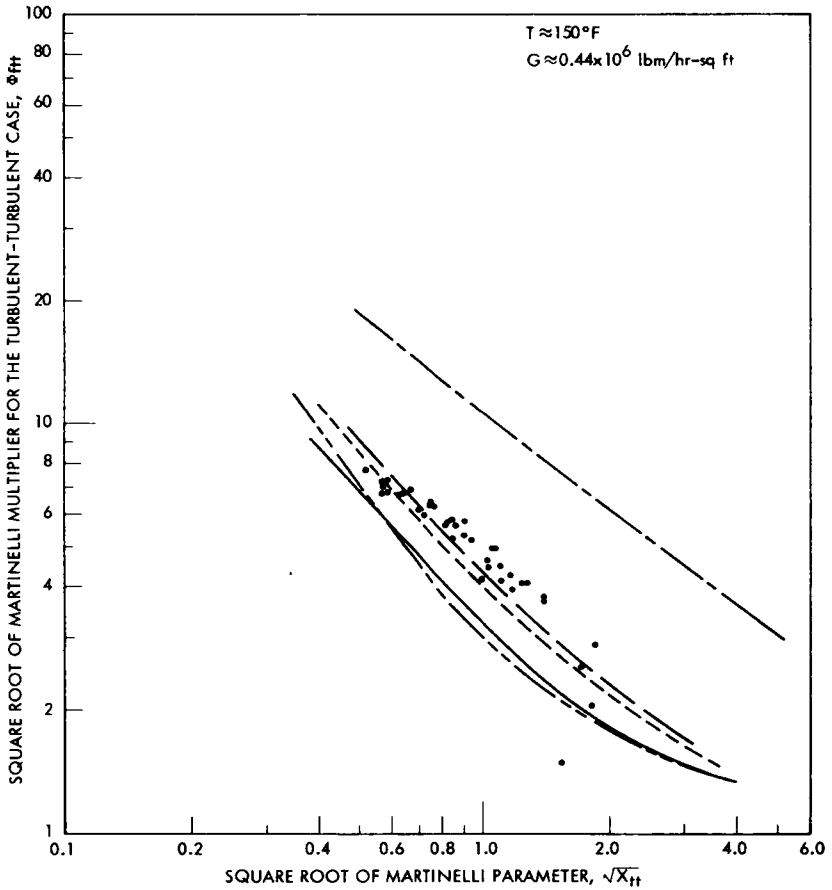


(a)

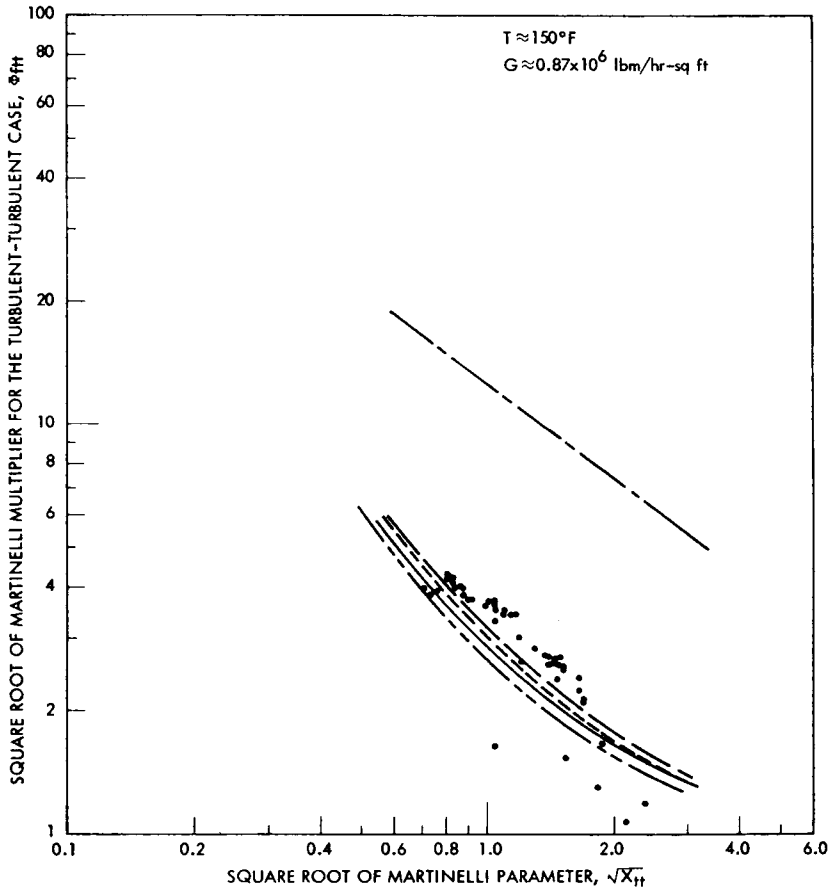


(b)

Figure IV-59. COMPARISON OF EXPERIMENTAL PRESSURE DROP RESULTS WITH VARIOUS CORRELATIONS, T ≈ 150°F.

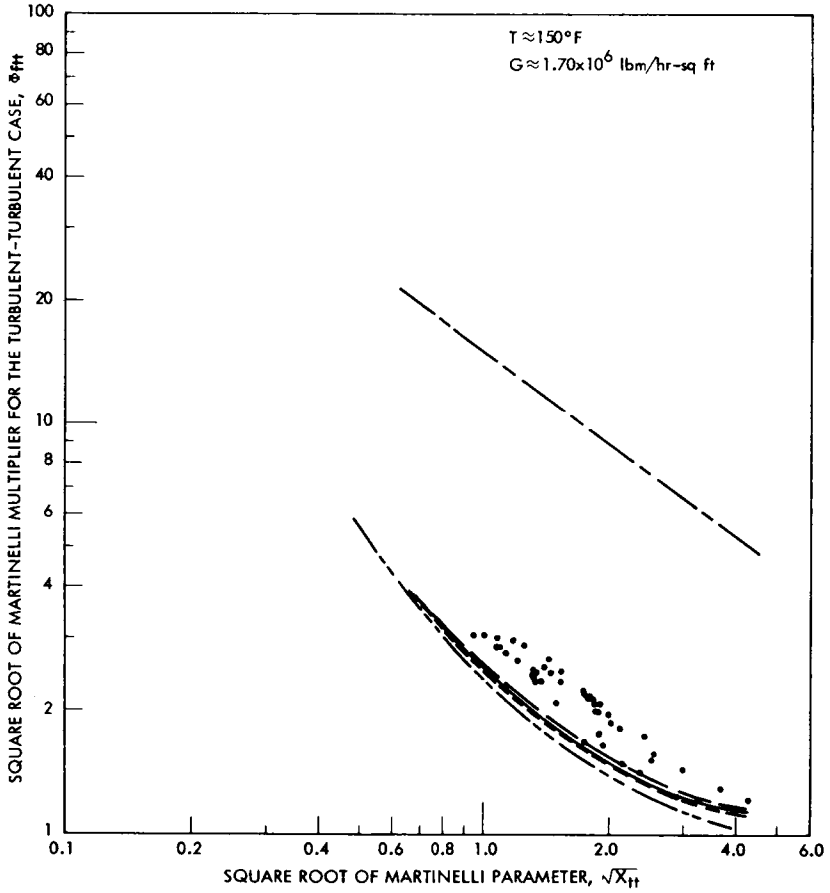


(c)

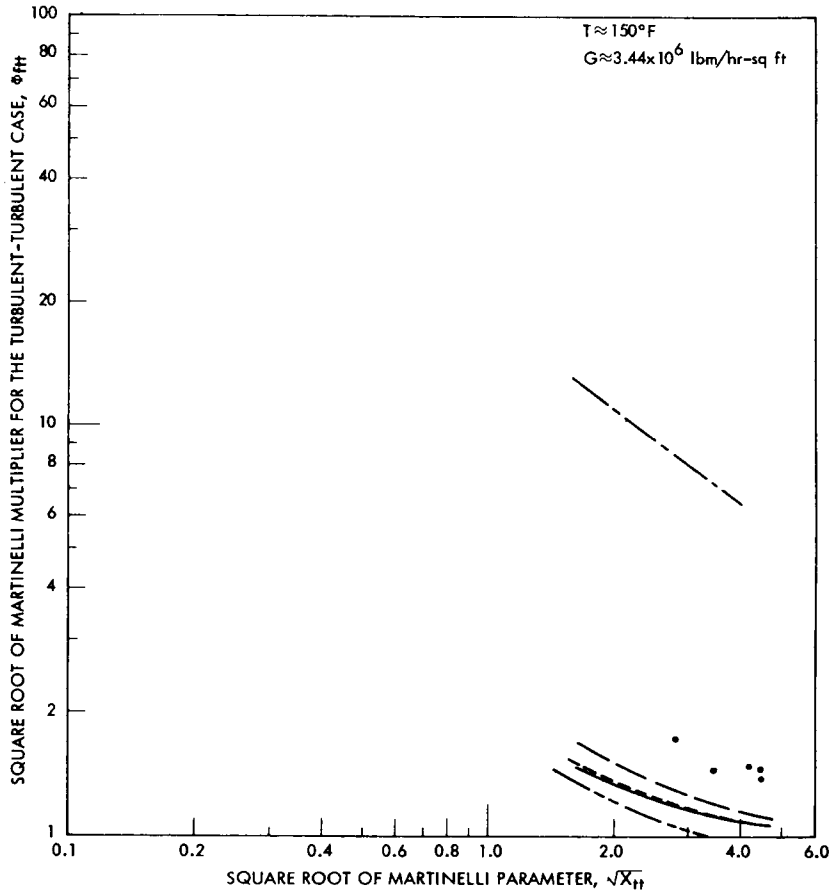


(d)

Figure IV-59. (continued)

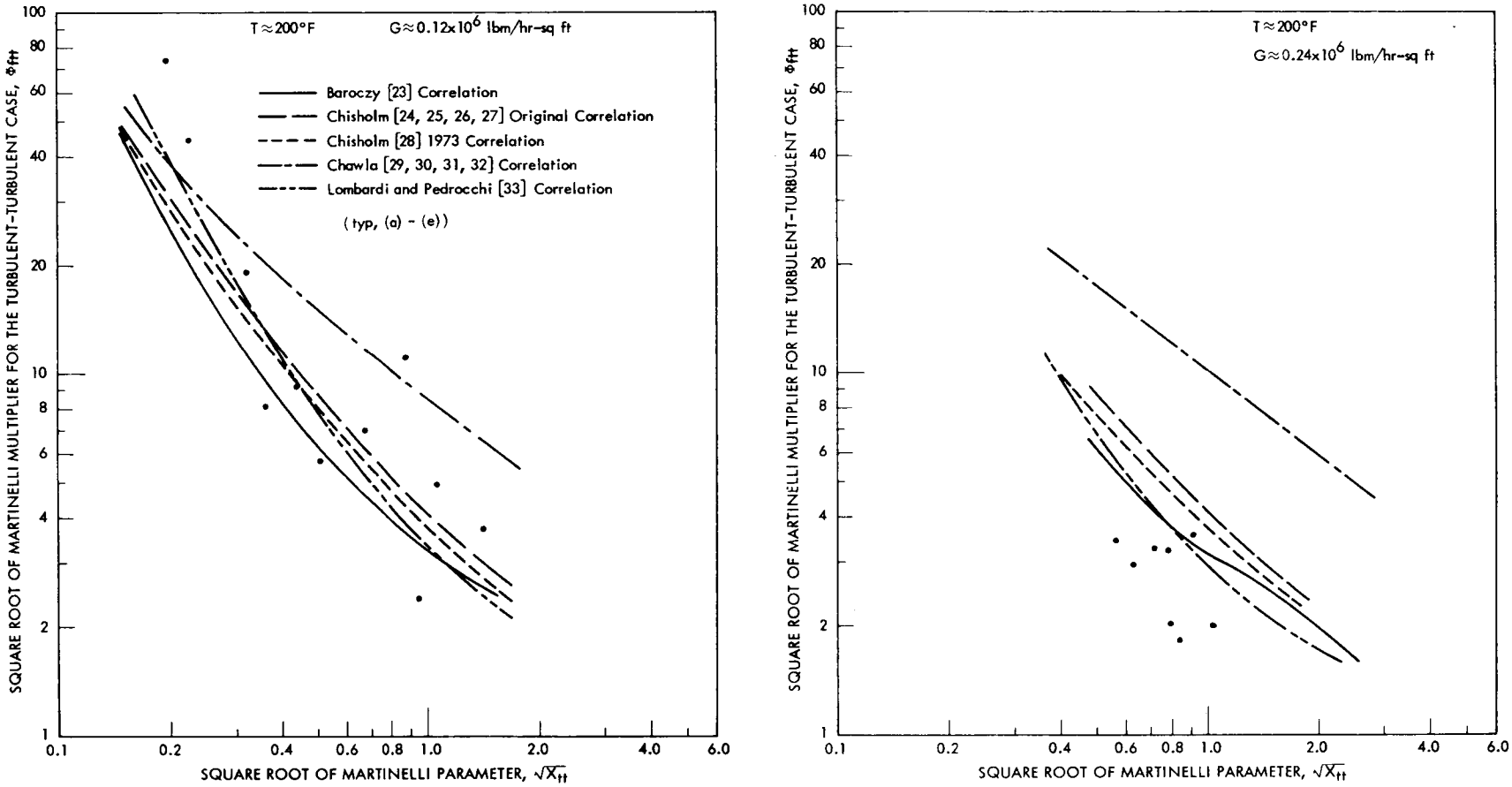


(e)



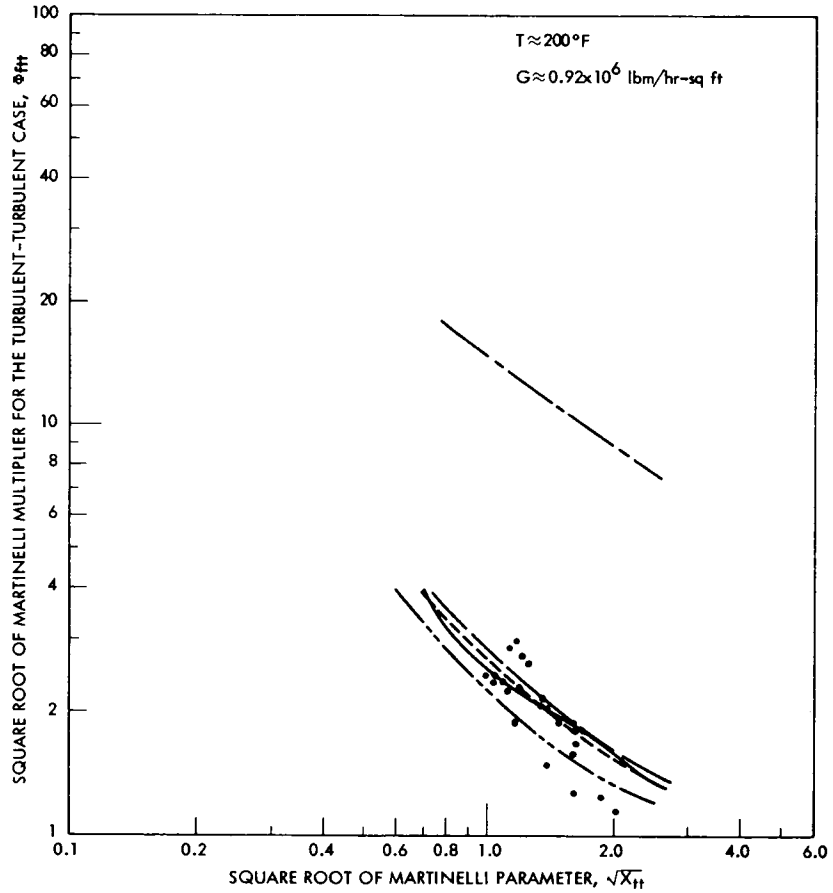
(f)

Figure IV-59. (continued)

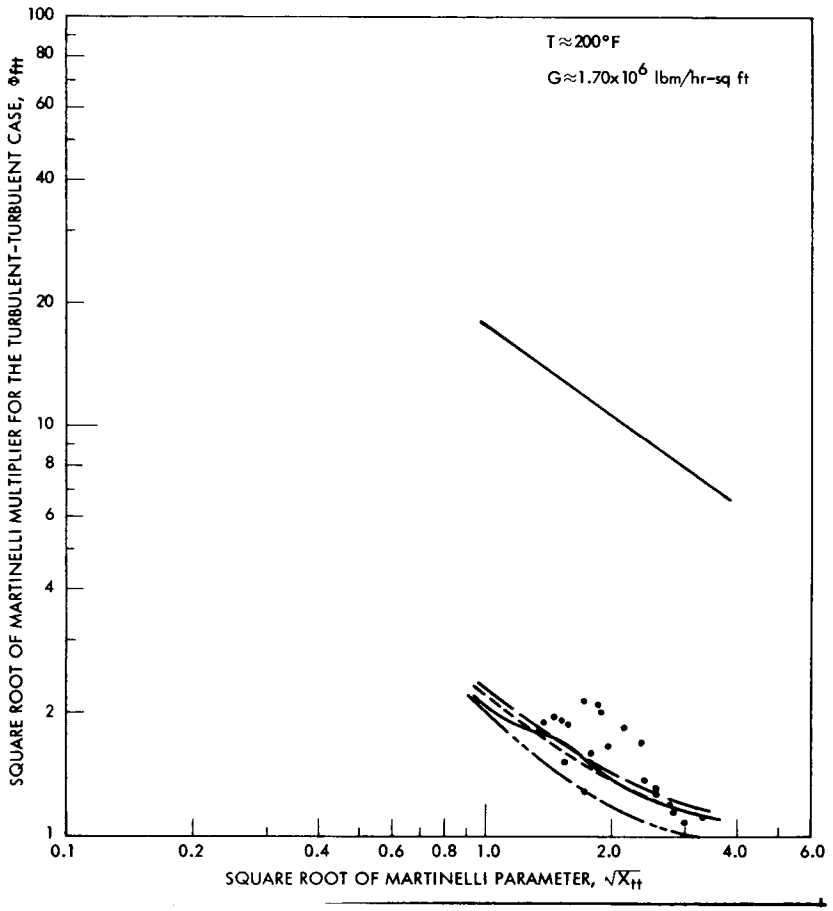


(a) (b)

Figure IV-60. COMPARISON OF EXPERIMENTAL PRESSURE DROP RESULTS WITH VARIOUS CORRELATIONS, T ≈ 200°F.

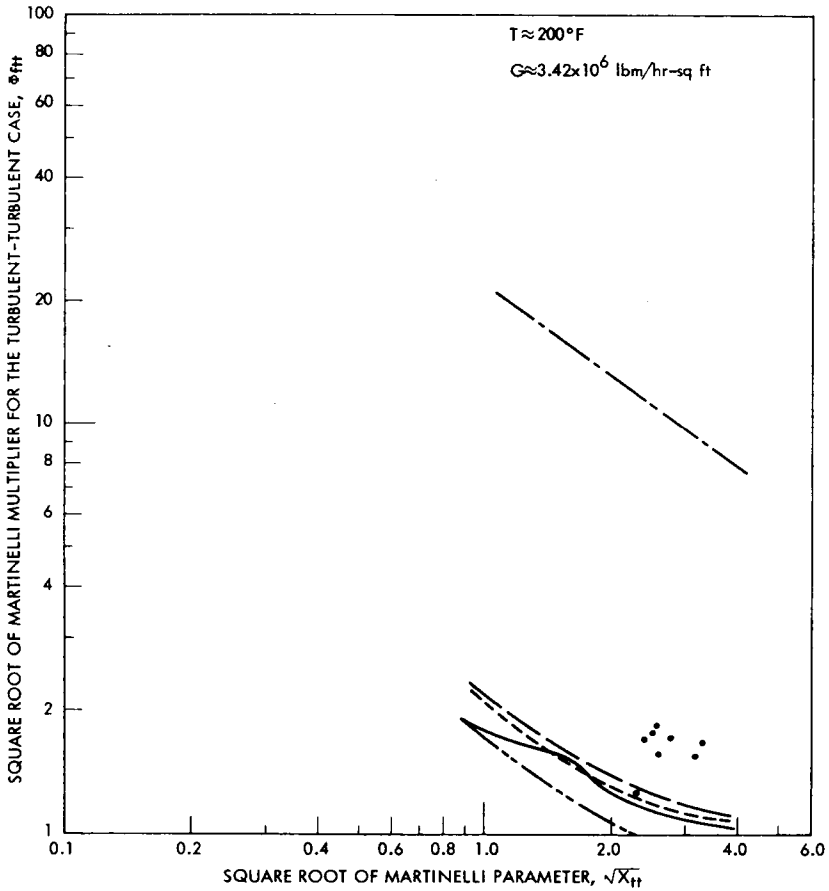


(c)



(d)

Figure IV-60. (continued)



(e)

Figure IV-60. (continued)

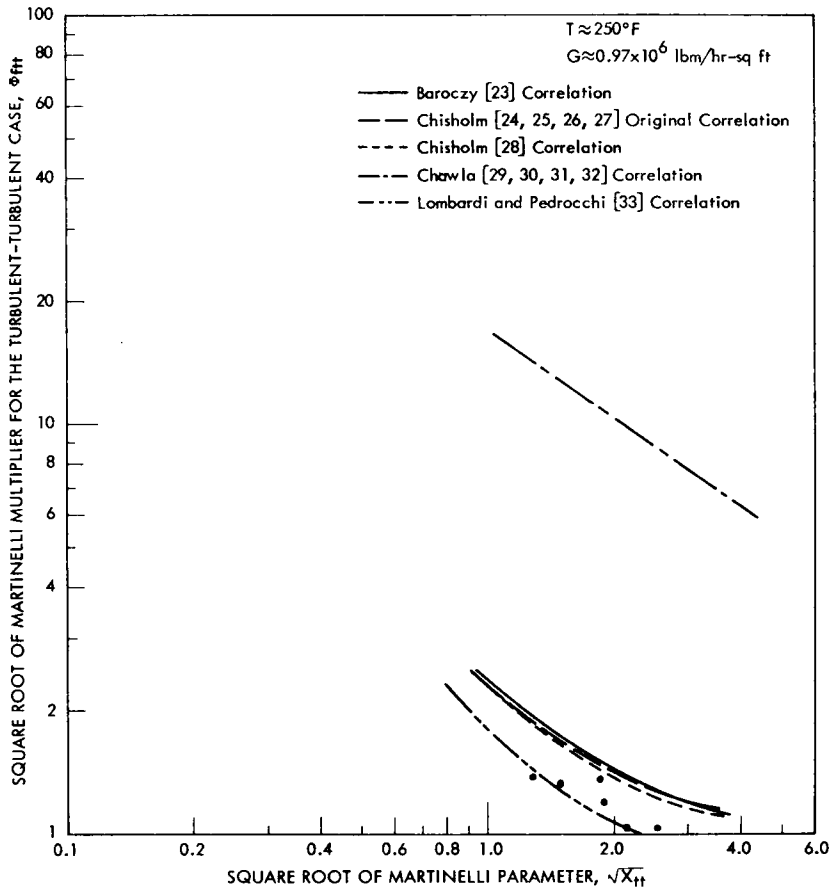


Figure IV-61. COMPARISON OF EXPERIMENTAL PRESSURE DROP RESULTS WITH VARIOUS CORRELATIONS, T ≈ 250°F.

Chawla [29, 30, 31, 32] Correlation. The results of this correlation, represented by Equation (2-23) and (2-24) are also shown in Figures IV-58 to IV-61. In general, the agreement was not good. Only the case of T ≈ 100°F and G ≈ 0.12 x 10^6 lbm/hr-sq ft gave good agreement with the experimental data. In order to attempt to explain this difference, it would be useful to examine the data on which this correlation was based. A study of the results in one of Chawla's [29] earlier publications indicates that the pressure drop in horizontal boiling of R-11 data were obtained in the ranges:

$$0.0104 \times 10^6 \leq G \leq 0.1855 \times 10^6 \text{ lbm/hr-sq ft}$$

$$288.4 \leq \frac{\rho_f}{\rho_g} \leq 617.6$$

Only the highest mass flow rate tested by Chawla [29, 30, 32] overlapped the lower range of the data in this study. The density ratio (or reduced pressure) range was very different from that at which the R-114 tests were made and corresponded to an R-114 boiling temperature range from 20 to -11°F. This would tend to explain why the best agreement was observed at low temperatures and low flow rates.

Lombardi and Pedrocchi [33] Correlation. This correlation represented by Equation (2-25) agreed quite well with much of the data, as shown in Figures IV-58 to IV-61.

In summary, it can be said that while all the frictional pressure drop models studied here, with the exception of the Chawla [29, 30, 31, 32] correlation gave reasonably good agreement with experimental data, some of these models are clearly less flexible. The Davis [34] correlation requires the use of an experimentally determined constant. The

Baroczy [23] correlation supplies values for the multiplier ratio, Ω, for only a limited range of mass fluxes. In addition, these curves are cumbersome for computer applications.

Experimental Results - Other Studies, Vertical Tests

In order for a correlation to be applied with confidence, it is necessary to show that it is in good agreement with a large body of experimental data. Thus, some of the pressure drop correlations discussed above, mainly the Martinelli-Nelson [4] model, the two Chisholm [24, 25, 26, 27, 28] correlations, Lombardi and Pedrocchi's [33] formulation, as well as Chawla's [29, 30, 31, 32] equation will now be applied to the results of other investigations.

As discussed in the literature survey, the only other experiment where sufficiently meaningful data were obtained with R-114 was undertaken by Cheshire and Stirling [36]. While only ten data points were recorded over the limited temperature range of 85 to 135°F, these results should be comparable with the findings of the present tests. The data are shown in Figures IV-62 to IV-64. Agreement between Cheshire and Stirling's [36] results and those of the present study is exceptionally good.

Another, rather extensive test program, using refrigerants in vertical tubes was undertaken by Napadensky [15] who boiled R-12 in a 0.9056 in. diameter stainless steel tube, 3.806 ft long. Napadensky [15] did not compare his results to the Martinelli-Nelson [4] model and since it is believed to be more applicable in this case than the Lockhart-Martinelli [19] model, the R-12 data were recomputed and compared to the various models. The modified Zuber et al [10] formulation

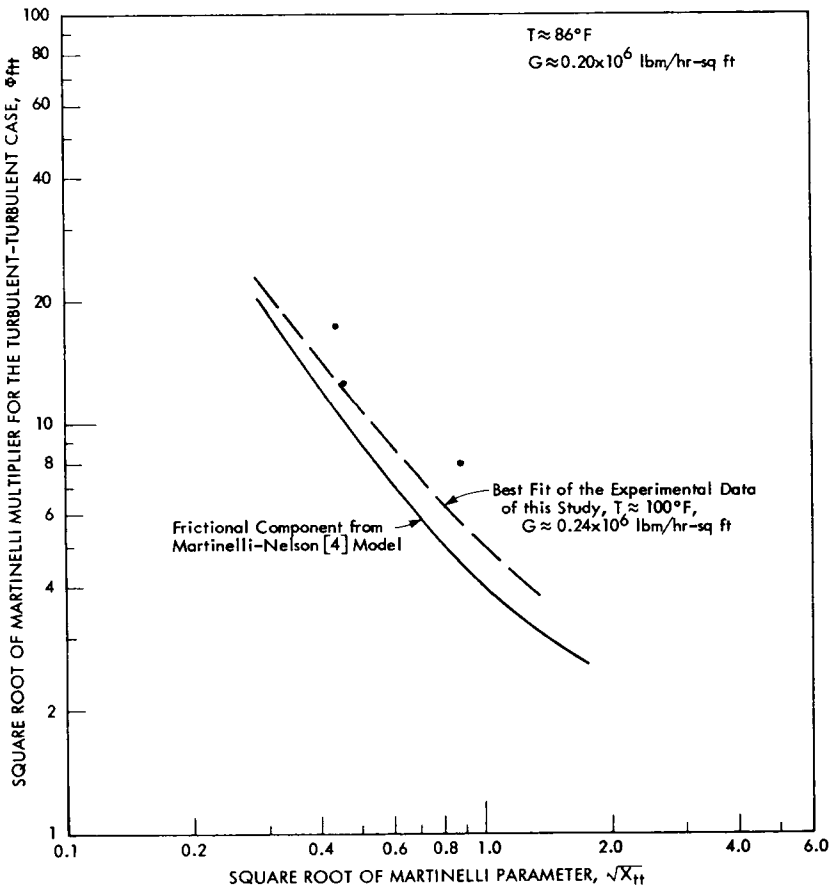


Figure IV-62. COMPARISON OF CHESHIRE AND STIRLING'S [36] R-114 EXPERIMENTAL PRESSURE DROP RESULTS WITH THOSE OF THIS STUDY, T ≈ 86°F.

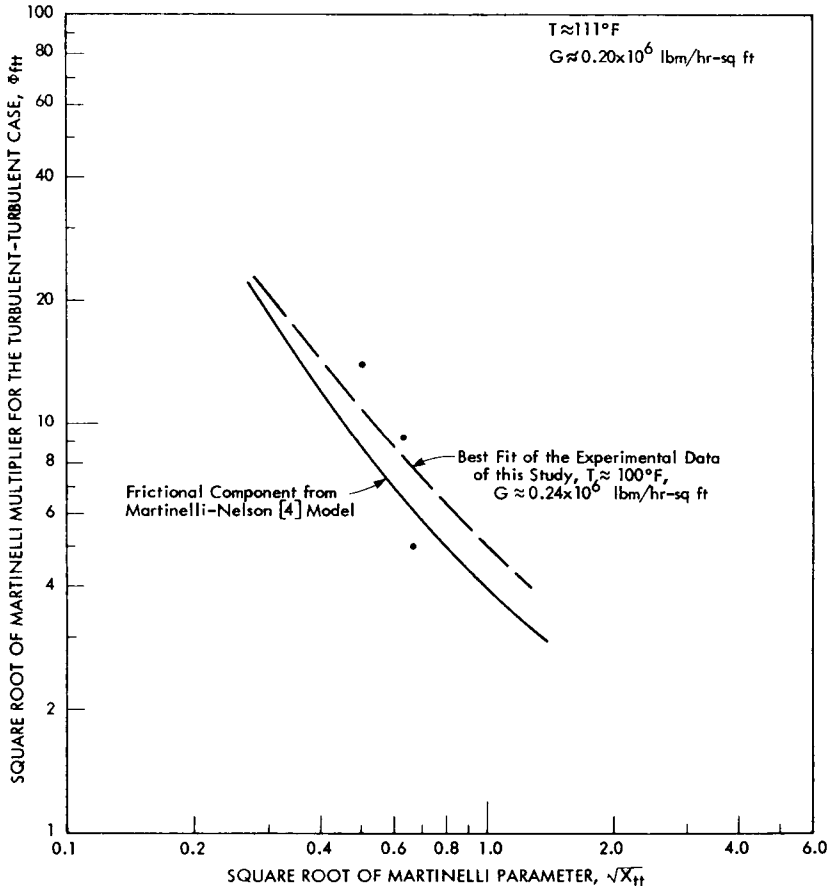


Figure IV-63. COMPARISON OF CHESHIRE AND STIRLING'S [36] R-114 EXPERIMENTAL PRESSURE DROP RESULTS WITH THOSE OF THIS STUDY, T ≈ 111°F.

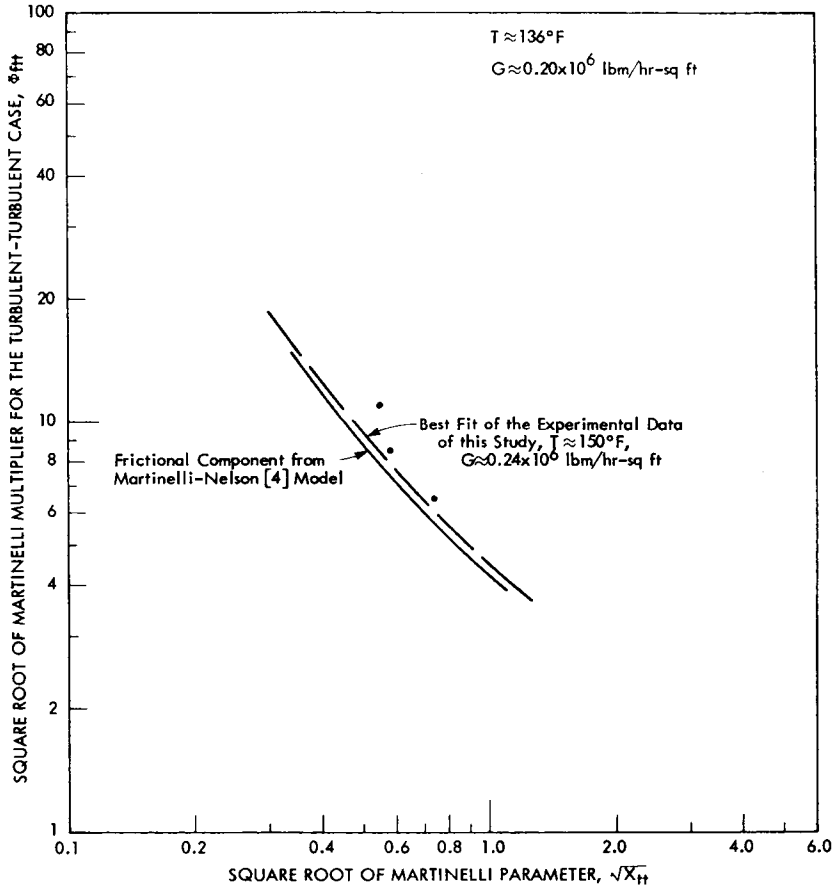


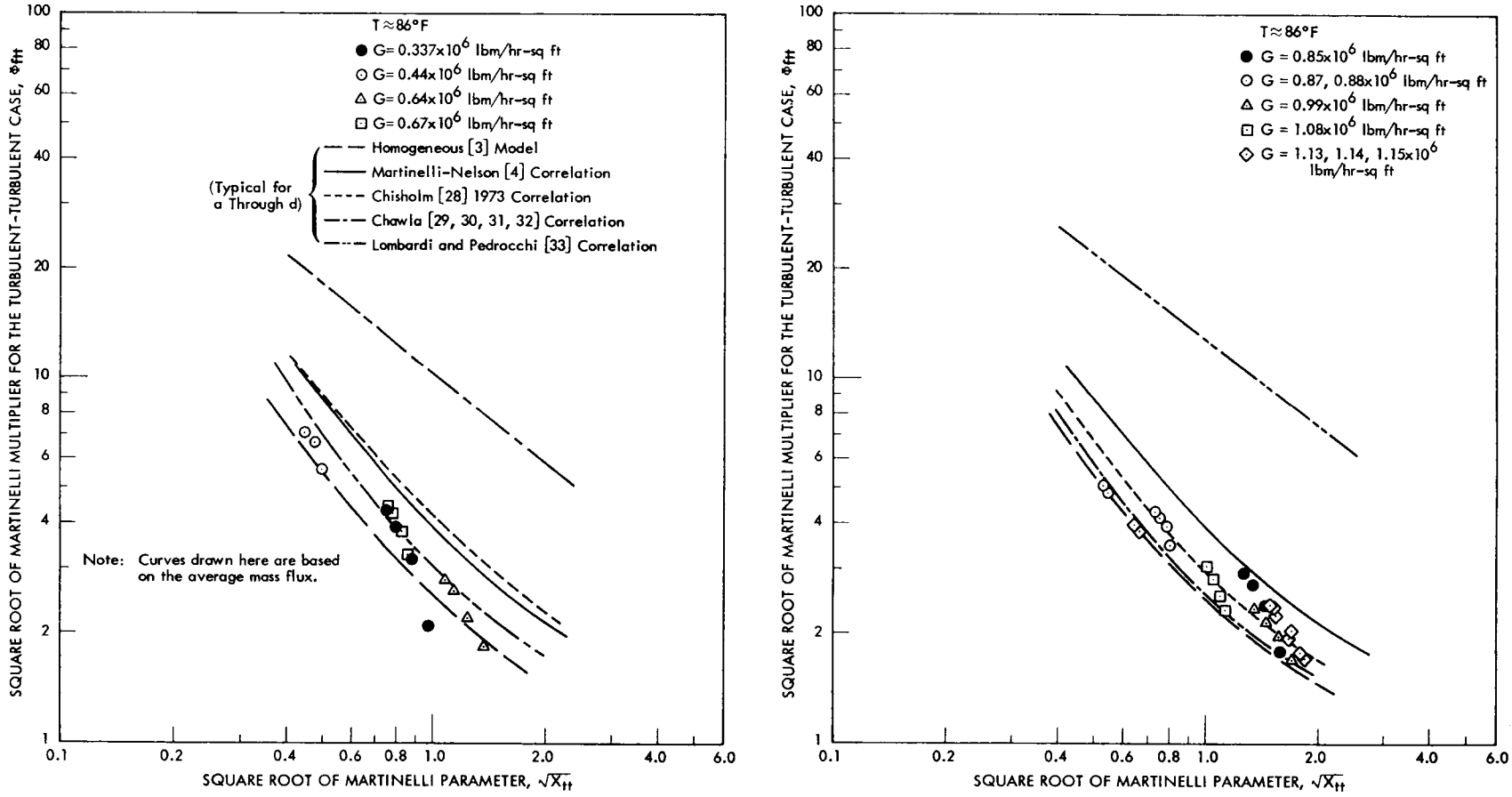
Figure IV-64. COMPARISON OF CHESHIRE AND STIRLING'S [36] R-114 EXPERIMENTAL PRESSURE DROP RESULTS WITH THOSE OF THIS STUDY, T≈136°F.

for the void fraction was used. The results are shown in Figures IV-65 to IV-67. It should be noted that Napadensky's [15] data lie in a narrow range of X_{tt} (and therefore quality). In all cases, low and high qualities were avoided. Also, while three boiling temperatures were investigated, the mass flux, G, was allowed to vary over a wide range. Thus, in order to minimize the number of plots, each graph in Figures IV-65 to IV-67 corresponded to a specific mass flux range.

Napadensky's [15] experimental data were compared to the frictional components predicted by the Martinelli-Nelson [4], Homogeneous [3], Lombardi and Pedrocchi [33], and Chisholm [28] 1973 correlations, as well as Chawla's [29, 30, 31, 32] equation. Chisholm's [28] 1973 correlation gave the best agreement. The other correlations exhibited the same trends with respect to the data as was observed in the R-114 tests of this study.

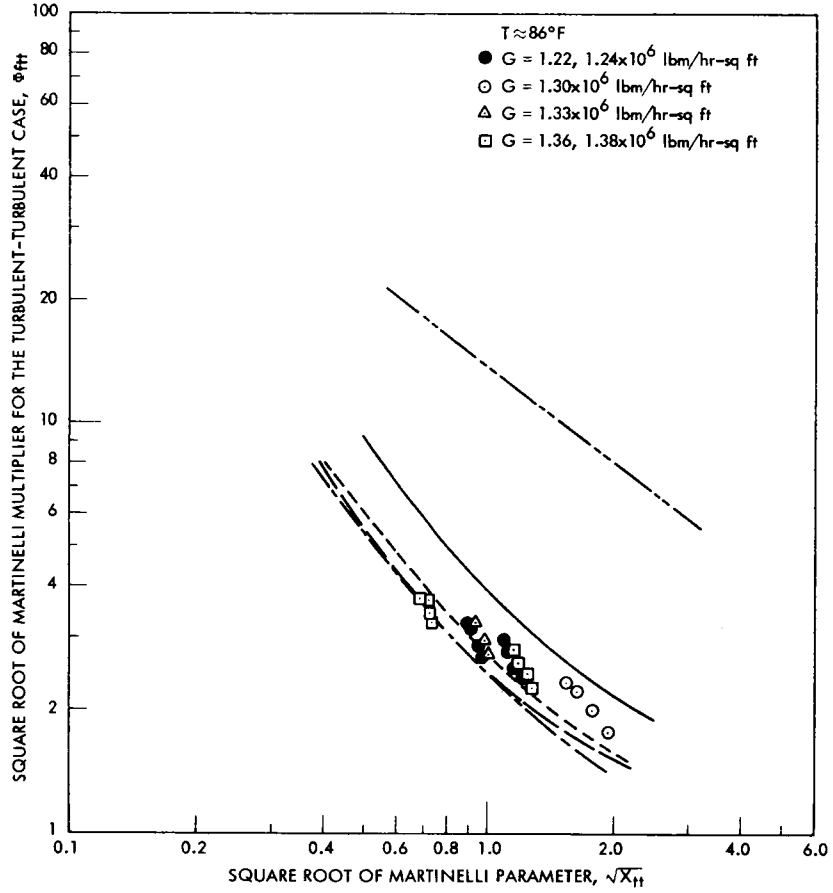
Experimental Results - Other Studies, Horizontal Tests

Tests conducted with tubes in the horizontal position generally yield results which can be analyzed more reliably. This is because the gravitational term in the total pressure drop equation is zero. Therefore, in the application of a separated flow model, such as Martinelli-Nelson [4], an accurate knowledge of the void fraction is not necessary. Consequently, it would be advantageous to reexamine the data from previous horizontal pressure drop tests and see how the experimental friction component compares with the results of the numerous models discussed above.

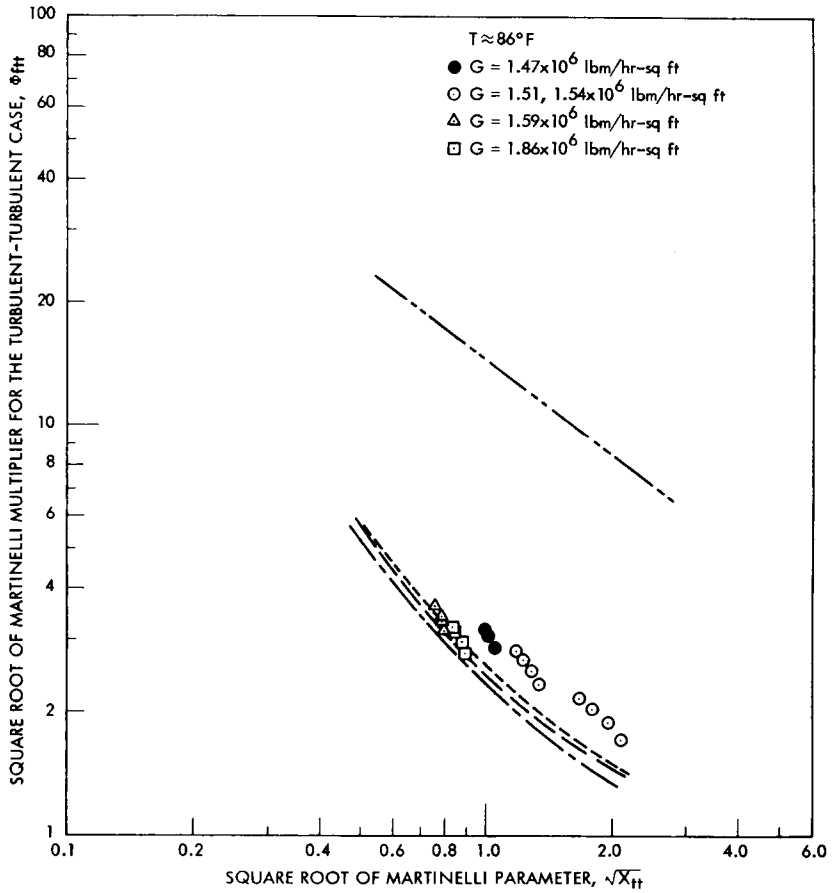


(a) (b)

Figure IV-65. COMPARISON OF NAPADENSKY'S [15] R-12 EXPERIMENTAL PRESSURE DROP RESULTS WITH VARIOUS CORRELATIONS, T≈86°F.

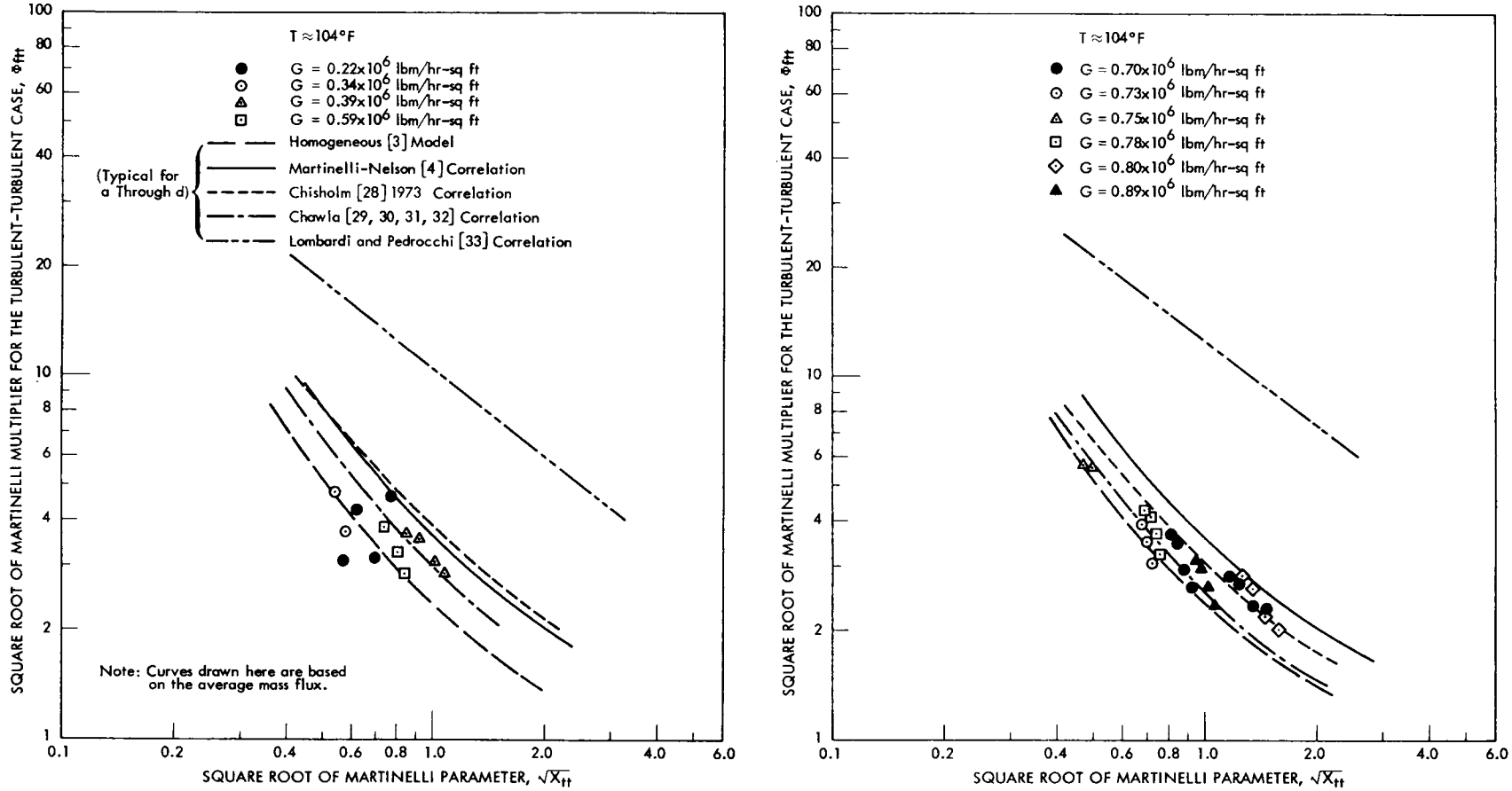


(c)



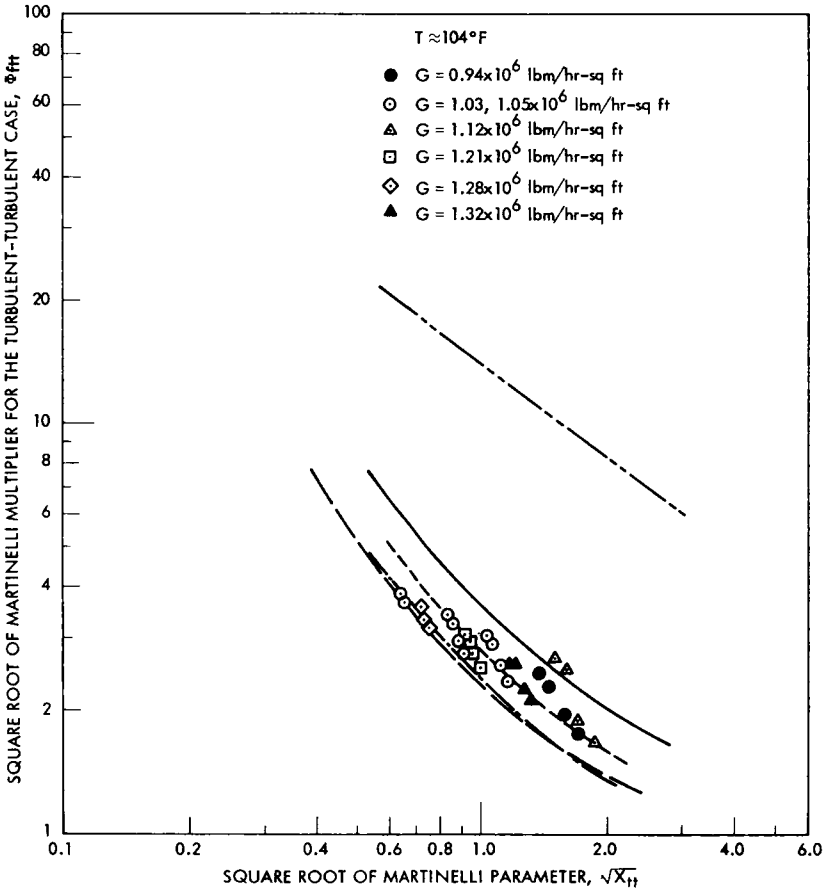
(d)

Figure IV-65. (continued)

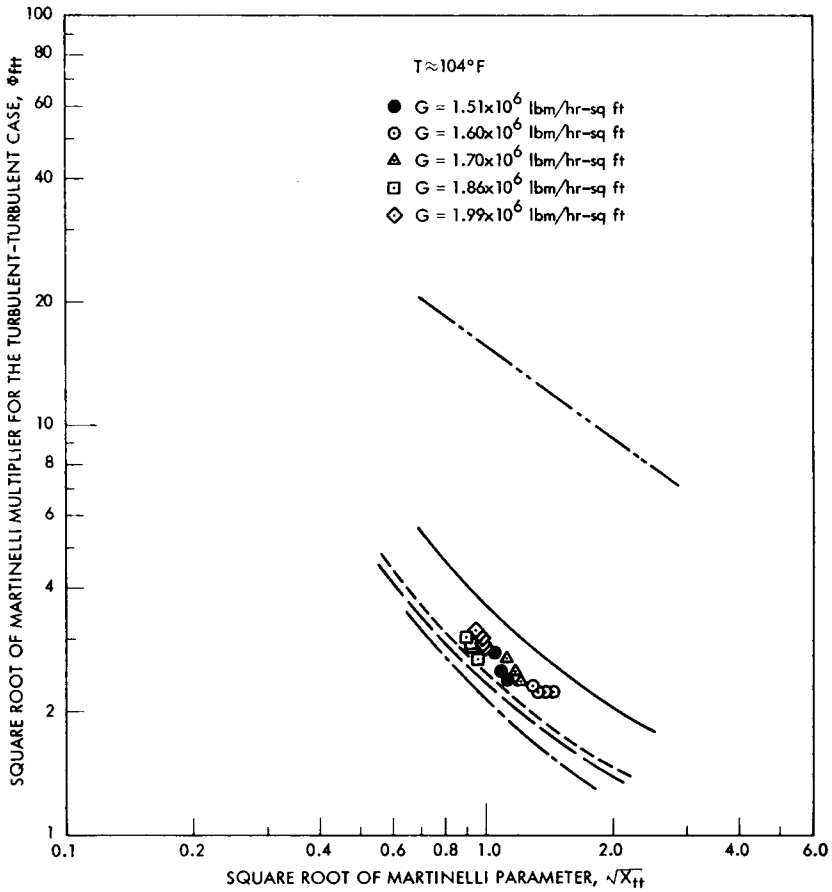


(a) (b)

Figure IV-66. COMPARISON OF NAPADENSKY'S [15] R-12 EXPERIMENTAL PRESSURE DROP RESULTS WITH VARIOUS CORRELATIONS, T≈104°F.

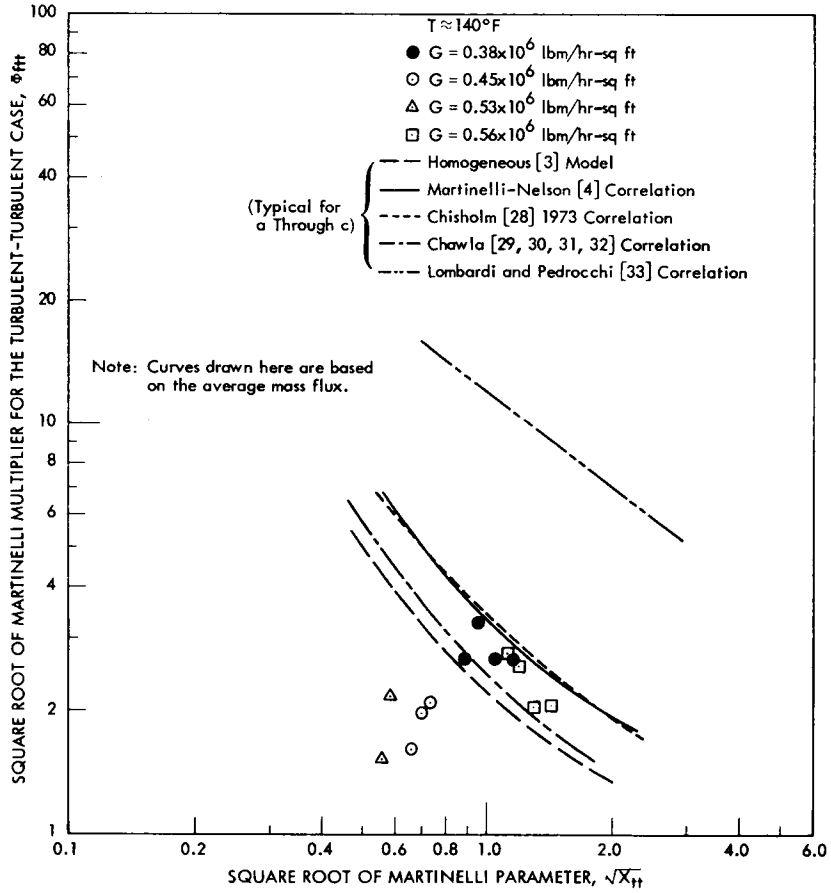


(c)

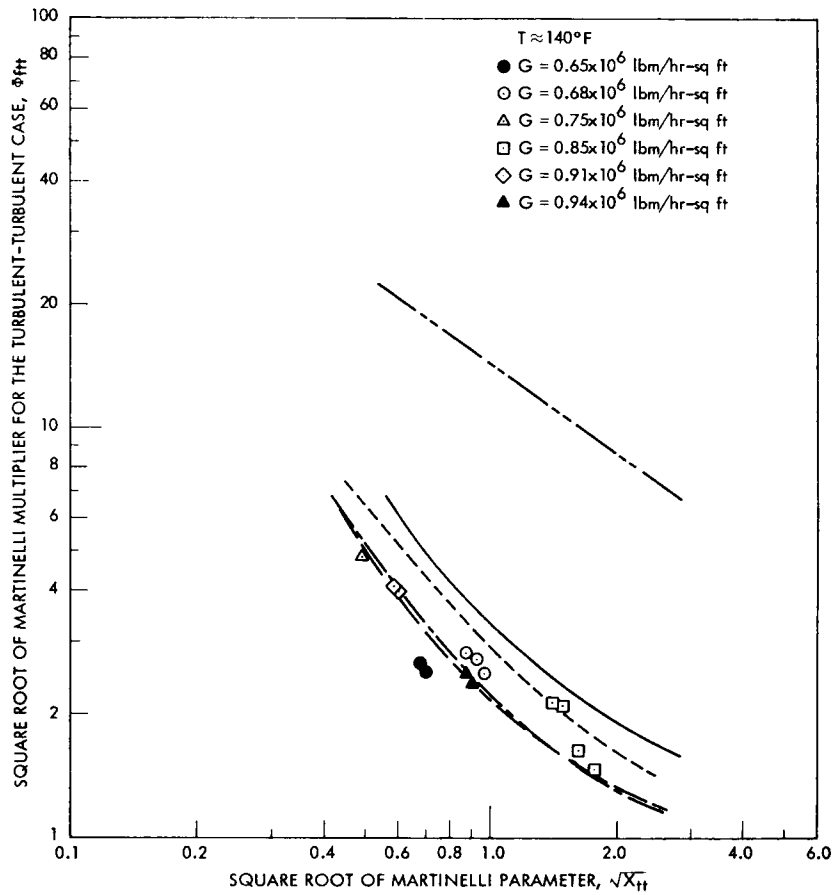


(d)

Figure IV-66. (continued)

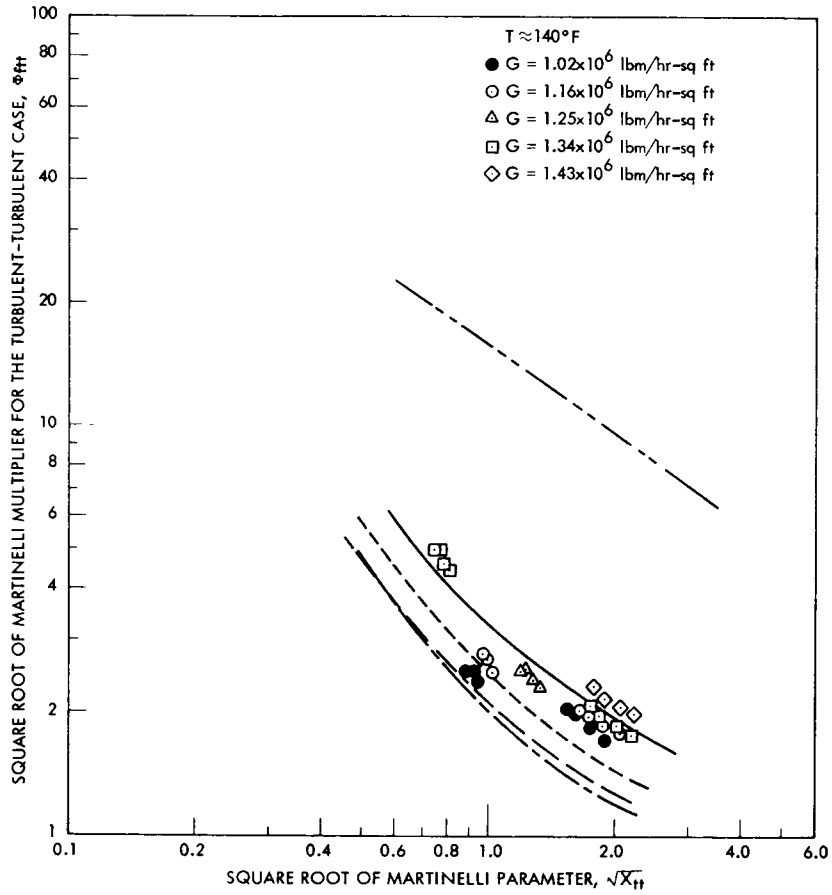


(a)



(b)

Figure IV-67. COMPARISON OF NAPADENSKY'S [15] R-12 EXPERIMENTAL PRESSURE DROP RESULTS WITH VARIOUS CORRELATIONS, T ≈ 140°F.



(c)

Figure IV-67. (continued)

As was noted in the literature survey, several studies on boiling refrigerants in horizontal tubes have been reported. Unfortunately, some of the authors such as Hatch and Jacobs [38] and Blatt and Adt [42] did not publish their data. Hatch and Jacobs [38] did however report that their results were 40% below the Martinelli-Nelson [4] model. This finding is not in agreement with the results of this study. However, since Hatch and Jacobs [38] did not specify how they modeled the Martinelli-Nelson [4] curve when applying it to R-11 data, no definitive conclusions can be made. Blatt and Adt [42] who ran tests in the low mass flux range ($G < 0.06 \times 10^6$ lbm/hr-sq ft) obtained agreement between the total pressure drop as predicted by Martinelli-Nelson [4] and the experimental data, in the quality range of 0.25 and above. The average deviation was 30%. Bryan and Seigel [39] who ran tests with R-11 in a horizontal 0.550-in.-ID tube did publish their data in the literature. Because both the boiling temperature and the mass flux were allowed to vary, plots of $\Phi_{ftt\ calculated}$ vs $\Phi_{ftt\ experimental}$ were the only meaningful way to analyze the data. In Figure IV-68 a comparison is made with the Martinelli-Nelson [4], Chawla [29, 30, 31, 32], Lombardi and Pedrocchi [33], and Chisholm [28] 1973 correlations. Of these, the Chisholm [28] 1973 and the Chawla [29, 30, 31, 32] correlations gave the best agreement. The Chisholm [28] correlation consistently overestimated the true frictional pressure drop. The Martinelli-Nelson [4] model gave the poorest agreement with the data.

Johnston and Chaddock [41] ran tests in a 0.460-in.-ID horizontal tube using both R-12 and R-22. The temperature range from approximately -60 to +1°F was investigated. Again, because both the boiling temperature

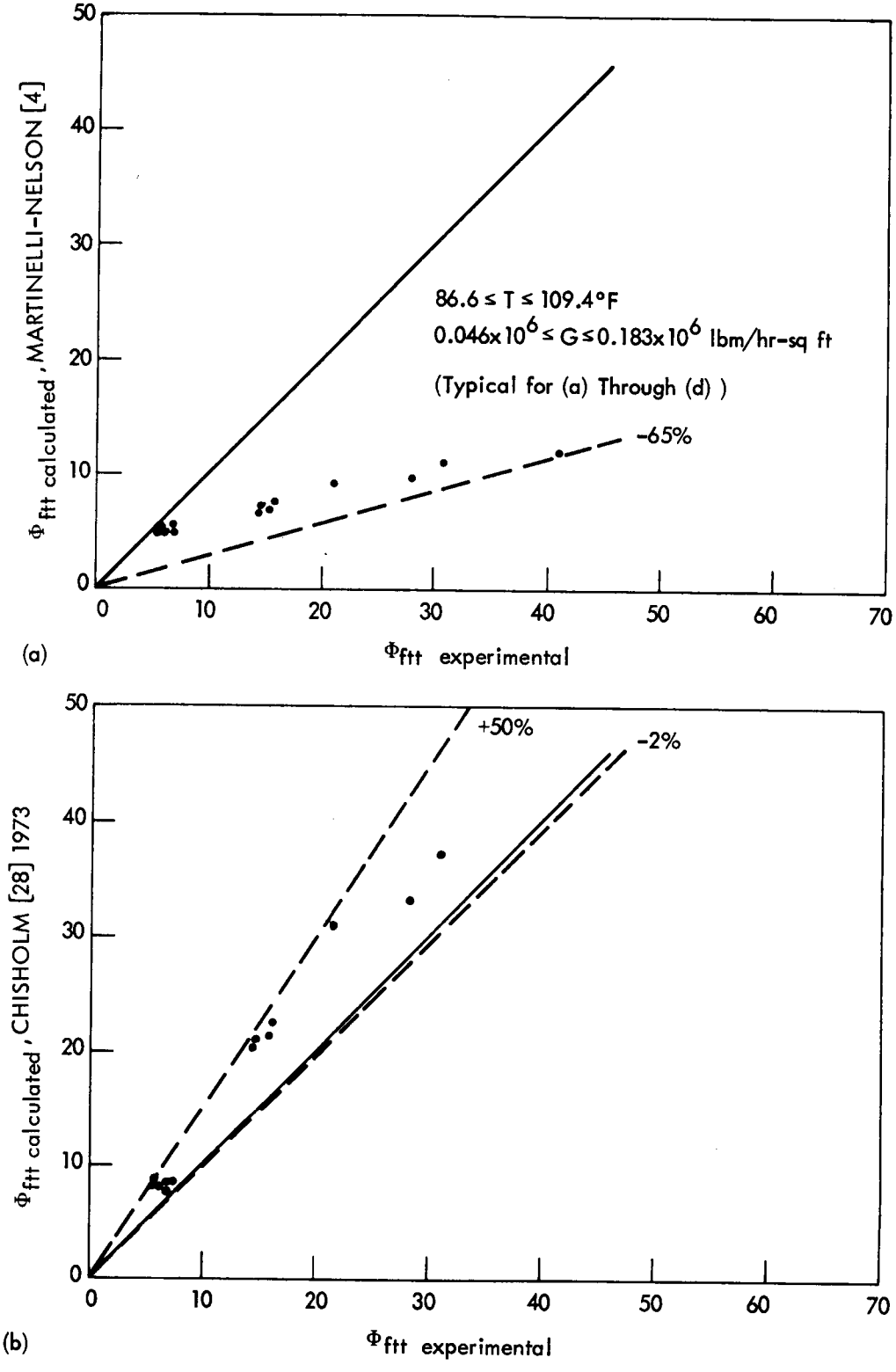
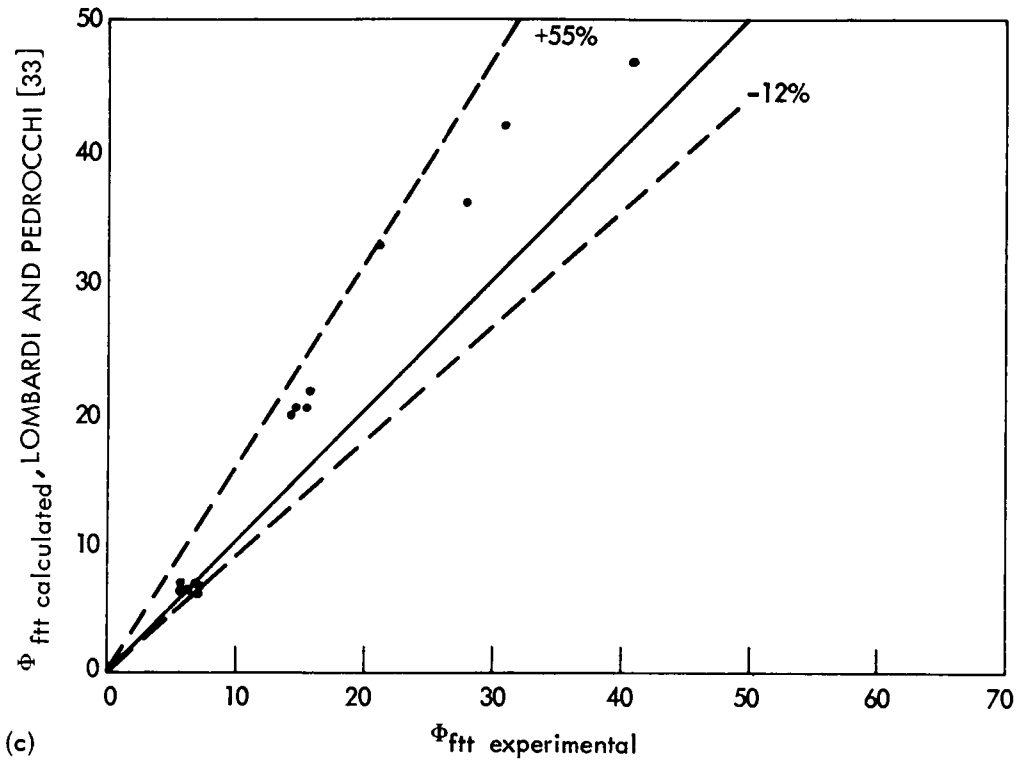
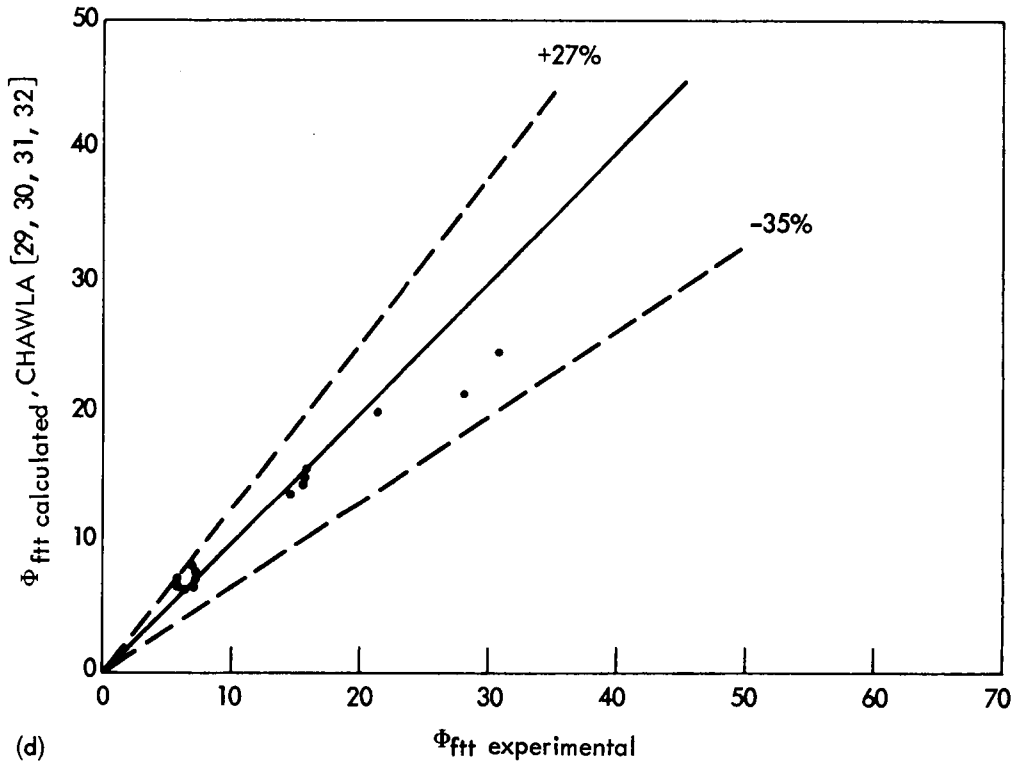


Figure IV-68. COMPARISON OF BRYAN AND SEIGEL'S [39] R-11 EXPERIMENTAL PRESSURE DROP RESULTS WITH VARIOUS CORRELATIONS. HORIZONTAL BOILING.



(c)



(d)

Figure IV-68. (continued)

and mass flux were not controlled, plots of $\Phi_{ftt\ calculated}$ vs $\Phi_{ftt\ experimental}$ were made as shown in Figures IV-69 and IV-70. For the R-12 results in Figure IV-69, the Martinelli-Nelson [4] and Chawla [29, 30, 31, 32] correlations were best. In contrast the Chisholm [28] 1973 correlation was poorest, overestimating the experimental Φ_{ftt} by as much as 340%. In contrast, for the R-22 results in Figure IV-70, the Lombardi and Pedrocchi [33] equation approximated the experimental data most closely.

Chaddock and Noerager [43] who boiled R-12 at 54°F, ran tests in the mass flux range of 0.89×10^5 to 4.3×10^5 lbm/hr-sq ft. The results shown in Figure IV-71 indicate that the Chisholm [28] 1973 correlation predicted the experimental results quite well.

It is worthwhile to note that Johnston and Chaddock's [41] results were the only ones presented so far for which Chisholm's [28] 1973 correlation was not among the best. One reason for this may be the operating conditions. These tests were run in the range where the reduced pressure for R-12 was between 0.010 and 0.040. For R-22, the studies were made at reduced pressures of 0.097 and above, while the lowest reduced pressure Napadensky [15] encountered was 0.181. A close examination of the Johnston and Chaddock [41] results will indicate that as the boiling temperature increased, the deviation between the Chisholm [28] 1973 correlation and the experimental data decreased.

In Figure IV-72, a comparison of Chisholm's [28] 1973 correlation with the Chawla [29, 30, 31, 32] correlation was made in the range of Chawla's [29, 30, 31, 32] experimental data with R-11. As can be seen, the agreement between the two correlations improves as the boiling temperature and/or the mass flux increases.

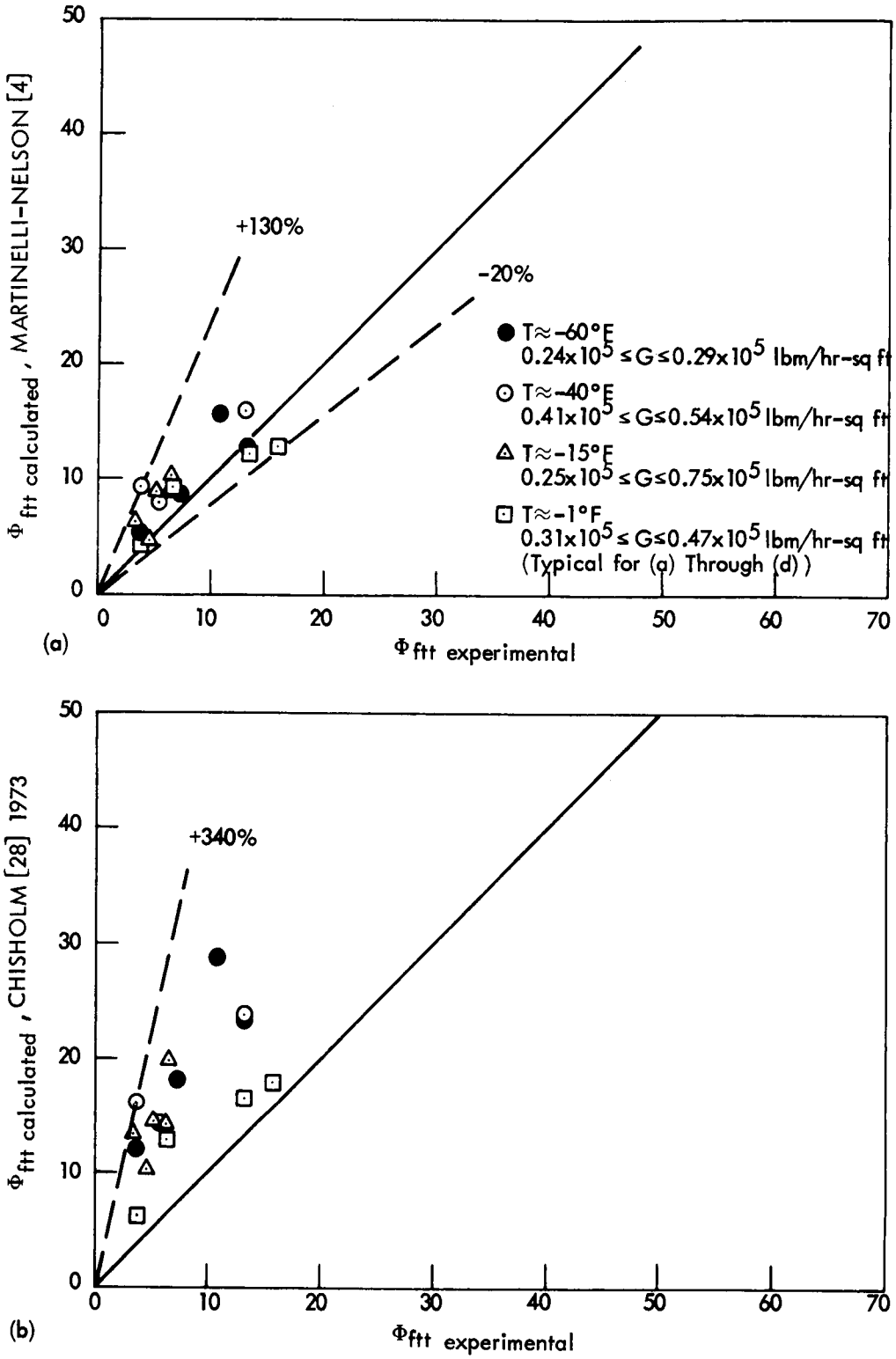
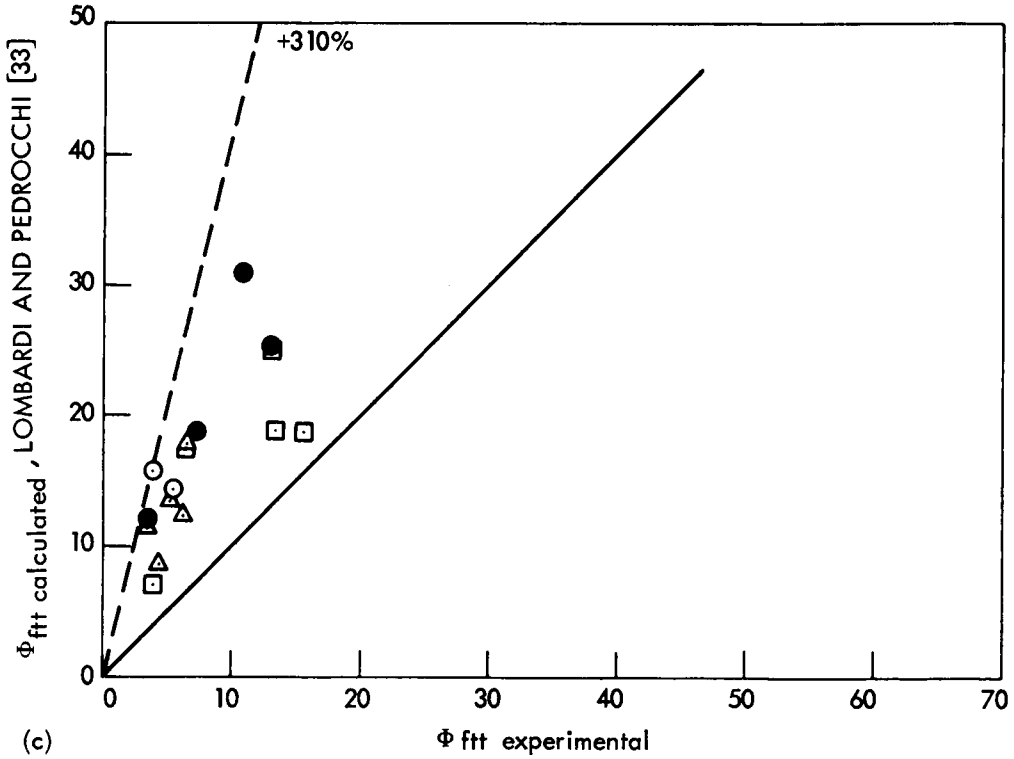


Figure IV-69. COMPARISON OF JOHNSTON AND CHADDOCK'S [41] R-12 EXPERIMENTAL PRESSURE DROP RESULTS WITH VARIOUS CORRELATIONS. HORIZONTAL BOILING.



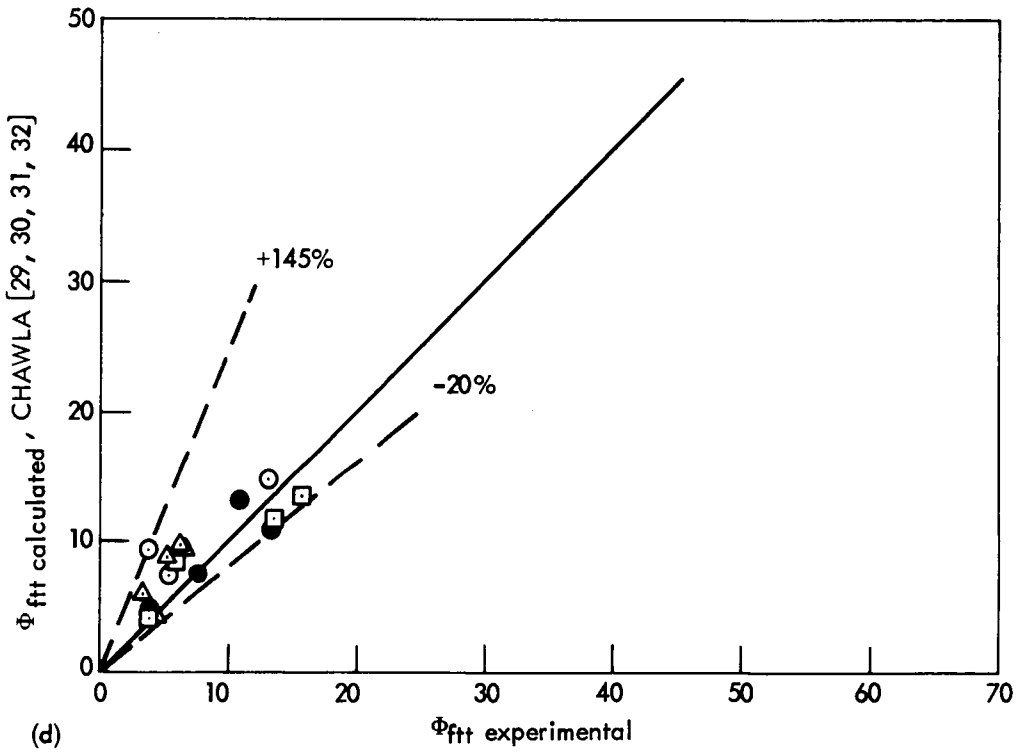


Figure IV-69. (continued)

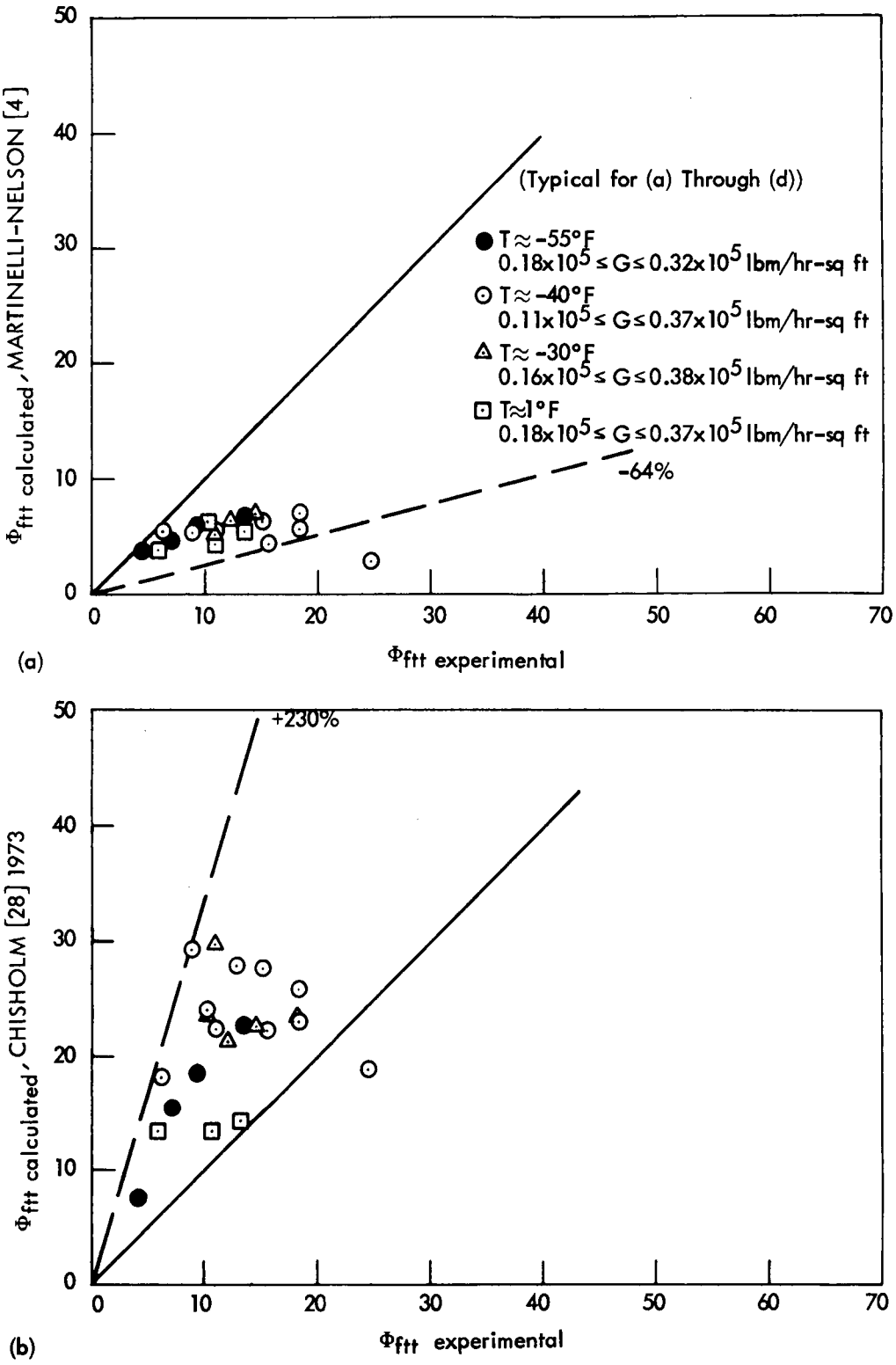
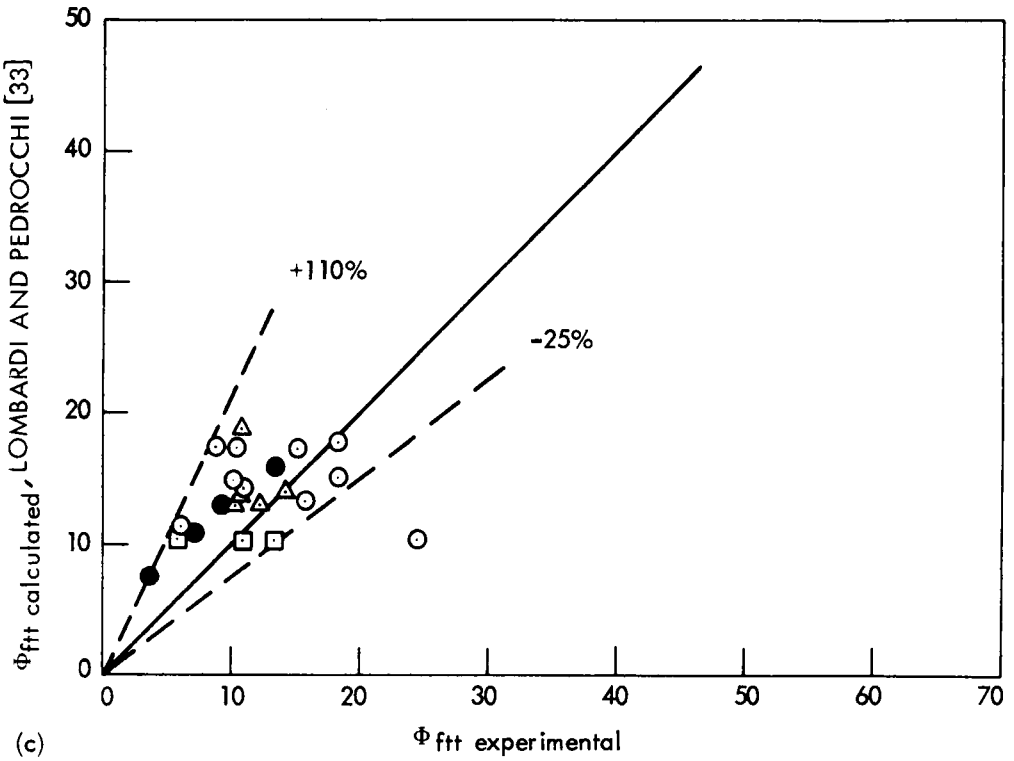


Figure IV-70. COMPARISON OF JOHNSTON AND CHADDOCK'S [41] R-22 EXPERIMENTAL PRESSURE DROP RESULTS WITH VARIOUS CORRELATIONS. HORIZONTAL BOILING.



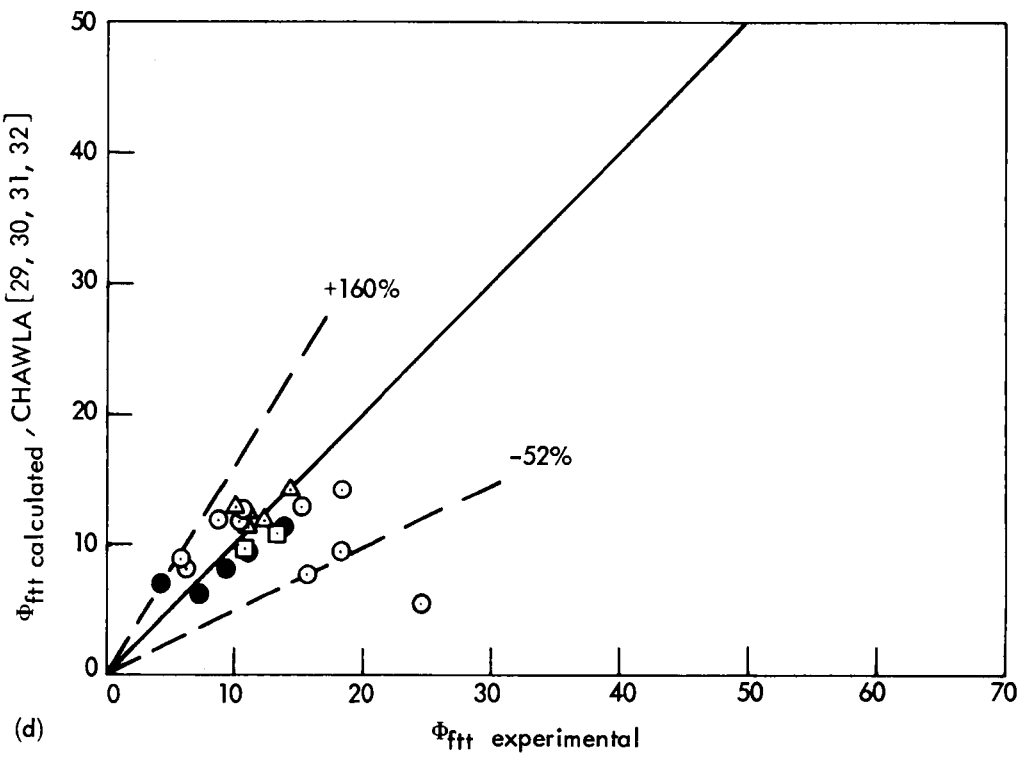


Figure IV-70. (continued)

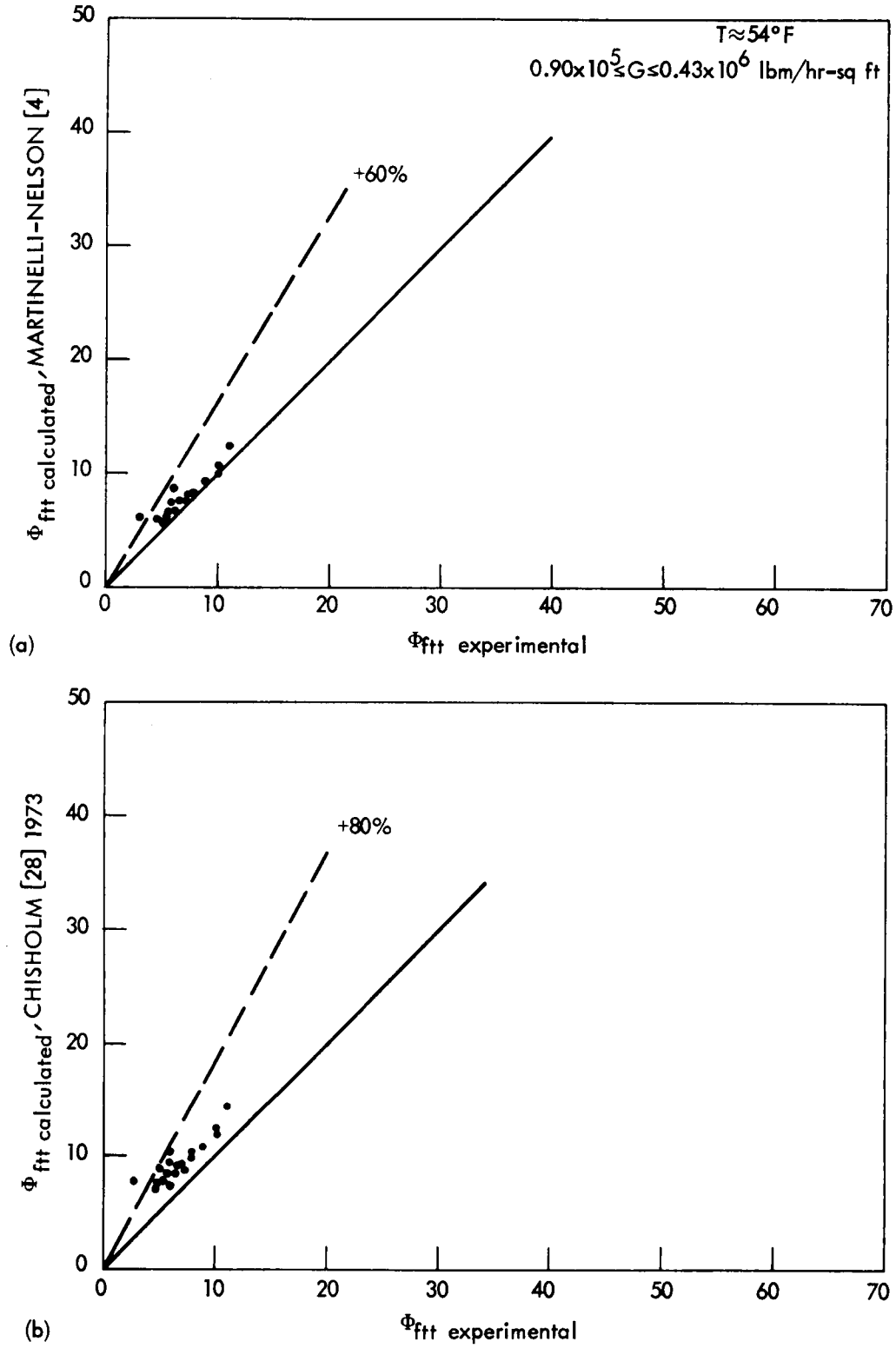
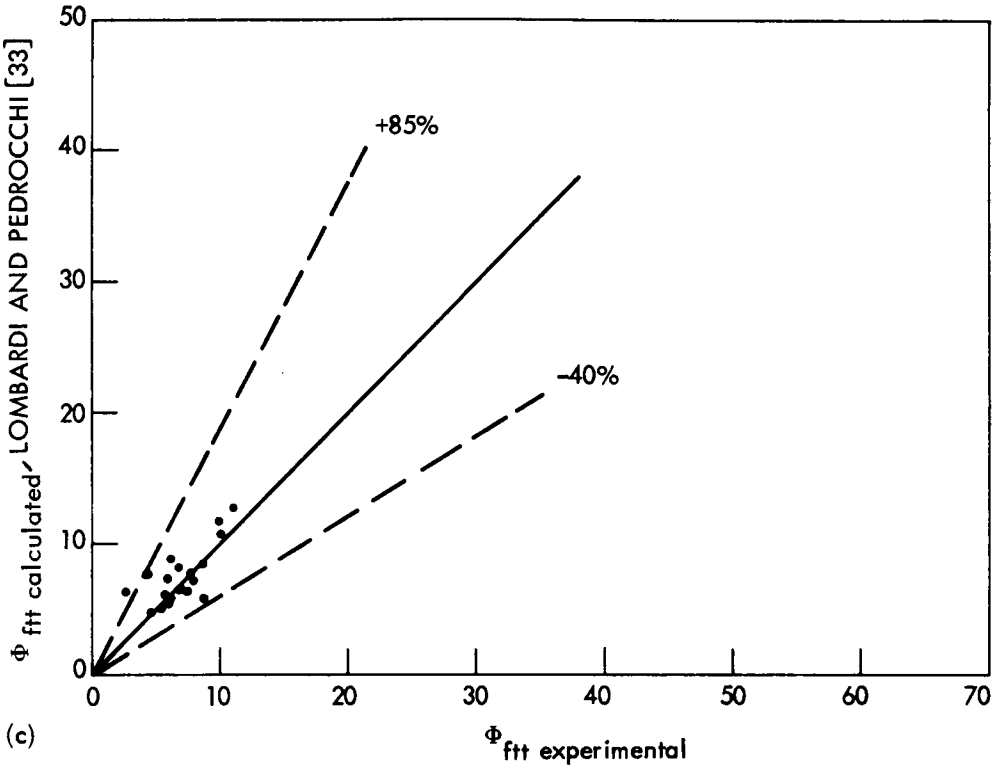


Figure IV-71. COMPARISON OF CHADDOCK AND NOERAGER'S [43] R-12 EXPERIMENTAL PRESSURE DROP RESULTS WITH VARIOUS CORRELATIONS. HORIZONTAL BOILING.



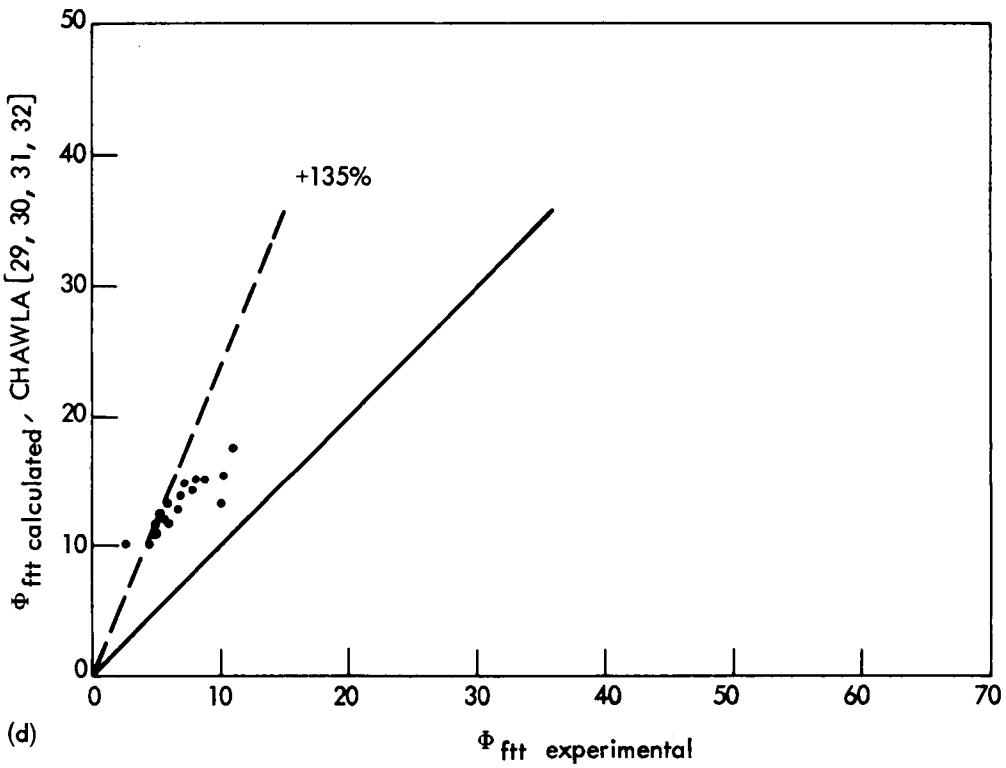
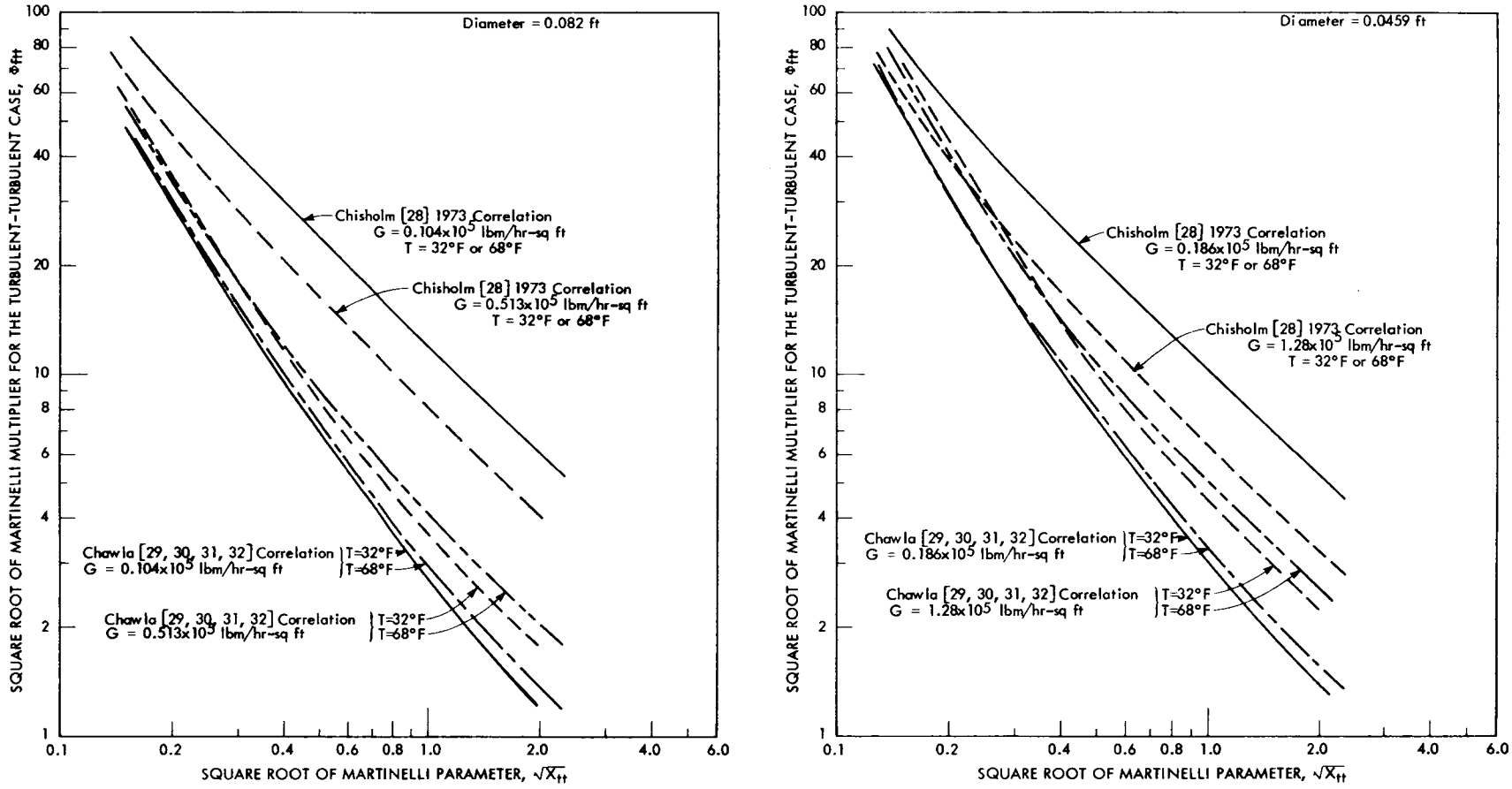
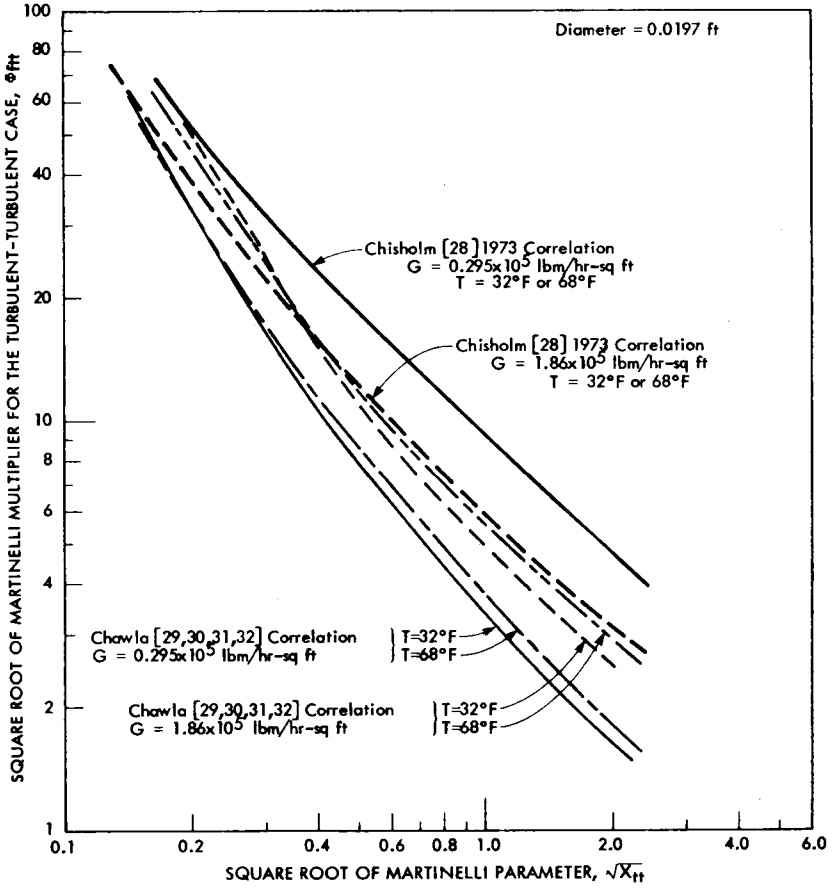


Figure IV-71. (continued)



(a) (b)

Figure IV-72. COMPARISON OF THE CHISHOLM [28] 1973 AND CHAWLA [29, 30, 31, 32] CORRELATIONS.



(c)

Figure IV-72. (continued)

In summary, it can be stated that the Chisholm [28] 1973 correlation represented by equations (2-21) and (2-22) gives the best agreement with experimental data. Originally derived for water and other non-refrigerants, this correlation was found applicable for R-11, R-12, R-22, and R-114 over a very wide range of boiling temperatures and flow rates. Only at very low temperatures and flow rates was this Chisholm [28] correlation found to be inaccurate. In this range, the Chawla [29, 30, 31, 32] correlation was better. The amount of data on which this observation is based is, however, meager and more tests need to be run in both the vertical and horizontal modes over a wide range of operating conditions to more firmly establish the limits of applicability of the available correlations. On the basis of the data obtained to date with refrigerants, the Chisholm [28] 1973 correlation is recommended for reduced pressures of 0.05 and above provided the mass flux is 0.2×10^5 lbm/hr-sq ft or greater. For a reduced pressure of less than 0.05 and a mass flux of less than 0.5×10^5 lbm/hr-sq ft, especially in horizontal flow, the Chawla [29, 30, 31, 32] correlation would probably be better. Outside the range of the above limitations, insufficient data exist to formulate any recommendations. It should, however, be pointed out that the application of the Chisholm [28] correlation will always yield a conservative design.

C. HEAT TRANSFER COEFFICIENTS

Introduction

Heat transfer coefficients were measured in the range described in Chapter III, Section C. A total of 445 runs were analyzed. While

ten heat transfer coefficient measurements--one in every zone--were obtainable under each set of operating conditions, only those runs in which a zone contained fluid with an average quality of greater than two percent were analyzed. This limitation was necessary because of the experimental error associated with obtaining the quality and the sensitivity of many of the correlations to small variations in quality in this region. In addition, for several of the runs, the critical heat flux occurred somewhere along the length of the tube. This section will be limited to the analysis of only those heat transfer coefficients occurring below the critical heat flux.

All heat transfer coefficient results were reduced on a digital computer. A sample calculation, including a discussion of the calibration curves used is shown in Appendix D. The runs undertaken were conducted in both the natural and forced circulation modes. Natural circulation was used in most of the runs in the lower mass flux range ($0.12 \times 10^6 \leq G \leq 0.90 \times 10^6$ lbm/hr-sq ft) while only forced circulation was used in the higher mass flux range ($0.90 \times 10^6 \leq G \leq 3.47 \times 10^6$ lbm/hr-sq ft). The latter restriction was due to the fact that sufficient head could not be generated in the system to accommodate the higher flows. Some forced circulation runs were also conducted in the lower flow range in order to compare with the natural circulation data. In all cases, natural and forced circulation operation gave the same heat transfer and critical heat flux results--enabling one to conclude that the mode of operation of the system had no effect on the results. Consequently, no distinction was made in the data analysis between natural and forced circulation operation.

Experimental Results - This Study

The simplest and most straightforward type of data presentation involves the plotting of the heat flux or the heat transfer coefficient versus the wall-to-bulk temperature difference. This type of plot is shown in Figures IV-73 to IV-78. In the q/A vs ΔT plots in Figures IV-73 to IV-75, the wall-to-bulk temperature difference increases with heat flux in much the same way one would expect it to in pool boiling. For the 100°F boiling runs, the slope is initially small and increases up to the $\Delta T \approx 8°F$ portion of the curve where it becomes approximately constant and remains so until the critical heat flux is achieved. The slope of the curve then decreases markedly. The same trend is evident in the 150 and 200°F runs. Curves representing the best fit through the data at the various mass fluxes are also shown.

Looking at the h vs ΔT plots in Figures IV-76 to IV-78, it is initially noted that considerably more scatter exists in the data. This can be attributed to two reasons. First, a plot of h vs ΔT is too simplified to account for variations in other parameters, such as quality and flow rate. Secondly, there exists an uncertainty in the heat flux and temperature measurements. Since these studies were conducted on one tube divided into ten zones, some zone-to-zone variations can be expected to increase the experimental error.

From the 100, 150, and 200°F plots in Figures IV-73 to IV-78, the following trends were observed:

(1) There is a mass flux effect. As G was increased, higher q/A vs ΔT and h vs ΔT curves were obtained.

(2) There is an effect of quality on the heat transfer coefficient. As x was increased, h decreased.

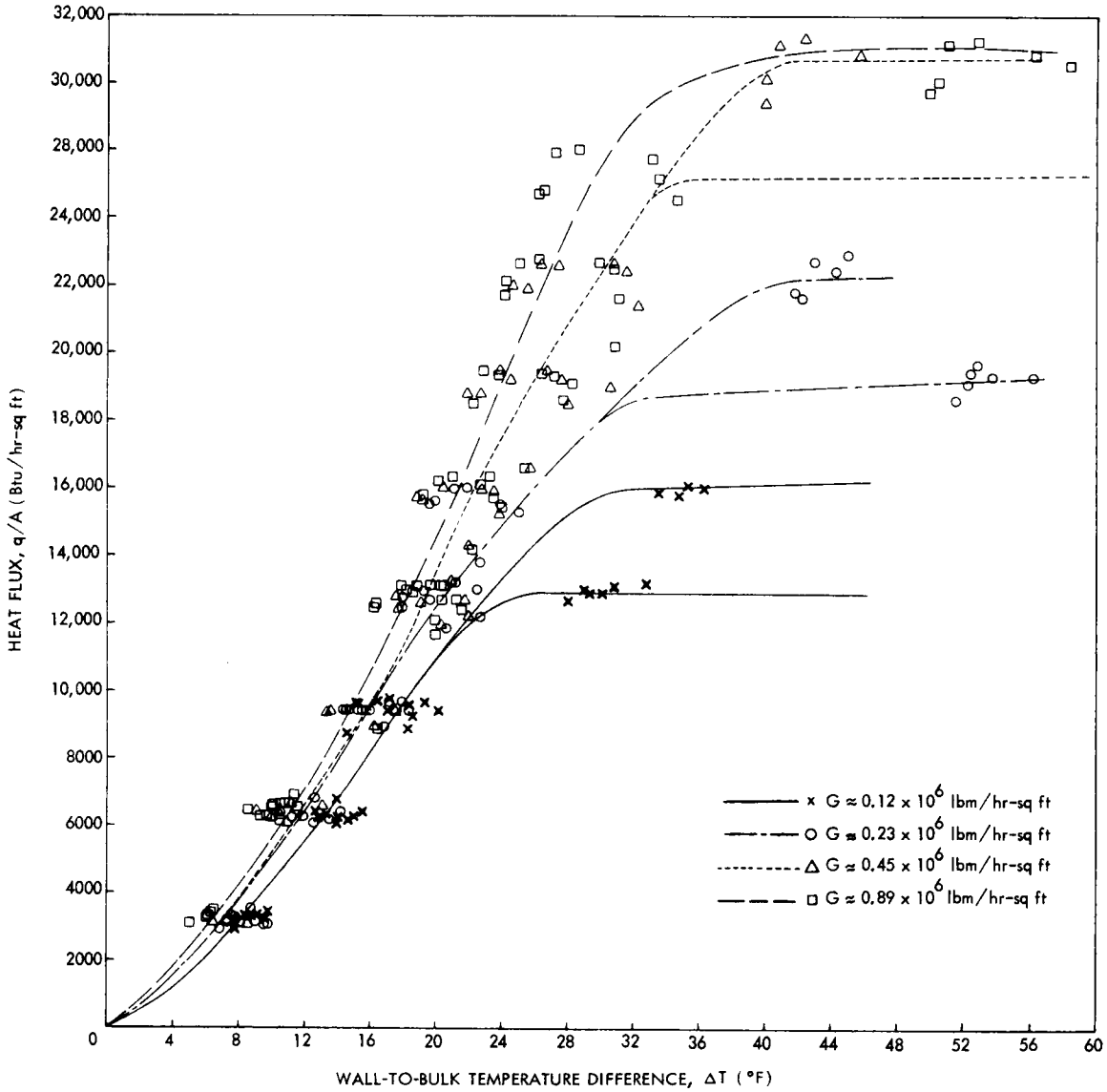


Figure IV-73. PLOT OF THE HEAT FLUX VERSUS THE WALL-TO-BULK TEMPERATURE DIFFERENCE FOR THE FORCED CONVECTIVE BOILING OF R-114, T≈100°F.

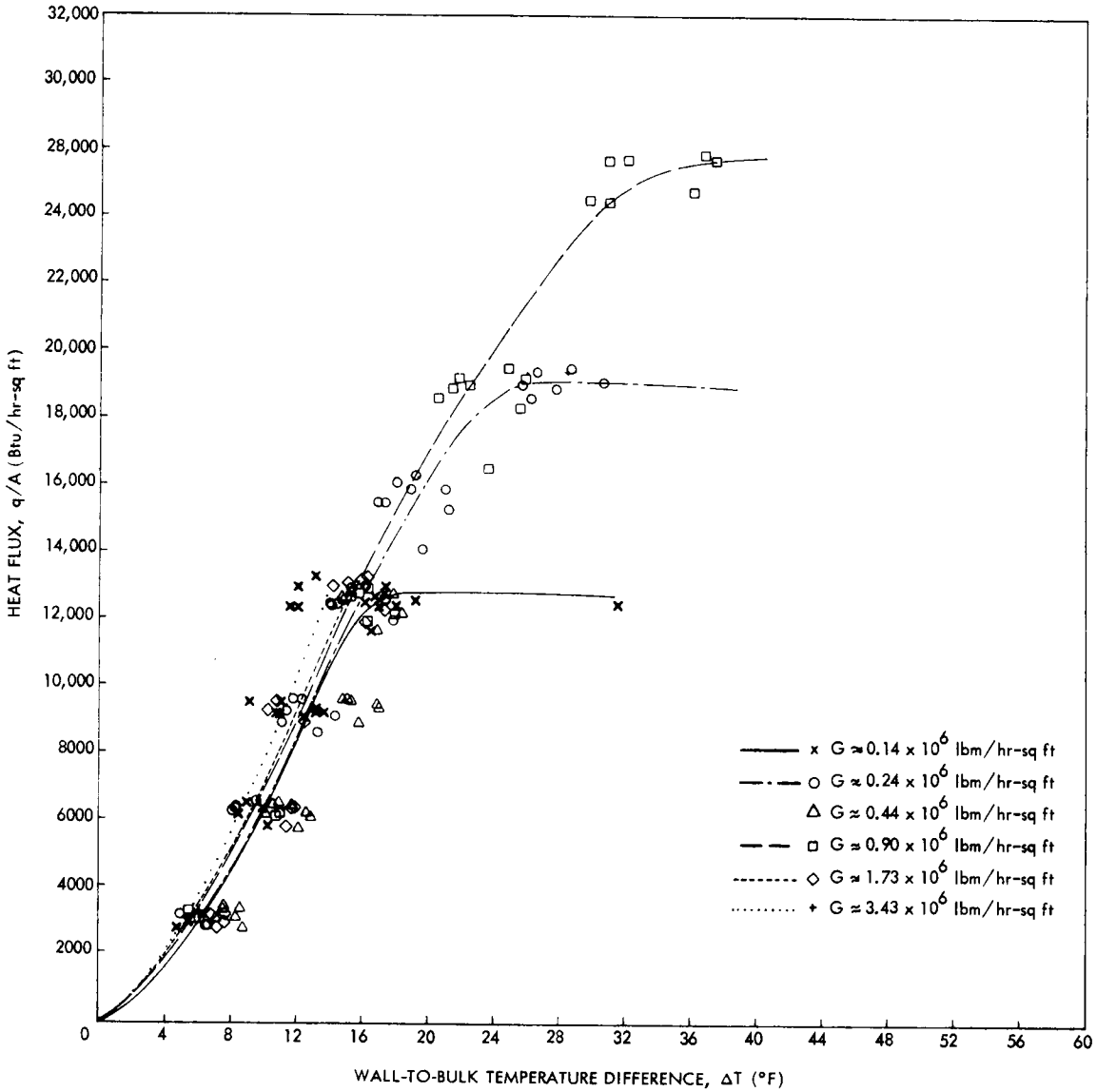


Figure IV-74. PLOT OF THE HEAT FLUX VERSUS THE WALL-TO-BULK TEMPERATURE DIFFERENCE FOR THE FORCED CONVECTIVE BOILING OF R-114, T≈150°F.

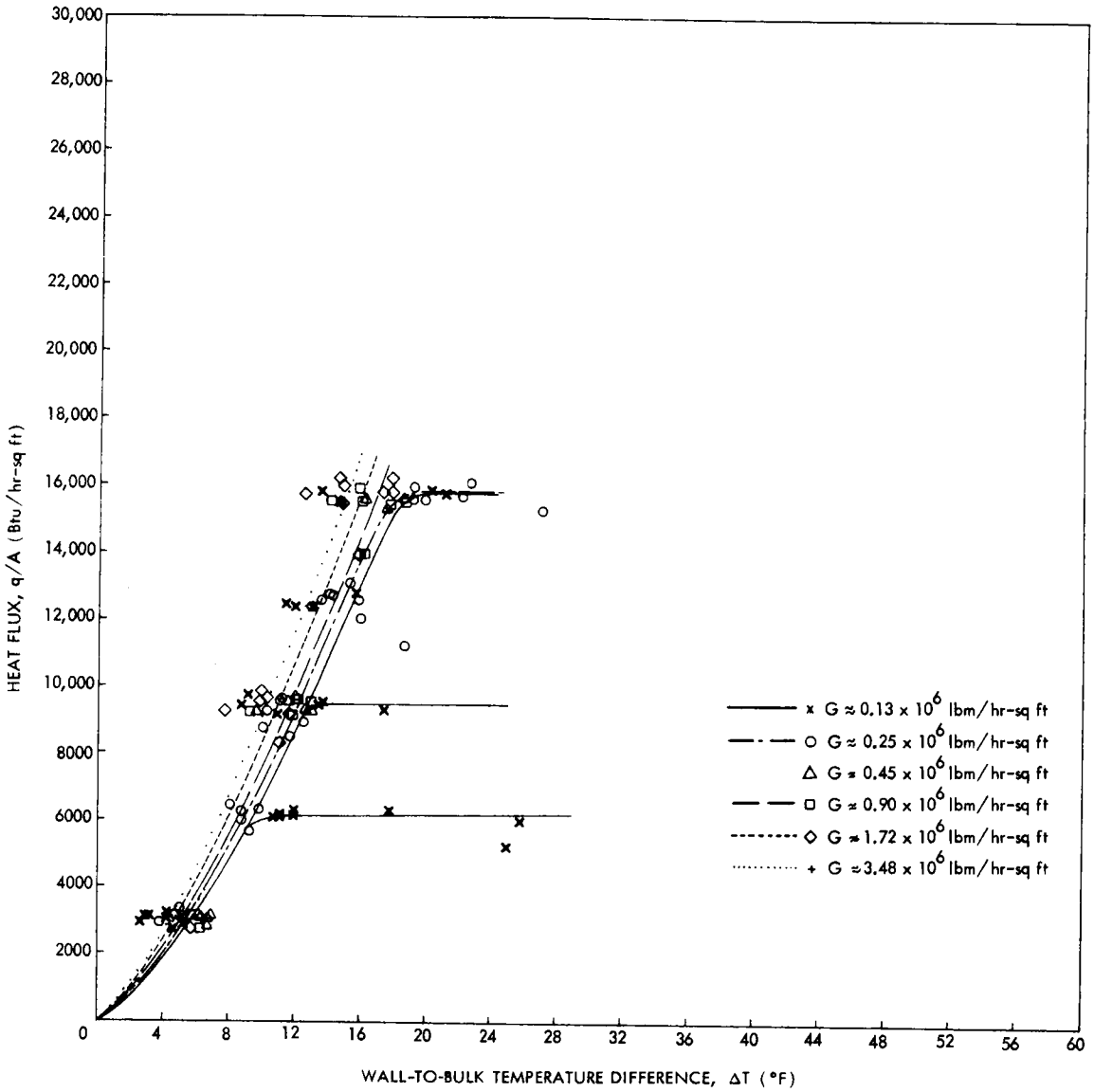


Figure IV-75. PLOT OF THE HEAT FLUX VERSUS THE WALL-TO-BULK TEMPERATURE DIFFERENCE FOR THE FORCED CONVECTIVE BOILING OF R-114, T≈200°F.

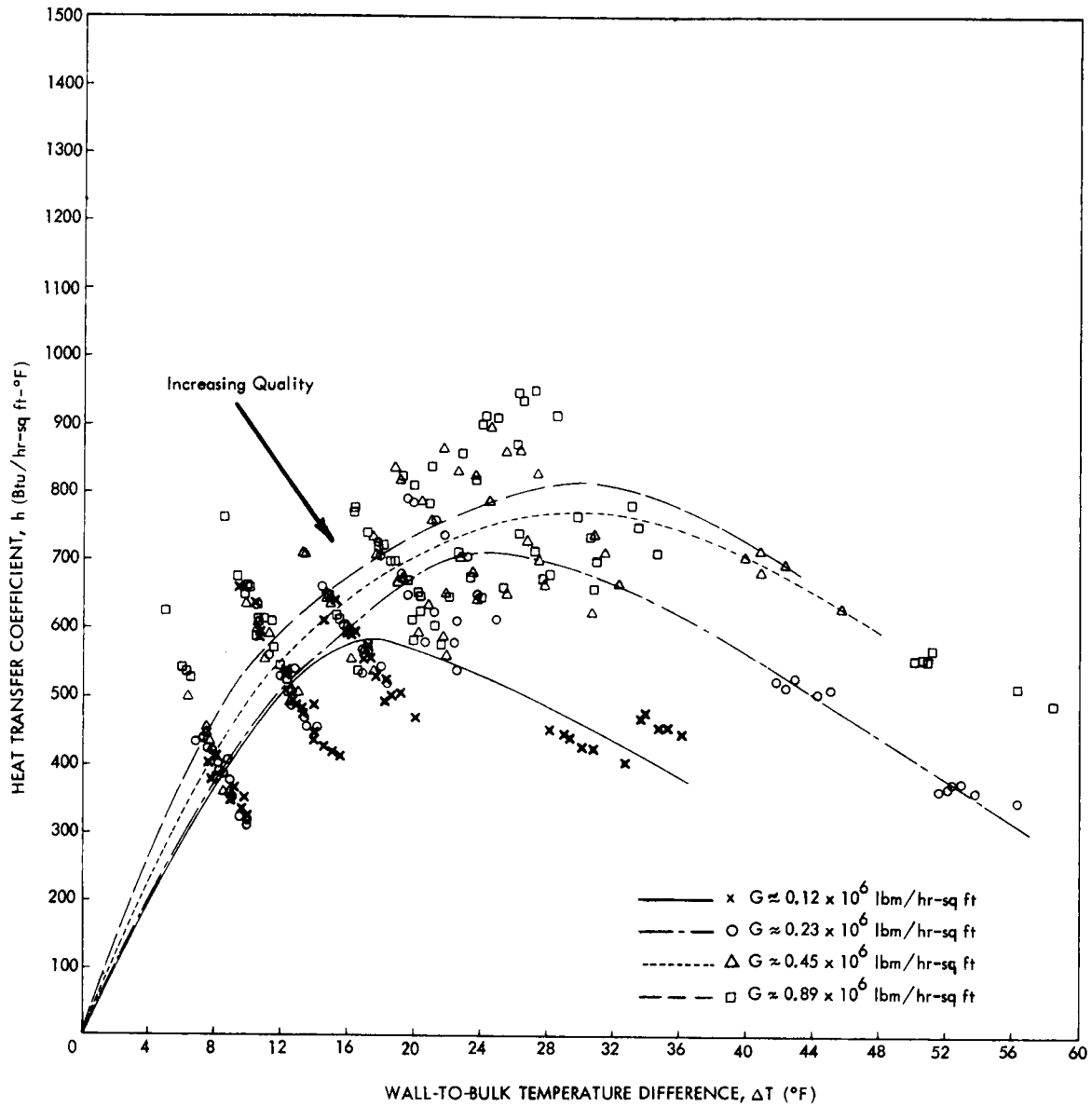


Figure IV-76. PLOT OF THE HEAT TRANSFER COEFFICIENT VERSUS THE WALL-TO-BULK TEMPERATURE DIFFERENCE FOR THE FORCED CONVECTIVE BOILING OF R-114, T≈100°F.

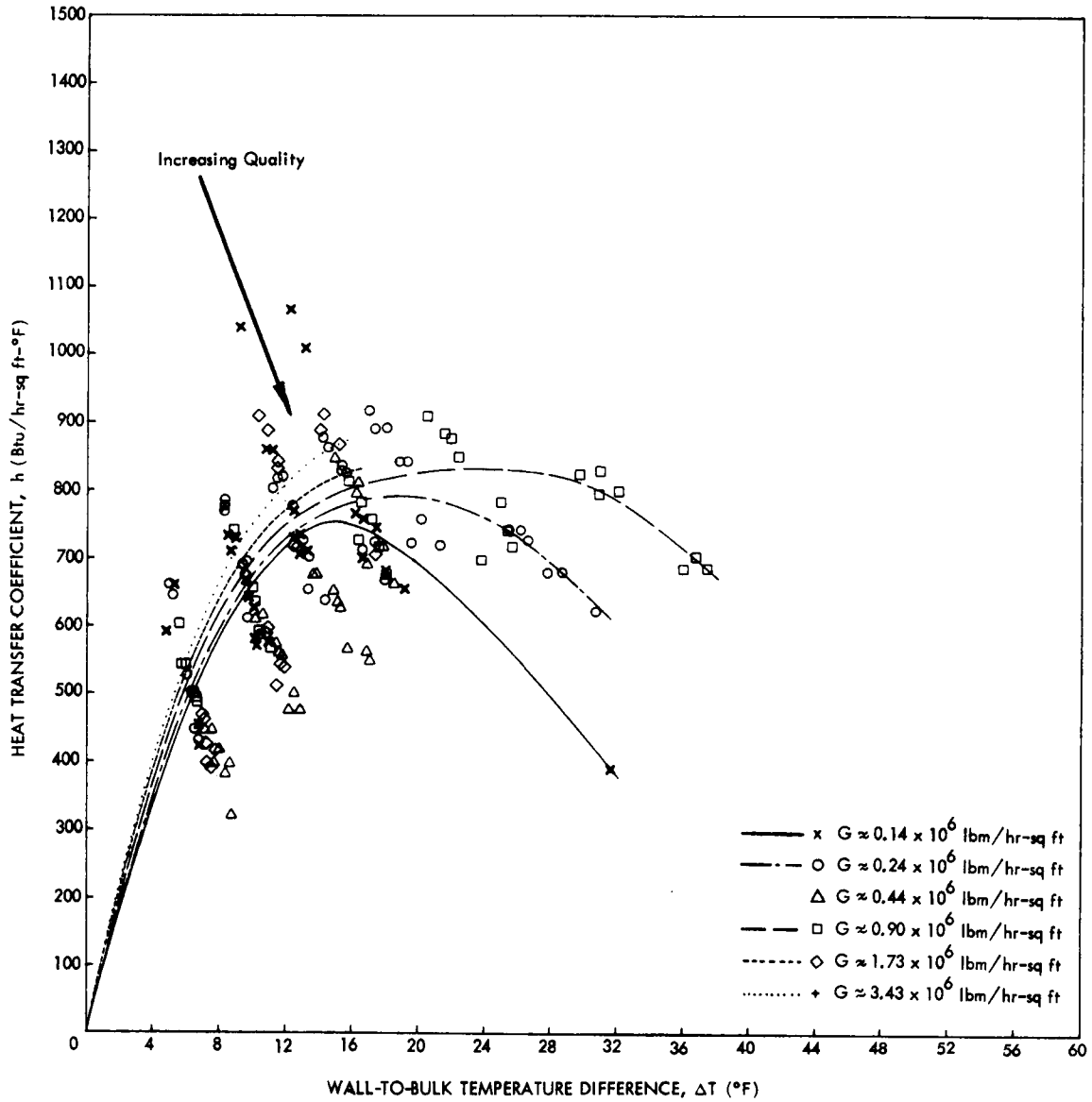


Figure IV-77. PLOT OF THE HEAT TRANSFER COEFFICIENT VERSUS THE WALL-TO-BULK TEMPERATURE DIFFERENCE FOR THE FORCED CONVECTIVE BOILING OF R-114, T≈150° F.

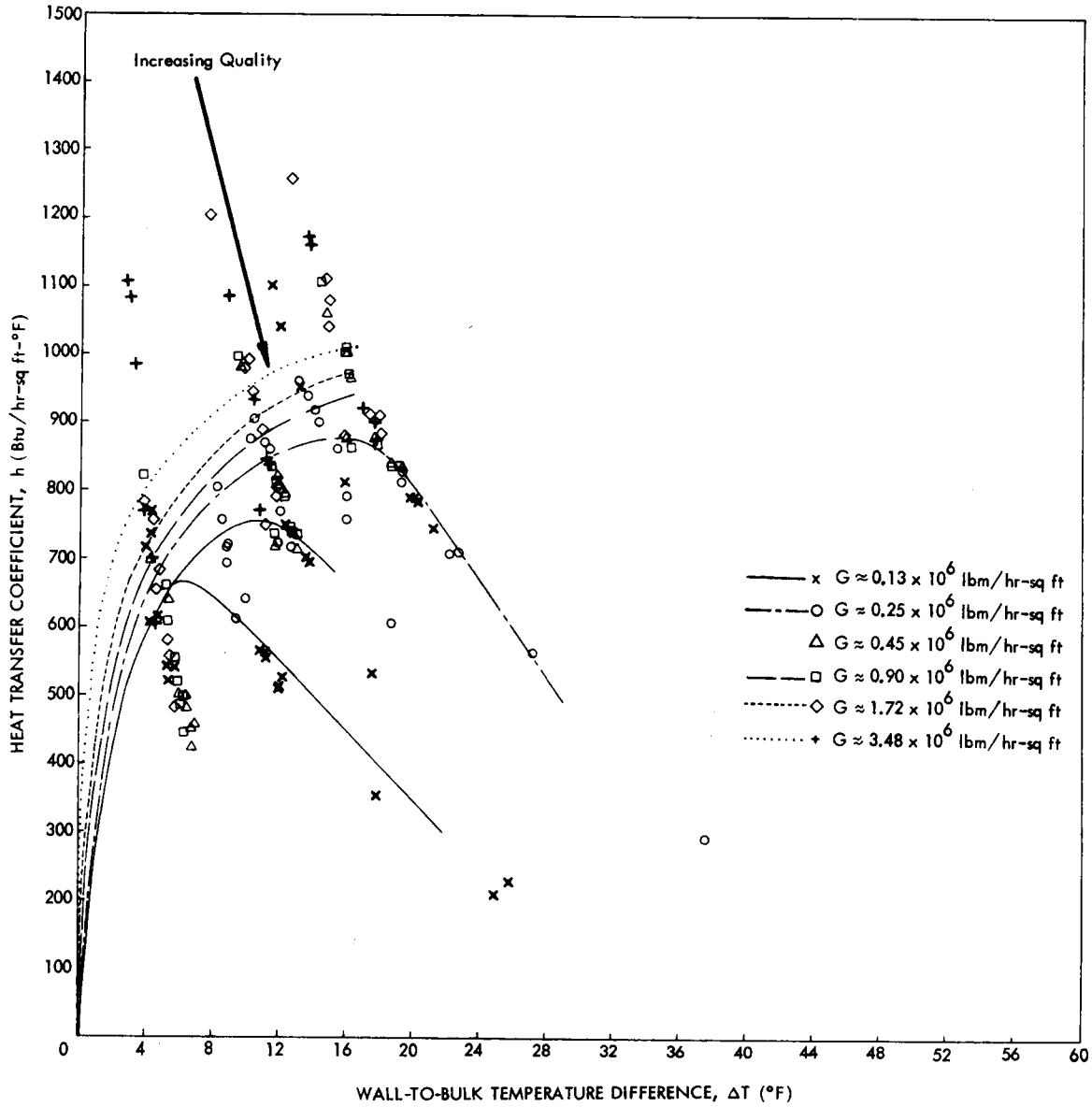


Figure IV-78. PLOT OF THE HEAT TRANSFER COEFFICIENT VERSUS THE WALL-TO-BULK TEMPERATURE DIFFERENCE FOR THE FORCED CONVECTIVE BOILING OF R-114, T≈200°F.

(3) As the boiling temperature increased, a much higher h vs ΔT curve was obtained.

(4) The critical heat flux seemed to occur at a considerably lower q/A but a slightly higher h in the 200°F runs than in the 100°F runs.

Quite apparently, more refined forms of correlating the heat transfer coefficient-preferably based on sound heat transfer principles are desirable in order to quantify some of the trends noted above. A comparison of a representative sample of the results obtained in this study with some of the correlations described in Chapter II, Section C will now be made. This representative sample, consisting of 318 data points, covers the entire range of test parameters and was chosen in order to reduce the amount of plotting involved. It, however, was sufficient to clearly delineate the trends obtained with all the correlations. Only for the case of the Chen [80] correlation, which will be extensively studied later on, were all the 445 data points plotted. As discussed in the literature survey, correlations obtained for boiling in horizontal tubes were found to hold equally well for vertical tubes. Consequently, no distinction based on test section orientation will be made in applying the correlations.

Comparison of Experimental Results With Various Correlations

Cheshire and Stirling [36] Correlation. A comparison of the Cheshire and Stirling [36] correlation represented by Equation (2-71) with the present results is shown in Figures IV-79 to IV-81. As can be seen, agreement in general is not good, with the correlation overestimating a large percentage of the data. Cheshire and Stirling [36]

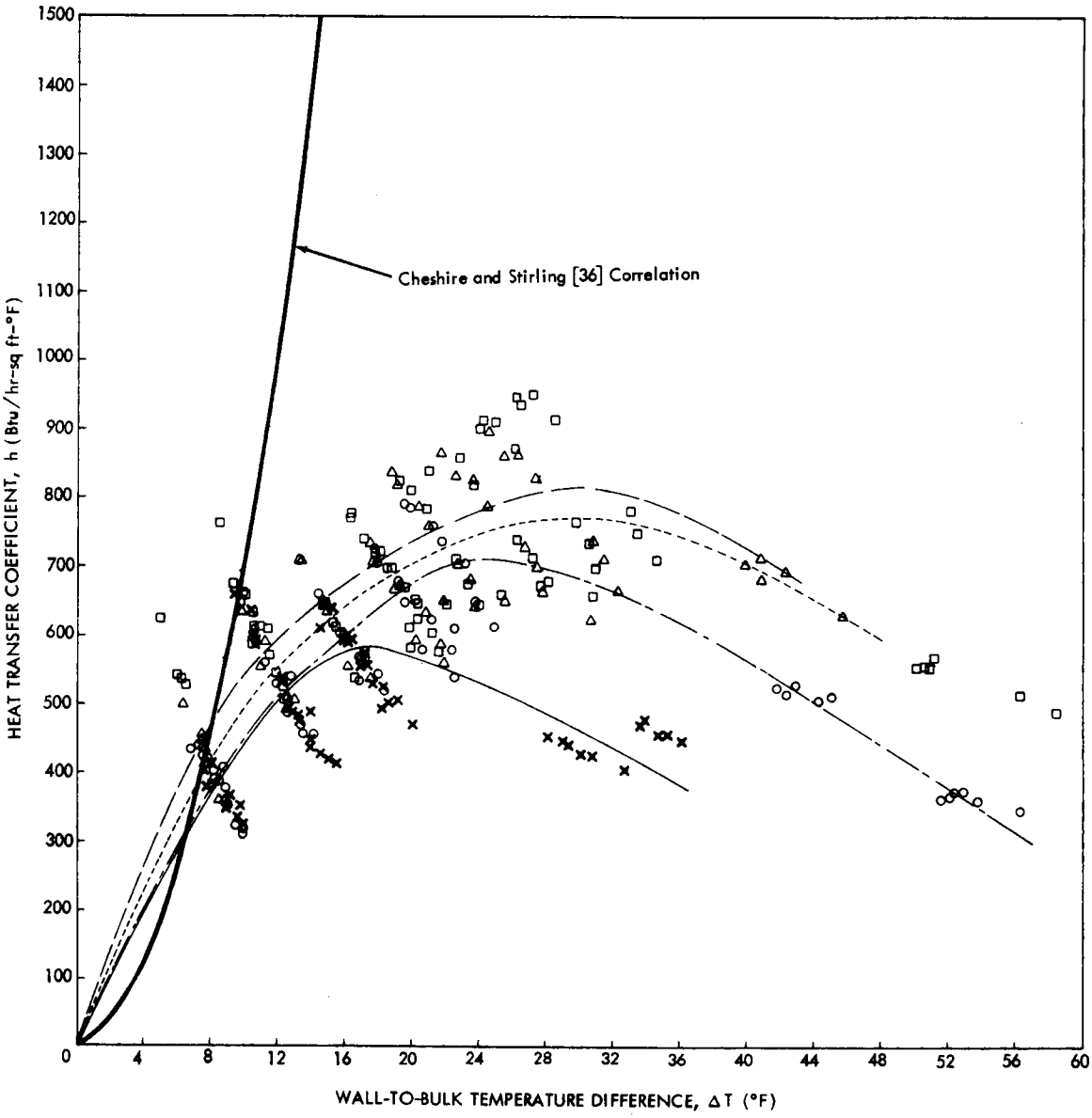


Figure IV-79. COMPARISON OF THE EXPERIMENTAL HEAT TRANSFER COEFFICIENTS WITH THE CHESHIRE AND STIRLING [36] CORRELATION, T≈100°F.

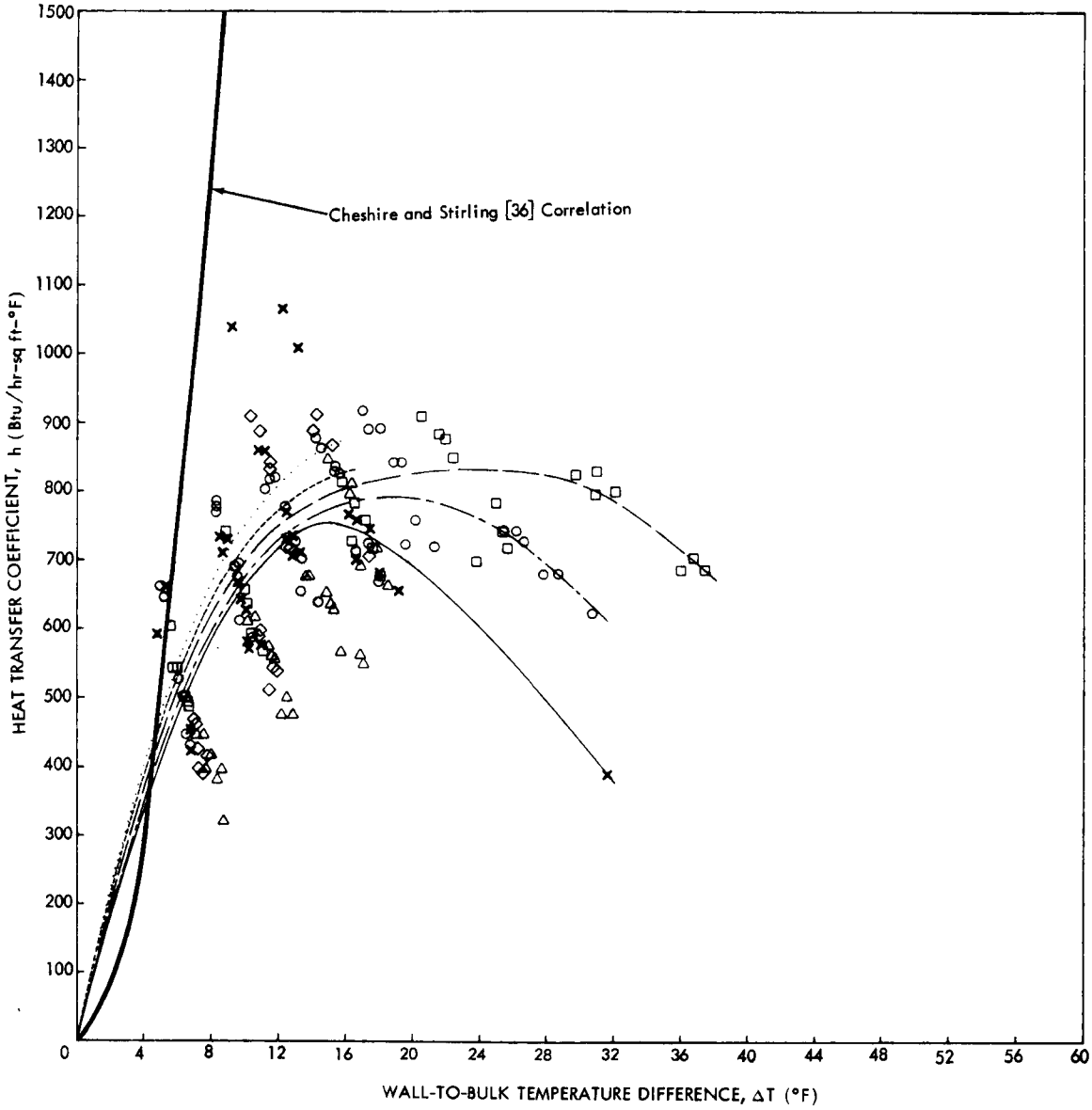


Figure IV-80. COMPARISON OF THE EXPERIMENTAL HEAT TRANSFER COEFFICIENTS WITH THE CHESHIRE AND STIRLING [36] CORRELATION, T≈150°F.

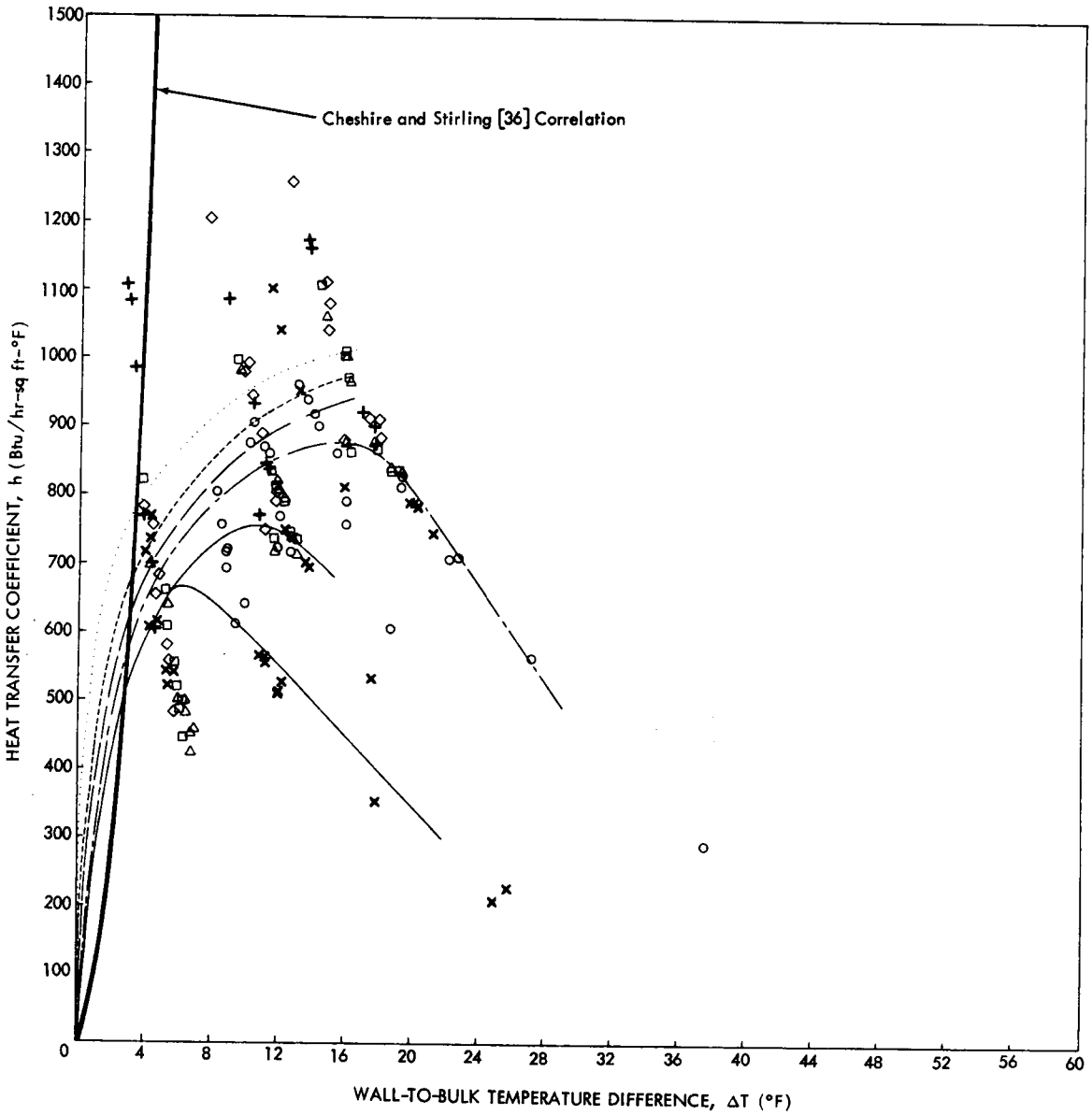


Figure IV-81. COMPARISON OF THE EXPERIMENTAL HEAT TRANSFER COEFFICIENTS WITH THE CHESHIRE AND STIRLING [36] CORRELATION, T≈200°F.

based their equation on data obtained in the range of operating conditions given in Table II-4 on page 73. For the 100°F boiling temperature, agreement between the correlation and experimental data occurred only in the narrow range of wall-to-bulk temperature differences of 6 to 10°F. For the 150 and 200°F boiling temperatures, agreement was even more limited with progressively greater deviations occurring as the boiling temperature was increased. This may be attributed, to a certain degree, to the surface tension term in the denominator of the correlation. For temperatures significantly above those at which Cheshire and Stirling [36] ran their tests, the surface tension term in the denominator decreases and goes to zero at the critical point. Thus, one would not expect the heat transfer coefficient to be accurately predicted at these high temperatures.

From the data at 100°F, it is apparent that even in the range where the operating conditions of Cheshire and Stirling [36] and this study overlapped, significant discrepancies exist in the heat transfer coefficient values obtained. Cheshire and Stirling [36] obtained coefficients as high as 2000 Btu/hr-sq ft-°F for the 110°F run while the highest coefficient observed in this study at the 100°F boiling temperature was 950 Btu/hr-sq ft-°F. These differences could be attributed to variations between the two systems and quite possibly to the surface characteristics of the boiling test sections used. It should be noted that Cheshire and Stirling [36] in their tests, experienced a variety of heat transfer coefficient levels for the same operating condition, depending on whether the system was flushed with cold acid, hot acid, or polished with emery cloth. In addition, it is possible that some

of the wall thermocouples used may have been damaged by the overheating that the test section was subjected to during the thermocouple installation process. Cheshire and Stirling [36] never ran a calibration test similar to the one outlined in Appendix C to check whether the wall-to-bulk fluid temperature difference was being accurately recorded.

O'Donnell, Robinson, and Webb [85] Correlation. O'Donnell, Robinson, and Webb [85], using the same apparatus and test section as Cheshire and Stirling [36], obtained a boiling correlation in a slightly different form as shown in Equation (2-72). For R-114, their equation reduced to that obtained by Cheshire and Stirling [36]. Therefore the curves in Figures IV-79 to IV-81 also represent the O'Donnell, Robinson, and Webb [85] correlation.

Altman, Norris, and Staub [40] Correlation. A comparison of the present data with the Altman, Norris, and Staub [40] correlation is shown in Figure IV-82. While this correlation is a considerable improvement over that of Cheshire and Stirling [36] and O'Donnell, Robinson, and Webb [85], it does consistently underpredict the experimental results. The majority of the data lie between 0 and -70% with the greatest deviations occurring at low qualities. In addition, a large fraction of the data could not be correlated because they lay in the $Re^2_f K_f$ range beyond that shown in Table II-7 on page 77 for which this set of equations was applicable. This greatly limited the usefulness of the Altman, Norris, and Staub [40] correlation.

Davis and David [81] Correlation. While Davis and David [81] were able to successfully correlate their results using a Dittus-Boelter

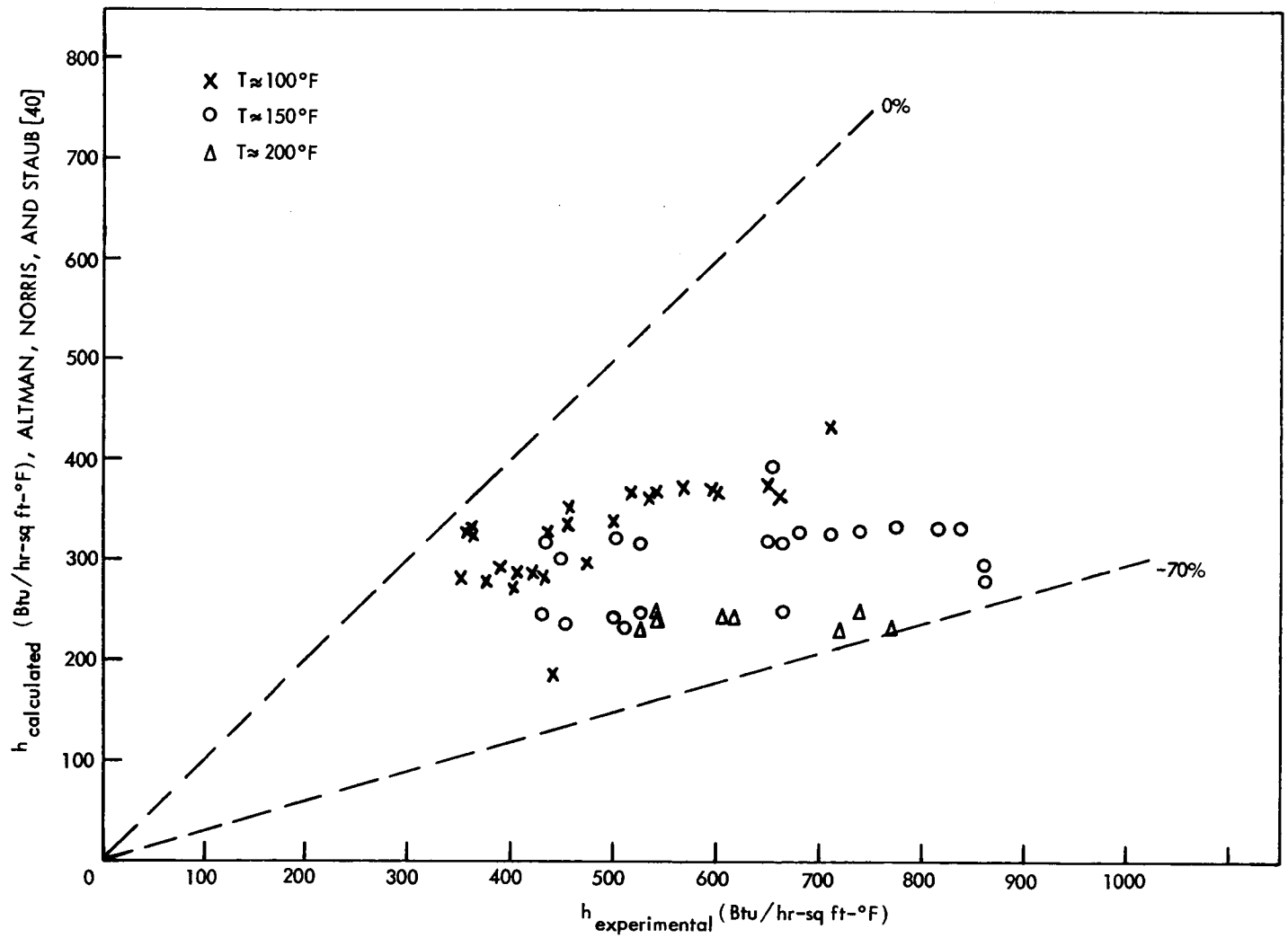


Figure IV-82. COMPARISON OF THE EXPERIMENTAL HEAT TRANSFER COEFFICIENTS WITH THE ALTMAN, NORRIS, AND STAUB [40] CORRELATION.

type of equation, neither their annular flow model nor their homogeneous flow model was successful when applied to the R-114 data obtained in this study, possibly due to the wide range of qualities covered here. In Figures IV-83 to IV-85, comparisons of the experimental and calculated heat transfer coefficients are shown for the Davis and David [81] separated-annular flow model. As can be seen, the data were correlated between +92 and - 96%. The greatest discrepancies occurred at the low flows and low qualities where the xG term in Equation (2-64) was small. Application of the Davis and David [81] homogeneous model is shown in Figures IV-86 to IV-88 for the 100, 150, and 200°F boiling temperatures, respectively. For all these boiling temperatures, the correlation was between > +300 and -83%. Again, the greatest discrepancies occurred in the low quality range, especially at low mass fluxes. In addition, at high qualities, the vapor viscosity assumed a predominant role in Equation (2-66) and since μ_g was more than an order of magnitude less than μ_f, the calculated values for the heat transfer coefficient in Equation (2-65) rose rapidly, causing the correlation to overpredict the true boiling coefficient by more than 300% in some cases.

One quite popular way of correlating the boiling coefficient is with formulations of the type given in Equations (2-59) and (2-60). A comparison of some of these correlations with the present experimental data will now be made.

Dengler and Addoms [78] Correlation. This correlation which was presented in the form of:

$$\frac{h_{TP}}{h_{fo}} = 3.5\left(\frac{1}{X_{tt}}\right)^{0.50} \qquad (2\text{-}60)$$

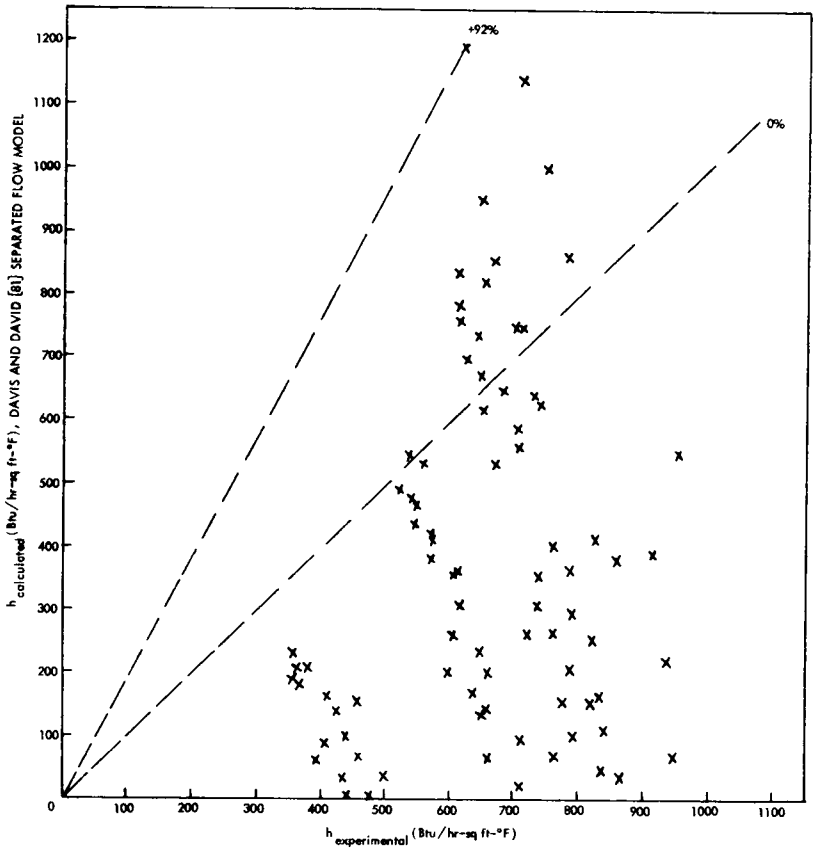


Figure IV-83. COMPARISON OF THE EXPERIMENTAL HEAT TRANSFER COEFFICIENTS WITH THE DAVIS AND DAVID [81] SEPARATED FLOW MODEL, T≈100°F.

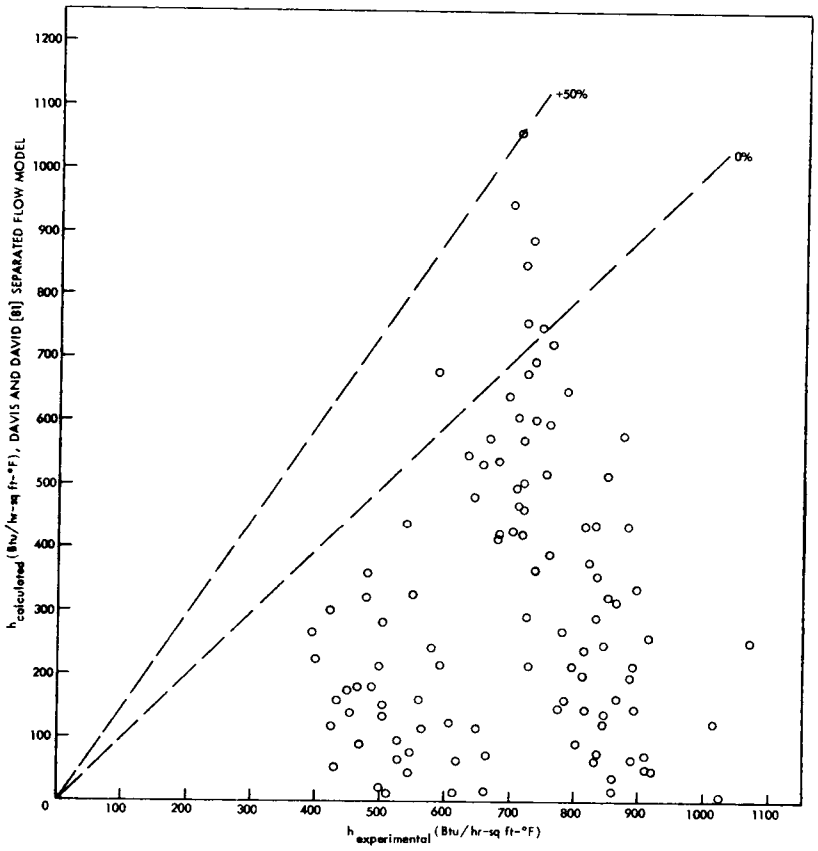


Figure IV-84. COMPARISON OF THE EXPERIMENTAL HEAT TRANSFER COEFFICIENTS WITH THE DAVIS AND DAVID [81] SEPARATED FLOW MODEL, T≈150°F.

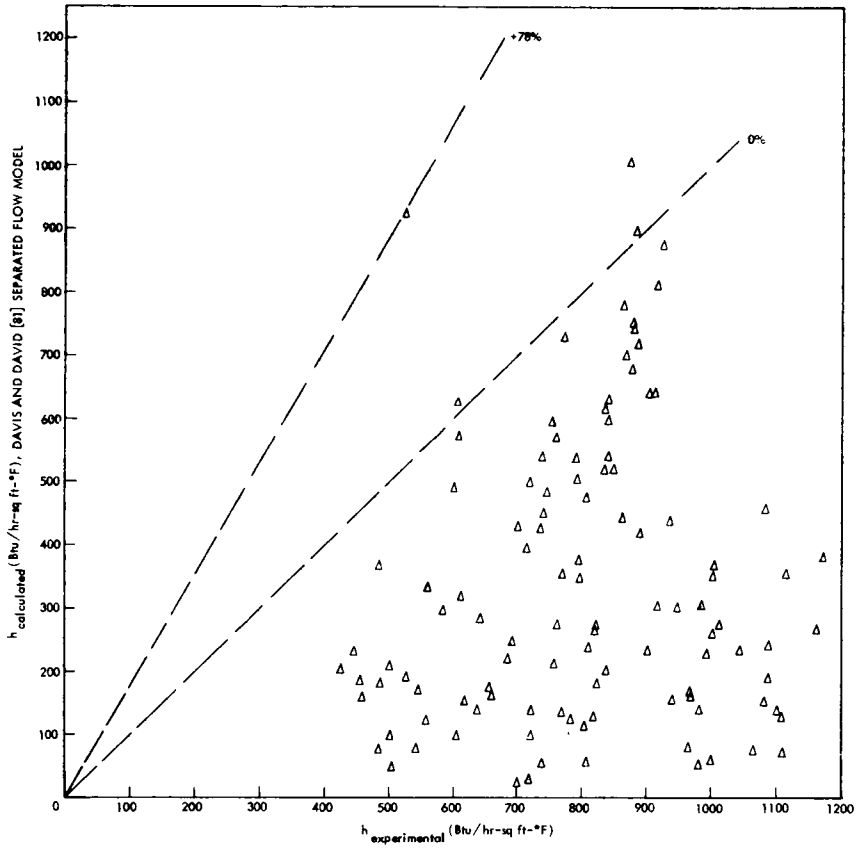


Figure IV-85. COMPARISON OF THE EXPERIMENTAL HEAT TRANSFER COEFFICIENTS WITH THE DAVIS AND DAVID [81] SEPARATED FLOW MODEL, T≈200°F.

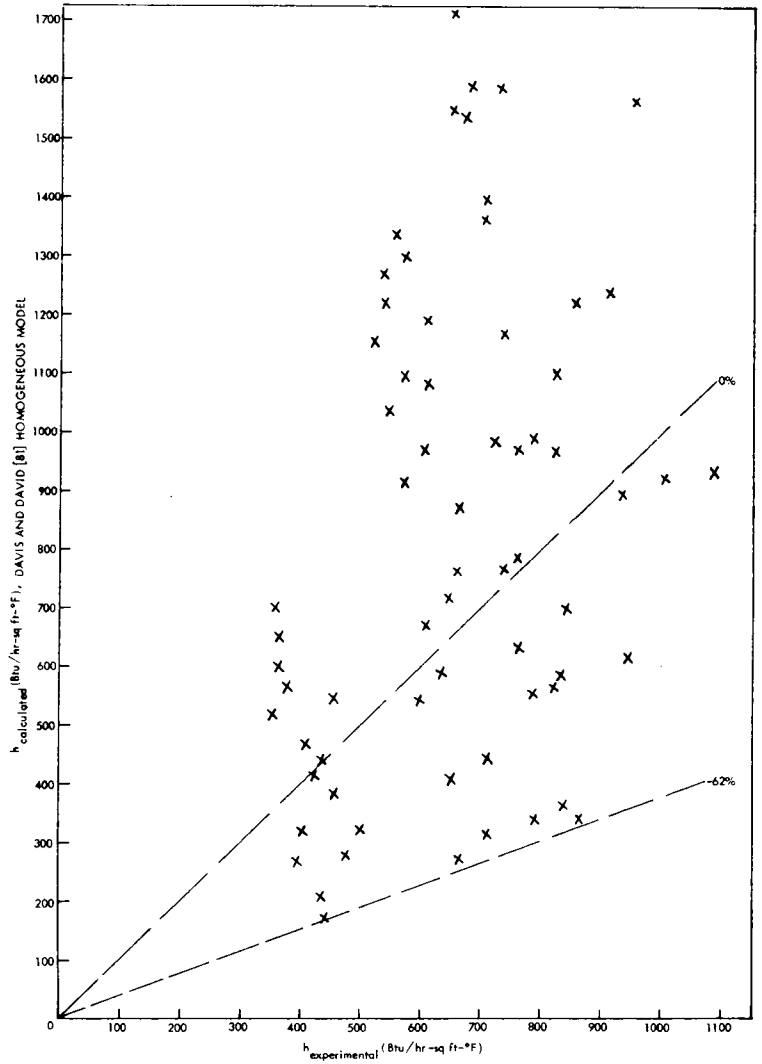


Figure IV-86. COMPARISON OF THE EXPERIMENTAL HEAT TRANSFER COEFFICIENTS WITH THE DAVIS AND DAVID [81] HOMOGENEOUS MODEL, T≈100°F.

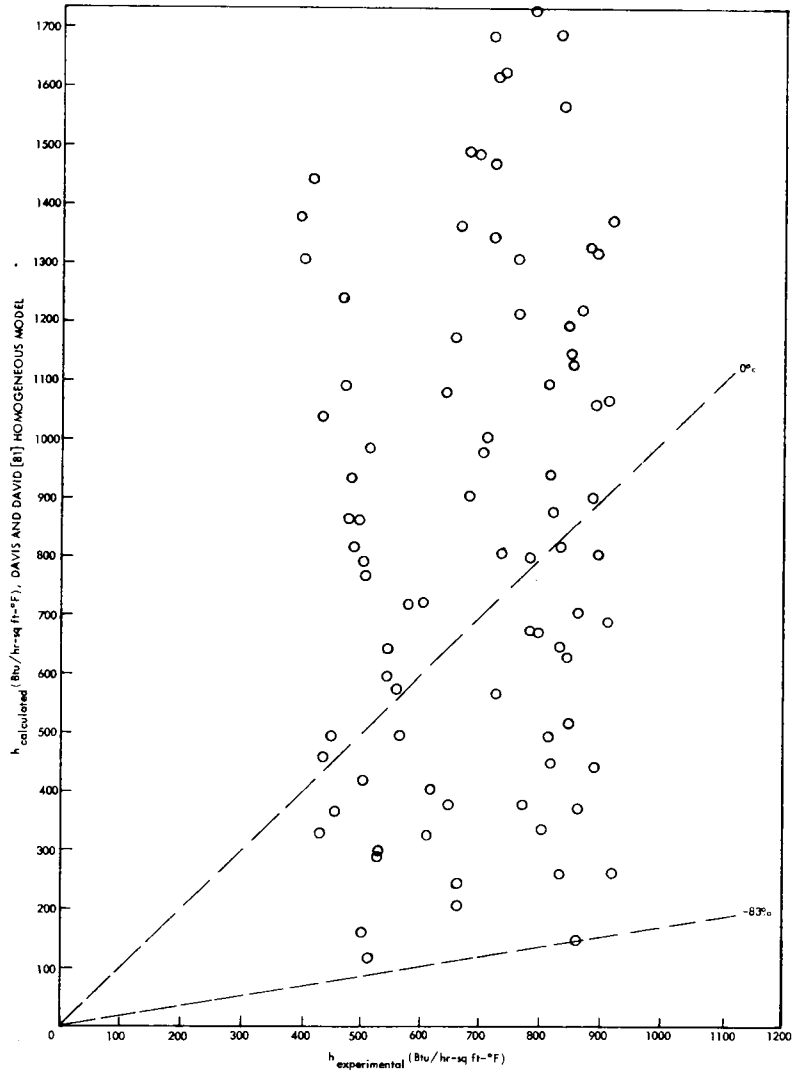


Figure IV-87. COMPARISON OF THE EXPERIMENTAL HEAT TRANSFER COEFFICIENTS WITH THE DAVIS AND DAVID [81] HOMOGENEOUS MODEL, T≈150°F.

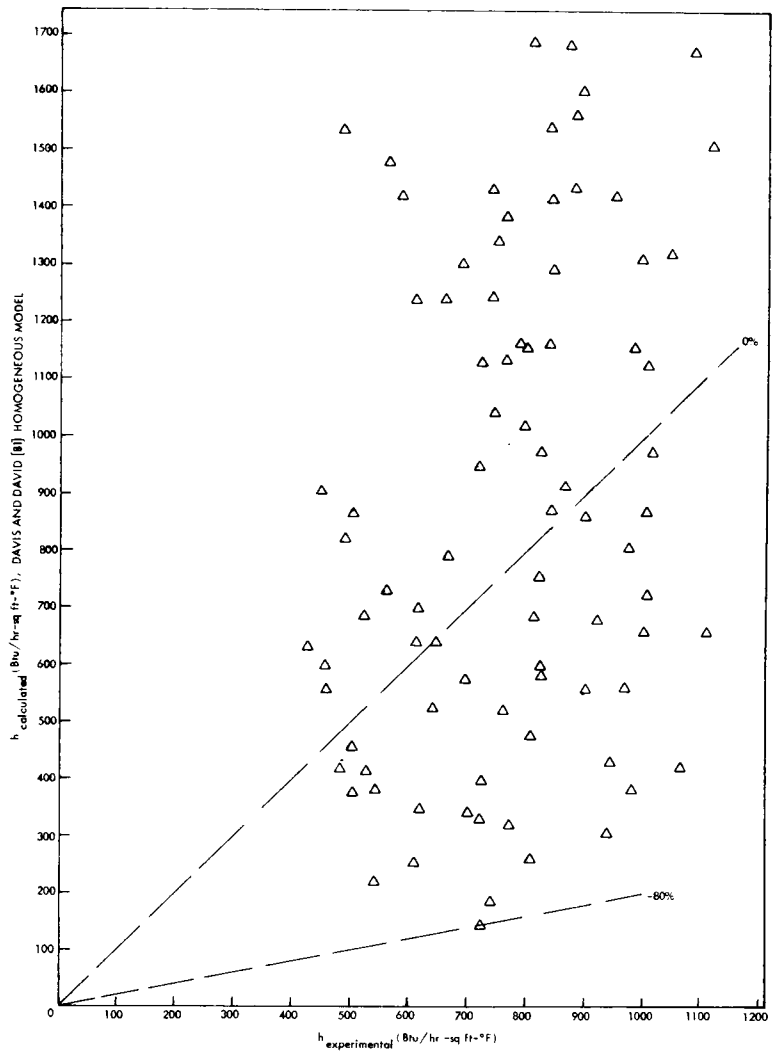


Figure IV-88. COMPARISON OF THE EXPERIMENTAL HEAT TRANSFER COEFFICIENTS WITH THE DAVIS AND DAVID [81] HOMOGENEOUS MODEL, T≈200°F.

was compared with the results from the present experimental investigation in Figure IV-89 for the 100°F case. The correlation was not very satisfactory and considerable scatter existed. A careful point-by-point study indicated that this scatter was due, to a large degree, to the zone-by-zone analysis performed in this investigation. The first portion of the test section containing the low quality fluid yielded results which were on the left hand portion of Figure IV-89. As the quality increased, the data tended to move to the right and eventually approached the Dengler and Addoms [78] line. Thus, instead of analyzing the results on a zone-by-zone basis, the average conditions along the entire tube were examined. Quite different results were obtained as shown in Figure IV-90 for the 100, 150, and 200°F boiling temperatures. The wide band of scatter was reduced considerably and a more clearly defined trend was observable. The best fit to the experimental data was:

$$\frac{h_{TP}}{h_{fo}} = 6.22\left(\frac{1}{X_{tt}}\right)^{0.64} \qquad (4\text{-}6)$$

with a spread of +74%, -42% for all but four points. This scatter should not be attributed completely to experimental error since a study of the data yielded the following trends:

(1) As the average quality (or heat flux) in the tube increased, h_{TP}/h_{fo} decreased.

(2) As the mass flux, G, increased, h_{TP}/h_{fo} decreased.

(3) As the boiling temperature increased, h_{TP}/h_{fo} increased.

Again here, as had been observed in the comparison with the Davis and David [81] and Altman, Norris, and Staub [40] correlations previously,

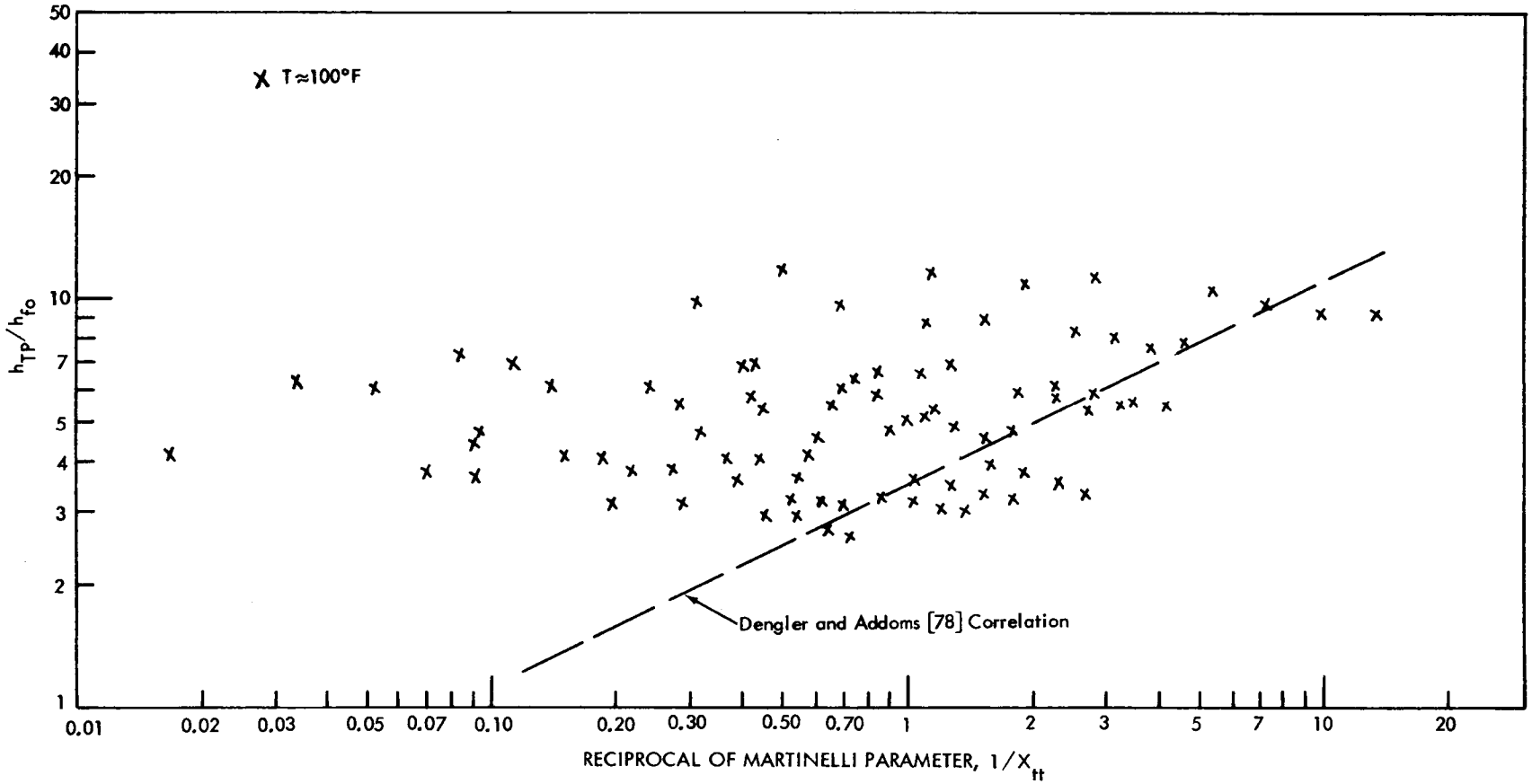


Figure IV-89. COMPARISON OF THE EXPERIMENTAL HEAT TRANSFER COEFFICIENTS WITH THE DENGLER AND ADDOMS [78] CORRELATION.

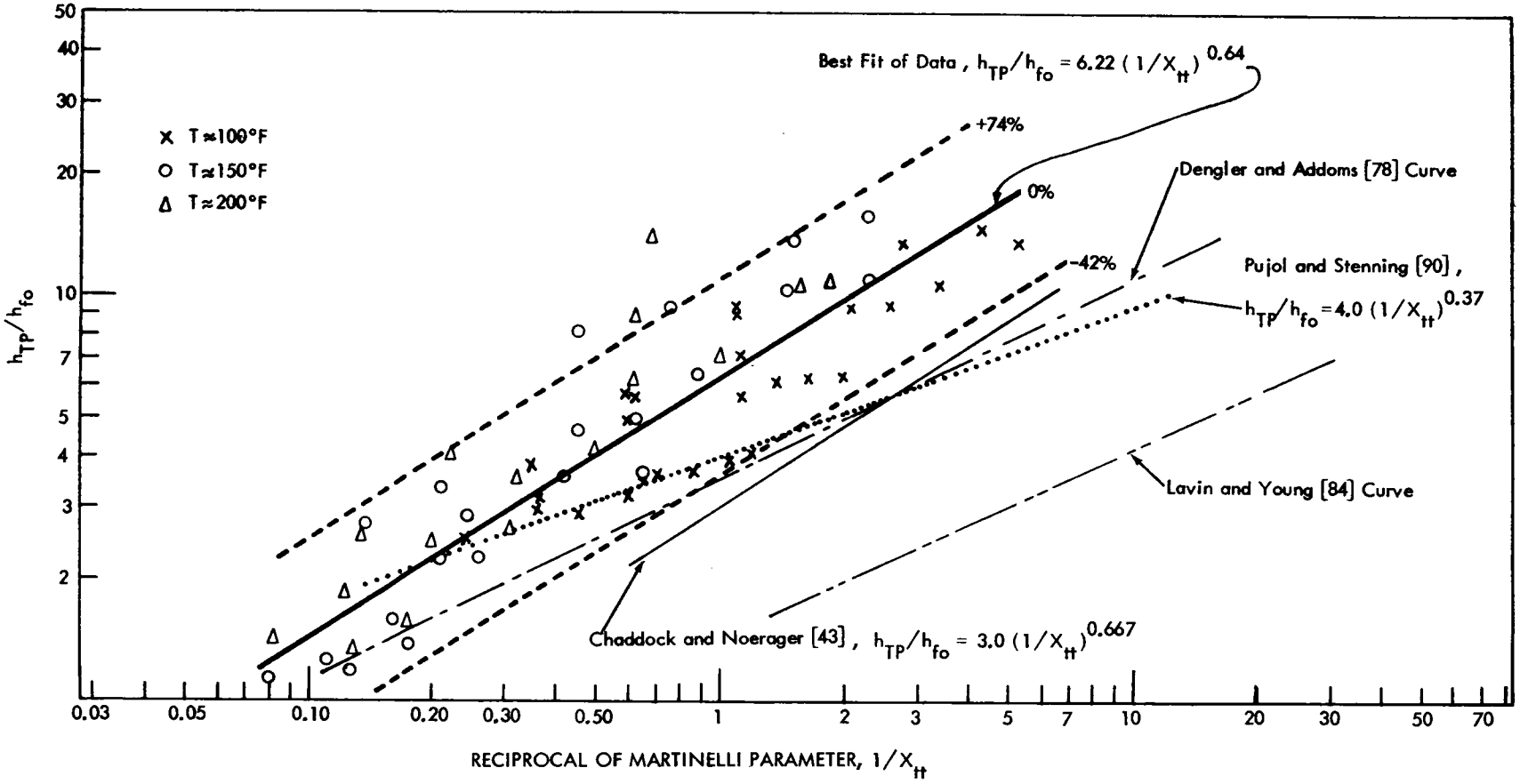


Figure IV-90. COMPARISON OF THE AVERAGE EXPERIMENTAL HEAT TRANSFER COEFFICIENTS ALONG THE LENGTH OF THE BOILING TEST SECTION WITH THE DENGLER AND ADDOMS [78] CORRELATION.

the experimental heat transfer coefficients obtained with R-114 were higher than those predicted by the correlations. Also shown in Figure IV-90 are the curves obtained by Pujol and Stenning [90] with R-113 for the nucleation suppressed region [Equation (2-79)], Chaddock and Noerager [43] for the horizontal flow boiling of R-12, and Lavin and Young [84] for the vertical flow boiling of R-12.

Guerrieri and Talty [77] Correlation. Another form of Equation (2-60), this time utilizing the ratio of the two-phase heat transfer coefficient to the single-phase coefficient assuming liquid alone flows through the tube was given by Guerrieri and Talty [77]. Again, as shown in Figure IV-91, comparison on a zone-by-zone basis yielded a wide scatter in the data. Using the average conditions over the whole test section in each run, the results in Figure IV-92 were obtained. The best fit to the data was:

$$\frac{h_{TP}}{h_{fa}} = 7.60 \left(\frac{1}{X_{tt}}\right)^{0.78} \qquad (4\text{-}7)$$

with a spread of from +113 to -47% for all but one point. This spread was more than the one obtained with the Dengler and Addoms [78] correlation. The same trends regarding the effect of average quality (or heat flux), mass flux, and boiling temperature observed with the Dengler and Addoms [78] correlation applied to Guerrieri and Talty [77] too. Also shown in Figure IV-92 was a comparison of the experimental data with the results of Chaddock and Noerager [43]. The best fit of the experimental data of this study was seen to lie above Chaddock and Noerager's [43] results. Napadensky's [15] results, an example of which was shown in Figure II-23 on page 72, were found to be strongly

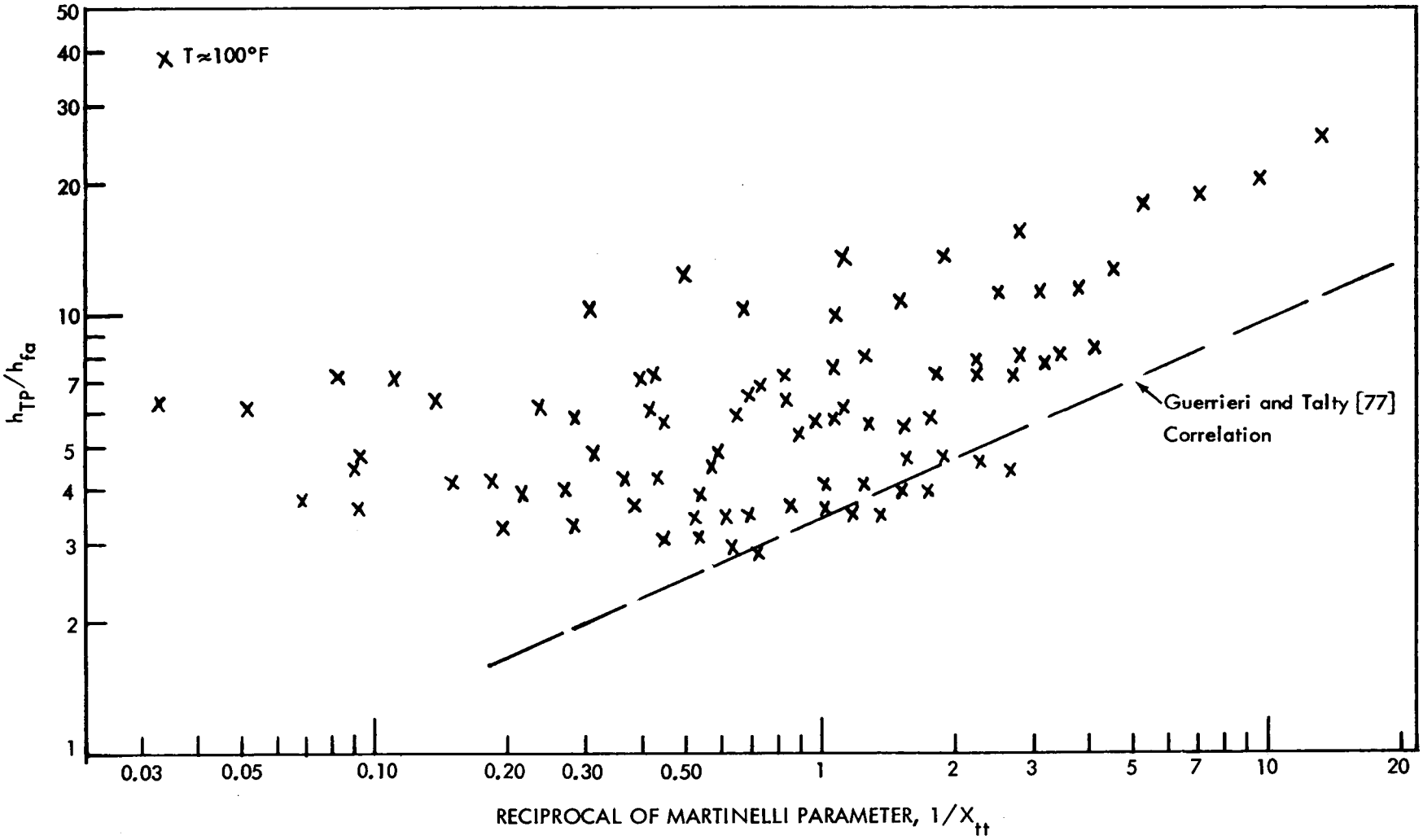


Figure IV-91. COMPARISON OF THE EXPERIMENTAL HEAT TRANSFER COEFFICIENTS WITH THE GUERRIERI AND TALTY [77] CORRELATION.

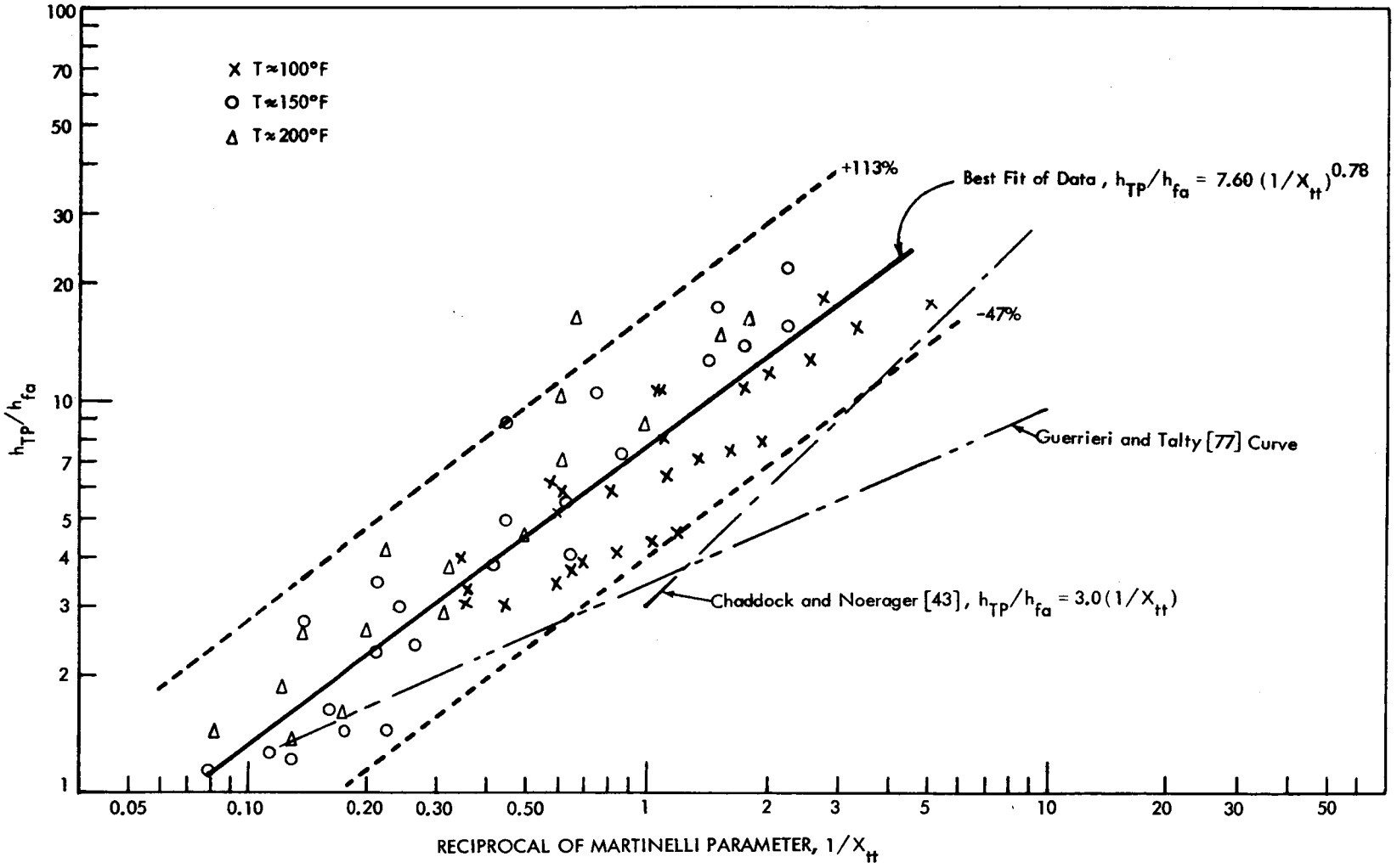


Figure IV-92. COMPARISON OF THE AVERAGE EXPERIMENTAL HEAT TRANSFER COEFFICIENTS ALONG THE LENGTH OF THE BOILING TEST SECTION WITH THE GUERRIERI AND TALTY [77] CORRELATION.

dependent on heat flux. All the vertical tube R-12 results were found to lie within the limits:

$$\frac{h_{TP}}{h_{fa}} = 1.42\left(\frac{1}{X_{tt}}\right)^{0.858} \tag{4-8}$$

for a heat flux of 4750 Btu/hr-sq ft and

$$\frac{h_{TP}}{h_{fa}} = 3.10\left(\frac{1}{X_{tt}}\right)^{0.545} \tag{4-9}$$

for a heat flux of 29,500 Btu/hr-sq ft.

Bennett et al [79] Correlation. Bennett et al [79] extended the Guerrieri and Talty [77] form of the equation to attempt to correct for one of the trends noted above, mainly the effect of the heat flux. He did this by adding a q/A term raised to a power and obtained Equation (2-61). A plot of $\left[h_{TP}/h_{fa}\ (q/A)^{-0.11}\right]$ vs $1/X_{tt}$ using the average conditions over the whole test section is shown in Figure IV-93. From the plot, it appears that the heat flux correction does not lead to any improvement in the correlation. A scatter of from +105 to -46% existed on both sides of the relation:

$$\frac{h_{TP}}{h_{fa}} = 2.80\left(\frac{1}{X_{tt}}\right)^{0.74}\left(\frac{q}{A}\right)^{0.11}. \tag{4-10}$$

Schrock and Grossman [82] Correlation. Another form of the Bennett et al [79] correlation, embodying more empirical constants, was presented by Schrock and Grossman [82] and given in Equation (2-67). This equation can be rewritten in the form:

$$\frac{h_{TP}}{h_{fa}} = 7391\left[\frac{q/A}{Gh_{fg}} + 1.50 \times 10^{-4}\left(\frac{1}{X_{tt}}\right)^{2/3}\right]. \tag{4-11}$$

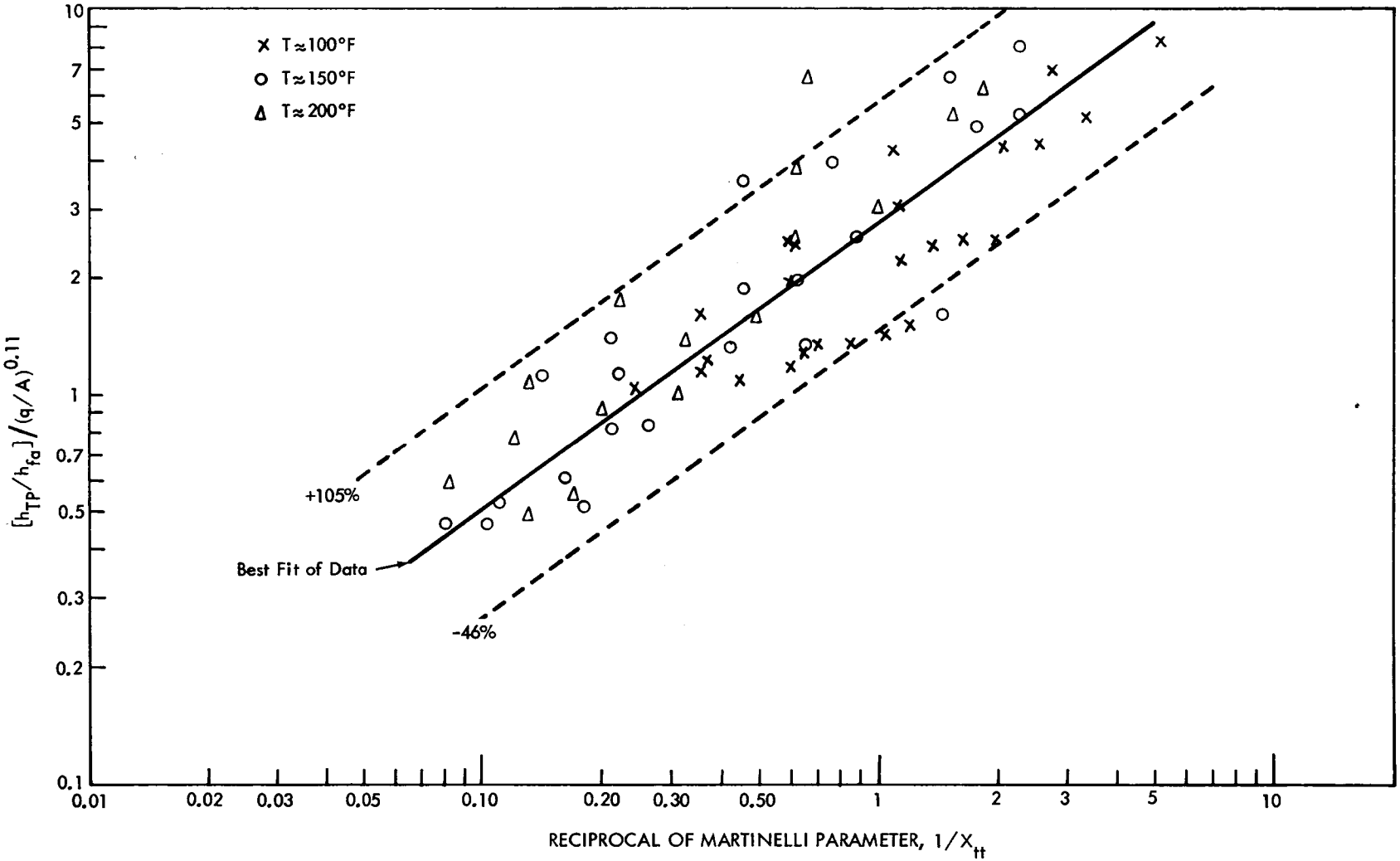


Figure IV-93. COMPARISON OF THE AVERAGE EXPERIMENTAL HEAT TRANSFER COEFFICIENTS ALONG THE LENGTH OF THE BOILING TEST SECTION WITH THE BENNETT ET AL [79] CORRELATION.

A comparison of the present data with the correlation is shown in Figures IV-94 to IV-96. As can be seen, the correlation was best for the 100°F boiling temperature runs and underestimated the experimental results to an increasingly greater extent with increasing temperature. The use of average conditions over the whole test section rather than the individual zone values did not reduce the scatter in the data. Purcupile, Riedle, and Schmidt [94] also compared their R-11 data for vertical flow with the Schrock and Grossman [82] correlation. As shown in Figure II-32 on page 87, the agreement was similar to that observed with R-114 in the present tests. Collier and Pulling [83] found better agreement with their data when they used the formulation:

$$\frac{h_{TP}}{h_{fa}} = 6700\left[\frac{q/A}{Gh_{fg}} + 3.50 \times 10^{-4}\left(\frac{1}{X_{tt}}\right)^{2/3}\right] . \qquad (4\text{-}12)$$

A comparison of this equation with some of the R-114 data is shown in Figures IV-97 to IV-99. No significant improvement was noted in the correlation.

Riedle and Purcupile [95] Correlation. Riedle and Purcupile [95] presented a simple expression for the wall superheat. As given in Purcupile, Riedle, and Schmidt's [94] recent publication, the correlation can be rearranged to give:

$$h = \frac{(q/A)^{0.7}}{28.3977\left(\frac{\rho_g}{\rho_f}\right)^{0.25}(D)^{0.6}} . \qquad (4\text{-}13)$$

The results shown in Figures IV-100 to IV-102 indicated that the correlation underestimated the experimental heat transfer coefficient at all temperature levels, especially the higher ones.

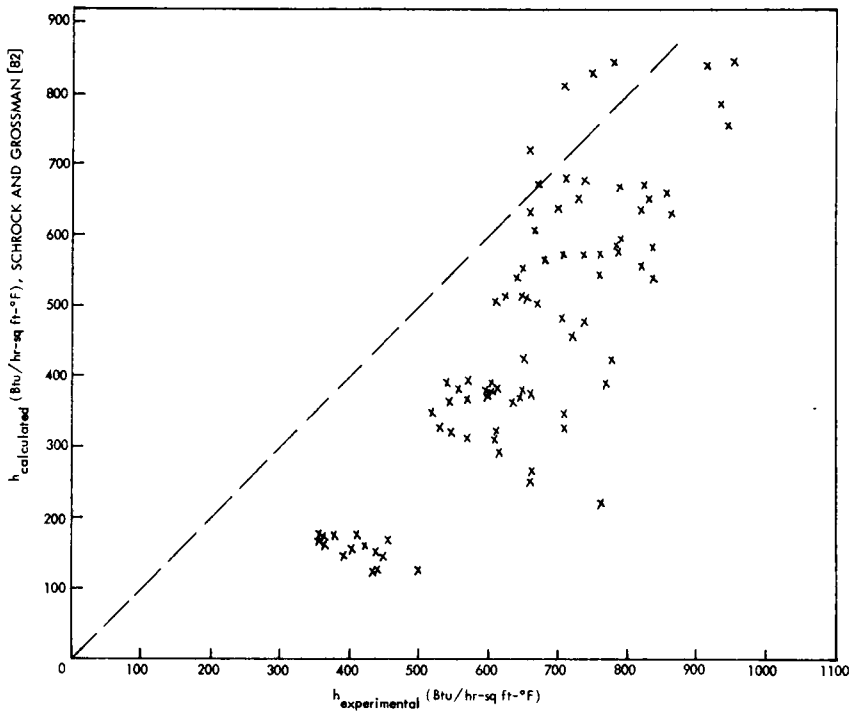


Figure IV-94. COMPARISON OF THE EXPERIMENTAL HEAT TRANSFER COEFFICIENTS WITH THE SCHROCK AND GROSSMAN [82] CORRELATION, T≈100°F.

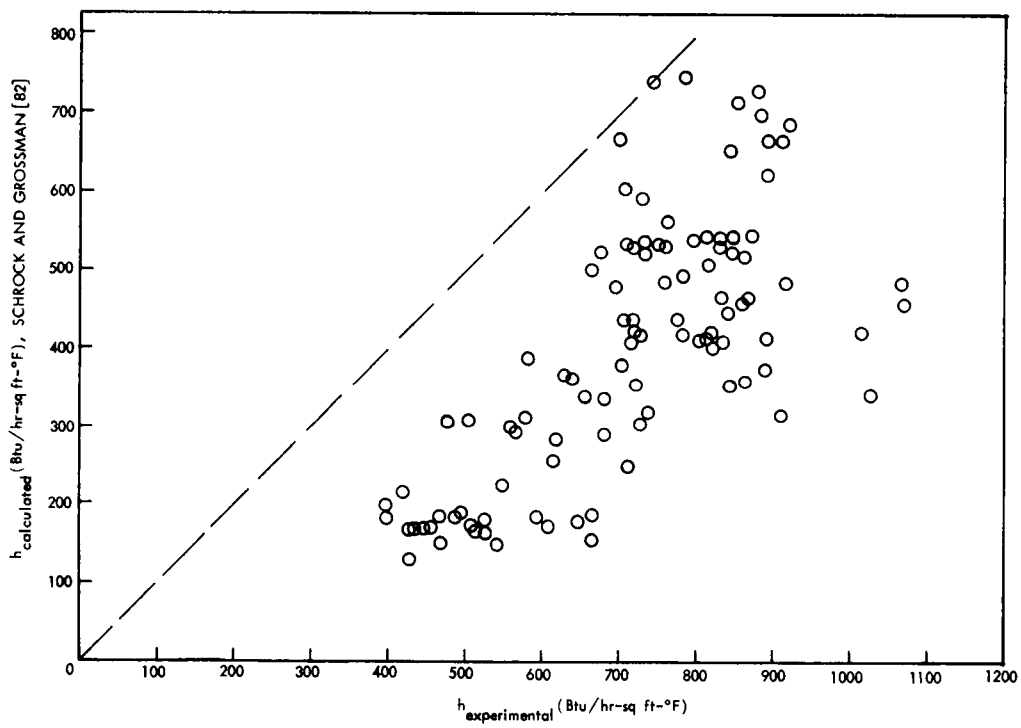


Figure IV-95. COMPARISON OF THE EXPERIMENTAL HEAT TRANSFER COEFFICIENTS WITH THE SCHROCK AND GROSSMAN [82] CORRELATION, T≈150°F.

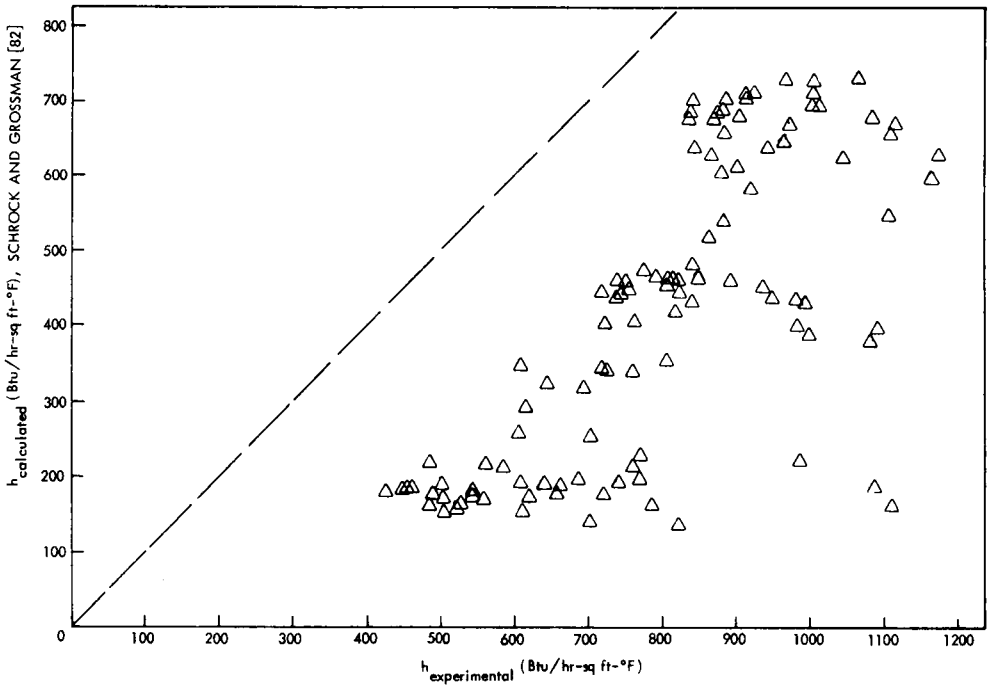


Figure IV-96. COMPARISON OF THE EXPERIMENTAL HEAT TRANSFER COEFFICIENTS WITH THE SCHROCK AND GROSSMAN [82] CORRELATION, T≈200°F.

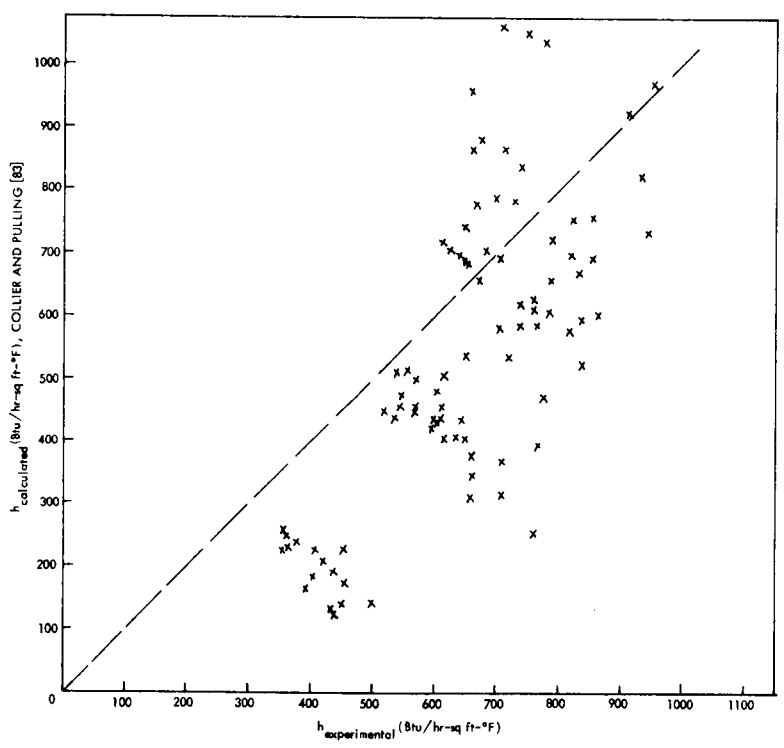


Figure IV-97. COMPARISON OF THE EXPERIMENTAL HEAT TRANSFER COEFFICIENTS WITH THE COLLIER AND PULLING [83] CORRELATION, T≈100°F.

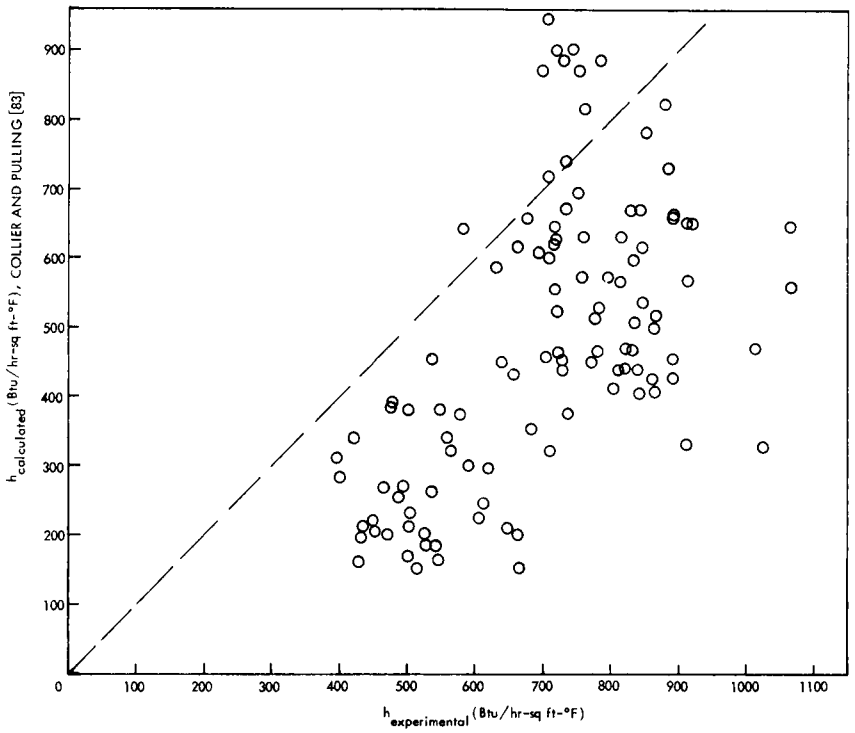


Figure IV-98. COMPARISON OF THE EXPERIMENTAL HEAT TRANSFER COEFFICIENTS WITH THE COLLIER AND PULLING [83] CORRELATION, T≈150°F.

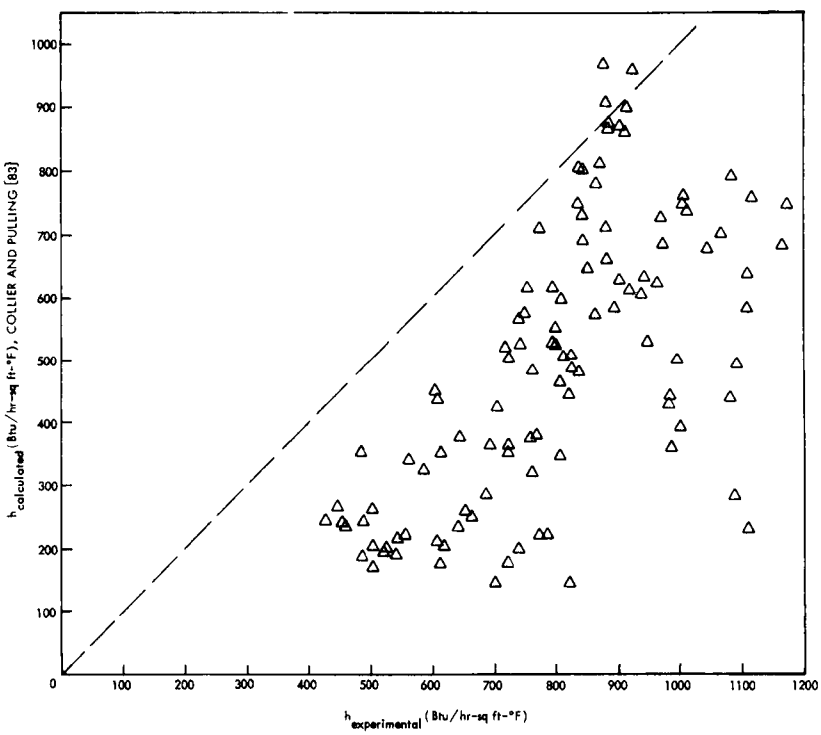


Figure IV-99. COMPARISON OF THE EXPERIMENTAL HEAT TRANSFER COEFFICIENTS WITH THE COLLIER AND PULLING [83] CORRELATION, T≈200°F.

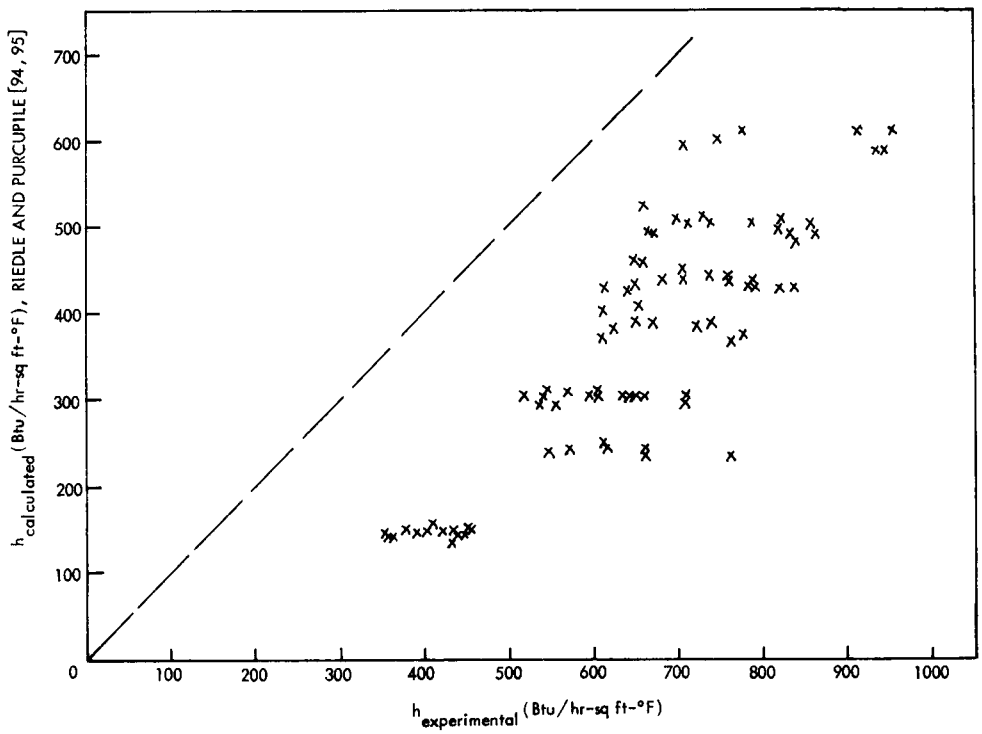


Figure IV-100. COMPARISON OF THE EXPERIMENTAL HEAT TRANSFER COEFFICIENTS WITH THE RIEDLE AND PURCUPILE [94, 95] CORRELATION, T≈100°F.

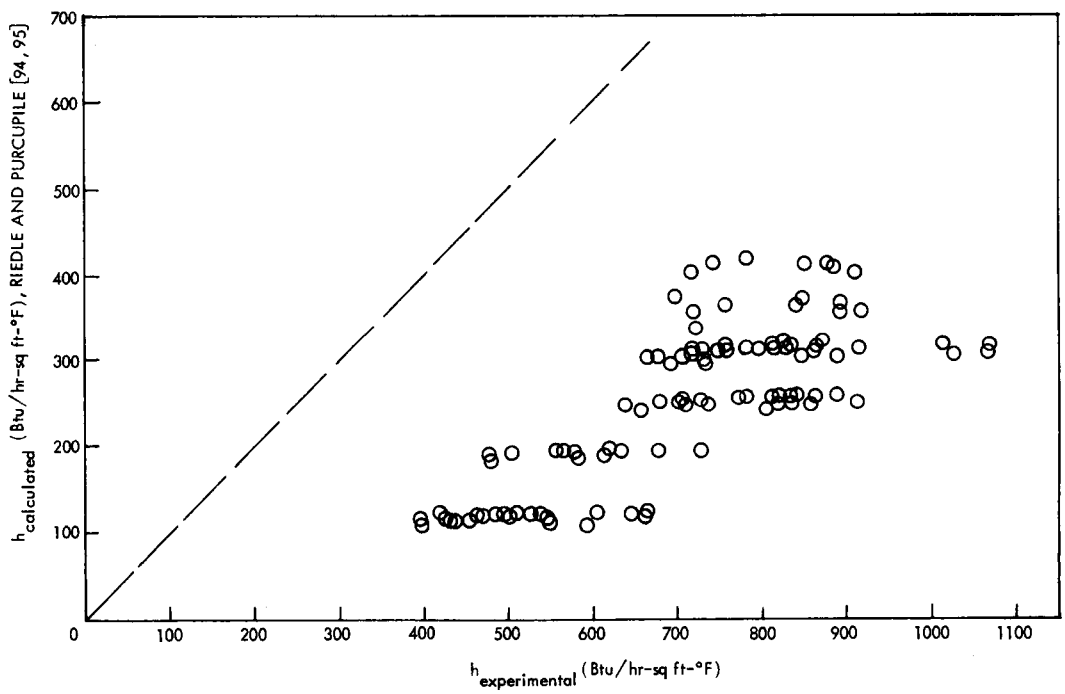


Figure IV-101. COMPARISON OF THE EXPERIMENTAL HEAT TRANSFER COEFFICIENTS WITH THE RIEDLE AND PURCUPILE [94, 95] CORRELATION, T≈150°F.

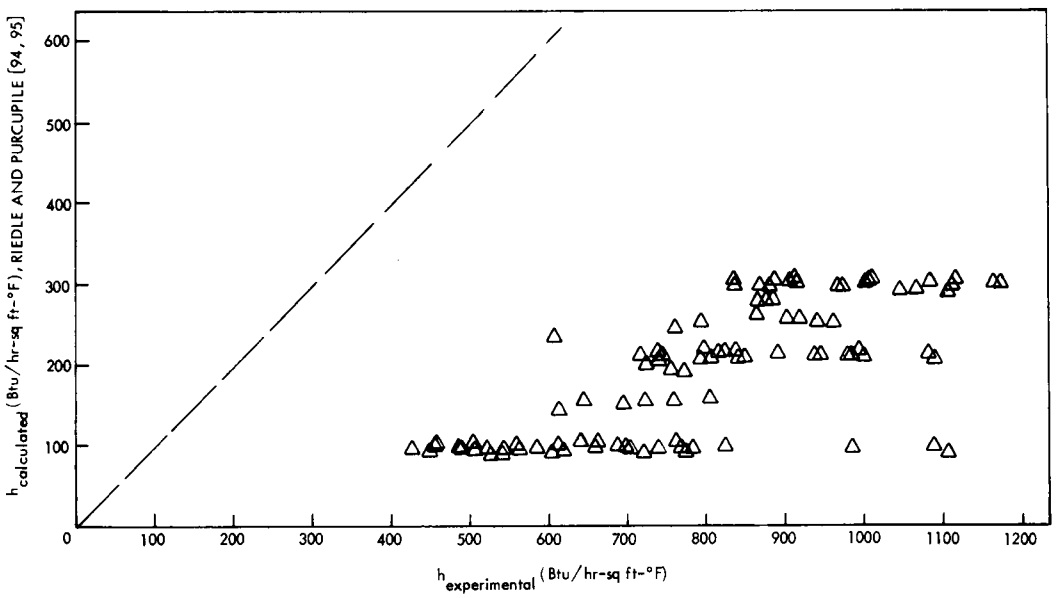


Figure IV-102. COMPARISON OF THE EXPERIMENTAL HEAT TRANSFER COEFFICIENTS WITH THE RIEDLE AND PURCUPILE [94, 95] CORRELATION, T≈200°F.

Chen [80] Correlation. The final correlation to be considered is the Chen [80] correlation which assumes that the convective and boiling components are additive. It was compared to data for water, methanol, cyclohexane, benzene, heptane, and pentane by Chen [80] and was found to give better overall agreement than the Dengler and Addoms [78], Guerrieri and Talty [77], Bennett et al [79], and Schrock and Grossman [82] correlations. When compared to all the present data on a zone-by-zone basis as shown in Figures IV-103 to IV-105, 82% of the data lay between +0 and -50%. While this spread is still large, it is worth noting that it is smaller than that obtained with any of the previously considered correlations. When the average conditions along the length of the tube are used, 97% (all but two) of the points were within the +0 and -50% tolerance limits. No change in the accuracy of the experimental results was observed when the average results along a test section

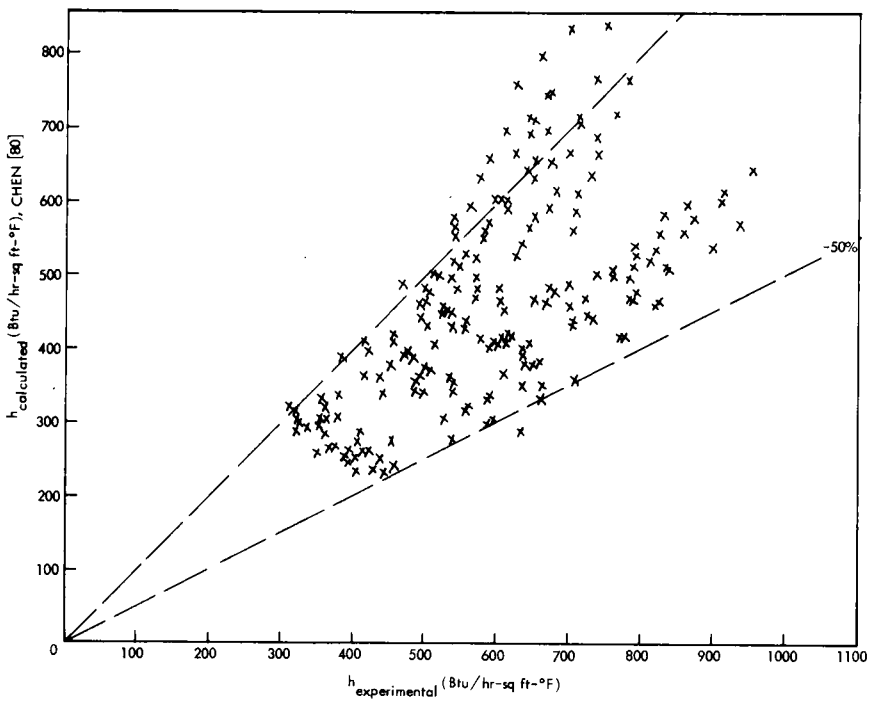


Figure IV-103. COMPARISON OF THE EXPERIMENTAL HEAT TRANSFER COEFFICIENTS WITH THE CHEN [80] CORRELATION, T≈100°F.

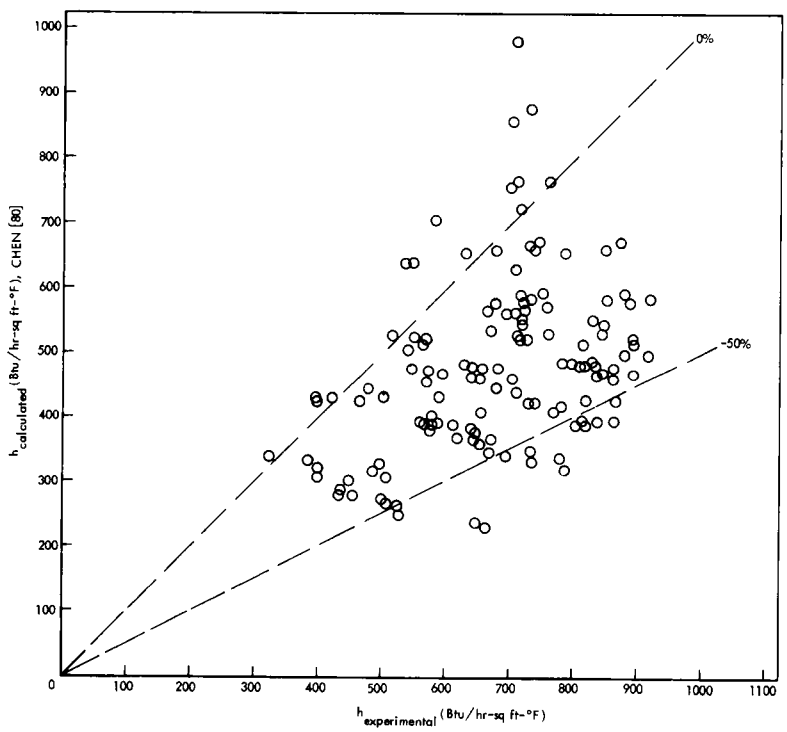


Figure IV-104. COMPARISON OF THE EXPERIMENTAL HEAT TRANSFER COEFFICIENTS WITH THE CHEN [80] CORRELATION, T≈150°F.

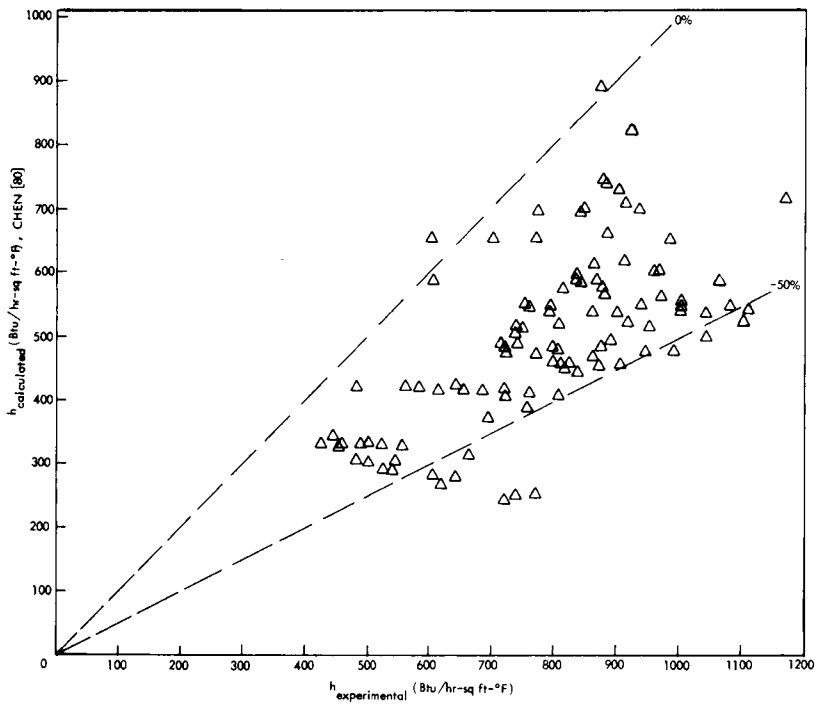


Figure IV-105. COMPARISON OF THE EXPERIMENTAL HEAT TRANSFER COEFFICIENTS WITH THE CHEN [80] CORRELATION, T≈ 200°F.

were used (Figure IV-106) or when a zone-by-zone analysis was made. In this respect therefore, Chen's [80] correlation is superior to those in the form of Equations (2-59) and (2-60).

Several other experimenters compared their boiling refrigerant data with the Chen [80] correlation. Gouse and Coumou's [91] results, shown in Figure II-24 on page 80, indicated that the Chen [80] correlation predicted boiling coefficients which were slightly, but consistently too low. The same trend was noted by Gouse and Dickson [93] in Figure II-26 on page 83. Probably one of the most extensive comparisons of refrigerant flow boiling coefficients with the Chen [80] correlation was shown in Figure II-33 on page 88. Purcupile, Riedle, and Schmidt's [94] data for R-11, R-12, and R-113 exhibited the same trend as that noted in the R-114 results of this study and illustrated in Figures IV-103 to IV-106.

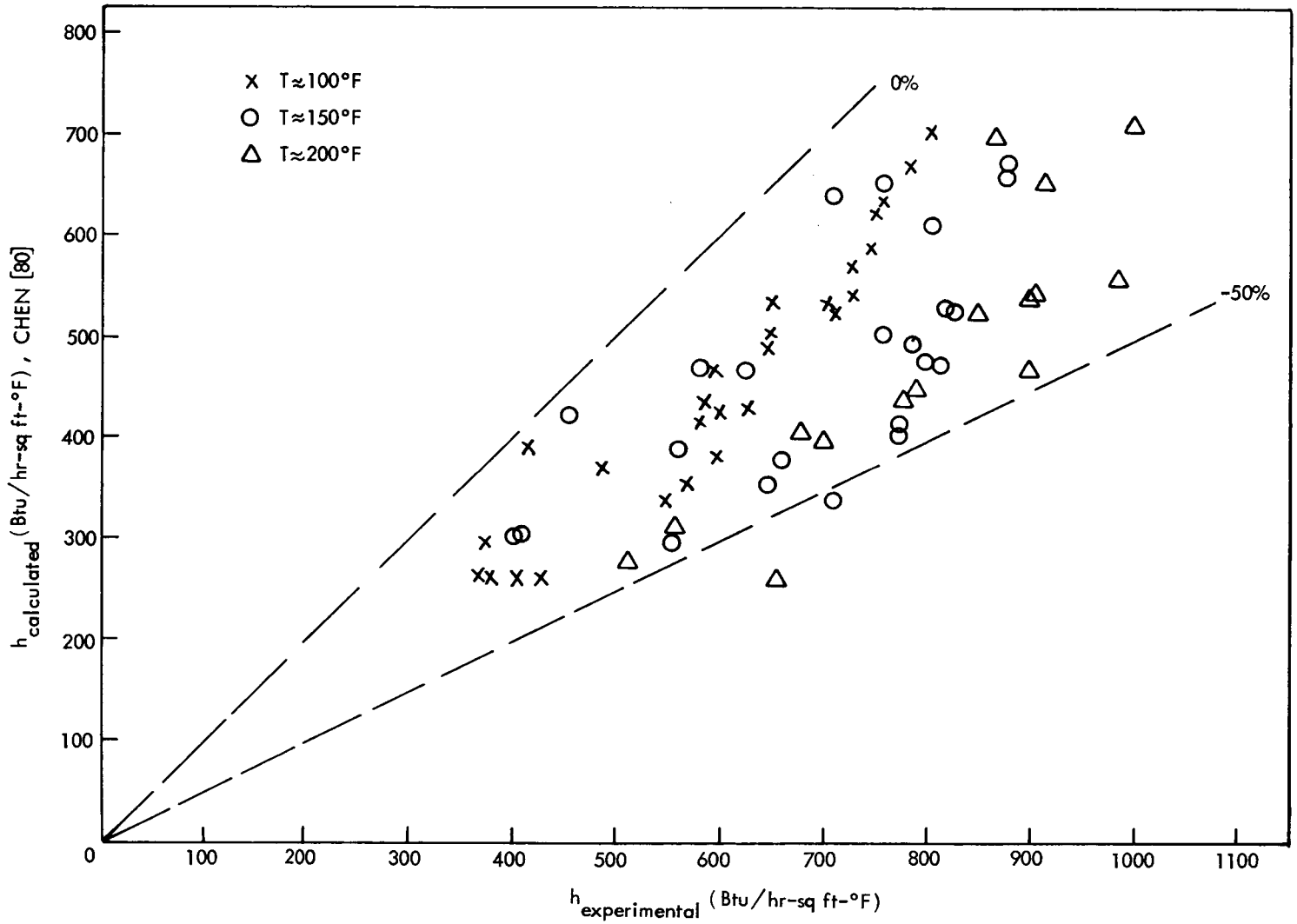


Figure IV-106. COMPARISON OF THE AVERAGE EXPERIMENTAL HEAT TRANSFER COEFFICIENTS ALONG THE LENGTH OF THE BOILING TEST SECTION WITH THE CHEN [80] CORRELATION.

In summary, it can be said that none of the correlations presented here has proved to be entirely satisfactory. While several of them were found to reliably predict the boiling coefficients of water and some other non-refrigerants, they generally underestimated the boiling coefficients of refrigerants. Cheshire and Stirling [36], O'Donnell, Robinson, and Webb [85], and Davis and David's [81] homogeneous model were exceptions to this trend. The Chen [80] correlation exhibited the least amount of deviation and scatter of all the correlations studied here. In addition, this deviation and scatter was not found to be biased by the boiling temperature. This correlation is inherently simple to use and is based on the plausible concept of superposition. The high-speed pictures obtained by Zuber et al [10] attest to the possibility of the existence of nucleation in annular flow and the dominant role played by the nucleation process. The use of empirical curves such as those for S, especially when they are not backed by analytical work or a large and broadly based body of experimental data, lead to questions as to the generality of this correlation.

In the next section, an attempt will be made to more carefully analyze the different components in the Chen [80] correlation and to see if they can be modified to successfully correlate the data on boiling refrigerants.

Derivation of An Improved Forced Convective Boiling Correlation

Since the Chen [80] correlation proved to be the most satisfactory over a wide range of working fluids and since it was based on the plausible heat transfer concept of superposition, a more careful study of this correlation is worthwhile. The four components of the equation are:

(1) The single-phase convective component.

(2) The pool boiling term.

(3) The multiplication factor, F.

(4) The suppression factor, S.

The Single-Phase Convective Component. The single-phase convective component, represented by the Dittus-Boelter equation will be assumed to be valid for refrigerants, as well as for other fluids. The extensive body of data on single-phase convective flow in the world literature, as well as the wall thermocouple calibrations in this study and those of Purcupile, Riedle, and Schmidt [94] confirm the validity of the Dittus-Boelter equation.

The Pool Boiling Term. In this correlation, Chen [80] used the Forster-Zuber [52] equation for the pool boiling component. While this equation has the obvious advantage of not requiring the input of a variable empirical coefficient, the validity of this correlation along with some of the others discussed in the literature survey has not been demonstrated for refrigerants. Obtaining a reliable pool boiling equation is therefore of primary importance.

Shown in Appendix A is data on the pool boiling of R-114, R-113, and R-11 obtained at the Oak Ridge Gaseous Diffusion Plant (ORGDP). The experimental heat transfer coefficients are compared with the Forster-Zuber [52] pool boiling equation in Table IV-1. As can be seen, the Forster-Zuber [52] correlation significantly underestimates the true pool boiling heat transfer coefficient. However, changing the constant in Equation (2-48) from 0.172 to 0.326 for R-114, to 0.213 for

Table IV-1

COMPARISON OF ORGDP POOL BOILING DATA WITH VARIOUS CORRELATIONS

$h_{experimental}$ (Btu/hr-sq ft)	Forster-Zuber [52] Correlation		Kutateladze [57] Correlation		Borishanskiy-Minchenko [58] Correlation		Hughmark [56] Correlation	
	$h_{calculated}$ (Btu/hr-sq ft-°F)	$\left(\frac{h_{experimental}}{h_{calculated}}\right)$	$h_{calculated}$ (Btu/hr-sq ft-°F)	$\left(\frac{h_{experimental}}{h_{calculated}}\right)$	$h_{calculated}$ (Btu/hr-sq ft-°F)	$\left(\frac{h_{experimental}}{h_{calculated}}\right)$	$h_{calculated}$ (Btu/hr-sq ft-°F)	$\left(\frac{h_{experimental}}{h_{calculated}}\right)$
R-114:								
820	455.1	1.802	320.1	2.562	693.3	1.183	640.0	1.281
1085	559.3	1.940	446.7	2.429	967.7	1.121	761.7	1.424
1320	683.5	1.931	584.6	2.258	1266.3	1.042	901.3	1.465
1520	818.3	1.858	723.1	2.102	1566.3	0.970	1046.9	1.452
1845	927.5	1.989	897.8	2.055	1944.8	0.949	1161.0	1.589
2020	1080.7	1.869	1052.2	1.920	2279.2	0.886	1315.9	1.535
		average = 1.898						
R-113:								
495	360.3	1.374	208.7	2.372	519.2	0.953	353.0	1.402
555	538.4	1.031	289.6	1.916	720.5	0.770	491.0	1.130
710	658.4	1.078	387.4	1.833	963.8	0.737	577.4	1.230
896	724.0	1.238	482.3	1.858	1199.8	0.747	622.2	1.440
1065	807.8	1.319	578.3	1.842	1438.6	0.740	680.8	1.564
1290	920.0	1.402	711.0	1.814	1769.0	0.729	758.5	1.701
		average = 1.240						
R-11:								
730	365.9	1.995	270.4	2.700	537.5	1.358	439.5	1.661
748	628.1	1.191	389.8	1.919	774.9	0.965	679.0	1.102
925	784.6	1.179	518.3	1.785	1030.4	0.898	808.2	1.145
1120	897.1	1.249	643.3	1.741	1278.7	0.876	896.1	1.250
1340	995.6	1.346	777.9	1.723	1546.4	0.867	970.2	1.381
1550	1130.4	1.371	926.1	1.674	1840.9	0.842	1067.6	1.452
		average = 1.389						

R-113 and to 0.239 for R-11 yields a correlation which gives much better agreement with most of the pool boiling data.

The choice of a different constant for the coefficient in Equation (2-48) does not result in a modification of the Forster and Zuber [52] analysis since the 0.172 value was experimentally determined. This coefficient is partially dependent on the time constant chosen. As shown in Equation (2-47), Forster and Zuber [52] used:

$$\left(\frac{2\sigma}{\Delta P}\right)^{1/2} \left(\frac{\rho_f}{\Delta P}\right)^{1/4}.$$

Substituting in the expression

$$\Delta P = \frac{2\sigma}{R_o} \tag{4-14}$$

where R_o is the initial radius of a bubble, one obtains

$$\left(R_o\right)^{1/2} \left(\frac{\rho_f R_o}{2\sigma}\right)^{1/4}$$

for the time constant. Assuming that the various surfaces used in the data analyzed by Forster and Zuber [52] had approximately the same sizes and types of cavities, and since the fluids analyzed had similar values for the physical properties ρ_f and σ, the choice of approximately the same number for the time constant was satisfactory. When one considers refrigerants, however, this situation is no longer true. The values for the surface tension of refrigerants are considerably lower than those of ordinary fluids such as water. Examining the ratio $(\rho_f/2\sigma)^{1/4}$ for water and R-114 at the same reduced pressure:

$$\frac{\left(\frac{\rho_f}{2\sigma}\right)^{1/4}_{\text{R-114 at 112°F}}}{\left(\frac{\rho_f}{2\sigma}\right)^{1/4}_{\text{water at 435°F}}} = 1.504 \tag{4-15}$$

it can be observed that a larger numerical value is obtained with refrigerants than with water. Variation of the exponent on the $(\rho_f/2\sigma)$ term can increase the ratio from 1.504 to the 1.898 value observed for $(h_{experimental}/h_{calculated})$ with R-114 in Table IV-1. The importance of ρ_f, σ, and R_o in the evaluation of the time constant implies that the fluid, the type of surface and the surface finish are important in evaluating the pool boiling coefficient.

One of the most widely used pool boiling correlations is the one developed by Rohsenow [61] and given in Equation (2-45). Using the standard value of 1.7 for s, a plot of $\left(\frac{c_{pf}\,\Delta T}{h_{fg}\,Pr^{1.7}}\right)$ vs $\left(\frac{q/A}{\mu_f h_{fg}}\sqrt{\frac{\sigma}{g\Delta\rho}}\right)$ was made and the results obtained for the R-114, R-113, and R-11 cases are given in Table IV-2. These results are also illustrated in Figure IV-107.

Table IV-2

VALUES OBTAINED FOR THE COEFFICIENTS OF THE ROHSENOW [61] CORRELATION USING THE ORGDP POOL BOILING DATA

Fluid	C_{sf}	r'
R-114	0.00481	0.427
R-113	0.00479	0.347
R-11	0.00760	0.408

These boiling results for R-114, R-113, and R-11 were also compared with some of the other pool boiling correlations in the literature including those by Kutateladze [57], Borischanskiy-Minchenko [58], and Hughmark [56]. A comparison is shown in Table IV-1. Of the equations examined,

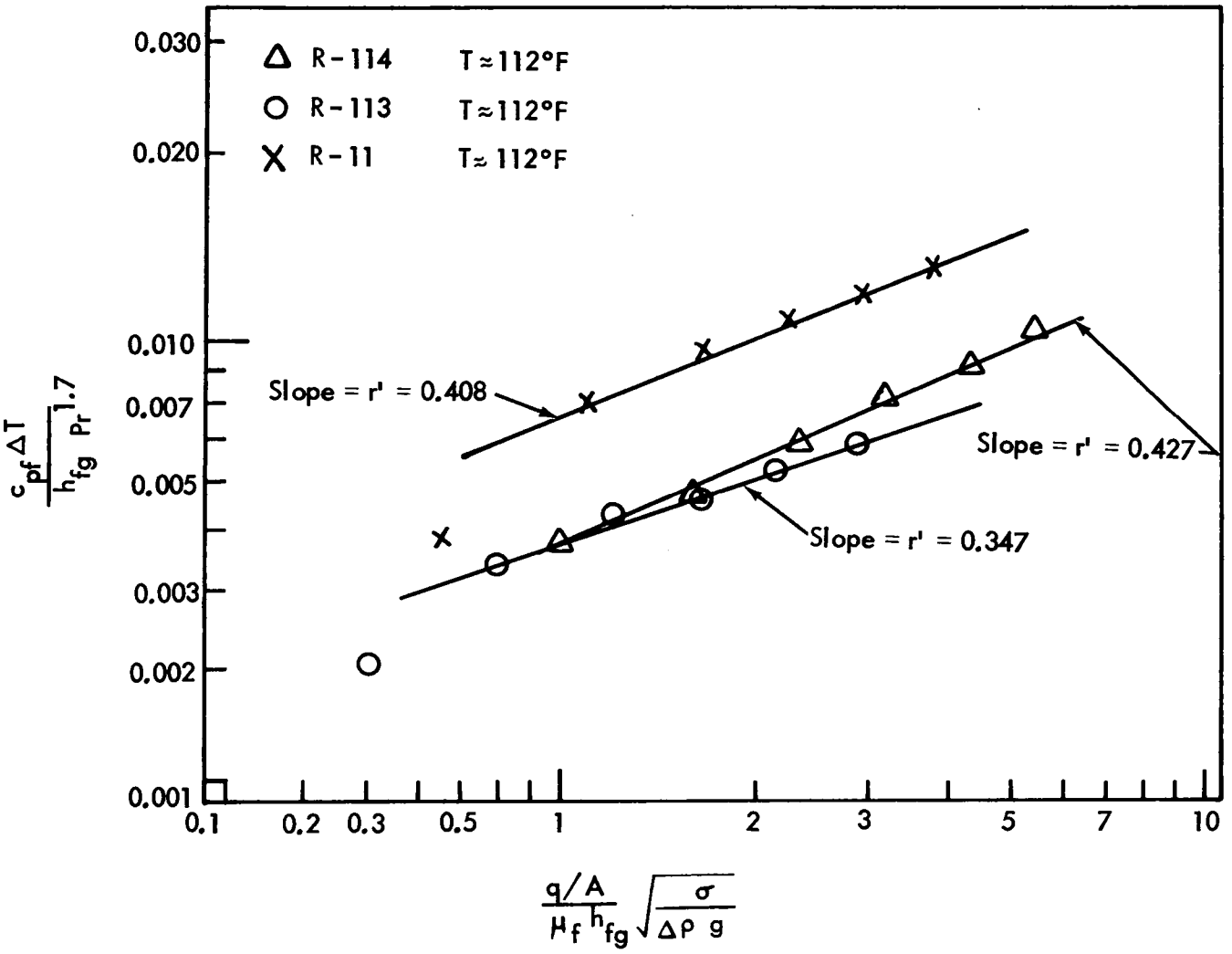


Figure IV-107. CORRELATION OF THE ORGDP POOL BOILING DATA WITH THE ROHSENOW [61] EQUATION.

only the Borishanskiy-Minchenko [58] correlation was satisfactory. For the R-114 case, however, none of these equations can be said to represent an improvement over the Forster-Zuber [52] correlation with a variable coefficient. The Gilmour [54] correlation could not be used since the diameter was not known.

The pool boiling data obtained by Furse [74] were also compared with the correlations mentioned above. A tabulation of this comparison is shown in Table IV-3 for the R-11 results. As can be seen, only the Borishanskiy-Minchenko [58] correlation performed satisfactorily. The same trend was also noted with the R-12 data. A comparison of the same results with the Rohsenow [61] correlation is shown in Figures IV-108 and IV-109 for R-11 and R-12, respectively. The R-11 results were correlated quite well with a C_{sf} of 0.0055 and an r' of 0.216 in Equation (2-45). The R-12 results did not correlate as well. With the exception of the 50°F boiling runs, the other points did not lie on a straight line and a different C_{sf} was obtained for each boiling temperature. For the 50°F boiling case, a C_{sf} of 0.00715 and an r' of 0.192 for Equation (2-45) were satisfactory.

Lippert and Dougall [76] in their experimental studies of the temperature profile in the thermal sublayer also correlated their pool boiling results. Using the Rohsenow [61] equation, they obtained a C_{sf} of 0.0048 and an r' of approximately 0.20 for R-113 boiling from a horizontal copper surface. Chapman [73] who boiled R-113 from a vertically and horizontally oriented copper surface lapped with 400-grit corundum obtained a C_{sf} of 0.00272 and an r' of 0.092.

A considerable amount of pool boiling information with refrigerants was obtained by Hesse [75]. Data were generated over the entire

Table IV-3

COMPARISON OF FURSE'S [74] R-11 POOL BOILING DATA WITH VARIOUS CORRELATIONS

	Forster-Zuber [52] Correlation		Kutateladze [57] Correlation		Borishanskiy-Minchenko [58] Correlation		Gilmour [54] Correlation		Hughmark [56] Correlation	
$h_{experimental}$ (Btu/hr-sq ft)	$h_{calculated}$ (Btu/hr-sq ft-°F)	$\left(\frac{h_{experimental}}{h_{calculated}}\right)$	$h_{calculated}$ (Btu/hr-sq ft-°F)	$\left(\frac{h_{experimental}}{h_{calculated}}\right)$	$h_{calculated}$ (Btu/hr-sq ft-°F)	$\left(\frac{h_{experimental}}{h_{calculated}}\right)$	$h_{calculated}$ (Btu/hr-sq ft-°F)	$\left(\frac{h_{experimental}}{h_{calculated}}\right)$	$h_{calculated}$ (Btu/hr-sq ft-°F)	$\left(\frac{h_{experimental}}{h_{calculated}}\right)$
1660	511.3	3.247	631.4	2.629	1345.0	1.234	1066.4	1.557	467.6	3.550
980	429.7	2.281	394.9	2.482	840.7	1.166	667.4	1.468	406.7	2.410
580	376.4	1.541	252.7	2.295	538.5	1.077	426.5	1.360	365.3	1.588
360	334.2	1.077	167.0	2.156	356.0	1.011	281.7	1.278	332.0	1.084
170	265.2	0.641	87.6	1.941	186.6	0.911	148.0	1.149	276.4	0.615
100	200.4	0.499	49.7	2.012	106.0	0.943	83.96	1.191	219.8	0.455
1410	491.9	2.867	563.2	2.504	1255.3	1.123	877.8	1.606	399.7	3.528
880	389.0	2.262	354.6	2.482	790.5	1.113	552.2	1.594	331.3	2.656
460	329.0	1.398	204.4	2.250	455.9	1.009	318.3	1.445	289.4	1.589
250	281.2	0.889	122.4	2.042	273.2	0.915	190.2	1.314	254.2	0.984
140	242.0	0.579	75.79	1.847	169.0	0.828	118.0	1.186	225.6	0.621
80	198.9	0.402	43.93	1.821	97.9	0.817	68.51	1.168	193.0	0.415

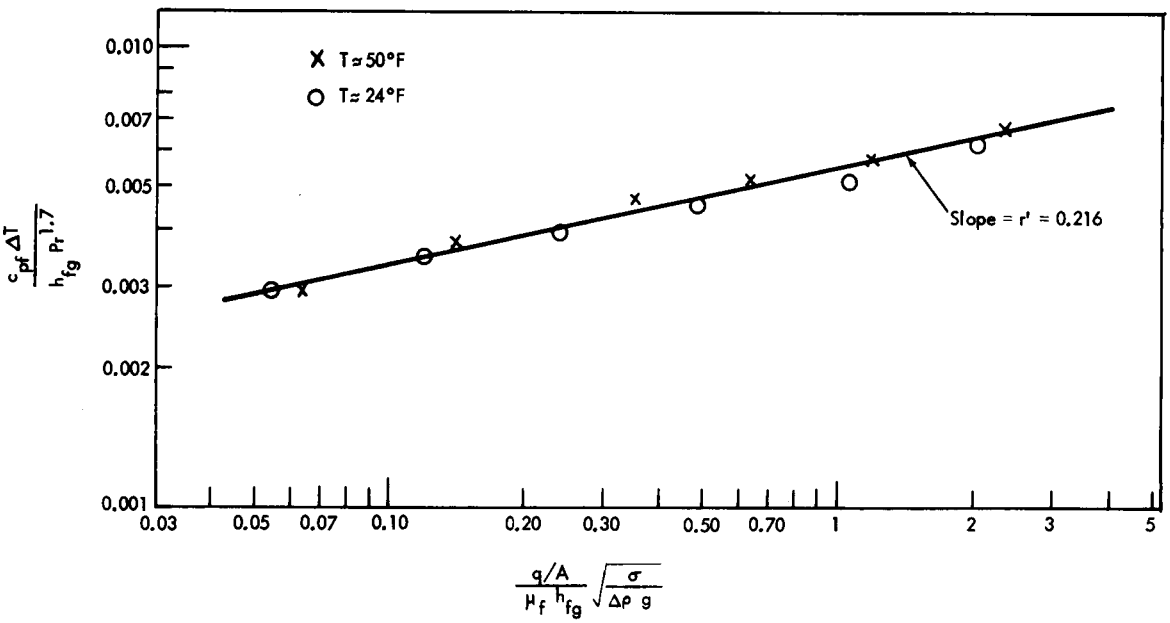


Figure IV-108. CORRELATION OF FURSE'S [74] R-11 DATA WITH THE ROHSENOW [61] EQUATION.

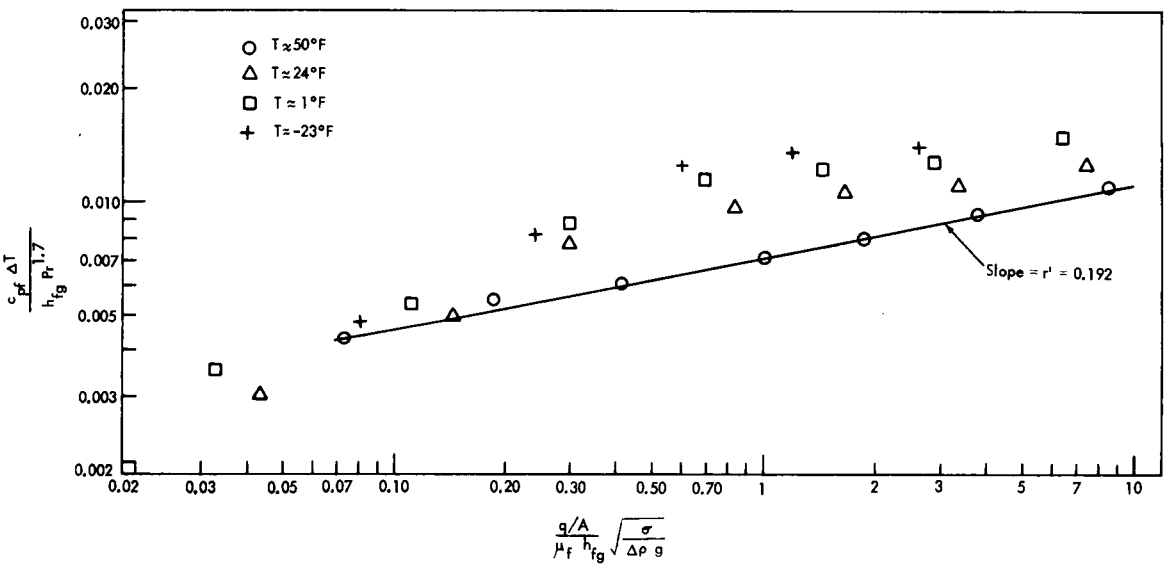


Figure IV-109. CORRELATION OF FURSE'S [74] R-12 DATA WITH THE ROHSENOW [61] EQUATION.

range from single-phase heat transfer to film boiling, as shown in Figure II-6 on page 25. The boiling surfaces consisted of two nickel tubes, one smooth and one finned. The data obtained before critical heat flux was attained were analyzed and a Rohsenow [61] type correlated attempted. The results for R-12, R-113, and R-114 are shown in Figures IV-110 to IV-112, respectively. None of the three fluids correlated satisfactorily. A large part of the non-linearity of the relationship in Figures IV-110 to IV-112 could be attributed to the fact that at the higher heat fluxes, the bubbles began to interfere with each other and thereby affected the heat transfer results. Only for the R-113 case could the correlation be meaningfully applied. A C_{sf} of 0.00303 and an r' of 0.143 were obtained.

In summary, it appears that the amount of information in the literature on the pool boiling of refrigerants is quite meager. The Forster-Zuber [52], Borishanskiy-Minchenko [58], and Rohensow [61] equations were the most satisfactory, at least when applied to the ORGDP data. For the Forster-Zuber [52] and Borishanskiy-Minchenko [58] equations, the coefficients were found to vary from the values originally recommended.

The Rohsenow [61] pool boiling equation was found to correlate the ORGDP data in addition to some of the results of other experimenters quite well, because it contained more parameters which could be varied. For example, a sizeable amount of variation was obtained for the r' value in Equation (2-45). The ORGDP data gave the highest value of 0.427 for R-114 while Chapman [73] noted values as low as 0.092. This parameter, r', is sensitive to the surface finish as discussed in the

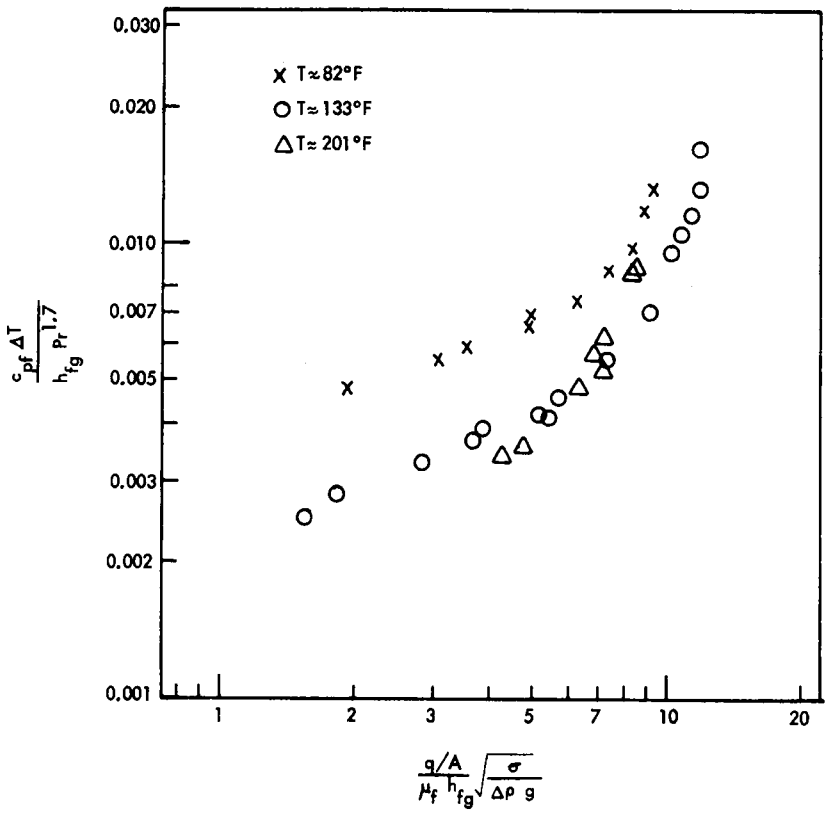


Figure IV-110. CORRELATION OF HESSE'S [75] R-12 DATA WITH THE ROHSENOW [61] EQUATION.

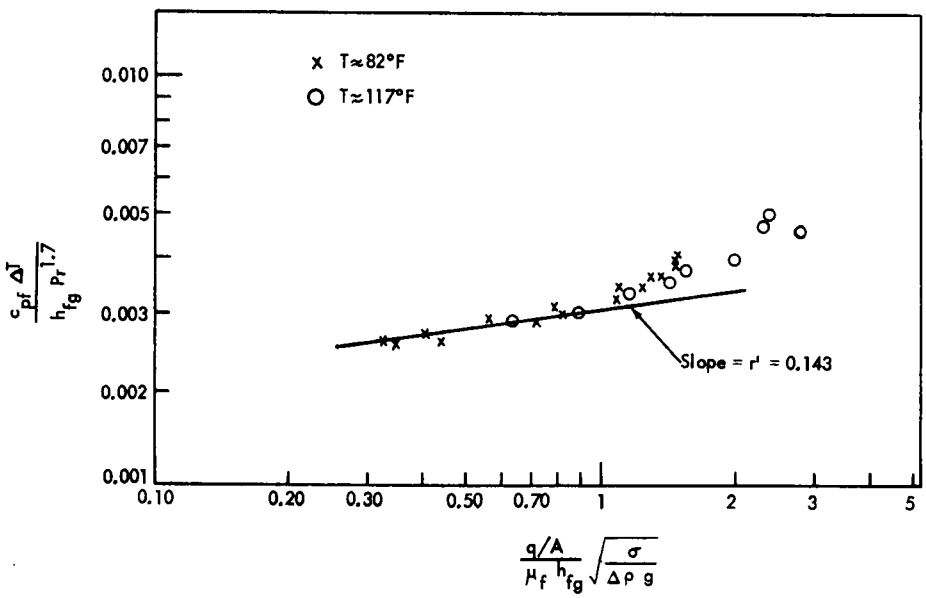


Figure IV-111. CORRELATION OF HESSE'S [75] R-113 DATA WITH THE ROHSENOW [61] EQUATION.

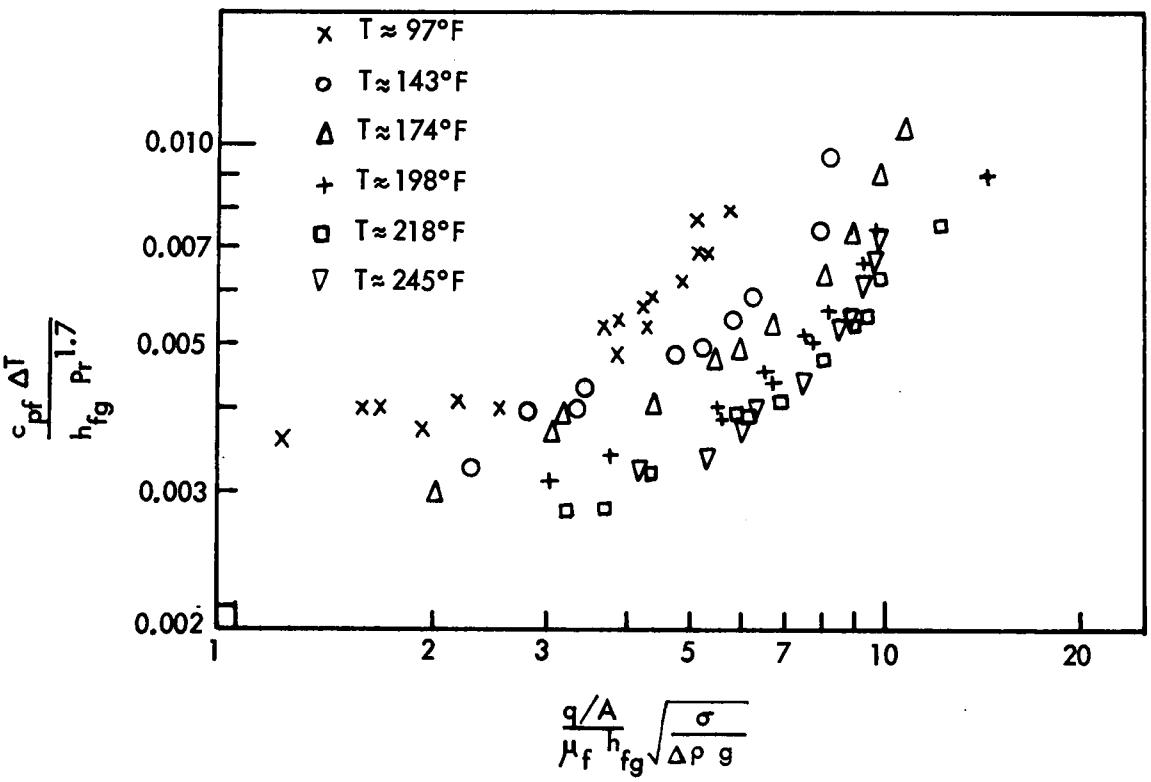


Figure IV-112. CORRELATION OF HESSE'S [75] R-114 DATA WITH THE ROHSENOW [61] EQUATION.

literature survey. Values of C_{sf} for a variety of surface-fluid combinations were also obtained. For R-11 boiling from a copper surface, 0.0076 and 0.00539 based on the ORGDP data and the results of Furse [74] were calculated for C_{sf}. For R-113, both the ORGDP data and Lippert and Dougall's [76] results were correlated with a C_{sf} of 0.0048. Hesse's [75] data yielded a C_{sf} of 0.00303 while Chapman calculated 0.00272. Furse's [74] R-12 results were correlated by a C_{sf} of anywhere from 0.00715 to 0.0135. For R-114 boiling from a copper surface, a C_{sf} value of 0.0048 based on the ORGDP data is recommended.

In the present study, the Forster-Zuber [52] and Rohsenow [61] equations with variable coefficients will be used as they are two of the most widely used pool boiling correlations. It should be remembered that the Borishanskiy-Menchenko [58] equation satisfactorily correlated refrigerant pool boiling data. Since, however, this correlation has not been extensively used in the past, additional confirmation of its applicability needs to be obtained before it can be used with confidence.

In the application of the Rohsenow [61] pool boiling correlation to flow boiling results, the value of 0.33, as originally recommended by Rohsenow [61], will be used for the exponent r'. Variations in the value of this parameter will affect the results to a smaller extent in flow boiling than in pool boiling.

The Multiplication Factor F. In his original publication, Chen [80] explained an iterative procedure he used to determine F as a function of $1/X_{tt}$. Kunz and Yerazunis [117], on the other hand, undertook a thorough analysis of the turbulent film that would exist in annular two-phase flow to determine F. Using the equation:

$$St^* = \frac{0.147}{Re_f^{0.1}\ Pr_f^{0.6}} \tag{4-16}$$

for $Pr_f \geq 1.0$ and the relation:

$$f = \frac{0.184}{Re_f^{0.2}} \tag{4-17}$$

where St* is the Stanton Number based on the frictional velocity and f is the Darcy-Weisbach friction factor, one can obtain the relationship:

$$h_{mac} = 0.0224 \left(\frac{(1 - x)\ GD}{\mu_f}\right)^{0.8} (Pr_f)^{0.4} \frac{k_f}{D} \left(\frac{1}{1 - \alpha}\right)^{0.90} \tag{4-18}$$

comparing this to the single-phase component of Equation (2-62) one obtains:

$$F = \left(\frac{1}{1 - \alpha}\right)^{0.90} \tag{4-19}$$

Chen [80] in his momentum analysis came up with the result:

$$F = (\Phi'_{ftt})^{0.89} \tag{4-20}$$

where Φ'_{ftt} was the square root of the Martinelli multiplier based on the Lockhart-Martinelli [19] correlation. Using the approximation

$$\Phi'_{ftt} \approx \left(\frac{1}{1 - \alpha}\right) \tag{4-21}$$

one obtains

$$F \approx \left(\frac{1}{1 - \alpha}\right)^{0.89} \tag{4-22}$$

which is almost identical to the result obtained above in Equation (4-19).

In order for this analysis to be applicable over a wide range of operating parameters, the square root of the Martinelli parameter Φ_{ftt}

based on the Martinelli-Nelson [4] correlation will be used instead of Φ'_{ftt}. In Figure IV-113, a comparison of the F function calculated by momentum transfer analogy with Chen's [80] empirical curve is shown. In Figures IV-114 to IV-116 a comparison of the original Chen [80] curve for F and Equation (4-19) is presented. As can be noted, a deviation exists between Chen's [80] curve and the present analysis in all ranges of X_{tt} except for $X_{tt} \simeq 1.0$. At low values of X_{tt}, the present analysis yields a curve that is higher, while at high values of X_{tt}, the Chen curve is higher. The void fraction formulation used was the modified version of the Zuber et al [10] general equation illustrated in Figure IV-46 on page 182. It is interesting to note that one of the assumptions Chen [80] made in his original work involved the statement that F was solely a function of $1/X_{tt}$. As it turned out, the terms ρ_f, ρ_g, and x in the Zuber et al [10] general void fraction equation were also present in the Martinelli parameter X_{tt}. The void fraction correlation did not however contain a viscosity effect but did include a dependence on surface tension and mass flux. A comparison of Chen's [80] empirical curve with the relationship

$$F = \left(\Phi_{ftt}\right)^{0.89} \tag{4-23}$$

is also shown in Figures IV-114 to IV-116.

The Suppression Factor, S. Chen [80], in his correlation, applied a suppression factor to the pool boiling component of his expression. This function, which lies between one (no suppression) and zero (total suppression) is supposed to reduce the pool boiling contribution to the total heat transfer coefficient in order to account for the

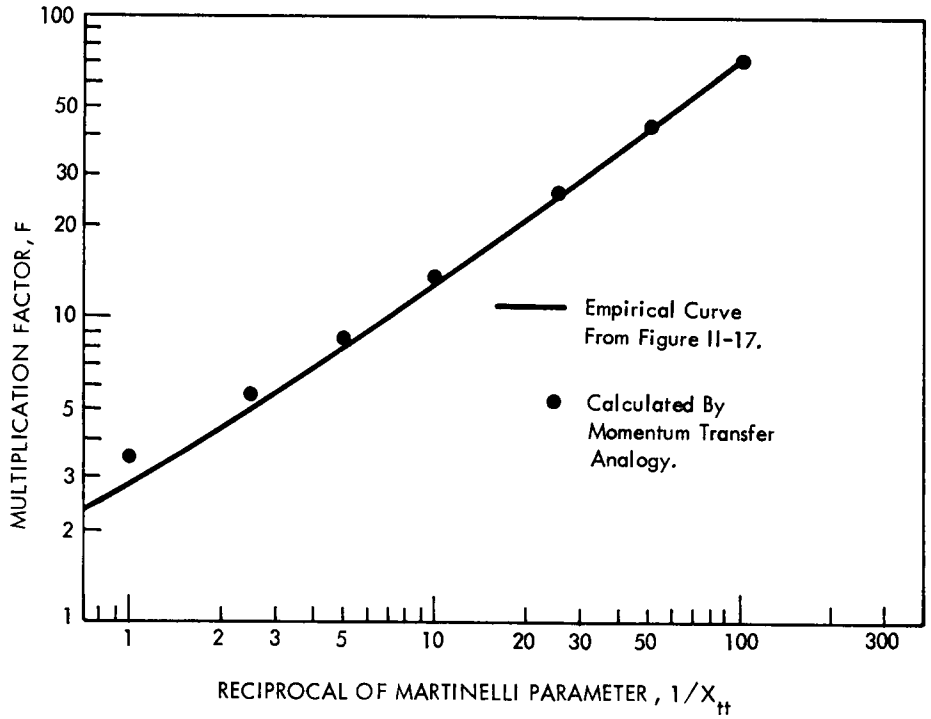


Figure IV-113. COMPARISON OF F FUNCTION CALCULATED BY MOMENTUM TRANSFER ANALOGY WITH EMPIRICAL CURVE, CHEN [80].

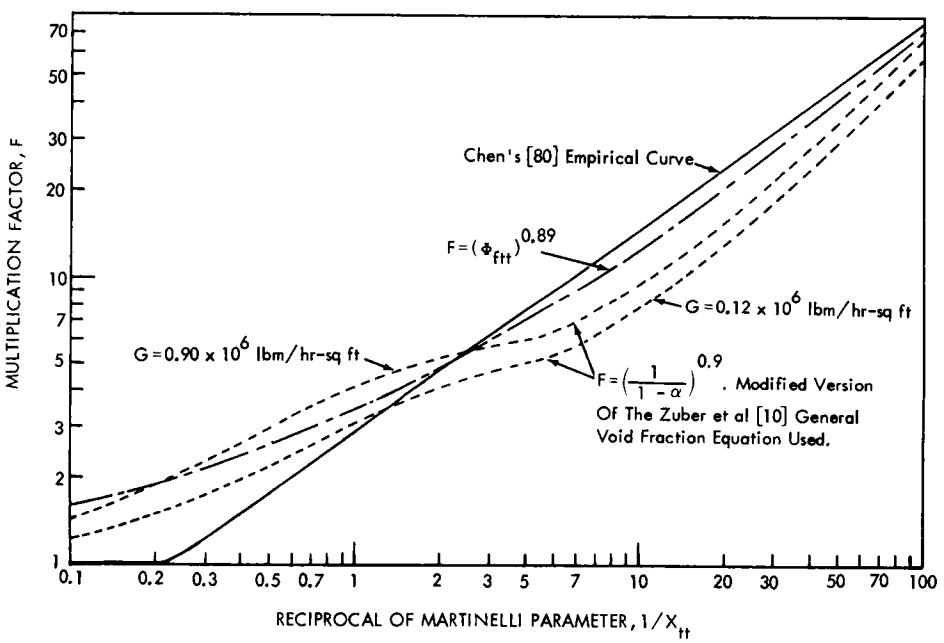


Figure IV-114. COMPARISON OF CHEN'S [80] EMPIRICAL CURVE WITH VARIOUS FORMULATIONS FOR THE MULTIPLICATION FACTOR F. T=100°F.

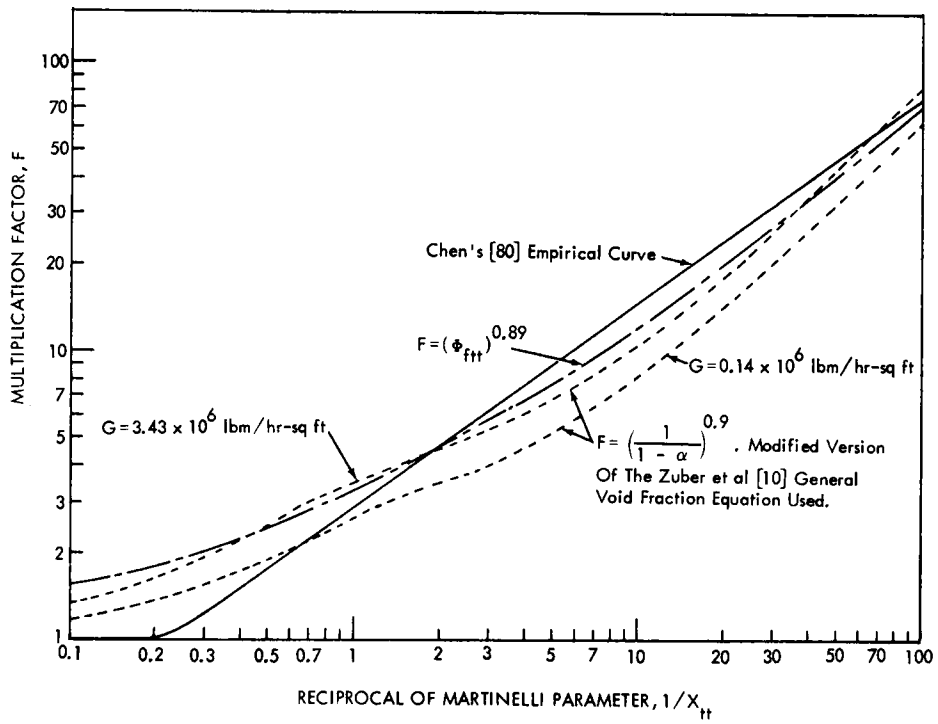


Figure IV-115. COMPARISON OF CHEN'S [80] EMPIRICAL CURVE WITH VARIOUS FORMULATIONS FOR THE MULTIPLICATION FACTOR F. T=150°F.

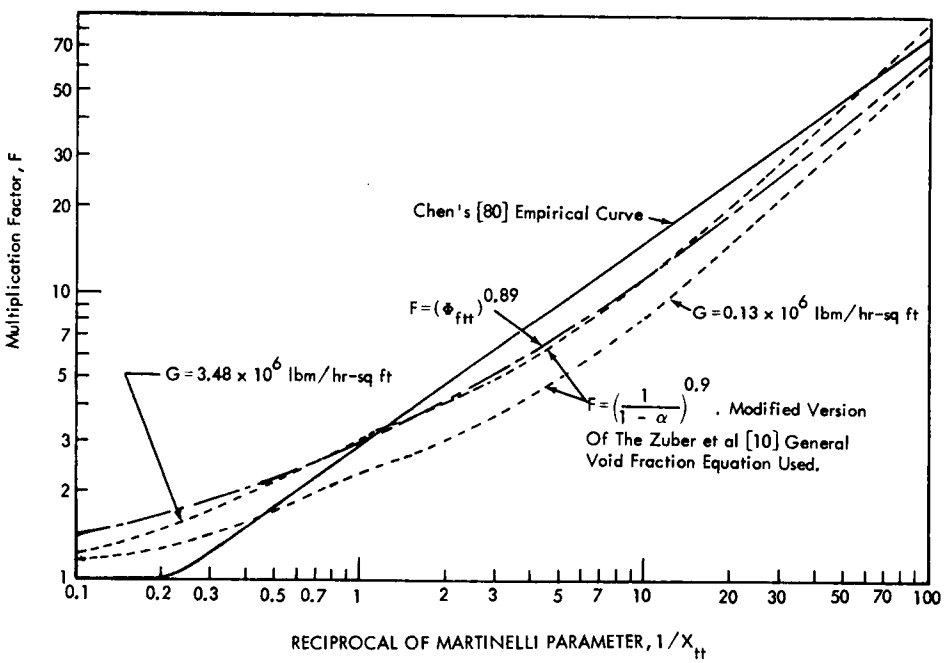


Figure IV-116. COMPARISON OF CHEN'S [80] EMPIRICAL CURVE WITH VARIOUS FORMULATIONS FOR THE MULTIPLICATION FACTOR F. T=200°F.

effect of the flow over the boiling surface. Chen [80] attributed this reduction in pool boiling "effectiveness" to the steeper temperature gradients close to the wall that exist in forced convection. In pool boiling, free convection effects brought about by buoyancy forces due to density variations in the fluid result in small temperature gradients and, therefore, thick boundary layers. The steep temperature gradients in forced convection decrease the superheat between the bubbles and the saturated liquid, $\Delta T_{2,conv}$ in Figure IV-117, and slow down the growth of the bubble. The suppression factor curve, shown in Figure II-18 on page 64 was experimentally determined, from the data Chen [80] analyzed, using an iterative procedure. In order to attempt to obtain a reliable mathematical expression for the suppression factor, an analytical solution will now be undertaken. Two models will be discussed. One will assume a steady state boundary layer while in the other, a transient boundary layer analysis will be attempted.

Steady State Solution: In order to gain a greater insight into the concept of suppression, it is worthwhile to consider a model on bubble initiation which has been discussed by numerous authors including Hsu [118] and Han and Griffith [119]. When a vapor bubble is in equilibrium with a liquid, the vapor-liquid interface behaves as if it is in tension and the vapor in the bubble is at a greater pressure than the liquid surrounding it. A simple force balance on a hemisphere yields the result:

$$\Delta P = \frac{2\sigma}{r} \qquad (4\text{-}24)$$

where r is the bubble radius and ΔP is the pressure difference corresponding to the temperature difference between the bubble and the

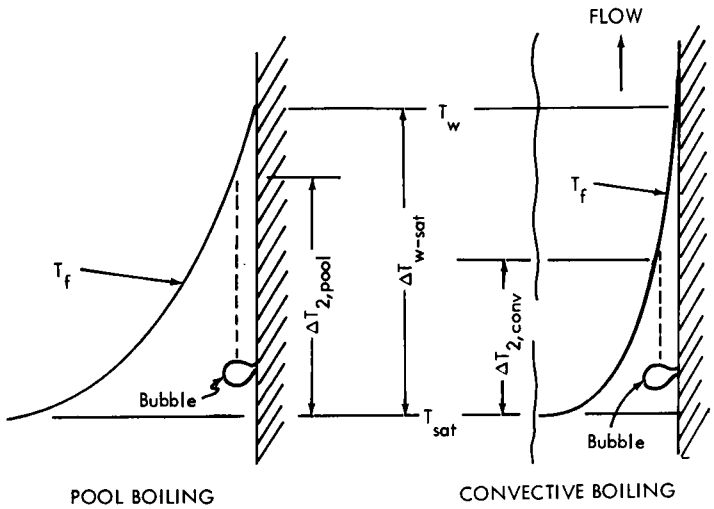


Figure IV-117. TEMPERATURE PROFILES FOR POOL BOILING AND FOR CONVECTIVE BOILING WITH THE SAME TOTAL SUPERHEAT, CHEN [80].

surrounding liquid. Shown in Figure IV-118a is an idealized conical cavity. When the wall is heated to a temperature in excess of the saturation temperature of the fluid, the minute amount of gas or vapor that is usually found to exist in cavities serves as a nucleation site where a bubble can grow. This initial volume of gas or vapor is needed to achieve a reasonably low value of $1/r$. If no gas or vapor existed, a theoretical value of $1/r = \infty$ corresponding to an infinite superheat would be needed to initiate nucleation. As heat is transferred from the wall to the nucleation site, the bubble increases in size. When a given volume is attained, corresponding to point b in Figure IV-118b a local maxima in $1/r$ is reached. For volumes greater than those represented by point b, the $1/r$ term is monotonically decreasing--leading to a corresponding monotonic decrease in the degree of superheat required. Thus, it can be said that as soon as point b is reached, the maximum superheat necessary would have been attained and the bubble may con-

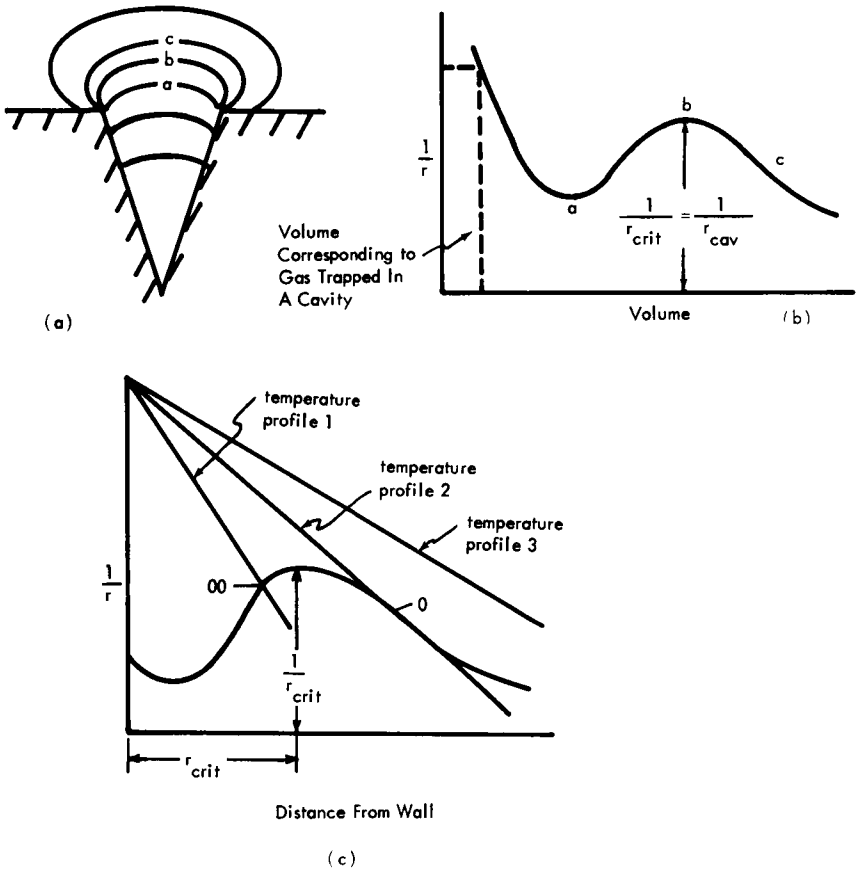


Figure IV-118. RADIUS OF CURVATURE VERSUS VAPOR VOLUME AND DISTANCE FROM THE WALL IN A CAVITY.

tinue to grow. It should be noted that while achieving a hemispherical bubble is a necessary requirement for bubble growth, it is not a sufficient one. A plot of 1/r versus distance from the wall is shown in Figure IV-118c. Since 1/r is proportional to ΔT, three temperature gradients of the fluid close to the wall are shown. Temperature Profile 1 illustrates the case where at distance of r_{crit} from the wall where the reciprocal of the radius achieves a local maxima, insufficient superheat exists for the bubble to grow and it is therefore suppressed. In temperature Profile 2, sufficient superheat exists for the bubble to grow beyond its hemispherical shape. However, at a certain point, marked by the intersection of the two curves (point 0), the bubble can no

longer grow. If this point lies beyond the breakoff diameter of the bubble, then nucleation will not be affected. Otherwise, bubble growth will be suppressed to some degree. The breakoff diameter is a complex function of fluid, surface, temperature, and flow effects. Profile 3 does not interfere with the bubble growth. For simplification, therefore, it will be assumed that temperature gradients of the type represented by Profile 3 in Figure IV-118c exist only. The validity of this assumption cannot be readily assessed since the 1/r versus distance from the wall curve is difficult to establish because of the many body and surface forces which act to change the shape of the bubble.

The intersection points 0 and 00 in Figure IV-118c represent the points where the tip of a growing bubble is no longer in contact with sufficiently superheated fluid. Quite possibly, the amount of heat transferred to the bubble from the wall could exceed the amount lost to the fluid and the bubble would continue to grow. In this study, a conservative assumption will be made and it will be assumed that the bubble grows little after coming in contact with fluid at a temperature below that corresponding to the degree of superheat needed to maintain the bubble. Thus, in the forthcoming analysis, the variable y representing the normal distance from the wall can replace the variable r corresponding to the bubble or cavity radius. Hsu [118] in contrast used the criterion $y = 2r_{crit}$ while Han and Griffith [119] used $y = 1.5r_{crit}$.

One of the assumptions made in the above discussion was that a minute amount of vapor gas existed in a cavity to act as a nucleation center. In certain cases, if great pains are taken to completely de-gas or to obtain a high degree of smoothness on a heated surface, high

superheats will be required to initiate boiling. In addition, certain fluid-surface combinations exhibit great wettability characteristics and the liquid completely fills or "floods" all but the very tiniest of cavities thus requiring a large amount of superheat to initiate boiling. Refrigerants on most surfaces exhibit very good wettability characteristics and thus require sizeable superheats to initiate boiling. This phenomena was clearly illustrated in an experiment conducted with R-113 by Murphy and Bergles [120] and illustrated in Figure IV-119. They showed that once boiling starts, the nucleation sites remain active and the curve therefore exhibits a hysteresis effect. The reason the nucleation sites remain active is thought to be due to a portion of the preceding bubble remaining trapped in the cavity and forming the nucleus of the next bubble. In this analysis, it will be assumed that none of the nucleation sites are "flooded."

The curve represented by the Gaussian expression for surface tension, $\Delta P = 2\sigma/r$ can be modified by using the Clausius-Clapeyron expression to yield (see Figure IV-120):

$$\Delta T_2 = \frac{2\sigma\, T_{sat}\, v_{fg}}{r\, h_{fg}} \qquad (4\text{-}25)$$

where ΔT_2 is the temperature difference between the vapor and the saturated liquid.

It will be assumed here that the bubble growth occurs in the thermal sublayer and the heat transfer is by conduction. Therefore:

$$\frac{q}{A} = -k_f \left(\frac{dT}{dy}\right)_{y=0} \approx -k_f \left(\frac{\Delta T}{\Delta y}\right)_{y=0} \qquad (4\text{-}26)$$

and:

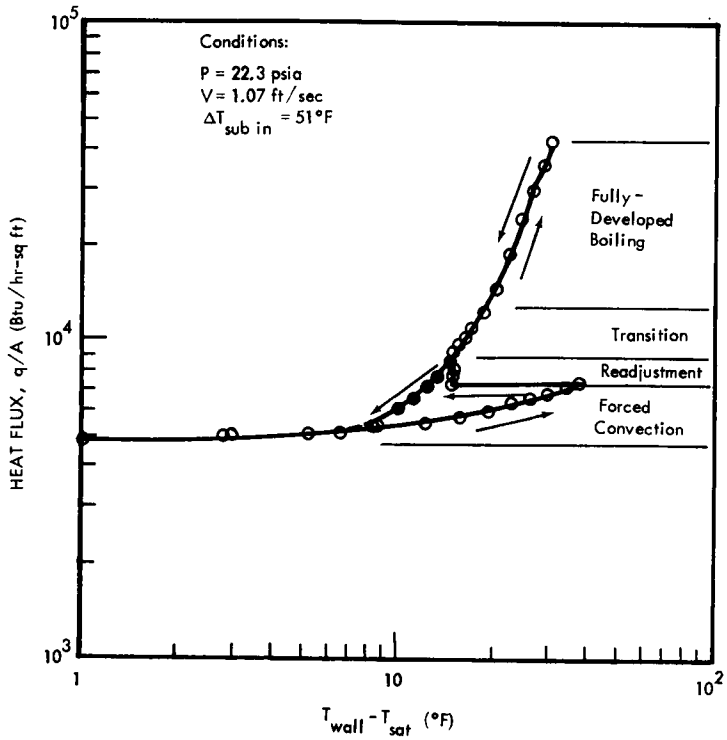


Figure IV-119. SUBCOOLED FLOW BOILING CURVE FOR R-113 IN A STAINLESS STEEL TUBE, MURPHY AND BERGLES [120].

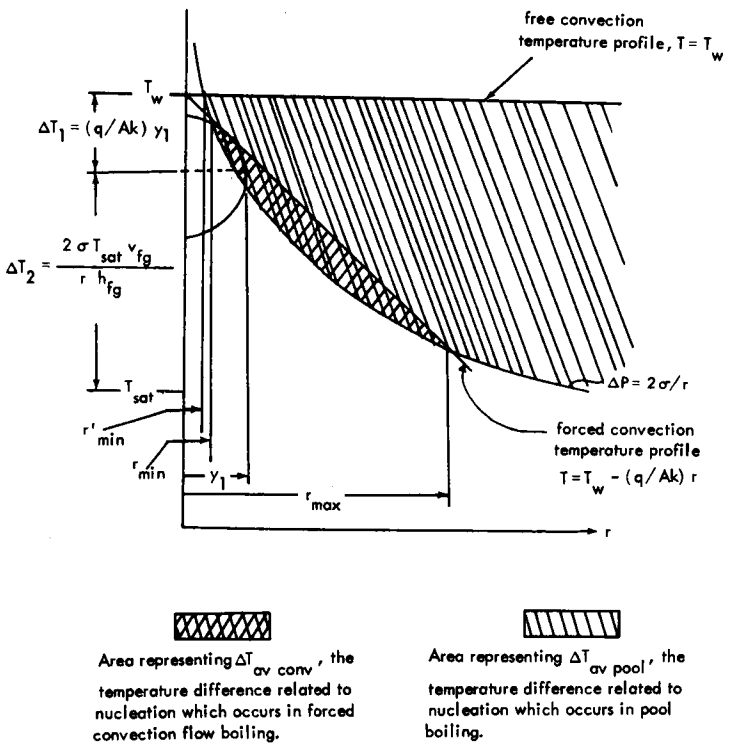


Figure IV-120. TEMPERATURE PROFILES IN THE VICINITY OF A BUBBLE IN POOL BOILING AND FLOW BOILING.

$$\Delta T_l = \left(\frac{q}{A}\right) \frac{y_l}{k_f} \cdot \tag{4-27}$$

In order to determine the range of available cavity radii, we combine Equations (4-25) and (4-27), replace y with r, and assume no subcooling to obtain:

$$T_w - T_{sat} - \frac{2\, T_{sat}\, \sigma v_{fg}}{h_{fg}\, r} = \left(\frac{q}{A}\right) \frac{r}{k} \tag{4-28}$$

which, on rearranging becomes:

$$\left(\frac{q}{Ak}\right) r^2 - (T_w - T_{sat})\, r + \frac{2\, T_{sat}\, \sigma v_{fg}}{h_{fg}} = 0. \tag{4-29}$$

Solving for r:

$$r_{\substack{max,\\min}} = \frac{T_w - T_{sat}}{2} \left(\frac{Ak}{q}\right) \pm \sqrt{\frac{(T_w - T_{sat})^2 k^2}{4\left(\frac{q}{A}\right)^2} - \frac{2\, T_{sat}\, \sigma k v_{fg}}{h_{fg} \left(\frac{q}{A}\right)}} \cdot \tag{4-30}$$

Here, r_{max} and r_{min} are the maximum and minimum cavity radii that are active. Applying Newton's law of cooling,

$$\frac{q}{A} = h(T_w - T_{sat}) \tag{4-31}$$

$$r_{\substack{max,\\min}} = \frac{k}{2h} \pm \sqrt{\frac{k^2}{4h^2} - \frac{2T_{sat}\, \sigma\, k\, v_{fg}}{h_{fg}\, h(T_w - T_{sat})}} \cdot \tag{4-32}$$

For the case of a saturated fluid Hsu [118], using a similar analysis but the expression y = 2r, obtained:

$$r_{\substack{max,\\min}} = \frac{\delta}{4} \pm \sqrt{\frac{\delta^2}{16} - \frac{0.8\, \sigma \delta T_{sat}}{\rho_g\, h_{fg}\, (T_w - T_{sat})}} \tag{4-33}$$

where δ was the boundary layer thickness. Using the approximation:

$$\delta \approx \frac{k}{h} \tag{4-34}$$

and since $\frac{1}{\rho_g} = v_g \approx v_{fg}$

$$r_{\substack{max,\\min}} = \frac{k}{4h} \pm \sqrt{\frac{k^2}{16h^2} - \frac{0.8\ T_{sat}\ \sigma k v_{fg}}{h_{fg}\ h(T_w - T_{sat})}} \qquad (4\text{-}35)$$

The Han and Griffith [119] solution, using the simplification in Equation (4-32) and the expression y = 1.5r yielded:

$$r_{\substack{max,\\min}} = \frac{k}{3h} \pm \sqrt{\frac{k^2}{9h^2} - \frac{4\ T_{sat}\ \sigma k v_{fg}}{3\ h_{fg}\ h(T_w - T_{sat})}} \qquad (4\text{-}36)$$

Except for the constants, Equation (4-35) and (4-36) are quite similar to Equation (4-32).

In order to find the average fluid temperature surrounding the bubbles, it is necessary to know the cavity size distribution. For example, if the sizes are such that the majority of them are concentrated in the small cavity range, the average fluid temperature would be higher than if the cavity sizes had been concentrated in the larger sized range. Brown [121] in a Ph.D. thesis in 1967 ran tests to study the bubble nucleation from different surfaces with various finishes. In the results, also discussed by Mikic and Rohsenow [122], the cavity size distribution was approximated by the power law:

$$n = C_1 \left(\frac{r_s}{r}\right)^m \qquad (4\text{-}37)$$

where n is the number of sites per unit area with radii larger than r, r_s is the radius for which n would be one per unit area, C_1 is a dimensional constant and m is the exponent. This equation can be differentiated to yield:

$$dn = Ndr = -C_1\ m\ r_s^m \left(\frac{1}{r}\right)^{m+1} dr \qquad (4\text{-}38)$$

Here, Ndr is the number of sites per unit area with radii between r and r + dr. The mean fluid temperature can therefore be defined as:

$$T_{avg} = \frac{1}{\int NAdr} \int T_f \, NAdr \qquad (4\text{-}39)$$

where T_{avg} is the average fluid temperature surrounding the bubbles and T_f is the fluid temperature. Since y = r and

$$T_f = T_w - \left(\frac{q}{Ak}\right) r \qquad (4\text{-}40)$$

from Figure IV-120 it can be observed that the temperature difference of interest is:

$$\Delta T_{avg\ conv} = \frac{1}{\int NAdr} \int \left[T_f - \left(T_{sat} + \frac{2\sigma\, T_{sat}\, v_{fg}}{r\, h_{fg}} \right) \right] NAdr \qquad (4\text{-}41)$$

or

$$\Delta T_{avg\ conv} = \frac{1}{\int_{r_{min}}^{r_{max}} -\pi C_1 m r_s^m\, r^{-m+1}\, dr}$$

$$\int_{r_{min}}^{r_{max}} \left[T_w - T_{sat} - \frac{q}{Ak} r - \frac{2\sigma\, T_{sat}\, v_{fg}}{r\, h_{fg}} \right]$$

$$\left(-\pi C_1 m r_s^m\, r^{-m+1}\, dr \right) \cdot \qquad (4\text{-}42)$$

This yields:

$$\Delta T_{avg\ conv} = (T_w - T_{sat}) - \frac{q}{Ak} \left(\frac{2-m}{3-m} \right) r_{max} \frac{1 - \left(\frac{r_{min}}{r_{max}} \right)^{3-m}}{1 - \left(\frac{r_{min}}{r_{max}} \right)^{2-m}}$$

$$- \frac{2\sigma\, T_{sat}\, v_{fg}}{h_{fg}} \left(\frac{2-m}{1-m} \right) \frac{1}{r_{max}} \frac{1 - \left(\frac{r_{min}}{r_{max}} \right)^{1-m}}{1 - \left(\frac{r_{min}}{r_{max}} \right)^{2-m}} \qquad (4\text{-}43)$$

where $\Delta T_{avg\ conv}$ is the average difference between the liquid temperature and the temperature needed for nucleation sites to be active in the range of radii where active nucleation sites exist.

For the case of pool boiling, a similar group of equations exists. In this case, because the temperature gradient near the wall is very small, the fluid can, for all practical purposes, be assumed to be equal to the wall temperature. Thus:

$$\Delta T_{avg\ pool} = (T_w - T_{sat}) - \frac{2\sigma\, T_{sat}\, v_{fg}}{h_{fg}} \left(\frac{2-m}{1-m}\right) \frac{1}{r'_{min}} \qquad (4\text{-}44)$$

r'_{min} is as shown in Figure IV-120 on page 294 and in this case r_{max} is taken to be infinite. Since:

$$S_1 = \left(\frac{\Delta T_{avg\ conv}}{\Delta T_{avg\ pool}}\right)^{0.99} \qquad (4\text{-}45)$$

and

$$r'_{min} = \frac{2\sigma\, T_{sat}\, v_{fg}}{h_{fg}\,(T_w - T_{sat})} \quad , \qquad (4\text{-}46)$$

$$S_1 = \left[\frac{(T_w - T_{sat}) - \left(\frac{q}{Ak}\right)\left(\frac{2-m}{3-m}\right) r_{max} \left\{ \frac{1 - \left(\frac{r_{min}}{r_{max}}\right)^{3-m}}{1 - \left(\frac{r_{min}}{r_{max}}\right)^{2-m}} \right\}}{\frac{1}{m-1}\,(T_w - T_{sat})} - \frac{\frac{2\sigma\, T_{sat}\, v_{fg}}{h_{fg}} \left(\frac{2-m}{1-m}\right) \frac{1}{r_{max}} \left\{ \frac{1 - \left(\frac{r_{min}}{r_{max}}\right)^{1-m}}{1 - \left(\frac{r_{min}}{r_{max}}\right)^{2-m}} \right\}}{\frac{1}{m-1}\,(T_w - T_{sat})} \right]^{0.99} \qquad (4\text{-}47)$$

for $m > 2$. For $m \leq 2$ the denominator is simply $(T_w - T_{sat})$. It should be noted that Equations (4-47) or (2-63) account for the suppression of a bubble due to the fact that, unlike the case of pool boiling, the liquid temperature around the bubble is significantly different from that of the wall. This suppression, however, only affects the active nucleation sites and therefore only the fraction of the heat transfer area containing cavities in the size range between r_{min} and r_{max}. Another suppression factor needs to be introduced to account for the reduced percentage of area that is active:

$$S_2 = \frac{\int_{r_{min}}^{r_{max}} Nadr}{\int_{r'_{min}}^{\infty} Nadr} \tag{4-48}$$

$$S_2 = \left(\frac{2\sigma T_{sat} v_{fg}}{(T_w - T_{sat}) h_{fg}} \right)^{m-2} \left[(r_{min})^{2-m} - (r_{max})^{2-m} \right] \tag{4-49}$$

for $m > 2$. Otherwise $S_2 = 0$. Thus, the total suppression is:

$$S_{tot} = S_1 S_2 \tag{4-50}$$

The expression for r_{max} and r_{min} is given in Equation (4-32). Looking at the variables which affect S_{tot}:

$$S_{tot} = S_{tot} (m, h, T_{sat}, \Delta T, \text{fluid properties})$$

The term, h, is taken here as the same heat transfer coefficient as that used for h_{mac} in the Chen [80] correlation, or:

$$h_{mac} = 0.023 (Re)_{fa}^{0.8} (Pr)_f^{0.4} \left(\frac{k_f}{D} \right) F \tag{4-51}$$

Thus:

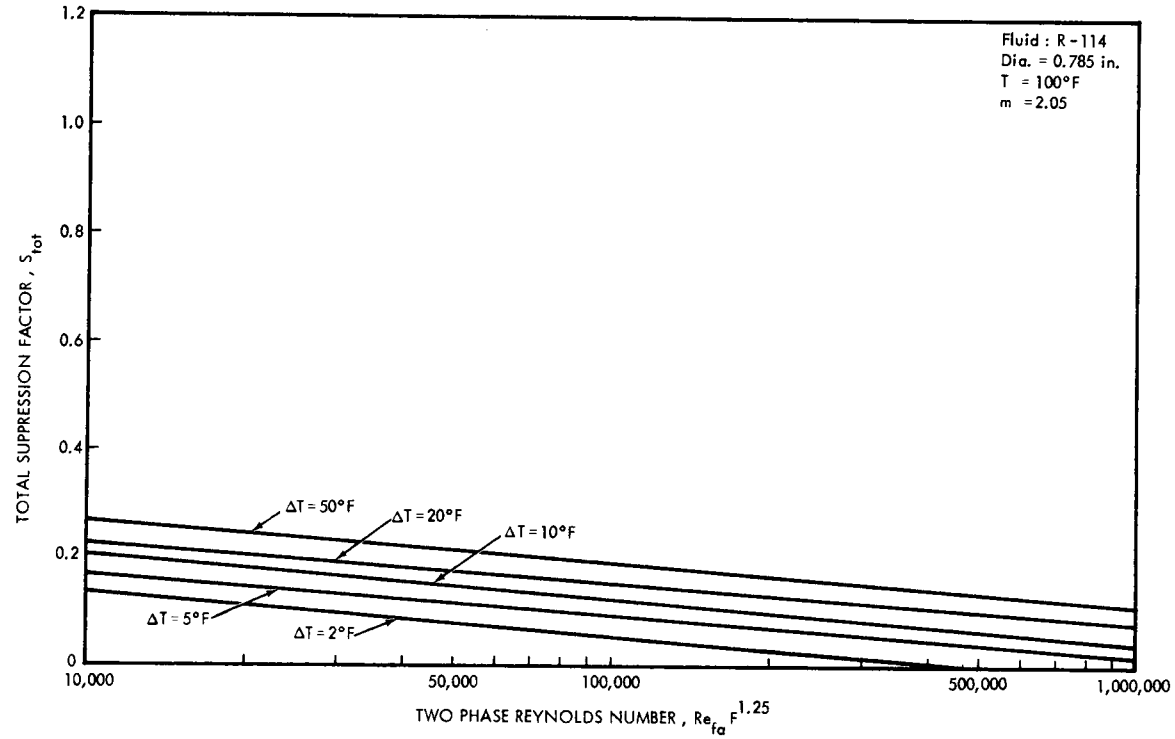
$$S_{tot} = S_{tot} (m, T_{sat}, \Delta T, Re_{fa}^{0.8} F, D, \text{fluid properties}) \tag{4-52}$$

In Chen's [80] analysis, the suppression factor was only a function of $Re_{fa} F^{1.25}$. In this analysis it is found to be a function of this parame-

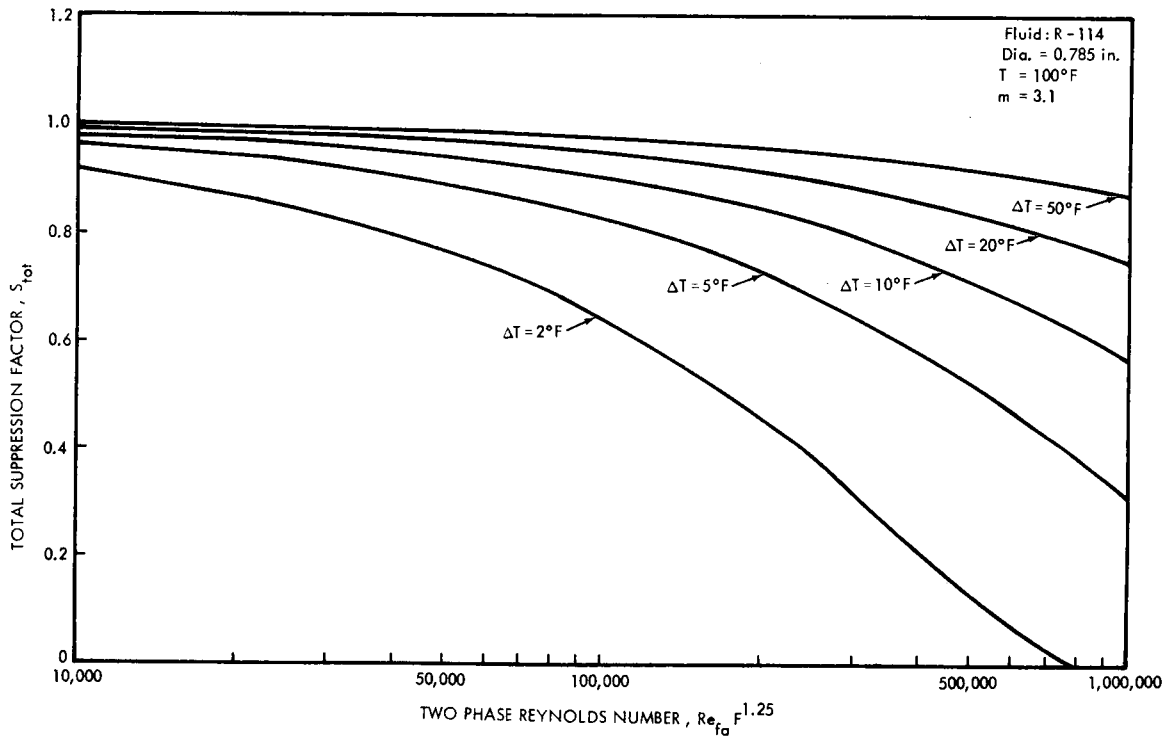
ter too, but also dependent on the boiling temperature, the wall-to-bulk temperature difference, the fluid properties, the tube diameter and the characteristics of the tube surface.

Plots of S_{tot} vs $Re_{fa}F^{1.25}$ are presented for the case of R-114 at 100°F, flowing in a 0.785 in. ID tube. ΔT was varied from 2 to 50°F. Values for m of 2.05, 3.1, 5.0, and 8.0 were tested. The plots obtained are shown in Figure IV-121. As can be seen, as m increases, the suppression factor approaches one. In Figure IV-122, the effect of the boiling temperature on the suppression factor for a constant m and ΔT is shown. As the boiling temperature increases, so does the suppression factor. Shown in Figure IV-123 are some of the results Brown [121] obtained experimentally with distilled degassed water for the number of active nucleation sites as a function of cavity size. The slopes of the lines which also represent the values for m in Equation (4-37) are seen to go as high as 4.04. For this range of m values, the model is seen to predict suppression factors which differ from those experimentally obtained by Chen [80]. For example while Chen's [80] suppression factor curve predicted an S value of 0.1 at a two-phase Reynolds number of approximately 400,000, the steady state model shows that in many cases, this value of S is not reached until a two-phase Reynolds number of several million. In addition, the analytical model shows a strong dependence of suppression factor on the wall-to-bulk temperature difference. No such trend was observed by Chen [80]. Because of these significant differences, it must be assumed that the steady state model is inadequate.

Transient Solution: Two of the basic assumptions implicit in the steady state solution were:

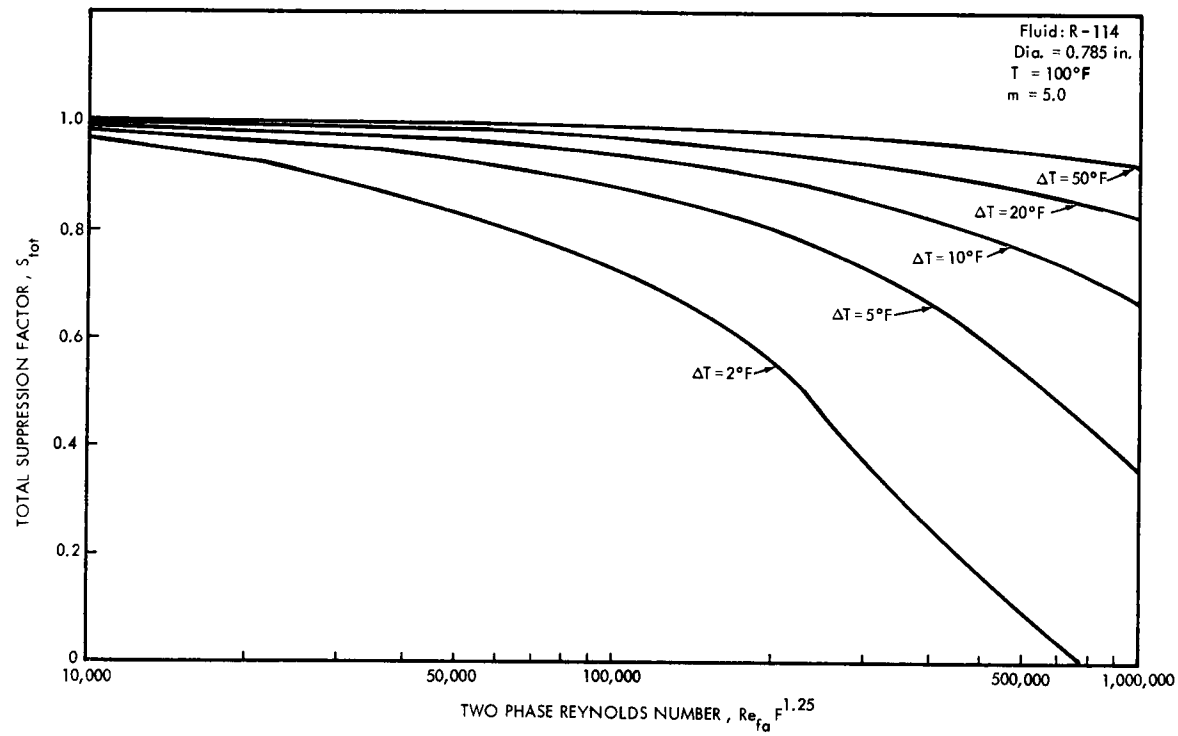


(a)

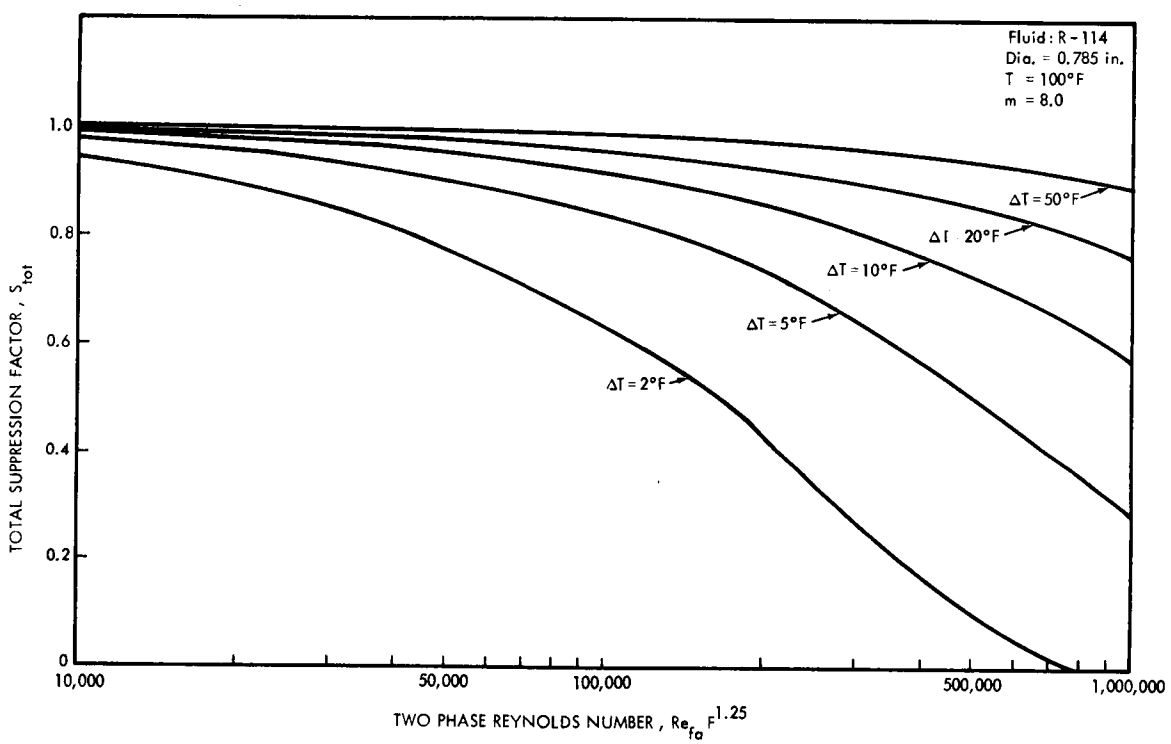


(b)

Figure IV-121. STEADY STATE SOLUTION FOR THE SUPPRESSION FACTOR FOR VARIOUS VALUES OF WALL-TO-BULK TEMPERATURE DIFFERENCES AND m .



(c)



(d)

Figure IV-121. (continued)

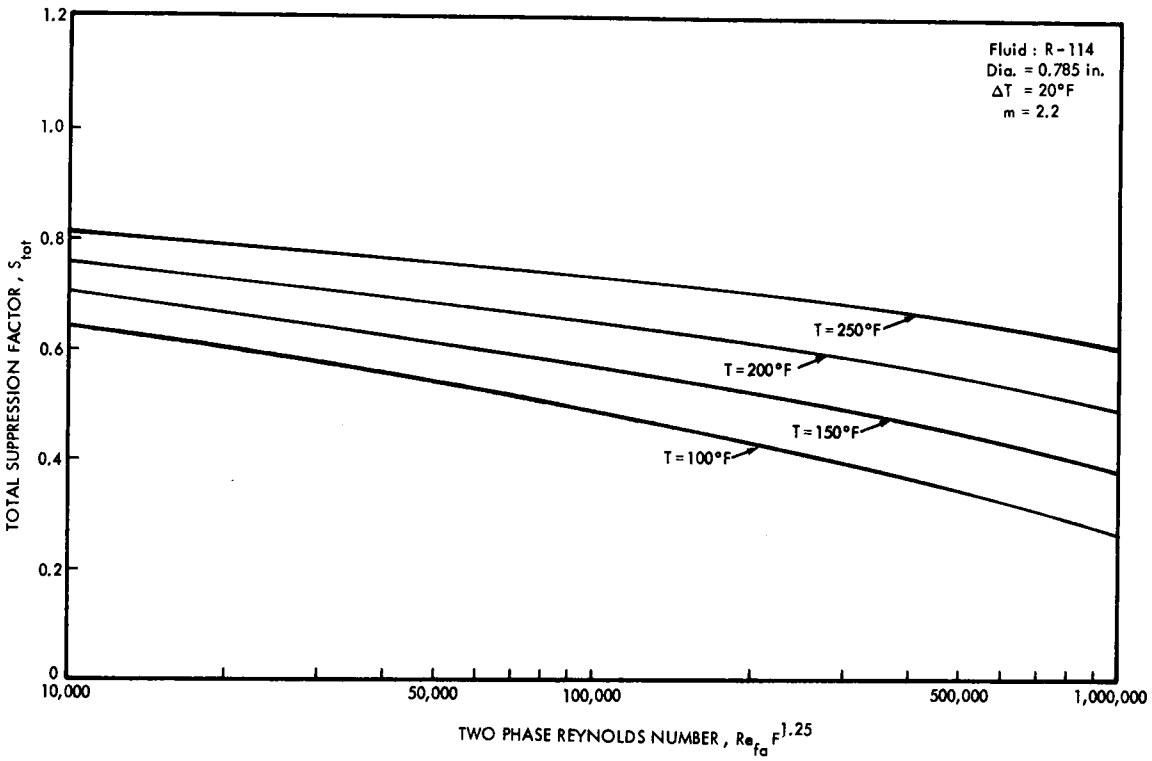


Figure IV-122. EFFECT OF BOILING TEMPERATURE ON THE SUPPRESSION FACTOR ACCORDING TO THE STEADY STATE SOLUTION.

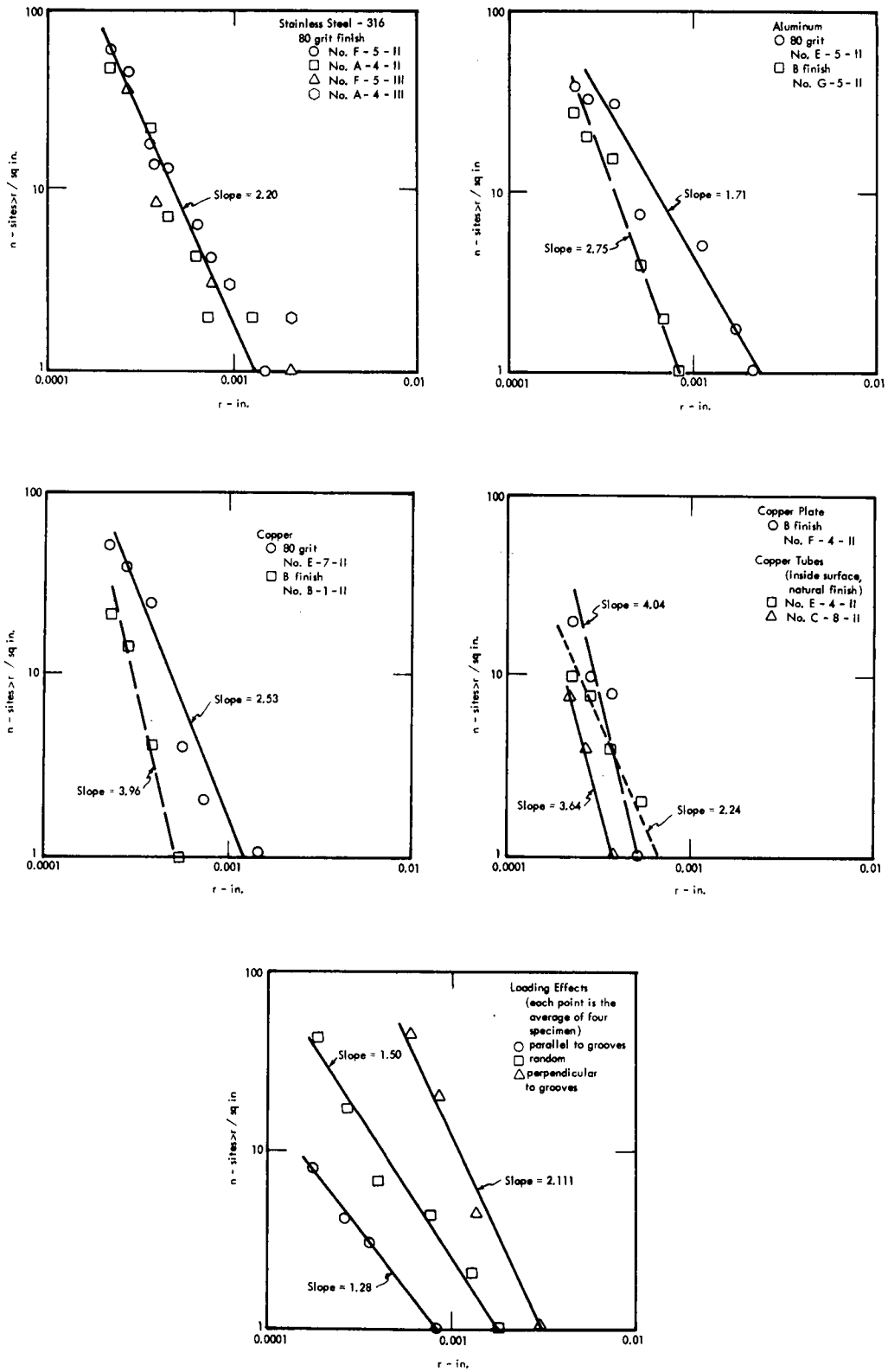


Figure IV-123. PLOT OF THE NUMBER OF ACTIVE NUCLEATION SITES VERSUS CAVITY SIZE FOR A VARIETY OF MATERIALS AND SURFACE FINISHES, BROWN [121].

(1) The temperature profile of the fluid close to the wall is steady and can be represented by:

$$\Delta T_l = \left(\frac{q}{A}\right) \frac{y_l}{k_f} \quad \text{and,} \tag{4-27}$$

(2) All the cavity sizes between r_{min} and r_{max} in Equation (4-32) are active and generate bubbles--assuming these sizes exist on the boiling surface.

A closer study of the hydrodynamics of the boundary layer indicates that in reality it is not steady. Bubbles are constantly forming on the boiling surface, growing, and eventually leaving it. As this occurs, the colder fluid beyond the boundary layer rushes in to fill the space created by the recently departed bubbles. As this cold fluid is heated, another bubble is formed on the wall. It grows and departs and more cold fluid replaces it. Thus, in reality, the boundary layer is constantly reforming. The temperature profile of the fluid next to the wall can therefore be represented by the transient heat conduction equation:

$$\frac{\partial \theta'}{\partial t} = \frac{k_f}{\rho_f \, c_{pf}} \left(\frac{\partial^2 \theta'}{\partial z_o^2}\right) \tag{4-53}$$

where

$$\theta' = T - T_{sat} \tag{4-54}$$

$$z_o = \delta - y \tag{4-55}$$

For the constant surface temperature case, Hsu [118] applied the following boundary conditions:

$$T = T_{sat} \text{ at } t = 0 \tag{4-56}$$

$$T = T_{sat} \text{ at } z_o = 0 \; (y = \delta) \tag{4-57}$$

and at $t > 0$:

$$\theta' = \theta'_w \text{ at } z_o = \delta \ (y = 0) \text{ for constant } \theta_w \tag{4-58}$$

The temperature profile for this differential equation is:

$$\frac{T - T_{sat}}{T_w - T_{sat}} = \eta + \frac{2}{\pi} \sum_{u=1}^{\infty} \frac{\cos u\pi}{u} \sin u\pi\eta e^{-u^2\pi^2\tau} \tag{4-59}$$

where

$$\tau = \frac{k_f t}{\rho_f c_{pf} \delta^2} \tag{4-60}$$

and

$$\eta = 1 - \frac{y}{\delta} \tag{4-61}$$

Han and Griffith [119] solved the differential equation

$$\frac{\partial \theta'}{\partial t} = \frac{k_f}{\rho_f \ c_{pf}} \left(\frac{\partial^2 \theta'}{\partial y^2} \right) \tag{4-62}$$

with the conditions:

$$T = T_w \text{ at } y = 0, \ t \geq 0 \tag{4-63}$$

$$T = T_{sat} \text{ at } y > 0, \ t = 0 \tag{4-64}$$

$$T = T_{sat} \text{ at } y = \infty, \ t > 0 \tag{4-65}$$

This set of initial and boundary conditions was slightly different from the one Hsu [118] used. Instead of assuming that the temperature of the fluid was the same as the saturation temperature at a distance $y = \delta$ from the wall, Han and Griffith [119] assumed that this occurred at $y = \infty$. In addition at $t = 0$, Hsu [118] postulated that the fluid at the wall had the same temperature as the saturated fluid. Han and Griffith [119], on the other hand, assumed this fluid had the same temperature as the wall. Their solution to Equation (4-62) was:

$$T - T_{sat} = (T_w - T_{sat}) \operatorname{erfc} \frac{y}{2\left(\frac{k_f t}{\rho_f c_{pf}}\right)^{1/2}} \qquad (4\text{-}66)$$

Of the two mathematical solutions, represented by Equations (4-59) and (4-66), the Han and Griffith [119] solution is believed to more accurately model the physical phenomena occurring. The boundary condition $T = T_w$ at all times at $y = 0$ is more reasonable since a microlayer of liquid has been observed to form underneath a bubble. This microlayer results in the fluid next to the wall remaining at the same temperature as the wall. The observation of a microlayer in pool boiling has been reported by numerous investigators including Cooper and Lloyd [123], Jawurek [124], and Katto and Shoji [125]. It should be mentioned at this time that both Hsu [118] and Han and Griffith [119] made the implicit assumption that the wall temperature was constant at all times. This is not completely true. The wall temperature has been observed to undergo frequent dips associated with the bubble departure in pool boiling. Madsen [126] and Tolubinskiy et al [127] among others have studied this phenomenon. It is, however, believed that in forced convection boiling, since only a portion of the heat transfer is associated with the bubble behavior, the fluctuations in the wall temperature will be considerably smaller.

Shown in Figure IV-124 are the curves representing Equation (4-66) for various values of t. Also shown is Equation (4-24). From a physical point of view, the behavior of the fluid can be described in this manner: as the cold fluid rushes close to the wall to fill up the space left by a departed bubble, the fluid temperature is the same as that of the fluid in the stream everywhere except adjacent to the wall.

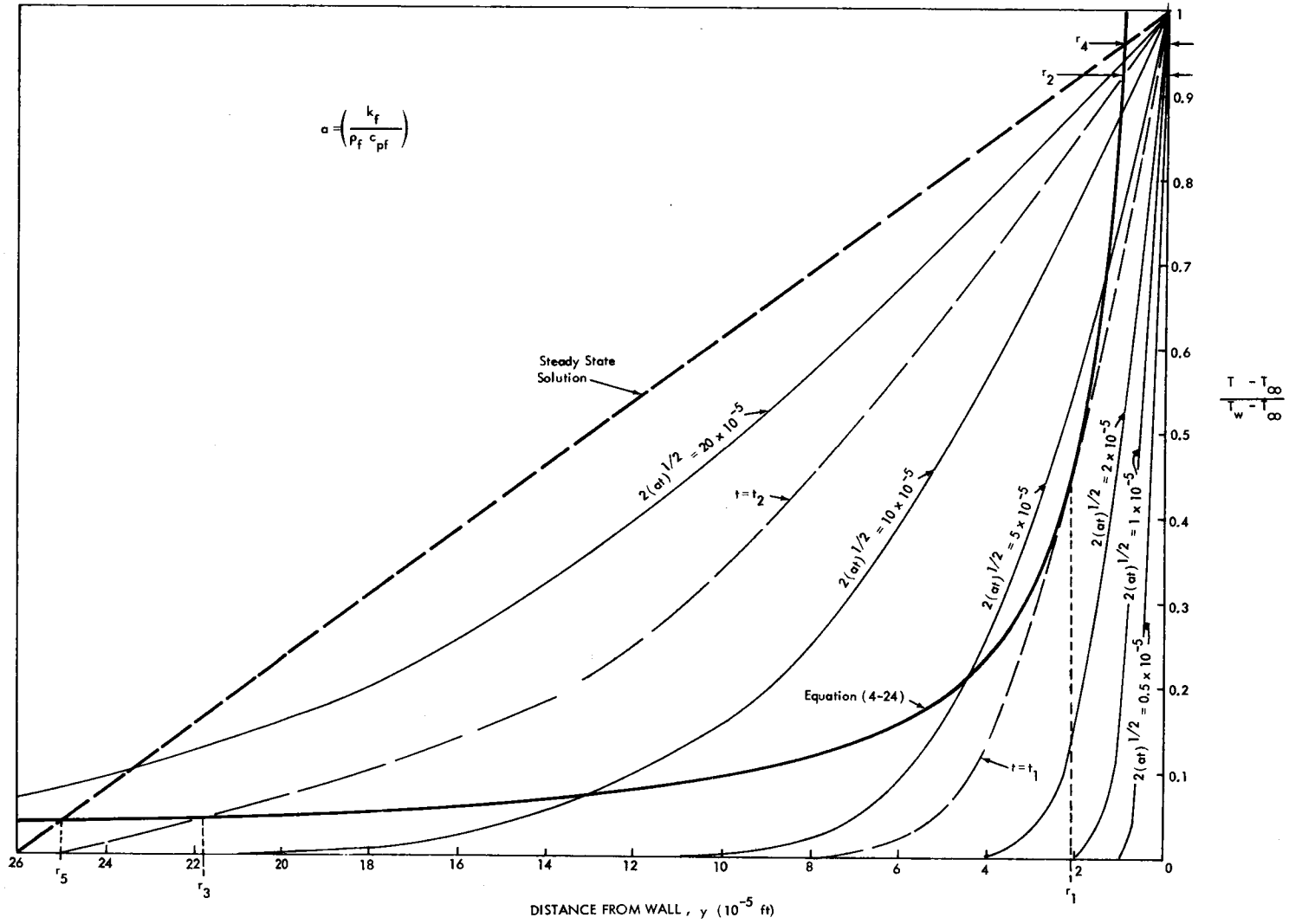


Figure IV-124. TRANSIENT BEHAVIOR OF THE THERMAL BOUNDARY LAYER IN THE VICINITY OF AN ACTIVE NUCLEATION SITE.

As the time, t, increases, the fluid near the wall is heated. Eventually, the temperature profile touches the curve representing Equation (4-24) at time t_1. At that instant, bubbles of radius r_1 start growing. As the time increases further, the range of active nucleation sites increases. As soon as the bubbles at radius r_1 start leaving the surface at time t_2, the turbulence created causes the bubbles from all the active nucleation sites to break off. The fluid from the mainstream rushes in and fills up the void created by the departing bubbles and the process repeats itself. At time t_2, the range of cavity sizes which are active is $r_2 \leq r \leq r_3$. This is less than the range $r_4 \leq r \leq r_5$ that would have been active in the steady state case. The time from $t = 0$ to $t = t_1$ is called the waiting time. The frequency of bubble departure is $1/t_2$.

Writing the mathematical equations:

$$T_{avg} = \frac{1}{\int NAdr} \int T_f \, NAdr \tag{4-39}$$

Since

$$T_f = (T_w - T_{sat}) \, \text{erfc} \, \frac{r}{2(at)^{1/2}} + T_{sat} \tag{4-67}$$

The temperature difference of interest is:

$$\Delta T_{avg\ conv} = \frac{1}{\int_{r_{min}}^{r_{max}} Nadr} \int_{r_{min}}^{r_{max}} \left[(T_w - T_{sat}) \, \text{erfc} \, \frac{r}{2(at)^{1/2}} - \frac{2\sigma \, T_{sat} \, v_{fg}}{r \, h_{fg}} \right] NAdr. \tag{4-68}$$

Letting

$$\xi = \frac{r}{2(at)^{1/2}} \tag{4-69}$$

and expanding the complimentary error function in Equation (4-68) in a Taylor Series:

$$\Delta T_{avg\ conv} = \frac{T_w - T_{sat}}{\int_{r_{min}}^{r_{max}} r^{-m+1} dr} \int_{r_{min}}^{r_{max}} r^{-m+1} \left[1 - \frac{2}{\sqrt{\pi}} \left(\xi - \frac{1}{3}\xi^3 + \frac{1}{10}\xi^5 - \frac{1}{42}\xi^7 \pm \ldots\right)\right] dr - \frac{2\sigma\, T_{sat}\, v_{fg}}{h_{fg} \int_{r_{min}}^{r_{max}} r^{-m+1} dr} \int_{r_{min}}^{r_{max}} r^{-m} dr \qquad (4\text{-}70)$$

$$\Delta T_{avg\ conv} = \frac{\left(T_w - T_{sat}\right)(2-m)}{\left(r_{max}\right)^{2-m} - \left(r_{min}\right)^{2-m}} \left\{ \int_{r_{min}}^{r_{max}} \left[r^{1-m} - \frac{2}{\sqrt{\pi}} \left(\frac{r^{2-m}}{2(at)^{1/2}} - \frac{1}{3} \frac{r^{4-m}}{2^3 (at)^{3/2}} + \frac{1}{10} \frac{r^{6-m}}{2^5 (at)^{5/2}} - \frac{1}{42} \frac{r^{8-m}}{2^7 (at)^{7/2}} \pm \ldots \right) \right] dr \right\} - \frac{2\sigma\, T_{sat}\, v_{fg}\, (2-m)}{h_{fg} \left(r_{max}^{2-m} - r_{min}^{2-m} \right)} \int_{r_{min}}^{r_{max}} r^{-m} dr \qquad (4\text{-}71)$$

$$\Delta T_{avg\ conv} = T_w - T_{sat} - \frac{2(T_w - T_{sat})(2-m)}{\sqrt{\pi}} \left\{ \frac{r_{max}}{2(3-m)(at)^{1/2}} \frac{1 - \left(\frac{r_{min}}{r_{max}}\right)^{3-m}}{1 - \left(\frac{r_{min}}{r_{max}}\right)^{2-m}} \right.$$

$$- \frac{r_{max}^{3}}{(3)(2^3)(5-m)(at)^{3/2}} \frac{1 - \left(\frac{r_{min}}{r_{max}}\right)^{5-m}}{1 - \left(\frac{r_{min}}{r_{max}}\right)^{2-m}}$$

$$+ \frac{r_{max}^{5}}{(10)(2^5)(7-m)(at)^{5/2}} \frac{1 - \left(\frac{r_{min}}{r_{max}}\right)^{7-m}}{1 - \left(\frac{r_{min}}{r_{max}}\right)^{2-m}} \mp \cdots\cdots \Bigg\}$$

$$- \frac{2\sigma\, T_{sat}\, v_{fg}\, (2-m)}{h_{fg}\, (1-m)} \frac{1}{r_{max}} \frac{1 - \left(\frac{r_{min}}{r_{max}}\right)^{1-m}}{1 - \left(\frac{r_{min}}{r_{max}}\right)^{2-m}} \qquad (4\text{-}72)$$

Since

$$S_1 = \left(\frac{\Delta T_{avg\ conv}}{\Delta T_{avg\ pool}}\right)^{0.99} \qquad (4\text{-}45)$$

$$S_1 = \Bigg\{ m-1 - \frac{2(2-m)(m-1)}{\sqrt{\pi}\left[1 - \left(\frac{r_{min}}{r_{max}}\right)^{2-m}\right]} \Bigg\{ \frac{r_{max}}{2(3-m)(at)^{1/2}} \left[1 - \left(\frac{r_{min}}{r_{max}}\right)^{3-m}\right]$$

$$- \frac{r_{max}^{3}}{(3)(2^3)(5-m)(at)^{3/2}} \left[1 - \left(\frac{r_{min}}{r_{max}}\right)^{5-m}\right]$$

$$+ \frac{r_{max}^{5}}{(10)(2^5)(7-m)(at)^{5/2}} \left[1 - \left(\frac{r_{min}}{r_{max}}\right)^{7-m}\right] \mp \cdots\cdots \Bigg\}$$

$$- \frac{2\sigma\, T_{sat}\, v_{fg}}{h_{fg}\, (T_w - T_{sat})} (m-2) \frac{1}{r_{max}} \left[\frac{1 - \left(\frac{r_{min}}{r_{max}}\right)^{1-m}}{1 - \left(\frac{r_{min}}{r_{max}}\right)^{2-m}}\right] \Bigg\}^{0.99} \qquad (4\text{-}73)$$

Equation (4-73) can be reduced to the form:

$$S_1 = \Bigg\{ (m-1) - \frac{2(2-m)(m-1)}{\sqrt{\pi}\left[1 - \left(\frac{r_{min}}{r_{max}}\right)^{2-m}\right]} \left\{ \sum_{u=1}^{\infty} \frac{(-1)^{u+1}}{(2u-1)(u-1)!} \left(\frac{r_{max}}{2(at)^{1/2}}\right)^{2u-1} \left[\frac{1 - \left(\frac{r_{min}}{r_{max}}\right)^{2u+1-m}}{(2u+1-m)}\right] \right\} - \frac{2\sigma\, T_{sat}\, v_{fg}\, (m-2)}{h_{fg}\, (T_w - T_{sat})\, r_{max}} \left[\frac{1 - \left(\frac{r_{min}}{r_{max}}\right)^{1-m}}{1 - \left(\frac{r_{min}}{r_{max}}\right)^{2-m}}\right] \Bigg\}^{0.99} \qquad (4\text{-}74)$$

It can be noted that in Equation (4-73), some of the terms reduce to the 0/0 form for given values of m. Looking, for example, at the second term in the brackets in Equation (4-73) and applying L'Hopital's rule:

$$\lim_{m \to 5} \frac{2(2-m)(m-1)\, r_{max}^{\,3} \left[1 - \left(\frac{r_{min}}{r_{max}}\right)^{5-m}\right]}{\sqrt{\pi}\left[1 - \left(\frac{r_{min}}{r_{max}}\right)^{2-m}\right] 3(2)^3\, (5-m)(at)^{3/2}}$$

$$= \frac{r_{max}^{\,3} \ln\left(\frac{r_{min}}{r_{max}}\right)}{\sqrt{\pi}(at)^{3/2}\left[1 - \left(\frac{r_{max}}{r_{min}}\right)^3\right]} \qquad (4\text{-}75)$$

The limit does not cause the term to go to infinity and the series converges. S_2 is the same for the transient case as it is for steady state, with:

$$S_2 = \left(\frac{2\sigma\, T_{sat}\, v_{fg}}{(T_w - T_{sat})\, h_{fg}}\right)^{m-2} \left[(r_{min})^{2-m} - (r_{max})^{2-m}\right] \qquad (4\text{-}49)$$

and

$$S_{tot} = S_1 S_2 \qquad (4\text{-}50)$$

Unfortunately, no simple equation can be obtained for r_{max} and r_{min}. They are a function of t_2 and therefore dependent on the frequency of the bubble departure. While the study of bubble dynamics is beyond the scope of this investigation, numerous studies performed over the years have resulted in a limited but significant understanding of the phenomena for the case of pool boiling. Mikic and Rohsenow [122] presented a brief summary of some of the earlier studies. For the case of flow boiling, considerably less has been done. Koumoutsos et al [128] have studied the effect of flow on the bubble departure diameter. The empirical nature of the correlation obtained limited the applicability of the results to water at conditions similar to those encountered during their tests. A recent paper by Abdelmessih et al [129] who studied the effect of fluid velocity on the growth and collapse of vapor bubbles in slightly subcooled water was the only other relevant publication found in the literature.

Before attempting to go further in obtaining an expression for S_{tot} it may be worthwhile to compare the waiting periods predicted by this model with some of the experimental results obtained in the literature. Hsu [118], in comparing his analytical solution, which was similar to the present one, with experimental flow boiling data from McAdams and coworkers [130] obtained good agreement. Abdelmessih et al [129] also measured waiting periods for the flow boiling mode. For the case of a heat flux of 1.3×10^5 Btu/hr-sq ft and a Reynolds number of 5.82×10^4, a wall-to-bulk temperature difference of 17.3°F was found to occur. The boiling temperature of the water was 215°F and the

experimentally measured waiting period was approximately 0.3 ms. This situation is shown plotted in Figure IV-125. The temperature profile that is seen to lie tangent to the curve representing Equation (4-24) was for the case of $2(at)^{1/2} = 4.6 \times 10^{-5}$ ft. Since at 215°F, for water, the thermal diffusivity, a, is 0.00654 ft^2/hr, a waiting time of 0.291 ms is obtained which is in very good agreement with the experimentally measured value. In addition to the above run three other runs were presented in Figure 4 of the Abdelmessih et al [129] publication. In each of those cases, the heat flux was kept constant and the Reynolds number was increased. In all cases, the experimentally measured waiting times were approximately 0.3 ms although it was mentioned that increasing the liquid velocity resulted in increased waiting times. All the analytical results obtained are summarized in Table IV-4. They verify the fact that at the relatively low heat flux of 5.94×10^4 Btu/hr-sq ft, the waiting time does increase slightly with increasing liquid velocity.

In addition to waiting times, growth times were also measured by Abdelmessih et al [129]. For the case of Re = 5.82×10^4 and a $(T_w - T_{bulk})$ of 17.3°F, a growth time of 0.3 ms was experimentally noted. When this is added to the waiting time of also 0.3 ms, a total time of 0.6 ms corresponding to a $2(at)^{1/2}$ of 6.5×10^{-5} ft is obtained. This line is shown in Figure IV-125, to intersect the curve representing Equation (4-24) at two points yielding an r_{max} of 6.55×10^{-5} ft and an r_{min} of 1.31×10^{-5} ft. This range is considerably smaller than the $r_{max} = 24.94 \times 10^{-5}$ ft and $r_{min} = 1.104 \times 10^{-5}$ ft predicted for the steady state case by Equation (4-32) for the above set of operating

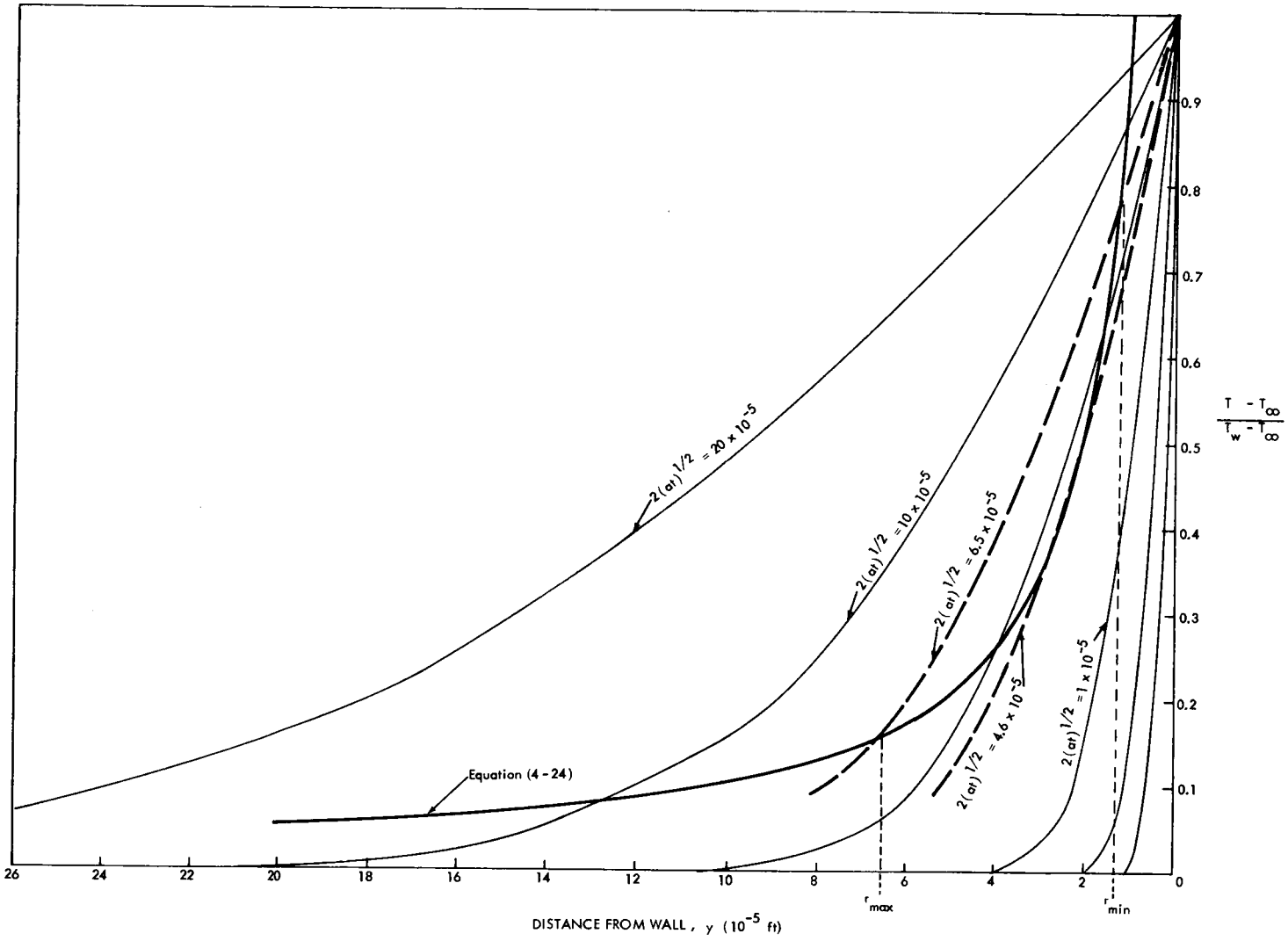


Figure IV-125. TRANSIENT BEHAVIOR OF THE THERMAL BOUNDARY LAYER IN THE VICINITY OF THE WALL FOR ONE OF THE TESTS CONDUCTED BY ABDELMESSIH ET AL [129].

Table IV-4

COMPARISON OF AN ANALYTICAL MODEL FOR WAITING TIME WITH THE ABDELMESSIH ET AL [129] EXPERIMENTAL RESULTS FOR THE CASE OF $q/A = 5.94 \times 10^4$ Btu/hr-sq ft

Run Characteristics	Waiting Time, ms	
	Calculated	Experimental
$Re = 5.82 \times 10^4$ $T_w - T_f = 17.3°F$	0.291	approximately 0.3
$Re = 6.98 \times 10^4$ $T_w - T_f = 16.9°F$	0.330	approximately 0.3
$Re = 8.14 \times 10^4$ $T_w - T_f = 16.5°F$	0.344	approximately 0.3
$Re = 9.32 \times 10^4$ $T_w - T_f = 15.6°F$	0.358	approximately 0.3

conditions. It should be noted that in the transient calculation above, the heat flux used was the single phase heat flux computed from the macroconvective portion of the Chen [80] correlation. A pencil and paper exercise indicates that in the Abdelmessih et al [129] tests, the qualities encountered were small. Therefore, the multiplication factor F was assumed equal to one. The Dittus-Boelter equation for the fluid alone was used to compute the heat flux. This calculation yielded a q/A of 26,150 Btu/hr-sq ft.

Having obtained r_{max} and r_{min} for the transient case, it is possible to obtain S_{tot}. These tests were run on a stainless steel surface and from Figure IV-123, on page 304, an m of 2.20 is reasonable. For this particular case, using Equation (4-74):

$$S_1 = 0.1207 \tag{4-76}$$

and from Equation (4-49)

$$S_2 = 0.2637 \tag{4-77}$$

Therefore,

$$S_{tot} = 0.0318 \tag{4-78}$$

Under the same set of conditions, the Chen [80] correlation yielded a suppression factor of 0.5343. If an m of 3.5 were used instead of 2.20, the suppression factors obtained would have been:

$$S_1 = 0.7516 \tag{4-79}$$

$$S_2 = 0.6605$$

and

$$S_{tot} = 0.4964 \tag{4-81}$$

Considering the scatter in the values of S which Chen [80] had obtained, and the uncertainty of the values of m and r_{min} and r_{max} in the present studies, the differences are understandable. In addition,

it should be remembered that in computing the suppression factor according to Chen [80] for Abdelmessih et al's [129] data, it was assumed that the multiplication factor F was equal to one. If F was actually higher, this would have affected the value of the Chen [80] suppression factor and lowered it considerably. Therefore, while no claim to the accuracy of this model can be made on the basis of Abdelmessih et al's [129] results it can be seen that the S curve is probably dependent on more parameters than simply the $(Re)_{fa}F^{1.25}$ term used in Figure II-18 on page 64. For the time being, no analytically based improvements can be made to Chen's [80] suppression factor curve. When more data on bubble dynamics are obtained, the results from the present model can be further compared with experimentally observed suppression factor curves over a wide range of operating conditions and numerous working fluids.

Application of An Improved Forced Convection Correlation to Refrigerant and Non-Refrigerant Data

From the results obtained in the previous section, the following general comments can be made:

(1) The use of the Forster-Zuber [52] pool boiling correlation in its original form is, possibly, the primary cause of the deviation of the Chen [80] correlation from actual experimental data for refrigerants. The use of the Forster-Zuber [52] equation with a variable coefficient or the use of the Rohsenow [61] correlation should be contemplated.

(2) A variation of the F term used in the Chen [80] correlation should be attempted. Based on the Zuber et al [10] void fraction correlation this may lead to closer agreement between this modified form

of the Chen [80] correlation and experimental data. Any improvements obtained, however, will probably be on a smaller scale than those from (1) above.

(3) The suppression factor curve, as given by Chen [80] will have to be used for now because of the lack of experimental information to verify the analytical model derived in the previous section.

Modification of the Chen [80] correlation will now be undertaken in an orderly step-by-step process so as to individually study the effect of the components discussed in (1) and (2) above. The multiplication factor F will be examined first.

Application of a Different Multiplication Factor F to the Chen [80] Correlation. In order to be able to better study the effect of F on the boiling correlation, the Foster-Zuber [52] pool boiling term will be replaced by the Rohsenow [61] equation. The validity of using the Rohsenow [61] pool boiling equation in the Chen [80] correlation will be shown in the next section. Since an additional unknown here is the C_{sf} term, plots of the experimentally determined C_{sf} value vs. the two-phase Reynolds number are presented in Figures IV-126 to IV-128 for the 100, 150, and 200°F boiling temperatures, respectively. If this modification to the Chen [80] correlation is to strictly apply, C_{sf} must be independent of the two-phase Reynolds number and a horizontal line should be obtained. It is noted that this is approximately so. The increase in C_{sf} at high values of the two-phase Reynolds number for the 100 and 150°F boiling runs is attributed to an inaccuracy in the suppression factor curve. In order to determine if Equation (4-19) represents a more accurate form of the multiplication factor F, it will be

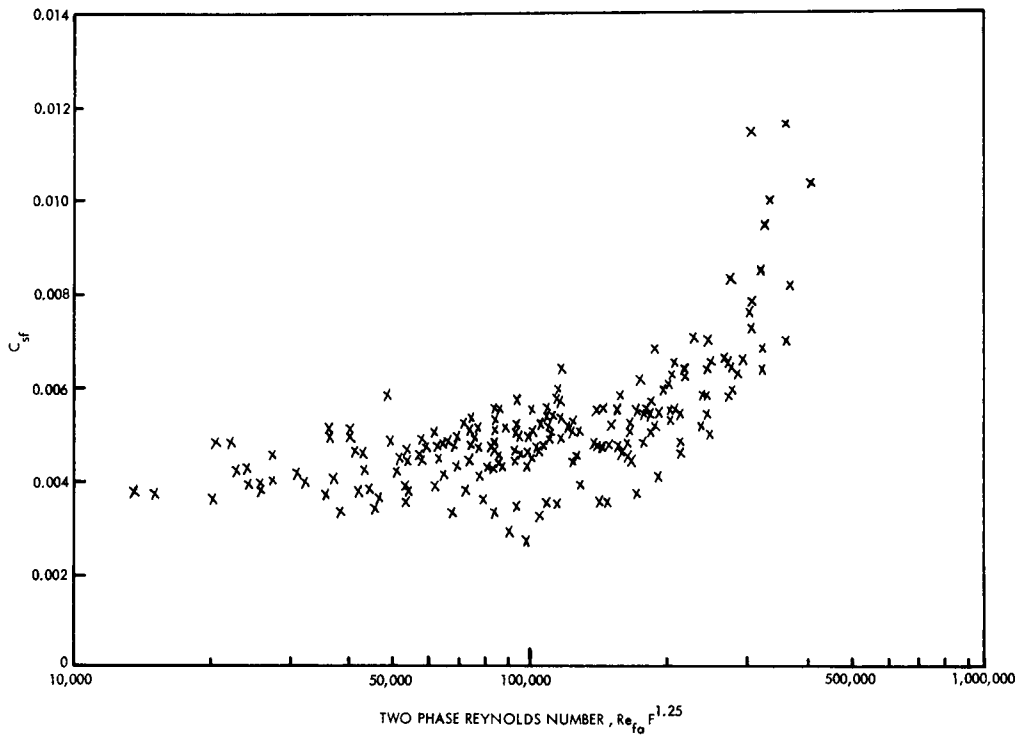


Figure IV-126. PLOT OF THE EXPERIMENTALLY DETERMINED C_{sf} VALUES VERSUS THE TWO-PHASE REYNOLDS NUMBER USING THE ORIGINAL MULTIPLICATION FACTOR F. T≈100°F.

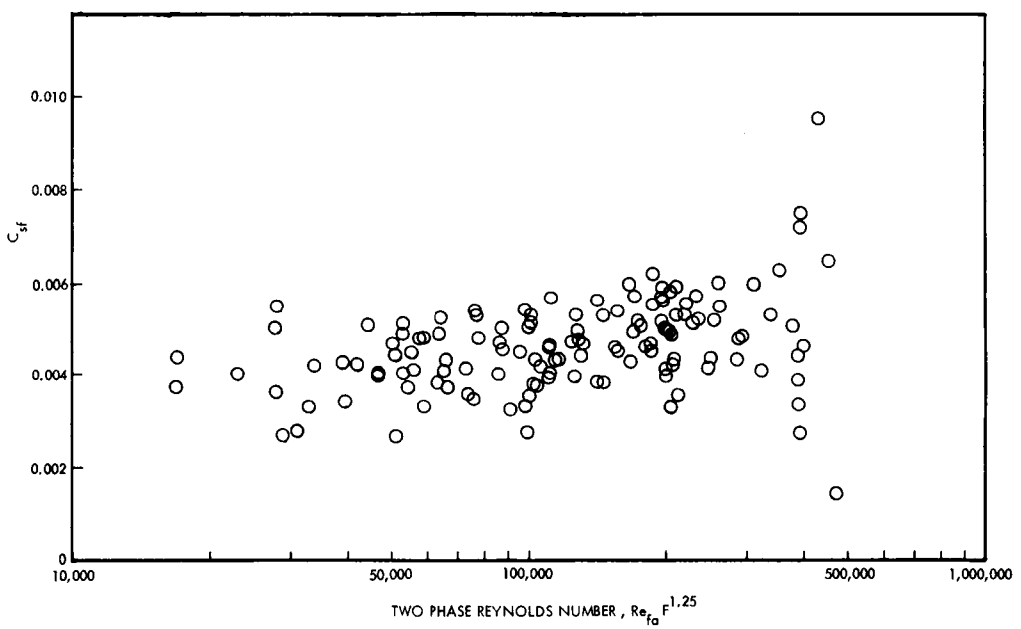


Figure IV-127. PLOT OF THE EXPERIMENTALLY DETERMINED C_{sf} VALUES VERSUS THE TWO-PHASE REYNOLDS NUMBER USING THE ORIGINAL MULTIPLICATION FACTOR F. T≈150°F.

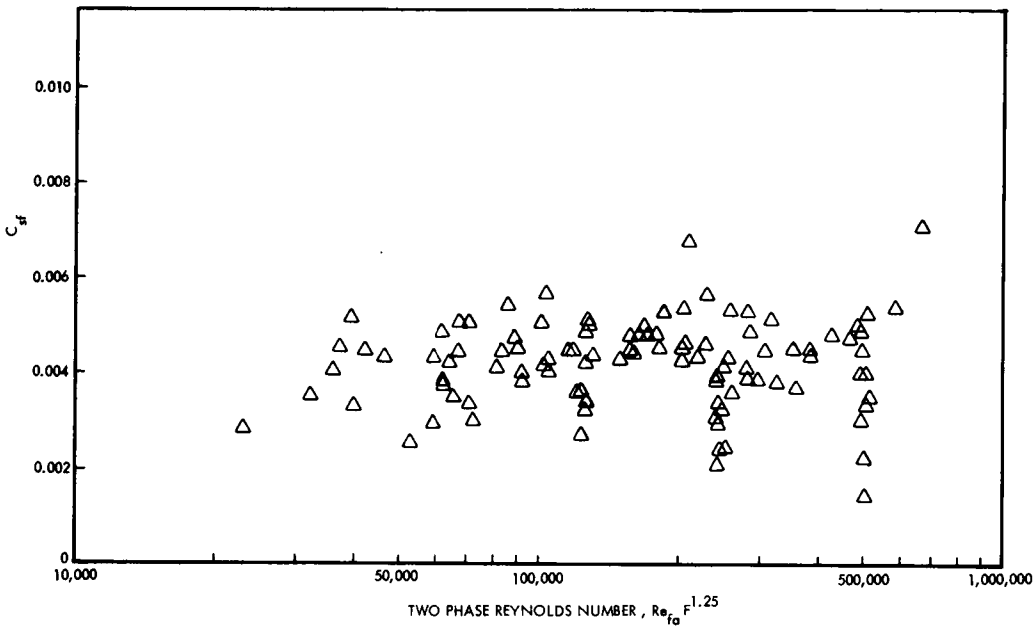


Figure IV-128. PLOT OF THE EXPERIMENTALLY DETERMINED C_{sf} VALUES VERSUS THE TWO-PHASE REYNOLDS NUMBER USING THE ORIGINAL MULTIPLICATION FACTOR F. T≈200°F.

seen if application of this equation results in less scatter in the data. The results of this are shown in Figures IV-129 to IV-131. As can be seen, the scatter is greater and thus Equation (4-19) is not satisfactory. A careful point-by-point examination of the plots in Figures IV-126 to IV-131 indicates that for the low quality runs, below approximately x = 0.20, Equation (4-19) is superior. Thus, in order to accommodate the best of Chen's [80] original F curve in the high $1/X_{tt}$ range and the higher F curve of Equation (4-19) in the low $1/X_{tt}$ range, Equation (4-23) will be considered. The C_{sf} vs. two-phase Reynolds number plots obtained are shown in Figures IV-132 to IV-134. An improvement is noted over the previous curves, especially for the 200°F boiling runs. It should be remembered at this point that

$$\Phi_{ftt} \approx \frac{1}{1 - \alpha} \qquad (2\text{-}28)$$

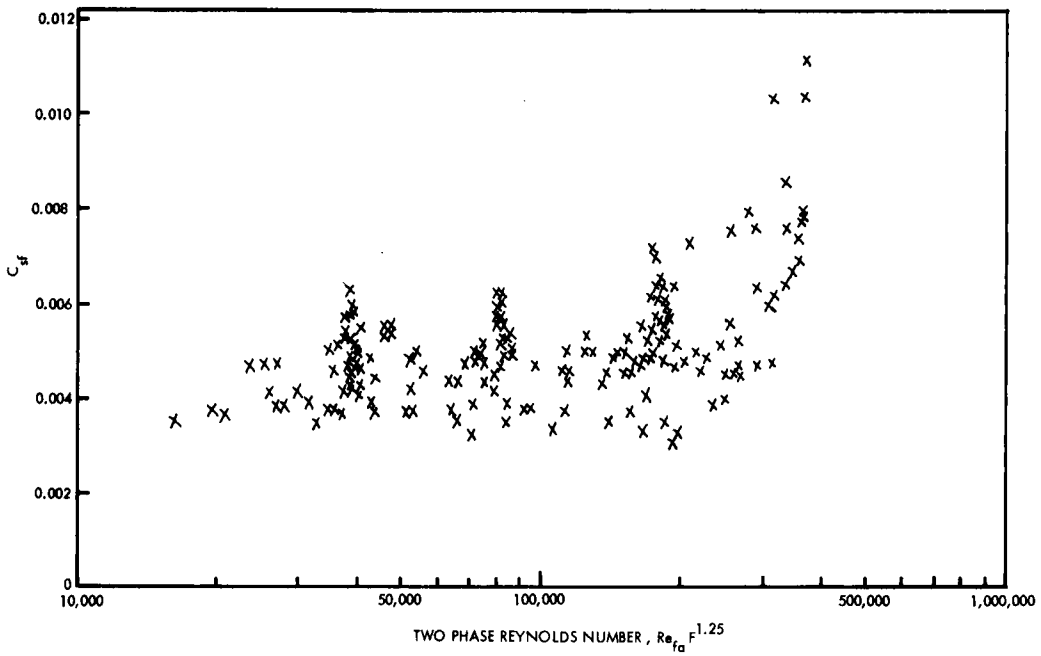


Figure IV-129. PLOT OF EXPERIMENTALLY DETERMINED C_{sf} VALUES VERSUS THE TWO-PHASE REYNOLDS NUMBER USING $F = (1/1-\alpha)^{0.9}$ AND THE MODIFIED ZUBER ET AL [10] VOID FRACTION FORMULATION. T ≈ 100°F.

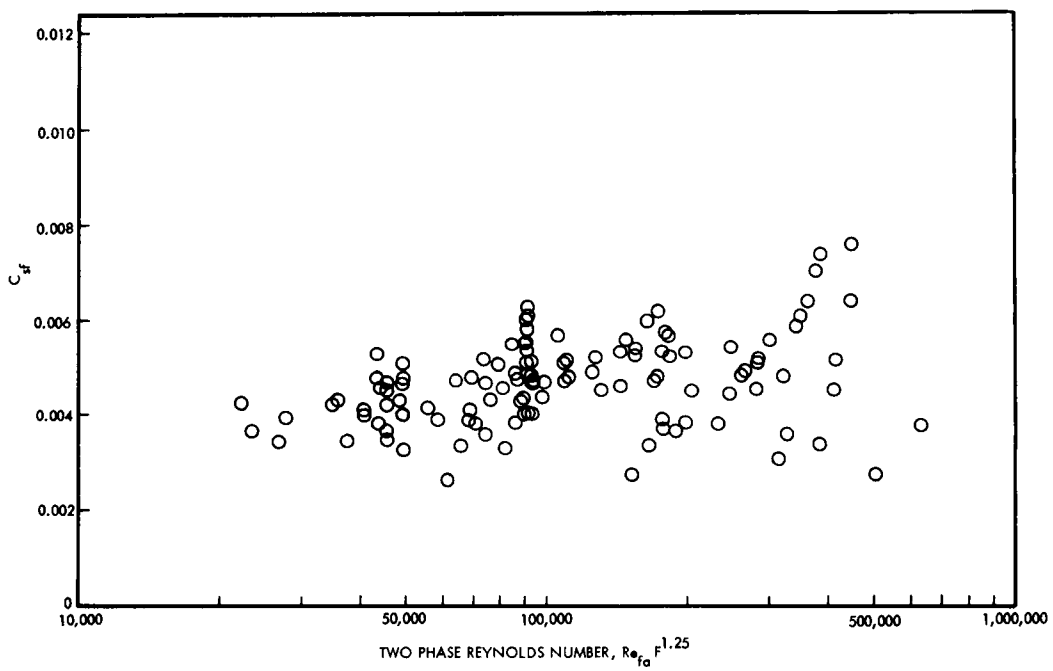


Figure IV-130. PLOT OF EXPERIMENTALLY DETERMINED C_{sf} VALUES VERSUS THE TWO-PHASE REYNOLDS NUMBER USING $F = (1/1-\alpha)^{0.9}$ AND THE MODIFIED ZUBER ET AL [10] VOID FRACTION FORMULATION. T ≈ 150°F.

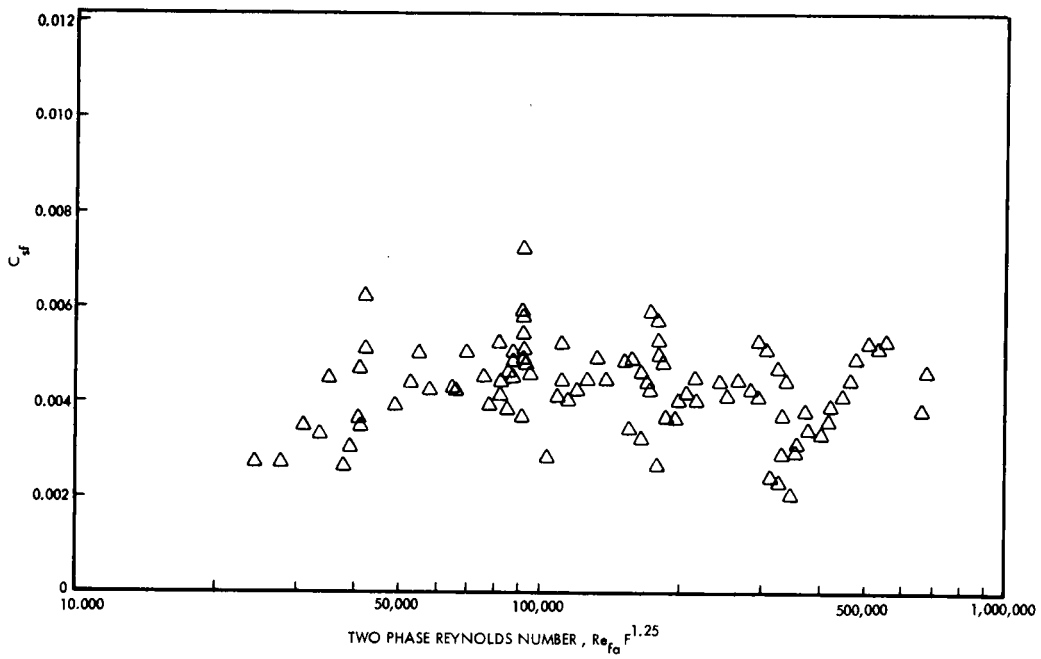


Figure IV-131. PLOT OF EXPERIMENTALLY DETERMINED C_{sf} VALUES VERSUS THE TWO-PHASE REYNOLDS NUMBER USING $F=(1/1-\alpha)^{0.9}$ AND THE MODIFIED ZUBER ET AL [10] VOID FRACTION FORMULATION. T≈200°F.

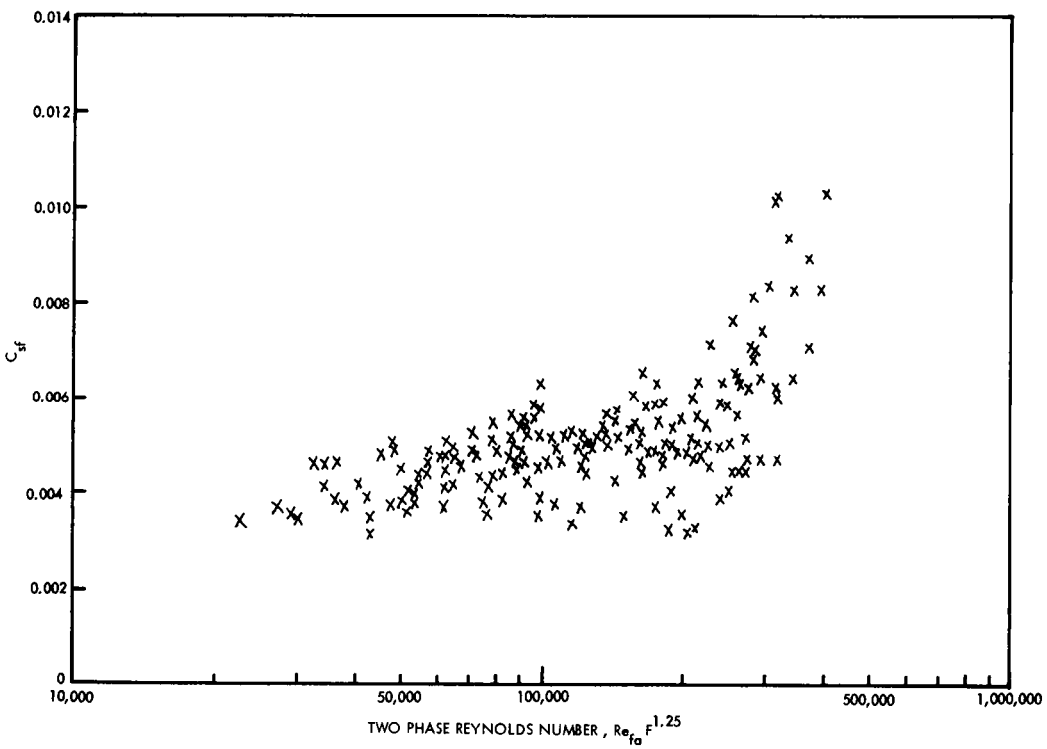


Figure IV-132. PLOT OF THE EXPERIMENTALLY DETERMINED C_{sf} VALUES VERSUS THE TWO-PHASE REYNOLDS NUMBER USING $F=(\Phi_{ftt})^{0.89}$. T≈100°F.

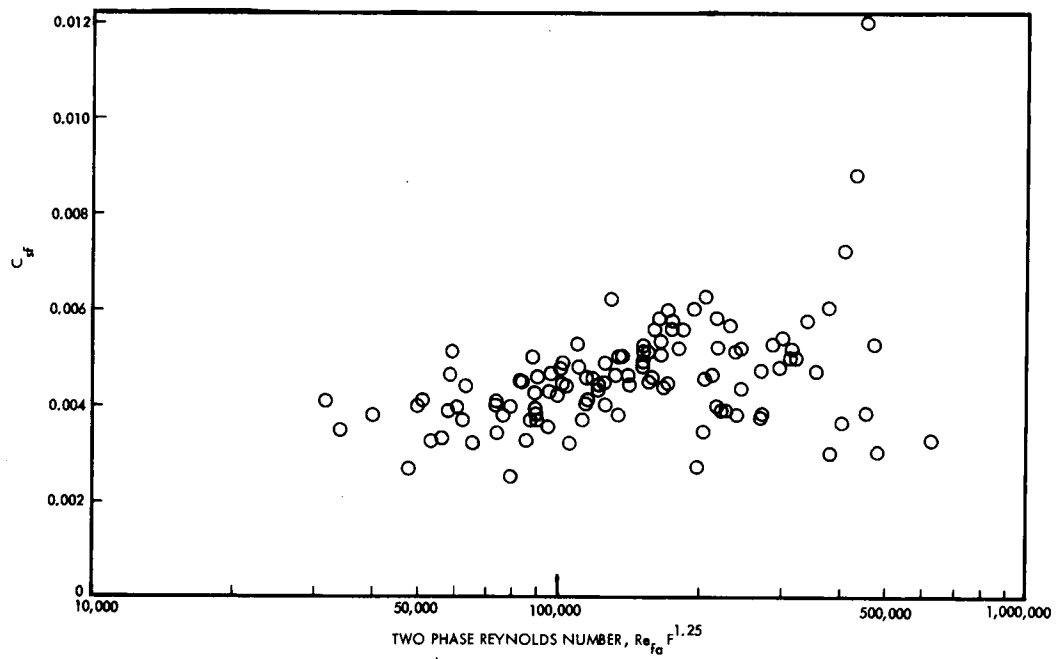


Figure IV-133. PLOT OF THE EXPERIMENTALLY DETERMINED C_{sf} VALUES VERSUS THE TWO-PHASE REYNOLDS NUMBER USING $F = (\Phi_{ftt})^{0.89}$. $T \approx 150°F$.

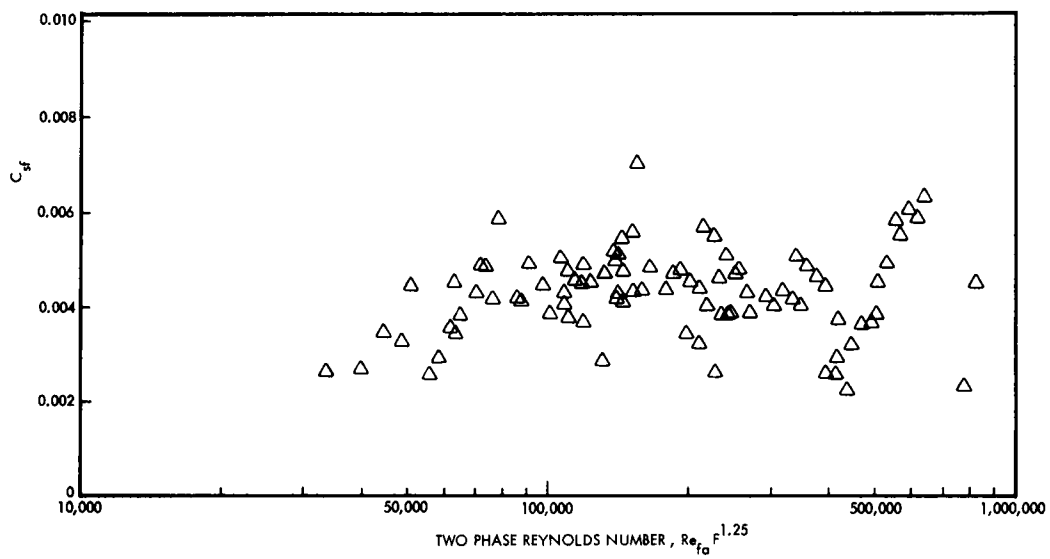


Figure IV-134. PLOT OF THE EXPERIMENTALLY DETERMINED C_{sf} VALUES VERSUS THE TWO-PHASE REYNOLDS NUMBER USING $F = (\Phi_{ftt})^{0.89}$. $T \approx 200°F$.

and thus, this equation differs little from Equation (4-19). In Equation (2-28), the Martinelli-Nelson [4] void fraction was used while in Equation (4-19) the modified Zuber et al [10] void fraction formulation was utilized. The differences between the two were shown in Figure II-46 on page 183. This result seems to reinforce the conclusion reached in the discussion on two-phase pressure drop, namely that the range of applicability of the Zuber et al [10] void fraction correlation is in question. For the present, however, Equation (4-23) will be used for F.

Application of a Different Pool Boiling Term to the Chen [80] Correlation. In a previous section, it was shown that the Forster-Zuber [52] pool boiling correlation with a variable coefficient, and the Rohsenow [61] equation were better at correlating the meager amount of data on the pool boiling of refrigerants than most of the other correlations attempted. By a trial-and-error method, it is found that the use of the coefficient 0.3802 rather than the value of 0.172 as originally recommended by Forster and Zuber [52] gives a satisfactory correlation with the experimental data of this study. The pool boiling data obtained at ORGDP for R-114 boiling on a copper surface yielded a coefficient of 0.326. This is 14% lower than the coefficient obtained in this study. A sizeable portion of the difference can probably be attributed to variations in the finish of the copper surfaces. Using the prefix 0.3802 in Equation (2-48), experimental suppression factor curves can be generated. These experimental curves are shown in Figures IV-135 to IV-137.

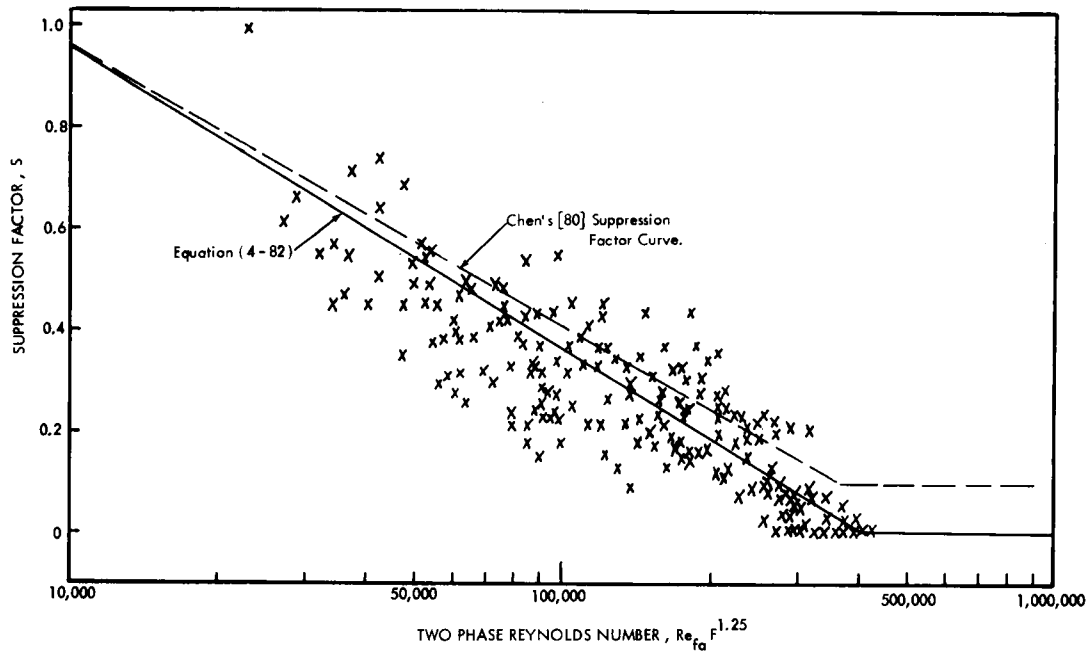


Figure IV-135. PLOT OF THE EXPERIMENTALLY DETERMINED SUPPRESSION FACTOR VERSUS THE TWO-PHASE REYNOLDS NUMBER USING THE FORSTER-ZUBER [52] POOL BOILING CORRELATION WITH A 0.3802 COEFFICIENT. T ≈ 100°F.

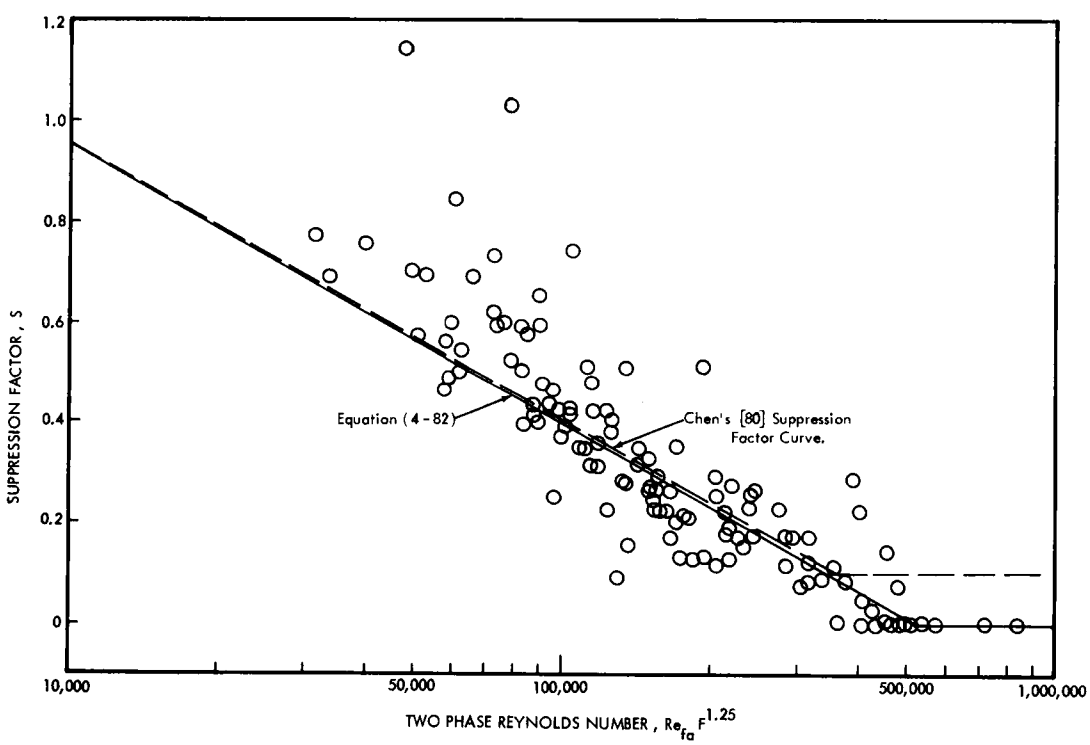


Figure IV-136. PLOT OF THE EXPERIMENTALLY DETERMINED SUPPRESSION FACTOR VERSUS THE TWO-PHASE REYNOLDS NUMBER USING THE FORSTER-ZUBER [52] POOL BOILING CORRELATION WITH A 0.3802 COEFFICIENT. T≈150°F.

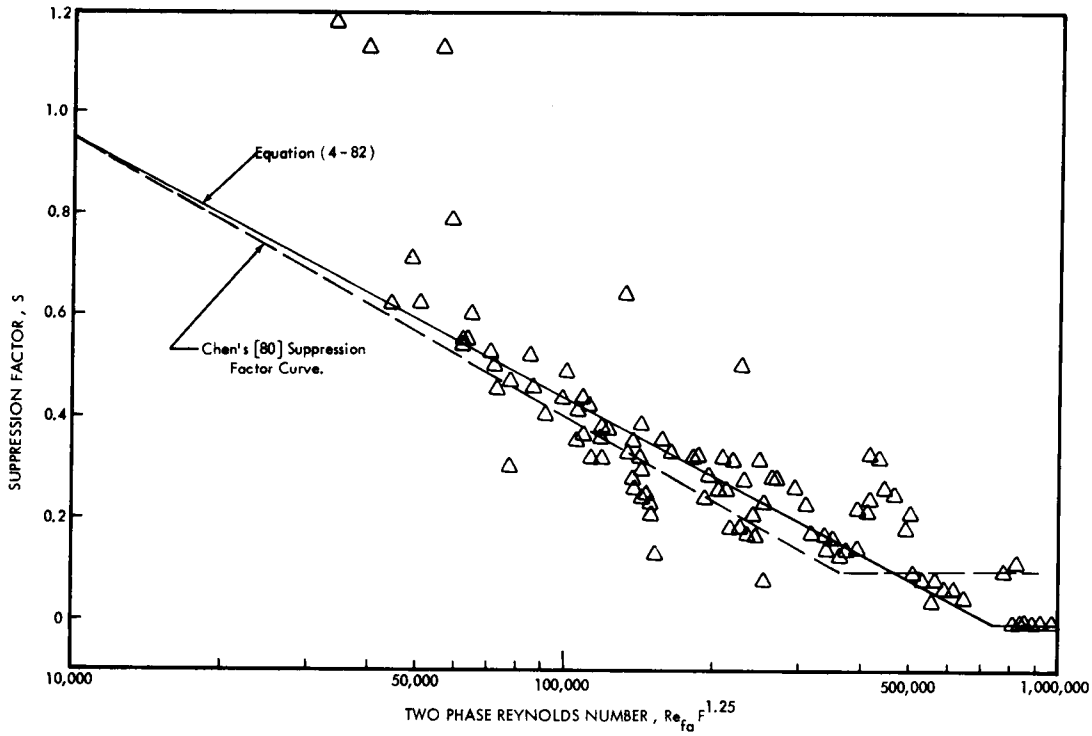


Figure IV-137. PLOT OF THE EXPERIMENTALLY DETERMINED SUPPRESSION FACTOR VERSUS THE TWO-PHASE REYNOLDS NUMBER USING THE FORSTER-ZUBER [52] POOL BOILING CORRELATION WITH A 0.3802 COEFFICIENT. T≈ 200°F.

As can be seen, there is a temperature effect on the suppression factor. For example, at 100°F, total suppression is obtained at a two-phase Reynolds number of 405,000. At 150°F, it occurs at 525,000 and at 200°F total suppression is not obtained until a two-phase Reynolds number of 735,000 is reached. It was found that a good fit to the suppression factor curves could be obtained with the following equation:

$$S = -0.2074\ (P_r)^{-0.0899}\ \ln\ (Re_{fa}F^{1.25}) + 2.85568\ (P_r)^{-0.06203} \quad (4\text{-}82)$$

where P_r is the reduced pressure and ln is the natural logarithm. If this equation yields a suppression factor greater than one, it should be set equal to one. Similarly, if this equation yields a negative

suppression factor, it should be set equal to zero. It can be noted that the suppression factor curve obtained here is a function of the reduced pressure. Chen [80] did not report any effect of boiling temperature or pressure on his suppression factor results. When one notes that the data he analyzed were at relatively low reduced pressures (less than 0.04 in all cases except Schrock and Grossman's [82] water results which went as high as 0.158), this is understandable. The experimental suppression factor curve obtained in this study for the 150°F boiling runs is seen to agree very well with Chen's [80] S curve in all ranges except the very high two-phase Reynolds number region. Here, the S curve obtained goes to zero while that of Chen [80] remains at about 0.1 up to a two-phase Reynolds number of about 900,000. The trend observed here of a higher S curve with increasing temperature is not totally unexpected. The analytically derived S curves obtained in a previous section for the steady state solution and shown in Figure IV-122 on page 303, while they did not predict the suppression factor well, did show higher S curves with increasing boiling temperature. The Chen [80] correlation with the prefix 0.3802 for the Forster-Zuber [52] pool boiling term and the suppression factor curves represented by Equation (4-82) were compared with the experimental heat transfer coefficients obtained in this study. The results are shown in Figures IV-138 to IV-140. Agreement is quite good in all temperature ranges and flow ranges except for the case of $G \simeq 3.5 \times 10^6$ lbm/hr-sq ft, the highest flow rate tested. Here the modified Chen [80] correlation overpredicted the experimentally measured heat transfer coefficient. These runs all occurred at sufficiently high two-phase Reynolds numbers so that the

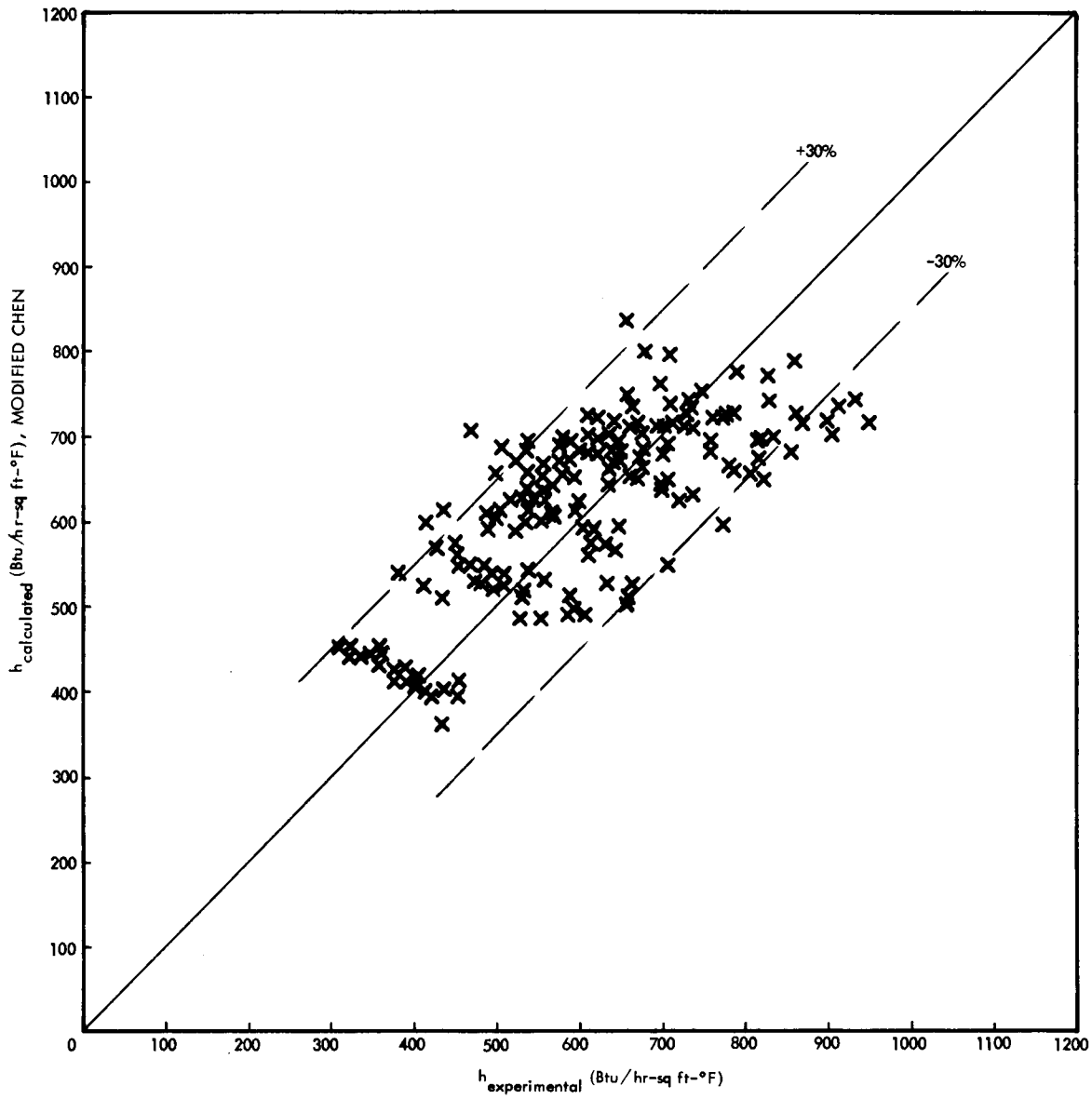


Figure IV-138. COMPARISON OF THE EXPERIMENTAL HEAT TRANSFER COEFFICIENTS WITH A MODIFIED FORM OF THE CHEN [80] CORRELATION USING THE FORSTER-ZUBER [52] POOL BOILING EQUATION WITH A 0.3802 COEFFICIENT. T ≈ 100°F.

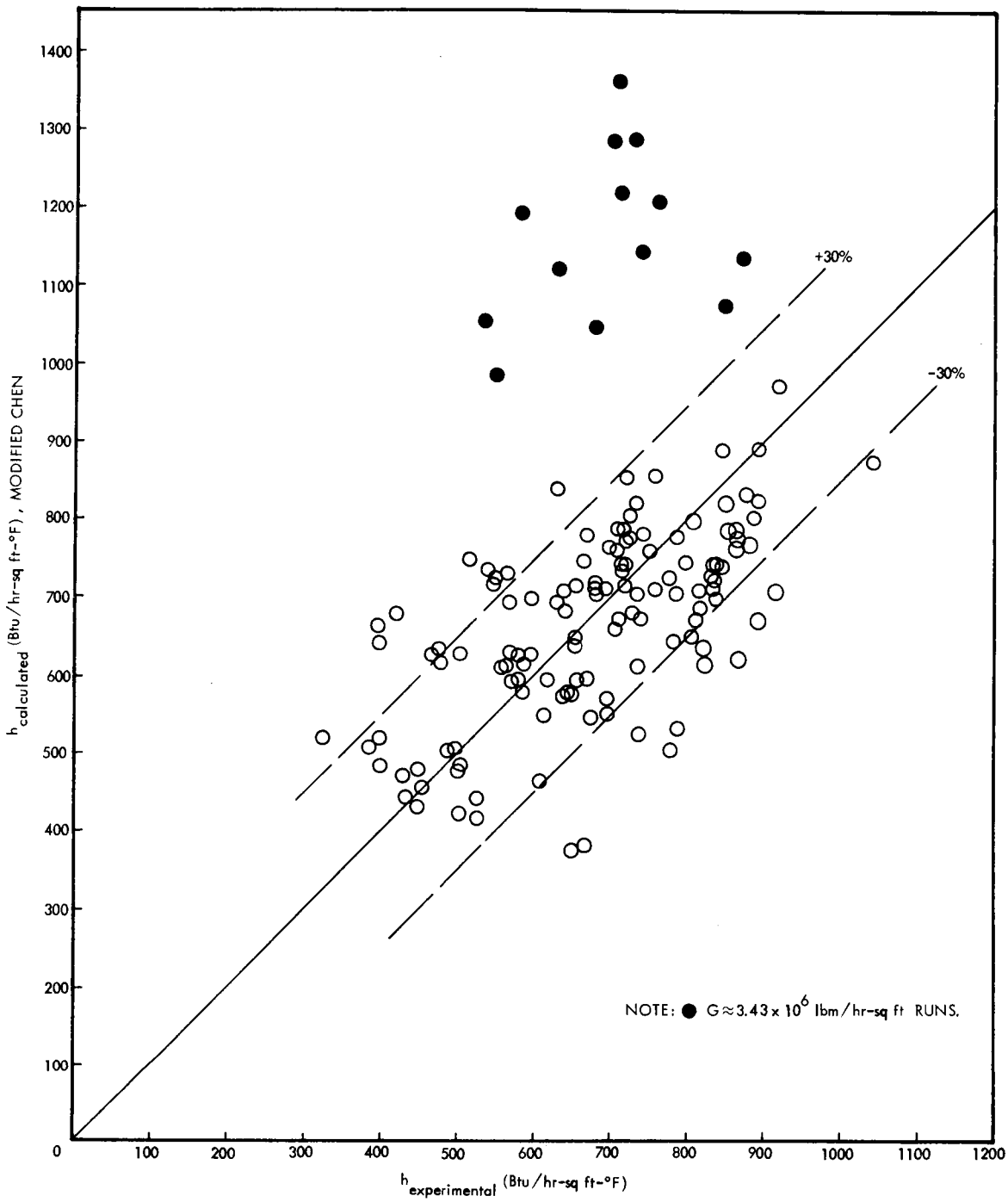


Figure IV-139. COMPARISON OF THE EXPERIMENTAL HEAT TRANSFER COEFFICIENTS WITH A MODIFIED FORM OF THE CHEN [80] CORRELATION USING THE FORSTER-ZUBER [52] POOL BOILING EQUATION WITH A 0.3802 COEFFICIENT. T≈150°F.

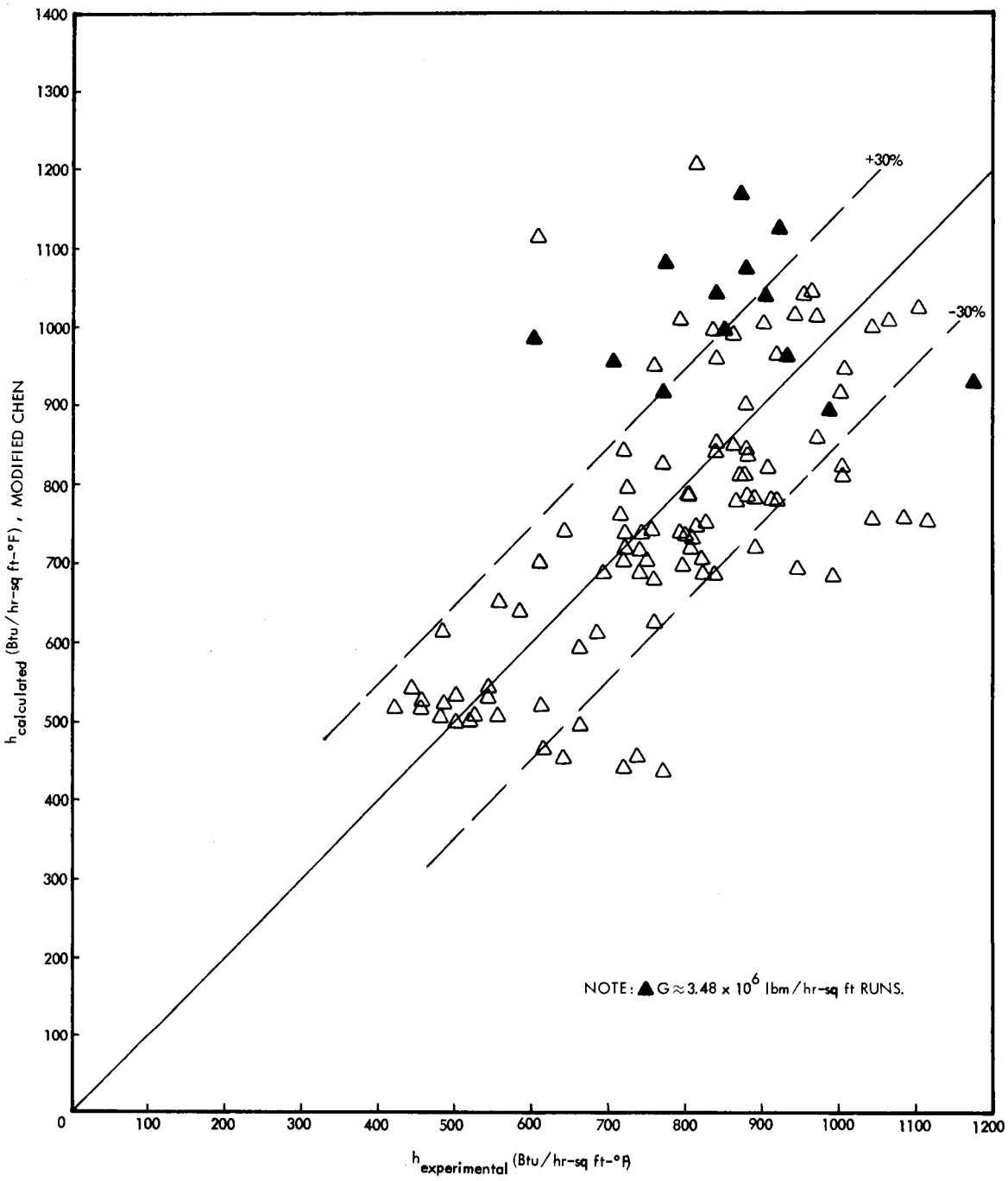


Figure IV-140. COMPARISON OF THE EXPERIMENTAL HEAT TRANSFER COEFFICIENTS WITH A MODIFIED FORM OF THE CHEN [80] CORRELATION USING THE FORSTER-ZUBER [52] POOL BOILING EQUATION WITH A 0.3802 COEFFICIENT. T ≈ 200°F.

pool boiling component was totally suppressed. Also, the qualities were, in all cases, below 0.10. From the flow regime studies made, it is not believed that annular flow existed. Therefore, the F term used here may not have been applicable since the wall was not completely covered with liquid as it was in annular flow. For the runs at mass fluxes of approximately 1.7 x 10^6 lbm/hr-sq ft and less, the modified Chen [80] correlation was applicable. The results in Figures IV-138 to IV-140 indicate that at a boiling temperature of 100°F, 91% of the data lie between ± 30% of the correlation. At 150°F, 83% of the data lie between ± 30% and at 200°F, 80% of the data lie between ± 30%.

From an application of the Rohsenow [61] pool boiling equation in the previous section to determine the best value of the multiplication factor F, it can be seen that a C_{sf} of 0.0047 satisfactory represents the data (see Figures IV-132 to IV-134 on pages 323 and 324). This compares well with the 0.00481 value which correlated the ORGDP data for the pool boiling of R-114 on a copper surface (see Table IV-2 on page 276). Using the 0.0047 value, experimental suppression factor curves were obtained and they are shown in Figures IV-141 to IV-143. These compare favorably with the experimental S curves obtained using the Forster-Zuber [52] pool boiling equation and are well represented by Equation (4-82). Using Equation (4-82) for S, and a C_{sf} of 0.0047, calculated values for the heat transfer coefficient can be obtained. Plots of the calculated vs. the experimental heat transfer coefficients for the 100, 150, and 200°F boiling temperatures are shown in Figures IV-144 to IV-146. Again, this correlation predicted the experimental results well, but with more scatter than in the cases where the Forster-Zuber [52] equation was used. At 100°F,

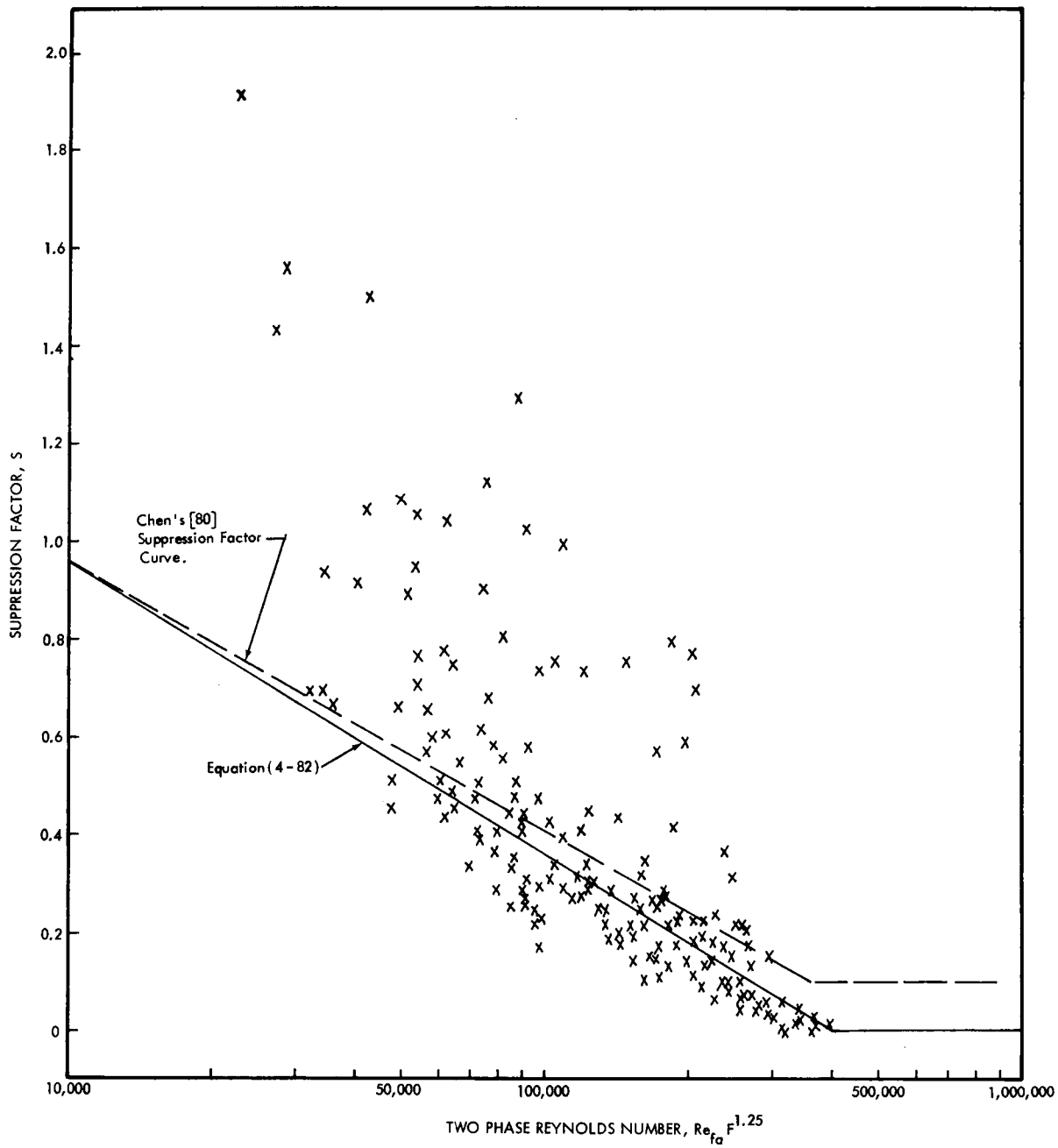


Figure IV-141. PLOT OF EXPERIMENTALLY DETERMINED SUPPRESSION FACTOR VERSUS TWO-PHASE REYNOLDS NUMBER USING THE ROHSENOW [61] POOL BOILING CORRELATION WITH $C_{sf} = 0.0047$. $T \approx 100°F$.

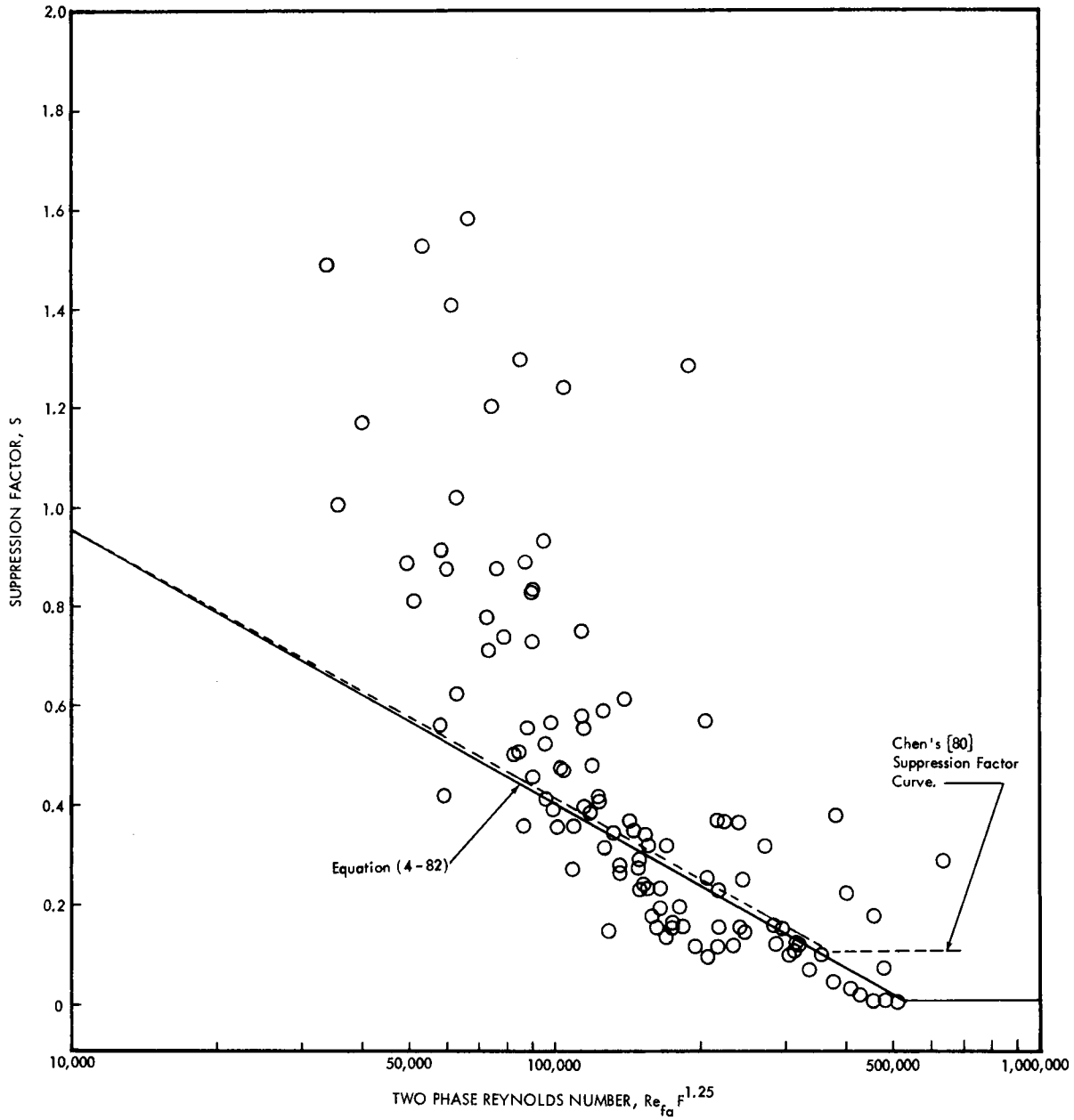


Figure IV-142. PLOT OF EXPERIMENTALLY DETERMINED SUPPRESSION FACTOR VERSUS TWO-PHASE REYNOLDS NUMBER USING THE ROHSENOW [61] POOL BOILING CORRELATION WITH $C_{sf} = 0.0047$. $T \approx 150°F$.

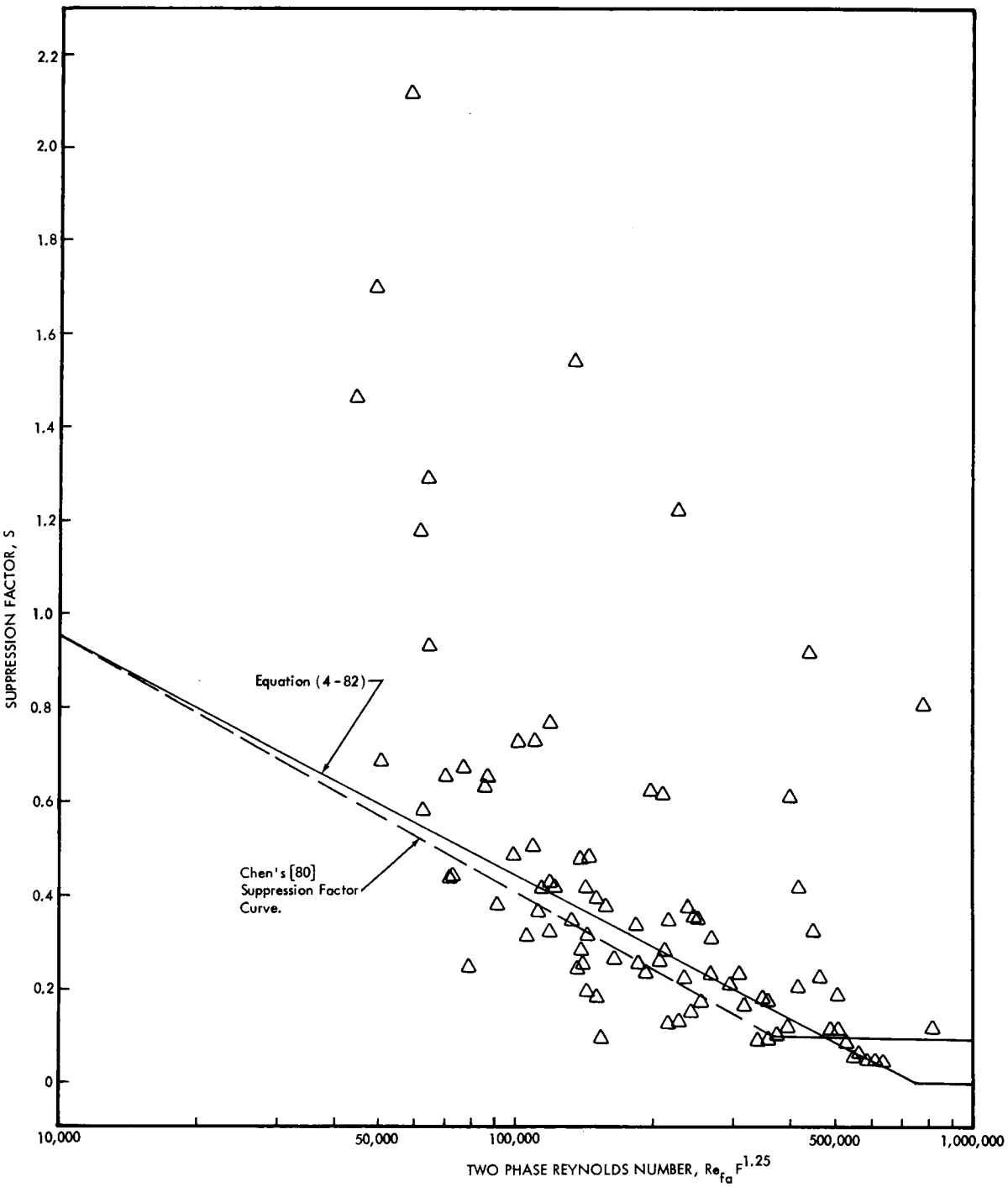


Figure IV-143. PLOT OF EXPERIMENTALLY DETERMINED SUPPRESSION FACTOR VERSUS TWO-PHASE REYNOLDS NUMBER USING THE ROHSENOW [61] POOL BOILING CORRELATION WITH $C_{sf} = 0.0047$. $T \approx 200°F$.

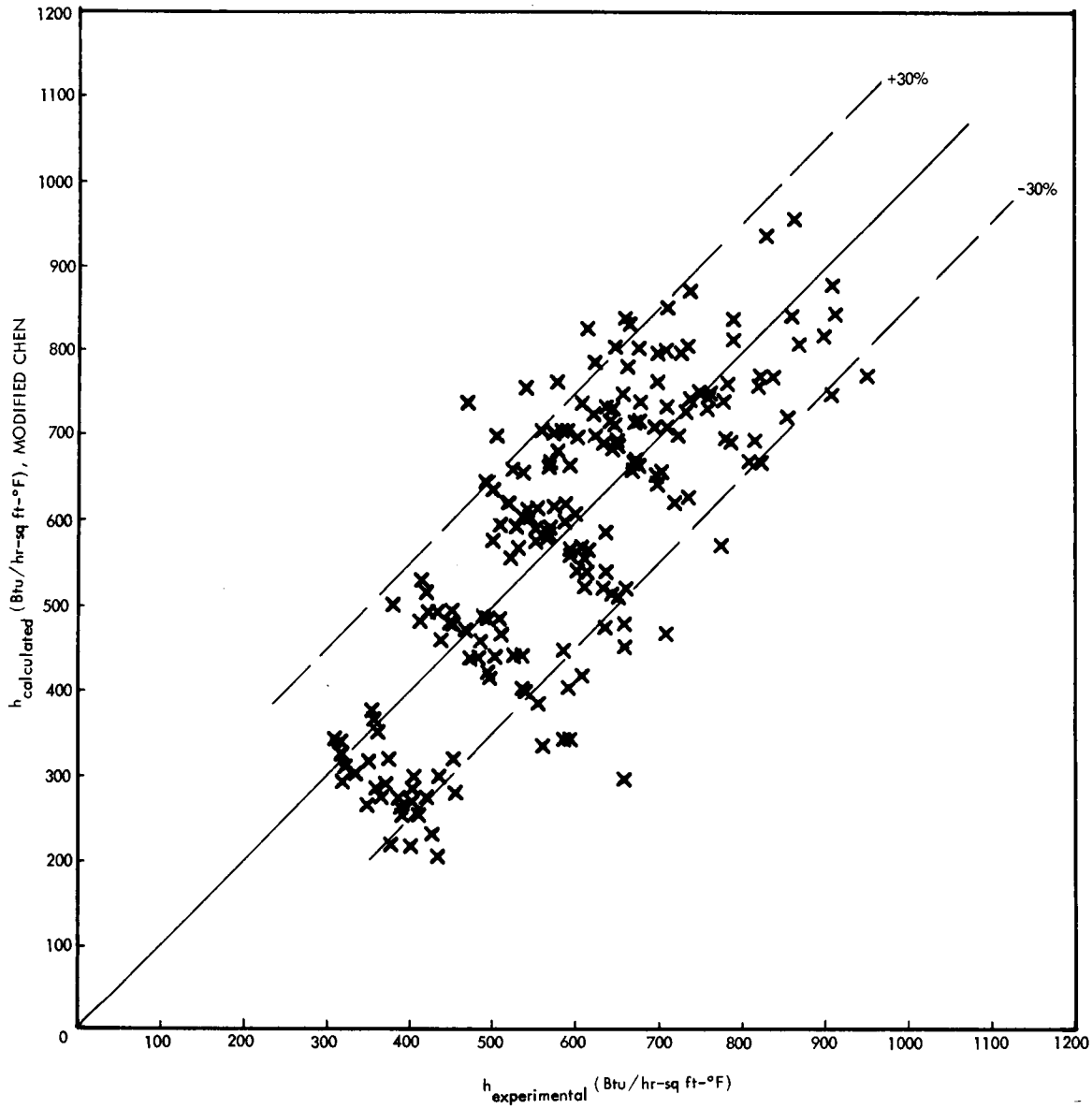


Figure IV-144. COMPARISON OF THE EXPERIMENTAL HEAT TRANSFER COEFFICIENTS WITH A MODIFIED FORM OF THE CHEN [80] CORRELATION USING THE ROHSENOW [61] POOL BOILING EQUATION WITH $C_{sf} = 0.0047$. $T \approx 100°F$.

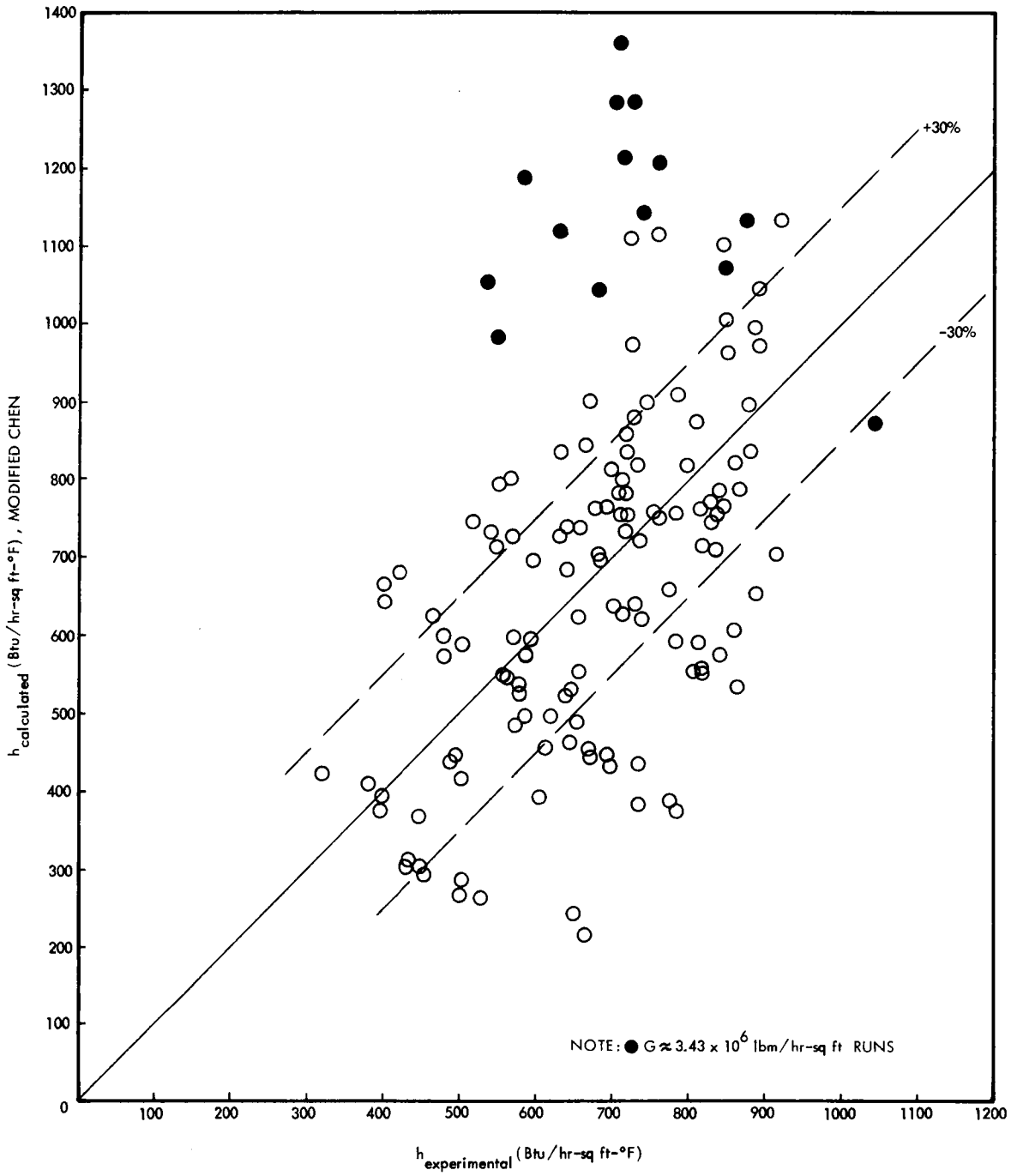


Figure IV-145. COMPARISON OF THE EXPERIMENTAL HEAT TRANSFER COEFFICIENTS WITH A MODIFIED FORM OF THE CHEN [80] CORRELATION USING THE ROHSENOW [61] POOL BOILING EQUATION WITH $C_{sf} = 0.0047$. $T \approx 150°F$.

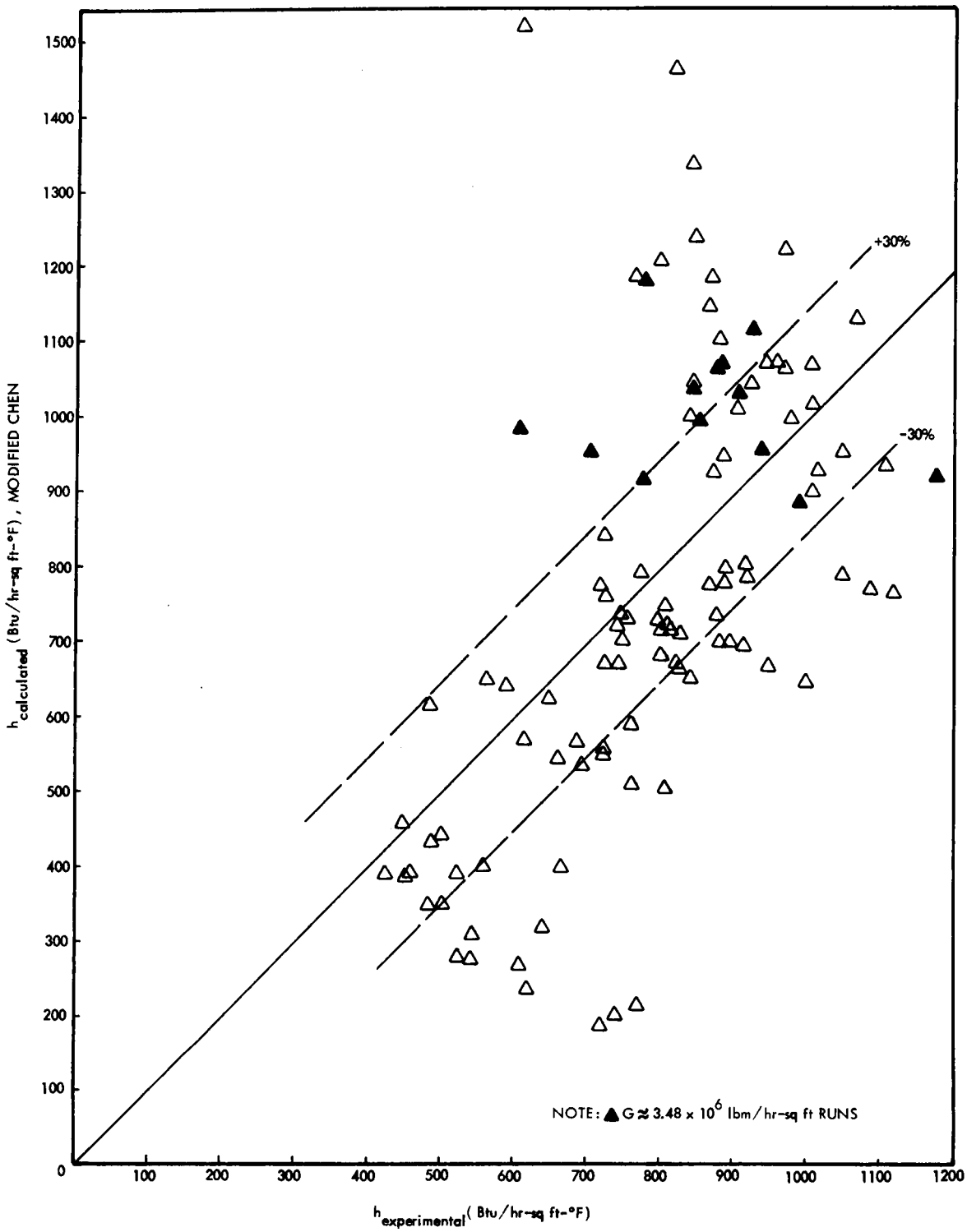


Figure IV-146. COMPARISON OF THE EXPERIMENTAL HEAT TRANSFER COEFFICIENTS WITH A MODIFIED FORM OF THE CHEN [80] CORRELATION USING THE ROHSENOW [61] POOL BOILING EQUATION WITH $C_{sf} = 0.0047$. $T \approx 200°F$.

87% of the data lay within ± 30%. At 150 and 200°F, only 60% lay within ± 30%.

In summary, it can be said that a modification of the Chen [80] correlation results in an improvement in predicting the heat transfer coefficient in annular flow. The major part of the improvement is obtained by modifying the coefficient in the Forster-Zuber [52] pool boiling component or by using the Rohsenow [61] pool boiling equation which already has a variable C_{sf} value for a prefix. The equations recommended for R-114 boiling in a vertical copper tube are:

$$h_{TP} = 0.023\ (Re)_{fa}^{0.8}\ (Pr)_{f}^{0.4}\ \left(\frac{k_f}{D}\right) F + 0.3802 \left(\frac{k_f^{0.79}\ c_{pf}^{0.45}\ \rho_f^{0.49}}{h_{fg}^{0.24}\ \rho_g^{0.24}\ \sigma^{0.5}\ \mu_f^{0.29}} \right) (\Delta T)^{0.24}\ (\Delta P)^{0.75}\ S \qquad (4\text{-}83)$$

or:

$$h_{TP} = 0.023\ (Re)_{fa}^{0.8}\ (Pr)_{f}^{0.4}\ \left(\frac{k_f}{D}\right) F + \left(\frac{k_f^{5.1}\ (\Delta\rho)^{0.5}\ g^{0.5}}{(0.0047)^3\ c_{pf}^{2.1}\ \mu_f^{4.1}\ \sigma^{0.5}\ h_{fg}^{2}\ g_c^{0.5}} \right) (\Delta T)^2\ S \qquad (4\text{-}84)$$

The coefficient in the Forster-Zuber [52] pool boiling correlation and the C_{sf} value used here were close to the values measured from an independent test of pool boiling R-114 from a copper surface. In addition, the use of Equations (4-23) for the multiplication factor F and (4-82) for the suppression factor S is recommended. The use of the Forster-Zuber [52] pool boiling correlation with the coefficient 0.3802 yielded less scatter in the correlation of the experimental results and

the error analysis in Appendix G explains why. More experimental data is needed, however, before the question of which pool boiling component should be used can be settled with certainty.

One interesting sideline of the correlation obtained above deals with the change in the boiling heat transfer coefficient along the length of the tube. Bennett et al's [79] correlation given in Equation (2-61), as well as much of the data on water indicates that the heat transfer coefficient increases along the length of the tube. Some refrigerant boiling studies such as those of Purcupile, Riedle, and Schmidt [94], Gouse and Coumou [91], and Gouse and Dickson [93] show the same trend. Johnston and Chaddock [41], Chaddock and Noerager [43], and Chawla [29] indicate that the heat transfer coefficient increases along the length of the tube at high mass fluxes, but may decrease at the lower flows. This is best illustrated in Figure 11a of Chawla's [29] publication. The results of the present study indicate that the heat transfer coefficient decreases along the length of the tube in all cases. To study this question a little more clearly, the Chen [80] correlation with the Forster-Zuber [52] pool boiling term as modified here, will be investigated. Using:

$$h_{TP} = 0.023 \left(\frac{GD(1-x)}{\mu_f}\right)^{0.8} (Pr)_f^{0.4} \left(\frac{k_f}{D}\right) F + C_5 \left(\frac{k_f^{0.79}\, c_{pf}^{0.45}\, \rho_f^{0.49}}{h_{fg}^{0.24}\, \rho_g^{0.24}\, \sigma^{0.5}\, \mu_f^{0.29}}\right) (\Delta T)^{0.24}\, (\Delta P)^{0.75}\, S \qquad (4\text{-}85)$$

where C_5 is the coefficient appropriate for the given fluid surface combination. Combining some of the fluid properties, dimensions, and constants to simplify the equation yields:

$$h_{TP} = C_6(1-x)^{0.8}\ F + C_7(\Delta T)^{0.24}\ (\Delta P)^{0.75}\ S. \qquad (4\text{-}86)$$

Applying the Clausius-Clapeyron relationship:

$$\frac{\Delta P}{\Delta T} \approx \frac{h_{fg} J}{T_{sat}\ v_{fg}} \qquad (4\text{-}87)$$

yields:

$$h_{TP} = C_6(1-x)^{0.8}\ F + C_8(\Delta T)^{0.99}\ S. \qquad (4\text{-}88)$$

Differentiating this with respect to x; since x changes along the length of the tube and remembering that C_6 and C_8 are positive numbers:

$$\frac{\partial h_{TP}}{\partial x} = -0.8\ C_6(1-x)^{-0.2}\ F + C_6(1-x)^{0.8}\ \frac{\partial F}{\partial x}$$

$$+ 0.99\ C_8 S(\Delta T)^{-0.01}\ \frac{\partial(\Delta T)}{\partial x} + C_8(\Delta T)^{0.99}\ \frac{\partial S}{\partial x}. \qquad (4\text{-}89)$$

From Newton's law of cooling, for a constant heat flux:

$$\frac{\partial h_{TP}}{\partial x} = -\frac{(q/A)\ \frac{\partial(\Delta T)}{\partial x}}{(\Delta T)^2}. \qquad (4\text{-}90)$$

Combining Equations (4-89) and (4-90) and rearranging:

$$\frac{\partial(\Delta T)}{\partial x}\left(-\frac{(q/A)}{(\Delta T)^2} - \frac{0.99\ C_8 S}{(\Delta T)^{0.01}}\right) = C_6(1-x)^{0.8}\left\{\frac{\partial F}{\partial x} - \frac{0.8F}{(1-x)}\right\}$$

$$+ C_8(\Delta T)^{0.99}\ \frac{\partial S}{\partial x}. \qquad (4\text{-}91)$$

Using Equation (4-82) for S, differentiating and plugging into equation (4-91):

$$\frac{\partial(\Delta T)}{\partial x}\left(-\frac{(q/A)}{(\Delta T)^2} - \frac{0.99\ C_8 S}{(\Delta T)^{0.01}}\right) = \frac{1}{F}\left(\frac{\partial F}{\partial x} - \frac{0.8F}{(1-x)}\right)\left\{C_6(1-x)^{0.8}\ F - 0.25925\right.$$

$$\left.(P_r)^{-0.0899}\ C_8(\Delta T)^{0.99}\right\}. \qquad (4\text{-}92)$$

A simple hand calculation can show that $\partial F/\partial x$ is always greater than $0.8F/(1-x)$. Now, if the term $C_6(1-x)^{0.8}\ F - 0.25925\ (P_r)^{-0.0899}$

$C_8(\Delta T)^{0.99}$ is positive, then $\partial(\Delta T)/\partial x$ is negative and h_{TP} increases along the length of a tube. If it is negative, then h_{TP} decreases along the length of the tube.

Looking for example, at Run 398-3 (see Appendix F), for this case:

$$C_6(1-x)^{0.8} F = 87.37 \text{ Btu/hr-sq ft-}^{\circ}\text{F}$$

and

$$0.25925 (P_r)^{-0.0899} C_8(\Delta T)^{0.99} = 152.08 \text{ Btu/hr-sq ft-}^{\circ}\text{F}.$$

Thus, the term: $C_6(1-x)^{0.8} F - 0.25925 (P_r)^{-0.0899} C_8(\Delta T)^{0.99}$ is negative and h_{TP} should decrease along the length of the tube. Looking now at a high flow rate run; Run 409.5:

$$C_6(1-x)^{0.8} F = 339.93 \text{ Btu/hr-sq ft-}^{\circ}\text{F}$$

and

$$0.25925 (P_r)^{-0.0899} C_8(\Delta T)^{0.99} = 409.34 \text{ Btu/hr-sq ft-}^{\circ}\text{F}.$$

Again, a decrease of h_{TP} with length is correctly predicted.

For the case of water, the situation is quite different. Looking at Sani's [131] data for downflow water, for Run 40, L = 1,

$$C_6(1-x)^{0.8} F = 4481.95 \text{ Btu/hr-sq ft-}^{\circ}\text{F}$$

and

$$0.25925 (P_r)^{-0.0899} C_8(\Delta T)^{0.99} = 422.80 \text{ Btu/hr-sq ft-}^{\circ}\text{F}.$$

An increase in h_{TP} with length is predicted and is indeed the case.

It should be noted that the expression $C_6(1-x)^{0.8} F - 0.25925 (P_r)^{-0.0899} C_8(\Delta T)^{0.99}$ is mass flux dependent. As the flow rate increases, $C_6(1-x)^{0.8} F$ increases, thereby making the expression more positive and tending to make $\partial(\Delta T)/\partial x$ negative in order to yield an h_{TP} that increases along the length of the tube.

Experimental Results - Other Studies, Vertical Tests

Only Allen [88] and Napadensky [15] presented convenient and sufficiently detailed heat transfer results to enable a correlation to be attempted. Allen [88] who boiled R-114 in a 3-ft long 3/4-in.-ID copper tube obtained heat transfer coefficients which were considerably higher than those measured in this study. An attempt to correlate these results using the modified Chen [80] correlation with the Forster-Zuber [52] pool boiling term was unsuccessful. The use of the Rohsenow [61] pool boiling equation with a C_{sf} of 0.0026 did yield a satisfactory correlation. A comparison of the calculated and experimental heat transfer coefficients is shown in Figure IV-147. Twelve of the 24 data points lay within ± 30% of the correlation. The C_{sf} value of 0.0026 was well below that predicted for pool boiling and the difference can be attributed only to markedly different surface characteristics or to experimental error. It is worth mentioning that additional unpublished data by Allen for boiling R-114 in a 16-ft long 0.258-in. by 0.450-in. rectangular aluminum channel yielded heat transfer coefficients of less than 725 Btu/hr-sq ft-°F in all cases.

An attempt was also made to correlate the results of Napadensky [15]. Use of the modified Chen [80] correlation with either pool boiling equations yielded considerable scatter in the results. It should be noted that Napadensky [15] took data at high flows only and no two-phase Reynolds numbers of less than 143,000 were encountered.

Experimental Results - Other Studies, Horizontal Tests

Bryan and Seigel [39], Johnston and Chaddock [41], and Chaddock and Noerager [43] were a few of the experimenters who presented heat transfer

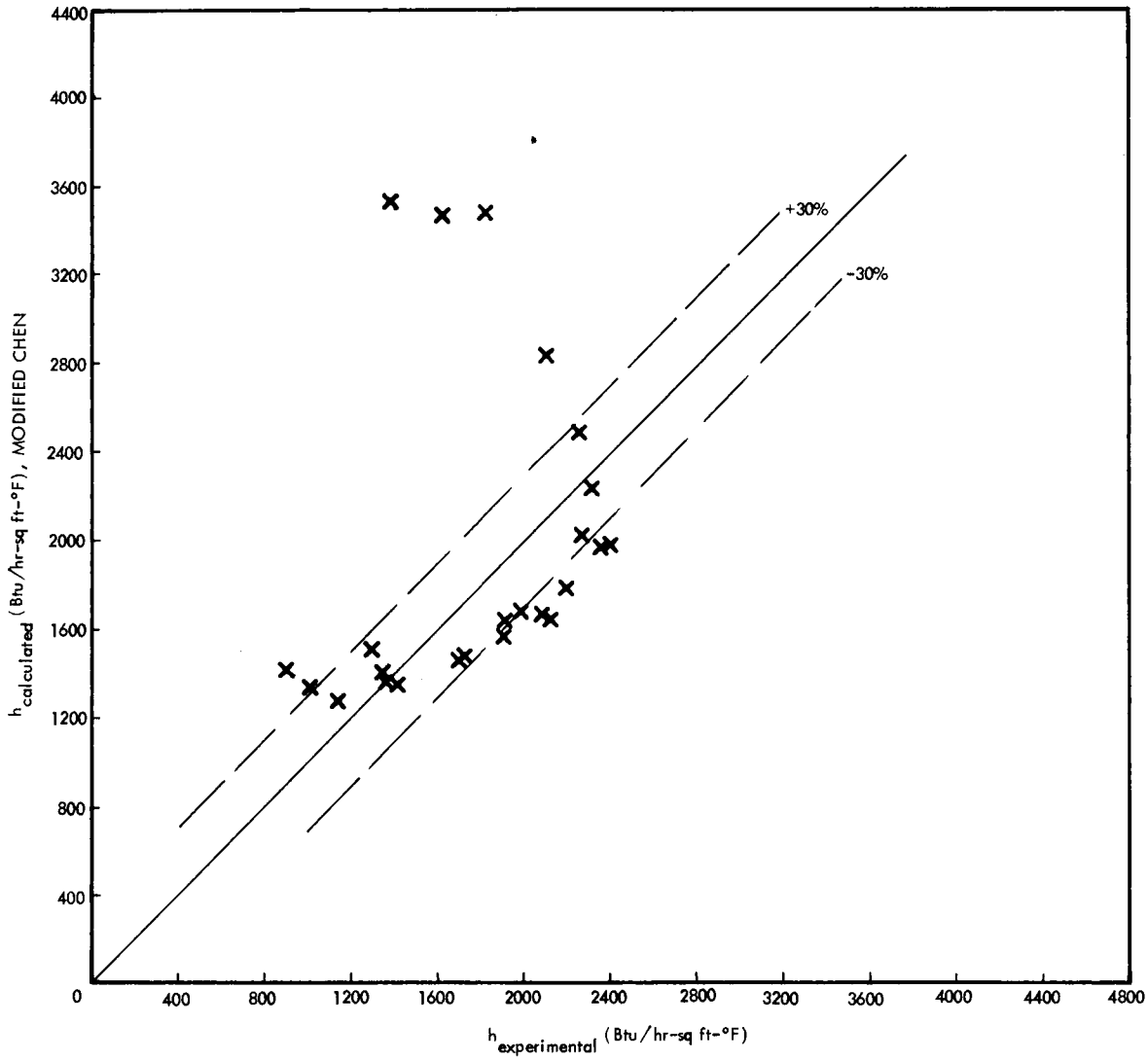


Figure IV-147. COMPARISON OF ALLEN'S [88] EXPERIMENTAL HEAT TRANSFER COEFFICIENTS FOR R-114 WITH A MODIFIED FORM OF THE CHEN [80] CORRELATION USING THE ROHSENOW [61] POOL BOILING EQUATION WITH C_{sf} = 0.0026. T≈160°F.

coefficients for boiling R-11, R-12, and R-22 in horizontal test sections. In this case, the problem is more complex than that encountered in vertical flow. Flow regime studies of boiling in horizontal tubes has shown that at sufficiently low flow rates, stratification can occur. Since this no longer leads to an annular type of flow and the wall of the tube is not completely covered with liquid, one of the basic hypotheses of the Chen [80] correlation is violated. It is this phenomena which is believed to be at least partially responsible for the discrepancies in some of the results obtained. While a detailed analysis of boiling in horizontal tubes is beyond the scope of this study, the results of Chaddock and Noerager [43] for R-12 will serve as an illustrative example. As shown in Figures IV-148 and IV-149, only at the higher flow rates is there reasonable agreement between experiment and correlation.

In summary, it should be noted that no completely satisfactory correlation existed in the literature to adequately predict the heat transfer coefficients of R-114 in a vertical tube. The Chen [80] correlation came the closest. Because of the success of this correlation in predicting the boiling coefficients of water and other fluids, each of its components was studied. It was found that while the multiplication factor F was satisfactory over a wide range of the Martinelli parameter X_{tt}, at very low qualities, an improvement could be obtained by using a slightly higher F curve. It was felt that F can be well represented over the entire quality range by the use of Equation (4-23). The greatest improvement in the correlation dealt with the pool boiling component. The pool boiling correlations in the literature generally underestimated the coefficients for refrigerants. The Forster-Zuber [52] and Rohsenow [61] equations were chosen as the two correlations

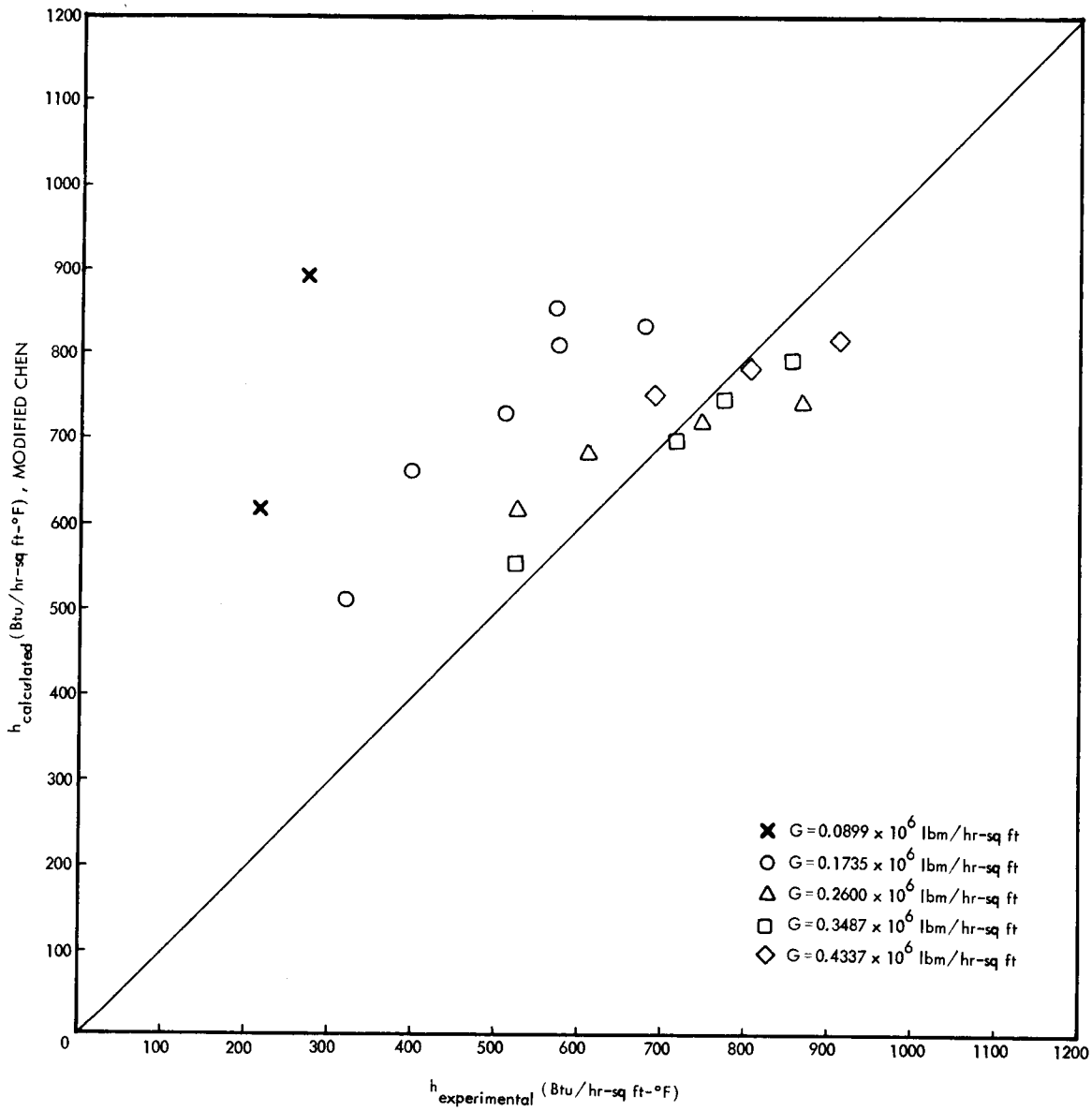


Figure IV-148. COMPARISON OF CHADDOCK AND NOERAGER'S [43] EXPERIMENTAL HEAT TRANSFER COEFFICIENTS FOR R-12 WITH A MODIFIED FORM OF THE CHEN [80] CORRELATION USING THE FORSTER-ZUBER [52] POOL BOILING EQUATION WITH A COEFFICIENT OF 0.292. T≈54°F.

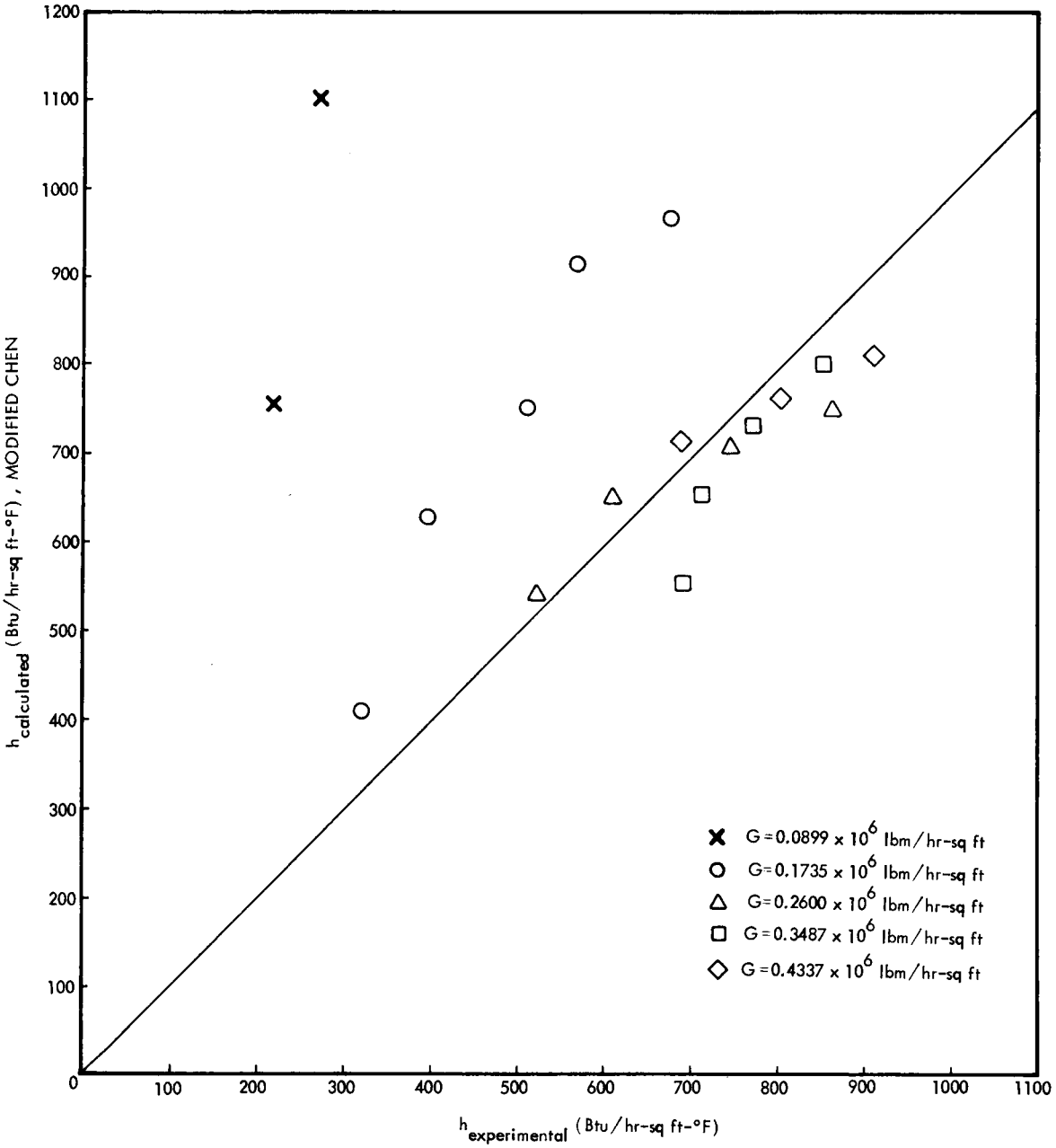


Figure IV-149. COMPARISON OF CHADDOCK AND NOERAGER'S [43] EXPERIMENTAL HEAT TRANSFER COEFFICIENTS FOR R-12 WITH A MODIFIED FORM OF THE CHEN [80] CORRELATION USING THE ROHSENOW [61] POOL BOILING EQUATION WITH $C_{sf} = 0.007$. $T \approx 54°F$.

performing most satisfactorily although some data were found which could not be properly correlated. Using Equations (4-83) or (4-84), most of the R-114 data obtained in this study were correlated quite satisfactorily. A modification in the S curve was necessary, mainly at high two-phase Reynolds numbers. In addition, the S curve was found to be dependent on pressure. Two analytical solutions were attempted for S. The steady state solution did not yield satisfactory results. A transient type of solutions which is believed to more realistically model the phenomena occurring was also attempted. The results, however, were inconclusive. This was due to the fact that this solution was dependent on the frequency of bubble departure in a forced flow system. Since information on this is quite scant at the present time, considerably more research in boiling is required before a theoretical basis for the suppression factor is obtained.

D. CRITICAL HEAT FLUX

Introduction

Critical heat flux data were taken in the range described in Chapter III, Section C. A total of 150 runs were obtained. While tests were conducted in both the natural and forced circulation modes, no differences in the results were noted and consequently, no differentiation between these two modes will be made. This is consistent with the findings for pressure drop and heat transfer coefficients.

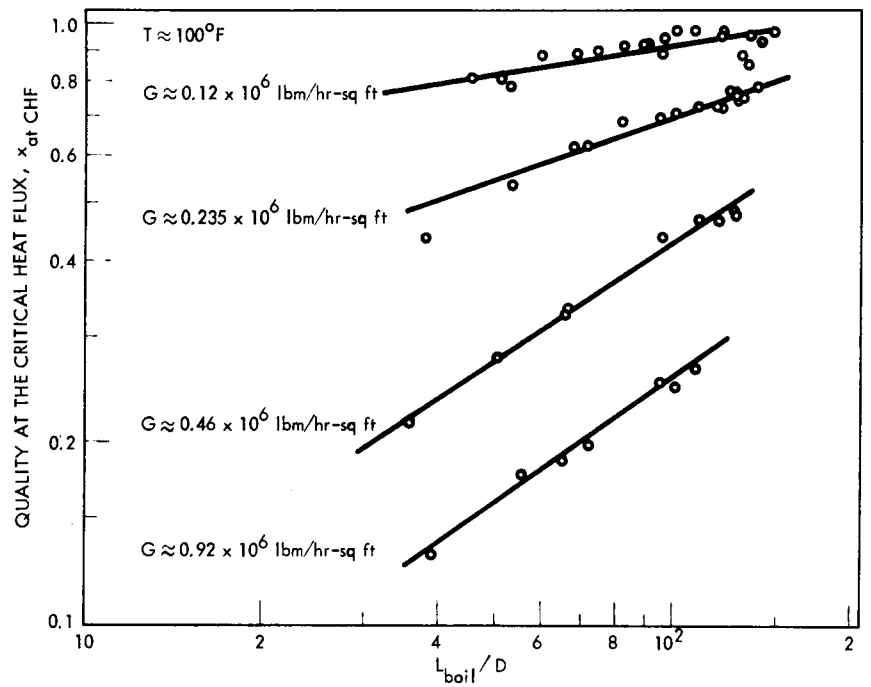
Experimental Results - This Study

As was described above, in all the runs conducted in this study, the fluid entering the tube was slightly subcooled. The degree of subcooling was, in all cases, quite small and the subcooled length was on

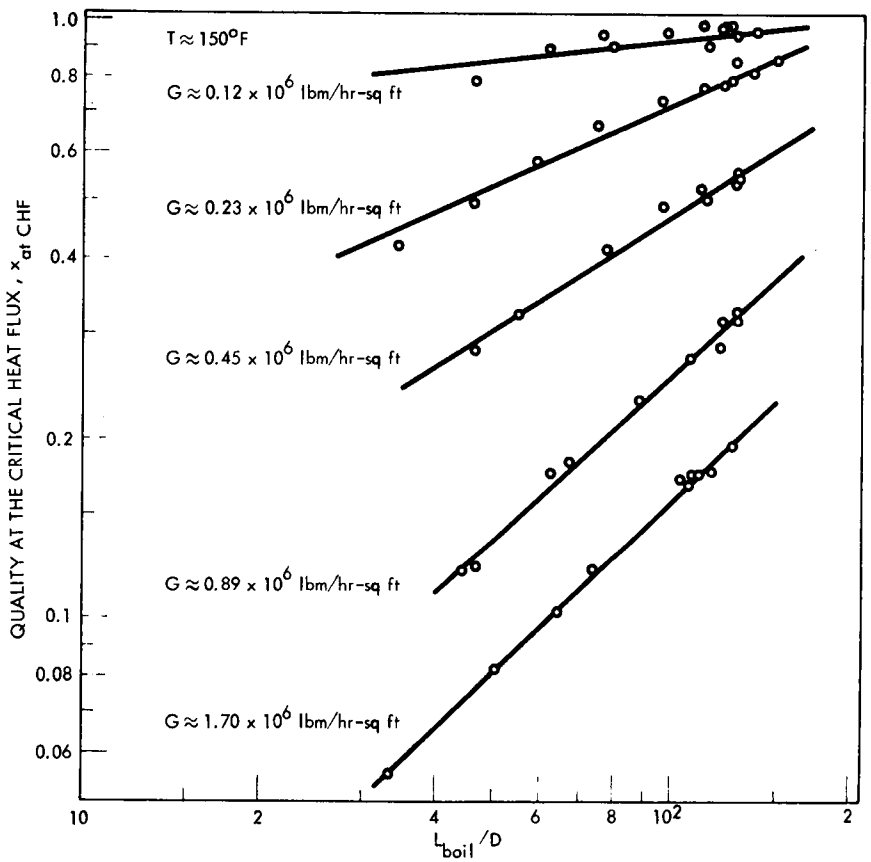
the order of several inches. This subcooled length was subtracted out and only the saturated length was considered. This technique of subtracting out the subcooled length was suggested by Staub [110] who was able to successfully use it to correlate his results. The tabulation of the results obtained in this study is given in Appendix F.

One of the most empirical ways of presenting critical heat flux information is in the form of graphs illustrating the effect of the L/D ratio, the mass flux, and the boiling temperature on the quality at which critical heat flux occurs. This is shown in Figures IV-150 and IV-151. In Figure IV-150 it can be seen that at a constant heat flux as the L/D ratio decreased, the critical heat flux occurred at a lower quality. Also, at a constant L/D ratio, the higher mass flux meant a lower quality at which critical heat flux occurred. The effect of the boiling temperature is best illustrated in Figure IV-151. There was little difference between the critical heat flux quality at the 100 and 150°F boiling temperatures. As the temperature increased, however, and the liquid to vapor density ratio decreased, the quality at which critical heat flux occurred decreased also. The critical heat flux corresponding to the qualities given in Figures IV-150 and IV-151 can be obtained from Equation (2-82).

The scaling law presented by Barnett and Wood [105] and given in Equation (2-80) enables one to compare the critical heat fluxes of two different fluids. In this case, by applying the scaling law, one is attempting to model the R-114 critical heat flux results obtained in this study by using water. In order to accomplish this, one must model each of the individual dimensionless groupings in Equation (2-80).

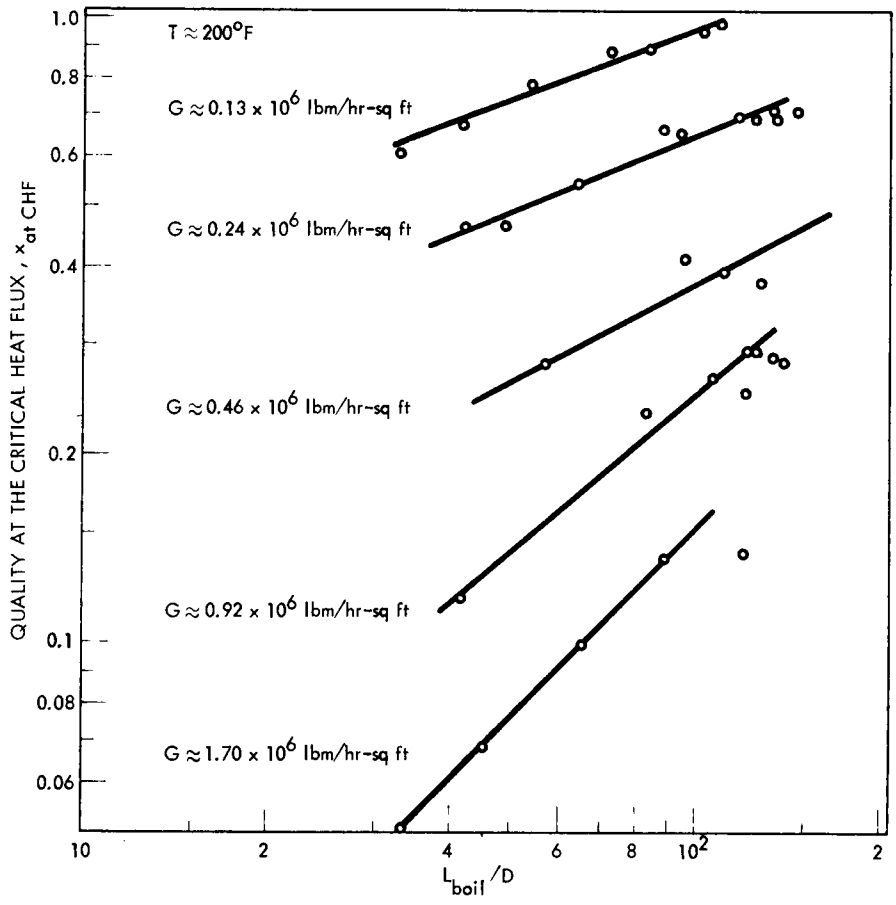


(a)

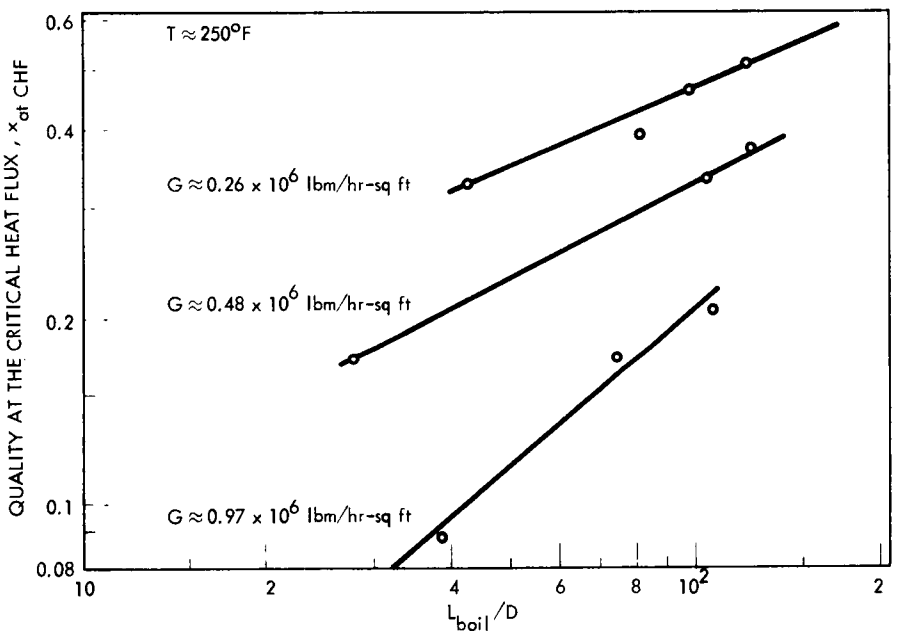


(b)

Figure IV-150. PLOT OF THE EXIT QUALITY AT WHICH THE CRITICAL HEAT FLUX OCCURS VERSUS THE L/D RATIO FOR VARIOUS MASS FLUXES.



(c)



(d)

Figure IV - 150. (continued)

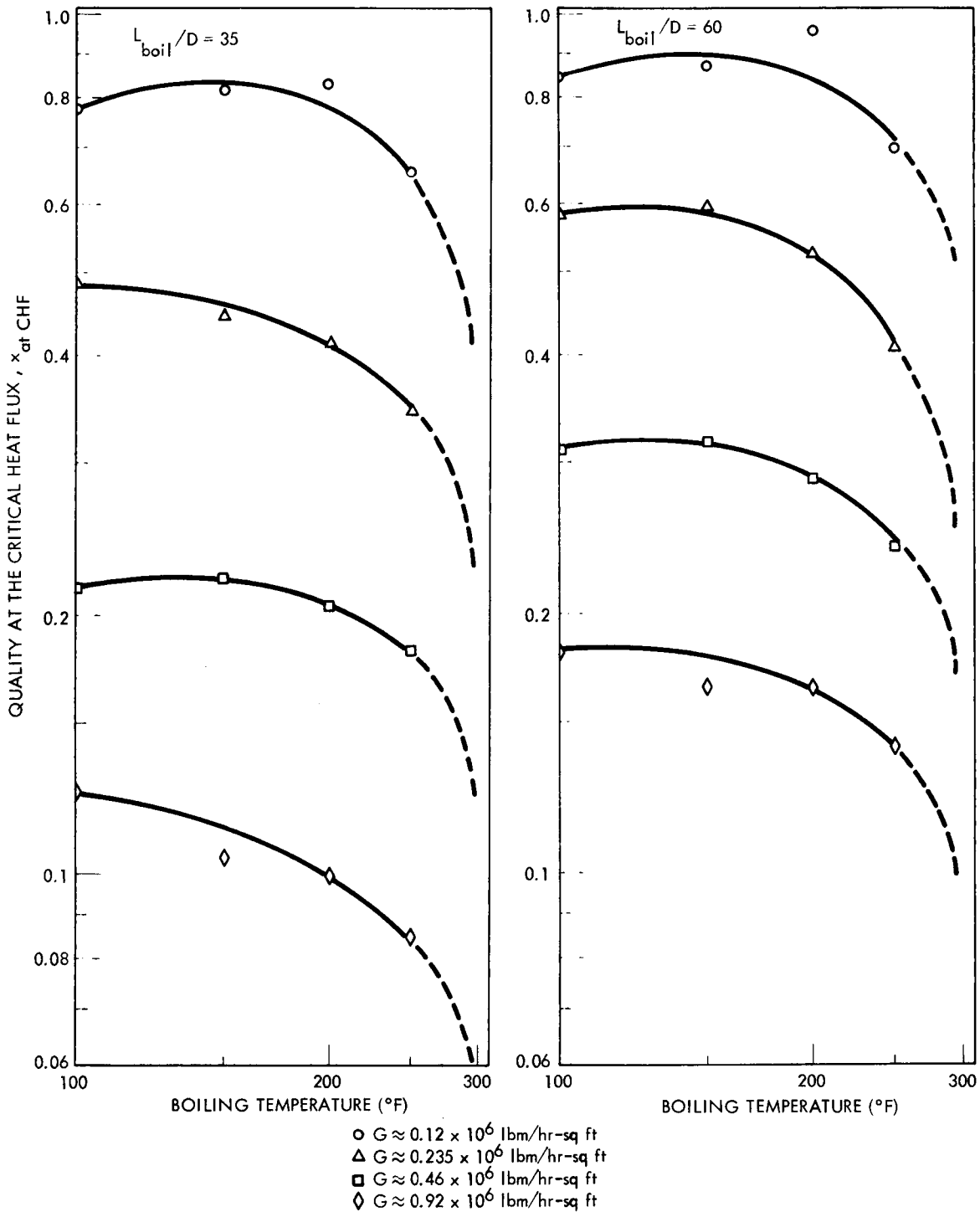


Figure IV-151. PLOT OF THE EXIT QUALITY AT WHICH THE CRITICAL HEAT FLUX OCCURS VERSUS THE BOILING TEMPERATURE FOR VARIOUS MASS FLUXES.

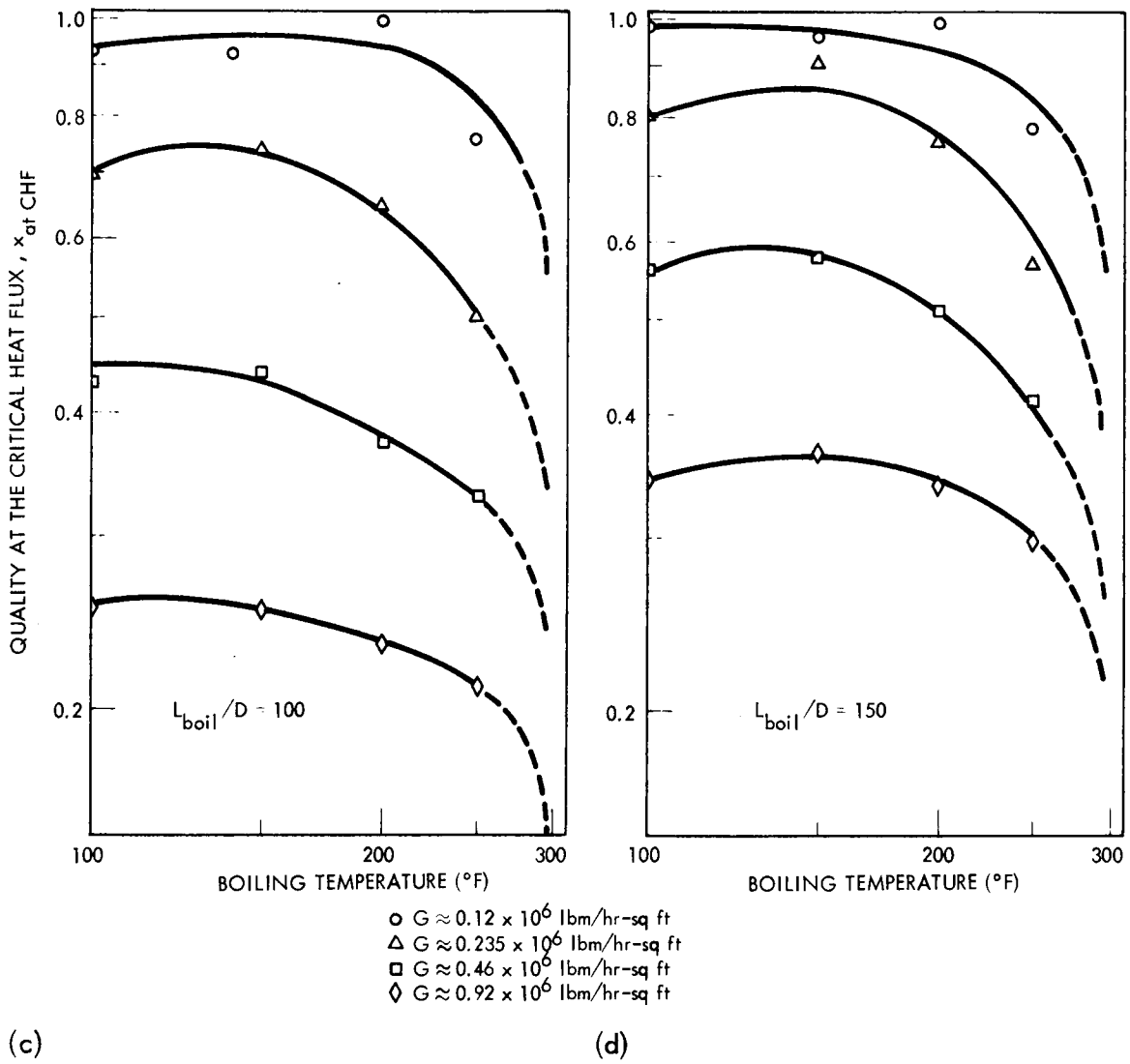


Figure IV-151. (continued)

First of all, the density ratio (ρ_f/ρ_g) is made the same. Thus for R-114 at 100°F, a corresponding boiling temperature of 442°F for water is needed. Once the water temperature is determined, equating the $\left(G\gamma^{1/2}/\rho_f{}^{1/2}\right)$ terms yields the mass flux of the water in the model. Setting the term $\left(Dc_{pf}\ \rho_f{}^{1/2}/k_f\gamma^{1/2}\right)$ equal for both fluids determines the corresponding diameter for the tube in the model. Finally, since L/D must be the same, the length of the model tube is determined. One can now use a critical heat flux correlation for water (such as the Macbeth [101] or Biasi et al [112] correlations) to determine $(q/A)_{crit}$ for the water model. This can then be inserted into the $\left[(q/A)_{crit}\ \gamma^{1/2}/\rho_f{}^{1/2}\ h_{fg}\right]$ dimensionless term to obtain the critical heat flux in the R-114 prototype.

This was precisely what was done in this case with the present results. Both the Macbeth [101] and Biasi et al [112] correlations were used to compute the critical heat fluxes for the scaled water tests. A sample calculation is given in Appendix D. Plots comparing the critical heat fluxes experimentally measured and those predicted using the scaling law approach described above are given in Figures IV-152 to IV-155. From these plots, it is seen that the model generally yielded critical heat fluxes which underestimated the measured ones. This deviation was smallest at the high L/D ratios and low mass fluxes. Generally, the Biasi et al [112] critical heat flux correlation yielded results which were closer to the experimental values than the Macbeth [101] high mass flux correlation. In Figure IV-153b, the data lay on the borderline between the high and low mass flux regions of the Macbeth [101] correlation. The deviation between these two regions is seen to increase significantly as the L/D ratio decreases.

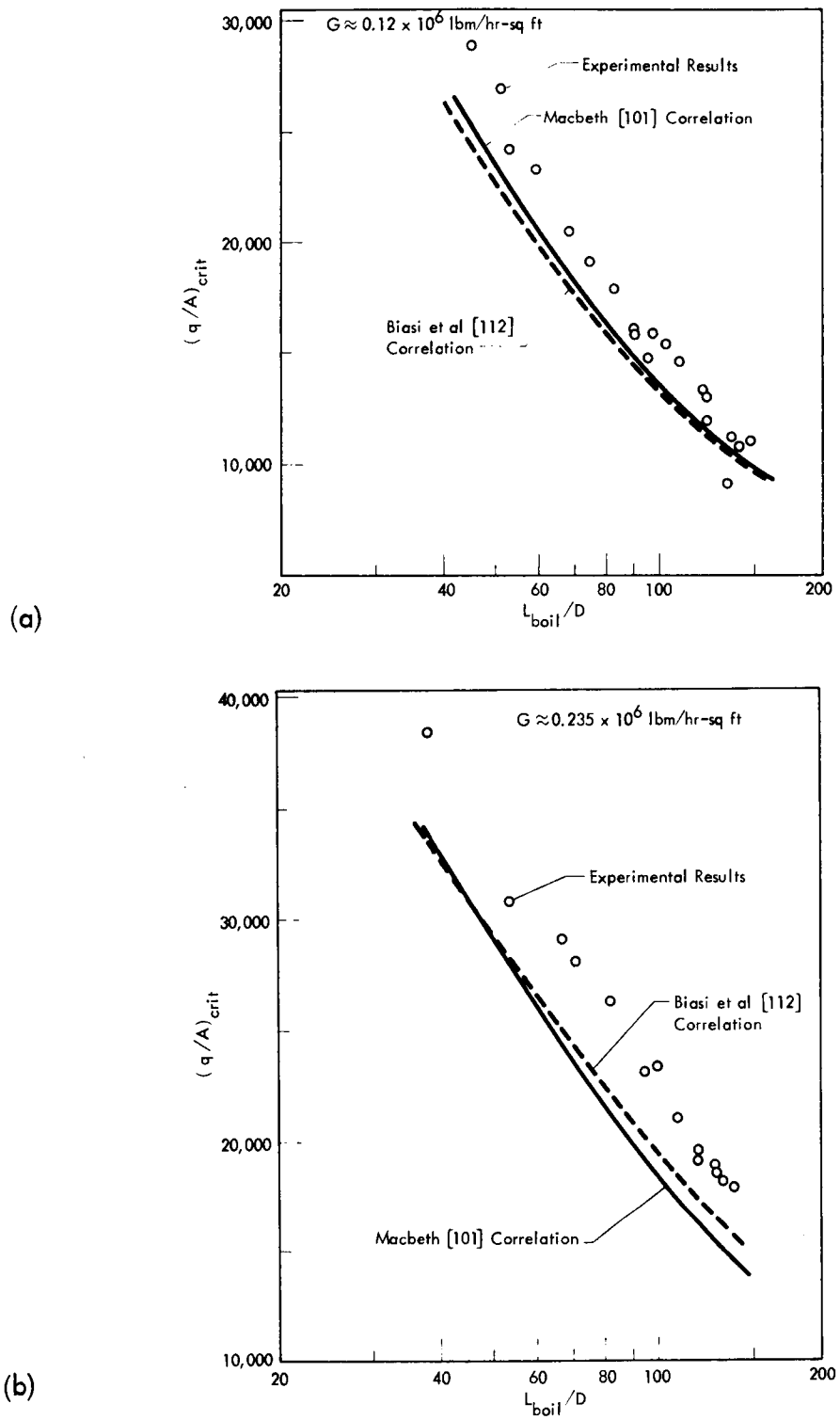
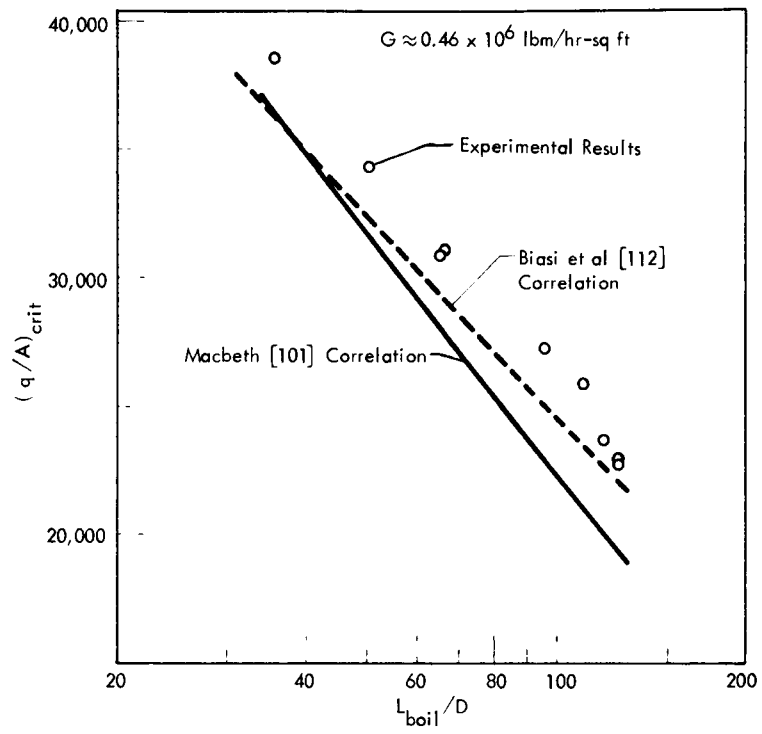
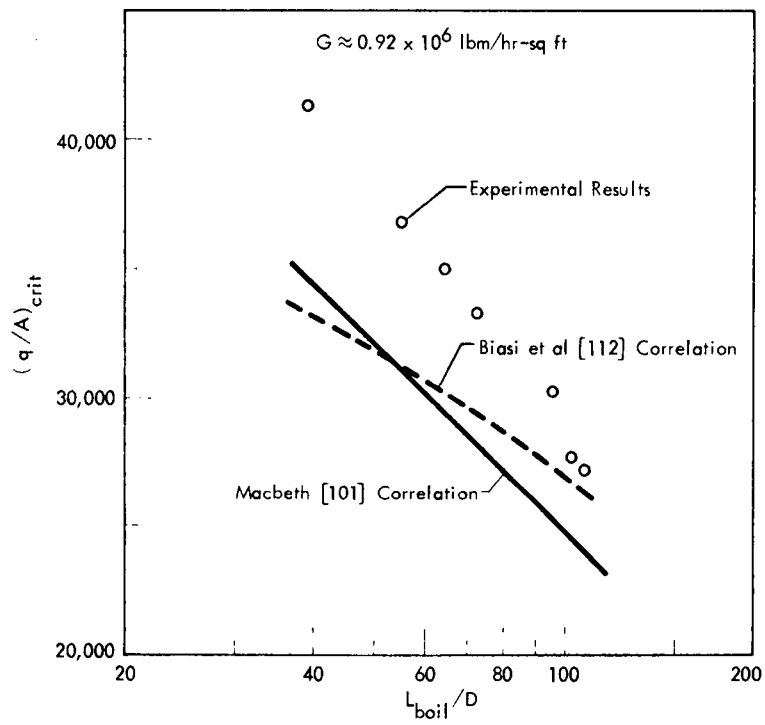


Figure IV-152. COMPARISON OF THE EXPERIMENTALLY DETERMINED CRITICAL HEAT FLUXES WITH VALUES OBTAINED USING THE MACBETH [101] AND BIASI ET AL [112] CORRELATIONS AND THE SCALING LAWS OF BARNETT AND WOOD [105]. T ≈ 100°F.

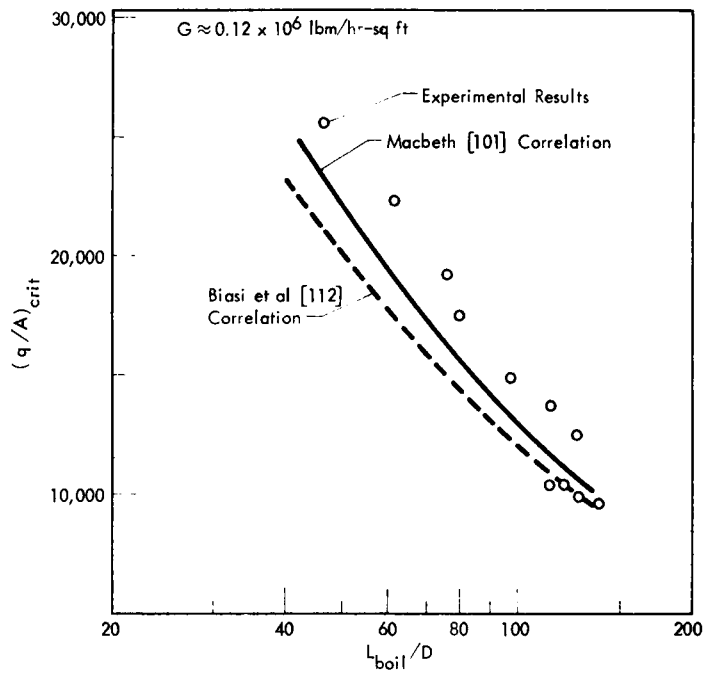


(c)

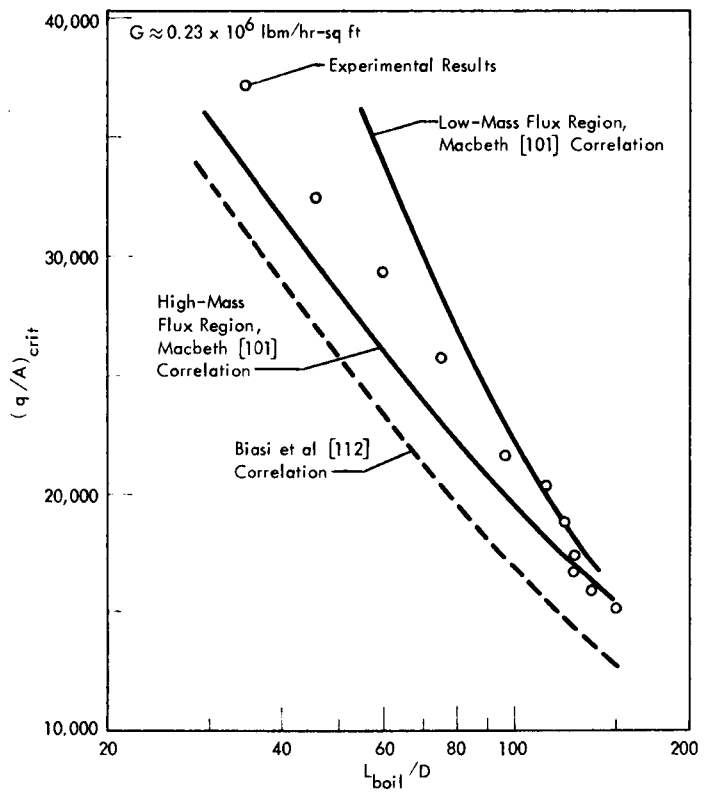


(d)

Figure IV-152. (continued)

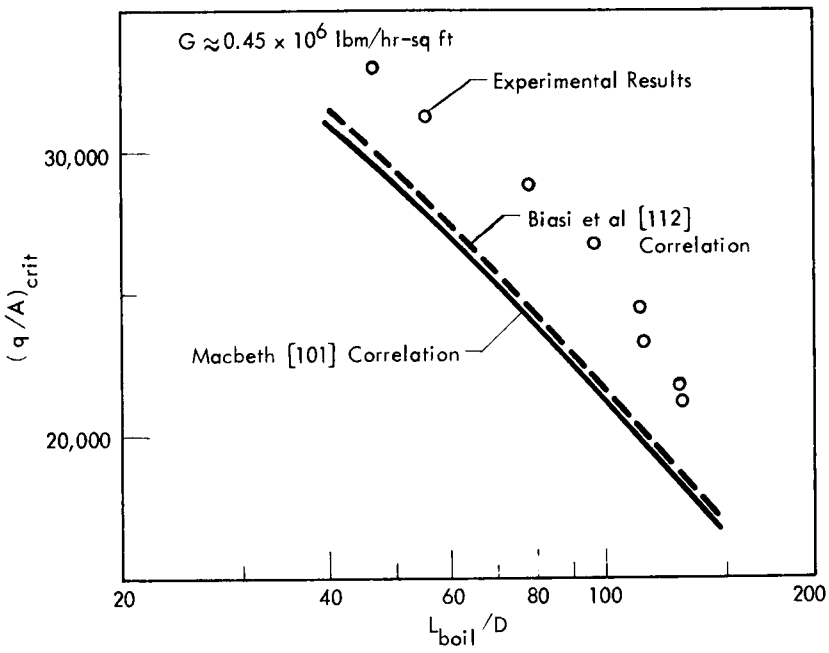


(a)

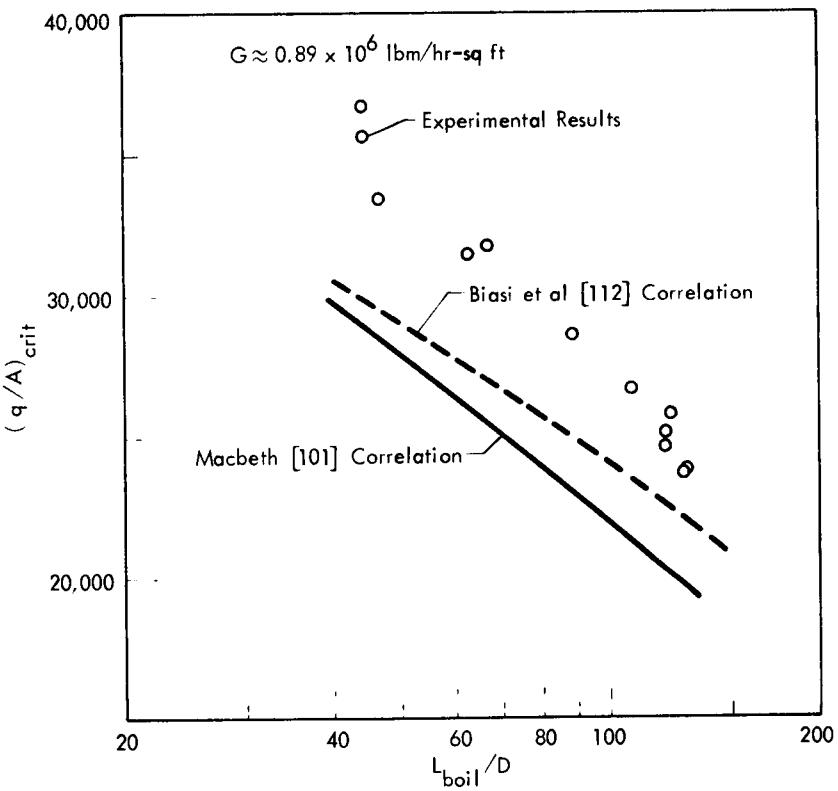


(b)

Figure IV-153. COMPARISON OF THE EXPERIMENTALLY DETERMINED CRITICAL HEAT FLUXES WITH VALUES OBTAINED USING THE MACBETH [101] AND BIASI ET AL [112] CORRELATIONS AND THE SCALING LAWS OF BARNETT AND WOOD [105]. T≈150°F.

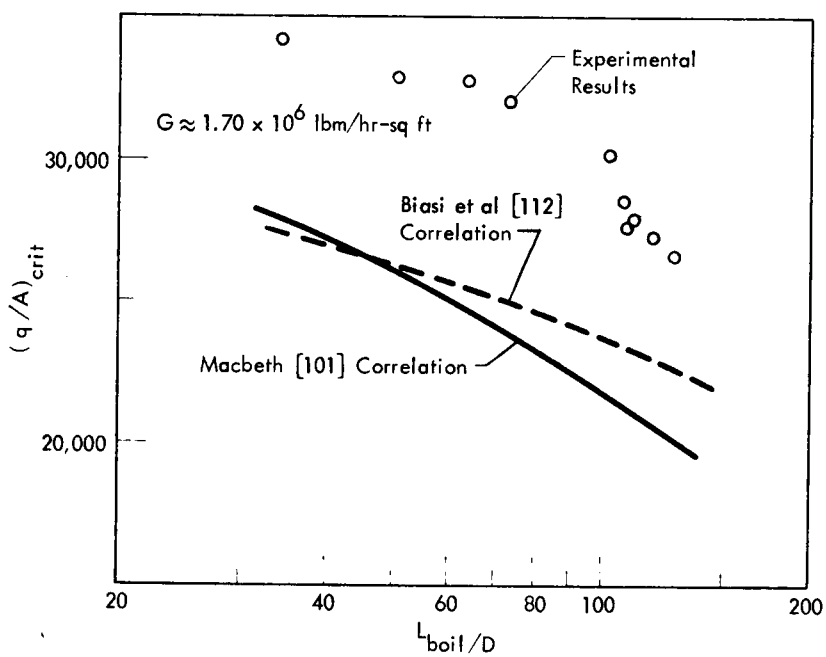


(c)



(d)

Figure IV-153. (continued)



(e)

Figure IV-153. (continued)

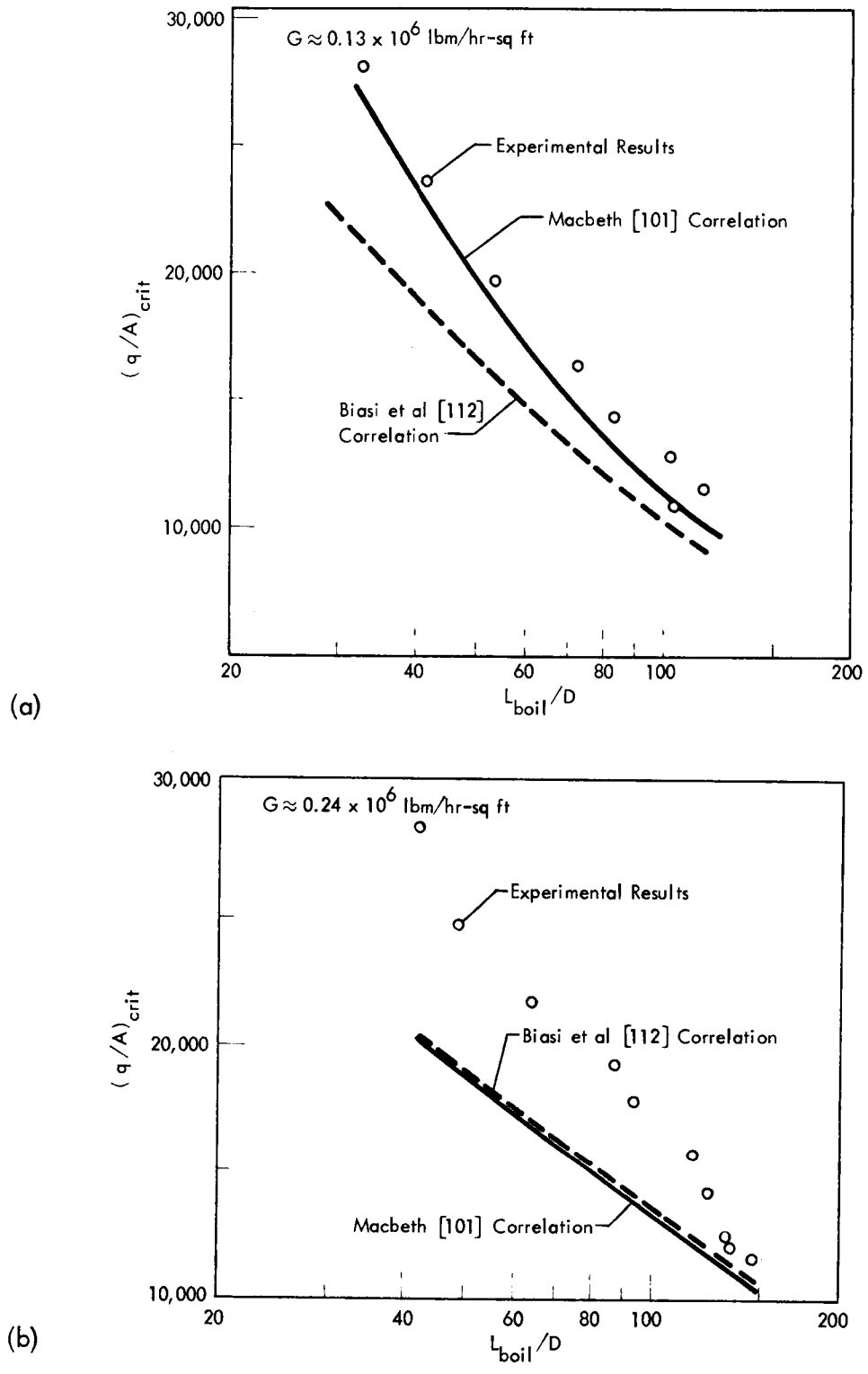
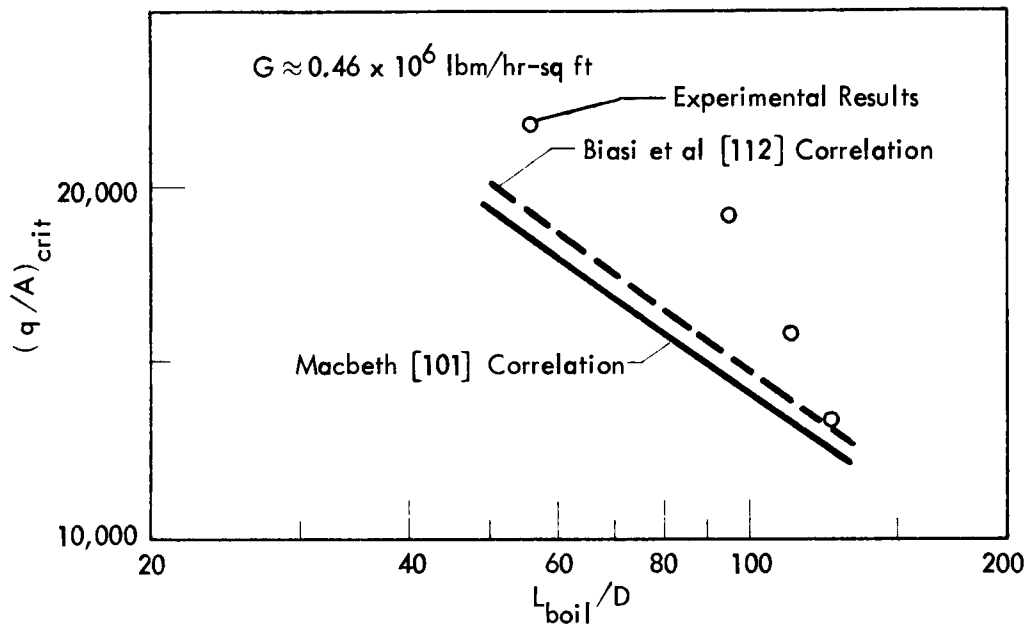
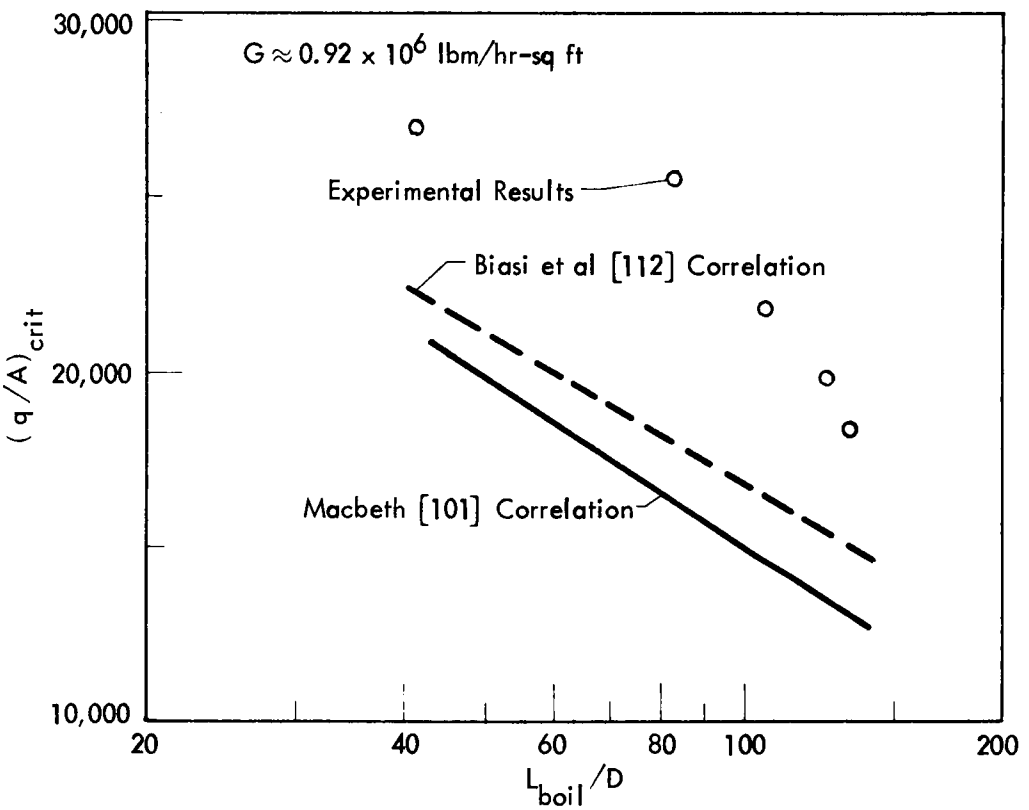


Figure IV-154. COMPARISON OF THE EXPERIMENTALLY DETERMINED CRITICAL HEAT FLUXES WITH VALUES OBTAINED USING THE MACBETH [101] AND BIASI ET AL [112] CORRELATIONS AND THE SCALING LAWS OF BARNETT AND WOOD [105]. $T \approx 200°F$.

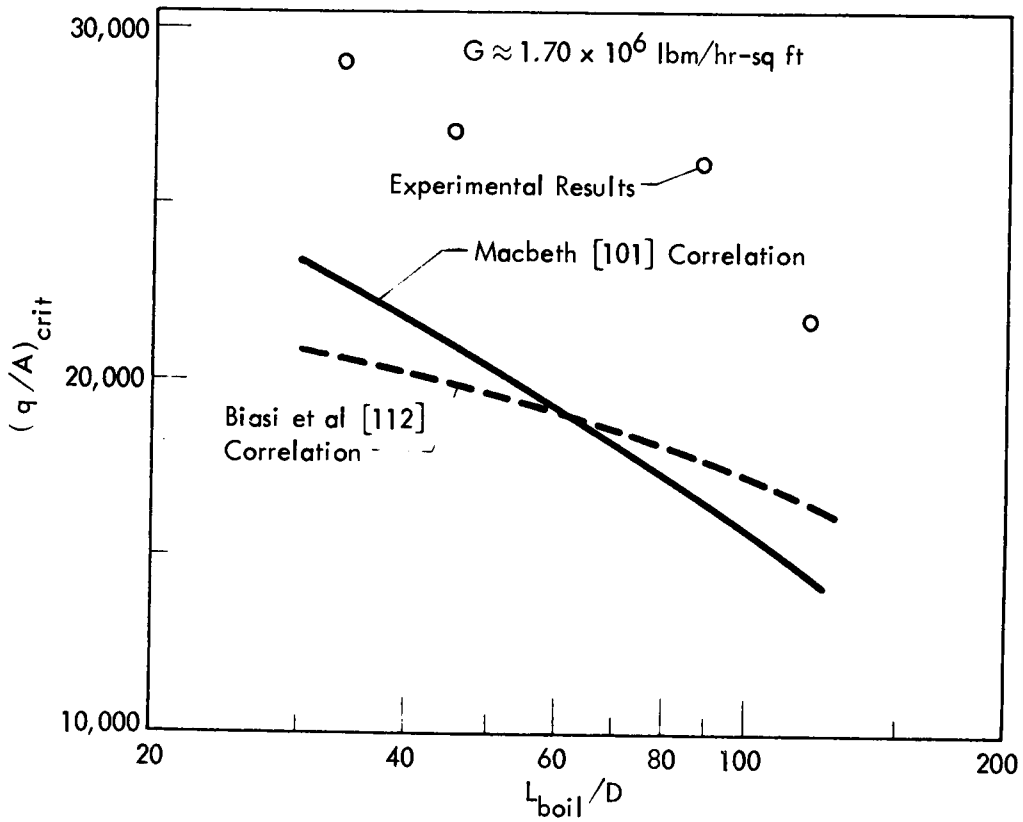


(c)



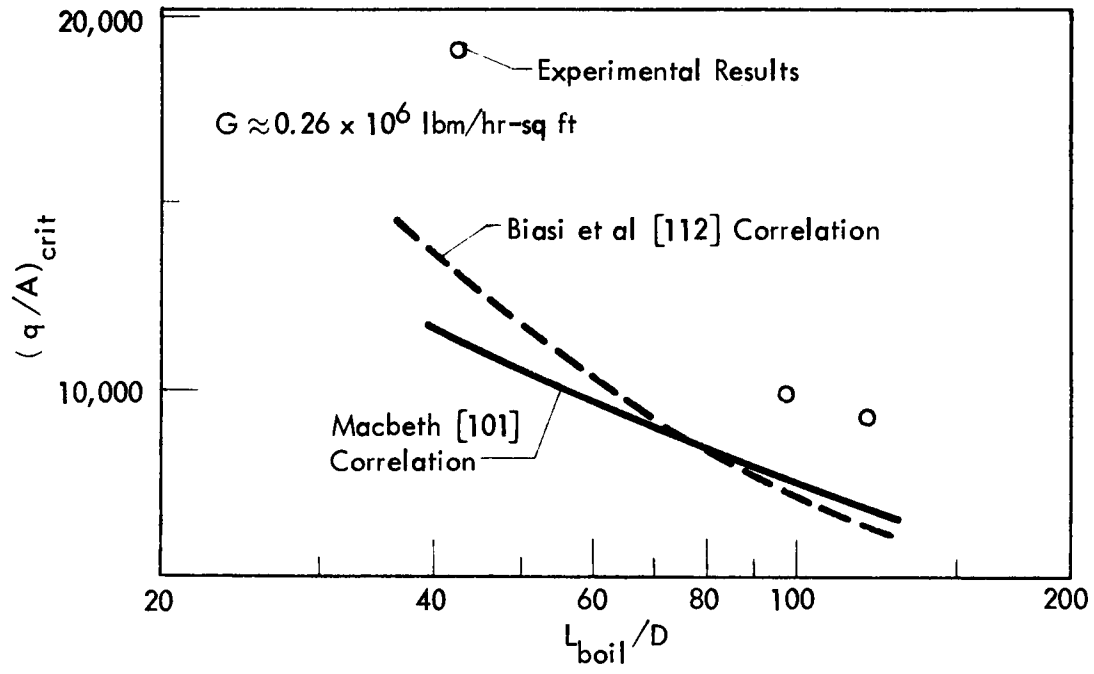
(d)

Figure IV-154. (continued)

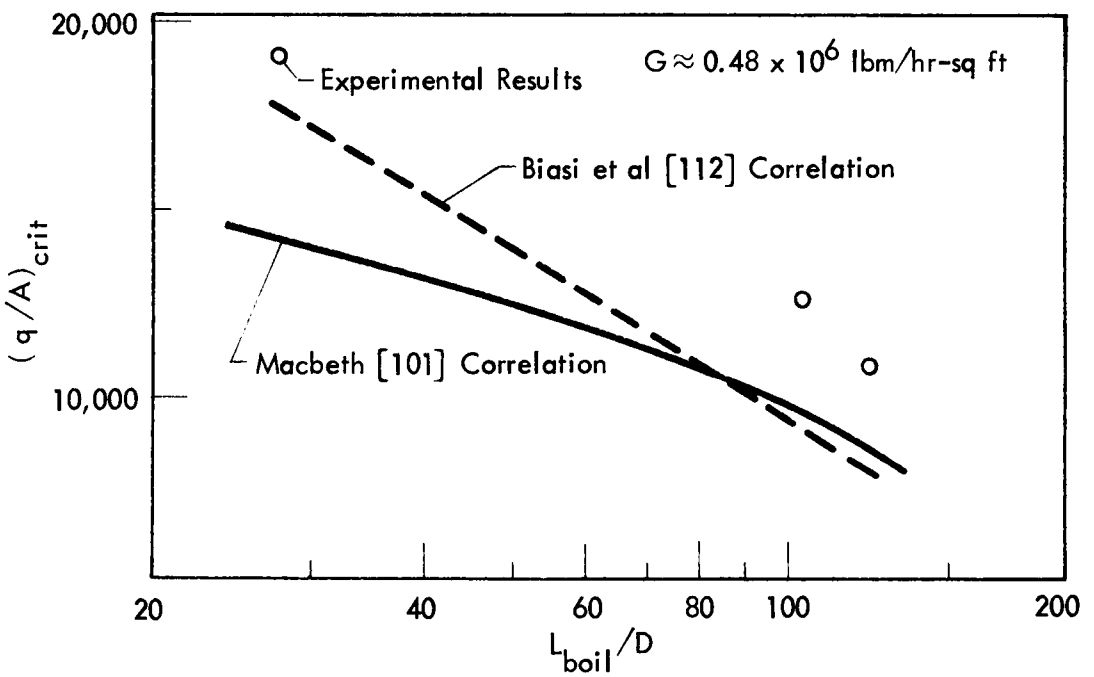


(e)

Figure IV-154. (continued)

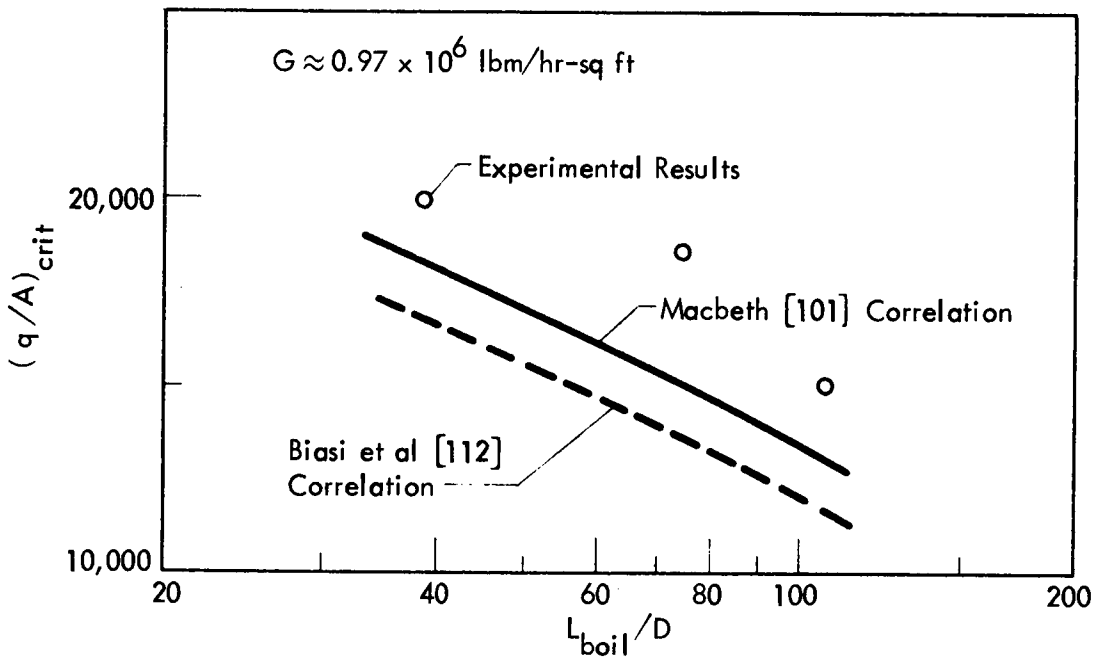


(a)



(b)

Figure IV-155. COMPARISON OF THE EXPERIMENTALLY DETERMINED CRITICAL HEAT FLUXES WITH VALUES OBTAINED USING THE MACBETH [101] AND BIASI ET AL [112] CORRELATIONS AND THE SCALING LAWS OF BARNETT AND WOOD [105]. T ≈ 250°F.



(c)

Figure IV-155. (continued)

Instead of the scaling law method of Barnett and Wood [105], the scaling factor approach as discussed by Stevens and Kirby [107] may be applied. In this case, a plot of the quality at which critical heat flux was obtained vs. the term E_s, given in Equation (2-83) is made as illustrated in Figure II-37 on page 98. The results of this study are shown in Figures IV-156 to IV-159. Also shown in these figures is the curve obtained by Stevens and Kirby [107] as modified by Staub [110] for the case of $\Delta h/h_{fg} = 0$. As can be seen, this curve overestimated the actual data especially at the 200 and 250°F boiling temperatures.

In addition to the R-114 results, critical heat flux data for water in the same sized tube at a temperature corresponding to the same density ratio as the R-114 results can be generated. Using the Biasi et al [112] correlation, plots of $x_{at\ CHF}$ vs. $E_s = K_s G(D)^{1/4}\ (D/L)^{0.59} \times 10^{-4}$ can be made. The K_s value used was 0.658 as suggested by Stevens and Kirby [107]. These plots are shown in Figures IV-160 to IV-163. The displacement in the data at $G \approx 0.12 \times 10^6$ lbm/hr-sq ft for the 100°F boiling temperature runs shown in Figure IV-160 was due to a limitation on the Biasi et al [112] correlation for $G < 0.22 \times 10^6$ lbm/hr-sq ft as discussed in the sample calculation in Appendix D.

From Figures IV-160 to IV-163, it can be seen that the corresponding water critical heat fluxes are not exactly modeled by the constant $K_s = 0.658$. For example, at 100°F, the equivalent water results shown in Figure IV-160 overestimated the R-114 results in Figure IV-156. The opposite was true at the 250°F temperature. In addition, there was a mass flux and an L/D effect. This is most clearly observable at the 150°F boiling temperature. Here, at low values of E_s, the water results

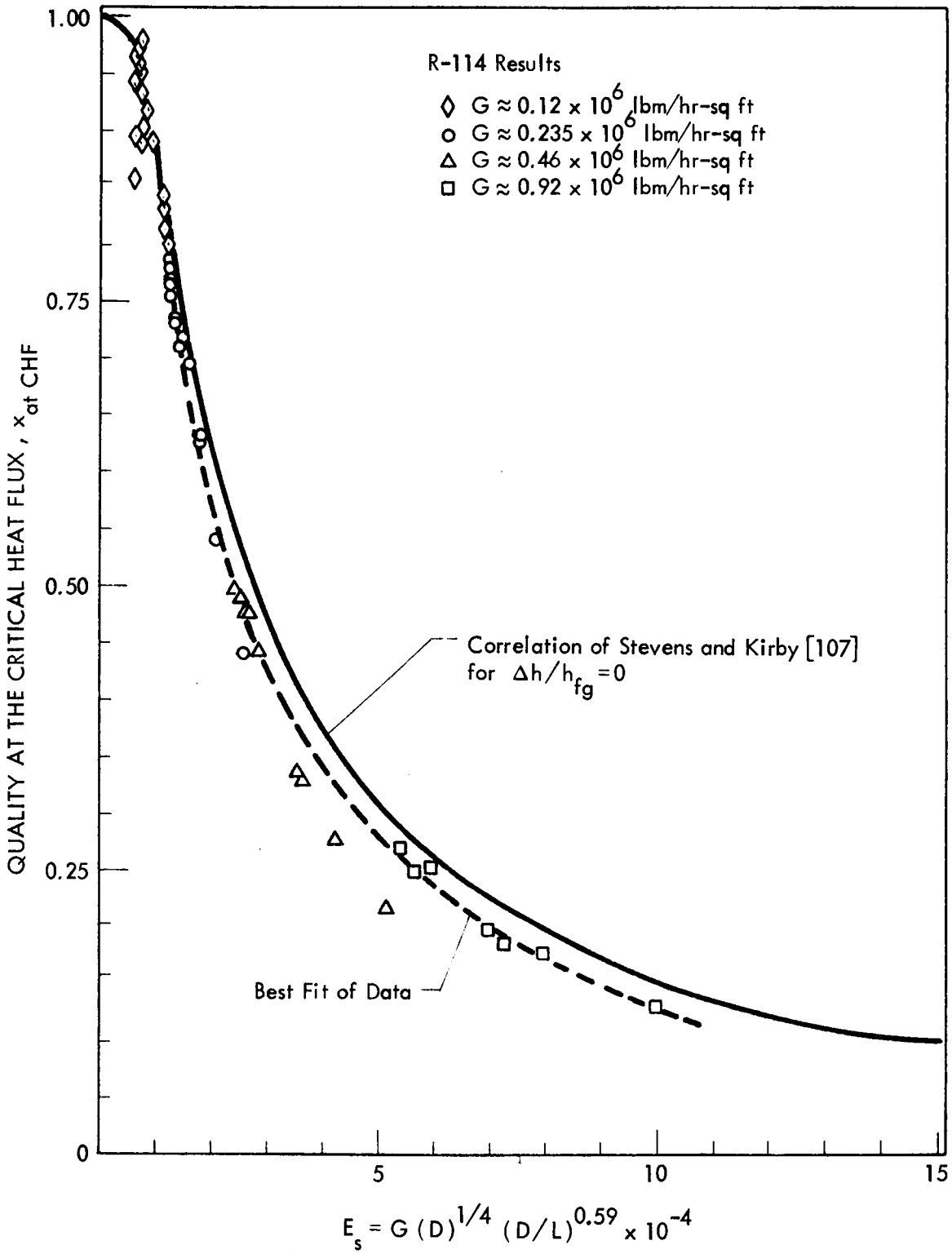


Figure IV-156. COMPARISON OF THE EXPERIMENTALLY DETERMINED QUALITIES AT THE CRITICAL HEAT FLUX WITH THE CORRELATION OF STEVENS AND KIRBY [107] AS MODIFIED BY STAUB [110] FOR THE CASE OF $\Delta h/h_{fg} = 0$. T ≈ 100°F.

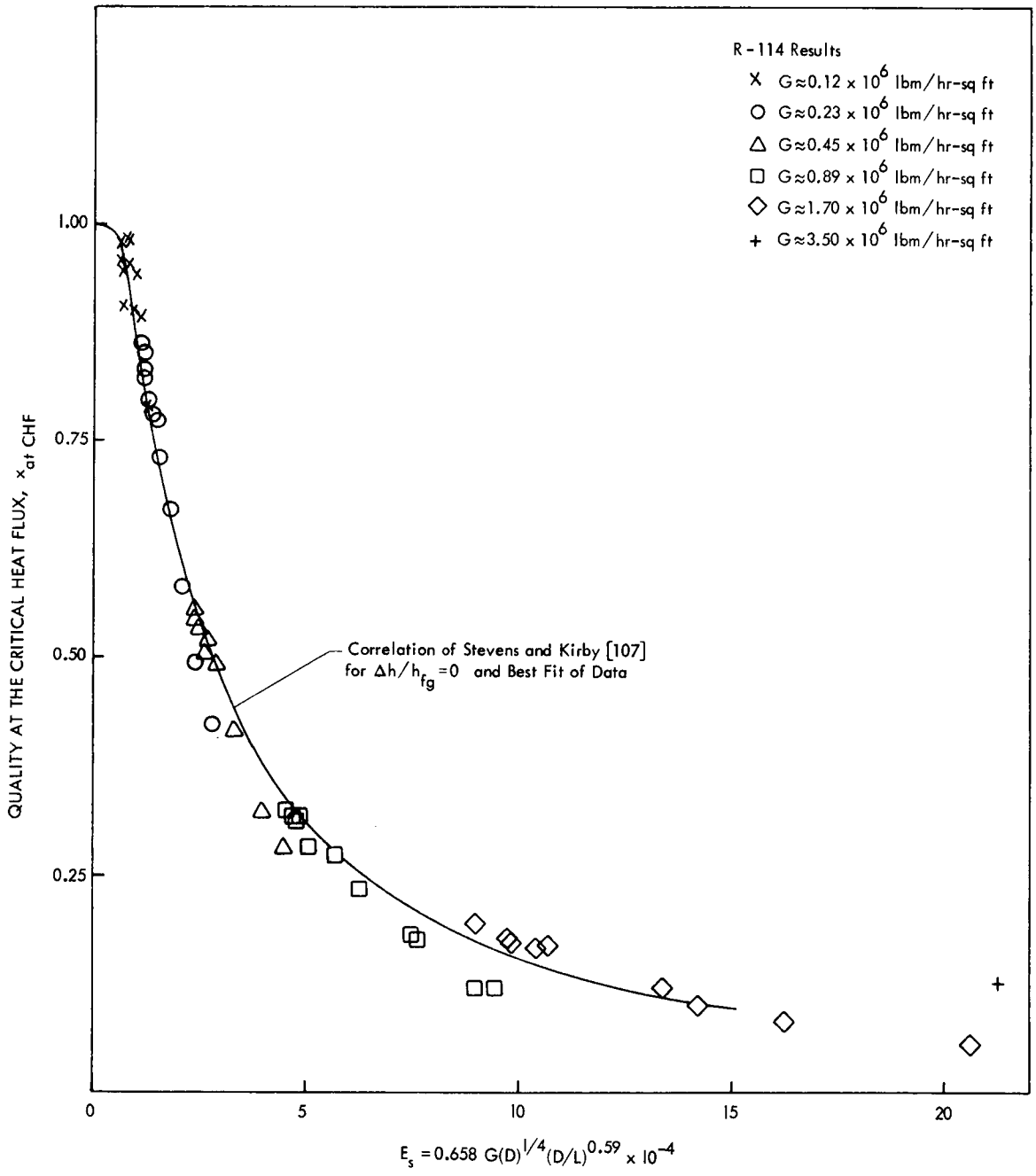


Figure IV-157. COMPARISON OF THE EXPERIMENTALLY DETERMINED QUALITIES AT THE CRITICAL HEAT FLUX WITH THE CORRELATION OF STEVENS AND KIRBY [107] AS MODIFIED BY STAUB [110] FOR THE CASE OF $\Delta h/h_{fg}=0$. $T \approx 150°F$.

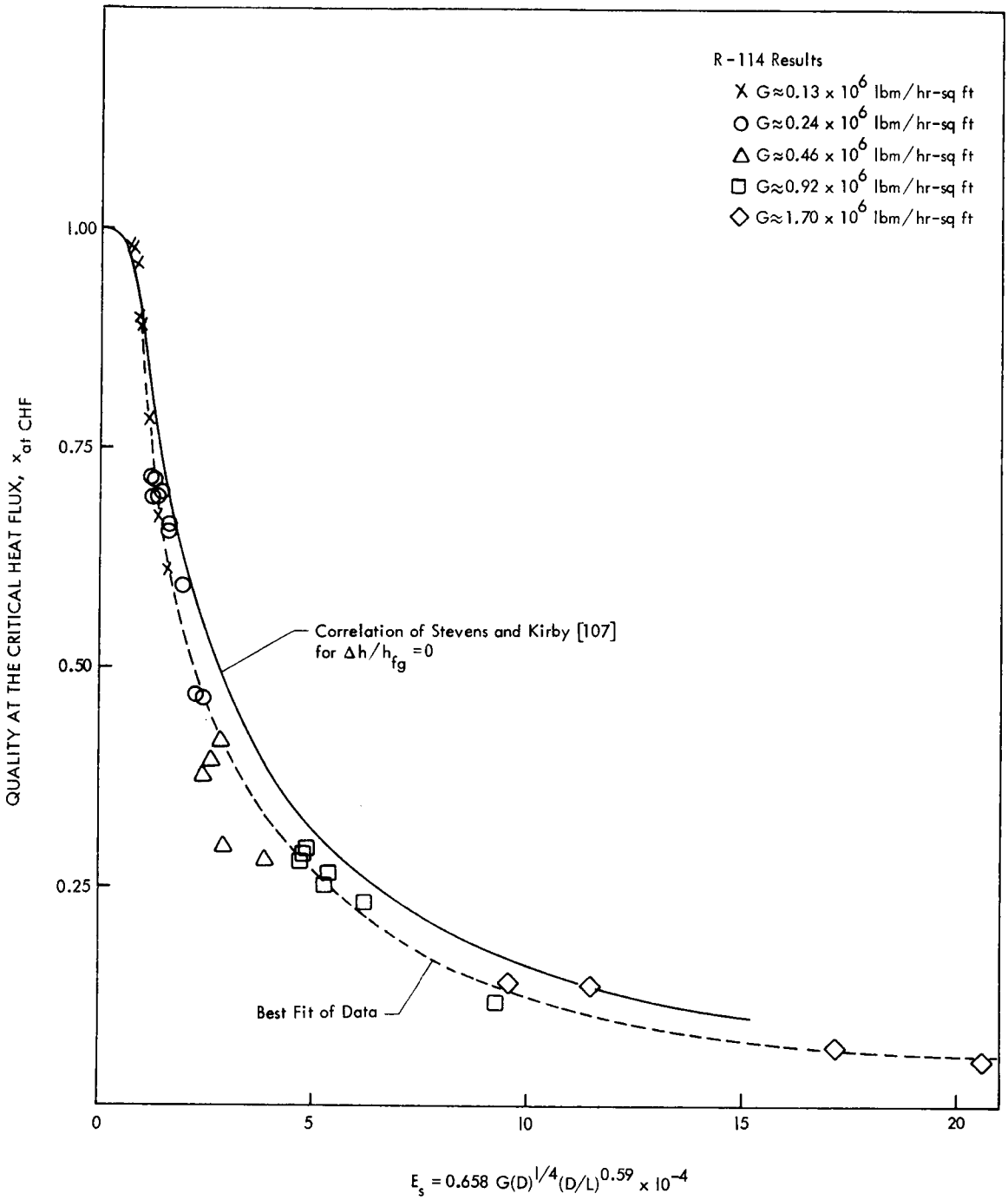


Figure IV-158. COMPARISON OF THE EXPERIMENTALLY DETERMINED QUALITIES AT THE CRITICAL HEAT FLUX WITH THE CORRELATION OF STEVENS AND KIRBY [107] AS MODIFIED BY STAUB [110] FOR THE CASE OF $\Delta h/h_{fg} = 0$. $T \approx 200°F$.

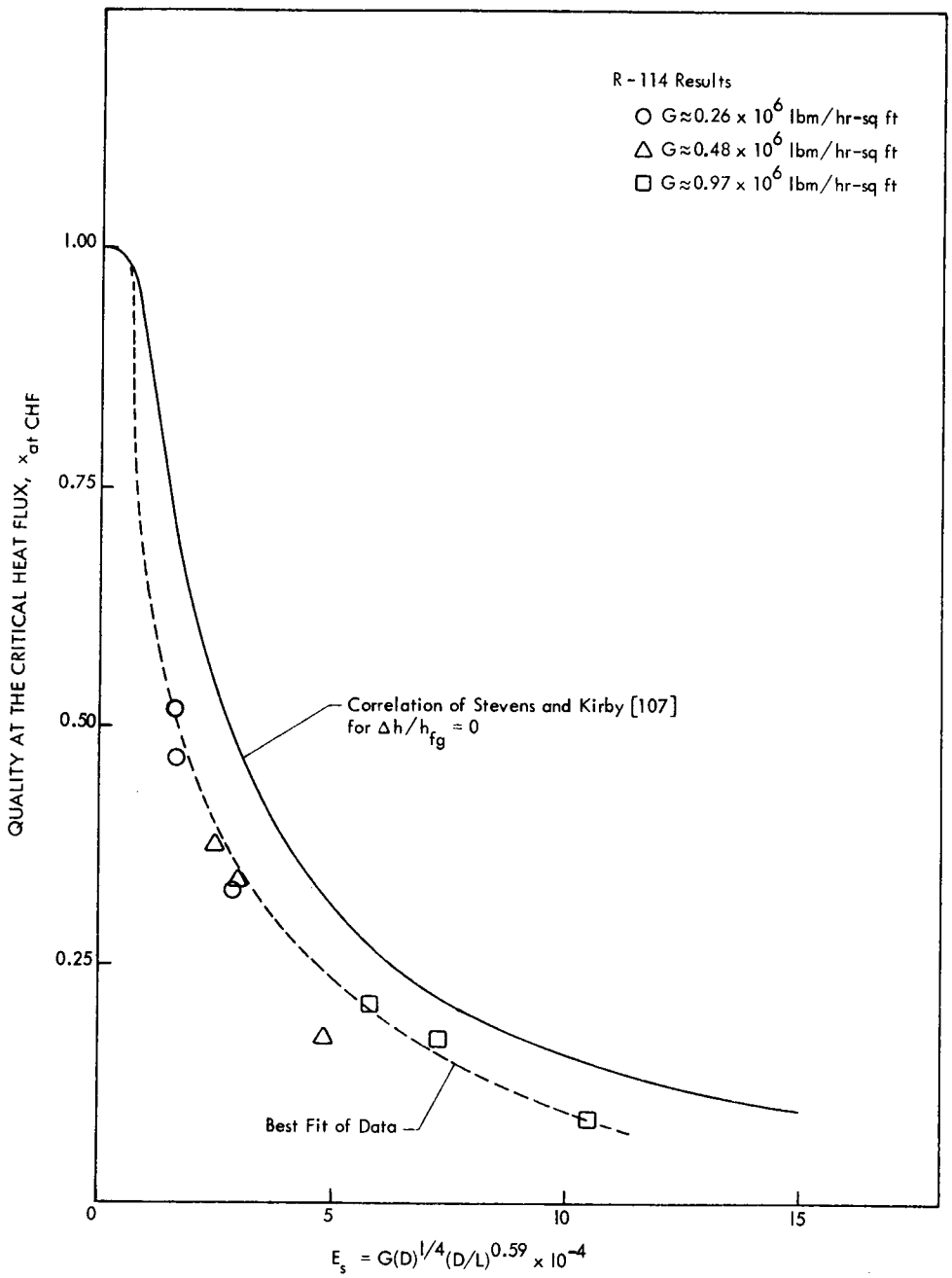


Figure IV-159. COMPARISON OF THE EXPERIMENTALLY DETERMINED QUALITIES AT THE CRITICAL HEAT FLUX WITH THE CORRELATION OF STEVENS AND KIRBY [107] AS MODIFIED BY STAUB [110] FOR THE CASE OF $\Delta h/h_{fg} = 0$. $T \approx 250°F$.

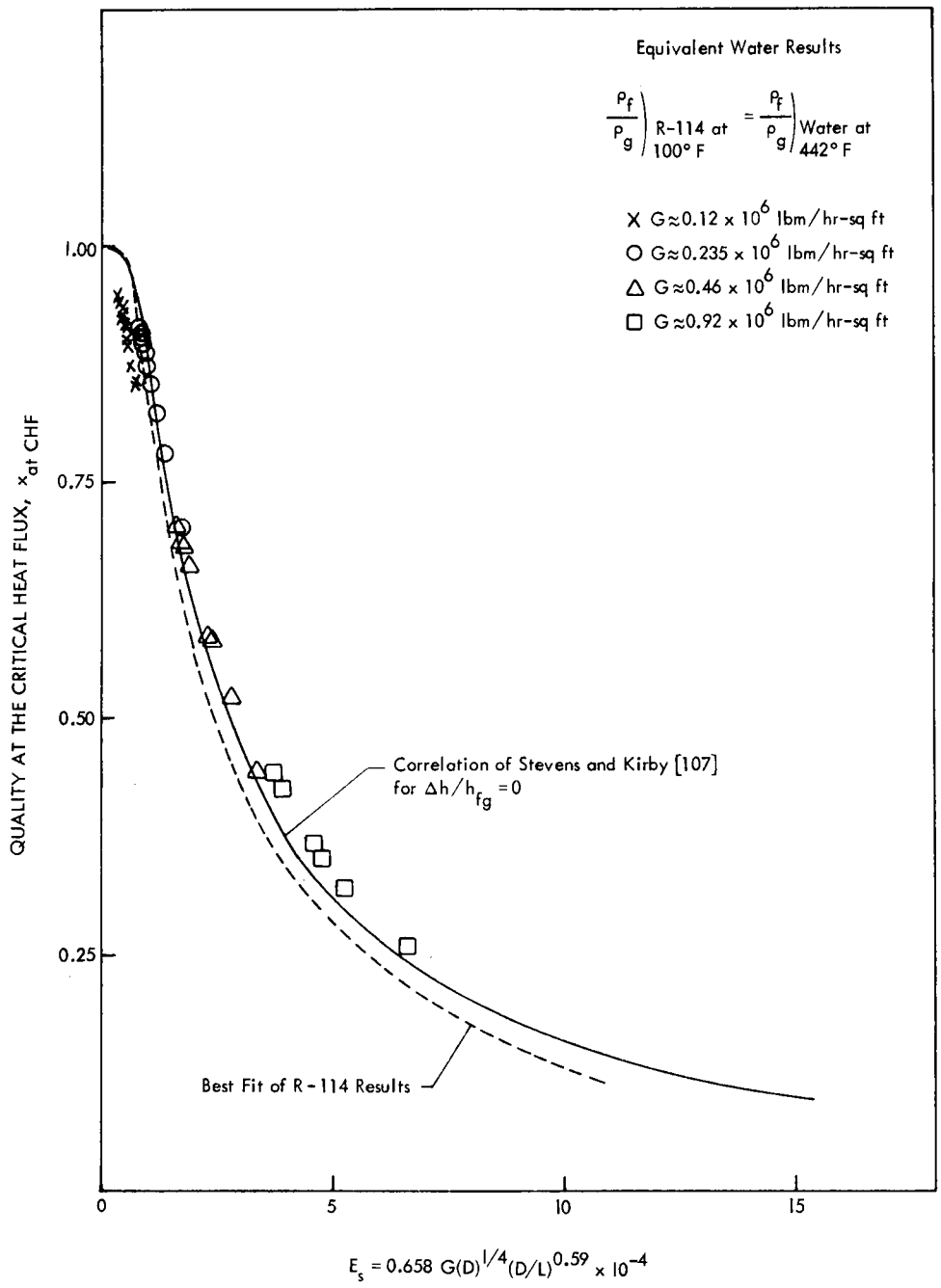


Figure IV-160. COMPARISON OF THE CRITICAL HEAT FLUX QUALITIES OBTAINED FOR WATER AT 442°F USING THE BIASI ET AL [112] CORRELATION WITH THE CORRELATION OF STEVENS AND KIRBY [107] AS MODIFIED BY STAUB [110] FOR THE CASE OF $\Delta h/h_{fg} = 0$. $K_s = 0.658$.

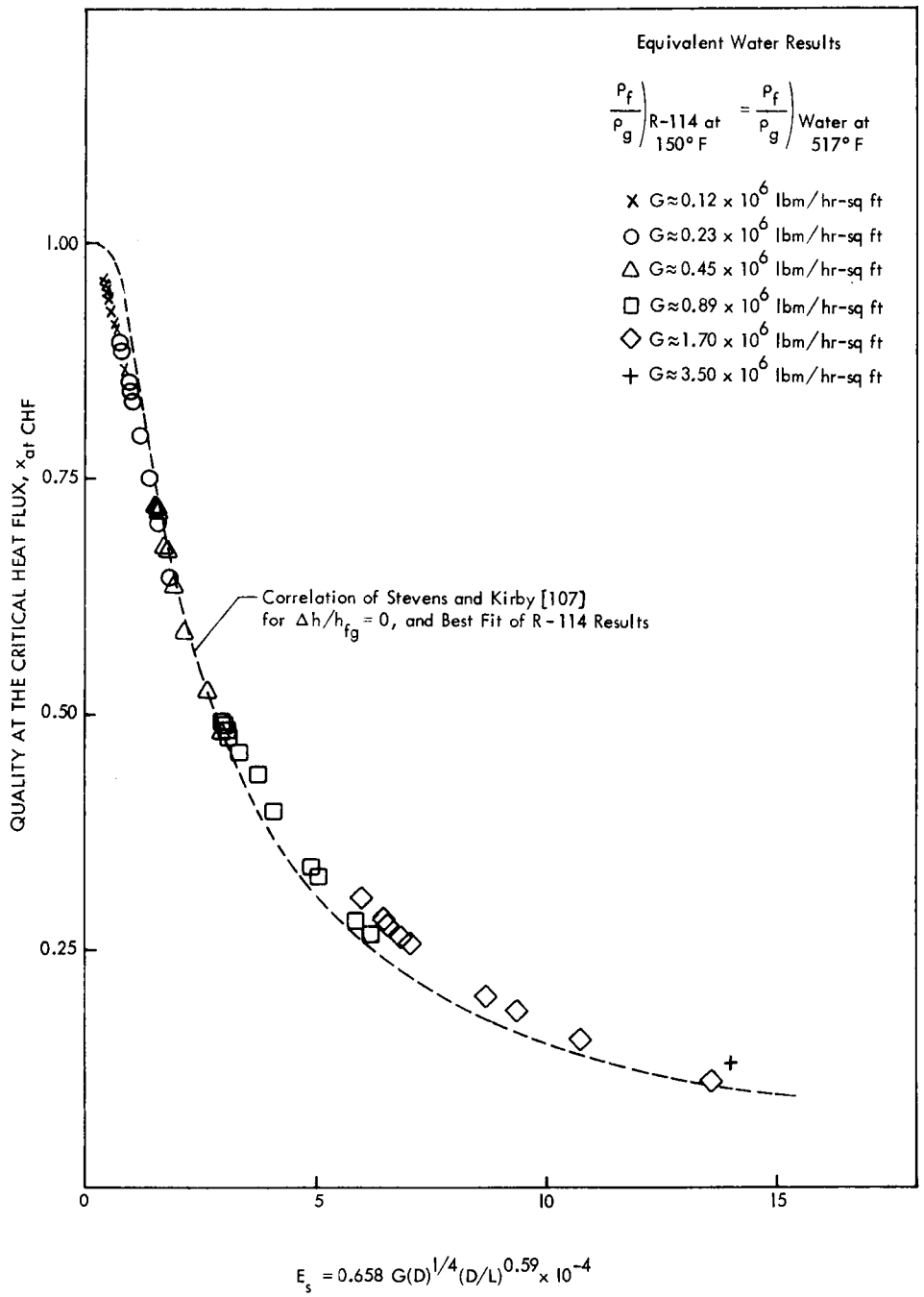


Figure IV-161. COMPARISON OF THE CRITICAL HEAT FLUX QUALITIES OBTAINED FOR WATER AT 517°F USING THE BIASI ET AL [112] CORRELATION WITH THE CORRELATION OF STEVENS AND KIRBY [107] AS MODIFIED BY STAUB [110] FOR THE CASE OF $\Delta h/h_{fg} = 0$. $K_s = 0.658$.

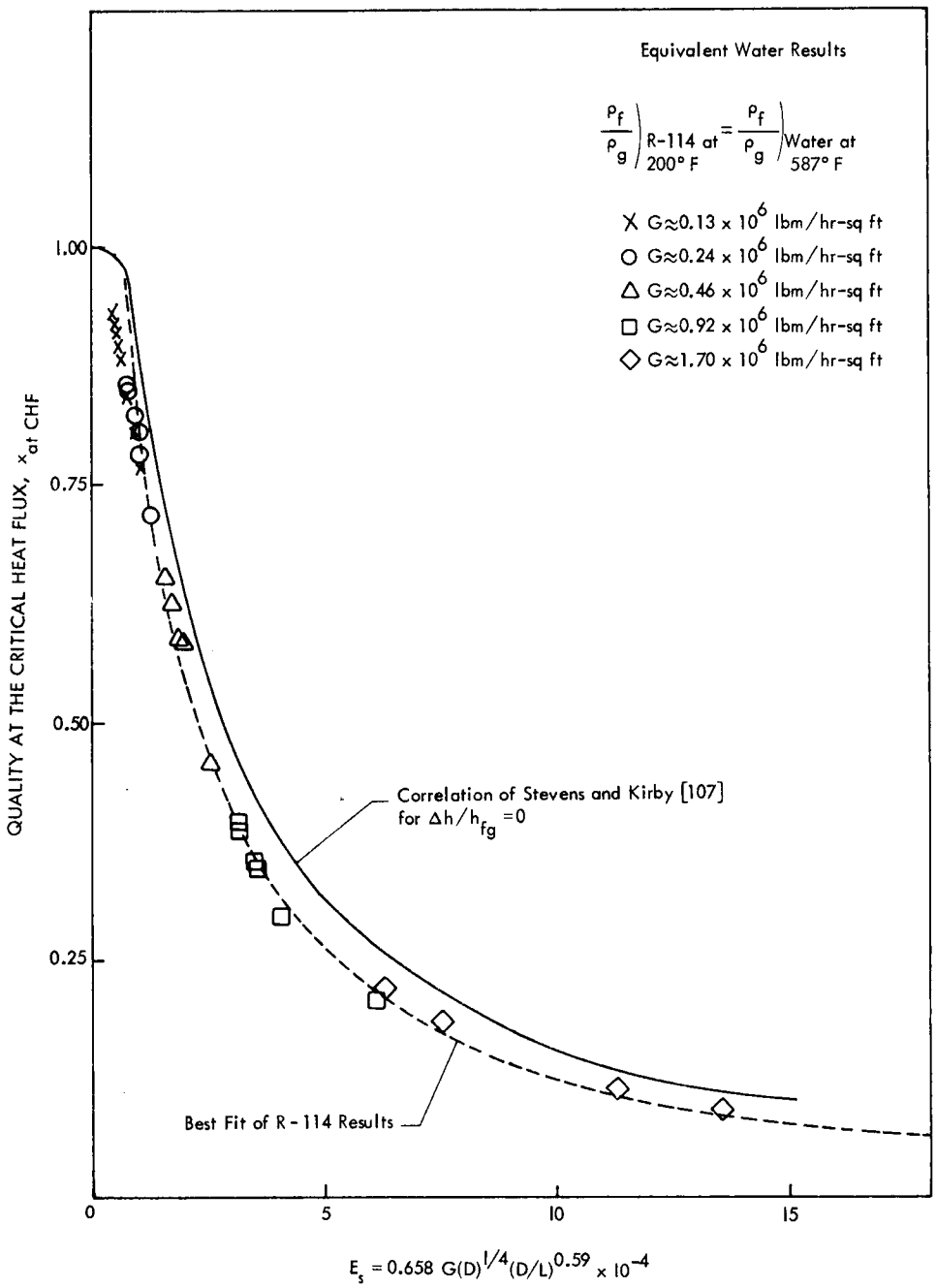


Figure IV-162. COMPARISON OF THE CRITICAL HEAT FLUX QUALITIES OBTAINED FOR WATER AT 587°F USING THE BIASI ET AL [112] CORRELATION WITH THE CORRELATION OF STEVENS AND KIRBY [107] AS MODIFIED BY STAUB [110] FOR THE CASE OF $\Delta h/h_{fg}=0$. $K_s = 0.658$.

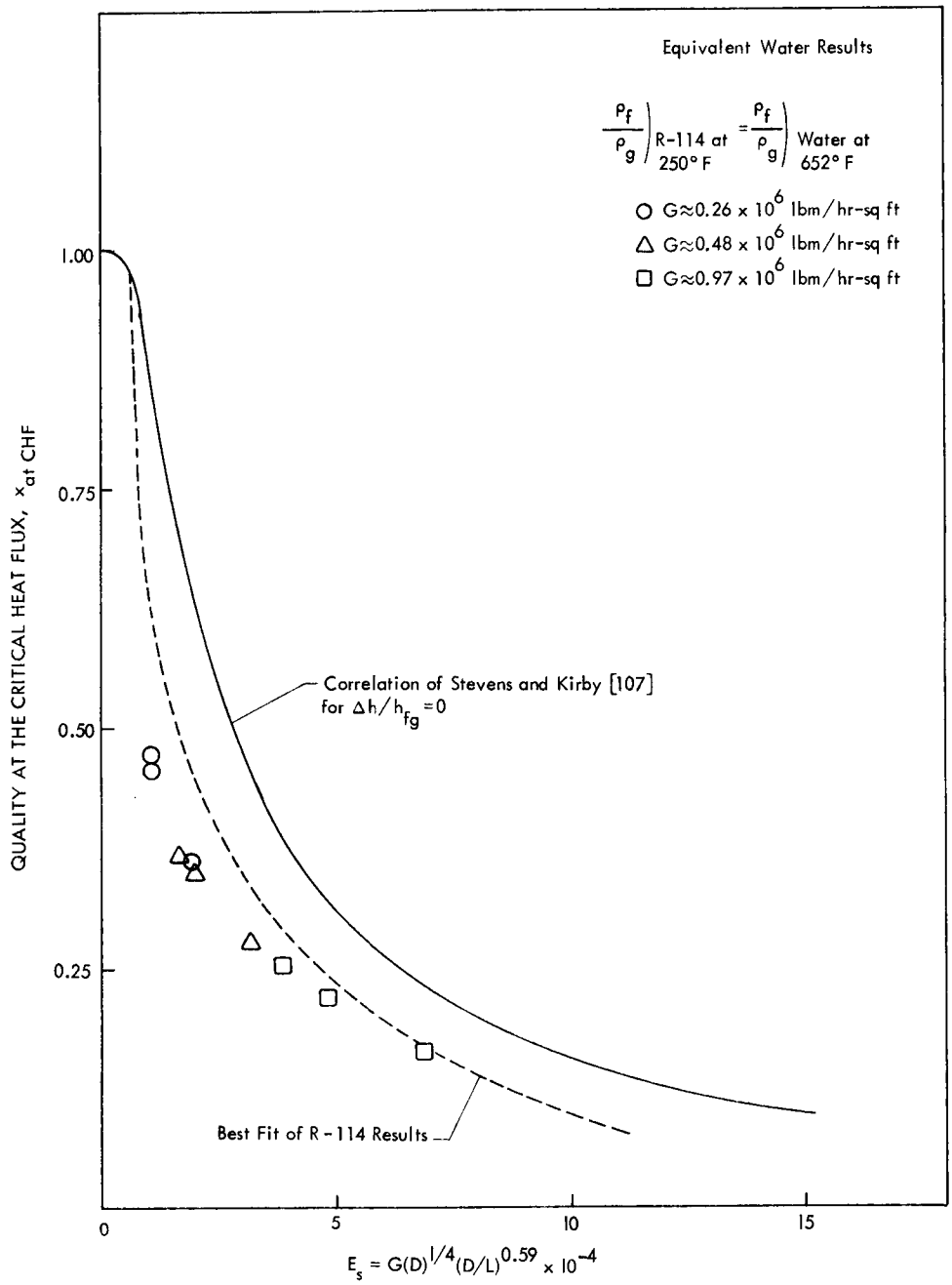


Figure IV-163. COMPARISON OF THE CRITICAL HEAT FLUX QUALITIES OBTAINED FOR WATER AT 652°F USING THE BIASI ET AL [112] CORRELATION WITH THE CORRELATION OF STEVENS AND KIRBY [107] AS MODIFIED BY STAUB [110] FOR THE CASE OF $\Delta h/h_{fg}=0$, $K_s=0.658$.

were lower than the best curve fit of the R-114 results. At high E_s values, the water results were higher. Dix [111] who ran critical heat flux tests in round tubes with R-114 also noted that K_s was not a constant but a function of various parameters. For the range of variables given in Table II-9 on page 99, Dix [111] found that Equation (2-84) modeled his R-114 results quite well. Application of Equation (2-84) to the present data led to unsatisfactory results at low pressures. Dix [111] who was aware of this compared the effect of his $(1.41 - 0.02\ \rho_f/\rho_g)$ term to the pressure effect terms generated by other experimenters. This is shown in Figure IV-164. In the present series of tests, the pressure effect was satisfactorily modeled by the term $0.95\ (1 + \rho_g/\rho_f)^2$. This curve is also shown in Figure IV-164 and compares well with other formulations for the pressure effect. Therefore, using the equation

$$K_s = 0.703(1.00 - 0.09 \times 10^{-6}\ G_{water})(1.04 - 0.0005\ L/D)$$
$$(1 + \rho_g/\rho_f)^2 \qquad (4\text{-}93)$$

for the multiplication factor, the water equivalents were recomputed and the new results given in Figures IV-165 to IV-168. As can be seen, there was little improvement in the 100°F water equivalent results while at the 250°F boiling temperature, the improvement was considerable. Since there was very good agreement between the actual R-114 data and the water equivalent results at 150°F and 200°F as shown in Figures IV-166 and IV-167 and since these two plots represented data taken at pressures closest to the range covered by Dix [111], one can conclude that there is good agreement between the critical heat flux results of this study and those of Dix [111].

The final model to be considered is the compensated distortion model of Ahmad [116]. Here, for the case of zero inlet subcooling, it

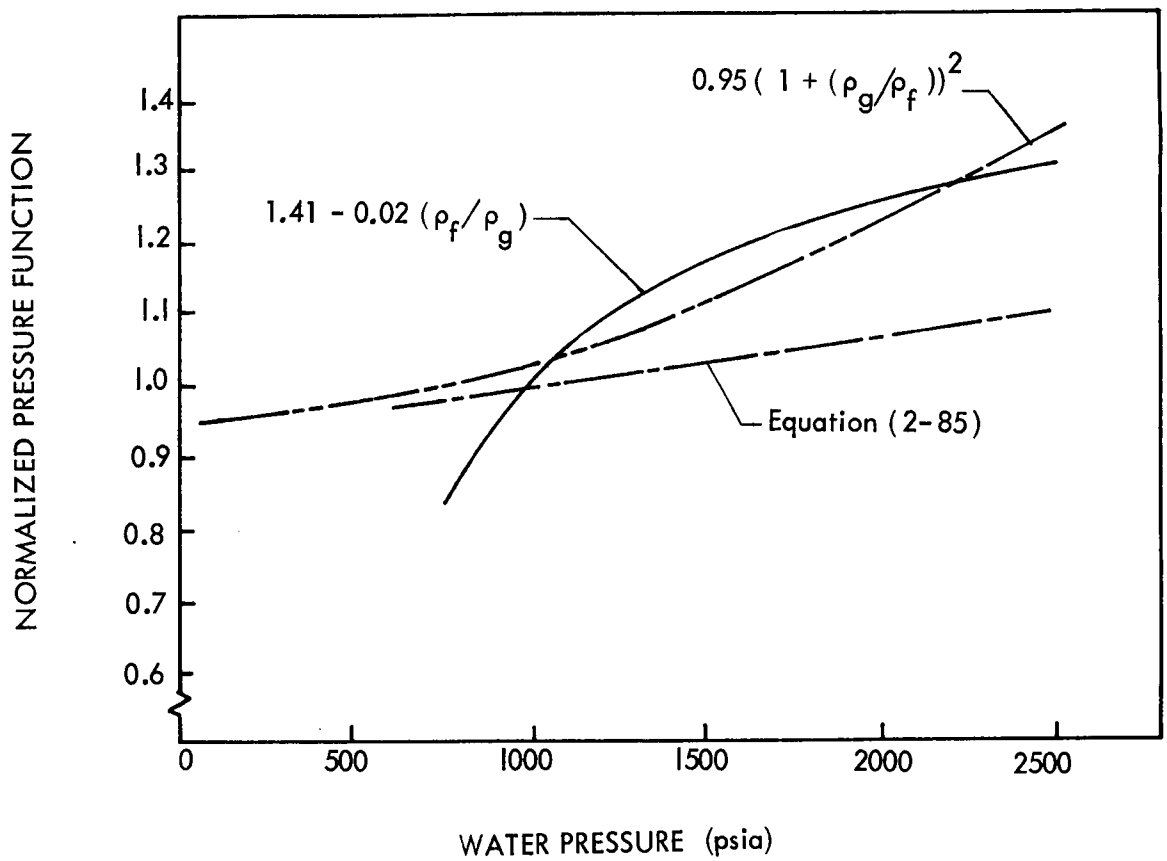


Figure IV-164. NORMALIZED PRESSURE EFFECT ON MASS VELOCITY MODELING.

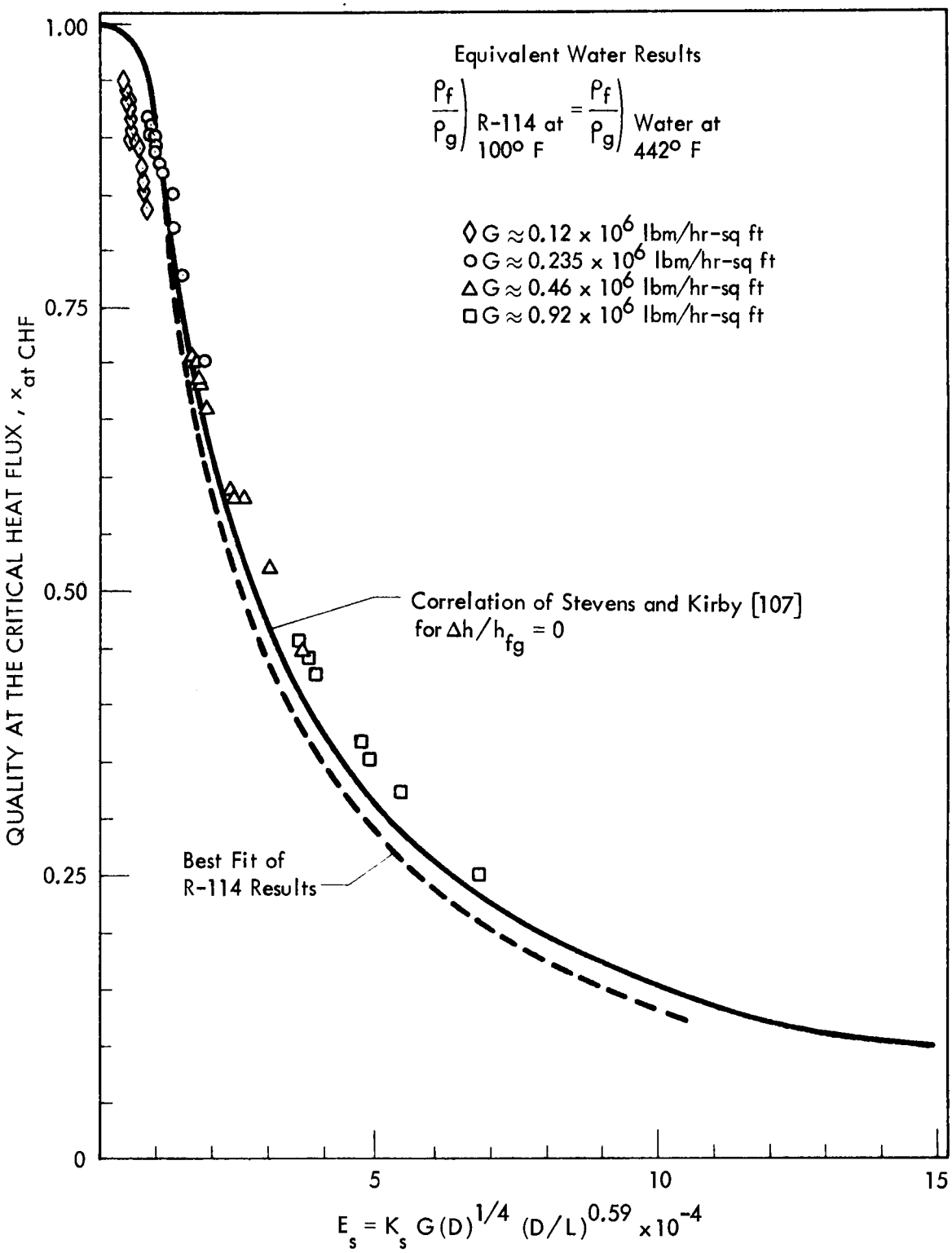


Figure IV-165. COMPARISON OF THE CRITICAL HEAT FLUX QUALITIES OBTAINED FOR WATER AT 442°F USING THE BIASI ET AL [112] CORRELATION WITH THE CORRELATION OF STEVENS AND KIRBY [107] AS MODIFIED BY STAUB [110] FOR THE CASE OF $\Delta h/h_{fg} = 0$. K_s IS AS DEFINED IN EQUATION (4-93).

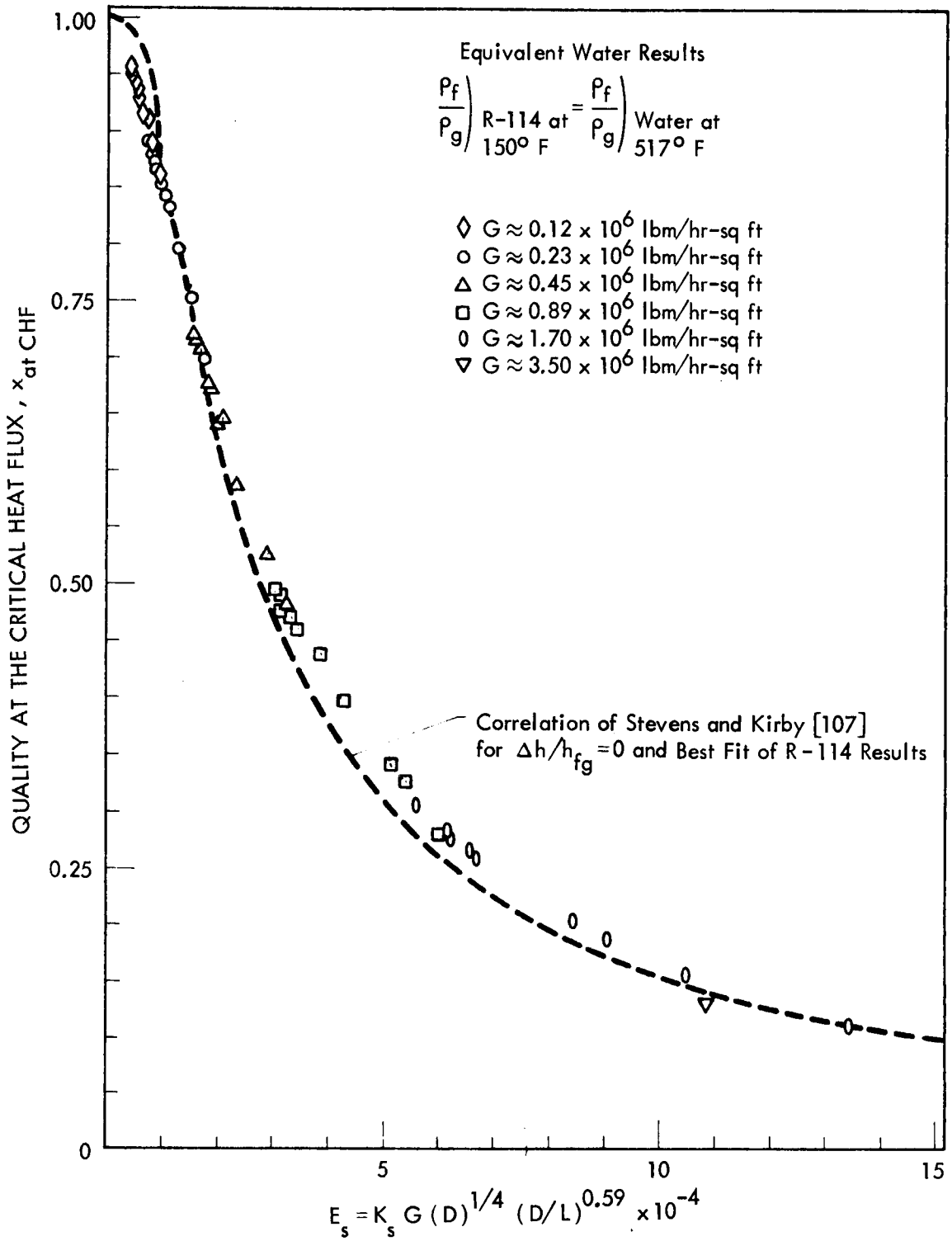


Figure IV-166. COMPARISON OF THE CRITICAL HEAT FLUX QUALITIES OBTAINED FOR WATER AT 517°F USING THE BIASI ET AL [112] CORRELATION WITH THE CORRELATION OF STEVENS AND KIRBY [107] AS MODIFIED BY STAUB [110] FOR THE CASE OF $\Delta h/h_{fg} = 0$. K_s IS AS DEFINED IN EQUATION (4-93).

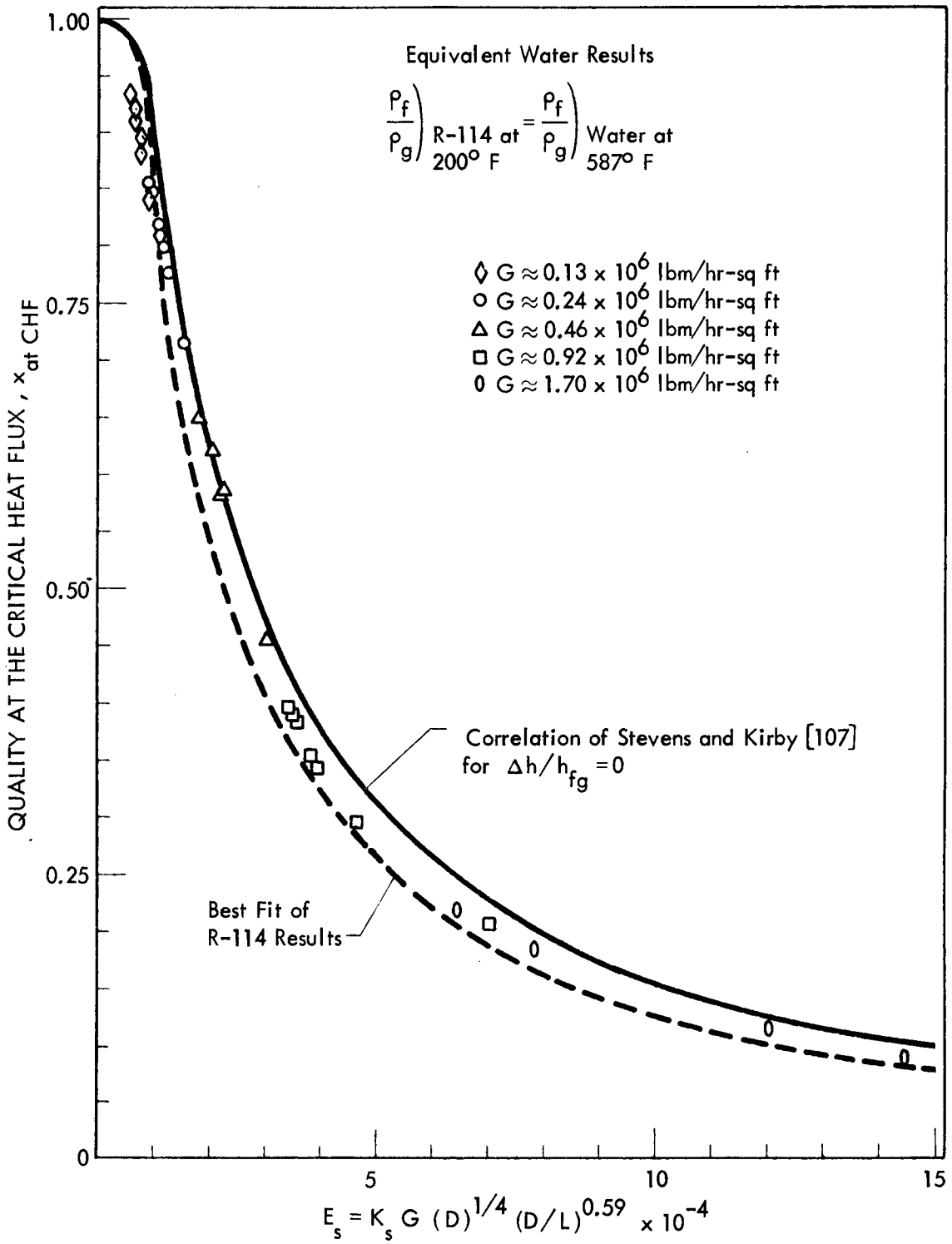


Figure IV-167. COMPARISON OF THE CRITICAL HEAT FLUX QUALITIES OBTAINED FOR WATER AT 587°F USING THE BIASI ET AL [112] CORRELATION WITH THE CORRELATION OF STEVENS AND KIRBY [107] AS MODIFIED BY STAUB [110] FOR THE CASE OF $\Delta h/h_{fg} = 0$. K_s IS AS DEFINED IN EQUATION (4-93).

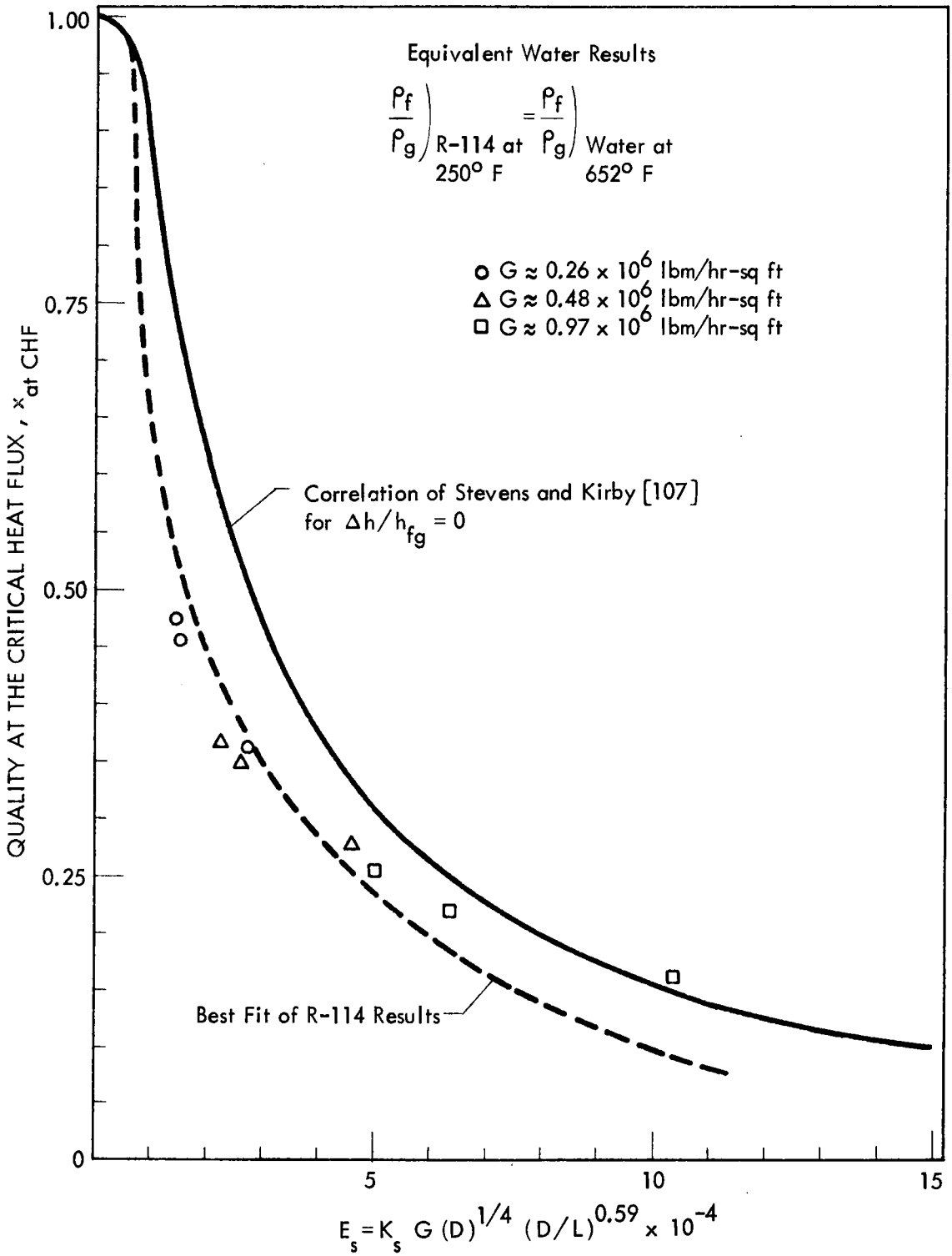


Figure IV-168. COMPARISON OF THE CRITICAL HEAT FLUX QUALITIES OBTAINED FOR WATER AT 652°F USING THE BIASI ET AL [112] CORRELATION WITH THE CORRELATION OF STEVENS AND KIRBY [107] AS MODIFIED BY STAUB [110] FOR THE CASE OF $\Delta h/h_{fg} = 0$. K_s IS AS DEFINED IN EQUATION (4-93).

was claimed that a unique plot of the exit quality at critical heat flux vs. $\Psi\ (D/L)^{0.6}$ existed for a given liquid to vapor density ratio. In Figures IV-169 to IV-172, such plots are presented for the R-114 critical heat flux results obtained in this study. As can be seen, this model correlated the results about as well as the scaling factor approach of Stevens and Kirby [107]. The compensated distortion model was also applied to the water equivalent data generated by using the Biasi et al [112] correlation. The same tube dimensions and flow rates were used for water as existed in the R-114 results and the liquid to vapor density ratios were modeled. The results are shown in Figures IV-173 to IV-176. Also shown in these figures is the best fit of the R-114 data at the same density ratio. As can be seen, with the exception of the 100°F runs, the R-114 and water equivalent results were modeled extremely well. Indeed, this compensated distortion model resulted in a better overall correlation and fluid model than the scaling factor approach of Stevens and Kirby with either a constant or a variable value for K_s as shown in Figures IV-156 to IV-163 and IV-165 to IV-168.

A regression type of analysis was performed on the data in this study and the following equations were found to best represent the results:

$$x_{at\ CHF} = 1-e^{y^+} \tag{4-94}$$

where

$$y^+ = -0.04299 \left(\frac{\rho_f}{\rho_g} - 1\right)^{0.5819} \Bigg/ \left[\Psi\left(\frac{D}{L}\right)^{0.7106}\right]^{1.0959} . \tag{4-95}$$

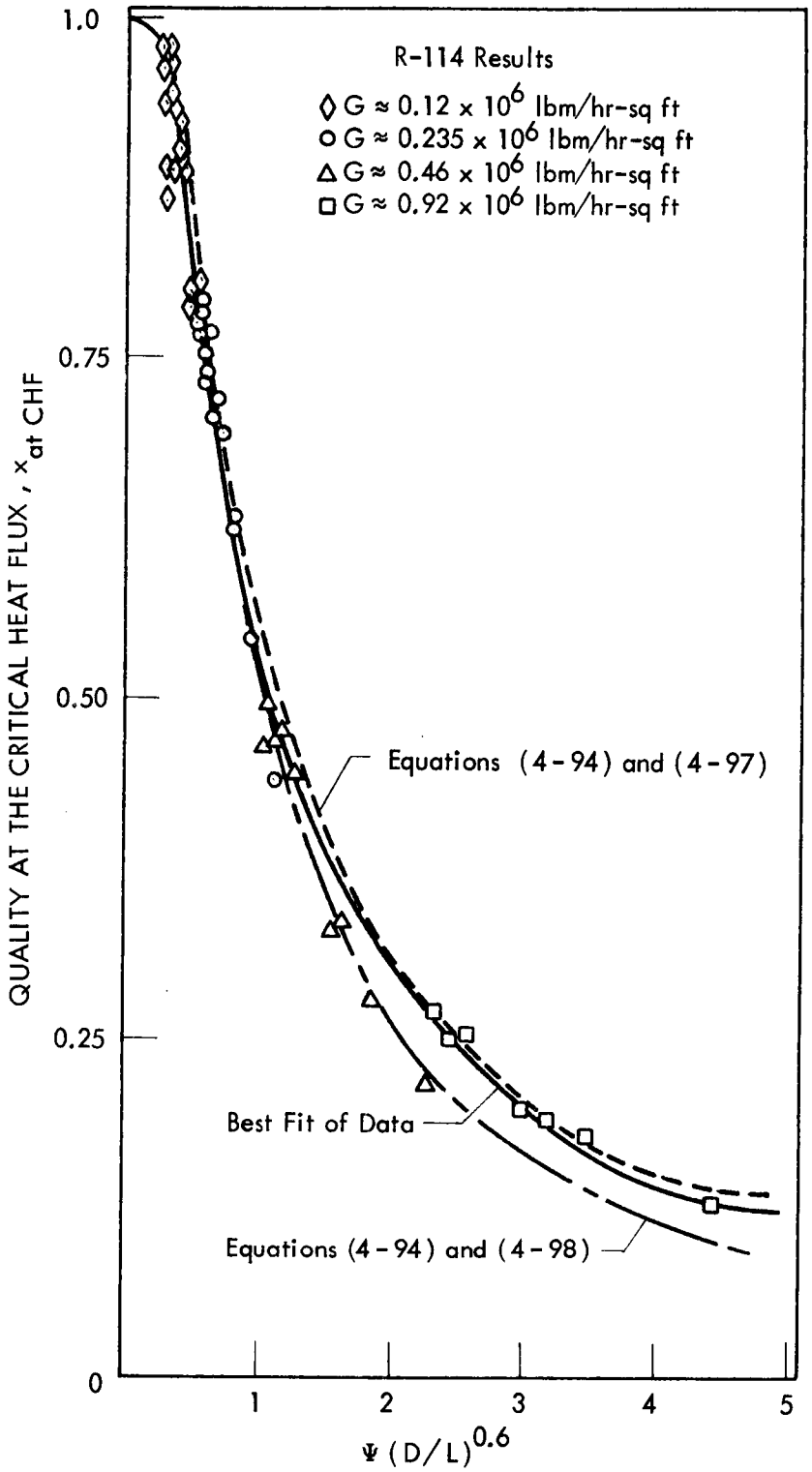


Figure IV-169. COMPARISON OF THE EXPERIMENTALLY DETERMINED QUALITIES AT THE CRITICAL HEAT FLUX WITH THE COMPENSATED DISTORTION MODEL OF AHMAD [116] . T ≈ 100° F.

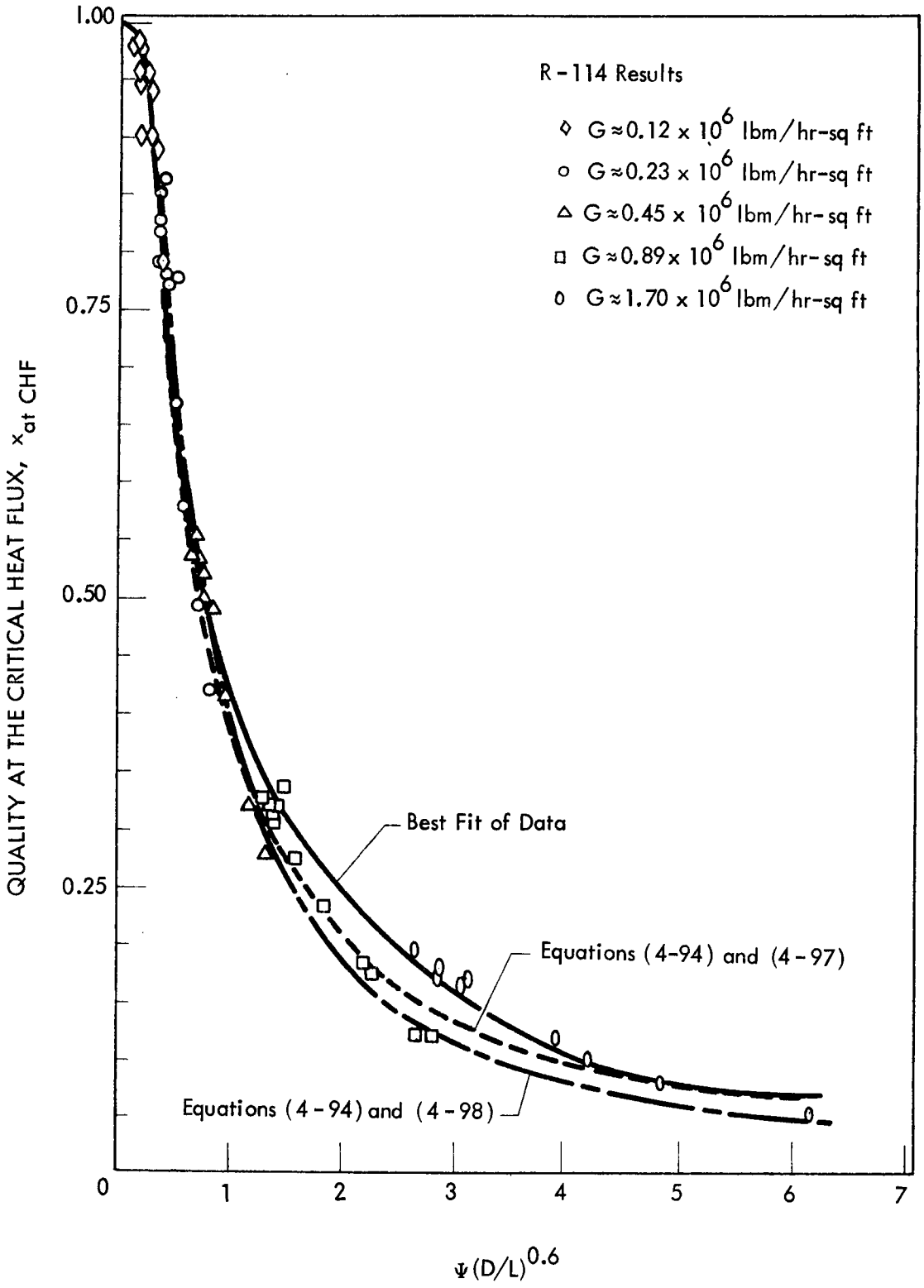


Figure IV-170. COMPARISON OF THE EXPERIMENTALLY DETERMINED QUALITIES AT THE CRITICAL HEAT FLUX WITH THE COMPENSATED DISTORTION MODEL OF AHMAD [116]. T ≈ 150°F.

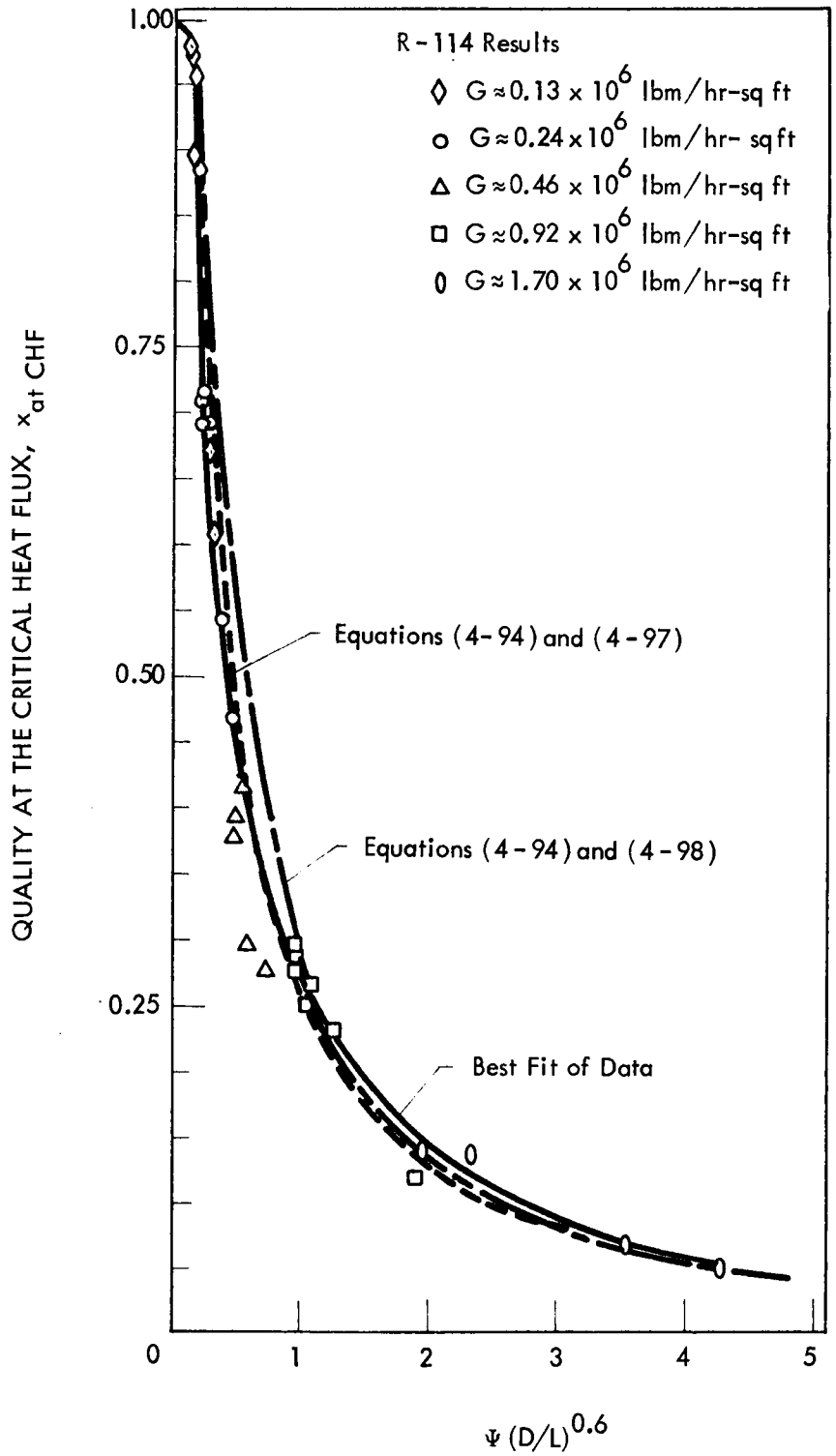


Figure IV-171. COMPARISON OF THE EXPERIMENTALLY DETERMINED QUALITIES AT THE CRITICAL HEAT FLUX WITH THE COMPENSATED DISTORTION MODEL OF AHMAD [116]. T≈ 200°F.

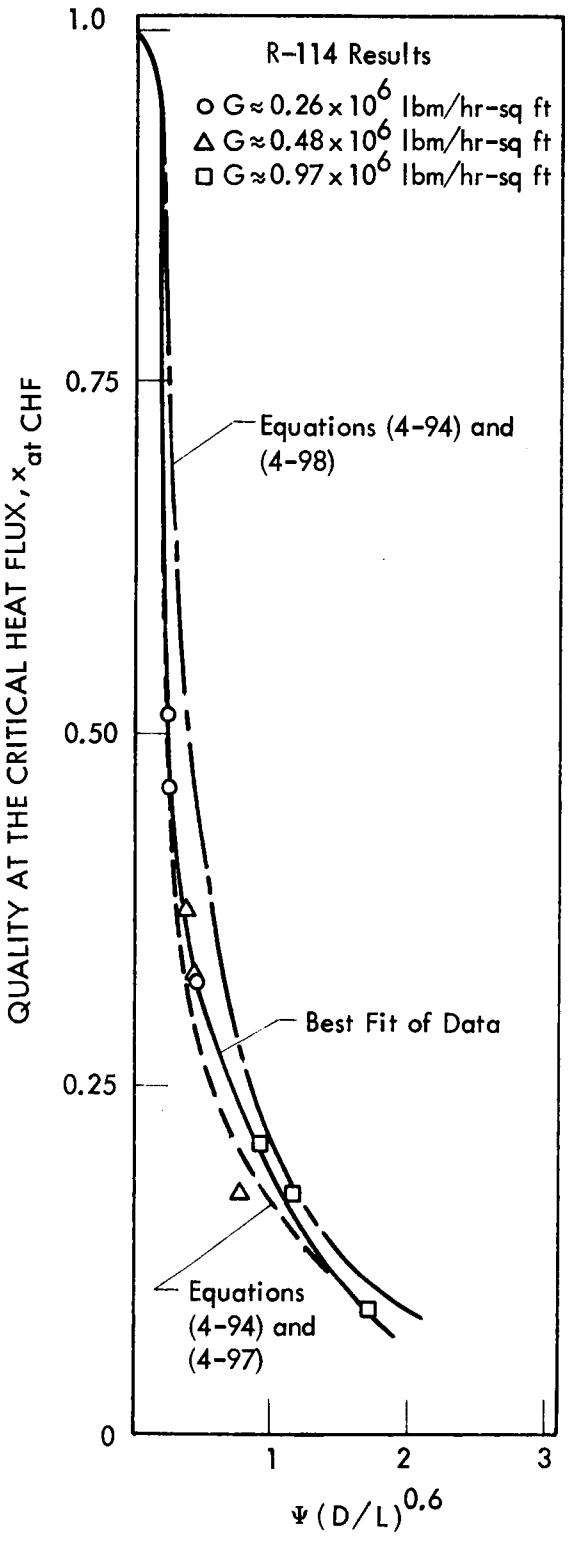


Figure IV-172. COMPARISON OF THE EXPERIMENTALLY DETERMINED QUALITIES AT THE CRITICAL HEAT FLUX WITH THE COMPENSATED DISTORTION MODEL OF AHMAD [116]. T ≈ 250° F.

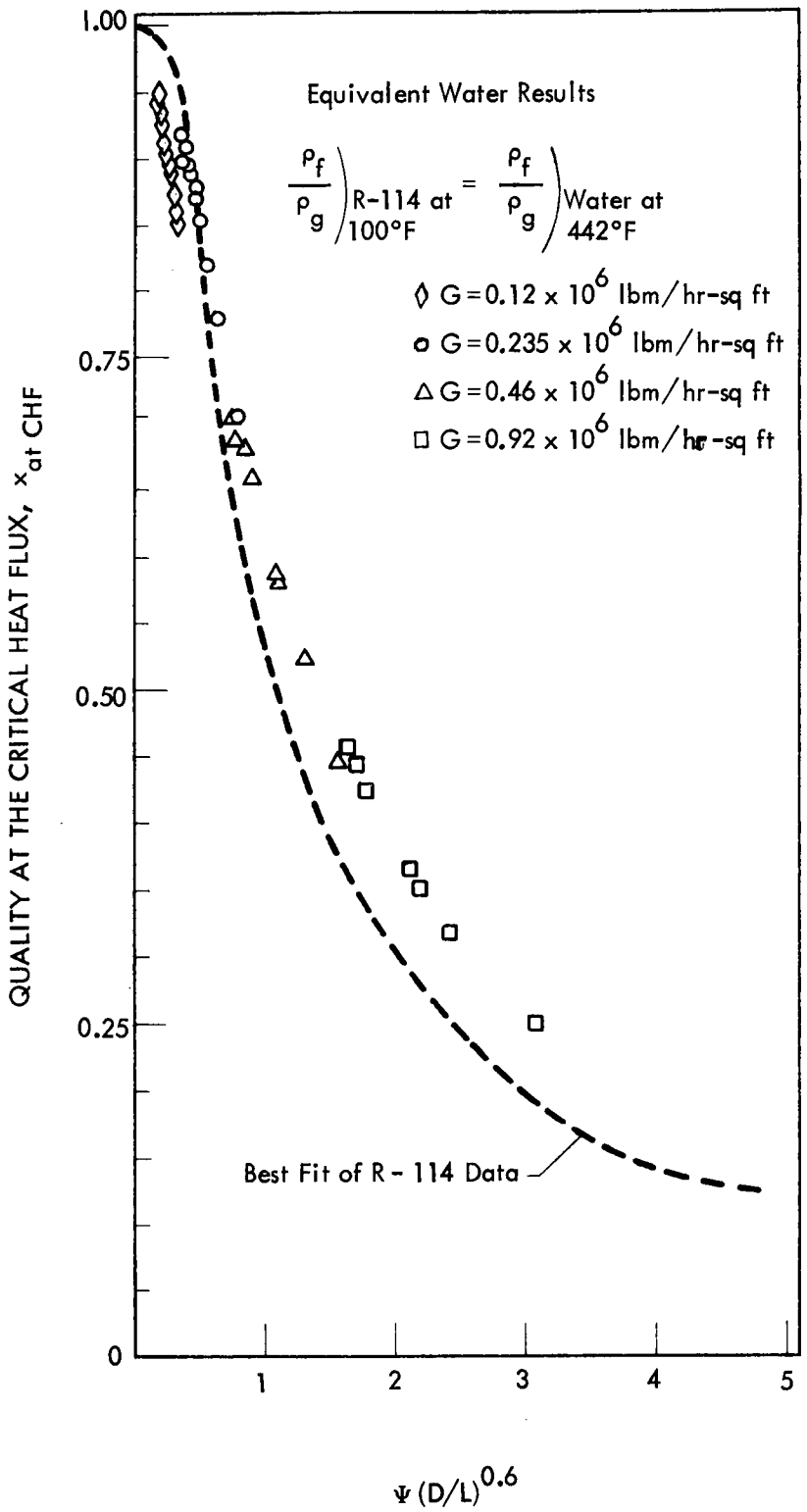


Figure IV-173. COMPARISON OF THE CRITICAL HEAT FLUX QUALITIES OBTAINED FOR WATER AT 442°F USING THE BIASI ET AL [112] CORRELATION WITH THE COMPENSATED DISTORTION MODEL OF AHMAD [116].

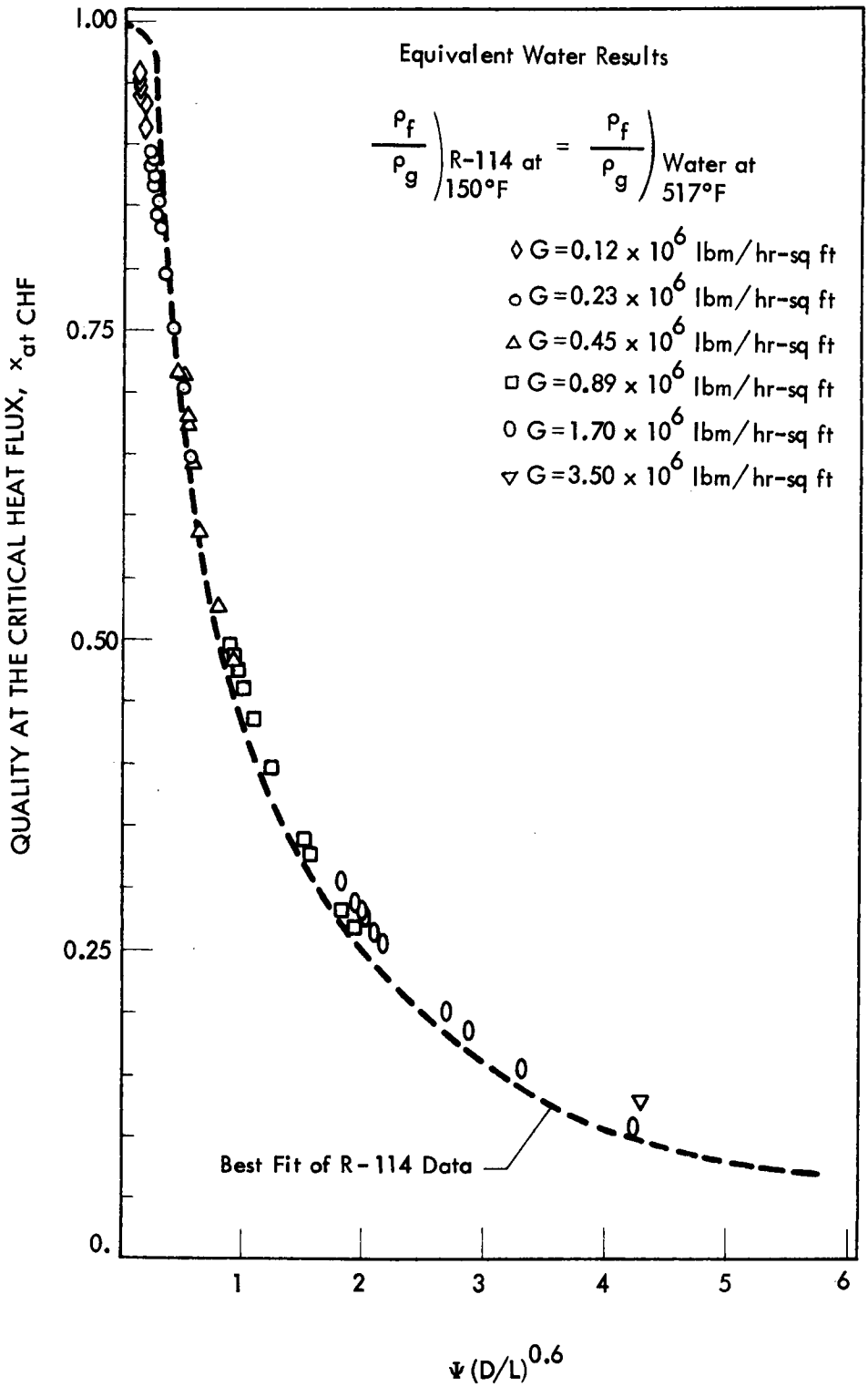


Figure IV-174. COMPARISON OF THE CRITICAL HEAT FLUX QUALITIES OBTAINED FOR WATER AT 517°F USING THE BIASI ET AL [112] CORRELATION WITH THE COMPENSATED DISTORTION MODEL OF AHMAD [116].

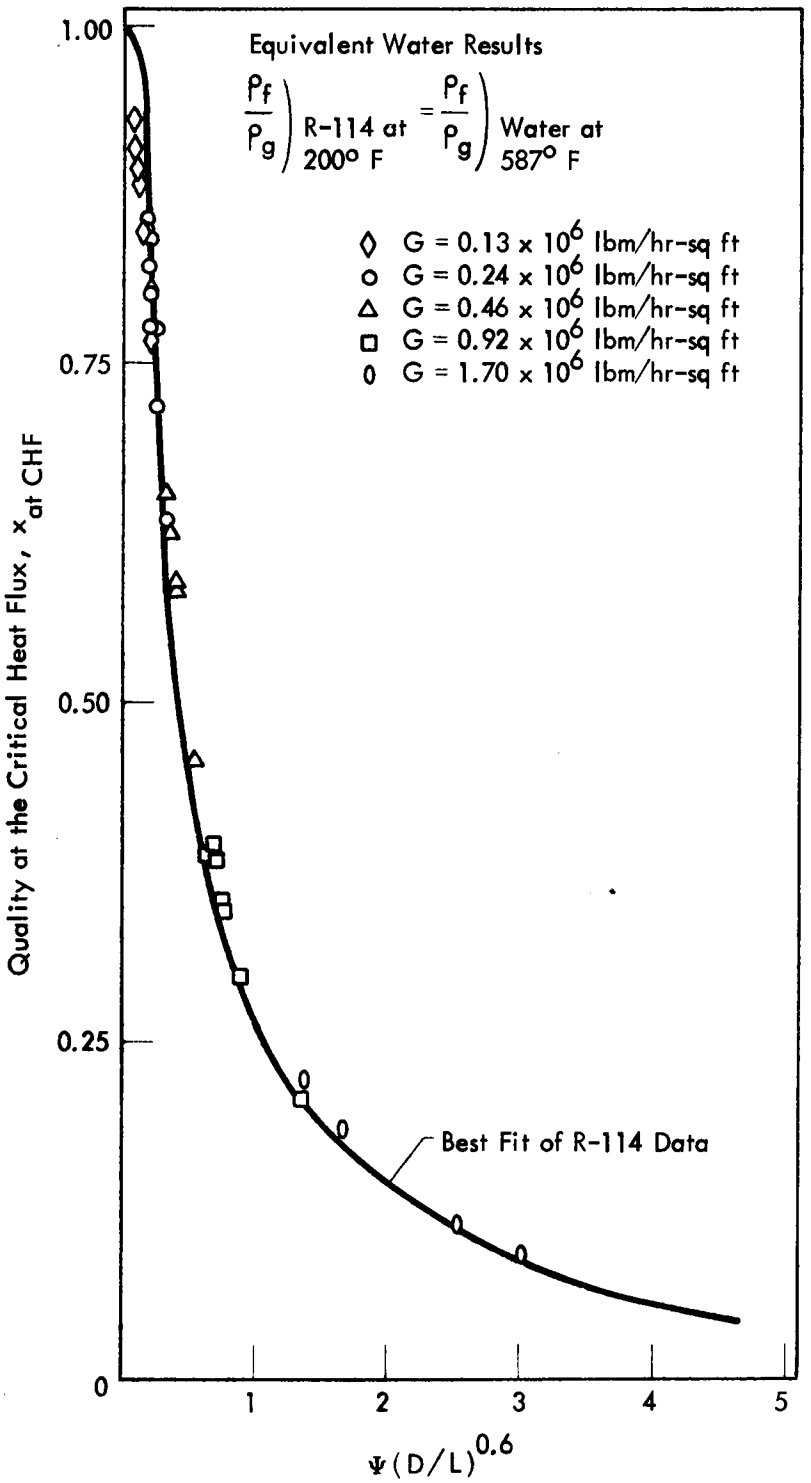


Figure IV-175. COMPARISON OF THE CRITICAL HEAT FLUX QUALITIES OBTAINED FOR WATER AT 587°F USING THE BIASI ET AL [112] CORRELATION WITH THE COMPENSATED DISTORTION MODEL OF AHMAD [116].

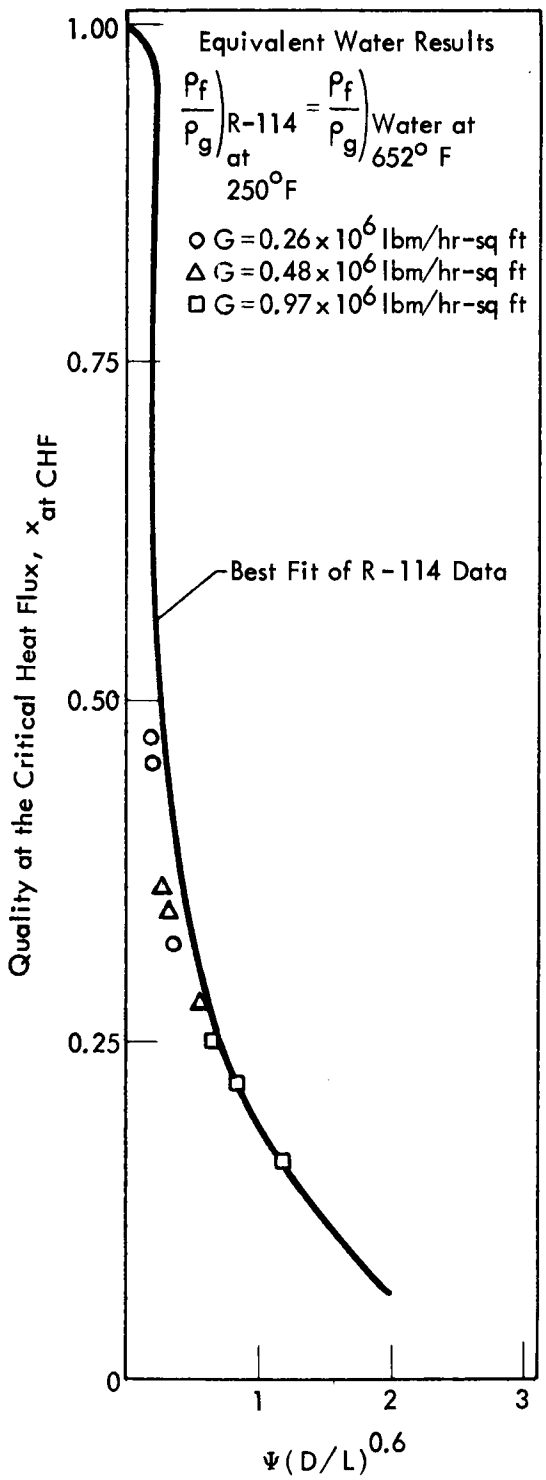


Figure IV-176. COMPARISON OF THE CRITICAL HEAT FLUX QUALITIES OBTAINED FOR WATER AT 652°F USING THE BIASI ET AL [112] CORRELATION WITH THE COMPENSATED DISTORTION MODEL OF AHMAD [116].

It should be noted here that the exponent on the (D/L) term is different from the 0.6 power claimed by Ahmad [116] or the 0.59 power used by Stevens and Kirby [107] as shown in Figures IV-156 to IV-163 and IV-165 to IV-168.

The results of Dix [111] for R-114 were anlayzed in a similar way. Since however, his results included a subcooled length, this was subtracted out and only the saturated length was used. This yielded the correlation:

$$y^+ = -0.1004 \left(\frac{\rho_f}{\rho_g} - 1 \right)^{0.3427} \Big/ \left[\Psi \left(\frac{D}{L} \right)^{0.6905} \right]^{1.1970} \qquad (4\text{-}96)$$

which when substituted into Equation (4-94) yielded the quality at which critical heat flux occurred. Again, it is noted that the exponent of the (D/L) term is not 0.60 but is quite similar to the value experimentally obtained in this study. To determine the sensitivity of the regression analysis to the exponent of the (D/L) term, the 0.60 power was "forced on" and the following result obtained:

$$y^+ = -\ 0.0711 \left(\frac{\rho_f}{\rho_g} - 1 \right)^{0.5918} \Big/ \left[\Psi \left(\frac{D}{L} \right)^{0.6} \right]^{1.1150} \qquad (4\text{-}97)$$

for the present data, and

$$y^+ = -0.1127 \left(\frac{\rho_f}{\rho_g} - 1 \right)^{0.4623} \Big/ \left[\Psi \left(\frac{D}{L} \right)^{0.6} \right]^{1.2963} \qquad (4\text{-}98)$$

for Dix's [111] data. The parameter Ψ can be recast into the form:

$$\Psi = \Psi^* \, G(D)^{1/3}. \qquad (4\text{-}99)$$

For R-114 in the 100 to 250°F temperature range, Ψ^* is represented by the equation:

$$\Psi^* = \left(135.209 - 1.53764\ T + 0.88672 \times 10^{-2}\ T^2 - 0.26636 \times 10^{-4}\ T^3 + 0.32853 \times 10^{-7}\ T^4 \right) \times 10^{-6}. \qquad (4\text{-}100)$$

Here, T is in °F, G is in lbm/hr-sq ft, and D is in inches. Only a small increase was noted in the rms error between the correlations where the exponent of the (D/L) term was held constant at 0.6 and where it was allowed to vary. Appendix G should be consulted for additional information on the error analysis.

Equations (4-97) and (4-98), inserted into Equation (4-94) are shown plotted in Figures IV-169 to IV-172. The agreement between the present data and Dix's [111] data is seen to be best in the region around 200°F. Remembering that Dix's [111] data were taken in the range of 169.5 to 213.5°F, this is not surprising.

In order for the results from Equations (4-94) and (4-95) to be easily applicable, Figures IV-177 to IV-180 were generated. Since the four interrelated parameters are the boiling temperature (i.e., fluid properties), the mass flux, the critical heat flux, and the exit quality, the graphs in Figures IV-177 to IV-180 can be easily used by design engineers. It should be noted that these graphs are valid only for R-114 flowing in a 0.785-in.-dia tube. For different sized tubes, Equations (4-94) and (4-95) should be used to generate the particular graphs of interest.

In summary, it can be said that the compensated distortion model presented by Ahmad [116] was generally better at modeling the critical heat fluxes of different fluids than either the scaling law or scaling factor approach. In addition, this compensated distortion model resulted in the attainment of good agreement between the results of this study and those of Dix [111]. In so doing, the assumption that the analysis of the critical heat flux in tubes with subcooled boiling lengths can be undertaken by subtracting the subcooled length has been

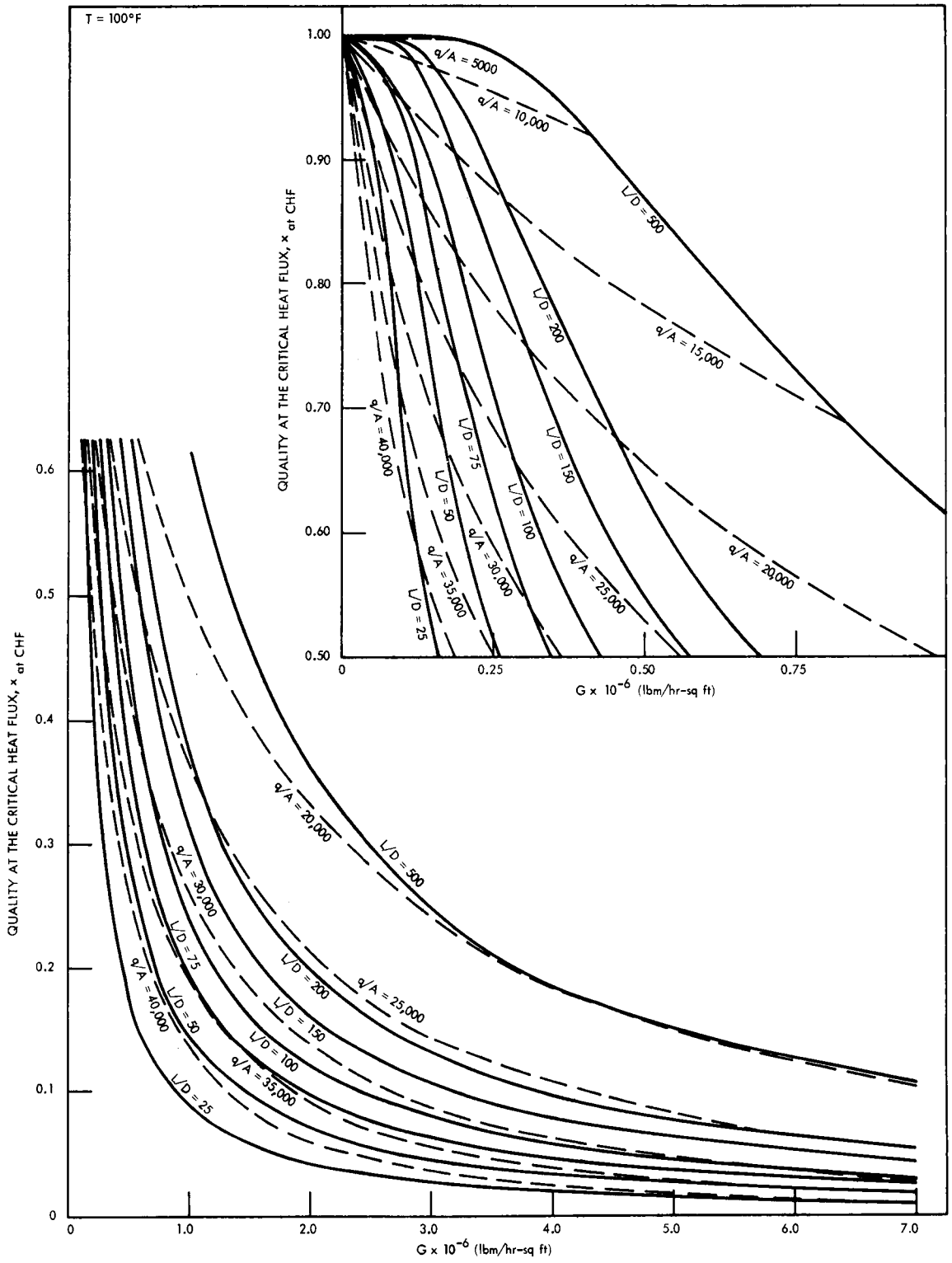


Figure IV-177. PLOT OF THE COMPENSATED DISTORTION MODEL FOR R-114 BOILING IN A 0.785-IN.-I D TUBE. T = 100°F.

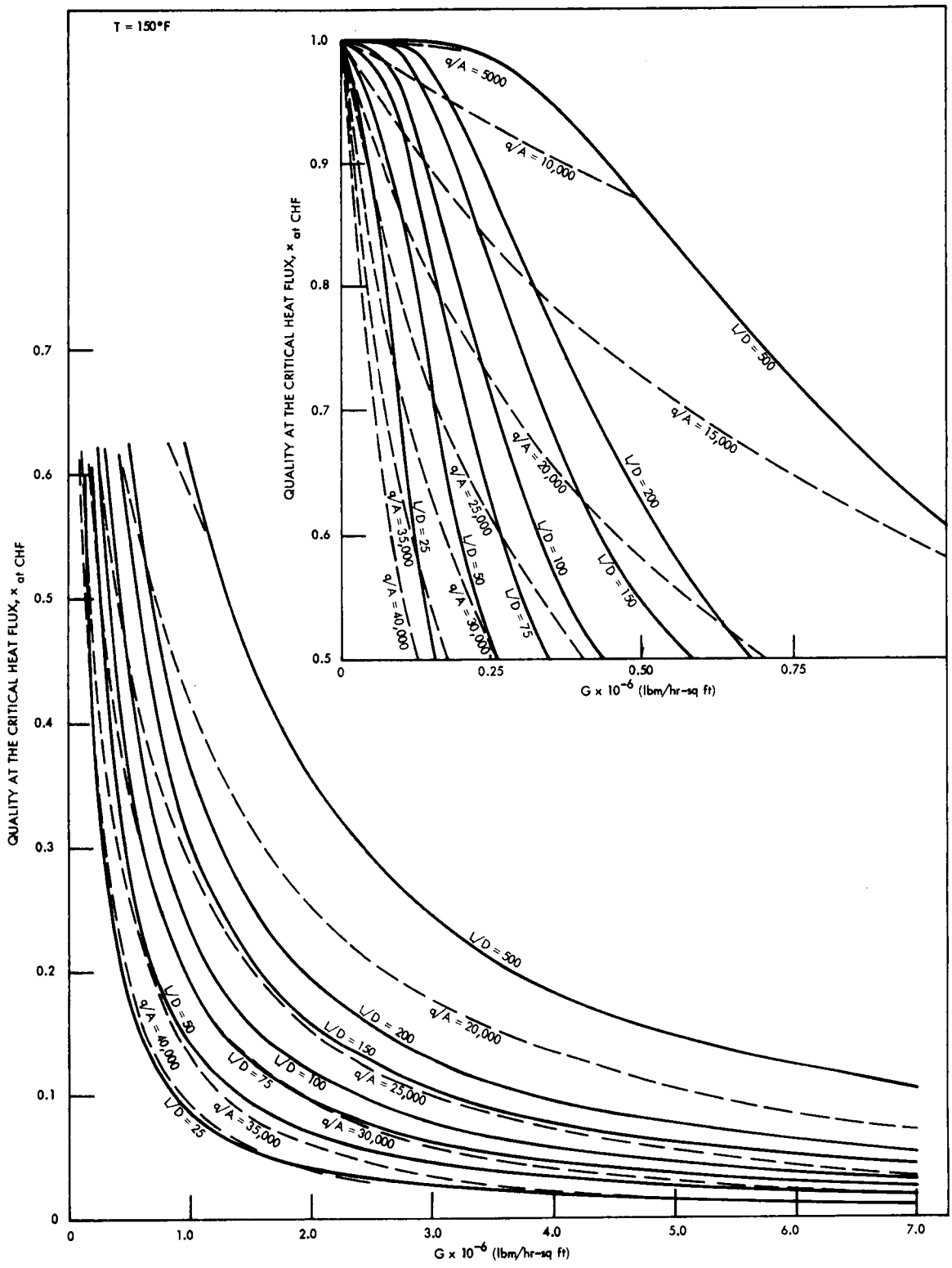


Figure IV-178. PLOT OF THE COMPENSATED DISTORTION MODEL FOR R-114 BOILING IN A 0.785 IN.-ID-TUBE. T=150°F.

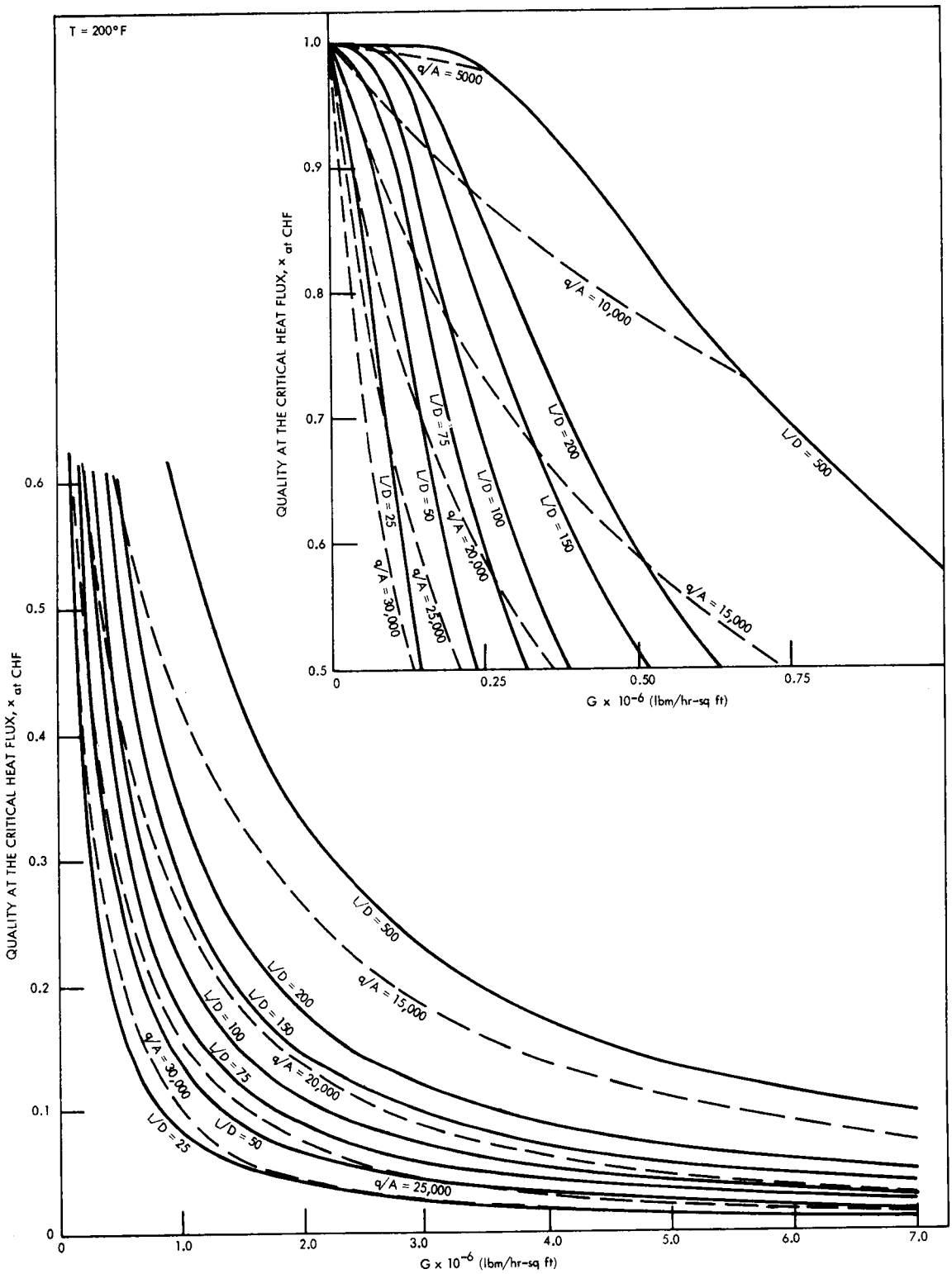


Figure IV-179. PLOT OF THE COMPENSATED DISTORTION MODEL FOR R-114 BOILING IN A 0.785-IN.-I D TUBE. T = 200°F.

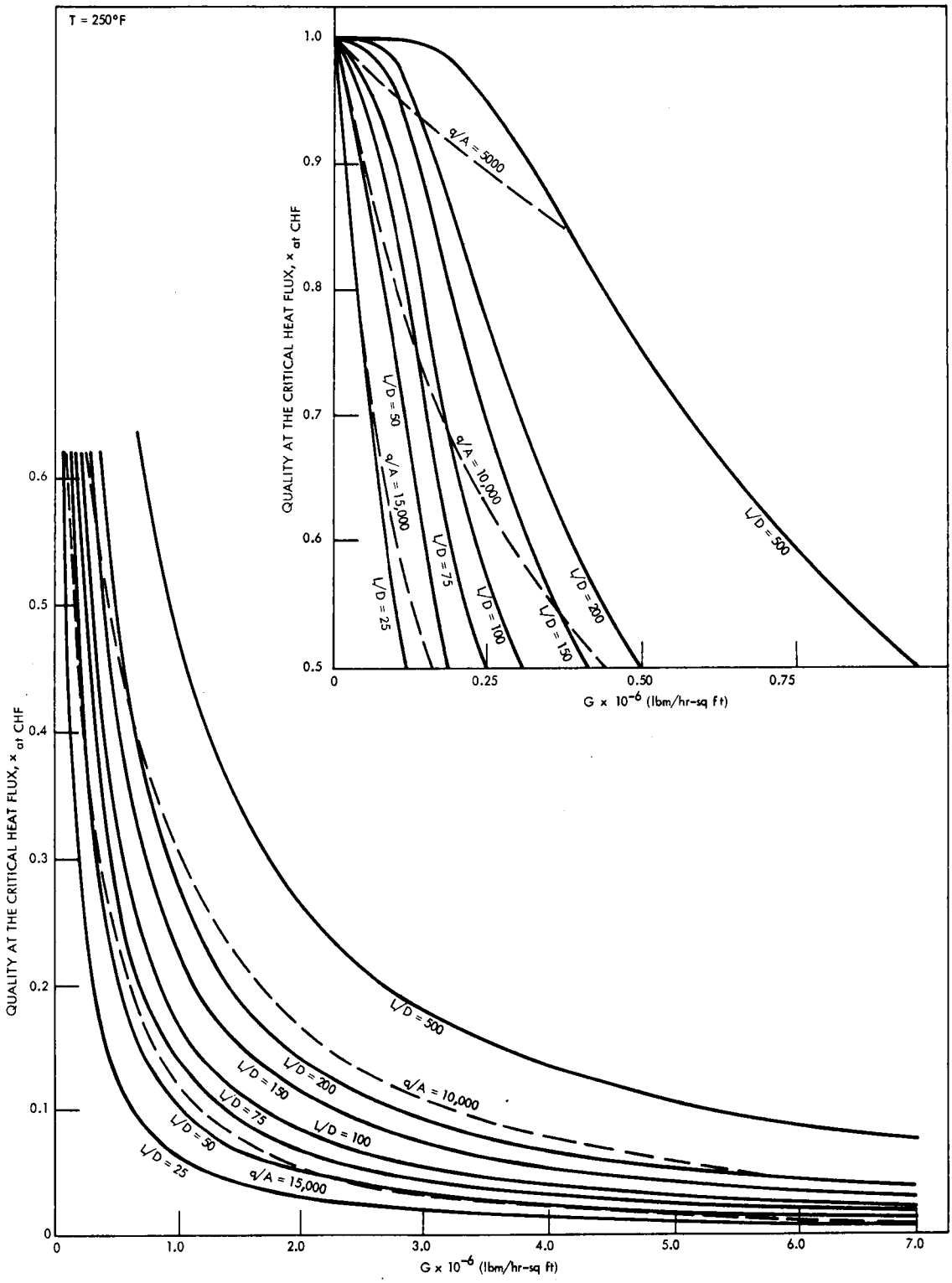


Figure IV-180. PLOT OF THE COMPENSATED DISTORTION MODEL FOR R-114 BOILING IN A 0.785-IN.-ID TUBE. T=250°F.

reinforced for the range of L/D ratios studied here. This technique was previously used by Staub [110]. For the case of R-114, Equations (4-94) and (4-95) are recommended for evaluation of the critical heat flux. A similar form of the equation with possibly different coefficients is believed to hold true for other fluids.

TWO-PHASE FLOW PRESSURE DROP AND HEAT TRANSFER CHARACTERISTICS OF REFRIGERANTS IN VERTICAL TUBES

A Dissertation

Presented for the

Doctor of Philosophy

Degree

The University of Tennessee

Philip A. Jallouk

December 1974

CHAPTER V

SUMMARY, CONCLUSIONS, AND RECOMMENDATIONS

Summary and Conclusions

A comprehensive study of the behavior of boiling R-114 in a vertical tube has been undertaken. Analytic and experimental techniques have been used to investigate the heat transfer and pressure drop characteristics. From this, an improvement in the prediction of the system behavior has been obtained and the discrepancies between the behavior of boiling refrigerants and other working fluids has been explained. New equations were developed or existing ones verified so that design engineers requiring information on the flow regime, pressure drop, heat transfer coefficient, and critical heat flux characteristics of boiling refrigerants in vertical tubes at operating conditions not too different from those studied here may use the equations presented here. The limitations of each equation are also presented. The four interrelated areas of endeavor will be explained below:

Flow Regimes. The flow regime information obtained indicated that at low mass fluxes and boiling temperatures, the major part of the flow was in the annualr type of flow regime. As the boiling temperature increased, the range of the bubbly flow regime was found to increase significantly. With increasing flow rate, however, there was a decrease in the size of the bubbly and weak annular flow regimes and a corresponding increase in the region of unidentifiable flow. Insufficient information was available to make a definite judgment as to the effect of adiabatic vs. diabatic boundary conditions or critical flux vs. non-critical heat flux operation.

1175404

Comparison of the experimental observations made in this study with the Baker [5] map and the Quandt [7] analysis did not yield any satisfactory agreement. Zuber et al [10] and J. L. L. Baker [17] presented additional equations for the boundaries between various adiabatic and diabatic flow regimes. Only the J. L. L. Baker [17] equations were found to be accurate. Thus, Equations (2-8) to (2-10), as well as the scaling of the experimental flow regimes obtained with one fluid to another on an equal density ratio basis were found to give the closest albeit not entirely satisfactory agreement.

Pressure Drop. In the pressure drop, as well as the heat transfer coefficient and critical heat flux studies, no differences were observed between runs conducted in the natural and forced circulation modes. In attempting to separate out the gravitational, frictional, and acceleration components of the pressure drop, it was noted that insufficiently accurate information was available on the void fraction of R-114. The Zuber et al [10] void fraction correlation, modified here in the high quality region, was not totally satisfactory. This was due to the fact that using this void fraction correlation, the sum of the calculated gravitational and acceleration terms were, in some cases, larger than the experimentally measured total pressure drop. Also, the use of the modified Zuber et al [10] void fraction correlation in computing the multiplication factor F in the Chen [80] correlation yielded inaccurate results. The use of the Martinelli-Nelson [4] void fraction results modeled for refrigerants on an equal density ratio basis yielded reasonable values.

Comparison of the frictional components of the pressure drop formulated in terms of the Martinelli multiplier for the turbulent-turbulent

case, Φ_{ftt}, indicated that at low flow rates and low boiling temperatures, the frictional component from the Martinelli-Nelson [4] model was more accurate than the one from the Homogeneous [3] model. As the mass flux was increased at a constant boiling temperature, the experimental Martinelli multiplier values began to decrease and approach those of the Homogeneous [3] model curve. Also, at a constant flow rate, as the boiling temperature increased, the experimental results approached those of the Homogeneous [3] model.

A comparison of the results of this study with numerous other correlations indicated that the equations developed by Chisholm [28] in 1973 gave the best agreement with the experimental results. In this correlation:

$$\Phi_{ftt} = 1 + (\Gamma^2 - 1)\left\{ Bx^{0.9}\,(1 - x)^{0.9} + x^{1.8} \right\} \qquad (2\text{-}21)$$

where

$$\Gamma = \left(\frac{\rho_f}{\rho_g}\right)^{0.5} \left(\frac{\mu_g}{\mu_f}\right)^{0.1} \qquad (2\text{-}22)$$

and B is given in Table II-1 on page 33.

This correlation was also found to agree well with the experimental data for R-11 and R-12 over a very wide range of boiling temperatures and flow rates in both vertical and horizontal flow. Only at very low temperatures and flow rates was the Chawla [29, 30, 31, 32] correlation given in Equations (2-23) and (2-24) found to be better. The results in this range of operation were however meager. It should be noted that the use of the Chisholm [28] 1973 correlation will always yield a conservative answer.

In the critical heat flux region, the data were found to correlate differently from those in the non-critical heat flux region. At low qualities where a vapor binding type of critical heat flux with bubbles forming an insulating layer on the wall was believed to have occurred, the Martinelli multiplier was below that observed in the non-critical heat flux regime. At high qualities where a film dryout type of critical heat flux took place, the multiplication factor was the same as that existing at non-critical heat flux conditions.

Heat Transfer Coefficients. The experimental heat transfer coefficients obtained in this study were compared to the ones predicted by numerous heat transfer correlations in the literature. None was found to be satisfactory. The Chen [80] correlation, however, exhibited the least amount of scatter and the smallest deviation. This correlation, which was found to reliably predict the boiling coefficients of water and some other fluids, generally underestimated the boiling coefficients of refrigerants. A detailed analysis of the different components of the Chen [80] correlation indicated that the pool boiling term was not applicable to refrigerants. A modification of the coefficient in the Forster-Zuber [52] pool boiling equation to 0.3802 from 0.172 or the use of the Rohsenow [61] pool boiling equation with a $C_{sf} = 0.0047$ yielded a considerable improvement in correlating the heat transfer coefficients. These coefficients were very close to those experimentally obtained from an independent pool boiling test of R-114 on a copper surface. In addition the modification of the multiplication factor F yielded an additional albeit much smaller improvement. An experimental suppression factor curve was obtained which was quite similar to that

Chen [80] obtained although an effect of pressure was noted. The following equations were found to best predict the heat transfer coefficients of R-114 boiling in a vertical copper tube:

$$h_{TP} = 0.023\ (Re)_{fa}^{0.8}\ (Pr)_f^{0.4}\ \frac{k_f}{D}\ F$$

$$+ 0.3802 \left(\frac{k_f^{0.79}\ c_{pf}^{0.45}\ \rho_f^{0.49}}{h_{fg}^{0.24}\ \rho_g^{0.24}\ \sigma^{0.5}\ \mu_f^{0.29}} \right) (\Delta T)^{0.24}\ (\Delta P)^{0.75}\ S \qquad (4\text{-}83)$$

or:

$$h_{TP} = 0.023\ (Re)_{fa}^{0.8}\ (Pr)_f^{0.4}\ \frac{k_f}{D}\ F$$

$$+ \left(\frac{k_f^{5.1}((\Delta\rho)^{0.5}\ g^{0.5}}{(0.0047)^3 c_{pf}^{2.1}\ \mu_f^{4\ 1}\ \sigma^{0.5}\ h_{fg}^2\ g_c^{0.5}} \right) (\Delta T)^2\ S \qquad (4\text{-}84)$$

Equation (4-82) should be used for the suppression factor S and Equation (4-23) for the multiplication factor F. For other fluid-surface combinations, different coefficients may be applicable. These equations should be used only in the range of $G \leq 1.7 \times 10^6$ lbm/hr-sq ft.

Two analytical solutions were presented for the suppression factor S. The transient analysis was found to give more reasonable agreement with experimental results than the steady state solution. The necessity of knowing the frequency of bubble departure from the boiling surface limited the applicability or even definite confirmation of this analytical model since information on the bubble frequency in forced convection boiling is practically non-existent.

An interesting extension of the modified Chen [80] correlation having practical importance dealt with the change in the heat transfer coefficient along the length of the tube. This was mathematically analyzed by taking the derivative with respect to quality of the heat transfer coefficient defined by the modified Chen [80] correlation. From this, the wide variation found in the literature of the slope of the heat transfer coefficient along the length of the tube could be predicted and meaningfully understood.

Little additional data on the boiling of refrigerants in vertical tubes was found in the literature in convenient and sufficiently detailed form to enable a correlation to be attempted. For the data that did exist, the use of correlations in the form of equations (4-83) and (4-84) were not very successful. For flow in horizontal tubes the problem is more complex and for sufficiently low mass fluxes, annular flow does not exist and the application of the modified Chen [80] correlation breaks down.

Critical Heat Flux. The critical heat flux results obtained in this study were compared to those for water using the scaling laws of Barnett and Wood [105]. The results obtained were not satisfactory and the critical heat flux values for water were generally lower than the corresponding R-114 case. The application of the scaling factor method of Stevens and Kirby [107] resulted in an improved correlation at all boiling temperatures except for the 250°F case. There, the modified correlation of Stevens and Kirby [107] overestimated the exit quality at the critical heat flux. The same trend was noted in the equivalent

water results when a value of 0.658 was substituted for K. A variable value for K_s, given in Equation (4-93) yielded a slight improvement.

The compensated distortion model of Ahmad [116] was better at modeling the critical heat flux than either the scaling law or scaling factor approach. In addition, it yielded good agreement between the results of this study and those of Dix [111] and reinforced the assumption that the subcooled length can be subtracted out in the critical heat flux analysis. The R-114 results were correlated by the equations:

$$x_{\text{at CHF}} = 1 - e^{y^+} \tag{4-94}$$

where

$$y^+ = -0.04299 \left(\frac{\rho_f}{\rho_g} - 1\right)^{0.5819} \Bigg/ \left[\psi\left(\frac{D}{L}\right)^{0.7106}\right]^{1.0959} \tag{4-95}$$

A correlation similar to Equation (4-95) but with possibly different coefficients is believed to hold true for other fluids.

Recommendations

Based on the results of this study, the following recommendations are made:

(1) An extension of the Quandt [7] analysis should be undertaken. At present, the analysis is limited to the case of fully developed homogeneous flow. Modification would require the addition of an acceleration term to the analysis of the forces on an element of liquid along with the use of the more reasonable separated flow model for the wave, as well as the dispersed annular-rivulet flow regime.

(2) Additional flow regime information with R-114 and other fluids needs to be obtained to increase the amount of knowledge and to

further check on the feasibility of comparing flow regime studies from numerous fluids on an equal density ratio basis. Flow regimes in horizontal flow should be considered too. To aid in this endeavor, a uniform set of flow regime terminologies and their definitions should be established.

(3) Additional reliable information on the void fraction of R-114 is needed. Shiralkar [50], who has obtained the only set of measurements, took data at only one boiling temperature and at qualities of less than 0.45. Information over a large range of boiling temperatures, flow rates, and qualities is needed so that a proper void fraction formulation, possibly based on the Zuber et al [10] void fraction correlation can be developed.

(4) At the present time, the use of the Chisholm [28] correlation obtained in 1973 as given in Equations (2-21) and (2-22) and Table II-1 on page 33 is recommended for reduced pressures of 0.05 and above provided the mass flux is 0.25×10^5 lbm/hr-sq ft or greater. For reduced pressures of less than 0.05 and a mass flux of less than 0.5×10^5 lbm/hr-sq ft, the Chawla [29, 30, 31, 32] correlation would probably be better. Outside the range of the above limitations, insufficient data exist to formulate any recommendations. The use of Chisholm's [28] 1973 correlation for design purposes will, however, always yield a conservative answer. Additional experimental work needs to be done to more clearly delineate the limits on the Chisholm [28] 1973 correlation and Chawla's [29, 30, 31, 32] equations. In addition, a close study of Chisholm's [28] 1973 correlation should be made to see if its applicability can be extended to the low flow rate and low reduced pressure region.

(5) Additional pressure drop tests with R-114 in a horizontal tube of the same dimensions as the one used in this study are recommended. Such experimental results will have the advantage of not containing a gravitational component and consequently should yield quite accurate frictional pressure drop results. In addition, any deviation between vertical and horizontal flow frictional pressure drops at low flow rates where stratification is expected to occur can be observed. This may shed further light on why the Chisholm [28] 1973 correlation broke down at the low flow rates. These tests should be supplemented with observations of the flow regime occurring.

(6) A considerable amount of heat transfer coefficient data on the forced convective boiling of refrigerants exists in the literature today. Much of it is not in a convenient form to use. It is recommended that these data be reanalyzed and a correlation of the type given in Equations (4-83) and (4-84) with variable coefficients be attempted. The results of Chawla [29, 30, 31, 32] and Purcupile, Riedle, and Schmidt [94] are but two publications where a large amount of potentially valuable data exist.

(7) Additional heat transfer tests with R-114 in a horizontal tube of the same dimensions as the one used in this study are also recommended. The differences in the heat transfer coefficients between vertical and horizontal flow observed in the results of Chaddock and Noerager [43] and attributed to stratification can be studied. Supplementing these tests with flow regime observations is highly desirable.

(8) An extensive, detailed, and carefully executed series of pool boiling tests with refrigerants on a variety of pool boiling surfaces of

different finishes needs to be undertaken. The pool boiling results already in the literature are meager and in some cases could not be satisfactorily correlated by equations which have been found to work well for other fluids. From this series of tests, reliable pool boiling correlations should be obtained with an extensive catalog of coefficients for the various fluid-surface combinations. The validity of the Borishanskiy-Minchenko [58] equation, especially, needs to be verified for refrigerants.

(9) Carefully run forced convection tests should be conducted in conjunction with pool boiling tests utilizing test sections made from the same piece of stock and having identically the same surface finish. This should further reinforce the concept of the pool boiling and forced convective superposition.

(10) Information on the frequency of bubble generation from a surface under forced convective boiling conditions needs to be obtained to verify the transient solution for the suppression factor represented in Chapter IV above.

(11) The modified Chen [80] correlation given above in Equations (4-83) and (4-84) should be expanded to the case of subcooled boiling and boiling in augmented heat transfer cases. The single phase convective component can probably be modified so that a coefficient representing the subcooled portion can be included. For the augmented heat transfer case, the single and two-phase Reynolds numbers would have to be modified to account for both the linear and angular velocity components. Moles and Shaw [132] who have pursued this approach for subcooled organic and inorganic liquids obtained encouraging results.

(12) The critical heat flux results in the literature for the various refrigerants should be reanalyzed and an attempt to correlate them using the compensated distortion model of Ahmad [116] should be attempted.

(13) The effect of tube orientation on the critical heat flux is not known. A series of tests to measure the critical heat flux in a horizontal tube containing R-114 should serve to supplement the vertical test section results of Dix [111] and those of this study. Again here, flow regime may be an important parameter.

REFERENCES

REFERENCES

1. "Properties and Applications of the 'Freon' Fluorinated Hydrocarbons," Du Pont Technical Bulletin B-2, E. I. du Pont de Nemours and Company, Wilmington, Delaware, 1966.

2. "ASHRAE Handbook of Fundamentals," American Society of Heating, Refrigerating, and Air-Conditioning Engineers, Inc., New York, 1972, pp. 246-7.

3. Collier, J. G. and Wallis, G. B., "Two-Phase Flow and Heat Transfer," Notes for a Summer Course, July 24 - August 4, 1967, Department of Mechanical Engineering, Stanford University, Stanford, California.

4. Martinelli, R. C. and Nelson, D. B., "Prediction of Pressure Drop During Forced-Circulation Boiling of Water," Trans. ASME, Vol. 70, No. 6, August 1948, pp. 695-702.

5. Baker, D., "Simultaneous Flow of Oil and Gas," The Oil and Gas Journal, Vol. 53, No. 12, July 26, 1954, pp. 185-195.

6. Kozlov, B. K., "Regimes and Types of Flow for an Air-Water Mixture In Vertical Tubes," Hydrodynamics and Heat Transfer During Boiling In High Pressure Boilers, edited by M. A. Styrikovich. Translated from a Publication of the Academy of Sciences of the USSR, Moscow, 1955, AEC-tr-4490, pp. 7-18.

7. Quandt, E., "Analysis of Gas-Liquid Flow Patterns," Chemical Engineering Progress Symposium Series, Heat Transfer-Boston, Vol. 61, No. 57, 1965, pp. 128-135.

8. Wallis, G. B. and Griffith, P., "Liquid and Gas Distributions In A Two-Phase Boiling Analogy," DSR7-7673, 1958, Division of Industrial Cooperation, Massachusetts Institute of Technology, Cambridge, Massachusetts.

9. Hsu, Y. Y. and Graham, R. W., "A Visual Study of Two-Phase Flow In a Vertical Tube With Heat Addition," TN D-1564, January 1963, National Aeronautics and Space Administration, Lewis Research Center, Cleveland, Ohio.

10. Zuber, N., Staub, F. W., Bijwaard, G., and Kroeger, P. G., "Steady State and Transient Void Fraction In Two-Phase Flow Systems - Final Report for the Program of Two-Phase Flow Investigation," Vol. I, GEAP-5417, January 1967, Joint U.S.-Euratom Research and Development Program, General Electric Co., San Jose, California.

11. Bergles, A. E. and Suo, M., "Investigation of Boiling Water Flow Regimes at High Pressure," 1966 Heat Transfer and Fluid Mechanics Institute. Paper No. 6, pp. 79-99.

12. Bergles, A. E., Roos, J. P., and Bourne, J. G., "Investigation of Boiling Flow Regimes and Critical Heat Flux," NYO-3304-13, July 1968, Dynatech Corporation, New York.

13. Bergles, A. E., Lopina, R. F., and Fiori, M. P., "Critical-Heat-Flux and Flow-Pattern Observations for Low-Pressure Water Flowing in Tubes," Trans. ASME, Journal of Heat Transfer, Vol. 89, No. 1, February 1967, pp. 69-74.

14. Hosler, E. R., "Flow Patterns in High Pressure Two-Phase (Steam-Water) Flow With Heat Addition," Chemical Engineering Progress Symposium Series, Heat Transfer - Seattle, Vol. 64, No. 82, 1968, pp. 54-66.

15. Napadensky, J. R., "Pressure Drop and Heat Transfer in the Two-Phase Flow of Freon-12," Ph.D. Thesis, Swiss Federal Institute of Technology, Zurich, 1969.

16. Isbin, H. S., Moen, R. H., Wickey, R. O., Mosher, D. R., and Larson, H. C., "Two-Phase Steam-Water Pressure Drops," Chemical Engineering Progress Symposium Series, Nuclear Engineering - Part VI, Vol. 55, No. 23, 1959, pp. 75-84.

17. Baker, J. L. L., "Flow-Regime Transitions At Elevated Pressures In Vertical Two-Phase Flow," Report 7093, September 1965, Argonne National Laboratory, Argonne, Illinois.

18. Haberstroh, R. D. and Griffith, D., "The Slug-annular Two-phase Flow Regime Transition," ASME Paper 65-HT-52, 1965.

19. Lockhart, R. W. and Martinelli, R. C., "Proposed Correlation of Data For Isothermal Two-Phase, Two-Component Flow In Pipes," Chemical Engineering Progress, Vol. 45, No. 1, January 1949, pp. 39-48.

20. Dukler, A. E., Wicks, Moye III, and Cleveland, R. G., "Frictional Pressure Drop in Two-Phase Flow: A. A Comparison of Existing Correlations for Pressure Loss and Holdup," A.I.Ch.E. Journal, Vol. 10, No. 1, January 1964, pp. 38-43.

21. Dukler, A. E., Wicks, Moye III, and Cleveland, R. G., "Frictional Pressure Drop in Two-Phase Flow: B. An Approach Through Similarity Analysis," A.I.Ch.E. Journal, Vol. 10, No. 1, January 1964, pp. 44-51.

22. Muscettola, M., "Two-Phase Pressure Drop--Comparison of the 'Momentum Exchange Model' and Martinelli and Nelson's Correlation With Experimental Measurements," AEEW-R-284, May 1963, Atomic Energy Establishment, Winfrith, England.

23. Baroczy, C. J., "A Systematic Correlation For Two-Phase Pressure Drop," Chemical Engineering Progress Symposium Series, Heat Transfer - Los Angeles, Vol. 62, No. 64, 1966, pp. 232-249.

24. Chisholm, D. and Laird, A. D. K., "Two-Phase Flow In Rough Tubes," Transactions ASME, Vol. 80, No. 2, February 1958, pp. 276-286.

25. Chisholm, D., "The Influence of Mass Velocity On Friction Pressure Gradients During Steam-Water Flow," Thermodynamics and Fluid Mechanics Convention, Proceedings of the Institution of Mechanical Engineers, Vol. 184, Pt. 3H, 1967-68, pp. 336-341.

26. Chisholm, D., "A Theoretical Basis for the Lockhart-Martinelli Correlation for Two-Phase Flow," International Journal oi Heat and Mass Transfer, Vol. 10, No. 12, December 1967, pp. 1767-1778.

27. Chisholm, D. and Sutherland, L. A., "Prediction of Pressure Gradients In Pipeline Systems During Two-Phase Flow," Thermodynamics and Fluid Mechanics Symposium, Proceedings of the Institution of Mechanical Engineers, Vol. 184, Pt. 3C, 1969-70, pp. 24-32.

28. Chisholm, D., "Pressure Gradients Due to Friction During The Flow of Evaporating Two-Phase Mixtures In Smooth Tubes and Channels," International Journal of Heat and Mass Transfer, Vol. 16, No. 2, February 1973, pp. 347-358.

29. Chawla, J. M., "Heat Transfer and Pressure Drop In Horizontal Tubes In Flow Of Evaporating Refrigerants," Translated from VDI-Forschungsheft 523, Dusseldorf, 1967, pp. 5-36. ORNL-tr-2695.

30. Chawla, J. M., "Frictional Pressure Drop In Flow of Liquid-Gas Mixtures In Horizontal Pipes," Translated from Forschung Im Ingenieurwesen, 34, No. 2, 1968, pp. 47-54. ORNL-tr-2696.

31. Chawla, J. M., "Liquid Holdup In Pipes For Gas-Liquid Mixtures In Two-Phase Flow," Translated from Chemie-Ingenieur-Technik, 41, 1969, pp. 328-330. ORNL-tr-2697.

32. Chawla, J. M., "Correlation of Convective Heat Transfer Coefficient For Two-Phase Liquid-Vapour Flow," Heat Transfer, 1970. Papers Presented at the Fourth International Heat Transfer Conference; Paris-Versailles 1970, Vol. V, Elsevier Publishing Co., Amsterdam, 1970, Paper B5.7.

33. Lombardi, C. and Pedrocchi, E., "A Pressure Drop Correlation In Two-Phase Flow,: Energia Nucleare, Vol. 19, No. 2, February 1972, pp. 91-99.

34. Davis, W. J., "The Effect of the Froude Number In Estimating Vertical Two-Phase Gas-Liquid Friction Losses," British Chemical Engineering, Vol. 8, No. 7, July 1963, pp. 462-465.

35. Thom, J. R. S., "Prediction of Pressure Drop During Forced Circulation Boiling of Water," International Journal of Heat and Mass Transfer, Vol. 7, No. 7, July 1964, pp. 709-724.

36. Cheshire, J. R. and Stirling, R. G., Jr., "Boiling Film Coefficients and Pressure Drops In a Natural-Circulation Evaporator," M.S. Thesis, Massachusetts Institute of Technology, Cambridge, Massachusetts, 1949.

37. Foltz, H. L. and Murray, R. G., "Two-Phase Flow Rates and Pressure Drops In Parallel Tubes," Chemical Engineering Progress Symposium Series, Heat Transfer - Storrs, Vol. 56, No. 30, 1960, pp. 83-94.

38. Hatch, M. R. and Jacobs, R. B., "Prediction of Pressure Drop in Two-Phase Single-Component Fluid Flow," A.I.Ch.E. Journal, Vol. 8, No. 1, March 1962, pp. 18-25.

39. Bryan, W. L. and Seigel, L. G., "Heat Transfer Coefficients In Horizontal Tube Evaporators," Refrigerating Engineering, Vol. 63, No. 5, May 1955, pp. 36-45, 120.

40. Altman, M., Norris, R. H., and Staub, F. W., "Local and Average Heat Transfer and Pressure Drop for Refrigerants Evaporating in Horizontal Tubes," Trans. ASME, Journal of Heat Transfer, Vol. 82, No. 3, August 1960, pp. 189-198.

41. Johnston, R. C., Jr. and Chaddock, J. B., "Heat Transfer and Pressure Drop of Refrigerants Evaporating In Horizontal Tubes," ASHRAE Transactions, Vol. 70, No. 1875, 1964, pp. 163-172.

42. Blatt, T. A. and Adt, R. R., Jr., "An Experimental Investigation of Boiling Heat Transfer and Pressure-Drop Characteristics of Freon 11 and Freon 113 Refrigerants," A.I.Ch.E. Journal, Vol. 10, No. 3, May 1964, pp. 369-373.

43. Chaddock, J. B. and Noerager, J. A., "Evaporation of Refrigerant 12 in a Horizontal Tube with Constant Wall Heat Flux," ASHRAE Transactions, Vol. 72, No. 1966, 1966, pp. 90-103.

44. Levy, S., "Steam Slip-Theoretical Prediction From Momentum Model," Trans. ASME, Journal of Heat Transfer, Vol. 82, No. 2, May 1960, pp. 113-124.

45. Bankoff, S. G., "A Variable Density Single-Fluid Model for Two-Phase Flow With Particular Reference to Steam-Water Flow," Trans. ASME, Journal of Heat Transfer, Vol. 82, No. 4, November 1960, pp. 265-272.

46. Hughmark, G. A., "Holdup In Gas-Liquid Flow," Chemical Engineering Progress, Vol. 58, No. 4, April 1962, pp. 62-65.

47. Marchaterre, J. F. and Hoglund, B. M., "Correlation For Two-Phase Flow," Nucleonics, Vol. 20, No. 8, August 1962, p. 142.

48. Baroczy, C. J., "Correlation of Liquid Fraction In Two-Phase Flow With Application To Liquid Metals," Chemical Engineering Progress Symposium Series, Heat Transfer - Boston, Vol. 61, No. 57, 1965, pp. 179-191.

49. Kowalczewski, J. J., "Vapor Slip In Two-Phase Fluid Flow," ASHRAE Transactions, Vol. 72, No. 1968, 1966, pp. 115-129.

50. Shiralkar, B. S., "Local Void Fraction Measurements In Freon-114 With a Hot-Wire Anemometer," Core Development Technical Memorandum 70-15, December 1970, General Electric Co., San Jose, California.

51. Chang, Y. P., "An Empirical Modification of Nucleation Theory and Its Application to Boiling Heat Transfer," ANL-6304, February 1961, Argonne National Laboratory, Argonne, Illinois.

52. Forster, H. K. and Zuber, N., "Dynamics of Vapor Bubbles and Boiling Heat Transfer," A.I.Ch.E. Journal, Vol. 1, No. 4, December 1955, pp. 531-535.

53. Forster, H. K. and Grief, R., "Heat Transfer to a Boiling Liquid-Mechanism and Correlations," Trans. ASME, Journal of Heat Transfer, Vol. 81, No. 1, February 1959, pp. 43-53.

54. Gilmour, C. H., "Nucleate Boiling - A Correlation," Chemical Engineering Progress, Vol. 54, No. 10, October 1958, pp. 77-79.

55. Hara, T., "The Mechanism of Nucleate Boiling Heat Transfer," International Journal of Heat and Mass Transfer, Vol. 6, No. 11, November 1963, pp. 959-969.

56. Hughmark, G. A., "A Statistical Analysis of Nucleate-Pool-Boiling Data," International Journal of Heat and Mass Transfer, Vol. 5, No. 5, July 1962, po. 667-672.

57. Kutateladze, S. S., "Heat Transfer in Condensation and Boiling," Translated from a Publication of the State Scientific and Technical Publishers of Literature on Machinery, Moscow-Leningrad, 1952, AEC-tr-3770, p. 129.

58. Cess, R. D., ed., "Fundamentals of Heat Transfer," Academic Press, New York, 1963, pp. 362.

59. Levy, S., "Generalized Correlation of Boiling Heat Transfer," Trans. ASME, Journal of Heat Transfer, Vol. 81, No. 1, February 1959, pp. 37-42.

60. Nishikawa, K. and Yamagata, K., "On the Correlation of Nucleate Boiling Heat Transfer," International Journal of Heat and Mass Transfer, Vol. 1, No. 2,3,1960, pp. 219-235.

61. Rohsenow, W. M., "A Method of Correlating Heat-Transfer Data For Surface Boiling of Liquids," Trans. ASME, Vol. 74, No. 6, August 1952, pp. 969-976.

62. Zuber, N., "Nucleate Boiling. The Region of Isolated Bubbles and the Similarity With Natural Convection," International Journal of Heat and Mass Transfer, Vol. 6, No. 1, January 1963, pp. 53-78.

63. Krieth, F., "Principles of Heat Transfer," 2nd ed., International Textbook Company, Scranton, Pennsylvania, 1965, pp. 445.

64. Tong, L. S., "Boiling Heat Transfer and Two-Phase Flow," 1st ed., John Wiley and Sons, New York, 1965, pp. 29.

65. Rohsenow, W. M. and Hartnett, J. P., ed., "Handbook of Heat Transfer," 1st ed., McGraw-Hill, New York, 1973, Section 13.

66. Vachon, R. I., Nix, G. H., and Tanger, G. E., "Evaluation of Constants for the Rohsenow Pool-Boiling Correlation," Trans. ASME, Journal of Heat Transfer, Vol. 90, No. 2, May 1968, pp. 239-247.

67. Vachon, R. I., Tanger, G. E., Davis, D. L., and Nix, G. H., "Pool Boiling on Polished and Chemically Etched Stainless-Steel Surfaces," Trans. ASME, Journal of Heat Transfer, Vol. 90, No. 2, May 1968, pp. 231-238.

68. Vachon, R. I., Nix, G. H., Tanger, G. E., and Cobb, R. O., "Pool Boiling Heat Transfer From Teflon-Coated Stainless Steel," Trans. ASME, Journal of Heat Transfer, Vol. 91, No. 3, August 1969, pp. 364-370.

69. Nix, G. H. and Vachon, R. I., "Surface and Pressure Effects On Pool Boiling From Chemically Etched Surfaces," Paper Presented at a Two-Phase Flow Short Course, University of Tennessee Space Institute, Tullahoma, Tenneseee, January 1970.

70. Kosky, P. G. and Lyon, D. N., "Pool Boiling Heat Transfer to Cryogenic Liquids; I. Nucleate Regime Data and a Test of Some Nucleate Boiling Correlations," A.I.Ch.E Journal, Vol. 14, No. 3, May 1968, pp. 372-387.

71. Zuber, N., "On the Stability of Boiling Heat Transfer," Trans. ASME, Vol. 80, No. 3, April 1958, pp. 711-720.

72. Corty, C. and Foust, A. S., "Surface Variables in Nucleate Boiling," Chemical Engineering Progress Symposium Series, Heat Transfer - St. Louis, Vol. 51, No. 17, 1955, pp. 1-12a.

73. Chapman, R. H., "Saturated Pool and Flow Boiling Studies With Freon-113 and Water at Atmospheric Pressure," Ph.D. Thesis, University of Tennessee, Knoxville, Tennessee, March 1974.

74. Furse, F. G., "Heat Transfer to Refrigerants 11 and 12 Boiling over a Horizontal Copper Surface," ASHRAE Transactions, Vol. 71, No. 1934, 1965, pp. 231-237.

75. Hesse, G., "Heat Transfer in Nucleate Boiling, Maximum Heat Flux and Transition Boiling," International Journal of Heat and Mass Transfer, Vol. 16, No. 8, August 1973, pp. 1611-1627.

76. Lippert, T. E. and Dougall, R. S., "A Study of the Temperature Profiles Measured in the Thermal Sublayer of Water, Freon-113, and Methyl Alcohol During Pool Boiling," Trans. ASME, Journal of Heat Transfer, Vol. 90, No. 3, August 1968, pp. 347-352.

77. Guerrieri, S. A. and Talty, R. D., "A Study of Heat Transfer to Organic Liquids in Single-tube, Natural-circulation Vertical-tube Boilers," Chemical Engineering Progress Symposium Series, Heat Transfer - Louisville, Vol. 52, No. 18, 1956, pp. 69-77.

78. Dengler, C. E. and Addoms, J. N., "Heat Transfer Mechanism for Vaporization of Water in a Vertical Tube," Chemical Engineering Progress Symposium Series, Heat Transfer - Louisville, Vol. 52, No. 18, 1956, pp. 95-103.

79. Bennett, J. A. R., Collier, J. G., Pratt, H. R. C., and Thornton, J. D., "Heat Transfer to Two-Phase Gas-Liquid Systems. Part I: Steam-Water Mixtures in the Liquid-Dispersed Region in an Annulus," Transactions of the Institution of Chemical Engineers, Vol. 39, 1961, pp. 113-126.

80. Chen, J. C., "Correlation for Boiling Heat Transfer to Saturated Fluids in Convective Flow," I & EC Process Design and Development, Vol. 5, No. 3, July 1966, pp. 322-329.

81. Davis, E. J. and David, M. M., "Heat Transfer to High-Quality Steam-Water Mixtures Flowing in a Horizontal Rectangular Duct," The Canadian Journal of Chemical Engineering, Vol. 39, June 1961, pp. 99-105.

82. Schrock, V. E. and Grossman, L. M., "Forced Convection Boiling in Tubes," Nuclear Science and Engineering, Vol. 12, No. 4, April 1962, pp. 474-481.

83. Collier, J. G. and Pulling, D. J., "Heat Transfer to Two-Phase Gas-Liquid Systems; Part II - Further Data on Steam/Water Mixtures in the Liquid Dispersed Region in an Annulus," AERE-R-3809, March 1962, Atomic Energy Research Establishment, Harwell, Berkshire.

84. Lavin, J. G. and Young, E. H., "Heat Transfer to Evaporating Refrigerants in Two-Phase Flow," A.I.Ch.E. Journal, Vol. 11, No. 6, November 1965, pp. 1124-1132.

85. O'Donnell, J. F., Robinson, J. B., Jr., and Webb, R. P., "Heat Transfer to Boiling Liquids in Natural-Circulation Evaporation," M.S. Thesis, Massachusetts Institute of Technology, Cambridge, Massachusetts, 1950.

86. Wasserman, A. A., Erickson, A. J., and Mann, W. L., "A Study of Surface Boiling Heat Transfer to Freon 113," K-963, September 1952, Carbide and Carbon Chemical Company, Oak Ridge, Tennessee.

87. Baker, M., Touloukian, Y. S., and Hawkins, G. A., "Heat Transfer Film Coefficients for Refrigerants Boiling Inside Tubes," Refrigerating Engineering, Vol. 61, No. 9, September 1953, pp. 986-991.

88. Allen, C. F., "Boiling of Freon-114 in a Three-Foot Straight Tube Evaporator," K-1487, October 1961, Union Carbide Nuclear Company, Oak Ridge, Tennessee.

89. Pierre, B., "The Coefficient of Heat Transfer for Boiling Freon 12 in Horizontal Tubes," S. F. Review, Vol. 2, No. 1, 1955, pp. 55-68.

90. Pujol, L. and Stenning, A. H., "Effect of Flow Direction on the Boiling Heat Transfer Coefficient in Vertical Tubes," Proceedings of an International Symposium on Research in Cocurrent Gas-Liquid Flow Held at the University of Waterloo, September 18-19, 1968, Plenum Press, New York, 1969, pp. 401-453.

91. Gouse, S. W., Jr. and Coumou, K. G., "Heat Transfer and Fluid Flow Inside a Horizontal Tube Evaporator: Phase I," ASHRAE Transactions, Vol. 71, No. 1957, 1965, pp. 152-161.

92. Bergles, A. E. and Rohsenow, W. M., "The Determination of Forced-Convection Surface-Boiling Heat Transfer," Trans. ASME, Journal of Heat Transfer, Vol. 86, No. 3, August 1964, pp. 365-372.

93. Gouse, S. W., Jr. and Dickson, A. J., "Heat Transfer and Fluid Flow Inside a Horizontal Tube Evaporator: Phase II," ASHRAE Transactions, Vol. 72, No. 1967, 1966, pp. 104-114.

94. Purcupile, J. C., Riedle, K., and Schmidt, F. K., "Experimental Investigation Boiling Heat Transfer In Evaporator Tubes-Vertical Flow," A.I.Ch.E. Preprint 18. Presented at the Fourteenth National Heat Transfer Conference, Atlanta, Georgia, August 5-8, 1973.

95. Riedle, K. and Purcupile, J. C., "Experimental and Analytical Investigation - Boiling Heat Transfer in Evaporator Tubes - Horizontal Flow," Presented at ASHRAE Semi-Annual Meeting, Chicago, Illinois, January 1973.

96. Danilova, G. N., "Correlation of Boiling Heat Transfer Data for Freons," Heat Transfer - Soviet Research, Vol. 2, No. 2, March 1970, pp. 73-78.

97. Ratiani, G. V. and Shekriladze, I. G., "Study of the Process of Fully Developed Boiling of Liquids," Heat Transfer - Soviet Research, Vol, 4, No. 4, July-August 1972, pp. 126-141.

98. Tong, L. S., "Boiling Crisis and Critical Heat Flux," TID-25887, August 1972, AEC Critical Review Series, National Technical Information Center, Springfield, Virginia.

99. Macbeth, R. V., "Burnout Analysis. 3. The Low-Velocity Burnout Regime," AEEW-R-222, 1963, Atomic Energy Establishment, Winfrith, England.

100. Macbeth, R. V., "Burnout Analysis. 4. Application of a Local Condition Hypothesis To World Data For Uniformly Heated Round Tubes and Rectangular Channels," AEEW-R-267, 1963, Atomic Energy Establishment, Winfrith, England.

101. Macbeth, R. V., "The Burn-Out Phenomenon In Forced-Convection Boiling," Advances in Chemical Engineering, Academic Press, New York, 1968, pp. 207-293.

102. Tong, L. S. and Hewitt, G. F., "Overall Viewpoint of Flow Boiling CHF Mechanisms," ASME Paper 72-HT-54, 1972.

103. Farber, E. A., "Free Convection Heat Transfer From Electrically Heated Wires," Journal of Applied Physics, Vol. 22, No. 12, December 1951, pp. 1437-1438.

104. Gambill, W. R., "Generalized Prediction of Burnout Heat Flux For Flowing Subcooled Wetting Liquids," Chemical Engineering Progress Symposium Series, Heat Transfer - Houston, Vol. 59, No. 41, 1963, pp. 71-87.

105. Barnett, P. G. and Wood, R. W., "An Experimental Investigation to Determine the Scaling Laws of Forced Convection Boiling Heat Transfer. Part 2: An Examination of Burnout Data for Water, Freon 12, and Freon 21 in Uniformly Heated Round Tubes," AEEW-R-443, August 1965, Atomic Energy Establishment, Winfrith, England.

106. Barnett, P. G., "Scaling of Burn-Out in Forced Convection Boiling Heat Transfer," Thermodynamics and Fluid Mechanics Symposium, Proceedings of the Institution of Mechanical Engineers, Vol. 180, Pt. 3C, 1965-66, pp. 16-26.

107. Stevens, G. F. and Kirby, G. J., "A Quantitative Comparison Between Burnout Data for Water at 1000 psia and Freon-12 at 155 psia Uniformly Heated Round Tubes, Vertical Flow," AEEW-R-327, 1964, Atomic Energy Establishment, Winfrith, England.

108. Coffield, R. D., Jr., Rohrer, W. M., Jr., and Tong, L. S., "An Investigation of Departure From Nucleate Boiling (DNB) in a Crossed-Rod Matrix With Normal Flow of Freon-113 Coolant," Nuclear Engineering and Design, Vol. 6, 1967, pp. 147-154.

109. Tong, L. S., Motley, F. E., and Cermak, J. O., "Scaling Law of Flow-Boiling Crisis," Heat Transfer, 1970. Papers Presented at the Fourth International Heat Transfer Conference, Paris-Versailles 1970, Vol. VI, Elsevier Publishing Co., Amsterdam, 1970, Paper B6.12.

110. Staub, F. W., "Two-Phase Fluid Modeling - the Critical Heat Flux," Nuclear Science and Engineering, Vol. 35, No. 2, February 1969, pp. 190-199.

111. Dix, G. E., "Freon-Water Modeling of CHF in Round Tubes," ASME Paper 70-HT-26, 1970.

112. Biasi, L., Clerici, G. C., Garribba, S., Sala, R., and Tozzi, A., "Studies on Burnout, Part 3 - A New Correlation for Round Ducts and Uniform Heating and its Comparison with World Data," Energia Nucleare, Vol. 14, No. 9, September 1967, pp. 530-536.

113. Paleev, I. I. and Filippovich, B. S., "Phenomena of Liquid Transfer in Two-Phase Dispersed Annular Flow," International Journal of Heat and Mass Transfer, Vol. 9, No. 10, October 1966, pp. 1089-1093.

114. Stevens, G. F. and Macbeth, R. V., "The Use of Freon 12 to Model Forced Convection Burnout in Water: The Restriction on the Size of the Model," ASME Paper 70-HT-20, 1970.

115. Groeneveld, D. C., "Freon Dryout Correlations and their Applicability to Water," AECL-3418, September 1969, Atomic Energy of Canada Limited, Chalk River, Ontario.

116. Ahmad, S. Y., "Fluid to Fluid Modeling of Critical Heat Flux: A Compensated Distortion Model," International Journal of Heat and Mass Transfer, Vol. 16, No. 3, March 1973, pp. 641-662.

117. Kunz, H. R. and Yerazunis, S., "An Analysis of Film Condensation, Film Evaporation, and Single-Phase Heat Transfer for Liquid Prandtl Numbers From 10^{-3} to 10^{4}," Trans. ASME, Journal of Heat Transfer, Vol. 91, No. 3, August 1969, pp. 413-420.

118. Hsu, Y. Y., "On the Size Range of Active Nucleation Cavities on a Heating Surface," Trans. ASME, Journal of Heat Transfer, Vol. 84, No. 3, August 1962, pp. 207-216.

119. Han, C. and Griffith, P., "The Mechanism of Heat Transfer in Nucleate Pool Boiling - Part I," International Journal of Heat and Mass Transfer, Vol. 8, No. 6, June 1965, pp. 887-904.

120. Murphy, R. W. and Bergles, A. E., "Subcooled Flow Boiling of Fluorocarbons--Hysteresis and Dissolved Gas Effects on Heat Transfer," Proceedings of the 1972 Heat Transfer and Fluid Mechanics Institute, Paper No. 24, pp. 400-416.

121. Brown, W. T., Jr., "A Study of Flow Surface Boiling," Ph.D. Thesis, Massachusetts Institute of Technology, Cambridge, Massachusetts, January 1967.

122. Mikic, B. B. and Rohsenow, W. M., "A New Correlation of Pool Boiling Data Including the Effect of Heating Surface Characteristics," ASME Paper 68-WA/HT-22, 1968.

123. Cooper, M. G. and Lloyd, A. J. P., "The Microlayer in Nucleate Pool Boiling," International Journal of Heat and Mass Transfer, Vol. 12, No. 8, August 1969, pp. 895-913.

124. Jawurek, H. H., "Simultaneous Determination of Microlayer Geometry and Bubble Growth in Nucleate Boiling," International Journal of Heat and Mass Transfer, Vol. 12, No. 8, August 1969, pp. 843-848.

125. Katto, Y, and Shoji, M., "Principal Mechanism of Micro-Liquid-Layer Formation on a Solid Surface with a Growing Bubble in Nucleate Boiling," International Journal of Heat and Mass Transfer, Vol. 13, No. 8, August 1970, pp. 1299-1311.

126. Madsen, N., "Temperature Fluctuation at a Heated Surface Supporting Pool Boiling of Water," Thermodynamics and Fluid Mechanics Symposium, Proceedings of the Institution of Mechanical Engineers, Vol. 180, Pt. 3C, 1965-66, pp. 150-159.

127. Tolubinskiy, V. I., Kriveshko, A. A., and Ostrovskiy, Y. N., "On Fluctuations of the Temperature of the Heated Surface at an Active Nucleation Site," Heat Transfer - Soviet Research, Vol. 4, No. 6, November-December 1972, pp. 30-35.

128. Koumoutsos, N., Moissis, R., and Spyridonos, A., "A Study of Bubble Departure in Forced-Convection Boiling," Trans. ASME Journal of Heat Transfer, Vol. 90, No. 2, May 1968, pp. 223-230.

129. Abdelmessih, A. H., Hooper, F. C., and Nangia, S., "Flow Effects on Bubble Growth and Collapse in Surface Boiling," International Journal of Heat and Mass Transfer, Vol. 15, No. 1, January 1972, pp. 115-125.

130. McAdams, W. H., Addoms, J. N., and Kennel, W. E., "Heat Transfer at High Rates to Water With Surface Boiling," ANL-4268 or AECU-200 Department of Chemical Engineering, Massachusetts Institute of Technology, Cambridge, Massachusetts, December 1948.

131. Sani, R. L., "Downflow Boiling and Non-Boiling Heat Transfer in a Uniformly Heated Tube," University of California Radiation Laboratory, Report UCRL-9023, 1960.

132. Moles, F. D. and Shaw, J. F. G., "Boiling Heat Transfer to Sub-Cooled Liquids Under Conditions of Forced Convection," Transactions of the Institution of Chemical Engineers, Vol. 50, No. 1, January 1972, pp. 76-84.

133. Benedict, R. P., "Fundamentals of Temperature, Pressure, and Flow Measurements," 1st ed., John Wiley and Sons, Inc., New York, 1969, Chapter 7.

134. "Variable Area Flowmeter Handbook, Vol. II," Catalog 10A 1022, Publication 16548a, 1969, Fisher and Porter Co., Warminster, Pennsylvania.

135. Collier, J. G., "Convective Boiling and Condensation," 1st ed., McGraw-Hill Book Co. Ltd., London, 1972, pp. 28-35.

136. "Thermodynamic Properties of Freon 114 Refrigerant," Du Pont Technical Bulletin T-114D, E. I. du Pont de Nemours and Company, Wilmington, Delaware, 1966.

137. Dr. Paul Liley, Purdue University, Lafayette, Indiana, Private Communication, 1972.

138. Perry, J. H., ed., "Chemical Engineers' Handbook," 4th ed., McGraw-Hill Book Co., New York, 1963, pp. 3-222 to 3-224.

139. Beers, Y., "Introduction to the Theory of Error," 2nd ed., Addison-Wesley Book Co., Reading, Massachusetts, 1962, p. 5.

140. Westley, G. W. and Watts, J. A., ed., "The Computing Technology Center Numerical Analysis Library," CTC-39, October 1970, Union Carbide Corporation, Nuclear Division, Oak Ridge, Tennessee.

APPENDIXES

APPENDIX A

POOL BOILING RESULTS FOR R-11, R-113, AND R-114

The results from a series of pool boiling tests conducted at the Oak Ridge Gaseous Diffusion Plant are presented here. The system used to measure the coefficients utilized an electrically heated copper disk immersed in a pool of liquid refrigerant. The temperature of the heating element was measured with nine thermocouples embedded approximately 1/16 in. below the surface. The liquid temperature was measured with thermocouples located approximately 1/16 in. from the surface of the heating element.

All tests were conducted at the same boiling temperature of 112°F. The heat flux was varied from 12,000 to 70,000 Btu/hr-sq ft. R-114 required the lowest temperature difference between the heating element and the liquid to start boiling, while R-113 required the highest temperature difference. The results are given in Table A-1.

Table A-1

POOL BOILING COEFFICIENTS FOR R-11, R-113, AND R-114

Refrigerant	Heat Flux (Btu/hr-sq ft)	Temperature Difference (°F)	Boiling Coefficient (Btu/hr-sq ft-°F)	Pressure (psia)
11	11,800	16.2	730	29.1
11	19,900	26.6	748	29.1
11	29,900	32.4	925	29.1
11	40,700	36.4	1120	29.1
11	53,400	39.8	1340	29.1
11	68,500	44.3	1550	29.1
113	12,150	24.5	495	13.3
113	19,400	34.9	555	13.3
113	29,400	41.4	710	13.3
113	40,200	44.8	896	13.3
113	52,100	49.0	1065	13.3
113	70,000	54.4	1290	13.3
114	11,800	14.4	820	56.1
114	19,000	17.5	1085	56.1
114	27,900	21.1	1320	56.1
114	37,800	24.9	1520	56.1
114	51,500	27.9	1845	56.1
114	64,600	32.0	2020	56.1

APPENDIX B

DESCRIPTION OF BOILING TEST FACILITY AND ASSOCIATED INSTRUMENTATION

A. BOILING FACILITY

A detailed diagram of the boiling facility located in the K-1401 building at ORGDP is shown in Figure B-1. This loop, constructed primarily of Schedule 40 carbon steel, is capable of operating at pressures of up to 300 psig and temperatures of up to 250°F. A listing of all the major components in the boiling facility, except the test section and its instruments, is given in Table B-1.

In the natural circulation mode, the R-114 working fluid, after leaving the storage tank, traveled through one of two turbine flowmeters. The low flow range meter, FE 105B, was capable of accurately measuring flows in the 0.5-to-6.0 gpm range. The high flow range meter, FE 105A, was accurate in the 3-to-90 gpm range. Once past the flowmeters, the fluid entered the preheater. This unit, with a 30-kW capacity, heated the fluid either to the saturation temperature or to the desired degree of subcooling. From there, the fluid traveled through a 1-in.-diameter, 3-11/16-ft-long straightener into the 10-ft test section. After being boiled, the two-phase mixture traveled through a flow visualization section sketched in detail in Figure III-9 on page 115 and into two entrainment separators. Care was taken to ensure that a minimum amount of interference occurred between the test section exit and the flow visualization section. In addition, the pressure drop between the test section outlet and the entrainment separators was kept as low as possible

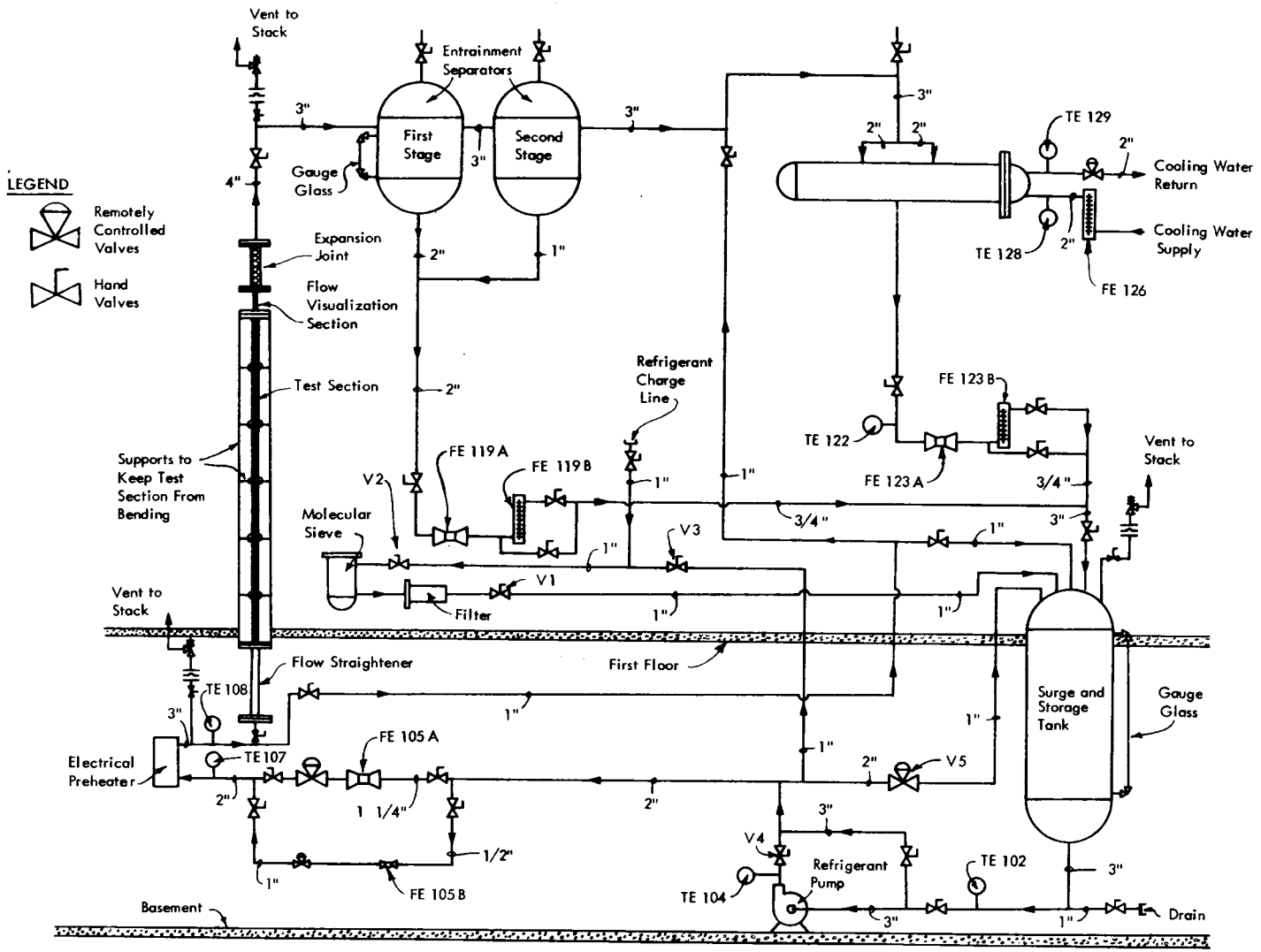


Figure B-1. DETAILED SCHEMATIC DRAWING OF THE BOILING FACILITY.

Table B-1

LISTING OF ALL MAJOR COMPONENTS IN THE BOILING FACILITY

Instrument	Description
Pump	Eastern Industries, canned rotor, Mod. No. A1LG; 300-psig system pressure; 200°F operating temperature; 15 hp, 3-phase, 60 cycle; 85 gpm.
FE 105A	Cox Instruments, turbine Type 20 Mod. I-1 1/4-600; range 3.0 to 90.0 gpm ± 0.5%; internal body Type 300 SS, Type 416 SS rotor.
FE 105B	Same as FE 105A except range 0.5 to 6.0 gpm; Type 20 Mod. I-1/2(8-6)-600.
FE 119A	Same as FE 105A.
FE 123A	Same as FE 105A except range 1.0 to 15.0 gpm; Type 20 Mod. I-3/4(10)-600.
Condenser	Struthers Wells Corp., Type 12-6U14-6H; shell M.A.W.P 300 psig, tube M.A.W.P. 150 psig; shell and tube maximum temperature 250°F.
Separators	Centrifix, Div. of Burgess Ind., Type V, M.A.W.P. 300 psig, maximum temperature 250°F.
Remote Control Valves	Skinner Uniflow Valve Div., Type 1020, for service at 200°F, 300 psig, c_v = 12 and c_v = 80.
Wattmeter	General Electric Watt-Hour Meter Standard, Type IB-10, Mod. AAA1; 120-240V, 1-5-12.5-50 amps.
Filter	Mueller Brass Co., Drymaster Micro-Guard Filter-Drier Mod. SD 14411.
Molecular Sieve	Linde Corp., Type 4A beads.
Pressure Transmitters	Foxboro Co., Mod. M-11GM, M.A.W.P. 750 psig; range 0-300 psi.
Preheater	E. L. Wiegand Co., Mod. GCH 83001; 30 kW, 480 V, 3-phase, M.A.W.P. 300 psig at 250°F.

Table B-1 (continued)

Instrument	Description
FE 123B	Fischer & Porter Co.; rotameter Mod. 10A1735Z; range 0.01-1.05 gpm; M.A.W.P. 290 psig at 100°F.
FE 119B	Brooks Instrument Div.; rotameter Type 1110-09H3B1A; range 0.2-3.2 gpm (H_2O, S.G. = 1), M.A.W.P 240 psig at 200°F.
FE 126	Schutte and Koerting Co.; Series 18000 "Safeguard" Rotameter; Tube: 4-HCFB; SS float 40-J; maximum recommended pressure 300 psig at 200°F.
SCR Unit	Robicon Corp.; SCR Type, 6KVA, 120 V, single-phase, zero voltage firing.
Flow Visualization Section	The Johnson Corp., regular type for 1 in. pipe 0-150 psig; modified for 0.785-in. ID and 300 psig.
L&N Controllers	Leeds & Northrup Co.; Mod. 6432-6-40XX-200-0-20-206; 0-300°F range w/Type E thermocouples.
Loop Thermocouples	Conax Corp., Type E, 0.125-in.-OD SS sheath, grounded.
Piping	All piping schedule 40 CRS 1/2 to 4 in.
Ball Valves	Contromatics, 300 series, 1000 psi. maximum, Teflon seats and gaskets.
Pipe Insulation	Hydrous Calcium Silicate, 70-1200°F, 2-in. thick.

by using relatively large 3- and 4-in.-diameter piping and ensuring that the valve downstream of the test section was always in the wide-open position. The occurrence of any significant pressure drop would have decreased the saturation temperature and caused a change in the quality of the two-phase mixture. In the two entrainment separators, connected in series, the liquid and vapor were separated with a high degree of efficiency. The liquid fraction flowed through either FE 119A or FE 119B into the storage tank. The Cox turbine meter, FE 119A, was accurate in the 3- to 90-gpm range. The Brooks rotameter, FE 119B, was accurate in the 0.2- to 3.2-gpm range. The vapor fraction traveled to the condenser where it was condensed, and its flow rate measured either by a 1- to 15-gpm Cox turbine meter (FE 123A) or a 0.01- to 1.05-gpm Fisher-Porter rotameter (FE 123B). It then flowed back into the storage tank. Table B-1 should be consulted for additional details about the equipment and instrumentation.

From this system, the following mass and heat balances could be obtained:

1. Mass Balance: The mass flow rate measured by FE 105A or FE 105B must equal the sum of FE 119A or FE 119B plus FE 123A or FE 123B. From these flow measurements, the quality at the tube exit could be computed.

2. Heat Balance: The heat input from the preheater and the test section must equal the heat output to the cooling water in the condenser. The heat input from the preheater can be obtained from the measurement of FE 105A or FE 105B and TE 107 and TE 108. When the fluid was not boiled in the preheater, the formulation

$$q = \dot{m}\, c_{pf}\, (T_{TE\ 108} - T_{TE\ 107}) \qquad \text{(B-1)}$$

sufficed. The heat input to the test section minus the heat losses was easily obtained and is described in Section B below. The heat output to the water in the condenser was calculated from the flowrate of the water and the inlet and outlet temperatures.

In the forced circulation mode, the operation was quite similar with the exception that the valves in the pump bypass and filter lines, Valves V1 to V5 in Figure B-1, were open to varying degrees. In the natural circulation mode, they were always closed. The pump bypass line along with the filter lines enabled the excess portion of the 85-gpm flow not needed in the test section to be sent back to the storage tank. A certain flow was always passed through the molecular sieve and filters to continuously remove moisture and iron oxide that were found to accumulate with time in minute quantities in the R-114. This will be discussed in further detail in Section C below, dealing with the operating procedures and problems encountered. In the heat balance calculations for the forced circulation mode, the rise in temperature of the 85 gpm of R-114 as it passed through the pump was calculated from the readings of TE 104 and TE 102.

B. TEST SECTION AND ASSOCIATED INSTRUMENTATION

Detailed, dimensionalized drawings of the test section were shown in Figures III-2 to III-7 on pages 105 and 107 to 111. The test section, made of drawn copper, had a 0.785-in. ID, a 1.750-in. OD, and 10-ft heated length. On each end, a 1/2-in.-thick copper flange with a 6-5/8-in. bolt circle was welded to the test section. To this flange, a 1-in.-thick

carbon steel slip flange was tacked. This procedure was undertaken because of the necessity of having a flange of a hard material to bolt on to the rest of the system. Welding of the carbon steel flange to the copper tube was not done because the different coefficients of expansion of the two materials would have resulted in an unnecessary stress on the welded joint and, quite possibly, a crack.

The 10-ft test section was divided into 10 zones, each individually heated. Between each zone, a 1/2-in.-wide groove was cut into the copper to a depth of 0.382-in. so that only a 0.100-in.-thick wall remained. This groove was then filled with a high-temperature epoxy. This groove effectively isolated each zone, since only 14% of the original cross-sectional area was left to allow conduction. This reduction in conduction was helpful not only during the heat transfer coefficient tests, but also during the critical heat flux runs where steep temperature gradients existed along the axis of the tube. A sketch of one of the grooves was given in Figure III-4 on page 108. After installation, the test section was properly braced to minimize the bending stresses it was subjected to.

Heat Input System

Heat was inputed to the test section by Chromalox calrod heaters. Each heater was capable of an output of 1120 watts. Three of these heaters were helically wound around the copper tube in each zone, as shown in Figure III-3 on page 107. Thus, each zone had a maximum heating capability of 3360 watts or 55,800 Btu/hr-sq ft. The heaters were of the stainless steel sheathed type and capable of withstanding a continuous sheath temperature of 1200°F. In practice, care was taken to make sure that

the sheath temperature rarely exceeded 800°F and then only during some of the critical heat flux runs. The heaters were covered with a 3/8-in.-thick layer of Thermon heat conducting cement and 2 in. of insulation.

The heat input control system to each of the 10 zones was rather unique, since it was desirable to have the option of operating the system in two modes. In one case, it was necessary to be able to impose a constant heat flux or a known heat flux distribution. In the other case, it was desirable to be able to set a uniform or known temperature distribution. To accommodate this, a feedback system consisting of an L&N controller and a potentiometer in parallel, connected to a Robicon zero-firing SCR was utilized for each zone, as shown in Figure B-2. If it was desirable to set a given wall temperature distribution, a number corresponding to that temperature was dialed in on the controller which then sent out a 0- to 5-ma signal corresponding to this temperature. This signal activated the SCR which rapidly fired on and off several times per second and allowed current to flow to the heaters. If the amount of heat being inputed resulted in too high a wall temperature, a feedback signal from a thermocouple embedded in the surface of the test section to the controller resulted in a reduced 0- to 5-ma signal to the zero-firing SCR. If the wall temperature was too low, the signal from the controller to the zero-firing SCR increased. In the circuit diagram shown in Figure B-2, the 820-ohm resistor placed between the controller and the zero-firing SCR matched the impedance of the two systems such that with a full 5-ma output from the controller, the zero-firing SCR was continuously on. When the SCR units were received from Robicon

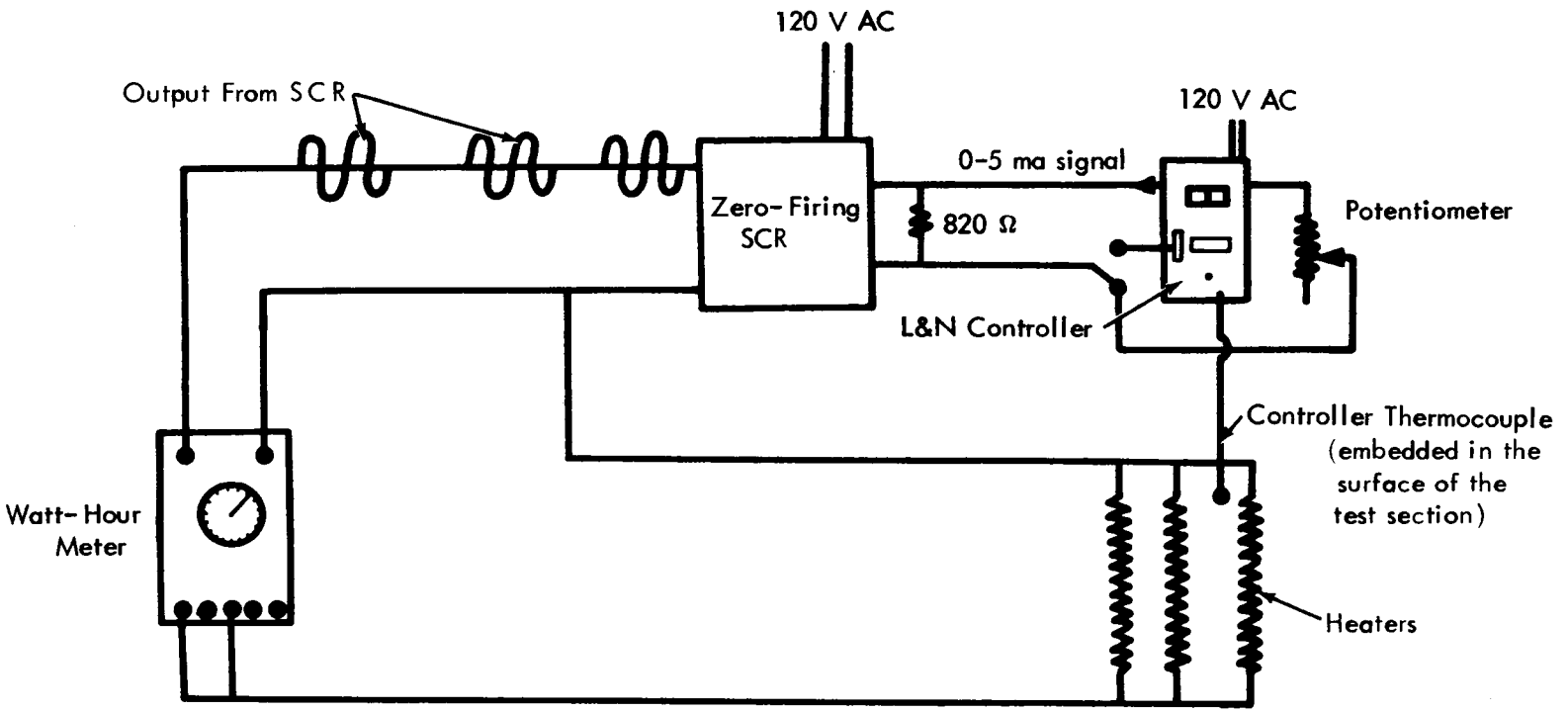


Figure B-2. CIRCUIT DIAGRAM FOR HEAT INPUT CONTROL SYSTEM. SHOWN HERE IN THE HEAT FLUX CONTROL POSITION.

Corp., the existing capacitors were replaced with new ones having a smaller capacitance so that the SCRs could fire on and off more rapidly. A quick calculation showed that the 0.4825-in.-thick copper wall effectively damped out the periodic heater cycling and resulted in a smooth heat input to the boiling fluid in the test section.

If, instead of setting a wall temperature, it was desirable to input a uniform heat flux or a heat flux of known distribution, it was possible to switch out a portion of the controller circuitry and switch in instead a potentiometer. This potentiometer could be adjusted so that any fraction of the 0- to 5-ma signal could be fed to the zero-firing SCR. It should be noted that in case a given heat flux or temperature distribution was desired, it was at best only possible to approximate it by 10 step function increments. Within each of these increments, only a constant heat flux condition was possible. In all the tests reported here, the system was operated in the uniform heat flux mode. In certain instances when the critical heat flux was attained in some of the upper zones of the test section, the heaters in the zones downstream of the one where critical heat flux occurred were shut off, or considerably lowered, in order to prevent the tube wall from getting too hot. This action prevented the possible damage of the heaters or the occurrence of a fundamental change in the surface characteristics of the copper tube.

Pressure Drop Measuring System

A sketch of the locations of the pressure taps in the test section can be found in Figure III-8 on page 112. Four interconnected pressure taps were located at the test section inlet and four at the outlet. This

enabled the average of the circumferential pressure readings to be obtained at these two locations. No differences between the reading from one tap on the wall or from four interconnected taps was noted in the pressure drop results--indicating that the pressure was uniform in the circumferential direction. These 12 taps were located in the test section so that it was possible to measure the pressure drops in five increments along the length of the test section. The distances between taps are also given in Figure III-8 on page 112. In constructing the pressure taps, 1/16-in.-diameter holes were drilled all the way through and 1/8-in.-diameter holes countersunk to a depth of 1/4 in. with a flat-bottom drill. Care was taken to make sure that the holes drilled were perpendicular to the surface of the tube and that no burrs existed on the inside surface of the tube. The ratio of the height to the diameter of the holes was the optimum size suggested by Benedict [133]. Inside the countersunk holes, 1/4-in.-OD soft copper tubes were silver soldered. Again here, care was taken to make sure that no solder or flux got into the pressure tap holes. The copper tube lines extending from the pressure tap holes were at a slight downward angle. The reason for this was to make sure that any vapor on noncondensable gas which may get into the lines would be moved by buoyancy forces into the test section, thereby not accumulating in the pressure tap lines and affecting the pressure drop readings. These lines, after extending 36 in. from the test section continued down to the basement and were connected to a pressure tap board where solenoid valves actuated from the control panel opened and closed the necessary valves to obtain the pressure drop reading from the desired sets of taps. From this board, two lines-- one representing the high side and one representing the low side--were connected

to a DP cell, where the pressure drop signal, which had a range of -175 in. water to +100 in. water was converted to a 3- to 15-psi. signal and read on a 0- to 100-division receiver gage. Details for the calibration are given in Appendix C.

In addition to the pressure drops along the length of the test section, the gage pressure at the test section inlet was also measured. This was done by recording the reading obtained on either one of two calibrated gages. One had a scale of 0 to 100 psig, while the other had a 0 to 300-psig range. The 0- to 100-psig instrument had a resolution of 0.5 psi., while the 0- to 300-psig gage had a resolution of 1.0 psi. These gage readings, along with a barometric reading, enabled the absolute pressure at the test section inlet to be determined.

Temperature Measuring System

In Figures III-5 to III-7 on pages 109 to 111, diagrams of all thermocouples located in a zone are shown. The wall thermocouples were made of 24-gage Chromel-Constantan thermocouple wire. They were placed in the 0.070-in.-diameter, 3/8-in.-deep holes with a 0.144-in.-diameter, 1/8-in.-deep countersink. Each thermocouple was covered by a 0.093-in.-ID, 0.140-in.-OD piece of ceramic insulation 3 in. long. The purpose of this ceramic insulation was to prevent contact between the thermocouple wire and the heaters. This heat, when conducted to the thermocouple bead, would have resulted in an erroneous voltage signal. Initially, these thermocouples were held in place by Loctite* quick-set adhesive. This strong adhesive prevented the wall thermocouples from accidentally

*Loctite Corp., Newington, Connecticut 06111.

falling out. During the runs, it was found that while this adhesive performed satisfactorily at first, it soon began to char and prevented good thermal contact between the test section wall and the thermocouple bead. Thus, all wall thermocouples were remounted and attached to the wall with a 30% tin, 70% lead solder. All heat transfer coefficient runs were then redone. Good contact between the wall and thermocouple bead was obtained, as will be illustrated in Appendix C.

The 10 in-stream thermocouples, one located in the center of each zone, were attached to the tube by stainless steel fittings with Teflon inserts as shown in Figure III-6 on page 110. These sheathed thermocouples were inserted to a depth so that the tip of the thermocouple sheath was in the center of each tube. The 10 control thermocouples which fed the signal to the controllers were peened into the copper tube surface at a depth of 3/8 in.

All thermocouples with the exception of those 10 that provided a feedback of the wall termperature to the controllers were connected using a zone-box circuit to a Vidar 521 Integrating Digital Voltmeter using thermal-free solder. A diagram of the thermocouple connections is given in Figure B-3. The relative advantages and disadvantages of the zone-box circuit are discussed in detail by Benedict [133]. A listing of all the components and instrumentation associated with the test section is given in Table B-2.

System Startup

When the construction of this boiling facility was complete, but before the test section was put in place, it was necessary to clean the system to remove welding slag and iron oxide. A 9 to 10% solution of

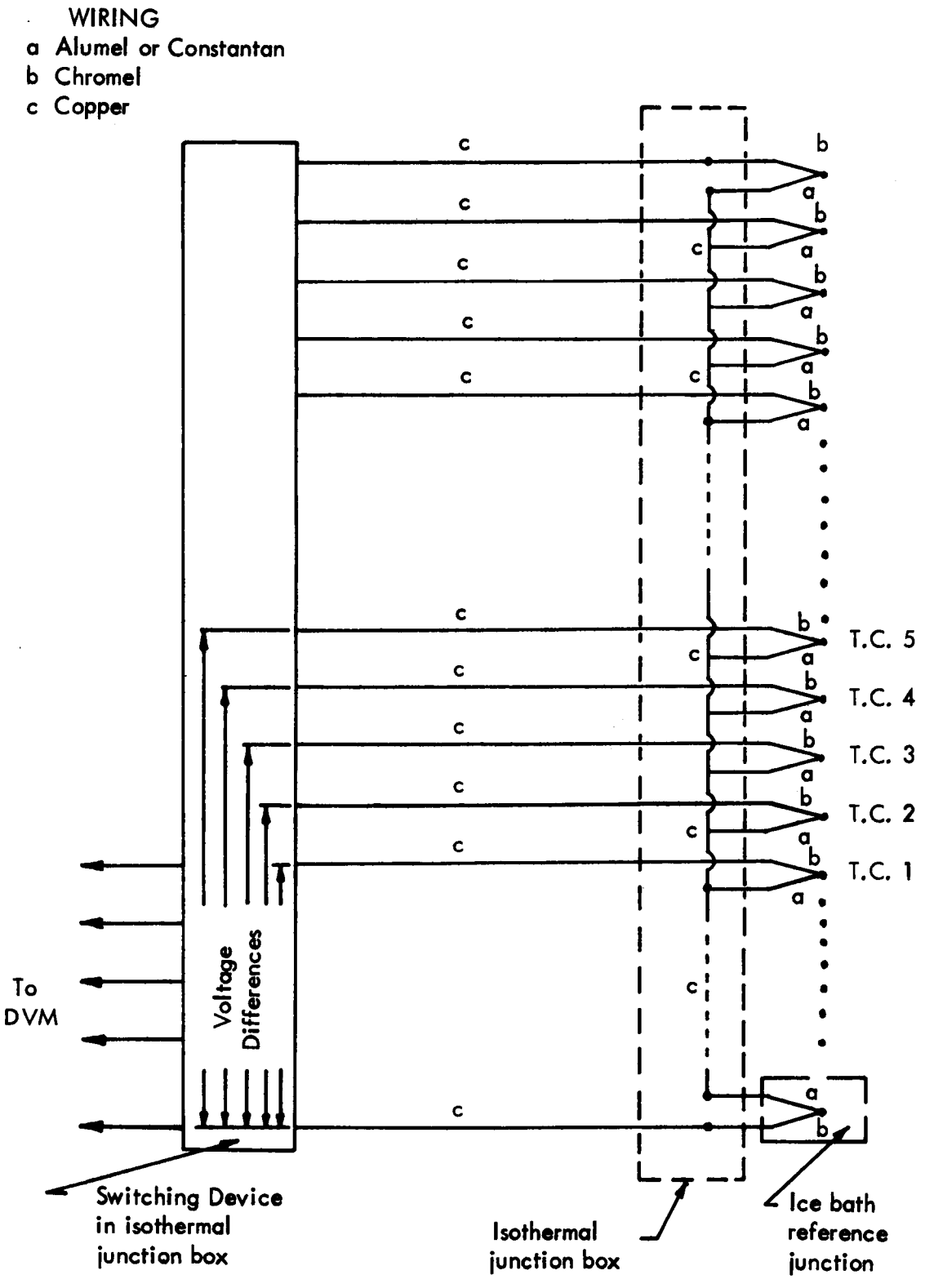


Figure B-3. THERMOCOUPLE WIRING DIAGRAM.

Table B-2

LISTING OF ALL THE COMPONENTS AND INSTRUMENTATION ASSOCIATED WITH THE TEST SECTION

Instrument	Description
Tube	Wolverine Tube Division; CDA copper No. 122, Type DHP, fully annealed temperature; finish comparable to tubes produced under ASTM B-111; 1.750-in. OD, 0.785-in. ID
TE, Wall	Claude S. Gordon Co.; Type E, Chromel-Constantan, B & S gage No. 24, Duplex, glass braid insulated each conductor.
Insulators	CGS/Thermodynamics; high-temperature, porcelain, one-hole, round, 0.140-in. OD, 0.093-in. ID, 3-in. long.
TE, In-stream	Conax Corp.; 304 SS sheathed, Type K, Chromel-Alumel, ungrounded, 0.040-in. OD, 12-in. long.
TE, Heater Control	Same as TE, Wall.
Heaters	E. L. Wiegand Co.; Chromlox Type TSSM-40, 115 V, 1120 W, 37-in. heated length.
Heat Transfer Cement	Thermon Mfg. Co.; high-temperature heat transfer cement, Grade T-63.
Differential Pressure Transmitter	Foxboro Co.; Type 13A, M.A.W.P. 1500-psi. range 0-100 in. water, modified to -170 to 100 in. water.
0-100 and 0-300 psi. Gages	Robertshaw Acragages; 0-100-psi. gage had a 0.5-psi. resolution. 0-300-psi. gage had a 1-psi. resolution.
Pressure Tap Lines	1/4-in.-OD copper tubing from taps to hand valves. 3/8-in.-OD copper tubing from hand valves to DP cell.
0-100 Division Gage	Ashcroft receiver gage. 3-15-psi. input, 0-100% output.
Solenoid Valves	1/4-in. pipe size, 3/64-in. orifice, 110 V normally closed, Automatic Switch Company, Florham Park, N. Y.

Table B-2 (continued)

Instrument	Description
Hand Valves	Hoke 1/4-in.-OD tubing connections, primary rating 3000 psi. at 70°F, brass body with stainless steel stem.
Digital Voltmeter	Vidar 521-01 Integrating Digital Voltmeter with bipolar integration. Resolution was 1 μv during tests, integration period was 16-2/3 msec. Also used was a Vidar 604 master scanner, Vidar 610 slave scanners, and Vidar 661 digital printer.

Oakite M.O.R.* cleaning agent was mixed with 480 gal of water and pumped into the boiling facility. This solution, at temperatures from 130 to 170°F was circulated for 7 hours, then recirculated at a pH of 9.5 and a temperature of about 100°F for 30 min. The system was then drained and refilled with water containing Calgon CS** corrosion inhibitor in order to stop the corrosion of the highly-activated steel surfaces. After draining and rinsing, air was blown through the system. Unsaturated R-113 was then circulated through the loop to remove residual water by extraction and drained out. Nitrogen at approximately 30 psig was blown through the system before it was evacuated and kept under vacuum for about 3 days. The R-114 was finally added to the system with a small Chempump which was constantly covered with dry ice to prevent vapor lock.

Operating Procedure and Problems Encountered

The range of operating conditions, as well as the repetition of certain runs to assure the accuracy of the data taken were discussed in sufficient detail in the main body of the thesis. This section will concentrate on the details of operating the system to achieve the desired set of testing conditions. A discussion of the major problems encountered is also included.

When a new set of parameters was to be obtained, the first variable in the boiling system to be set up was the heat flux to the

---

*Oakite Products, Inc., 50 Valley Road, Berkeley Heights, New Jersey 07922.

**Calgon Corp., Pittsburgh, Pennsylvania 15230.

test section. After the desired heat input was obtained and checked with the watt-hour meter, the flow rate through the test section was adjusted. The necessary preheater setting was obtained so that the liquid entering the test section was, in most cases, slightly subcooled. The last parameter to be set was the boiling temperature. This was accomplished by increasing or decreasing the flow of water to the condenser. Because of the mass of the system and associated thermal lag, it usually took from 30 to 120 min to settle out at the desired boiling temperature. Since the boiling temperature constantly changed along the length of the test section, an in-stream thermocouple in Zones 5 or 6 was usually taken as representative of the average of the test section. Only in the cases of very high velocities were the temperature gradients appreciable and even then, the maximum deviation between inlet and outlet was only 5 or 7°F. After the desired boiling temperature was obtained, the flow rate was again checked and any drift that had occurred was corrected.

Once all the adjustments to the system were made, a minimum of at least a half-hour's wait was allowed before any data were taken. In case the boiling temperature or the flow rate began to drift, the necessary adjustments were made and the half-hour wait begun all over again. As a criterion, a drift of less than 1/2°F per hour or a variation in flow of less than 5% from the original set point was allowable. In instances where a significant change in heat flux--either upwards or downwards--was made from one run to another, a waiting period of at least two hours between runs was allowed. This was done so that the temperature gradient and consequently the heat loss through the insulation could approach the steady state case.

Little maintenance had to be performed on the boiling system. It was necessary, however, from time to time to add small amounts of R-114 to the system. Small leaks at the flanges between the instruments and the carbon steel piping of the system were detected. They could not all be eliminated, despite the fact that CaF-impregnated Teflon gaskets were used and the bolts were tightened to a high torque. Additional maintenance was performed on the refrigerant filters and molecular sieve. They were replaced at approximately 1-month intervals.

In addition to the problems regarding the thermocouples mentioned earlier, another problem encountered had to do with the integrity of the test section itself. Because of the necessity of minimizing axial conduction, the grooves were cut to a depth such that a sufficient wall thickness was left to accommodate any stresses that developed due to the hydrostatic pressure inside the test section. However, at the 200 and 250°F boiling temperatures, when significant thermal expansion occurred, the test section did bend slightly because the expansion joint in the system had a high spring constant. Thus, when the system was cooled down, a crack developed in the boundaries downstream of Zones 4, 5, or 6. When these cracks were sealed by welding, this necessitated heating an area of several inches on both sides of where this crack occurred to about 700°F.

The test section cracked less than half a dozen times, and in all cases very late in the testing program. Several of the boiling runs and wall thermocouple calibrations were repeated to detect any changes in the boiling characteristics of the zones affected. None were found.

Another problem of a minor nature involved the Cox turbine meters that were used. In numerous instances, the turbine which rotated inside the meter and whose rpm was translated into the flow rate reading was found to jam. Very fine particles of iron oxide were usually responsible. It was therefore necessary to replace the bearings in some of these turbine meters rather frequently. A check at one time showed no effect on calibration due to the new bearings in the meters. It was not possible to oil or in any other way lubricate the bearings because R-114 readily absorbs oil and, therefore, any amount used would afford protection for only a very short period of time and would instead contribute to the contamination of the refrigerant.

To check the purity of the R-114 in the system, samples were periodically removed and checked for water, oil, and iron oxide content. A water content of as high as 30 ppm was sometimes measured. The quantities of oil and iron oxide were negligible.

General Observations

During the operation of the system, the following observations of interest were made:

1. In the pressure drop readings at 100°F, a fluctuation of approximately ± 0.7 units on the 0-to-100 gage, corresponding to approximately ± 1.8 in. water was noted during most runs. At the 150°F boiling temperature, the fluctuations were considerably smaller and of the order of ± 0.8 in. water. No fluctuations were noted at the 200 and 250°F boiling temperatures.

2. In addition to the above fluctuations, at very high flow rates where low qualities were encountered, the pressure drop reading

along the length of the tube was found to drift from time to time by some rather large amounts of about 40 in. water. This was believed to be due to the fact that the point of inception of the boiling was varying along the length of the tube because of the very small quality gradient. Since the void fraction changes appreciably with quality in this range, small changes in the point of boiling inception could have resulted in the drift in the pressure drop readings.

3. Relatively good heat balances (within ± 10%) and mass balances (within ± 7%) were obtained at the 100°F run. The balances were not as good at the 150°F runs and became increasingly poorer at the higher boiling temperatures. The reason for the poor heat balances was the less-than-perfect insulation on the boiling system. As the boiling temperature increased, so did the heat loss through the insulation so that it was necessary for the water flowing through the condenser to remove less heat. This trend of a greater measured heat input than a measured heat output was noted on all high temperature runs. The loss of a significant portion of the heat through the insulation also affected the mass balances. A little thought and the study of Figure B-1 on page 424 would indicate that the amount of vapor condensed was not strictly dependent on the amount of heat generated in the boiling test section but was solely dependent on the amount of heat removed by the water in the condenser. If the vapor on its way from the test section exit to the condenser lost some of its heat and a fraction of that vapor condensed, then the amount of condensed vapor measured by FE 123A or FE 123B would have been lower than the true quantity of vapor exiting the test section.

Because of the uncertainty of the experimentally measured qualities, all qualities used in the data reduction and analysis were calculated from the in-stream thermocouples. In all runs, a slightly subcooled liquid entered the test section. This fluid increased in temperature until it reached its saturated point in Zone 1 or Zone 2. Beyond this point, the fluid decreased slightly in saturation pressure due to the small pressure drop along the length of the tube. From the temperatures in both the subcooled and saturated portions, it was possible to determine the point within the tube where the quality was zero. From there, one could calculate the quality at each point in the test section. Very good agreement between the calculated and measured qualities was obtained in those ranges where the heat loss through the insulation was minimal.

4. Operation of the system at the 250°F boiling temperature presented a unique set of operating problems not encountered at the other boiling temperatures. Since the operating temperature was above the boiling point of the water in the condenser, it was not possible to easily maintain the 250°F operating temperature for the R-114. Consequently, in many of the pressure drop and critical heat flux runs undertaken, a steady state waiting period of 1/2 hour was the exception rather than the rule. Judicious control of the water flow was necessary since the amount of liquid fed to the condenser had to equal the amount boiled away. Thus, the quantity of water involved was exceedingly small. Sometimes, an accidental discharge of a slug of water would result in a 20 to 30°F drop in the boiling temperature and necessitate a wait of as long as 4 to 6 hours for the system to return to its original

operating temperature. This situation could have been avoided had a closed, pressurized system for the coolant water been utilized.

APPENDIX C

CALIBRATION TECHNIQUES

A calibration was performed on each piece of instrumentation used in conjunction with the boiling test facility. The instrumentation was used to measure the pressure drops, temperatures, flow rates, and heat fluxes in various parts of the system.

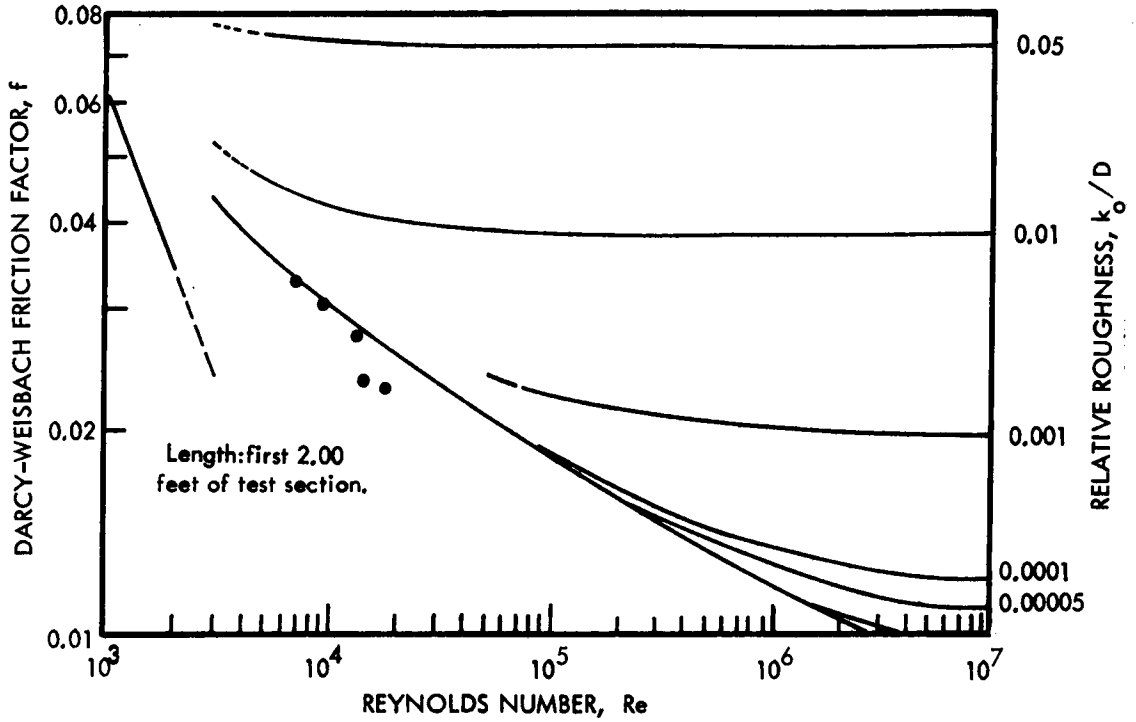
Pressure Drop

Pressure Taps. The care with which the pressure taps of the 10-ft section were made was briefly discussed in Appendix B. In the final analysis, a test needs to be conducted to experimentally verify the soundness of the pressure tap construction. This was done before the test section was installed in the boiling facility. Water at various velocities was pumped through the 10-ft tube while it was in the horizontal position. The pressure drop at approximately 2-, 4-, 6-, 8-, and 10-ft increments was measured with an inclined manometer. This data was reduced in the form of friction factor versus Reynolds number. The results are shown in Figure C-1. As can be seen, the data points lie close to the curve representing the friction factor for drawn tubing. A good fit to the data in the range of interest was

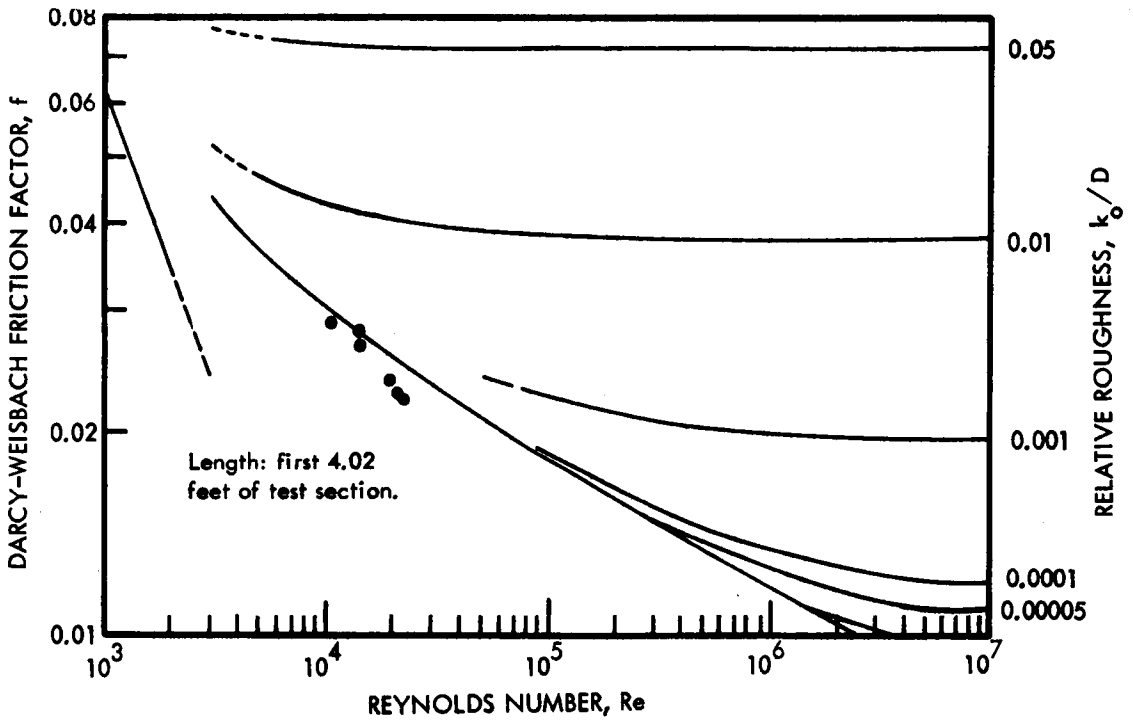
$$1/4\ f = f' = 0.0674\ (Re)^{-0.2349} \qquad (C\text{-}1)$$

Here, f' is the Fanning friction factor and f is the Darcy-Weisbach friction factor.

Pressure Drop Measuring System. Having determined the soundness of the pressure tap construction, it is now necessary to make sure that

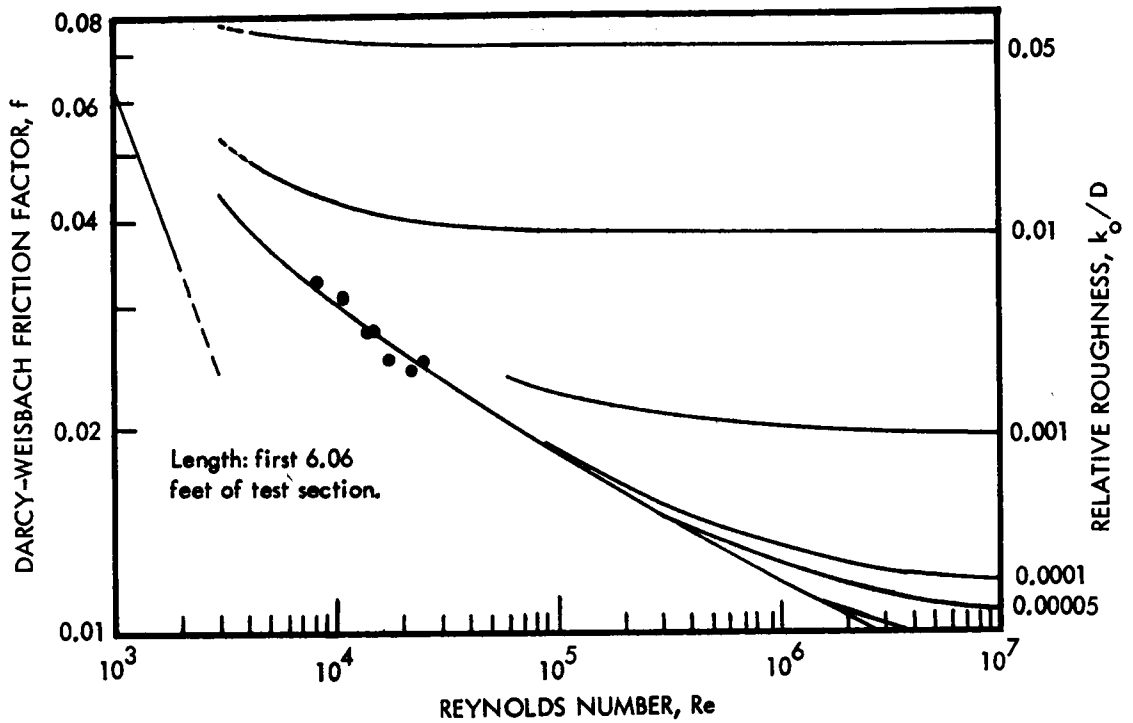


(a)

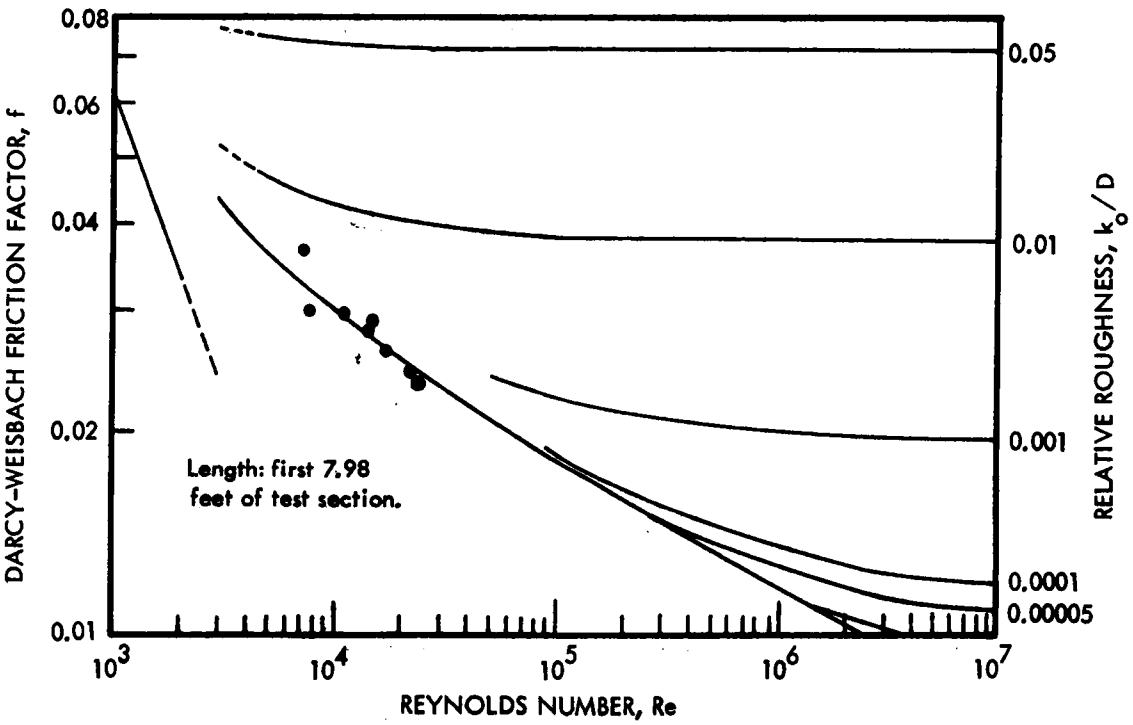


(b)

Figure C-1. EXPERIMENTALLY DETERMINED FRICTION FACTORS FOR SINGLE-PHASE FLOW OF WATER INSIDE TEST SECTION.

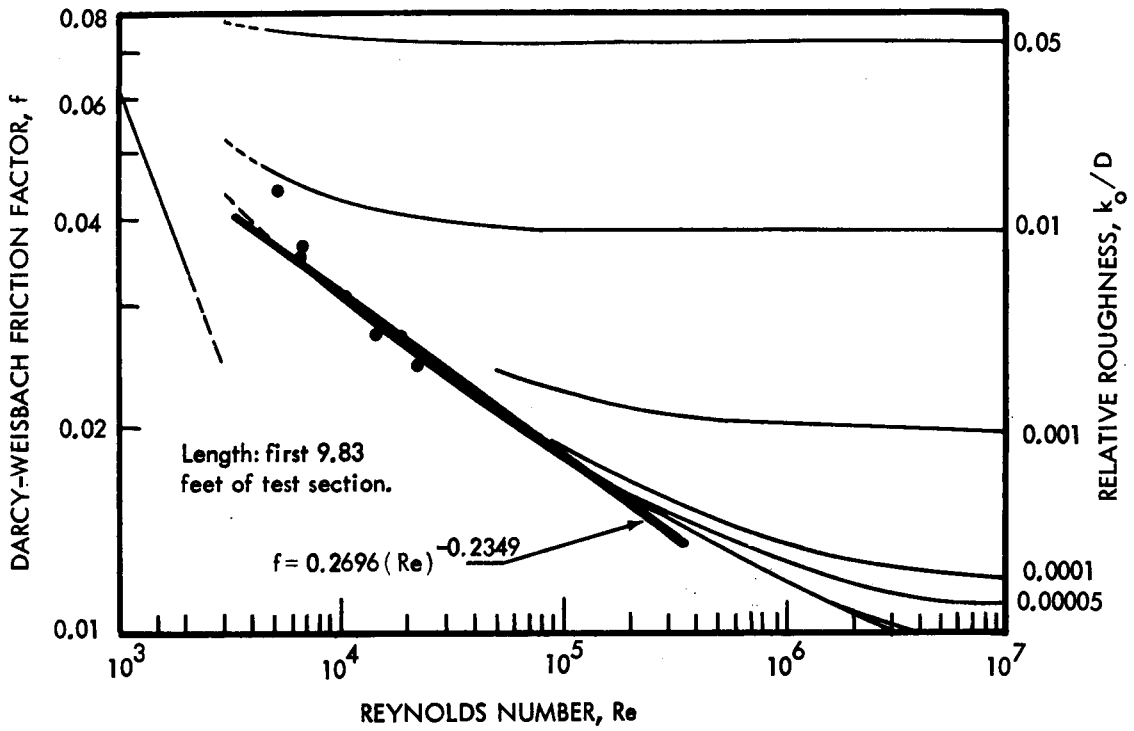


(c)



(d)

Figure C-1. (continued)



(e)

Figure C - 1. (continued)

the pressure drop is accurately sensed by the DP cell and correctly indicated on the 0 to 100 division gage. For maximum accuracy, the various pressure drop measuring components were calibrated as one system. A constant and accurately known pressure was inputed on one side of the DP cell while the other side of the DP cell was open to the atmosphere. The deflection on the 0 to 100 receiver gage was recorded. This was done in the range of -175 to +100 in. of water. This range was necessary because as can be observed in Figure III-8 on page 112, the pressure drop across the DP cell was the same as the pressure drop across two pressure taps on the wall plus the pressure increase due to a length of liquid in the pressure tap line equal to the distance between the two pressure taps. The sum of the gravitational, acceleration, and frictional pressure drops in the boiling test section was sometimes greater than and sometimes less than the hydrostatic pressure increase due to the liquid in the pressure tap line. The calibration for this system is given in Figure C-2.

Flow Rates

Turbine Meters. All Cox turbine meters were calibrated by pumping a constant flow rate of water through them, and collecting the water in a barrel mounted on a scale. The amount of water entering the barrel within a specified period of time was measured and the flow rate readily determined. FE 105B was the only turbine meter where the digital readout of gallons per minute varied appreciably from the true flow rate measured during the calibration. The calibration curves of all four turbine meters are given in Figures C-3 to C-6. Least squares fits of the calibration curves were used in the data reduction codes. Once the

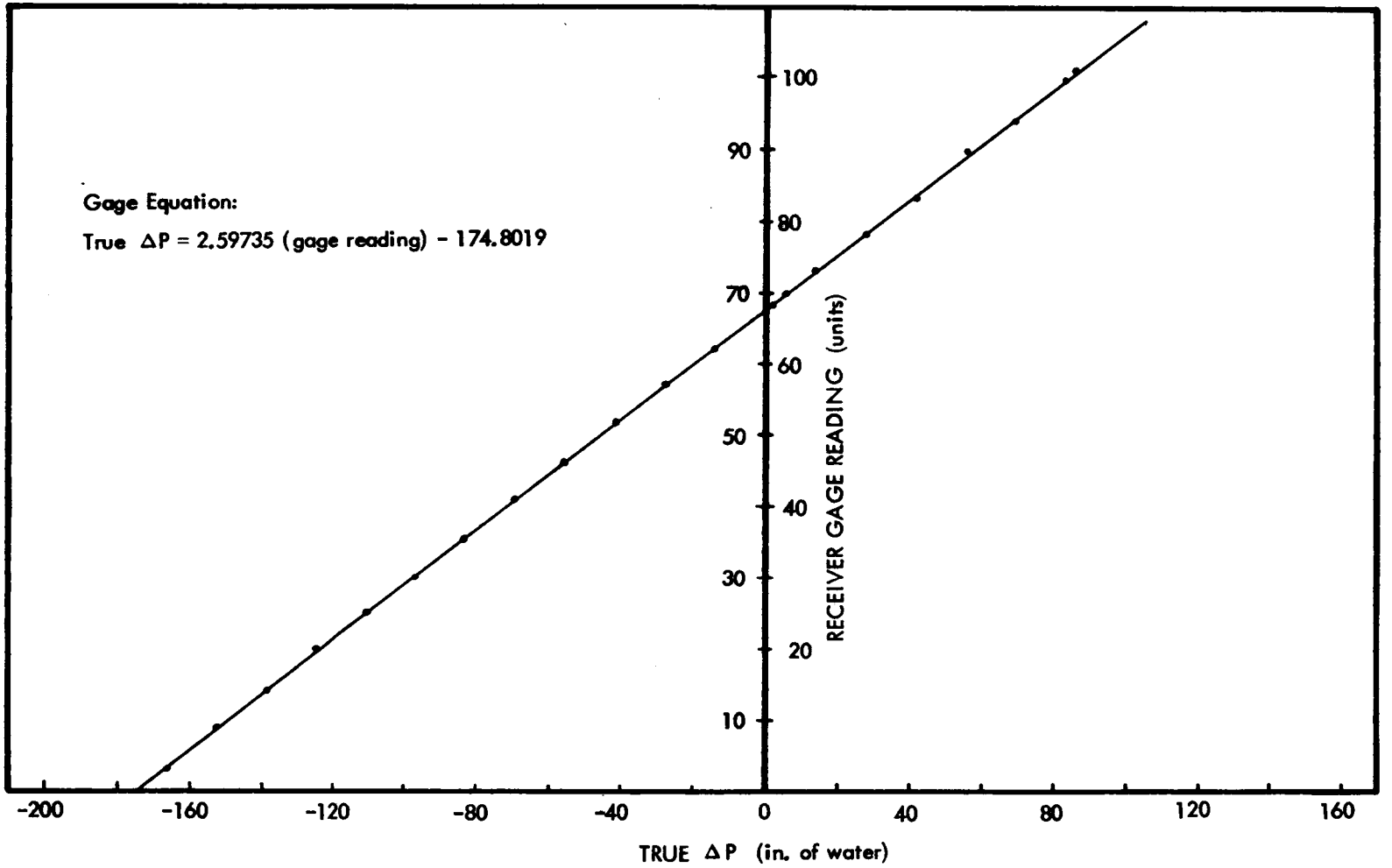


Figure C-2. CALIBRATION CURVE FOR THE DP CELL AND RECEIVER GAGE.

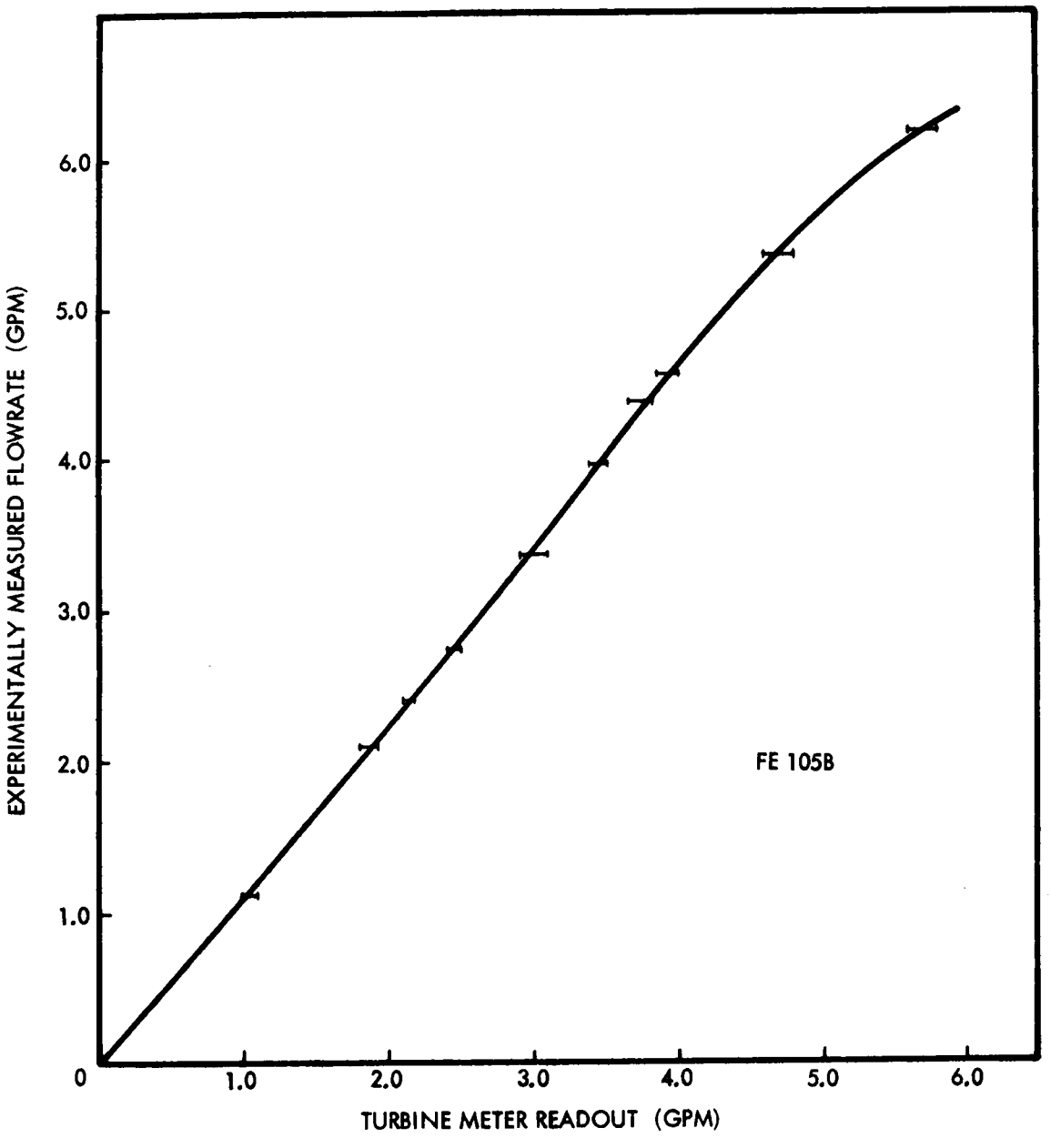


Figure C - 3. CALIBRATION CURVE FOR FE 105B.

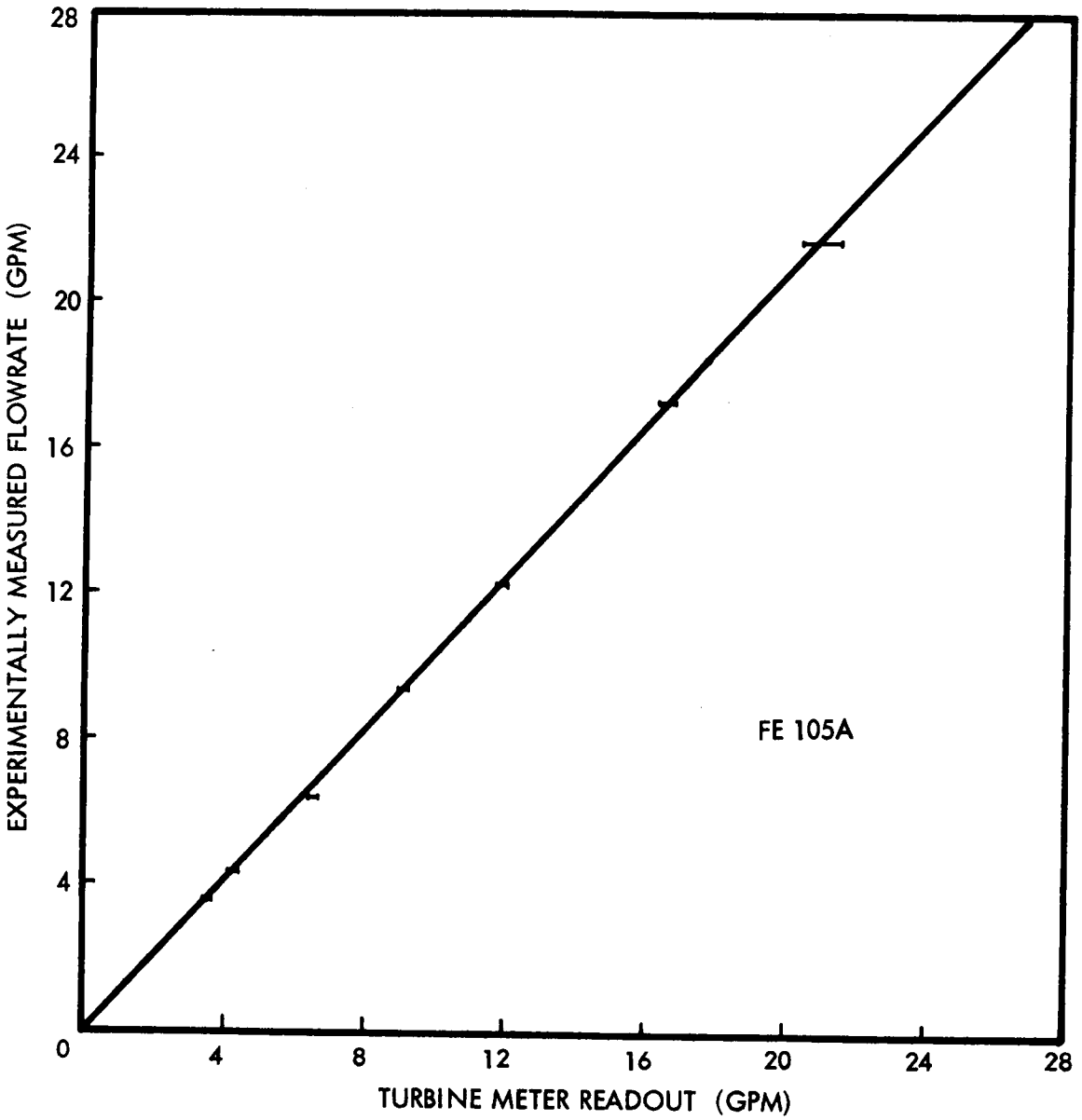


Figure C-4. CALIBRATION CURVE FOR FE105A.

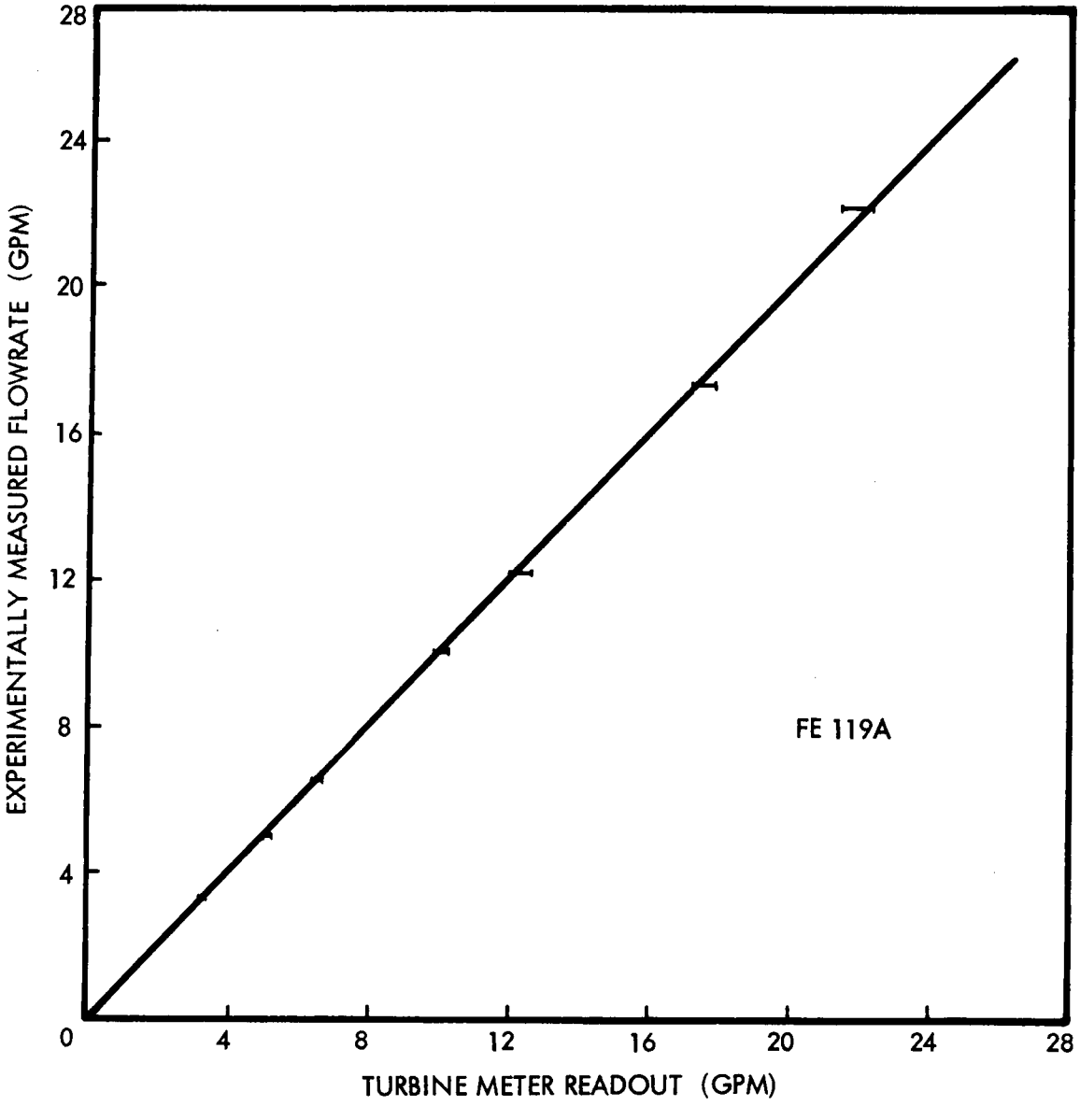


Figure C - 5. CALIBRATION CURVE FOR FE 119 A.

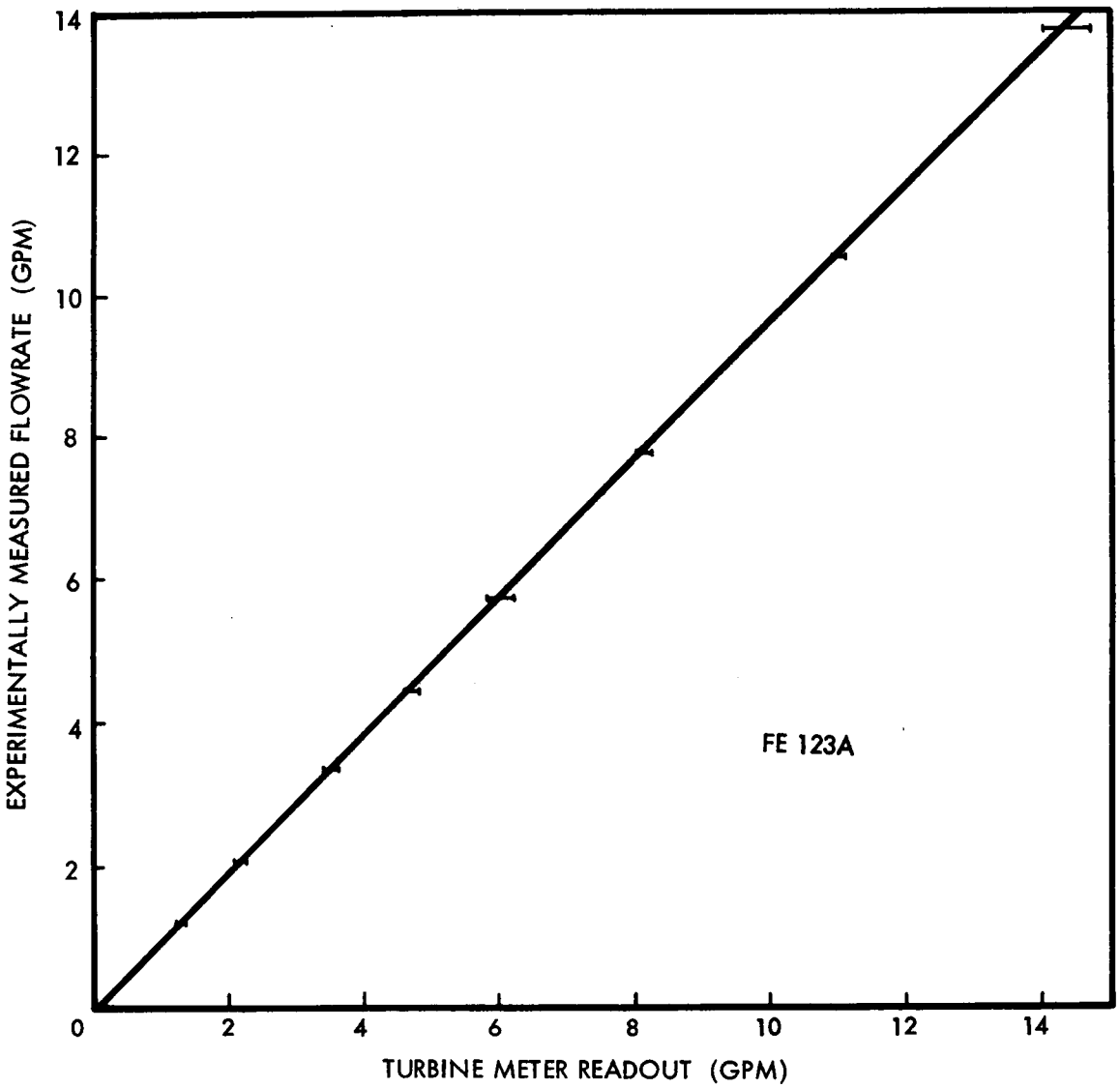


Figure C-6. CALIBRATION CURVE FOR FE 123A.

true flow rate, as well as the fluid temperature were known, multiplying the cu ft per minute by the fluid density in lbm/cu ft yielded the flow rate in lbm/min.

Rotameters. The flow of a liquid through a rotameter is found to be well predicted by the equation [134]:

$$Q = A_w C' \left[\frac{2v_f'(\rho_{float} - \rho_f)}{A_{float}\,\rho_f}\right]^{1/2} \qquad (C\text{-}2)$$

where Q is the volumetric flow rate, A_w is the area of the annular orifice, C' is the discharge coefficient, ρ_{float} is the density of the float material, v_f' is the volume of the float, A_{float} is the area of the float, and ρ_f is the fluid density. If a rotameter that is calibrated for a given fluid and temperature is used for a different fluid or at a significantly different temperature:

$$Q_2 = Q_1 \left[\frac{(\rho_{float} - \rho_2)\rho_1}{(\rho_{float} - \rho_1)\rho_2}\right]^{1/2} \qquad (C\text{-}3)$$

allows the necessary correction to be made. Here ρ_1, is the fluid density for which the rotameter has been calibrated and ρ_2 is the new fluid density. Rewriting this,

$$Q_2 = K'' \left[\frac{\rho_{float}}{\rho_2} - 1\right]^{1/2} R' \qquad (C\text{-}4)$$

where K'' is a constant and R' is the scale reading on the rotameter. This equation can be used for any fluid at any temperature as long as ρ_2 is known. Thus, a calibration for water is sufficient. All the rotameters used in this experiment were calibrated with water. These curves are shown in Figures C-7 to C-9. There was very good agreement

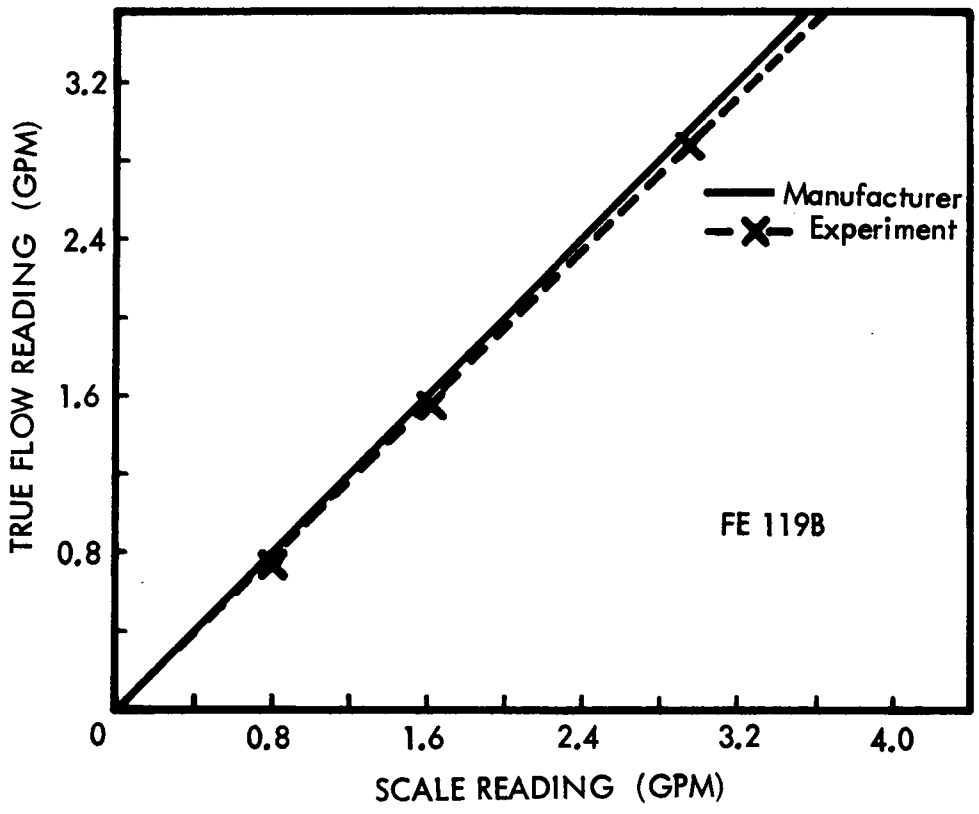


Figure C - 7. CALIBRATION CURVE FOR FE 119 B.

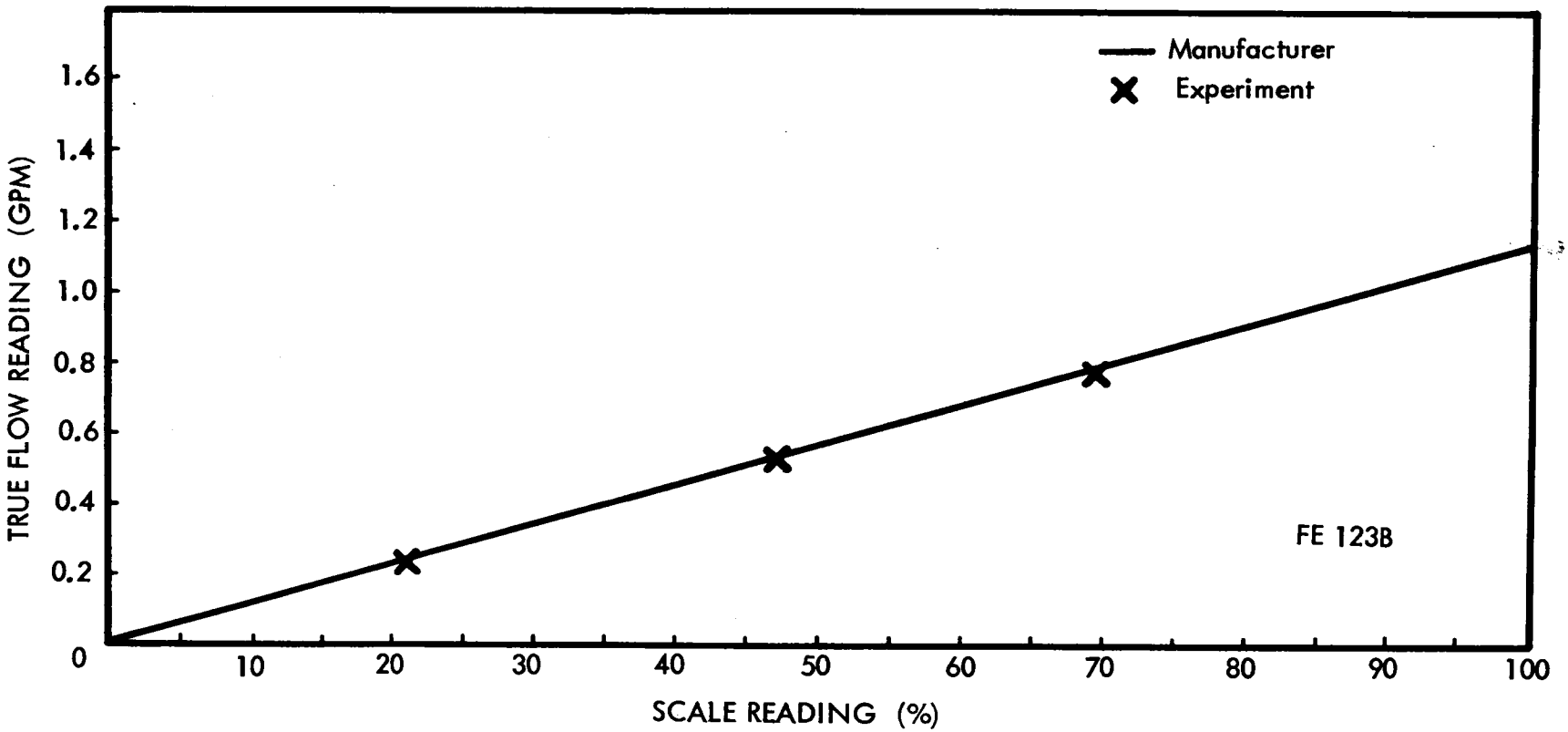


Figure C - 8. CALIBRATION CURVE FOR FE 123B.

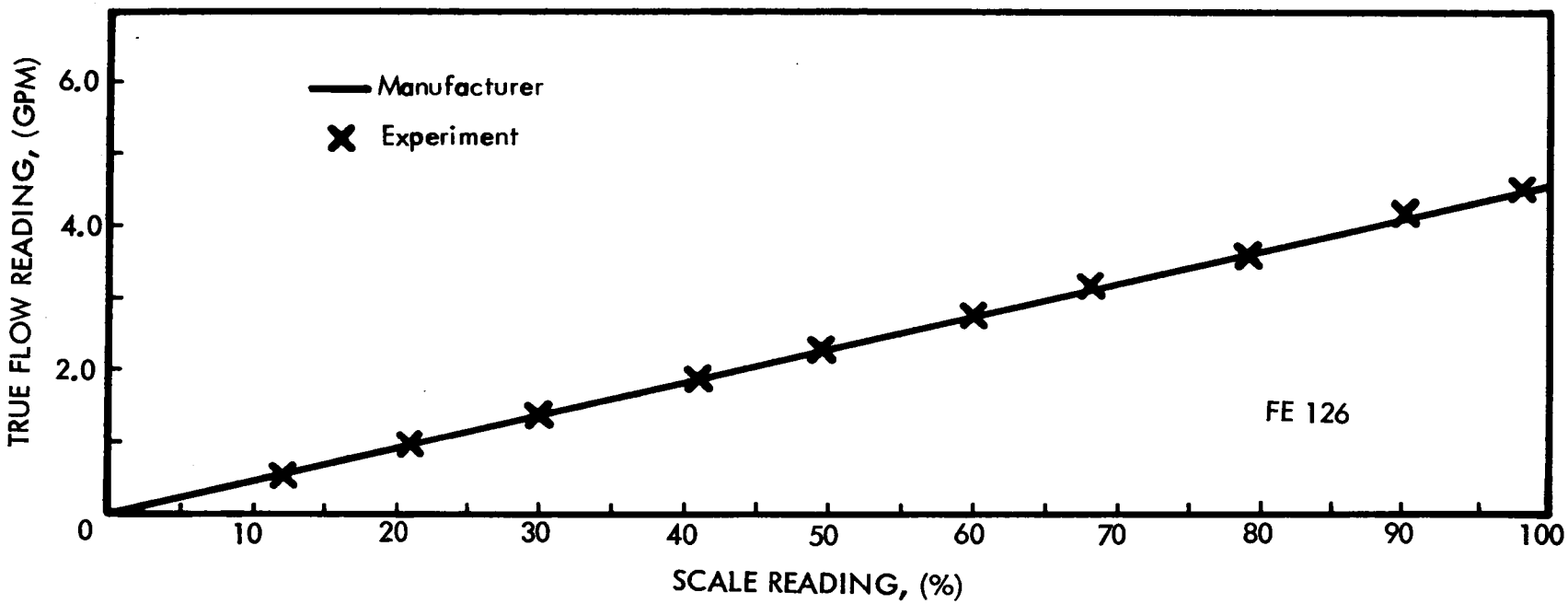


Figure C-9. CALIBRATION CURVE FOR FE 126.

with the manufacturer's curve. Thus, the following equations were used in the data reduction code:

For FE 119B:

$$GPM = 0.35813\left(\frac{499.66}{\rho_f} - 1\right)^{1/2} R' \qquad (C\text{-}5)$$

for FE 123B:

$$GPM = 0.0042385\left(\frac{499.66}{\rho_f} - 1\right)^{1/2} R' \qquad (C\text{-}6)$$

and for FE 126:

$$GPM = 0.017515\left(\frac{499.66}{\rho_f} - 1\right)^{1/2} R' \qquad (C\text{-}7)$$

Heat Input to Test Section

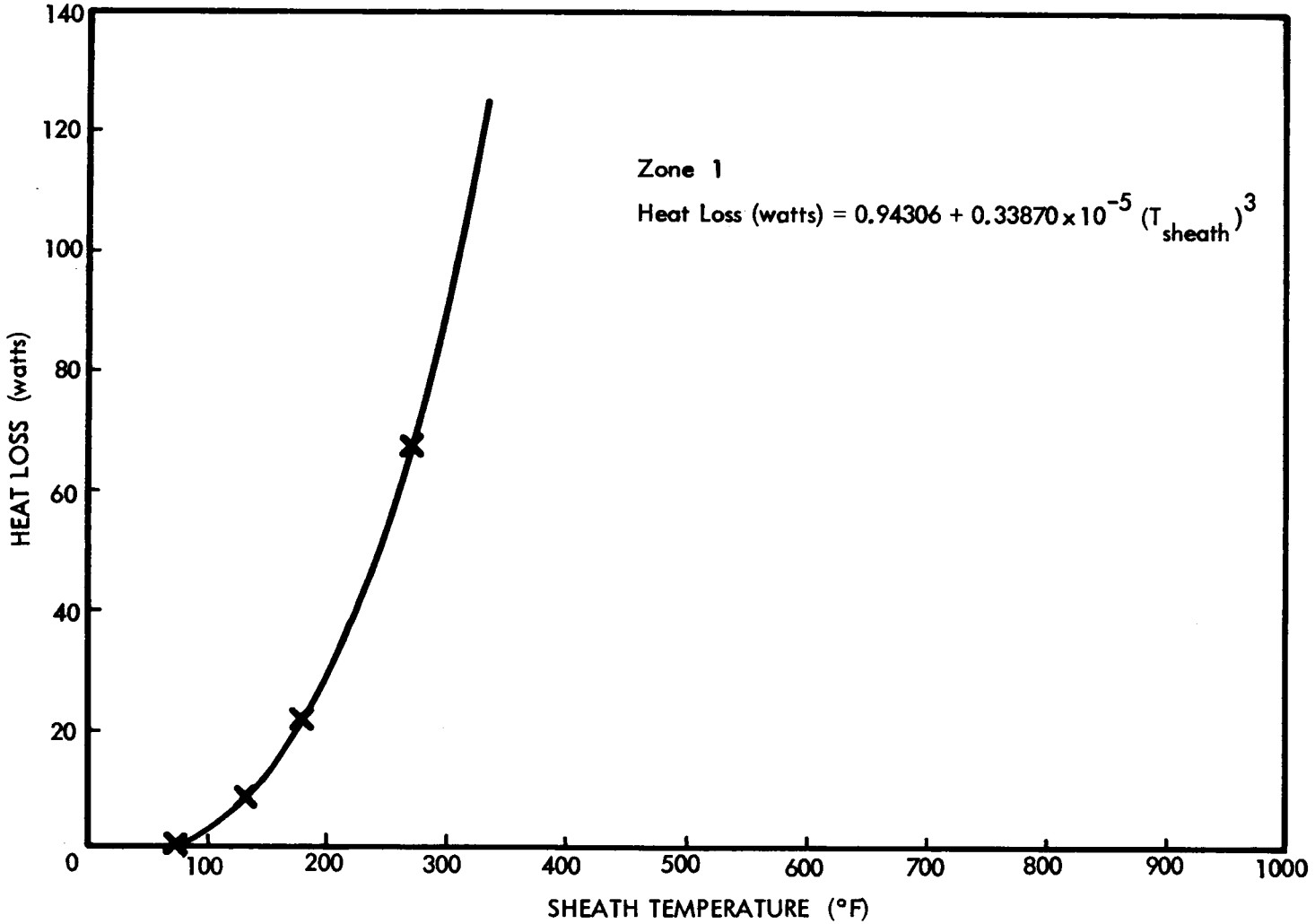
Heat Loss Through Insulation. Despite the fact that 2 in. of insulation was placed on the heaters, a fraction of the heat generated by the Chromalox heaters did not go to the refrigerant. The loss of heat was mainly:

(1) Through the insulation.

(2) By conduction through the copper ends to the adjacent parts of the system.

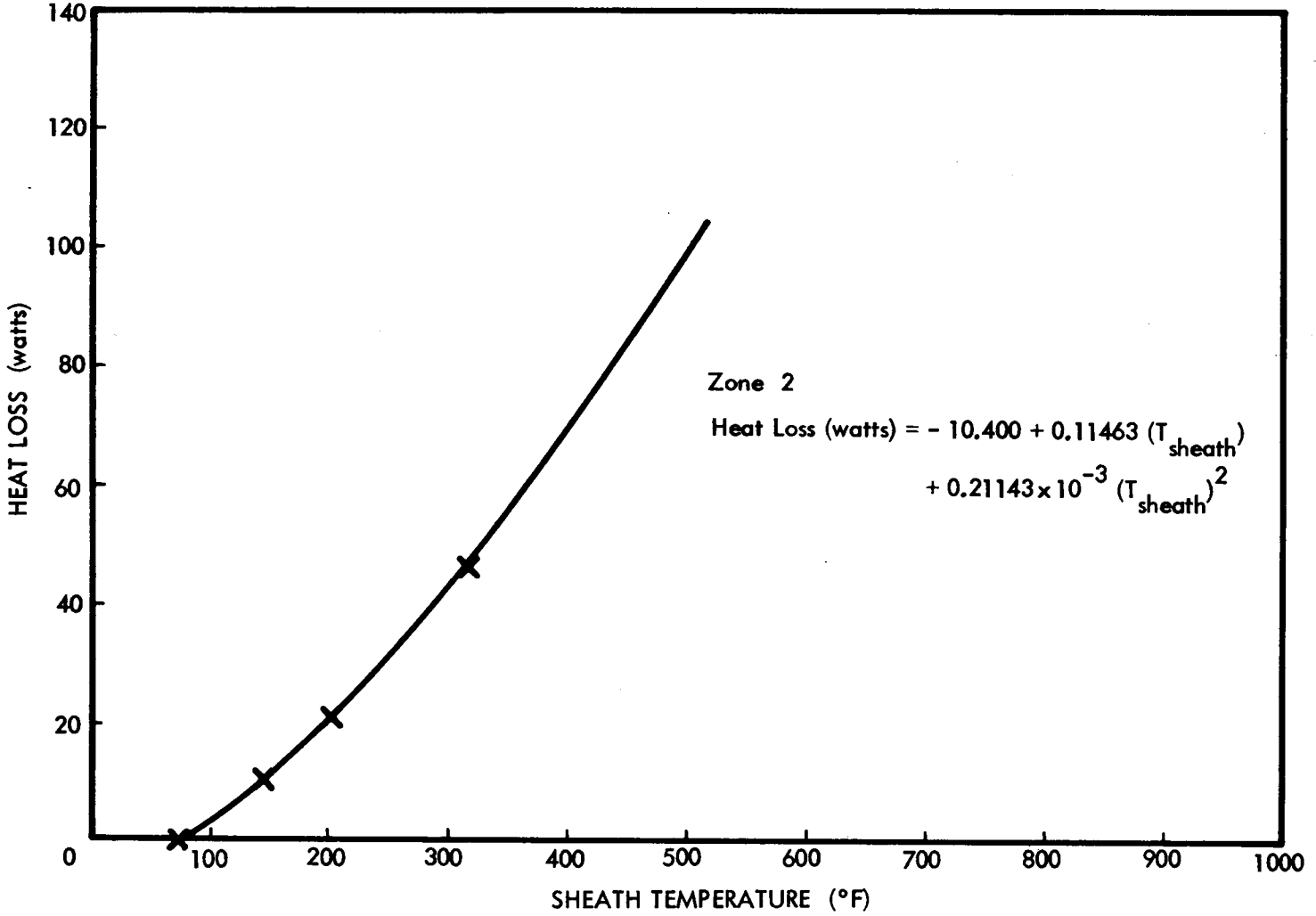
(3) Via the thermocouples and pressure tap lines.

In order to experimentally determine the heat loss, the system was evacuated using a vacuum pump. This was done so that there could be no convective heat transfer. A small heat flux was then uniformly applied to all 10 zones. At least 8 hours were allowed for the system to reach steady state. The heat input and the heater sheath temperatures in each zone were then recorded. Plots of the heat loss versus the heater sheath temperatures are shown in Figure C-10. It can be



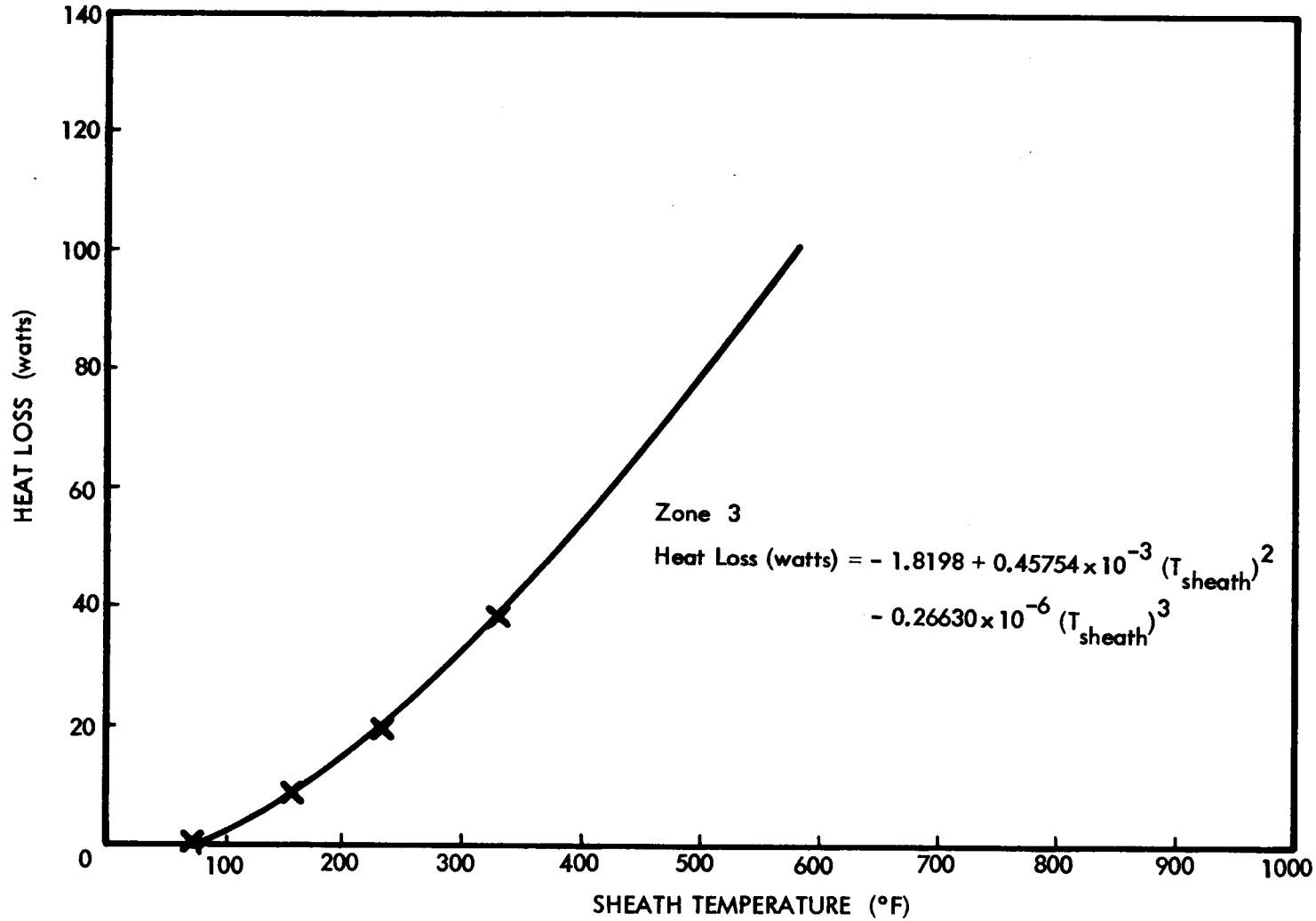
(a)

Figure C - 10. HEAT LOSS CALIBRATION RESULTS.



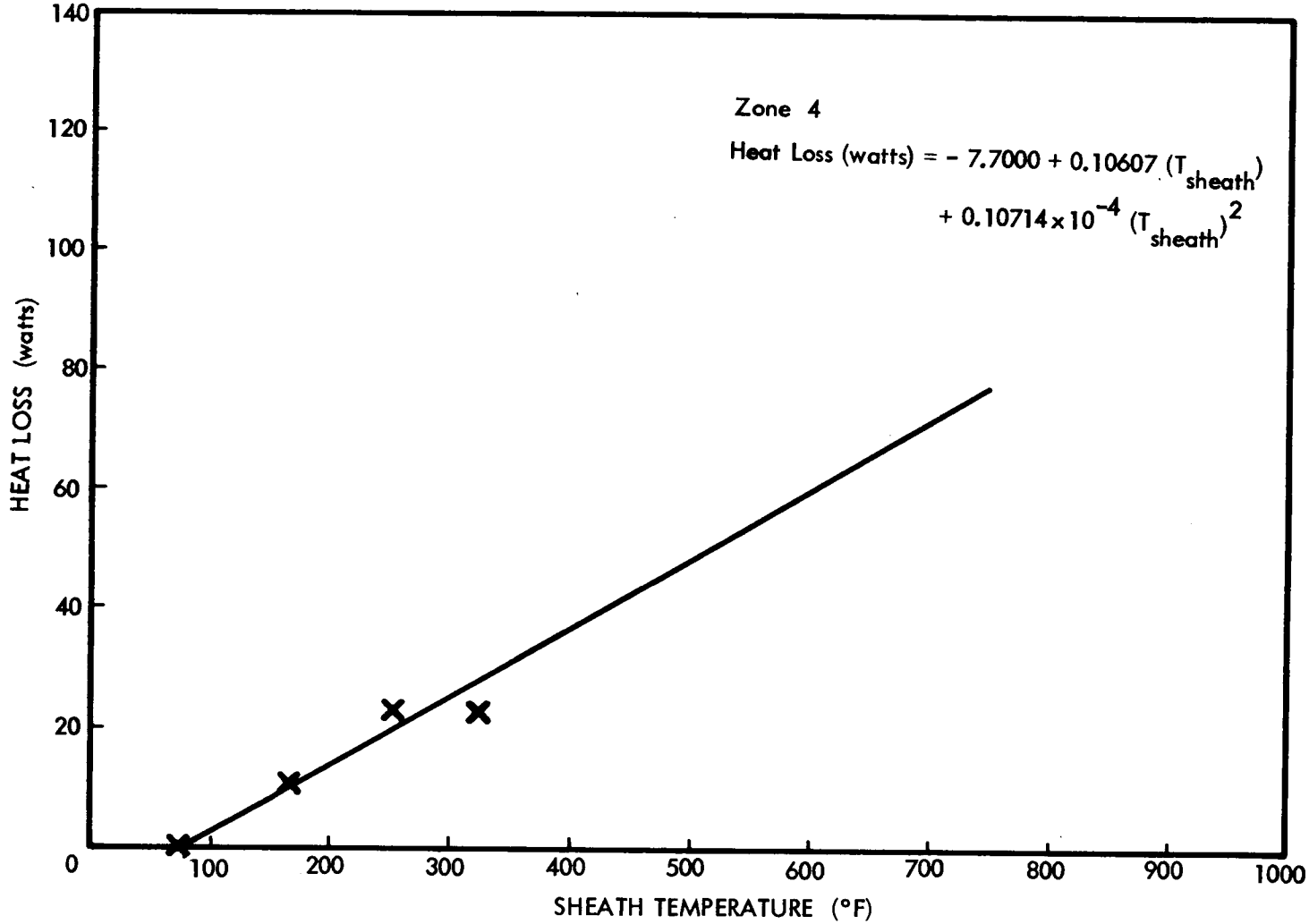
(b)

Figure C - 10. (continued)



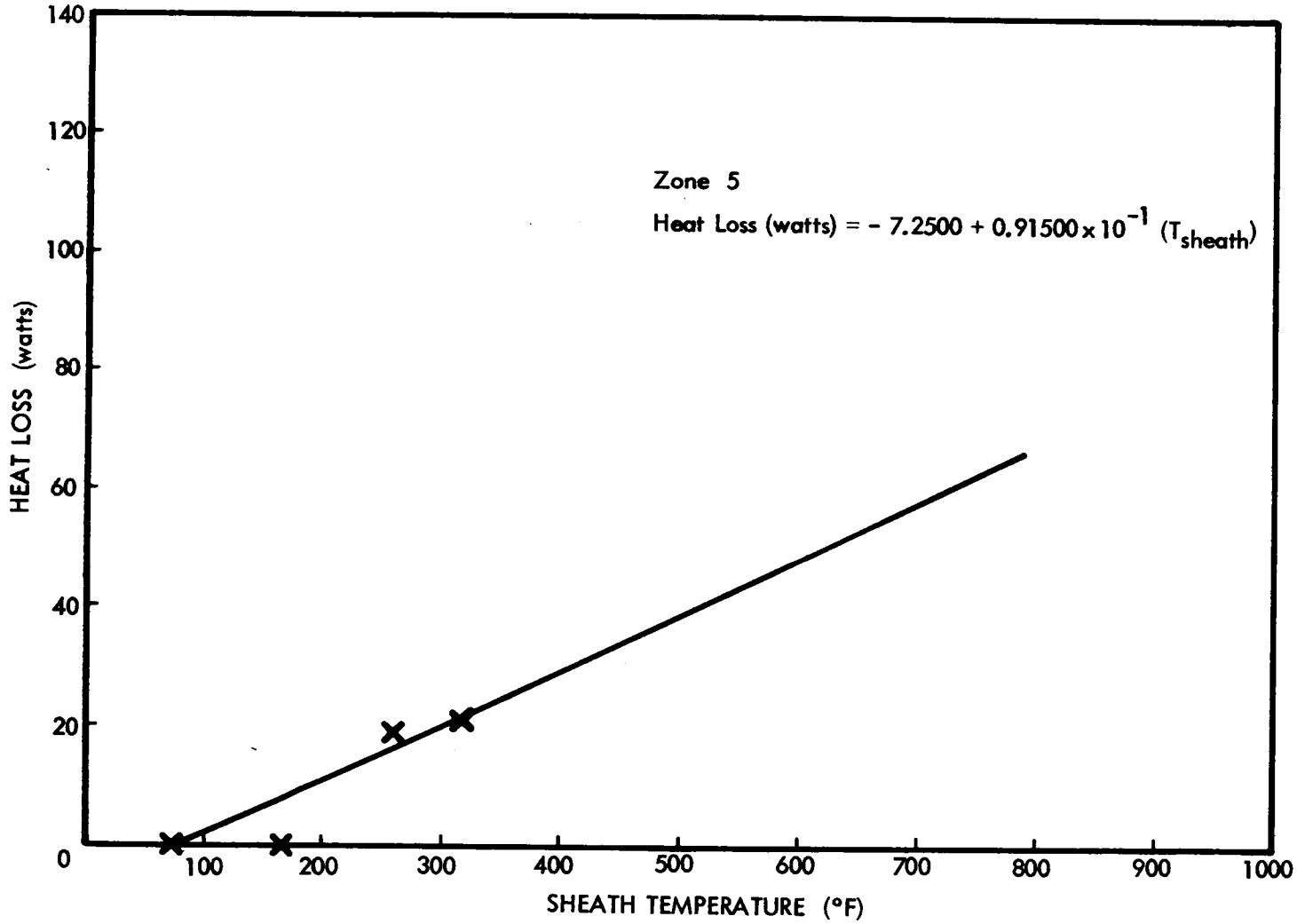
(c)

Figure C - 10. (continued)



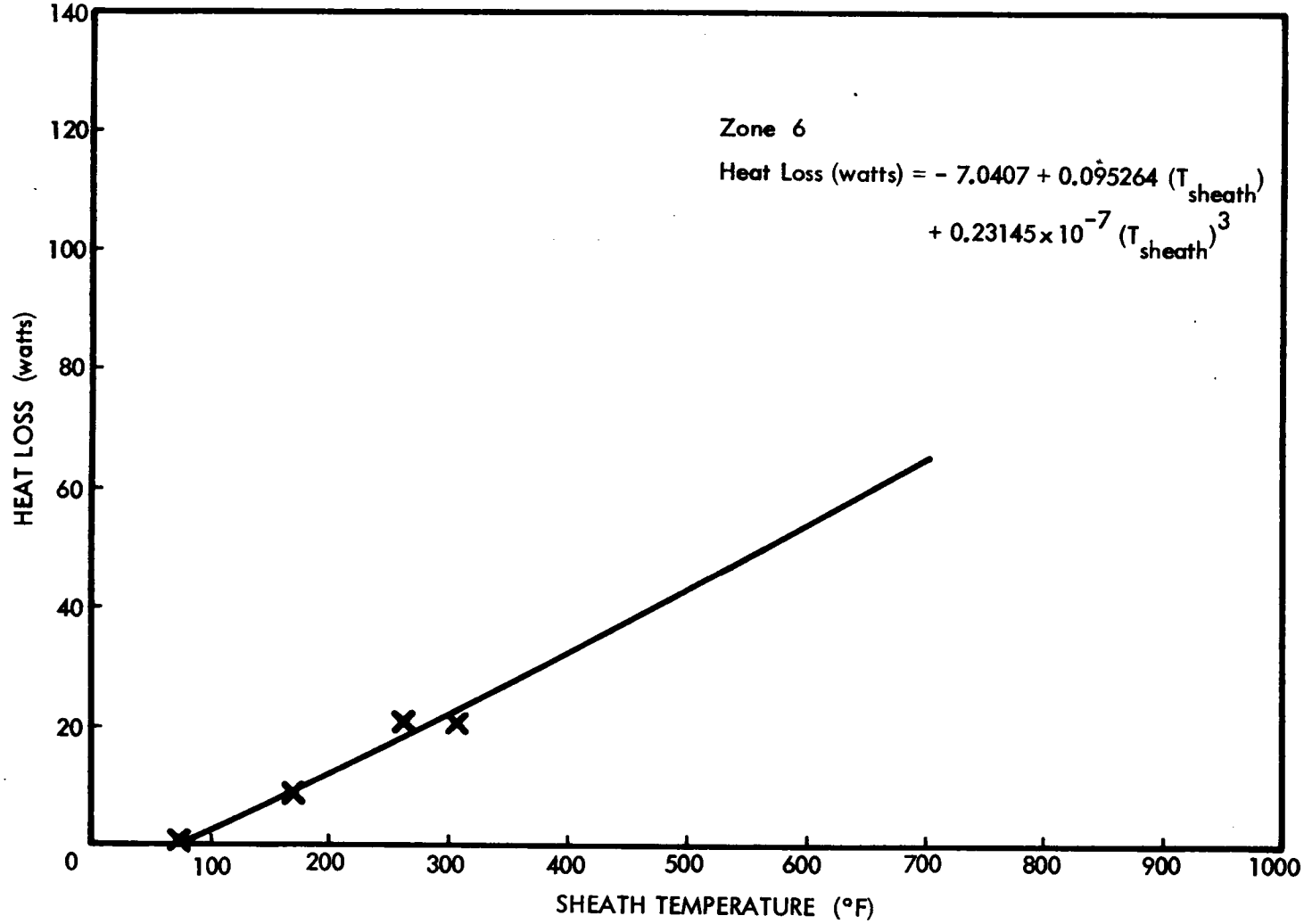
(d)

Figure C - 10. (continued)



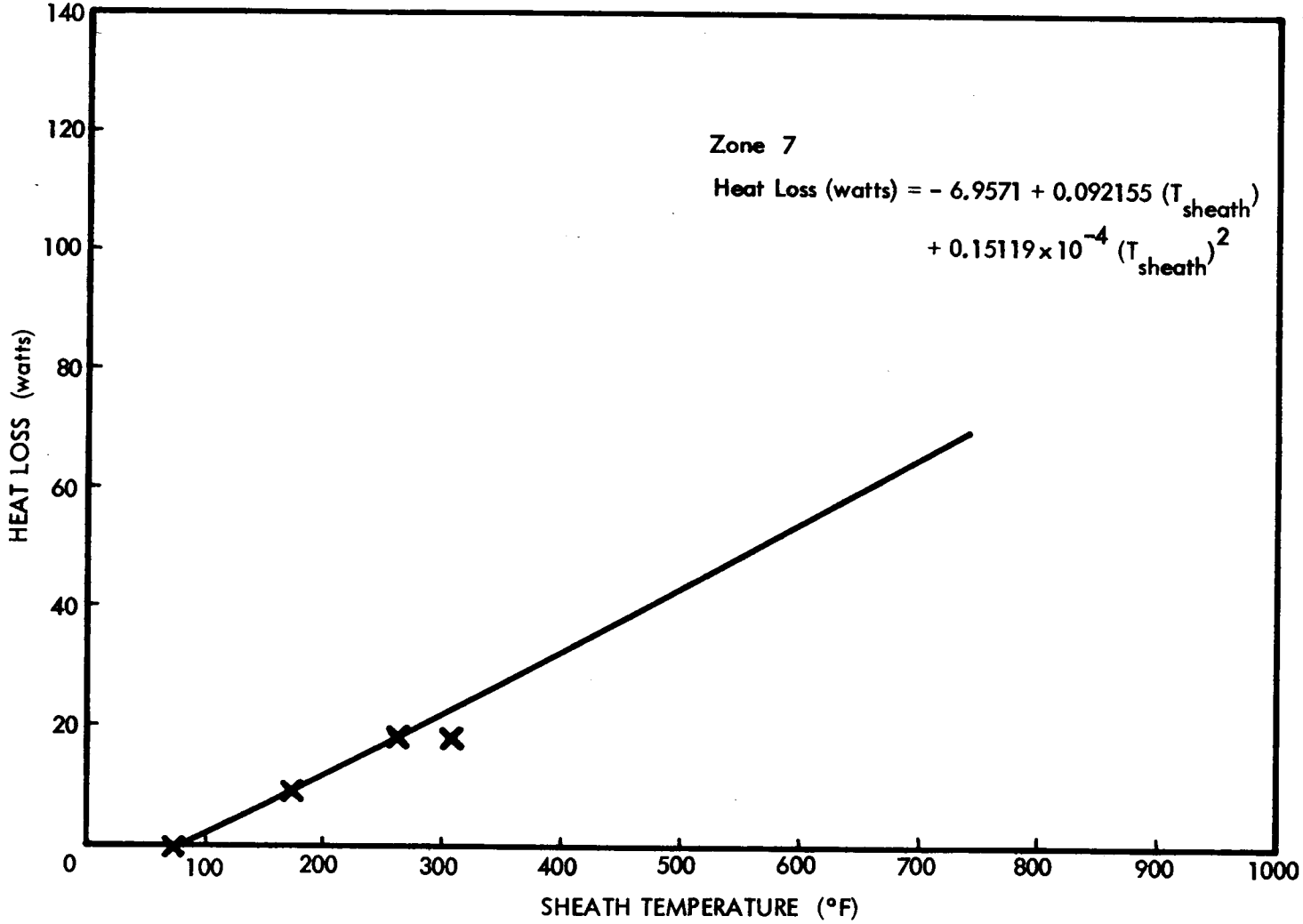
(e)

Figure C - 10. (continued)



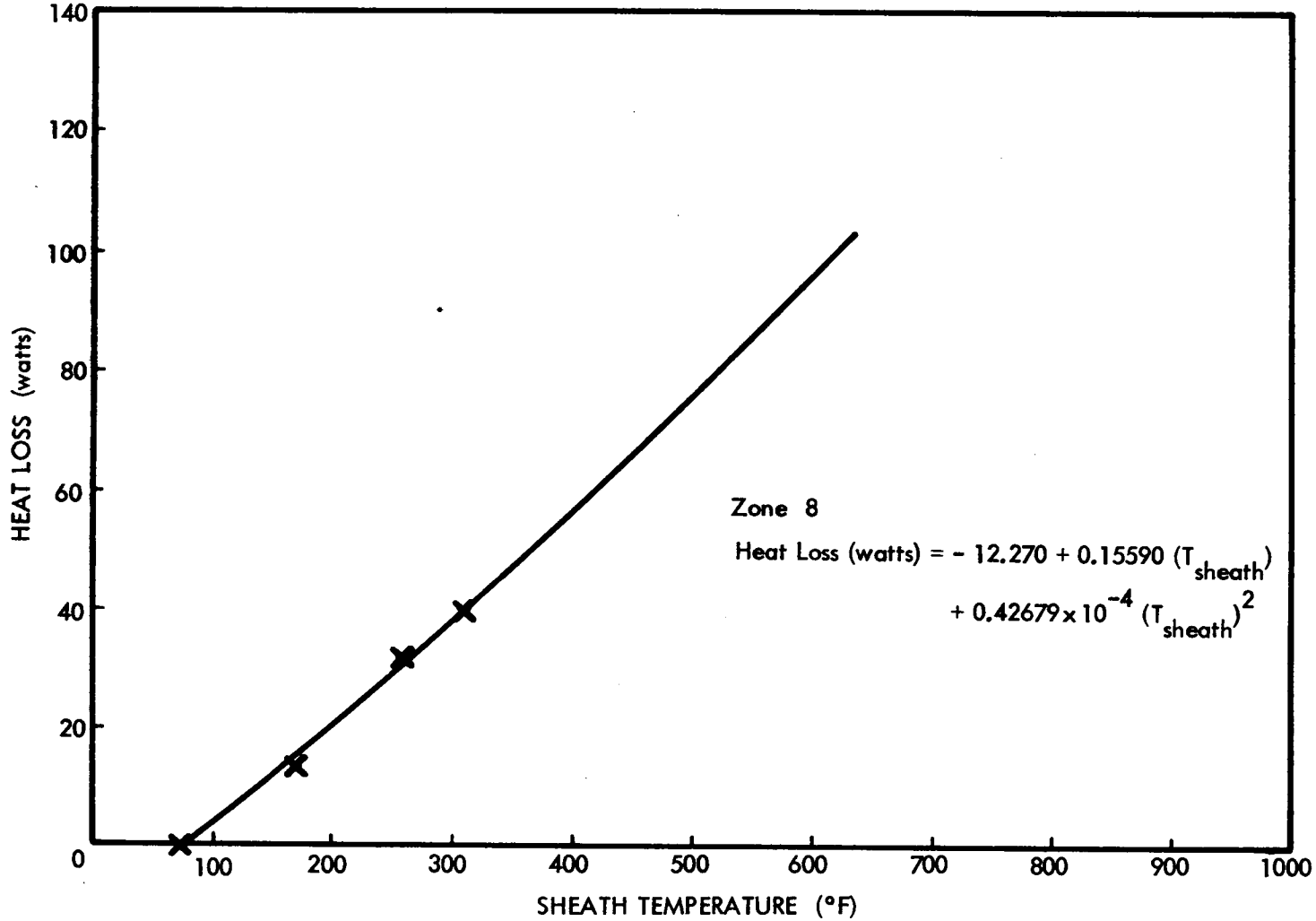
(f)

Figure C - 10. (continued)



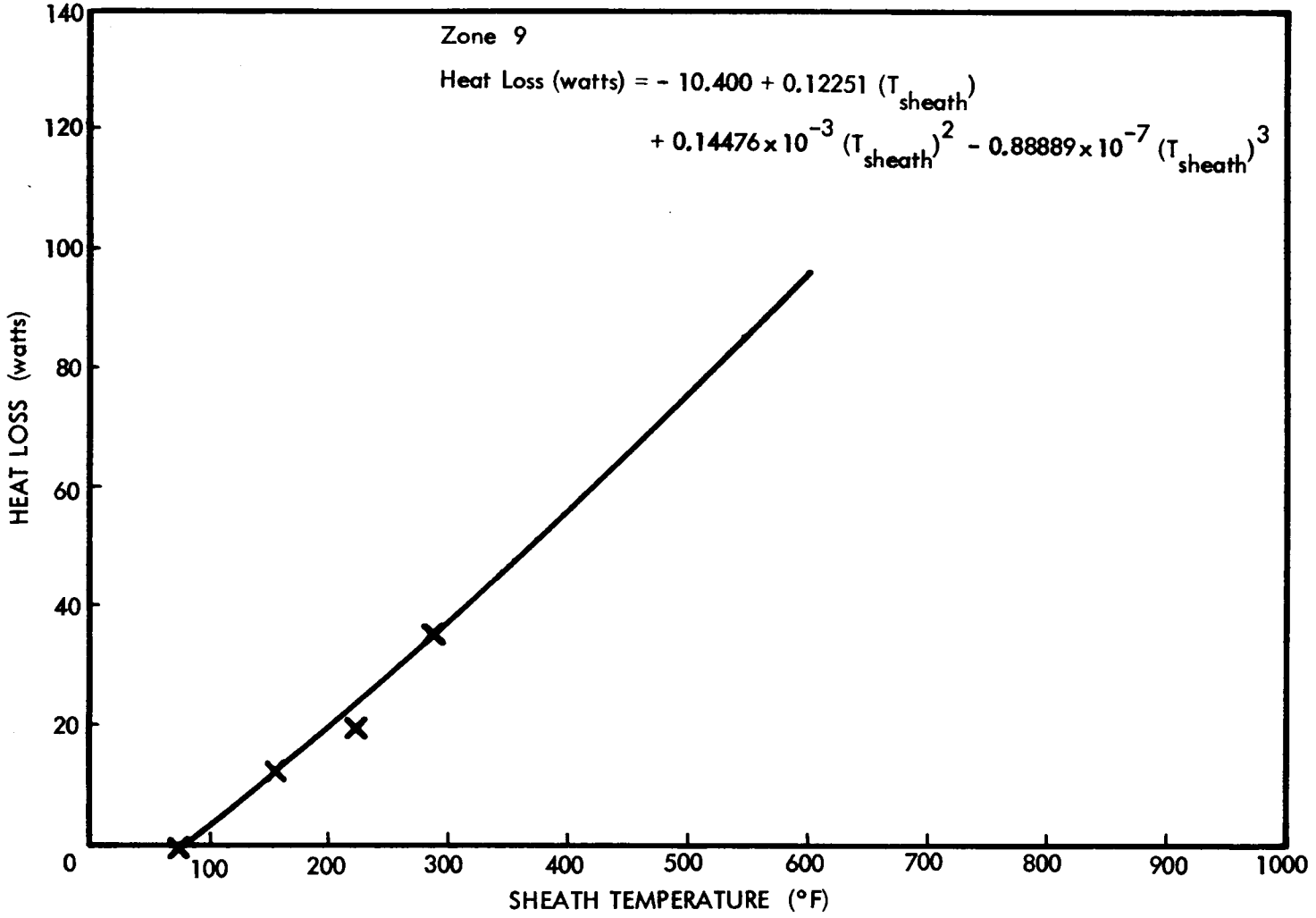
(g)

Figure C - 10. (continued)



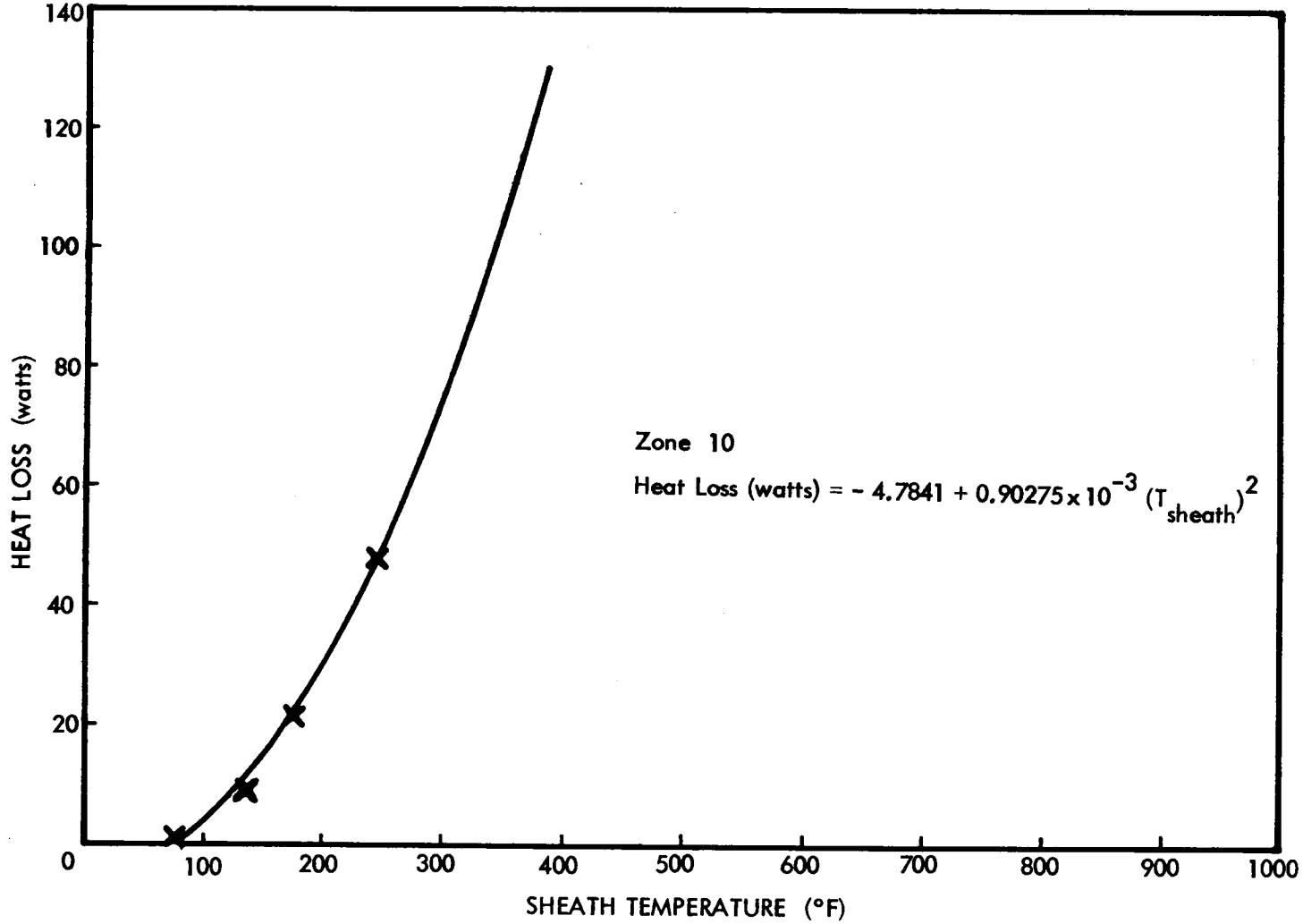
(h)

Figure C - 10. (continued)



(i)

Figure C - 10. (continued)



(j)

Figure C - 10. (continued)

noted that the heat lost in Zones 1 and 10 was greater than that in other zones. This was due to the fact that a significant portion of the heat lost is by conduction through the flanges.

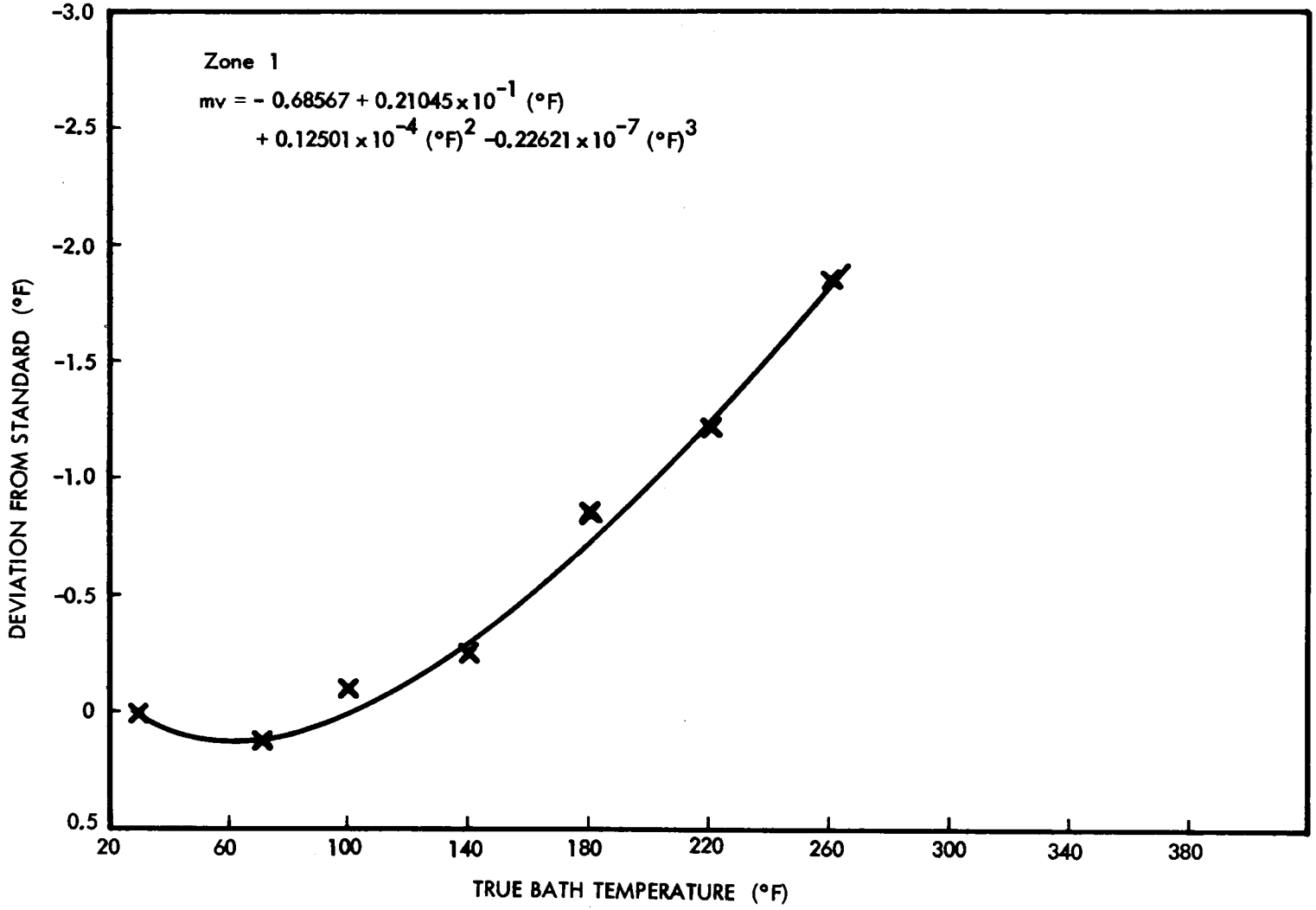
Watt-Hour Meter Standard Calibration. Because the watt-hour meter used was a standard and factory calibrated, very small errors were anticipated. Calibration data enclosed with the watt-hour meter indicated that less than 0.30% error was measured in all current and voltage ranges.

Thermocouple Calibrations

All the sheathed Chromel-Alumel in-stream thermocouples used were calibrated before installation. The calibrations were performed in an oil bath in the 32 to 260°F temperature range. Plots of the deviation from the standard curve versus the temperature are shown for each of the 10 zones in Figure C-11. This type of plot is considered to be superior to the mv versus °F curve, since small deviations can be more easily seen. The best fit through the calibration data points are also given in Figure C-11. The form of the equation mv = mv(°F) was preferred to the inverse of this equation because of the smaller rms error generated by the least square fit. A Newton-Raphson technique was used to determine the °F corresponding to a given mv reading.

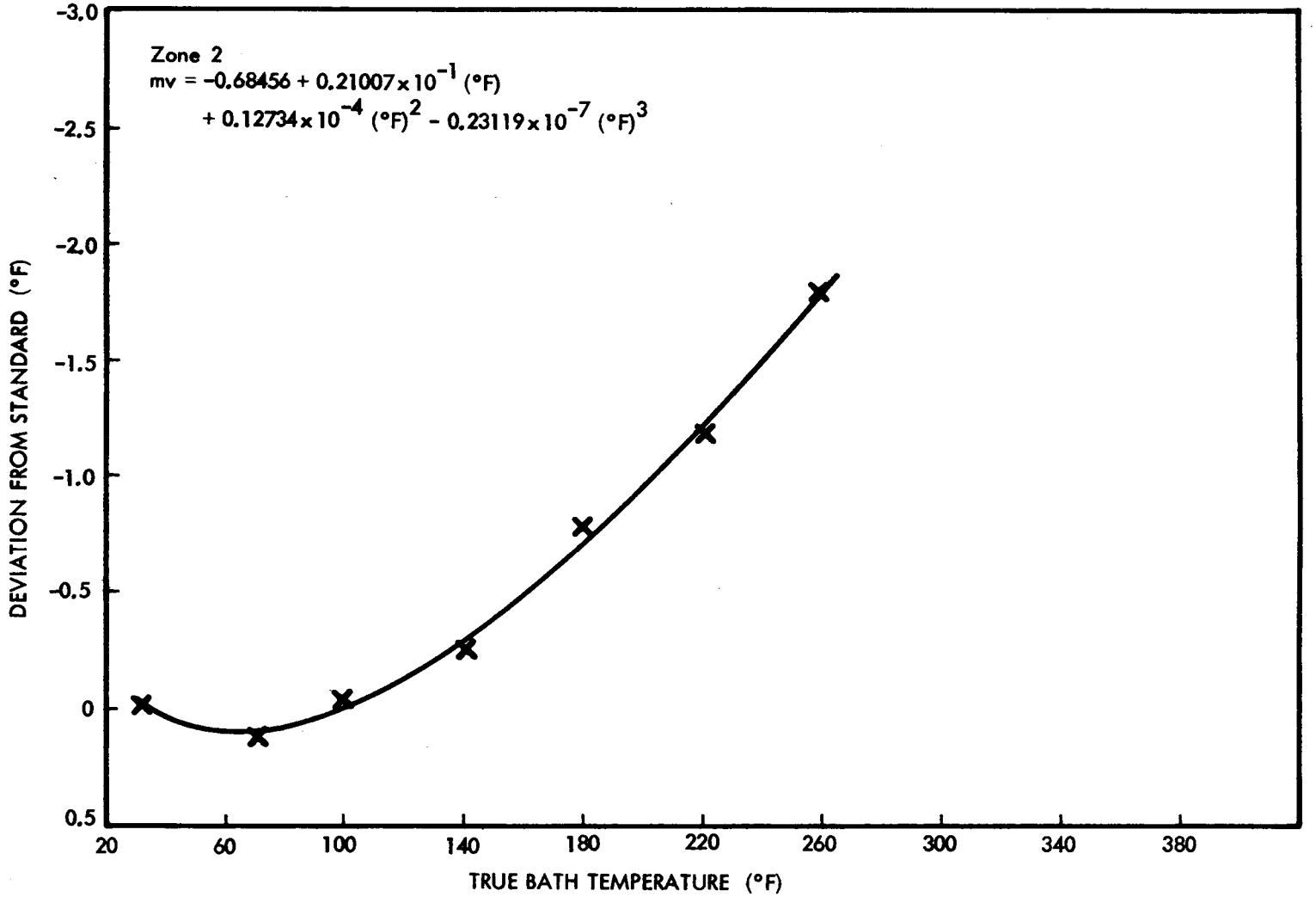
For the unsheathed Chromel-Constantan wall thermocouples, all the wire used was taken from the same spool. Only the first and last pieces of wire were calibrated, and no differences between the two were detected. The best fit through the bare wire calibration data was:

$$mv = -1.0207 + 3.1273 \times 10^{-2} (°F) + 1.7629 \times 10^{-5} (°F)^2 - 9.4550 \times 10^{-9} (°F)^3 \qquad (C-8)$$



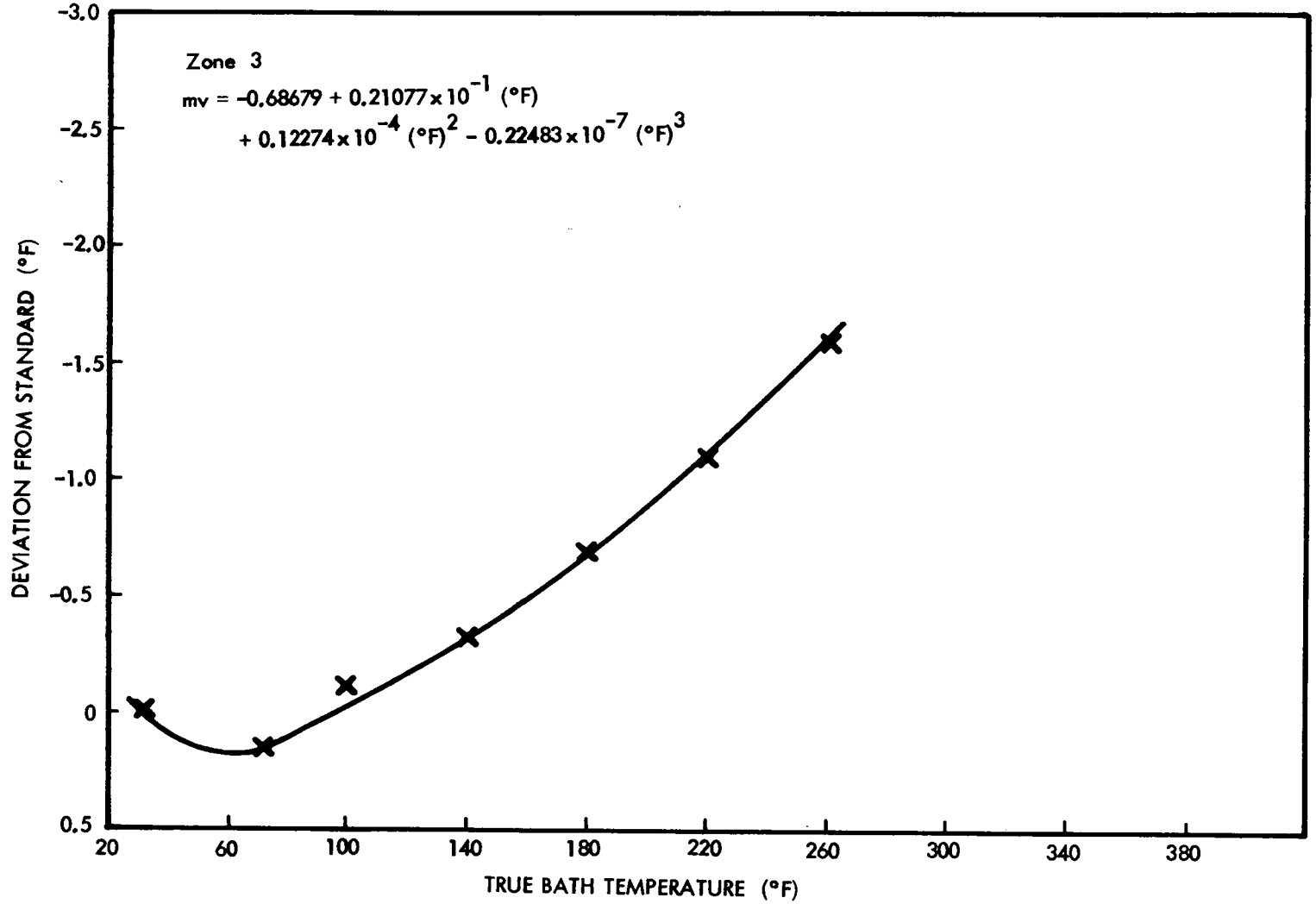
(a)

Figure C-11. IN-STREAM THERMOCOUPLE CALIBRATION RESULTS.



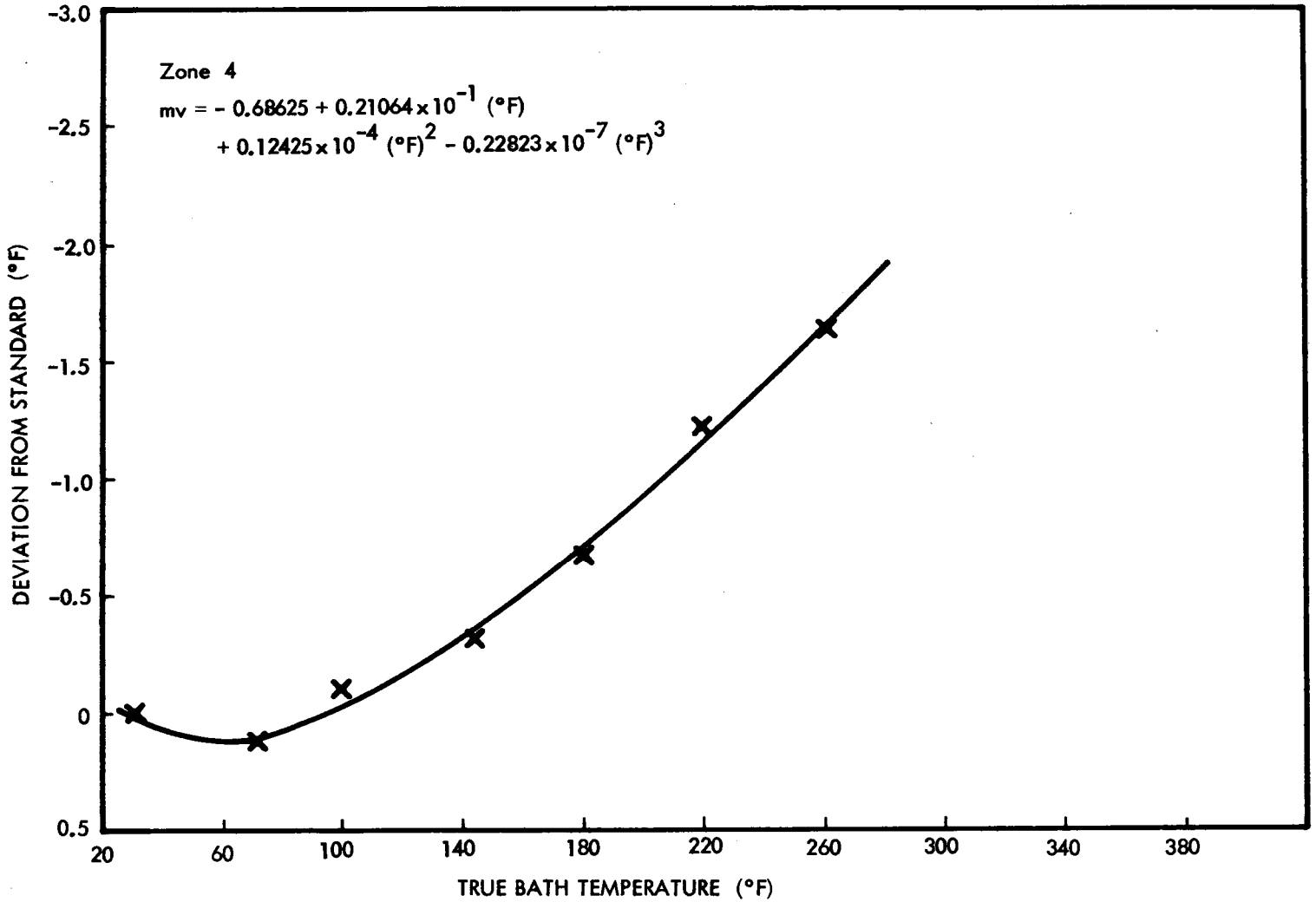
(b)

Figure C-11. (continued)



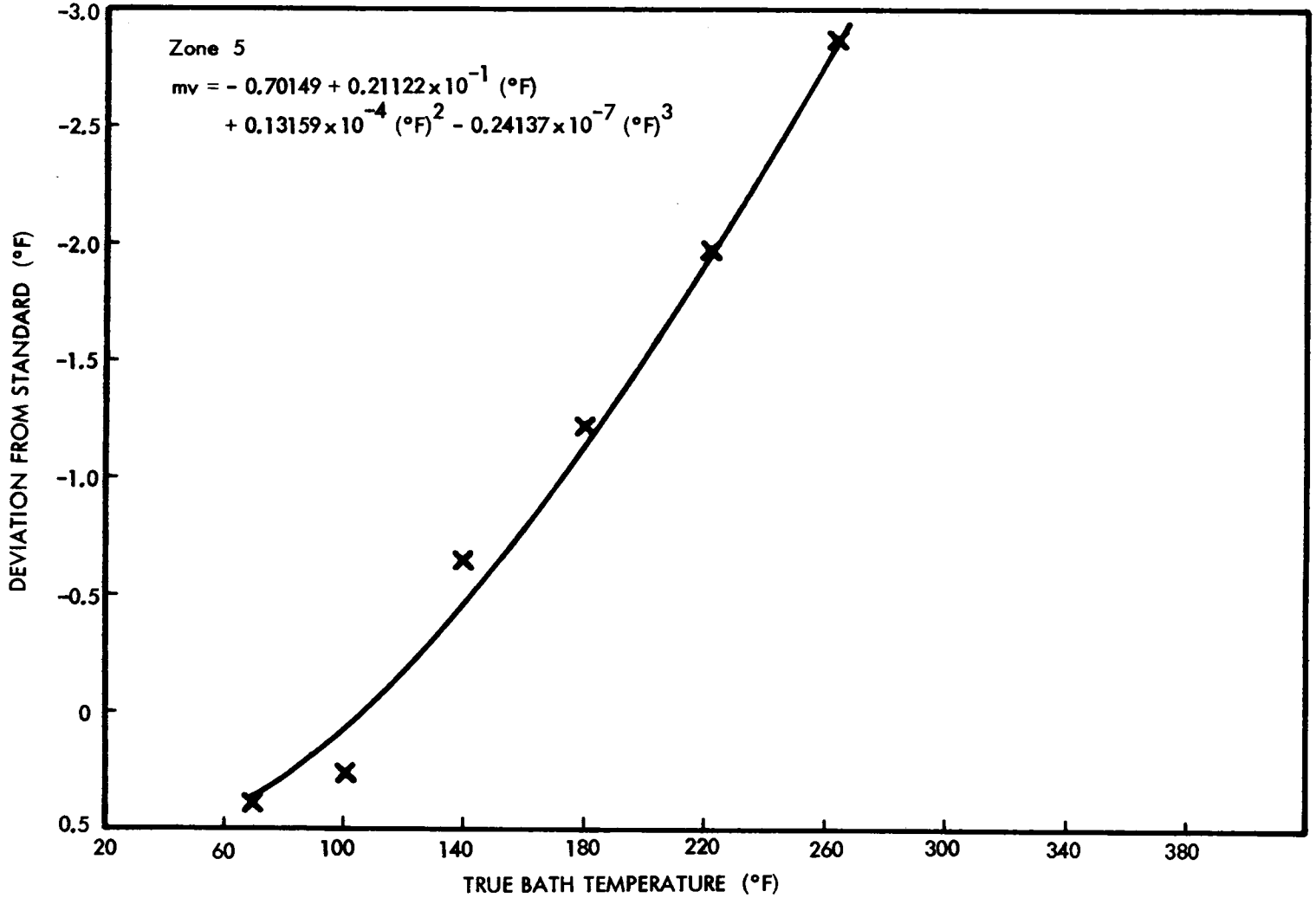
(c)

Figure C - 11. (continued)



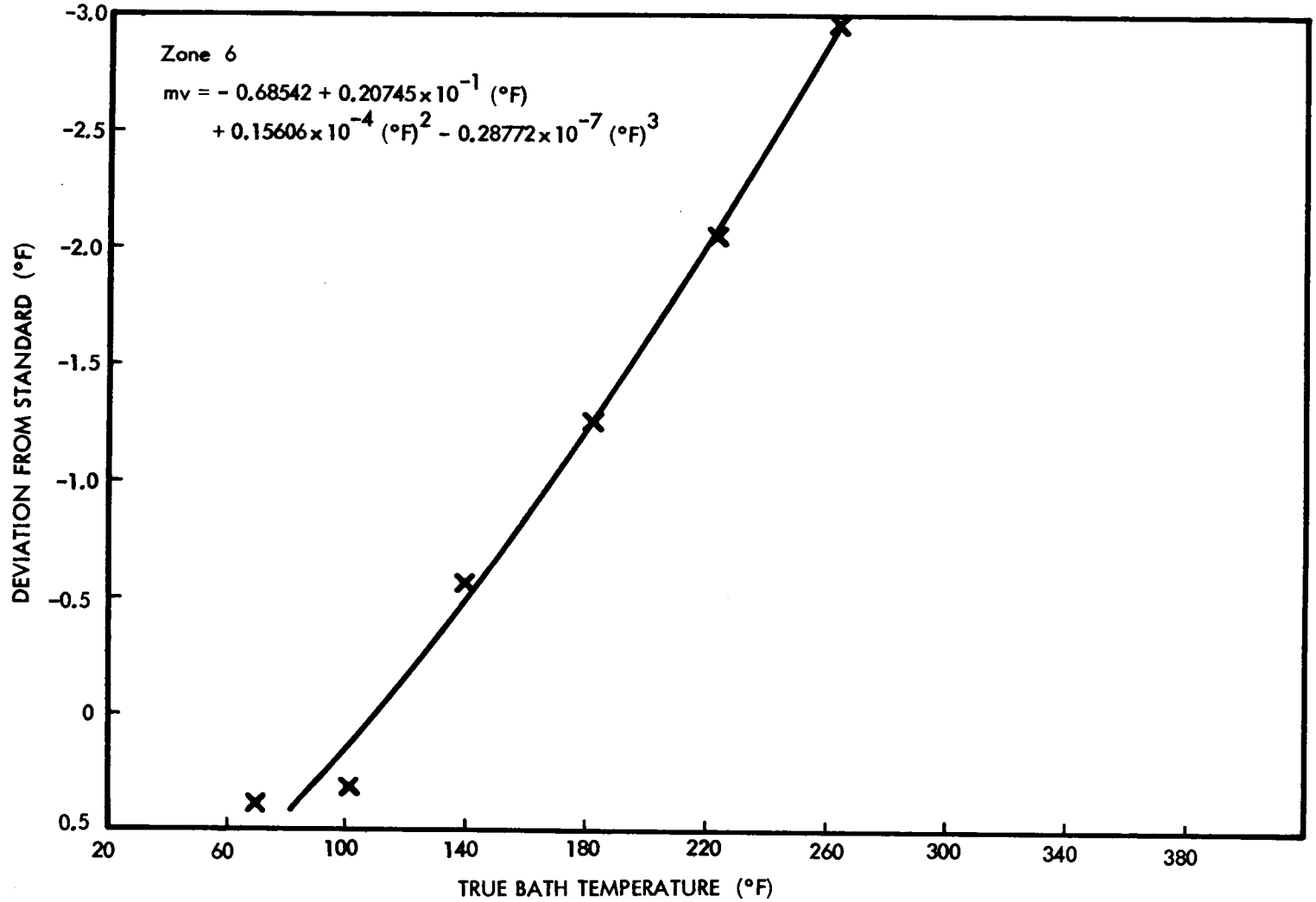
(d)

Figure C - 11. (continued)



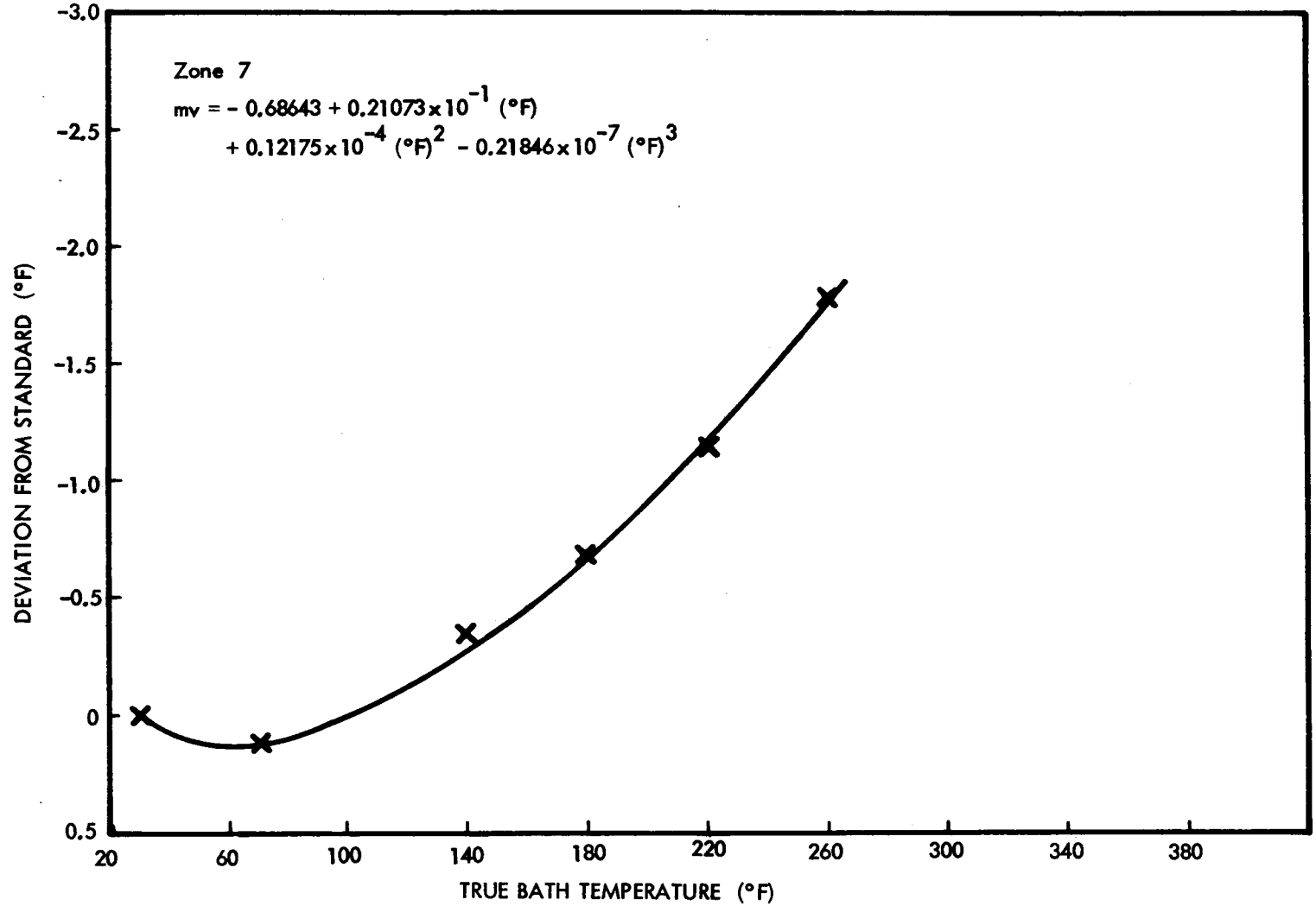
(e)

Figure C - 11. (continued)



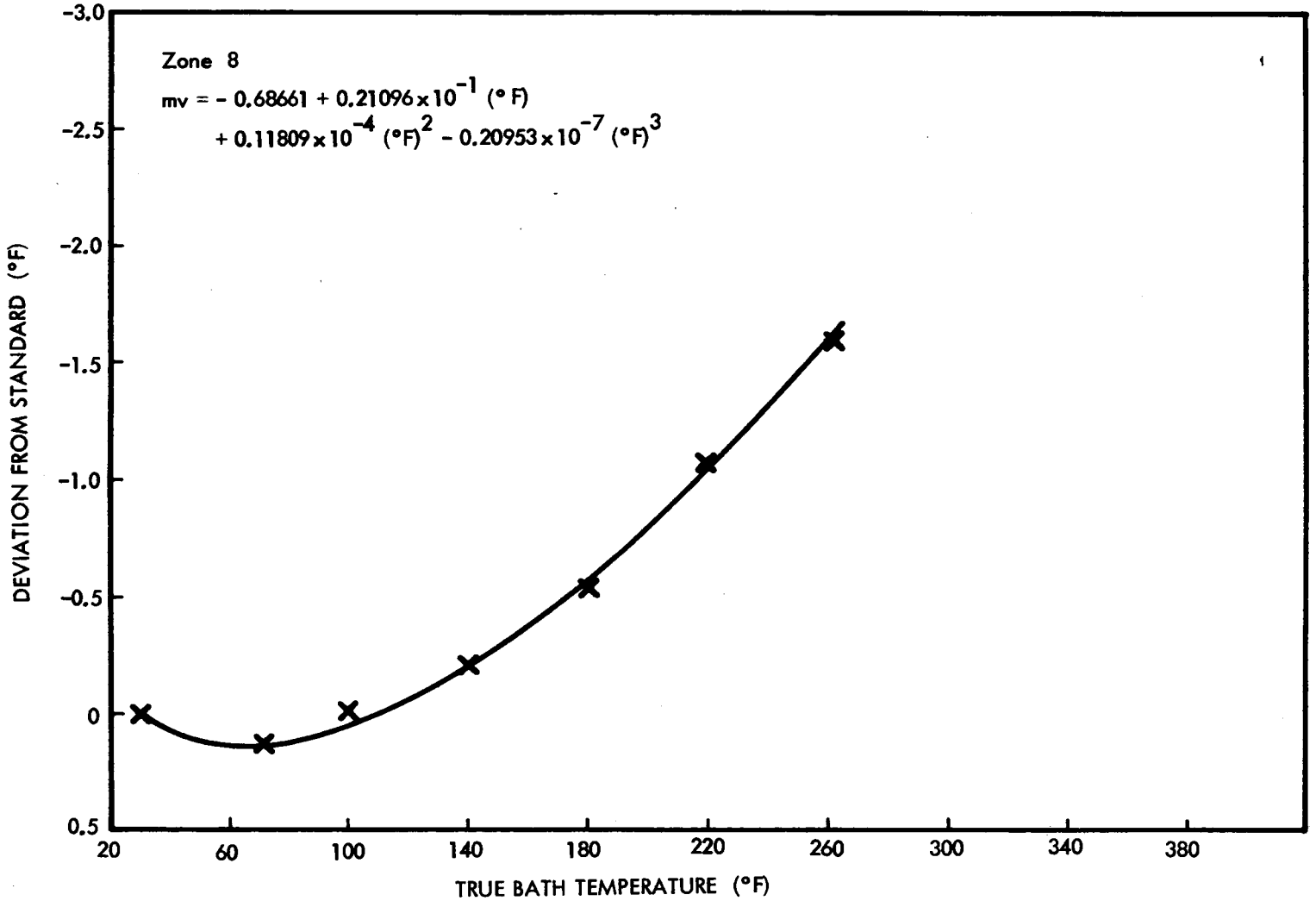
(f)

Figure C - 11. (continued)



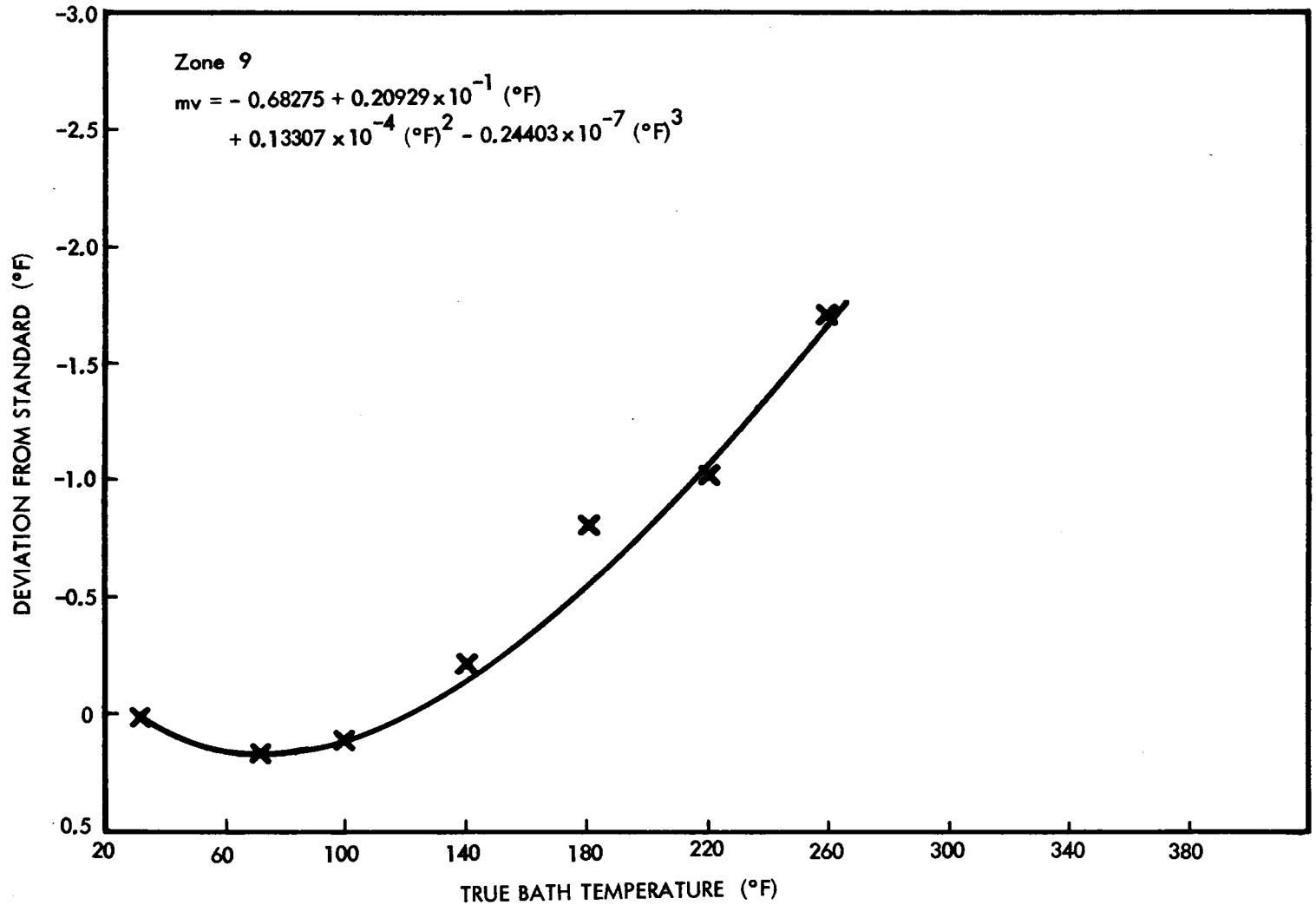
(g)

Figure C - 11. (continued)



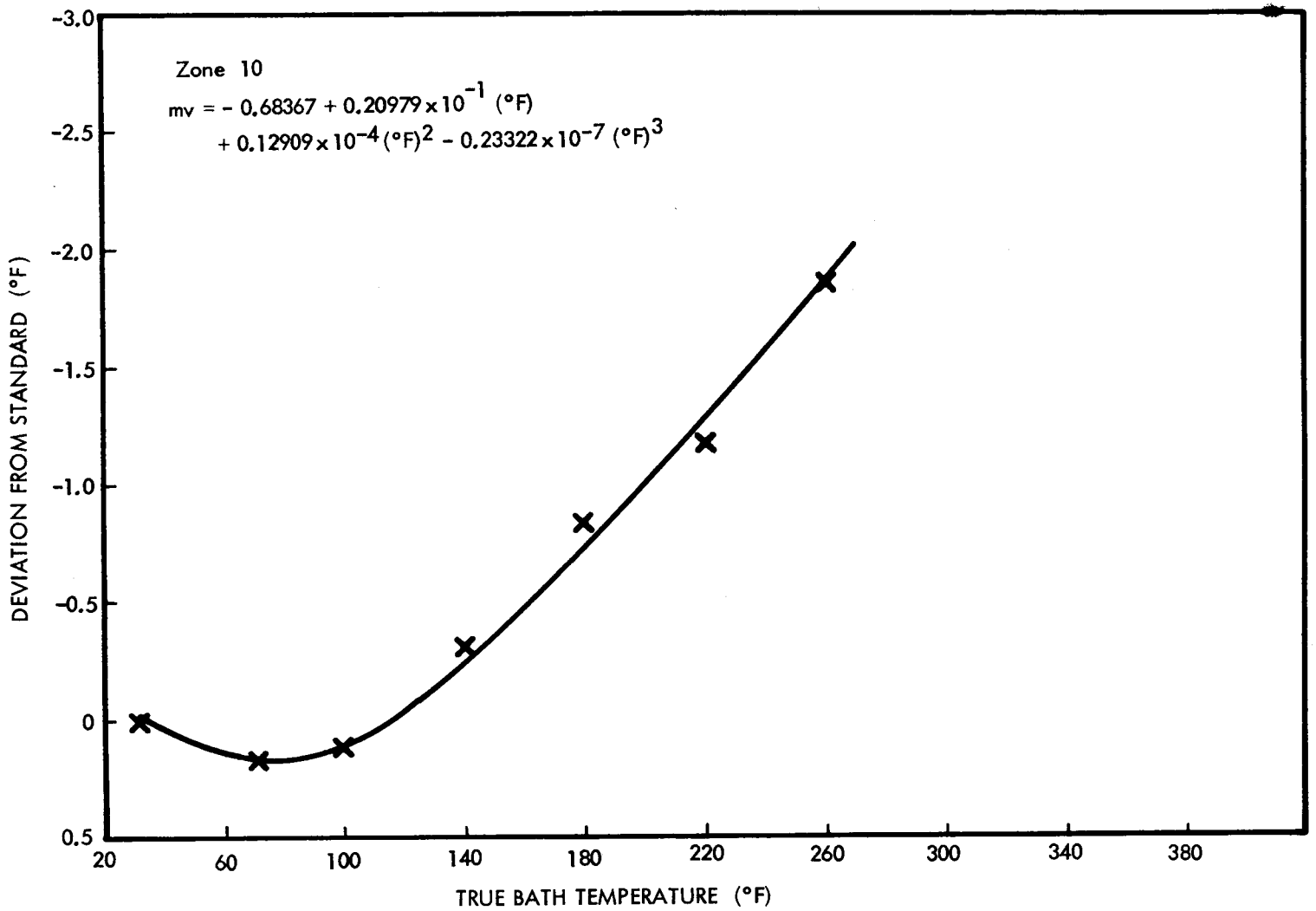
(h)

Figure C - 11. (continued)



(i)

Figure C - 11. (continued)

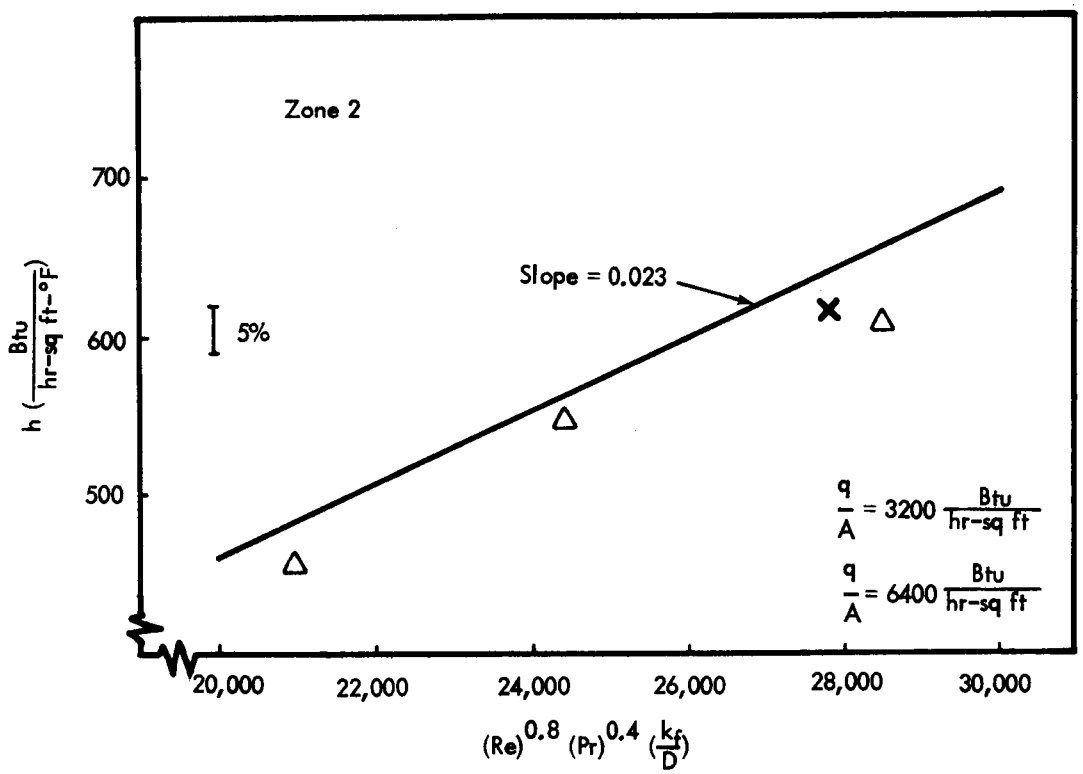


(j)

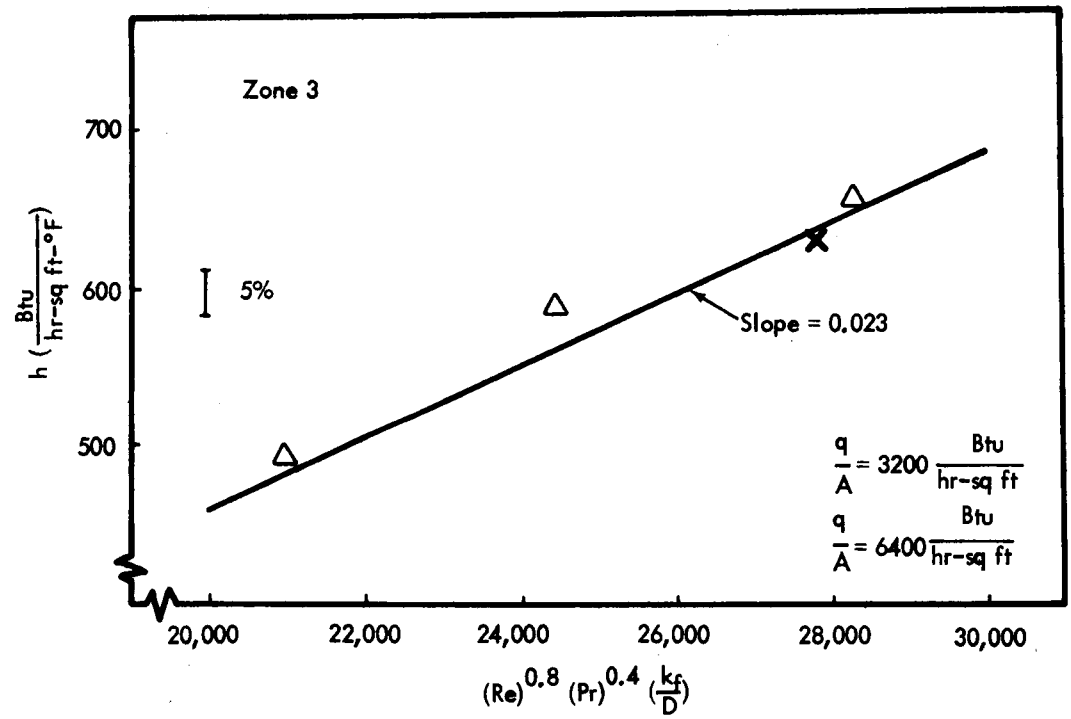
Figure C - 11. (continued)

Overall Calibration

Having calibrated the turbine meters, rotameters, and system thermocouples, as well as having measured the heat loss through the insulation, one additional in-place calibration needs to be performed to check the overall accuracy of the system. One basic measurement of importance in the heat transfer coefficient is the wall-to-bulk temperature difference. While both wall and in-stream thermocouples were calibrated, an additional test needs to be performed to make sure that the wall thermocouples are properly attached to the wall and are measuring the wall temperature accurately. The simplest way to do this is to pump single-phase fluid through the heated test section and determine how closely the experimental heat transfer coefficients agree with those predicted by the Dittus-Boelter equation. This was done for all 10 zones, and the results are shown in Figure C-12. Quite a bit of difficulty was encountered in trying to keep the R-114 in the system in the single-phase mode. In almost all the runs, some bubbles were seen in the flow visualization section at the tube exit and this is believed to account for the abnormally high experimental heat transfer coefficients in Zones 9 and 10. During the boiling tests, the heat transfer coefficients obtained from Zones 9 and 10 were similar to those obtained from the other zones. The results from Zone 6 are not given since they were not satisfactory because of the difficulty encountered in reattaching those thermocouples with the 30% tin - 70% lead solder. This was due to the relative inaccessability of that portion of the test section.

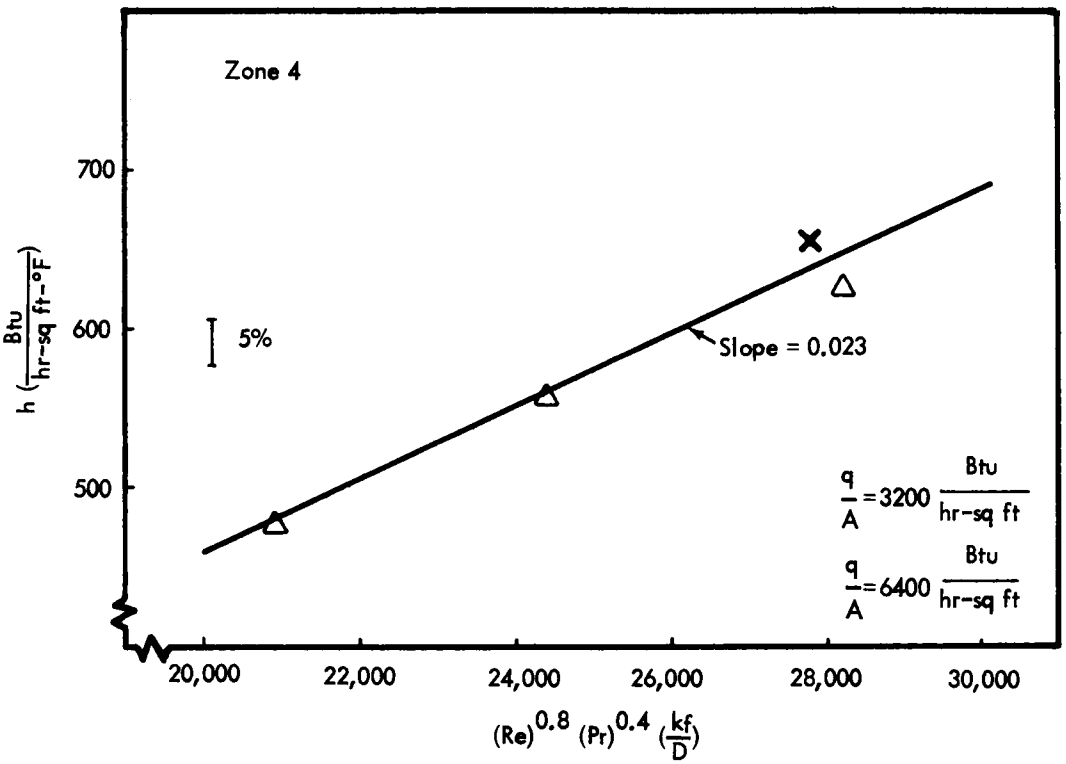


(a)

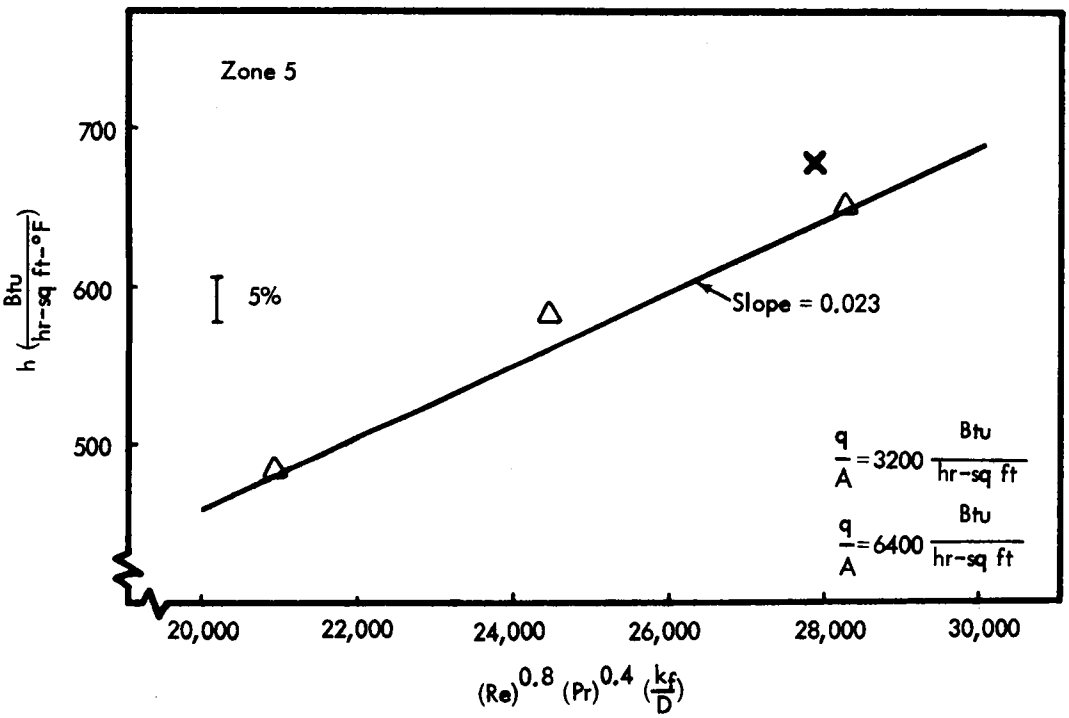


(b)

Figure C-12. OVERALL CALIBRATION OF INSTRUMENTATION.

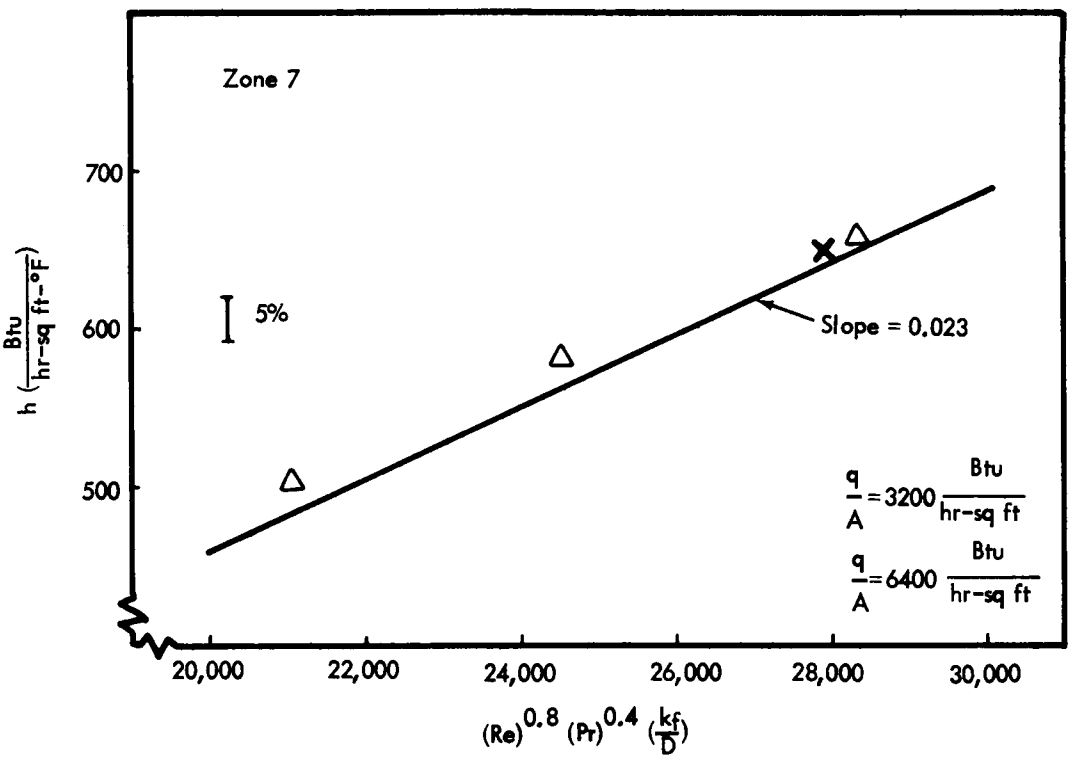


(c)

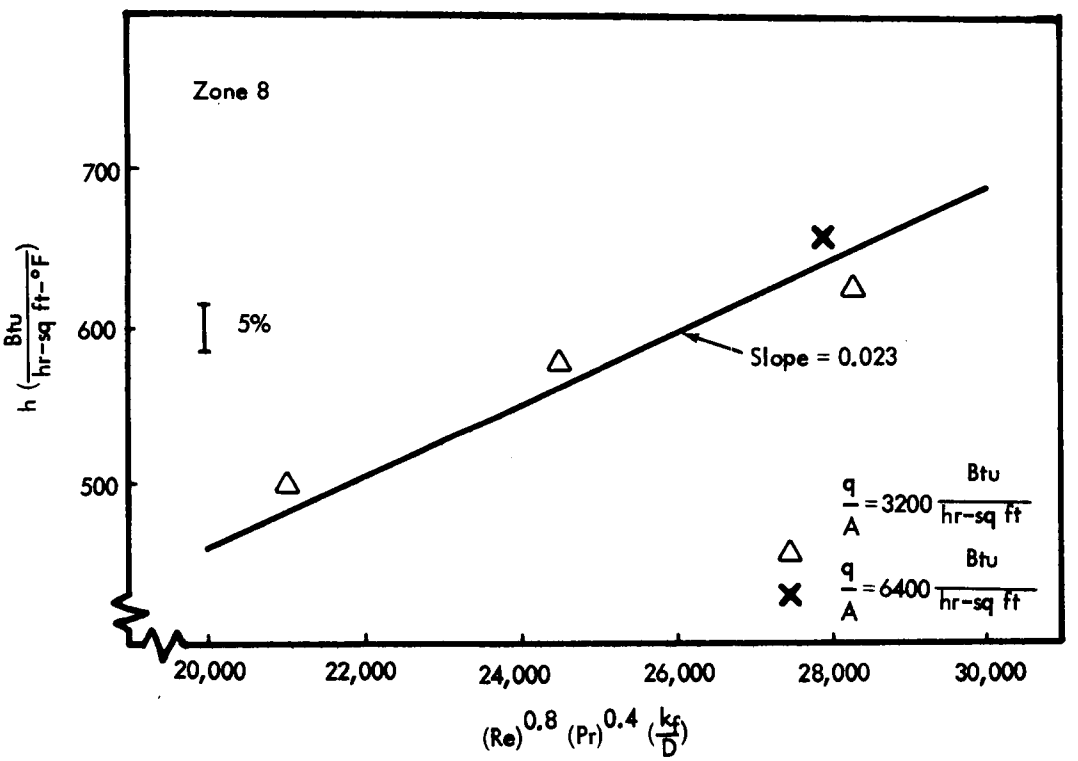


(d)

Figure C - 12. (continued)

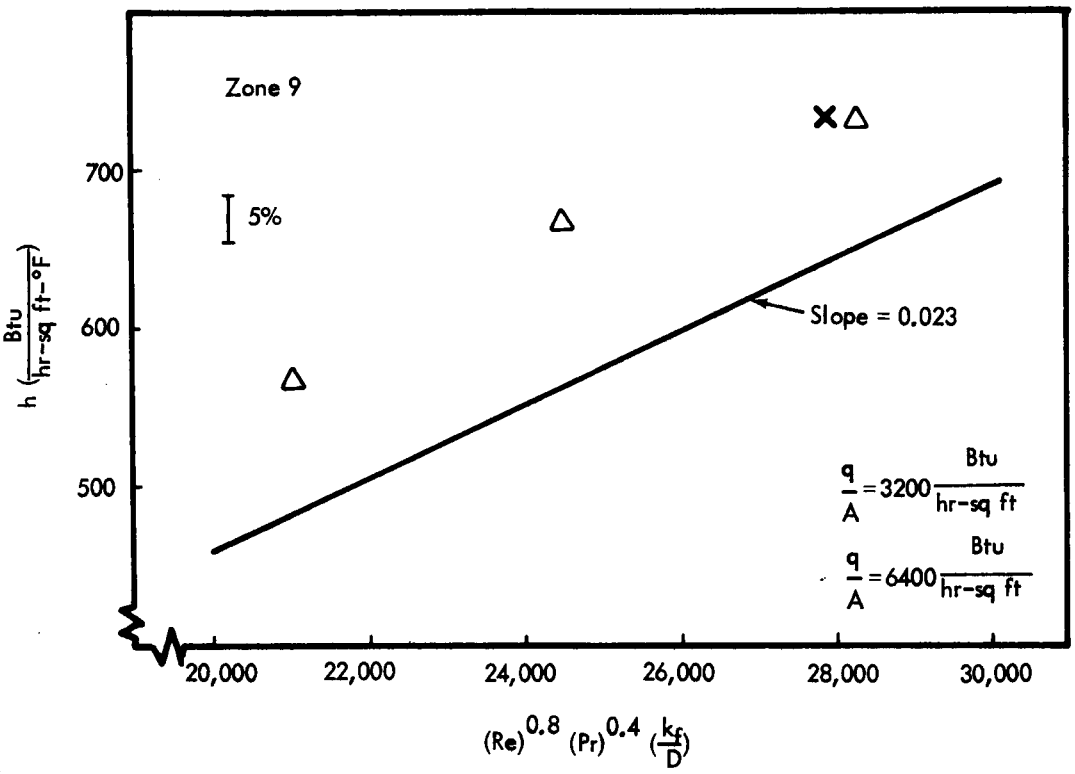


(e)

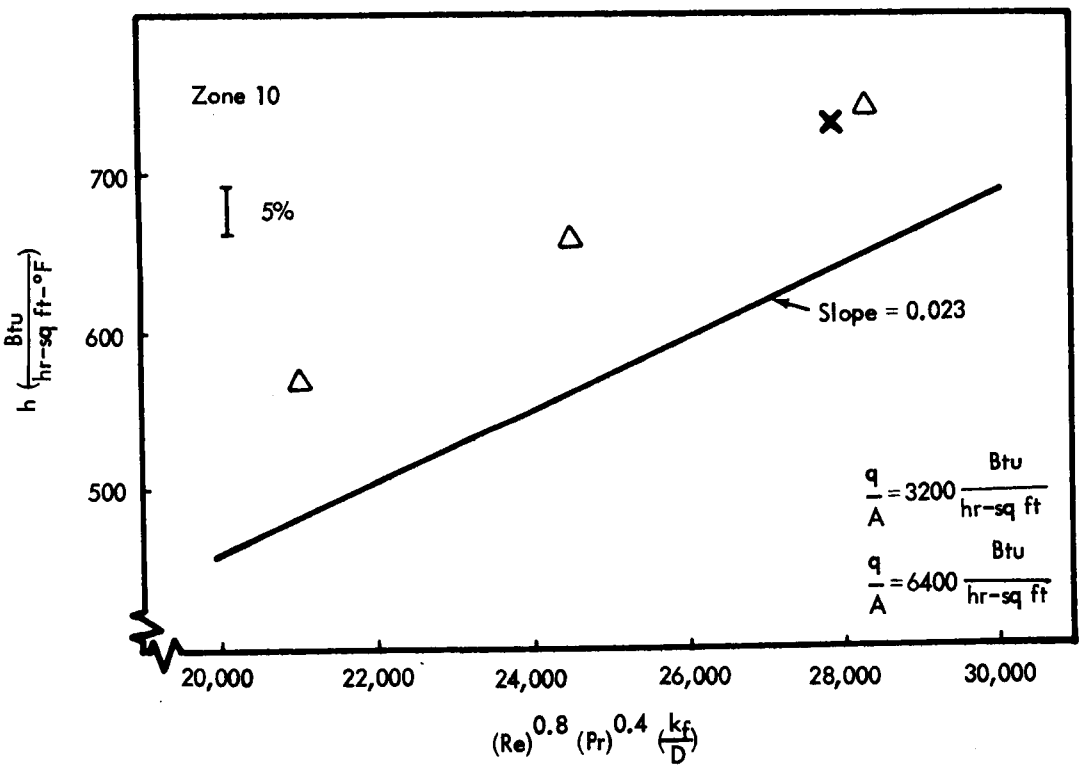


(f)

Figure C - 12. (continued)



(g)



(h)

Figure C - 12. (continued)

APPENDIX D

SAMPLE CALCULATIONS

The purpose of the sample calculations presented here is twofold:

1. To illustrate how the data obtained from the boiling facility were reduced and correlated.

2. To assist the design engineer in correctly using the correlation discussed in this study.

Flow Regimes - Application of Quandt [7] Analysis

The application of the Quandt [7] analysis is quite straightforward and is explained satisfactorily in the original publication. The only deviation made here involved the calculation of the two-phase friction factor, f_{TP}. While Quandt [7] assumed a value of 0.02, a more refined approach was attempted here. In Appendix C, it was shown that the experimentally determined single-phase friction factor was:

$$f = 0.2696\ (Re)^{-0.2349} \qquad (C\text{-}1)$$

For the two-phase case, one method of determining f_{TP} is to use the two-phase Reynolds number in Equation (C-1) and the McAdams formulation for the two-phase viscosity as given in Equation (2-66). Thus, for a 0.785-in.-diameter tube, with R-114 at 100°F, a quality of 0.05 and a mass flux, G, of 0.1 x 10^6 lbm/hr-sq ft, one obtains:

$$f_{TP} = 0.2696\ (GD)^{-0.2349} \left[\frac{x}{\mu_g} + \frac{(1 - x)}{\mu_f}\right]^{-0.2349}$$

$$f_{TP} = 0.2696\ (0.12697)(0.76982) = 0.02635$$

At the same conditions as above, but a mass flux, G, of 1.0 x 10^6 lbm/hr-sq ft:

$$f_{TP} = 0.01534$$

Thus, it can be seen that f_{TP} varies with the mass flux (and quality), but is still of the same magnitude as the 0.02 value assumed by Quandt [7].

Data Reduction - Pressure Drop

A sample calcuation of the pressure drop data reduction will be shown for Run 17.

1. R-114 Flowmeter Readouts, gpm

Inlet (FE 105B)	1.010 at 78°F
Liquid from entrainment separators (FE 119B)	0.430 at 97°F
Condensed vapor (FE 123A)	0.904 at 80°F

2. Water Flow to Condenser:

(FE 126) 59.0 units

$T_{H_2O\ in} = 47°F$; $T_{H_2O\ out} = 74°F$

3. Gross Heat Input to Test Section, watts

Zone 1	1072.08
Zone 2	1040.40
Zone 3	1060.20
Zone 4	1033.92
Zone 5	1058.40
Zone 6	1056.60
Zone 7	1054.44
Zone 8	1045.44
Zone 9	1051.92
Zone 10	1060.56

4. Heater Sheath Temperatures, °F:

Zone 1	150
Zone 2	190
Zone 3	190
Zone 4	205
Zone 5	195
Zone 6	165
Zone 7	205
Zone 8	205
Zone 9	215
Zone 10	270

5. Pressure Tap Line Thermocouple Readings:

T.C. 1	1.046 mv; 79.3°F
T.C. 2	1.047 mv; 79.4°F
T.C. 3	1.042 mv; 79.3°F

6. In-Stream Thermocouple Readings, mv:

Zone 1	1.495
Zone 2	1.520
Zone 3	1.516
Zone 4	1.501
Zone 5	1.498
Zone 6	1.496
Zone 7	1.492
Zone 8	1.482
Zone 9	1.473
Zone 10	1.470

7. Receiver Gage Readings for Pressure Drop Across DP Cell:

First 2.00 ft	60.0
First 4.02 ft	51.0
First 6.06 ft	42.5
First 7.99 ft	35.0
Total 9.84 ft	27.5

Reducing the results given in the seven sections above:

8. R-114 Flow Rates:

at 78°F, ρ_f = 90.79 lbm/cu ft

at 80°F, ρ_f = 90.6 lbm/cu ft

at 97°F, ρ_f = 88.7 lbm/cu ft

For FE 105B, the true flow rate (from Figure C-3 on page 452) is 1.12 gpm. The mass flow is therefore:

$$(1.12)(0.1337)(90.79)(60) = 815.7 \text{ lbm/hr}$$

For FE 119B, the true flow rate (Equation C-5 on page 454) is:

$$0.35813\left(\frac{499.66}{88.7} - 1\right)^{0.5}(0.430) = 0.331 \text{ gpm.}$$

The mass flow is therefore:

$$(0.331)(0.1337)(88.7)(60) = 235.9 \text{ lbm/hr}$$

For FE 123A, the true flow rate (from Figure C-6 on page 455) is 0.872 gpm. The mass flow is therefore:

$$(0.872)(0.1337)(90.6)(60) = 633.4 \text{ lbm/hr}$$

9. Water Flow Rate to Condenser:

For FE 126, the mass flow rate (from Figure C-9 on page 459) is:

$$(2.736)(0.1337)(62.4)(60) = 1369 \text{ lbm/hr}$$

10. Net Heat Input to Test Section:

Gross heat input is 1072.08 watts for Zone 1. With a sheath temperature of 150°F, the heat loss (from Figure C-10 on page 461) is:

Heat Loss (watts) = $0.94306 + 0.3387 \times 10^{-5} (150)^3$

= 12.374 watts

Net heat input is 1059.7 watts

The inside heat transfer is πDL, or

$$\pi \left(\frac{0.785}{12}\right)(1) = 0.20551 \text{ sq ft}$$

The heat flux in Zone 1 is:

$$(1059.7)(3.4129)\left(\frac{1}{0.2055}\right) = 17{,}599 \text{ Btu/hr-sq ft}$$

For all ten zones, the net heat flux is, Btu/hr-sq ft:

Zone 1	17,599
Zone 2	16,963
Zone 3	17,393
Zone 4	16,930
Zone 5	17,401
Zone 6	17,402
Zone 7	17,303
Zone 8	17,005
Zone 9	17,109
Zone 10	16,600

11. In-Stream Temperature Readings:

In Zone 1 (from Figure C-11 on page 472)

$$mv = -0.68567 + 0.21045 \times 10^{-1} (°F) + 0.12501 \times 10^{-4} (°F)^2 - 0.22621 \times 10^{-7} (°F)^3$$

By an iterative technique, for a reading of 1.495 mv, a temperature of 98.85°F is obtained. Using a similar procedure for the other nine zones, the temperatures obtained in °F are:

Zone 1	98.85
Zone 2	99.99
Zone 3	99.76
Zone 4	99.10
Zone 5	99.12
Zone 6	99.11
Zone 7	98.74
Zone 8	98.33
Zone 9	97.99
Zone 10	97.81

12. Pressure Drop:

In the first 2.0 ft, the receiver gage reading was 60.0. From Figure C-2 on page 451, the true pressure drop across the DP cell is:

$$2.59735 (60.0) - 174.8019 = -18.961 \text{ in. of water}$$

By looking at Figure III-8 on page 112, it can be seen that the pressure drop across the DP cell is not the same as the pressure drop along the first 2.0 ft of the test section. The pressure exerted by the 2.0 ft of liquid in the pressure tap lines needs to be subtracted out

The pressure tap thermocouples average out to 79.33°F where the liquid density is 90.6 lbm/cu ft. The liquid leg exerts a pressure of

$$\rho_f g\ L/g_c = (90.6)(32.174)(0.19224)$$

$$(2)/(32.174) = 34.845 \text{ in. water}$$

Therefore $\Delta P = 34.845 - 18.961 = 15.884$ in. water or 0.5740 lbf/sq in.

To find the pressure drop in the next 2.02 ft, one uses the above procedure to obtain the pressure drop in the first 4.02 ft and then subtracts out the pressure drop in the first 2.0 ft. The final results obtained in lbf/sq in. are:

First 2.00 ft	0.5740
Second 2.02 ft	0.4276
Third 2.04 ft	0.4876
Fourth 1.93 ft	0.5093
Fifth 1.85 ft	0.4634

13. Heat and Mass Balances:

From the experimental results, the following heat balances are obtained:

Heat in:

From preheater: (815.74)(0.2456)(99-77) =

4407.96 Btu/hr

From test section: Sum of the net heat in =

35,286 Btu/hr

Total heat in = 39,694 Btu/hr

Heat out:

Water in condenser: $(1369)(1.032)(74-47) =$

$38,155$ Btu/hr

$$\text{Percent error} = \frac{39,694 - 38,155}{39,694} \times 100 = 3.877\%$$

The following mass balances were also obtained:

Flow in: 815.74 lbm/hr

Flow out = sum of flow from downcomer of entrainment separators and flow of condensed vapor =

$235.90 + 633.44 = 869.34$ lbm/hr

$$\text{Percent error} = \frac{869.34 - 815.74}{869.34} \times 100 = 6.166\%$$

14. Qualities:

From the flow rate into the test section and the flow rate from the condenser, one obtains:

$$x_o = \frac{633.44}{815.74} = 0.7765$$

From the flow rate into the test section and the flow rate from the downcomer of the entrainment separators:

$$x_o = 1 - \frac{235.90}{815.74} = 0.7108$$

From the flow rate to the condenser and the flow from the downcomer of the entrainment separators:

$$x_o = \frac{633.44}{633.44 + 235.90} = 0.7286$$

The average of the above three qualities is 0.7387.

Now, there is another way of determining the exit quality without depending on the accuracy of the mass flow

measurements. Shown in Figure D-1, are the in-stream temperatures measured. As can be seen, a "break" occurs in the profile approximately 60% of the way through Zone 1. This break signifies that the quality at this point is zero. From this information, the quality at any point downstream can be calculated from the equation:

$$x = \frac{4L}{D} \frac{(q/A)}{Gh_{fg}} \qquad (D\text{-}1)$$

Thus, the quality at the center of Zone 2 is:

$$x = \frac{4(0.90)}{\left(\frac{0.785}{12}\right)} \frac{[0.4(17{,}599) + 0.5(16{,}963)]}{\left(\frac{815.74}{0.785\ D^2}\right)(52.9)} = 0.0665$$

This calculation can be performed for all zones. For the test section exit, this yields 0.7700 which is quite close

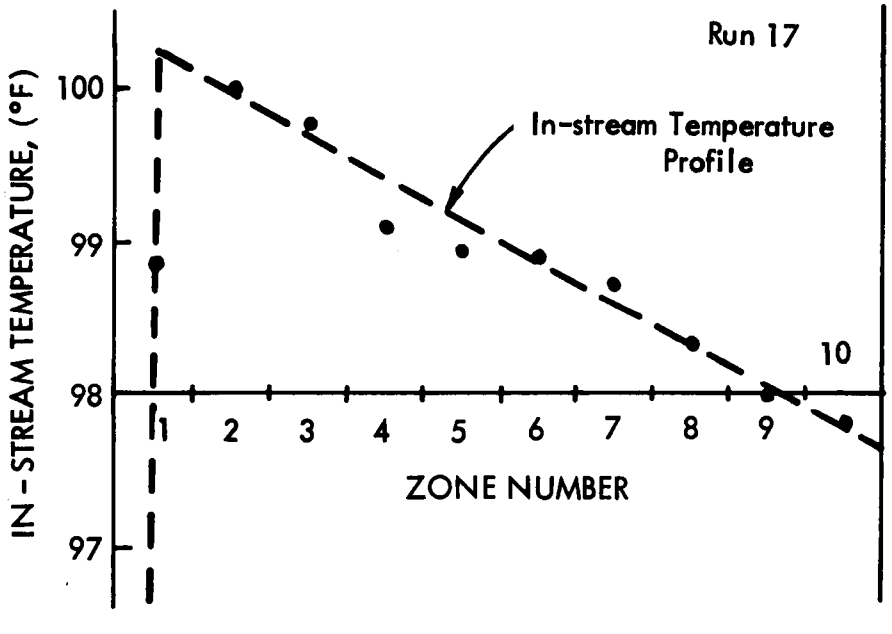


Figure D - 1. IN - STREAM TEMPERATURE PROFILE FOR RUN 17.

to the average exit quality based on the mass flow measurement which is 0.7387. The difference can be attributed to experimental error. In all the calculations done in this study, the temperature profile based on the in-stream thermocouple readings was always used to determine the quality at any point.

Data Analysis - Pressure Drop

Looking now in great detail at the third section which is 2.042 ft long, for Run 17, the following information is known:

$$T = 99.1°F$$

$$P = 43.46 \text{ psia}$$

$$x_i = 0.2774$$

$$x_o = 0.4428$$

$$G = 0.2427 \times 10^6 \text{ lbm/hr-sq ft}$$

$$L = 2.042 \text{ ft}$$

$$\Delta P = 0.4876 \text{ psi.}$$

It should be remembered that the data reduction was done on a computer and the 2.042-ft length was divided into 24 increments. As this is very tedious to do by hand for the sample calculation, the section will be considered as one increment. The answers obtained will then be compared to those calculated by the computer.

1. Homogeneous [3] Model. In the Homogeneous [3] model, the liquid and vapor phases are assumed to flow at the same velocity. The pressure drop equations are given in Collier and Wallis' [3] Notes or by Equation (2-34) of the more recent book by Collier [135].

$$-\frac{dp}{dz} = \frac{\dfrac{2f'_{TP}G^2v_f}{D}\left[1 + x\left(\dfrac{v_{fg}}{v_f}\right)\right] + G^2v_f\left(\dfrac{v_{fg}}{v_f}\right)\dfrac{dx}{dz} + \dfrac{g\cos\theta}{v_f\left[1 + x\left(\dfrac{v_{fg}}{v_f}\right)\right]}}{1 + G^2x\left(\dfrac{dv_g}{dp}\right)} \qquad \text{(D-2)}$$

Assuming no flashing exists, the denominator is equal to one. The three components in the numerator of Equation (D-2) are the frictional, acceleration, and gravitational components. Thus

$$-\left(\frac{dp}{dz}\right)_{acc} = G^2v_{fg}\frac{dx}{dz} \qquad \text{(D-3)}$$

and

$$-\left(\frac{dp}{dz}\right)_{grav} = \frac{g\cos\theta}{v_f\left[1 + x\left(\dfrac{v_{fg}}{v_f}\right)\right]} \qquad \text{(D-4)}$$

From Equation (D-3):

$$-\Delta P \approx G^2v_{fg}\,\Delta x = (0.2427 \times 10^6)(0.69551)(0.1654)\left(\frac{1}{32.174}\right)\left(\frac{1}{(3600)^2}\right)$$

$$= 16.2503 \text{ lbf/sq ft}$$

The computer program gave an answer of 16.826 lbf/sq ft.

From Equation (D-4):

$$-\Delta p \approx \frac{g\cos\theta\,\Delta z}{v_f\left[1 + x\left(\dfrac{v_{fg}}{v_f}\right)\right]} = \frac{(32.174)(1)(2.042 \text{ ft})}{0.0113\left[1 + 0.3601\left(\dfrac{0.6955}{0.0113}\right)\right](32.174)}$$

$$= 7.8014 \text{ lbf/sq ft}$$

The computer gave an answer of 7.649 lbf/sq ft.

Using the computer values, the sum of the acceleration and gravitational terms is 24.475 lbf/sq ft or 0.16997 lbf/sq in. Since the measured total pressure drop was 0.4876 lbf/sq in.,

$$-\Delta p_{TPF} = 0.3176 \text{ lbf/sq in.} \qquad \text{(D-5)}$$

The single-phase pressure drop is:

$$-\Delta p_{\text{single phase}} = f' \left(\frac{4L}{D}\right)\left(\frac{G^2}{2\rho_f}\right) \qquad \text{(D-6)}$$

From Equation (C-1), Appendix C, the Fanning friction factor was experimentally determined. Thus:

$$f' = 0.0674 \left[\frac{(0.2427 \times 10^6)\left(\frac{0.785}{12}\right)}{0.71648}\right]^{-0.2349}$$

$$= 0.006425$$

$$-\Delta p_{\text{single phase}} = (0.006425)\left[\frac{4(2.042)(12)}{0.785}\right]\left[\frac{(0.2427 \times 10^6)^2}{(2)(88.516)}\right]$$

$$\left(\frac{1}{32.174}\right)\left(\frac{1}{3600}\right)^2 = 0.6401 \text{ lbf/sq ft}$$

$$= 0.004445 \text{ lbf/sq in.}$$

$$\Phi_{fo}^2 = \frac{\left(\frac{dp}{dz}\right)_{TPF}}{\left(\frac{dp}{dz}\right)_{fo}} = \frac{0.3176}{0.00445} = 71.4438$$

$$\Phi_{fo} = 8.4524$$

$$\Phi_{ftt} = \frac{\Phi_{fo}}{(1 - x)^{0.9}} = \frac{8.4524}{(1 - 0.3601)^{0.9}} = 12.6322$$

The computer gave an answer of 12.611.

2. Martinelli-Nelson [4] Model. In the Martinelli-Nelson [4] model, the two phases are assumed to be separate. The pressure drop is most clearly defined by Equation (2-46) of Collier's [135] book:

$$-\left(\frac{dp}{dz}\right) = -\left(\frac{dp}{dz}\right)_{TPF} + G^2 \frac{d}{dz}\left[\frac{x^2 v_g}{\alpha} + \frac{(1 - x)^2 v_f}{(1 - \alpha)}\right]$$

$$+ g \cos \theta \left[\alpha\rho_g + (1 - \alpha)\ \rho_f\right] \qquad \text{(D-7)}$$

This can be rewritten as:

$$- \left(\frac{\Delta P}{L}\right) \simeq -\left(\frac{\Delta P}{L}\right)_{TPF} + \frac{G2}{L} \left\{ \left[\frac{x^2 v_g}{\alpha} + \frac{(1 - x)^2\ v_f}{(1 - \alpha)}\right]_{\substack{\text{end of} \\ \text{section}}} \right.$$

$$\left. - \left[\frac{x^2 v_g}{\alpha} + \frac{(1 - x)^2\ v_f}{(1 - \alpha)}\right]_{\substack{\text{start of} \\ \text{section}}} \right\}$$

$$+ g \cos \theta \left[\alpha\rho_g + (1 - \alpha)\ \rho_f\right] \qquad \text{(D-8)}$$

The three terms are the frictional, acceleration, and gravitational terms, respectively. For this sample calculation, the Zuber et al [10] modified void fraction correlation will be used. Here:

$$\alpha = \langle\alpha\rangle = \frac{x}{C_o \left(\frac{\Delta\rho}{\rho_f}\right) x + \left[C_o + \bar{V}_{gj}/V_{fo}\right](\rho_g/\rho_f)} \qquad \text{(2-32)}$$

where

$$C_o \simeq 1.13 \qquad \text{(2-42)}$$

$$\bar{V}_{gj} = 1.41 \left[\frac{\sigma g\ \Delta\rho}{\rho_f^2}\right]^{1/4} \qquad \text{(2-43)}$$

for $x \leq 0.40$. For $x > 0.40$, a linear relationship is assumed between $x = 0.40$ and $x = 1.0$. For this case, $x_{avg} = 0.3601$.

Thus

$$\bar{V}_{gj} = 1.41 \left[\frac{(0.00078388)(87.101)(32.174)^2}{(88.516)^2}\right]^{1/4}$$

$$= 0.43454 \text{ ft/sec}$$

$$V_{fo} = G/\rho_f = \frac{0.2427 \times 10^6}{88.516} = 2741.877 \text{ ft/hr}$$

$$= 0.7616325 \text{ ft/sec}$$

$$\alpha = \frac{0.3601}{1.13\left(\frac{87.101}{88.516}\right)(0.3601) + \left[1.13 + \frac{0.43454}{0.76163}\right]\left(\frac{1.4149}{88.516}\right)}$$

$$= 0.84216$$

Using this value of α, the gravitational term is:

$$-\left(\frac{dp}{dz}\right)_{grav} = \frac{32.174(1)}{32.174}\left[(0.84216)(1.4149) + (0.15784)(88.516)\right]$$

$$= 15.1629$$

$$-\Delta p = (15.1629)(2.042) = 30.9626 \text{ lbf/sq ft}$$

The computer code gave an answer of 30.6971 lbf/sq ft.

To determine the acceleration term:

The void fraction at the entrance is 0.82650.

The void fraction at the exit is 0.85841.

Thus the acceleration term is:

$$-\Delta p = \frac{(0.2427 \times 10^6)^2}{(32.174)(3600)^2}\left\{\left[\frac{(0.4428)^2\,(0.7068)}{(0.85841)} + \frac{(0.5572)^2\,(0.011297)}{(0.14159)}\right]\right.$$

$$\left. - \left[\frac{(0.2774)^2\,(0.7068)}{(0.8265)} + \frac{(0.7226)^2\,(0.011297)}{(0.1735)}\right]\right\} = 12.2064 \text{ lbf/sq ft}$$

The computer code gave an answer of 12.7679 lbf/sq ft.

Using the computer values, the sum of the acceleration and gravitational terms is 43.4650 lbf/sq ft or 0.3018 lbf/sq in. Since the measured total pressure drop was 0.4876 lbf/sq in.,

$$-\Delta p_{TPF} = 0.18576 \text{ lbf/sq in.}$$

Therefore

$$\Phi_{fo}^2 = \frac{0.18576}{0.00445} = 41.7438$$

$$\Phi_{fo} = 6.46094$$

$$\Phi_{ftt} = 9.65595$$

The computer code gave an answer of 9.644.

To determine the Martinelli Parameter:

$$X_{tt} = \left(\frac{1 - x}{x}\right)^{0.9} \left(\frac{\rho_g}{\rho_f}\right)^{0.5} \left(\frac{\mu_f}{\mu_g}\right)^{0.1}$$

$$= \left(\frac{1 - 0.3601}{0.3601}\right)^{0.9} \left(\frac{1.4149}{88.516}\right)^{0.5} \left(\frac{0.71648}{0.029164}\right)^{0.1}$$

$$= 0.292151$$

Therefore $\sqrt{X_{tt}} = 0.54051$.

Application of Pressure Drop Results to Design Calculations

The sample calculations above helped to illustrate how each of the experimentally determined pressure drop results was subdivided into its corresponding gravitational, acceleration, and frictional components. In the separated flow model, the Zuber et al [10] modified void fraction correlation was used. Any other void fraction correlation could have been substituted instead. In a design calculation, the reverse of the order used in the above sample calculation would be employed. If the desired flow conditions are known, the corresponding Φ_{ftt} term can be determined by any of the models discussed in Chapter IV (such as the Chisholm [28] 1973 correlation given by Equations (2-21) and (2-22), as well as Table II-1 on page 33). The gravitational and acceleration terms as illustrated in the above sample calculations can then be added to the frictional pressure drop term to determine the total pressure drop.

Data Reduction - Heat Transfer Coefficients

A sample calculation for the heat transfer coefficient data reduction will be shown for Run 454. The flow rate, heat flux, in-stream

temperatures and qualities are computed in identically the same way as illustrated above for the pressure drop run. For Zone 5, the following readings were obtained:

$$\text{Mass flow} = 402.095 \text{ lbm/hr}$$

$$G = 0.1196 \times 10^6 \text{ lbm/hr-sq ft}$$

$$(q/A)_{net} = 6595 \text{ Btu/hr-sq ft}$$

$$x_{avg} = 0.2724$$

$$T = 98.65°F$$

The readings of the four wall thermocouples in mv are:

TC 5-1	2.642
TC 5-2	2.667
TC 5-3	2.645
TC 5-4	2.651

By using Equation (C-8), Appendix C, the above mv readings can be converted to °F to yield:

TC 5-1	110.63
TC 5-2	111.35
TC 5-3	110.71
TC 5-4	110.89

The average is 110.90°F. Thus, the average wall to bulk temperature difference is

$$110.90 - 98.65 = 12.25°F$$

The heat transfer coefficient is:

$$h_{exp} = \frac{q/A}{\Delta T} = \frac{6595}{12.25} = 538.4 \text{ Btu/hr-sq ft-°F}$$

For all the other zones, the same technique applies.

Data Analysis - Heat Transfer Coefficients

Only for the modified Chen [80] correlation will a sample calculation be presented. The other correlations discussed in Chapter IV are presented in sufficient detail in the original publication and the designer is referred there. For Run 454, Zone 5, the following information is known:

$$T = 98.65°F$$

$$P = 45.0 \text{ lbf/sq in.}$$

$$T_{wall} = 110.90°F$$

$$(q/A) = 6595 \text{ Btu/hr-sq ft}$$

$$x_{avg} = 0.2724$$

$$G = 0.1196 \times 10^6 \text{ lbm/hr-sq ft}$$

$$h_{exp} = 538.4 \text{ Btu/hr-sq ft-°F}$$

Since $X_{tt} = 0.4194$ and $P_r = 0.09514$, $\Phi_{ftt} = 6.535$ from the Martinelli-Nelson [4] curves using the same reduced pressure for R-114 and water. Therefore,

$$F = (\Phi_{ftt})^{0.89} = 5.316$$

$$(Re)_{fa} = \frac{(1 - x)GD}{\mu_f} = \frac{(0.7276)(0.1196 \times 10^6)\left(\frac{0.785}{12}\right)}{(0.71648)} = 7945.26$$

Plugging into Equation (4-82):

$$S = -0.2074(0.09514)^{-0.0899} \ln \left|(7945.26)(5.316)^{1.25}\right|$$

$$+ 2.85568(0.09514)^{-0.06203} = 0.4680$$

The pressure difference, Δp, corresponding to a ΔT of 12.25°F is 9.618 lbf/sq in. Thus, plugging into Equation (4-83):

$$h_{TP} = 0.023(7945.3)^{0.8}\ (5.015)^{0.4} \left(\frac{0.035429}{(0.785/12)}\right) (5.316)$$

$$+ 0.3802 \left(\frac{(0.03543)^{0.79}\ (0.2486)^{0.45}\ (88.516)^{0.49}}{(53.008)^{0.24}\ (1.4149)^{0.24}\ (0.0007839)^{0.5}\ (0.71648)^{0.29}}\right)$$

$$(12.25)^{0.24} \left((9.618)(144)\right)^{0.75} (0.4680)$$

$$= 519.9 \text{ Btu/hr-sq ft-}^{\circ}\text{F}$$

Using instead, Equation (4-84)

$$h_{TP} = 166.41 + \left(\frac{(0.03543)^{5.1}(87.101)^{0.5}}{(0.0047)^{3}(0.24856)^{2.1}(0.71648)^{4.1}(0.0007839)^{0.5}(53.008)^{2}}\right)$$

$$(12.25)^2\ (0.4680) = 400.55 \text{ Btu/hr-sq ft-}^{\circ}\text{F}$$

Application of Heat Transfer Results to Design Calculations

In applying the modified Chen [80] correlation as represented by Equations (4-83) or (4-84), it can be seen that the boiling temperature, flow rates, and qualities need to be known. This information is usually available to the design engineer. However, it is also necessary to know the wall-to-bulk temperature difference. This quantity is seldom known although the heat flux usually is. Therefore, it is necessary to perform a trial-and-error solution. A wall-to-bulk temperature difference is assumed and the corresponding heat transfer coefficient is determined using Equations (4-83) or (4-84). This is compared to the heat transfer coefficient obtained from $h = (q/A)/\Delta T$. If the two values are different, a second choice of ΔT is made and the procedure is repeated until the same heat transfer coefficient values are obtained.

Data Reduction - Critical Heat Flux

For the critical heat flux runs the boiling temperature, flow rate, heat flux, and quality measurements were performed in identically the same manner as the pressure drop and heat transfer coefficient runs. To determine the point where the critical heat flux occurred, the wall temperatures which were measured at 6-in. intervals were closely observed. The point where the wall temperature began to increase sharply was taken as the point where critical heat flux occurred. The quality at that point, as well as the length from the point where the quality was zero were then determined. For Run CHF 7, the following information was obtained:

$$T = 99.53°F$$

$$G = 0.2400 \times 10^6 \text{ lbm/hr-sq ft}$$

$$x_{\text{at CHF}} = 0.7652$$

$$(q/A)_{\text{crit}} = 18{,}218 \text{ Btu/hr-sq ft}$$

$$L/D = 132.24$$

Data Analysis - Critical Heat Flux

Barnett and Wood [105] Scaling Law. At 100°F

$$\frac{\rho_f}{\rho_g} = 61.511$$

The same density ratio exists for water at 442°F.

Looking at the individual terms in Equation (2-80):

(a) $\dfrac{G\gamma^{1/2}}{\rho_f{}^{1/2}}$ term: $\gamma = -\dfrac{d\left(\dfrac{\rho_f}{\rho_g}\right)}{dp}$

for R-114:

at 98°F: $\frac{\rho_f}{\rho_g} = 63.6375$ $\quad p = 44.377$ lbf/sq in.

at 102°F: $\frac{\rho_f}{\rho_g} = 59.4639$ $\quad p = 47.362$ lbf/sq in.

$$\gamma = -\frac{(63.6375 - 59.4639)}{(44.377 - 47.362)} = 1.3982 \text{ sq in./lbf}$$

for water:

at 440°F: $\frac{\rho_f}{\rho_g} = 63.11068$ $\quad p = 381.59$ lbf/sq in.

at 444°F: $\frac{\rho_f}{\rho_g} = 60.36918$ $\quad p = 397.61$ lbf/sq in.

$$\gamma = -\frac{(63.11068 - 60.36918)}{(381.59 - 397.61)} = 0.17113 \text{ sq in./lbf}$$

$$\text{Thus } G_{\substack{\text{water}\\\text{equivalent}}} = \left(\frac{G\gamma^{1/2}}{\rho_f^{1/2}}\right)_{\text{R-114}} \left(\frac{\rho_f^{1/2}}{\gamma^{1/2}}\right)_{\text{water}}$$

$$= \left(\frac{(0.24 \times 10^6)(1.1825)}{9.4023}\right)\left(\frac{7.1947}{0.4137}\right)$$

$$= 0.5249 \times 10^6 \text{ lbm/hr-sq ft}$$

(b) $\frac{D\, c_{pf}\, \rho_f^{1/2}}{k_f\, \gamma^{1/2}}$ term:

$$D_{\substack{\text{water}\\\text{equivalent}}} = \left(\frac{D\, c_{pf}\, \rho_f^{1/2}}{k_f\, \gamma^{1/2}}\right)_{\text{R-114}} \left(\frac{k_f\, \gamma^{1/2}}{c_{pf}\, \rho_f^{1/2}}\right)_{\text{water}}$$

$$= \left(\frac{(0.785)(0.2489)(9.4023)}{(0.03535)(1.1825)}\right)\left(\frac{(0.3702)(0.4137)}{(1.1201)(7.1947)}\right)$$

$$= 0.8351 \text{ in.}$$

(c) L/D term:

$$L_{\substack{\text{water}\\\text{equivalent}}} = (132.24)(0.8351) = 110.43 \text{ in.}$$

Thus, for the water equivalent tube based on the Barnett and Wood [105] scaling law:

$$T = 442°F$$

$$G = 0.5249 \times 10^6 \text{ lbm/hr-sq ft}$$

$$L = 110.43 \text{ in.}$$

$$D = 0.8351 \text{ in.}$$

To find the critical heat flux corresponding to this set of conditions, either the Macbeth [101], Biasi et al [112] or any other critical heat flux correlation applicable to water can be used. For the above set of conditions the Macbeth [101] high velocity region correlation is applicable. Thus, for no subcooling,

$$(q/A)_{crit} \times 10^{-6} = \frac{A_1}{1 + C_{11}L}$$

where

$$A_1 = y_o D^{y_1} (G \times 10^{-6})^{y_2}$$

$$C_{11} = y_3 D^{y_4} (G \times 10^{-6})^{y_5}$$

values for y_o ....y_5 can be found in Macbeth's [101] original publication. For this case,

$$y_0 = 1.67$$

$$y_1 = -0.559$$

$$y_2 = -0.294$$

$$y_3 = 0.0147$$

$$y_4 = -1.4$$

$$y_5 = -0.837$$

Thus, $A_1 = 1.67(0.835)^{-0.559}\ (0.5249)^{-0.294} = 2.2325$

$C_{11} = (0.0147)(0.835)^{-1.4}\ (0.5249)^{-0.837} = 0.03245$

Therefore, $(q/A)_{crit} = 0.48708 \times 10^6$ Btu/hr-sq ft.

(d) $\dfrac{(q/A)_{crit}\ \gamma^{1/2}}{\rho_f^{1/2}\ h_{fg}}$ term:

$$(q/A)_{\substack{crit\ R\text{-}114\\ equivalent}} = \left(\frac{(q/A)_{crit}\ \gamma^{1/2}}{\rho_f^{1/2}\ h_{fg}}\right)_{water} \left(\frac{\rho_f^{1/2}\ h_{fg}}{\gamma^{1/2}}\right)_{R\text{-}114}$$

$$= \left(\frac{(0.48708 \times 10^6)(0.4137)}{(7.1947)(783.27)}\right) \left(\frac{(9.4023)(52.905)}{1.1825}\right)$$

$$= 15{,}042 \text{ Btu/hr-sq ft}$$

This compares to the experimentally determined $(q/A)_{crit}$ value of 18,218 Btu/hr-sq ft.

If instead of the Macbeth [101] correlation, the Biasi et al [112] correlation is used:

For the low quality region:

$$(q/A)_{crit} = \frac{1.883 \times 10^3}{(D)^{0.4}\ (G)^{1/6}} \left[\frac{f(p)}{(G)^{1/6}} - x(z)\right] \qquad \text{(D-9)}$$

where

$$f(p) = 0.7249 + 0.099p \exp(-0.032p) \qquad \text{(D-10)}$$

For the high quality region

$$(q/A)_{crit} = \frac{3.78 \times 10^3\ h(p)}{(D)^{0.4}\ (G)^{0.6}} \left[1 - x(z)\right] \qquad \text{(D-11)}$$

where

$$h(p) = -1.159 + 0.149\ p \exp(-0.019\ p) + \frac{8.99\ p}{10 + p^2} \qquad \text{(D-12)}$$

In the above equations, D is in cm, G is in gm/sq cm-sec, (q/A) is in watts/sq cm, and p is in bars. They are applicable for the case of $D \geq 1$ cm. Plugging into Equation (D-1) and using English units:

$$(q/A)_{crit} = \frac{25{,}243.5\ f(p)}{(D)^{0.4}\ G^{1/3}} \Bigg/ \left[\frac{1}{3170.38} + \frac{22{,}887.2\ L}{(D)^{1.4}\ G^{1.1667}\ h_{fg}}\right] \qquad \text{(D-13)}$$

where

$$f(p) = 0.7249 + 0.006828\ p \exp(-0.002207\ p). \qquad \text{(D-14)}$$

$$(q/A)_{crit} = \frac{544{,}725\ h(p)}{(D)^{0.4}\ (G)^{0.6}} \Bigg/ \left[\frac{1}{3170.38} + \frac{2.1789 \times 10^6\ L\ h(p)}{(D)^{1.4}\ (G)^{1.6}\ h_{fg}}\right] \qquad \text{(D-15)}$$

where

$$h(p) = -1.159 + 0.010276\ p \exp(-0.00131\ p) + \frac{0.62\ p}{10 + 0.00476\ p^2} \qquad \text{(D-16)}$$

In Equations (D-13) to (D-16) D and L are in inches, G is lbm/hr-sq ft, (q/A) is in Btu/hr-sq ft, h_{fg} is in Btu/lbm, and p is in lbf/sq in. To determine the critical heat flux, both Equations (D-13) and (D-15) are used. The higher of the two values is taken as the answer. The only exception is in the range of $G < 0.2212 \times 10^6$ lbm/hr-sq ft. Here, the correlation for the high quality region is always used. Thus, for Run CHF 7:

$$f(p) = 1.8507$$

$$(q/A)_{crit} = \frac{(25{,}243.5)(1.8507)}{(0.8351)^{0.4}(0.5249 \times 10^6)^{1/3}} \Bigg/ \left[\frac{1}{3170.38} + \frac{(22{,}887.2)(110.43)}{(0.83509)^{1.4}(0.5249 \times 10^6)^{1.1667}(783.27)}\right]$$

$$= 520{,}327 \text{ Btu/hr-sq ft}$$

Using the equation for the high-quality region

$$h(p) = 1.5741$$

$$(q/A)_{crit} = \frac{(544{,}725)(1.5741)}{(0.8351)^{0.4}(0.5249 \times 10^6)^{0.6}} \Bigg/ \left[\frac{1}{3170.38} + \frac{(2.1789 \times 10^6)(110.43)(1.5741)}{(0.8351)^{1.4}(0.5249 \times 10^6)^{1.6}(783.27)}\right]$$

$$= 452{,}054 \text{ Btu/hr-sq ft}$$

Since the high quality, region yields the higher critical heat flux, it is considered the correct answer. Thus:

$$(q/A)_{\substack{crit\ R\text{-}114 \\ equivalent}} = 16{,}069 \text{ Btu/hr-sq ft}$$

This compares to the experimentally determined $(q/A)_{crit}$ value of 18,218 Btu/hr-sq ft.

Stevens and Kirby [107] Scaling Factor. For the application of the scaling factor approach of Stevens and Kirby [107], a plot of

$$x_{at\ CHF} \text{ vs } G(D)^{1/4}\ (D/L)^{0.59}$$

is made. For the above example,

$$G(D)^{1/4}\ (D/L)^{0.59} = (0.2400 \times 10^6)(0.785)^{1/4}\left(\frac{1}{132.24}\right)^{0.59}$$

$$= 0.01266 \times 10^6 \frac{\text{lbm in.}^{1/4}}{\text{hr-sq ft}}$$

$x_{at\ CHF}$ is 0.7652.

For the water equivalent case, the critical heat flux is obtained by using the Biasi et al [112] correlation for the flow of water in a 0.785

in. ID tube. The water is at 442°F and G = 0.2400 x 10^6 lbm/hr-sq ft. Thus, the conditions are the same as those in the R-114 case; the only exception being that the density ratios are modeled. The critical heat flux quality is obtained by plugging into Equation (D-1). Using the Biasi et al [112] value for the critical heat flux, which for this case is 322,820 Btu/hr-sq ft.

$$x_{\substack{\text{at CHF} \\ \text{water} \\ \text{equivalent}}} = 4(132.24)\,\frac{322{,}800}{(0.2400 \times 10^6)(783.27)} = 0.9083$$

Thus, for the water equivalent case, a plot is made of $x_{\substack{\text{at CHF water} \\ \text{equivalent}}}$ vs $K_s G(D)^{1/4}\,(D/L)^{0.59}$ where K_s is either the 0.658 value Stevens and Kirby [107] recommended or a more complex formulation such as Equation (4-93) or Equation (2-84).

Compensated Distortion Model. In the application of the compensated distortion model, for the case of no inlet subcooling, a plot of

$$x_{\text{at CHF}} \text{ vs } \Psi\,(D/L)^{0.6}$$

is made where:

$$\Psi = \left\{\left(\frac{GD}{\rho_f}\right)\left(\frac{\gamma^{1/2}\,\mu_f}{\sqrt{g}\,D\,\rho_f{}^{1/2}}\right)^{2/3}\left(\frac{\mu_f}{\mu_g}\right)^{1/8}\right\} \qquad (2\text{-}95)$$

For Run CHF 7:

$$\Psi = \left\{\left(\frac{(0.2400 \times 10^6)\left(\frac{0.785}{12}\right)}{0.71232}\right)\left(\frac{(1.1825)(0.71232)}{(20{,}419.97)(0.785)(9.4023)}\right)^{2/3}\left(\frac{0.71232}{0.02921}\right)^{1/8}\right\} = 10.3472$$

Therefore:

$$\Psi\ (D/L)^{0.6} = 0.5521$$

and

$$x_{\text{at CHF}} = 0.7652$$

Application of Critical Heat Flux Results to Design Calculations

The scaling law of Barnett and Wood [105], the scaling factor approach of Stevens and Kirby [107], or the compensated distortion model of Ahmad [116] can be directly applied to determine under what conditions critical heat flux will occur. It should be remembered that Equation (4-95) is valid only for R-114 and additional data need to be obtained for other fluids.

APPENDIX E

PHYSICAL PROPERTIES OF R-114

Whenever the experimental results of any boiling experiment are analyzed, it is very important to know as accurately as possible the thermodynamic and transport properties of the working fluid. This is particularly necessary if one is attempting to meaningfully correlate the results as certain equations, such as the Rohsenow [61] pool boiling correlation given in Equation (2-52), are particularly sensitive to fluid properties.

Thermodynamic Properties

The thermodynamic properties of R-114 used in this study were obtained from a recent du Pont publication [136].

Vapor Pressure. The vapor pressure can be obtained from this equation:

$$\log_{10}(P) = 27.07131 - (5113.702/T) - 6.308676\,(\log_{10} T) + 6.913003 \times 10^{-4}\,T + 0.781421\,[(768.35 - T)/T]\,\log_{10}(768.35 - T) \quad \text{(E-1)}$$

where T is the temperature in degrees Rankine, and the vapor pressure is in lbf/sq in. absolute.

Vapor Density. The vapor density can be obtained from the equation of state:

$$P = \frac{0.062780807T}{(v_g - b_a)} + \frac{-2.3856704 + 1.0801207 \times 10^{-3}T - 6.5643648e^{HT}}{(v_g - b_a)^2}$$

$$+ \frac{0.034055687 - 5.3336494 \times 10^{-6}T + 0.16366057e^{HT}}{(v_g - b_a)^3} - \frac{3.857481 \times 10^{-4}}{(v_g - b_a)^4}$$

$$+ \frac{1.6017659 \times 10^{-6} + 6.2632341 \times 10^{-10}T - 1.0165314 \times 10^{-5}e^{HT}}{(v_g - b_a)^5} \quad \text{(E-2)}$$

where v_g is the specific volume of the vapor in cu ft/lbm and T is in degrees Rankine. The values for the constants are:

$$b_a = 0.005914907 \quad \text{(E-3)}$$

$$H = -3.9790437 \times 10^{-3} \quad \text{(E-4)}$$

The specific volume is obtained from Equation (E-2) using an iterative technique such as the Newton-Raphson method. The vapor density is the reciprocal of the specific volume. The vapor density is in lbm/cu ft.

Liquid Density. This property can be obtained from the equation:

$$\text{Liquid Density} = 36.32 + 6.71826\,(753.95 - T)^{1/3} + 0.63649\,(753.95 - T)^{1/2} + 0.021776\,(753.95 - T) + 1.97 \times 10^{-6}\,(753.95 - T)^2 \quad \text{(E-5)}$$

T here is in degrees Rankine. The liquid density is in lbm/cu ft.

Enthalpy of Vapor. The vapor enthalpy can be obtained from:

$$h_g = 0.0175T + 1.745 \times 10^{-4}T^2 - 5.566666667 \times 10^{-8}T^3 + 25.33966211 + J'Pv_g - \frac{0.4414754645}{(v_g - b_a)} + \frac{3.151053523 \times 10^{-3}}{(v_g - b_a)^2} - \frac{2.379461438 \times 10^{-5}}{(v_g - b_a)^3} + \frac{7.410289627 \times 10^{-8}}{(v_g - b_a)^4} + \left[\frac{-1.214755399}{(v_g - b_a)} + \frac{0.01514293973}{(v_g - b_a)^2} - \frac{4.702804629 \times 10^{-7}}{(v_g - b_a)^4}\right](1 - HT)e^{HT} \quad \text{(E-6)}$$

$$J' = 0.185053 \quad \text{(E-7)}$$

The vapor enthalpy is in Btu/lbm. T is in degrees Rankine.

Latent Heat of Vaporization. The latent heat of vaporization can be obtained from:

$$h_{fg} = \left\{[2.17895 \times 10^3 - 255.8327 \log_{10} (768.35 - T)]/T - 1.312044 + 2.94563 \times 10^{-4} T\right\} P \left(v_g - \frac{1}{\rho_f}\right) \qquad \text{(E-8)}$$

h_{fg} is in Btu/lbm. T is in degrees Rankine.

Liquid Enthalpy. The liquid enthalpy is equal to the vapor enthalpy minus the latent heat of vaporization:

$$h_f = h_g - h_{fg} \qquad \text{(E-9)}$$

Vapor Heat Capacity at Constant Pressure. From the relation:

$$c_p = c_v - J'T \left[\frac{\left(\frac{\partial P}{\partial T}\right)_v^2}{\left(\frac{\partial P}{\partial v}\right)_T}\right] \qquad \text{(E-10)}$$

where c_v, the vapor heat capacity at constant volume is:

$$c_v = 0.0175 + 3.49 \times 10^{-4}T - 1.67 \times 10^{-7}T^2 + T \left[\frac{1.923296567 \times 10^{-5}}{(v_g - b_a)} - \frac{2.397549664 \times 10^{-7}}{(v_g - b_a)^2} + \frac{7.44585124 \times 10^{-12}}{(v_g - b_a)^4}\right] e^{HT} \qquad \text{(E-11)}$$

Here $\left(\frac{\partial P}{\partial T}\right)_v$ and $\left(\frac{\partial P}{\partial v}\right)_T$ can be obtained by differentiating Equation (E-2) with respect to the proper variable to yield:

$$\left(\frac{\partial P}{\partial T}\right)_v = \frac{0.062780807}{(v_g - b_a)} + \frac{1.0801207 \times 10^{-3}}{(v_g - b_a)^2} - \frac{5.3336494 \times 10^{-6}}{(v_g - b_a)^3} + \frac{6.2632341 \times 10^{-10}}{(v_g - b_a)^5} + \left[\frac{0.02611989442}{(v_g - b_a)^2}\right.$$

$$- \frac{6.512125605 \times 10^{-4}}{(v_g - b_a)^3} + \frac{4.044822866 \times 10^{-8}}{(v_g - b_a)^5} \Bigg] e^{HT} \qquad \text{(E-12)}$$

$$\left(\frac{\partial P}{\partial v}\right)_T = \frac{-0.0627808T}{(v_g - b_a)^2} + \frac{4.7713408 - 2.1602414 \times 10^{-3}T + 13.1287296e^{HT}}{(v_g - b_a)^3}$$

$$+ \frac{-0.102167061 + 1.60009482 \times 10^{-5}T - 0.49098171e^{HT}}{(v_g - b_a)^4}$$

$$+ \frac{1.5429924 \times 10^{-3}}{(v_g - b_a)^5} - \frac{8.0088295 \times 10^{-6}}{(v_g - b_a)^6}$$

$$- \frac{3.13161705 \times 10^{-9}T - 5.082657 \times 10^{-5}e^{HT}}{(v_g - b_a)^6} \qquad \text{(E-13)}$$

Again here, T is in degrees Rankine. c_p and c_v are in Btu/lbm-°F.

Liquid Heat Capacity. The liquid specific heat can be obtained from:

$$\text{Liquid } c_p = 0.224074 + 1.844997 \times 10^{-4}\ T + 7.582739 \times 10^{-7}\ T^2 - 1.247439 \times 10^{-9}\ T^3 \qquad \text{(E-14)}$$

where T is in degrees Fahrenheit and c_p is in Btu/lbm-°F.

Transport Properties

All the transport properties listed here with the exception of the surface tension were supplied by Dr. Paul Liley [137] of Purdue University. They also appear in the ASHRAE Handbook of Fundamentals [2].

Liquid Viscosity. In the range of $170 < T < 360$°K:

$$\mu_f = 2.39026 \left[e^{-4.4636 + 1011.47/T}\right] \qquad \text{(E-15)}$$

In the range $350 < T < 410$°K:

$$\mu_f = 2.39026\ [8.98644 - 0.07248\ T + 2.02802 \times 10^{-4}\ T^2 - 1.92593 \times 10^{-7}\ T^3] \qquad \text{(E-16)}$$

The viscosity is in lbm/ft-hr and the temperature is in degrees Kelvin.

Vapor Viscosity. In the temperature range $270° < T < 410°K$:

$$\mu_g = 2.39026 \left[-0.14274 + 1.4201 \times 10^{-3} T - 4.43555 \times 10^{-6} T^2 + 4.73144 \times 10^{-9} T^3\right]. \quad \text{(E-17)}$$

The viscosity is in lbm/ft-hr and the temperature is in degrees Kelvin.

Liquid Thermal Conductivity.

$$k_f = 4.43750 \times 10^{-2} - 9.900167 \times 10^{-5} T + 8.482783 \times 10^{-8} T^2 + 2.0877 \times 10^{-10} T^3 - 1.858469 \times 10^{-12} T^4. \quad \text{(E-18)}$$

The liquid thermal conductivity is in Btu/hr-ft-°F and the temperature is in degrees Fahrenheit.

Surface Tension. Very meager information on surface tension was found in the literature.

$$\frac{\sigma_2}{\sigma_1} = \left(\frac{T_{crit} - T_2}{T_{crit} - T_1}\right)^{1.2} \quad \text{(E-19)}$$

recommended by Perry et al [138] was used to extrapolate a known value of σ to other temperatures. Since the surface tension at 77°F is 13 dynes/cm or 0.000891 lbf/ft [1],

$$\sigma = 0.000891 \left(\frac{294.3 - T}{217.3}\right)^{1.2} \quad \text{(E-20)}$$

can be used to obtain the surface tension at other temperatures. Here, σ is in lbf/ft and T is in degrees Fahrenheit.

Tabulation of Results

A brief tabulation of the above mentioned properties is given in Table E-1. All the equations discussed yield accurate property values in the 100 to 250°F range.

Table E-1

TABULATION OF PHYSICAL PROPERTIES OF R-114

	100°F	150°F	200°F	250°F
Vapor Pressure (psia)	45.851	96.053	178.42	304.87
Vapor Density (lbm/cu ft)	1.4372	2.9778	5.7295	11.052
Liquid Density (lbm/cu ft)	88.404	82.381	75.144	65.286
Enthalpy of Vapor (Btu/lbm)	84.706	91.845	98.342	103.25
Latent Heat of Vaporization (Btu/lbm)	52.905	47.197	40.148	30.474
Liquid Enthalpy (Btu/lbm)	31.801	44.648	58.194	72.780
Liquid c_p (Btu/lbm-°F)	0.24886	0.26460	0.28133	0.29810
Vapor c_p (Btu/lbm-°F)	0.17927	0.19447	0.21761	0.27797
Liquid Viscosity (lbm/ft-hr)	0.71232	0.54553	0.43551	0.31385
Vapor Viscosity (lbm/ft-hr)	0.029208	0.031676	0.035506	0.042173
Liquid Thermal Conductivity (Btu/hr-ft-°F)	0.035346	0.031197	0.026664	0.020929
Surface Tension (lbf/ft)	0.00077906	0.00054516	0.00032720	0.00013216

APPENDIX F

TABULATION OF DATA

The experimental results obtained in this study are tabulated in Tables F-1 to F-54. Table F-1 contains the flow regime data. Tables F-2 to F-19 contain the experimental pressure drop data, while Tables F-20 to F-37 contain the correlated pressure drop results using the Homogeneous [3] and Martinelli-Nelson [4] models. The Martinelli-Nelson [4] model is used in conjunction with both the Martinelli-Nelson [4] and Zuber et al [10] modified void fraction correlations. Tables F-38 to F-53 contain the experimental heat transfer coefficient results, while Table F-54 contains the critical heat flux data.

Table F-1

TABULATION OF FLOW REGIME DATA

Run No.	G (lbm/hr-sq ft)	Quality, x	T (°F)	Regime
V2	0.235×10^6	0.0024	105.4	Bubbly
V3	0.235×10^6	0.0056	107.4	Bubbly-Slug
V4	0.234×10^6	0.0224	108.7	Transition
V5	0.234×10^6	0.0373	107.9	Weak Annular
V6	0.232×10^6	0.0941	107.8	Weak Annular
V7	0.231×10^6	0.1579	107.7	Weak Annular
V8	0.231×10^6	0.2849	108.1	Weak Annular
V9	0.230×10^6	0.5021	108.3	Strong Annular, Annular-Mist
V10	0.233×10^6	0.4646	108.8	Strong Annular, Annular-Mist
V11	0.234×10^6	0.6603	108.3	Strong Annular, Annular-Mist
V12	0.230×10^6	0.6104	108.3	Strong Annular, Annular-Mist
V13	0.229×10^6	0.7141	108.3	Strong Annular, Annular-Mist
V14	0.217×10^6	0.9247	107.5	Strong Annular, Annular-Mist
V16	0.233×10^6	0.0076	107.9	Transition
V17	0.232×10^6	0.0092	107.9	Transition
V18	0.233×10^6	0.0031	108.1	Bubbly
V19	0.234×10^6	0.0204	108.1	Transition
V20	0.238×10^6	0.0429	108.1	Weak Annular
V21	0.232×10^6	0.1109	108.2	Weak Annular
V22	0.237×10^6	0.0357	108.1	Transition
V23	0.230×10^6	0.1439	108.3	Weak Annular
V24	0.240×10^6	0.1813	108.0	Weak Annular
V25	0.237×10^6	0.2144	108.2	Weak Annular
V26	0.235×10^6	0.2585	108.0	Weak Annular
V27	0.234×10^6	0.3089	108.0	Weak Annular
V28	0.228×10^6	0.0581	108.2	Weak Annular
V29	0.230×10^6	0.0342	108.1	Weak Annular
V30	0.227×10^6	0.0221	108.3	Transition
V31	0.231×10^6	0.3915	107.9	Weak Annular
V32	0.232×10^6	0.4896	108.0	Strong Annular, Annular-Mist
V33	0.230×10^6	0.5842	108.1	Strong Annular, Annular-Mist
V34	0.228×10^6	0.6850	107.8	Strong Annular, Annular-Mist
V35	0.230×10^6	0.7329	108.4	Strong Annular, Annular-Mist
V36	0.229×10^6	0.7862	108.0	Strong Annular, Annular-Mist
V37	0.230×10^6	0.8383	107.6	Strong Annular, Annular-Mist
V38	0.231×10^6	0.8654	108.6	Strong Annular, Annular-Mist
V39	0.113×10^6	0.0068	108.1	Bubbly
V40	0.115×10^6	0.0059	108.6	Bubbly
V41	0.114×10^6	0.0808	108.2	Weak Annular
V42	0.113×10^6	0.1652	108.3	Weak Annular

Table F-1 (continued)

Run No.	G (lbm/hr-sq ft)	Quality, x	T (°F)	Regime
V43	0.117×10^6	0.2171	108.1	Weak Annular
V44	0.114×10^6	0.2847	108.0	Weak Annular
V45	0.114×10^6	0.3973	108.4	Weak Annular
V46	0.118×10^6	0.5162	107.9	Weak Annular
V47	0.115×10^6	0.6680	108.3	Strong Annular, Annular-Mist
V48	0.116×10^6	0.7502	108.2	Strong Annular, Annular-Mist
V49	0.120×10^6	0.7929	108.0	Strong Annular, Annular-Mist
V50	0.115×10^6	0.9013	107.8	Strong Annular, Annular-Mist
V51	0.459×10^6	0.2187	108.0	Weak Annular
V52	0.469×10^6	0.1885	107.3	Weak Annular
V53	0.457×10^6	0.1407	108.8	Weak Annular
V54	0.457×10^6	0.1153	108.6	Weak Annular
V55	0.452×10^6	0.0651	107.9	Weak Annular
V56	0.469×10^6	0.0503	107.4	Weak Annular
V57	0.471×10^6	0.0366	108.3	Weak Annular
V58	0.469×10^6	0.0198	108.2	Transition
V59	0.464×10^6	0.0126	107.9	Transition
V60	0.460×10^6	0.0051	107.7	Bubbly
V61	0.465×10^6	0.3117	108.1	Weak Annular
V62	0.468×10^6	0.3809	108.3	Strong Annular, Annular-Mist
V63	0.463×10^6	0.4560	108.0	Unidentifiable
V64	0.463×10^6	0.5933	108.1	Unidentifiable
V65	0.473×10^6	0.5709	108.1	Unidentifiable
V66	0.710×10^6	0.0170	107.1	Bubbly
V67	0.706×10^6	0.0468	108.1	Weak Annular
V68	0.706×10^6	0.1082	108.3	Strong Annular, Annular-Mist
V69	0.707×10^6	0.1473	108.1	Unidentifiable
V70	0.707×10^6	0.2305	108.3	Unidentifiable
V71	0.707×10^6	0.2602	108.3	Unidentifiable
V72	0.710×10^6	0.2994	108.2	Unidentifiable
V73	0.706×10^6	0.3670	108.3	Unidentifiable
V74	0.707×10^6	0.5531	108.3	Unidentifiable
V75	0.706×10^6	0.6000	108.8	Unidentifiable
V76	0.172×10^7	0.0013	108.4	Bubbly
V77	0.176×10^7	0.0030	107.6	Bubbly
V78	0.175×10^7	0.0693	108.1	Unidentifiable
V79	0.178×10^7	0.1072	107.6	Unidentifiable
V80	0.173×10^7	0.1522	108.3	Unidentifiable
V81	0.175×10^7	0.1818	108.1	Unidentifiable
V82	0.177×10^7	0.2509	108.1	Unidentifiable

Table F-1 (continued)

Run No.	G (lbm/hr-sq ft)	Quality, x	T (°F)	Regime
V83	0.178×10^7	0.3302	107.9	Unidentifiable
V84	0.350×10^7	0.0021	108.9	Bubbly
V85	0.352×10^7	0.0023	108.6	Transition
V86	0.350×10^7	0.0042	108.0	Transition
V87	0.347×10^7	0.0052	108.1	Transition
V88	0.353×10^7	0.0061	107.5	Unidentifiable
V89	0.351×10^7	0.0098	110.1	Unidentifiable
V90	0.350×10^7	0.0144	108.6	Unidentifiable
V91	0.359×10^7	0.0174	108.1	Unidentifiable
V92	0.356×10^7	0.0185	108.0	Unidentifiable
V96	0.892×10^6	0.0119	194.0	Bubbly
V97	0.894×10^6	0.0199	194.1	Weak Annular
V98	0.893×10^6	0.0319	193.7	Weak Annular
V99	0.898×10^6	0.0352	193.2	Strong Annular, Annular-Mist
V100	0.919×10^6	0.0456	195.0	Strong Annular, Annular-Mist
V101	0.908×10^6	0.0491	196.3	Strong Annular, Annular-Mist
V102	0.911×10^6	0.0541	198.9	Strong Annular, Annular-Mist
V103	0.914×10^6	0.0568	201.5	Unidentifiable
V104	0.930×10^6	0.0886	199.8	Unidentifiable
V105	0.951×10^6	0.0952	201.8	Unidentifiable
V106	0.956×10^6	0.1366	202.8	Unidentifiable
V107	0.910×10^6	0.2362	201.9	Unidentifiable
V108	0.919×10^6	0.2609	201.5	Unidentifiable
V109	0.911×10^6	0.2846	201.6	Unidentifiable
V110	0.924×10^6	0.3065	198.5	Unidentifiable
V111	0.116×10^6	0.0161	146.7	Bubbly
V112	0.123×10^6	0.0282	147.5	Bubbly
V113	0.111×10^6	0.0726	154.0	Transition
V114	0.122×10^6	0.2913	152.9	Weak Annular
V115	0.114×10^6	0.4357	153.1	Weak Annular
V116	0.113×10^6	0.6395	153.4	Weak Annular
V117	0.119×10^6	0.7759	153.8	Strong Annular, Annular-Mist
V118	0.118×10^6	0.8437	153.5	Strong Annular, Annular-Mist
V119	0.116×10^6	0.9023	151.9	Strong Annular, Annular-Mist
V120	0.247×10^6	0.0077	152.3	Bubbly
V121	0.212×10^6	0.0117	148.4	Bubbly
V122	0.232×10^6	0.0148	148.2	Bubbly
V123	0.228×10^6	0.0150	149.1	Bubbly
V124	0.241×10^6	0.0330	149.8	Transition
V125	0.231×10^6	0.0569	149.7	Weak Annular

Table F-1 (continued)

Run No.	G (lbm/hr-sq ft)	Quality, x	T (°F)	Regime
V126	0.252×10^6	0.0836	150.1	Weak Annular
V127	0.229×10^6	0.1367	149.8	Weak Annular
V128	0.231×10^6	0.2310	149.9	Weak Annular
V129	0.219×10^6	0.3261	150.3	Weak Annular
V130	0.235×10^6	0.3760	150.6	Weak Annular
V131	0.232×10^6	0.4660	150.5	Weak Annular
V132	0.237×10^6	0.5573	150.4	Weak Annular
V133	0.214×10^6	0.6936	150.0	Strong Annular, Annular-Mist
V134	0.227×10^6	0.7290	149.4	Strong Annular, Annular-Mist
V135	0.209×10^6	0.8910	150.1	Strong Annular, Annular-Mist
V136	0.454×10^6	0.0129	150.6	Bubbly
V137	0.453×10^6	0.0149	152.3	Bubbly
V138	0.436×10^6	0.0343	149.9	Transition
V139	0.447×10^6	0.0510	149.3	Transition
V140	0.491×10^6	0.0647	150.7	Weak Annular
V141	0.456×10^6	0.1128	151.9	Weak Annular
V142	0.447×10^6	0.1619	151.4	Weak Annular
V143	0.445×10^6	0.1976	151.3	Weak Annular
V144	0.445×10^6	0.2393	151.5	Weak Annular
V145	0.454×10^6	0.2735	151.6	Weak Annular
V146	0.446×10^6	0.3191	152.0	Weak Annular
V147	0.453×10^6	0.3566	151.9	Weak Annular
V148	0.452×10^6	0.3959	151.4	Weak Annular
V149	0.448×10^6	0.4399	151.6	Strong Annular, Annular-Mist
V150	0.458×10^6	0.4680	152.2	Strong Annular, Annular-Mist
V151	0.447×10^6	0.5299	152.5	Strong Annular, Annular-Mist
V152	0.887×10^6	0.0043	154.0	Bubbly
V153	0.896×10^6	0.0020	151.4	Bubbly
V154	0.918×10^6	0.0032	151.2	Bubbly
V155	0.112×10^7	0.0103	152.1	Transition
V156	0.918×10^6	0.0268	151.2	Weak Annular
V157	0.935×10^6	0.0280	150.7	Weak Annular
V158	0.950×10^6	0.0339	151.1	Weak Annular
V159	0.919×10^6	0.0595	151.9	Weak Annular
V160	0.944×10^6	0.0914	151.2	Weak Annular
V161	0.905×10^6	0.1487	151.7	Weak Annular
V162	0.911×10^6	0.1883	151.6	Strong Annular, Annular-Mist
V163	0.901×10^6	0.2296	151.8	Strong Annular, Annular-Mist
V164	0.902×10^6	0.2448	151.3	Unidentifiable
V165	0.882×10^6	0.2703	149.4	Unidentifiable

Table F-1 (continued)

Run No.	G (lbm/hr-sq ft)	Quality, x	T (°F)	Regime
V166	0.881×10^6	0.2870	149.8	Unidentifiable
V167	0.885×10^6	0.3088	151.0	Unidentifiable
V168	0.330×10^7	0.0099	150.9	Strong Annular
V169	0.115×10^6	0.0389	192.2	Bubbly
V170	0.121×10^6	0.0766	193.5	Bubbly
V171	0.124×10^6	0.1144	191.7	Weak Annular
V172	0.120×10^6	0.2322	188.3	Weak Annular
V173	0.124×10^6	0.2657	188.0	Weak Annular
V174	0.125×10^6	0.6100	182.3	Weak Annular
V175	0.121×10^6	0.8231	178.3	Strong Annular, Annular-Mist
V176	0.121×10^6	0.8742	179.1	Strong Annular, Annular-Mist
V177	0.122×10^6	0.9001	178.8	Strong Annular, Annular-Mist
V178	0.232×10^6	0.0258	187.3	Bubbly
V179	0.232×10^6	0.0287	186.6	Bubbly
V181	0.231×10^6	0.1243	184.9	Weak Annular
V182	0.237×10^6	0.3283	182.4	Weak Annular
V183	0.228×10^6	0.4590	183.7	Weak Annular
V184	0.229×10^6	0.5390	185.9	Weak Annular
V185	0.227×10^6	0.6424	188.0	Strong Annular, Annular-Mist
V186	0.226×10^6	0.7200	190.3	Strong Annular, Annular-Mist
V187	0.224×10^6	0.8101	193.1	Strong Annular, Annular-Mist
V188	0.445×10^6	0.0187	190.9	Bubbly
V189	0.448×10^6	0.0182	188.1	Bubbly
V190	0.442×10^6	0.0509	184.1	Transition
V191	0.457×10^6	0.0569	185.7	Weak Annular
V192	0.462×10^6	0.0962	182.2	Weak Annular
V193	0.470×10^6	0.1217	182.9	Weak Annular
V194	0.468×10^6	0.1719	182.5	Weak Annular
V195	0.459×10^6	0.2117	183.3	Strong Annular, Annular-Mist
V196	0.457×10^6	0.2528	185.5	Strong Annular, Annular-Mist
V197	0.458×10^6	0.2885	187.9	Strong Annular, Annular-Mist
V198	0.456×10^6	0.3550	190.0	Strong Annular, Annular-Mist
V199	0.439×10^6	0.4615	193.5	Unidentifiable
V200	0.443×10^6	0.4932	196.7	Unidentifiable
V201	0.489×10^6	0.3434	247.8	Unidentifiable
V202	0.100×10^7	0.1240	247.3	Unidentifiable
V203	0.949×10^6	0.2307	249.1	Unidentifiable
V204	0.968×10^6	0.2263	248.7	Unidentifiable
V205	0.981×10^6	0.2086	245.7	Unidentifiable
V206	0.955×10^6	0.1330	243.4	Unidentifiable

Table F-1 (continued)

Run No.	G (lbm/hr-sq ft)	Quality, x	T (°F)	Regime
V207	0.262×10^6	0.3266	243.4	Unidentifiable
V208	0.281×10^6	0.5991	249.7	Unidentifiable
V209	0.257×10^6	0.5375	245.0	Unidentifiable
V210	0.277×10^6	0.4617	241.8	Unidentifiable
V211	0.449×10^6	0.4317	244.1	Unidentifiable
V212	0.484×10^6	0.3644	244.0	Unidentifiable
V213	0.362×10^6	0.3316	246.9	Unidentifiable

Table F-2

PRESSURE DROP -- EXPERIMENTAL DATA

$G \approx 0.12 \times 10^6$ lbm/hr-sq ft T≈100°F

RUN #	G (LBM/HR-SQ FT)	T BOIL (DEG F)	X IN	X OUT	LENGTH (FT)	ΔP TOTAL (PSI)
1- 2	0.1204E 06	99.5	0.037	0.105	2.0208	0.5728
1- 3	0.1204E 06	98.9	0.105	0.167	2.0417	0.3983
1- 4	0.1204E 06	98.6	0.167	0.230	1.9271	0.3259
1- 5	0.1204E 06	98.3	0.230	0.290	1.8542	0.2798
3- 3	0.1166E 06	98.9	0.236	0.371	2.0417	0.3513
3- 4	0.1166E 06	98.6	0.371	0.506	1.9271	0.1850
3- 5	0.1166E 06	98.4	0.506	0.637	1.8542	0.1389
4- 2	0.1196E 06	98.3	0.129	0.322	2.0208	0.2836
4- 3	0.1196E 06	97.7	0.322	0.512	2.0417	0.2967
4- 4	0.1196E 06	97.6	0.512	0.702	1.9271	0.1778
4- 5	0.1196E 06	97.3	0.702	0.886	1.8542	0.2259
5- 2	0.1200E 06	97.4	0.150	0.355	2.0208	0.2945
5- 3	0.1200E 06	96.6	0.355	0.558	2.0417	0.2608
5- 4	0.1200E 06	96.6	0.558	0.767	1.9271	0.1882
5- 5	0.1200E 06	96.2	0.767	0.968	1.8542	0.1420
6- 2	0.1203E 06	96.8	0.202	0.409	2.0208	0.2488
6- 3	0.1203E 06	96.0	0.409	0.615	2.0417	0.2620
6- 4	0.1203E 06	95.8	0.615	0.821	1.9271	0.1894
6- 5	0.1203E 06	95.6	0.821	1.014	1.8542	0.0962
7- 2	0.1183E 06	99.5	0.173	0.377	2.0208	0.2456
7- 3	0.1183E 06	98.8	0.377	0.576	2.0417	0.2587
7- 4	0.1183E 06	98.5	0.576	0.774	1.9271	0.1863
8- 2	0.1200E 06	99.7	0.131	0.288	2.0208	0.2930
8- 3	0.1200E 06	99.0	0.288	0.443	2.0417	0.2123
8- 4	0.1200E 06	98.9	0.443	0.600	1.9271	0.2102
8- 5	0.1200E 06	98.7	0.600	0.753	1.8542	0.1641
53- 2	0.1190E 06	100.1	0.121	0.331	2.0208	0.2866
53- 3	0.1190E 06	99.3	0.331	0.540	2.0417	0.2904
53- 4	0.1190E 06	99.1	0.540	0.746	1.9271	0.1525
53- 5	0.1190E 06	98.8	0.746	0.944	1.8542	0.2005
54- 2	0.1198E 06	99.0	0.144	0.368	2.0208	0.4100
54- 3	0.1198E 06	98.2	0.368	0.590	2.0417	0.2917
54- 4	0.1198E 06	97.9	0.590	0.808	1.9271	0.1820
55- 3	0.1190E 06	98.4	0.148	0.372	2.0417	0.3029
55- 4	0.1190E 06	98.2	0.372	0.594	1.9271	0.2541
55- 5	0.1190E 06	97.9	0.594	0.807	1.8542	0.2315
56- 2	0.1179E 06	100.7	0.181	0.425	2.0208	0.2643
56- 3	0.1179E 06	99.7	0.425	0.665	2.0417	0.2352
56- 4	0.1179E 06	99.4	0.665	0.903	1.9271	0.1817
57- 3	0.1172E 06	99.3	0.128	0.370	2.0417	0.3110

Table F-2 (continued)

RUN #	G (LBM/HR-SQ FT)	T BOIL (DEG F)	X IN	X OUT	LENGTH (FT)	ΔP TOTAL (PSI)
57- 4	0.1172E 06	99.2	0.370	0.610	1.9271	0.2481
57- 5	0.1172E 06	98.9	0.610	0.840	1.8542	0.2491
58- 3	0.1171E 06	99.8	0.139	0.398	2.0417	0.2763
58- 4	0.1171E 06	99.5	0.398	0.653	1.9271	0.1804
58- 5	0.1171E 06	99.4	0.653	0.901	1.8542	0.2736
59- 3	0.1173E 06	96.9	0.0	0.238	2.0417	0.4436
59- 4	0.1173E 06	99.5	0.238	0.495	1.9271	0.2539
59- 5	0.1173E 06	99.2	0.495	0.740	1.8542	0.2314
60- 3	0.1190E 06	101.0	0.120	0.402	2.0417	0.3082
60- 4	0.1190E 06	100.8	0.402	0.680	1.9271	0.2361
60- 5	0.1190E 06	100.5	0.680	0.945	1.8542	0.2372
61- 3	0.1194E 06	99.0	0.169	0.462	2.0417	0.2854
61- 4	0.1194E 06	98.9	0.462	0.752	1.9271	0.2743
62- 3	0.1177E 06	100.1	0.069	0.387	2.0417	0.3922
62- 4	0.1177E 06	100.3	0.387	0.707	1.9271	0.2028
63- 4	0.1178E 06	99.4	0.380	0.702	1.9271	0.2498
64- 4	0.1201E 06	99.9	0.259	0.636	1.9271	0.2275
65- 4	0.1183E 06	99.0	0.089	0.556	1.9271	0.2784
73- 2	0.1188E 06	100.1	0.016	0.082	2.0208	0.6616
73- 3	0.1188E 06	99.2	0.082	0.144	2.0417	0.5339
73- 4	0.1188E 06	98.6	0.144	0.206	1.9271	0.3679
73- 5	0.1188E 06	98.0	0.206	0.269	1.8542	0.2751
74- 2	0.1185E 06	99.5	0.088	0.216	2.0208	0.4290
74- 3	0.1185E 06	98.9	0.216	0.341	2.0417	0.3013
74- 4	0.1185E 06	98.7	0.341	0.468	1.9271	0.2291
74- 5	0.1185E 06	98.2	0.468	0.589	1.8542	0.2300
75- 2	0.1187E 06	100.4	0.132	0.321	2.0208	0.3340
75- 3	0.1187E 06	99.9	0.321	0.506	2.0417	0.2532
75- 4	0.1187E 06	99.5	0.506	0.693	1.9271	0.1811
75- 5	0.1187E 06	99.1	0.693	0.875	1.8542	0.2290
76- 2	0.1136E 06	99.4	0.181	0.400	2.0208	0.2937
76- 3	0.1136E 06	98.8	0.400	0.615	2.0417	0.2646
76- 4	0.1136E 06	98.4	0.615	0.826	1.9271	0.2205
76- 5	0.1136E 06	98.0	0.826	1.036	1.8542	0.1839
77- 2	0.1146E 06	99.5	0.160	0.390	2.0208	0.2930
77- 3	0.1146E 06	98.8	0.390	0.617	2.0417	0.2592
77- 4	0.1146E 06	98.5	0.617	0.845	1.9271	0.2337
268- 2	0.1299E 06	99.5	0.048	0.240	2.0208	0.3855
268- 3	0.1299E 06	99.2	0.240	0.431	2.0417	0.3048
268- 4	0.1299E 06	98.8	0.431	0.621	1.9271	0.2324

Table F-2 (continued)

RUN #	G (LBM/HR-SQ FT)	T BOIL (DEG F)	X IN	X OUT	LENGTH (FT)	ΔP TOTAL (PSI)
268- 5	0.1299E 06	98.3	0.621	0.807	1.8542	0.2614
269- 2	0.1266E 06	100.0	0.060	0.304	2.0208	0.3169
269- 3	0.1266E 06	99.5	0.304	0.547	2.0417	0.3489
269- 4	0.1266E 06	99.0	0.547	0.790	1.9271	0.2297
270- 2	0.1267E 06	100.3	0.098	0.354	2.0208	0.3372
270- 3	0.1267E 06	99.9	0.354	0.608	2.0417	0.3128
270- 4	0.1267E 06	99.3	0.608	0.856	1.9271	0.2686
271- 3	0.1219E 06	100.4	0.421	0.703	2.0417	0.3504
271- 4	0.1219E 06	99.9	0.703	0.982	1.9271	0.2311
272- 2	0.1199E 06	99.6	0.176	0.479	2.0208	0.2883
272- 3	0.1199E 06	99.2	0.479	0.779	2.0417	0.3390
273- 2	0.1217E 06	99.7	0.189	0.495	2.0208	0.2879
273- 3	0.1217E 06	99.3	0.495	0.801	2.0417	0.3011
274- 2	0.1203E 06	100.3	0.230	0.577	2.0208	0.3072
274- 3	0.1203E 06	99.9	0.577	0.927	2.0417	0.3391
275- 2	0.1171E 06	99.9	0.292	0.697	2.0208	0.3269
276- 2	0.1201E 06	99.8	0.330	0.790	2.0208	0.3396

Table F-3

PRESSURE DROP -- EXPERIMENTAL DATA

$G \approx 0.24 \times 10^6$ lbm/hr-sq ft T≈100°F

RUN #	G (LBM/HR-SQ FT)	T BOIL (DEG F)	X IN	X OUT	LENGTH (FT)	ΔP TOTAL (PSI)
9- 2	0.2346E 06	102.1	0.018	0.051	2.0208	0.6603
9- 3	0.2346E 06	101.5	0.051	0.083	2.0417	0.5795
9- 4	0.2346E 06	101.2	0.083	0.118	1.9271	0.4136
9- 5	0.2346E 06	100.7	0.118	0.153	1.8542	0.4147
10- 2	0.2387E 06	99.2	0.045	0.113	2.0208	0.4736
10- 3	0.2387E 06	98.6	0.113	0.178	2.0417	0.4398
10- 4	0.2387E 06	98.3	0.178	0.245	1.9271	0.3442
10- 5	0.2387E 06	97.9	0.245	0.312	1.8542	0.3453
11- 2	0.2379E 06	99.1	0.018	0.113	2.0208	0.5074
11- 3	0.2379E 06	99.0	0.113	0.207	2.0417	0.4503
11- 4	0.2379E 06	98.8	0.207	0.302	1.9271	0.3776
11- 5	0.2379E 06	98.4	0.302	0.396	1.8542	0.3313
12- 2	0.2396E 06	99.4	0.024	0.134	2.0208	0.5048
12- 3	0.2396E 06	99.0	0.134	0.245	2.0417	0.4476
12- 4	0.2396E 06	98.7	0.245	0.357	1.9271	0.3751
12- 5	0.2396E 06	98.1	0.357	0.468	1.8542	0.4228
13- 2	0.2406E 06	99.6	0.075	0.202	2.0208	0.4789
13- 3	0.2406E 06	99.0	0.202	0.329	2.0417	0.4451
13- 4	0.2406E 06	98.7	0.329	0.457	1.9271	0.3727
13- 5	0.2406E 06	98.3	0.457	0.581	1.8542	0.4675
14- 2	0.2417E 06	99.9	0.089	0.236	2.0208	0.4708
14- 3	0.2417E 06	98.9	0.236	0.380	2.0417	0.4370
14- 4	0.2417E 06	98.6	0.380	0.525	1.9271	0.5059
14- 5	0.2417E 06	98.0	0.525	0.670	1.8542	0.4601
15- 2	0.2412E 06	99.3	0.099	0.260	2.0208	0.4274
15- 3	0.2412E 06	98.3	0.260	0.418	2.0417	0.4874
15- 4	0.2412E 06	98.0	0.418	0.579	1.9271	0.5092
15- 5	0.2412E 06	97.2	0.579	0.740	1.8542	0.5102
16- 2	0.2389E 06	98.9	0.115	0.284	2.0208	0.4767
16- 3	0.2389E 06	97.9	0.284	0.453	2.0417	0.4899
16- 4	0.2389E 06	97.4	0.453	0.622	1.9271	0.4645
16- 5	0.2389E 06	96.7	0.622	0.785	1.8542	0.4185
17- 2	0.2427E 06	99.9	0.111	0.277	2.0208	0.4276
17- 3	0.2427E 06	99.1	0.277	0.443	2.0417	0.4876
17- 4	0.2427E 06	98.9	0.443	0.609	1.9271	0.5093
17- 5	0.2427E 06	98.1	0.609	0.770	1.8542	0.4634
18- 2	0.2390E 06	100.0	0.113	0.291	2.0208	0.4264
18- 3	0.2390E 06	99.2	0.291	0.468	2.0417	0.4865
18- 4	0.2390E 06	98.8	0.468	0.643	1.9271	0.5083
19- 2	0.2402E 06	99.1	0.120	0.304	2.0208	0.4786

Table F-3 (continued)

RUN #	G (LBM/HR-SQ FT)	T BOIL (DEG F)	X IN	X OUT	LENGTH (FT)	ΔP TOTAL (PSI)
19- 3	0.2402E 06	98.0	0.304	0.485	2.0417	0.4448
19- 4	0.2402E 06	97.5	0.485	0.668	1.9271	0.5602
20- 2	0.2417E 06	99.3	0.123	0.312	2.0208	0.3757
20- 3	0.2417E 06	98.3	0.312	0.500	2.0417	0.5765
20- 4	0.2417E 06	97.8	0.500	0.688	1.9271	0.5516
21- 2	0.2400E 06	101.7	0.116	0.299	2.0208	0.4680
21- 3	0.2400E 06	100.8	0.299	0.479	2.0417	0.4811
21- 4	0.2400E 06	100.3	0.479	0.658	1.9271	0.4093
22- 2	0.2400E 06	100.3	0.108	0.282	2.0208	0.4352
22- 3	0.2400E 06	99.1	0.282	0.453	2.0417	0.5188
22- 4	0.2400E 06	98.7	0.453	0.623	1.9271	0.4462
22- 5	0.2400E 06	98.2	0.623	0.791	1.8542	0.4704
68- 3	0.2438E 06	101.3	0.209	0.399	2.0417	0.5329
68- 4	0.2438E 06	100.8	0.399	0.586	1.9271	0.5547
68- 5	0.2438E 06	100.1	0.586	0.761	1.8542	0.3681
69- 3	0.2421E 06	99.5	0.098	0.331	2.0417	0.5405
69- 4	0.2421E 06	98.9	0.331	0.560	1.9271	0.5149
69- 5	0.2421E 06	98.3	0.560	0.770	1.8542	0.4688
70- 3	0.2374E 06	97.4	0.015	0.253	2.0417	0.5391
70- 4	0.2374E 06	100.2	0.253	0.506	1.9271	0.5606
71- 4	0.2413E 06	100.5	0.156	0.437	1.9271	0.5602
71- 5	0.2413E 06	99.7	0.437	0.693	1.8542	0.4672
72- 4	0.2380E 06	98.8	0.051	0.354	1.9271	0.5013
72- 5	0.2380E 06	99.7	0.354	0.641	1.8542	1.4413
78- 2	0.2462E 06	100.2	0.076	0.199	2.0208	0.4259
78- 3	0.2462E 06	99.6	0.199	0.320	2.0417	0.4860
78- 4	0.2462E 06	99.0	0.320	0.442	1.9271	0.3670
78- 5	0.2462E 06	98.3	0.442	0.563	1.8542	0.4619
79- 2	0.2419E 06	99.9	0.101	0.257	2.0208	0.4772
79- 3	0.2419E 06	99.2	0.257	0.414	2.0417	0.4904
79- 4	0.2419E 06	98.6	0.414	0.569	1.9271	0.4650
79- 5	0.2419E 06	97.8	0.569	0.716	1.8542	0.4190
80- 2	0.2424E 06	99.8	0.104	0.277	2.0208	0.4307
80- 3	0.2424E 06	99.1	0.277	0.450	2.0417	0.7254
80- 4	0.2424E 06	98.4	0.450	0.621	1.9271	0.3246
80- 5	0.2424E 06	97.4	0.621	0.783	1.8542	0.4663
81- 2	0.2432E 06	100.0	0.124	0.313	2.0208	0.4307
81- 3	0.2432E 06	99.2	0.313	0.499	2.0417	0.5846
81- 4	0.2432E 06	98.4	0.499	0.683	1.9271	0.5123
82- 2	0.2478E 06	100.1	0.118	0.309	2.0208	0.4780

Table F-3 (continued)

RUN #	G (LBM/HR-SQ FT)	T BOIL (DEG F)	X IN	X OUT	LENGTH (FT)	ΔP TOTAL (PSI)
82- 3	0.2478E 06	99.2	0.309	0.501	2.0417	0.5851
82- 4	0.2478E 06	98.3	0.501	0.692	1.9271	0.5127
278- 2	0.2336E 06	101.1	0.081	0.275	2.0208	0.4799
278- 3	0.2336E 06	100.9	0.275	0.471	2.0417	0.5870
278- 4	0.2336E 06	100.0	0.471	0.663	1.9271	0.4676
279- 2	0.2335E 06	101.3	0.094	0.294	2.0208	0.4611
279- 3	0.2335E 06	100.9	0.294	0.494	2.0417	0.5119
279- 4	0.2335E 06	100.0	0.494	0.693	1.9271	0.5614
280- 2	0.2349E 06	101.7	0.103	0.315	2.0208	0.4332
280- 3	0.2349E 06	101.2	0.315	0.527	2.0417	0.5872
280- 4	0.2349E 06	100.1	0.527	0.736	1.9271	0.5147
281- 2	0.2336E 06	102.2	0.127	0.359	2.0208	0.4669
281- 3	0.2336E 06	101.8	0.359	0.593	2.0417	0.5738
282- 2	0.2336E 06	101.6	0.170	0.433	2.0208	0.5605
282- 3	0.2336E 06	100.9	0.433	0.696	2.0417	0.6205
283- 2	0.2330E 06	101.7	0.192	0.483	2.0208	0.5697
284- 2	0.2326E 06	100.6	0.225	0.542	2.0208	0.6163

Table F-4

PRESSURE DROP -- EXPERIMENTAL DATA

$G \approx 0.47 \times 10^6$ lbm/hr-sq ft $T \approx 100°F$

RUN #	G (LBM/HR-SQ FT)	T BOIL (DEG F)	X IN	X OUT	LENGTH (FT)	ΔP TOTAL (PSI)
83- 3	0.4748E 06	99.2	0.017	0.036	2.0417	0.7712
83- 4	0.4748E 06	98.3	0.036	0.056	1.9271	0.6051
83- 5	0.4748E 06	97.3	0.056	0.075	1.8542	0.5122
84- 2	0.4801E 06	100.0	0.021	0.058	2.0208	0.7119
84- 3	0.4801E 06	98.8	0.058	0.091	2.0417	0.6782
84- 4	0.4801E 06	98.0	0.091	0.125	1.9271	0.6059
84- 5	0.4801E 06	97.1	0.125	0.159	1.8542	0.5129
85- 2	0.4740E 06	100.0	0.032	0.084	2.0208	0.6651
85- 3	0.4740E 06	98.9	0.084	0.134	2.0417	0.6782
85- 4	0.4740E 06	98.1	0.134	0.185	1.9271	0.6059
85- 5	0.4740E 06	97.1	0.185	0.234	1.8542	0.6068
86- 2	0.4738E 06	99.7	0.040	0.107	2.0208	0.7132
86- 3	0.4738E 06	98.6	0.107	0.173	2.0417	0.6325
86- 4	0.4738E 06	97.6	0.173	0.240	1.9271	0.7479
86- 5	0.4738E 06	96.5	0.240	0.305	1.8542	0.6080
87- 2	0.4651E 06	99.5	0.051	0.136	2.0208	0.7227
87- 3	0.4651E 06	98.4	0.136	0.218	2.0417	0.7546
87- 4	0.4651E 06	97.2	0.218	0.301	1.9271	0.7855
87- 5	0.4651E 06	96.0	0.301	0.382	1.8542	0.8333
88- 2	0.4755E 06	100.2	0.055	0.155	2.0208	0.7421
88- 3	0.4755E 06	99.0	0.155	0.253	2.0417	0.8773
88- 4	0.4755E 06	97.8	0.253	0.353	1.9271	0.8588
88- 5	0.4755E 06	96.3	0.353	0.447	1.8542	0.8903
89- 2	0.4672E 06	100.3	0.068	0.177	2.0208	0.7895
89- 3	0.4672E 06	98.9	0.177	0.284	2.0417	0.8871
89- 4	0.4672E 06	97.7	0.284	0.393	1.9271	0.9086
89- 5	0.4672E 06	96.1	0.393	0.494	1.8542	0.9751
90- 2	0.4709E 06	100.0	0.069	0.185	2.0208	0.8089
90- 3	0.4709E 06	98.8	0.185	0.301	2.0417	0.9535
90- 4	0.4709E 06	97.1	0.301	0.417	1.9271	0.9749
90- 5	0.4709E 06	95.5	0.417	0.523	1.8542	0.8912
91- 2	0.4723E 06	99.8	0.073	0.198	2.0208	0.8376
91- 3	0.4723E 06	98.0	0.198	0.321	2.0417	0.9822
91- 4	0.4723E 06	97.0	0.321	0.446	1.9271	1.0130
92- 2	0.4684E 06	100.1	0.070	0.192	2.0208	0.8088
92- 3	0.4684E 06	98.6	0.192	0.312	2.0417	0.9722
92- 4	0.4684E 06	97.1	0.312	0.434	1.9271	0.9936
93- 2	0.4714E 06	99.9	0.068	0.188	2.0208	0.8088
93- 3	0.4714E 06	98.3	0.188	0.303	2.0417	0.9534
93- 4	0.4714E 06	97.0	0.303	0.421	1.9271	0.9935

Table F-4 (continued)

RUN #	G (LBM/HR-SQ FT)	T BOIL (DEG F)	X IN	X OUT	LENGTH (FT)	ΔP TOTAL (PSI)
93- 5	0.4714E 06	95.2	0.421	0.529	1.8542	0.8817
149- 2	0.4570E 06	100.5	0.066	0.190	2.0208	0.8535
149- 3	0.4570E 06	99.6	0.190	0.316	2.0417	0.9136
149- 4	0.4570E 06	98.0	0.316	0.442	1.9271	1.0289
150- 2	0.4643E 06	99.5	0.075	0.209	2.0208	0.8088
150- 3	0.4643E 06	98.3	0.209	0.344	2.0417	1.0097
150- 4	0.4643E 06	96.8	0.344	0.478	1.9271	1.1250
151- 2	0.4542E 06	99.6	0.082	0.226	2.0208	0.8447
151- 3	0.4542E 06	98.3	0.226	0.371	2.0417	0.9987
153- 2	0.4576E 06	99.3	0.094	0.256	2.0208	0.9255
154- 2	0.4598E 06	99.3	0.100	0.278	2.0208	0.9908

Table F-5

PRESSURE DROP -- EXPERIMENTAL DATA

$G \approx 0.90 \times 10^6$ lbm/hr-sq ft $T \approx 100°F$

RUN #	G (LBM/HR-SQ FT)	T BOIL (DEG F)	X IN	X OUT	LENGTH (FT)	ΔP TOTAL (PSI)
23- 2	0.9174E 06	99.5	0.005	0.029	2.0208	0.9976
23- 3	0.9174E 06	99.6	0.029	0.057	2.0417	0.9639
23- 4	0.9174E 06	98.7	0.057	0.085	1.9271	0.8444
23- 5	0.9174E 06	98.0	0.085	0.115	1.8542	0.7513
24- 3	0.8971E 06	100.5	0.055	0.092	2.0417	1.0460
24- 4	0.8971E 06	99.5	0.092	0.132	1.9271	0.9741
24- 5	0.8971E 06	98.1	0.132	0.171	1.8542	0.9753
25- 3	0.9062E 06	99.5	0.015	0.029	2.0417	0.9560
25- 4	0.9062E 06	98.3	0.029	0.042	1.9271	0.8369
26- 2	0.9074E 06	99.1	0.019	0.042	2.0208	0.8997
26- 3	0.9074E 06	97.6	0.042	0.063	2.0417	0.8659
26- 4	0.9074E 06	96.5	0.063	0.085	1.9271	0.7936
26- 5	0.9074E 06	95.5	0.085	0.106	1.8542	0.7945
94- 2	0.8862E 06	100.6	0.006	0.022	2.0208	1.0410
94- 3	0.8862E 06	98.9	0.022	0.035	2.0417	0.8664
94- 4	0.8862E 06	97.8	0.035	0.051	1.9271	0.7472
94- 5	0.8862E 06	96.3	0.051	0.063	1.8542	0.7012
95- 2	0.8885E 06	99.9	0.007	0.030	2.0208	0.9468
95- 3	0.8885E 06	98.5	0.030	0.052	2.0417	0.8661
95- 4	0.8885E 06	97.3	0.052	0.076	1.9271	0.7938
95- 5	0.8885E 06	96.0	0.076	0.097	1.8542	0.7009
96- 2	0.8730E 06	100.0	0.019	0.051	2.0208	0.9000
96- 3	0.8730E 06	98.6	0.051	0.081	2.0417	0.8662
96- 4	0.8730E 06	97.4	0.081	0.112	1.9271	0.8878
96- 5	0.8730E 06	96.2	0.112	0.143	1.8542	0.7479
97- 2	0.8918E 06	99.9	0.022	0.062	2.0208	0.9494
97- 3	0.8918E 06	98.5	0.062	0.100	2.0417	1.0095
97- 4	0.8918E 06	97.1	0.100	0.141	1.9271	0.9843
97- 5	0.8918E 06	95.6	0.141	0.179	1.8542	0.9379
98- 2	0.8940E 06	100.2	0.024	0.072	2.0208	0.9973
98- 3	0.8940E 06	98.8	0.072	0.119	2.0417	1.1044
98- 4	0.8940E 06	97.3	0.119	0.168	1.9271	1.0788
98- 5	0.8940E 06	95.6	0.168	0.215	1.8542	1.0796
99- 2	0.8907E 06	100.2	0.028	0.084	2.0208	1.0417
99- 3	0.8907E 06	98.8	0.084	0.141	2.0417	1.2425
99- 4	0.8907E 06	97.1	0.141	0.199	1.9271	1.2171
99- 5	0.8907E 06	95.1	0.199	0.255	1.8542	1.3588
100- 2	0.8951E 06	100.1	0.031	0.098	2.0208	1.0887
100- 3	0.8951E 06	98.3	0.098	0.161	2.0417	1.3365
100- 4	0.8951E 06	96.7	0.161	0.229	1.9271	1.3111

Table F-5 (continued)

RUN #	G (LBM/HR-SQ FT)	T BOIL (DEG F)	X IN	X OUT	LENGTH (FT)	ΔP TOTAL (PSI)
100- 5	0.8951E 06	94.5	0.229	0.291	1.8542	1.4528
101- 3	0.8951E 06	98.8	0.101	0.171	2.0417	1.3839
101- 4	0.8951E 06	96.9	0.171	0.244	1.9271	1.4025
101- 5	0.8951E 06	94.6	0.244	0.311	1.8542	1.4974
102- 3	0.8962E 06	100.9	0.108	0.181	2.0417	1.3800
102- 4	0.8962E 06	99.1	0.181	0.259	1.9271	1.4017
102- 5	0.8962E 06	96.6	0.259	0.328	1.8542	1.4496
156- 2	0.9139E 06	104.0	0.019	0.096	2.0208	1.2221
156- 3	0.9139E 06	102.5	0.096	0.174	2.0417	1.4229
156- 4	0.9139E 06	100.6	0.174	0.252	1.9271	1.3978
157- 2	0.9217E 06	100.1	0.036	0.113	2.0208	1.2750
157- 3	0.9217E 06	98.5	0.113	0.191	2.0417	1.4758
158- 2	0.9261E 06	101.7	0.042	0.127	2.0208	1.2767
158- 3	0.9261E 06	99.8	0.127	0.210	2.0417	1.5245

Table F-6

PRESSURE DROP -- EXPERIMENTAL DATA

$G \approx 1.77 \times 10^6$ lbm/hr-sq ft T≈100°F

RUN #	G (LBM/HR-SQ FT)	T BOIL (DEG F)	X IN	X OUT	LENGTH (FT)	ΔP TOTAL (PSI)
103- 4	0.1787E 07	99.6	0.006	0.025	1.9271	1.7874
103- 5	0.1787E 07	96.5	0.025	0.042	1.8542	1.3848
104- 3	0.1766E 07	99.8	0.003	0.023	2.0417	1.7301
104- 4	0.1766E 07	97.2	0.023	0.044	1.9271	1.7610
104- 5	0.1766E 07	94.5	0.044	0.065	1.8542	1.5460
105- 3	0.1756E 07	100.5	0.007	0.029	2.0417	1.8071
105- 4	0.1756E 07	98.2	0.029	0.055	1.9271	1.7346
105- 5	0.1756E 07	95.5	0.055	0.080	1.8542	1.6604
106- 3	0.1760E 07	102.3	0.013	0.040	2.0417	2.0426
106- 4	0.1760E 07	99.8	0.040	0.070	1.9271	1.6415
106- 5	0.1760E 07	97.2	0.070	0.100	1.8542	1.8958
107- 3	0.1819E 07	106.0	0.013	0.046	2.0417	1.9299
107- 4	0.1819E 07	103.2	0.046	0.081	1.9271	1.6707

Table F-7

PRESSURE DROP -- EXPERIMENTAL DATA

$G \approx 0.12 \times 10^6$ lbm/hr-sq ft T ≈ 150°F

RUN #	G (LBM/HR-SQ FT)	T BOIL (DEG F)	X IN	X OUT	LENGTH (FT)	ΔP TOTAL (PSI)
27- 2	0.1184E 06	149.1	0.101	0.249	2.0208	0.4269
27- 3	0.1184E 06	148.3	0.249	0.391	2.0417	0.3461
27- 4	0.1184E 06	148.4	0.391	0.532	1.9271	0.2271
27- 5	0.1184E 06	148.3	0.532	0.670	1.8542	0.1812
28- 2	0.1166E 06	148.4	0.157	0.376	2.0208	0.3347
28- 3	0.1166E 06	147.6	0.376	0.589	2.0417	0.3009
28- 4	0.1166E 06	147.6	0.589	0.801	1.9271	0.1349
29- 2	0.1139E 06	149.7	0.178	0.420	2.0208	0.3102
29- 3	0.1139E 06	149.0	0.420	0.662	2.0417	0.2013
29- 4	0.1139E 06	149.0	0.662	0.904	1.9271	0.1101
30- 2	0.1148E 06	150.7	0.151	0.382	2.0208	0.3707
30- 3	0.1148E 06	150.0	0.382	0.611	2.0417	0.2468
30- 4	0.1148E 06	150.0	0.611	0.836	1.9271	0.1772
31- 2	0.1158E 06	149.1	0.013	0.085	2.0208	0.7582
31- 3	0.1158E 06	148.7	0.085	0.156	2.0417	0.5366
31- 4	0.1158E 06	148.4	0.156	0.226	1.9271	0.4174
31- 5	0.1158E 06	148.3	0.226	0.295	1.8542	0.3715
108- 2	0.1098E 06	148.9	0.110	0.263	2.0208	0.4390
108- 3	0.1098E 06	148.3	0.263	0.413	2.0417	0.3439
108- 4	0.1098E 06	148.2	0.413	0.567	1.9271	0.2297
108- 5	0.1098E 06	147.9	0.567	0.711	1.8542	0.2306
109- 2	0.1123E 06	149.5	0.163	0.385	2.0208	0.3545
109- 3	0.1123E 06	149.1	0.385	0.605	2.0417	0.2550
109- 4	0.1123E 06	149.1	0.605	0.811	1.9271	0.1827
109- 5	0.1123E 06	148.7	0.811	1.019	1.8542	0.1367
110- 2	0.1096E 06	148.9	0.179	0.430	2.0208	0.3365
110- 3	0.1096E 06	148.5	0.430	0.676	2.0417	0.2558
110- 4	0.1096E 06	148.4	0.676	0.921	1.9271	0.1365
286- 2	0.1329E 06	149.4	0.160	0.409	2.0208	0.3489
286- 3	0.1329E 06	148.7	0.409	0.656	2.0417	0.2588
286- 4	0.1329E 06	148.5	0.656	0.898	1.9271	0.2051
287- 2	0.1334E 06	149.8	0.178	0.449	2.0208	0.3341
287- 3	0.1334E 06	149.1	0.449	0.719	2.0417	0.2722
287- 4	0.1334E 06	148.9	0.719	0.984	1.9271	0.1931
288- 2	0.1279E 06	149.9	0.198	0.500	2.0208	0.3078
288- 3	0.1279E 06	149.4	0.500	0.803	2.0417	0.2553
289- 2	0.1297E 06	150.3	0.241	0.594	2.0208	0.2737
289- 3	0.1297E 06	149.8	0.594	0.947	2.0417	0.2464
290- 2	0.1288E 06	149.4	0.267	0.654	2.0208	0.2797
291- 2	0.1294E 06	150.2	0.325	0.782	2.0208	0.2469

Table F-8

PRESSURE DROP -- EXPERIMENTAL DATA

$G \approx 0.24 \times 10^6$ lbm/hr-sq ft $T \approx 150°F$

RUN #	G (LBM/HR-SQ FT)	T BOIL (DEG F)	X IN	X OUT	LENGTH (FT)	ΔP TOTAL (PSI)
32- 3	0.2375E 06	148.9	0.033	0.069	2.0417	0.6830
32- 4	0.2375E 06	148.8	0.069	0.105	1.9271	0.5732
32- 5	0.2375E 06	148.5	0.105	0.139	1.8542	0.4661
33- 2	0.2377E 06	149.4	0.042	0.115	2.0208	0.5317
33- 3	0.2377E 06	148.5	0.115	0.187	2.0417	0.5542
33- 4	0.2377E 06	148.4	0.187	0.259	1.9271	0.3694
33- 5	0.2377E 06	148.3	0.259	0.329	1.8542	0.2765
34- 2	0.2477E 06	150.0	0.021	0.126	2.0208	0.5788
34- 3	0.2477E 06	149.0	0.126	0.228	2.0417	0.4606
34- 4	0.2477E 06	148.9	0.228	0.328	1.9271	0.3602
34- 5	0.2477E 06	148.9	0.328	0.428	1.8542	0.3236
35- 2	0.2493E 06	149.7	0.088	0.229	2.0208	0.4572
35- 3	0.2493E 06	148.6	0.229	0.365	2.0417	0.3765
35- 4	0.2493E 06	148.5	0.365	0.501	1.9271	0.3512
35- 5	0.2493E 06	148.5	0.501	0.631	1.8542	0.2677
36- 2	0.2383E 06	149.7	0.127	0.310	2.0208	0.4289
36- 3	0.2383E 06	148.4	0.310	0.486	2.0417	0.4045
36- 4	0.2383E 06	148.5	0.486	0.662	1.9271	0.3792
36- 5	0.2383E 06	148.3	0.662	0.833	1.8542	0.2206
37- 2	0.2294E 06	149.2	0.144	0.342	2.0208	0.4001
37- 3	0.2294E 06	148.0	0.342	0.535	2.0417	0.3288
37- 4	0.2294E 06	148.0	0.535	0.727	1.9271	0.3129
38- 2	0.2321E 06	150.0	0.184	0.374	2.0208	0.3507
38- 3	0.2321E 06	148.9	0.374	0.561	2.0417	0.3451
38- 4	0.2321E 06	148.8	0.561	0.745	1.9271	0.3387
39- 2	0.2289E 06	149.8	0.179	0.368	2.0208	0.3586
39- 3	0.2289E 06	148.6	0.368	0.552	2.0417	0.3623
39- 4	0.2289E 06	148.6	0.552	0.735	1.9271	0.2528
40- 2	0.2248E 06	149.5	0.177	0.362	2.0208	0.3880
40- 3	0.2248E 06	148.3	0.362	0.541	2.0417	0.3354
40- 4	0.2248E 06	148.2	0.541	0.717	1.9271	0.2822
111- 2	0.2236E 06	150.1	0.079	0.233	2.0208	0.4397
111- 3	0.2236E 06	149.3	0.233	0.381	2.0417	0.3590
111- 4	0.2236E 06	149.2	0.381	0.530	1.9271	0.3149
111- 5	0.2236E 06	148.8	0.530	0.671	1.8542	0.2783
112- 2	0.2207E 06	149.6	0.122	0.312	2.0208	0.4021
112- 3	0.2207E 06	148.8	0.312	0.499	2.0417	0.3683
112- 4	0.2207E 06	148.5	0.499	0.684	1.9271	0.2772
112- 5	0.2207E 06	148.2	0.684	0.861	1.8542	0.2781
113- 2	0.2204E 06	149.9	0.130	0.342	2.0208	0.4031

Table F-8 (continued)

RUN #	G (LBM/HR-SQ FT)	T BOIL (DEG F)	X IN	X OUT	LENGTH (FT)	ΔP TOTAL (PSI)
113- 3	0.2204E 06	149.0	0.342	0.550	2.0417	0.3599
113- 4	0.2204E 06	148.8	0.550	0.756	1.9271	0.2876
293- 2	0.2433E 06	149.4	0.051	0.223	2.0208	0.4700
293- 3	0.2433E 06	149.3	0.223	0.395	2.0417	0.4081
293- 4	0.2433E 06	148.8	0.395	0.564	1.9271	0.3544
293- 5	0.2433E 06	148.7	0.564	0.726	1.8542	0.2990
294- 2	0.2526E 06	149.3	0.093	0.292	2.0208	0.4239
294- 3	0.2526E 06	149.0	0.292	0.492	2.0417	0.4277
294- 4	0.2526E 06	148.4	0.492	0.689	1.9271	0.3458
295- 2	0.2524E 06	149.9	0.138	0.351	2.0208	0.4234
295- 3	0.2524E 06	149.6	0.351	0.564	2.0417	0.4178
295- 4	0.2524E 06	149.0	0.564	0.774	1.9271	0.3547
296- 2	0.2362E 06	149.4	0.131	0.369	2.0208	0.4030
296- 3	0.2362E 06	149.2	0.369	0.609	2.0417	0.3880
297- 2	0.2349E 06	149.7	0.102	0.385	2.0208	0.4104
297- 3	0.2349E 06	149.5	0.385	0.670	2.0417	0.4329
298- 2	0.2403E 06	150.0	0.110	0.426	2.0208	0.4272
299- 2	0.2385E 06	149.0	0.143	0.495	2.0208	0.4549

Table F-9

PRESSURE DROP -- EXPERIMENTAL DATA

$G \approx 0.44 \times 10^6$ lbm/hr-sq ft $T \approx 150°F$

RUN #	G (LBM/HR-SQ FT)	T BOIL (DEG F)	X IN	X OUT	LENGTH (FT)	ΔP TOTAL (PSI)
114- 3	0.4466E 06	149.3	0.022	0.043	2.0417	0.7990
114- 4	0.4466E 06	148.6	0.043	0.065	1.9271	0.6892
114- 5	0.4466E 06	148.1	0.065	0.086	1.8542	0.5681
115- 2	0.4493E 06	149.6	0.034	0.073	2.0208	0.7378
115- 3	0.4493E 06	149.0	0.073	0.112	2.0417	0.6570
115- 4	0.4493E 06	148.6	0.112	0.151	1.9271	0.5473
115- 5	0.4493E 06	148.0	0.151	0.188	1.8542	0.5108
116- 2	0.4471E 06	149.3	0.032	0.091	2.0208	0.6905
116- 3	0.4471E 06	148.8	0.091	0.148	2.0417	0.6285
116- 4	0.4471E 06	148.4	0.148	0.206	1.9271	0.5094
116- 5	0.4471E 06	147.8	0.206	0.262	1.8542	0.5105
117- 2	0.4412E 06	149.5	0.053	0.132	2.0208	0.6710
117- 3	0.4412E 06	148.7	0.132	0.207	2.0417	0.5902
117- 4	0.4412E 06	148.4	0.207	0.284	1.9271	0.5557
117- 5	0.4412E 06	147.8	0.284	0.356	1.8542	0.5098
118- 2	0.4389E 06	148.6	0.061	0.161	2.0208	0.6628
118- 3	0.4389E 06	147.9	0.161	0.256	2.0417	0.6102
118- 4	0.4389E 06	147.5	0.256	0.353	1.9271	0.5381
118- 5	0.4389E 06	146.8	0.353	0.445	1.8542	0.5391
119- 2	0.4405E 06	148.5	0.074	0.191	2.0208	0.6495
119- 3	0.4405E 06	147.7	0.191	0.305	2.0417	0.6064
119- 4	0.4405E 06	147.2	0.305	0.420	1.9271	0.5621
119- 5	0.4405E 06	146.5	0.420	0.526	1.8542	0.5066
120- 2	0.4378E 06	150.6	0.087	0.225	2.0208	0.6780
120- 3	0.4378E 06	149.9	0.225	0.360	2.0417	0.6254
120- 4	0.4378E 06	149.2	0.360	0.495	1.9271	0.5529
121- 3	0.4389E 06	149.0	0.224	0.354	2.0417	0.6362
121- 4	0.4389E 06	148.4	0.354	0.484	1.9271	0.5448
163- 2	0.4477E 06	149.6	0.082	0.212	2.0208	0.6558
163- 3	0.4477E 06	149.3	0.212	0.344	2.0417	0.6502
163- 4	0.4477E 06	148.5	0.344	0.474	1.9271	0.5591
164- 2	0.4532E 06	150.4	0.077	0.215	2.0208	0.6367
164- 3	0.4532E 06	149.9	0.215	0.353	2.0417	0.6686
164- 4	0.4532E 06	149.1	0.353	0.489	1.9271	0.5588
165- 2	0.4537E 06	149.0	0.125	0.270	2.0208	0.6556
165- 3	0.4537E 06	148.4	0.270	0.415	2.0417	0.6688
166- 2	0.4523E 06	148.8	0.132	0.290	2.0208	0.7022
166- 3	0.4523E 06	148.4	0.290	0.449	2.0417	0.6403
167- 2	0.4562E 06	148.6	0.144	0.314	2.0208	0.6819
168- 2	0.4492E 06	147.3	0.137	0.324	2.0208	0.7001

Table F-10

PRESSURE DROP -- EXPERIMENTAL DATA

$G \approx 0.87 \times 10^6$ lbm/hr-sq ft T≈150°F

RUN #	G (LBM/HR-SQ FT)	T BOIL (DEG F)	X IN	X OUT	LENGTH (FT)	ΔP TOTAL (PSI)
41- 2	0.8609E 06	149.2	0.013	0.032	2.0208	0.9473
41- 3	0.8609E 06	147.4	0.032	0.044	2.0417	0.8478
41- 4	0.8609E 06	146.9	0.044	0.056	1.9271	0.8036
41- 5	0.8609E 06	146.5	0.056	0.068	1.8542	0.6544
42- 3	0.8378E 06	148.4	0.020	0.042	2.0417	0.8374
42- 4	0.8378E 06	148.0	0.042	0.065	1.9271	0.7181
42- 5	0.8378E 06	147.5	0.065	0.087	1.8542	0.6346
43- 2	0.8739E 06	151.4	0.014	0.049	2.0208	0.8863
43- 3	0.8739E 06	150.3	0.049	0.080	2.0417	0.7961
43- 4	0.8739E 06	149.9	0.080	0.111	1.9271	0.7334
43- 5	0.8739E 06	149.4	0.111	0.140	1.8542	0.6406
44- 2	0.8817E 06	150.7	0.021	0.066	2.0208	0.8765
44- 3	0.8817E 06	149.5	0.066	0.106	2.0417	0.7864
44- 4	0.8817E 06	149.1	0.106	0.146	1.9271	0.7519
44- 5	0.8817E 06	148.7	0.146	0.186	1.8542	0.6779
45- 2	0.8272E 06	150.5	0.027	0.083	2.0208	0.8295
45- 3	0.8272E 06	149.4	0.083	0.136	2.0417	0.7863
45- 4	0.8272E 06	149.0	0.136	0.189	1.9271	0.7236
45- 5	0.8272E 06	148.5	0.189	0.239	1.8542	0.6778
46- 2	0.8460E 06	150.1	0.056	0.125	2.0208	0.8492
46- 3	0.8460E 06	148.6	0.125	0.187	2.0417	0.8341
46- 4	0.8460E 06	148.2	0.187	0.248	1.9271	0.7808
46- 5	0.8460E 06	147.7	0.248	0.306	1.8542	0.6974
47- 2	0.8558E 06	149.3	0.067	0.145	2.0208	0.8686
47- 3	0.8558E 06	147.5	0.145	0.216	2.0417	0.8724
47- 4	0.8558E 06	147.1	0.216	0.286	1.9271	0.8190
47- 5	0.8558E 06	146.6	0.286	0.351	1.8542	0.6980
48- 2	0.8786E 06	150.3	0.051	0.127	2.0208	0.8935
48- 3	0.8786E 06	148.6	0.127	0.195	2.0417	0.8879
48- 4	0.8786E 06	148.3	0.195	0.263	1.9271	0.8530
48- 5	0.8786E 06	147.9	0.263	0.328	1.8542	0.7130
49- 2	0.8718E 06	150.5	0.056	0.140	2.0208	0.9144
49- 3	0.8718E 06	149.0	0.140	0.220	2.0417	0.8993
49- 4	0.8718E 06	148.6	0.220	0.299	1.9271	0.8929
50- 2	0.8491E 06	150.4	0.053	0.139	2.0208	0.8825
50- 3	0.8491E 06	148.7	0.139	0.219	2.0417	0.8864
50- 4	0.8491E 06	148.3	0.219	0.297	1.9271	0.8421
51- 2	0.8418E 06	150.0	0.053	0.137	2.0208	0.8714
51- 3	0.8418E 06	148.4	0.137	0.215	2.0417	0.8939
51- 4	0.8418E 06	147.9	0.215	0.291	1.9271	0.8216

Table F-10 (continued)

RUN #	G (LBM/HR-SQ FT)	T BOIL (DEG F)	X IN	X OUT	LENGTH (FT)	ΔP TOTAL (PSI)
52- 2	0.8345E 06	150.8	0.045	0.126	2.0208	0.8824
52- 3	0.8345E 06	149.4	0.126	0.203	2.0417	0.8674
52- 4	0.8345E 06	148.9	0.203	0.277	1.9271	0.8044
122- 2	0.8703E 06	149.8	0.045	0.115	2.0208	0.8914
122- 3	0.8703E 06	149.2	0.115	0.184	2.0417	0.8952
122- 4	0.8703E 06	148.5	0.184	0.255	1.9271	0.8416
122- 5	0.8703E 06	147.6	0.255	0.319	1.8542	0.7768
123- 2	0.8484E 06	149.8	0.049	0.127	2.0208	0.8836
123- 3	0.8484E 06	149.0	0.127	0.203	2.0417	0.9052
123- 4	0.8484E 06	148.3	0.203	0.282	1.9271	0.8149
123- 5	0.8484E 06	147.4	0.282	0.351	1.8542	0.6937
124- 2	0.8607E 06	149.5	0.050	0.128	2.0208	0.8830
124- 3	0.8607E 06	148.7	0.128	0.205	2.0417	0.8868
124- 4	0.8607E 06	147.9	0.205	0.282	1.9271	0.8143
301- 2	0.9124E 06	149.8	0.027	0.097	2.0208	0.9315
301- 3	0.9124E 06	149.4	0.097	0.170	2.0417	0.9823
301- 4	0.9124E 06	148.5	0.170	0.241	1.9271	0.8534
301- 5	0.9124E 06	147.8	0.241	0.305	1.8542	0.7885
302- 2	0.9054E 06	150.1	0.027	0.102	2.0208	0.9333
302- 3	0.9054E 06	149.6	0.102	0.179	2.0417	0.9652
302- 4	0.9054E 06	148.6	0.179	0.254	1.9271	0.8457
303- 2	0.8985E 06	149.6	0.042	0.123	2.0208	0.9715
303- 3	0.8985E 06	148.9	0.123	0.205	2.0417	0.9753
303- 4	0.8985E 06	147.9	0.205	0.285	1.9271	0.9027
304- 2	0.9297E 06	149.6	0.025	0.108	2.0208	1.0182
304- 3	0.9297E 06	148.9	0.108	0.192	2.0417	0.9939
305- 2	0.9311E 06	150.8	0.021	0.110	2.0208	1.0159
306- 2	0.9451E 06	150.7	0.053	0.143	2.0208	0.9952
307- 2	0.9158E 06	149.2	0.031	0.124	2.0208	1.0217

Table F-11

PRESSURE DROP -- EXPERIMENTAL DATA

$G \approx 1.70 \times 10^6$ lbm/hr-sq ft T≈150°F

RUN #	G (LBM/HR-SQ FT)	T BOIL (DEG F)	X IN	X OUT	LENGTH (FT)	ΔP TOTAL (PSI)
125- 2	0.1696E 07	149.7	0.003	0.014	2.0208	1.3500
125- 3	0.1696E 07	148.6	0.014	0.025	2.0417	1.2505
125- 4	0.1696E 07	147.3	0.025	0.036	1.9271	1.1783
125- 5	0.1696E 07	146.3	0.036	0.045	1.8542	0.9821
126- 2	0.1701E 07	150.5	0.005	0.019	2.0208	1.3313
126- 3	0.1701E 07	149.8	0.019	0.035	2.0417	1.2693
126- 4	0.1701E 07	148.6	0.035	0.051	1.9271	1.2346
126- 5	0.1701E 07	147.5	0.051	0.066	1.8542	1.0384
127- 2	0.1706E 07	149.5	0.008	0.029	2.0208	1.3435
127- 3	0.1706E 07	148.4	0.029	0.049	2.0417	1.3003
127- 4	0.1706E 07	147.3	0.049	0.069	1.9271	1.2936
127- 5	0.1706E 07	146.3	0.069	0.090	1.8542	1.0973
128- 2	0.1685E 07	150.8	0.013	0.040	2.0208	1.3629
128- 3	0.1685E 07	149.5	0.040	0.064	2.0417	1.3292
128- 4	0.1685E 07	148.5	0.064	0.091	1.9271	1.3130
128- 5	0.1685E 07	147.2	0.091	0.116	1.8542	1.1730
129- 2	0.1663E 07	151.6	0.014	0.045	2.0208	1.3905
129- 3	0.1663E 07	150.6	0.045	0.076	2.0417	1.3943
129- 4	0.1663E 07	149.3	0.076	0.107	1.9271	1.3312
129- 5	0.1663E 07	148.2	0.107	0.136	1.8542	1.2382
130- 2	0.1656E 07	150.1	0.020	0.058	2.0208	1.2482
130- 3	0.1656E 07	148.8	0.058	0.094	2.0417	1.4772
130- 4	0.1656E 07	147.6	0.094	0.131	1.9271	1.4518
130- 5	0.1656E 07	146.3	0.131	0.164	1.8542	1.2649
131- 2	0.1696E 07	149.1	0.023	0.066	2.0208	1.4827
131- 3	0.1696E 07	147.6	0.066	0.106	2.0417	1.6179
131- 4	0.1696E 07	146.3	0.106	0.148	1.9271	1.5456
131- 5	0.1696E 07	144.9	0.148	0.185	1.8542	1.4056
132- 3	0.1691E 07	148.4	0.076	0.120	2.0417	1.4784
132- 4	0.1691E 07	147.3	0.120	0.167	1.9271	1.4342
132- 5	0.1691E 07	145.8	0.167	0.209	1.8542	1.3599
133- 2	0.1671E 07	150.2	0.027	0.079	2.0208	1.5303
133- 3	0.1671E 07	148.6	0.079	0.125	2.0417	1.4309
133- 4	0.1671E 07	147.6	0.125	0.175	1.9271	1.4242
134- 2	0.1674E 07	151.2	0.025	0.078	2.0208	1.5201
134- 3	0.1674E 07	149.5	0.078	0.126	2.0417	1.4206
134- 4	0.1674E 07	148.3	0.126	0.177	1.9271	1.5172
135- 2	0.1674E 07	150.9	0.026	0.078	2.0208	1.5228
135- 3	0.1674E 07	149.3	0.078	0.127	2.0417	1.4234
135- 4	0.1674E 07	148.1	0.127	0.177	1.9271	1.5198

Table F-11 (Continued)

RUN #	G (LBM/HR-SQ FT)	T BOIL (DEG F)	X IN	X OUT	LENGTH (FT)	ΔP TOTAL (PSI)
136- 2	0.1680E 07	151.5	0.023	0.073	2.0208	1.3685
136- 3	0.1680E 07	149.8	0.073	0.118	2.0417	1.4191
136- 4	0.1680E 07	148.8	0.118	0.167	1.9271	1.3938
136- 5	0.1680E 07	147.3	0.167	0.209	1.8542	1.3478
170- 3	0.1731E 07	149.2	0.063	0.110	2.0417	1.5974
170- 4	0.1731E 07	147.7	0.110	0.160	1.9271	1.5157
171- 2	0.1741E 07	150.6	0.024	0.076	2.0208	1.4608
171- 3	0.1741E 07	148.9	0.076	0.124	2.0417	1.5397
172- 2	0.1747E 07	155.1	0.028	0.080	2.0208	1.6109
172- 3	0.1747E 07	154.0	0.080	0.132	2.0417	1.5865
173- 2	0.1760E 07	152.9	0.023	0.077	2.0208	1.7319
173- 3	0.1760E 07	151.8	0.077	0.129	2.0417	1.6418
174- 2	0.1749E 07	149.4	0.026	0.080	2.0208	1.7220
175- 2	0.1740E 07	146.7	0.029	0.082	2.0208	1.6958

Table F-12

PRESSURE DROP -- EXPERIMENTAL DATA

$G \approx 3.44 \times 10^6$ lbm/hr-sq ft $T \approx 150°F$

RUN #	G (LBM/HR-SQ FT)	T BOIL (DEG F)	X IN	X OUT	LENGTH (FT)	ΔP TOTAL (PSI)
137- 3	0.3406E 07	152.0	0.002	0.014	2.0417	2.2680
137- 4	0.3406E 07	149.9	0.014	0.028	1.9271	2.4776
138- 3	0.3459E 07	150.5	0.002	0.016	2.0417	2.4023
139- 3	0.3471E 07	151.4	0.000	0.015	2.0417	2.4041
140- 3	0.3449E 07	151.1	0.005	0.026	2.0417	2.4955

Table F-13

PRESSURE DROP -- EXPERIMENTAL DATA

$G \approx 0.12 \times 10^6$ lbm/hr-sq ft T≈200°F

RUN #	G (LBM/HR-SQ FT)	T BOIL (DEG F)	X IN	X OUT	LENGTH (FT)	ΔP TOTAL (PSI)
253- 3	0.1126E 06	195.3	0.085	0.171	2.0417	0.6360
253- 4	0.1126E 06	195.1	0.171	0.256	1.9271	0.4883
253- 5	0.1126E 06	194.8	0.256	0.329	1.8542	0.4609
254- 2	0.1176E 06	199.0	0.029	0.189	2.0208	0.6156
254- 3	0.1176E 06	199.1	0.189	0.355	2.0417	0.4598
254- 4	0.1176E 06	199.0	0.355	0.515	1.9271	0.3590
254- 5	0.1176E 06	198.9	0.515	0.667	1.8542	0.2658
255- 2	0.1164E 06	198.4	0.044	0.288	2.0208	0.5313
255- 3	0.1164E 06	198.5	0.288	0.537	2.0417	0.3662
255- 4	0.1164E 06	198.4	0.537	0.778	1.9271	0.2560
255- 5	0.1164E 06	198.4	0.778	1.010	1.8542	0.1628
256- 2	0.1190E 06	199.6	0.053	0.334	2.0208	0.4756
256- 3	0.1190E 06	198.8	0.334	0.612	2.0417	0.3386
256- 4	0.1190E 06	198.6	0.612	0.882	1.9271	0.2096
257- 2	0.1183E 06	199.1	0.022	0.270	2.0208	0.5667
257- 3	0.1183E 06	200.6	0.270	0.534	2.0417	0.3640
257- 4	0.1183E 06	200.3	0.534	0.793	1.9271	0.2257
257- 5	0.1183E 06	200.3	0.793	1.042	1.8542	0.1795
335- 2	0.1362E 06	197.7	0.012	0.227	2.0208	0.5748
335- 3	0.1362E 06	199.4	0.227	0.461	2.0417	0.4002
335- 4	0.1362E 06	199.1	0.461	0.686	1.9271	0.2526
335- 5	0.1362E 06	199.1	0.686	0.901	1.8542	0.2065
336- 2	0.1364E 06	200.1	0.039	0.298	2.0208	0.4806
336- 3	0.1364E 06	200.7	0.298	0.563	2.0417	0.3530
336- 4	0.1364E 06	200.4	0.563	0.821	1.9271	0.2242
337- 2	0.1364E 06	200.2	0.058	0.346	2.0208	0.4620
337- 3	0.1364E 06	200.3	0.346	0.637	2.0417	0.3062
337- 4	0.1364E 06	200.0	0.637	0.923	1.9271	0.1868
338- 2	0.1334E 06	199.6	0.074	0.400	2.0208	0.4262
338- 3	0.1334E 06	199.5	0.400	0.732	2.0417	0.2705
339- 2	0.1313E 06	199.8	0.086	0.460	2.0208	0.4074
339- 3	0.1313E 06	199.8	0.460	0.841	2.0417	0.2517

Figure F-14

PRESSURE DROP -- EXPERIMENTAL DATA

$G \approx 0.24 \times 10^6$ lbm/hr-sq ft T≈200°F

RUN #	G (LBM/HR-SQ FT)	T BOIL (DEG F)	X IN	X OUT	LENGTH (FT)	ΔP TOTAL (PSI)
258- 2	0.2401E 06	200.2	0.048	0.170	2.0208	0.6006
258- 3	0.2401E 06	199.6	0.170	0.293	2.0417	0.4542
258- 4	0.2401E 06	199.4	0.293	0.413	1.9271	0.3631
258- 5	0.2401E 06	199.4	0.413	0.523	1.8542	0.2983
259- 3	0.2379E 06	199.6	0.269	0.413	2.0417	0.3310
259- 4	0.2379E 06	199.4	0.413	0.552	1.9271	0.2493
259- 5	0.2379E 06	199.5	0.552	0.685	1.8542	0.1845
260- 2	0.2368E 06	199.3	0.132	0.289	2.0208	0.4121
260- 3	0.2368E 06	198.9	0.289	0.442	2.0417	0.3220
260- 4	0.2368E 06	198.8	0.442	0.591	1.9271	0.2309
261- 3	0.2351E 06	198.2	0.303	0.464	2.0417	0.3237
261- 4	0.2351E 06	197.9	0.464	0.620	1.9271	0.2513
262- 3	0.2345E 06	198.5	0.308	0.474	2.0417	0.3517
343- 3	0.2505E 06	199.4	0.201	0.360	2.0417	0.4454
343- 4	0.2505E 06	199.0	0.360	0.514	1.9271	0.3166
343- 5	0.2505E 06	199.1	0.514	0.660	1.8542	0.2516
344- 2	0.2541E 06	200.9	0.084	0.258	2.0208	0.4768
344- 3	0.2541E 06	201.0	0.258	0.437	2.0417	0.3867
344- 4	0.2541E 06	200.5	0.437	0.613	1.9271	0.3051
345- 2	0.2588E 06	200.4	0.114	0.303	2.0208	0.4580
345- 3	0.2588E 06	200.3	0.303	0.491	2.0417	0.3772
345- 4	0.2588E 06	199.8	0.491	0.676	1.9271	0.2580
346- 3	0.2515E 06	200.4	0.354	0.573	2.0417	0.3196
347- 2	0.2426E 06	199.8	0.100	0.342	2.0208	0.4258
347- 3	0.2426E 06	199.8	0.342	0.586	2.0417	0.3169
348- 2	0.2433E 06	199.3	0.137	0.410	2.0208	0.4167
349- 2	0.2413E 06	199.4	0.157	0.467	2.0208	0.4212

Table F-15

PRESSURE DROP — EXPERIMENTAL DATA

$G \approx 0.92 \times 10^6$ lbm/hr-sq ft $T \approx 200°F$

RUN #	G (LBM/HR-SQ FT)	T BOIL (DEG F)	X IN	X OUT	LENGTH (FT)	ΔP TOTAL (PSI)
263- 3	0.9663E 06	201.9	0.057	0.086	2.0417	0.7252
263- 4	0.9663E 06	201.9	0.086	0.119	1.9271	0.6529
263- 5	0.9663E 06	201.5	0.119	0.149	1.8542	0.5881
264- 3	0.9202E 06	200.7	0.080	0.123	2.0417	0.7348
264- 4	0.9202E 06	200.5	0.123	0.165	1.9271	0.6719
264- 5	0.9202E 06	200.4	0.165	0.203	1.8542	0.5602
265- 2	0.9087E 06	200.8	0.036	0.091	2.0208	0.8145
265- 3	0.9087E 06	200.4	0.091	0.148	2.0417	0.7431
265- 4	0.9087E 06	199.9	0.148	0.201	1.9271	0.6615
265- 5	0.9087E 06	199.7	0.201	0.250	1.8542	0.5779
266- 2	0.9297E 06	199.6	0.042	0.107	2.0208	0.8053
266- 3	0.9297E 06	199.4	0.107	0.172	2.0417	0.7715
266- 4	0.9297E 06	198.9	0.172	0.235	1.9271	0.6523
267- 2	0.9354E 06	199.3	0.030	0.097	2.0208	0.8239
267- 3	0.9354E 06	199.0	0.097	0.163	2.0417	0.7713
267- 4	0.9354E 06	198.5	0.163	0.228	1.9271	0.6521
358- 2	0.9045E 06	200.4	0.059	0.127	2.0208	0.8085
358- 3	0.9045E 06	200.0	0.127	0.194	2.0417	0.7934
358- 4	0.9045E 06	199.5	0.194	0.258	1.9271	0.6182
359- 2	0.8868E 06	199.4	0.059	0.134	2.0208	0.8035
359- 3	0.8868E 06	198.6	0.134	0.204	2.0417	0.7885
359- 4	0.8868E 06	198.5	0.204	0.277	1.9271	0.6037
360- 2	0.8922E 06	198.6	0.059	0.140	2.0208	0.8143
360- 3	0.8922E 06	197.8	0.140	0.217	2.0417	0.8180
361- 2	0.8922E 06	200.1	0.054	0.144	2.0208	0.8061
361- 3	0.8922E 06	199.6	0.144	0.233	2.0417	0.8098

Table F-16

PRESSURE DROP -- EXPERIMENTAL DATA

$G \approx 1.70 \times 10^6$ lbm/hr-sq ft $T \approx 200°F$

RUN #	G (LBM/HR-SQ FT)	T BOIL (DEG F)	X IN	X OUT	LENGTH (FT)	ΔP TOTAL (PSI)
363- 2	0.1705E 07	196.8	0.010	0.034	2.0208	1.1844
363- 3	0.1705E 07	195.7	0.034	0.055	2.0417	1.2633
363- 4	0.1705E 07	195.0	0.055	0.074	1.9271	1.0781
363- 5	0.1705E 07	194.5	0.074	0.093	1.8542	0.8537
364- 2	0.1709E 07	198.0	0.013	0.041	2.0208	1.1659
364- 3	0.1709E 07	197.2	0.041	0.069	2.0417	1.3105
364- 4	0.1709E 07	196.2	0.069	0.093	1.9271	1.0315
364- 5	0.1709E 07	196.0	0.093	0.117	1.8542	0.8915
365- 2	0.1696E 07	200.6	0.021	0.056	2.0208	1.1755
365- 3	0.1696E 07	199.7	0.056	0.089	2.0417	1.3107
365- 4	0.1696E 07	198.9	0.089	0.119	1.9271	1.0505
365- 5	0.1696E 07	198.7	0.119	0.147	1.8542	0.9387
366- 2	0.1700E 07	200.6	0.014	0.053	2.0208	1.2039
366- 3	0.1700E 07	199.9	0.053	0.091	2.0417	1.3391
366- 4	0.1700E 07	199.0	0.091	0.127	1.9271	1.0789
366- 5	0.1700E 07	198.8	0.127	0.157	1.8542	0.9107
367- 2	0.1698E 07	200.5	0.011	0.053	2.0208	1.2227
367- 3	0.1698E 07	200.3	0.053	0.097	2.0417	1.3954
367- 4	0.1698E 07	199.4	0.097	0.140	1.9271	1.0976
368- 2	0.1714E 07	200.5	0.013	0.063	2.0208	1.2739
368- 3	0.1714E 07	200.2	0.063	0.113	2.0417	1.4185
369- 2	0.1728E 07	198.6	0.017	0.068	2.0208	1.3006

Table F-17

PRESSURE DROP — EXPERIMENTAL DATA

$G \approx 3.42 \times 10^6$ lbm/hr-sq ft T≈200°F

RUN #	G (LBM/HR-SQ FT)	T BOIL (DEG F)	X IN	X OUT	LENGTH (FT)	ΔP TOTAL (PSI)
371- 3	0.3444E 07	199.9	0.013	0.031	2.0417	2.5353
371- 4	0.3444E 07	198.5	0.031	0.044	1.9271	2.0887
371- 5	0.3444E 07	197.8	0.044	0.056	1.8542	1.6210
372- 3	0.3407E 07	201.1	0.016	0.034	2.0417	2.3317
372- 4	0.3407E 07	199.9	0.034	0.052	1.9271	2.3167
373- 3	0.3423E 07	199.0	0.021	0.043	2.0417	2.5925
374- 3	0.3362E 07	199.9	0.027	0.052	2.0417	2.6309
375- 3	0.3440E 07	200.8	0.025	0.053	2.0417	2.8937

Table F-18

PRESSURE DROP -- EXPERIMENTAL DATA

$G \approx 0.47 \times 10^6$ lbm/hr-sq ft $T \approx 250°F$

RUN #	G (LBM/HR-SQ FT)	T BOIL (DEG F)	X IN	X OUT	LENGTH (FT)	ΔP TOTAL (PSI)
377- 2	0.4869E 06	248.4	0.044	0.126	2.0208	0.7073
377- 3	0.4869E 06	247.7	0.126	0.201	2.0417	0.5983
377- 4	0.4869E 06	247.7	0.201	0.272	1.9271	0.4700
377- 5	0.4869E 06	248.0	0.272	0.343	1.8542	0.4148
387- 3	0.4495E 06	243.7	0.160	0.258	2.0417	0.5217
387- 4	0.4495E 06	243.4	0.258	0.350	1.9271	0.4117

Table F-19

PRESSURE DROP -- EXPERIMENTAL DATA

$G \approx 0.97 \times 10^6$ lbm/hr-sq ft T≈250°F

RUN #	G (LBM/HR-SQ FT)	T BOIL (DEG F)	X IN	X OUT	LENGTH (FT)	ΔP TOTAL (PSI)
378- 3	0.1003E 07	247.0	0.022	0.053	2.0417	0.8900
378- 4	0.1003E 07	247.5	0.053	0.090	1.9271	0.7522
378- 5	0.1003E 07	247.4	0.090	0.124	1.8542	0.6501
379- 2	0.9496E 06	249.4	0.022	0.079	2.0208	0.8407
379- 3	0.9496E 06	249.0	0.079	0.132	2.0417	0.7881
379- 4	0.9496E 06	249.1	0.132	0.185	1.9271	0.6596
379- 5	0.9496E 06	248.9	0.185	0.231	1.8542	0.5762
380- 3	0.9689E 06	248.5	0.047	0.111	2.0417	0.8168
380- 4	0.9689E 06	248.3	0.111	0.173	1.9271	0.6601
381- 3	0.9817E 06	245.9	0.062	0.136	2.0417	0.8078
382- 2	0.9554E 06	243.0	0.017	0.090	2.0208	0.8813

Table F-20

PRESSURE DROP -- CORRELATED RESULTS

$G \approx 0.12 \times 10^6$ lbm/hr-sq ft $T \approx 100°F$

RUN #	SQRT (X_{tt})	HOMOGENEOUS [3] MODEL			MARTINELLI-NELSON [4] MODEL			MARTINELLI-NELSON [4] MODEL WITH ZUBER ET AL [10] GENERAL VOID FRACTION MODEL		
		ΔP (ACC+GRAV) (PSI)	ΔP (FRICTION) (PSI)	Φ_{ftt}	ΔP (ACC+GRAV) (PSI)	ΔP (FRICTION) (PSI)	Φ_{ftt}	ΔP (ACC+GRAV) (PSI)	ΔP (FRICTION) (PSI)	Φ_{ftt}
1- 2	1.3310	0.2554	0.0054	16.823	0.4306	0.0105	11.263	0.5078	0.0076	7.615
1- 3	0.9589	0.1433	0.0086	16.017	0.3189	0.0177	8.938	0.3630	0.0134	5.956
1- 4	0.7811	0.0980	0.0108	16.675	0.2454	0.0230	9.913	0.2871	0.0162	6.884
1- 5	0.6663	0.0749	0.0127	17.320	0.2003	0.0279	10.790	0.2470	0.0174	6.930
3- 3	0.6061	0.0846	0.0147	20.461	0.2082	0.0328	14.988	0.2677	0.0180	11.454
3- 4	0.4660	0.0625	0.0183	17.323	0.1529	0.0425	8.869	0.2219	0.0167	*******
3- 5	0.3660	0.0519	0.0216	18.981	0.1206	0.0503	8.713	0.1780	0.0169	*******
4- 2	0.7249	0.1171	0.0125	14.437	0.2537	0.0269	6.121	0.3010	0.0175	*******
4- 3	0.4829	0.0785	0.0200	21.225	0.1763	0.0459	15.768	0.2468	0.0191	10.145
4- 4	0.3415	0.0625	0.0251	22.646	0.1314	0.0580	14.371	0.1867	0.0192	*******
4- 5	0.2260	0.0539	0.0296	50.437	0.1045	0.0644	42.376	0.1319	0.0211	37.282
5- 2	0.6764	0.1108	0.0135	15.607	0.2400	0.0295	8.498	0.2904	0.0182	2.337
5- 3	0.4474	0.0774	0.0214	20.671	0.1681	0.0495	14.694	0.2390	0.0192	7.130
5- 4	0.3053	0.0639	0.0268	26.906	0.1267	0.0614	18.917	0.1748	0.0199	8.817
5- 5	0.1771	0.0554	0.0316	53.193	0.0991	0.0643	37.417	0.1148	0.0237	29.811
6- 2	0.5991	0.0978	0.0157	15.081	0.2146	0.0350	7.178	0.2723	0.0191	*******
6- 3	0.4040	0.0735	0.0235	23.029	0.1564	0.0545	17.239	0.2246	0.0196	10.259
6- 4	0.2710	0.0615	0.0287	31.969	0.1188	0.0647	23.745	0.1589	0.0208	15.615
6- 5	0.1396	0.0512	0.0334	58.329	0.0845	0.0604	29.697	0.0928	0.0278	15.911
7- 2	0.6472	0.1043	0.0138	14.244	0.2293	0.0304	4.836	0.2837	0.0178	*******
7- 3	0.4353	0.0735	0.0210	21.743	0.1623	0.0490	15.685	0.2333	0.0184	8.056
7- 4	0.3001	0.0602	0.0259	28.347	0.1216	0.0595	20.302	0.1682	0.0192	10.741
8- 2	0.7616	0.1179	0.0115	14.488	0.2622	0.0247	6.075	0.3084	0.0167	*******
8- 3	0.5352	0.0793	0.0176	15.315	0.1878	0.0403	6.578	0.2550	0.0189	*******
8- 4	0.4013	0.0617	0.0218	21.482	0.1393	0.0509	14.839	0.2030	0.0182	4.727
8- 5	0.2990	0.0524	0.0255	27.028	0.1103	0.0586	18.747	0.1548	0.0190	7.798
53- 2	0.7298	0.1212	0.0121	14.460	0.2575	0.0262	6.064	0.3059	0.0169	*******
53- 3	0.4698	0.0797	0.0201	21.566	0.1746	0.0464	15.989	0.2455	0.0187	9.953
53- 4	0.3206	0.0632	0.0255	21.816	0.1292	0.0588	11.147	0.1802	0.0192	*******
53- 5	0.1946	0.0546	0.0302	60.250	0.1024	0.0627	49.401	0.1215	0.0221	44.317
54- 2	0.6748	0.1141	0.0135	19.918	0.2418	0.0296	15.016	0.2929	0.0180	12.529
54- 3	0.4324	0.0783	0.0220	23.182	0.1665	0.0511	17.758	0.2367	0.0192	11.772
54- 4	0.2846	0.0640	0.0278	29.086	0.1252	0.0631	20.182	0.1681	0.0203	9.985
55- 3	0.6665	0.1133	0.0137	16.038	0.2413	0.0300	9.143	0.2940	0.0180	3.469
55- 4	0.4293	0.0752	0.0206	22.137	0.1573	0.0479	16.280	0.2236	0.0178	9.139
55- 5	0.2839	0.0614	0.0263	35.934	0.1199	0.0597	29.105	0.1612	0.0192	23.103
56- 2	0.6116	0.1048	0.0147	15.729	0.2220	0.0328	8.104	0.2805	0.0178	*******
56- 3	0.3858	0.0753	0.0232	23.010	0.1555	0.0540	16.242	0.2214	0.0188	6.771
56- 4	0.2342	0.0628	0.0289	39.921	0.1181	0.0631	29.199	0.1481	0.0209	21.228
57- 3	0.6867	0.1203	0.0126	16.088	0.2506	0.0278	9.057	0.3038	0.0168	3.133

Table F-20 (continued)

RUN #	SQRT (X_{tt})	HOMOGENEOUS [3] MODEL ΔP (ACC+GRAV) (PSI)	HOMOGENEOUS [3] MODEL ΔP (FRICTION) (PSI)	HOMOGENEOUS [3] MODEL Φ_{ftt}	MARTINELLI-NELSON [4] MODEL ΔP (ACC+GRAV) (PSI)	MARTINELLI-NELSON [4] MODEL ΔP (FRICTION) (PSI)	MARTINELLI-NELSON [4] MODEL Φ_{ftt}	MARTINELLI-NELSON [4] MODEL WITH ZUBER ET AL [10] GENERAL VOID FRACTION MODEL ΔP (ACC+GRAV) (PSI)	MARTINELLI-NELSON [4] MODEL WITH ZUBER ET AL [10] GENERAL VOID FRACTION MODEL ΔP (FRICTION) (PSI)	MARTINELLI-NELSON [4] MODEL WITH ZUBER ET AL [10] GENERAL VOID FRACTION MODEL Φ_{ftt}
57- 4	0.4252	0.0765	0.0199	22.260	0.1579	0.0464	16.144	0.2241	0.0171	8.328
57- 5	0.2696	0.0620	0.0258	41.351	0.1184	0.0581	34.565	0.1560	0.0188	29.164
58- 3	0.6573	0.1170	0.0134	15.062	0.2417	0.0297	6.995	0.2973	0.0171	*******
58- 4	0.3997	0.0765	0.0210	18.489	0.1543	0.0489	9.271	0.2183	0.0173	*******
58- 5	0.2386	0.0635	0.0272	52.467	0.1180	0.0596	45.031	0.1479	0.0197	40.377
59- 3	1.0192	0.2623	0.0076	13.575	0.3975	0.0158	6.846	0.4653	0.0110	*******
59- 4	0.5353	0.0928	0.0158	17.722	0.1913	0.0362	11.042	0.2544	0.0168	*******
59- 5	0.3368	0.0688	0.0226	28.590	0.1340	0.0524	22.123	0.1863	0.0174	15.060
60- 3	0.6720	0.1271	0.0132	15.692	0.2517	0.0293	8.762	0.3067	0.0171	1.428
60- 4	0.3906	0.0804	0.0215	22.981	0.1567	0.0503	16.415	0.2189	0.0178	7.648
60- 5	0.2172	0.0663	0.0283	54.904	0.1191	0.0603	45.647	0.1429	0.0210	40.775
61- 3	0.5915	0.1138	0.0156	16.323	0.2261	0.0351	9.597	0.2864	0.0183	*******
61- 4	0.3430	0.0795	0.0241	29.500	0.1497	0.0558	23.594	0.2050	0.0188	17.601
62- 3	0.7265	0.1505	0.0117	17.596	0.2794	0.0256	12.018	0.3350	0.0154	8.562
62- 4	0.3858	0.0865	0.0213	20.291	0.1624	0.0497	11.964	0.2240	0.0175	*******
63- 4	0.3883	0.0879	0.0223	23.660	0.1650	0.0515	17.121	0.2272	0.0180	8.835
64- 4	0.4603	0.1074	0.0196	16.960	0.1922	0.0451	9.189	0.2554	0.0183	*******
65- 4	0.5831	0.1462	0.0146	15.004	0.2427	0.0331	7.793	0.3006	0.0161	*******
73- 2	1.5899	0.3520	0.0041	16.467	0.5055	0.0079	11.694	0.6186	0.0053	6.136
73- 3	1.0549	0.1651	0.0075	19.038	0.3480	0.0151	13.517	0.3961	0.0115	11.639
73- 4	0.8368	0.1061	0.0099	17.626	0.2617	0.0205	11.228	0.3015	0.0150	8.877
73- 5	0.7027	0.0792	0.0119	16.680	0.2111	0.0257	9.532	0.2548	0.0168	5.367
74- 2	0.9075	0.1455	0.0089	17.502	0.3085	0.0184	11.409	0.3547	0.0135	8.962
74- 3	0.6409	0.0892	0.0141	17.417	0.2190	0.0313	10.851	0.2740	0.0184	6.245
74- 4	0.4964	0.0654	0.0177	18.720	0.1617	0.0408	12.014	0.2293	0.0173	*******
74- 5	0.3954	0.0530	0.0209	24.496	0.1269	0.0487	18.693	0.1880	0.0171	11.936
75- 2	0.7296	0.1167	0.0120	16.621	0.2542	0.0260	10.070	0.3029	0.0168	6.283
75- 3	0.4903	0.0778	0.0190	19.056	0.1771	0.0439	12.555	0.2479	0.0184	3.319
75- 4	0.3488	0.0614	0.0238	22.850	0.1310	0.0553	14.785	0.1874	0.0185	*******
75- 5	0.2337	0.0532	0.0281	49.244	0.1034	0.0617	41.622	0.1322	0.0203	36.546
76- 2	0.6253	0.0999	0.0135	17.625	0.2213	0.0299	10.773	0.2801	0.0165	4.664
76- 3	0.4115	0.0714	0.0207	24.326	0.1560	0.0483	18.242	0.2262	0.0172	10.845
76- 4	0.2719	0.0574	0.0255	38.316	0.1147	0.0577	30.867	0.1555	0.0183	24.197
76- 5	0.1289	0.0435	0.0302	127.658	0.0739	0.0513	113.012	0.0815	0.0253	109.032
77- 2	0.6473	0.1066	0.0131	16.829	0.2305	0.0291	9.745	0.2870	0.0165	3.024
77- 3	0.4146	0.0742	0.0209	23.452	0.1594	0.0486	17.227	0.2296	0.0175	9.376
77- 4	0.2657	0.0607	0.0262	40.544	0.1183	0.0589	33.109	0.1573	0.0188	26.936
268- 2	0.9330	0.1794	0.0102	13.651	0.3317	0.0211	6.971	0.3755	0.0158	3.005
268- 3	0.5679	0.0957	0.0194	17.188	0.2069	0.0437	11.760	0.2665	0.0227	7.353
268- 4	0.3978	0.0725	0.0256	20.974	0.1506	0.0597	15.003	0.2121	0.0218	7.472

Table F-20 (continued)

RUN #	SQRT (X_{tt})	HOMOGENEOUS [3] MODEL			MARTINELLI-NELSON [4] MODEL			MARTINELLI-NELSON [4] MODEL WITH ZUBER ET AL [10] GENERAL VOID FRACTION MODEL		
		ΔP (ACC+GRAV) (PSI)	ΔP (FRICTION) (PSI)	Φ_{ftt}	ΔP (ACC+GRAV) (PSI)	ΔP (FRICTION) (PSI)	Φ_{ftt}	ΔP (ACC+GRAV) (PSI)	ΔP (FRICTION) (PSI)	Φ_{ftt}
268- 5	0.2757	0.0624	0.0312	37.602	0.1216	0.0706	31.509	0.1597	0.0233	26.879
269- 2	0.8236	0.1621	0.0115	12.602	0.3026	0.0243	3.829	0.3473	0.0170	*******
269- 3	0.4786	0.0919	0.0221	22.207	0.1872	0.0508	17.616	0.2550	0.0215	13.422
269- 4	0.3044	0.0744	0.0294	29.144	0.1414	0.0674	21.975	0.1879	0.0223	15.125
270- 2	0.7297	0.1393	0.0133	14.970	0.2692	0.0290	8.774	0.3154	0.0189	4.969
270- 3	0.4335	0.0888	0.0238	22.698	0.1767	0.0554	17.693	0.2447	0.0214	12.514
270- 4	0.2660	0.0723	0.0310	39.630	0.1340	0.0696	32.818	0.1711	0.0232	27.926
271- 3	0.3750	0.0846	0.0248	29.815	0.1637	0.0579	24.990	0.2268	0.0202	20.333
271- 4	0.1970	0.0708	0.0320	59.800	0.1261	0.0661	48.413	0.1461	0.0244	43.553
272- 2	0.5781	0.1131	0.0163	16.776	0.2216	0.0366	10.354	0.2818	0.0186	3.224
272- 3	0.3295	0.0826	0.0269	34.477	0.1563	0.0621	29.102	0.2120	0.0206	24.259
273- 2	0.5619	0.1123	0.0172	16.900	0.2176	0.0388	10.695	0.2787	0.0192	3.866
273- 3	0.3175	0.0845	0.0281	32.806	0.1570	0.0645	26.756	0.2097	0.0214	21.314
274- 2	0.4999	0.1093	0.0191	19.814	0.2047	0.0438	14.260	0.2700	0.0191	8.587
274- 3	0.2543	0.0876	0.0311	48.949	0.1569	0.0682	41.662	0.1934	0.0229	37.259
275- 2	0.4230	0.1060	0.0208	24.884	0.1908	0.0481	19.531	0.2567	0.0182	14.024
276- 2	0.3755	0.1143	0.0235	27.850	0.1945	0.0543	22.350	0.2550	0.0195	17.062

Table F-21

PRESSURE DROP -- CORRELATED RESULTS

$G \approx 0.24 \times 10^6$ lbm/hr-sq ft $T \approx 100°F$

RUN #	SQRT (X_{tt})	HOMOGENEOUS [3] MODEL			MARTINELLI-NELSON [4] MODEL			MARTINELLI-NELSON [4] MODEL WITH ZUBER ET AL [10] GENERAL VOID FRACTION MODEL		
		ΔP (ACC+GRAV) (PSI)	ΔP (FRICTION) (PSI)	Φ_{ftt}	ΔP (ACC+GRAV) (PSI)	ΔP (FRICTION) (PSI)	Φ_{ftt}	ΔP (ACC+GRAV) (PSI)	ΔP (FRICTION) (PSI)	Φ_{ftt}
9- 2	1.8848	0.4405	0.0109	7.506	0.5618	0.0208	5.024	0.6313	0.0167	2.729
9- 3	1.3760	0.2681	0.0169	9.168	0.4415	0.0332	6.104	0.4555	0.0314	5.785
9- 4	1.1278	0.1861	0.0211	8.334	0.3525	0.0424	4.318	0.3525	0.0426	4.319
9- 5	0.9671	0.1421	0.0254	9.638	0.2951	0.0520	6.384	0.2946	0.0522	6.398
10- 2	1.2626	0.2595	0.0199	7.609	0.4186	0.0390	3.858	0.4244	0.0387	3.646
10- 3	0.9254	0.1667	0.0310	9.145	0.3213	0.0636	6.025	0.3197	0.0638	6.065
10- 4	0.7528	0.1262	0.0387	9.043	0.2543	0.0824	5.806	0.2645	0.0737	5.469
10- 5	0.6383	0.1053	0.0459	10.476	0.2148	0.1009	7.726	0.2388	0.0757	6.978
11- 2	1.3790	0.3423	0.0169	6.618	0.4721	0.0332	3.061	0.4998	0.0314	1.418
11- 3	0.8799	0.1788	0.0321	9.292	0.3176	0.0671	6.497	0.3193	0.0650	6.454
11- 4	0.6762	0.1329	0.0427	10.112	0.2431	0.0937	7.497	0.2624	0.0749	6.939
11- 5	0.5515	0.1115	0.0522	11.033	0.2037	0.1184	8.407	0.2426	0.0719	7.010
12- 2	1.2615	0.3104	0.0195	7.229	0.4418	0.0387	4.116	0.4580	0.0378	3.547
12- 3	0.8032	0.1744	0.0371	9.563	0.3000	0.0787	7.028	0.3058	0.0728	6.889
12- 4	0.6095	0.1351	0.0494	10.539	0.2338	0.1102	8.087	0.2628	0.0776	7.208
12- 5	0.4881	0.1175	0.0605	14.169	0.2017	0.1394	12.057	0.2506	0.0707	10.639
13- 2	0.9527	0.2220	0.0291	8.789	0.3503	0.0598	6.220	0.3499	0.0592	6.227
13- 3	0.6599	0.1588	0.0479	10.657	0.2653	0.1056	8.445	0.2874	0.0818	7.909
13- 4	0.5068	0.1342	0.0610	11.891	0.2210	0.1399	9.485	0.2691	0.0747	7.836
13- 5	0.4021	0.1194	0.0727	18.057	0.2000	0.1695	15.829	0.2495	0.0734	14.290
14- 2	0.8759	0.2173	0.0330	8.923	0.3340	0.0688	6.555	0.3350	0.0662	6.532
14- 3	0.6007	0.1622	0.0543	10.975	0.2588	0.1213	8.836	0.2910	0.0833	8.000
14- 4	0.4541	0.1406	0.0687	16.080	0.2241	0.1591	14.123	0.2771	0.0752	12.725
14- 5	0.3482	0.1318	0.0821	20.490	0.2168	0.1908	17.640	0.2617	0.0770	15.928
15- 2	0.8288	0.2160	0.0354	8.313	0.3247	0.0746	5.794	0.3279	0.0697	5.704
15- 3	0.5624	0.1669	0.0581	12.372	0.2571	0.1314	10.489	0.2970	0.0818	9.537
15- 4	0.4168	0.1488	0.0737	17.325	0.2308	0.1715	15.227	0.2836	0.0761	13.706
15- 5	0.3080	0.1398	0.0882	25.351	0.2281	0.2031	22.125	0.2668	0.0795	20.550
16- 2	0.7801	0.2086	0.0376	9.654	0.3123	0.0805	7.561	0.3190	0.0722	7.404
16- 3	0.5297	0.1685	0.0610	13.020	0.2554	0.1390	11.123	0.3016	0.0794	9.968
16- 4	0.3875	0.1494	0.0770	17.572	0.2315	0.1794	15.110	0.2828	0.0761	13.343
16- 5	0.2806	0.1385	0.0916	25.176	0.2285	0.2083	20.739	0.2617	0.0805	18.839
17- 2	0.7952	0.2136	0.0378	8.454	0.3168	0.0806	6.082	0.3225	0.0731	5.925
17- 3	0.5411	0.1700	0.0609	12.611	0.2577	0.1388	10.729	0.3018	0.0816	9.644
17- 4	0.3984	0.1505	0.0768	18.069	0.2339	0.1792	15.829	0.2855	0.0776	14.269
17- 5	0.2907	0.1403	0.0915	25.580	0.2324	0.2090	21.630	0.2673	0.0817	19.930
18- 2	0.7776	0.2157	0.0377	8.579	0.3158	0.0807	6.217	0.3233	0.0716	6.001
18- 3	0.5210	0.1704	0.0615	13.115	0.2566	0.1408	11.184	0.3044	0.0786	9.954
18- 4	0.3773	0.1518	0.0778	19.347	0.2360	0.1815	16.910	0.2861	0.0762	15.276
19- 2	0.7546	0.2154	0.0392	9.654	0.3120	0.0844	7.682	0.3210	0.0735	7.471

Table F-21 (continued)

RUN #	SQRT (X_{tt})	HOMOGENEOUS [3] MODEL ΔP (ACC+GRAV) (PSI)	HOMOGENEOUS [3] MODEL ΔP (FRICTION) (PSI)	HOMOGENEOUS [3] MODEL Φ_{ftt}	MARTINELLI-NELSON [4] MODEL ΔP (ACC+GRAV) (PSI)	MARTINELLI-NELSON [4] MODEL ΔP (FRICTION) (PSI)	MARTINELLI-NELSON [4] MODEL Φ_{ftt}	MARTINELLI-NELSON [4] MODEL WITH ZUBER ET AL [10] GENERAL VOID FRACTION MODEL ΔP (ACC+GRAV) (PSI)	MARTINELLI-NELSON [4] MODEL WITH ZUBER ET AL [10] GENERAL VOID FRACTION MODEL ΔP (FRICTION) (PSI)	MARTINELLI-NELSON [4] MODEL WITH ZUBER ET AL [10] GENERAL VOID FRACTION MODEL Φ_{ftt}
19- 3	0.5043	0.1731	0.0638	12.375	0.2562	0.1466	10.311	0.3062	0.0789	8.839
19- 4	0.3612	0.1572	0.0804	21.397	0.2388	0.1876	19.108	0.2873	0.0776	17.607
20- 2	0.7436	0.2195	0.0411	7.445	0.3124	0.0883	4.738	0.3219	0.0761	4.369
20- 3	0.4942	0.1786	0.0668	15.149	0.2619	0.1534	13.471	0.3133	0.0804	12.320
20- 4	0.3502	0.1633	0.0847	21.688	0.2514	0.1969	19.069	0.2987	0.0800	17.504
21- 2	0.7705	0.2167	0.0392	9.397	0.3145	0.0839	7.345	0.3228	0.0737	7.143
21- 3	0.5150	0.1720	0.0639	13.103	0.2600	0.1463	11.081	0.3094	0.0795	9.766
21- 4	0.3707	0.1565	0.0808	16.670	0.2485	0.1878	13.293	0.2979	0.0777	11.064
22- 2	0.7941	0.2146	0.0358	8.680	0.3186	0.0769	6.310	0.3255	0.0691	6.121
22- 3	0.5337	0.1672	0.0585	13.536	0.2530	0.1344	11.769	0.2983	0.0780	10.720
22- 4	0.3896	0.1484	0.0739	17.013	0.2256	0.1734	14.643	0.2761	0.0750	12.857
22- 5	0.2802	0.1385	0.0879	27.576	0.2194	0.2009	23.981	0.2517	0.0795	22.384
68- 3	0.6117	0.1959	0.0530	11.995	0.2829	0.1190	10.331	0.3130	0.0826	9.689
68- 4	0.4262	0.1671	0.0724	17.592	0.2497	0.1690	15.607	0.3025	0.0766	14.190
68- 5	0.3026	0.1499	0.0891	20.023	0.2452	0.2047	15.028	0.2818	0.0811	12.593
69- 3	0.7498	0.2560	0.0407	9.949	0.3357	0.0879	8.441	0.3455	0.0744	8.237
69- 4	0.4605	0.2002	0.0669	14.736	0.2742	0.1550	12.888	0.3258	0.0757	11.421
69- 5	0.3058	0.1735	0.0879	22.898	0.2665	0.2021	18.951	0.3045	0.0800	17.079
70- 3	0.9607	0.3440	0.0296	7.675	0.4124	0.0614	6.185	0.4270	0.0564	5.817
70- 4	0.5234	0.2191	0.0582	14.109	0.2885	0.1327	12.594	0.3322	0.0743	11.538
71- 4	0.6197	0.2586	0.0493	11.673	0.3156	0.1097	10.511	0.3417	0.0756	9.936
71- 5	0.3723	0.2110	0.0783	16.906	0.2990	0.1819	13.697	0.3479	0.0757	11.535
72- 4	0.7727	0.3134	0.0364	8.332	0.3596	0.0786	7.235	0.3715	0.0640	6.925
72- 5	0.4202	0.2293	0.0687	32.720	0.3032	0.1598	31.708	0.3545	0.0716	30.985
78- 2	0.9584	0.2228	0.0305	7.652	0.3507	0.0625	4.658	0.3486	0.0627	4.721
78- 3	0.6704	0.1596	0.0496	11.075	0.2680	0.1086	9.051	0.2879	0.0862	8.628
78- 4	0.5190	0.1340	0.0627	11.320	0.2236	0.1431	8.880	0.2696	0.0791	7.317
78- 5	0.4143	0.1216	0.0747	16.973	0.2048	0.1738	14.754	0.2548	0.0767	13.241
79- 2	0.8314	0.2134	0.0354	9.261	0.3233	0.0748	7.074	0.3267	0.0698	6.995
79- 3	0.5684	0.1660	0.0575	12.356	0.2576	0.1299	10.467	0.2564	0.0820	9.555
79- 4	0.4233	0.1443	0.0727	16.093	0.2265	0.1693	13.879	0.2793	0.0760	12.247
79- 5	0.3190	0.1301	0.0863	21.393	0.2145	0.1997	18.000	0.2546	0.0789	16.138
80- 2	0.8030	0.2202	0.0370	8.363	0.3224	0.0787	6.000	0.3273	0.0718	5.861
80- 3	0.5375	0.1741	0.0610	16.716	0.2607	0.1391	15.346	0.3052	0.0813	14.593
80- 4	0.3906	0.1526	0.0779	12.764	0.2360	0.1818	9.162	0.2872	0.0778	8.948
80- 5	0.2821	0.1396	0.0926	26.745	0.2294	0.2111	22.775	0.2626	0.0823	21.119
81- 2	0.7436	0.2192	0.0414	8.626	0.3116	0.0893	6.474	0.3215	0.0766	6.197
81- 3	0.4960	0.1783	0.0667	15.224	0.2620	0.1535	13.564	0.3132	0.0809	12.442
81- 4	0.3530	0.1590	0.0843	20.445	0.2455	0.1962	17.765	0.2928	0.0804	16.113
82- 2	0.7541	0.2289	0.0418	9.155	0.3189	0.0900	7.317	0.3268	0.0786	7.133

Table F-21 (continued)

RUN #	SQRT (X_{tt})	HOMOGENEOUS [3] MODEL			MARTINELLI-NELSON [4] MODEL			MARTINELLI-NELSON [4] MODEL WITH ZUBER ET AL [10] GENERAL VOID FRACTION MODEL		
		ΔP (ACC+GRAV) (PSI)	ΔP (FRICTION) (PSI)	Φ_{ftt}	ΔP (ACC+GRAV) (PSI)	ΔP (FRICTION) (PSI)	Φ_{ftt}	ΔP (ACC+GRAV) (PSI)	ΔP (FRICTION) (PSI)	Φ_{ftt}
82- 3	0.4965	0.1873	0.0688	14.803	0.2695	0.1584	13.185	0.3201	0.0840	12.082
82- 4	0.3492	0.1695	0.0877	20.066	0.2579	0.2042	17.289	0.3047	0.0837	15.622
278- 2	0.8380	0.2364	0.0325	9.165	0.3366	0.0692	7.031	0.3432	0.0626	6.867
278- 3	0.5314	0.1768	0.0571	15.102	0.2627	0.1309	13.428	0.3091	0.0745	12.429
278- 4	0.3712	0.1546	0.0744	18.953	0.2390	0.1741	16.199	0.2885	0.0726	14.338
279- 2	0.7994	0.2293	0.0345	9.104	0.3266	0.0740	6.934	0.3351	0.0653	6.712
279- 3	0.5105	0.1768	0.0593	14.077	0.2616	0.1367	12.167	0.3112	0.0740	10.894
279- 4	0.3534	0.1566	0.0767	22.821	0.2420	0.1791	20.272	0.2893	0.0734	18.711
280- 2	0.7675	0.2313	0.0367	8.597	0.3229	0.0794	6.355	0.3333	0.0680	6.048
280- 3	0.4861	0.1819	0.0628	16.045	0.2654	0.1456	14.297	0.3180	0.0746	13.076
280- 4	0.3290	0.1630	0.0812	23.102	0.2529	0.1887	19.930	0.2966	0.0758	18.192
281- 2	0.7049	0.2296	0.0405	9.742	0.3133	0.0890	7.839	0.3302	0.0705	7.394
281- 3	0.4406	0.1884	0.0681	17.202	0.2729	0.1590	15.199	0.3285	0.0739	13.713
282- 2	0.6157	0.2331	0.0480	12.303	0.3066	0.1077	10.835	0.3364	0.0734	10.178
282- 3	0.3742	0.2043	0.0785	21.127	0.2971	0.1832	18.623	0.3503	0.0769	17.024
283- 2	0.5713	0.2431	0.0519	12.919	0.3123	0.1178	11.469	0.3493	0.0734	10.612
284- 2	0.5201	0.2541	0.0576	14.544	0.3215	0.1321	13.120	0.3664	0.0738	12.081

Table F-22

PRESSURE DROP -- CORRELATED RESULTS

$G \approx 0.47 \times 10^6$ lbm/hr-sq ft $T \approx 100°F$

RUN #	SQRT (X_{tt})	HOMOGENEOUS [3] MODEL			MARTINELLI-NELSON [4] MODEL			MARTINELLI-NELSON [4] MODEL WITH ZUBER ET AL [10] GENERAL VOID FRACTION MODEL		
		ΔP (ACC+GRAV) (PSI)	ΔP (FRICTION) (PSI)	Φ_{ftt}	ΔP (ACC+GRAV) (PSI)	ΔP (FRICTION) (PSI)	Φ_{ftt}	ΔP (ACC+GRAV) (PSI)	ΔP (FRICTION) (PSI)	Φ_{ftt}
83- 3	2.1152	0.5296	0.0340	4.170	0.6886	0.0567	2.439	0.7252	0.0515	1.820
83- 4	1.6314	0.3455	0.0453	4.531	0.5592	0.0768	1.905	0.5511	0.0832	2.066
83- 5	1.3720	0.2596	0.0558	4.642	0.4859	0.0957	1.497	0.4630	0.1143	2.050
84- 2	1.7692	0.4732	0.0418	4.174	0.5675	0.0793	3.247	0.5839	0.0800	3.057
84- 3	1.2959	0.3074	0.0664	5.354	0.4449	0.1292	4.247	0.4175	0.1554	4.489
84- 4	1.0735	0.2318	0.0821	5.724	0.3629	0.1630	4.613	0.3326	0.2032	4.893
84- 5	0.9310	0.1976	0.0975	5.546	0.3152	0.1977	4.391	0.2902	0.2399	4.661
85- 2	1.4700	0.4105	0.0530	4.438	0.5059	0.1022	3.510	0.4981	0.1150	3.594
85- 3	1.0741	0.2860	0.0844	5.748	0.3996	0.1685	4.857	0.3690	0.2078	5.117
85- 4	0.8789	0.2325	0.1055	6.099	0.3306	0.2173	5.237	0.3072	0.2550	5.455
85- 5	0.7534	0.2036	0.1259	6.827	0.2922	0.2665	6.030	0.2812	0.2796	6.135
86- 2	1.3085	0.4024	0.0624	4.980	0.4788	0.1217	4.326	0.4619	0.1437	4.479
86- 3	0.9422	0.2982	0.1012	5.497	0.3814	0.2064	4.764	0.3527	0.2480	5.029
86- 4	0.7601	0.2541	0.1280	7.393	0.3251	0.2711	6.841	0.3107	0.2862	6.957
86- 5	0.6428	0.2299	0.1535	7.131	0.2995	0.3351	6.442	0.3031	0.2927	6.403
87- 2	1.1652	0.3993	0.0713	5.263	0.4546	0.1411	4.793	0.4314	0.1704	4.996
87- 3	0.8317	0.3108	0.1161	6.694	0.3713	0.2424	6.222	0.3481	0.2721	6.407
87- 4	0.6642	0.2744	0.1474	8.134	0.3305	0.3206	7.675	0.3292	0.2907	7.685
87- 5	0.5544	0.2553	0.1767	9.799	0.3207	0.3961	9.229	0.3434	0.2742	9.022
88- 2	1.0992	0.4287	0.0792	5.144	0.4563	0.1589	4.912	0.4317	0.1917	5.119
88- 3	0.7704	0.3484	0.1319	7.386	0.3839	0.2808	7.134	0.3644	0.2967	7.273
88- 4	0.6046	0.3155	0.1692	8.997	0.3588	0.3760	8.656	0.3679	0.2998	8.583
88- 5	0.4957	0.2933	0.2044	10.619	0.3603	0.4672	10.005	0.3984	0.2688	9.639
89- 2	1.0168	0.4196	0.0852	5.778	0.4406	0.1733	5.611	0.4137	0.2069	5.824
89- 3	0.7177	0.3519	0.1395	7.781	0.3830	0.3017	7.551	0.3705	0.2965	7.644
89- 4	0.5617	0.3244	0.1774	9.585	0.3699	0.3998	9.204	0.3904	0.2830	9.027
89- 5	0.4574	0.3006	0.2137	12.261	0.3765	0.4932	11.551	0.4208	0.2581	11.116
90- 2	0.9982	0.4412	0.0889	5.746	0.4466	0.1812	5.703	0.4190	0.2155	5.916
90- 3	0.6952	0.3732	0.1470	8.167	0.3948	0.3196	8.013	0.3844	0.3043	8.088
90- 4	0.5377	0.3472	0.1890	10.155	0.3903	0.4284	9.801	0.4176	0.2819	9.569
90- 5	0.4345	0.3205	0.2279	11.716	0.4037	0.5278	10.829	0.4488	0.2652	10.316
91- 2	0.9636	0.4539	0.0934	5.906	0.4479	0.1913	5.952	0.4195	0.2259	6.166
91- 3	0.6663	0.3951	0.1562	8.356	0.4077	0.3420	8.266	0.4015	0.3094	8.311
91- 4	0.5127	0.3704	0.2003	10.611	0.4162	0.4567	10.225	0.4507	0.2788	9.926
92- 2	0.9819	0.4433	0.0900	5.780	0.4455	0.1840	5.763	0.4178	0.2178	5.978
92- 3	0.6805	0.3808	0.1497	8.368	0.3996	0.3268	8.234	0.3915	0.3030	8.292
92- 4	0.5239	0.3566	0.1925	10.476	0.4016	0.4379	10.099	0.4330	0.2763	9.827
93- 2	0.9942	0.4444	0.0893	5.719	0.4478	0.1819	5.693	0.4201	0.2165	5.907
93- 3	0.6910	0.3741	0.1489	8.169	0.3946	0.3239	8.023	0.3848	0.3060	8.093
93- 4	0.5350	0.3533	0.1907	10.280	0.3957	0.4323	9.934	0.4237	0.2823	9.698

Table F-22 (continued)

RUN #	SQRT (X_{tt})	HOMOGENEOUS [3] MODEL			MARTINELLI-NELSON [4] MODEL			MARTINELLI-NELSON [4] MODEL WITH ZUBER ET AL [10] GENERAL VOID FRACTION MODEL		
		ΔP (ACC+GRAV) (PSI)	ΔP (FRICTION) (PSI)	Φ_{ftt}	ΔP (ACC+GRAV) (PSI)	ΔP (FRICTION) (PSI)	Φ_{ftt}	ΔP (ACC+GRAV) (PSI)	ΔP (FRICTION) (PSI)	Φ_{ftt}
93- 5	0.4305	0.3251	0.2305	11.649	0.4085	0.5340	10.740	0.4537	0.2665	10.214
149- 2	0.9967	0.4423	0.0838	6.244	0.4470	0.1720	6.208	0.4214	0.2014	6.401
149- 3	0.6812	0.3766	0.1415	8.161	0.3967	0.3103	8.007	0.3898	0.2856	8.060
149- 4	0.5196	0.3489	0.1833	11.160	0.3948	0.4193	10.777	0.4283	0.2601	10.488
150- 2	0.9400	0.4637	0.0926	5.724	0.4495	0.1916	5.841	0.4216	0.2218	6.064
150- 3	0.6418	0.4012	0.1552	8.818	0.4113	0.3439	8.744	0.4100	0.2965	8.754
150- 4	0.4867	0.3773	0.2006	12.102	0.4224	0.4622	11.732	0.4633	0.2641	11.385
151- 2	0.9006	0.4612	0.0939	6.231	0.4446	0.1961	6.365	0.4174	0.2219	6.578
151- 3	0.6112	0.4075	0.1576	9.114	0.4184	0.3527	9.030	0.4250	0.2828	8.978
153- 2	0.8406	0.4960	0.1052	6.700	0.4560	0.2219	7.004	0.4285	0.2427	7.207
154- 2	0.8038	0.5326	0.1117	7.003	0.4729	0.2385	7.445	0.4461	0.2516	7.636

Table F-23

PRESSURE DROP -- CORRELATED RESULTS

$G \approx 0.90 \times 10^6$ lbm/hr-sq ft $T \approx 100°F$

RUN #	SQRT (X_{tt})	HOMOGENEOUS [3] MODEL			MARTINELLI-NELSON [4] MODEL			MARTINELLI-NELSON [4] MODEL WITH ZUBER ET AL [10] GENERAL VOID FRACTION MODEL		
		ΔP (ACC+GRAV) (PSI)	ΔP (FRICTION) (PSI)	Φ_{ftt}	ΔP (ACC+GRAV) (PSI)	ΔP (FRICTION) (PSI)	Φ_{ftt}	ΔP (ACC+GRAV) (PSI)	ΔP (FRICTION) (PSI)	Φ_{ftt}
23- 2	2.5701	0.8565	0.0877	1.776	0.8148	0.1522	2.022	0.9017	0.1346	1.464
23- 3	1.6850	0.6001	0.1394	2.907	0.6041	0.2685	2.890	0.6131	0.3040	2.854
23- 4	1.3241	0.4637	0.1843	3.143	0.4863	0.3613	3.049	0.4601	0.4704	3.158
23- 5	1.1173	0.3996	0.2263	3.169	0.4653	0.4272	2.857	0.4309	0.5819	3.024
24- 3	1.3135	0.5560	0.1968	3.541	0.5380	0.3829	3.606	0.5191	0.5072	3.672
24- 4	1.0613	0.4753	0.2521	3.821	0.4643	0.5013	3.863	0.4300	0.6883	3.991
24- 5	0.9030	0.4400	0.3085	4.205	0.4356	0.6276	4.222	0.3989	0.8232	4.363
25- 3	2.3046	0.6404	0.0940	2.683	0.8046	0.1388	1.858	0.8462	0.1277	1.583
25- 4	1.8485	0.4589	0.1179	3.059	0.6872	0.1770	1.925	0.6909	0.1931	1.901
26- 2	1.9810	0.6261	0.1090	2.528	0.7155	0.1839	2.074	0.7483	0.1860	1.880
26- 3	1.5225	0.4617	0.1617	3.121	0.6148	0.2779	2.460	0.5997	0.3441	2.533
26- 4	1.2893	0.3738	0.1939	3.341	0.5337	0.3367	2.629	0.5051	0.4536	2.770
26- 5	1.1335	0.3266	0.2268	3.672	0.4849	0.3984	2.987	0.4521	0.5546	3.142
94- 2	2.8454	0.8423	0.0680	2.167	0.9008	0.0954	1.820	0.9860	0.0757	1.140
94- 3	2.0293	0.5428	0.1063	2.788	0.7576	0.1586	1.617	0.7756	0.1607	1.477
94- 4	1.6760	0.4076	0.1282	2.980	0.6602	0.1932	1.508	0.6529	0.2250	1.570
94- 5	1.4590	0.3247	0.1532	3.241	0.5952	0.2325	1.719	0.5746	0.2993	1.879
95- 2	2.4783	0.7968	0.0799	1.887	0.8188	0.1303	1.743	0.8968	0.1129	1.089
95- 3	1.7126	0.5242	0.1333	2.894	0.6573	0.2267	2.261	0.6601	0.2603	2.246
95- 4	1.3853	0.4011	0.1686	3.261	0.5557	0.2901	2.539	0.5344	0.3790	2.651
95- 5	1.1915	0.3317	0.2047	3.295	0.4938	0.3568	2.467	0.4632	0.4936	2.644
96- 2	1.8698	0.6556	0.1107	2.482	0.6475	0.2087	2.523	0.6806	0.2211	2.352
96- 3	1.3734	0.4867	0.1748	3.169	0.5229	0.3374	3.014	0.5001	0.4381	3.113
96- 4	1.1337	0.3977	0.2177	3.821	0.4825	0.4049	3.474	0.4489	0.5564	3.616
96- 5	0.9810	0.3565	0.2602	3.590	0.4403	0.4928	3.183	0.4047	0.6706	3.362
97- 2	1.7182	0.6923	0.1286	2.514	0.6414	0.2449	2.752	0.6703	0.2760	2.620
97- 3	1.2433	0.5322	0.2069	3.539	0.5196	0.4044	3.586	0.4914	0.5425	3.687
97- 4	1.0127	0.4657	0.2632	3.950	0.4504	0.5264	4.008	0.4104	0.7182	4.155
97- 5	0.8687	0.4233	0.3186	4.181	0.4169	0.6519	4.207	0.3780	0.8394	4.361
98- 2	1.6050	0.7228	0.1399	2.609	0.6378	0.2688	2.985	0.6630	0.3143	2.879
98- 3	1.1471	0.5803	0.2307	3.754	0.5231	0.4574	3.954	0.4895	0.6194	4.066
98- 4	0.9266	0.5199	0.2968	4.191	0.4650	0.6048	4.391	0.4214	0.7999	4.545
98- 5	0.7885	0.4810	0.3609	4.655	0.4445	0.7547	4.795	0.4060	0.9034	4.938
99- 2	1.4948	0.7717	0.1548	2.615	0.6385	0.2984	3.196	0.6591	0.3658	3.113
99- 3	1.0571	0.6400	0.2599	4.108	0.5363	0.5198	4.447	0.4972	0.7060	4.569
99- 4	0.8462	0.5898	0.3375	4.582	0.5007	0.6970	4.896	0.4549	0.8784	5.051
99- 5	0.7138	0.5489	0.4143	5.658	0.5002	0.8805	5.826	0.4648	0.9523	5.945
100- 2	1.3984	0.8250	0.1703	2.594	0.6441	0.3298	3.368	0.6602	0.4173	3.306
100- 3	0.9813	0.7072	0.2923	4.253	0.5579	0.5908	4.731	0.5116	0.7918	4.870
100- 4	0.7827	0.6632	0.3796	4.767	0.5459	0.7946	5.181	0.4980	0.9432	5.340

Table F-23 (continued)

RUN #	SQRT (X_{tt})	HOMOGENEOUS [3] MODEL			MARTINELLI-NELSON [4] MODEL			MARTINELLI-NELSON [4] MODEL WITH ZUBER ET AL [10] GENERAL VOID FRACTION MODEL		
		ΔP (ACC+GRAV) (PSI)	ΔP (FRICTION) (PSI)	Φ_{ftt}	ΔP (ACC+GRAV) (PSI)	ΔP (FRICTION) (PSI)	Φ_{ftt}	ΔP (ACC+GRAV) (PSI)	ΔP (FRICTION) (PSI)	Φ_{ftt}
100- 5	0.6568	0.6205	0.4679	5.938	0.5670	1.0099	6.126	0.5357	0.9812	6.234
101- 3	0.9586	0.7467	0.3023	4.299	0.5755	0.6131	4.845	0.5279	0.8155	4.986
101- 4	0.7568	0.7129	0.3986	4.987	0.5809	0.8399	5.443	0.5322	0.9639	5.602
101- 5	0.6313	0.6652	0.4935	6.068	0.6183	1.0732	6.237	0.5896	0.9830	6.338
102- 3	0.9356	0.7699	0.3088	4.251	0.5883	0.6355	4.842	0.5396	0.8286	4.989
102- 4	0.7382	0.7246	0.4042	5.007	0.5976	0.8641	5.457	0.5506	0.9604	5.614
102- 5	0.6145	0.6727	0.5000	5.975	0.6384	1.1033	6.106	0.6137	0.9638	6.198
156- 2	1.4937	0.9868	0.1608	2.391	0.7190	0.3128	3.496	0.7689	0.3812	3.318
156- 3	0.9766	0.8264	0.3016	4.089	0.6138	0.6169	4.762	0.5703	0.8158	4.889
156- 4	0.7568	0.7756	0.4077	4.680	0.6279	0.8694	5.205	0.5780	0.9850	5.371
157- 2	1.3020	0.9396	0.1980	2.879	0.6703	0.3879	3.865	0.6807	0.5042	3.832
157- 3	0.9039	0.8448	0.3417	4.248	0.6180	0.7024	4.953	0.5623	0.9118	5.112
158- 2	1.2323	0.9637	0.2096	2.796	0.6730	0.4177	3.884	0.6745	0.5430	3.879
158- 3	0.8595	0.8850	0.3599	4.335	0.6405	0.7555	5.097	0.5802	0.9444	5.268

Table F-24

PRESSURE DROP -- CORRELATED RESULTS

$G \approx 1.77 \times 10^6$ lbm/hr-sq ft $T \approx 100°F$

RUN #	SQRT (X_{tt})	HOMOGENEOUS [3] MODEL			MARTINELLI-NELSON [4] MODEL			MARTINELLI-NELSON [4] MODEL WITH ZUBER ET AL [10] GENERAL VOID FRACTION MODEL		
		ΔP (ACC+GRAV) (PSI)	ΔP (FRICTION) (PSI)	Φ_{ftt}	ΔP (ACC+GRAV) (PSI)	ΔP (FRICTION) (PSI)	Φ_{ftt}	ΔP (ACC+GRAV) (PSI)	ΔP (FRICTION) (PSI)	Φ_{ftt}
103- 4	2.7263	0.9411	0.2068	2.469	1.0951	0.1579	2.233	1.1599	0.1250	2.126
103- 5	1.8851	0.5739	0.3437	2.504	0.9143	0.3183	1.907	0.9663	0.3519	1.799
104- 3	2.9492	1.1841	0.2103	1.943	1.1250	0.2840	2.045	1.2301	0.2253	1.859
104- 4	1.8836	0.7579	0.3452	2.762	0.8144	0.5135	2.683	0.8878	0.5611	2.577
104- 5	1.4824	0.5985	0.4857	2.790	0.7096	0.7290	2.622	0.7472	0.9859	2.562
105- 3	2.5305	1.1544	0.2498	2.165	1.0092	0.4057	2.371	1.1459	0.3502	2.159
105- 4	1.6964	0.8211	0.3895	2.670	0.7500	0.6639	2.772	0.8184	0.7789	2.674
105- 5	1.3414	0.6972	0.5423	2.863	0.6516	0.9344	2.930	0.6739	1.3096	2.898
106- 3	2.1364	1.1545	0.3041	2.516	0.9592	0.5133	2.779	1.1013	0.4955	2.590
106- 4	1.5045	0.9065	0.4639	2.419	0.7562	0.8050	2.655	0.8206	1.0262	2.557
106- 5	1.2089	0.8009	0.6253	3.098	0.6789	1.1001	3.266	0.6935	1.5834	3.246
107- 3	2.0642	1.3356	0.3403	2.055	1.0160	0.5752	2.485	1.2041	0.5783	2.216
107- 4	1.4246	1.0503	0.5415	2.177	0.8157	0.9412	2.556	0.9256	1.2544	2.386

Table F-25

PRESSURE DROP -- CORRELATED RESULTS

$G \approx 0.12 \times 10^6$ lbm/hr-sq ft T ≈150°F

RUN #	SQRT (X_{tt})	HOMOGENEOUS [3] MODEL			MARTINELLI-NELSON [4] MODEL			MARTINELLI-NELSON [4] MODEL WITH ZUBER ET AL [10] GENERAL VOID FRACTION MODEL		
		ΔP (ACC+GRAV) (PSI)	ΔP (FRICTION) (PSI)	Φ_{ftt}	ΔP (ACC+GRAV) (PSI)	ΔP (FRICTION) (PSI)	Φ_{ftt}	ΔP (ACC+GRAV) (PSI)	ΔP (FRICTION) (PSI)	Φ_{ftt}
27- 2	1.0070	0.2196	0.0052	15.302	0.3497	0.0124	9.338	0.4388	0.0074	*******
27- 3	0.7022	0.1318	0.0078	18.417	0.2521	0.0197	12.199	0.3280	0.0104	5.346
27- 4	0.5364	0.0916	0.0096	18.594	0.1840	0.0244	10.481	0.2570	0.0103	*******
27- 5	0.4158	0.0710	0.0112	22.402	0.1402	0.0279	13.671	0.1973	0.0106	*******
28- 2	0.7892	0.1619	0.0066	15.730	0.2851	0.0165	8.427	0.3636	0.0091	*******
28- 3	0.5150	0.0989	0.0102	23.159	0.1929	0.0259	16.930	0.2691	0.0107	9.193
28- 4	0.3443	0.0710	0.0126	21.597	0.1304	0.0301	5.711	0.1769	0.0113	*******
29- 2	0.7374	0.1511	0.0068	16.051	0.2700	0.0170	8.068	0.3503	0.0089	*******
29- 3	0.4653	0.0930	0.0104	19.295	0.1785	0.0262	8.849	0.2507	0.0102	*******
29- 4	0.2811	0.0671	0.0129	24.595	0.1146	0.0292	*******	0.1469	0.0114	*******
30- 2	0.7950	0.1516	0.0071	17.961	0.2781	0.0174	11.677	0.3539	0.0097	4.977
30- 3	0.5062	0.0909	0.0113	21.144	0.1846	0.0283	13.356	0.2593	0.0113	*******
30- 4	0.3262	0.0655	0.0140	31.619	0.1265	0.0327	21.300	0.1679	0.0121	9.103
31- 2	1.9084	0.5359	0.0024	14.209	0.5739	0.0052	12.937	0.7613	0.0028	*******
31- 3	1.2250	0.2805	0.0040	16.280	0.4090	0.0094	11.493	0.5207	0.0055	4.058
31- 4	0.9581	0.1813	0.0051	17.348	0.3112	0.0123	11.635	0.3908	0.0074	5.820
31- 5	0.8003	0.1341	0.0060	19.221	0.2534	0.0150	13.556	0.3230	0.0085	8.686
108- 2	0.9731	0.2073	0.0047	17.502	0.3390	0.0114	11.497	0.4325	0.0066	2.934
108- 3	0.6769	0.1242	0.0072	20.647	0.2422	0.0181	14.225	0.3240	0.0089	6.871
108- 4	0.5090	0.0861	0.0089	21.493	0.1745	0.0224	13.328	0.2492	0.0089	*******
108- 5	0.3862	0.0659	0.0103	32.021	0.1300	0.0254	25.030	0.1850	0.0092	16.859
109- 2	0.7787	0.1582	0.0063	17.489	0.2808	0.0157	10.716	0.3624	0.0084	*******
109- 3	0.5061	0.0968	0.0097	21.657	0.1891	0.0244	13.978	0.2663	0.0098	*******
109- 4	0.3366	0.0581	0.0118	31.077	0.1252	0.0282	22.012	0.1705	0.0104	10.148
109- 5	0.1720	0.0511	0.0138	83.047	0.0735	0.0251	71.374	0.0836	0.0135	65.424
110- 2	0.7269	0.1468	0.0065	18.253	0.2652	0.0163	11.188	0.3482	0.0082	*******
110- 3	0.4544	0.0895	0.0101	25.333	0.1730	0.0252	17.879	0.2452	0.0095	6.394
110- 4	0.2691	0.0645	0.0124	35.135	0.1097	0.0277	21.443	0.1401	0.0107	*******
286- 2	0.7592	0.1653	0.0065	14.780	0.2827	0.0214	8.873	0.3523	0.0122	*******
286- 3	0.4721	0.1013	0.0135	19.975	0.1873	0.0339	13.457	0.2533	0.0143	3.736
286- 4	0.2855	0.0740	0.0167	36.471	0.1238	0.0380	28.724	0.1541	0.0159	22.746
287- 2	0.7154	0.1594	0.0089	14.906	0.2726	0.0225	8.843	0.3428	0.0124	*******
287- 3	0.4302	0.0987	0.0141	23.224	0.1772	0.0350	17.180	0.2377	0.0145	10.347
287- 4	0.2280	0.0727	0.0175	49.786	0.1113	0.0365	40.793	0.1295	0.0176	35.772
288- 2	0.6657	0.1477	0.0089	15.535	0.2564	0.0225	8.806	0.3295	0.0115	*******
288- 3	0.3786	0.0926	0.0140	27.361	0.1622	0.0341	20.693	0.2152	0.0136	13.582
289- 2	0.5845	0.1350	0.0103	15.619	0.2343	0.0260	8.091	0.3053	0.0124	*******
289- 3	0.2914	0.0881	0.0162	38.803	0.1428	0.0363	31.401	0.1760	0.0156	25.884
290- 2	0.5391	0.1279	0.0110	17.806	0.2218	0.0277	10.996	0.2912	0.0126	*******
291- 2	0.4568	0.1186	0.0129	19.331	0.2021	0.0320	11.423	0.2642	0.0136	*******

Table F-26

PRESSURE DROP -- CORRELATED RESULTS

$G \approx 0.24 \times 10^6$ lbm/hr-sq ft $T \approx 150°F$

RUN #	SQRT (X_{tt})	HOMOGENEOUS [3] MODEL			MARTINELLI-NELSON [4] MODEL			MARTINELLI-NELSON [4] MODEL WITH ZUBER ET AL [10] GENERAL VOID FRACTION MODEL		
		ΔP (ACC+GRAV) (PSI)	ΔP (FRICTION) (PSI)	Φ_{ftt}	ΔP (ACC+GRAV) (PSI)	ΔP (FRICTION) (PSI)	Φ_{ftt}	ΔP (ACC+GRAV) (PSI)	ΔP (FRICTION) (PSI)	Φ_{ftt}
32- 3	1.8696	0.5119	0.0088	6.593	0.5628	0.0191	5.525	0.6779	0.0129	1.141
32- 4	1.4439	0.3386	0.0111	8.227	0.4398	0.0253	6.203	0.5032	0.0189	4.495
32- 5	1.2164	0.2549	0.0130	8.243	0.3708	0.0305	5.538	0.4119	0.0242	4.177
33- 2	1.5185	0.4090	0.0108	5.758	0.4936	0.0243	3.210	0.5742	0.0178	*******
33- 3	1.0877	0.2519	0.0164	9.683	0.3789	0.0390	7.373	0.4162	0.0315	6.542
33- 4	0.8773	0.1766	0.0201	8.617	0.2969	0.0493	5.284	0.3256	0.0394	4.108
33- 5	0.7413	0.1376	0.0234	8.132	0.2469	0.0585	3.753	0.2783	0.0432	*******
34- 2	1.5711	0.4610	0.0111	5.415	0.5218	0.0248	3.766	0.6120	0.0182	*******
34- 3	1.0000	0.2386	0.0193	8.230	0.3603	0.0467	5.533	0.3921	0.0382	4.572
34- 4	0.7693	0.1625	0.0248	8.994	0.2729	0.0619	5.978	0.3028	0.0471	4.848
34- 5	0.6269	0.1269	0.0295	10.459	0.2229	0.0748	7.484	0.2621	0.0481	5.850
35- 2	1.0649	0.2767	0.0178	7.266	0.3863	0.0426	4.553	0.4233	0.0347	3.147
35- 3	0.7370	0.1761	0.0277	8.960	0.2670	0.0694	5.990	0.3202	0.0513	4.750
35- 4	0.5646	0.1330	0.0341	11.680	0.2238	0.0866	8.924	0.2695	0.0510	7.191
35- 5	0.4439	0.1086	0.0398	12.929	0.1843	0.0998	9.357	0.2251	0.0518	6.688
36- 2	0.8913	0.2309	0.0203	8.467	0.3108	0.0720	6.539	0.3730	0.0392	4.496
36- 3	0.6025	0.1544	0.0314	11.973	0.2529	0.0796	9.321	0.2987	0.0489	7.788
36- 4	0.4376	0.1216	0.0385	17.069	0.2000	0.0963	14.238	0.2430	0.0492	12.411
36- 5	0.3068	0.1030	0.0451	18.826	0.1663	0.1052	12.797	0.1909	0.0529	9.462
37- 2	0.8367	0.2155	0.0204	8.696	0.3242	0.0505	5.576	0.3587	0.0384	4.117
37- 3	0.5582	0.1473	0.0314	11.232	0.2414	0.0797	7.791	0.2908	0.0457	5.139
37- 4	0.3925	0.1165	0.0385	17.537	0.1898	0.0948	13.884	0.2290	0.0468	11.463
38- 2	0.7705	0.1943	0.0226	8.283	0.3020	0.0571	4.623	0.3371	0.0420	2.444
38- 3	0.5310	0.1413	0.0333	12.360	0.2333	0.0845	9.152	0.2832	0.0469	6.808
38- 4	0.3768	0.1134	0.0401	19.660	0.1851	0.0980	16.232	0.2218	0.0484	14.158
39- 2	0.7802	0.1952	0.0221	8.509	0.3040	0.0550	4.917	0.3393	0.0406	2.923
39- 3	0.5377	0.1401	0.0323	12.904	0.2332	0.0821	9.835	0.2834	0.0456	7.687
39- 4	0.3836	0.1120	0.0389	15.358	0.1849	0.0955	10.669	0.2229	0.0469	7.083
40- 2	0.7864	0.1940	0.0211	9.375	0.3042	0.0525	6.160	0.3402	0.0387	4.654
40- 3	0.5459	0.1385	0.0308	12.161	0.2323	0.0781	8.797	0.2829	0.0437	6.277
40- 4	0.3941	0.1102	0.0370	16.643	0.1826	0.0910	12.664	0.2222	0.0447	9.832
111- 2	1.0758	0.2780	0.0144	7.550	0.3885	0.0345	4.250	0.4341	0.0269	1.404
111- 3	0.7234	0.1678	0.0232	9.760	0.2794	0.0582	6.797	0.3186	0.0409	4.487
111- 4	0.5435	0.1230	0.0289	12.499	0.2126	0.0733	9.125	0.2609	0.0406	6.629
111- 5	0.4172	0.0998	0.0339	16.228	0.1717	0.0844	12.543	0.2123	0.0417	9.880
112- 2	0.8956	0.2278	0.0176	8.490	0.3388	0.0431	5.109	0.3763	0.0330	3.262
112- 3	0.5953	0.1486	0.0276	12.139	0.2474	0.0700	9.006	0.2962	0.0416	6.955
112- 4	0.4236	0.1140	0.0342	15.107	0.1898	0.0851	11.052	0.2330	0.0421	7.857
112- 5	0.2882	0.0955	0.0400	27.600	0.1533	0.0917	22.816	0.1757	0.0459	20.665
113- 2	0.8527	0.2216	0.0184	8.864	0.3299	0.0456	5.629	0.3676	0.0341	3.922

Table F-26 (continued)

RUN #	SQRT (X_{tt})	HOMOGENEOUS [3] MODEL			MARTINELLI-NELSON [4] MODEL			MARTINELLI-NELSON [4] MODEL WITH ZUBER ET AL [10] GENERAL VOID FRACTION MODEL		
		ΔP (ACC+GRAV) (PSI)	ΔP (FRICTION) (PSI)	Φ_{fft}	ΔP (ACC+GRAV) (PSI)	ΔP (FRICTION) (PSI)	Φ_{fft}	ΔP (ACC+GRAV) (PSI)	ΔP (FRICTION) (PSI)	Φ_{fft}
113- 3	0.5525	0.1461	0.0292	12.785	0.2398	0.0741	9.584	0.2905	0.0416	7.286
113- 4	0.3766	0.1137	0.0363	18.098	0.1845	0.0886	13.933	0.2221	0.0432	11.103
293- 2	1.1488	0.3247	0.0155	6.514	0.4198	0.0368	3.827	0.4690	0.0293	0.543
293- 3	0.7208	0.1826	0.0271	9.860	0.2890	0.0680	7.164	0.3247	0.0488	5.994
293- 4	0.5199	0.1337	0.0349	12.955	0.2193	0.0885	10.135	0.2655	0.0490	8.222
293- 5	0.3828	0.1100	0.0416	17.248	0.1804	0.1021	13.665	0.2159	0.0511	11.438
294- 2	0.9566	0.2695	0.0205	6.895	0.3697	0.0500	4.084	0.4031	0.0403	2.528
294- 3	0.6104	0.1718	0.0340	11.405	0.2675	0.0863	9.022	0.3105	0.0547	7.717
294- 4	0.4244	0.1338	0.0432	15.245	0.2106	0.1075	12.175	0.2515	0.0556	10.165
295- 2	0.8347	0.2335	0.0241	8.127	0.3341	0.0598	5.571	0.3647	0.0465	4.517
295- 3	0.5421	0.1624	0.0379	12.633	0.2533	0.0961	10.139	0.3004	0.0555	8.564
295- 4	0.3652	0.1304	0.0471	19.007	0.2045	0.1144	15.556	0.2386	0.0580	13.675
296- 2	0.8228	0.2310	0.0218	8.253	0.3317	0.0541	5.313	0.3662	0.0407	3.817
296- 3	0.5114	0.1563	0.0354	13.467	0.2451	0.0896	10.574	0.2943	0.0491	8.564
297- 2	0.8366	0.2532	0.0212	7.866	0.3473	0.0524	4.985	0.3841	0.0390	3.216
297- 3	0.4777	0.1640	0.0371	15.638	0.2504	0.0932	12.883	0.2988	0.0494	11.045
298- 2	0.7906	0.2547	0.0235	8.317	0.3436	0.0585	5.792	0.3802	0.0424	4.342
299- 2	0.7048	0.2403	0.0265	9.974	0.3263	0.0665	7.721	0.3652	0.0451	6.447

Table F-27

PRESSURE DROP -- CORRELATED RESULTS

$G \approx 0.44 \times 10^6$ lbm/hr-sq ft $T \approx 150°F$

RUN #	SQRT (X_{tt})	HOMOGENEOUS [3] MODEL ΔP (ACC+GRAV) (PSI)	HOMOGENEOUS [3] MODEL ΔP (FRICTION) (PSI)	HOMOGENEOUS [3] MODEL Φ_{ftt}	MARTINELLI-NELSON [4] MODEL ΔP (ACC+GRAV) (PSI)	MARTINELLI-NELSON [4] MODEL ΔP (FRICTION) (PSI)	MARTINELLI-NELSON [4] MODEL Φ_{ftt}	MARTINELLI-NELSON [4] MODEL WITH ZUBER ET AL [10] GENERAL VOID FRACTION MODEL ΔP (ACC+GRAV) (PSI)	MARTINELLI-NELSON [4] MODEL WITH ZUBER ET AL [10] GENERAL VOID FRACTION MODEL ΔP (FRICTION) (PSI)	MARTINELLI-NELSON [4] MODEL WITH ZUBER ET AL [10] GENERAL VOID FRACTION MODEL Φ_{ftt}
114- 3	2.3073	0.6524	0.0222	3.435	0.6993	0.0410	2.833	0.8039	0.0289	*******
114- 4	1.8144	0.4693	0.0263	4.419	0.5828	0.0516	3.075	0.6414	0.0405	2.060
114- 5	1.5407	0.3655	0.0303	4.416	0.5122	0.0612	2.320	0.5651	0.0522	1.487
115- 2	1.8334	0.5245	0.0274	4.224	0.5646	0.0596	3.806	0.6396	0.0465	2.881
115- 3	1.4007	0.3743	0.0376	5.026	0.4697	0.0860	4.091	0.4983	0.0768	3.766
115- 4	1.1697	0.2788	0.0441	5.246	0.3870	0.1036	4.054	0.3971	0.0989	3.923
115- 5	1.0204	0.2243	0.0502	5.754	0.3341	0.1205	4.519	0.3384	0.1175	4.464
116- 2	1.7098	0.5089	0.0295	3.945	0.5507	0.0647	3.462	0.6156	0.0525	2.535
116- 3	1.2314	0.3367	0.0434	5.270	0.4356	0.1014	4.285	0.4520	0.0950	4.099
116- 4	0.9989	0.2494	0.0527	5.442	0.3526	0.1271	4.226	0.3573	0.1234	4.162
116- 5	0.8509	0.2006	0.0614	6.463	0.3013	0.1510	5.311	0.3066	0.1424	5.242
117- 2	1.4037	0.4321	0.0355	4.817	0.4891	0.0811	4.117	0.5254	0.0717	3.684
117- 3	1.0238	0.2882	0.0529	5.718	0.3881	0.1271	4.678	0.3946	0.1226	4.602
117- 4	0.8295	0.2218	0.0639	6.747	0.3178	0.1579	5.695	0.3243	0.1463	5.616
117- 5	0.7008	0.1844	0.0742	7.457	0.2750	0.1865	6.335	0.2900	0.1548	6.129
118- 2	1.2766	0.4019	0.0395	5.049	0.4681	0.0912	4.362	0.4946	0.0835	4.053
118- 3	0.9104	0.2765	0.0598	6.306	0.3685	0.1462	5.367	0.3735	0.1391	5.311
118- 4	0.7227	0.2190	0.0734	7.135	0.3047	0.1840	6.103	0.3174	0.1565	5.935
118- 5	0.5978	0.1852	0.0859	8.740	0.2662	0.2176	7.674	0.2940	0.1537	7.274
119- 2	1.1650	0.3867	0.0429	5.464	0.4499	0.1015	4.500	0.4696	0.0943	4.272
119- 3	0.8220	0.2742	0.0657	6.569	0.3563	0.1631	5.700	0.3629	0.1491	5.624
119- 4	0.6423	0.2212	0.0807	7.946	0.2960	0.2045	7.021	0.3175	0.1564	6.732
119- 5	0.5217	0.1889	0.0943	9.285	0.2578	0.2397	8.217	0.2914	0.1539	7.642
120- 2	1.0780	0.3755	0.0460	5.706	0.4357	0.1105	5.106	0.4511	0.1032	4.942
120- 3	0.7485	0.2730	0.0711	7.161	0.3494	0.1787	6.356	0.3608	0.1539	6.223
120- 4	0.5722	0.2250	0.0877	8.628	0.2967	0.2234	7.627	0.3278	0.1531	7.148
121- 3	0.7510	0.2699	0.0710	7.279	0.3468	0.1785	6.469	0.3577	0.1545	6.347
121- 4	0.5791	0.2233	0.0871	8.420	0.2938	0.2219	7.440	0.3239	0.1539	6.979
163- 2	1.1070	0.3845	0.0477	5.251	0.4427	0.1136	4.654	0.4577	0.1073	4.487
163- 3	0.7704	0.2812	0.0738	7.079	0.3579	0.1844	6.301	0.3667	0.1631	6.206
163- 4	0.5904	0.2313	0.0916	8.225	0.3067	0.2328	7.217	0.3355	0.1636	6.793
164- 2	1.1147	0.3980	0.0480	4.856	0.4506	0.1145	4.296	0.4670	0.1080	4.102
164- 3	0.7620	0.2896	0.0759	7.151	0.3628	0.1899	6.423	0.3717	0.1668	6.329
164- 4	0.5782	0.2388	0.0946	8.193	0.3127	0.2411	7.184	0.3427	0.1669	6.731
165- 2	0.9421	0.3493	0.0590	5.824	0.4089	0.1438	5.227	0.4245	0.1367	5.167
165- 3	0.6711	0.2774	0.0874	7.836	0.3498	0.2208	7.074	0.3675	0.1756	6.875
166- 2	0.9059	0.3539	0.0618	6.326	0.4086	0.1514	5.808	0.4134	0.1427	5.761
166- 3	0.6357	0.2846	0.0926	7.784	0.3558	0.2344	6.962	0.3787	0.1769	6.675
167- 2	0.9642	0.3593	0.0669	6.169	0.4085	0.1647	5.678	0.4126	0.1533	5.636
168- 2	0.8571	0.3755	0.0667	6.284	0.4174	0.1637	5.865	0.4215	0.1515	5.822

Table F-28

PRESSURE DROP -- CORRELATED RESULTS

$G \approx 0.87 \times 10^6$ lbm/hr-sq ft $T \approx 150°F$

RUN #	SQRT (X_{tt})	HOMOGENEOUS [3] MODEL			MARTINELLI-NELSON [4] MODEL			MARTINELLI-NELSON [4] MODEL WITH ZUBER ET AL [10] GENERAL VOID FRACTION MODEL		
		ΔP (ACC+GRAV) (PSI)	ΔP (FRICTION) (PSI)	Φ_{ftt}	ΔP (ACC+GRAV) (PSI)	ΔP (FRICTION) (PSI)	Φ_{ftt}	ΔP (ACC+GRAV) (PSI)	ΔP (FRICTION) (PSI)	Φ_{ftt}
41- 2	2.7380	0.8252	0.0575	1.749	0.8342	0.0872	1.683	0.9417	0.0608	0.374
41- 3	2.1277	0.6256	0.0744	2.383	0.7393	0.1250	1.665	0.8044	0.0970	1.054
41- 4	1.8679	0.5106	0.0800	2.849	0.6598	0.1387	1.996	0.7008	0.1155	1.687
41- 5	1.6846	0.4357	0.0855	2.539	0.6076	0.1512	1.175	0.6333	0.1335	0.789
42- 3	2.3530	0.7312	0.0653	1.676	0.7483	0.1199	1.594	0.8369	0.0893	0.116
42- 4	1.8197	0.5324	0.0787	2.330	0.6113	0.1544	1.767	0.6593	0.1307	1.311
42- 5	1.5359	0.4250	0.0910	2.579	0.5374	0.1844	1.756	0.5593	0.1718	1.546
43- 2	2.3529	0.7816	0.0689	1.611	0.7163	0.1400	2.053	0.8270	0.1048	1.213
43- 3	1.6764	0.5512	0.0988	2.530	0.5710	0.2192	2.426	0.6168	0.1963	2.165
43- 4	1.3876	0.4276	0.1164	3.000	0.4763	0.2667	2.751	0.4918	0.2652	2.666
43- 5	1.2014	0.3555	0.1328	3.045	0.4182	0.3117	2.689	0.4193	0.3286	2.683
44- 2	2.0293	0.7298	0.0792	1.914	0.6758	0.1676	2.238	0.7671	0.1335	1.652
44- 3	1.4553	0.5206	0.1156	2.670	0.5396	0.2634	2.574	0.5663	0.2528	2.430
44- 4	1.1981	0.4127	0.1376	3.234	0.4513	0.3237	3.044	0.4526	0.3384	3.037
44- 5	1.0357	0.3500	0.1578	3.380	0.3983	0.3794	3.122	0.3898	0.4088	3.169
45- 2	1.9144	0.6853	0.0791	2.029	0.6413	0.1722	2.318	0.7166	0.1449	1.796
45- 3	1.2377	0.4403	0.1185	3.053	0.5108	0.2758	2.946	0.5237	0.2774	2.876
45- 4	1.0477	0.3959	0.1436	3.495	0.4294	0.3455	3.311	0.4225	0.3676	3.350
45- 5	0.8983	0.3375	0.1665	3.644	0.3804	0.4087	3.594	0.3692	0.4304	3.661
46- 2	1.4221	0.5892	0.1075	2.766	0.5664	0.2453	2.885	0.6014	0.2355	2.700
46- 3	1.0707	0.4628	0.1542	3.517	0.4779	0.3690	3.445	0.4721	0.3927	3.473
46- 4	0.8890	0.3927	0.1823	3.964	0.4176	0.4478	3.836	0.4039	0.4716	3.907
46- 5	0.7680	0.3472	0.2083	4.123	0.3822	0.5203	3.912	0.3727	0.5121	3.970
47- 2	1.3104	0.5920	0.1206	2.868	0.5579	0.2787	3.040	0.5827	0.2785	2.916
47- 3	0.9856	0.4790	0.1742	3.681	0.4788	0.4215	3.682	0.4665	0.4514	3.739
47- 4	0.8146	0.4173	0.2065	4.152	0.4284	0.5120	4.096	0.4134	0.5226	4.172
47- 5	0.7004	0.3709	0.2361	4.158	0.3983	0.5945	3.980	0.3926	0.5451	4.017
48- 2	1.4352	0.6433	0.1428	2.620	0.5927	0.2569	2.873	0.6347	0.2457	2.664
48- 3	1.0593	0.5026	0.1680	3.485	0.4950	0.4036	3.519	0.4875	0.4315	3.552
48- 4	0.8637	0.4346	0.2010	4.033	0.4397	0.4959	4.008	0.4239	0.5189	4.084
48- 5	0.7381	0.3856	0.2318	3.945	0.4080	0.5817	3.809	0.3980	0.5584	3.871
49- 2	1.3684	0.6556	0.1190	2.708	0.5917	0.2736	3.022	0.6284	0.2692	2.846
49- 3	0.9916	0.5261	0.1792	3.525	0.5057	0.4336	3.620	0.4948	0.4646	3.670
49- 4	0.8024	0.4597	0.2175	4.288	0.4595	0.5405	4.286	0.4439	0.5467	4.363
50- 2	1.3815	0.6652	0.1108	2.649	0.5888	0.2543	2.966	0.6266	0.2466	2.750
50- 3	0.9944	0.5088	0.1681	3.625	0.4947	0.4071	3.692	0.4838	0.4233	3.743
50- 4	0.8040	0.4407	0.2041	4.215	0.4423	0.5081	4.207	0.4270	0.5126	4.286
51- 2	1.3852	0.6373	0.1096	2.648	0.5853	0.2514	2.928	0.6225	0.2443	2.731
51- 3	1.0021	0.4985	0.1655	3.726	0.4906	0.4000	3.763	0.4804	0.4267	3.810
51- 4	0.8129	0.4318	0.2005	4.160	0.4388	0.4978	4.123	0.4240	0.5054	4.201

Table F-28 (continued)

RUN #	SQRT (X_{tt})	HOMOGENEOUS [3] MODEL			MARTINELLI-NELSON [4] MODEL			MARTINELLI-NELSON [4] MODEL WITH ZUBER ET AL [10] GENERAL VOID FRACTION MODEL		
		ΔP (ACC+GRAV) (PSI)	ΔP (FRICTION) (PSI)	Φ_{ftt}	ΔP (ACC+GRAV) (PSI)	ΔP (FRICTION) (PSI)	Φ_{ftt}	ΔP (ACC+GRAV) (PSI)	ΔP (FRICTION) (PSI)	Φ_{ftt}
52- 2	1.4621	0.6506	0.1004	2.631	0.5985	0.2284	2.911	0.6450	0.2146	2.662
52- 3	1.0428	0.4975	0.1535	3.586	0.4923	0.3696	3.611	0.4858	0.3913	3.643
52- 4	0.8417	0.4244	0.1872	4.075	0.4326	0.4640	4.030	0.4189	0.4766	4.108
122- 2	1.5101	0.6567	0.1067	2.536	0.6033	0.2415	2.810	0.6512	0.2270	2.566
122- 3	1.0973	0.5145	0.1575	3.449	0.5056	0.3768	3.490	0.5032	0.4007	3.500
122- 4	0.8856	0.4346	0.1920	3.969	0.4416	0.4716	3.934	0.4269	0.4979	4.005
122- 5	0.7509	0.3772	0.2246	4.349	0.4012	0.5623	4.216	0.3908	0.5466	4.275
123- 2	1.4410	0.6436	0.1063	2.610	0.5940	0.2422	2.900	0.6372	0.2307	2.679
123- 3	1.0389	0.5089	0.1595	3.668	0.4970	0.3836	3.720	0.4896	0.4075	3.754
123- 4	0.8348	0.4351	0.1941	4.027	0.4376	0.4810	4.013	0.4221	0.4946	4.095
123- 5	0.7053	0.3781	0.2267	4.304	0.3972	0.5716	3.978	0.3907	0.5267	4.021
124- 2	1.4309	0.6562	0.1104	2.540	0.5966	0.2522	2.855	0.6380	0.2423	2.640
124- 3	1.0335	0.5142	0.1650	3.510	0.5000	0.3972	3.576	0.4920	0.4238	3.613
124- 4	0.8315	0.4413	0.2012	3.942	0.4420	0.4984	3.942	0.4259	0.5133	4.026
301- 2	1.7040	0.7659	0.1006	2.009	0.6714	0.2225	2.518	0.7467	0.1964	2.122
301- 3	1.2644	0.5722	0.1571	3.378	0.5270	0.3720	3.520	0.5419	0.3899	3.500
301- 4	0.9197	0.4759	0.1969	3.607	0.4603	0.4823	3.680	0.4440	0.5144	3.756
301- 5	0.7754	0.4145	0.2322	3.965	0.4174	0.5805	3.950	0.4035	0.5785	4.029
302- 2	1.6753	0.7695	0.0999	2.016	0.6719	0.2216	2.547	0.7466	0.1961	2.152
302- 3	1.1356	0.5736	0.1582	3.346	0.5349	0.3765	3.508	0.5369	0.3950	3.499
302- 4	0.8934	0.4810	0.1988	3.613	0.4601	0.4894	3.715	0.4423	0.5169	3.800
303- 2	1.4840	0.7157	0.1145	2.581	0.6292	0.2556	2.986	0.6814	0.2403	2.749
303- 3	1.0432	0.5619	0.1730	3.549	0.5224	0.4167	3.715	0.5145	0.4437	3.748
303- 4	0.8283	0.4821	0.2144	4.041	0.4506	0.5325	4.148	0.4403	0.5485	4.238
304- 2	1.6473	0.8152	0.1068	2.197	0.6919	0.2374	2.785	0.7696	0.2132	2.431
304- 3	1.0927	0.6151	0.1743	3.245	0.5520	0.4166	3.509	0.5500	0.4427	3.518
305- 2	1.6657	0.8576	0.1065	1.935	0.7144	0.2365	2.670	0.7983	0.2123	2.269
306- 2	1.3680	0.7544	0.1367	2.432	0.6367	0.3153	2.970	0.6792	0.3117	2.786
307- 2	1.5289	0.8235	0.1164	2.223	0.6818	0.2620	2.911	0.7490	0.2491	2.613

Table F-29

PRESSURE DROP -- CORRELATED RESULTS

$G \approx 1.70 \times 10^6$ lbm/hr-sq ft $T \approx 150°F$

RUN #	SQRT (X_{tt})	HOMOGENEOUS [3] MODEL			MARTINELLI-NELSON [4] MODEL			MARTINELLI-NELSON [4] MODEL WITH ZUBER ET AL [10] GENERAL VOID FRACTION MODEL		
		ΔP (ACC+GRAV) (PSI)	ΔP (FRICTION) (PSI)	Φ_{ftt}	ΔP (ACC+GRAV) (PSI)	ΔP (FRICTION) (PSI)	Φ_{ftt}	ΔP (ACC+GRAV) (PSI)	ΔP (FRICTION) (PSI)	Φ_{ftt}
125- 2	4.2556	1.0845	0.1550	1.400	1.1127	0.1298	1.323	1.1500	0.0950	1.215
125- 3	2.8977	0.8822	0.1909	1.657	0.9659	0.2158	1.457	1.0455	0.1546	1.236
125- 4	2.3527	0.6986	0.2131	1.967	0.8819	0.2378	1.546	0.9385	0.1839	1.391
125- 5	2.0624	0.5841	0.2337	1.844	0.8446	0.2464	1.084	0.8839	0.2057	0.916
126- 2	3.6269	1.0621	0.1697	1.410	1.0172	0.2339	1.524	1.1063	0.1653	1.289
126- 3	2.5181	0.8642	0.2127	1.745	0.8708	0.3386	1.731	0.9689	0.2533	1.503
126- 4	2.0220	0.6809	0.2437	2.132	0.7475	0.4130	2.000	0.8142	0.3439	1.858
126- 5	1.7434	0.5688	0.2754	2.031	0.6744	0.4829	1.788	0.7173	0.4426	1.680
127- 2	2.9771	1.0499	0.1858	1.478	0.9572	0.3097	1.696	1.0697	0.2212	1.428
127- 3	2.1166	0.8235	0.2483	1.910	0.7866	0.4690	1.983	0.8759	0.3806	1.802
127- 4	1.7337	0.6670	0.2845	2.298	0.6720	0.5618	2.288	0.7239	0.5111	2.191
127- 5	1.4932	0.5698	0.3244	2.193	0.6006	0.6584	2.128	0.6256	0.6582	2.074
128- 2	2.5551	1.0260	0.2014	1.611	0.9215	0.3567	1.844	1.0396	0.2641	1.579
128- 3	1.8555	0.8071	0.2744	2.045	0.7651	0.5359	2.125	0.8421	0.4663	1.975
128- 4	1.5244	0.6700	0.3176	2.394	0.6605	0.6440	2.412	0.6999	0.6290	2.338
128- 5	1.3171	0.5774	0.3657	2.411	0.5908	0.7608	2.383	0.6016	0.8091	2.361
129- 2	2.4364	1.0547	0.2056	1.632	0.8819	0.4130	2.009	1.0137	0.3127	1.729
129- 3	1.7339	0.8376	0.2661	2.153	0.7099	0.6305	2.387	0.7909	0.5699	2.242
129- 4	1.4098	0.6949	0.3401	2.443	0.5985	0.7787	2.622	0.6331	0.7954	2.559
129- 5	1.2163	0.6077	0.3935	2.557	0.5675	0.8749	2.637	0.5738	0.9609	2.625
130- 2	2.1216	1.0494	0.2286	1.273	0.8511	0.4780	1.799	0.9809	0.3852	1.476
130- 3	1.5436	0.8495	0.3243	2.332	0.6958	0.7301	2.600	0.7591	0.7107	2.493
130- 4	1.2650	0.7295	0.3856	2.669	0.6007	0.8970	2.897	0.6190	0.9694	2.866
130- 5	1.0928	0.6433	0.4479	2.619	0.5398	1.0657	2.828	0.5296	1.2119	2.848
131- 2	1.9946	1.0999	0.2536	1.738	0.8644	0.5372	2.208	1.0006	0.4496	1.950
131- 3	1.4477	0.9103	0.3692	2.447	0.7154	0.8386	2.763	0.7776	0.8562	2.666
131- 4	1.1842	0.7981	0.4432	2.698	0.6311	1.0382	2.984	0.6455	1.1632	2.960
131- 5	1.0200	0.7110	0.5179	2.766	0.5797	1.2403	3.016	0.5645	1.4353	3.044
132- 3	1.3570	0.9516	0.3928	2.142	0.7245	0.9050	2.563	0.7735	0.9495	2.478
132- 4	1.1122	0.8462	0.4688	2.442	0.6489	1.1125	2.821	0.6500	1.2577	2.819
132- 5	0.9573	0.7466	0.5476	2.667	0.5929	1.3291	2.983	0.5652	1.5235	3.036
133- 2	1.8456	1.1500	0.2637	1.769	0.8736	0.5693	2.324	1.0106	0.4944	2.068
133- 3	1.3337	0.9712	0.3936	2.030	0.7322	0.9095	2.503	0.7804	0.9628	2.415
133- 4	1.0894	0.8661	0.4718	2.420	0.6608	1.1234	2.830	0.6599	1.2749	2.832
134- 2	1.8780	1.1785	0.2589	1.670	0.8931	0.5572	2.263	1.0351	0.4778	1.990
134- 3	1.3371	0.9790	0.3892	1.986	0.7365	0.9000	2.472	0.7865	0.9455	2.380
134- 4	1.0859	0.8793	0.4713	2.586	0.6649	1.1252	2.989	0.6617	1.2720	2.995
135- 2	1.8608	1.1720	0.2614	1.694	0.8871	0.5638	2.281	1.0268	0.4860	2.015
135- 3	1.3315	0.9771	0.3910	1.998	0.7345	0.9048	2.482	0.7823	0.9523	2.394
135- 4	1.0825	0.8786	0.4725	2.595	0.6633	1.1285	2.999	0.6587	1.2762	3.007

Table F-29 (continued)

RUN #	SQRT (X_{tt})	HOMOGENEOUS [3] MODEL			MARTINELLI-NELSON [4] MODEL			MARTINELLI-NELSON [4] MODEL WITH ZUBER ET AL [10] GENERAL VOID FRACTION MODEL		
		ΔP (ACC+GRAV) (PSI)	ΔP (FRICTION) (PSI)	Φ_{ftt}	ΔP (ACC+GRAV) (PSI)	ΔP (FRICTION) (PSI)	Φ_{ftt}	ΔP (ACC+GRAV) (PSI)	ΔP (FRICTION) (PSI)	Φ_{ftt}
136- 2	1.9420	1.1640	0.2514	1.284	0.8950	0.5364	1.954	1.0371	0.4506	1.635
136- 3	1.3817	0.9605	0.3771	2.004	0.7311	0.8683	2.455	0.7854	0.8974	2.356
136- 4	1.1227	0.8573	0.4531	2.342	0.6546	1.0768	2.749	0.6584	1.2066	2.742
136- 5	0.9617	0.7456	0.5319	2.658	0.5911	1.2933	2.979	0.5639	1.4742	3.033
170- 3	1.4496	1.0423	0.3760	2.129	0.7750	0.8563	2.591	0.8514	0.8658	2.468
170- 4	1.1517	0.9209	0.4667	2.383	0.6842	1.1023	2.818	0.6959	1.2347	2.798
171- 2	1.8873	1.2133	0.2716	1.373	0.9141	0.5836	2.041	1.0557	0.4946	1.757
171- 3	1.3440	1.0183	0.4053	2.082	0.7484	0.9381	2.565	0.7916	0.9734	2.494
172- 2	1.8605	1.2255	0.2832	1.711	0.9133	0.6145	2.302	1.0650	0.5312	2.036
172- 3	1.3319	1.0450	0.4178	2.124	0.7758	0.9713	2.599	0.8427	1.0178	2.489
173- 2	1.9109	1.3157	0.2877	1.744	0.9644	0.6188	2.369	1.1300	0.5323	2.098
173- 3	1.3404	1.1246	0.4354	2.038	0.8108	1.0080	2.583	0.8857	1.0648	2.464
174- 2	1.8340	1.3194	0.2956	1.748	0.9504	0.6397	2.420	1.1133	0.5699	2.150
175- 2	1.7813	1.3174	0.3064	1.707	0.9369	0.6666	2.418	1.0926	0.6099	2.156

Table F-30

PRESSURE DROP -- CORRELATED RESULTS

$G \approx 3.44 \times 10^6$ lbm/hr-sq ft $T \approx 150°F$

RUN #	SQRT (X_{tt})	HOMOGENEOUS [3] MODEL			MARTINELLI-NELSON [4] MODEL			MARTINELLI-NELSON [4] MODEL WITH ZUBER ET AL [10] GENERAL VOID FRACTION MODEL		
		ΔP (ACC+GRAV) (PSI)	ΔP (FRICTION) (PSI)	Φ_{ftt}	ΔP (ACC+GRAV) (PSI)	ΔP (FRICTION) (PSI)	Φ_{ftt}	ΔP (ACC+GRAV) (PSI)	ΔP (FRICTION) (PSI)	Φ_{ftt}
137- 3	4.4324	1.2319	0.5054	1.485	1.4642	0.0668	1.308	1.2767	0.0536	1.453
137- 4	2.8088	0.9322	0.5998	1.891	1.1778	0.1114	1.734	1.1851	0.0801	1.730
138- 3	4.1483	1.3667	0.5386	1.467	1.5252	0.4725	1.350	1.3625	0.3561	1.470
139- 3	4.4621	1.5194	0.5359	1.350	1.8752	0.5248	1.044	1.4758	0.4089	1.383
140- 3	3.2279	1.5452	0.5975	1.417	1.4686	0.8237	1.473	1.4893	0.5888	1.459

Table F-31

PRESSURE DROP -- CORRELATED RESULTS

$G \approx 0.12 \times 10^6$ lbm/hr-sq ft $T \approx 200°F$

RUN #	SQRT (X_{tt})	HOMOGENEOUS [3] MODEL			MARTINELLI-NELSON [4] MODEL			MARTINELLI-NELSON [4] MODEL WITH ZUBER ET AL [10] GENERAL VOID FRACTION MODEL		
		ΔP (ACC+GRAV) (PSI)	ΔP (FRICTION) (PSI)	Φ_{ftt}	ΔP (ACC+GRAV) (PSI)	ΔP (FRICTION) (PSI)	Φ_{ftt}	ΔP (ACC+GRAV) (PSI)	ΔP (FRICTION) (PSI)	Φ_{ftt}
253- 3	1.3914	0.4152	0.0025	15.351	0.4816	0.0058	12.835	0.6231	0.0032	3.706
253- 4	1.0544	0.2733	0.0031	17.110	0.3682	0.0076	12.788	0.4703	0.0042	4.948
253- 5	0.8715	0.2054	0.0036	20.921	0.3027	0.0090	16.465	0.3888	0.0048	11.118
254- 2	1.5273	0.4891	0.0024	11.004	0.5227	0.0054	9.378	0.6714	0.0030	*******
254- 3	0.9251	0.2591	0.0039	16.542	0.3601	0.0096	11.656	0.4557	0.0052	2.364
254- 4	0.6682	0.1668	0.0049	20.922	0.2579	0.0122	15.175	0.3380	0.0057	6.923
254- 5	0.5031	0.1242	0.0058	24.491	0.1957	0.0139	17.229	0.2580	0.0059	5.741
255- 2	1.2258	0.3903	0.0029	12.446	0.4558	0.0068	9.109	0.5821	0.0038	*******
255- 3	0.6953	0.1897	0.0050	18.989	0.2869	0.0123	12.728	0.3733	0.0059	*******
255- 4	0.4417	0.1209	0.0064	27.814	0.1864	0.0148	19.961	0.2412	0.0063	9.212
255- 5	0.2270	0.0865	0.0076	61.199	0.1097	0.0139	51.050	0.1230	0.0080	44.192
256- 2	1.1276	0.3585	0.0033	11.460	0.4318	0.0077	7.010	0.5481	0.0043	*******
256- 3	0.6233	0.1726	0.0056	19.898	0.2640	0.0137	13.337	0.3443	0.0063	*******
256- 4	0.3643	0.1113	0.0072	30.522	0.1642	0.0158	20.737	0.2028	0.0070	8.011
257- 2	1.3141	0.4297	0.0028	11.839	0.4814	0.0065	9.342	0.6116	0.0037	*******
257- 3	0.7136	0.1993	0.0049	17.785	0.2961	0.0120	11.416	0.3819	0.0059	*******
257- 4	0.4392	0.1238	0.0065	24.180	0.1883	0.0148	14.645	0.2411	0.0064	*******
257- 5	0.2017	0.0772	0.0078	87.503	0.0957	0.0131	79.212	0.1060	0.0082	74.200
335- 2	1.4531	0.4802	0.0033	8.455	0.5161	0.0075	6.662	0.6437	0.0045	*******
335- 3	0.7949	0.2252	0.0058	14.900	0.3244	0.0142	9.809	0.4030	0.0079	*******
335- 4	0.5197	0.1400	0.0076	18.144	0.2159	0.0181	10.354	0.2756	0.0084	*******
335- 5	0.3239	0.1031	0.0091	34.069	0.1477	0.0193	25.696	0.1741	0.0095	19.058
336- 2	1.2220	0.3971	0.0038	8.346	0.4589	0.0089	4.252	0.5703	0.0053	*******
336- 3	0.6777	0.1923	0.0066	16.183	0.2869	0.0161	10.380	0.3613	0.0083	*******
336- 4	0.4146	0.1230	0.0085	22.992	0.1844	0.0193	14.419	0.2280	0.0090	*******
337- 2	1.1069	0.3558	0.0042	9.760	0.4293	0.0099	5.417	0.5320	0.0058	*******
337- 3	0.6057	0.1734	0.0072	16.297	0.2625	0.0175	9.343	0.3331	0.0086	*******
337- 4	0.3370	0.1125	0.0093	26.687	0.1614	0.0198	15.600	0.1908	0.0098	*******
338- 2	1.0067	0.3200	0.0044	10.369	0.4013	0.0105	5.024	0.4986	0.0061	*******
338- 3	0.5276	0.1564	0.0076	17.783	0.2376	0.0181	9.553	0.3019	0.0085	*******
339- 2	0.9252	0.2924	0.0046	11.422	0.3775	0.0112	5.826	0.4709	0.0062	*******
339- 3	0.4501	0.1425	0.0081	21.419	0.2133	0.0186	12.695	0.2667	0.0086	*******

Table F-32

PRESSURE DROP -- CORRELATED RESULTS

$G \approx 0.24 \times 10^6$ lbm/hr-sq ft $T \approx 200°F$

RUN #	SQRT (X_{tt})	HOMOGENEOUS [3] MODEL			MARTINELLI-NELSON [4] MODEL			MARTINELLI-NELSON [4] MODEL WITH ZUBER ET AL [10] GENERAL VOID FRACTION MODEL		
		ΔP (ACC+GRAV) (PSI)	ΔP (FRICTION) (PSI)	Φ_{ftt}	ΔP (ACC+GRAV) (PSI)	ΔP (FRICTION) (PSI)	Φ_{ftt}	ΔP (ACC+GRAV) (PSI)	ΔP (FRICTION) (PSI)	Φ_{ftt}
258- 2	1.5331	0.4922	0.0086	5.423	0.5259	0.0192	4.502	0.6212	0.0131	*******
258- 3	1.0204	0.2995	0.0128	7.367	0.3931	0.0310	4.629	0.4428	0.0229	2.003
258- 4	0.7808	0.2073	0.0155	8.883	0.3013	0.0384	5.595	0.3427	0.0268	3.218
258- 5	0.6301	0.1599	0.0179	10.178	0.2441	0.0441	6.366	0.2866	0.0274	2.954
259- 3	0.8007	0.2338	0.0154	6.756	0.3312	0.0379	*******	0.3754	0.0267	*******
259- 4	0.6136	0.1699	0.0182	7.814	0.2543	0.0443	*******	0.2983	0.0273	*******
259- 5	0.4785	0.1354	0.0206	8.247	0.2037	0.0486	*******	0.2391	0.0280	*******
260- 2	1.0784	0.3286	0.0116	5.372	0.4127	0.0277	*******	0.4681	0.0203	*******
260- 3	0.7613	0.2204	0.0162	7.179	0.3177	0.0400	1.477	0.3627	0.0275	*******
260- 4	0.5763	0.1609	0.0191	7.834	0.2430	0.0465	*******	0.2865	0.0279	*******
261- 3	0.7338	0.2112	0.0167	7.803	0.3082	0.0414	2.895	0.3541	0.0278	*******
261- 4	0.5485	0.1539	0.0198	9.775	0.2337	0.0481	4.156	0.2764	0.0282	*******
262- 3	0.7240	0.2092	0.0168	8.900	0.3056	0.0417	5.064	0.3518	0.0277	*******
343- 3	0.9090	0.2715	0.0153	7.978	0.3665	0.0374	5.375	0.4098	0.0277	3.609
343- 4	0.6660	0.1852	0.0190	8.931	0.2729	0.0469	5.134	0.3151	0.0305	0.961
343- 5	0.5074	0.1433	0.0222	10.898	0.2161	0.0532	6.250	0.2529	0.0313	*******
344- 2	1.2161	0.3905	0.0116	4.907	0.4561	0.0273	2.401	0.5199	0.0200	*******
344- 3	0.7938	0.2402	0.0175	7.890	0.3352	0.0431	4.676	0.3770	0.0308	2.029
344- 4	0.5704	0.1686	0.0216	10.437	0.2493	0.0523	6.674	0.2902	0.0320	3.444
345- 2	1.0876	0.3437	0.0135	5.794	0.4215	0.0323	3.275	0.4739	0.0242	*******
345- 3	0.7197	0.2184	0.0200	8.686	0.3124	0.0492	5.546	0.3547	0.0338	3.270
345- 4	0.5116	0.1579	0.0242	9.901	0.2343	0.0581	4.820	0.2720	0.0347	*******
346- 3	0.6376	0.1951	0.0210	8.614	0.2894	0.0516	4.309	0.3340	0.0330	*******
347- 2	1.0498	0.3388	0.0125	5.434	0.4158	0.0301	1.845	0.4714	0.0220	*******
347- 3	0.6355	0.1999	0.0199	8.774	0.2898	0.0488	4.222	0.3356	0.0308	*******
348- 2	0.9228	0.2979	0.0143	6.744	0.3821	0.0348	3.638	0.4308	0.0251	*******
349- 2	0.8493	0.2815	0.0150	7.734	0.3660	0.0366	4.863	0.4135	0.0257	1.817

Table F-33

PRESSURE DROP -- CORRELATED RESULTS

$G \approx 0.92 \times 10^6$ lbm/hr-sq ft $T \approx 200°F$

		HOMOGENEOUS [3] MODEL			MARTINELLI-NELSON [4] MODEL			MARTINELLI-NELSON [4] MODEL WITH ZUBER ET AL [10] GENERAL VOID FRACTION MODEL		
RUN #	SQRT (X_{tt})	ΔP (ACC+GRAV) (PSI)	ΔP (FRICTION) (PSI)	Φ_{ftt}	ΔP (ACC+GRAV) (PSI)	ΔP (FRICTION) (PSI)	Φ_{ftt}	ΔP (ACC+GRAV) (PSI)	ΔP (FRICTION) (PSI)	Φ_{ftt}
253- 3	1.8974	0.6474	0.0862	1.287	0.6220	0.1831	1.482	0.7007	0.1416	0.722
253- 4	1.5918	0.5265	0.0928	1.741	0.5344	0.2065	1.686	0.5857	0.1715	1.269
263- 5	1.3880	0.4419	0.1009	1.971	0.4732	0.2318	1.748	0.5049	0.2048	1.487
254- 3	1.5943	0.5772	0.0904	1.971	0.5759	0.2011	1.979	0.6326	0.1665	1.587
264- 4	1.3307	0.4622	0.1003	2.446	0.4901	0.2324	2.277	0.5201	0.2083	2.081
264- 5	1.1660	0.3873	0.1098	2.364	0.4335	0.2610	2.023	0.4491	0.2458	1.895
265- 2	2.0043	0.7242	0.0732	1.461	0.6664	0.1525	1.872	0.7599	0.1151	1.136
265- 3	1.4655	0.5579	0.0953	2.201	0.5612	0.2168	2.182	0.6093	0.1862	1.871
265- 4	1.1986	0.4385	0.1088	2.636	0.4719	0.2576	2.430	0.4928	0.2400	2.292
265- 5	1.0366	0.3679	0.1209	2.763	0.4179	0.2928	2.412	0.4267	0.2829	2.344
266- 2	1.8525	0.7115	0.0807	1.476	0.6551	0.1723	1.867	0.7411	0.1341	1.221
266- 3	1.3506	0.5461	0.1071	2.430	0.5499	0.2480	2.409	0.5885	0.2212	2.189
266- 4	1.0981	0.4326	0.1233	2.648	0.4643	0.2960	2.449	0.4780	0.2833	2.359
267- 2	1.9950	0.7618	0.0771	1.182	0.6891	0.1607	1.742	0.7853	0.1219	0.932
267- 3	1.3977	0.5690	0.1049	2.268	0.5637	0.2411	2.297	0.6074	0.2121	2.042
267- 4	1.1210	0.4481	0.1221	2.516	0.4732	0.2922	2.356	0.4886	0.2783	2.252
358- 2	1.6626	0.6487	0.0827	2.009	0.6147	0.1809	2.213	0.6840	0.1463	1.773
358- 3	1.2556	0.5097	0.1074	2.855	0.5258	0.2507	2.773	0.5538	0.2286	2.623
358- 4	1.0355	0.4095	0.1220	2.713	0.4463	0.2938	2.462	0.4546	0.2827	2.402
359- 2	1.6283	0.6506	0.0806	2.007	0.6150	0.1768	2.229	0.6831	0.1436	1.782
359- 3	1.2149	0.5018	0.1068	2.950	0.5184	0.2508	2.864	0.5419	0.2308	2.736
359- 4	0.9951	0.4058	0.1215	2.736	0.4408	0.2936	2.482	0.4464	0.2829	2.439
360- 2	1.5958	0.6558	0.0826	2.041	0.6167	0.1821	2.279	0.6834	0.1491	1.855
360- 3	1.1753	0.5048	0.1110	3.101	0.5177	0.2620	3.037	0.5379	0.2436	2.933
361- 2	1.6109	0.6815	0.0818	1.807	0.6318	0.1795	2.137	0.7018	0.1468	1.653
361- 3	1.1490	0.5190	0.1124	3.017	0.5255	0.2655	2.983	0.5451	0.2481	2.878

Table F-34

PRESSURE DROP -- CORRELATED RESULTS

$G \approx 1.70 \times 10^6$ lbm/hr-sq ft $T \approx 200°F$

RUN #	SQRT (X_{tt})	HOMOGENEOUS [3] MODEL			MARTINELLI-NELSON [4] MODEL			MARTINELLI-NELSON [4] MODEL WITH ZUBER ET AL [10] GENERAL VOID FRACTION MODEL		
		ΔP (ACC+GRAV) (PSI)	ΔP (FRICTION) (PSI)	Φ_{ftt}	ΔP (ACC+GRAV) (PSI)	ΔP (FRICTION) (PSI)	Φ_{ftt}	ΔP (ACC+GRAV) (PSI)	ΔP (FRICTION) (PSI)	Φ_{ftt}
363- 2	3.2519	0.9953	0.1690	1.169	0.9229	0.2575	1.375	1.0122	0.1828	1.116
363- 3	2.3400	0.8368	0.2019	1.785	0.7873	0.3587	1.886	0.8821	0.2627	1.687
363- 4	1.9508	0.6954	0.2152	1.775	0.6814	0.4076	1.807	0.7504	0.3175	1.643
363- 5	1.7183	0.6052	0.2292	1.486	0.6161	0.4514	1.453	0.6648	0.3727	1.295
364- 2	2.9704	0.9948	0.1770	1.114	0.9146	0.2832	1.351	1.0093	0.2011	1.066
364- 3	2.1276	0.8342	0.2141	1.900	0.7830	0.3921	1.999	0.8748	0.2954	1.817
364- 4	1.7576	0.6840	0.2339	1.714	0.6716	0.4567	1.744	0.7325	0.3731	1.590
364- 5	1.5434	0.5925	0.2508	1.660	0.6061	0.5069	1.622	0.6466	0.4407	1.502
365- 2	2.5360	0.9598	0.1871	1.272	0.8376	0.3528	1.592	0.9492	0.2551	1.303
365- 3	1.8775	0.8020	0.2290	2.007	0.7105	0.4827	2.180	0.7970	0.3818	2.017
365- 4	1.5643	0.6674	0.2508	1.851	0.6065	0.5575	1.993	0.6585	0.4802	1.872
365- 5	1.3780	0.5779	0.2709	1.887	0.5403	0.6212	1.983	0.5697	0.5697	1.908
366- 2	2.7230	1.0346	0.1817	1.118	0.9068	0.3323	1.481	1.0123	0.2391	1.190
366- 3	1.8842	0.8481	0.2293	1.966	0.7373	0.4825	2.177	0.8295	0.3815	2.003
366- 4	1.5273	0.7004	0.2563	1.845	0.6223	0.5725	2.027	0.6750	0.4985	1.906
366- 5	1.3318	0.5969	0.2812	1.772	0.5472	0.6493	1.908	0.5732	0.6056	1.838
367- 2	2.7714	1.0777	0.1815	1.035	0.9442	0.3315	1.435	1.0453	0.2395	1.145
367- 3	1.8474	0.8803	0.2318	2.023	0.7542	0.4902	2.257	0.8498	0.3909	2.082
367- 4	1.4663	0.7236	0.2646	1.854	0.6321	0.5964	2.068	0.6840	0.5296	1.950
368- 2	2.5576	1.0985	0.1908	1.135	0.9466	0.3578	1.551	1.0543	0.2614	1.270
368- 3	1.7124	0.8956	0.2495	2.045	0.7548	0.5386	2.304	0.8437	0.4446	2.145
369- 2	2.3974	1.0982	0.2019	1.218	0.9251	0.3935	1.659	1.0465	0.2898	1.365

Table F-35

PRESSURE DROP -- CORRELATED RESULTS

$G \approx 3.42 \times 10^6$ lbm/hr-sq ft $T \approx 200°F$

RUN #	SQRT (X_{tt})	HOMOGENEOUS [3] MODEL			MARTINELLI-NELSON [4] MODEL			MARTINELLI-NELSON [4] MODEL WITH ZUBER ET AL [10] GENERAL VOID FRACTION MODEL		
		ΔP (ACC+GRAV) (PSI)	ΔP (FRICTION) (PSI)	Φ_{ftt}	ΔP (ACC+GRAV) (PSI)	ΔP (FRICTION) (PSI)	Φ_{ftt}	ΔP (ACC+GRAV) (PSI)	ΔP (FRICTION) (PSI)	Φ_{ftt}
371- 3	3.2896	1.1540	0.5864	1.688	1.0990	0.7905	1.721	1.1554	0.5638	1.687
371- 4	2.5670	0.9756	0.6299	1.583	0.9135	0.9670	1.626	1.0173	0.7034	1.553
371- 5	2.2290	0.8647	0.6605	1.347	0.8671	0.9372	1.344	0.9670	0.7092	1.252
372- 3	3.1101	1.2079	0.5913	1.540	1.1337	0.8230	1.590	1.1997	0.5868	1.546
372- 4	2.3974	1.0584	0.6370	1.708	0.9465	1.0617	1.782	1.0657	0.7842	1.703
373- 3	2.7505	1.2485	0.6300	1.690	1.1039	1.0453	1.779	1.2090	0.7506	1.715
374- 3	2.5033	1.2794	0.6378	1.734	1.1029	1.0955	1.843	1.2261	0.7994	1.767
375- 3	2.5334	1.3839	0.6580	1.793	1.1837	1.1199	1.908	1.3069	0.8159	1.838

Table F-36

PRESSURE DROP -- CORRELATED RESULTS

$G \approx 0.47 \times 10^6$ lbm/hr-sq ft $T \approx 250°F$

RUN #	SQRT (X_{tt})	HOMOGENEOUS [3] MODEL			MARTINELLI-NELSON [4] MODEL			MARTINELLI-NELSON [4] MODEL WITH ZUBER ET AL [10] GENERAL VOID FRACTION MODEL		
		ΔP (ACC+GRAV) (PSI)	ΔP (FRICTION) (PSI)	Φ_{ftt}	ΔP (ACC+GRAV) (PSI)	ΔP (FRICTION) (PSI)	Φ_{ftt}	ΔP (ACC+GRAV) (PSI)	ΔP (FRICTION) (PSI)	Φ_{ftt}
377- 2	2.0493	0.6799	0.0212	1.383	0.6627	0.0345	1.765	0.7212	0.0278	*******
377- 3	1.4641	0.5388	0.0255	2.200	0.5704	0.0455	1.506	0.6010	0.0396	*******
377- 4	1.1905	0.4277	0.0275	2.372	0.4810	0.0509	*******	0.4956	0.0467	*******
377- 5	1.0138	0.3585	0.0293	2.661	0.4213	0.0553	*******	0.4295	0.0520	*******
337- 3	1.2619	0.4767	0.0247	2.165	0.5253	0.0465	*******	0.5500	0.0411	*******
337- 4	1.0053	0.3669	0.0272	2.495	0.4324	0.0530	*******	0.4444	0.0486	*******

Table F-37

PRESSURE DROP -- CORRELATED RESULTS

$G \approx 0.97 \times 10^6$ lbm/hr-sq ft $T \approx 250°F$

RUN #	SQRT (X_{tt})	HOMOGENEOUS [3] MODEL			MARTINELLI-NELSON [4] MODEL			MARTINELLI-NELSON [4] MODEL WITH ZUBER ET AL [10] GENERAL VOID FRACTION MODEL		
		ΔP (ACC+GRAV) (PSI)	ΔP (FRICTION) (PSI)	Φ_{ftt}	ΔP (ACC+GRAV) (PSI)	ΔP (FRICTION) (PSI)	Φ_{ftt}	ΔP (ACC+GRAV) (PSI)	ΔP (FRICTION) (PSI)	Φ_{ftt}
378- 3	3.0246	0.8185	0.0690	1.123	0.7689	0.1020	1.462	0.8339	0.0819	0.995
378- 4	2.2306	0.6947	0.0705	1.070	0.6635	0.1134	1.329	0.7178	0.0927	0.827
378- 5	1.8264	0.5954	0.0739	1.102	0.5878	0.1257	1.177	0.6254	0.1073	0.741
379- 2	2.6462	0.7998	0.0632	0.906	0.7523	0.0948	1.331	0.8144	0.0768	0.727
379- 3	1.8505	0.6737	0.0733	1.590	0.6600	0.1230	1.633	0.7035	0.1053	1.368
379- 4	1.5002	0.5555	0.0771	1.649	0.5683	0.1360	1.544	0.5910	0.1238	1.338
379- 5	1.2908	0.4743	0.0814	1.757	0.5048	0.1481	1.471	0.5138	0.1419	1.375
380- 3	2.1316	0.7442	0.0718	1.213	0.7063	0.1175	1.496	0.7653	0.0960	1.022
380- 4	1.5859	0.5896	0.0782	1.311	0.5893	0.1386	1.314	0.6209	0.1236	0.878
381- 3	1.8898	0.7160	0.0776	1.377	0.6847	0.1326	1.595	0.7381	0.1117	1.200
382- 2	2.5215	0.8166	0.0661	1.141	0.7601	0.1055	1.562	0.8279	0.0846	1.036

Table F-38

HEAT TRANSFER -- EXPERIMENTAL DATA

$G \approx 0.12 \times 10^6$ lbm/hr-sq ft T≈100 °F

RUN #	G (LBM/HR-SQ FT)	T BOIL (DEG F)	X IN	X OUT	ΔT (DEG F)	HEAT FLUX (BTU/HR-SQ FT)	H EXP (BTU/HR-SQ FT-DEG F)
398- 3	0.1197E 06	101.7	0.024	0.058	7.61	3066.5	402.9
398- 4	0.1197E 06	100.8	0.058	0.092	8.44	3308.8	392.0
398- 5	0.1197E 06	100.6	0.092	0.125	8.63	3367.7	390.0
398- 7	0.1197E 06	100.1	0.159	0.192	8.06	3316.6	411.3
398- 8	0.1197E 06	99.7	0.192	0.224	9.37	2982.1	318.3
398- 9	0.1197E 06	99.3	0.224	0.256	9.84	3185.7	323.7
398-10	0.1197E 06	98.9	0.256	0.287	9.72	3109.5	319.8
402- 3	0.1360E 06	102.1	0.025	0.079	12.82	6237.2	486.4
402- 4	0.1360E 06	101.2	0.079	0.134	13.89	6055.6	435.9
402- 5	0.1360E 06	101.4	0.134	0.189	13.91	6811.5	489.7
402- 7	0.1360E 06	101.1	0.246	0.301	14.11	6357.3	450.6
402- 8	0.1360E 06	101.0	0.301	0.356	14.98	6263.7	418.2
402- 9	0.1360E 06	100.5	0.356	0.411	15.48	6415.0	414.5
402-10	0.1360E 06	100.5	0.411	0.465	14.59	6205.3	425.3
404- 1	0.1197E 06	102.8	0.011	0.098	14.45	8811.7	609.9
404- 2	0.1197E 06	102.8	0.098	0.190	15.94	9384.0	588.6
404- 3	0.1197E 06	102.3	0.190	0.284	16.10	9456.2	587.3
404- 4	0.1197E 06	101.5	0.284	0.377	17.58	9427.0	536.4
404- 5	0.1197E 06	101.7	0.377	0.468	16.98	9426.0	555.2
404- 7	0.1197E 06	101.5	0.563	0.658	18.27	9607.1	525.7
404- 8	0.1197E 06	101.6	0.658	0.752	19.18	9696.9	505.6
404- 9	0.1197E 06	101.1	0.752	0.844	20.14	9455.4	469.4
404-10	0.1197E 06	101.0	0.844	0.932	18.16	8929.0	491.6
450- 3	0.1160E 06	99.8	0.020	0.054	7.79	2940.3	377.5
450- 4	0.1160E 06	98.5	0.054	0.088	8.93	3109.9	348.4
450- 5	0.1160E 06	98.6	0.088	0.121	9.14	3354.4	366.8
450- 7	0.1160E 06	98.4	0.154	0.188	8.44	3307.0	391.8
450- 8	0.1160E 06	98.1	0.188	0.221	9.21	3299.5	358.3
450- 9	0.1160E 06	97.8	0.221	0.255	9.60	3222.3	335.7
450-10	0.1160E 06	97.5	0.255	0.290	9.79	3447.4	352.3
454- 2	0.1197E 06	100.4	0.050	0.111	10.69	6282.9	587.9
454- 3	0.1197E 06	100.0	0.111	0.177	10.79	6402.0	593.5
454- 4	0.1197E 06	98.4	0.177	0.242	12.66	6324.6	499.7
454- 5	0.1197E 06	98.6	0.242	0.304	12.25	6593.7	538.4
454- 7	0.1197E 06	98.4	0.369	0.433	12.29	6545.5	532.5
454- 8	0.1197E 06	98.3	0.433	0.495	12.72	6335.6	498.2
454- 9	0.1197E 06	98.2	0.495	0.556	13.16	6348.2	482.5
454-10	0.1197E 06	98.0	0.556	0.618	13.27	6306.3	475.1
455- 2	0.1171E 06	99.2	0.024	0.112	15.16	9677.3	638.2
455- 3	0.1171E 06	98.9	0.112	0.212	15.13	9661.2	636.4

Table F-38 (continued)

RUN #	G (LBM/HR-SQ FT)	T BOIL (DEG F)	X IN	X OUT	ΔT (DEG F)	HEAT FLUX (BTU/HR-SQ FT)	H EXP (BTU/HR-SQ FT-DEG F)
455- 4	0.1171E 06	97.4	0.212	0.311	17.12	9846.6	575.0
455- 5	0.1171E 06	97.6	0.311	0.406	16.38	9741.6	594.7
455- 7	0.1171E 06	97.3	0.504	0.600	17.32	9625.6	555.9
455- 8	0.1171E 06	97.3	0.600	0.694	17.69	9488.4	536.3
455- 9	0.1171E 06	97.0	0.694	0.786	18.54	9278.9	500.4
455-10	0.1171E 06	96.9	0.786	0.878	17.61	9337.3	530.4

Table F-39

HEAT TRANSFER -- EXPERIMENTAL DATA

$G \approx 0.23 \times 10^6$ lbm/hr-sq ft T≈100°F

RUN #	G (LBM/HR-SQ FT)	T BOIL (DEG F)	X IN	X OUT	ΔT (DEG F)	HEAT FLUX (BTU/HR-SQ FT)	H EXP (BTU/HR-SQ FT-DEG F)
396- 3	0.2208E 06	103.5	0.010	0.030	7.56	3222.0	426.4
396- 4	0.2208E 06	102.5	0.030	0.050	8.59	3322.6	386.8
396- 5	0.2208E 06	102.2	0.050	0.069	8.87	3310.9	373.1
396- 7	0.2208E 06	101.7	0.087	0.106	8.35	3378.0	404.5
396- 8	0.2208E 06	101.4	0.106	0.124	9.47	3065.8	323.9
396- 9	0.2208E 06	100.9	0.124	0.143	9.90	3157.7	318.9
396-10	0.2208E 06	100.6	0.143	0.160	9.83	3048.5	310.2
403- 3	0.2269E 06	107.5	0.016	0.050	11.15	6225.3	558.1
403- 4	0.2269E 06	106.6	0.050	0.085	12.46	6046.4	485.4
403- 5	0.2269E 06	106.4	0.085	0.118	12.64	6811.5	538.9
403- 7	0.2269E 06	106.1	0.153	0.187	12.56	6357.3	506.1
403- 8	0.2269E 06	106.1	0.187	0.221	13.38	6263.7	468.3
403- 9	0.2269E 06	105.5	0.221	0.255	14.05	6386.4	454.5
403-10	0.2269E 06	105.3	0.255	0.288	13.50	6142.3	455.1
405- 2	0.2272E 06	104.0	0.015	0.062	14.29	9426.1	659.8
405- 3	0.2272E 06	103.3	0.062	0.114	14.56	9446.8	648.7
405- 4	0.2272E 06	102.5	0.114	0.164	15.92	9481.4	595.4
405- 5	0.2272E 06	102.5	0.164	0.213	15.62	9437.9	604.3
405- 7	0.2272E 06	102.1	0.264	0.315	16.88	9585.3	567.9
405- 8	0.2272E 06	102.0	0.315	0.365	17.87	9699.4	542.7
405- 9	0.2272E 06	101.6	0.365	0.414	18.26	9441.0	517.0
405-10	0.2272E 06	101.3	0.414	0.462	16.77	8970.9	534.8
410- 2	0.2272E 06	103.4	0.025	0.088	17.73	12835.3	724.1
410- 3	0.2272E 06	103.0	0.088	0.156	17.83	12553.1	704.0
410- 4	0.2272E 06	101.7	0.156	0.224	19.61	12688.7	647.1
410- 5	0.2272E 06	101.8	0.224	0.289	19.19	13023.4	678.6
410- 7	0.2272E 06	101.3	0.356	0.424	21.13	13178.5	623.6
410- 8	0.2272E 06	101.4	0.424	0.490	22.37	12970.5	579.8
410- 9	0.2272E 06	100.8	0.490	0.554	22.57	12175.0	539.3
410-10	0.2272E 06	100.6	0.554	0.616	20.61	11919.1	578.4
412- 2	0.2246E 06	103.5	0.026	0.102	19.57	15469.8	790.4
412- 3	0.2246E 06	103.0	0.102	0.187	19.93	15630.9	784.1
412- 4	0.2246E 06	101.9	0.187	0.272	21.80	16043.5	735.9
412- 5	0.2246E 06	101.8	0.272	0.354	21.05	15966.6	758.3
412- 7	0.2246E 06	101.0	0.439	0.523	23.19	16301.1	702.9
412- 8	0.2246E 06	101.3	0.523	0.604	23.78	15448.2	649.7
412- 9	0.2246E 06	100.6	0.604	0.683	24.90	15253.5	612.5
412-10	0.2246E 06	100.3	0.683	0.757	22.58	13786.9	610.6
451- 4	0.2361E 06	99.9	0.025	0.043	8.30	3237.8	390.0
451- 5	0.2361E 06	99.9	0.043	0.060	8.26	3314.1	401.3
451- 7	0.2361E 06	99.6	0.077	0.095	7.80	3278.7	420.5
451- 8	0.2361E 06	99.3	0.095	0.113	8.71	3545.0	406.8
451- 9	0.2361E 06	98.8	0.113	0.131	9.03	3175.3	351.6
451-10	0.2361E 06	98.6	0.131	0.148	8.89	3344.2	376.0

Table F-40

HEAT TRANSFER -- EXPERIMENTAL DATA

$G \approx 0.45 \times 10^6$ lbm/hr-sq ft T≈100°F

RUN #	G (LBM/HR-SQ FT)	T BOIL (DEG F)	X IN	X OUT	ΔT (DEG F)	HEAT FLUX (BTU/HR-SQ FT)	H EXP (BTU/HR-SQ FT-DEG F)
397- 4	0.4278E 06	101.8	0.016	0.028	7.44	3384.2	455.1
397- 5	0.4278E 06	101.5	0.028	0.038	7.63	3318.4	435.0
397- 7	0.4278E 06	100.7	0.049	0.060	7.46	3378.0	452.9
397- 8	0.4278E 06	100.3	0.060	0.071	8.49	3073.6	361.9
397- 9	0.4278E 06	99.8	0.071	0.081	8.89	3196.2	359.6
397-10	0.4278E 06	99.5	0.081	0.091	8.94	3174.0	355.1
401- 4	0.4481E 06	100.9	0.028	0.048	10.92	6070.3	555.7
401- 5	0.4481E 06	100.6	0.048	0.065	11.20	6614.3	590.7
401- 7	0.4481E 06	99.7	0.084	0.103	10.54	6401.2	607.2
401- 8	0.4481E 06	99.5	0.103	0.121	12.51	6399.6	511.6
401- 9	0.4481E 06	98.8	0.121	0.141	12.96	6583.2	507.8
401-10	0.4481E 06	98.3	0.141	0.159	12.45	6143.2	493.5
406- 3	0.4502E 06	104.5	0.015	0.043	13.36	9464.7	708.5
406- 4	0.4502E 06	103.4	0.043	0.071	14.98	9505.3	634.6
406- 5	0.4502E 06	103.3	0.071	0.096	14.68	9461.8	644.5
406- 7	0.4502E 06	102.5	0.123	0.150	15.90	9609.2	604.3
406- 8	0.4502E 06	102.5	0.150	0.176	16.96	9649.1	568.8
406- 9	0.4502E 06	101.8	0.176	0.203	17.49	9405.1	537.9
406-10	0.4502E 06	101.5	0.203	0.227	16.17	8976.9	555.2
409- 3	0.4390E 06	105.1	0.025	0.063	17.69	12483.2	705.8
409- 4	0.4390E 06	104.0	0.063	0.099	18.96	12623.3	665.9
409- 5	0.4390E 06	103.8	0.099	0.133	19.27	12972.1	673.3
409- 7	0.4390E 06	102.9	0.170	0.207	20.82	13206.8	634.2
409- 8	0.4390E 06	102.9	0.207	0.242	21.70	12722.5	586.3
409- 9	0.4390E 06	102.2	0.242	0.277	21.90	12237.5	558.7
409-10	0.4390E 06	101.8	0.277	0.310	20.22	12014.8	594.1
411- 3	0.4586E 06	105.5	0.029	0.073	19.13	15636.3	817.5
411- 4	0.4586E 06	104.3	0.073	0.117	21.03	15971.8	759.5
411- 5	0.4586E 06	104.1	0.117	0.158	20.43	16050.2	785.8
411- 7	0.4586E 06	103.0	0.201	0.245	22.70	15998.5	704.8
411- 8	0.4586E 06	103.1	0.245	0.286	23.44	15947.4	680.3
411- 9	0.4586E 06	102.3	0.286	0.327	23.76	15211.6	640.1
411-10	0.4586E 06	101.7	0.327	0.366	21.90	14262.9	651.2
415- 3	0.4598E 06	102.8	0.028	0.080	22.61	18788.7	830.8
415- 4	0.4598E 06	101.5	0.080	0.132	24.43	19245.5	787.8
415- 5	0.4598E 06	101.1	0.132	0.181	23.67	19478.9	822.8
415- 7	0.4598E 06	99.8	0.233	0.285	26.73	19458.9	727.8
415- 8	0.4598E 06	100.0	0.285	0.334	27.49	19221.3	699.3
415- 9	0.4598E 06	99.0	0.334	0.383	27.86	18522.8	664.9
415-10	0.4598E 06	98.4	0.383	0.428	25.55	16594.8	649.4

Table F-40 (continued)

RUN #	G (LBM/HR-SQ FT)	T BOIL (DEG F)	X IN	X OUT	ΔT (DEG F)	HEAT FLUX (BTU/HR-SQ FT)	H EXP (BTU/HR-SQ FT-DEG F)
416- 3	0.4607E 06	103.5	0.038	0.098	25.45	21892.9	860.1
416- 4	0.4607E 06	102.3	0.098	0.159	27.37	22639.6	827.1
416- 5	0.4607E 06	101.9	0.159	0.216	26.32	22650.4	860.5
416- 7	0.4607E 06	100.2	0.277	0.337	30.80	22676.7	736.2
416- 8	0.4607E 06	100.5	0.337	0.395	31.46	22363.3	710.8
416- 9	0.4607E 06	99.3	0.395	0.450	32.24	21426.8	664.7
416-10	0.4607E 06	99.0	0.450	0.501	30.51	18998.6	622.7

Table F-41

HEAT TRANSFER -- EXPERIMENTAL DATA

G≈0.89 x 10^6 lbm/hr-sq ft T=100°F

RUN #	G (LBM/HR-SQ FT)	T BOIL (DEG F)	X IN	X OUT	ΔT (DEG F)	HEAT FLUX (BTU/HR-SQ FT)	H EXP (BTU/HR-SQ FT-DEG F)
399- 7	0.8999E 06	98.7	0.031	0.038	6.43	3383.9	526.1
399- 8	0.8999E 06	98.3	0.038	0.044	7.54	3313.7	439.6
399- 9	0.8999E 06	97.6	0.044	0.051	7.76	3198.8	412.2
399-10	0.8999E 06	97.1	0.051	0.057	8.03	3063.9	381.4
400- 4	0.8828E 06	101.5	0.017	0.028	10.46	6122.3	585.5
400- 5	0.8828E 06	101.2	0.028	0.038	10.53	6680.0	634.2
400- 7	0.8828E 06	99.9	0.050	0.062	10.59	6471.3	611.1
400- 8	0.8828E 06	99.6	0.062	0.072	12.27	6423.5	523.6
400- 9	0.8828E 06	98.7	0.072	0.084	12.62	6309.6	500.1
400-10	0.8828E 06	98.2	0.084	0.094	12.38	6268.3	506.4
407- 4	0.9030E 06	104.7	0.014	0.029	15.38	9445.5	614.2
407- 5	0.9030E 06	104.5	0.029	0.042	15.25	9418.4	617.6
407- 7	0.9030E 06	103.3	0.058	0.073	16.00	9615.2	600.8
407- 8	0.9030E 06	103.3	0.073	0.087	17.08	9708.9	568.3
407- 9	0.9030E 06	102.4	0.087	0.102	17.59	9480.4	539.1
407-10	0.9030E 06	101.9	0.102	0.116	16.53	8888.2	537.6
408- 4	0.8887E 06	106.2	0.023	0.044	18.50	12933.0	699.0
408- 5	0.8887E 06	105.8	0.044	0.062	18.78	13092.1	697.2
408- 7	0.8887E 06	104.6	0.082	0.102	20.36	13081.2	642.6
408- 8	0.8887E 06	104.5	0.102	0.121	21.13	12716.7	601.9
408- 9	0.8887E 06	103.7	0.121	0.140	21.50	12377.3	575.6
408-10	0.8887E 06	103.0	0.140	0.158	19.88	11665.0	586.7
413- 3	0.8822E 06	106.1	0.004	0.029	19.23	15788.5	821.1
413- 4	0.8822E 06	104.6	0.029	0.054	20.90	16332.7	781.6
413- 5	0.8822E 06	104.4	0.054	0.076	20.00	16184.7	809.1
413- 7	0.8822E 06	102.8	0.101	0.125	22.61	16057.0	710.1
413- 8	0.8822E 06	102.7	0.125	0.149	23.39	15717.7	672.0
413- 9	0.8822E 06	101.7	0.149	0.172	23.94	15385.0	642.6
413-10	0.8822E 06	101.1	0.172	0.194	22.07	14233.4	644.8
414- 3	0.8933E 06	105.8	0.005	0.032	22.10	18508.3	837.5
414- 4	0.8933E 06	104.3	0.032	0.061	23.67	19385.2	819.1
414- 5	0.8933E 06	104.0	0.061	0.087	22.84	19546.0	855.6
414- 7	0.8933E 06	102.3	0.116	0.145	26.27	19419.7	739.1
414- 8	0.8933E 06	102.2	0.145	0.173	27.06	19250.9	711.4
414- 9	0.8933E 06	101.0	0.173	0.201	27.65	18561.3	671.3
414-10	0.8933E 06	100.3	0.201	0.226	25.29	16643.1	658.1
417- 3	0.8831E 06	105.9	0.013	0.045	24.08	21670.1	899.9
417- 4	0.8831E 06	104.4	0.045	0.079	26.17	22793.1	870.9
417- 5	0.8831E 06	104.1	0.079	0.110	24.99	22681.8	907.5

Table F-41 (continued)

RUN #	G (LBM/HR-SQ FT)	T BOIL (DEG F)	X IN	X OUT	ΔT (DEG F)	HEAT FLUX (BTU/HR-SQ FT)	H EXP (BTU/HR-SQ FT-DEG F)
417- 7	0.8831E 06	101.9	0.145	0.178	29.79	22735.7	763.3
417- 8	0.8831E 06	102.1	0.178	0.210	30.65	22517.9	734.7
417- 9	0.8831E 06	100.8	0.210	0.243	30.97	21628.7	698.4
417-10	0.8831E 06	100.0	0.243	0.271	28.16	19121.7	679.1
418- 3	0.8727E 06	106.5	0.022	0.059	26.53	24767.1	933.6
418- 4	0.8727E 06	105.1	0.059	0.098	28.56	26016.5	911.0
418- 5	0.8727E 06	104.5	0.098	0.134	27.23	25886.3	950.6
418- 7	0.8727E 06	102.3	0.173	0.211	33.01	25696.3	778.5
418- 8	0.8727E 06	102.6	0.211	0.247	33.47	25065.0	749.0
418- 9	0.8727E 06	101.2	0.247	0.283	34.60	24506.8	708.3
418-10	0.8727E 06	100.4	0.283	0.315	30.80	20267.5	657.9
452- 4	0.9268E 06	99.7	0.016	0.029	10.06	6615.3	657.6
452- 5	0.9268E 06	99.5	0.029	0.038	9.96	6583.2	660.7
452- 7	0.9268E 06	98.3	0.049	0.061	10.83	6656.3	614.7
452- 8	0.9268E 06	98.0	0.061	0.071	11.34	6911.7	609.6
452- 9	0.9268E 06	97.3	0.071	0.083	11.48	6546.1	570.2
452-10	0.9268E 06	96.6	0.083	0.094	11.82	6450.4	545.9
453- 3	0.8976E 06	102.2	0.015	0.037	16.26	12601.6	775.0
453- 4	0.8976E 06	100.4	0.037	0.058	18.06	13007.7	720.1
453- 5	0.8976E 06	100.1	0.058	0.076	17.81	13121.0	736.6
453- 7	0.8976E 06	98.6	0.096	0.117	19.59	13131.8	670.5
453- 8	0.8976E 06	98.3	0.117	0.136	20.18	13122.2	650.3
453- 9	0.8976E 06	97.6	0.136	0.155	20.33	12694.4	624.3
453-10	0.8976E 06	96.8	0.155	0.174	19.85	12113.5	610.2

Table F-42

HEAT TRANSFER -- EXPERIMENTAL DATA

$G \approx 0.14 \times 10^6$ lbm/hr-sq ft T≈150°F

RUN #	G (LBM/HR-SQ FT)	T BOIL (DEG F)	X IN	X OUT	ΔT (DEG F)	HEAT FLUX (BTU/HR-SQ FT)	H EXP (BTU/HR-SQ FT-DEG F)
456- 5	0.1444E 06	150.6	0.015	0.044	6.42	3217.2	501.0
456- 7	0.1444E 06	150.7	0.073	0.103	5.20	3451.4	663.9
456- 8	0.1444E 06	150.7	0.103	0.134	6.25	3288.5	525.9
456- 9	0.1444E 06	150.1	0.134	0.164	6.98	2999.7	430.0
456-10	0.1444E 06	150.0	0.164	0.192	6.77	3067.0	453.1
457- 3	0.1345E 06	150.0	0.032	0.097	9.00	6603.3	733.6
457- 4	0.1345E 06	149.2	0.097	0.162	9.96	6496.4	652.6
457- 5	0.1345E 06	149.3	0.162	0.223	9.60	6414.8	668.2
457- 7	0.1345E 06	149.5	0.285	0.347	8.47	6229.1	735.8
457- 8	0.1345E 06	149.6	0.347	0.408	9.81	6321.4	644.5
457- 9	0.1345E 06	149.0	0.408	0.470	10.98	6352.2	576.4
457-10	0.1345E 06	148.9	0.470	0.528	10.28	5898.3	573.9
458- 2	0.1438E 06	150.1	-.008	0.055	10.75	9267.6	861.7
458- 3	0.1438E 06	149.7	0.055	0.142	11.03	9251.0	838.6
458- 4	0.1438E 06	148.9	0.142	0.229	12.40	9596.4	774.2
458- 5	0.1438E 06	149.0	0.229	0.315	11.76	9567.3	813.4
458- 7	0.1438E 06	149.2	0.401	0.487	11.09	9568.6	863.0
458- 8	0.1438E 06	149.6	0.487	0.571	12.46	9188.5	737.5
458- 9	0.1438E 06	149.0	0.571	0.655	13.65	9288.9	680.6
458-10	0.1438E 06	148.8	0.655	0.738	12.77	9065.5	710.0

Table F-43

HEAT TRANSFER -- EXPERIMENTAL DATA

$G \approx 0.24 \times 10^6$ lbm/hr-sq ft T≈150°F

RUN #	G (LBM/HR-SQ FT)	T BOIL (DEG F)	X IN	X OUT	ΔT (DEG F)	HEAT FLUX (BTU/HR-SQ FT)	H EXP (BTU/HR-SQ FT-DEG F)
460- 5	0.2453E 06	146.9	0.039	0.056	6.07	3194.9	526.2
460- 7	0.2453E 06	146.8	0.074	0.091	5.13	3323.1	647.2
460- 8	0.2453E 06	146.9	0.091	0.109	6.21	3126.8	503.8
460- 9	0.2453E 06	146.3	0.109	0.127	6.79	2944.5	433.5
460-10	0.2453E 06	146.2	0.127	0.142	6.47	2899.3	447.9
461- 3	0.2442E 06	150.0	0.018	0.056	8.28	6503.3	785.8
461- 4	0.2442E 06	149.0	0.056	0.094	9.57	6646.3	694.7
461- 5	0.2442E 06	149.0	0.094	0.127	9.32	6467.1	693.7
461- 7	0.2442E 06	149.1	0.161	0.195	8.25	6405.7	776.6
461- 8	0.2442E 06	149.3	0.195	0.229	9.45	6345.3	671.1
461- 9	0.2442E 06	148.8	0.229	0.263	10.53	6175.2	586.4
461-10	0.2442E 06	148.7	0.263	0.295	9.71	5937.1	611.7
462- 2	0.2462E 06	149.9	0.041	0.089	11.13	8945.7	803.8
462- 3	0.2462E 06	149.6	0.089	0.141	11.36	9304.8	819.1
462- 4	0.2462E 06	148.5	0.141	0.193	12.96	9424.1	727.2
462- 5	0.2462E 06	148.6	0.193	0.242	12.31	9613.6	780.7
462- 7	0.2462E 06	148.8	0.293	0.343	11.79	9673.5	820.2
462- 8	0.2462E 06	149.0	0.343	0.393	13.32	9355.8	702.6
462- 9	0.2462E 06	148.4	0.393	0.442	14.33	9175.3	640.2
462-10	0.2462E 06	148.2	0.442	0.489	13.26	8691.5	655.5
463- 2	0.2410E 06	149.4	0.005	0.063	14.14	12415.0	878.1
463- 3	0.2410E 06	149.1	0.063	0.134	14.46	12495.7	864.4
463- 4	0.2410E 06	148.1	0.134	0.205	16.08	12994.2	808.0
463- 5	0.2410E 06	148.2	0.205	0.273	15.34	12861.5	838.5
463- 7	0.2410E 06	148.2	0.341	0.410	15.69	12957.6	826.1
463- 8	0.2410E 06	148.5	0.410	0.478	17.37	12600.2	725.2
463- 9	0.2410E 06	147.9	0.478	0.544	17.94	12027.8	670.6
463-10	0.2410E 06	147.8	0.544	0.608	16.54	11816.8	714.4
464- 2	0.2421E 06	149.4	-.001	0.069	16.90	15521.7	918.7
464- 3	0.2421E 06	149.0	0.069	0.156	17.34	15460.5	891.5
464- 4	0.2421E 06	148.2	0.156	0.243	18.88	15917.9	843.1
464- 5	0.2421E 06	148.1	0.243	0.327	18.00	16078.2	893.3
464- 7	0.2421E 06	148.0	0.414	0.500	19.23	16292.4	847.1
464- 8	0.2421E 06	148.5	0.500	0.585	20.96	15874.1	757.3
464- 9	0.2421E 06	147.9	0.585	0.667	21.23	15296.6	720.4
464-10	0.2421E 06	147.7	0.667	0.745	19.56	14146.4	723.3

Table F-44

HEAT TRANSFER -- EXPERIMENTAL DATA

$G \approx 0.44 \times 10^6$ lbm/hr-sq ft T≈150°F

RUN #	G (LBM/HR-SQ FT)	T BOIL (DEG F)	X IN	X OUT	ΔT (DEG F)	HEAT FLUX (BTU/HR-SQ FT)	H EXP (BTU/HR-SQ FT-DEG F)
419- 5	0.4301E 06	150.6	0.020	0.030	8.57	3418.9	399.1
419- 7	0.4301E 06	150.3	0.040	0.051	7.59	3405.4	449.0
419- 8	0.4301E 06	150.3	0.051	0.062	7.62	3045.6	399.7
419- 9	0.4301E 06	149.6	0.062	0.074	8.76	2832.3	323.5
419-10	0.4301E 06	149.4	0.074	0.085	8.33	3186.1	382.6
424- 3	0.4383E 06	149.0	0.014	0.037	10.57	6531.5	617.8
424- 4	0.4383E 06	147.9	0.037	0.059	11.55	6523.0	564.8
424- 5	0.4383E 06	148.0	0.059	0.078	11.65	6508.9	558.6
424- 7	0.4383E 06	148.0	0.097	0.117	11.40	6573.7	576.6
424- 8	0.4383E 06	148.0	0.117	0.137	12.55	6298.5	501.9
424- 9	0.4383E 06	147.3	0.137	0.157	12.89	6142.2	476.6
424-10	0.4383E 06	147.2	0.157	0.176	12.18	5838.5	479.4
425- 3	0.4570E 06	150.3	0.018	0.048	13.83	9401.9	679.8
425- 4	0.4570E 06	149.4	0.048	0.078	14.82	9667.1	652.4
425- 5	0.4570E 06	149.3	0.078	0.105	15.10	9655.3	639.5
425- 7	0.4570E 06	149.4	0.132	0.159	15.25	9603.3	629.9
425- 8	0.4570E 06	149.5	0.159	0.188	16.86	9503.1	563.7
425- 9	0.4570E 06	148.8	0.188	0.216	17.02	9373.1	550.9
425-10	0.4570E 06	148.6	0.216	0.243	15.78	8965.7	568.1
430- 2	0.4477E 06	151.8	0.000	0.032	14.78	12731.3	861.2
430- 3	0.4477E 06	151.6	0.032	0.072	14.87	12573.4	845.7
430- 4	0.4477E 06	150.6	0.072	0.113	16.24	12934.3	796.2
430- 5	0.4477E 06	150.5	0.113	0.150	15.60	12994.4	832.8
430- 7	0.4477E 06	150.1	0.188	0.227	16.30	13266.3	813.9
430- 8	0.4477E 06	150.6	0.227	0.265	17.85	12832.4	719.1
430- 9	0.4477E 06	149.7	0.265	0.303	18.43	12236.8	664.0
430-10	0.4477E 06	149.6	0.303	0.337	16.87	11711.3	694.1

Table F-45

HEAT TRANSFER -- EXPERIMENTAL DATA

G≈0.90 x 10^6 lbm/hr-sq ft T≈150°F

RUN #	G (LBM/HR-SQ FT)	T BOIL (DEG F)	X IN	X OUT	ΔT (DEG F)	HEAT FLUX (BTU/HR-SQ FT)	H EXP (BTU/HR-SQ FT-DEG F)
466- 3	0.9309E 06	150.5	0.026	0.057	21.42	18959.0	885.0
466- 4	0.9309E 06	149.5	0.057	0.086	22.38	19037.3	850.6
466- 5	0.9309E 06	149.6	0.086	0.112	21.84	19196.1	879.0
466- 7	0.9309E 06	148.9	0.141	0.169	24.81	19452.8	784.1
466- 8	0.9309E 06	149.4	0.169	0.197	25.77	19170.1	743.8
466- 9	0.9309E 06	148.4	0.197	0.225	25.53	18324.6	717.8
466-10	0.9309E 06	148.2	0.225	0.249	23.64	16515.4	698.6
468- 4	0.8818E 06	148.5	0.023	0.044	16.42	12859.6	783.4
468- 5	0.8818E 06	148.5	0.044	0.063	15.75	12836.2	815.1
468- 7	0.8818E 06	148.2	0.082	0.101	17.14	13018.4	759.4
468- 8	0.8818E 06	148.6	0.101	0.121	17.53	12591.2	718.1
468- 9	0.8818E 06	147.7	0.121	0.142	18.02	12204.4	677.4
468-10	0.8818E 06	147.4	0.142	0.161	16.31	11958.9	733.3
469- 4	0.9687E 06	148.5	0.021	0.033	10.07	6415.4	637.1
469- 5	0.9687E 06	148.4	0.033	0.041	9.83	6355.0	646.4
469- 7	0.9687E 06	148.2	0.051	0.060	9.87	6468.3	655.5
469- 8	0.9687E 06	148.3	0.060	0.070	10.56	6201.8	587.5
469- 9	0.9687E 06	147.5	0.070	0.081	11.01	6262.5	568.9
469-10	0.9687E 06	147.3	0.081	0.090	10.38	6137.5	591.5
470- 7	0.8441E 06	149.5	0.024	0.030	5.53	3349.8	606.0
470- 8	0.8441E 06	149.5	0.030	0.037	6.22	3139.0	504.8
470- 9	0.8441E 06	148.8	0.037	0.045	6.68	3248.9	486.2
470-10	0.8441E 06	148.5	0.045	0.051	6.55	3246.3	495.3

Table F-46

HEAT TRANSFER -- EXPERIMENTAL DATA

G≈1.73 x 10^6 lbm/hr-sq ft T≈150°F

RUN #	G (LBM/HR-SQ FT)	T BOIL (DEG F)	X IN	X OUT	ΔT (DEG F)	HEAT FLUX (BTU/HR-SQ FT)	H EXP (BTU/HR-SQ FT-DEG F)
420- 7	0.1710E 07	148.2	0.018	0.023	7.00	3252.1	464.6
420- 8	0.1710E 07	148.0	0.023	0.028	7.15	2852.1	399.1
420- 9	0.1710E 07	147.1	0.028	0.033	7.59	2995.6	394.9
420-10	0.1710E 07	146.8	0.033	0.037	7.75	3246.3	419.1
423- 7	0.1759E 07	147.2	0.030	0.036	10.87	6460.1	594.3
423- 8	0.1759E 07	147.2	0.036	0.043	11.66	6376.3	547.0
423- 9	0.1759E 07	146.2	0.043	0.051	11.87	6411.3	540.3
423-10	0.1759E 07	145.8	0.051	0.058	11.41	5874.4	514.9
426- 5	0.1760E 07	148.7	0.019	0.028	10.80	9607.6	889.7
426- 7	0.1760E 07	147.7	0.037	0.046	11.48	9573.4	833.8
426- 8	0.1760E 07	147.6	0.046	0.055	12.68	9084.4	716.3
426- 9	0.1760E 07	146.7	0.055	0.066	13.41	9481.5	706.8
426-10	0.1760E 07	146.2	0.066	0.076	12.53	8977.6	716.4
429- 5	0.1710E 07	150.1	0.024	0.035	14.18	12967.5	914.6
429- 7	0.1710E 07	148.9	0.048	0.060	15.99	13230.4	827.6
429- 8	0.1710E 07	149.3	0.060	0.072	17.07	12823.4	751.1
429- 9	0.1710E 07	148.1	0.072	0.085	17.39	12306.8	707.8
429-10	0.1710E 07	147.6	0.085	0.097	16.19	11872.8	733.3

Table F-47

HEAT TRANSFER -- EXPERIMENTAL DATA

G≈3.43 x 10^6 lbm/hr-sq ft T≈150°F

RUN #	G (LBM/HR-SQ FT)	T BOIL (DEG F)	X IN	X OUT	ΔT (DEG F)	HEAT FLUX (BTU/HR-SQ FT)	H EXP (BTU/HR-SQ FT-DEG F)
421- 9	0.3429E 07	147.6	0.015	0.023	5.48	3009.3	549.1
421-10	0.3429E 07	146.5	0.023	0.030	6.12	3275.9	535.6
422- 8	0.3461E 07	147.7	0.021	0.029	9.42	6384.7	678.1
422- 9	0.3461E 07	146.1	0.029	0.039	10.04	6330.9	630.5
422-10	0.3461E 07	145.0	0.039	0.047	10.15	5911.5	582.5
427- 5	0.3436E 07	150.8	0.006	0.014	9.18	9568.7	1042.1
427- 7	0.3436E 07	148.2	0.025	0.034	11.38	9647.9	847.8
427- 8	0.3436E 07	147.5	0.034	0.043	12.83	9464.1	737.5
427- 9	0.3436E 07	146.0	0.043	0.054	13.30	9469.5	712.0
427-10	0.3436E 07	144.8	0.054	0.064	13.20	9261.4	701.4
428- 7	0.3443E 07	146.7	0.031	0.042	15.08	13140.7	871.6
428- 8	0.3443E 07	146.1	0.042	0.053	16.62	12644.2	761.0
428- 9	0.3443E 07	144.3	0.053	0.066	17.04	12435.3	729.8
428-10	0.3443E 07	142.9	0.066	0.078	16.56	11712.8	707.3

Table F-48

HEAT TRANSFER -- EXPERIMENTAL DATA

$G \approx 0.13 \times 10^6$ lbm/hr-sq ft T≈200°F

RUN #	G (LBM/HR-SQ FT)	T BOIL (DEG F)	X IN	X OUT	ΔT (DEG F)	HEAT FLUX (BTU/HR-SQ FT)	H EXP (BTU/HR-SQ FT-DEG F)
471- 2	0.1310E 06	200.7	0.022	0.055	3.96	2847.4	719.7
471- 3	0.1310E 06	200.6	0.055	0.094	4.20	3103.3	739.1
471- 4	0.1310E 06	199.6	0.094	0.131	5.25	2847.1	542.0
471- 5	0.1310E 06	199.7	0.131	0.167	5.18	3143.1	607.3
471- 7	0.1310E 06	200.2	0.203	0.237	4.23	3256.2	770.1
471- 8	0.1310E 06	200.6	0.237	0.273	4.61	2854.2	619.3
471- 9	0.1310E 06	199.8	0.273	0.309	5.69	3090.2	543.0
471-10	0.1310E 06	199.9	0.309	0.342	5.28	2770.7	525.0
474- 2	0.1326E 06	200.1	0.095	0.226	11.39	12554.3	1102.1
474- 3	0.1326E 06	200.0	0.226	0.372	11.87	12370.9	1042.2
474- 4	0.1326E 06	199.2	0.372	0.517	13.04	12447.5	954.8
474- 5	0.1326E 06	199.3	0.517	0.652	15.74	12817.0	814.2

Table F-49

HEAT TRANSFER -- EXPERIMENTAL DATA

G=0.25 x 10^6 lbm/hr-sq ft T=200°F

RUN #	G (LBM/HR-SQ FT)	T BOIL (DEG F)	X IN	X OUT	ΔT (DEG F)	HEAT FLUX (BTU/HR-SQ FT)	H EXP (BTU/HR-SQ FT-DEG F)
475- 3	0.2502E 06	202.2	0.021	0.059	8.03	6469.6	805.2
475- 4	0.2502E 06	201.5	0.059	0.101	8.73	6281.6	719.8
475- 5	0.2502E 06	201.5	0.101	0.139	8.75	6312.0	721.5
475- 7	0.2502E 06	201.6	0.177	0.214	8.40	6373.0	758.4
475- 8	0.2502E 06	202.2	0.214	0.253	8.67	6023.1	694.5
475- 9	0.2502E 06	201.0	0.253	0.294	9.82	6328.4	644.3
475-10	0.2502E 06	201.0	0.294	0.329	9.23	5659.4	613.1
476- 2	0.2557E 06	201.2	0.028	0.077	10.02	8775.6	876.1
476- 3	0.2557E 06	201.2	0.077	0.135	10.22	9265.4	906.2
476- 4	0.2557E 06	200.4	0.135	0.194	11.22	9674.6	862.4
476- 5	0.2557E 06	200.5	0.194	0.251	10.98	9566.2	871.5
476- 8	0.2557E 06	201.1	0.363	0.419	11.87	9153.5	770.9
476- 9	0.2557E 06	200.1	0.419	0.475	12.51	8985.3	718.2
476-10	0.2557E 06	200.0	0.475	0.527	11.74	8495.6	723.7
477- 2	0.2548E 06	201.8	0.028	0.096	12.86	12366.1	961.9
477- 3	0.2548E 06	201.4	0.096	0.174	13.45	12641.0	939.9
477- 4	0.2548E 06	200.9	0.174	0.252	14.16	12753.1	900.7
477- 5	0.2548E 06	200.9	0.252	0.328	13.95	12805.2	918.2
477- 7	0.2548E 06	200.8	0.405	0.481	15.22	13116.3	861.7
477- 8	0.2548E 06	201.6	0.481	0.557	15.82	12562.1	794.0
477- 9	0.2548E 06	200.6	0.557	0.631	15.86	12046.2	759.6
477-10	0.2548E 06	200.6	0.631	0.699	18.55	11258.3	606.8

Table F-50

HEAT TRANSFER -- EXPERIMENTAL DATA

G≈0.45 x 10^6 lbm/hr-sq ft T≈200°F

RUN #	G (LBM/HR-SQ FT)	T BOIL (DEG F)	X IN	X OUT	ΔT (DEG F)	HEAT FLUX (BTU/HR-SQ FT)	H EXP (BTU/HR-SQ FT-DEG F)
540- 4	0.4549E 06	185.1	0.024	0.036	6.33	3059.5	483.1
540- 5	0.4549E 06	185.0	0.036	0.047	6.24	3129.8	501.4
540- 7	0.4549E 06	184.8	0.057	0.067	5.22	3342.6	640.5
540- 8	0.4549E 06	185.1	0.067	0.079	6.89	3152.5	457.3
540- 9	0.4549E 06	184.2	0.079	0.091	6.67	3026.1	453.7
540-10	0.4549E 06	184.2	0.091	0.101	6.68	2840.8	425.2
541- 3	0.4484E 06	191.6	0.033	0.068	11.74	9448.2	804.8
541- 4	0.4484E 06	190.8	0.068	0.103	11.63	9582.3	823.6
541- 5	0.4484E 06	190.8	0.103	0.134	11.89	9648.7	811.2
541- 7	0.4484E 06	190.6	0.166	0.197	12.11	9650.8	797.0
541- 8	0.4484E 06	191.1	0.197	0.229	12.96	9279.1	715.9
541- 9	0.4484E 06	190.1	0.229	0.262	12.54	9299.1	741.4
541-10	0.4484E 06	190.0	0.262	0.291	11.60	8363.5	720.9
544- 2	0.4597E 06	199.3	0.012	0.051	14.60	15533.6	1063.8
544- 3	0.4597E 06	198.9	0.051	0.106	16.09	15566.8	967.4
544- 4	0.4597E 06	198.2	0.106	0.161	15.82	15867.9	1003.0
544- 5	0.4597E 06	198.1	0.161	0.213	15.85	15881.7	1001.7
544- 7	0.4597E 06	197.6	0.267	0.319	19.22	16057.1	835.4
544- 8	0.4597E 06	198.6	0.319	0.370	18.52	15605.9	842.5
544- 9	0.4597E 06	197.6	0.370	0.423	17.45	15325.5	878.4
544-10	0.4597E 06	197.5	0.423	0.470	15.77	13892.1	880.7

Table F-51

HEAT TRANSFER -- EXPERIMENTAL DATA

G≈0.90 x 10^6 lbm/hr-sq ft T≈200°F

RUN #	G (LBM/HR-SQ FT)	T BULK (DEG F)	X IN	X OUT	ΔT (DEG F)	HEAT FLUX (BTU/HR-SQ FT)	H EXP (BTU/HR-SQ FT-DEG F)
539- 4	0.8933E 06	189.0	0.016	0.024	5.78	3014.0	521.5
539- 5	0.8933E 06	188.9	0.024	0.030	5.65	3147.6	557.1
539- 7	0.8933E 06	188.8	0.036	0.040	5.03	3334.4	663.4
539- 8	0.8933E 06	189.0	0.040	0.046	5.93	2895.4	488.5
539- 9	0.8933E 06	188.2	0.046	0.054	6.05	3029.2	500.5
539-10	0.8933E 06	188.0	0.054	0.060	6.20	2763.6	446.1
542- 3	0.9219E 06	191.2	0.018	0.038	11.65	9519.4	817.1
542- 4	0.9219E 06	190.2	0.038	0.057	11.35	9518.1	838.5
542- 5	0.9219E 06	189.9	0.057	0.073	11.66	9588.9	822.2
542- 7	0.9219E 06	189.6	0.090	0.104	12.11	9631.9	795.5
542- 8	0.9219E 06	190.2	0.104	0.121	12.89	9506.3	737.2
542- 9	0.9219E 06	189.2	0.121	0.139	12.44	9309.7	746.5
542-10	0.9219E 06	189.0	0.139	0.154	11.59	8564.7	738.9
543- 3	0.8951E 06	198.6	0.026	0.057	15.96	15493.1	971.0
543- 4	0.8951E 06	197.6	0.057	0.087	15.75	15929.6	1011.1
543- 5	0.8951E 06	197.6	0.087	0.114	15.77	15823.4	1003.1
543- 7	0.8951E 06	196.9	0.143	0.169	19.03	15980.2	839.7
543- 8	0.8951E 06	197.8	0.169	0.196	18.58	15537.3	836.5
543- 9	0.8951E 06	196.8	0.196	0.225	17.70	15367.4	868.1
543-10	0.8951E 06	196.5	0.225	0.251	16.13	13939.9	864.1

Table F-92

HEAT TRANSFER -- EXPERIMENTAL DATA

G≈1.72 x 10^5 lbm/hr-sq ft T≈200°F

RUN #	G (LBM/HR-SQ FT)	T BOIL (DEG F)	X IN	X OUT	ΔT (DEG F)	HEAT FLUX (BTU/HR-SQ FT)	H EXP (BTU/HR-SQ FT-DEG F)
537- 3	0.1717E 07	197.9	0.021	0.041	14.79	15447.3	1044.2
537- 4	0.1717E 07	196.7	0.041	0.060	14.55	16216.3	1114.4
537- 5	0.1717E 07	196.5	0.060	0.075	14.79	16002.9	1082.1
537- 7	0.1717E 07	195.7	0.092	0.106	17.80	16233.8	911.8
537- 8	0.1717E 07	196.5	0.106	0.120	17.89	15842.3	885.4
537- 9	0.1717E 07	195.4	0.120	0.138	17.25	15767.8	914.0
537-10	0.1717E 07	195.2	0.138	0.152	15.71	13868.5	882.7
A538- 4	0.1714E 07	197.6	0.024	0.037	9.94	9874.2	993.5
A538- 5	0.1714E 07	197.4	0.037	0.048	10.19	9639.7	946.4
A538- 7	0.1714E 07	196.8	0.057	0.065	10.78	9601.3	890.5
A538- 8	0.1714E 07	197.4	0.065	0.075	11.63	9386.7	807.4
A538- 9	0.1714E 07	196.3	0.075	0.087	11.60	9185.0	792.0
A538-10	0.1714E 07	196.1	0.087	0.096	11.00	8297.6	754.0
B538- 4	0.1736E 07	193.9	0.018	0.025	4.49	2950.5	656.9
B538- 5	0.1736E 07	193.6	0.025	0.031	4.65	3188.0	685.7
B538- 7	0.1736E 07	193.1	0.035	0.037	4.36	3308.9	759.7
B538- 8	0.1736E 07	193.3	0.037	0.042	5.24	3060.4	584.3
B538- 9	0.1736E 07	192.4	0.042	0.049	5.33	2990.5	560.7
B538-10	0.1736E 07	192.1	0.049	0.053	5.70	2756.5	483.6

Table F-53

HEAT TRANSFER -- EXPERIMENTAL DATA

G≈3.48 x 10^6 lbm/hr-sq ft T≈200°F

RUN #	G (LBM/HR-SQ FT)	T BOIL (DEG F)	X IN	X OUT	ΔT (DEG F)	HEAT FLUX (BTU/HR-SQ FT)	H EXP (BTU/HR-SQ FT-DEG F)
534- 7	0.3454E 07	197.2	0.020	0.022	3.16	3113.4	985.2
534- 8	0.3454E 07	197.2	0.022	0.028	3.80	2929.0	770.1
534- 9	0.3454E 07	196.0	0.028	0.034	4.28	3002.4	701.3
534-10	0.3454E 07	195.6	0.034	0.038	4.58	2767.2	604.4
535- 7	0.3508E 07	198.4	0.029	0.034	10.23	9565.5	934.6
535- 8	0.3508E 07	198.6	0.034	0.043	11.08	9413.6	849.3
535- 9	0.3508E 07	197.1	0.043	0.053	10.93	9187.3	840.9
535-10	0.3508E 07	196.7	0.053	0.060	10.69	8263.8	773.3
536- 5	0.3455E 07	198.7	0.023	0.032	13.53	15863.8	1172.1
536- 7	0.3455E 07	197.0	0.045	0.054	17.57	15876.0	903.4
536- 8	0.3455E 07	197.6	0.054	0.064	17.61	15491.7	879.8
536- 9	0.3455E 07	196.1	0.064	0.077	16.62	15541.8	923.8
536-10	0.3455E 07	195.5	0.077	0.087	15.97	13970.5	874.7

Table F-54

CRITICAL HEAT FLUX - EXPERIMENTAL DATA

RUN NO.		T (DEG F)	L/D	X - AT CHF	G (LBM/HR-SQ FT)
CHF	1	96.15	140.96	0.9435	120000.
CHF	2	95.52	133.01	0.8952	120300.
CHF	3	98.40	133.78	0.8695	118300.
CHF	4	97.70	139.43	0.7928	239000.
CHF	5	96.67	128.42	0.7558	240200.
CHF	6	96.94	120.76	0.7349	241700.
CHF	7	99.53	132.24	0.7652	240000.
CHF	8	147.68	137.29	0.9579	116600.
CHF	9	148.90	114.70	0.9046	113900.
CHF	10	149.94	128.38	0.9456	114800.
CHF	11	147.72	126.90	0.7963	229400.
CHF	12	148.56	137.58	0.8328	232100.
CHF	13	148.36	136.86	0.8224	228900.
CHF	14	148.12	149.04	0.8642	224800.
CHF	15	97.72	136.04	0.9655	119800.
CHF	16	99.22	122.46	0.9613	117900.
CHF	17	98.41	95.95	0.8921	119400.
CHF	18	100.04	90.94	0.9371	117700.
CHF	19	98.99	90.17	0.9322	117800.
CHF	20	99.43	74.98	0.9057	120100.
CHF	21	99.83	59.54	0.8933	118300.
CHF	22	100.00	51.12	0.8089	120100.
CHF	23	97.94	100.56	0.7209	242200.
CHF	24	99.39	71.59	0.6336	241300.
CHF	25	97.70	147.72	0.9817	114600.
CHF	26	97.63	128.44	0.7703	243200.
CHF	27	97.16	119.26	0.7378	247800.
CHF	28	94.88	119.29	0.4762	472300.
CHF	29	94.98	126.87	0.4891	468400.
CHF	30	148.12	121.93	0.9801	109700.
CHF	31	148.47	127.66	0.8528	220400.
CHF	32	148.49	128.08	0.5568	437800.
CHF	33	147.65	129.81	0.5445	438900.
CHF	34	146.76	128.12	0.3178	860800.
CHF	35	145.71	127.61	0.1970	1671000.
CHF	36	147.00	109.90	0.1767	1674000.
CHF	37	146.76	110.83	0.1775	1674000.
CHF	38	144.07	102.67	0.1261	3477000.
CHF	39	96.59	125.66	0.4986	457000.
CHF	40	95.18	111.31	0.4781	464300.
CHF	41	95.85	96.01	0.4449	454200.
CHF	42	99.16	66.06	0.3374	451800.
CHF	43	98.84	65.79	0.3306	457600.
CHF	44	98.13	50.47	0.2786	459800.
CHF	45	98.62	35.93	0.2178	452600.
CHF	46	98.13	108.74	0.2706	913900.
CHF	47	94.77	102.52	0.2513	921700.
CHF	48	96.62	95.44	0.2549	926100.
CHF	49	98.68	72.31	0.2004	929400.
CHF	50	101.40	64.97	0.1897	904000.
CHF	51	97.25	55.17	0.1793	898400.
CHF	52	97.00	39.00	0.1317	925600.
CHF	53	148.36	127.50	0.5330	447700.
CHF	54	148.51	114.11	0.5055	453200.
CHF	55	147.04	112.41	0.5245	453700.
CHF	56	147.35	96.47	0.4909	452300.
CHF	57	148.88	77.52	0.4165	456200.
CHF	58	147.07	55.04	0.3242	449200.
CHF	59	142.80	46.65	0.2835	459300.
CHF	60	146.53	117.76	0.1782	1731000.
CHF	61	146.46	107.01	0.1690	1741000.
CHF	62	151.30	103.36	0.1729	1748000.
CHF	63	151.00	73.80	0.1216	1780000.
CHF	64	148.76	64.11	0.1028	1750000.
CHF	65	145.84	50.11	0.0822	1740000.
CHF	66	143.17	33.20	0.0557	1734000.
CHF	67	147.82	122.05	0.3191	871800.
CHF	68	147.61	121.13	0.3172	849100.
CHF	69	147.15	129.16	0.3282	841800.
CHF	70	198.50	109.35	0.9805	119000.
CHF	71	199.00	145.52	0.7144	236800.
CHF	72	197.97	134.80	0.6943	235100.
CHF	73	198.40	133.74	0.7154	234500.
CHF	74	199.30	139.82	0.2827	929700.
CHF	75	198.10	120.16	0.2519	939400.
CHF	76	98.42	122.29	0.9626	126600.
CHF	77	98.91	121.87	0.9726	126700.
CHF	78	99.21	109.78	0.9816	121900.
CHF	79	98.16	102.00	0.9828	119900.
CHF	80	98.38	96.55	0.9527	121700.
CHF	81	100.06	82.55	0.9267	120300.
CHF	82	100.70	68.35	0.8957	117100.
CHF	83	100.09	53.06	0.7905	120100.
CHF	84	98.75	45.40	0.8126	119900.
CHF	85	99.25	127.48	0.7772	233600.
CHF	86	99.26	125.03	0.7852	233600.
CHF	87	99.22	109.76	0.7358	234900.
CHF	88	100.00	95.09	0.7097	233600.
CHF	89	100.50	82.40	0.6964	233600.
CHF	90	101.62	67.41	0.6260	233000.
CHF	91	100.24	53.59	0.5420	232600.
CHF	92	98.10	38.10	0.4416	235900.
CHF	93	148.48	126.26	0.9843	132900.
CHF	94	148.68	113.06	0.9845	133400.
CHF	95	148.79	97.82	0.9559	127900.
CHF	96	150.35	79.04	0.9029	129700.
CHF	97	149.94	75.68	0.9441	128800.
CHF	98	151.05	61.15	0.8946	129400.
CHF	99	150.50	46.32	0.7940	126600.
CHF	100	148.50	123.78	0.7807	252600.

Table F-54 (continued)

RUN NO.	T (DEG F)	L/D	X - AT CHF	G (LBM/HR-SQ FT)
CHF 101	148.63	113.12	0.7741	252400.
CHF 102	148.38	95.98	0.7303	236200.
CHF 103	149.44	74.58	0.6702	234900.
CHF 104	150.66	59.26	0.5816	240300.
CHF 105	148.82	45.86	0.4952	238500.
CHF 106	147.75	34.35	0.4230	235400.
CHF 107	148.19	120.78	0.2867	905400.
CHF 108	147.30	107.31	0.2755	898500.
CHF 109	147.42	88.50	0.2358	929700.
CHF 110	150.32	62.16	0.1772	931100.
CHF 111	150.79	67.23	0.1842	945100.
CHF 112	149.44	46.74	0.1236	915900.
CHF 113	148.42	44.26	0.1221	936000.
CHF 114	200.65	116.09	0.9755	136400.
CHF 115	199.90	102.07	0.9583	136400.
CHF 116	199.15	83.60	0.8982	133400.
CHF 117	199.69	72.13	0.8891	131300.
CHF 118	202.15	53.35	0.7824	133800.
CHF 119	202.09	41.22	0.6731	135000.
CHF 120	202.18	32.69	0.6102	135000.
CHF 121	200.67	124.25	0.6956	254100.
CHF 122	199.70	116.18	0.6995	258900.
CHF 123	199.83	93.85	0.6543	251500.
CHF 124	199.15	87.83	0.6634	242600.
CHF 125	199.84	64.03	0.5439	243300.
CHF 126	199.53	48.74	0.4672	241300.
CHF 127	200.91	41.76	0.4649	237800.
CHF 128	199.95	121.23	0.2955	525900.
CHF 129	200.85	126.58	0.3799	451700.
CHF 130	200.76	112.31	0.3956	450400.
CHF 131	200.59	95.86	0.4176	447600.
CHF 132	199.98	56.75	0.2796	448500.
CHF 133	199.40	133.29	0.2882	904500.
CHF 134	197.59	125.35	0.2959	886800.
CHF 135	197.50	106.24	0.2656	892200.
CHF 136	199.33	82.60	0.2328	892200.
CHF 137	197.64	41.29	0.1189	886900.
CHF 138	198.95	118.01	0.1403	1697700.
CHF 139	199.39	88.15	0.1381	1714400.
CHF 140	198.01	45.10	0.0685	1727700.
CHF 141	198.34	33.59	0.0505	1742700.
CHF 142	248.59	106.73	0.2093	969000.
CHF 143	245.87	74.36	0.1731	981700.
CHF 144	243.78	38.31	0.0896	955400.
CHF 145	249.05	120.41	0.5177	281500.
CHF 146	245.03	97.21	0.4653	257700.
CHF 147	241.78	42.23	0.3288	277600.
CHF 148	243.36	122.74	0.3762	449500.
CHF 149	244.37	104.73	0.3389	484300.
CHF 150	246.97	27.58	0.1733	363200.

APPENDIX G

ERROR ANALYSIS

Monte Carlo Error Analysis Code

Most computer codes require the input of measured and/or calculated data. These data may be questionable in one or more of the following ways:

1. The data may contain errors associated with judgment. For example, instruments read visually are routinely rounded to the nearest whole division of the instrument's scale.
2. Data readings are subject to fluctuating conditions in the physical system, such as ambient temperatures and atmospheric pressures.
3. The instruments can pick up extraneous signals, such as mechanical vibrations or spurious signals from nearby electrical equipment.
4. The data may have error introduced by definition or by imprecise definition. For example, height of a system is not an exact quantity. The edges are not perfectly smooth nor exactly parallel; therefore, the measurement will have error simply by definition [139].

A computer program that accepts a set of data ($X'_1, X'_2, \ldots, X'_N$) and calculates a set of dependent variables ($Y_1, Y_2, \ldots, Y_M$) can be denoted mathematically by the following relation:

$$(Y_1, Y_2, \ldots, Y_M) = f_1(X'_1, X'_2, \ldots, X'_N) \qquad \text{(G-1)}$$

The statistical error in each dependent variable Y_i in Equation (G-1) is difficult to calculate directly because of the possible

complexity of $f_1(X'_1,X'_2,\ldots,X'_N)$. However, if a large amount of data is obtained, the standard deviation for each Y_i can be evaluated directly using

$$\sigma'_i = \sqrt{\frac{\sum_{j=1}^{k'} (Y_{ij} - \bar{Y}_i)^2}{k' - 1}} \qquad \text{(G-2)}$$

where $\bar{Y}_i$ is the average value of the i^{th} dependent variable and k' is the total number of observations. In general, it is not practical to accumulate the large amounts of observed data needed to evaluate Equation (G-2). However, estimates on the range of the deviation in the independent variables, $X'_1,X'_2,\ldots,X'_N$, can be established.

The MONTE code accomplishes this evaluation using Monte Carlo techniques. The Monte Carlo analyzer inputs data to any computer code by making it a subprogram called EVAL. The analyzer accepts the error range of each independent variable, minimum, mid, and maximum percentages, as well as the type of distribution associated with each variable--uniform, exponential, normal--or any distribution described by array values (optional input).

The function, f_1, is then evaluated k' times using random numbers, varying in the range specified [140]. Therefore, Equation (G-2) can be evaluated using actual calculated values for the dependent variables. The calling program MONTE inputs independent variables, $X'_1,X'_2,\ldots,X'_N$, and tabulates the dependent variable output, $Y_1,Y_2,\ldots,Y_N$. Each of the input and output numbers are generated within an error range about some mean value.

Pressure Drop

For the pressure drop results, 17 independent variables were used and each of them was assigned limits. These limits were taken so as to

include fluctuations in the readings, as well as the limits of accuracy of the instruments. In addition, uncertainities were assigned to fluid properties and void fraction. This error analysis was conducted on several runs covering the low, medium, and high flow ranges. These are shown in Figure G-1. As can be seen, the standard deviation σ' decreases with increasing quality and with increasing mass flux. This is because the frictional component becomes a greater percentage of the total pressure drop.

Heat Transfer Coefficients

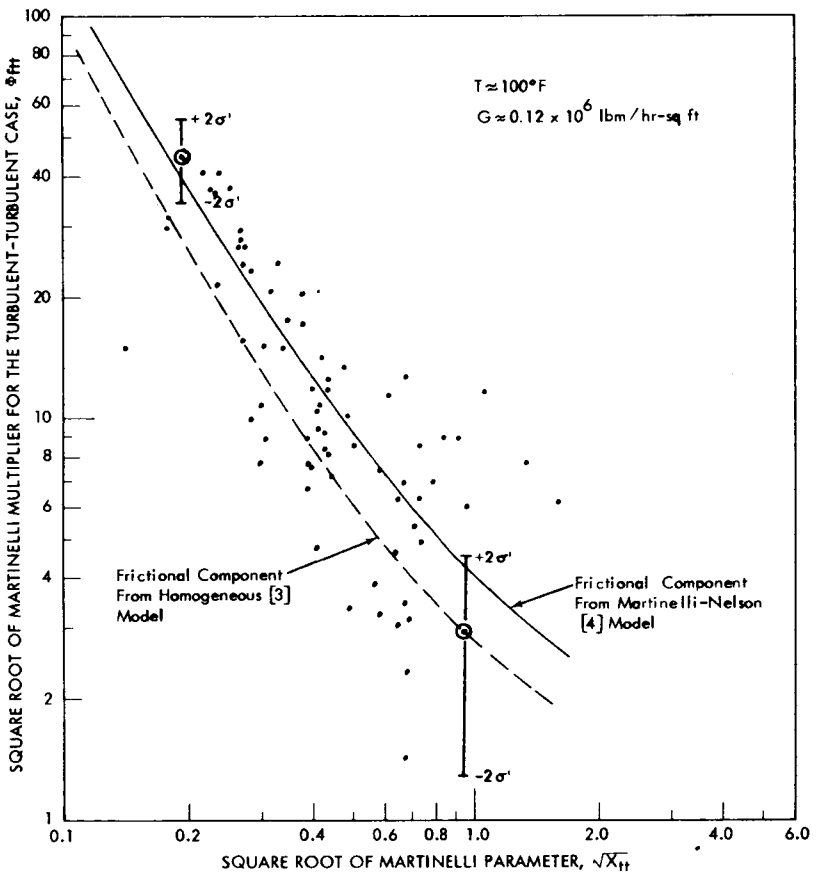
The same procedure used for the pressure drop results was also applied in the error analysis of the heat transfer coefficients. The results for the modified Chen [80] correlation with the Forster-Zuber [52] and Rohsenow [61] pool boiling correlations are given in Figures G-2 and G-3, respectively. As shown, the standard deviation is greater with the Rohsenow [61] pool boiling correlation because the heat transfer coefficient is proportional to $(\Delta T)^2$. In the Forster-Zuber [52] equation, the heat transfer coefficient is proportional to ΔT only.

Critical Heat Flux

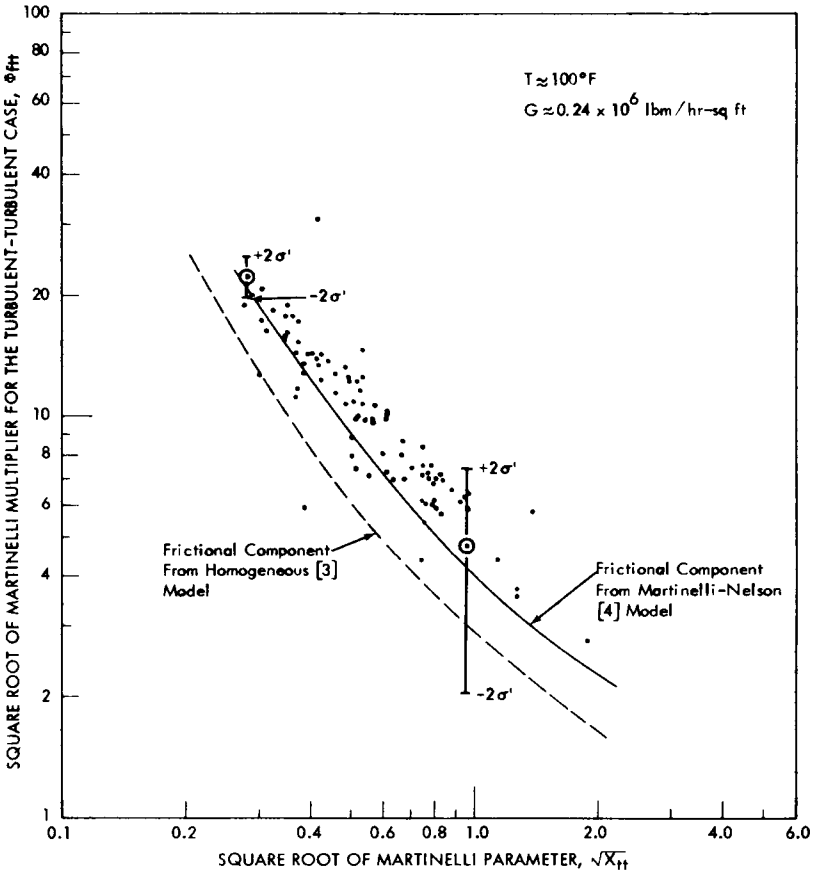
For the critical heat flux runs of this study, a sensitivity analysis of the least squares fit represented by Equations (4-95) and (4-97) was made. For the case where (D/L) is allowed to vary to any power [Equations (4-95)], the rms error was found to be:

$$\text{RMS 1} = 4.21068 \tag{G-3}$$

Now when the power of the (D/L) term is constrained to the 0.6 value, the rms error was found to be:

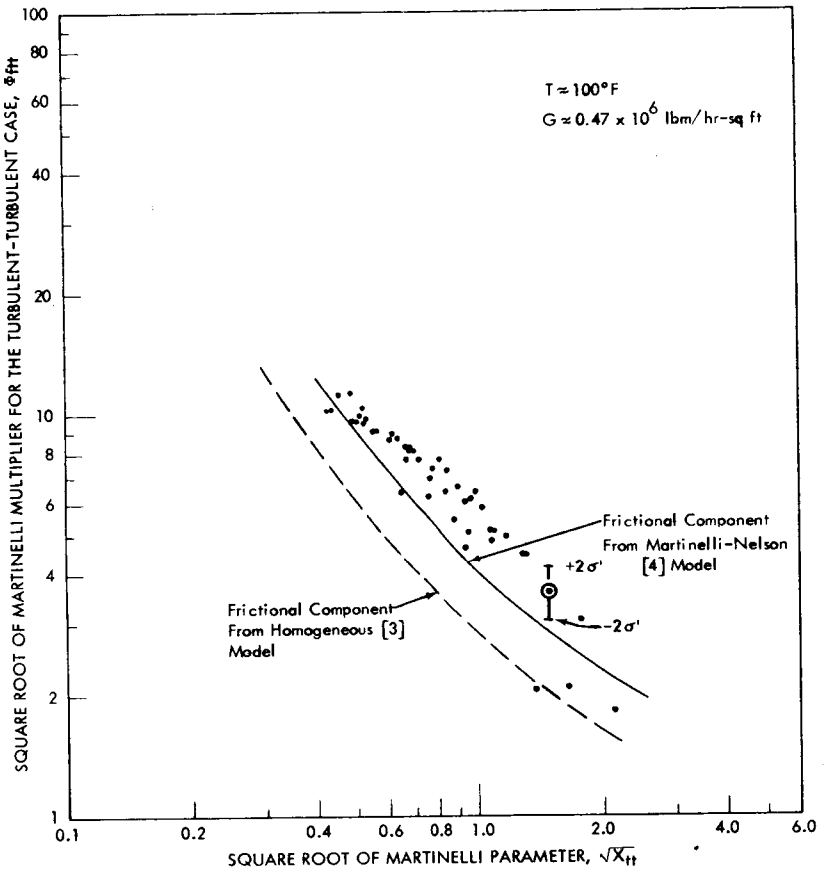


(a)

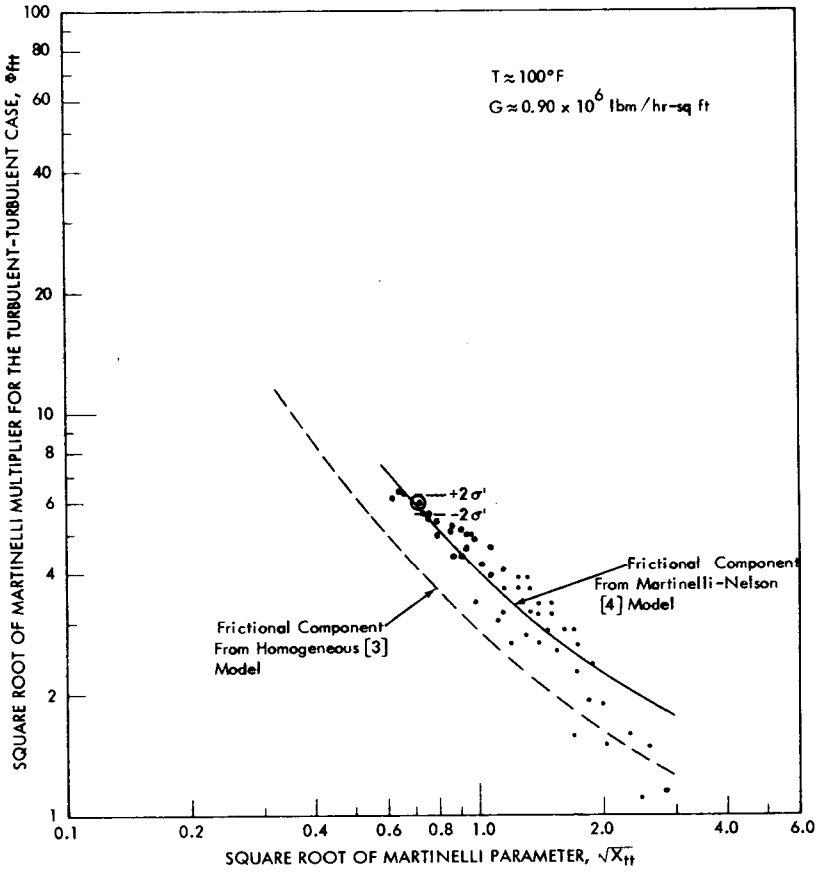


(b)

Figure G-1. EXPERIMENTAL UNCERTAINTY IN FRICTIONAL PRESSURE DROP RESULTS. MARTINELLI-NELSON [4] MODEL WITH ZUBER ET AL [10] MODIFIED VOID FRACTION CORRELATION.

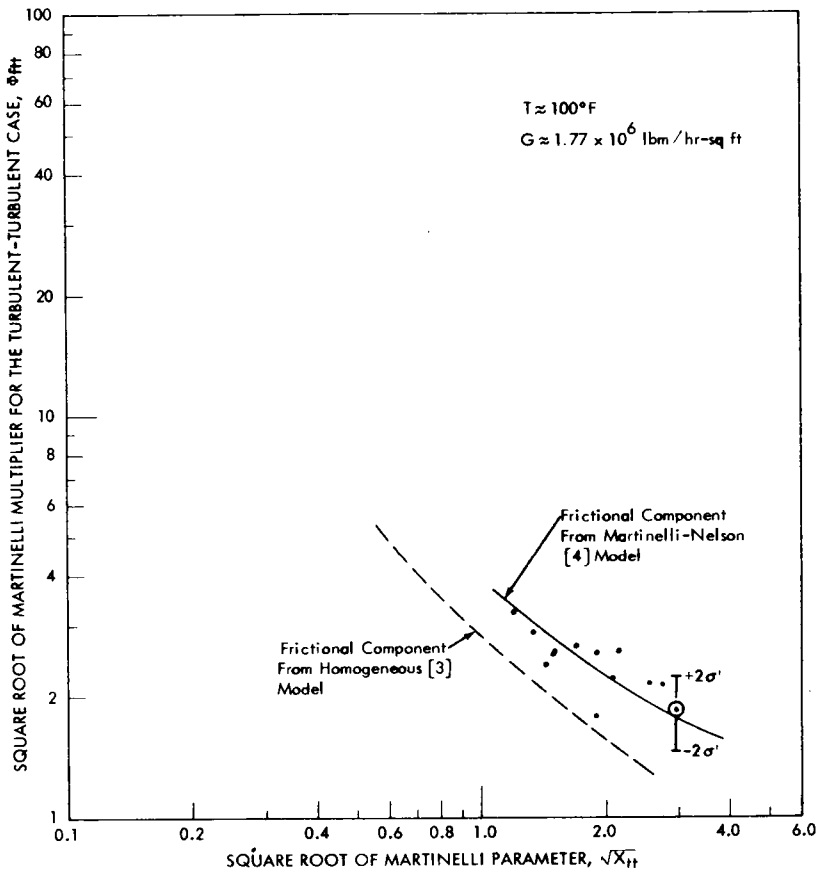


(c)



(d)

Figure G-1. (continued)



(e)

Figure G-1. (continued)

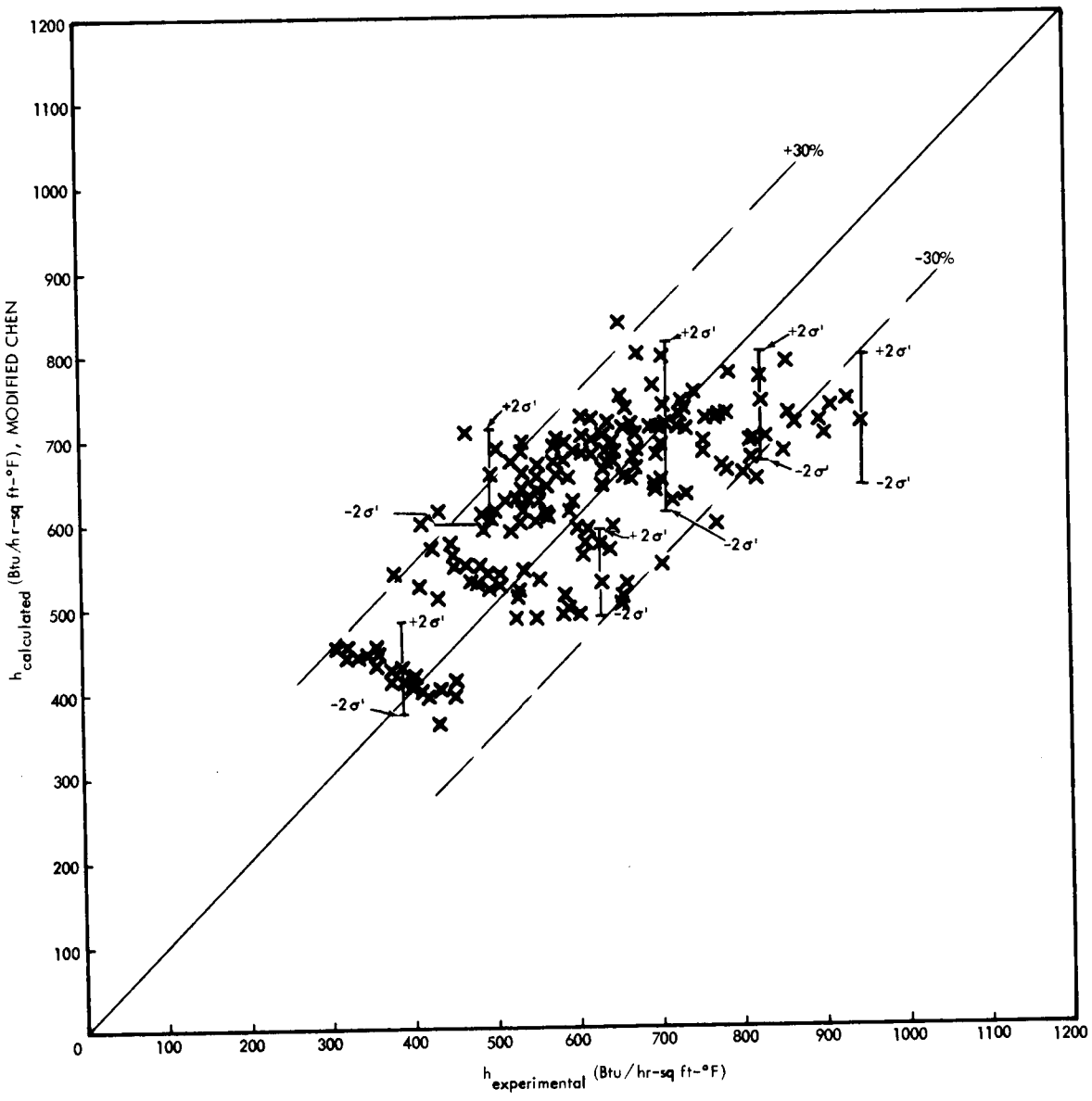


Figure G-2. EXPERIMENTAL UNCERTAINTY IN HEAT TRANSFER COEFFICIENT RESULTS. CHEN [80] CORRELATION USING THE FORSTER-ZUBER [52] POOL BOILING EQUATION WITH A COEFFICIENT OF 0.3802 . T≈100°F.

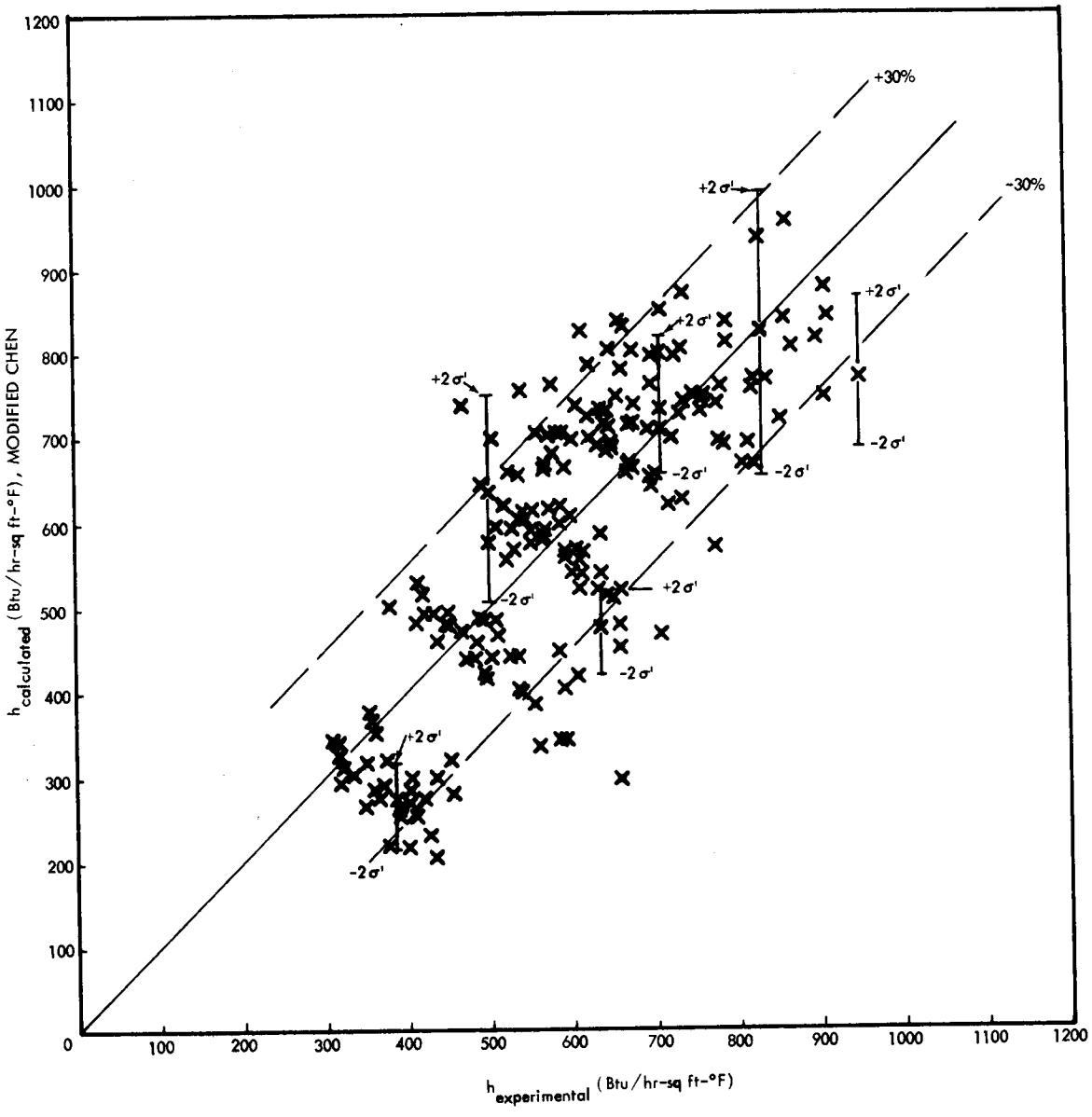


Figure G-3. EXPERIMENTAL UNCERTAINTY IN HEAT TRANSFER COEFFICIENT RESULTS. CHEN [80] CORRELATION USING THE ROHSENOW [61] POOL BOILING EQUATION WITH $C_{sf}=0.0047$. $T \approx 100°F$.

$$\text{RMS } 2 = 4.5460. \tag{G-4}$$

Thus, based on the 150 data points available, little additional error is introduced by constraining the exponent of the (D/L) term. For Dix's [111] data, a similar sensitivity analysis yielded the results

$$\text{RMS } 1 = 7.87543 \tag{G-5}$$

for the case where (D/L) is allowed to vary to any power, and

$$\text{RMS } 2 = 8.70318 \tag{G-6}$$

when the exponent of (D/L) is constrained to the 0.6 value. This was based on 419 data points.

VITA

Philip A. Jallouk was born on June 23, 1945 in Jerusalem, Palestine. He came to the United States in August 1956 and became a U.S. citizen in November 1963. In June 1963, he graduated from Brooklyn Technical High School in Brooklyn, New York. He then enrolled at the Cooper Union School of Engineering and Science in New York City and was graduated in June 1967 with a Bachelor of Science Degree in Mechanical Engineering. He went on to do graduate work at Purdue University from which he received a Master of Science Degree in Mechanical Engineering in June 1969. He subsequently went to work as a Development Engineer for the Nuclear Division of Union Carbide Corporation at the Oak Ridge Gaseous Diffusion Plant where he is presently employed. He is a member of the American Society of Mechanical Engineers and is a registered professional engineer in the State of Tennessee